ASTES

Advances in Science, Technology & Engineering Systems Journal

VOLUME 4-ISSUE 2|MAR-APR 2019

www.astesj.com

ISSN: 2415-6698

Editorial

Advances in Science, Technology and Engineering Systems Journal (ASTESJ) is an online-only journal dedicated to publishing significant advances covering all aspects of technology relevant to the physical science and engineering communities. The journal regularly publishes articles covering specific topics of interest.

Current Issue features key papers related to multidisciplinary domains involving complex system stemming from numerous disciplines; this is exactly how this journal differs from other interdisciplinary and multidisciplinary engineering journals. This issue contains 52 accepted papers in Software Engineering domain.

Editor-in-chief
Prof. Passerini Kazmersk

ADVANCES IN SCIENCE, TECHNOLOGY AND ENGINEERING SYSTEMS JOURNAL

Volume 4 Issue 2 **March-April 2019**

CONTENTS

ASTES

Advances in Science, Technology and Engineering Systems Journal
Vol. 4, No. 2, 01-07 (2019)
www.astesj.com
Special Issue on Multidisciplinary Sciences and Engineering

ASTES Journal
ISSN: 2415-6698

The Chimera and the Cyborg

Hybrid Compute: In vivo HPC, Cloud and Container Implementations

Lev Lafayette[*,1], Bernd Wiebelt[2], Dirk von Suchdoletz[2], Helena Rasche[3], Michael Janczyk[2], Daniel Tosello[1]

[1]*University of Melbourne, Department of Infrastructure, Melbourne, Australia*

[2]*University of Freiburg, High Performance Computing, Freiburg, Germany*

[3]*University of Freiburg, de.NBI, Freiburg, Germany*

ARTICLEINFO

Article history:
Received: 15 August, 2018
Accepted: 03 February, 2019
Online: 10 March, 2019

Keywords:
Hybrid HPC/Cloud
High Performance Computing
Cloud Computing
High Throughput Computing
Containers

ABSTRACT

High Performance Computing (HPC) systems offer excellent metrics for speed and efficiency when using bare metal hardware, a high speed interconnect, and massively parallel applications. However, this leaves out a significant portion of scientific computational tasks, namely high throughput computing tasks that can be trivially parallelized and scientific workflows that require their own well defined software environments. Cloud computing provides such management and implementation flexibility at the expense of a tolerable fraction of performance. We show two approaches to make HPC resources available in a dynamically reconfigurable hybrid HPC/Cloud architecture. Both can be achieved with few modifications to existing HPC/Cloud environments. The first approach, from the University of Melbourne, generates a consistent compute node operating system image with variation in the virtual hardware specification. The second approach, from the University of Freiburg, deploys a cloud-client on the HPC compute nodes, so the HPC hardware can run Cloud-Workloads using the scheduling and accounting facilities of the HPC system. Extensive use of these production systems provide evidence of the validity of either approach.

1 Motivation

Modern research institutions increasingly employ digital methods and workflows, which require a corresponding increase in the amount of computational resources. As data sets grow the researchers' own machines or large workstations no longer suffice, and they must turn to other resources such as High Performance Compute (HPC) and Cloud resources. Procurement, installation, and operation of these compute resources are demanding tasks which cannot be handled by individual researchers and work groups any more. Centralization of resources and administration can leverage economies of scale, but comes with compromises regarding hardware and software configurations that can cater to the needs of a growing user base. Currently neither HPC nor Cloud computing in isolation can mesh the the demands of users with the needs and resources of the compute centers.

University centers must find new, efficient ways to cater to user desires of tailored infrastructures that meets their computational needs. Any new solution should provide comparable offerings regarding features and pricing while avoiding overstretching existing personnel resources. Often demands for hardware arise with short notice and for project durations well below the normal cost amortization period of five to six years. The typical challenges of university computer centers are rooted in the very diversity of their scientific communities; wide ranging requirements for software, services, workflows, and compute resources.

Virtualization is a key technology from two fronts; it can permit accommodating diverse user requirements with a largely centralized resource, and it can help to isolate the different software environments and hardware configurations. As many resources in research infrastructures are inconsistently utilized, tapping into cloud strategies can help to significantly save on energy, personnel investment, and hardware resources.

[*]Corresponding Author: Lev Lafayette, University of Melbourne, lev.lafayette@unimelb.edu.au

https://dx.doi.org/10.25046/aj040201

This paper explores the possibility to overcome the dichotomy of cloud and HPC with a single cohesive system, and how such a setup can provide the performance of an HPC system as well as the flexibility of a cloud compute environment. Furthermore, the paper discusses if such a single system can deliver the best possible result for overall throughput and make better use of computational resources. We examine two practical approaches to make HPC resources available in a dynamically reconfigurable hybrid HPC/Cloud setup, both of which can be achieved with few modifications to existing HPC/Cloud environments. The first approach (University of Melbourne) generates a consistent compute node operating system image with variation in the virtual hardware specification. The second approach (University of Freiburg) deploys a cloud-client on the HPC compute nodes, so the HPC hardware can run Cloud-Workloads for backfilling free compute slots. This paper is an extension of work originally presented in the 2017 IEEE 13th International Conference on e-Science [1], with a new exploration of container implementations in such environments.

2 The HPC/Cloud Conflict

HPC systems running massively parallel jobs require a fairly static software environment, running on bare metal hardware, with a high speed interconnect in order to reach their full potential. Even then, they only offer linear performance scaling for cleverly designed applications. Massively parallel workloads need to be synchronized. Fitting several of these jobs into the individual nodes' schedules will necessarily leave gaps, since jobs have to wait until a sufficient number of nodes become available. The scheduler is "playing Tetris" with large, incompatible pieces, which can lead to under-utilization of the whole system. In contrast, cloud workloads typically consist of small tasks, each only using fractions of the available compute resources, but often in large quantities. Cloud computing offers flexible operating system and software environments which can be optimally leveraged in cases of embarrassingly parallel workloads that do not suffer from slow inter-node connections. A cloud environment offers more flexibility at the expense of the virtualization overhead and the loss of efficient, multi-node high-speed low-latency communication.

Large scale projects, e.g. the Large Hadron Collider from the particle physicist community, have a tendency to develop extremely large and complex software stacks. There exists a well-founded lay-assumption that a computational experiment that deals with objective values ought to be reproducible by other researchers. However this is often not the case as researchers are unaware of the details of their operating environment (operating system, application, and dependencies etc) [2]. One potential solution to the reproducibility issue is to be found in containerisation technology, which permits encapsulation of the entire operating environment. Unfortunately this approach has a couple costs; there is a modest performance penalty, and it requires that the container owner manages be the entire environment.

In addition to the more general problems of HPC and Cloud workloads, finding a truly optimal hybrid system should also consider resource allocation issues. An often encountered instance of this problem is when one parallel application on a HPC system requests 51% of the available resources while another application needs 50% of said resources. It is impossible to co-locate these workloads, which unfortunately leave a large portion of nodes idle if those are the only two tasks scheduled. Another resource allocation problem arises in the scheduling of jobs which different behaviours. In the case where two types of jobs (single-node, short term vs. multi-node, longer term) are submitted to a job scheduler with backfilling to maximise resource utilisation, the overall system can still experience sub-optimal utilization. The single node jobs, request fewer resources and will have priority over the multinode jobs, thereby reducing the cost-effectiveness of the expensive high-speed interconnect and resulting in idle cluster resources.

When looking for a hybrid system which offers flexibility and performance in the face of such problems, it is also worth noting that applications and their datasets usually have varied and characteristic computational workflows that are more or less appropriate for different computational architectures. It is certainly preferable from a user's perspective that a single system is capable of adapting to these diverse requirements, rather than requiring the user to migrate data between different systems depending on the task. A hybrid system must be found in order to address these sub-optimal resource utilization issues.

3 Hybrid Architectures

Both Melbourne and Freiburg Universities have been operating various compute clusters for more than two decades. While the variation in hardware architecture has decreased, new possibilities have arisen from X86 hardware virtualization becoming ubiquitous. It has allowed both sites to host multiple operating systems on a single server and to strictly separate their complete operating environments. Hardware and software stacks are decoupled. While widespread in computer center operation, virtualization is still underutilized in HPC environments. Projects like hybrid cluster approaches and the use of Virtualized Research Environments (VRE) drastically changes the landscape.

3.1 HPC with Compute Nodes as Cloud VMs

The University of Melbourne approach consists of a traditional HPC cluster with a high speed interconnect in one partition (or queue), and an alternative partition providing virtual machines (VM) managed through OpenStack as compute nodes. Using the Slurm Workload Manager multiple partitions are accessible; the bare metal partition in place for a traditional HPC architecture), while the National eResearch Collaboration Tools and Resources project (NeCTAR) research cloud provides generic virtual machines). Additionally there are private departmental partitions (the "water" and "ashley" partitions) , a specialist proteomics partition ("punim0095"), a general GPU partition, a large general-purpose graphics processing (GPGPU) partition for recipients of a specific Linkage, Infrastructure, Equipment, and Facilities (LIEF) grant from the Australian Research Council, and others. In total there are 24 partitions, including those used for debugging and testing purposes, and nodes can belong to multiple partitions simultaneously. Despite their heterogenous high level use cases, the general hardware specifications can be summarised as follows (Fig. 1):

- Physical partition: 12 core, Intel Xeon CPU E5-2643 v3, 3.40GHz, 256GB RAM.
- Cloud partition: 8 core, Intel Haswell, 2.3GHz, 64GB RAM.
- GPGPU partition: 24 core, Intel Xeon E5-2650 v4, 2.20GHz, 128GB RAM, 4 Tesla P100 cards.
- Ceph filesystem: 4.5PB for /home, /project, and /scratch storage.
- Network varies by partition; cloud partition on 10GbE with Cisco Nexus and physical partition with Mellanox ConnectX4 cards and SN2100 switch.

The VMs on the cloud partition use a common image just like the traditional HPC compute nodes, but with differing virtual hardware based on the results of job profiling and user requests. Each of these have an nodelist and are generated by VM images. Deployment of compute node according to partition is carried out with a simple script which invokes the OpenStack Nova service to deploy specific images. These can be deployed as either a static definition, or dynamically using Slurm's cloud-bursting capabilities. In addition the login and management nodes are also deployed as virtual machines.

Jobs are submitted to the Slurm workload manager, specifying which partition that they wish to operate on. The collection of virtual machines comes from the Melbourne share of the Australian-wide NeCTAR research cloud [3]. The VMs, with different virtual hardware, can be configured flexibly into different partitions in accordance with user needs. However, unlike a lot of VM deployments, overcommitment of resources is used. Early testing indicated that whilst there is good boundary separation through the virtualisation model, overcommit usage resulted in unexpected time mismatch errors on concurrent compute tasks. As a result the entire virtual machine architecture operates with a 1:1 ratio with physical machines. While this removes the normal advantages of overcommit for scheduling low utilization processes, it instead simplifies deployment and offers significant flexibility in extending or reducing the size of partition as required.

Of particular importance is assuring that the HPC "physical" partition has a high-speed interconnect. Mellanox 2100 switches with 16 x 100Gb ports with a mixture of 25/50/100Gb, maximum of 64 x 25Gb connections with RDMA over Ethernet and Cumulus Linux OS. An Message Passing Interface (MPI) "ping-pong" test was conducted between two compute nodes on separate infrastructure, with 40GbE RDMA over ethernet receiving better latency results than 56Gb Infiniband FDR14 on a comparable system [4].

3.2 HPC with Cloud VMs on Compute Nodes

The University of Freiburg runs an HPC cluster for Tier-3 users coming from different scientific communities and fields of interest. After a primary installation of 752 nodes in 2016 the cluster now commands more than 1000 compute nodes equipped with dual socket 10 core plus HT Intel Xeon E5-2650 v4, 2.20GHz CPUs and 128GB of memory each. The local operating system is remotely booted over the 1Gb Ethernet interface which also handles most of the user traffic. The cluster is equipped with 100Gb OmniPath offering 44 node islands which are aggregated by 4 100 Gb links. This high speed low latency network provides both MPI functionality for HPC jobs and access to the BeeGFS parallel filesystem.

Standard bare metal jobs are scheduled by Adaptive Moab. On top of the standard HPC jobs (bare metal jobs), it enables users to run virtual machines as standard compute jobs (VM jobs). In order to run VMs on a compute node, a virtualization hypervisor is installed on every compute node using the standard Linux Kernel-based Virtual Machine (KVM) hypervisor. This architecture enables users to run both bare metal and VM jobs on the same hardware, through the same resource manager, without partitioning the cluster into isolated parts. Users that require a special software environment and do not need direct access to hardware can use the VM jobs which provide Virtual Research Environments (VRE). A VRE in this instance is a container image with a complete software stack installed and configured by the user [5]. Thus, the file system of a virtual machine or VRE is a disk image presented as a single file. From the operator's perspective this image is a "black box" requiring no involvement, provisioning, updating, nor any other management effort. From the researcher's perspective the VRE is an individual virtual node whose operating system, applications and configurations as well as certain hardware-level parameters, e.g. CPU and RAM, can be configured fully autonomously by the researcher.

On typical HPC clusters the resource management is orchestrated through a scheduler. Since researchers using a hybrid compute resource are allowed both to submit jobs to the scheduler for bare metal computation and initiate VRE jobs, it is necessary that the scheduler is also responsible for the resources requested by virtual machines. If VMs are executed on the cluster without the knowledge of the scheduler, resources could get overbooked. A special workflow was developed to submit a request for a VM as a normal cluster job and let the scheduler handle the request for a new virtual machine. Thus, the hybrid HPC cluster concept becomes flexible and independent of the actual scheduler deployed.

The hybrid cluster setup is not without additional costs. For the orchestration of the virtual machines on the cluster the OpenStack framework is installed. If a compute job is designed to run in a virtual environment (VM) the Moab scheduler is configured to instantiate this VM through the OpenStack API. OpenStack is selected for its modular architecture to allow to choose the components needed for the cluster virtualization, such as network, image handling or a web interface and omit the rest. While introducing additional management and operational overheads, this allows building a virtualization environment for the cluster that meets the specific objectives. Four infrastructure nodes are dedicated to running the OpenStack services and preparing VM images. These nodes are not part of the compute resources available to the user.

3.3 Containerization

A further elaboration of the hybrid architecture is the use of containers in either aforementioned model. Whilst virtual machines simulate the hardware environment (even in a 1:1 environment), a container virtualizes at the operating system level. As containers can be imported with a exact level of consistency this is seen as solution to reproducibility issues in computation.

The most well-known application for containerisation is Docker. However Docker is not a good fit for the common tasks in research computing [6]. Docker is primarily designed for micro-services on an enterprise level, or during software development on local systems. Additionally, the Docker daemon runs as root, and the group with root privileges, which has security implications, e.g. when mounting file systems. These scaling and security issues leads HPC system administrators to be resistant to the installation of Docker. As an alternative, Singularity can be deployed without the issues of Docker, to obtain the benefits of containerisation [7]. Singularity is used at the University of Melbourne as it has good integration with the Slurm Workload Manager and MPI. Security issues are mitigated by ensuring that user privileges inside the system are the same as the privileges outside the system (i.e., as a user on an HPC) and that there are no root-owned daemons or root-level privileges for the group. Another container technology that also is considered appropriate for high performance compute environments is Shifter [8]. In either case, these containers can run on HPC nodes, whether they are bare-metal or virtualized, leading to the interesting situation of a virtualized operating environment (singularity) on a VM with its own operating environment, which is running on real hardware with an additional operating environment. The saying “that there is no cloud, there is just somebody else’s computer” is doubly applicable for containers.

The following is a simple example to illustrate the use of the container within a Slurm job script that makes use of an existing container.

```
#!/bin/bash
#SBATCH --partition cloud
module load Singularity/2.4-GCC-6.2.0
singularity \
 exec vsoch-hello-world-master.simg \
 echo "Hello from inside my container!" \
 > output.txt
```

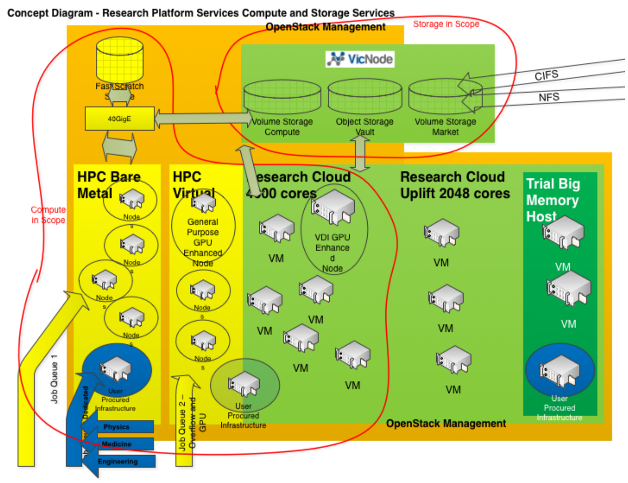

Figure 1: Concept diagram of the hybrid research platform services, combining bare metal and OpenStack resources at the University of Melbourne depicting the various partitions.

4 Workflow Design

Given the two competing primary compute resource variants, HPC scheduling and Cloud scheduling, it is necessary to orchestrate both systems through a mediator. In a hybrid approach one needs to define a primary scheduler which controls which jobs should run on which worker node and instruct the other scheduler to run within the boundaries of the other scheduler, especially respecting the scheduling decision of the other. The mediator could be a special service daemon which waits for requests from users and administrators and translates it to the OpenStack API and vice versa.

The University of Melbourne uses a traditional HPC workflow where job submission with Slurm Workload Manager occurs on different partitions according to whether they are based on physical or cloud architectures. At the University of Freiburg three workflows are present; job submission via Moab scheduler without running a resource manager client in the VM, job Submission via Moab scheduler with a resource manager client, The Terascale Open-source Resource and QUEue Manager (TORQUE) running in the VM, and job submission via OpenStack Dashboard/API.

4.1 Job Submission with Slurm Scheduler for different Partitions

A standard batch job submission workflow is a key part of the architecture. This follows the well-known path in HPC for job submission. As a unique feature, the placement of the virtual machine on the cluster nodes is scheduled by Moab and the job lifetime is coupled to the lifetime of the VM. This allows for a seamless integration with the jobs sent by other user groups and honors the fairshare policies of the cluster. A batch script makes resource requests on a particular partition. Based on the resource request, the information received from resource manager daemons, and the fairshare policies in place, the scheduler will allocate a time when the job will run which may change if other jobs finish early etc. At the appropriate time, the job will launch on one or more compute nodes, run, and write the relevant processed data and output to the directories as specified. The developed thin integration layer between OpenStack and Moab can be adapted to other batch servers and virtualization systems, making the concept also applicable for other cluster operators.

In the University of Melbourne model, the Slurm workload manager acts as the job scheduler and resource manager. Different partitions refer to the queues which a user may submit jobs and are varied by the physical or virtual hardware that have been provisioned (e.g., `#SBATCH --partition=cloud` or `#SBATCH --partition=physical`). For single node jobs, whether single or multi-core, a low speed (Ethernet) network and virtual machines are suitable, whereas for multinode jobs the physical partition with a high-speed interconnect is used. Thus, the physical architecture is optimised for the type of computational task required, increasing overall throughput and more efficiently allocating resource.

4.2 Job Submission via Moab Scheduler without running a Resource Manager Client in the VM

At the University of Freiburg, one use case is where users provide their VM images themselves. These VM images cannot be trusted and therefore they are not allowed to access cluster resources like parallel storage or user home directories. It is expected that the user is working with an external resource manager or is using the cloud-init procedure to start compute jobs within the VM. In this case the user's workflow is to submit a cluster job through the scheduler msub/qsub and, if resources are available, the job launches a virtual machine via the OpenStack API. When the VM boots data and compute instructions have to be injected by an external resource manager or through cloud-init into the virtual machine (possibly injecting the aforementioned cluster job script).

4.3 Job Submission via Moab Scheduler with a Resource Manager Client (TORQUE) running in the VM

A second use case at the University of Freiburg is when the user submits classic compute jobs to a different software environment on the cluster (Fig. 2, left branch). The software environment is represented by a VM in this case. This makes it necessary to install and run a TORQUE client in the virtual machine. In this use case the workflow begins with the user submitting a job through the scheduler (msub/qsub) with a specified image and job-script (e.g., msub -l image=¡id¿ job-script.sh). The job is then scheduled like any other bare metal job. If and when resources are available this job will trigger the start of a new virtual machine environment through the OpenStack API. When the virtual machine is booted the TORQUE client connects to the TORQUE server and receives the job which then is started within the VM. If this software environment is provided by an external source (user virtual machine) all necessary data has to be injected as well. This could be achieved for example with the stagein and stageout options from TORQUE.

4.4 Job Submission via OpenStack Dashboard/API

The third use case from the University of Freiburg is when the user submits compute jobs simply by creating a VM via the OpenStack web interface (Horizon) or OpenStack API (Fig. 2, right branch). These virtual machines then should be represented as a compute job in the Moab scheduler. The compute job script is injected via cloud-init into the virtual machine during boot and is executed in the virtual machine after the boot process is finished. In this use case the workflow is initiated by the user starting a virtual machine instance on the compute partition. OpenStack schedules this VM as any other bare metal job and, when and if resources are available, OpenStack will start up the virtual machine on the resources previously assigned by the Moab scheduler. When the virtual machine boots data and compute instructions have to be injected by an external resource manager or through cloud-init into the virtual machine.

4.5 Script and Data Injection

In the University of Melbourne case the injection of scripts and data to the virtual machine is not a significant issue, as the virtual machines are simply another node on the HPC system. The issues faced here are the same as other HPC environments. Primarily this means the need to firmly encourage users to manage their data so that it is physically close to the site of computation. Grace Hopper's famous reminder [9] to "mind your nanoseconds" is applicable even to many research scientists who ask whether remote data can have a mount-point on a HPC system in order to speed up their computational time, and even across all compute nodes which are normally do not have access outside of the system network for security reasons. A more genuine issue is the access speed of shared mount points across a system, and education on the need for staging actions on local (e.g., `/var/local/tmp`) disk or faster shared storage (e.g., `/scratch`) before copying data to slower shared directories.

For Freiburg's architecture the situation is more complex. There are there possibilities to inject job scripts into a VM: cloud-init, TORQUE client and an external resource manager client.

- cloud-init: This is the easiest way to inject job scripts into a VM. A job script has to be specified when instantiating the VM. After booting the VM the script gets executed automatically.
- TORQUE Resource Manager Client: Since the Cluster uses the TORQUE resource manager new "virtual" clients can be added dynamically and so the job script will be injected directly through the resource manager to the client. The only challenge is to signal the TORQUE Client running the bare metal job not to execute the job script.
- External Resource Manager: If external scheduling and resource managers are implemented by a research group they can be used to inject job scripts into the VM. Once the virtual resource pops up after starting a VM on the bare metal cluster it registers at its external resource manager and then can be used as every other resource of this Resource Manager.

The nature of the VM image defines the difficulty of injecting data into the booted virtual environment. Usually virtual research environments are built by research groups containing the configuration and software which is necessary to solve the problems of that specific research groups. Since these VM images are externally built, the instantiated environments can't be trusted. In such environments mounting home and work directories is not allowed, so other methods for data injection and result retrieval from these environments must be available. There are two possibilities to do so:

- The job script can provide information on how to transfer data by copying or streaming it through the network
- The resource manager client features can be used to stage data into the VM and stage out the results. TORQUE supports staging data by specifying the options "stagein" and "stageout", the job output is copied to the remote site automatically if not specified otherwise in the TORQUE client config (`$usecp`).

For trusted virtual environments provided by cluster administrators, these issues are not present. For example replicating a modules software environment for experimental particle physicists. These virtual environments are fully controlled by the same people running the bare metal environment and so can be trusted. In these environments, home and work directories can be mounted, and users can be identified and authorized through the same mechanisms as in the underlying bare metal environment. They can be simply leveraged by users as special software environments with no difference to the bare metal system (ignoring the fact, that it wouldn't support multi-node usage).

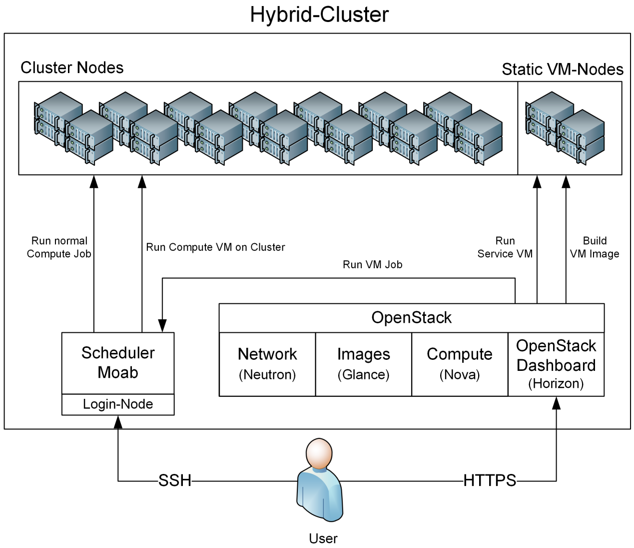

Figure 2: The Freiburg HPC cluster user has multiple options to submit compute jobs, either via the traditional way submitting it to the scheduler (left branch) or interactively by starting an appropriate virtual machine containing the relevant workflow (right branch).

5 Conclusions

Hybrid clusters make research groups more independent from the base software environment defined by the cluster operators. Operating VREs brings additional advantages like scientific reproducibility but may introduce caveats like lost cycles or a layered job scheduling. However, the advantages of this approach makes HPC resources more easily available for broader scientific communities. Both models are meant to be easily extensible by additional resources brought in by further research groups.

The two models - HPC with Cloud VMs on Compute Nodes, and HPC with Compute Nodes as Cloud VMs - represent different hybrid systems to solve different problems. In effect, the University of Freiburg model provides a "cyborg", where the HPC compute nodes are replaced with cloud virtual machines, whereas the University of Melbourne model provides a "chimera", a multi-headed beast where the virtual machines have become new cloud nodes. In the former case there was a desire to make existing compute nodes available to researchers for their particular configurations. In the latter case there was a desire to make virtual machines accessible to an HPC system to increase cost efficiency and improve throughput.

The two approaches illustrate the importance of HPC-Cloud hybrids in general purpose research computing.

Migrating complex and diverse software stacks to new HPC systems every few years constitutes a major effort in terms of human resources. By virtualization of these complex software environments, one sacrifices a fraction of performance, but one gains the possibility to run these complex software environments in cloud systems and thus literally anytime, anywhere and on any scale. This flexibility, in many cases, outweighs the loss in performance [10, 11, 12].

For future developments, the University of Melbourne plans to extend their model to provide the ability to include cloud bursting to external providers (e.g., Amazon, Azure), and hosting highly varied X86 configurations on the same system, although this requires equivalent real or virtual hardware, partial replication of the operating environment, and accounting for latency between the local and remote sites. A further option of HPC cloud-bursting that will be subject to further investigation is Moab/NODUS cloud-bursting by Adaptive Computing. The principles used by NODUS are similar to the exploration here; a workload queue has an elastic trigger that uses an API key to an template image which then invokes nodes, deploys upon them and potentially cluster nodes simultaneously, completes the job, and transfers the data as necessary. The ability for fine-grained task parallel workloads across local HPC and remote cloud providers suggests an obvious difficulty.

The University of Freiburg model is rather complex and took a while to mature. It is in production since the official start of the cluster in mid 2016. The HPC/cloud group hopes to improve their model, mapping Moab commands to OpenStack commands allowing to pause/hibernate and resume the virtual machine for preemption or maintenance instead of killing a job. In addition the possibility of mapping the live migration of virtual machine to Moab during runtime will give the opportunity to migrate compute jobs during runtime to optimize the overall cluster utilization. For the next generation HPC cluster we will reconsider the options to reduce the complexity of the VRE scheduling. Following the Melbourne model a distinct cloud partition for the future system is definitely an option.

Acknowledgment Lev Lafayette would like to thank Bernard Meade, Linh Vu, Greg Sauter, and David Perry from the University of Melbourne for their contributions to this document. The authors from Freiburg University would like to thank the Ministry of Science, Research and the Arts of Baden-Württemberg (MWK) and the German Research Foundation (DFG) which funded both the research infrastructure NEMO and the ViCE eScience project on Virtual Research Environments.

References

[1] L. Lafayette and B. Wiebelt, "Spartan and NEMO: Two HPC-cloud hybrid implementations," in *13th International Conference on e-Science*, IEEE, oct 2017.

[2] V. V. Sochat, C. J. Prybol, and G. M. Kurtzer, "Enhancing reproducibility in scientific computing: Metrics and registry for singularity containers," *PLOS ONE*, vol. 12, p. e0188511, nov 2017.

[3] Z. Li, R. Ranjan, L. O'Brien, H. Zhang, M. A. Babar, A. Y. Zomaya, and L. Wang, "On the communication variability analysis of the NeCTAR research cloud system," *IEEE Systems Journal*, vol. 12, pp. 1506–1517, jun 2018.

[4] B. Meade, L. Lafayette, G. Sauter, and D. Tosello, "Spartan HPC-Cloud Hybrid: Delivering performance and flexibility," 2017.

[5] M. Janczyk, B. Wiebelt, and D. von Suchodoletz, "Virtualized research environments on the bwForCluster NEMO," in *Proceedings of the 4th bwHPC Symposium*, 2017.

[6] G. Kurtzer, "Singularity: Containers for science, reproducibility, and high performance computing." Keynote at Stanford Conference, 2017.

[7] G. M. Kurtzer, V. Sochat, and M. W. Bauer, "Singularity: Scientific containers for mobility of compute," *PLOS ONE*, vol. 12, p. e0177459, may 2017.

[8] D. M. Jacobsen and R. S. Canon, "Contain this, unleashing docker for HPC," in *Proceedings of the Cray User Group*, 2015.

[9] L. Gilbert, *Particular Passions: Grace Murray Hopper (Women of Wisdom)*. Lynn Gilbert Inc., 2012.

[10] A. Gupta and D. Milojicic, "Evaluation of HPC applications on cloud," in *Sixth Open Cirrus Summit*, IEEE, oct 2011.

[11] P. Church and A. Goscinski, "Iaas clouds vs. clusters for hpc: a performance study," in *Cloud Computing 2011 : The 2nd International Conference on Cloud Computing, GRIDS, and Virtualization*, pp. 39–45, IARIA, 2011.

[12] A. Marathe, R. Harris, D. K. Lowenthal, B. R. de Supinski, B. Rountree, M. Schulz, and X. Yuan, "A comparative study of high-performance computing on the cloud," in *Proceedings of the 22nd international symposium on High-performance parallel and distributed computing - HPDC '13*, ACM Press, 2013.

ASTES

Advances in Science, Technology and Engineering Systems Journal
Vol. 4, No. 2, 8-16 (2019)
www.astesj.com
Special Issue on Recent Advances in Engineering Systems

ASTES Journal
ISSN: 2415-6698

Robust synchronization of nonfragile control of complex dynamical network with stochastic coupling and time-varying delays

Fehrs Adu-Gyamfi[*,1,2], Yuhua Cheng[1], Chun Yin[1]

[1] *University of Electronic Science and Technology of China (UESTC), School of Automation,611731, Chengdu - P.R. China*

[2] *Koforidua Technical University (KTU), Mechanical Engineering Department, Faculty of Engineering, KF 981, Koforidua-Ghana*

ARTICLEINFO

Article history:
Received: 04 December, 2018
Accepted: 22 February, 2019
Online: 10 March, 2019

Keywords:
Complex dynamical networks
Extended Jensen's integral inequality
Nonfragile control
Robust
Stochastic coupling
Synchronization

ABSTRACT

This paper explores the problem of robust synchronization of complex dynamical network with stochastic coupling and time-varying delays through the application of nonfragile control. A well defined Lyapunov Krasovskii functional is established and by employing the widely acknowledged extended Jensen's integral inequality and the Bernoulli's distribution sequences, the stochastic nature of network coupling is modeled which entails the occurrence of randomness in the controller gain uncertainties are presented. Sufficient delay dependent conditions are given for the purposes of synchronization. Additionally, a nonfragile controller is designed based on linear matrix inequalities (LMIs). Two numerical examples are finally given to exhibit the effectiveness and usefulness of the proposed theoretical results.

1 Introduction

This article is an extension of a paper previously presented in the international conference of ubiquitous and future networks 2018 (ICUFN 2018) [1]. The great works of Watts and Strogatz [2] which focused on investigation of complex networks have witnessed a tremendous attention from many scientific communities because of the theoretical importance and practical implementation of such outcome in areas such as computer networks, social networks, biological networks, communication networks, electric power grid, food webs and transportation networks [3, 4, 5, 6, 7, 8]. Complex dynamical networks (CDNs) are large number of interconnected nodes with each node having some defined contents. Majority of these networks display some level of complexities in their overall topology as well as dynamical properties [9]. Amongst the important collective behaviors of CDNs is synchronization problem. This behavior has been investigated by many profound researchers [10, 11]. Synchronization of a network is related to subsystems been represented as nodes in coupled systems in which the various nodes with different initial conditions converge to a common behavioral trajectory. Many control methodologies have been proposed to ensure the solution to synchronization problems, amongst such control methods are pinning control [12], sampled data control [13], sliding mode control [14], impulsive control [15] and so on. The tendencies of sudden changes in network coupling which can emanate from internal and external environmental factors such as unexpected change of working environment, random link failures and repairs on network connectivity result in stochastic behavior in the network coupling. Additionally, the practical implementation of control design might not be precise because of limited information speed, round-off error of numerical computations, aging of system components, analogy to digital conversions (ADC) and Digital to analogy conversion (DAC) [13]. Controller fragility refers to the variation effects on the control parameters as cited in [16]. This problem is addressed in the design of a nonfragile control

[*] Corresponding Author: Fehrs Adu-Gyamfi, UESTC and KTU, Email: fehrs.adugyamfi@ktu.edu.gh

https://dx.doi.org/10.25046/aj040202

scheme which is presented to address controller gain fluctuation based on the aforementioned shortfalls as presented in [17, 18].
Time delays which are ubiquitous in nature and present in CDNs, possess the ability to destroy synchronization performance which can lead to oscillation and instability of the network, hence the need to consider it when addressing synchronization issues of CDNs. It is very important to also note that, there exit time delays in the exchange of information resulting from finite transmission speed in the network, memory effect, limited bandwidth and so on [19]. From the aforementioned discussions, we are motivated in this paper to seek solutions to CDNs synchronization with nonfragile control design scheme, taking into consideration the stochastic coupling nature of the network. The important contributions of this paper are summarized as follows:

1. The problem of CDNs robust synchronization with stochastic coupling and time-varying delays is studied permitting some level of control gain uncertainties.

2. Control scheme with non-fragile characteristics is designed and presented which guarantee the system error synchronization.

3. A suitable Lyapunov Krasovskii functional (LKF) is chosen which applied the extended Jensen's integral inequality.

4. Given are two numerical examples which indicate the usefulness of our proposed control approach.

2 Model description and Preliminaries

In this paper, standard notations are used. $\mathbb{R}^n$ shows the Euclidean n- dimensional space, $\mathbb{R}^{m\times n}$ denotes the set of all $m \times n$ real matrices. I and 0 represent identity and zero matrices with appropriate dimensions, respectively. $P > 0$ is a real positive symmetric definite matrix. The superscript "T" indicates transposition. Also, an asterisk($*$) is used to show the symmetric terms and diag{....} represent a diagonal block matrix. All other matrices without given dimensions are considered to be of compatible dimensions. In this paper, the robust synchronization of CDNs which entail the stochastic coupling of N identical nodes with time varying delays is described as follows:

$$\begin{aligned}\dot{\tilde{r}}_i(t) =& A\tilde{r}_i(t) + Bf(\tilde{r}_i(t)) + (1-\bar{\delta}_1(t))\sum_{j=1}^{N}\bar{c}_{ij}\Gamma\tilde{r}_j(t)\\ &+ \bar{\delta}_1(t)\sum_{j=1}^{N}\bar{c}_{ij}\Gamma\tilde{r}_j(t-\ddot{\gamma}(t)) + \hat{u}_i(t),\\ &i = 1,2,\dots,N,\end{aligned} \tag{1}$$

Where, $\tilde{r}_i(t) = (\tilde{r}_{i1}(t), \tilde{r}_{i2}(t), ..., \tilde{r}_{in}(t))^T \in \mathbb{R}^n$ denotes the state vector of the i^{th} node, $\hat{u}_i(t) \in \mathbb{R}^n$. A, B are known real constant matrices and they are assumed to be stabilizable, $f : \mathbb{R}^n \to \mathbb{R}^n$ indicate a smooth nonlinear function, $\Gamma \in \mathbb{R}^{n\times n}$ is the inner coupling matrix of the nodes and $\bar{C} = (\bar{c}_{ij})_{N\times N}$ represent the outer coupling configuration of the network. If there is a connection from node i to node j ($i \neq j$), then the coupling matrix $\bar{c}_{ij} \neq 0$; otherwise $\bar{c}_{ij} = 0$. Furthermore, the diagonal elements are defined as $\bar{c}_{ii} = -\sum_{j=1,j\neq i}^{N}\bar{c}_{ij}$. $\ddot{\gamma}(t)$ represent time-varying delay which is considered to be a differentiable function that satisfies the following conditions:

$$0 \le \ddot{\gamma}_1 \le \ddot{\gamma}(t) \le \ddot{\gamma}_2, \qquad \dot{\ddot{\gamma}}(t) \le \tilde{\mu}. \tag{2}$$

$\bar{\delta}_1(t) \in \mathbb{R}$ denotes a stochastic variable, which is in the form of a Bernoulli distribution sequence defined by

$$\bar{\delta}_1(t) = \begin{cases}1 & \text{presence of delay in information exchange,}\\ 0 & \text{no delay in information exchanges}\end{cases}$$

Below indicates the stochastic probability variable $\bar{\delta}_1(t)$:

$$Pr\{\bar{\delta}_1(t) = 1\} = \bar{\delta}_1,$$
$$Pr\{\bar{\delta}_1(t) = 0\} = 1 - \bar{\delta}_1,$$

where $\bar{\delta}_1 \in [0,1]$ is a known constant.
Then, the supposed initial condition for (1) is given by $\tilde{r}_i(t) = \bar{\psi}_i(t)$, $t \in [-\ddot{\gamma}_2, 0]$ and $i = 1,\dots,N$.

Assumption 2.1 *[20] The continuous vector valued function $f(\bullet) : \mathbb{R}^n \to \mathbb{R}^n$ is considered which satisfies $f(0) = 0$, hence this sector-bounded condition stands:*

$$[f(x)-f(y)-Z_1(x-y)]^T[f(x)-f(y)-Z_2(x-y)] \le 0, \tag{3}$$

given that Z_1 and Z_2 are constant matrices of appropriate size. From (1) and using kronecker properties, we have

$$\begin{aligned}\dot{\tilde{r}}(t) =& (I_N \otimes A)\tilde{r}(t) + (I_N \otimes B)g(\tilde{r}(t)) + (1-\bar{\delta}_1(t))(\bar{C}\otimes\Gamma)\\ &\times \tilde{r}(t) + \bar{\delta}_1(t)(\bar{C}\otimes\Gamma)\tilde{r}(t-\ddot{\gamma}(t)) + \hat{u}(t)\end{aligned}$$

Where,

$$\tilde{r}(t) = [\tilde{r}_1^T(t), \tilde{r}_2^T(t), \dots, \tilde{r}_N^T(t)]^T,$$
$$g(\tilde{r}(t)) = [f^T(\tilde{r}_1(t)), f^T(\tilde{r}_2(t)), \dots, f^T(\tilde{r}_N(t))]^T,$$
$$\hat{u}(t) = [\hat{u}_1^T(t), \hat{u}_2^T(t), \dots, \hat{u}_N^T(t)]^T.$$

Lemma 2.1 *([21] Jensen inequality) Given a matrix $H = H^T > 0$, of an appropriate dimension and a vector function $\bar{\alpha}(\cdot) : [0 \quad \bar{\gamma}] \to \mathbb{R}^n$ for a scalar $\bar{\gamma} > 0$, the integration is defined as follows:*

$$\bar{\gamma}\int_0^{\bar{\gamma}}\bar{\alpha}^T(s)H\bar{\alpha}(s)ds \ge \left[\int_0^{\bar{\gamma}}\bar{\alpha}(s)ds\right]^T H\left[\int_0^{\bar{\gamma}}\bar{\alpha}(s)ds\right] \tag{4}$$

Lemma 2.2 *[22] For constant matrices* $L = \begin{pmatrix} L_{11} & L_{12} \\ L_{21} & L_{22} \end{pmatrix}$, $L \in \mathbb{R}^{2n\times 2n}$, $\tilde{U} = \tilde{U}^T > 0$, $\tilde{U} \in \mathbb{R}^{n\times n}$, *a continuous function satisfying* $d_1 \le d(t) \le d_2$, *and a continuously differentiable function* $x : [-d_2, 0] \to \mathbb{R}^n$ *such that the integration is properly defined, hence the following inequality holds:* $\int_{t-d_2}^{t-d_1} \dot{x}^T(s)\tilde{U}\dot{x}(s)ds \ge \frac{1}{d_{12}} v^T(t)\Psi v(t)$
where

$$
\begin{aligned}
&v(t) = [\ v_1^T(t) \quad v_2^T(t) \quad v_3^T(t) \quad v_4^T(t)\ ]^T \\
&d_{12} = d_2 - d_1 \\
&v_1(t) = x(t-d_1) - x(t-d(t)) \\
&v_2(t) = x(t-d_1) + x(t-d(t)) - \frac{2}{d(t)-d_1}\int_{t-d(t)}^{t-d_1} x(s)ds \\
&v_3(t) = x(t-d(t)) - x(t-d_2) \\
&v_4(t) = x(t-d(t)) + x((t-d_2) - \frac{2}{d_2-d(t)}\int_{t-d_2}^{t-d(t)} x(s)ds \\
&\Psi = \begin{bmatrix} \tilde{U} & 0 & L_{11} & L_{12} \\ * & 3\tilde{U} & L_{21} & L_{22} \\ * & * & \tilde{U} & 0 \\ * & * & * & 3\tilde{U} \end{bmatrix} \ge 0.
\end{aligned}
\tag{5}
$$

Remark 1. The Lemma (2.2) is derived from the reciprocal convex combination techniques with Jensen inequality resulting in the less conservativeness of our results. The detailed proof is omitted but can be referred from [22].

Lemma 2.3 *(Schur Complement [23]): For a given matix*

$$\Lambda = \begin{pmatrix} \Lambda_{11} & \Lambda_{12} \\ * & \Lambda_{22} \end{pmatrix} < 0,$$

any of the inequalities below is equivalent to Λ :

1. $\Lambda_{11} < 0, \quad \Lambda_{22} - \Lambda_{12}^T \Lambda_{11}^{-1} \Lambda_{12} < 0$
2. $\Lambda_{22} < 0, \quad \Lambda_{11} - \Lambda_{12} \Lambda_{22}^{-1} \Lambda_{12}^T < 0$

Lemma 2.4 *[6], Suppose* $Q = Q^T$, R *and* T *been real appropriate dimension matrices and the function* $F(t)$ *which satisfies the condition* $F^T(t)F(t) < I$. *Accordingly,* $Q + RF(t)T + T^T F^T(t)R^T < 0$ *when a given scalar* $\epsilon > 0$ *exist. Then,*

$$\begin{bmatrix} Q & R & \epsilon T^T \\ * & -\epsilon I & 0 \\ * & * & -\epsilon I \end{bmatrix} < 0.$$

Definition 1 *The CDNs* (1) *is synchronized when the condition below holds:*

$$\lim_{t\to\infty} [\tilde{r}_i(t) - s(t)] = 0.$$

Consider the dynamics of an isolated unforced node $s(t)$ to be $\dot{s}(t) = As(t) + Bf(s((t)))$. $s(t)$ can be taken as an equilibrium point, periodic orbit, or even a chaotic attractor.
Let the i^{th} node error system be given as $e_i(t) = \tilde{r}_i(t) - s(t)$. Consequently, error dynamics of CDNs (1) is given by:

$$
\begin{aligned}
\dot{e}_i(t) &= Ae_i(t) + Bg(e_i(t)) + (1-\bar{\delta}_1(t))\sum_{j=1}^{N} \bar{c}_{ij}\Gamma e_j(t) \\
&+ \bar{\delta}_1(t)\sum_{j=1}^{N} \bar{c}_{ij}\Gamma e_j(t-\ddot{\gamma}(t)) + \hat{u}_i(t)
\end{aligned}
\tag{6}
$$

Note: $g(e_i(t)) \equiv f(\tilde{r}_i(t)) - f(s(t))$.
The designed control scheme to guarantee synchronization of the CDNs is:

$$\hat{u}_i(t) = (k_i + \sigma(t)\triangle k_i(t))e(t) + k_\tau e(t-\ddot{\gamma}(t)), \quad i = 1, 2, \ldots, N. \tag{7}$$

Consider $k_i, k_\tau \in \mathbb{R}^{n\times n}$ as the feedback controller gain matrices which are yet to be estimated. Also, $\triangle k_i$ represent the gain fluctuation, where $\triangle k_i(t)$ is known as follows:

$$\triangle k_i(t) \equiv H_i \Upsilon_i(t) W_i$$

where $\Upsilon_i(t) \in \mathbb{R}^{k\times l}$, is an unknown time-varying matrix which satisfies the condition: $\Upsilon_i(t)^T \Upsilon_i(t) \le I$, H_i and W_i are matrices of known parameters. The probability variable $\sigma(t)$ shows controller gains fluctuations. The random occurring fluctuations of the gain obeys the Bernoulli distribution with the following definition

$$\sigma(t) = \begin{cases} 1 & \text{Gain fluctuation occur,} \\ 0 & \text{Gain fluctuation does not occur} \end{cases}$$

and the probability of stochastic parameter $\sigma(t)$ is given as:

$$
\begin{aligned}
&Pr\{\sigma(t) = 1\} = \sigma \\
&Pr\{\sigma(t) = 0\} = 1 - \sigma; \quad \sigma \in [0, 1]
\end{aligned}
$$

Closed loop of the error dynamics (6) of the CDNs yields:

$$
\begin{aligned}
\dot{e}_i(t) &= Ae_i(t) + Bg(e_i(t)) + (1-\bar{\delta}_1(t))\sum_{j=1}^{N} \bar{c}_{ij}\Gamma e_j(t) \\
&+ \bar{\delta}_1(t)\sum_{j=1}^{N} \bar{c}_{ij}\Gamma e_j(t-\ddot{\gamma}(t)) + (k_i + \sigma(t)\triangle k_i(t))e_i(t) \\
&+ k_\tau e_i(t-\gamma(t)) \\
&= (A + k_i + \sigma(t)\triangle k_i(t))e_i(t) + Bg(e_i(t)) \\
&+ (1-\bar{\delta}_1(t))\sum_{j=1}^{N} \bar{c}_{ij}\Gamma e_j(t) + \bar{\delta}_1(t)\sum_{j=1}^{N} \bar{c}_{ij}\Gamma \\
&\times e_j(t-\ddot{\gamma}(t)) + k_\tau e_i(t-\ddot{\gamma}(t))
\end{aligned}
$$

$$
\begin{aligned}
&= (A + k + \sigma H_i \Upsilon_i W_i)e_i(t) + ((\sigma(t) - \sigma)H_i \Upsilon_i W_i)e_i(t) \\
&\quad + Bg(e_i(t)) + (1 - \bar{\delta}_1)\sum_{j=1}^{N} \bar{c}_{ij}\Gamma e_j(t) + (\bar{\delta}_1 - \bar{\delta}_1(t))\sum_{j=1}^{N} \\
&\quad \times \bar{c}_{ij}\Gamma e_j(t) + \bar{\delta}_1 \sum_{j=1}^{N} \bar{c}_{ij}\Gamma e_j(t - \ddot{\gamma}(t)) + (\bar{\delta}_1(t) - \bar{\delta}_1) \\
&\quad \times \sum_{j=1}^{N} \bar{c}_{ij}\Gamma e_j(t - \ddot{\gamma}(t)) \\
&\quad + k_\tau e_i(t - \ddot{\gamma}(t)); \quad (i = 1, 2, \ldots, N)
\end{aligned}
\tag{8}
$$

$$
\begin{aligned}
\dot{e}(t) &= (\bar{A} + \bar{k} + \sigma \bar{H}\bar{\Upsilon}\bar{W})e(t) + (\sigma(t) - \sigma)\bar{H}\bar{\Upsilon}\bar{W}e(t) \\
&\quad + \bar{B}G(e(t)) + (1 - \bar{\delta}_1)(\bar{C} \otimes \Gamma)e(t) + (\bar{\delta}_1 - \bar{\delta}_1(t)) \\
&\quad \times (\bar{C} \otimes \Gamma)e(t) + \bar{\delta}_1(\bar{C} \otimes \Gamma)(e(t) - \int_{t-\ddot{\gamma}(t)}^{t} \dot{e}(s)\,\mathrm{d}s) \\
&\quad + (\bar{\delta}_1(t) - \bar{\delta}_1)(\bar{C} \otimes \Gamma)(e(t) - \int_{t-\ddot{\gamma}(t)}^{t} \dot{e}(s)\,\mathrm{d}s) \\
&\quad + \bar{k}_\tau(e(t) - \int_{t-\ddot{\gamma}(t)}^{t} \dot{e}(s)\,\mathrm{d}s)
\end{aligned}
\tag{9}
$$

where,
$\bar{A} \equiv I_N \otimes A$
$\bar{k} \equiv diag(k_1, k_2, \ldots, k_N)$
$\bar{H} \equiv diag(H_1, H_2, \ldots, H_N)$
$\bar{\Upsilon} \equiv diag(\Upsilon_1, \Upsilon_2, \ldots, \Upsilon_N)$
$\bar{W} \equiv diag(W_1, W_2, \ldots, W_N)$
$e(t) \equiv [e_1^T(t), e_2^T(t), \ldots, e_N^T(t)]^T$
$G(e(t)) \equiv [g^T(e_1(t)), g^T(e_2(t)), \ldots, g^T(e_N(t))]^T$
$\bar{k}_\tau \equiv I_N \otimes k_\tau$
$\bar{B} \equiv I_N \otimes B$

$$
\begin{aligned}
\dot{e}(t) &= (\bar{A} + \bar{k} + \sigma \bar{H}\bar{\Upsilon}\bar{W} + (\bar{C} \otimes \Gamma))e(t) + ((\sigma(t) - \sigma) \\
&\quad \times \bar{H}\bar{\Upsilon}\bar{W})e(t) + \bar{B}G(e(t)) - \bar{\delta}_1(\bar{C} \otimes \Gamma)e(t) + \bar{\delta}_1(\bar{C} \otimes \Gamma) \\
&\quad \times (e(t) - \int_{t-\ddot{\gamma}(t)}^{t} \dot{e}(s)\,\mathrm{d}s + (\bar{\delta}_1 - \bar{\delta}_1(t))(\bar{C} \otimes \Gamma)e(t) \\
&\quad + (\delta_1(t) - \bar{\delta}_1)(\bar{C} \otimes \Gamma)(e(t) - \int_{t-\ddot{\gamma}(t)}^{t} \dot{e}(s)\,\mathrm{d}s + \bar{k}_\tau(e(t) \\
&\quad - \int_{t-\ddot{\gamma}(t)}^{t} \dot{e}(s)\,\mathrm{d}s \\
&= (\bar{A} + \bar{k} + \sigma \bar{H}\bar{\Upsilon}\bar{W} + (\bar{C} \otimes \Gamma) + \bar{k}_\tau)e(t) + (\sigma(t) - \sigma) \\
&\quad \times \bar{H}\bar{\Upsilon}\bar{W}e(t) + \bar{B}G(e(t)) - (\bar{k}_\tau + \bar{\delta}_1(\bar{C} \otimes \Gamma)) \\
&\quad \times \int_{t-\ddot{\gamma}(t)}^{t} \dot{e}(s)\,\mathrm{d}s - (\bar{\delta}_1(t) - \bar{\delta}_1)(\bar{C} \otimes \Gamma)\int_{t-\ddot{\gamma}(t)}^{t} \dot{e}(s)\,\mathrm{d}s
\end{aligned}
\tag{10}
$$

3 Main results

This section establishes sufficient condition for the synchronization purposes of the CDNs. Additionally, the method for designing the synchronization controllers are presented in terms of LMIs.

Theorem 1 *Suppose Assumption 1 holds. For given scalars $\sigma \in [0,1], \bar{\delta}_1, \ddot{\gamma}_1, \ddot{\gamma}_2$, and $\tilde{\mu} < 1$, the closed-loop error system* (10) *is synchronized with controller gains $k_i, k_{\tau i}(i = 1, 2, \ldots, N)$. If some positive definite matrices $P, \hat{S}, W_1, W_2, Z \in \mathbb{R}^{nN \times nN}$ exist and any given matrices $\begin{bmatrix} L_{11} & L_{12} \\ * & L_{22} \end{bmatrix}$ such that*

$$
\Psi = \begin{bmatrix} \hat{S} & 0 & L_{11} & L_{12} \\ * & 3\hat{S} & L_{21} & L_{22} \\ * & * & \hat{S} & 0 \\ * & * & * & 3\hat{S} \end{bmatrix} \geq 0,
$$

Then

$$
\begin{bmatrix} \Phi_1 & N & \varepsilon W_*^T \\ * & -\varepsilon I & 0 \\ * & * & -\varepsilon I \end{bmatrix} < 0,
\tag{11}
$$

holds, as

$$
\Phi_1 = \begin{bmatrix} \Omega_1 & M_{1*}^T P & \sqrt{\sigma(1-\sigma)} M_2^T P & 0 \\ * & \Theta - 2P & 0 & 0 \\ * & * & \Theta - 2P & 0 \\ * & * & * & \Theta - 2P \end{bmatrix}
$$

$N^T = \begin{bmatrix} \sigma(P\bar{H})^T & \underbrace{0 \cdots 0}_{8\,elements} & \sigma(P\bar{H})^T & 0 & \hat{\omega} \end{bmatrix}$

$W_* = \begin{bmatrix} W & \underbrace{0 \cdots 0}_{11\,elements} \end{bmatrix}$

$M_1 = \begin{bmatrix} \bar{Z} & \bar{B} & -(k_\tau + \bar{\delta}_1(\bar{C} \otimes \Gamma)) & \underbrace{0 \cdots 0}_{6\,elements} \end{bmatrix}$

$\bar{Z} = \bar{A} + \bar{k} + \sigma \bar{H}\bar{\Upsilon}\bar{W} + \bar{C} \otimes \Gamma + \bar{k}_\tau$

$M_{1*} = M_1 - \begin{bmatrix} \sigma \bar{H}\bar{\Upsilon}\bar{W} & \underbrace{0 \cdots 0}_{8\,elements} \end{bmatrix}$,

$M_2 = \begin{bmatrix} 0 & 0 & \bar{C} \otimes \Gamma & \underbrace{0 \cdots 0}_{6\,elements} \end{bmatrix}$, $\Omega_1 \equiv \begin{bmatrix} \Omega_1^1 & \Omega_1^2 \\ * & \Omega_1^3 \end{bmatrix}$

$- \frac{1}{\ddot{\gamma}_{12}} \Pi^T \Psi \Pi$, $\Omega_1^1 \equiv \begin{bmatrix} ß_1 + ß_2 & P\bar{B} + F_2 \\ * & -I \end{bmatrix}$,

$ß_1 = P\bar{A} + \bar{A}^T P + P\bar{k} + \bar{k}^T P + P(\bar{C} \otimes \Gamma) + (\bar{C} \otimes \Gamma)^T P$

$ß_2 = P\bar{k}_\tau + \bar{k}_\tau^T P + W_1 + \ddot{\gamma}_1 W_2 - F_1$

$$
\Omega_1^2 \equiv \begin{bmatrix} -\bar{\delta}_1 P(\bar{C} \otimes \Gamma) - P\bar{k}_\tau & \underbrace{0 \cdots 0}_{6\,elements} \\ 0 & \underbrace{0 \cdots 0}_{6\,elements} \end{bmatrix},
$$

$$
\Omega_1^3 \equiv \begin{bmatrix} -\frac{1-\tilde{\mu}}{\ddot{\gamma}_2} Z & 0 & 0 & 0 & 0 & 0 & 0 \\ 0 & 0 & 0 & 0 & 0 & 0 & 0 \\ 0 & 0 & \tilde{\Delta}_1 & 0 & 0 & 0 & 0 \\ 0 & 0 & 0 & 0 & 0 & 0 & 0 \\ 0 & 0 & 0 & 0 & 0 & 0 & 0 \\ 0 & 0 & 0 & 0 & 0 & 0 & 0 \\ 0 & 0 & 0 & 0 & 0 & 0 & -\frac{1}{\ddot{\gamma}_1} W_2 \end{bmatrix}
$$

Where:
$\Theta = \ddot{\gamma}_{12}\hat{S} + \ddot{\gamma}_2 Z$, $\tilde{\Delta}_1 = -(1-\tilde{\mu})W_1 - F_1$,
$\hat{\omega} = \sqrt{\sigma(1-\sigma)}(P\tilde{H})^T$, $F_1 = I_N \otimes \frac{U_1^T U_2 + U_2^T U_1}{2}$,
$F_2 = I_N \otimes \frac{U_1^T + U_2^T}{2}$

Proof. The following candidate of Lyapunov-Krasovskii functional is considered

$$\bar{V}(t) = \bar{V}_1(t) + \bar{V}_2(t) + \bar{V}_3(t) \tag{12}$$

Where

$$\bar{V}_1(t) = e^T(t)Pe(t)$$
$$\bar{V}_2(t) = \int_{t-\ddot{\gamma}(t)}^{t} e^T(s)W_1e(s)\mathrm{d}s + \int_{-\ddot{\gamma}_1}^{0}\int_{t+\phi}^{t} e^T(s)W_2e(s) \times \mathrm{d}s\mathrm{d}\phi$$

$$\bar{V}_3(t) = \int_{-\ddot{\gamma}_2}^{-\ddot{\gamma}_1}\int_{t+\delta}^{t} \dot{e}^T(s)\hat{S}\dot{e}(s)\mathrm{d}s\mathrm{d}\delta + \int_{-\ddot{\gamma}(t)}^{0}\int_{t+\delta}^{t} \dot{e}^T(s) \times Ze(s)\mathrm{d}s\mathrm{d}\delta$$

Finding infinitesimal operator $Ł$ on $\bar{V}(t)$ results in the following:
$Ł\bar{V}(t) = \lim_{\triangle\to 0^+} \frac{1}{\triangle}\{\mathbf{E}\{\bar{V}(t+\triangle)\} - \bar{V}(t)\}$
One should take note of the following expectation:
$\mathbf{E}\{\bar{\delta}_1(t) - \bar{\delta}_1\} = 0, \quad \mathbf{E}\{(\bar{\delta}_1(t) - \bar{\delta}_1)^2\} = \bar{\delta}_1(1-\bar{\delta}_1),$
$\mathbf{E}\{\sigma(t) - \sigma\} = 0, \quad \mathbf{E}\{(\sigma(t) - \sigma)^2\} = \sigma(1-\sigma).$
$\dot{\bar{V}}(t)$ is calculated based on the trajectory of error system (10)

$$\begin{aligned}\mathbf{E}\{L\bar{V}_1(t)\} = \mathbf{E}\{&2e^T(t)P[(\bar{A} + \bar{k} + \sigma\bar{H}\bar{\Upsilon}\bar{W} + (\bar{C}\otimes\Gamma) \\ &+ \bar{k}_\tau)e(t) + \bar{B}G(e(t)) - \bar{\delta}_1(\bar{C}\otimes\Gamma)\int_{t-\ddot{\gamma}(t)}^{t}\dot{e}(s)\mathrm{d}s \\ &- \bar{k}_\tau\int_{t-\ddot{\gamma}(t)}^{t}\dot{e}(s)\mathrm{d}s]\}\end{aligned} \tag{13}$$

$$\begin{aligned}\mathbf{E}\{L\bar{V}_2(t)\} \le \mathbf{E}\{&e^T(t)(W_1 + \ddot{\gamma}_1W_2)e(t) - (1-\tilde{\mu}) \\ &\times e^T(t-\ddot{\gamma}(t))W_1e(t-\ddot{\gamma}(t)) - \frac{1}{\ddot{\gamma}_1} \\ &\times\left(\int_{t-\ddot{\gamma}_1}^{t} e(\theta)\mathrm{d}\theta\right)^T W_2\left(\int_{t-\ddot{\gamma}_1}^{t} e(\theta)\mathrm{d}\theta\right)\}\end{aligned} \tag{14}$$

$$\begin{aligned}\mathbf{E}\{L\bar{V}_3(t)\} \le \mathbf{E}\{&(\ddot{\gamma}_2 - \ddot{\gamma}_1)\dot{e}^T(t)\hat{S}\dot{e}(t) + \ddot{\gamma}_2\dot{e}^T(t)Z\dot{e}(t) \\ &- \int_{t-\ddot{\gamma}_2}^{t-\ddot{\gamma}_1}\dot{e}^T(\delta)\hat{S}\dot{e}(\delta)\mathrm{d}\delta - (1-\tilde{\mu})\int_{t-\ddot{\gamma}(t)}^{t} \\ &\times \dot{e}^T(s)Z\dot{e}(s)\mathrm{d}s\}\end{aligned} \tag{15}$$

Based on lemma (2.2) and from (15), the integral component satisfies the following inequality:

$$-\int_{t-\ddot{\gamma}_2}^{t-\ddot{\gamma}_1}\dot{e}^T(\delta)\hat{S}\dot{e}(\delta)\mathrm{d}\delta \le -\zeta^T(t)\frac{1}{\ddot{\gamma}_{12}}\Pi^T\Psi\Pi\zeta(t) \tag{16}$$

Where,

$$\ddot{\gamma}_{12} = \ddot{\gamma}_2 - \ddot{\gamma}_1$$

$$v(t) = \begin{pmatrix} \underbrace{0\cdots 0}_{3\,elements} & I & -I & 0 & 0 & 0 & 0 \\ \underbrace{0\cdots 0}_{3\,elements} & I & I & 0 & -2I & 0 & 0 \\ \underbrace{0\cdots 0}_{3\,elements} & 0 & I & -I & 0 & 0 & 0 \\ \underbrace{0\cdots 0}_{3\,elements} & 0 & I & I & 0 & -2I & 0 \end{pmatrix}\zeta(t) = \Pi\zeta(t) \tag{17}$$

Let,

$$\begin{aligned}\zeta(t) = [&e^T(t), G^T(e(t)), \int_{t-\ddot{\gamma}(t)}^{t}\dot{e}^T(s)\mathrm{d}s, e^T(t-\ddot{\gamma}_1), \\ &e^T(t-\ddot{\gamma}(t)), e^T(t-\ddot{\gamma}_2), \frac{1}{\ddot{\gamma}(t)-\ddot{\gamma}_1}\int_{t-\ddot{\gamma}(t)}^{t-\ddot{\gamma}_1}e^T(\omega)\mathrm{d}\omega, \\ &\frac{1}{\ddot{\gamma}_2-\ddot{\gamma}(t)}\int_{t-\ddot{\gamma}_2}^{t-\ddot{\gamma}(t)}e^T(\omega)\mathrm{d}\omega, \int_{t-\ddot{\gamma}_1}^{t}e^T(\theta)\mathrm{d}\theta]^T\end{aligned}$$

$$M_1 = [\bar{A} + \bar{k} + \sigma\bar{H}\bar{\Upsilon}\bar{W} + \bar{C}\otimes\Gamma + \bar{k}_\tau, \bar{B}, -(k_\tau + \bar{\delta}_1(\bar{C}\otimes\Gamma)), \underbrace{0\cdots 0}_{6\,elements}]$$

$$\dot{e}(t) = M_1\zeta(t) + (\sigma(t)-\sigma)\bar{H}\bar{\Upsilon}\bar{W}e(t) + (\bar{\delta}_1 - \bar{\delta}_1(t))(\bar{C}\otimes\Gamma) \times \int_{t-\ddot{\gamma}(t)}^{t}\dot{e}(s)\mathrm{d}s$$

From (15), we represent

$$M_2 = \begin{bmatrix} 0 & 0 & (\bar{C}\otimes\Gamma) & 0 & 0 & 0 & \underbrace{0\cdots 0}_{3\,elements} \end{bmatrix}$$

$$M_3 = \begin{bmatrix} \bar{H}\bar{\Upsilon}\bar{W} & 0 & 0 & 0 & \underbrace{0\cdots 0}_{5\,elements} \end{bmatrix}$$

Hence,

$$\begin{aligned}\mathbf{E}\{L\bar{V}_3(t)\} \le \mathbf{E}\{&\zeta^T(t)(M_1^T(\ddot{\gamma}_{12}\hat{S} + \ddot{\gamma}_2Z)M_1 + \bar{\delta}_1(1-\bar{\delta}_1)M_2 \\ &\times(\ddot{\gamma}_{12}\hat{S} + \ddot{\gamma}_2Z)M_2^T + \sigma(1-\sigma)M_3^T(\ddot{\gamma}_{12}\hat{S} \\ &+ \ddot{\gamma}_2Z)M_3) - \frac{1}{\ddot{\gamma}_{12}}\Pi^T\Psi\Pi)\zeta(t)\} \\ &- \frac{1-\tilde{\mu}}{\ddot{\gamma}_2}(\int_{t-\ddot{\gamma}(t)}^{t}\dot{e}(s)\mathrm{d}s)^TZ(\int_{t-\ddot{\gamma}(t)}^{t}\dot{e}(s)\mathrm{d}s)\}\end{aligned} \tag{18}$$

From some simple computations, Assumption (2.1) can be presented as:

$$-\begin{bmatrix} e(t) \\ G(e(t)) \end{bmatrix}^T \begin{bmatrix} F_1 & -F_2 \\ * & I \end{bmatrix}\begin{bmatrix} e(t) \\ G(e(t)) \end{bmatrix} \ge 0, \tag{19}$$

$$F_1 = I_N \otimes \frac{Z_1^TZ_2 + Z_2^TZ_1}{2}, F_2 = I_N \otimes \frac{Z_1^T + Z_2^T}{2}$$

combining equations (13)-(14), (18)-(19), hence the following:

$$\mathbf{E}\{L\bar{V}(t)\} \le \mathbf{E}\{\zeta^T(t)\Phi\zeta(t)\} \tag{20}$$

This conclude $\mathbf{E}\{L\bar{V}(t)\} < 0$, if $\mathbf{E}\{\zeta^T(t)\Phi\zeta(t)\} < 0$, holds when $\Phi < 0$:
$\Phi = \Omega_1 + M_1^T\Theta M_1 + \bar{\delta}_1(1-\bar{\delta}_1)M_2^T\Theta M_2 + \sigma(1-\sigma)M_3^T\Theta M_3 + \Omega_2 + \Omega_2^T$
From theorem (1), we represent

$$\Omega_2 = \begin{bmatrix} \sigma P\bar{H}\bar{\Upsilon}\bar{W} \\ 0_{8n\times n} \end{bmatrix} \begin{bmatrix} I & \underbrace{0\cdots 0}_{8\,elements} \end{bmatrix}, \Theta = \ddot{\gamma}_{12}\hat{S} + \ddot{\gamma}_2 Z$$

The application of Schur complements formula yeilds the following:

$$\tilde{\Phi} = \begin{bmatrix} \Omega_z & M_1^T P & \Omega_{zz} & \sqrt{\sigma(1-\sigma)}M_3^T P \\ * & -\Theta^{-1} & 0 & 0 \\ * & * & -\Theta^{-1} & 0 \\ * & * & * & -\Theta^{-1} \end{bmatrix} < 0 \tag{21}$$

where, $\Omega_z = \Omega_1 + \Omega_2 + \Omega_2^T$, $\Omega_{zz} = \sqrt{\bar{\delta}_1(1-\bar{\delta}_1)}M_2^T P$. By using the method of congruence transformation with $diag\{\underbrace{I, I, \ldots, I}_{9}, P, P, P\}$ on (21) and utilizing $P\Theta^{-1}P \geq 2P - \Theta$, ensures $\tilde{\Phi} < 0$. Applying simple computations considering Lemma (2.4), let $\Phi_1 = \begin{bmatrix} \Omega_1 & M_{1*}^T P & \Omega_{zz} & 0 \\ * & \Theta - 2P & 0 & 0 \\ * & * & \Theta - 2P & 0 \\ * & * & * & \Theta - 2P \end{bmatrix}$, $M_{1*} = M_1 - \begin{bmatrix} \sigma\bar{H}\bar{\Upsilon}\bar{W} & \underbrace{0\cdots 0}_{8\,elements} \end{bmatrix}$

$N^T = \begin{bmatrix} \sigma(P\bar{H})^T & 0_{n,8n} & \sigma(P\bar{H})^T & 0 & \sqrt{\sigma(1-\sigma)}(P\bar{H})^T \end{bmatrix}$
$W_* = \begin{bmatrix} W & 0_{n,11n} \end{bmatrix}$. Then we have

$$\begin{bmatrix} \Phi_1 & N & \varepsilon W_*^T \\ * & -\varepsilon I & 0 \\ * & * & -\varepsilon I \end{bmatrix} < 0 \tag{22}$$

Based on Lemma (2.4), if the conclusion $\tilde{\Phi} < 0$ is true, then $\mathbf{E}\{LV(t)\} < 0$. Hence, the synchronized error system is asymptotically stable. This completes the proof. □

The following theorem is presented based on the above results in addressing the nonfragile control design problem.

Theorem 2 *Let $\ddot{\gamma}_1, \bar{\delta}_1, \ddot{\gamma}_2, \sigma \in [0,1]$, and $\tilde{\mu} < 1$, be some given scalars. The given CDNs is synchronized, when some symmetric positive definite matrices $P = diag\{P_1, P_2, \ldots, P_N\}, \hat{S} = diag\{\hat{S}_1, \hat{S}_2, \ldots, \hat{S}_N\}$ and any matrices $Y_1 = diag\{Y_1^1, Y_2^1, \ldots, Y_N^1\} \in \mathbb{R}^{nN\times nN}$ and $Y_2 = diag\{Y_1^2, Y_2^2, \ldots, Y_N^2\} \in \mathbb{R}^{nN\times nN}$ exit with the positive scalar ε, hence $\bar{\Omega} < 0$, where*

$$\bar{\Omega} \equiv \begin{bmatrix} \bar{\Omega}_1 & \bar{\Omega}_2 \\ * & \bar{\Omega}_3 \end{bmatrix} < 0, \tag{23}$$

$$\bar{\Omega}_1 \equiv \begin{bmatrix} \bar{\Omega}_1^1 & \bar{\Omega}_1^2 \\ * & \bar{\Omega}_1^3 \end{bmatrix},$$

$$\bar{\Omega}_1^1 \equiv \begin{bmatrix} \bar{\Omega}*_1^1 & P\bar{B} + F_2 & -\bar{\delta}_1 P(\bar{C}\otimes\Gamma) - Y_2 \\ * & -I & 0 \\ * & * & -\frac{1-\tilde{\mu}}{\ddot{\gamma}_2}Z \end{bmatrix},$$

$$\bar{\Omega}_1^2 \equiv \begin{bmatrix} 0 & 0 & 0 & 0 & 0 & 0 & \bar{\Omega}*_1^2 & 0 \\ 0 & 0 & 0 & 0 & 0 & 0 & \bar{B}^T P & 0 \\ 0 & 0 & 0 & 0 & 0 & 0 & -\bar{\delta}_1(\bar{C}\otimes\Gamma)^T & \wp \end{bmatrix},$$

$$\bar{\Omega}_1^3 \equiv \begin{bmatrix} \bar{\Omega}_1^{31} & \bar{\Omega}_1^{32} \end{bmatrix}, \bar{\Omega}_2 \equiv \begin{bmatrix} 0 & \sigma P\bar{H} & \varepsilon\bar{W}^T \\ 0 & 0 & 0 \\ \bar{K}_\tau^T & 0 & 0 \\ 0_{6n\times n} & 0_{6n\times n} & 0_{6n\times n} \\ 0 & \sigma P\bar{H} & 0 \\ 0 & \tilde{\varpi} & 0 \end{bmatrix},$$

$$\bar{\Omega}_3 \equiv \begin{bmatrix} -\Theta^{-1} & 0 & 0 \\ * & -\varepsilon I & 0 \\ * & * & -\varepsilon I \end{bmatrix}$$

$$\bar{\Omega}_1^{31} \equiv \begin{bmatrix} -4\hat{S} & \Delta & \Delta_1 & 6\hat{S} & \varpi_1 \\ * & \Delta_2 & \tilde{\Delta}_1 & \tilde{\Delta}_2 & \tilde{\Delta} \\ * & * & -4\hat{S} & \varpi_2 & 6\hat{S} \\ * & * & * & -12\hat{S} & -4L_{22} \\ * & * & * & * & -12\hat{S} \\ * & * & * & * & * \\ * & * & * & * & * \\ * & * & * & * & * \end{bmatrix}$$

$$\bar{\Omega}_1^{32} \equiv \begin{bmatrix} 0_{5n\times n} & 0_{5n\times n} & 0_{5n\times n} \\ -\frac{1}{\ddot{\gamma}_1}W_2 & 0 & 0 \\ * & \varpi_3 & 0 \\ * & * & -\Theta^{-1} \end{bmatrix},$$

Where:
$\bar{\Omega}*_1^2 = \bar{A}^T P + Y_1^T + (\bar{C}\otimes\Gamma)^T P + Y_2^T$
$\bar{\Omega}*_1^1 = P\bar{A} + \bar{A}^T P + Y_1 + Y_1^T + P(\bar{C}\otimes\Gamma) + (\bar{C}\otimes\Gamma)^T P + Y_2 + Y_2^T + W_1 + \ddot{\gamma}_1 W_2 - F_1$, $\tilde{\Delta} = 6\hat{S} - 2L_{12} + 2L_{22}$
$\wp = \sqrt{\sigma(1-\sigma)}(\bar{C}\otimes\Gamma)^T$, $\tilde{\Delta}_1 = -2\hat{S} + L_{21} - L_{22} - L_{11} + L_{12}$
$\varpi_1 = 2L_{22} + 2L_{12}$, $\varpi_2 = 2L_{22}^T - L_{12}^T$, $\varpi_3 = \Theta - 2P$
$\tilde{\Delta}_2 = 2L_{12}^T + 6\hat{S} + 2L_{22}^T$, $\tilde{\varpi} = \sqrt{\sigma(1-\sigma)}\hat{S}\bar{H}$
$\Delta = -2\hat{S} - L_{11} - L_{12} - L_{21} - L_{22}$; $\Delta_1 = L_{11} - L_{12} + L_{21} - L_{22}$;
$\Delta_2 = -(1-\tilde{\mu})W_1 - F_1 - 8\hat{S} + L_{11} - L_{11}^T + L_{12} - L_{12}^T + L_{21}^T - L_{22}^T - L_{21} - L_{22}$;
Let $Y_1 = P\bar{k}$ and $Y_2 = P\bar{k}_\tau$. The control gains can be derived as $\bar{k} = P^{-1}Y_1$ and $\bar{k}_\tau = P^{-1}Y_2$. The proof is directly obtained from Theorem (1).

4 Numerical Simulations

The objective of this section is to exhibit the correctness of our synchronization schemes in Section (3).

Example 1. The CDNs (1) is considered which comprises of five nodes with each node been two dimensional, such that $N = 5$ and $n = 2$. The other parameters involved are:

$$\text{A}=\begin{bmatrix} 0.7 & 0.2 \\ 0.5 & 1.0 \end{bmatrix}, \quad \bar{C} = \begin{bmatrix} -1 & 1 & 0 & 0 & 0 \\ 0 & -1 & 1 & 0 & 0 \\ 0 & 0 & -1 & 1 & 0 \\ 0 & 0 & 0 & -1 & 1 \\ 1 & 0 & 0 & 0 & -1 \end{bmatrix},$$
$$\Gamma = 0.5I_n$$

$$B = \begin{bmatrix} 1.50 & -0.82 \\ 5.15 & 2.50 \end{bmatrix},$$

The controller gain fluctuations made to satisfy $\triangle k_i(t)$ are defined as

$$H_1 = 0.5I_n, H_2 = 0.6I_n, H_3 = 0.7I_n, H_4 = 0.8I_n,$$
$$H_5 = 0.9I_n, W_1 = 0.6I_n, W_2 = 0.5I_n, W_3 = 0.4I_n,$$
$$W_4 = 0.3I_n, W_5 = 0.2I_n$$

Let $f(\tilde{r}_i(t))$ be represented as

$$f(\tilde{r}_i(t)) = \begin{bmatrix} 0.2\tilde{r}_{i1} - \tanh(0.1\tilde{r}_{i1}) \\ 0.1\tilde{r}_{i2} \end{bmatrix}.$$

The above $f(\tilde{r}_i(t))$, satisfies the sector-bounded condition in assumption (2.1) with

$$Z_1 = \begin{bmatrix} 0.1 & 0 \\ 0 & 0.1 \end{bmatrix}, \; Z_2 = \begin{bmatrix} 0.2 & 0 \\ 0 & 0.1 \end{bmatrix}.$$

Considering this example, we set $\sigma = 0.5$, $\bar{\delta}_1 = 0.5$, $\tilde{\mu} = 0.2$, $\ddot{\gamma}_1 = 0$, $\ddot{\gamma}_2 = 0.5$.
From MATLAB LMI toolbox, Theorem (2) is verified, where feasible solution of the LMIs in Theorem (2) is obtained. The controller gain matrices obtained are:

$$K_1 = \begin{bmatrix} -1.3647 & -0.3460 \\ -0.1196 & -1.5990 \end{bmatrix},$$
$$K_2 = \begin{bmatrix} -1.3121 & -0.3079 \\ -0.0990 & -1.4745 \end{bmatrix},$$
$$K_3 = \begin{bmatrix} -1.2755 & -0.3126 \\ -0.0893 & -1.3825 \end{bmatrix},$$
$$K_4 = \begin{bmatrix} -1.2436 & -0.3139 \\ -0.0836 & -1.3191 \end{bmatrix},$$
$$K_5 = \begin{bmatrix} -1.2226 & -0.3139 \\ -0.0780 & -1.2753 \end{bmatrix},$$
$$K_{1\tau} = \begin{bmatrix} -0.2735 & -0.1907 \\ -0.0188 & -0.1500 \end{bmatrix},$$
$$K_{2\tau} = \begin{bmatrix} -0.3101 & -0.1871 \\ -0.0325 & -0.2592 \end{bmatrix},$$
$$K_{3\tau} = \begin{bmatrix} -0.3163 & -0.1580 \\ -0.0335 & -0.3072 \end{bmatrix}$$
$$K_{4\tau} = \begin{bmatrix} -0.3192 & -0.1247 \\ -0.0292 & -0.3276 \end{bmatrix},$$
$$K_{5\tau} = \begin{bmatrix} -0.3251 & -0.11251 \\ -0.0263 & -0.3376 \end{bmatrix}.$$

Using the following initial conditions, $\tilde{r}_1(0) = [3,-1]^T$, $\tilde{r}_2(0) = [0,1]^T$, $\tilde{r}_3(0) = [-6,2]^T$, $\tilde{r}_4(0) = [3,-2]^T$, $\tilde{r}_5(0) = [-1,1]^T$, and $s(0) = [2,3]^T$. The error trajectories (10) is shown in figure (1) without control input. The control inputs and error system trajectories with control inputs are shown in figures (2) and (3) respectively .

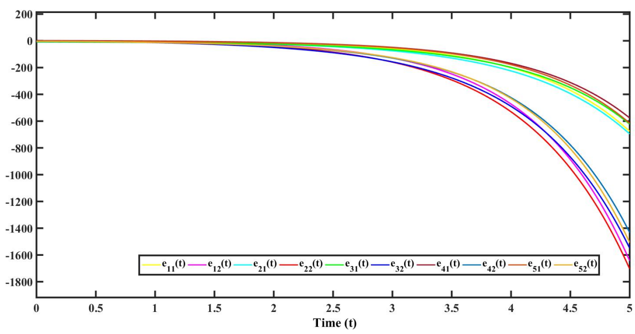

Figure 1: Error synchronization without control inputs $\hat{u}(t)$ in Example 1.

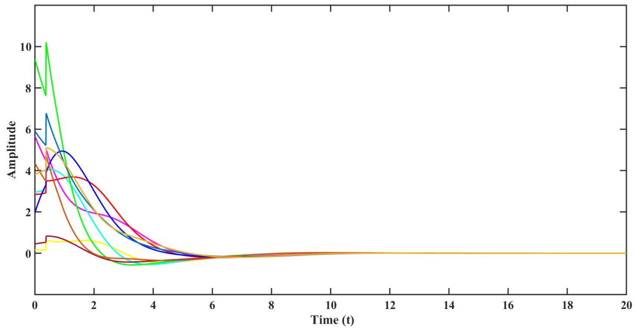

Figure 2: Control inputs $\hat{u}(t)$ in Example 1.

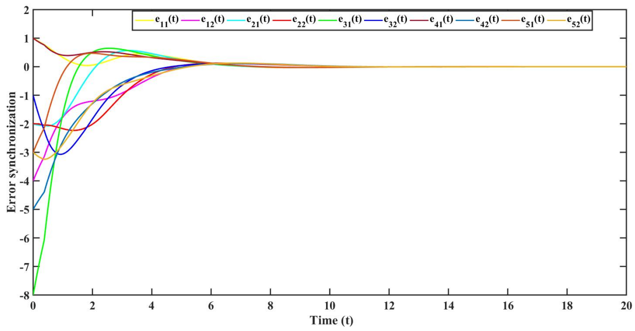

Figure 3: Error synchronization with control inputs $\hat{u}(t)$ in Example 1.

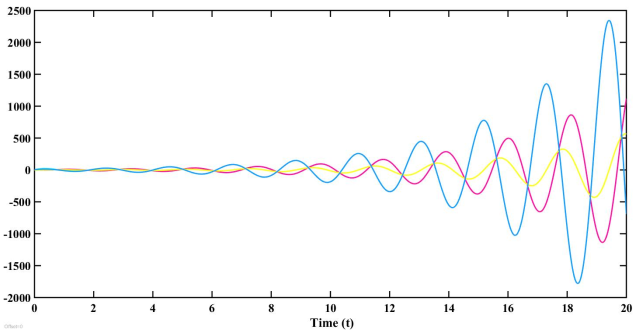

Figure 4: Error synchronization without control inputs $\hat{u}(t)$ in Example 2.

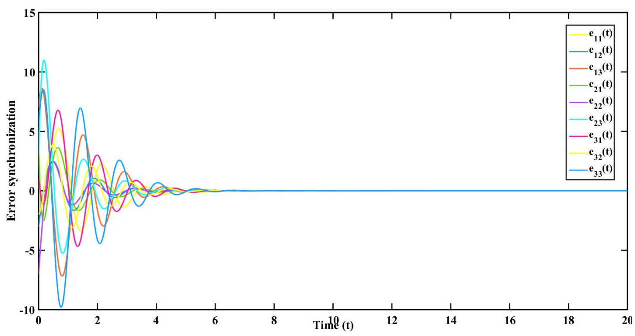

Figure 5: Error synchronization with control inputs $\hat{u}(t)$ in Example 2.

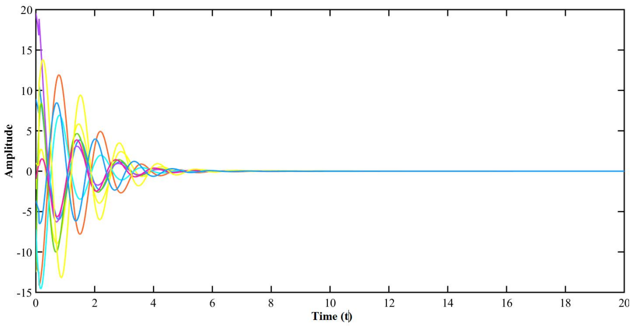

Figure 6: Control inputs $\hat{u}(t)$ in Example 2.

Example 2. Chua's circuit is adopted in this example as an isolated node which is decribed by the following equation:

$$\begin{cases} \dot{s}_1 = & \bar{\kappa}(s_2 - s_1 + \bar{\varphi}(s_1)) \\ \dot{s}_2 = & s_1 - s_2 + s_3 \\ \dot{s}_3 = & -\bar{b}s_2. \end{cases} \tag{24}$$

Let $A = 0$, $B = I_3$, $\delta_1 = 0.1$, $\bar{\kappa}$ =10, $\bar{b}$ =14.87 and $\bar{\varphi}(s_1) = \tilde{\omega}_1 s_1 + \frac{1}{2}(\tilde{\omega}_2 - \tilde{\omega}_1)\bar{\psi}(s_1)$ where $\tilde{\omega}_1 = -0.68$, $\tilde{\omega}_2 = -1.27$, and $\bar{\psi}(s_1) = (|s_1+1| - |s_1-1|)$. Denote $s = [s_1, s_2, s_3]^T$, $\bar{\phi} = -\frac{1}{2}(\tilde{\omega}_2 - \tilde{\omega}_1)$, where

$$f(s) = \begin{bmatrix} -\bar{\kappa}(1-\tilde{\omega}_1) & \bar{\kappa} & 0 \\ 1 & -1 & 1 \\ 0 & -\bar{b} & 0 \end{bmatrix} + \begin{bmatrix} \bar{\phi}\bar{\psi}(s_1) & 0 & 0 \\ 0 & 0 & 0 \\ 0 & 0 & 0 \end{bmatrix}.$$

From Assumption(2.1),

$$Z_1 = \begin{bmatrix} 2.7 & 10 & 0 \\ 1 & -1 & 1 \\ 0 & -14.87 & 0 \end{bmatrix}, Z_2 = \begin{bmatrix} -3.2 & 10 & 0 \\ 1 & -1 & 1 \\ 0 & -14.87 & 0 \end{bmatrix}.$$

The inner coupling Γ and network topology $\bar{C}$ matrices are given as

$$\Gamma = \begin{bmatrix} 1 & 0 & 0 \\ 0 & 1 & 0 \\ 0 & 0 & 1 \end{bmatrix}, \bar{C} = \begin{bmatrix} -1 & 0 & 1 \\ 1 & -1 & 0 \\ 1 & 1 & -2 \end{bmatrix}.$$

The parameters considered are: $\ddot{\gamma}_1 = 0.01, \ddot{\gamma}(t) = 0.4 + 0.01\sin(10t), \ddot{\gamma}_2 = 0.41, \tilde{\mu} = 0.1, \sigma = 0$. MATLAB LMI toolbox is used on Theorem (1). The obtained controller gain matrices are

$$k_1 = \begin{bmatrix} -1.6520 & 0.3835 & 0.0811 \\ 0.6663 & -0.9311 & 0.7839 \\ 0.0602 & 0.43138 & -1.3760 \end{bmatrix},$$

$$k_2 = \begin{bmatrix} -2.6121 & 0.3850 & 0.2110 \\ 0.5820 & -1.9887 & 1.1084 \\ 0.0163 & 0.5489 & -1.1378 \end{bmatrix},$$

$$k_3 = \begin{bmatrix} -0.7934 & 0.3540 & 0.0905 \\ 0.7406 & 0.6739 & 0.2685 \\ 0.0820 & 0.2063 & -0.5514 \end{bmatrix},$$

$$k_{\tau 1} = \begin{bmatrix} -0.1015 & 0.0165 & -0.0144 \\ -0.0051 & -0.5132 & 0.3061 \\ -0.0022 & 0.1375 & -0.1897 \end{bmatrix},$$

$$k_{\tau 2} = \begin{bmatrix} -0.0967 & -0.0076 & -0.0082 \\ -0.0175 & -0.3802 & -0.0082 \\ -0.0007 & -0.0081 & -0.1502 \end{bmatrix},$$

$$k_{\tau 3} = \begin{bmatrix} -0.0810 & 0.0670 & -0.0145 \\ -0.0070 & -1.2975 & 1.2294 \\ -0.0177 & 0.5618 & -0.0825 \end{bmatrix}.$$

Assume the following initial conditions are considered for the system: $s(0) = [0,-1,1]^T$ $\tilde{r}_1(0) = [1,-2,8]^T, \tilde{r}_2(0) = [4,-6,4]^T$, *and* $\tilde{r}_3(0) = [1,-1,7]^T$. The simulation result given in figure (4) indicates state error trajectories without control input, whereas that of figures (5) and (6) depict the synchronized closed-loop error system and the control input signals respectively.

5 Conclusion

This paper shows how an appropriate Lyapunov Krasovskii functional is used to address a non fragile synchronization control problem for a stochastic coupling complex dynamical networks with time-varying delays and control gain perturbations. The application of extended version of Jensen's inequality ensured the LMIs to be feasible. Finally, numerical examples with simulations are shown to illustrate the validity and applicability of our proposed control scheme.

Conflict of Interest The authors declare no conflict of interest.

Acknowledgment The authors would like to express their profound gratitude to Professor Zhong Shouming of UESTC for his immense support and contributions.

References

[1] F. A. Gyamfi, Y. Cheng, C. Yin and S. Zhong, Synchronization of complex dynamical networks with randomly coupling via nonfragile control, 2018 Tenth International Conference on Ubiquitonus and Future Networks (ICUFN), Prague, 2018, pp. 497 - 502.

[2] D. J. Watts and S. H. Strogatz,Collective dynamics of small-world networks.Nature,393(6684)(1998) 440 - 442.

[3] W. Yu, G. Chen, J. Lü, On pinning synchronization of complex dynamical networks , Automatica 45 (2) (2009) 429 - 435.

[4] R. Rakkiyappan, G. Velmurugan, J. Nicholas George, R. Selvamani, Exponential synchronization of Lur'e complex dynamical networks with uncertain inner coupling and pinning impulsive control, Applied maths. and Comput., 307(2017) 217 - 231.

[5] J. Wang, H. Zhang, Z. Wang and B. Wang, Local exponential synchronization in complex dynamical networks with time-varying and hybrid coupling,Applied Mathematics and Computation,225(2013) 16 - 32.

[6] D. Li, Z. Wang and G. Ma, Controlled synchronization for complex dynamical networks with random delayed information exchanges:A non-fragile approach. Neurocomputing,171(2016) 1047 - 1052.

[7] M. Fang, Synchronization for complex dynamical networks with time delay and discrete-time information. Applied Mathematics and Computation,258(2015) 1 - 11.

[8] M. J. Park, O. M. Kwon, J. H. Park, S. M. Lee and E. J. Cha, On synchronization criterion for coupled discrete-time neural networks with interval time-varying delays. Neurocomputing, 99(2013) 188 - 196.

[9] Y. Wang, Y. Ma, A. Chen, Exponential synchronization of Markovian jump complex dynamical networks with partially uncertain transition rates and stochastic disturbances. Neurocomputing 304 (2018) 30 - 46.

[10] Y. Tang, F. Qian, H. Gao and J. Kurths, Synchronization in complex networks and its application- A survey of recent advances and challenges. Annual reviews in control 38(2) (2014) 184 - 198.

[11] A. Arenas, A. Diaz - Guilera, J. Kurths, Y. Moreno and C. Zhou, Synchronization in complex networks, Physics Reports 469 (2008) 93 - 153.

[12] M. Xu, J - L. Wang, Y - L. Huang, P - C. Wei and S - X. Wang, Pinning sychronization of complex dynamical networks with and without time-varying delay. Neurocomputing, 266(2017) 263 - 273.

[13] F. Adu - Gyamfi, Y. Cheng, C. Yin and S. Zhong, Exponential H_∞ synchronization of non-fragile sampled-data controlled complex dynamical networks with random coupling and time varying delay. System Science and Control Engineering, 6(1) (2018), 370 - 387.

[14] M. Syed Ali, J. Yogambigai and J. Cao, Synchronization of master-slave markovian switching complex dynamical networks with time-varying delays in nonlinear function via sliding mode control. Acta Mathematica Scientia, 37(2)(2017) 368 - 384.

[15] M. Yang, Y -W. Wang, J - W. Xiao and Y. Huang, Robust synchronization of singular complex switched networks with parameteric uncertainities and unknown coupling topologies via impulsive control. Communications in Nonlinear Science and Numerical Simulation, 17(11) (2012), 4404 - 4416.

[16] V. M. Alfaro, R. Vilanova and O. Arrieta, Fragility analysis of PID controllers. IEEE Control Applications, (CCA) Intelligent Control, (ISIC), (2009) 725-730.

[17] Y. Liu, B - Z. Guo, J. .H. Park and S - M. Lee, Nonfragile exponential synchronization of delayed complex dynamical networks with memory sampled-data control. IEEE Transactions on Neural Networks and Learning Systems. 29(1) (2018) 118 - 128.

[18] R. Zhang, D. Zeng, J. .H. Park, Y. Liu and S. Zhong, Nonfragile sampled-data synchronization for delayed complex dynamical networks with randomly occurring controller gain fluctuation. IEEE Transactions on Systems, Man and Cybernetics: Systems, 48(12)(2018) 2271 - 2281.

[19] E. Gyurkovics, K. Kiss and A. Kazemy, Non-fragile exponential synchronization of delayed complex dynamical networks with transmission delay via sampled-data control. Journal of the Franklin Institute, 355(17)(2018), 8934 - 8956.

[20] V. M. Revathi, P. Balasubramaniam and K. Ratnavelu, Delay-dependent H 1 filtering for complex dynamical networks with time-varying delays in nonlinear function and network couplings. Signal Processing,118(2016) 122 - 132.

[21] X. Li and X. Fu, Effect of leakage time varying delay on stability of nonlinear differential systems. Journal of the Franklin institute, 350(6)(2012) 1335 - 1344.

[22] H. Zhang, J. Wang, Z. Wang and H. Liang, Mode-Dependent stochastic synchronization for Markovian coupled neural networks with time-varying mode-delays. IEEE Transactions on Neural Networks and Learning systems,26(11)(2015) 2621 - 2634.

[23] H. Bao, J .H. Park and J. Cao, Exponential synchronization of coupled stochastic memristor-based neural networks with time-varying probabilitic delay coupling and impulsive delay. IEEE Transactions on Neural Networks and Learning Systems,27(1)(2015) 190 - 201.

Advances in Science, Technology and Engineering Systems Journal Vol. 4, No. 2, 17-22 (2019)

www.astesj.com

Special Issue on Recent Advances in Engineering Systems

ASTESJ

ISSN: 2415-6698

High-Temperature Optical Characterization of Wide Band Gap Light Emitting Diodes and Photodiodes for Future Power Module Application

Syam Madhusoodhanan[1], Abbas Sabbar[1], Sattar Al-Kabi[1], Stanley Atcitty[2], Robert Kaplar[2], Binzhong Dong[3], Jiangbo Wang[3], Shui-Qing Yu[1], Zhong Chen[*,1]

[1]*Department of Electrical Engineering, University of Arkansas, Fayetteville, Arkansas 72701, USA*

[2]*Sandia National Laboratories, Albuquerque, New Mexico 87185, USA*

[3]*HC SemiTek (Suzhou), 28 Chenfeng Road, Zhangjiagang, Jiangsu, P. R. 215600, China*

A R T I C L E I N F O

Article history:
Received: 20 December, 2018
Accepted: 22 February, 2019
Online : 06 March, 2019

Keywords:
High-Density Power Module,
High-Temperature Optocouplers,
Light Emitting Diodes,
Optical Characterization,
Photodiodes,
Wide Bandgap

A B S T R A C T

A systematic study of wide bandgap (WBG) based light emitting diodes (LEDs) and photodiodes (PDs) were conducted for the assessment of modular integration of optoelectronic devices into power modules. The temperature dependence of the photoluminescence (PL) efficiency of Indium gallium nitride/Gallium nitride (InGaN/GaN) multiple quantum wells (MQWs) material was studied from 10 to 800 K. The photoluminescence efficiency is calculated using the power law relation connecting the integrated photoluminescence signal and the excitation pump power. A peak PL efficiency of 43.97 % was recorded at 800 K. Electroluminescence (EL) study was conducted on Gallium nitride (GaN) based LEDs in the temperature range of 300 – 800 K. An intensity drop of three orders of magnitude is recorded at 800 K as compared to room temperature. The full width half maximum (FWHM) of the spectra was also calculated from the EL measurements. The S-shaped shift of FWHM at high temperature indicates a strong localization effect. High-temperature spectral response analysis of 4H-Silicon carbide (4H-SiC) pn-junction photodiode is performed at zero voltage bias condition. Enhancement of spectral response is observed at higher wavelengths due to increased phonon population at higher temperatures.

1. Introduction

This paper is an extension of work originally presented in Conference on Lasers and Electro-Optics (CLEO): Applications and Technology 2018 titled 'Investigation of High-Temperature Photoluminescence Efficiency from InGaN/GaN MQWs' [1]. Power electronic system plays a significant role in renewable energy, energy storage, and electric or hybrid electric vehicles. As an integral part of the power electronic system, power modules provide a highly efficient form of power conversion. In the last two decades, the field of power conversion is going through a transformation where the application often demands extreme operating environments. Advancement in the field of hybrid electric vehicles, aerospace and deep oil-gas exploration necessitate the development of power modules based on WBG devices to operate in extreme environments where the ambient temperature exceeds 200oC. Compared to silicon (Si) devices, wide bandgap materials like SiC and GaN can withstand higher current densities, exhibit lower switching losses and possess higher breakdown voltages [2-3].

Power modules based on WBG materials enhance reliability and considerably reduce cooling requirements that lead to a significant reduction in total system cost and weight. Although these innovative properties lead power modules to higher power density [4], some concerns still need to be addressed to take full advantage of wide bandgap based modules. For example, the use of bulky transformers used as a galvanic isolation system to float the high voltage gate driver limit further size reduction of the high-temperature power modules [5]. Bulky transformers can be replaced by integrating high-temperature optocouplers to scale down power modules further and achieve disrupting performance

[*]Zhong Chen, University of Arkansas, chenz@uark.edu

in terms of thermal management, power efficiency, power density, operating environments, and reliability. However, regular semiconductor optoelectronic materials and devices have major difficulty functioning in high-temperature environments. The motivation for this study is to develop optoelectronic devices, specifically optocouplers that can be integrated into high-density power modules. A detailed study on optoelectronic devices at high temperature enables us to explore the possibility of scaling high-density power modules by integrating high-temperature optoelectronic devices into the power module.

Modular integration of optoelectronic devices into high-temperature power modules is restricted due to the significant optical efficiency drop at elevated temperatures. The quantum efficiency and long-term reliability of optoelectronic devices decrease at elevated temperatures. Thermal studies show that high junction temperature will significantly lower the lifetime of the LED [6-7]. Performance, as well as the useful life period of the LEDs, will significantly go down under high temperatures. It was also found that high leakage current [8-13], dark spot generation [10,11], and degradation of the metal contacts [9,12,13] at high temperatures can often lead to the degradation of light intensity. These factors limit the application of LEDs in high-temperature environments.

Photodiodes (PDs) based on SiC has lower leakage current and better stability at high-temperature operation. Brown et al. demonstrated a 6H-SiC pn-junction based PD operation at temperatures up to 350oC [13]. Several groups have reported 6H-SiC pn-junction photodiodes in the past [15-17]. Schottky-barrier PDs are also tested for high-temperature environments in recent years. Different groups have studied and characterized 4H-SiC Schottky-barrier and pn-junction PDs at high temperatures [18,19]. Although high quantum efficiency was reported up to 350oC, no groups have ever reported a detailed study on the temperature dependence of the spectral response of SiC pn-junction photodiodes for a wide range of temperatures. In this paper, we report on the performance degradation of InGaN based LED material and LED devices at high temperatures. Also, a study on the temperature dependence of the response in SiC-based pn-junction PDs up to 527oC (800 K) is presented.

2. Experiment

High-temperature photoluminescence studies were conducted on the InGaN/GaN MQW structure as described in the sketch of Fig. 1. The InGaN/GaN MQW structures were grown on sapphire substrates. The quantum well structure comprised of 10 periods of 3 nm undoped InGaN wells and 12.5 nm Si-doped GaN barriers grown on a 0.4 µm thick n-GaN layer. Vertically structured GaN-based bare die blue LEDs, fabricated at Cree, were subjected to high-temperature electroluminescence studies. The LED structures were grown on SiC substrate with both contact layers were formed by highly reflective electrodes. Optical responsivity measurements were conducted on 4H-SiC pn-junction PDs purchased from ifw Optronics GmbH. The material and device selection for this study are based on the demonstrated high quality, performance, and reliability.

Temperature-dependent measurements on materials and devices were performed using a Janis ST-100 cryostat. The cryostat can reach temperatures up to 800 K. Temperature-dependent PL measurements were carried out using a customary off-axis configuration. The excitation source was a continuous wave laser operating at 395 nm laser beam diameter of 64µm. The power instance of the sample was changed from 1.0 – 110.0 mW. A Horiba 550 spectrometer combined with a photomultiplier tube is used to collect PL and EL spectra. A Lakeshore 335 temperature controller is used to vary the temperature. Vacuum environment is maintained inside the cryostat throughout the measurements using a Janis TS-75-W turbopump. The injection current during the EL measurements was limited to 1.0 mA to avoid the device burn out due to the high current density. A Keithley 2450 source measurement unit is used for precise injection of current to the device. Temperature-dependent optical responsivity measurements on 4H-SiC PDs were carried out using Spex 270M rapid scanning imaging monochromator coupled with a deuterium lamp. The wavelength was changed from 250 to 400 nm.

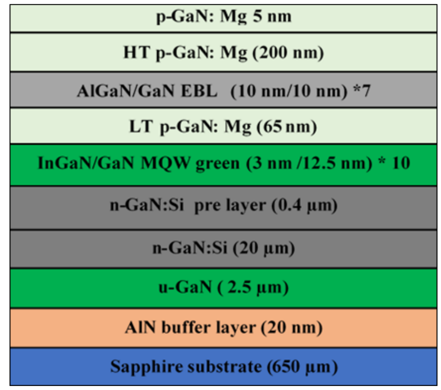

Figure 1. A sketch represents the InGaN/GaN MQWs structure.

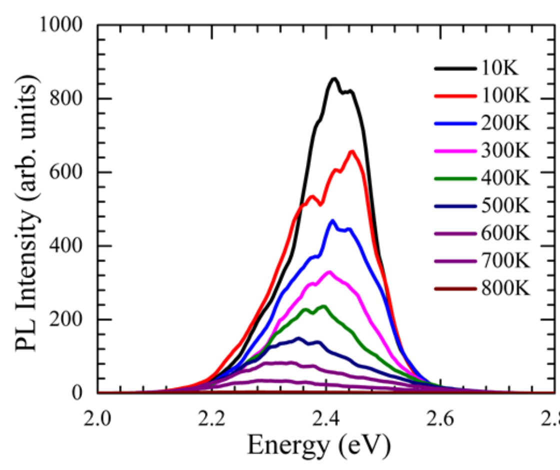

Figure 2. Temperature-dependent photoluminescence spectra of InGaN/GaN MQW were taken in the temperature range of 10 – 800 K.

3. Results and Discussion

The photoluminescence efficiency of the InGaN/GaN MQW structure was measured using the power law relation connecting the integrated PL intensity and the excitation pumping power of the spectrum [20]. Figure 2 shows PL spectra for the InGaN/GaN MQWs for a temperature range from 10 to 800 K. A gradual reduction in the intensity is observed on the high energy side of the PL spectra at elevated temperatures. It is observed from the plot that the PL band of InGaN/GaN MQWs become wider at elevated temperatures. A strong Indium (In) segregation can be attributed to the temperature independent behavior of the low energy side [21]. The strong In segregation leads to the formation of In-rich quantum dot-like regions [22]. The spectral peak positions were redshifted from 2.41 eV at 10 K to 2.32 eV at 800 K. Varshni empirical equation explain the redshift due to the bandgap shrinkage [23].

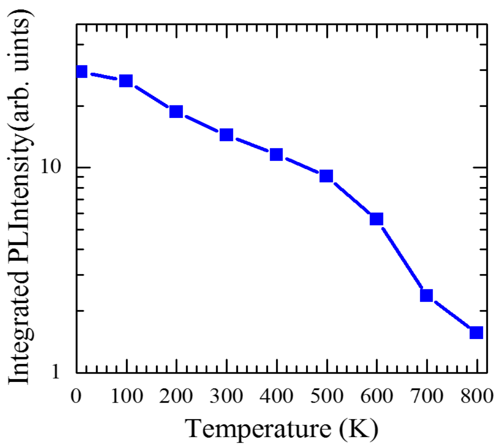

Figure 3. Integrated photoluminescence intensity of InGaN/GaN MQW is plotted as a function of temperature.

Figure 3 shows the integrated PL intensity for the InGaN-related PL emission for different temperatures. A reduction of one magnitude in the integrated PL intensity at 800 K compared to 77 K suggests a high PL efficiency even at elevated temperatures. Domination of non-radiative recombination at higher temperature causes a reduction in PL intensity. Carrier escape at higher temperature due to high thermal energy and the high rate of non-radiative recombination in QWs lead to the intensity drop at high temperature.

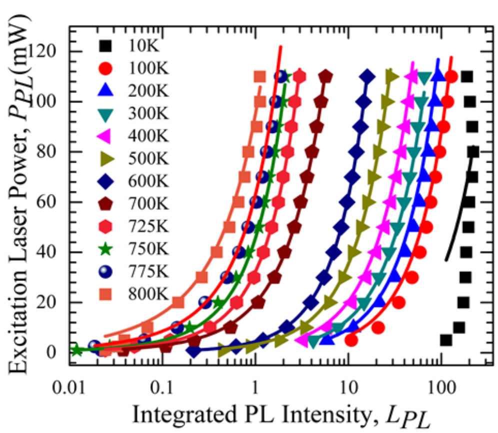

Figure 4. Excitation laser power is plotted against integrated PL intensity from InGaN/GaN MQW at different temperatures. The solid curves are fits of power law model to the data.

The extraction of PL efficiency by the power-law equation is explained in Ref. [19]. Excitation power dependent PL measurements were taken with pump power ranging from 1.0 mW to 110.0 mW. The results are plotted in terms of excitation pump power as a function of integrated PL intensity in Fig. 4. The dots are the experiment results while the solid curves are the fits of Eq. (1) from Ref. [19] to the data.

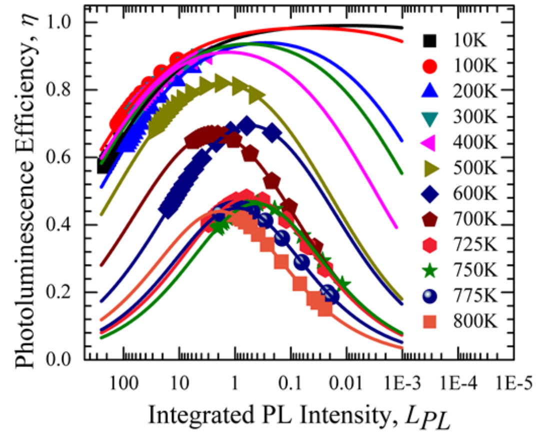

Figure 5. Photoluminescence efficiency is plotted as a function of integrated PL intensity at different temperatures. The solid lines are the simulated data for injection levels above and below the experiment limitations.

Figure (5) shows the temperature-dependent PL efficiency versus integrated PL intensity. The laser injection level where the peak PL efficiency is observed increases as the temperature increases. At 800 K, the peak PL efficiency is observed at an injection level above 110.0 mW. This behavior indicates that the non-radiative recombination rates are dominant even at a low injection rate under room temperature. At elevated temperatures, non-radiative recombinations along with thermally activated carrier escape from the QWs cause the PL efficiency to drop. These results indicate that the Auger and Shockley-Read-Hall (SRH) recombination rates are dependent on temperature and injection level.

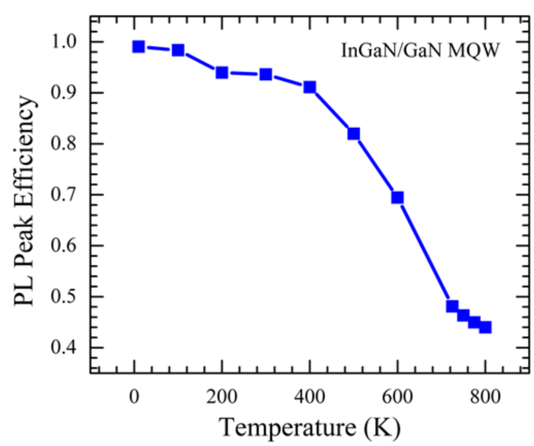

Figure 6. PL peak efficiency of InGaN/GaN MQW is plotted as a function of temperature.

The peak PL efficiency was plotted against temperature as shown in Fig. 6. The peak PL efficiency is almost unity at 10 K. At elevated temperatures, the peak PL efficiency decreases. As mentioned earlier, the drop in the Pl efficiency is caused by the domination of nonradiative recombinations in the active region of the quantum wells. At high temperatures, both SRH and Auger recombinations suppress the radiative recombination resulting in a PL efficiency drop. Another reason for the drop in PL efficiency is due to the carrier escape from the quantum wells as a result of high thermal energy. A PL efficiency of 44% is observed for the sample at 800 K. The temperature independent behavior of PL efficiency up to 400 K indicates high thermal stability.

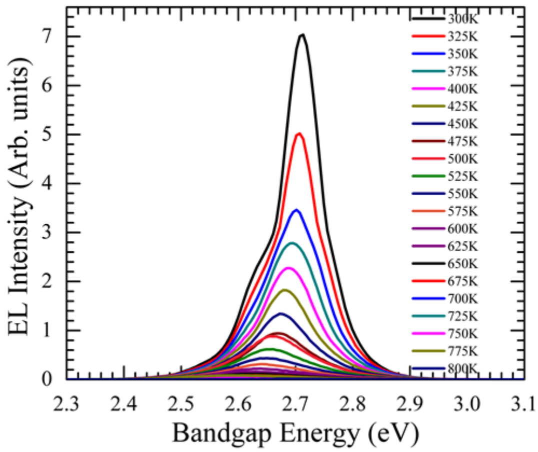

Figure 7. Electroluminescence spectra of InGaN/GaN single quantum well LED measured at different temperatures ranging from 300 – 800 K.

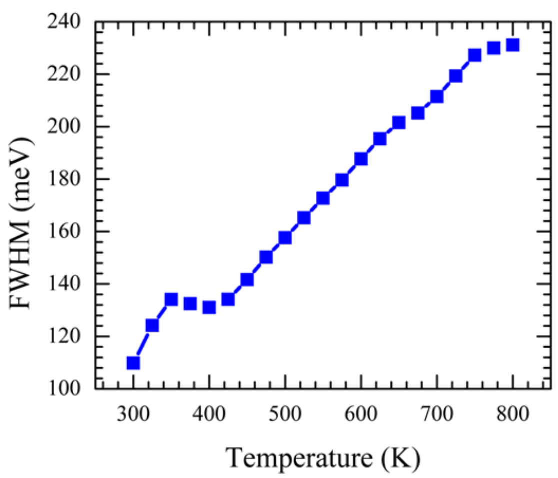

Figure 8. The full width half maximum of the electroluminescence spectra is calculated and plotted against temperature for InGaN/GaN single quantum well LED from 300 – 800 K.

Temperature-dependent electroluminescence spectra of the InGaN/GaN single quantum well (SQW) LED at an injection current of 1 mA is shown in Fig. 7. The spectral intensity of the LED is decreased as the temperature is increased from 300 to 800 K. The EL peak energy is measured to be 2.71 eV at 300 K. The Indium composition is approximated to be as 16 % from the EL peak energy [24]. The EL peak energy changes from 2.72 to 2.60 eV as the temperature increased from 300 to 800 K. The EL spectra are fitted using a Gaussian model to calculate the full-width half maximum (FWHM). It is found that the FWHM of the spectra increased from 109.11 meV at 300 K to 230.11 meV at 800 K. Temperature dependence of the FWHM of the EL spectra for InGaN/GaN LED is shown in Fig. 8. The FWHM shows an S-shaped shift when the temperature increases. The S-shaped shift again indicates a strong localization effect [25].

The FWHM of the spectra increased from 109.11 meV at 300 K to 230.11 meV at 800 K. The FWHM increases from 300 - 350 K due to carrier relaxation in the localized states. The further increase in the temperature results in a drop in the FWHM until the temperature reaches 400 K. The drop in the FWHM when the temperature further increases to 400 K suggests that nonradiative recombination centers capture a part of the carriers before reaching the lower energy tail states. The FWHM increases when the temperature increases above 400 K. This monotonic increase in FWHM is caused by the coupling of the excitons to acoustic phonons and longitudinal optical (LO) phonons [26].

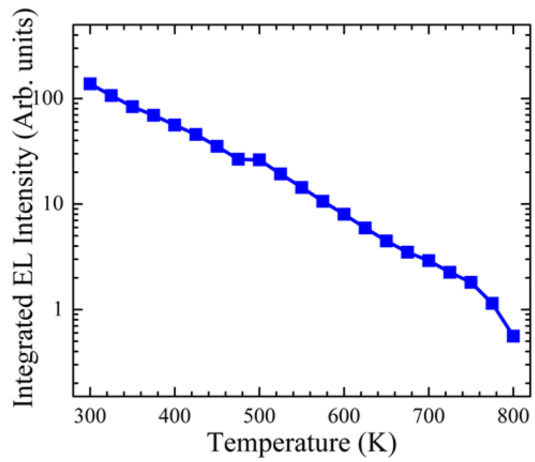

Figure 9. The integrated intensity of the electroluminescence spectra at each temperature is calculated and plotted as a function of temperature for InGaN/GaN single quantum well LED.

Figure 9 shows the change in the integrated intensity of the InGaN/GaN SQW LED over the temperature range of 300 – 800 K. The integrated intensity decreases when the temperature increases. The integrated intensity remains the same in the temperature range of 475 – 500 K. An intensity drop of three orders of magnitude is recorded at 800 K as compared to room temperature. The three orders of magnitude drop in the intensity suggest the presence of shallow QWs in the InGaN/GaN structure. The reduced intensity at a high temperature is due to the domination of the nonradiative recombination. At elevated temperature, the injected carriers gain high thermal energy. Carrier escape due to high thermal energy leads to the intensity drop at high temperature.

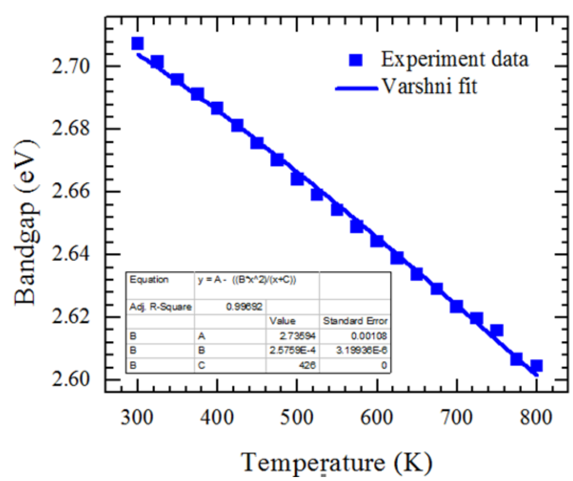

Figure 10. Energy bandgap of InGaN/GaN single quantum well LED is measured and plotted against temperature.

Figure 10 shows the change in the EL peak energy of the InGaN/GaN SQW LED concerning temperature. The EL peak energy decreases when the temperature increases. The rate of change in EL peak energy remains almost constant during the temperature range of 300 – 750 K. The EL peak energy changes from 2.71 to 2.60 eV over the temperature range of 300 - 800 K. The temperature dependence of the EL peak energy is described by the Varshni relation [23].

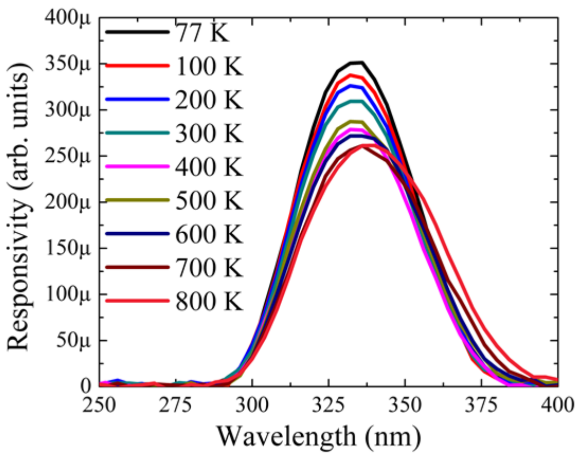

Figure 11. The spectral response characteristics of 4H-SiC pn-junction photodiode at different temperatures under 0 V bias.

Figure 11 shows the spectral response characteristics of the 4H-SiC detector measured as a function of temperature from 77 K to 800 K at zero biased condition. The photodetectors spectral response is wavelength dependent on the incident light. This is caused by a different energy absorption rate at each wavelength. The spectral response curves shift towards longer wavelength, and the responsivity at a wavelength above 350 nm is improved at higher temperatures. The redshift is caused by thermally induced bandgap narrowing effect. The observed spectral enhancement at higher wavelengths can be attributed to the increased phonon population at higher temperatures. Phonons assisted photon absorption is necessary at longer wavelengths as the corresponding photon energy is smaller than the direct energy spacing of 4H-SiC [19]. Interestingly, the responsivity at a lower wavelength (<320nm) exhibits less temperature dependent. The responsivity spectra of the photodiode at lower wavelength merges indicating that at this region temperature has less influence on the responsivity. More studies are necessary to understand the degradation of detectors under high temperature thoroughly.

4. Conclusion

Performance degradation of GaN-based LED material, and devices are studied for a wide range of temperature. Spectral responsivity of a 4H-SiC pn-junction photodiode is evaluated for the temperature range of 77 -800 K. The InGaN/GaN MQW structure shows temperature independent PL efficiency up to 400 K, signifying high thermal stability and displays a peak PL efficiency of 44 % at 800 K. The EL intensity of the LED device was decreased by three orders of magnitude at high temperatures as compared to room temperature. The reduced EL intensity is caused by the carrier escape from the quantum well due to high thermal energy. A strong localization effect is speculated due to the S-shaped FWHM curve. Initial studies on the 4H-SiC pn-junction photodiode show a temperature independent spectral response at lower wavelengths. These results serve as a strong foundation for future studies in the field of high-temperature optoelectronics in the applications of future ultra-high density power modules.

Conflict of Interest

The authors declare no conflict of interest.

Acknowledgment

The authors acknowledge financial support from the United States Department of Energy, DOE (Grant No. DE-SC0016485), program manager Dr. Imre Gyuk. Sandia National Laboratories is a multi-program laboratory managed and operated by National Technology Engineering Solutions of Sandia, LLC (NTESS), a wholly owned subsidiary of Honeywell Corporation, for the U.S. Department of Energy's National Nuclear Security Administration under contract DE- NA0003525. The views expressed in this article do not necessarily represent the views of the U.S. Department of Energy or the United States Government.

References

[1] Sabbar, A., Madhusoodhanan, S., Al-Kabi, S., Dong, B., Wang, J., Yu, S., & Chen, Z. (2018). Investigation of High-Temperature Photoluminescence Efficiency from InGaN/GaN MQWs. Conference on Lasers and Electro-Optics. doi:10.1364/cleo_at.2018.jth2a.79

[2] Homberger, J., Lostetter, A., Olejniczak, K., Mcnutt, T., Lal, S., & Mantooth, A. (n.d.). Silicon-carbide (SiC) semiconductor power electronics for extreme high-temperature environments. 2004 IEEE Aerospace Conference Proceedings (IEEE Cat. No.04TH8720). doi:10.1109/aero.2004.1368048

[3] Nomura, T., Masuda, M., Ikeda, N., & Yoshida, S. (2008). Switching Characteristics of GaN HFETs in a Half Bridge Package for High Temperature Applications. IEEE Transactions on Power Electronics, 23(2), 692-697. doi:10.1109/tpel.2007.915671

[4] Katsis, D. C., & Zheng, Y. (2008). Development of an extreme temperature range silicon carbide power module for aerospace applications. 2008 IEEE Power Electronics Specialists Conference. doi:10.1109/pesc.2008.4591943

[5] Rowden, B., Mantooth, A., Ang, S., Lostetter, A., Hornberger, J., & Mcpherson, B. (2009). High Temperature SiC Power Module Packaging. Volume 5: Electronics and Photonics. doi:10.1115/imece2009-12883

[6] Narendran, N., & Gu, Y. (2005). Life of LED-Based White Light Sources. Journal of Display Technology, 1(1), 167-171. doi:10.1109/jdt.2005.852510

[7] Huang, F., Yin, L., Li, S., Xu, G., Yan, H., Chen, Y., . . . Zhang, J. (2011). Study on the reliability of high-power LEDs under temperature cycle. 2011 12th International Conference on Electronic Packaging Technology and High Density Packaging. doi:10.1109/icept.2011.6067024

[8] Cao, X., Sandvik, P., Leboeuf, S., & Arthur, S. (2003). Defect generation in InGaN/GaN light-emitting diodes under forward and reverse electrical stresses. Microelectronics Reliability, 43(12), 1987-1991. doi:10.1016/j.microrel.2003.06.001

[9] Osiński, M., Zeller, J., Chiu, P., Phillips, B. S., & Barton, D. L. (1996). AlGaN/InGaN/GaN blue light emitting diode degradation under pulsed current stress. Applied Physics Letters, 69(7), 898-900. doi:10.1063/1.116936

[10] Cao, X., Teetsov, J., Shahedipour-Sandvik, F., & Arthur, S. (2004). Microstructural origin of leakage current in GaN/InGaN light-emitting diodes. Journal of Crystal Growth, 264(1-3), 172-177. doi:10.1016/j.jcrysgro.2004.01.031

[11] Egawa, T., Jimbo, T., & Umeno, M. (1997). Characteristics of InGaN/AlGaN light-emitting diodes on sapphire substrates. Journal of Applied Physics, 82(11), 5816-5821. doi:10.1063/1.366450

[12] Bulashevich, K. A., Evstratov, I. Y., Mymrin, V. F., & Karpov, S. Y. (2007). Current spreading and thermal effects in blue LED dice. Physica Status Solidi (c), 4(1), 45-48. doi:10.1002/pssc.200673502

[13] Cao, X., Stokes, E., Sandvik, P., Taskar, N., Kretchmer, J., & Walker, D. (2002). Optimization of current spreading metal layer for GaN/InGaN-based light emitting diodes. Solid-State Electronics, 46(8), 1235-1239. doi:10.1016/s0038-1101(02)00023-0

[14] Brown, D., Downey, E., Ghezzo, M., Kretchmer, J., Saia, R., Liu, Y., . . . Schneider, W. (1993). Silicon carbide UV photodiodes. IEEE Transactions on Electron Devices, 40(2), 325-333. doi:10.1109/16.182509
[15] Campbell, R., & Chang, H. (1966). Detection of ultraviolet radiation using silicon carbide P-N junctions. 1966 International Electron Devices Meeting. doi:10.1109/iedm.1966.187651
[16] Glasow, P., Ziegler, G., Suttrop, W., Pensl, G., & Helbig, R. (1988). SiC-UV-Photodetectors. Optoelectronic Technologies for Remote Sensing from Space. doi:10.1117/12.943598
[17] Edmond, J., Kong, H., Suvorov, A., Waltz, D., & Carter, J. C. (1997). 6H-Silicon Carbide Light Emitting Diodes and UV Photodiodes. Physica Status Solidi (a), 162(1), 481-491. doi:10.1002/1521-396x(199707)162:13.0.co;2-o
[18] Watanabe, N., Kimoto, T., & Suda, J. (2012). 4H-SiC pn Photodiodes with Temperature-Independent Photoresponse up to 300oC. Applied Physics Express, 5(9), 094101. doi:10.1143/apex.5.094101
[19] Blank, T. V., Goldberg, Y. A., Kalinina, E. V., Konstantinov, O. V., Konstantinov, A. O., & Hallén, A. (2005). Temperature dependence of the photoelectric conversion quantum efficiency of 4H–SiC Schottky UV photodetectors. Semiconductor Science and Technology, 20(8), 710-715. doi:10.1088/0268-1242/20/8/010
[20] Johnson, S. R., Ding, D., Wang, J., Yu, S., & Zhang, Y. (2007). Excitation dependent photoluminescence measurements of the nonradiative lifetime and quantum efficiency in GaAs. Journal of Vacuum Science & Technology B: Microelectronics and Nanometer Structures, 25(3), 1077. doi:10.1116/1.2720864
[21] Shchekin, O. B., Epler, J. E., Trottier, T. A., Margalith, T., Steigerwald, D. A., Holcomb, M. O. et al Krames, M. R. (2006). High performance thin-film flip-chip InGaN–GaN light-emitting diodes. Applied Physics Letters, 89(7), 071109. doi:10.1063/1.2337007
[22] Bogdanov, M. V., Bulashevich, K. A., Khokhlev, O. V., Evstratov, I. Y., Ramm, M. S., & Karpov, S. Y. (2010). Current crowding effect on light extraction efficiency of thin-film LEDs. Physica Status Solidi (c), 7(7-8), 2124-2126. doi:10.1002/pssc.200983415
[23] Y. P. Varshni, ``Temperature dependence of the energy gap in semiconductors," Physica, (Utrecht), no. 34, pp. 149 -154, 1967, http://dx.doi.org/10.1016/0031-8914(67)90062-6
[24] Wu, J., Walukiewicz, W., Yu, K. M., Ager, J. W., Haller, E. E., Lu, H., & Schaff, W. J. (2002). Small band gap bowing in In1−xGaxN alloys. Applied Physics Letters, 80(25), 4741-4743. doi:10.1063/1.1489481
[25] Lu, T., Ma, Z., Du, C., Fang, Y., Wu, H., Jiang, Y., . . . Chen, H. "Temperature-dependent photoluminescence in light-emitting diodes, Scientific Reports, 2014, http://dx.doi.org/10.1038/srep06131
[26] Franssen, G., Litwin-Staszewska, E., Piotrzkowski, R., Suski, T., & Perlin, P. (2003). Optical and electrical properties of homoepitaxially grown multiquantum well InGaN/GaN light-emitting diodes. Journal of Applied Physics, 94(9), 6122-6128. doi:10.1063/1.1616637

Advances in Science, Technology and Engineering Systems Journal Vol. 4, No. 2, 23-33 (2019)

www.astesj.com

Special Issue on Recent Advances in Engineering Systems

ASTESJ

ISSN: 2415-6698

Design of an Additively Manufacturable Multi-Material Light-Weight Gripper with integrated Bellows Actuators

Gabriel Dämmer[1,2,*], Sven Gablenz[1], Alexander Hildebrandt[1], Zoltan Major[2]

[1]*Festo AG & Co. KG, Advanced Mechatronic Systems, 73734, Germany*

[2]*Johannes Kepler University Linz, Institute of Polymer Product Engineering, 4040, Austria*

A R T I C L E I N F O

Article history:
Received: 22 December, 2018
Accepted: 09 February, 2019
Online: 06 March, 2019

Keywords:
Printed Robotics
Multi-Material Additive Manufacturing Structural Optimization
Pneumatic Actuators
Pneumatic Robots
Functional Integration
PolyJet™

A B S T R A C T

Combining state-of-the-art additive manufacturing technologies with structural optimization has the potential to produce geometrically complex multi-material components with integrated functionalities and desired structural behavior. In this article, the simulation-driven design process of a multi-material light-weight gripper with an integrated pneumatic bellows actuator is described. The design of the bellows structure is based on a previously published contribution to the RoboSoft2018 conference in Livorno, Italy. The conference paper contains the shape optimization and experimental investigations of the structural and fatigue behavior of linear type multi-material PolyJet bellows actuators. In this extended version, the main findings of the conference paper are translated into the design of a rotary type bellows actuator that is finally integrated into a multi-material light-weight gripper. In order to define the lay-out of the gripper's support structure, a density-based topology optimization is performed and the application on a PolyJet printed light-weight robot is demonstrated. The presented design approach and results are useful for researchers and engineers involved in the development of multi-material additive manufacturing, simulation-driven design and functionally integrated structures for pneumatic robotic systems.

1. Introduction

Recent advances in material science and manufacturing technologies allows for the production of geometrically complex [1], [2] multi-material structures that were not manufacturable until recently [3]. At the same time, an increasing demand for short lead times, large product variety and flexible production processes will influence the design of future robotic systems. Particularly interesting components for future light-weight robots may result from the combination of multi-material additive manufacturing (AM) and pneumatic actuation.

1.1. "Low Inertia and Compliant Elements" Approach

An approach for increased flexibility in future production processes is to combine human and robotic strengths in human-robot collaboration scenarios. The associated abolition of safety cages—that typically enclose robot workspaces today—leads to alternative safety concepts. In general, various measures can be applied to reduce the severity of injuries or damage caused by an unintended collision [4]. Thereby, the addition of compliant elements to the kinematic chain and the reduction of manipulator link inertia contributes to an inherently safe design [4], [5]. In the described work, novel materials and manufacturing technologies are combined with structural optimization to create compliant and light-weight components for light-weight robots.

1.2. Topology Optimization and Additive Manufacturing

The term topology optimization (TO) covers mathematical methods that allow for the definition of an optimum material distribution (also "material lay-out" [6]) within a given design space. Typical optimization set-ups are the minimization of structural compliance (or "global stiffness", [6]) with a constraint volume or the minimization of used material (volume) respecting a stress constraint. The underlying concept and fundamentals of todays TO have already been proposed in the 1990s (see [7], [8]).

* Gabriel Dämmer, Festo AG & Co.KG, gabriel.daemmer@festo.com

https://dx.doi.org/10.25046/aj040204

However, the field of TO has recently attracted a lot of attention. This actuality may (at least partly) be explained by an increasing degree of practical applicability of the optimization results through additive manufacturing of single material [9], [10], [11] as well as multi-material structures [3], [12]. Most AM processes allows for very complex geometries and therefore facilitate simulation-driven design processes. Thereby, light-weight design is especially relevant for robotic components close to the payload as their motion results in comparatively large inertial loads which in turn reduce the robot's performance and safety. Hence, considering AM technologies for the development of robot components makes sense in many ways [13]. Moreover, users of optimization approaches based on a given material layout, such as shape optimization (SO) and sizing optimization [14], can as well benefit from the absence of conventional manufacturing constraints as a result of the layer-wise material deposition inherent to many AM technologies.

1.3. Pneumatic Bellows Actuators

As a result of high gear ratios, typical electro-mechanical drive systems show little compliance when subjected to abrupt external loadings. Against the background of human-robot collaboration, mechanical designs have been developed that overcome this behavior i.e. can reduce the stiffness of electro-mechanical drive systems by the addition of compliant elements between the motor and torque output [15]. The use of nonlinear springs even allows for adjustment of the stiffness level [16], [17] so that the compliance of the system can be tuned according to a specific application. However, these measures come along with an inevitable increase in weight and mechanical complexity. The use of pneumatic actuators presents an alternative approach. Due to the relatively low compression modulus of air, pneumatic actuators show inherently compliant behavior and can easily be arranged to antagonistic pairs with adjustable compliance [17], [18], [19]. However, conventional pneumatic actuators (e.g. pneumatic cylinders) include dynamic seals and require smooth surfaces and close manufacturing tolerances [20]. Considering AM for the production of pneumatic actuators, alternative concepts such as bellows actuators are more promising. The structural behavior of bellows actuators can easily be modified by shape and material variations. Bellows actuators have been realized by various AM technologies such as selective laser sintering [21], PolyJet™ printing [20], [22] and Digital Mask Projection Stereolithography [23]. Numerous publications demonstrate the silicone molding process of bellow-like bending actuators utilizing additively manufactured molds (e.g. [24]). Also, detailed reviews of bellows actuators in the context of articulated robotic systems [25], 3D printing [26] and soft robotics [27] have been published. In continuum manipulators such as the "Bionic Handling Assistant" [21], bellows structures are not only used for actuation but also as a support structure.

1.4. The DIMAP Project

The main objective of the EU founded research project "Digital Materials for 3D Printing" (DIMAP) was the development of novel functional materials for PolyJet™ technology (http://www.dimap-project.eu). In PolyJet™ printing, three-dimensional objects are created from layers of small droplets of resin that are cured via ultra-violet light. Using this technology, multi-material structures with highly complex geometries can be manufactured. In order to narrow down the possible applications of the materials and technology in industry-like environments, a PolyJet-printable light-weight robot was developed.

1.5. Aim and Structure of this article

PolyJet™ printing is an interesting option for the manufacturing of highly geometrically complex and functionally integrated multi-material structures. These capabilities may be used to produce robotic components with desired structural behavior such as maximum stiffness (for light-weight structures) and inherent compliance (for actuators). Despite the existence of multiple examples of AM-related advanced structural optimization methods and multiple examples for AM of bellows structures, there is a lack of knowledge on the design and use of functional multi-material structures in industrial-near applications. This is especially the case for PolyJet™ printing. Thereby, the absence of sufficient knowledge on the achievable performance and sustainability [28] of PolyJet bellows actuators holds back the exploitation of the technological possibilities. The aim of this work is therefore to develop a complex pneumatic-mechanical multi-material component in the context of the development of a PolyJet printable light-weight robot for the DIMAP project. The chosen component is a multi-material light-weight gripper that comprises a geometrically complex bellows actuator and a numerically optimized light-weight structure. By means of the gripper development, structural and material properties are investigated, and suitable design strategies are proposed. With the final design and application to a functional light-weight robot an example is given that may inspire and encourage others for the application of the proposed materials, manufacturing technology and design approaches.

1.6. Design Approach and Concept

The structure of the gripper development is displayed in Figure 1. In a first step a conceptual design (A) is presented that already considers the functional principle of the gripper and adjacent construction in the robot. Moreover, standard parts (bearings, machined parts) are already defined at this stage. The further development is separated into the design of the bellows actuator and the support structure. This separation does not only take place on a component but also on a methodical level as the bellows actuator is (at least for the linear case) optimized via SO and the support structure via TO. Further, the development process of the bellows actuator is divided into a linear (B) and rotary (C) phase. The content of the linear phase was already presented in the conference paper [1] and contains the design and SO of linear PolyJet bellows actuators. Finite elements analysis (FEA) and experiments are conducted to understand the effects of shape and material on the number of endured cycles under repeated loading conditions. The main findings of (B), in particular an initial wall thickness distribution, the selection of an elastomeric material and a respective strain limit for repeated loading conditions, are translated into the design of a rotary type bellows actuator (C).

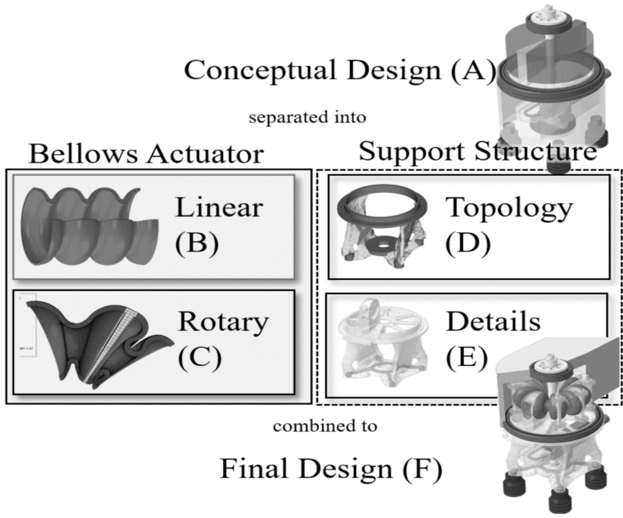

Figure 1: Development approach utilized for the design and development of a PolyJet-printed multi-material light-weight vacuum gripper.

The support structure is investigated separately in (D) and (E). Therefore, the fundamentals of density-based minimum (weighted) compliance TO are developed (D) and applied to the gripper's support structure. The optimization result is smoothened and completed with design features (E). Finally, the rotary bellows actuator and the light-weight structure are combined to the final design (F) and the application of the gripper on a PolyJet printed light-weight robot is demonstrated.

1.7. Conceptual Design

The work described in this paper contributes to the development of a PolyJet-printable vacuum gripper for a pneumatically actuated light-weight robot. When mounted to the robot as shown in Figure 2, the gripper has to fulfill two main functions. First: an object has to be gripped i.e. lifted and carried in a pick and place application. Second: the orientation of the gripped object has to be modifiable i.e. the gripper has to perform a rotatory motion. To drive the design and development process into the direction of an industry-grade performance, a payload of 1 kg and a minimum of 10000 sustainable load cycles are set as requirements. In Figure 2 the conceptual design of the light-weight gripper is displayed. The main components are a rotary bellows actuator on top of the gripper (1), a support structure (2) and a vacuum nozzle (4a) with an adapter (4b). To rotate the gripper, a pressure differential is applied to its two deformable pressure chambers (1a, 1b) that results in a torque about the main axis of the hollow shaft (8). The two antagonistically arranged chambers (1a, 1b) are attached to a fixed (1c) and a movable flange (1d) so that, depending on the external loading condition, a rotatory motion of the gripper relative to the robot (3) can be achieved. In order to grip the payload, a vacuum is created in a vacuum nozzle (Festo VN-05-H-T2, Festo AG & Co. KG, Germany) and guided through the structure to four suction cups (5, Festo ESS-20-CN, Festo AG & Co. KG).

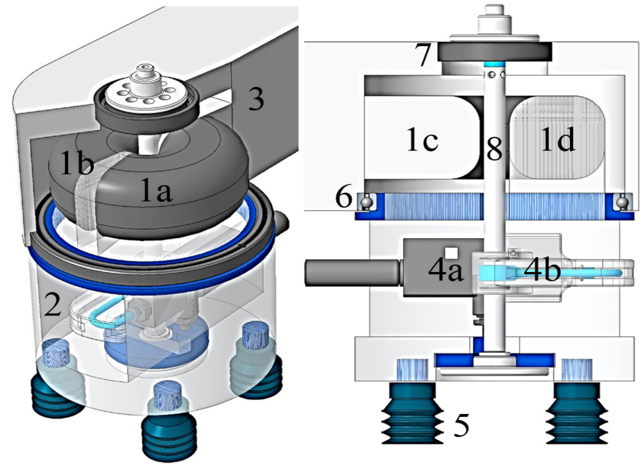

Figure 2: Conceptual design of a PolyJet-printable light-weight gripper with integrated bellows actuator. The main components are the bellows actuator (1), the support structure (2) and a vacuum nozzle (4).

Therefore, compressed air is guided through the hollow shaft (8) into the adapter (4b) and the vacuum nozzle (4a). The hollow shaft (8) is pretensioned against a lower (6) and an upper bearing (7). In order to minimize the contact pressure at the polymeric bearing seats of the attached structural component (3) and keep the weight down, thin section ball bearings (Schaeffler AG, Germany) are chosen. The bottom bearing is a INA CSCA 030 (76,2x88,9x6,35 mm^3, Schaeffler AG) and the top bearing is a CSCAA 010 TN (25x37x7 mm^3, Schaeffler AG).

2. Bellows Actuators

2.1. Linear Bellows Actuators

The behaviour of linear type bellows actuators is investigated first, as their structural behaviour is simpler to analyse by FEA. Linear bellows actuators were designed (Figure 3), comprised of an elastomeric bellows structure and thermosetting flanges.

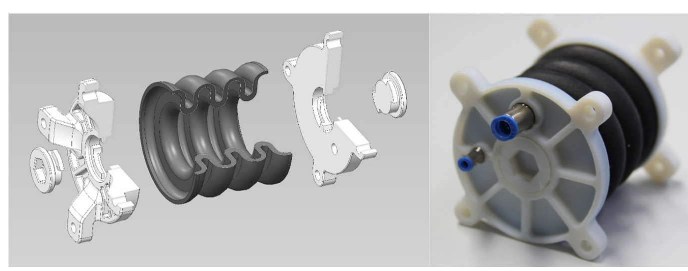

Figure 3: CAD drawing (left) and photograph (right) of a multi-material linear bellows actuator. The bellows structure and flanges are printed in one piece.

The bellows structure and flanges were printed as one monolithic piece and complemented with closing caps and pneumatic connectors (Figure 3). The elastomeric materials TangoBlackPlus™ (TB+) and Agilus30™ (A30) were used. For the flanges VeroWhitePlus™ (VW+) was selected. Actuators with bellows structures made of TB+ were provided by cirp GmbH (Römerstraße 8, 71296 Heimsheim, Germany) and actuators with bellows structures made of A30 by Stratasys® (Haim Holtsman St. 1, 7612401 Rehovot, Israel).

The linear deflection x and "effective force" F_{eff} of a pneumatic actuator depend on multiple factors including the actuator geometry, actuator material and the components of the surrounding pneumatic-mechatronic actuation system. Assuming frictionless guiding and quasi-static conditions, the effective force F_{eff} can be expressed as a function (1) of the pressure force F_p and the structural force F_s that is caused by the bellows deformation.

$$F_{eff} = F_p - F_s \tag{1}$$

Thereby, F_p can easily be determined ($F_p=(\Delta p)\cdot A_{eff}$) by multiplying the relative pressure Δp ($\Delta p = p_i - p_a$) and the effective area A_{eff} of the pneumatic chamber. The structural force F_s however, depends on the displacement x and Δp and typically results from an FEA. The curve characteristics of F_s (x, Δp) depend on the specific bellows geometry and material. Therefore, a geometrical representation and a material model for elastomeric structures of linear bellows actuators are described below.

2.2. Finite Elements Analysis of Linear Bellows

The geometric model is reduced to the bellows structure because the elastic modulus of the flange material is significantly larger than the modulus of the used elastomers (> 1000 MPa [29], compared to 0.5 MPa [30]). In the FEA described below, the flange is represented by boundary conditions applied to the bellows structure's mesh. For the axisymmetric linear bellows structure (Figure 4), a u-shaped design is chosen that consists of semicircles and parallel lines. The entire bellows structure is defined by 7 design parameters (Figure 4, left). In Figure 4 (right), parameter values (in mm) for an initial (V1) and optimized version (V2) are given and will be referred to in the following.

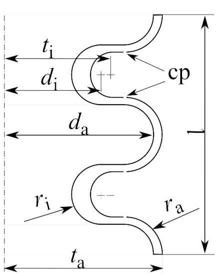

Param.	Geom. V1	Geom. V2
d_a	30	30
r_i	7.5	5.0
r_a	7.5	6.5
t_a	32.0	32.1
t_i	24.5	21.4
d_i	24.5	20.5
l	52	52

Figure 4: Left: Parameterization of a linear bellows shape with non-constant wall thickness. Control points (cp) are for the evaluation of the distances to adjacent half-waves. Right: Parameter values (Param.) in mm for an initial geometry (Geom. V1) and an optimized geometry (Geom. V2).

The structural force F_s, exerted by the deformed bellows structure, originates in the strive of the molecular chains in the elastomeric material to return to their initial configuration. Typically, a strain energy function U is utilized to describe this entropic elasticity in elastomers on a macroscopic scale [31]. In the polynomial form (2) [32], U is expressed as a function of the first and second invariant (I_1, I_2) of the left Cauchy-Green deformation tensor and—in case of compressibility—of the elastic volume strain J_{el} as

$$U = \sum_{i+j=1}^{N} C_{ij}(I_1-3)^i(I_2-3)^j + \sum_{i=1}^{N} \frac{1}{D_i}(J_{el}-1)^{2i}. \tag{2}$$

Thereby, C_{ij} and D_i are constants that are related to the deviatoric and volumetric material behavior respectively. Reducing the general polynomial form (2) to the first order (N=1), the Mooney-Rivlin form for compressible materials [32] is obtained as

$$U=C_{10}(I_1-3)+C_{01}(I_2-3)+\frac{1}{D_1}(J_{el}-1)^2. \tag{3}$$

Mooney-Rivlin model (3) to uniaxial tensile and compression test data of TB+ with Abaqus' (Dassault Systèmes) internal fitting procedure, the material constants (C_{10}=0.11 MPa, C_{01}=4.52 MPa, D_1 = 2.28 MPa) were determined. A FEA is carried out utilizing the described geometrical and material model. In order to verify the FEA, the effective force F_{eff} for given pressures Δp and deflections x, was measured and compared to simulated results. Figure 5 shows a TB+ bellows actuator mounted to an actuator test bench in three states of enforced displacement. In the testing procedure, the applied pressure difference Δp is controlled by a Festo VPPM pressure control valve (0-2 bar), F_{eff} is measured using a Burster 8523-50 force sensor (+/- 50 N) and the linear displacement x is enforced by a Festo EGSA-50-100 linear axis.

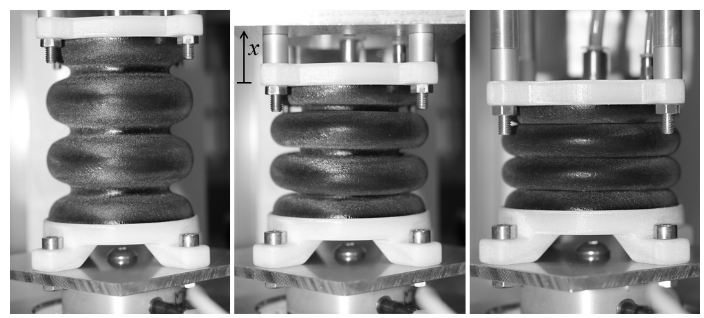

Figure 5: Measuring effective forces F_{eff} of linear bellows actuators for given pressures and enforced displacements. Extension (left), initial (middle) and compression (right) states were tested.

In the experimental procedure, relative pressures Δp were varied in 20 mbar steps from 0 mbar to 140 mbar. Displacements were varied between 20 mm of compression and 30 mm of extension. Noticeably, the effective force was observed to increase for almost 30 s after the enforced displacement states and pressures were reached. Therefore, effective forces at all displacement-pressure combinations were measured after waiting for 30 s. In Figure 6 the experimental and simulated force-pressure-deflection characteristics of a linear bellows actuator are compared. As expected, the effective force F_{eff} exerted by the actuator increases with an increase in relative pressure Δp but generally decreases with an increase in deflection x. For compressions (x < 0), the effective force F_{eff} remains almost constant. Remarkably, none of the interpolated lines covers the full deflection range. Low pressures shift the static force equilibrium (2) and limit the maximum extension. At higher pressures, compression is limited because the waves of the bellows geometry touch adjacent waves ("self-contact", see Figure 5, right). Results from FEA are generally in good agreement with the experimental results. However, Figure 6 indicates, that deviations correlate with high pressures or elongations i.e. increase with increasing strains. For improved significance of the material model, additional stress states (pure shear, bi-axial) should be considered in the fitting procedure of the constitutive model.

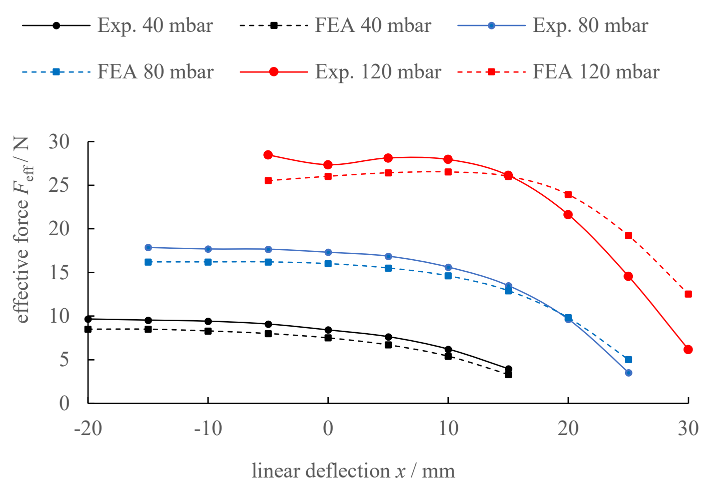

Figure 6: Comparison of the simulated (dashed lines) and experimental results (solid lines) of the effective actuator force F_{eff} as a function of given pressures and forced displacements. Simulations are generally in good accordance with the experiments. Lines are interpolated between measuring points.

2.3. Shape Optimization of Linear Bellows

The underlying concept of a bellows actuator is, that the deformation of a pressurized chamber is utilized to create a linear or rotatory motion. This implies not only the absence of holes in the bounding surface but also leads inevitably to folded structures in which the total actuator displacement is “distributed” into relatively small strains. Consequently, an optimum material lay-out or topology is known a priori (folded structure without holes). Therefore, optimizing a bellows structure can be reduced to the optimization of its shape.

In elastomers that undergo repeated strains [33], [34], material imperfections—also typical for AM materials [28]—cause local strain peaks that can lead to the formation and propagation of microscopic cracks and may eventually result in fatigue failure. In the experiments described above, the bellows structures failed after undergoing repeated deformations i.e. strain. To find an improved bellows design (V2), that reaches similar effective force F_{eff} and deflection x as the initial geometry (V1) but sustains an increased number of load cycles, a numerical optimization routine was developed. Thereby, maximum (logarithmic) principal strain $\varepsilon_{\mathrm{ln,\,max}}$ was considered as a fatigue life indicator [35] in the strain objective function

$$Q_{\varepsilon}(\mathrm{x})=(\varepsilon_{\mathrm{ln,\,max}}(x)\text{-}\varepsilon_{\max})^2. \tag{5}$$

During the optimization process, various designs are created. Sets of design parameters in the design vectors x that lead to simulated strains $\varepsilon_{\mathrm{ln,\,max}}$ larger than a reference strain $\varepsilon_{\max}$ result in large values of the objective function. To achieve a required deflection and avoid self-contact, the specific objective functions for the deflection and self-contact $Q_{\mathrm{ld}}(x)$ and $Q_{\mathrm{sc}}(x)$ are stated analogous to $Q_{\varepsilon}(x)$. The quality of a design is described by the weighted sum of specific objective functions. The resulting multiple criteria objective function is

$$Q(x)=w_{\varepsilon}\cdot Q_{\varepsilon}(x)+w_{\mathrm{ld}}\cdot Q_{\mathrm{ld}}(x)+w_{\mathrm{sc}}\cdot Q_{\mathrm{sc}}(x) \tag{6}$$

with w_{ε}, w_{ld} and w_{sc} being weighting factors for the specific objective functions. Therefore, a bellows design is fully described by the design vector

$$x=[r_{\mathrm{i}}\quad r_{\mathrm{a}}\quad t_{\mathrm{i}}\quad t_{\mathrm{a}}\quad d\quad \Delta p]^{\mathrm{T}}. \tag{7}$$

Note that Δp has to be variable and is a component of the design vector because the required effective force F_{eff} is implemented as a hard constraint. Additionally, an integer parameter n_{hw} is defined to quantify the (even) number of half-waves that describe the bellows structure. To account for bounds and secondary constraints (their exhaustive description is beyond the scope of this article), a constraint vector $g(n_{\mathrm{hw}}, x)$ is defined. Therefore, the constraint mixed integer bellows optimization problem is

$$\min_{n_{\mathrm{hw}}}\left\{\min_{x}\{Q(n_{\mathrm{hw}}, x)|g(n_{\mathrm{hw}}, x)\leq 0\}\right\}. \tag{8}$$

In order to solve the optimization problem (8), an optimization routine was realized that contains the structural simulation and parameterization described above.

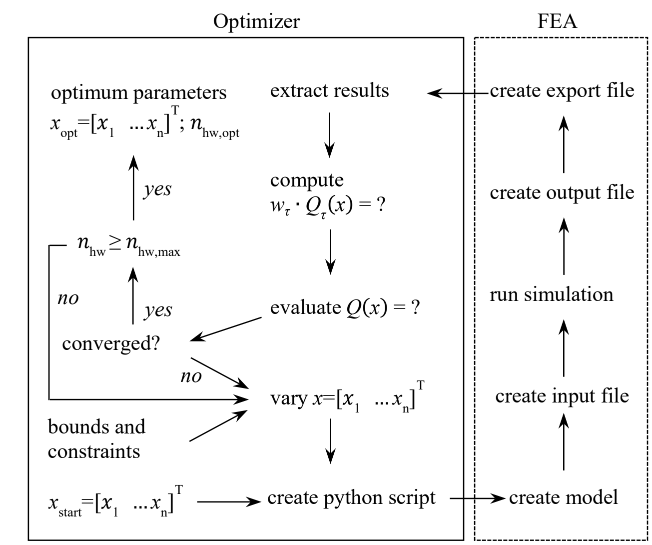

Figure 7: Optimization routine of linear bellows actuators with Matlab (MathWorks) and Abaqus (Dassault Systèmes). The optimization routine finds an optimum bellows shape and corresponding relative pressure concerning a required effective force at defined displacement. Maximum principal strain is minimized in order to increase the fatigue life of the bellows actuator.

Abaqus (Dassault Systèmes) and Matlab (MathWorks) were connected utilizing python scripts as shown in Figure 7. Starting with the initial parameters x_{start} and $n_{\mathrm{hw,start}}$ the optimization routine terminates with the output of the optimum parameters x_{opt} and $n_{\mathrm{hw,\,opt}}$. The Matlab function *fmincon* with default settings (gradient based optimizer) was chosen for convenient implementation of bounds and secondary constraints. The optimization routine was run with a maximum strain reference of $\varepsilon_{\max}$ = 0,2 and a force requirement of 12 N at 30 mm linear deflection. In Figure 8 the max. principal strain distribution of the initial (top left) and the optimized bellows geometry (top right) are displayed. The corresponding shape parameters can be found in Figure 7 (right). The initial geometry (V1) is based on an intuitive design process and comprises four half-waves with constant wall thickness. Applying 140 mbar of relative pressure results in an effective force of 12 N at 30 mm deflection. The corresponding deformation induces a (simulated) maximum principal strain of 65 % that occurs at the inner diameter of the structure (red). The optimized geometry (V2) consists of six half-waves. Wall thickness is non-constant with thickened regions at the inner diameter. Applying 100 mbar at a linear deflection of 30 mm, the effective force is above 12 N. Under these conditions, the (simulated) max. principal strain is 24 % and maximum principal strains are distributed more evenly if compared to the initial geometry (V1) i.e. respective values at the inner and outer diameter are almost equal.

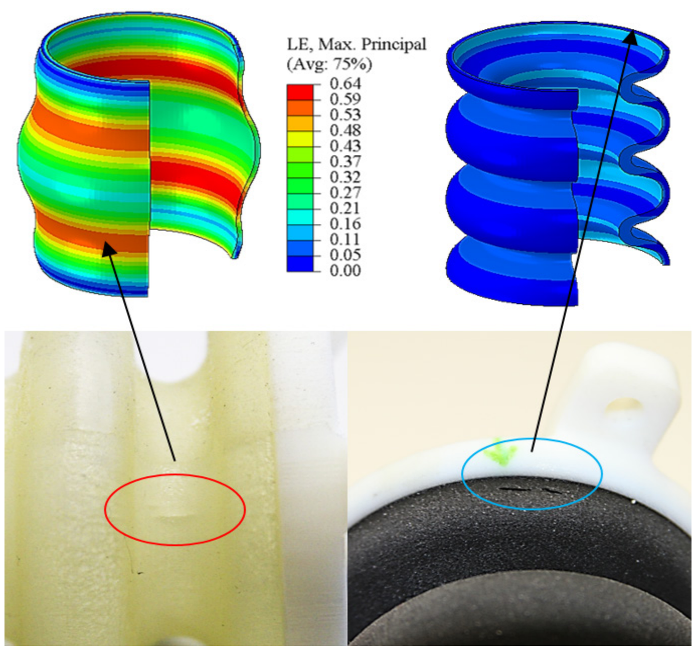

Figure 8: Comparison of the max. principal strain distribution and failures. Cracks in the bellows structure of the initial geometry "V1" (left) are oriented in axial direction occur at the inner diameter. Cracks in the bellows structure of the optimized geometry "V2" (right) are oriented in tangential direction and occur next to the flange. Our observations in the experiments match the locations and are perpendicular to the directions of max. principal strain in the FEA.

Figure 9 shows a comparison of the pressure-force-deflection characteristics of the initial (V1) and optimized (V2) bellows geometry. Noticeably, the effective force of the initial geometry (V1) is significantly more dependent on its deflection. The loss of effective force at increased deflections in Figure 8 is caused by the increased strain in the structure. In the optimized actuator (V2), lower pressures result in similar forces at large displacements. The optimized geometry (V2) satisfies the force constraint of 12 N at 30 mm. Considering the significant reduction of the (simulated) maximum principal strain (from 64 % to 24 %) and fatigue data from literature [28], an increased sustainability of the optimized actuators can be expected.

2.4. Fatigue Testing

In order to examine the hypothesis of an extended fatigue life of the optimized geometry and for comparison of the materials TB+ and A30, endurance runs were performed with the linear bellows actuators. A30 is a recently released PolyJet elastomer with similar hardness range (Shore A 30-35 compared to 26-28 for TB+) as well as a higher elongation at break and tear resistance [36]. Due to superior properties in the data-sheet [36], an increased fatigue life was expected if compared to TB+. The same geometries and material parameters were used for both the TB+ and A30 bellows actuators because no sufficient material data of A30 were available at this time. Therefore, A30 results should be interpreted with care and are presented here for comparison only.

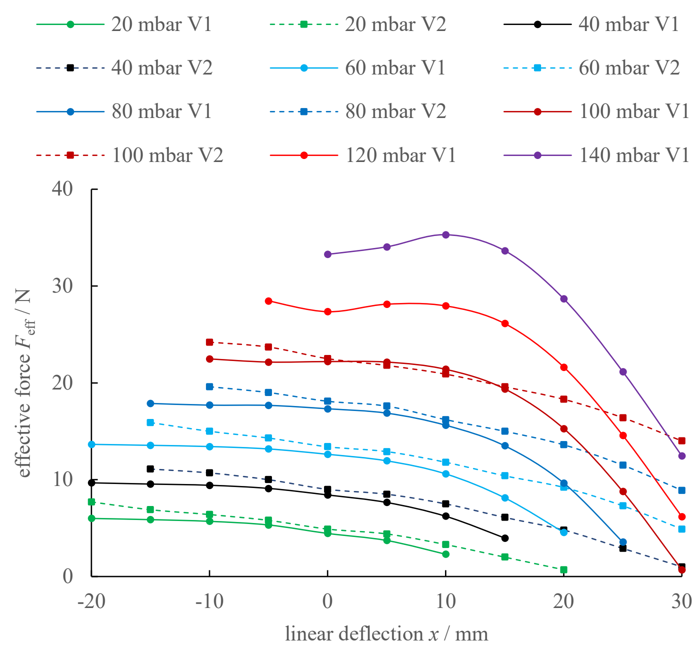

Figure 9: Experimental comparison of the pressure-force-deflection characteristics of the initial (V1, solid lines) and the optimized (V2, dashed lines) bellows geometry. Actuators with the optimized geometry (V2) require significantly less pressure to reach the required forces at 30 mm deflection. Lines are interpolated between measuring points.

In Figure 10, the endurance test bench is displayed. During the test, the right side of the actuator was attached to the test bench (Figure 10). The left side is constrained to horizontal translation by four PTFE-lubricated guiding bolts. The translation was mechanically restrained to 30 mm. In the procedure, a differential pressure of 140 mbar (V1) or 100 mbar (V2) was applied for 30 s. The actuators were vented for another 30 s before the cycle was repeated. Volume flow was measured during the 30 s period to detect possible failure of the bellows structure. The experiment was stopped in case that 2 Nl/min were exceeded.

In Figure 10 the cycles to failure of the tested actuators are displayed. Thereby, cycles to failure range from below 20 (TB+, V1) to more than 30000 (A30, V2). A30 bellows with the initial geometry (V1) endured 143 load cycles in average. With the optimized geometry (V2), A30 bellows endured an average of 24104 load cycles. Despite the relatively small number of specimen (each point in Figure 10 corresponds to a single endurance run), our results indicate that the optimized geometry (V2) sustains significantly more cycles until failure if compared to the initial geometry (V1). Moreover, we conclude that bellows made from A30 can endure more cycles to failure compared to those manufactured from TB+. Noticeably, different geometries lead to two consistent categories (i.e. modes and locations) of failures. As shown in Figure 8 (bottom), all specimens of the initial geometry (V1) show axial cracks at the inner diameter of the structure (Figure 8, bottom left). In the corresponding FEA, maximum principal strains are oriented perpendicular to the observed cracks and located at the inner diameter. Actuators with the optimized shape (V2) consistently show tangential cracks (i.e. perpendicular to axial strains) near the flanges as shown in Figure 8 (bottom right). To reduce strains at the flange region of the optimized shape (V2) additional shape parameters could be introduced in the optimization routine.

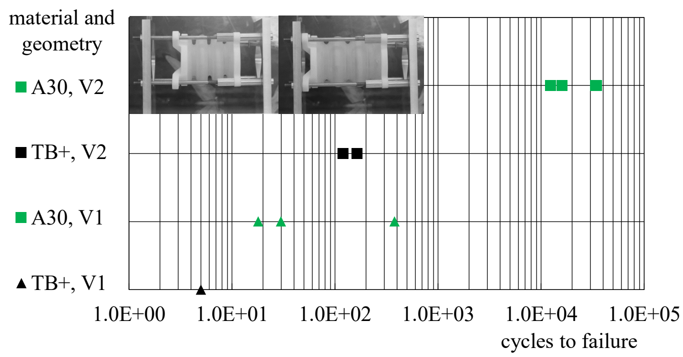

Figure 10: Endurance run with linear bellows actuators load cycles to failure of PolyJet printed linear type bellows actuators. Cycles of pressurization (extension) and ventilation (contraction) were performed until a threshold volume flow was exceeded as an indicator of structural failure. Most cycles to failure were obtained from the combination of Agilus30 (A30) with an optimized bellows shape (V2).

2.5. Rotary Bellows Actuators

The investigations described above pose an intermediate step in the development process of a PolyJet light-weight gripper with integrated elastomeric bellows actuators (number (2) in Figure 8). Three main findings can be formulated as a basis for the initial design of a rotary type bellows actuator.

1. A constant wall thickness leads to extensive strains at the inner diameter of the bellows structure. Thickening this area (as proposed by the shape optimization algorithm), may lead to an increased number of sustainable cycles.
2. A30 should be used instead of TB+ as we observed significantly increased fatigue life for the same geometries and loading conditions.
3. In the performed endurance runs, modes and locations of failure largely corresponded with maximum principal strain in our FEA. Reducing this value to 20 – 25 % delivered acceptable sustainability.

As already displayed in the conceptual gripper model (Figure 2) one rotary actuator comprises two antagonistic (i.e. separate) chambers (1a, 1b). Following this concept and based on the findings of the previous section, an initial geometry was defined in Creo (PTC Inc.) and imported into Abaqus CAE (Dassault Systèmes) for structural analysis and refinement of the bellows shape. The final design of a single chamber for the rotary bellows actuator is displayed in Figure 11. In contrast to existing designs, buckling of the deformable structure is prevented by a roller guiding system and radial forces are supported by the surrounding structure.

As displayed in Figure 12 (top), each chamber is built up from four equal elastomeric segments (1). Between the elastomeric sections, rigid frames (2) are placed that hold rotatable rollers (3). The fixed flange can be attached to the robot link and the movable flange (5) to the gripper's support structure which is pivoted as shown in Figure 2. Under extension or compression, each segment (within one chamber) undergoes the same deformation.

Figure 11: Single chamber for a rotary type bellows actuator. The main components are the soft bellows segments (1), frames (2), rollers (3) and flanges (4,5). The rollers prevent buckling of the bellows structure. The frame-roller combination at the end of each bellows segment subdivide the design into equal design features which facilitates structural analysis and scalability.

As displayed in Figure 12 (top), each chamber is built up from four equal elastomeric segments (1). Between the elastomeric sections, rigid frames (2) are placed that hold rotatable rollers (3). The fixed flange can be attached to the robot link and the movable flange (5) to the gripper's support structure which is pivoted as shown in Figure 2. Under extension or compression, each segment (within one chamber) undergoes the same deformation.

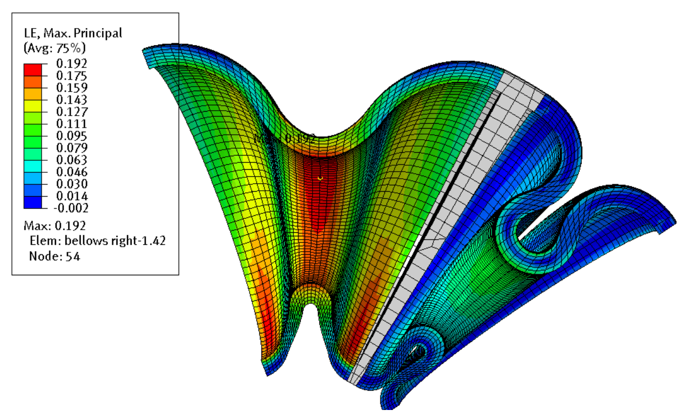

Figure 12: In the printed actuator (top), four identical segments are arranged in series to one of two counteracting chambers. In the corresponding FEA (bottom), two segments are considered because the expansion of one chamber denotes the compression of the antagonistic chamber.

This is due to the serial arrangement within a chamber and the roller guiding system that inhibits buckling. However, the expansion of one chamber denotes the compression of the antagonistic chamber. In the corresponding FE model, the roller guiding system was modelled by constraining the motion of the frame to the rotational degree of freedom (DOF) about the center axis. Hence, the FE model (Figure 12, bottom) was reduced to one half of a bellows segment of one agonist and one antagonist chamber. Nodes at the left and right side are constrained in all DOF. The geometry was meshed so that the bellows structures thickness was represented by 6 (quadratic) elements. For the bellows structure, the hyper-elastic Mooney-Rivlin material model was used as described in paragraph 3 whereas the frame was modelled as a rigid body. A linearly increasing pressure load was applied to the inner surface of the left bellows segment and left surface of the flange. The analysis type was set to non-linear quasi-static. The occurring (logarithmic, maximum principle) strains were interpreted as a fatigue life indicator. The geometry was then optimized by iteratively adding material at locations of extensive strain and removing material from less strained sections. The final geometry was defined after 5 iterations of re-design in Creo (PTC Inc.) and re-analysis in Abaqus (Dassault Systèmes) and provides a good compromise between the estimated max. rotation angle (95°) at 90 mbar and estimated max. principal strain (19 %). The described FEA does not consider any inertial loads or friction in the roller guiding system and bearings (Figure 2). Therefore, the simulated angular deflection should be interpreted as an upper limit. In initial measurements, a maximum deflection of 50-60° at 90 mbar was observed. The described actuator reaches a theoretical maximum torque of 86 Nmm at 90 mbar and 0° deflections. Apparently, overcoming the frictional torque of the rollers and bearings requires already a considerable fraction of the theoretical torque.

3. Light-Weight Structure

3.1. Density Based Topology Optimization

For the optimization of the bellows shape, a boundary variation approach was applied that is based on an a priori known optimum (or at least very reasonable) material lay-out. However, concerning the light-weight structure of the gripper, no reasonable initial shape can be defined based on intuition or examples. This is due to the complexity of the design space and expected loads and because discontinuities ("holes") in the structure are permissible. The general task for the design of the gripper's support structure is to determine the optimum spatial material distribution within the design space (as shown in Figure 2) that results in a maximum stiffness considering typical or critical loads and boundary conditions. This is exactly what is known today under the term "topology optimization" (TO). In the following, some of the fundamental concepts and equations for density-based minimum (weighted) compliance TO are explained. Detailed descriptions and exemplary Matlab code of density-based TO can be found in [6] and [37].

In typical TO approaches, the objective (and constraint) functions are structural responses from a corresponding FEA. Therefore, an FE model is set up with the discretized geometry being subdivided into design- and non-design regions. The task of the optimizer is to decide for each element of the design region if it should be void or material. As this is clearly an integer problem [8] and the optimization of a large number of discrete variables is computationally time-consuming [38], in popular algorithms ([8], [38]), continuous pseudo densities ρ_e are introduced for each element. Moreover, the stiffness of each element is coupled to its pseudo density that can continuously be varied (9) between 0 (void) and 1 (solid material) by the optimizer. Hence, the design variables of (density based) topology optimization are the continuous pseudo element densities coupled to the elements in the design space.

$$0 < \rho_e \leq 1 \tag{9}$$

However, intermediate densities i.e. values for ρ_e that are not 0 or 1, can generally not be translated into fractions of real-world structures. In the so-called "power-law" or "SIMP" (Solid Isotropic Material with Penalization) approach the stiffness of each element is coupled to its pseudo density in a nonlinear manner (10). $\widetilde{K}_e(\rho)$ is the pseudo or penalized stiffness matrix of an element, ρ_e^p is the elements pseudo density to the power of a penalization factor p (p > 1) and K_e is the initial/non-penalized stiffness matrix of an element.

$$\widetilde{K}_e(\rho) = \rho_e^p K_e \tag{10}$$

By choosing p > 1, intermediate densities become "uneconomical" [6] because the cost (volume or mass) of an element is high, compared to its penalized stiffness. If the individual element stiffness matrices $\widetilde{K}_e(\rho)$ are assembled to a global stiffness matrix $\widetilde{K}$ of the structure, the compliance C can be defined as a reciprocal measure of the structures stiffness as

$$C(\rho) = \frac{1}{2} u^T \widetilde{K} u. \tag{11}$$

In (11), u is the displacement vector. In order to rate the compliance of a structure subjected to multiple load cases i in a single scalar value, the sum of the compliances C_w, of each individual load case C_i is built using weighting factors w_i as shown in (12).

$$C_w(\rho) = \sum_{i=1}^{n} w_i C_i \tag{12}$$

The minimum weighted compliance optimization problem can now be formulated as

$$\min_{\rho} \quad C_w \quad \text{subject to} \tag{13}$$

$$\widetilde{K} u = f \tag{14}$$

$$0 < \rho_{min} \leq \rho \leq 1 \tag{15}$$

$$v = V_{d,c} / V_{d,i} \tag{16}$$

with (14) expressing the equilibrium of external (f) and internal forces for a static load case that has to be satisfied for each FEA iteration and (15) defining the value range for the design variables ρ. The volume fraction v constrains the amount of used volume in the design space $V_{d,c}$ in relation to the initial volume of the design space $V_{d,i}$ (16).

3.2. Optimization of Support Structure

For the TO of the gripper's light-weight structure, HyperWorks software was used (Altair Engineering Inc.) with HyperMesh, OptiStruct and HyperView for pre-processing, solving FEA iterations/optimization and post-processing the results respectively. In OptiStruct, the above described SIMP method was implemented [38]. As the objective function value is computed from the structural responses of an FEA, a suitable FE model was set up first. For an initial analysis, the conceptual geometry (as displayed in Figure 2) was reduced to one fourth and imported to Hypermesh (Figure 13). The geometry was discretized with 43096 CTETRA elements from which 38354 belong to the design space (transparent) and 4742 to the non-design space (blue). As strains were expected to be small and contacts were modelled with rigid body elements, a linear static analysis was set up (this also corresponds to the described approach in section 3.1). Uni-axial tensile testing of VW+ specimen revealed that for small strains the material behavior can be assumed to be linear and isotropic with an elastic modulus of 1809.00 MPa and a Poisson's ratio of 0.42.

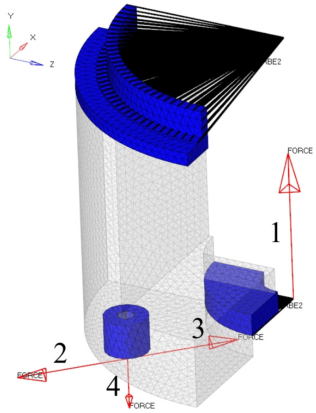

Figure 13: FEA of a light-weight gripper. One fourth of the gripper is modelled including the design space (transparent) and the non-design space (blue).

As shown in Figure 13 loads were applied for pretension of the bearing (force 1: 50.0 N), lifting the payload (force 4: 17.0 N) as well as centrifugal forces resulting from the rotational motion of the whole robot (forces 2 and 3: 35.4 N each). Loads were applied to the independent nodes of 1D RBE2 elements (black). The dependent nodes of the RBE2 elements were attached to the respective nodes in the non-design space with all DOF constrained. It must be pointed out, that the definition of two symmetry planes was made to reduce time in the development (computational time and time for design interpretation). The two planes of symmetry are valid for the load cases "pretension" and "lift" but not for the loads resulting from the rotation of the robotic arm. However, loads in radial direction were considered to drive the design towards a structure that is less sensitive to actual dynamic loads in operation. A TO was performed based on the above described FE model and according to the problem definition ((13)-(16)). The volume fraction was set to v=0.15 (16) and the four loads were weighted equally in the weighted compliance calculation (12). ρ_{min} was set to 0.01 (default). OptiStruct uses gradient-based optimization algorithms [38] in which the sensitivity of the response (C_{w}) is calculated with respect to the design variables ρ. In this case, convergence was reached within 29 iterations. In Figure 14 (top left) the optimization result is shown. For the illustration, the obtained geometry is mirrored by the (assumed) planes of symmetry. Noticeably, the main feature of the structure is a straight connection from the base-plate at the bottom to the bearing seat at the top. Smaller Features are the connections from the attachment points of the suction cups to the base plate and bearing seat. This result seems meaningful because the dominant load (load 1 in Figure 13) results in a compression of the structure between the base plate and the bearing seat. The features connecting the attachment points of the suction cups to the rest of the structure are generally in accordance with the directions of applied loads (loads 2 and 3: radial; load 4: vertical).

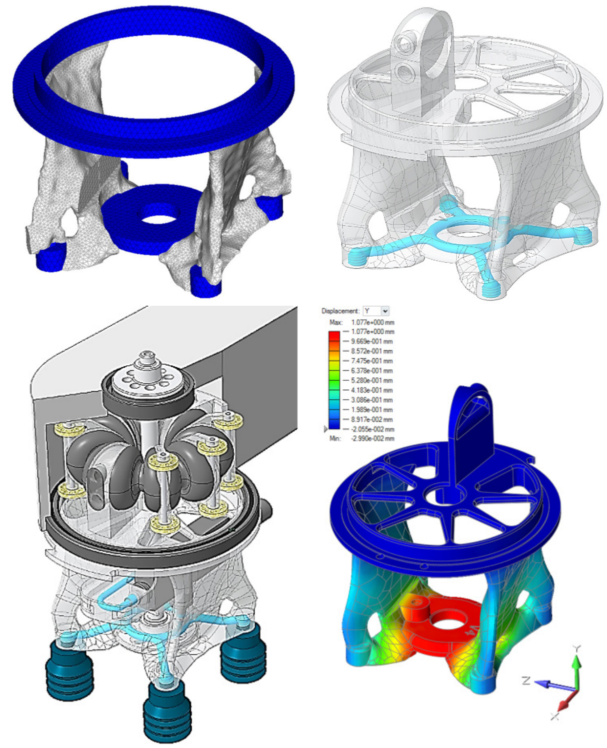

Figure 14: Optimization results and final design. Results of topology optimization (top left) were interpreted with Altair Inspire PolyNurbs (top right). Details were added to achieve the final design (bottom left) and the final structure was re-analyzed (bottom right).

The structure was remodeled using PolyNurbs functionality of Altair Inspire. Moreover, the geometry was re-imported to Creo (PTC Inc.) and features such as threads for the suction cups, internal air guidings (blue colored in Figure 14, top right) and an attachment for the bellows actuator were added. A CAD drawing of the gripper assembly is displayed in Figure 14 (bottom left). A re-analysis was performed (Figure 14, bottom right) and the structure was inspected for strain peaks. When interpreting the results, it must be mentioned, that the elastic modulus of VW+ is significantly rate-dependent which is typical for polymers. The choice of modulus might be considered less important when performing a minimum compliance TO, based on linear static load cases. However, rate-dependency of the modulus in combination with a mixture of long-term static (preload and lift and hold) and dynamic loads (rotatory motion of the robot) bring a certain vagueness to the computation of the weighted compliance (eq. 12) and re-analysis. In further research, the effect of rate-dependent material behavior on the optimization result should be considered.

4. Final Design and Application in Light-Weight Robot

Multiple Grippers were printed by Stratasys ® (Haim Holtsman St. 1, 7612401 Rehovot, Israel) and cirp (cirp GmbH Römerstraße 8, 71296 Heimsheim, Germany). In Figure 15 a prototype of the developed gripper is displayed. Including bottom and top bearing as well as the adapter with vacuum nozzle, the gripper has a weight of 263 g (Figure 15, left) of which the printed multi-material structure constitutes 102 g.

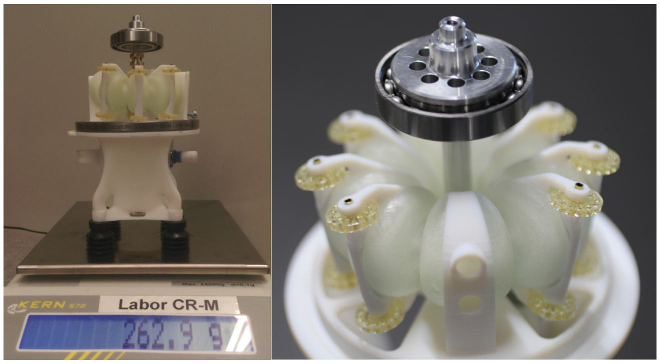

Figure 15: Prototype of a multi-material light-weight gripper with integrated elastomeric bellows actuator. Left: the printed light-weight structure and bellows contribute less than half of the total weight. Right: top-end of the gripper with roller guiding system.

A gripper was mounted to the PolyJet printed light-weight robot that was developed for the DIMAP project (Figure 16). The functioning robot was presented to the public at the formnext2018 faire (19.-22.11.2019, Frankfurt, Germany) at the cirp booth (cirp GmbH Römerstraße 8, 71296 Heimsheim, Germany).

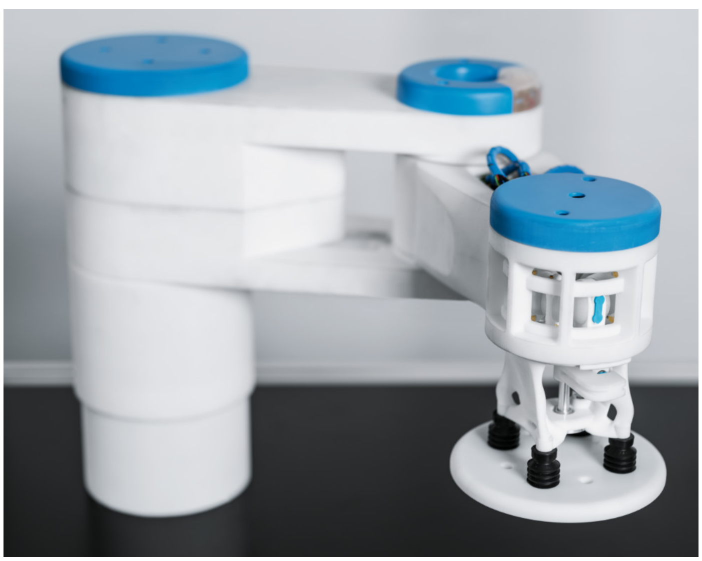

Figure 16: Light-weight gripper attached to the DIMAP SCARA (© Festo).

During the four days, no failure occurred and all the features (bellows actuator, vacuum system, light-weight structure) worked flawlessly. Figure 15 shows the PolyJet printed light-weight robot “DIMAP SCARA” with the attached gripper in a typical pick and place application. Objects of more than 1 kg can be lifted with the described configuration of vacuum nozzle and suction cups.

5. Conclusion

Additively manufactured bellows actuators pose an interesting option for the actuation of future robotic systems as their structural behavior is highly tunable by variations of shape and material. By using state-of-the-art AM technologies such as multi-material PolyJet™ printing, soft actuators can be integrated into stiff and light-weight support structures resulting in highly integrated and geometrically complex components. Though there are many publications that contain AM bellows actuators or suitable light-weight design approaches, the combination of both has hardly been investigated so far. In this article, the simulation-driven design process of a multi-material light-weight vacuum gripper with an integrated bellows actuator is described with the aim to demonstrate possible development approaches and the application in a printed light-weight robot. Based on a conceptual gripper design, investigations were separated into the actuator and support structure development. To understand the structural and fatigue behavior of elastomeric PolyJet bellows, linear type multi-material bellows actuators were designed using VeroWhitePlus™ (VW+) material for the rigid flanges and TangoBlackPlus™ (TB+) for the soft bellows structure. Starting from very few (below 50) sustainable load cycles, optimizing the bellows shape and using Agilus30™ (A30) instead of TB+ material, increased the fatigue life to more than 20.000. Based on these findings, a rotary type actuator was designed that consists of two antagonistic chambers with each chamber being a linear arrangement of equal bellows segments. If compared to existing solutions, the design of the novel guiding system facilitates structural analysis and scalability of the geometry. In order to develop the gripper’s support structure, the fundamentals of density-based minimum (weighted) compliance topology optimization were developed and applied to the conceptual gripper design. Considering multiple load cases, an optimum material lay-out was defined. By merging the rotary bellows actuator and the light-weight structure, a fully functional multi-material vacuum gripper was obtained that reaches rotatory deflections of more than 60°, can lift and hold objects of more than 1 kg and has a weight of 263 g of which the printed multi-material structure constitutes 102 g. Finally, the gripper was mounted to a PolyJet printed light-weight robot and its functionality was successfully presented to the public at the formnext2018 faire in Frankfurt, Germany. The described development steps and design solutions can be transferred to other manufacturing technologies.

Conflict of Interest

The authors declare no conflict of interest.

Acknowledgment

The authors of this paper thank for the opportunity to be involved in the DIMAP project funded as part of the Horizon 2020 Framework program for research and innovation under the grant agreement no 685937. Moreover, we thank the responsible persons for the organization of the 2018 IEEE international conference on Soft Robotics (RoboSoft) and publication of the conference paper [1]. The software used for the simulation-driven design of the light-weight structure was kindly provided by Altair Engineering Inc..

References

[1] G. Dämmer, S. Gablenz, A. Hildebrandt, and Z. Major “Design and Shape Optimization of PolyJet Bellows Actuators,” in *Proc. 2018 IEEE International Conference on Soft Robotics (RoboSoft)*, 2018. https://doi.org/10.1109/ROBOSOFT.2018.8404933

[2] A. Clausen, N. Aage, and O. Sigmund “Exploiting Additive Manufacturing Infill in Topology Optimization for Improved Buckling Load”. Engineering, vol. 2, no. 2, pp. 250-257, 2016. https://doi.org/10.1016/J.ENG.2016.02.006

[3] A. M. Mirzendehdel and K. Suresh “A Pareto-optimal approach to multimaterial topology optimization”. *Journal of Mechanical Design*, vol. 137, no. 10, pp. 101701-12, 2015. https://doi.org/10.1115/1.4031088
[4] DIN ISO/TS 15066:2017-04 “Robots and robotic devices - Collaborative robots,” 2017.
[5] M. Zinn, B. Roth, O. Khatib, and J. K. Salisbury “A new actuation approach for human friendly robot design”. The international journal of robotics research, vol. 23, no. 4-5, pp. 379—398, 2004. https://doi.org/10.1177/0278364904042193
[6] M. P. Bendsøe and O. Sigmund, Topology optimization: theory*, methods, and applications.* Springer Science+Business Media, 2013, ISBN 978-3-662-05086-6. https://doi.org/10.1007/978-3-662-05086-6
[7] R. V. Kohn and G. Strang “Optimal design and relaxation of variational problems, I”. *Communications on pure and applied mathematics,* vol. 39, no. 1, pp. 113-137, 1986. https://doi.org/10.1002/cpa.3160390107
[8] M. P. Bendsøe “Optimal Shape Design as a material distribution Problem”. *Structural and Multidisciplinary Optimization*, vol. 1, no. 4, pp. 193-202, 1989. https://doi.org/10.1007/BF01650949
[9] J. Liu, A. T. Gaynor, S. Chen, Z. Kang, K. Suresh, A. Takezawa, L. Li, J. Kato, J. Tang, W. Jinyuan et al. “Current and future trends in topology optimization for additive manufacturing”. *Structural and Multidisciplinary Optimization*, vol. 57, no. 6, pp. 2457-2483, 2018. https://doi.org/10.1007/s00158-018-1994-3
[10] J. Liu, and Y. Ma “A survey of manufacturing oriented topology optimization methods”. Advances in Engineering Software, vol. 100, pp. 161-175, 2016. https://doi.org/10.1016/j.advengsoft.2016.07.017
[11] T. Zegard and G. H. Paulino “Bridging topology optimization and additive manufacturing”. Structural and Multidisciplinary Optimization, vol. 53, no. 1, pp. 175-192, 2016. https://doi.org/doi:10.1007/s00158-015-1274-4
[12] A. T. Gaynor, N. A. Meisel, C. B. Williams, and J. K. Guest “Multiple-material topology optimization of compliant mechanisms created via PolyJet three-dimensional printing”, Journal of Manufacturing Science and Engineering, vol. 136, no. 6, pp. 0610151-10, 2014. https://doi.org/10.1115/1.4028439
[13] S. Junk, B. Klerch, L. Nasdala, and U. Hochberg “Topology optimization for additive manufacturing using a component of a humanoid robot,” in Proc. 28th CIRP Design Conference, pp. 102-107, 2018. https://doi.org/10.1016/j.procir.2018.03.270
[14] P. W. Christensen and A. Klarbring, *An Introduction to Structural Optimization*. Springer Science+Business Media, 2008, ISBN 978-1-4020-8666-3.
[15] T. Lens, J. Kunz, O. Von Stryk, C. Trommer, and A. Karguth “Biorob-arm: A quickly deployable and intrinsically safe, light-weight robot arm for service robotics applications,” in *Proc. 41st International Symposium on Robotics (ISR)* and *6th German Conference on Robotics (ROBOTIK)*, pp. 905-910, 2010.
[16] M. Grebenstein, A. Albu-Schäffer, T. Bahls, M. Chalon, O. Eiberger, W. Friedl, R. Gruber, S. Haddadin, U. Hagn, R. Haslinger et al. “The DLR hand arm system,” in *Proc. 2011 IEEE International Conference on Robotics and Automation (ICRA)*, pp. 3175-3182, 2011. https://doi.org/10.1109/ICRA.2011.5980371
[17] B. Vanderborght, A. Albu-Schäffer, A. Antonio, E. Burdet, D. G. Caldwell, R. Carloni, M. Catalano, O. Eiberger, W. Friedl, G. Ganesh et al. “Variable impedance actuators: A review”. *Robotics and autonomous systems*, vol. 61, no. 12, pp. 1601—1614, 2013. https://doi.org/doi:10.1016/j.robot.2013.06.009
[18] A. J. Veale and S. Q. Xie “Towards compliant and wearable robotic orthoses: A review of current and emerging actuator technologies”. *Medical engineering & physics*, vol. 38, no. 4, pp. 317-325, 2016. https://doi.org/doi:10.1016/j.medengphy.2016.01.010
[19] D. Baiden and O. Ivlev “Independent torque and stiffness adjustment of a pneumatic direct rotary soft-actuator for adaptable human-robot-interaction,” in *Proc. 23rd International Conference on Robotics in Alpe-Adria-Danube Region (RAAD)*, September 2014. https://doi.org/10.1109/RAAD.2014.7002257
[20] R. MacCurdy, R. Katzschmann, K. Youbin, and D. Rus “Printable Hydraulics: A Method for Fabricating Robots by 3D Co-Printing Solids and Liquids,” in *Proc. 2016 IEEE International Conference on Robotics and Automation (ICRA)*, 2016. https://doi.org/10.1109/ICRA.2016.7487576
[21] A. Grzesiak, R. Becker, and A. Verl “The bionic handling assistant: a success story of additive manufacturing”. *Assembly Automation*, vol. 31, no. 4, pp. 329—333, 2011. http://dx.doi.org/10.1108/01445151111172907
[22] D. Drotman, S. Jadhav, M. Karimi, M. T. Tolley et al. “3D printed soft actuators for a legged robot capable of navigating unstructured terrain,” in *Proc. 2017 IEEE International Conference on Robotics and Automation,* ICRA, pp. 5532-5538, 2017. http://dx.doi.org/10.1109/ICRA.2017.7989652
[23] B. N. Peele, T. J. Wallin, H. Zhao, R. F. Shepherd “3D printing antagonistic systems of artificial muscle using projection stereolithography”. *Bioinspiration & Biomimetics*, vol. 10, no. 5, 2015. http://dx.doi.org/10.1088/1748-3190/10/5/055003
[24] B. Mosadegh, P. Polygerinos, C. Keplinger, S. Wennstedt, R. F. Shepherd, U. Gupta, J. Shim, K. Bertoldi, C. J. Walsh, G. M. Whitesides “Pneumatic networks for soft robotics that actuate rapidly”. *Advanced Functional Materials*, vol. 24, no. 15, pp. 2163-2170, 2014. http://dx.doi.org/10.1002/adfm.201303288
[25] I. Gaiser, A. Andres, G. Bretthauer, H. Breitwieser, O. Ivlev, R. Wiegand, S. Schulz “Compliant robotics and automation with flexible fluidic actuators and inflatable structures,” *INTECH Open Access Publisher*, 2012. http://dx.doi.org/10.5772/51866
[26] A. Zolfagharian, A. Z. Kouzani, S. Y. Khoo, A. A. A. Moghadam, I. Gibson, A. Kaynak “Evolution of 3D printed soft actuators”. *Sensors and Actuators*, vol. 250, pp. 258-272, 2016. https://doi.org/10.1016/j.sna.2016.09.028
[27] P. Polygerinos, N. Correll, S. A. Morin, B. Mosadegh, C.D. Onal, K. Petersen, M. Cianchetti, M. T. Tolley, R. F. Shepherd “Soft Robotics: Review of Fluid-Driven Intrinsically Soft Devices; Manufacturing, Sensing, Control, and Applications in Human-Robot Interaction”. *Advanced Engineering Materials*, 2017. http://dx.doi.org/10.1002/adem.201700016
[28] J. P. Moore and C. B. Williams “Fatigue properties of parts printed by PolyJet material jetting”. *Rapid Prototyping Journal*, vol. 21, no. 6, pp. 675-685, 2015. http://dx.doi.org/10.1108/RPJ-03-2014-0031
[29] O. Sheikhnejad, F. Hiptmair, and Z. Major “Finite element simulation and mechanical modelling of nanoparticles reinforced composite,” in *Proc. 6th International Conference on Additive Technologies*, 2016.
[30] M. Reiter and Z. Major “A combined experimental and simulation approach for modelling the mechanical behaviour of heterogeneous materials using rapid prototyped microcells”. *Virtual and Physical Prototyping*, vol. 6, no. 2, pp. 111-120, 2011. http://dx.doi.org/10.1080/17452759.2011.586949
[31] R. W. Ogden, *Non-linear elastic deformations*. Dover Publications, Inc., Mineola, 1997, ISBN: 9780486696485.
[32] Dassault Systemes Simulia Corp “Abaqus Theory Guide. Version 6.14,”, 2014.
[33] A.N. Gent, P.B. Lindley, and A.G. Thomas “Cut growth and fatigue of rubbers. I. The relationship between cut growth and fatigue”. *Journal of Applied Polymer Science*, vol. 8, no. 1, pp. 455-466, 1964. https://doi.org/10.1002/app.1964.070080129
[34] G.J. Lake and P.B. Lindley “Cut growth and fatigue of rubbers. II. Experiments on a noncrystallizing rubber”. *Journal of Applied Polymer Science*, vol. 8, no. 2, pp. 707-721, 1964. https://doi.org/10.1002/app.1964.070080212
[35] Y. Zhou, “Fatigue Properties Of Magnetorheological Elastomers And The Design Of Interfacial Layers To Improve Fatigue Life.” Ph.D. thesis, Dublin Institute of Technology, Ireland, 2016. https://doi.org/doi:10.21427/D75315
[36] Stratasys Ltd, “PolyJet Materials DataSheet”, [Online]. Available: http://usglobalimages.stratasys.com/Main/Files/Material_Spec_Sheets/MS S_PJ_PJMaterialsDataSheet.pdf?v=635785205440671440. [Accessed: Feb. 26. 2018].
[37] O. Sigmund “A 99 line topology optimization code written in Matlab”. *Structural and Multidisciplinary Optimization*, vol. 21, no. 2, pp. 120-127, 2001. https://doi.org/10.1007/s001580050176
[38] OptiStruct, Altair “OptiStruct 11.0 user manual”, Altair Engineering Inc, Troy, MI Google Scholar, 2011.

Advances in Science, Technology and Engineering Systems Journal Vol. 4, No. 2, 34-39 (2019)

www.astesj.com

Special Issue on Recent Advances in Engineering Systems

ASTESJ

ISSN: 2415-6698

Technical and Economic Merits Resulting from Power Systems Interconnection

Abdullah Al-Shaalan*

Electrical Engineering Department, King Saud University, 11421, Riyadh, Kingdom of Saudi Arabia

A R T I C L E I N F O

Article history:
Received: 06 October, 2018
Accepted: 15 February, 2019
Online: 07 March, 2019

Keywords:
Load
Reliability
Energy
Cost
Interconnection
Planning

A B S T R A C T

In this paper, the impact of interconnection among isolated and dispersed electric power systems have been Investigated and analyzed. Therefore, the methodology proposed in this work is implemented in three real electric power systems in the western part of Saudi Arabia (designated as I, II and III). The outcome of this study revealed positive benefits resulting from power systems interconnection for reliability enhancement as well as cost saving.

1. Introduction

This paper is an extension of work originally presented in the "2017 9th IEEE-GCC Conference [1].

Power systems interconnection is an effective way of raising reliability levels and in the meantime lowering their static and spinning reserves. The diversity between various systems in their peak demand and load variations encourage these systems to be integrated and interconnected via one unified grid. Reliability evaluation techniques can be used to determine the optimal system reliability risk level. The systems interconnection provides mutual assistance among interconnected system as well as reducing their reserve capacity periodic additions. Also, systems interconnection will elevate the degree of coordination and cooperation by establishing efficient and more and more efficient and larger electric power facilities. This necessitates the advent and implementations of various modeling techniques and reliability methodologies [2-7]. The Loss of Load Expectation (LOLE) is considered to be the most widely adopted and utilized reliability measure by the electric utilities and system planners [3]. This index specifies the average length of time that unit(s) is being out of service causing power outages for a specified period of time. There is another complementary index known as the Expected Energy not Served (ϵENS) which evaluates the size of energy that is curtailed due to unexpected severe power outages occurrence) [8].

*Abdullah Al-Shaalan, Saudi Arabian Standards Organization (SASO), Email: shaalan@ksu.edu.sa

2. Review of Some Existing works on Power Systems Interconnection

For the purpose of exploring other methodologies, practices and experiences adopted in the process of power system interconnection, the following existing research works are overviewed and discussed. In [9], the environmental benefits have been assessed and evaluated based on power system interconnection point of view. The author showed analytical findings of reductions environmental reductions carbon and in CO_2 taxes, which can be obtained should power system interconnection achieved. In [10], the need for systems interconnection in developing countries has been highly emphasized through national grids and as a prerequisite with integrating with other neighboring countries. In [11,12] the authors discussed the interconnection among the Arab Gulf states and the potential benefits that accrue as a result of this historic milestone. In [13], the author proposed a probabilistic model to evaluate capacity assistant transfer between the interconnected systems to be ready against any unexpected deficit or emergency state. This model has been applied and substantiated on the IEEE Reliability Test System and gave promising results. In [14], the author demonstrated safety measures due to mutual system interconnection that can be abided by and utilized in power system reliability evaluation and utilization in cost/reliability benefit tradeoffs for long-range systems expansion plans and costs assessments process.

From the preceding review of the existing research works devoted and focused on systems interconnection, it is shown that the most widely adopted and applied is the reliability modeling and evaluation that ought to be considered at every stage of electric system installation, commissioning, operation, and interconnection nationally or internationally.

3. Interconnected Power Systems

Electric power systems can be interconnected in several configuration methods, as shown in Figure (1). These configurations are subject to systems site, size of power, peak loads occurrence, fuel proximity and level of mutual influence and impact. Figure (1) shows different ways of system interconnection arrangements.

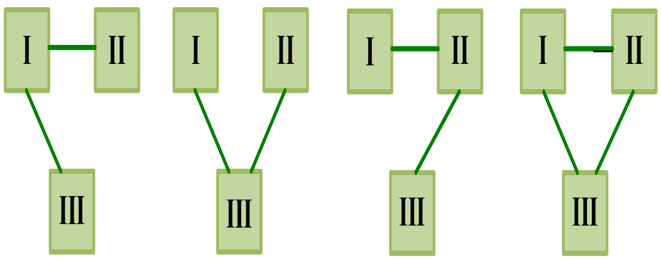

Figure 1: Configuration arrangements of interconnected systems

4. Reliability Evaluation of Interconnected Systems

In case of interconnected power systems, let us consider two integrated power electric systems, say, system (I) and system (II) where each one is maintaining its rated power capacity and demands, and along with the three postulates mentioned below:

- systems are ready to share their available spinning reserve to back up the other system if a tie-line exists.
- systems can assist each other's only if there are an adequate reserve and a connecting tie-line.
- the connecting tie-line has a capability to transfer the capacity assistance (C_T).

Figure (2) interprets the above three assumptions, as the deviation between: (i) with no tie-line and (ii) with tie-line is the capacity assistance (C_T) that is provided to system (I) by system (II) through the tie-line interconnection. This capacity assistance ((C_T)) substitutes the capacity shortfall in system (I) and enables it to cover its standing demands adequately rather being independent and isolated.

5. Adopted Criterion for the Case Under Study

In this case study, a criterion based on a simulation process has been established that can simulate the adopted criterion and its techniques applied for this case under study. Figure 3 and the subsequent steps explain the conceptual operations of the adopted computational Algorithm.

5.1. Systems are dispersed and independent:

- Prepare the data pertinent to the studied systems (ss).
- Use the ($\boldsymbol{FOR}$) for for all units residing in the system to establish the ($\boldsymbol{COPT}$) for the system.
- Combine the $\boldsymbol{COPT}$ with the load duration curve ($\boldsymbol{LDC}$) for process.
- Evaluate the ($\boldsymbol{LOLE_e}$) risk level for each separate system and compare it with the prescribed reliability level ($\boldsymbol{LOLE_P}$).
- If ($\boldsymbol{LOLE_e}$) is larger than ($\boldsymbol{LOLE_P}$), more units should be incorporated to the existing capacity up to the reliability risk level prescribed and decided upon by the executive management is attained and satisfied or else the process continues to the next following year, repeating the process with future annual load.
- Now, evaluate the expected energy not supplied ($\boldsymbol{\epsilon ENS}$). This index has two merits, firstly, it measures the degree of energy adequacy and secondly, can provide a substantiated methodology for energy production computation, particularly in case of interconnected power systems.
- Estimate the total system cost taking into account the units being added to the system in the planning process.

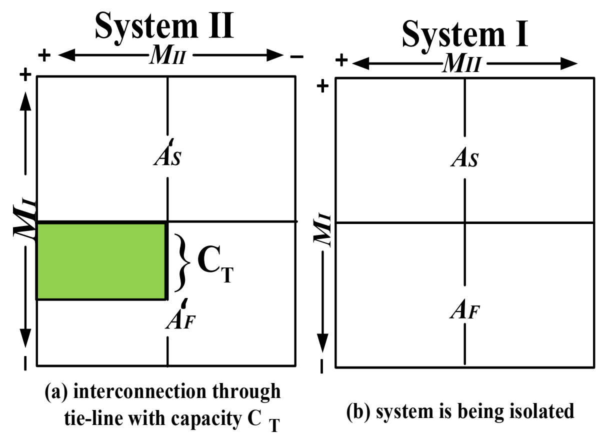

Figure 2: Capability of system B to assist system A

5.2. Case of interconnected systems:

- Prepare the data related to systems considered for the study.
- Build the ($\boldsymbol{COPT}$) for the interconnected systems.
- Repeat the preceding steps (c-g) mentioned in 4.1. The capacity assistance (C_T) is the available reserve that can be transmitted through the connecting line to the system being in deficit and viable to be assisted. For reliability evaluation, the system being assisted can then proceed as an isolated system for risk level evaluation.

6. Developed Approach to an Existing Systems

In order to substantiate the proposed preceding techniques, an existing real case study has been considered. This case represents three electric power systems in three large cities in a fast-developing country. These systems supply these cities and each system is designated as I, II and III respectively. These cities are facing tremendous future load increase as a result of population growth and industrial project expansion in realization to the Kingdom 2030 vision.

For the purpose of this study, a generation expansion planning spanning over the coming five-year period (2018-2023) to determine the appropriate timely capacity reinforcement schedule capacity-addition and evaluating the reliability level for each power system before and after the proposed interconnection commission. The target is to investigate and realize the resulting economic and technical benefits that may accrue due to electric power systems integration.

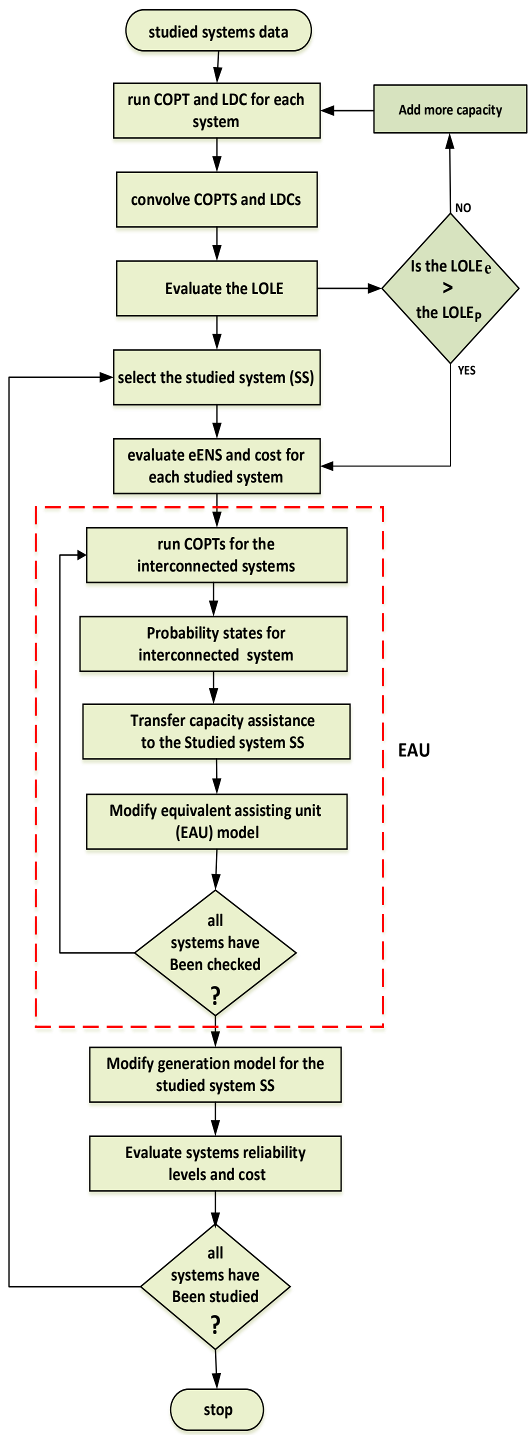

Figure 3: Simulation methodology applied in the proposed case study

6.1. Systems interconnection technical merits

This part tries to analyze and evaluate the risk levels for each electric power system separately for future specified period assuming that there are no capacity additions to the systems. With lack of capacity addition, the reliability level will deteriorate due to reserve reduction and capacity shortage. At each year the reliability level exceeds the prescribed limit either a new generating unit must be added or an interconnection with another adjacent power system may be a favorite solution. The results shown in Figure (4), display the outcome of the study pertinent to systems (I) and (II) as investigating their reliability risk levels while they are being isolated during the upcoming five years applying the LOLE reliability index. From the figure, it is obvious that if the prescribed level of the LOLE is set at 0.10 d/y, both systems will surpass the specified reliability prescribed limit. Hence, an additional capacity should be added to the existing capacity of each individual system to upgrade their reliability against any service deficit due to unexpected service interruptions and consequent power deficit and shortage. After envisioning of mutual interconnection among power systems, the process was performed again to the same systems. The outcome is displayed in Figure (4), and it is evident from the figure that risk limits for both systems have been enhanced when systems are being interconnected. Consequently, system (I) requires no unit(s) addition up to 2021, while system (II), it will go over its risk levels at 2022.

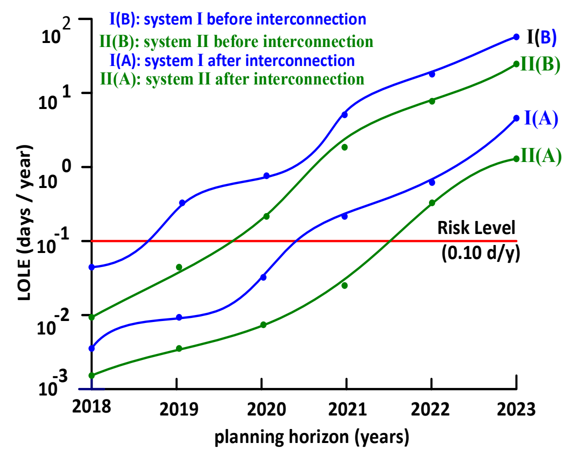

Figure 4: Systems LOLE before and after interconnection

To ascertain and exhibit the benefits accruing due to systems integration in improving and upgrading their reliability levels, the impact of interconnection for another essential complementary risk index (ϵENS) mentioned previously, has been evaluated. Systems (I) and (II) have been selected for this analysis and demonstration as being the largest among the three systems. The outcome is exhibited by Figure (5) where it indicates the size and amount of energy not supplied (ϵENS) that has been reduced after systems being interconnected.

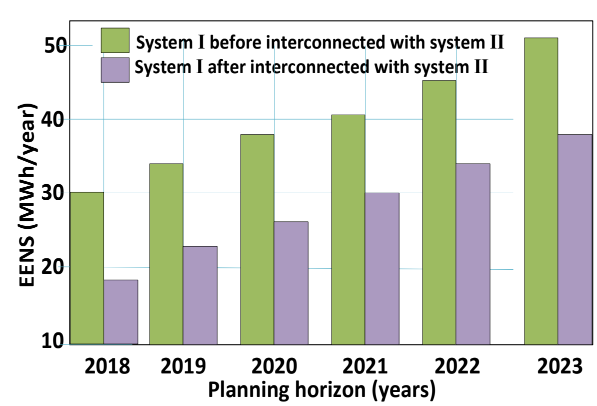

Figure 5: ϵENS before and after interconnection

6.2. Systems Interconnection economic merits

This analysis focusses on searching and exploring the possible economic merits that may accrue due to systems interconnection. The study covers the same period of study (2018-2023). The prescribed risk index (***LOLE***) has been fixed at 0.1 d/y for the three systems and considered to be steady over that planning horizon. The reliability level at the beginning year (i.e.***LOLE***) due to load demand increment. To maintain the reliability level at the prescribed limit specified previously by the utility executive management, unit(s) additions either should be added (in case of isolated system) or ought to be integrated with neighboring electric power systems. For assessing and estimating the unit(s) added cost for this process, the methodology demonstrated in Section 4 was applied. Figure (6) displays the analysis outcome of this study where it is evident that all systems will gain from the interconnection process where there will be substantial savings in fixed cost and variable costs. This can be observed as 55%, 51%, and 62% for systems I, II and III respectively. Moreover, the reliability level for each system will improve and attain better reliability levels as demonstrated in earlier sections.

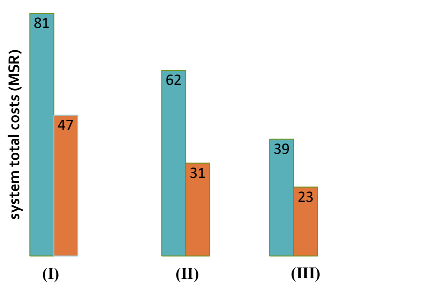

	(I)	(II)	(III)
Units (isol)	2	4	3
Costs (isol)	81	62	93
Units (inter)	1	2	1
Costs (inter)	47	31	23

Figure 6: Cost for isolated and interconnected systems

7. Searching for Optimal levels in Reliability evaluation

Searching for optimal levels in system planning process is a major endeavor and concern for all utilities, planners, engineers and economists to guarantee adequate and reliable supply at reasonable and acceptable tariff. Hence, extensive and rigorous factors investigations and analysis based on econometric indicators and variables related to units installation, transmission networks and operations should be conducted and explored. Therefore, the reliability indices, namely, the (LOLE) and the(ϵENS) have been applied to system (I) utilizing the concepts shown in the Appendices and the simulation process shown in Figure (3) above.

In order to obtain the optimal range of reliability levels, the system investment cost should be convolved with the anticipated outages losses [7]. The costs of system represent the expenditure for unit installation cost, and fuel and maintenance cost. Outages costs represent the losses cost borne by the consumers as a results of energy cease. The total system cost portrays the overall cost sustained by the consumers as a worth of uninterrupted energy flow. The outcome of the process yields the results shown by Figure 7 as system cost (SC) tends to increase as level of reliability level increases. In the meantime, the outage cost (OC) starts to decrease as system reliability improves with generating units' additions. The optimality of reliability levels varies between 0.16 and 0.27 days/year (see Fig. 7). However, adding new capacity in some cases may not imply the perfect resolution to encounter ever increasing load growth and preserve desirable levels of reliability. Hence, it may be better to improve unit's efficiency and performance by regular scheduled maintenance. Likewise, establishing a consistent co-ordination and co-operation between the demand-side and the supply-side may further improve energy consumption and reduce financial obligations.

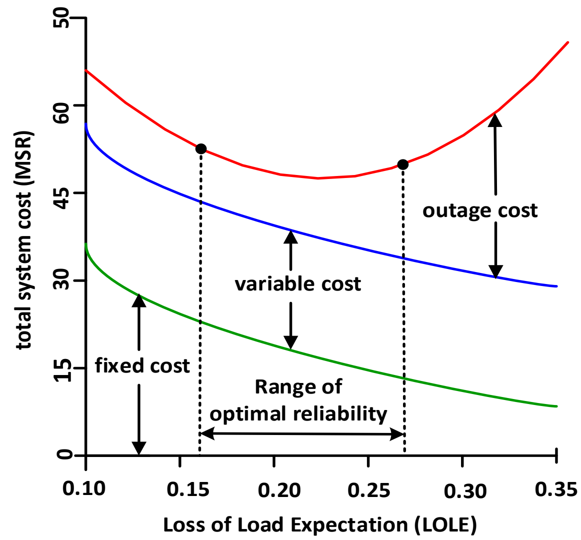

Figure 7: reliability levels Variation vs. variation of system cost

8. Conclusion

In this work, the merits of interconnection among isolated and dispersed electric power systems have been explored, analyzed and assessed using recent developed reliability criteria. The methodology proposed in this work was conducted for realistic electric power systems serving major cities in a fast-developing country. The outcome of this work revealed positive benefits that can be attained as a result of power systems interconnection. These benefits and merits can be interpreted in systems reliability improvement and cost saving.

References

[1] A. M. Al-Shaalan, "Management of Power Systems Interconnection to Realize Technical and Economical Potentials", 2017 9th IEEE-GCC Conference and Exhibition (GCCCE), Gulf Hotel, Manama, Bahrain, 8 -11 May 2017.

[2] R. Billinton, R. N. Allan, "Reliability Evaluation of Power Systems", (Book), Second Edition, Plenum Press, London, 1985.

[3] R. Billinton, "Reliability Assessment of Bulk Electric Systems," Power System Research Group, University of Saskatchewan, Canada, Publications No. 148, 2007, p. 75.

[4] J. Endrenyi, "Reliability Modelling in Electric Power Systems", Wiley International Publication, 1978.

[5] L. Leonard, L. Grigsby, "Power Systems", Power System Planning (Reliability Part 3), 2009 by Taylor and Francis Group, LLC.

[6] IEEE Bronze Book on Recommended Practice for Energy Conservation and Cost-Effective Planning in Industrial Facilities. New York: IEEE, 1993.

[7] A. M. Al-Shaalan, "Reliability/Cost Tradeoff Evaluation for Interconnected Electric Power Systems", International Journal of Computing and Digital Systems, ISSN (2210-142X), Int. J. Com. Dig. Sys. 6, No.6, pp. 371-374, Nov-2017.

[8] A. M. Al-Shaalan, "Reliability evaluation in generation expansion planning based on the expected energy not supplied", Journal of King Saud, Engineering Science, Vol. 24, No. 1, January 2012, pp. 11 – 18.

[9] Y. K. Jaeyoung, "Environmental impacts and benefits of regional power system interconnections for the Republic of Korea", IEEE Conference, Power Engineering Society General Meeting, Changwon, South Korea, 6-10 June 2004, pp. 427 – 433.

[10] A. M. Al-Shaalan, "Essential aspects of power system planning in developing countries", Journal of King Saud, Engineering Science, Vol. 23, No. 1, January 2011, pp. 28 – 32.

[11] E. S. Ibrahim, "Interconnection of electric power systems in the Arab world", IEEE Power Engineering Journal, Volume: 10, Issue: 3, 1996, pp. 121 -127.

[12] O. A. Al-Zeer, "Assessment of Economic and Technical Advantages of the Tie-Line Interconnection Among the GCC States Networks, MSc. Thesis, College of Engineering, King Saud University 2009.

[13] G. Hamoud, "Probabilistic assessment of interconnection assistance between power systems", IEEE Transactions on Power Systems, Volume: 13, Issue: 2, pp. 535 – 542, 1998.

[14] Mo-Shing Chen. "Security issues of power system interconnection", IEEE Power Engineering Society, General Meeting on System Improvement and Saving, June 12-16, 2005, pp. 1797 – 1800.

Appendix A - Power System Costs

The general aspects of power system costs can be documented as follows:

- Fixed Cost (*FC*): costs associated with establishing the power plant (site, generating units, transformers, protection and control facilities, auxiliaries, etc.):

$$FC_T = \sum_t \sum_k (CC_k \cdot CAP_k \cdot NU_k)^t$$

- Variable Cost (*VC*): cost related to the cost of operation and maintenance (fuel, scheduled maintenance, interim spare parts):

$$VC_T = \sum_t \sum_k (VOM_k \cdot CAP_k \cdot NU_k)^t$$

- Outages Cost (*OC*): cost that incurred by the consumers as a result of power interruptions and energy curtailment (this type of costs is not transferable and ought to be assessed and evaluated through public investigations and questionnaires):

$$OC_T = \sum_t (\epsilon ENS_t \cdot cost/kWh)^t$$

Hence, the above costs constitute the total system cost (TC), and can be expressed as:

Where,

CC_k : *capital cost of unit of type* k.
CAP_k: *unit capacity added to the system of type* k.
NU_k: *number of unit(s)added to the system of type* k.
VOM_k: *variable operation & maintenance to unit of type* k *(maianly cost of fuel).*
ϵENS_t: *expected energy not served to the consumers due to power outages.*
t: *interval period of time considered in the planning horiozon.*
T: *total number of years in the planning horizon.*

Appendix B- Some Pertinent Reliability Index

Loss of Load Expectation (LOLE)

The LOLE risk index is the most widely accepted and used probabilistic method in power system reliability evaluation of generation expansion planning. It is defined as: "the expected number of days in the specified

period in which the load levels will exceed the available system capacity". To evaluate this risk index, two models are required and employed. One is the Load Duration Curve (LDC) which the load levels are arranged in a descending order of magnitude, and the other one is the Capacity Outage Probability Table (COPT) which contains all capacity states of the generating units with their associated probabilities. These two models are convolved (combined) in the process. The unit of the LOLE is in days per year (d/y). The LOLE evaluation method is expressed in the following mathematical formula:

$$LOLE = \sum_{i=1}^{n} t_i \cdot p_i \quad (d/y) \qquad (outage > Reserve)$$

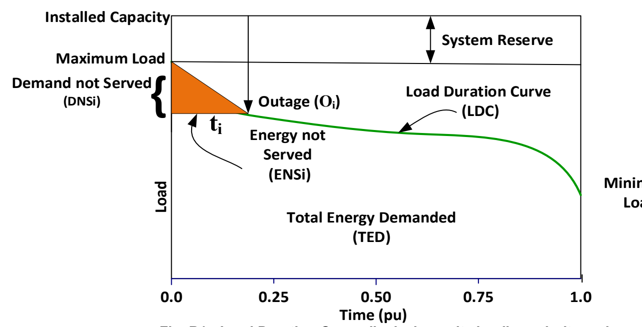

Fig. B1: Load Duration Curve displaying units loading priority and their energy shares according to their least operating costs

It is clear from the above load characteristics that those capacity outages less than the reserve will not cause a loss of load yielding a "Demand not Supplied" to the consumers. Consider now:

$o_i =$ the i^th^ outage(s) state in the COPT

$t_i =$ number of times unit(s) is unavailable

$p_i =$ the probability of this i^th^ unavailable

Expected Energy Not Supplied (*ϵENS*)

Since the un-supplied energy caused by power outages reflects great damages and heavy losses to the entire consumers' classes, so, another essential and most needed reliability index known as the **ϵENS** can be deduced as follows:

$$\epsilon ENS = \sum_{i=1}^{n} (ENS_i) \cdot p_i \quad MWh/year \quad (outage > Reserve)$$

Appendix C- Energy Production Methodology

The Expected Energy Supplied (ϵES) by each unit available and being operated in the system can be evaluated by using the above concept of the Expected Energy Not Supplied (ϵENS) as shown below:

$$\epsilon ES_i = \epsilon ENS_{i-1} - \epsilon ENS_i \qquad \text{MWh/year}$$

This method adopts a priority loading order, i.e. the generating units are loaded according to their least operation cost. Hence, operating, first, the most efficient and economical operating units (called the base units), followed by the more cost operating units (called the intermediate units), then the costliest operating units (called the peaker units), and so on. This means that the least cost operating units occupy the lower levels in the LDC, and the expensive operating units occupy the upper levels in the LDC respectively.

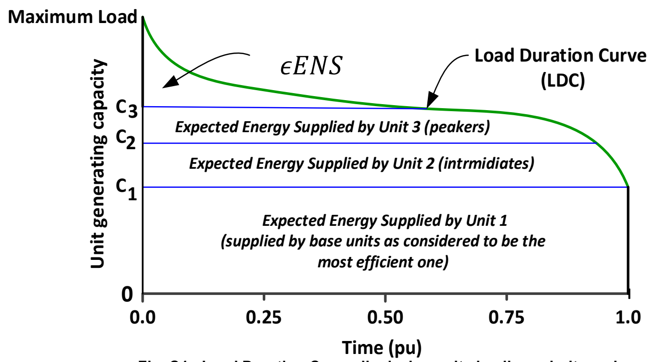

Fig. C1: Load Duration Curve displaying units loading priority and their energy shares according to their least operating costs

The above equation can be explained in the following process:

- The LDC (Load Duration Curve) is implemented, as it is the type of curve that is widely used in power system reliability evaluation and planning for its convenience and flexibility. It is derived from the ordinary load curve and hence can be defined as “the arrangement of all load levels in a descending order of magnitude.
- The expected energy not supplied (ϵENS_0) before any unit is operated = the total area under the LDC.
- When the first unit (C_1) is loaded according to the priority loading level # 1, it will occupy the green area (0 – C_1) and shifts the new expected energy not supplied (ϵENS_1) upward (i.e. above C_1. Therefore, the expected energy supplied by unit C_1 (ϵES_1) will: be $\epsilon ES_1 = \epsilon ENS_0$ - ϵENS_1.
- When the second unit (C_2) is loaded according to the priority loading level # 2, it will occupy the area (C_1 – C_2) and then shift the new expected energy not supplied (ϵENS_2) upward above C_2. Therefore, the expected energy supplied by unit C_2 (ϵES_2) will be $\epsilon ES_2 = \epsilon ENS_1$ - ϵENS_2.
- When the third unit (C_3) is operated according to the priority loading level # 3, it will occupy the area (C_2 – C_3) and then shift expected energy not supplied (ϵENS_3)above C_3, and then the process ends and the remaining expected energy not supplied will be above C_3. As such, the expected energy supplied by unit C_3 $(\epsilon ES_3) = \epsilon ENS_2 - \epsilon ENS_3$.

Advances in Science, Technology and Engineering Systems Journal Vol. 4, No. 2, 40-44 (2019)

www.astesj.com

ASTESJ

ISSN: 2415-6698

Coupling of Local and Global Quantities by A Subproblem Finite Element Method – Application to Thin Region Models

Dang Quoc Vuong[*,1] and Nguyen Duc Quang[2]

[1]*School of Electrical Engineering, Ha Noi University of Science and Technology, Viet Nam*

[2]*Faculty of Electrical Engineering, Electric Power University, Hanoi, Viet Nam*

A R T I C L E I N F O

Article history:
Received: 29 October, 2018
Accepted: 10 January, 2019
Online: 07 March, 2019

Keywords:
Finite element method (FEM)
Magnetostatics
Magnetodynamics
Subproblem method (SPM)
Coupled problems thin region
Magnetic fields

A B S T R A C T

A method for coupling of local and global fields related to currents, voltages and magnetic fields in magnetodynamic problems is developed in the frame of the finite subproblem finite element method. The method allows to correct the errors arising from thin conducting regions, that replace volume thin regions by surfaces but neglect border effects in the vicinity of geometrical discontinuities, edges and corners, increasing with the thickness, which limits their range of validity. This leads to errors when solving the thin shell finite element magnetic models in electrical machines and devices. It also permits to perform a natural coupling between local and global quantities weak formulations. A subproblem finite element method is developed to split a complete problem/model composed of local and global fields (some of these being thin regions) into a series of subproblems with the change of materials. Each subproblem is performed on its own separate domain and mesh.

1. Introduction

Many papers have been published about thin region finite element (FE) models [1]-[7]. Besides theoretical studies on the shielding effect and related to interface conditions (ICs), several finite element (FE) subproblem method (SPM) formulations for the thin shell (TS) models have been developed [1]-[7]. This means that instead of meshing the volume thin regions, the TS models can be considered as surfaces with ICs, that neglect errors on the computation of local electromagnetic quantities in the vicinity of geometrical discontinuities, edges and corners, increasing with the thickness [1] - [4].

In this paper, the FE SPM is herein extended for coupling of local fields (magnetic flux density, magnetic field and eddy current) and global quantities (currents, voltages Joule losses) associated with any conducting part of an electric system to correct the inherent errors of the local and global fields near eges and corners comming from the TS models. It is particularly the case with inductors driven by external sources. For such components, either a global current I_i or a global voltage V_i can be fixed (Figure 1), in a more general way, both of them must be taken into account when a coupling with circuit equation is performed.

*Dang Quoc Vuong, Hanoi Universtiy of Science and Technology,
Email: Vuong.dangquoc@hust.edu.vn

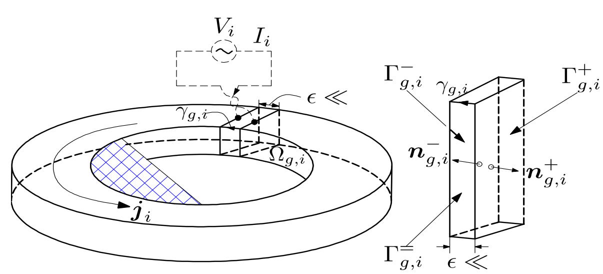

Figure 1. Generator $\Omega_{g,i}$ with associated global current I_i and voltage V_i.

The FE SPM allows to couple any changes from this problem to others via surface sources (SSs) and volume sources (VSs) and applied via a projection method [1]-[4]. The development of the method is proposed for the magnetic vector potential FE magneto dynamic formulation, paying special attention to the proper discretization of the constraints involved in each subproblem (SP) and to the resulting weak FE formulations. The method is validated on a practical test problem [8].

2. Coupled Magnetic Subproblem

2.1. Sequence of Subproblems

At the hearth of the SPM, a full problem is proposed to be divided into sequences of SPs: A problem involving global current driven stranded or massive inductors alone is first performed on a simplified mesh without any thin regions. The obtained solution considered as SSs for added TS problems via ICs [1] - [7]. The TS solution is then corrected by a correction problem via SSs and VSs, that overcomes the TS assumptions as presented in Section 1.

2.2. Canonical magnetodynamic problem

A canonical 3-D magnetodyanmic problem i, to be solved at step i of the SPM, is defined in a domain Ω_i, with boundary $\partial\Omega_i = \Gamma_i = \Gamma_{h,i} \cup \Gamma_{b,i}$. The eddy current defined in the conducting part and the non-conducting of Ω_i are respectively denoted $\Omega_{c,i}$ and $\Omega_{c,i}^C$, with $\Omega_i = \Omega_{c,i} \cup \Omega_{c,i}^C$. Stranded inductors belong to $\Omega_{c,i}^C$, whereas massive inductors belong to $\Omega_{c,i}$. The equations and material relations of SPs i are [9] - [11]:

$$\operatorname{curl} \boldsymbol{h}_i = \boldsymbol{j}_i, \quad \operatorname{div} \boldsymbol{b}_i = 0, \quad \operatorname{curl} \boldsymbol{e}_i = -\boldsymbol{\partial}_t \boldsymbol{b}_i \quad \text{(1a-b-c)}$$

$$\boldsymbol{h}_i = \mu_i^{-1} \boldsymbol{b}_i + \boldsymbol{h}_{s,i}, \quad \boldsymbol{j}_i = \sigma_i \boldsymbol{e}_i + \boldsymbol{j}_{s,i}, \quad \text{(2a-b)}$$

where $\boldsymbol{h}_i$ is the magnetic field, $\boldsymbol{b}_i$ is the magnetic flux density, $\boldsymbol{e}_i$ is the electric field, $\boldsymbol{j}_i$ is the electric current density, μ_i is the magnetic permeability and σ_i is the electric conductivity. Note that (1c) is only defined in $\Omega_{c,i}$, whereas it is reduced to the form (1b) in $\Omega_{c,i}^C$. Boundary conditions (BCs) are defined on complementary parts $\Gamma_{h,i}$ and $\Gamma_{b,i}$, i.e.

$$\boldsymbol{n} \times \boldsymbol{h}_i = \boldsymbol{j}_{f,i}, \quad \boldsymbol{n} \times \boldsymbol{b}_i|_{\Gamma_{b,i}} = \boldsymbol{f}_{f,i}, \quad \text{(3a-b)}$$

where $\boldsymbol{n}$ is the unit normal exterior to Ω_i. The surface fields $\boldsymbol{j}_{f,i}$ and $\boldsymbol{f}_{f,i}$ in (3a) and (3b) are SSs which comes from previous problems [2] - [6]. For the classical homogeneous BCs, they normally define as zero. However, they define as possible SSs in the thin region between γ_i^+ and γ_i^- [1] - [7]. This is the case when some field traces in a SP_u are forced to be discontinuous, whereas their continuity must be recovered via a SP_p. The SSs in SP_p are thus to be fixed as the opposite of the trace solution of SP_u.

In addition, global conditions on currents or voltages in inductors are considered. A typical inductor is shown in Figure 1 where a source of electromotive force $\Omega_{g,i}$ is defined between two electrodes very close to each other of voltage V_i and the current I_i following through surface $\Gamma_{g,i}$, i.e.

$$\oint_{\Gamma_i^-}^{\Gamma_i^+} \boldsymbol{e} \cdot dl = V_i \quad \text{and} \quad \oint_{\Gamma_i^-}^{\Gamma_i^+} n \cdot \boldsymbol{j}\, ds = I_i, \quad \text{(5a-b)}$$

where Γ_i is a path in $\Omega_{g,i}$ connecting its two electrodes. Surface $\Gamma_{g,i}$ is defined as a part of the boundary $\Gamma_{e,i}$ of the studied domain in presences symmetry conditions.

The fields $\boldsymbol{h}_{s,i}$ and $\boldsymbol{j}_{s,i}$ (fixes the global current in inductors) and in (2a) and (2b) are VSs which can be used for expressing changes of materials in each SP [1]-[4]. Indeed, for changes of permeability and conductivity in a region, from SP_u (i = u) to SP_p (i = p) are defined via VSs $\boldsymbol{h}_{s,i}$ and $\boldsymbol{j}_{s,i}$, i.e.

$$\boldsymbol{h}_{s,p} = (\mu_p^{-1} - \mu_u^{-1}) \boldsymbol{b}_u, \quad \boldsymbol{j}_{s,p} = (\sigma_p - \sigma_u) \boldsymbol{e}_u \quad \text{(4a-b)}$$

Each SP is constrained through the so defined SSs and VSs from the parts of the solutions of other SPs.

3. Finite Element Weak Formulation

3.1. Magnetic Vector Potential Formulation

We can define a vector potential $\boldsymbol{a}_i$ so that $\boldsymbol{b}_i = \operatorname{curl} \boldsymbol{a}_i$ and $\boldsymbol{e}_i = \sigma_i \partial_i \boldsymbol{a}_i - \sigma_i \operatorname{grad} v_i$. A weak formulation of SP_i ($i \equiv u, p$ or k) of the Ampère equation (1a) can be written as [1]-[4].

$$\begin{aligned}
&(\mu_i^{-1} \operatorname{curl} \boldsymbol{a}_i, \operatorname{curl} \boldsymbol{a}'_i)_{\Omega_i} + \left(\boldsymbol{h}_{s,i}, \operatorname{curl} \boldsymbol{a}'_i\right)_{\Omega_i} + \left(\boldsymbol{j}_{s,i}, \boldsymbol{a}'_i\right)_{\Omega_i} \\
&\quad + (\sigma_i \partial_i \boldsymbol{a}_i, \boldsymbol{a}'_i)_{\Omega_{c,i}} + (\sigma_i \operatorname{grad} v_i, \boldsymbol{a}'_i)_{\Omega_{c,i}} \\
&\quad + < \boldsymbol{n} \times \boldsymbol{h}_i, \boldsymbol{a}'_i >_{\Gamma_{h,i} - \Gamma_{t,i}} \\
&\quad + < [\boldsymbol{n} \times \boldsymbol{h}_i]_{\Gamma_{t,i}}, \boldsymbol{a}'_i >_{\Gamma_{t,i}} \\
&\qquad = (\boldsymbol{j}_i, \boldsymbol{a}'_i)_{\Omega_{s,i}}, \forall\, \boldsymbol{a}'_i \in F_i^1(\Omega_i) \quad (6)
\end{aligned}$$

where $F_i^1(\Omega)$ is a curl-conform function space defined in $\Omega_{c,i}$, gauged in $\Omega_{c,i}^C$, and containing the basis functions for $\boldsymbol{a}_i$ as well as for the test function $\boldsymbol{a}'_i$ (at the discrete level, this space is defined by edge FEs; the gauge is based on the tree-co-tree technique); $(\cdot,\cdot)_\Omega$ and $<\cdot,\cdot>_\Gamma$ respectively denote a volume integral in Ω and a surface integral on Γ of the product of their vector field arguments. The surface integral term on $\Gamma_{h,i}$ is considered as natural BCs of type (3a), usually zero. The electrical scalar potential v_i is only defined in the conducting regions $\Omega_{c,i}$. The weak formulation (6) implies, by taking $\boldsymbol{a}'_i = \operatorname{grad} v'_i$ as a test function, that

$$\begin{aligned}
&(\sigma_i \partial_t \boldsymbol{a}_i, \operatorname{grad} v'_i)_{\Omega_{c,i}} + (\sigma_i \operatorname{grad} v_i, \operatorname{grad} v'_i)_{\Omega_{c,i}} \\
&\quad + \left(\boldsymbol{h}_{s,i}, \operatorname{curl} \boldsymbol{a}'_i\right)_{\Omega_i} + \left(\boldsymbol{j}_{s,i}, \boldsymbol{a}'_i\right)_{\Omega_i} \\
&+ < [\boldsymbol{n} \times \boldsymbol{h}_i]_{\Gamma_{t,i}}, \boldsymbol{a}'_i >_{\Gamma_{t,i}} = < \boldsymbol{n} \cdot \boldsymbol{j}, v'_i >_{\Gamma_g}, \forall\, \boldsymbol{a}'_i \in F_i^1(\Omega_i) \quad (7)
\end{aligned}$$

where Γ_g is the part of the boundary of $\Omega_{c,i}$ which is crossed by a current (Γ_g is the union of all the surfaces $\Gamma_{g,i}$ resulting from the abstraction of the generators $\Omega_{g,i}$) (Fig. 1).

3.2. Current as weak global quantities and circuit relations

For the weak formulation in (6), the appearing of total current in a conductor is only expressed in a weak sense, e.g. as a natural global constraint, because it arises from Ampère law which is its self-expressed in a weak form. By solving the equation (7), the current I_i flowing in the part $\Gamma_{g,i}$ of an inductor can be obtained with v'_i equal to the source scalar potential $v_{s,i}$. Hence, with $v'_i = v_{s,i}$, the surface intergral term in (7) written for the inductor $\Omega_{m,i}$ gives

$$< \boldsymbol{n} \cdot \boldsymbol{j}, v_{s,i} >_{\Gamma_{g,i}} = < \boldsymbol{n} \cdot \boldsymbol{j}, 1 >_{\Gamma_{g,i}} = I_i, \quad (8)$$

and thus (7) becomes

$$\begin{aligned}
&\left(\sigma_i \partial_i \boldsymbol{a}_i, \operatorname{grad} v_{s,i}\right)_{\Omega_{m,i}} + \left(\sigma_i \operatorname{grad} v_i, \operatorname{grad} v_{s,i}\right)_{\Omega_{m,i}} \\
&\quad + \left(\boldsymbol{h}_{s,i}, \operatorname{curl} \boldsymbol{a}'_i\right)_{\Omega_i} + \left(\boldsymbol{j}_{s,i}, \boldsymbol{a}'_i\right)_{\Omega_i} \\
&\quad + < [\boldsymbol{n} \times \boldsymbol{h}_i]_{\Gamma_{t,i}}, \boldsymbol{a}'_i >_{\Gamma_{t,i}} = I_i, \quad (9)
\end{aligned}$$

or, with $v = V_i\, v_{s,i}$,

$$\begin{aligned}
&\left(\sigma_i \partial_i \boldsymbol{a}_i, \operatorname{grad} v_{s,i}\right)_{\Omega_{m,i}} + V_i \left(\sigma_i \operatorname{grad}\ v_{s,i}, \operatorname{grad} v_{s,i}\right)_{\Omega_{m,i}} \\
&\quad + \left(\boldsymbol{h}_{s,i}, \operatorname{curl} \boldsymbol{a}'_i\right)_{\Omega_i} + \left(\boldsymbol{j}_{s,i}, \boldsymbol{a}'_i\right)_{\Omega_i} \\
&\quad + < [\boldsymbol{n} \times \boldsymbol{h}_i]_{\Gamma_{t,i}}, \boldsymbol{a}'_i >_{\Gamma_{t,i}} = I_i. \quad (10)
\end{aligned}$$

Equation (10) is the circuit relation associated with the inductor $\Omega_{m,i}$, i.e. a relation between its voltage V_i and its current I_i.

3.3. Inductor alone "$\boldsymbol{SP}_{\boldsymbol{u}}$" - The added TS model "$\boldsymbol{SP}_{\boldsymbol{p}}$" - Volume correction "$\boldsymbol{SP}_{\boldsymbol{k}}$"

The weak form of an SP_u with the inductor alone is first solved via the volume integrals in (10) ($i \equiv u$) where I_u is the fixed current density in on $\Omega_{m,i}$, i.e.

$$\left(\sigma_i \partial_i \boldsymbol{a}_i, \operatorname{grad} v_{s,i}\right)_{\Omega_{m,i}} + V_i \left(\sigma_i \operatorname{grad}\ v_{s,i}, \operatorname{grad} v_{s,i}\right)_{\Omega_{m,i}} = I_i. \quad (11)$$

The added TS problem is defined via the second term in (11) ($i \equiv p$). The test function $\boldsymbol{a}'_p$ is divided into continuous and discontinuous parts $\boldsymbol{a}'_{c,p}$ and $\boldsymbol{a}'_{d,p}$ (with $\boldsymbol{a}'_{d,p}$ zero on Γ_p^-) [6]. One thus has

$$< [\boldsymbol{n} \times \boldsymbol{h}_p]_{\Gamma_{t,p}}, \boldsymbol{a}'_p >_{\Gamma_{t,p}} = \; < [\boldsymbol{n} \times \boldsymbol{h}_p]_{\Gamma_{t,p}}, \boldsymbol{a}'_{c,p} >_{\Gamma_{t,p}} + \; < \boldsymbol{n} \times \boldsymbol{h}_p|_{\Gamma_{t,p}^+}, \boldsymbol{a}'_{d,p} >_{\Gamma_{t,p}^+} \quad (12)$$

The terms of the right-hand side of (12) are developed from the TS models [6], i.e.

$$< [\boldsymbol{n} \times \boldsymbol{h}_p]_{\Gamma_{t,p}}, \boldsymbol{a}'_{c,p} >_{\Gamma_{t,p}} = \; < \sigma_p \beta_p \partial_t (2\boldsymbol{a}_{c,p} + \boldsymbol{a}_{d,p}), \boldsymbol{a}'_{c,p} >_{\Gamma_{t,p}} \quad (13)$$

$$< \boldsymbol{n} \times \boldsymbol{h}_p|_{\Gamma_{t,p}^+}, \boldsymbol{a}'_{d,p} >_{\Gamma_{t,p}^+} = - < \boldsymbol{n} \times \boldsymbol{h}_u|_{\Gamma_{t,p}^+}, \boldsymbol{a}'_{d,p} >_{\Gamma_{t,p}^+} + \frac{1}{2} < \sigma_p \beta_p \partial_t (2\boldsymbol{a}_{c,p} + \boldsymbol{a}_{d,p}) + 1/\sigma_p \beta_p, \boldsymbol{a}'_{d,p} >_{\Gamma_{t,p}}. \quad (14)$$

The surface integral term $- < \boldsymbol{n} \times \boldsymbol{h}_u|_{\Gamma_{t,p}^+}, \boldsymbol{a}'_{d,p} >_{\Gamma_{t,p}^+}$ in (14) is considered as a SS appeared from the weak formulation of SP_u (6), i.e.

$$- < \boldsymbol{n} \times \boldsymbol{h}_u|_{\Gamma_{t,p}^+}, \boldsymbol{a}'_{d,p} >_{\Gamma_{t,p}^+} = \left(\sigma_u \partial_u \boldsymbol{a}_u, \operatorname{grad} v_{s,u}\right)_{\Omega_{m,p^+}} + V_u \left(\sigma_u \operatorname{grad} \; v_{s,u}, \operatorname{grad} v_{s,u}\right)_{\Omega_{m,p^+}}. \quad (15)$$

At the discrete level, the first term on the right side of (15) is thus limited to a single layer of FEs on the side Ω_{m,p^+} touching $\Gamma_{t,p}^+$, because it occurs only the associated trace $\boldsymbol{n} \times \boldsymbol{a}'_{d,p}|_{\Gamma_{t,p}^+}$. Moreover, the source $\boldsymbol{a}_u$ obtained from the mesh of SP_u is then projected on the mesh of SP_p via a projection method [1] - [7].

Once achieved, the errors on the TS SP_p solution is then corrected by SP_k ($i \equiv k$) via the volume integrals $\left(\boldsymbol{h}_{s,k}, \operatorname{curl} \boldsymbol{a}'_k\right)_{\Omega_k}$ and $\left(\boldsymbol{j}_{s,k}, \boldsymbol{a}'_k\right)_{\Omega_k}$ in (10). The VSs $\boldsymbol{h}_{s,k}$ and $\boldsymbol{j}_{s,k}$ are given in (4a-b). In parallel with the VSs in (10), ICs recover the TS discontinuities to remove the TS representation via SSs opposed to previous TS ICs.

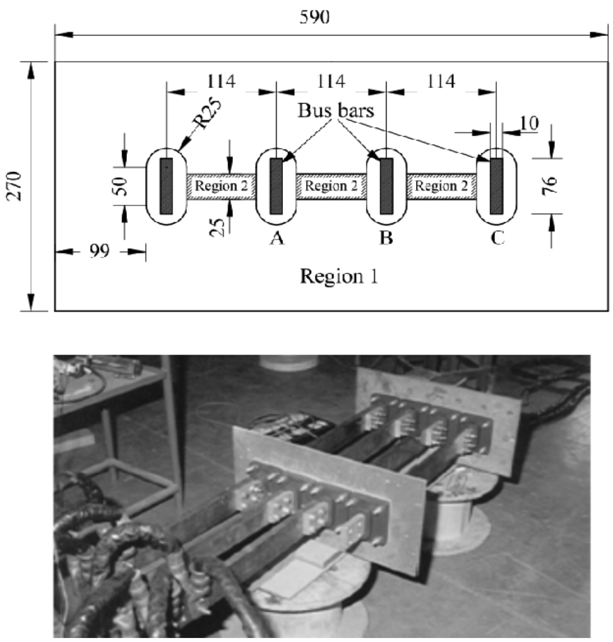

Figure 2. The geometry of the cover plate (*top*) and the experimental set-up (*bottom*) (all dimensions are in mm).

4. Application example

The illustrate and validate the SPM with global quantities, an actual test problem is a cover plate of a transformer with ratings from 500kVA upto 2000kVA. The geometry of the cover plate is shown in Figure 2 (*top*) and the experimental set - up developed by the authors in [8] is presented in Figure 2 (*bottom*).

The three bus bars carry adjustable balanced three – phase currents up to $I_a = I_{max} \sin(\omega t + 0)$, $I_b = I_{max} \sin\left(\omega t - \frac{2\pi}{3}\right)$ and $I_c = I_{max} \sin(\omega t + 2\pi/3)$. The distance between plates is 114mm and the plate dimensions are 270x590x6mm (Figure 2, *top*). The cover plate is made of two different regions and properties (magnetic and non-magnetic). The conductivities for the regions 1 and 2 are taken as σ_1 = 4.07 MS/m and σ_2 = 1.15 MS/m respectively and the relative permeabilties for the regions 1 and 2 are taken as $\mu_{r,1}$ = 300 and $\mu_{r,1}$ = 1, respectively.

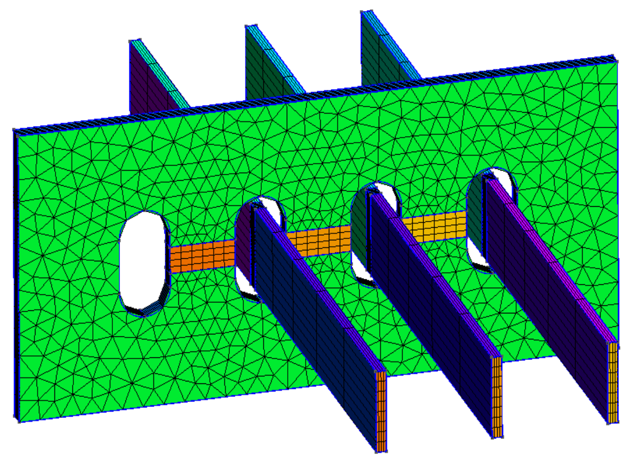

The problem herein is considered three SPs strategy. The field $\boldsymbol{b}_u$ computed in a simplified mesh in SP_u (with the bus bars considered as massive inductors) is shown in Figure 4 (*top*). A TS model SP_p (presenting the distribution of eddy current density $\boldsymbol{j}_p$ on the surface) is then added (Figure 4, *middle*). Finally, a SP_k replaces the TS model with volume correction covered by the actual plate and its neighborhood with an adequate refined mesh (Figure 4, *bottom*). By integrating the value of $\boldsymbol{j}_k$ (Figure 4, *bottom*) along the thickness of the cover plate and comparing the result to the TS solution $\boldsymbol{j}_p$, it is obtained. Thus, the TS inaccuracy on $\boldsymbol{j}_p$ can locally reach 47% (Fig. 4, *middle*) (d = 6 mm, f = 50Hz, skindepth $\delta = 2$ mm. The error on TS SP_p solution through the cover plate hole (Figure 5), and along the cover plate border and near the plate ends (Figure 6) can reach 37,5% and 50%, respectively. The Joule losses and the global currents flowing in the bus bars calculated for the mounting plate (with non-magnetic (region 2) inserted) by the SPM and the experimental method proposed by authors in [8], are given in Table 1. It can be shown that there is a very good agreement.

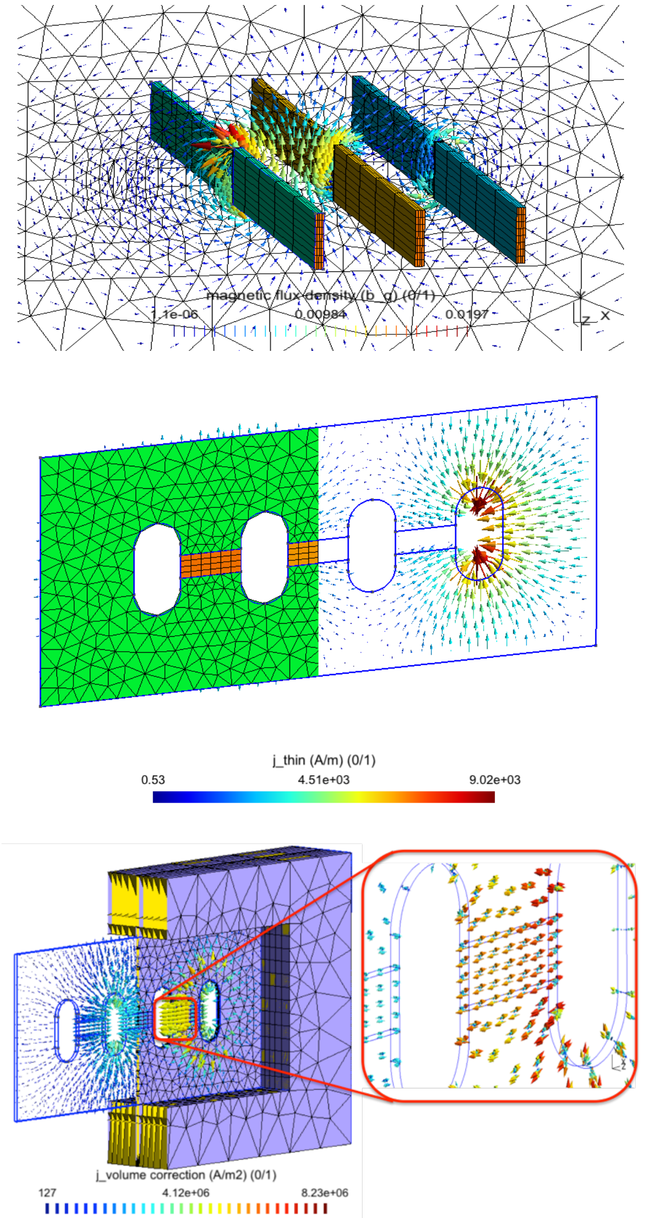

Figure 4. Magnetic flux density b_u (in a cut plane) generated by massive inductors (*top*), TS eddy current j_p (*middle*) and its volume correction j_k (*bottom*) (thickness d = 6mm, frequency f = 50Hz).

This test problem has helped to standardize the type and material of the cover plate for various current in transformers rated between 50kVA upto 2000kVA.

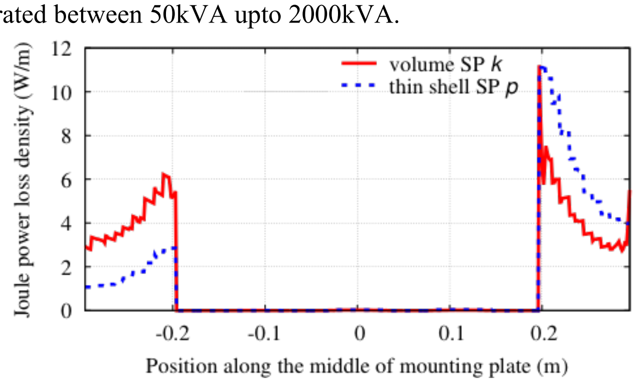

Figure 5. Joule power loss density for the TS and VS solution through the plate hole (I_{max} = 2kA).

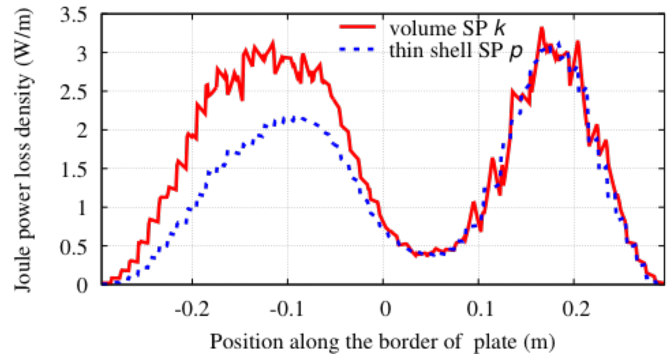

Current I (kA)	Frequency f (Hz)	Massive inductors		Measured values (W)
		Thin shell P_{thin} (W)	Volume P_{vol} (W)	
2000	50	51.8	62.58	65
2250	50	64.8	78.9	74
2500	50	80.8	97.5	95
2800	40	100.5	122.7	119

4. Conclusions

References

[2] Vuong Q. Dang, P. Dular, R.V. Sabariego, L. Krähenbühl, C. Geuzaine, "Subproblem approach for Thin Shell Dual Finite Element Formulations," IEEE Trans. Magn., vol. 48, no. 2, pp. 407–410, 2012.

[3] P. Dular, Vuong Q. Dang, R. V. Sabariego, L. Krähenbühl and C. Geuzaine, "Correction of thin shell finite element magnetic models via a subproblem method," IEEE Trans. Magn., Vol. 47, no. 5, pp. 158 –1161, 2011.

[4] Dang Quoc Vuong "A Subproblem Method for Accurate Thin Shell Models between Conducting and Non-Conducting Regions," The University of Da Nang Journal of Science and Technology, no 12 (109).2016.

[5] Tran Thanh Tuyen, Dang Quoc Vuong, Bui Duc Hung and Nguyen The Vinh "Computation of magnetic fields in thin shield magetic models via the Finite Element Method," The University of Da Nang Journal of Science and Technology, no 7 (104).2016.

[6] Dang Quoc Vuong "Modeling of Electromagnetic Systems by Coupling of Subproblems – Application to Thin Shell Finite Element Magnetic Models," PhD. Thesis (2013/06/21), University of Liege, Belgium, Faculty of Applied Sciences, June 2013.

[7] Dang Quoc Vuong, Bui Duc Hung and Khuong Van Hai "Using Dual Formulations for Correction of Thin Shell Magnetic Models by a Finite Element Subproblem Method," The University of Da Nang Journal of Science and Technology, no 6 (103).2016.

[8] S.V. Kulkarni, J.C. Olivares, R. Escarela-Prerez, V. K. Lakhiani and J. Turowski "Evaluation of Eddy Current Losses in the Cover Plates of Distribution Transformers," IEE Proc. Sci. Meas. Technol, Vol. 151, No. 5, September 2004.

[9] Dang Quoc Vuong "An iterative subproblem method for thin shell finite element magnetic models," The University of Da Nang Journal of Science and Technology, no 12 (121).2017.

[10] Tran Thanh Tuyen and Dang Quoc Vuong, "Using a Magnetic Vector Potential Formulation for Calculting Eddy Currents in Iron Cores of Transformer by A Finite Element Method," The University of Da Nang Journal of Science and Technology, no 3 (112), 2017 (Part I).

[11] S. Koruglu, P. Sergeant, R.V. Sabarieqo, Vuong. Q. Dang, M. De Wulf "Influence of contact resistance on shielding efficiency of shielding gutters for high-voltage cables," IET Electric Power Applications, Vol.5, No.9, (2011), pp. 715-720.

Advances in Science, Technology and Engineering Systems Journal
Vol. 4, No. 2, 45-64 (2019)
www.astesj.com
Special Issue on Recent Advances in Engineering Systems

ASTES Journal
ISSN: 2415-6698

W.A.S.T.E. R.E.D.U.C.E.: Waste Auditing Sensor Technology to Enhance the Reduction of Edible Discards in University Cafeterias & Eateries

Shiree Hughes*, Jiannan Zhai, Jason Hallstrom

Institute for Sensing and Embedded Network Systems Engineering, Florida Atlantic University, 33434, USA

ARTICLEINFO

Article history:
Received: 21 December, 2018
Accepted: 08 February, 2019
Online: 15 March, 2019

Keywords:
Internet of Things
Ambient displays
Food waste

ABSTRACT

Food waste disposal and food availability are both problems in the world today. The ability to monitor food waste is currently limited by the use of manual data collection and sparsity of monitoring. Using sensors to automate the process of measuring and collecting data on food waste would allow constant monitoring and provide a better dataset for analysis. This data can also be used to create ambient displays geared educate a target audience and produce behavioral changes. Student cafeterias serve as the focal point for data collection within this study, presenting both an abundance of data and unique challenges. We have created, deployed, and tested an autonomous, real-time system to collect data on food waste which includes an ambient display tailored to effect behavioral change in students.

1 Introduction

This paper is an extension of the work presented in *W.A.S.T.E. R.E.D.U.C.E.* [1].

In the U.S., approximately 40% of the food we cultivate goes to waste; yet, 1 in 6 people suffers from inconsistent access to food [2]. The cost of this waste is $165 billion per year, plus a large portion of methane emissions from U.S. landfills. Reducing the amount we waste by just 15% would generate enough food to feed approximately 25 million people, which would reduce food shortage problems by almost 50%[1]. It is imperative that we begin the task of educating society and encouraging changes in behavior.

Food waste studies are categorized based on where in the pipeline food is lost. Pre-consumer food waste is food that is discarded before reaching the end consumer; this includes food that is spoiled, dropped on the floor, or otherwise improperly handled. Post-consumer food waste consists of food that is prepared for and taken by a customer for consumption, but is eventually discarded; this would include leftover food on a customer's plate [2].

Educational institutions house future leaders; they are a desirable target to begin affecting change in food waste behavior. Campus cafeterias are typically the primary providers of meals to students, faculty, staff, and other visitors on college campuses across the nation. This makes them an ideal location for sampling post-consumer waste to get an accurate representation of food waste on a campus. As such, our first case study occurs in the main cafeteria on the Boca Raton campus of Florida Atlantic University (FAU), which services all students who have meal plans, plus drop-ins. Three different displays are introduced in the case study; each display conveys the amount of food wasted in real-time. A second case study was realized with one of the aforementioned displays in the cafeteria at A.D. Henderson University School, a laboratory school located on FAU's campus, which services elementary and middle school students. This location allows us to compare the effects of the display on different age ranges. We are also able to witness the effects of policies within different cafeterias that may aid (or hinder) food waste reduction.

Like many college cafeterias, FAU's dining hall is designed to be a la carte, allowing customers to pick and choose which sides and entrées they would like, including the choice of mixing and matching from the menu options. By allowing customers to choose their dishes, one might expect that it would reduce waste (e.g., a customer could request only the fries from a

*Shiree Hughes, 777 Glades Rd, Boca Raton, FL 33434, shughes2015@fau.edu
[1] This estimation was calculated using the current population of 324,121,843, as of July 31, 2016 [3].

https://dx.doi.org/10.25046/aj040207

burger-and-fries meal, which would eliminate wasting a burger). Yet, it is also possible that a customer may request a particular combination of dishes, be unsatisfied, and revisit the line for a more appetizing selection, leading the customer to waste the first plate. It is also possible that even if satisfied with the selection, the customer may still waste some of the food. U.S. portion sizes have been shown to be as much as 700% larger than the U.S. Department of Agriculture (USDA) recommendation, and as much as 263% larger than the Food and Drug Administration (FDA) recommendation [4]. While most research cites this as a contributing factor to obesity, it may also be a contributing factor to wastefulness. Information calling attention to this fact may caution students to ask for smaller portions.

Food waste audits are implemented in cafeterias of many institutions to generate information on how much food is wasted in their cafeterias for similar reasons to those noted above. However, most of these institutions only collect data for a short span of time, do not necessarily provide resolutions for reducing the waste that is found, and the process is not automated. An overview of food audits performed by institutions comparable to FAU can be found in Section 2. The purpose of WASTE REDUCE is to provide: (i) sustainable and on-going measurements of food waste; and (ii) visual cues designed to decrease the amount each customer wastes by encouraging more thoughtful choices.

The implementation of such a system has several challenges, related to both the implementation of the network and the visual cues used to evoke behavioral change. Cafeterias are dynamic environments and thus require a network that is able to withstand and/or adapt to sudden changes. Network reliability is a critical component to keeping the system operational and requires the network to adapt to communication issues such as interference or obstruction. To truly be an autonomous system, we must also ensure cafeteria employees are not required to change their behavior to use the system. This requires a robust design that withstands mishandling and minor leaks from garbage bags. The sensors must be power efficient, both for ease of use and for reliability. The devices within the network must also be compact enough to fit within a trash can. Most importantly, the sensors must be able to provide accurate, real-time data to create real-time feedback for the visual cues. The visual cues, which are implemented as a series of displays, must be seen by the target audience and the audience must be able to connect the information presented with their own behavior for change to take place. In addition, a display must resonate with the target audience to evoke change. After addressing each of these challenges, we designed and evaluated the use of three different displays with the system. Two of these displays were proven to evoke behavioral change in the target audience and reduced the amount of waste generated.

We present the design and implementation of **W**aste **A**uditing **S**ensor **T**echnology to **E**nhance the **R**eduction of **E**dible **D**iscards in **U**niversity **C**afeterias & **E**ateries (WASTE REDUCE), an automated method of measuring food waste and providing real-time feedback. We evaluate the system through a preliminary deployment and case studies. We also present the design and implementation of three ambient displays to provide visual cues to a targeted audience based on the real-time data provided through WASTE REDUCE. We evaluate the effectiveness of these displays on behavioral change through two case studies. [1].

Section 2 presents background and related work. Section 3 details our approach, including the hardware components, software implementation, and challenges for each component. Section 4 presents the results and evaluation of the case studies used to assess the effectiveness of the ambient display component of WASTE REDUCE and the associated displays. Section 5 concludes the work.

2 Background and Related Work

To better understand the design and implementation of each focus, we must first explore the background and related work concerning each area.

2.1 Campus Food Waste Auditing

Food waste is a major concern for society and many university cafeterias are engaging the issue through food waste audits. Food waste audits allow the cafeteria to collect sample data on how much food is being wasted in their dining halls and may or may not include campaigns to reduce this waste. Currently, these food waste audits are implemented manually. Highlighted below are methods and results from audits conducted by several universities around the country.

The University of California at Davis (UC-Davis) has an enrollment of approximately 35,000 students [5]. Using quarterly waste audits, UC-Davis saw a 30% decrease in food waste from 2012 to 2015. In the Fall of 2009, UC-Davis cafeterias saw an average of 3.6 oz (102.06 g) of waste per guest; this dropped to 1.6 oz (45.36 g) per guest by Spring of 2015. The primary goal of their food waste program is to have zero waste by 2020. A food waste audit is conducted in each of the university's cafeterias during lunch hours over 3 consecutive days each quarter. Part of the audit includes a visual display of the amount of food wasted, which is created by asking students to divide their waste into edible (e.g., leftover breadsticks), inedible (e.g., banana peels), and other (e.g., napkins). The edible food is then placed on display for guests to view and discuss. Other solutions implemented by UC-Davis include allowing students to ask for smaller portions, distributing samples for taste-testing, and donating unused food through the Food Recovery Network [6, 7]. (FAU also uses the Food Recovery Network to donate leftover food.) Since these audits only occur briefly during the semester and during one meal time, they can only provide a snapshot of the amount of waste generated. This snapshot may not reflect the average amount of daily waste generated.

Georgia Institute of Technology (GT) has an enrollment of approximately 25,000 [8]. GT uses the LeanPath tracking system in their cafeteria to monitor and inform staff about food waste [9]. LeanPath is a commercial system that allows kitchen staff to record information on waste, such as food type, weight, and reason for disposal, each time something is thrown away. This system measures pre-consumer food waste, and provides detailed graphs and reports, estimates on cost, and email alerts for disposed amounts valued over a set threshold [10]. While the tool increased awareness among staff members, LeanPath requires extra effort from each staff member. To generate a report, LeanPath requires a staff member to weigh the food they are throwing away and provide additional information, such as his or her name, the type of food (e.g., dairy), what the food is (e.g., yogurt), reason for disposal (e.g., expired), and what type of container is being disposed (e.g., carton). This method has four main drawbacks: (i) it is an extra burden for staff who may have their hands occupied with food preparation; (ii) staff can easily forget or neglect to record items; (iii) it introduces a higher likelihood of human error; and (iv) it does not include post-consumer waste.

Michigan State University (MSU) has an enrollment of approximately 50,000 students [11]. MSU's research on food waste focused on cafeteria food waste in addition to off-campus food waste. Researchers discovered that off-campus, the average amount of food wasted was approximately 1.54 lbs (0.7 kg) per week for a single person. Using the number of weeks students are in school, compounded by the number of students living off-campus, researchers scaled their findings to estimate a total of 3,669,120 lbs (1,664,284.8 kg) of food waste per year from off-campus housing. In addition, MSU found that approximately 14,131 lbs (6,409.7 kg) of food was wasted per day in their cafeterias, with over 9,500 lbs (4,309.1 kg) of this weight associated with post-consumer waste [12]. Solutions to help reduce waste were printed along with these findings in a brochure for students. Recommendations were also given to the students on how to handle waste, including information on composting, recycling, and local produce. In addition, MSU created a food waste program that implements composting, and a student organic farm to help students handle food waste [13].

Florida International University (FIU) serves approximately 45,000 students [14]. FIU conducted a general waste audit and found that on average, 25.6% of their waste, and 4.5% of their recyclables were from food waste. For the audit, researchers collected samples of general waste across campus, sorting it by type and location. Food waste was one of the top three contributors to waste in each of the locations, and the primary contributor in housing and auxiliary areas. However, only one of their fourteen proposed solutions to waste reduction focused on food waste [14]. There was no clear campaign defined in the report to inform students of the audit results or to reduce waste generated.

The University of Miami (UM) has an enrollment of approximately 17,000 students [15]. Like FAU, UM uses tray-less dining halls to reduce the amount of food students take to the table. UM also reduced the amount of solid waste it generates by using a bio-digester to convert pre-consumer food waste to liquid. While UM does have a composting program on its campus, it is not integrated with their food waste management program [16]. UM reports the total processed waste generated by the campus as part of their Green U website, but they do not specifically report food waste [17].

2.2 Data Analysis and Feedback

Extensive research has been conducted in data presentation and visualization. Behavioral change cannot be realized without effectively conveying data to the target audience–in this case, cafeteria customers. Effectively conveying data requires guarding against habituation, presenting the data in compliance with known human-computer interaction (HCI) standards, and creating a lasting impression that encourages retainment of the information.

Habituation is the "diminishing of an innate response to a frequently repeated stimulus" [18]. Habituation is frequently used in post traumatic stress recovery to desensitize patients to images or thoughts that trigger their discomfort [19]. Repetitive exposure to images trains the brain to normalize the discomfort and anxiety provoked by the image. This is the opposite of what is desired for this project. Cafeteria customers should get a renewed sense of urgency each time they view the feedback–large quantities of food waste should not be normalized. Varied presentations of data will be used to avoid habituation.

HCI research has generated a wealth of knowledge pertaining to engaging customers with information displayed via a monitor. Adhering to these principles is crucial in designing a display that is successful in capturing cafeteria customers' attention. Lin et al. [20] outline eight criteria that should be taken into account for optimal engagement: stimulus-response compatibility, consistency, flexibility, learnability, minimal action, minimal memory load, perceptual limitation, and user guidance. Stimulus-response *compatibility* occurs when users have faster and more accurate responses for a set of attributes because the attributes naturally correspond. An example would be using red to highlight an error in the system versus using green; a user would naturally attribute red to a problem, whereas green would naturally lead the user to assume that everything was fine. *Consistency*, both within the system and across different systems improves usability. This goes hand-in-hand with compatibility; the use of consistency creates a natural correspondence among certain symbols, icons, layouts, etc. *Flexibility* enables a system to adapt to users' needs. This can range from allowing a user to customize the interface (e.g., changing the color scheme) to adapting to unique environments automatically (e.g., website designs that work for PCs, tablets, and mobile phones). *Learnability* refers to the ease with which a person can learn to navigate an interface. The easier it is for a person to understand the format, the greater the user's satisfaction. *Minimal action* echoes the principle of learnability in the sense that users prefer interfaces that are straightforward and require minimal effort to complete a desired task. *Minimal memory load* addresses the working memory load required of the user to use the interface. Users perform better under minimal working memory loads. *Perceptual limitation* addresses the short-comings of human perception, such as color resolution. Designs should group like elements and use spatial and color resolution to ensure all details can be understood. *User guidance* refers to implementing cues and documentation, which gives the user information on how to use the system. Implemented correctly, user guidance aids with learnabiltiy and enabling a minimal memory load.

Creating a lasting impression in customers requires the information to be presented in a manner that achieves impact. Heath and Heath [21] outline six principles meant to enhance the "stickiness" of an idea. They define a "sticky" idea as one that remains with people over time. The six principles, which they refer to as SUCCES, are simplicity, unexpectedness, concreteness, credibility, emotions, and stories. *Simple* ideas are easier to remember than complex ideas; the authors argue that to make an idea stick in someone's mind, you have to reveal the core idea in simple terms. *Unexpected* information and surprises catch people off guard, which sparks curiosity and causes them to think about what they are being told. *Concreteness* refers to presenting clear ideas. Information that is abstract to the point of ambiguity is not likely to achieve impact. *Credibility* is needed to convince an audience that the information presented is accurate and reliable. *Emotions* have a way of controlling people when logic fails–in many cases invoking strong feelings of sympathy, regret, or anger. Heath and Heath give the example of persuading people to donate to specific people who are in need, which has a higher success rate than persuading people to donate to an anonymous group of people in need. *Stories* provide a plot and direction, which is often easier to remember than bulleted lists. Heath and Heath concede that each idea might not lend itself to every principle, but suggest that employing a number of these ideas will improve impact. We employ these techniques in the design of each display for WASTE REDUCE to ensure the magnitude of food wasted "sticks" in consumers minds to prompt a change in their behavior.

Stasko et al. [22] explore the technique of conveying information through art. The authors focus on ambient, peripheral displays. The displays are designed to smoothly adapt based on the underlying information being presented, while maintaining an aesthetically appealing appearance. Non-critical information, such as information on food waste, is usually the driving source of such displays. Critical information, such as a medical alert, is not ideal for these displays because the goal is to produce an informative, yet "calm," tool. The aim is to reduce cognitive disruptions so that seeking out the information does not require the user to completely shift his or her train of thought. Maintaining the calmness of the display allows the display to move from a user's periphery to focal attention, and then back to the periphery. Ambient displays began with the emergence of Dangling String [23], which conveyed information on how busy a network was by causing a dangling string to twitch each time bits of data were transmitted across the network.

Ariely [24] explores human behavior, specifically that of customers, in relation to information control. Information control refers to the ability of a user to control what information they receive. Research shows that there are both advantages and disadvantages to restricting users' control over the information presented. A key advantage is that users are able to choose topics that interest them the most. The key disadvantage is that this increases cognitive burden since users must configure what information is presented. In Ariely's studies, users who were able to choose the way in which information was presented learned the information better. Results suggest an improvement in users' decision making skills when information control is used.

2.3 Wireless Sensor Networks

Wireless sensor networks are formed by several sensors connected via wireless communication protocols [25, 26]. These networks allow specific information to be collected and transmitted to a central location for monitoring or analysis. There are a wide variety of sensors available for use, each able to provide specific information about an environment. A representative example of a sensor is a load cell, which can be used to determine the weight of an object. Such sensors can be used independently or in conjunction with other sensors to determine pertinent information about the environment in which the sensors are deployed (such as the weight of objects placed in a container, or water quality in a river). When connected to a wireless communication device, the information can be transmitted within the network. Networks usually have a *base station*, which receives the data transmitted by the sensors in the network, and then stores the information in a central location, such as a server. Users can then access the data without needing to physically interact with the environment. This is ideal for monitoring information in unpleasant locations, such as a garbage can, and for long-term monitoring, where it is infeasible for a person to be continually present to collect the data.

The sensors and radio are connected and controlled by a microcontroller. The microcontroller serves as a centralized controller and uses software modules, commonly known as drivers, to control the sensors, radio, and other peripherals. The overall device is typically small, embedded in the environment being monitored, and battery powered. As such, power and memory are typically limited [27]. To maximize the longevity of the battery, software must be written to take advantage of low-power and sleep modes for sensors and micro-controllers. To satisfy the memory constraints software must also be concise. A few example devices that could exist in a sensor network include the RaspberryPi [28], Aurdino [29], and BeagleBone Black [30].

Connectivity is a primary concern with sensor networks. Data is typically transmitted through small wireless packets. Packets contain additional information for the destination device, such as the source of the data, and a checksum to verify that the message has not been corrupted. Communication protocols must be robust enough to handle interference and failures within a network. The quality of links within the network, which is a predictor of system performance, is often analyzed to debug or enhance communication within a network. Two common methods of defining network quality are Received Signal Strength Indication (RSSI) [31] and packet reception rate. RSSI provides a measurement of the strength of a received transmission. Packet reception rate conveys the percentage of packets successfully transmitted with respect to the total number of packets transmitted. The higher the percentage, the better the link quality. We use RSSI and packet reception rate to examine the quality of the links within WASTE REDUCE.

2.4 Data-Driven Visualization

WASTE REDUCE is concerned with affecting behavioral change through dynamic displays, driven by automated data collection.

Current methods for collecting food waste data and presenting information for social norming campaigns, as discussed previously, involve manual collection of data and the use of static advertising material. Manual collection of data not only introduces human error—what if someone forgets to weigh the waste before emptying it?—but is difficult to sustain, as witnessed in the audits discussed previously. Static advertising doesn't account for changes in the data and risks habituation. Data collected over a short interval of time may or may not be indicative of normal behavior, and since data is only collected during the campaign, it is difficult to assess if the campaign was successful in raising awareness or reducing waste. This also makes it difficult to provide students with feedback about their progress in reducing waste. Campaigns are left with the option of either disseminating the same information until the next audit, which is likely to result in habituation, or place the responsibility of continuing the message on the students, who would need to remember and gauge their own behavior.

The cognitive burden of a target audience can be managed by presenting data to an audience in an appealing and informative manner. Since data-driven visualizations are controlled by data inputs, the display is more readily updated to reflect data changes or needs of the target audience. Data-driven displays can be used to analyze real-time data and change on the fly.

Plaue et al. [32] explore the efficacy of presenting information through peripheral displays through *InfoCanvas*. InfoCanvas is a form of information art in which the art is manipulated to communicate information. The authors chose 10 specific pieces of information, generally found on a home page, to present in a scene depicted by InfoCanvas. Each piece of information was mapped to an image within the picture, and the image changed based upon the information. For example, airfare prices were represented by a kite flying in the sky; when the kite is closer to the horizon, it signifies a low price, and when the kite is high in the sky, it signifies a higher price. Plaue et al. [32] compare users' ability to remember the information using the abstract InfoCanvas versus a text-only display and a typical web interface (containing a mix of text and graphics). After allowing users to view a display for 8 seconds, users were given a recall test to assess how well the information was retained. For 7 of the 10 elements of information, InfoCanvas had the highest rate of recall. Users were also given a survey to rank the 3 displays based on ease of information recall, effectiveness of data presented, and visual appeal. Users rated InfoCanvas highest for both ease of information recall and visual appeal. Some users expressed a preference for the web portal display citing it to be "more professional," "logical and precise," while others expressed a preference for InfoCanvas. Those who preferred the web portal and those who preferred InfoCanvas mentioned the need for adaptation to the InfoCanvas display.

Dahley et al. [33] compare the use of ambient displays to the cues we pick up in nature. Drawing inspiration from nature, the authors created *Water Lamp* and *Pinwheels*. Water Lamp is inspired by the creation of ripples from raindrops. Using data to simulate raindrops, computer-controlled solenoids are used to create ripples in a tray filled with water. A light shines from beneath the tray, displaying the ripple effect through light and shadow on the ceiling above. Water Lamp can be driven from multiple sources of information, enabling the display to behave as an indicator of the weather outside or a white-noise effect. Pinwheels was created to convey information on air flow. Air flow data is represented using pulse width modulation to control a motor, which spins a pinwheel at a speed reflective of air flow. Both devices function as a display and a physical reminder of the associated data. Identifying a physical representation that would convey information on food waste is a difficult task and not likely to be intuitive to our audience; we limit our display to the virtual world.

Mankoff et al. [34] create BusMobile and Daylight Display to evaluate the effectiveness of ambient displays. Both displays were created to provide information to college students in a window-less lab. The displays were created after surveying the students on which information was of most interest to them. BusMobile uses information from the published local bus schedules and the current time to inform students how near or far a bus is to its scheduled stop. Each bus is represented by a "bus token," which moves to the top of the display as it approaches the bus stop. Daylight Display was designed to inform students about outdoor lighting. A lamp was modified to brighten and dim according to the expected amount of light outside for the current time of day. Both displays use static data and will not be accurate if there is a deviation from the norm– e.g., a bus stuck in traffic, or a cloudy day when it becomes dark earlier than expected. Surveys from students revealed the Daylight Display was less effective than the BusMobile; many students assumed the lamp was broken and did not notice information being conveyed.

Heiner [35] et al. describe Information Percolator, a display created from tubes filled with water. Bubbles in the water are produced to behave as pixels, allowing the creation of an image across the tubes. One application for the device is a clock application. The clock application is designed to sync with a user's calendar and change the display to notify the user of an event. Information Percolator can also display specific information, such as the availability of a co-worker or current stock market trends. Heiner [35] et al. present a new and interesting way to convey information; however, the effectiveness of this method was not explored.

Snapshot [36] was developed to introduce data-driven visualization techniques to the game of hockey. Snapshot marries current hockey analytics with visualization and is designed to give both teams and fans a clearer picture of patterns within the game. In hockey, teams may be concerned with where on the court shots are most frequently taken by their opponent. To visualize this data, Snapshot uses a monochromatic heat map of the rink, where variations in color are determined by opacity. The opacity of a particular location is set based on the frequency of shots in the region with respect to the number of shots taken overall and the size of the region. Snapshot also provides visualization of shot distance using a radial heat map. Shots are divided into bins based on distance and mapped to rings of distance around the goal; each ring is colored based on the number of shots that fall in that ring. To determine the effectiveness of such a technique, Snapshot was evaluated by 3 professional hockey analysts. Each analyst discovered something unique while using the tool. The first analyst was able to pick up on patterns in multiple rinks that were previously thought to exist only in a particular rink. The second analyst found patterns related to how teams shoot and score at home versus away. The final analyst used Snapshot to investigate "sweet spots" in the rink and found that his hypothesis of shooting from a goalie's weak side did not yield more goals. All 3 analysts expressed interest in using the tool beyond the evaluation period to dig deeper into their theories. While Snapshot is not a real-time tool and is specific to hockey, it accomplishes our basic goal of conveying accurate data in a manner that stimulates interest.

Current solutions do not address the challenges associated with creating a network to monitor food waste data, nor do current ambient display techniques attempt to work in conjunction with a wireless sensor network to change behavior. The focus of ambient display research is on informing an audience rather than affecting the behavior of the audience. We present novel approaches to specific problems which were previously unaddressed.

3 Approach

We accomplish automated collection and analysis of food waste data through an accurate, robust, and efficient wireless sensor network. The method used to determine the amount of food wasted must be able to accurately detect small changes in weight for the system to provide a complete picture of waste accumulation over time. The system must be robust enough to maintain functionality despite unexpected events, such as mishandling of trash cans or network interference. Efficiency is necessary to minimize power consumption which will extend the lifetime of the battery and maintain functionality over long time periods. The device must also be compact enough to fit inside the trash cans used by the cafeteria.

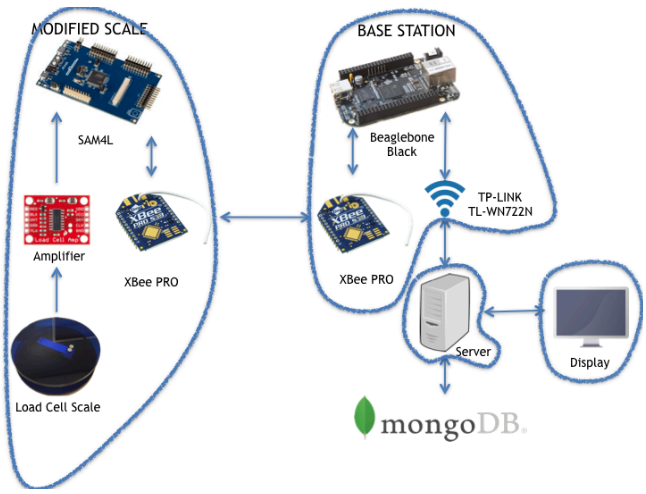

Figure 1: Food Waste Monitoring Architecture

3.1 Hardware

The system architecture, shown in Figure 1, consists of four main components: a modified scale (located within each trash can), a base station, a back-end server, and a front-end display.

3.1.1 Modified Scale

The modified scale was created using a 10kg wide-bar load cell [37], an HX711 [38] amplifier, an XBee-PRO 900HP S3B [39] radio, and a SAM4L Xplained Pro [40] board. The SAM4L Xplained Pro is a prototyping board for Atmel's SAM4L Cortex™-M4 based microcontroller. The load cell translates force exerted on the scale to an electrical signal, which is amplified by the HX711. This raw value is transmitted by the

XBee radio to a base station. A PCB board was designed for the XBee-PRO and HX711 to plug into the SAM4L Xplained Pro extension header. This enabled a compact, 4” x 5” design conducive to the limited space within each trash can.

3.1.2 Base Station

The base station is driven by a BeagleBone Black [30], which is connected to an XBee-PRO 900HP S3B [39] radio and a TL-WN722N 150 Mbps high-gain WiFi dongle [41]. A Java program is used to receive packets transmitted from the radios on each device, determine which device sent each packet, convert the payload of the packet to pounds, and transmit the human-readable information to a server.

3.1.3 Server

Collected data is stored in MongoDB [42] so that it may be queried for later use. Since the server is protected by a firewall and cannot be accessed remotely, we adopted a RESTful design. The RESTful design allows access to the data through text strings which can be passed from the server to the front-end. We developed a server-side function, called using HTTP-GET requests. The function queries MongoDB based on parameters supplied by the front-end and returns a JSON string containing the data.

3.1.4 Design Challenges

Detailed discussion of design challenges discovered and overcome during the initial deployment can be found in the original publication [43]. These challenges included both situations in our control, such as the antenna strength of the radios or reliability of the communication protocol, and out of our control, such as the reliability of the WiFi network in the deployment location or how the devices are handled.

3.2 Software

3.2.1 Modified Scale, SAM4L Implementation

Figure 2 illustrates the flow for the implementation of the modified scale. First, the SAM4L and all connected sensors are initialized. After initialization, the same series of steps are repeated for each cycle. The microcontroller and radio are brought to their active states. A sample is then taken. Once the sample is taken, local time is attached to the sample. Next, a packet containing the sample and necessary timestamp information is transmitted to the base station. Local time on the scale at the time of sampling and at the time of transmission is kept; therefore, if the network is experiencing interference, and it takes multiple retries to successfully transmit the data, delays that occurred between the time of sampling and the successful transmission to the base station can be accounted for. The SAM4L marks local time via an asynchronous timer, driven by a 32.767kHz crystal. The timer updates a counter which defines the local time in number of ticks since boot. This information is used to convert from local time to wall clock time at the base station, achieving time synchronization. If no acknowledgment is received from the base station, it is assumed the transmission was unsuccessful, and the sample is placed in a queue to be retransmitted during the next cycle. If an acknowledgment is received, the transmission is considered successful and the devices are put into sleep mode for 60 seconds before restarting the cycle. Placing the radio and microcontroller to sleep between cycles reduces power consumption. This is crucial since it is undesirable to change the batteries frequently. An analysis of power consumption can be found in Section 3.3.

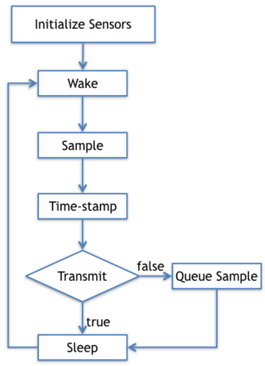

Figure 2: Modified Scale Implementation (SAM4L)

3.2.2 BeagleBone Implementation

Figure 3 depicts the flow of execution for the base station. First, the BeagleBone Black and XBee radio are initialized. Once initialized, the radio listens for packets from the modified scale. Once a packet is received, the local time from the modified scale is converted to wall clock time. Next, the base station transmits an acknowledgment to the scale to indicate receipt of the data. The scale then converts the sample from raw data to pounds. The final sample is then transmitted to the server over WiFi. If the sample cannot be successfully transmitted to the server, it is placed in a queue and the transmission is retried at a later time. After attempting the transmission, the radio once again listens for packets.

Time Conversion. Figure 4 depicts the process of timestamp conversion. The SAM4L marks local time using a counter driven by a 32.767kHz oscillator crystal. After a prescaler is applied, the effective increment of the clock is 1 millisecond. The counter is updated each time there is an overflow. From this, we know each counter increment represents 32,767 milliseconds. `transmissionTime` is approximately equivalent to the wall clock time at reception. Given this information, we can identify the local time at which the sample was taken (the difference between `transmissionTime` and `sampleTime`) and convert this into milliseconds elapsed. We can then add those milliseconds to the current wall clock time to estimate the wall clock equivalent of the sample time.

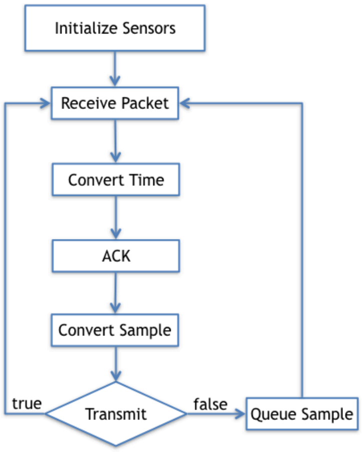

Figure 3: BeagleBone Black Implementation

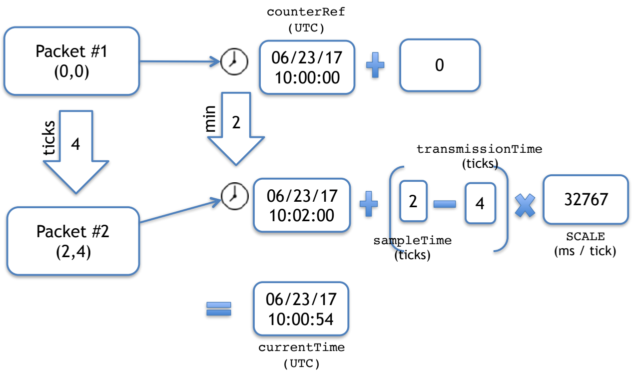

Figure 4: Time Conversion Flowchart

Raw Data Conversion. Equation 1 is used to convert raw data to pounds. The `offset` parameter is calculated by taking the average over 10 readings while nothing is placed on the scale. `scale` is calculated just prior to deployment using the calculated offset and an object of known weight. Averages over 10 readings are used[2], and the process is repeated with multiple objects of known weight to ensure the accuracy of the `scale` parameter.

$$knownWeight = (raw - offset)/scale \tag{1}$$

Tables 1 and 2 detail accuracy for each deployment. Accuracy of the scale varied negligibly between deployments due to differences in hardware mounting. Table 1 shows the accuracy, in pounds, for the case study carried out at Atlantic Dining Hall (Case Study #1). Table 2 shows the accuracy, in pounds, for the case study carried out at A.D. Henderson University School (Case Study #2). The objects of known weight were a power drill and a cell phone. Different cell phones were used between the pilots at the two schools. For the objects of known weight, and the case when the scale is empty, the tables show the average weight measured by the scale in each trash can followed by percent error. Percent error is calculated using Equation 2. As shown by the percent error, the scale is more accurate for heavier objects. This means we can be more confident as the amount of waste increases. We take this into consideration when identifying when the trash can was emptied; this is discussed in Section 3.4.1.

$$percent\_error = (measured - actual)/actual \tag{2}$$

3.3 Power Consumption

Power consumption is an important factor in most wireless sensor networks and especially in this network. Replacing the scale's battery requires removing the top plate of the scale to gain access to the enclosure, all of which are located in the bottom of the trash can. We seek to maximize the lifetime of the battery by taking advantage of the sleep features of the XBee and SAM4L to minimize power consumption and limit inconvenience.

Figure 5 illustrates power consumption over time (x-axis) in mA (y-axis) for 15 cycles. We observe that power consumption is generally consistent across cycles. There are three observable states within each cycle: sleep, sample, and transmit. The lowest power consumption occurs at approximately 5mA, while both the SAM4L and XBee are in their respective sleep modes. Next, the SAM4L wakes and takes a sample. This appears as a defined step and shows a consumption of approximately 21mA. At the end of the cycle, the radio is awakened, and the sample is transmitted. Power consumption is not consistent during this state in the cycle, but averages 107mA.

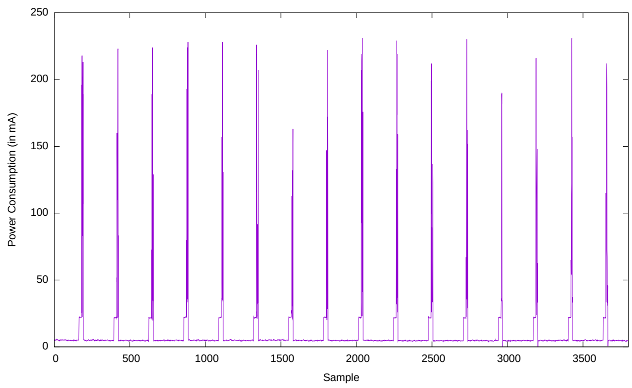

Figure 5: Power Consumption (in mA)

The average power consumption for each state is shown for 10 cycles in Figure 6. The x-axis shows the cycle, and the y-axis shows power consumption in mA. This confirms the variability of power consumed during transmission. We can estimate the average power consumption during each cycle by scaling the average power consumption of each state according to its duration and summing the values. In our case, the cycle is broken down as follows: 86% sleep, 8% sampling, and 6% transmission. Figure 7 shows the average power consumption for the 10 cycles. Again, the x-axis shows

[2] Each sample is based on 100 readings from the load cell as a result of the oversampling method discussed previously.

Table 1: Atlantic Dining Hall – Scale Accuracy (in lbs)

	Empty		Power Drill		Cell Phone	
	Measured	Error	Measured	Error	Measured	Error
Actual Weight	0.000	-	3.200	-	0.284	-
Trash Can #1	0.048	NaN	3.220	0.625%	0.345	21.479%
Trash Can #2	0.000	0.000%	3.200	0.000%	0.293	3.000%

Table 2: A.D. Henderson University School – Scale Accuracy (in lbs)

	Empty		Power Drill		Cell Phone	
	Measured	Error	Measured	Error	Measured	Error
Actual Weight	0.000	-	3.200	-	0.304	-
Trash Can #1	0.042	NaN	3.200	0.000%	0.359	18.092%
Trash Can #2	0.016	0.000%	3.199	-0.031%	0.336	10.526%

the cycle, and the y-axis shows power consumption in mA. On average, the current draw is 12mA. Using a 6000mAh battery the scale can be powered continuously for just under a month.

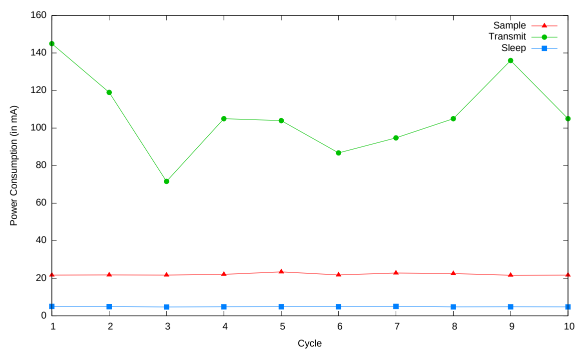

Figure 6: Average Power Consumption Per State

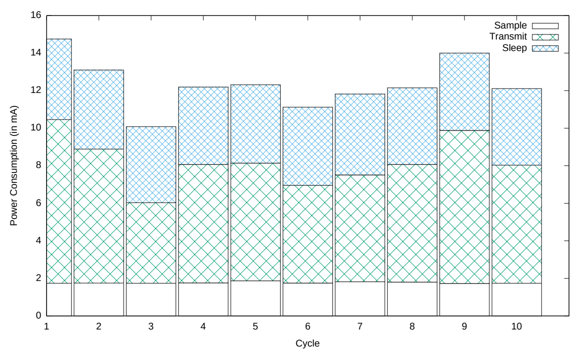

Figure 7: Power Consumption per Cycle by Active State

3.4 Front-End Display

Three front-end displays were designed to test whether ambient displays could be used to change behavior. The front-end displays are JavaScript-based web applications. Graphs were created using the open source Data-Driven Documents (D3) library [44]. The application fetches information from the server using an HTTP-GET request and uses the data to create displays.

3.4.1 Calculation of Total Waste

Figure 8 illustrates two ways to present the waste measured over time. The first is used to analyze the time periods when the most waste is generated and the second is shown in the display to inform of overall waste. The x-axis shows the time of day the sample was taken, and the y-axis shows the waste, in pounds. Since the modified scale reports the weight of waste *currently* in the trash can (Figure 8(a)), a method has to be devised to approximate the *total* waste over time (Figure 8(b)). Total waste should be the sum of the local maxima, which should occur just before the waste is emptied. However, there are two scenarios that must be taken into account: (i) the scale may never register as empty, and (ii) there may be a spike in the data from someone pressing down on the trash bag or bumping the trash can.

Based on the accuracy of the scale, discussed in Section 3.2.2, an *empty* scale should be defined as a measurement below 0.05 lbs. However, during peak hours, it was observed that students may crowd around the waste area and empty waste in the trash can immediately after it has been emptied. When this occurs, the scale never registers a zero value. To account for this, when calculating the total waste, we check if the current sample is significantly less than the previous sample to identify if the waste has been emptied. *Significantly less* is defined as a difference of 10 lbs or more based on observations from the preliminary data.

Figure 8(a) illustrates the second scenario involving an anomalous reading, just before 12:00 in both trash cans. Since this occurs in both cans, the anomaly is likely from someone lifting the trash bag to tie it just before emptying the waste. (If pressure were applied to cause the spike, the corresponding area would have a concave shape.) In this case, the maximum reading before the empty event is added to the total. (In the opposite case, we take the value after the local maxima.) When the algorithm checks if the current sample is less than the previous sample, it checks for this scenario as well. Between each empty event, we save the maximum observed sampled. This value is compared to the current sample. If the current sample is more than 1 pound less than the maximum observed sample, but

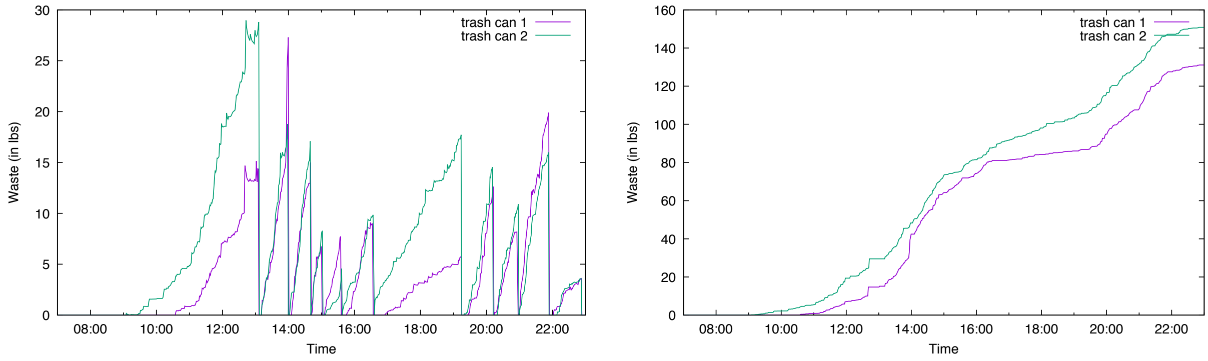

(a) Measured Weight

(b) Accumulated Waste

Figure 8: Finding the Total Waste

not more than 10 lbs, the current sample is considered the real maximum. The previously observed maximum is then subtracted from the total waste and the current sample is added. The maximum observed sample is then set to the current sample. This method accommodates cases like the one shown in Figure 8(a), since the waste settles at its original weight before being emptied. The calculated accumulated waste for each trash can using this method is shown in Figure 8(b).

3.4.2 Display Setup

Figure 9 show the display setup for each location. Figure 9(a) [43] illustrates the setup inside Atlantic Dining Hall. This cafeteria has a single point of entry for students. Our display is mounted right as students enter, beside the pay stations. The display was placed here for ease of installation and maximum visibility. The optimal location for the display would likely be near the trash cans. This would allow students to make a direct connection to the information presented and the waste filling up the cans. The trash cans are not located near a power supply; therefore, it wasn't feasible to place a monitor there. A battery powered tablet would have been the only option for that location. However, the tablet would be too small to capture attention and would require recharging each day. Excluding the space directly beside the trash cans, the entry point near the pay station has the maximum visibility for customers. Everyone who enters the cafeteria must pass this location, and many are forced to linger in the vicinity as they wait in line to pay, providing more time to view the display. The displays are updated every minute so students can view the increase in waste in real-time.

The display for Case Study #2, at A.D. Henderson University School, was closer to the trash cans, as shown in Figure 9(b). However, we were still unable to place the display directly behind the cans as desired. Instead, the display was located in the front of the room, directly opposite to the trash cans.

A total of three displays are evaluated in Case Study #1. There are several reasons to test multiple displays. Each display focuses on one concept. Display 1 focuses on simplicity, Display 2 focuses on context, and Display 3 focuses on humanizing the issue. The variety of displays allows us to investigate if one method has the more impact than another. Ideally, if WASTE REDUCE were a permanent fixture in a cafeteria, multiple displays would be used in randomized rotation to avoid habituation.

All three displays use the same basic layout. The top of the screen displays the date and location. The left side of the display contains an image, which is altered by the data provided by WASTE REDUCE. The right side of the display consists of 3 graphs: (i) a gauge comparing the current day's total food waste accumulation in comparison to the previous week's maximum total food waste accumulation, (ii) a gauge comparing the current day's total food waste accumulation in comparison to the previous week's minimum total food waste accumulation, and (iii) a line graph showing accumulation over time for that day. This allows students to compare their progress in reducing waste. The gauges were updated for each display based on feedback from cafeteria employees about student confusion on what information the gauges represented and conveyed. The goal of conveying the max and min waste values for the week remains the same throughout each display. These differences are discussed in detail below. Below the two gauges is a line graph of time versus total weight in pounds. The total amount of waste, starting at breakfast, seen by each trash can is plotted on the graph; this graph is present for all displays.

For each display, we adapted 4 principles from Heath and Heath's [21] SUCCES method. Table 3 identifies which principles were applied to each display.

Table 3: Application of SUCCES Principles

	Display 1	Display 2	Display 3
Simple	✓	✓	
Unexpected	✓	✓	
Concrete	✓		✓
Credible	✓	✓	✓
Emotional		✓	✓
Stories			✓

(a) Atlantic Dining Hall (b) A.D. Henderson University School

Figure 9: Displays

3.4.3 Display 1

An example of the first display is shown in Figure 10 [43]. This display is the most straight-forward. It was designed to illustrate the message of food waste reduction in the simplest terms. Since reducing the cognitive load is one of the goals of an ambient display, and there was no opportunity to introduce or explain the display to the target audience, a no-frills approach was deemed best for the initial display.

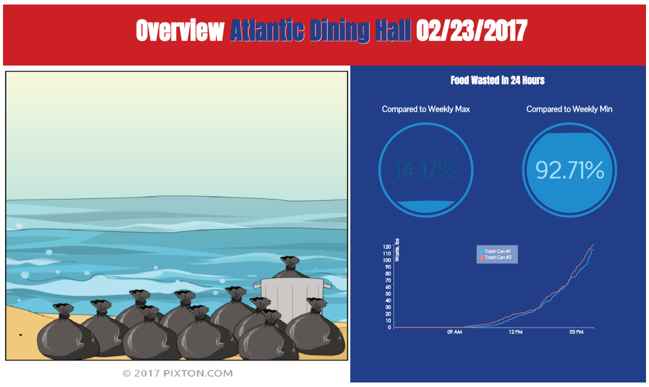

Figure 10: Display 1 for Case Study #1

The main section shows an image of the beach,[3] which becomes littered with trash bags in accordance with how much waste is generated. Preliminary data allowed us to estimate the average weight of the trash when emptied to be 20 lbs (9.07 kg). Therefore, for every 20 lbs wasted, a new trash bag is added to the beach scene in the display.

To the right of the main image is a sidebar of additional information. There are two gauges that show the amount of waste generated at present compared to the maximum and minimum observed waste over the previous week. The value shown is calculated by taking the current waste divided by the maximum and minimum, respectively. This allows us to present the current waste as a percentage of the highest and lowest waste observed the previous week. The gauges fill up according to percentage and the filled portion is animated to look like liquid.

3.4.4 Display 2

Figure 11 depicts a sample of the second display used for Case Study #1 and the only display used for Case Study #2. The display was designed to encourage customers to relate their waste to consumable food. Although this requires a slightly heavier cognitive burden than Display 1, since customers must connect the image of consumable food to wasted food, giving wasted food context in terms of consumable food is more likely to "stick" in consumer's minds. This display capitalizes on 4 out of 6 (67%) of Heath and Heath's [21] SUCCES method.

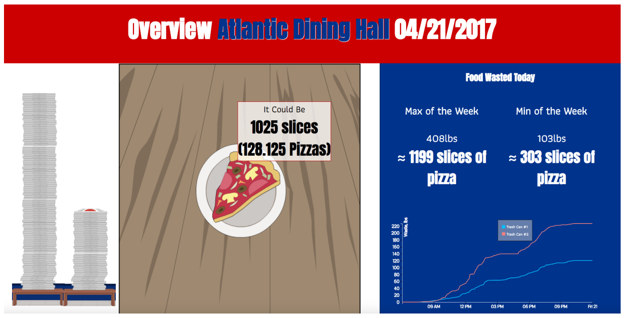

Figure 11: Display 2 for Case Study #1

Instead of using trash bags to depict how much was wasted, this display uses slices of pizza. Pizza was chosen as the food item to display because it is a common staple among college students.

The United States Department of Agriculture maintains a food composition database that provides the average weights of food items by serving size and brand [45]. Using this information, we determined the average weight of a slice of Papa John's *"Supreme Pizza"* to be approximately 0.34 lbs (.15 kg). We use Papa John's as the brand because the university has a contract with Papa John's; it is the pizza typically served on campus. In the pizza slice graphic used for

[3] The image was chosen due to the university's proximity to the ocean, and students' likelihood of relating to the image.

the display, the toppings present are similar to what is served on Papa John's Supreme Pizza.

A minor change to update the header of the display to reflect the new location was made before redeploying for Case Study #2. Since A.D. Henderson University School was too long to comfortably fit on one line, we simply called the page "Food Waste Overview."

Another change in the second display involved the gauges used for comparing weekly progress toward food waste reduction. The cafeteria staff expressed confusion, both among themselves and with the students, concerning what the original gauges were trying to convey. For clarification, the animated gauges were replaced with static text defining the maximum and minimum amount of waste generated for the week. These values were shown in both pounds and number of pizza slices.

3.4.5 Display 3

The main goal of Display 3 is to humanize the issue and remind customers that this issue is continuing in the background of our lives. Another goal for Display 3 is to avoid habituation. Although the other two displays update according to the data in real-time, the images will follow the same general pattern each day. This might cause students to lose interest in the display. Display 3 is guaranteed to have a different image each day, with the goal of preventing habituation and keeping customers interested in checking the display for new information.

Figure 12 depicts a sample of the third display for Case Study #1. There are two differences between this display and the previous displays. The focal image, featured to the left of the screen, depicts a story about 4 characters. The characters are designed to project diversity to ensure all customers feel included in the story. The story is driven by the amount of food wasted each day. Food waste for the day is compared to the average amount of food wasted over the previous week. When more food is wasted, the characters experience a bad day. When less food is wasted, the characters experience a positive day. As with the first display, trash bags appear in the scene to emphasize how much is currently being wasted.

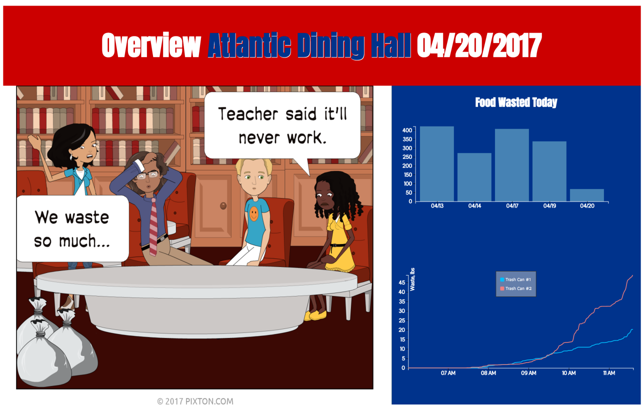

Figure 12: Display 3 for Case Study #1

Another change is in the depiction used to compare the maximum and minimum food wasted over the week. Since pizza slices were no longer being displayed, it no longer made sense to display weight in pizza slices as the maximum and minimum. Since the story follows the accumulation of waste each day, we thought a bar graph allowing customers to compare waste each day would be the most beneficial.

4 Case Studies

Two case studies were carried out to evaluate the efficacy of WASTE REDUCE to affect behavior change and reduce the amount of food wasted in a cafeteria setting. The first case study took place at a university cafeteria; it spanned 7 weeks and tested 3 displays. The second case study was carried out at a grade-school cafeteria over 2 weeks and tested 1 display. For each case study, we obtained a baseline of waste behavior during the first week.

4.1 Technical Difficulties

Although the system was thoroughly tested before beginning the case studies, there were still a few technical difficulties during the case studies. Otherwise, the data was collected over consecutive days and weeks.

4.1.1 Display 1

After the week of baseline data was collected, the cafeteria was closed a week for Spring Break. When the cafeteria reopened, there were technical difficulties the first two days and data could not be collected. This postponed the introduction of Display 1, but did not create a problem for the case study. Another technical difficulty occurred on the Monday during the second week the display was deployed (Week 3). The monitor that allows students to view the display experienced technical difficulties and was not visible until mid-afternoon for that day.

4.1.2 Display 3

Display 3 had one day of technical difficulties. The hotspot providing WiFi connectivity for the system malfunctioned several times during the Tuesday of the week this display was deployed (Week 6). The device could not maintain its connection to the cellular network; thus, the base station could not establish a WiFi connection. Data was not lost due to reboots of the device to troubleshoot and facilitate reconnection to the network.

4.2 Case Study #1

A case study was carried out in FAU's main campus dining hall to determine the efficacy of WASTE REDUCE. The data presented in this section was collected over seven weeks. The first week (Week 1) serves as a baseline for comparing the effects of the ambient display, and thus, only the monitoring system was active during this week. During the second and third weeks (Week 2 and Week 3), the first ambient display was also present in the cafeteria. During the fourth and sixth weeks data was collected but no display was present. This was done to reduce lingering effects of the previous display when the next display was introduced. Display 2 was shown during the fifth week (Week 5), and Display 3 was shown during the final week (Week 7). Due to the cafeteria closing for Spring Break, there is actually one week gap between Week 1 and Week 2.

The campus cafeteria provided the number of meals sold each day during this time period. This information is used to normalize the data by determining waste per meal sold. The number of meals sold is the best estimate of how many people contributed to the waste. This allows better comparison of a day in which the cafeteria may have wasted 500 lbs while serving 5,000 people, versus a day when the cafeteria wasted 500 lbs, but only served 3,000 people. Since the number of meals sold per day is available only as a total, we can only normalize the total waste for the day, and not the real-time data throughout the day.

The cafeteria was closed the weekend before and after Spring Break; therefore, we could not establish a baseline for Saturday and Sunday. In addition, the cafeteria has restricted hours, a different meal service, and receives significantly less traffic during the weekends. Saturday and Sunday are not included in the analysis.

As traffic increases in the cafeteria, the number of trash cans used to contain waste varies, a factor that was unclear in the initial deployment. Only two instrumented cans were used during the case study; however, these cans were always present for student waste. More trash cans may have been present during various times within the study. Thus, all results represent a minimum bound on food wasted in the cafeteria.

4.2.1 Display 1

We will briefly summarize the results of Display 1 for the sake of comparison. Greater detail for this display can be found in the original publication [1].

To determine changes in waste behavior, we examined both total and normalized waste per day for the baseline week (Week 1) and the days the display was present (Week 2 and Week 3). Figure 13 illustrates these results. The x-axis shows the day of the week and the y-axis shows amount of waste (in pounds). For Figure 13(a), the waste is total waste for the day and for Figure 13(b), the waste is waste per meal.

The observation on Friday illustrates why comparing the total waste generated is not sufficient to determine behavioral change. In Figure 13(a), Friday is the only day in which total waste did not decrease after the introduction of the display. This divergence from the trend is because Friday of Week 1 was also the beginning of Spring Break; fewer people ate in the cafeteria that day, leading to less overall food waste. We normalize the day by diving the total waste observed by account the number of meals sold that day, shown in Figure 13(b). The normalized data confirms waste per meal decreased after the introduction of the display even on Friday.

We expected waste for Week 3, the second week the display was present, to continue to decrease or remain the same as Week 2 (the first week the display was present). Figure 13(b) shows a slight decrease for majority of the days in Week 3 compared to Week 2. The increase in waste on Monday of Week 3 compared to Monday of Week 2 is likely due to the technical difficulties experienced with the monitor that day as discussed previously.

Overall, These figures show a consistent decrease in waste per meal for each day the display was present.

We calculated the mean over each week. To determine if the decrease in waste was significant, we applied a standard Z-Test to the normalized values. Calculation of the Z value is discussed in the original publication [1]. Using a Z-Table and the calculated Z-value for each week when the display was present, we are able to determine the p-value for each week and assess statistical significance. For Week 2 compared to Week 1, the p-value was determined to be .035; the results are significant at the .05 level. For Week 3 compared to Week 1, the p-value is .046; the results are also significant at the .05 level.

4.2.2 Display 2

The second display was deployed during Week 5 after a week without the display (Week 4). During Week 4 we collected data but did not include a display; this was done to reduce behavior effects from the previous display from overlapping with the new display. Week 5 introduced the new display.

Behavioral Results Figure 14 compares the waste generated during Week 5 with the waste generated during Weeks 1 and 4. In each graph, the x-axis shows the day of the week in which the data was collected. In Figures 14(a) and 14(c), the y-axis shows the overall amount of food wasted in pounds. In Figures 14(b) and 14(d), the y-axis shows food wasted (in pounds) per meal sold, to normalize the data. Compared to Week 4, when no display was present, customers actually wasted slightly more food–the opposite of the desired result. However, compared to the baseline before the first display was introduced, there was negligible change. Table 4 compares the impact of this display to the initial baseline (Week 1), the second week of the first display (Week 3), and the week just prior to deploying Display 2 (Week 4). None of these proved to be statistically significant for lowering waste.

There are two theories as to why this display was unsuccessful at lowering food waste. The first is the connotation of pizza, versus garbage. Garbage is undesirable; therefore, it is easy for customers to perceive the growing number of garbage bags on a screen as

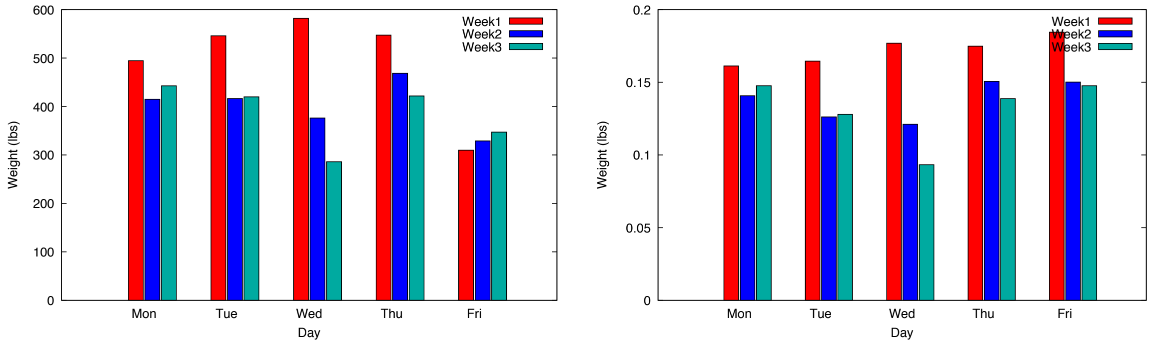

(a) Total Wasted per Day (lbs) (b) Normalized (waste per meal, lbs)

Figure 13: Food Waste With Respect To Display 1

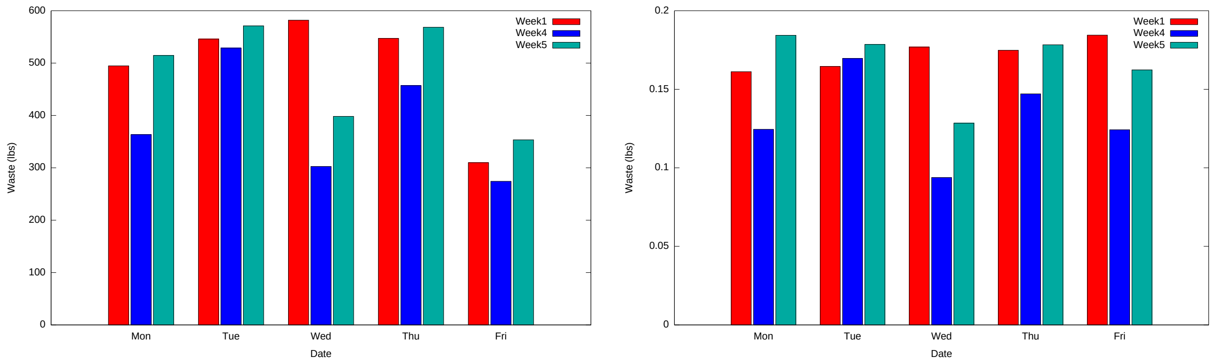

(a) Total Wasted per Day (lbs) (b) Normalized (waste per meal, lbs)

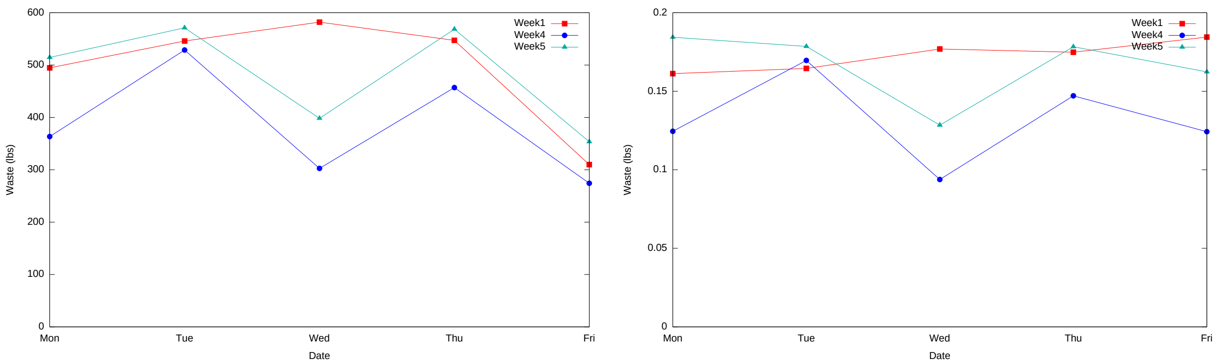

(c) Total Wasted per Day (lbs) (d) Normalized (waste per meal, lbs)

Figure 14: Food Waste With Respect To Display 2

Table 4: Comparing Display 2 (Week 5) to Weeks 1,3&4

	Week 1	Week 3	Week 4
Overall Mean (lbs)	0.16939954	0.148733991	0.14913039
Sample Mean (lbs)	0.16640566	0.16640566	0.16640566
Overall StdDev (lbs)	0.01673104	0.028363066	0.03031837
n (days)	5	5	5
Z	-0.40012464	1.393187366	1.27410199
p-value	0.3446	.9177	0.8980

something negative. Pizza, on the other hand, is desirable (especially among college students). The image of pizza multiplying on the display may invoke positive feelings, rather than a sense of alarm. In future work, it would be interesting to test this concept with a less desirable food.

4.2.3 Display 3

The third display for Case Study #1 was evaluated over Weeks 6 and 7, directly following the evaluation of Display 2. During Week 6, there was no display present. As before, this was done to eliminate behavioral effects associated with the previous display from overlapping with the new display. Week 7 introduced the new display. The purpose of this display is to test the "story" component of the SUCCES concepts (discussed in Section 2.2) and humanize the issue.

Behavioral Results Figure 15 compares the waste generated during Weeks 1, 6, and 7. The y-axis in Figures 15(a) and 15(c) shows total waste in pounds, while the y-axis in Figures 15(b) and 15(d) shows waste per meal. For all plots, the x-axis shows the day of the week in which the sample was collected. Week 1 is the baseline week; data was collected this week without a display and before any of the displays were introduced. Week 6 was the week just before this display was introduced; no display was present during this week. As with the previous evaluations, this was done to eliminate lingering effects from the previous display. Week 7 was the week this display was present. In general, the most waste was generated during Week 1, before any of the displays were introduced. An outlier is seen in the data collected on Tuesday of Week 6. This value is much lower due to the technical difficulties experienced that day, not because of an actual reduction in waste. Aside from this outlier, both the total and normalized waste was lowest each day for Week 7.

Table 5 shows the information used to calculate the p-value when comparing the normalized waste each day from Week 7 to the baseline data (Week 1), the first display week (Week 3), and the gap week preceding the display (Week 6). Once again, overall mean is the average for the display week and the comparison week, sample mean is the average for Week 7, overall standard deviation is the standard deviation for the samples across both weeks being compared, and n is the number of days included in the sample. We see that a statistically significant decrease was observed between the baseline week (Week 1, before any displays were introduced) and the week of the display (Week 7), with $p < .05$. There was not a statistically significant improvement from the display shown during Week 3 (Display 1), nor from the week just before the display was implemented (Week 6, no display after the introduction of displays). When comparing Week 6, we calculated the results both with and without the outlier. Neither confirmed $p < .05$; the results listed in the table are those with the outlier excluded.

4.2.4 Significance at Atlantic Dining Hall

To assess the overall affect of using the displays to affect behavioral change and reduce waste, we compare the two displays that had a significant impact compared to the baseline data. Using three weeks of data, in which two of the weeks used the display, and one week did not, would skew the average of the data toward the waste generated while the displays were present. Therefore, we add to the comparison an additional baseline week from the preliminary deployment in which there was no display, no technical difficulties, and there was a similar packet reception rate. We call this Week 0.

A test of statistical significance was carried out across Week 0 (pre-display), Week 1 (pre-display), Week 3 (display from Case Study #1), and Week 7 (display from Case Study #3). The results of the test are shown in Table 6. Week 0 was too far in the past for the cafeteria to provide us with the exact number of meals sold each day. To normalize the data from that week, we took the average, maximum, and minimum number of customers over the seven weeks data was collected and used those values for normalization. In the table, we show the statistical significance results using the average, maximum, and minimum values for normalization. Assuming the number of customers during that week was near the average, we found that $p = .0174$. If we assume the number of meals sold that week was closer to the maximum observed during the case studies, $p = .0244$. Finally, if we assume the number of meals sold was closer to the minimum observed during the case studies, $p = .0188$. In all three scenarios $p < .05$. Therefore, we can say with confidence at the $p < .05$ level that our displays generated a reduction of waste compared to the baseline.

4.3 Case Study #2

Ideally, WASTE REDUCE would be able to affect behavior in a variety of age groups and settings. We carried out a second case study in the cafeteria at A.D. Henderson University School. The school serves meals for students from kindergarten to eighth grade; however, on most days, only kindergarten through third grade eat in the cafeteria. (Secondary seating is located outside; therefore on rainy days other grades may eat inside.) Once again, we collect one week of data in which the display is not present to establish a baseline, and then collect data for one week with the display present. For this case study, we used Display 2 from Case Study #1 to see if changes in age may alter the effectiveness of the display.

Although this display was unsuccessful in Atlantic Dining Hall, it was believed that of the displays evaluated, the students would relate to this display the most. Display 1 was unlikely to engage young students, who may not have a concept of environmental protection to connect the concept of food waste littering the beach. The storyline for Display 3 was not developed with young children in mind. Although the text and plot

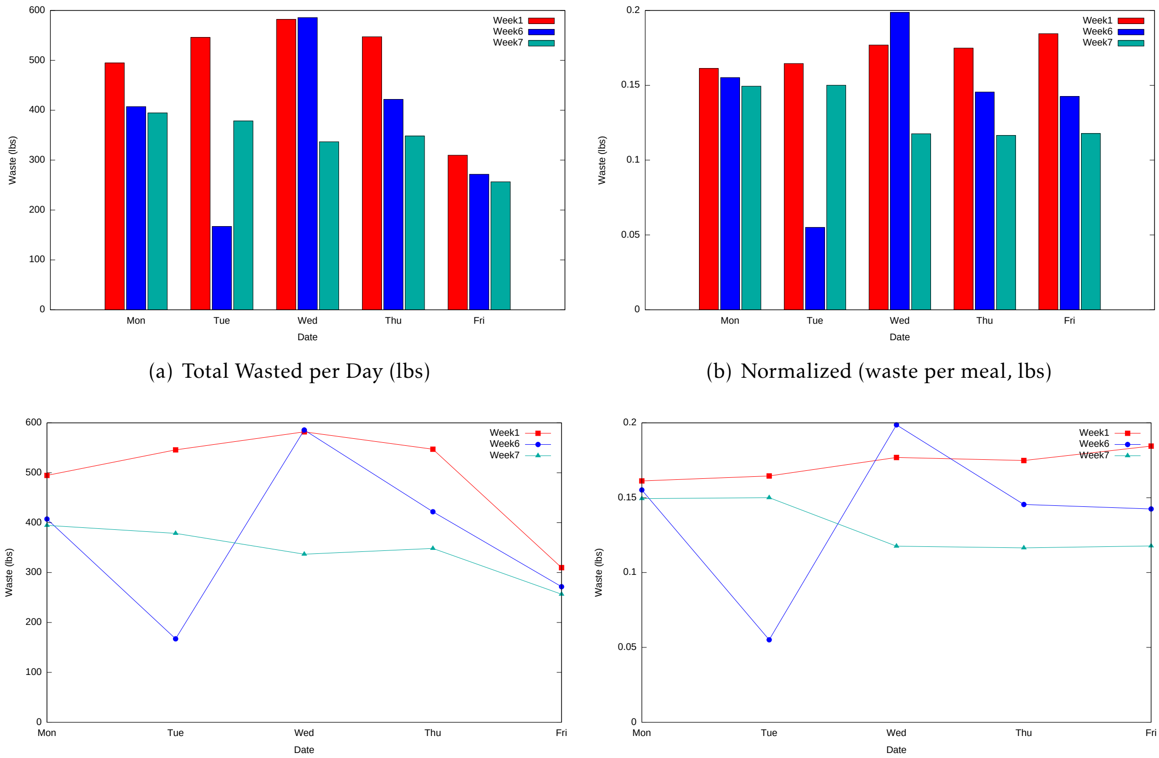

(a) Total Wasted per Day (lbs)

(b) Normalized (waste per meal, lbs)

(c) Total Wasted per Day (lbs)

(d) Normalized (waste per meal, lbs)

Figure 15: Food Waste With Respect To Display 3

Table 5: Comparing Display 3 (Week 7) to Weeks 1,3&6

	Week 1	Week 3	Week 6
Overall Mean (lbs)	0.15233164	0.1316661	0.14480004
Sample Mean (lbs)	0.13226988	0.13226988	0.13226988
Overall StdDev (lbs)	0.026049314	0.02047648	0.02628205
n (days)	5	5	5
Z	-1.722098	0.06593393	-1.0660622
p-value	0.0427	0.5239	0.1446

Table 6: Comparing Waste (Pre-Display vs. Post-Display)

	Average	Maximum	Minimum
Overall Mean (lbs)	0.149672203	0.145258053	0.16064566
Sample Mean (lbs)	0.121939527	0.121939527	0.121939527
Overall StdDev (lbs)	0.032224476	0.028959416	0.04561033
n (days)	5	5	5
Z	-2.108053109	-1.972363293	-2.0787016
p-value	0.0174	.0244	.0188

is fairly simple, it would likely be a challenge for students just learning to read. In addition, the storyline, which follows college or high-school aged students trying to complete a group project, is unlikely to appeal to such a young audience.

4.3.1 Scale Accuracy

Details concerning the accuracy of the scales are presented in Section 3.2.2, and a comparison of the observed versus expected weights of known objects for Case Study #2 is shown in Table 2. Trash Can #1 was found to be perfectly accurate at best, and .055 lbs at worst. Trash Can #2 was found to be accurate within .001 lbs best, and within .032 lbs at worst. This is sufficient to maintain high confidence in the readings from the scale.

4.3.2 Behavioral Significance

Figure 16 illustrates what is typically thrown away during the lunch hour at A.D. Henderson. Unlike Atlantic Dining Hall, there is a higher probability for food packaging, containers, and bottles to be disposed with the food. Also, A.D. Henderson uses disposable trays, which are thrown into the trash can with the food waste. In the figure, it can be observed that the trays, along with packaging containers are included in the waste. Although we were unable to estimate the weight of containers and bottles, we were able to estimate the weight of the trays. We measured the weight of an individual tray and discovered it weighed approximately 0.044 pounds (0.020 kg). Multiplying the number of students who purchased a meal each day by the weight of an individual tray allows us to estimate the total weight of tray waste and exclude it from the analysis.

Figure 16: Observed Waste (A.D. Henderson)

There was no significant change in behavior for the students at A.D. Henderson. Table 7 summarizes the waste accumulated during the case study. The first 3 columns show the total waste, tray waste, and normalized waste, respectively, for the first week of the case study. During this week, no display was present. This is our baseline for comparison. The next 3 columns show the same information for the week the display was present. Since tray waste is unavoidable, this value was subtracted from each day's total waste during the normalization process. Once again, we use the number of students who purchased a meal to estimate the tray waste, and then normalize the total waste to pounds per person. On average, the cafeteria generated 12.50 lbs (5.67 kg) of tray waste per day, and approximately 0.10 lbs (0.05 kg) of waste per person. When the display was present, the students wasted approximately 0.009 lbs more per person. This is not significant.

One thing that may have swayed the results was an incident that occurred during day 5 of the baseline week. On this day, the school was placed on a soft lock-down. During the lock-down, students were escorted to the cafeteria, where they picked up food, and were then escorted back to their classrooms to eat. All waste disposed by these students was deposited outside of the cafeteria. However, the number given for students purchasing meals that day includes both the students who ate in the cafeteria, and those who did not. This means that fewer trays and fewer students contributed to the 21.682 lbs of waste than we estimate. Based on this disturbance, it is likely that there was no change, or an insignificant decrease in behavior for the students.

There are several other differences between the case study at Atlantic Dining Hall and A.D. Henderson that may have affected these results. Everyone who dines at Atlantic Dining Hall eats a meal prepared by the dining hall. However, some of the students at A.D. Henderson bring their lunch from home. This creates three major differences: (i) packed lunches are likely the source of the food packaging containers, (ii) portion sizes for the food brought from home are not likely to be consistent, or to follow recommended guidelines, and (iii) these children are not included in the head count for meals sold.

Another difference is that the children at A.D. Henderson are required to take a full meal. This means they had less control over what they were given, and their ability to waste less. For example, during the case studies, students at Atlantic Dining Hall could view the display, decide they never finish their mashed potatoes, and begin requesting a smaller portion, or no portion at all to aid in reducing waste. Students at A.D. Henderson could not request smaller portions or decline portions of their meal. Therefore, students may have been impacted by the screen, but were powerless to change the outcome.

Age is another factor that may have played a role. Children are generally more inquisitive about changes in their surroundings and were visibly more curious about the changes as the equipment was being installed. However, children are also less likely to understand the significance of lowering food waste.

When food is disposed at Atlantic Dining Hall, cus-

Table 7: Waste at A.D. Henderson University School (in lbs)

	Baseline (No Display)			With Display		
	Total Waste	Tray Waste	Normalized	Total Waste	Tray Waste	Normalized
Day 1	48.401	11.220	0.146	36.258	13.552	0.074
Day 2	30.050	13.068	0.058	48.950	13.552	0.115
Day 3	48.911	12.848	0.124	40.012	12.056	0.146
Day 4	62.777	13.728	0.157	50.586	11.396	0.151
Day 5	27.401	11.748	0.059	33.907	11.704	0.083
Average	43.508	12.522	0.108	41.943	12.452	0.114

Table 8: Comparison of Food Waste by Grade

Time	Grade	Baseline (lbs)	With Display (lbs)
10:20-10:52	2nd Grade	13.0471711	15.8778712
10:37-11:11	Kindergarten	7.09731827	7.1770412
11:15-11:47	3rd Grade	10.9046479	8.88260616
11:56-12:30	1st Grade	16.4856573	10.0050221

tomers come and go intermittently. Due to the randomized nature of individuals entering and exiting the dining hall, the display is constantly updating, and customers can easily view their individual contribution to total waste. On the other hand, A.D. Henderson has set meal times for the students, and everyone disposes of their waste at the same time. A comparison of the daily waste curve for A.D. Henderson versus Atlantic Dining Hall can be seen in Figure 17. It can be observed that due to the organized nature of the meal times at A.D. Henderson, the graph follows a step pattern; waste increases rapidly as students dispose their waste at the end of their lunch, then flat-lines until the end of the next lunch. Since the display was located at the front of the room, and the trash cans were located at the rear, it is possible students only saw how much the classes before them wasted.

4.3.3 Breakdown By Grade

As noted previously, students at A.D. Henderson eat and dispose of their meals at set times. This allows us to more easily parse out data on food waste by grade. Lunch times and grades are provided in Table 8. Since the head count for meals provided does not include students who bring meals from home and is not broken up by grade level, the data presented is not normalized. Because the data is not normalized, we cannot make inferences across grade levels. For example, the kindergarten lunches produced the least amount of waste; however, they may also have the least number of students attending lunch. These numbers do, however, provide a better view of how the display affected each grade. As expected, there was little to no change for the kindergarten lunch. This age group was likely too young to understand the concept. The students from the second grade lunch appeared to waste about 2 lbs more, on average, after the display was implemented. The first and third grade students saw an average decrease in waste of approximately 2 lbs and 6 lbs, respectively. Although a decrease was viewed for these grades, when tested for statistical significance, it was found that for both groups, $p > .05$.

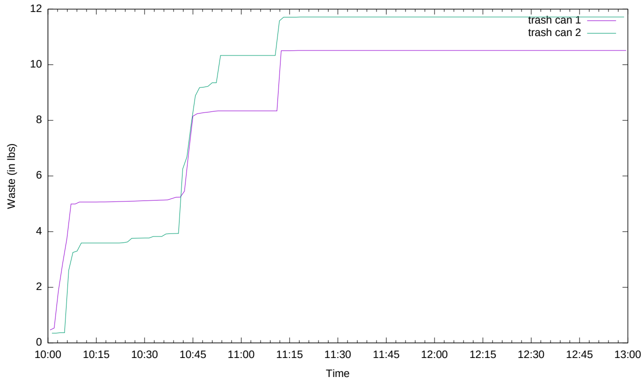

(a) A.D. Henderson University School

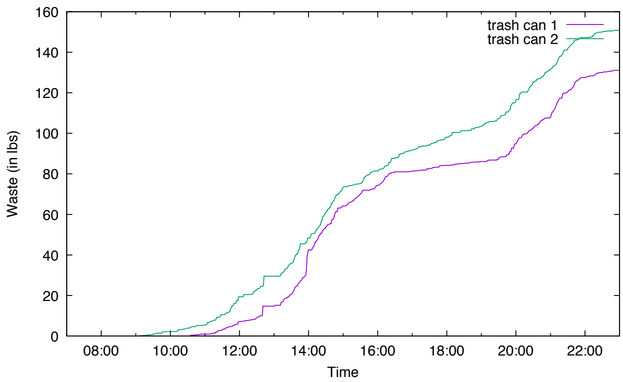

(b) Atlantic Dining Hall

Figure 17: Pattern of Waste Over a Day

5 Conclusion

We have presented WASTE REDUCE, which is a wireless sensor network to provide real-time data on post-consumer food waste. We address software and hardware challenges, such as the communication protocol, wireless connection stability, and power consumption, to ensure WASTE REDUCE is accurate, robust, and sustainable. We also provide three ambient displays designed to evoke behavior change in customers to reduce food waste. We conducted two case studies to evaluate the efficacy of these displays to generate a change in behavior among cafeteria customers. Analysis of the data before and after the displays were introduced confirms behavioral change was affected for two of the three displays developed for the system.

6 Acknowledgments

This work was supported by the NSF grant CNS-1541917. The authors would like to acknowledge Chancey Kelley and Nicholas Lee Yee for their work in designing the electronic enclosure. The authors would also like to thank Chartwells and A.D. Henderson University School for their assistance and cooperation in using their respective dining halls to carry out each case study.

References

[1] Shiree Hughes, Jiannan Zhai, and Jason O. Hallstrom. Waste auditing sensor technology to enhance the reduction of edible discards in university cafeterias & eateries. In *2018 IEEE International Conference on Smart Computing, SMARTCOMP 2018, Taormina, Sicily, Italy, June 18-20, 2018*, pages 344–349, 2018.

[2] Dana Gunders. Wasted: How america is losing up to 40 percent of its food from farm to fork to landfill. *Natural Resources Defense Council Issue Paper*, August 2012. IP: 12-06-B.

[3] U.S. and World Population Clock. U.S. Department of Commerce, 2016. http://www.census.gov/popclock/.

[4] Lisa R. Young and Marion Nestle. The contribution of expanding portion sizes to the us obesity epidemic. *American Journal of Public Health*, 92(2):246–249, 2002.

[5] UC-Davis. UC Davis profile, March 2016. https://www.ucdavis.edu/sites/default/files/upload/files/uc-davis-student-profile.pdf.

[6] Samantha Lubow, Shaina Forsman, Steganie Scott, Linnea Whitney, Isaac O'Leary, and Amy Wang. Love food, dont waste: Resident dining commons food waste report, 2015. http://dining.ucdavis.edu/documents/SP15WasteAuditReport.pdf.

[7] UC-Davis. Waste reduction and elimination, 2015. http://dining.ucdavis.edu/sus-recycling.html.

[8] GT. Admissions & enrollment, 2016. http://factbook.gatech.edu/quick-facts/admissions-enrollment/.

[9] GT. Campus services fall 2012 semester report, January 2013. http://campusservices.gatech.edu/publications/Documents/fallsemesterreport0113final.pdf.

[10] LeanPath. What is LeanPath?, 2015. http://www.leanpath.com/product-video/.

[11] MSU. Msu facts, 2016. https://msu.edu/about/thisismsu/facts.html.

[12] Simon Anderson, Alex Parker, Lisa Schindler, Lindsay Stolkey, and Kaite Ward. MSU: Wasted students? or wasted food. *Michigan State University*.

[13] Carla Iansiti, Allison Stawara, and Robbia Pipper. Food waste impacts msu, 2013. *National Association of College & University Food Services 2013 Regional Conference*. https://eatatstate.com/sites/default/files/pdf/2013%20NACUFS%20Regional%20Conference.pdf.

[14] FIU. Sustainability solutions opportunity assessment report. *Waste Management Sustainability Services*, May 2011. Florida International University. http://gogreen.fiu.edu/_assets/documents/topics/Waste-Audit-Report.pdf.

[15] UM. Student enrollment fall 2015, 2016. http://www.miami.edu/index.php/about_us/fast_facts/student_enrollment_--_fall_2015/.

[16] UM. Sustainability interim report, 2014. Office of Sustainability. https://umshare.miami.edu/web/wda/greenu/DOCUMENTS/Sustainability%20Interim%20Report%202013-2014_UMWeb.pdf.

[17] UM. Green waste - food waste, 2016. Office of Sustainability. http://www.miami.edu/finance/index.php/green_u/recycling/green_waste_-_food_waste/.

[18] Oxford English Dictionary. habitutation, n 1.1. https://en.oxforddictionaries.com/definition/habituation, 2016.

[19] Kevin Vaughan and Nicholas Tarrier. The use of image habituation training with post-traumatic stress disorders. *The British Journal of Psychiatry*, 161(5):658–664, 1992.

[20] Han X Lin, Yee-Yin Choong, and Gavriel Salvendy. A proposed index of usability: a method for comparing the relative usability of different software systems. *Behaviour & information technology*, 16(4-5):267–277, 1997.

[21] Chip Heath and Dan Heath. *Made to Stick: Why Some Ideas Survive and Others Die*. Random House, 2008.

[22] John Stasko, Todd Miller, Zachary Pousman, Christopher Plaue, and Osman Ullah. Personalized peripheral information awareness through information art. In *International Conference on Ubiquitous Computing*, pages 18–35. Springer, 2004.

[23] Mark Weiser and John Seely Brown. The coming age of calm technology. In *Beyond calculation*, pages 75–85. Springer, 1997.

[24] Dan Ariely. Controlling the information flow: Effects on consumers' decision making and preferences. *Journal of Consumer Research*, 27(2):233, 2000.

[25] Franck L Lewis et al. Wireless sensor networks. *Smart environments: technologies, protocols, and applications*, pages 11–46, 2004.

[26] Ian F Akyildiz and Mehmet Can Vuran. *Wireless sensor networks*, volume 4. John Wiley & Sons, 2010.

[27] Ian F Akyildiz, Weilian Su, Yogesh Sankarasubramaniam, and Erdal Cayirci. Wireless sensor networks: a survey. *Computer networks*, 38(4):393–422, 2002.

[28] Raspberry Pi Foundation. Raspberry pi. https://www.raspberrypi.org/, 2017.

[29] Massimo Banzi, David Cuartielles, Tom Igoe, Gianluca Martino, David Mellis, et al. Arduino. https://www.arduino.cc/, 2005.

[30] Beagleboard.org. Beaglebone black. https://beagleboard.org/black, 2016.

[31] Niels Reijers, Gertjan Halkes, and Koen Langendoen. Link layer measurements in sensor networks. In *Mobile Ad-hoc and Sensor Systems, 2004 IEEE International Conference on*, pages 224–234. IEEE, 2004.

[32] Christopher Plaue, Todd Miller, and John Stasko. Is a picture worth a thousand words?: An evaluation of information awareness displays. In *Proceedings of Graphics Interface 2004*, GI '04, pages 117–126, School of Computer Science, University of Waterloo, Waterloo, Ontario, Canada, 2004. Canadian Human-Computer Communications Society.

[33] Andrew Dahley, Craig Wisneski, and Hiroshi Ishii. Water lamp and pinwheels: Ambient projection of digital information into architectural space. In *CHI 98 Conference Summary on Human Factors in Computing Systems*, CHI '98, pages 269–270, New York, NY, USA, 1998. ACM.

[34] Jennifer Mankoff, Anind K. Dey, Gary Hsieh, Julie Kientz, Scott Lederer, and Morgan Ames. Heuristic evaluation of ambient displays. In *Proceedings of the SIGCHI Conference on Human Factors in Computing Systems*, CHI '03, pages 169–176, New York, NY, USA, 2003. ACM.

[35] Jeremy M Heiner, Scott E Hudson, and Kenichiro Tanaka. The information percolator: ambient information display in a decorative object. In *Proceedings of the 12th annual ACM symposium on User interface software and technology*, pages 141–148. ACM, 1999.

[36] Hannah Pileggi, Charles D Stolper, J Michael Boyle, and John T Stasko. Snapshot: Visualization to propel ice hockey analytics. *IEEE Transactions on Visualization and Computer Graphics*, 18(12):2819–2828, 2012.

[37] HT Sensor Technology Co. Limited. Tal201 parallel beam load cell. http://www.htc-sensor.com/products/87.html, 2016.

[38] AVIA Semiconductor (Xiamen) Co. LTD. Hx711: 24-bit analog-to-digital converter (adc) for weigh scales. http://www.aviaic.com/UpLoadFile/hx711_brief_en.pdf, 2016.

[39] Digi International Inc. Xbee-pro 900hp. https://www.digi.com/products/xbee-rf-solutions/modules/xbee-pro-900hp, 2016.

[40] Atmel Corporation. Sam4l xplained pro evaluation kit. http://www.atmel.com/tools/ATSAM4L-XPRO.aspx, 2016.

[41] TP-Link Technologies Co. Ltd. 150mbps high gain wireless usb adapter: Tl-wn722n. http://www.tp-link.com/en/products/details/cat-11_TL-WN722N.html, 2016.

[42] Inc. MongoDB. Mongodb. https://www.mongodb.com/, 2016.

[43] Author One, Author Two, and Author Three. Title of paper. In *Conference*, page Pages, Year.

[44] Mike Bostock. Data-driven documents. https://d3js.org/, 2015.

[45] Beltsville Human Nutrition Research Center. Usda food composition databases. *United States Department of Agriculture*. https://ndb.nal.usda.gov/ndb/, 2017.

ASTES

Advances in Science, Technology and Engineering Systems Journal
Vol. 4, No. 2, 65-69 (2019)
www.astesj.com
Special Issue on Recent Advances in Engineering Systems

ASTES Journal
ISSN: 2415-6698

A Relation Extraction System for Indian Languages

Ajees Arimbassery Pareed*, Sumam Mary Idicula

Department of Computer Science, CUSAT, 682022, India

ARTICLEINFO

Article history:
Received: 04 January, 2019
Accepted: 28 February, 2019
Online: 15 March, 2019

Keywords:
Convolutional Neural Networks
Natural Language Processing
Word embedding
Relation extraction.

ABSTRACT

Relation Extraction is an important subtask of Information Extraction that involves extracting significant facts from natural language text. Extracting structured information from the plaintext is the ultimate goal of IE systems. The Indian language content on the internet is increasing day to day. Extracting relevant information from this huge unstructured data is a challenging task especially when the business firms are interested in ascertaining public view on their products and processes. The primary objective of relation extraction systems is to find those entities which can be targeted through social networking and digital marketing. Cannibalisation of the product is nowadays done using these Social Networks. Different methods are proposed and experimented for Relation extraction problems. In this paper, we propose a Relation Extraction system using Convolutional Neural Networks. Deep learning based methods have produced state of the art results in many domains. Training and testing are conducted using the shared corpus provided by 'ARNEKT-IECSIL 2018' competition organisers. The evaluation results show that the proposed system could outperform most of the reported methods in the competition.

1 Introduction

Internet is the fastest growing resource on the planet. Lots of information are added to the web every second. However, this information is stored in an unstructured manner. Retrieving the relevant information from this unstructured text is a challenging task that invites the focus of Language researchers. Information extraction, a branch of Artificial Intelligence deals with this challenge [1]. IE transforms the unstructured text into a structured form that can be easily handled by machines. Relation Extraction is one of the subdomains of IE. It is the process of identifying the relation between two entities in a document. There are two major types of RE namely-closed domain and open domain RE. Closed domain RE considers only a closed set of relationships between two arguments while the open domain RE systems use an arbitrary phrase to specify a relationship [2].

Relation Extraction is one of the subtasks of Information Extraction. The occurrence of entities in a sentence is always through well-defined relationships. Automatic identification of such relationships is what we call as the task of relation extraction. Relation Extraction also helps in getting the structured information from the unstructured text. It is very similar to Information Extraction with the exception that IE additionally requires the removal of repeated relations. Applications of Relation Extraction systems include construction of knowledge bases, Question answering systems, text summarisation, etc. Construction of knowledge bases is a laborious, time-consuming project that demands domain expertise. Automatic extraction of relationships and concepts from text documents helps to reduce the time and domain expertise needed for the task. Question answering systems also make use of relation extraction systems since relations can provide a clue about the answers to most of the questions. Similarly, relation extraction systems can be employed in areas like textual entailment, gene-disease prediction, protein-protein interaction, etc.

Text classification is the primary area of research where the supervised machine learning algorithms are explored in Natural Language Processing. It is a very active research area both in industry and academia. Examples of such classification tasks include sentiment analysis from social media text, detection of spam emails, categorisation of customer queries, auto tag-

*Corresponding Author: Department of Computer Science, CUSAT, 9061859697 & ajeesap87@gmail.com

https://dx.doi.org/10.25046/aj040208

ging of news articles, etc. In this work, we have tried to move towards a direction which is not much explored in the case of Indian languages.

The structure of this article is as follows. Section 2 briefly reviews the related works and details about the dataset. Section 3 explains the proposed method and section 4 illustrates the experiments and results. Finally, section 5 concludes the article along with some routes for future works.

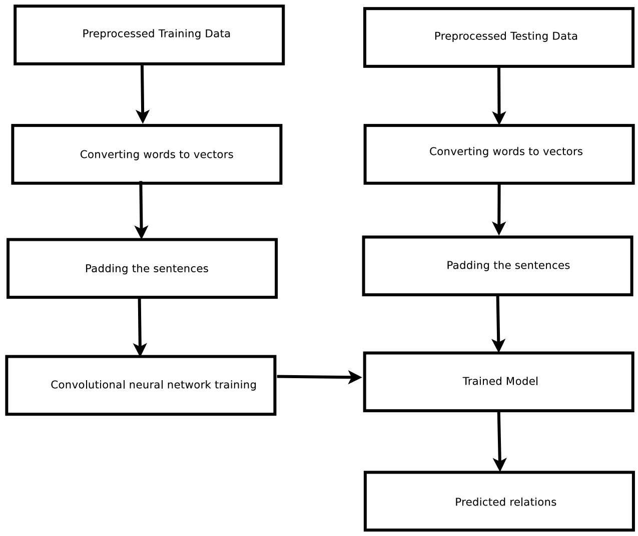

Figure 1: Architecture of the proposed system.

2 Related Works

Various studies are conducted to extract the semantic relations between entities in a text document. Starting from the straightforward rule-based approach to more complex supervised approaches and also semi-supervised approaches are explored in the literature [3]. Rule-based systems employ a naive approach towards the relation extraction task. They construct a set of possible rules for relation extraction by looking at some examples. Hearst, who applied this approach to find the hyponyms of words could achieve an accuracy of 66% on his task [4]. The major issue associated with this technique is that it needs a lot of rules to accomplish the task. We have to continuously update the rule set whenever we find an exception to the existing rules. And more notably, we have to redo this entire work for the other kinds of relations.

On the other hand, supervised relation extraction systems build the model with the help of already tagged corpus. Set of features are designed for each sample in the training data with the help of domain experts. This feature set act as input to the learning algorithms. The key idea behind the supervised learning algorithms is to model the relation extraction task as a classification problem and train the classifier with different algorithms (SVM, Naive Bayes, etc.) available for supervised learning. These classifiers can be trained using a different set of features selected after performing a textual analysis of the labeled data. Different features considered for the study include lexical features, syntactic features, dependency features, entity features, etc [3].

Supervised methods suffer from the problem of availability of enough labelled data. If we do not have enough labelled data to train our classifier, results will be poor. The solution to this issue is the bootstrapping technique. In this technique, we will start with some seed instances of training data, which is manually tagged data used for the first phase of training. We train our classifier with seed instances and learn the classifier. This classifier is used to test more unlabelled data, and get more train examples by adding the test results to the training set. Thus, the training set will expand up to a sufficient amount. This approach is called a semi-supervised learning. 'DIPRE' is an example of the semi-supervised system employed for the relation extraction task [5]. It tries to extract author-book relationship from web text. However, the current trend in relation extraction is based on reinforcement learning. Xiangrong Zeng et al.[6] reports an improvement of 13.36% over the baseline models with the help of reinforcement learning.

The shared task is divided into two subparts say task-A and task-B [7]. Task-A deals with the identification of named entities from the raw text and task-B deals with extracting relation amongst the entities in a sentence. Both these tasks come under the domain of Information Extraction (IE), which is an area under constant research. The growth of research in this area leads to the advancement of applications like information search, question answering, document summarization, etc. Five Indian languages are considered for this shared task. They are Tamil, Hindi, Kannada, Telugu, and Malayalam. It is well known that IE works significantly well with languages like English from applications like Google search, frameworks like Stanford CoreNLP, OpenNLP and many more. The same does not hold good for Indian Languages due to its morphologically rich nature and agglutinative structure. Hence, the objective of this shared task is to improve the Information Extraction systems for Indian languages.

The shared dataset contains data from five different Indian languages [8]. The training data for task-B is a set of files in plain text format. Each file consists of sentences and their corresponding labels. Each language has more than 25000 samples of training data. Statistics of the training data for the task-B is shown in figure 2. The testing data contains two files say test1 and test2. Test1 is for pre-evaluation, and test2 is for final evaluation. The statistics of the test data is given in table 1.

3 Proposed Method

The problem is framed as a sentence classification problem with classes as relations. The number of classes is equal to the number of relations in the tagged data. Convolutional neural networks are used to build the model. They are a class of neural networks that have

Table 1: Data statistics

Language	Train	Pre-eval	Final-eval
Hindi	56775	18925	18926
Kannada	6637	2213	2213
Malayalam	28287	9429	9429
Telugu	37039	12347	12347
Tamil	64833	21611	21612

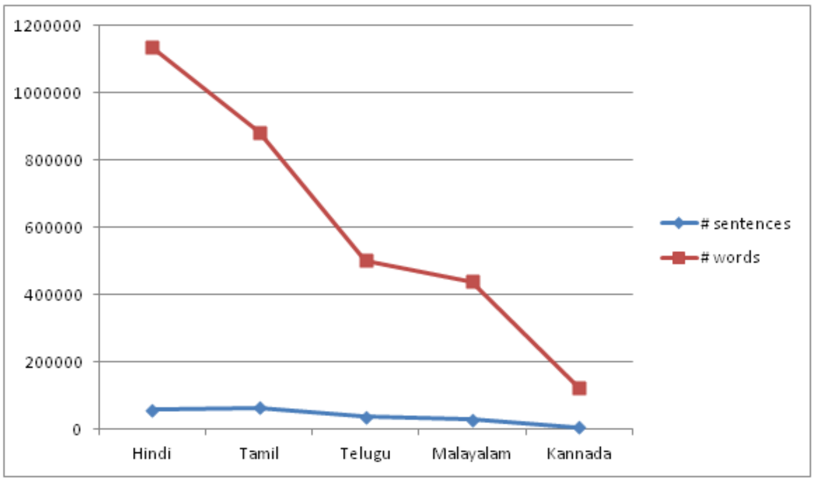

Figure 2: Statistics of the training data

proven very effective in areas such as image classification and pattern recognition. Figure 3 depicts the easiness of deep learning based text processing systems over the traditional machine learning approaches. They can capture the local texture within the text and can be used to find the representative patterns in a text document [9]. The most important property of CNN is preserving the 2D spatial orientation in computer vision problems. But these orientations have a one-dimensional structure in the case of texts.

The architecture of the proposed method is shown in figure 1. The first phase is the preprocessing phase, where words in each sentence are separated using NLTK word splitter. Since words are symbolic units, it can't be directly fed to neural networks. Hence words are converted into numeric values(vectors) using word2vec [10]. The sequences of vectors are then padded with zeros to make it of uniform length. Finally, the padded sentences and their corresponding labels are provided to CNN for training. After training, the model file is saved for testing. In the testing phase, the test data is passed through operations similar to that of the training data and are provided to the saved model for prediction. The model then predicts the label for each sentence indicating the relation within the sentences.

4 Experiments and Results

The preprocessing stage contains operation like trimming, stopword removal, etc. Trimming is the process of removing unwanted symbols from the text. And the most common words are removed in the stop word removal stage. Inputting sequences of raw human alike words will make no sense to computers. For that reason, the raw words are converted into vectors of numeric value using word2vec [11]. Word2vec model is built using a manually created corpus of 27 lakhs words. Skip-gram configuration of Word2vec is used to build the model. The model is constructed with a context window size of 10. The dimensionality of the word embedding is fixed as 100 to cope up with the processing power of the machine.

Keras sequential model is used to construct the classifier [12]. The configuration of the constructed convolutional neural network is shown in table 2. The network is designed with four convolutional layers, two max-pooling layers, and two dense layers. The first layer is a convolutional layer for its ability to capture the local context. The following layers are alternate max-pooling and convolutional layers for acquiring the hidden patterns within the sentence. We have used 'Relu' as the activation function to bring nonlinearity. The number of filters used in the first two convolutional layers is 756. And the kernel size is fixed at 7 for the first two convolutional layers and 3 for the remaining layers. The final dense layer is associated with softmax activation units. During the training phase, filters slide over full rows of the word embeddings. CNN automatically learns the values of its filters based on the labels on the training samples.

In our experiments, we have selected the first 90% of the sentences as training data, and the remaining is selected as the testing data. The batch size is fixed at 100. Categorical cross entropy is used as the loss function. We used Adam, the efficient gradient descent algorithm as the optimizer. Dropout is used to

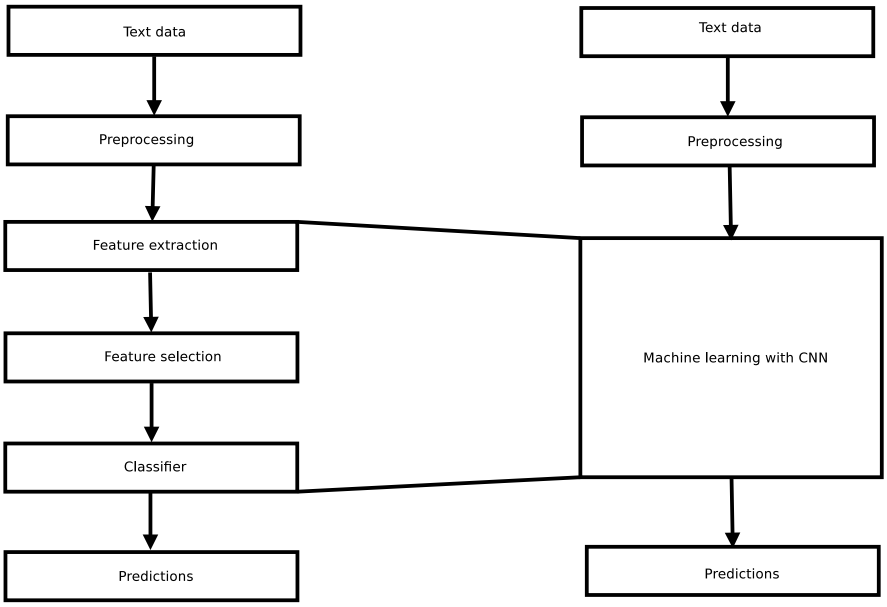

Figure 3: Comparative architecture of deep learning based and non-deep learning based systems

Table 2: Configuration of the CNN architecture

Layers	Output shape	Configuration
conv1d_1	30×756	$7 \times 1, strides 1$
max_pooling1d_1	15×756	$3 \times 1, strides 1$
conv1d_2	15×756	$7 \times 1, strides 1$
max_pooling1d_2	7×756	$3 \times 1, strides 1$
conv1d_3	7×256	$3 \times 1, strides 1$
conv1d_4	7×256	$3 \times 1, strides 1$
flatten_1	1792	–
dense_1	128	Relu activation
dropout_2	128	0.5
dense_2	14	Softmax activation

prevent overfitting [13]. Model is compiled using Tensorflow in the backend. The network is trained for five epochs, and the model file is saved for the testing. Due to the lack of pre-trained word embeddings, we could not complete our work on languages other than Malayalam using pre-trained word embeddings. For Malayalam, we were able to simulate word vectors using our corpus. Moreover, the publicly available pre-trained word embeddings were out of the scope of our machine memory. For languages other than Malayalam, we used an additional embedding layer in front of the convolutional layers.

The proposed system is tested with two test datasets(pre-evaluation and final evaluation). Our system predicts the relation in each input sentence. Table 3 demonstrates the results of our system on both the datasets. Since the final evaluation phase is not available for real-time evaluation, we were not able to get the results for test 2 dataset for languages other than Malayalam. It is clear from the results that our system performance is promising as compared with the performance of other methods reported in the competition. The performance of different relation extraction systems reported in the competition (on test 1) is shown in figure 4. Our system records an average accuracy of 85.62% on test-1 data. From the experimental results, it is obvious that the performance of the system increases with the increase in the training data size. This point is evident from the results of Kannada and other languages. Kannada, which contains the least number of training samples, records the least performance as compared with other languages in the dataset.

5 Conclusion

In this paper, we have discussed a CNN based Relation Extraction system for Indian languages. The exclusive feature of our technique is the use of CNN for relation extraction in Indian languages. The main reason we preferred CNN rather than other traditional feature-based methods is their ability to capture the relations within the sentences. Since deep learning methods require a sufficient amount of training data, the performance of the system can still be improved by increasing the training data size. The performance of the system can also be improved by incorporating word embedding based cluster features into the word vectors. Due to the lack of enough computational power, we could not accomplish that task. Apart from Rela-

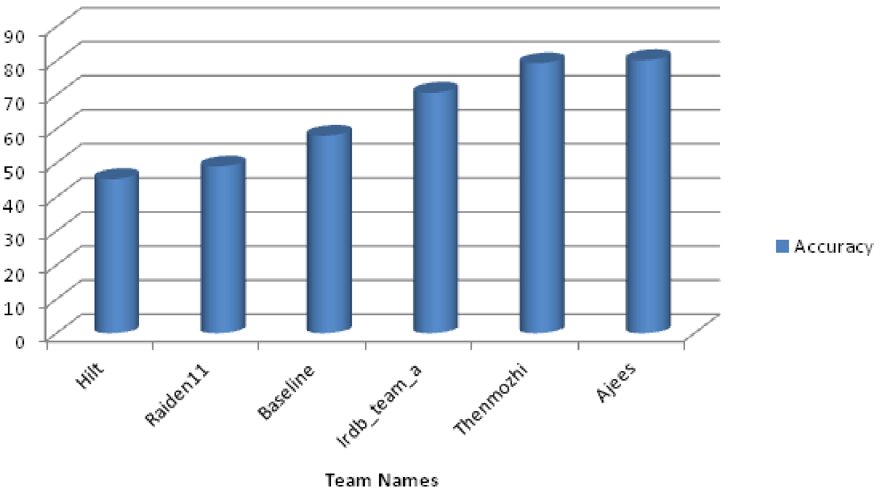

Figure 4: Performance of different relation extraction systems on the shared corpus

Table 3: Results

Test data	Hindi	Kannada	Malayalam	Tamil	Telugu	Average
Test 1 (Accuracy %)	94.72	50.64	80.46	85.76	84.76	85.62
Test 2 (Accuracy %)	NA	NA	77.77	NA	NA	15.55

tion Extraction, Convolutional Neural Networks based deep learning methods can also be applied to various NLP applications like Text classification, sentiment analysis, document labelling, etc.

References

[1] Nita Patil, Ajay S Patil, and BV Pawar. Survey of named entity recognition systems with respect to indian and foreign languages. *International Journal of Computer Applications*, 134(16), 2016.

[2] Manaal Faruqui and Shankar Kumar. Multilingual open relation extraction using cross-lingual projection. *arXiv preprint arXiv:1503.06450*, 2015.

[3] Kush Goyal and Pushpak Bhattacharyya. Literature survey on relation extraction and relational learning.

[4] Barbara Rosario and Marti Hearst. Classifying the semantic relations in noun compounds via a domain-specific lexical hierarchy. In *Proceedings of the 2001 Conference on Empirical Methods in Natural Language Processing*, 2001.

[5] Jinxiu Chen, Donghong Ji, Chew Lim Tan, and Zhengyu Niu. Relation extraction using label propagation based semi-supervised learning. In *Proceedings of the 21st International Conference on Computational Linguistics and the 44th annual meeting of the Association for Computational Linguistics*, pages 129–136. Association for Computational Linguistics, 2006.

[6] Zeng Xiangrong, Liu Kang, He Shizhu, Zhao Jun, et al. Large scaled relation extraction with reinforcement learning. 2018.

[7] HB Barathi Ganesh, KP Soman, U Reshma, Kale Mandar, Mankame Prachi, Kulkarni Gouri, and Kale Anitha. Overview of arnekt iecsil at fire-2018 track on information extraction for conversational systems in indian languages. In *FIRE (Working Notes)*, 2018.

[8] HB Barathi Ganesh, KP Soman, U Reshma, Kale Mandar, Mankame Prachi, Kulkarni Gouri, and Kale Anitha. Information extraction for conversational systems in indian languages - arnekt iecsil. In *Forum for Information Retrieval Evaluation*, 2018.

[9] Yoon Kim. Convolutional neural networks for sentence classification. *arXiv preprint arXiv:1408.5882*, 2014.

[10] Tomas Mikolov, Ilya Sutskever, Kai Chen, Greg S Corrado, and Jeff Dean. Distributed representations of words and phrases and their compositionality. In *Advances in neural information processing systems*, pages 3111–3119, 2013.

[11] Radim Řehůřek and Petr Sojka. Software Framework for Topic Modelling with Large Corpora. In *Proceedings of the LREC 2010 Workshop on New Challenges for NLP Frameworks*, pages 45–50, Valletta, Malta, May 2010. ELRA. http://is.muni.cz/publication/884893/en.

[12] François Chollet et al. Keras. 2015.

[13] Nitish Srivastava, Geoffrey Hinton, Alex Krizhevsky, Ilya Sutskever, and Ruslan Salakhutdinov. Dropout: A simple way to prevent neural networks from overfitting. *The Journal of Machine Learning Research*, 15(1):1929–1958, 2014.

ASTES
Advances in Science, Technology and Engineering Systems Journal
Vol. 4, No. 2, 70-77 (2019)
www.astesj.com
Special Issue on Recent Advances in Engineering Systems

ASTES Journal
ISSN: 2415-6698

A Spectrum Sharing based Metering Infrastructure for Smart Grid Utilizing LTE and WiFi

Imtiaz Parvez, Arif I. Sarwat *

Department of Electrical and Computer Engineering, Florida International University, Miami, FL 33174

A R T I C L E I N F O

Article history:
Received: 12 December, 2018
Accepted: 09 February, 2019
Online: 15 March, 2019

Keywords:
3.5 GHz
AMI
cognitive radio
LTE-U
CBRS
spectrum sharing
Internet of Things (IoT)
smart meter
licensed assisted access (LAA)
WiFi

A B S T R A C T

In advanced metering infrastructure (AMI) of smart grid, WiFi is an appropriate choice for its bidirectional communication requirement to transmit data to the billing center. But, WiFi functions in the free spectrum bands and LTE also requires to use the same free bands for its network expansion being licensed spectrum is limited and expansive. LTE and WiFi can operate simultaneously in the 3.5 GHz band (also known as citizen broadband radio service (CBRS)), which has large amount of free and clean spectrum. In this paper, we propose a smart grid metering infrastructure based on fixed duty cycled LTE and WiFi, where smart meters and its' data collectors (known as Access Point) use WiFi and LTE, respectively, for transferring data. Under a system level simulation environment, we investigated the LTE-WiFi coexistence performance in CBRS band considering a time division duplexing (TDD)-LTE associated with FTP traffic, and IEEE 802.11n (WiFi). The simulation performance demonstrates a good neighborhood coexistence between WiFi and LTE, which makes it a potential communication solution for the AMI.

1 Introduction

Smart grid is the advanced power and energy system that has been transformed from unidirectional power flow to bidirectional power flow. Moreover, it is employed with information communication technology among its entities for electricity supply to the consumers with reinforced control and efficiency [1, 2, 3, 4]. Advanced metering infrastructure (AMI) is an critical building block of smart grid as it builds communication bridge between metering data management service (MDMS) and consumer meters for consumption data transfer utilizing wireless networks [5, 6, 7, 8, 9]. The prominent communication standards for AMI are Zigbee, and WiFi, that use public frequency bands e.g. 5 GHz, 2.4 GHz, and 900 MHz [10]. Since unlicensed/public frequency bands will be shared, smart meters may need to coexist along with atypical techniques e.g. ZigBee and LTE in the same bands.

LTE is the long range broadband communication for exchanging voice and data [1, 11]. For the advancement of requirement, LTE requires to accommodate machine-to-machine (M2M) communication in addition to voice communication. Moreover, to satisfy the exponential increase of throughput requirement in LTE, spectrum shortage is a critical obstacle. In this regard, spectrum sharing among different wireless technologies could be a promising solution. However, this sharing approach has its own implementation hurdles. Additionally, public (license free) spectrum can be used in conjunction with licensed spectrum. In this regard, 3GPP working group is studying on the license assisted access (LAA) of LTE in the free bands [12].

WiFi[1] is a prominent short range communication protocol which utilizes a distributed coordination function (DCF). Its channel access mechanism performs four-way handshaking and carrier sensing [13]. The WiFi DCF mode utilizes clear channel assessment (CCA) technique for the packet transmission. The CCA includes energy detection and carrier sensing mechanism to detect the state of channel- whether it is in operation or not. WiFi node will cease transmission attempt for a random time period if the interference level crosses CCA threshold. This back-off method avoids packet collision that may happen due to coexisted LTE network transmission.

*Corresponding Author: Arif I. Sarwat, Department of Electrical and Computer Engineering, Florida International University, Miami, FL 33174, Email: asarwat@fiu.edu

[1] Unless or otherwise saying, IEEE 802.11n version will considered as WiFi in our study.

https://dx.doi.org/10.25046/aj040209

In contrast, the LTE technology is comparatively flexible and systematic. LTE utilities dynamic scheduling for its users. The main obstacle for coexisting WiFi and LTE system in the identical band is the data transmission technique. WiFi uses CSMA/CA protocol for the transmission of OFDM. On the other hand, LTE uses the dynamic scheduling in OFDM access through which data is transmitted to several UEs simultaneously at low rate with proper time and frequency allotment [14]. LTE reserves channels to make transmission simultaneously. On the other hand, WiFi implements carrier sensing before the packet transmission. Therefore, LTE transmission will block the WiFi transmission most likely in the coexistence scenario.

Recently, 3.5 GHz band (also known as citizen broadband radio service (CBRS)) has been released for public use, which is to be shared [15, 16]. According to the guideline, the users can be classified into three classes: first tier users, second tier users, and third tier (general) users. In general, third tier/general users access the CBRS spectrum, giving priority to the first and second tier users. In several cases, third/general users can use full 150 MHz of bandwidth in the absence of first and second tier users' activity [17]. At the worst case scenario, 80 MHz spectrum will always be available for third tier/general users when second tier users are active and operated outside of first tier users' zones. This large amount of spectrum can provide clean channels for various wireless communication applications such as smart grid metering data communication [18, 19, 20, 21]. WiFi and LTE use the CBRS band as the potential general (third tier) users in our study.

In this study, we expand our previous work in [22], which introduces a AMI architecture based on WiFi and LTE coexistence. In the architecture, WiFi is used in smart meters for transferring data to Access point (AP). After collecting data from a group of meters, AP transfers the data to MDMS utilizing the LTE. In our framework, we consider an integrated LTE-WiFi system where LTE BS and WiFi APs are connected through IP layer. Following this, we investigate the performance of LTE-WiFi coexistence in the CBRS band considering both conventional personal mobile communication and AMI communication. For system level simulation, a time division duplexing (TDD)-LTE and WiFi are considered in a seven cell hexagonal layout. LTE uses a fixed duty cycle of a transmission period for its transmission, and WiFi transmits in the remaining period, in contrast. The simulation performance exhibits a harmonious coexistence relationship between WiFi and LTE. Since CRBS posses a huge chunk of free and clean spectrum, AMI based on LTE-WiFi coexistence operating in CBRS can be a potential communication resolution for smart grid. The contributions of our work is as follows:

1) We introduce a smart grid metering infrastructure based on fixed duty cycled LTE and WiFi for the first time, where LTE and WiFi shares the same spectrum band.
2) Our proposed spectrum sharing method ensures good neighborhood spectrum sharing with an option of adjusting duty of LTE transmission.
3) Our spectrum sharing technique enhances the spectral efficiency significantly.
4) We propose the usage of recently release CRBS band for metering infrastructure which can provide large amount of free and clean spectrum.

The subsequent sections are arranged as follows. The literature review on LTE-WiFi coexistence and AMI communication is discussed in Section II. The coexisted system model of LTE-WiFi coexistence in 3.5 GHz band is illustrated in Section III. Deployment scenario and performance results are illustrated in Section IV. Lastly, Section V summarizes the whole work. Some of the acronyms used in this paper are presented in Table 1.

Table 1: List of Acronyms.

3GPP	3rd Generation Partnership
AMI	Advanced Metering Infrastructure
AP	Access Point
APP	application
CSMA/CA	Collision Sensed Multiple Access/Collision Avoidance
CCA	Clear Channel Assessment
CBRS	Citizen Broadband Radio Service
DCF	Decentralized Frequency Control
EDCA	Enhanced Distributed Channel Access
EPC	Evolved packet core
EPC	Enhanced Packet Core
FCC	Federal Communications Commission
FBE	Frame Based Equipment
GTP	GPRS tunneling protocol
PAL	Prioritized Access License
PHY	physical
PDPC	packet data convergence Protocol
GAA	General Authorized Access
IP	Internet Layer
LAA	Licensed Assisted Access
LBT	Listen Before Talk
LBE	Load Based Equipment
LLC	logic link control
LTE	Long Term Evolution
M2M	Machine-to-Machine
MDMS	Meter Data management Service
MAC	medium access control
OFDM	Orthogonal Frequency Division Multiplexing
PPDU	PLCP Protocol Data Unit
PL	Path Loss
RLC	radio link control
SINR	Signal-to-Interference-plus-Noise Ratio
TPC	Transmission Power Control
TTI	Transmission Time Interval
UE	User Equipment
UDP	user datagram protocol

2 Literature Review

The variants of LTE working in the public/free bands can be categorized into two groups: (1) LTE-U and (2) LTE-LAA [23]. LTE-U was developed by industry consortium [24]. It uses simple mechanism and excludes modification in the air interface structure of LTE system. It is founded on the LTE release 10-12 aggregation protocol and does not embrace LBT [25]. On the other hand, LTE-LAA is based on 3rd Generation

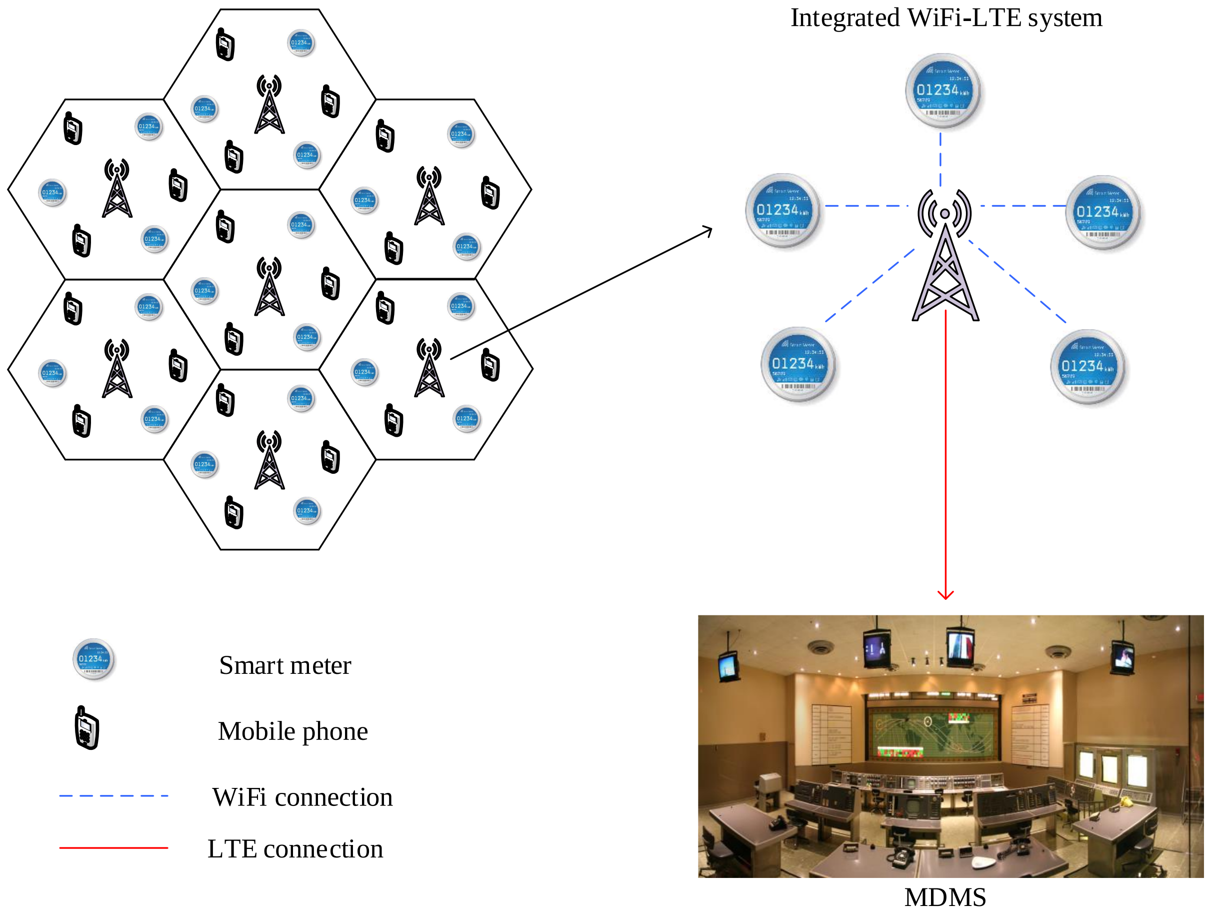

Figure 1: Architecture of smart grid metering infrastructure using LTE and WiFi on a collocated cell layout.

Partnership (3GPP) Release 13, which aims to develop a single global framework [26, 27].

In the literature, mainly three techniques have been proposed for coexistence between WiFi and LTE-U/LAA. They are- 1) listen before talk (LBT); 2) transmission gap; 3) dynamic channel selection. In [28], least congested channel search and adaptation of channel bandwidth are proposed for LTE[2]. Qualcomm proposed an interference level based effective channel selection technique in [29]. If the interference at the operating channel crosses the threshold value, LTE alters the channel with interference measurement before and during operation at both the network and equipment side. In Japan and Europe, LBT is compulsory for data transmission in the unlicensed band. The LBT techniques can be divided into two groups- frame based equipment (FBE) and load based equipment (LBE). In FBE based LBT, a fixed slot of frame is reserved for transmission where CCA is performed [30, 31]. If the channel is empty, the transmission is attempted. Otherwise, it will wait for the next frame. On the other hand, LBE based LBT is demand driven and the user equipment finds a clear channel for transmission [32, 33]. It performs extended CCA (ECCA) for clear channel access. Carrier aggression from licensed to public band is introduced in [34] using clear-to-send (CTS) and request-to-send (RTS) together with LBT. In [35], a technique of blank subframe allocation is introduced in LTE subframe, in which WiFi transmits. In [36], a identical approach is proposed, where n out of 5 sub-frames of LTE is reserved for the transmission of WiFi.

In [13], the coexistence performance of hot-spot indoor scenario is explored using a semi-static system level simulator. The study found that WiFi's performance deteriorated more significantly than the performance of LTE when operated in the same band. In [37], the similar result has been found for coexistence system of ZigBee and LTE, where the performance of ZigBee is affected more compared to that of LTE. [38] explored the usage of different communication networks and recommended to use LTE for low density scenarios (i.e. rural regions) and WiFi for high density scenarios (i.e. urban regions). Meter data communication using the hybrid WiFi/LTE configuration is introduced in [39], where LTE is kept on the upper layer and WiFi in the bottom layer. However, LTE and WiFi uses different spectrum bands in this architecture and there is no spectrum sharing aspect in this study.

In our study, we introduce a fixed duty cycle based coexistence for AMI of smart grid, where LTE and WiFi shares the same spectrum band. Additionally, we consider an integrated LTE-WiFi system where LTE BS and WiFi APs are connected through IP layer. WiFi is

[2] Unless and otherwise specified, LTE will be considered as LTE-U or LTE-LAA throughout this study.

used for meter-to-meter and meter-to-AP data communication. On the other hand, AP uses LTE to transfer data to MDMS. The duty of LTE transmission can be adjusted based on the data amount.

3 System Architecture

Let us assume, a coexisted network architecture consists of WiFi and LTE (LAA/LTE-U) operating in CBRS, as shown in the Fig. 1. Smart meters utilize WiFi and APs utilitie LTE for data transfer, in contrast. In addition, LTE BS and WiFi AP are attached together in the collocated environment. WiFi APs collect smart meters' data and forward them to the interconnected LTE BS. Afterwards, LTE BSs transfer data to MDMS through long range communication. Fig. 2 illustrates the protocol mapping of different components of LTE network and WiFi system. The PHY layers of WiFi AP and smart meters are connected together through wireless channel. Additionally, the IP layers of LTE BS and WiFi AP are integrated together in our proposed configuration. The data exchange among enhanced packet core (EPC), LTE BS, and MDMS are carried out according to standard LTE system [1].

We assume, the sets of LTE BS, WiFi STAs (i.e. smart meter), WiFi APs (i.e. collector of data from meters), and LTE UE (i.e. MDMS and other UEs) are marked as S_l, U_w^i, S_w, and U_l^j, respectively. Besides, LTE BS j, LTE UE/MDMS m, WiFi AP i, and meter/WiFi STA l transmission power are denoted by p_r^j, p_r^m, p_r^i, and p_r^l.

The channel gain values from LTE UE a to WiFi AP j, from WiFi STA/meter x to WiFi AP j, from LTE BS $b(i \neq b)$ to WiFi j and, from LTE BS i to WiFi AP j are $h_{j,r}^a$, $h_{j,r}^x$, $h_{j,r}^b$, and $h_{j,r}^i$ respectively.

During the data reception, the signal to interference plus noise ratio (SINR) of WiFi AP j from meter/WiFi STA x at the r the resource block [40] is

$$\mathrm{SINR}_{j,r}^x = \frac{h_{j,r}^x p_r^j}{\sum h_{j,r}^a p_r^a + \sum h_{j,r}^i p_r^i + \sum h_{j,r}^b p_r^b + \sigma^2}, \quad (1)$$

where σ^2 is the noise variance. A low SINR results poor throughput whereas high SINR ensures good throughput.

The received bit N_B^x at WiFi AP j from WiFi STA x [40] is given by

$$N_\mathrm{B}^x = \mathrm{BT} \sum \log_2(1 + \mathrm{SINR}_{j,r}^x), \quad (2)$$

where B and T (T=$\sum r$) are the bandwidth and transmission time, respectively. The received bit number is dependent on the SINR value.

The throughput of WiFi STA/meter x during the up link (UL) can be expressed [40] as

$$C^x = \frac{N_\mathrm{B}^x}{T_\mathrm{tx} + T_\mathrm{wait}}, \quad (3)$$

where T_wait and T_tx represent the wait time and transmission time of WiFi, respectively.

For down-link capacity calculation, similar equations: (1)-(3) are applicable.

The arrival rate of traffic for both WiFi and LTE is λ. The function relating delay of incoming packets (d) [40] is then

$$f(d) = \lambda e^{\lambda d}. \quad (4)$$

4 Deployment Scenario and Simulation Results

As illustrated in Fig. 1, a coexisted network layout of 7 cells is considered to investigate the system performance. A Matlab simulator founded on 3GPP standard was used for simulation similar to [13, 41]. For each integrated WiFi AP and LTE BS, 10 LTE UEs and 10 smart meters (WiFi STAs) are dropped randomly in each cell. One of the 10 LTE UEs is used as the MDMS. For both WiFi and LTE, the data arrival rate is kept same as $\lambda_\mathrm{WiFi} = \lambda_\mathrm{LTE} = 2.5$ packets/second. The PHY and MAC layer of IEEE 802.11n and LTE are enforced in the simulation scenario. Single UE is scheduled for DL/UL during a transmission time interval (TTI) and the corresponding SINR is sent to the BS. During one subframe of transmission, bandwidth is divided among all UEs based on request and waiting LTE UEs. TABLE 2 summarizes the simulation parameter for LTE, where values were chosen according to 3GPP LTE standard [12].

Enhanced distributed channel access (EDCA) and advanced clear channel assessment (CCA) have been enforced for WiFi channel access mechanism i.e. CSMA/CA. After receiving a beacon signal, all WiFi STAs (i.e. meters) with traffic will be in competition for accessing channel. Data transmission or reception will be at postponed without receiving a beacon signal.

Table 2: PHY and MAC Layer Parameters for LTE.

Parameter	Value
Frequency band	3.5 GHz
Bandwidth	20 MHz
Transmission power of DL transmission	15 dBm
Velocity of UEs	0 ms
Transmission power of UL transmission	PL Based TPC
Frame duration	10 ms
Type of scheduling	Round Robin
P_0	-106 dBm
TTI	1 ms
Packet arrival rate (λ)	2.5

The WiFi STA will sense for a free channel before any kind of transmission. Transmission will take place only if the channel is in idle, otherwise it will back off. After a randomly chosen back off time, next transmission

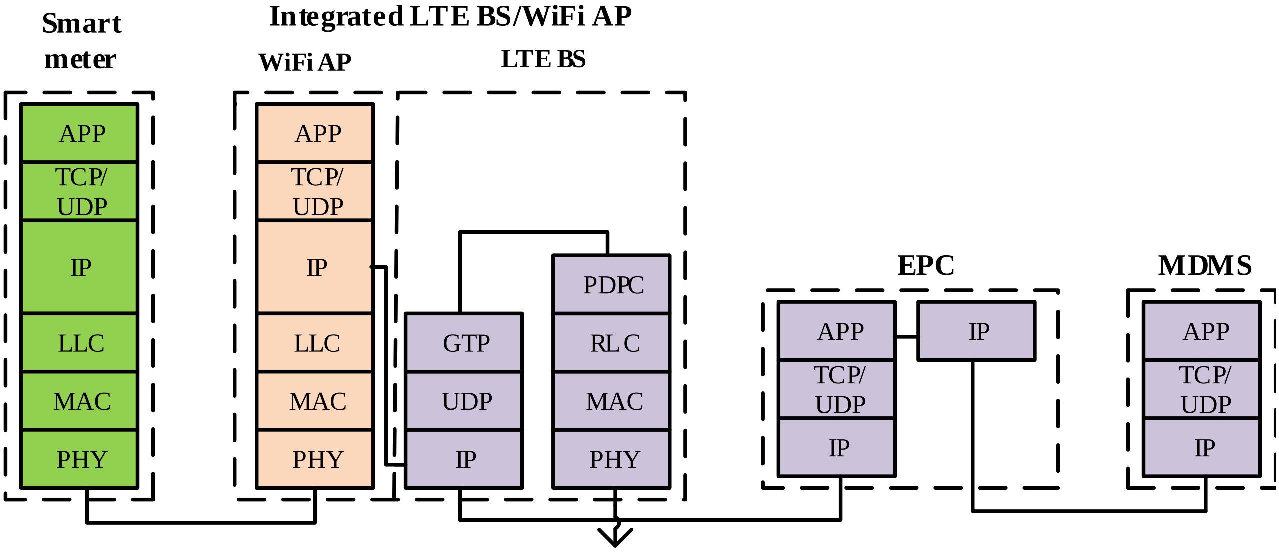

Figure 2: Protocol mapping among various entities of LTE and WiFi system.

will be attempted. TABLE 3 summarizes the WiFi simulation parameter used in the simulation [13, 18, 42].

The abstract of PHY layer is used for calculating Shannon capacity of LTE and WiFi at the $4\mu s$ granularity of WiFi OFDM symbol period. FTP traffic model-2 is applied for both LTE and WiFi traffic [43]. In this study, duty cycles- 20%, 40%, 60% and 80% of 50 ms time period are utilized for LTE transmission and the rest of 50 ms, i.e. 80%, 60%, 40% and 20% are used for WiFi transmission, respectively. The data rate performance of coexisting WiFi and LTE system is presented in Table 4. For 20% duty cycle, the LTE throughput is 10.3 Mbps and the throughput of WiFi is 155.2 Mpbs.

Table 3: PHY and MAC Layer Parameters for WiFi.

Parameter	Value
Frequency band	3.5 GHz
Bandwidth	20 MHz
Transmission power of Downlink/Uplink	23 dBm
Velocity of STA/meter	0 ms
Category of access	Best Effort
Protocol for MAC layer	EDCA
Sensing threshold of CCA	-82 dBm
Energy detection threshold of CCA	-65 dBm
Number of PPDU service bits	16 bits
Number of PPDU tail bits	12 bits
Window size for contention	$\mathcal{U}(0,31)$
Noise figure	6
Interval for beacon transmission	100 ms
Threshold of symbol detection in OFDM	10 dB
Threshold of beacon error ratio	15
Arrival rate of packets (λ)	2.5

For 40% duty cycle of LTE, the throughput of LTE and WiFi are 18.8 Mbps and 111.78 Mbps, respectively. For 60% duty cycle of LTE, the throughput of LTE and WiFi are 36.3 Mbps and 36.1 Mpbs, respectively. The throughput of LTE is boosted to 38.6 Mbps after increasing the duty cycle of LTE to 80%. However, WiFi capacity is reduced to 31.2 Mbps. Therefore, for increment of LTE transmission duty cycle, the LTE capacity is improved and WiFi is degraded drastically. The reason behind the WiFi throughput degradation is the increased transmission back off on the extended period of LTE transmission.

The energy efficiency (EE) performance of coexisted systems is demonstrated in Table 5. It is noted that the EE of LTE is improved with the increment of duty cycle of LTE. The EEs of LTE at 20% and 80% duty cycle are 3.32×10^8 bits/joule and 1.245×10^9 bits/joule, respectively. On the other hand, the EE of WiFi is degraded with the increase of LTE duty cycle. The EEs of WiFi at 20% and 80% duty cycle of LTE are 7.76×10^8 bits/joule and 1.56×10^8 bits/joule, respectively. More significantly, the overall EE of the coexisted system continues to improve with the increment of LTE transmission duty cycle. The overall EE is boosted from 1.008×10^9 bits/joule to 1.401×10^9 bits/joule. This reflects a good neighborhood relationship between LTE and WiFi regardless of degradation of overall throughput of the coexisted system.

The SINR distribution of coexisting LTE and WiFi system is illustrated in Fig. 3. For 20% and 40% duty cycle of LTE transmission, WiFi has better SINR distribution over LTE system. This is reflected in Fig. 3(a) and Fig. 3(b). For the increment of LTE duty cycle to 60% and 80%, the SINR of LTE system improves while the SINR of WiFi degrades consequently. This is demonstrated in Fig. 3(c) and Fig. 3(d), respectively.

In urban or suburban areas, large number of smart meters will use WiFi for sending consumption data to AP, and later the collected data will be sent to MDMS using LTE. Therefore, more opportunity of accessing channel by WiFi is desirable in this case. In this regard, 20% and 40% duty cycle of LTE transmission can be prudent choice for AMI infrastructure. On the other

Table 4: Capacity of the coexisted LTE-WiFi system

Duty cycle	LTE			WiFi		
	Down link (bits/second)	Up link (bits/second)	Total (bits/second)	Down link (bits/second)	Up link (bits/second)	Total (bits/second)
20%	9.15×10^{6}	1.153×10^{5}	1.030×10^{7}	8.343×10^{7}	7.176×10^{7}	1.552×10^{8}
40%	1.667×10^{7}	2.17×10^{6}	1.884×10^{7}	6.435×10^{7}	4.742×10^{7}	1.1178×10^{8}
60%	2.81×10^{7}	8.16×10^{6}	3.63×10^{7}	2.45×10^{7}	1.16×10^{7}	3.61×10^{7}
80%	2.71×10^{7}	1.15×10^{7}	3.86×10^{7}	1.66×10^{7}	1.46×10^{7}	3.12×10^{7}

Table 5: Energy efficiency performance of coexisted LTE-WiFi system

Duty cycle	LTE (bits/joule)	WiFi (bits/joule)	Total (bits/joule)
20%	3.32×10^{8}	7.76×10^{8}	1.008×10^{9}
40%	6.07×10^{8}	5.58×10^{8}	1.17×10^{9}
60%	1.171×10^{9}	1.80×10^{8}	1.351×10^{9}
80%	1.245×10^{9}	1.56×10^{8}	1.401×10^{9}

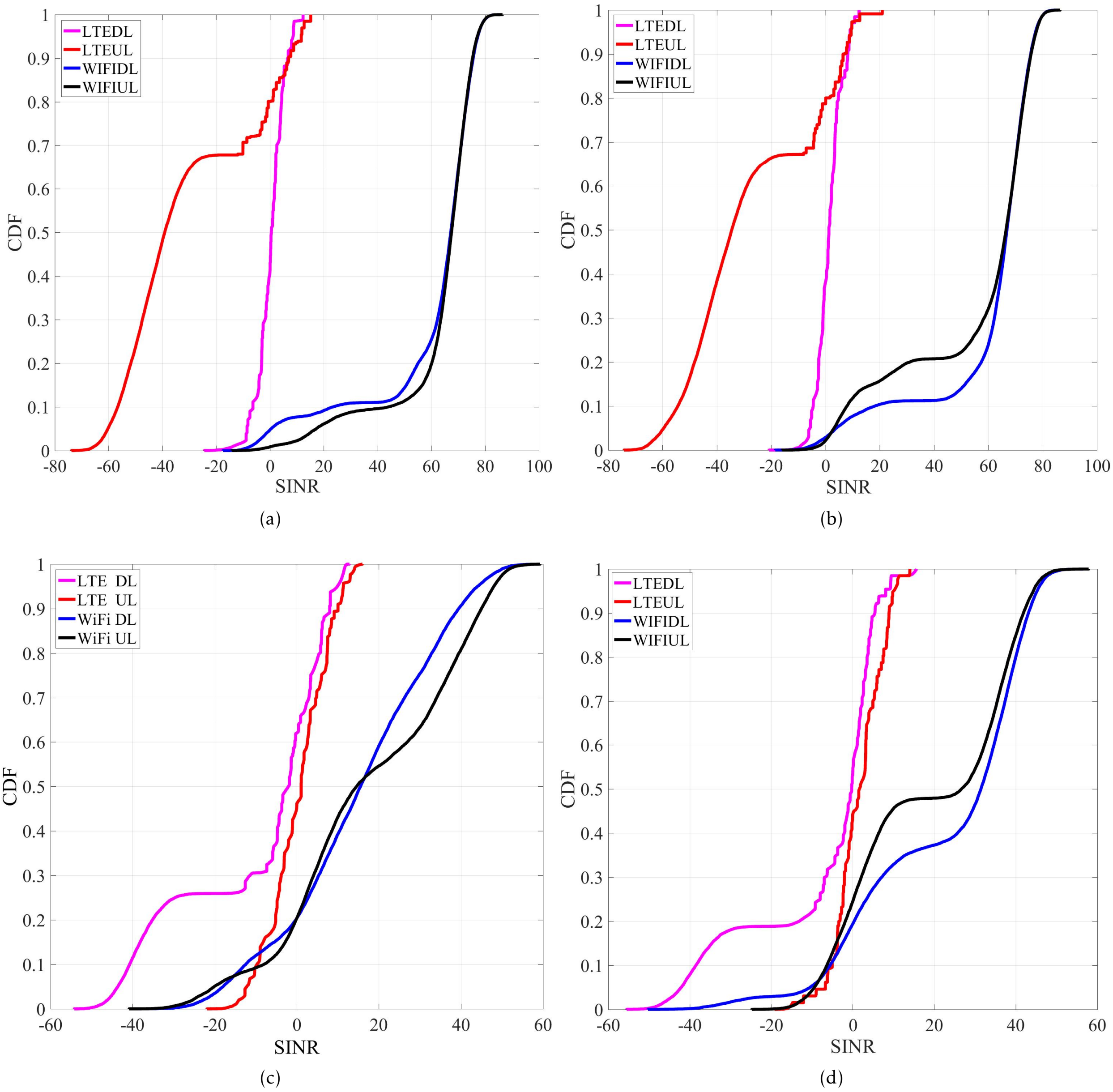

Figure 3: SINR distribution of coexisted LTE-WiFi system (a) SINR distribution at 20% duty cycle (b) SINR distribution at 40% duty cycle (c) SINR distribution at 60% duty cycle (d) SINR distribution at 80% duty cycle

hand, in the rural areas, scattered and limited number of meters will use WiFi. Therefore, in this case, more access can be given to LTE by selecting higher duty cycles such as 60% and 80%.

5 Conclusion

In this study, a collocated WiFi and LTE based advance metering infrastructure is proposed for smart grid. For meter-to-meter data communication, WiFi is proposed. On the other hand, for sending collected data from a group of meters to MDMS, LTE is proposed. A fixed duty cycle of a transmission time is reserved for LTE and the rest of the period is given to WiFi system. The simulation performance shows a harmonious neighborhood spectrum sharing between LTE and WiFi. With the increase of LTE duty cycle, the throughput, energy efficiency and SINR of LTE are improved along with degradation of those of WiFi.

The transmission duty cycle of LTE is adjustable based on the amount of data and number of smart meters. In particular, lower duty cycle of LTE transmission can be selected for urban and suburban areas where the density of smart meters are high and meters need more access to WiFi. On the other hand, higher duty of LTE transmission can be selected for rural areas where the density of smart meter is low. The CBRS band has a big amount of free, underutilized, and clean spectrum for wireless network. So, network consists of coexisting LTE and WiFi in CBRS band can be a viable communication solution for the metering infrastructure of smart grid.

Acknowledgment The work is a outcome of the research supported by the U.S. National Science Foundation under the grant CPS-1446570 and CAREER-1553494.

References

[1] A. F. Molisch, *3GPP LongTerm Evolution*. Wiley-IEEE Press, 2011, pp. 665–698. [Online]. Available: http://ieeexplore.ieee.org/xpl/articleDetails.jsp?arnumber=5635449

[2] I. Parvez, M. Jamei, A. Sundararajan, and A. I. Sarwat, "RSS based loop-free compass routing protocol for data communication in advanced metering infrastructure (AMI) of Smart Grid," in *2014 IEEE Symposium on Computational Intelligence Applications in Smart Grid (CIASG)*, Dec 2014, pp. 1–6.

[3] I. Parvez, A. I. Sarwat, J. Pinto, Z. Parvez, and M. A. Khandaker, "A gossip algorithm based clock synchronization scheme for smart grid applications," *CoRR*, vol. abs/1707.08216, 2017. [Online]. Available: http://arxiv.org/abs/1707.08216

[4] M. Jafari, T. O. Olowu, and A. I. Sarwat, "Optimal smart inverters volt-var curve selection with a multi-objective volt-var optimization using evolutionary algorithm approach," in *2018 North American Power Symposium (NAPS)*, Sep. 2018, pp. 1–6.

[5] I. Parvez, A. Islam, and F. Kaleem, "A key management-based two-level encryption method for ami," in *2014 IEEE PES General Meeting — Conference Exposition*, July 2014, pp. 1–5.

[6] I. Parvez, A. I. Sarwat, L. Wei, and A. Sundararajan, "Securing metering infrastructure of smart grid: A machine learning and localization based key management approach," *Energies*, vol. 9, no. 9, 2016.

[7] I. Parvez, F. Abdul, and A. I. Sarwat, "A location based key management system for advanced metering infrastructure of smart grid," in *2016 IEEE Green Technologies Conference (GreenTech)*, April 2016, pp. 62–67.

[8] M. O. Onibonoje and T. O. Olowu, "Real-time remote monitoring and automated control of granary environmental factors using wireless sensor network," in *2017 IEEE International Conference on Power, Control, Signals and Instrumentation Engineering (ICPCSI)*, Sep. 2017, pp. 113–118.

[9] T. O. Olowu, M. Jafari, and A. I. Sarwat, "A multi-objective optimization technique for volt-var control with high pv penetration using genetic algorithm," in *2018 North American Power Symposium (NAPS)*, Sep. 2018, pp. 1–6.

[10] I. Parvez, A. Sundararajan, and A. I. Sarwat, "Frequency band for HAN and NAN communication in Smart Grid," in *Proc. IEEE Symp. on Comp. Intel. App. in Smart Grid (CIASG)*, Dec 2014, pp. 1–5.

[11] I. Parvez, A. Rahmati, I. Güvenç, A. I. Sarwat, and H. Dai, "A Survey on Low Latency Towards 5G: RAN, Core Network and Caching Solutions," *CoRR*, vol. abs/1708.02562, 2017. [Online]. Available: http://arxiv.org/abs/1708.02562

[12] 3GPP, "Study on Licensed-Assisted Access using LTE," RP-141397, Tech. Rep., Sep. 2014.

[13] N. Rupasinghe and İ. Güvenç, "Licensed-assisted access for WiFi-LTE coexistence in the unlicensed spectrum," in *Proc. IEEE Glob. Work.(GC Wkshps)*. IEEE, 2014, pp. 894–899.

[14] F. Chaves, A. Cavalcante, E. Almeida, F. Abinader Jr, R. Vieira, S. Choudhury, and K. Doppler, "LTE/Wi-Fi coexistence: Challenges and mechanisms," in *2013, XXXI SIMPOSIO BRASILEIRO DE TELECOMUNICACOES–SBrT2013*, 2013.

[15] FCC, "Amendment of the Commissions Rules with Regard to Commercial Operations in the 3550-3650 MHz Band," Report and Order and Second Further Notice of Proposed Rulemaking, Apr. 2015.

[16] L. Stefani, "The FCC Raises the Curtain on the Citizens Broadband Radio Service," CommLawBlog Article, May 2015. [Online]. Available: http://www.commlawblog.com/2015/05/articles/unlicensed-operations-and-emer/the-fcc-raises-the-curtain-on-the-citizens-broadband-radio-service/

[17] G. Locke and L. E. Strickling, "An assessment of the near-term viability of accommodating wireless broadband systems in the 1675-1710 MHz, 1755-1780 MHz, 3500-3650 MHz, and 4200-4220 MHz, 4380-4400 MHz bands," Report, Oct. 2010. [Online]. Available: http://www.ntia.doc.gov/files/ntia/publications/fasttrackevaluation11152010.pdf

[18] I. Parvez, M. Sriyananda, İ. Güvenç, M. Bennis, and A. Sarwat, "Cbrs spectrum sharing between lte-u and wifi: A multiarmed bandit approach," *Mobile Information Systems*, vol. 2016, 2016.

[19] S. Rahman, M. Moghaddami, A. I. Sarwat, T. Olowu, and M. Jafaritalarposhti, "Flicker estimation associated with pv integrated distribution network," in *SoutheastCon 2018*, April 2018, pp. 1–6.

[20] I. Parvez, N. Chotikorn, and A. I. Sarwat, "Average quantized consensus building by gossip algorithm using 16 bit quantization and efficient data transfer method."

[21] Y. Mekonnen, M. Haque, I. Parvez, A. H. Moghadasi, and A. I. Sarwat, "LTE and wi-fi coexistence in unlicensed spectrum with application to smart grid: A review," *CoRR*, vol. abs/1708.09005, 2017. [Online]. Available: http://arxiv.org/abs/1708.09005

[22] I. Parvez, T. Khan, A. I. Sarwat, and Z. Parvez, "Laa-lte and wifi based smart grid metering infrastructure in 3.5 ghz band," in *2017 IEEE Region 10 Humanitarian Technology Conference (R10-HTC)*, Dec 2017, pp. 151–155.

[23] X. Wang, S. Mao, and M. X. Gong, "A survey of lte wi-fi coexistence in unlicensed bands," *GetMobile: Mobile Computing and Communications*, vol. 20, no. 3, pp. 17–23, 2017.

[24] A. Babaei, J. Andreoli-Fang, Y. Pang, and B. Hamzeh, "On the impact of LTE-U on Wi-Fi performance," *International Journal of Wireless Information Networks*, vol. 22, no. 4, pp. 336–344, 2015.

[25] M. Sriyananda, I. Parvez, I. Güvene, M. Bennis, and A. I. Sarwat, "Multi-armed bandit for LTE-U and WiFi coexistence," in *Proc. IEEE Wire. Commun. and Netw. Conf.* IEEE, 2016, pp. 1–6.

[26] G. RP-140808, "Review of regulatory requirements for unlicensed spectrum)," AlcatelLucent, Alcatel-Lucent Shanghai Bell, Ericsson, Huawei, HiSilicon, IAESI, LG, Nokia, NSN, Qualcomm, NTT Docomo, Tech. Rep., June 2014.

[27] Nokia, "Nokia LTE for unlicensed spectrum," AlcatelLucent, Alcatel-Lucent Shanghai Bell, Ericsson, Huawei, HiSilicon, IAESI, LG, Nokia, NSN, Qualcomm, NTT Docomo, Tech. Rep., June 2014.

[28] F. M. Abinader, E. P. L. Almeida, F. S. Chaves, A. M. Cavalcante, R. D. Vieira, R. C. D. Paiva, A. M. Sobrinho, S. Choudhury, E. Tuomaala, K. Doppler, and V. A. Sousa, "Enabling the coexistence of LTE and Wi-Fi in unlicensed bands," *IEEE Commun. Mag.*, vol. 52, no. 11, pp. 54–61, Nov. 2014.

[29] Qualcomm, "Qualcomm Research LTE in Unlicensed Spectrum: Harmonious Coexistence with WiFi," 3GPP RAN1 standard contribution, Tech. Rep., Jun. 2014.

[30] ZTE, "Frame structure design for LAA considering LBT," 3GPP TSG RAN WG1 Meeting no.80, Feb. 2015.

[31] R. Zhang, M. Wang, L. X. Cai, X. Shen, L.-L. Xie, and Y. Cheng, "Modeling and analysis of MAC protocol for LTE-U co-existing with Wi-Fi," in *Proc. IEEE Glob. Commun. Conf. (GLOBECOM)*. IEEE, 2015, pp. 1–6.

[32] O. El-Samadisy, M. Khedr, and A. El-Helw, "Performance Evaluation of MAC for IEEE 802.11 and LAA LTE," in *Proc. Intern. Conf. on Comput. Science and Comput. Intell. (CSCI)*, Dec 2016, pp. 923–928.

[33] A. k. Ajami and H. Artail, "Fairness in future licensed assisted access (laa) lte networks: What happens when operators have different channel access priorities?" in *Proc. IEEE Intern. Conf. on Commun. Works. (ICC Workshops)*, May 2017, pp. 67–72.

[34] R. Ratasuk, M. A. Uusitalo, N. Mangalvedhe, A. Sorri, S. Iraji, C. Wijting, and A. Ghosh, "License-exempt LTE deployment in heterogeneous network," in *Int. Symp. on Wireless Commun. Sys.*, Paris, France, Aug. 2012, pp. 246–250.

[35] E. Almeida, A. M. Cavalcante, R. C. D. Paiva, F. S. Chaves, F. M. Abinader, R. D. Vieira, S. Choudhury, E. Tuomaala, and K. Doppler, "Enabling LTE/WiFi coexistence by LTE blank subframe allocation," in *Proc.IEEE Int. Conf.*, Budapest, Hungary, Jun. 2013, pp. 5083–5088.

[36] T. Nihtil, V. Tykhomyrov, O. Alanen, M. A. Uusitalo, A. Sorri, M. Moisio, S. Iraji, R. Ratasuk, and N. Mangalvedhe, "System performance of LTE and IEEE 802.11 coexisting on a shared frequency band," in *Proc. IEEE Wireless Commun. and Net. Conf.(WCNC)*, Shanghai, China, Apr. 2013, pp. 1038–1043.

[37] I. Parvez, N. Islam, N. Rupasinghe, A. I. Sarwat, and . Gven, "LAA-based LTE and ZigBee coexistence for unlicensed-band smart grid communications," in *Proc. IEEE SoutheastCon conf.*, March 2016, pp. 1–6.

[38] F. Granelli, D. Domeniconi, N. L. S. D. Fonseca, and B. Tsetsgee, "On the usage of wifi and lte for the smart grid," in *2014 7th International Conference on Ubi-Media Computing and Workshops*, July 2014, pp. 1–5.

[39] F. Koohifar, N. Saputro, I. Guvenc, and K. Akkaya, "Hybrid wi-fi/lte aggregation architecture for smart meter communications," in *2015 IEEE International Conference on Smart Grid Communications (SmartGridComm)*, Nov 2015, pp. 575–580.

[40] N. Rupasinghe and . Gven, "Licensed-assisted access for wifi-lte coexistence in the unlicensed spectrum," in *2014 IEEE Globecom Workshops (GC Wkshps)*, Dec 2014, pp. 894–899.

[41] I. Parvez, N. Islam, N. Rupasinghe, A. I. Sarwat, and . Gven, "LAA-based LTE and ZigBee coexistence for unlicensed-band smart grid communications," in *SoutheastCon 2016*, March 2016, pp. 1–6.

[42] M. G. S. Sriyananda, I. Parvez, I. Gvene, M. Bennis, and A. I. Sarwat, "Multi-armed bandit for LTE-U and WiFi coexistence in unlicensed bands," in *2016 IEEE Wireless Communications and Networking Conference*, April 2016, pp. 1–6.

[43] 3GPP, "Evolved Universal Terrestrial Radio Access (E-UTRA); Further advancements for E-UTRA physical layer aspects (Release 9)," 3GPP Technical Report, Tech. Rep., Mar. 2010.

Advances in Science, Technology and Engineering Systems Journal Vol. 4, No. 2, 78-82 (2019)

www.astesj.com

Special Issue on Advanced Electrical and Communication Technologies

ASTESJ
ISSN: 2415-6698

Novel CPW-fed UWB antenna for X-band applications

Qaddi Mohamed Hamza*[1], Srifi Mohamed Nabil[1], Mharzi Hassan[2]

[1]*Telecommunication Systems Research Group, National School of Applied Sciences, Ibn Tofail University Kenitra, Morocco*

[2]*Laboratory of Electric Engineering, Computing and Mathematical Sciences National School of Applied Sciences, Ibn Tofail University Kenitra, Morocco*

A R T I C L E I N F O

Article history:
Received: 28 January, 2019
Accepted: 28 February, 2019
Online: 15 March, 2019

Keywords:
CPW-fed
Ultra-wide band (UWB)
X-band
Patch antenna
Slot

A B S T R A C T

An ultra-wideband (UWB) printed antenna (PMA) powered by a compact coplanar waveguide (CPW) is featured. The propounded antenna is supposed to cover the UWB range from 7 GHz to 10 GHz, with return loss values below −10 dB in the whole frequency range, for X-band applications, often used for dense satellite communications. The 30 x 35 x 1.6 mm3 antenna is mounted on a dielectric substrate named FR-4 with thickness h=1.6mm, relative permittivity εr=4.3 and loss tangent of 0.025. All the conception and simulated results are realized using the 3D Electromagnetic Simulator software CST Microwave Studio. The results show wide bandwidth and good omnidirectional radiation patterns in the operating band, with a very reduced size. The global satisfying achievement with a very simple structure and small size makes the propounded antenna attractive for use in ultra-wide band (UWB) systems, especially for X-band applications.

1. Introduction

In recent years, there have been new and different mobile standards established in the context of the explosive growth in wireless services that require both higher communication data rate and larger bandwidth. Ultra-Wide Band (UWB) antennas have shown a renewed interest since the allocation by the Federal Communication Commission (FCC) of the bandwidth from 3.1 to10.6 GHz in 2002 [1-2]. This allocation has excited antenna designers to seek for challenging designs of low-cost UWB antennas.

Ultra-wideband technology is potentially the most adequate technologies for future wireless communication system due to various satisfying factures such as ultra-wide bandwidth, low power consumption, high data rate transmission and admirable immunity to multi-patch interference.

A variety of antenna's models have been explored for UWB applications [3-5]. Nevertheless, the operating band of UWB communication systems includes other frequency bands. Therefore, UWB communication systems may generate interference with those bands. To overcome problems caused by electromagnetic interference (EMI) from UWB to other applications, a new antenna for X-band applications is introduced to avoid possible interferences with existing communication systems running over the whole range of UWB. Different methods for generating CP waves were investigated [6-7]. Coplanar waveguide (CPW) feed antennas with slots are broadly used in many applications because of their advantageous qualities like one metallic layer, simple integration and low profile and wide impedance bandwidth

The propounded antenna is designed utilizing slots of many forms in the radiating patch.

In this paper, a CPW-fed UWB antenna design method is presented, using U shape slot. The operating mechanism and design methodology of the antenna are investigated. The remaining of this paper organized as follows. Section 2 presents the configuration and the parametric study of our antenna. Simulation results accompanied with some discussions are presented in the third Section. In the end, Section 4 summarizes the paper.

2. Antenna Design and Configuration

Normally, the bandwidth of a micro-strip antennas is not very broad, they have narrow bandwidth. Therefore, to conceive an UWB antenna, the conventional technique consist on cutting slots of various forms in the radiating patch is required. The structure of

*Corresponding Author: QADDI Mohamed Hamza, 27 Bir Rami EST, Kenitra, Morocco, Cell No; +212 661634417, qaddihamza@gmail.com

the antenna is depicted in Figure 1. To improve the bandwidth of the propounded antenna, the radiating element is modified by cutting U-shaped slots on its middle [8-10]. Many methods have been already employed in the design in order to obtain wideband antennas by using Different slot shapes that are available and explored by various researchers [11-13]. Among rectangular slot, T-H-L shaped slots and many others, U-slot antennas have proven to be advantageous in that context [14-16]. Although, placement and design of the slots is more challenging than the other methods.

The antenna includes a rectangular patch which is fed by a common coplanar waveguide (CPW) transmission line, mounted on the dielectric substrate FR4-lossy, with thickness h=1.6 mm, relative permittivity εr=4.3 and loss tangent of 0.025, having dimensions of 30 x 35 x 1.6 mm3.

The choice of CPW is due to its easy unification with slots and also to its uniplanar and conformal shape. To ensure a 50-Ω characteristic impedance, the width of the CPW feeder line is fixed at 3.6 mm. A transmission line with characteristic impedance Z_0 can simply represent CPW in the equivalent circuit model. Closed-form expressions are given in [17] For the effective dielectric constant and characteristic impedance of CPW. The small gap between the radiating element and the ground plane is the main reason in the excessive capacitive coupling. The manufacturing of the antenna is very simple and inexpensive as both the radiating element and the ground plane are implemented on the same plane, only a single-sided metallization substrate with one layer is utilized [18].

The antenna's features have been optimized through CST Microwave Studio with Time-domain solver, a market-oriented electromagnetic simulator relying on finite integration technique. The optimized antenna's parameters of the are listed in Table 1 and the flow chart presenting the design methodology of the CPW-fed ultra-wideband antenna is depicted in Figure 2.

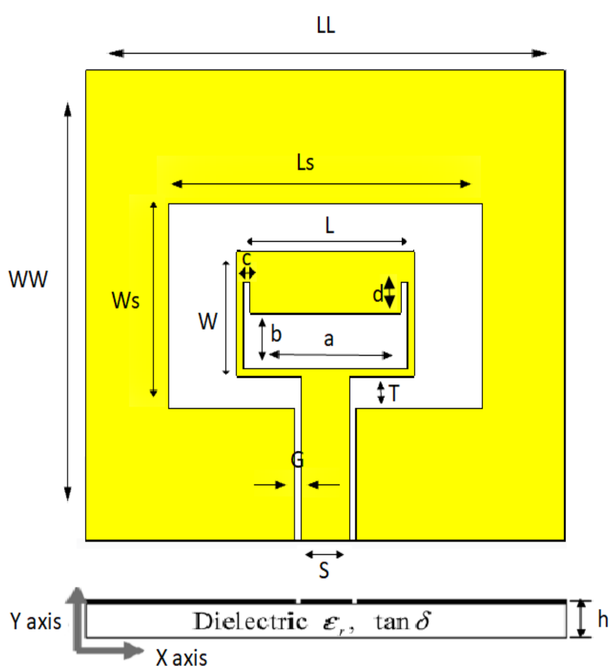

Figure 1 Propounded UWB antenna's structure

Table 1 parameter values of the propounded antenna

Parameters	Values (mm)
LL	35
WW	30
Ls	23
Ws	13
L	13
W	8
T	2
G	0.5
S	3.6
h	1.6
Mt	0.07
a	12
b	3.5
c	0.5
d	2

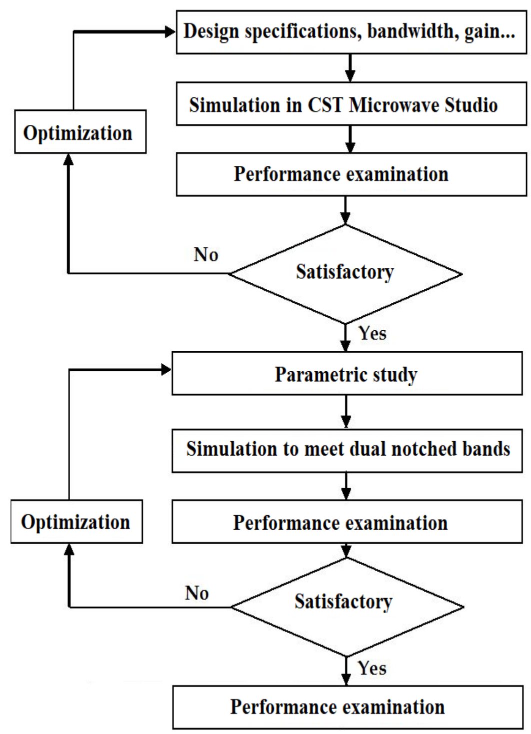

Figure 2 Flow chart of the CPW-fed Ultra-wideband antenna

3. Results and Discussions

Evidently, the simulation results provide a broadband with a -10dB from 7 to 9.9 GHz with two resonant frequencies at 7.65 and 9 GHz, respectively. Figure 3 illustrates the simulated reflection coefficient of the antenna. Apparently, the above achieved bandwidth covers the entire UWB spectrum for X-band applications.

The simulated result of our UWB antenna with and without slots is shown in Figure 4. The slots are made on the radiating element to get rid of the notched band.

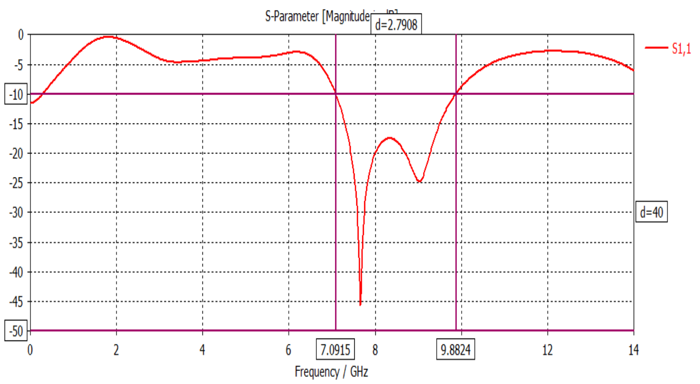

Figure 3 Simulated reflection coefficient of the propounded antenna

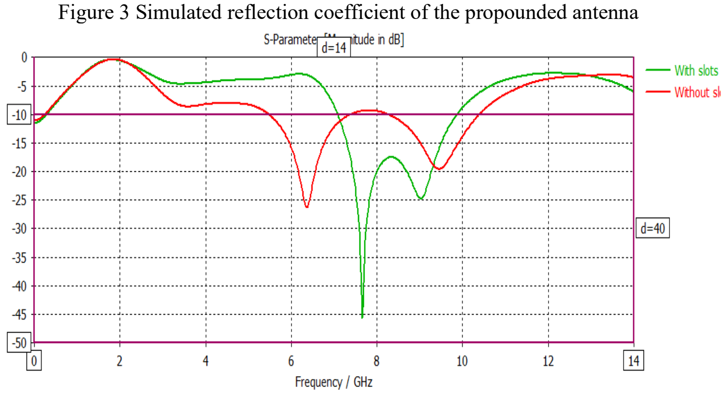

Figure 4 Simulated reflection coefficient of the propounded antenna with and without slots

By analyzing the effect of the width and the length of the slot in the radiating element, we aimed to determine the optimum parameters of the slot to achieve the right bandwidth for X-band applications. Figure 5 reveals the impact of the width "d" of the slot on the simulated reflection coefficient of the antenna. It may be noticed that the bandwidth increase as the width increases from 0 to 2mm to match with the X-band. Therefore, the slot width was fixed at 2 mm. Figure 6 illustrates the impact of the length "c" on the simulated reflection coefficient of the antenna. It can be seen that the suitable value of the slot length to match with X-band is 0.5mm. Higher return loss parameter values are observed when slot length increases from 0.5 to 0.75 mm. In summary, by reasonable selection of the length and width of the slot, we can obtain the desired bandwidth. Therefore, we decided on c=0.5mm and d=2mm as the optimum values of the slot.

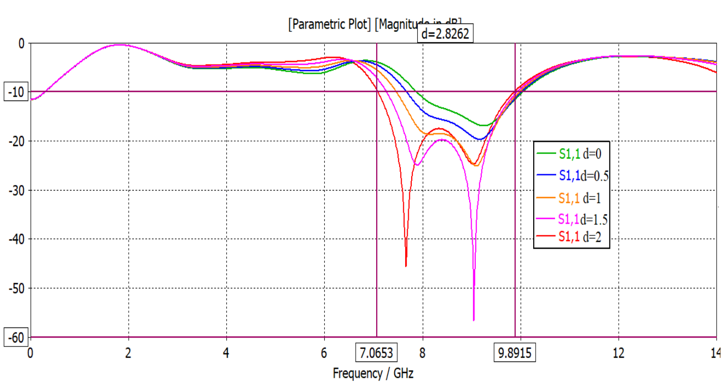

Figure 5 Simulated reflection coefficient response of the propounded antenna as a function of "d". All remaining parameters are identical to those in Table 1.

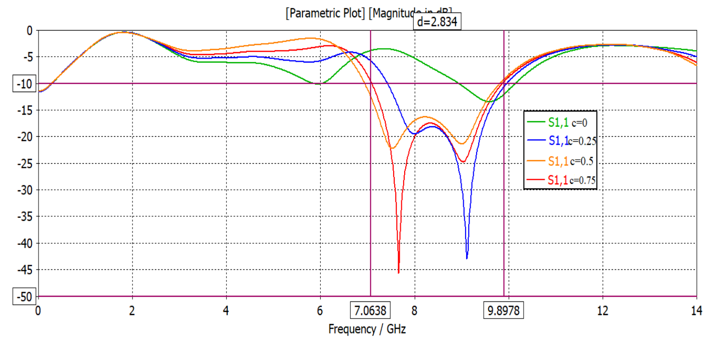

Figure 6 Simulated reflection coefficient response of the propounded antenna as a function of "c". All remaining parameters are identical to those in Table 1.

Regarding the radiation properties of the concept model, the antenna has quasi-invariant radiation characteristics, which is confirmed on the basis of the three-dimensional radiation patterns of the simulations in Figure 7.

From the Figure 8, that presents the E-Plane (XZ plane, Phi=0) radiation patterns at7.65 GHz and 9 GHz, the antenna has an approximate unchanged radiation pattern and the results match the characteristic of UWB systems, which should be possible to receive information signals from all directions. Furthermore, this is supported by the same diagrams of the surface current distributions in Figure 9.

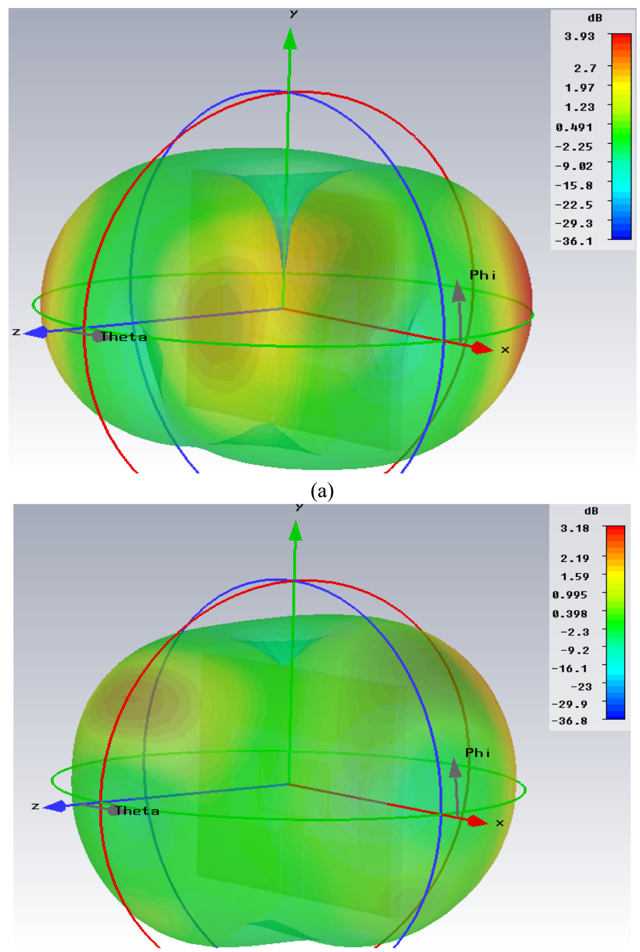

(a)

(b)

Figure 7 3D radiation patterns of the propounded antenna at (a) 7.65 and (b) 9 GHz.

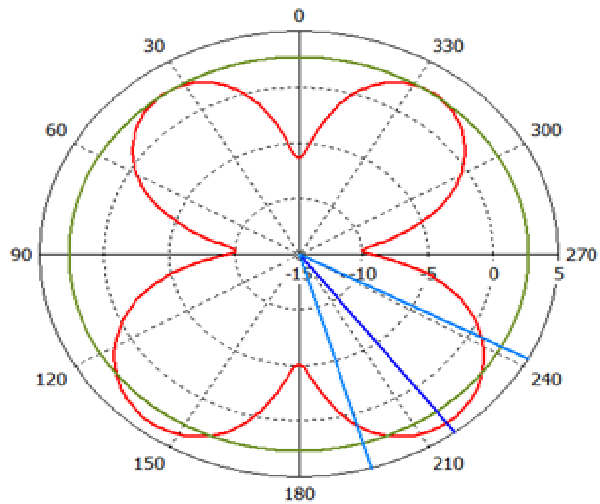

(a)

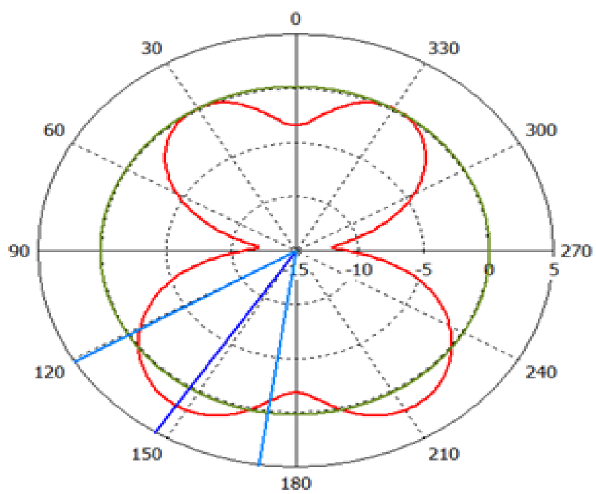

(b)

Figure 8 E-field radiation patterns of the antenna (XZ; Phi=0) at (a) 7.65 GHz and (b) 9GHz

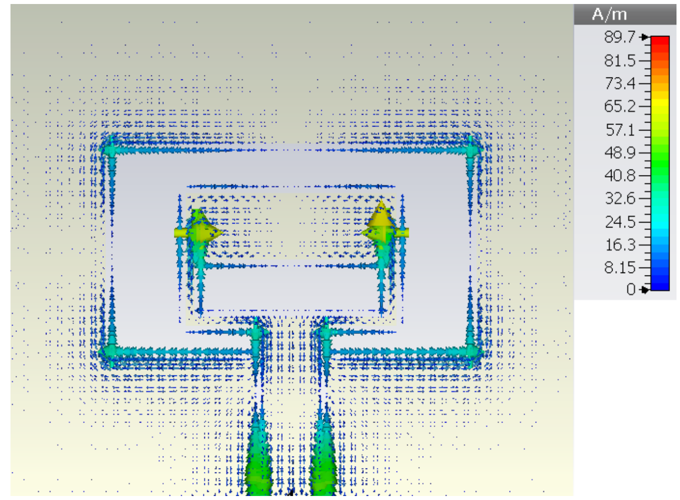

(a)

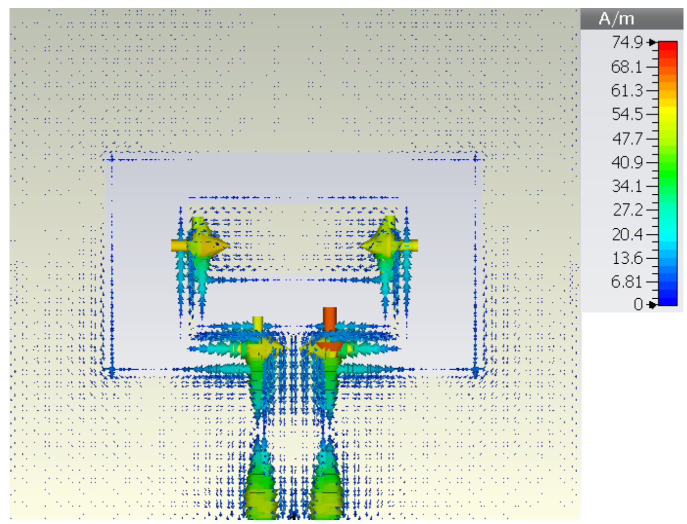

(b)

Figure 9 Surface Current distributions at (a) 7.65 GHz and (b) 9 GHz.

The current distribution over the antenna with slots is shown in Figure 9 at the two resonant frequencies (a) 7.65 and (b) 9 GHz. It can be seen that the current density is highly condensed at the edges of the slots. The currents flow from the feed point of the antenna to the upper part of the radiating element on the same channel for the two resonant frequencies. The current distributions flow principally through the transmission line. Patently, the distribution of the surface current is symmetric over the antenna.

Figure 10 illustrates the radiation efficiency of the CPW-fed UWB antenna. A maximum radiation efficiency of 83% and more than 79% throughout the entire frequency range is achieved by the antenna.

The evaluation of the antenna's performance compared other UWB antennas is demonstrated in Table 2 in terms of their dimensions, bandwidth, gain and applications, in order to support the concept of design. It is found that the propounded antenna shows broad bandwidth impedance, small size, and high gain characteristics which make the antenna appropriate for use in UWB applications, especially X-band applications.

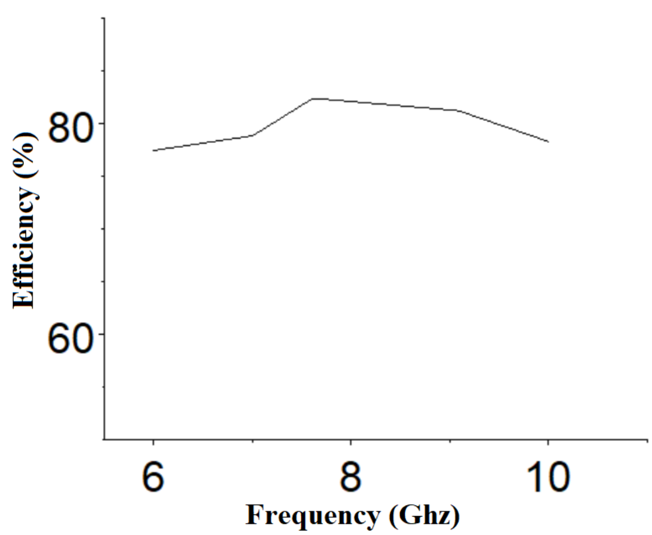

Figure 10 Simulated radiation efficiency of the propounded CPW-fed UWB antenna

Table 2: A summary of the propounded antenna and other previously released work.

References	Dimensions (in mm)	Bandwidth UWB	Gain at resonant frequency (dB)	Applications
[19]	30x29	5.5-12.5	5	UWB applications (C-X-band)
[20]	150x150	4.5-7.47	5	UWB applications (S-X-band)
[21]	20x35	8.15-9.08	‘.46	UWB applications (X-band)
Our work	30x35	7- 9.9	3.18 3.93	UWB applications (X-band)

4. Conclusion

An ultra-wide band (UWB) printed antenna (PMA) powered by a compact coplanar waveguide (CPW)-fed is proposed. The antenna having a total size of 30 x 35 mm² is printed on an inexpensive dielectric substrate named FR-4. The above conception skills are presented to achieve broad bandwidth supported by good impedance matching as well as constant radiation characteristics throughout the entire operating band (7-9.9 GHz). An analysis of the width and the length of the slots in the radiating patch has been given. The antenna design has been assessed through many numerical simulations. Therefore, the propounded antenna is supposed to be a strong competitor for a variety of UWB systems, especially for X-band applications.

References

[1] Federal Communications Commission (FCC) “New Public Safety Applications and Broadband Internet Access among Uses Envisioned by FCC Authorization of Ultra-Wideband Technology”, February 2002.

[2] Federal Communications Commission (FCC), “Revision of Part 15 of the Commission's Rules Regarding Ultra-Wideband Transmission Systems”, First Report & Order, Washington DC, February 2002.

[3] M. Naghshvarian Jahromi, A. Falahati and R.M. Edwards, “Application of fractal binary tree slot to design and construct a dual band-notch CPW-ground-fed ultra-wide band antenna”, *IET Microwaves, Antennas & Propagation,* Vol. 5, pp. 1424-1430, 2011. DOI: 10.1049/iet-map.2011.0025

[4] Y. Shen, C.L.Law, and Z. Shen “A CPW-fed circularly polarized antenna for lower Ultra Wideband application,” *Microwave Opt. Technol. Lett.*,Vol. 51, No. 10, Oct. 2009. https://doi.org/10.1002/mop.24629

[5] M. Hamza QADDI, Marko SONKKI, Sami MYLLYMAKI, Hassan MHARZI, M. Nabil SRIFI, and Heli JANTUNEN, “Novel compact patch antenna for Ultra-wideband (UWB) applications”, *International Journal Of Microwave And Optical Technology,* Vol. 13, pp. 343-350, July 2018.

[6] J. Y. Sze and S. P. Pan “Design of CPW-fed circularly polarized slot antenna with a miniature configuration,” IEEE Trans. Antennas and Wireless Propagation Lett., vol.10, pp.1465-1468, Oct. 2011. DOI: 10.1109/LAWP.2011.2179912

[7] J. Y. Sze and C. C. Chang, “Circularly polarized square slot antenna with a pair of inverted-L grounded strips,” IEEE Trans. Antennas and Wireless Propagation Lett., vol.7, pp.149-151, July 2008. DOI: 10.1109/LAWP.2008.921341

[8] Kharakhili, F. G., M. Fardis, G. Dadashzadeh, A. Ahmadi, and N. Hojjat, “Circular slot with a novel circular microstrip open ended microstrip feed for UWB applications,” Progress In Electromagnetics Research, Vol 68, pp. 161–167, 2007. doi:10.2528/PIER06071901

[9] Marqués, R.; Mesa, F.; Martel J.; Medina, F. “Comparative analysis of edge and broadside coupled split ring resonators for metamaterial design: Theory and experiment”. IEEE Transactions on Antennas and Propagation, Vol. 51, No. 10, pp. 2572-258, October 2003. DOI: 10.1109/TAP.2003.817562

[10] I. Latif, L. Shafai and S. K. Sharma, “Bandwidth Enhancement and Size Reduction of Microstrip Slot Antennas”. IEEE Transactions on Antennas and Propagation, Vol. 53, No. 3, pp. 994-1003, March 2005. DOI: 10.1109/TAP.2004.842674

[11] A. Ibrahim, M. A. Abdalla, and A. Boutejdar, “A Printed Compact Band-Notched Antenna Using Octagonal Radiating Patch and Meander Slot Technique for UWB Applications”, Progress In Electromagnetics Research M, Vol. 54, pp. 153–162, 2017. doi:10.2528/PIERM16122805

[12] Changzhou Hua, Yunlong Lu, and Taijun Liu, “UWB Heart-Shaped Planar Monopole Antenna with a Reconfigurable Notched Band”, Progress In Electromagnetics Research Letters, Vol. 65, pp. 123–130, 2017. doi:10.2528/PIERL16120203

[13] A. Pirooj, M. Naser Moghadasi, F. B. Zarrabi, and A Sharifi, “A Dual Band Slot Antenna for Wireless Applications with Circular Polarization”, Progress In Electromagnetics Research C, Vol. 71, pp. 69–77, 2017. doi:10.2528/PIERC16111401

[14] W. LUI, C. CHENG and H. ZHU, “Improved frequency notched ultra wideband slot antenna using square ring resonator”, IEEE Trans. Antennas Propag., vol 55, No. 9, pp. 2445–2450, 2007. DOI: 10.1109/TAP.2007.904090

[15] A. Farswan, A. K. Gautam, B. K. Kanaujia and K. Rambabu “Design of Koch Fractal Circularly Polarized Antenna for Handheld UHF RFID Reader Applications”, IEEE Transactions on Antennas and Propagation , Vol 64, No 2, Feb. 2016. DOI: 10.1109/TAP.2015.2505001

[16] S. Lakrit, H. Ammor and J. Terhzaz , “Design of H-slot Patch Antenna for Ultra Wideband”, European Journal of Scientific Research , Vol 106 No 2, pp:224-228, 2013.

[17] B. C. Wadell, *Transmission Line Design Handbook*. Boston, MA: Artech House, 1991, pp. 73–76.

[18] Y. C. Lin and K. J. Hung, “Compact ultrawideband rectangular aperture antenna and band-notched designs,” *IEEE Trans. Antennas Propag.*, vol. 54, pp. 3075–3081, Nov. 2006. DOI: 10.1109/TAP.2006.883982

[19] Abdelnasser A. Eldek, Atef Z. Elsherbeni and Charles E. Smith, “Wide-Band Modified Printed Bow-Tie Antenna With Single and Dual Polarization for C– and X-Band Applications”, IEEE TRANSACTIONS ON ANTENNAS AND PROPAGATION, VOL. 53, NO. 9, SEPTEMBER 2005. DOI: 10.1109/TAP.2005.851870

[20] Veeresh G. Kasabegoudar, Dibyant S. Upadhyay, and K. J. Vinoy, “Design Studies of Ultra-Wideband Microstrip Antennas with a Small Capacitive Feed”, International Journal of Antennas and Propagation, Volume 2007, Article ID 67503, 8 pages, 2007. http://dx.doi.org/10.1155/2007/67503

[21] Devesh Kumar, Manish Sharma and Sakshi Bansal , “Novel Design of Key-Shaped Fractal Antenna for UWB Applications”, 2014 Sixth International Conference on Computational Intelligence and Communication Networks, 14-16 Nov. 2014. DOI: 10.1109/CICN.2014.31

Advances in Science, Technology and Engineering Systems Journal Vol. 4, No. 2, 83-90 (2019)
www.astesj.com
Special Issue on Recent Advances in Engineering Systems
ASTESJ
ISSN: 2415-6698

LabVIEW Development for an Intelligent Management System of the Electrical Energy Free Market

Rodrigo Reina Muñoz*, Rafael Valim Xavier de Souza, Alex Soto da Silva

Center for Engineering, Modeling and Applied Social Sciences (CECS), Federal University of ABC - UFABC, ZIP Code, 09210-180, Santo André, Brazil

ARTICLE INFO

Article history:
Received: 05 January, 2019
Accepted: 28 February, 2019
Online: 15 March, 2019

Keywords:
Demand response
Intelligent management
Energy free market
LabVIEW

ABSTRACT

Consumers of electrical energy have looked more closely to the energy consumption in last years due to the successive increase of the electricity bill. Nowadays it is possible to notice that many consumers have been looking for ways to reduce their consumption or the value of their electricity bill. Such a cost reduction is obtained mainly by means of own generation, distributed generation, investment in electrical efficiency, migration to the open market, or intelligent demand management. Considering that there are opportunities to reduce the bill at the end of the month for consumers that opt for the Free Market, particularly companies that has the possibility to reduce their energy consumption, is proposed here the development of a system (hardware and software) implemented in LabVIEW and hardware resources of National Instruments company, to make an intelligent demand management system for a free consumer. The program looks optimize the financial results through the demand response concept taking advantage of the price difference in the spot market. A study was done for the Federal University of ABC - UFABC in Santo André Brazilian city looking for check the implemented system. Authors hope that the results obtained with this system can help companies and consulting firms in the decision-making process as some companies can eventually adopt the energy open market. Therefore, this article seeks contribute to the reduction of monthly costs of companies through the developed system. The importance of this system lies in the fact that it is possible to identify loads considered as non-priority and can therefore be temporarily disconnected in order to maintain energy consumption within the limits established in contracts with the energy concessionaire. The results presented here are quite promising taking into account that the intelligent management of demand in the free energy market is still underexplored.

1. Introduction

Nowadays, we see a race for energy consumption to be efficient and optimized, with companies in general (public or private sector) seeking the most diverse opportunities to reduce energy bills. In this context, there is an opportunity for some consumers to migrate to the free energy market. Migration allows a reduction in energy cost. However, it is possible to go further through intelligent management of energy demand. The migration to the free market causes the contracted energy price to be lower than the price practiced by the local distributor. However, within the energy market itself, there are times when the spot price (short-term price) is higher or lower than the contract price.

Through intelligent consumption management, it is possible to further reduce the value of the energy bill if demand responds to these prices. For these reasons, this work is inserted in an extremely current context. This work will present analyzes for a university campus in Brazil seeking to reduce its cost of electric energy through the intelligent and automatic management of demand, taking advantage of price changes in the free energy market to reduce consumption at the best times, so that the consumer not only benefits from the reduction itself but also receives a financial value for the reduction obtained. Therefore, a LabVIEW program for free energy consumers will be developed.

*Rodrigo Reina Muñoz, Center of Engineering and Applied Social Sciences, Federal University of ABC - UFABC, Santo Andre – SP, 09210-580, Brazil, Cel. 55 11 982422337, rodrigo.munoz@ufabc.edu.br

https://dx.doi.org/10.25046/aj040211

In the energy market, reference is made to the amount of energy as *MWmédio* (MWaverage). Generally, the contracts entered into in the free market have the energy amount in *MWmédio*. *MWmédio* is the volume in MWh divided by the hours of the analyzed period. That is, the average consumption per hour. Thus, a consumption of 1 *MWmédio*, for example in January (31 days * 24 hours = 744 hours), means 744 MWh.

1.1. The Free Energy Market

The Brazilian energy market is currently divided into the regulated contracting environment (ACR) and free contracting environment (ACL). Each of these environments are distinct models of the market that have certain rules foreseen by law. In ACR, the consumer pays for their energy consumption based on the energy tariff of their local distributor. The distributor, in turn, carries out the hiring at auctions held by the Electric Energy Trading Chamber (CCEE), operations that are formalized by regulated contracts, and only passes on the price of the contracts to its captive consumers. In this hiring environment, the consumer has no way to improve or manage the price of his contracted energy. In the ACR environment, consumers have as compulsory energy suppliers the distributor, at a regulated tariff, and are called captive consumers [1]. In the ACL, the consumer can contract his own energy from any generator or marketer of energy in the country through bilaterally negotiated contracts, being able to negotiate his own price and buy his energy in the moments in which the prices practiced are more attractive. Consumers operating in this market by purchasing electricity in freely negotiated bilateral contracts are called free consumers [2].

Part of the power generators can sell energy in both environments, and energy marketers can only sell energy in the ACL [2,3]. The main motivation for a captive consumer to become free consumer is the immediate cost reduction after migration from one environment to another. However, ACL is still restricted to large consumers. Only consumers with a demand contracted with the distributor over 500 kW can migrate to the free market. A key difference between the ACL and ACR for the consumer is that in the ACL is directly subject to the impacts of a spot price. This spot price is called the Spot Settlement Price (PLD) and is calculated weekly before the beginning of the operating week of the system. From the scheduling of the dispatch of the electric power plants the PLD is calculated, which corresponds to the marginal cost of operation of the system (CMO). This price targets the differences between generation (or consumption) and spot market contracts. Therefore, the PLD is calculated by evaluating the current and future state of the water stored in the reservoirs, the fuel cost of the thermoelectric plants, the optimal proportion of hydraulic generation, thermal and the interchange between subsystems considering an acceptable risk for the system.

1.2. Motivation

The reduction of energy costs to a consumer after the migration is immediate. In other words, the free market by itself provides financial savings for its consumers. However, there are still opportunities not used by consumers, such as intelligent demand management, taking advantage of the hourly variation of the PLD to maximize financial results. The present study was based on a Campus of the city of Santo André, state of São Paulo, Brazil. The algorithm developed in LabVIEW will be used to gauge the gain that could be obtained in the Campus if the migration to the ACL environment is done. It is important to mention that currently free market models are used in various parts of the world, such as in various markets in the United States, Canada, European Economic Community, Latin America, and in Asia, countries such as Australia, New Zealand, China and Japan, has adopted this model, and each market has its own peculiarities [4].

1.3. Objective

The objective of this work is to develop a LabVIEW algorithm and a system that allows to make the intelligent management of energy of a consumer in order to assist in decision making within the scope of demand response in the ACL. Intelligent demand management in this context is still little explored in the way it is proposed in this work. Therefore, we propose an experimental apparatus that was assembled using a National Instruments CompactDAQ as well as suitable interface modules that operate in connection with such hardware. The results of this experiment may help companies in decision making related to the management of loads (on or off loads), since the developed algorithm indicates when it is financially feasible to disconnect a load set to sell contracted energy surplus in the ACL. It is necessary to point out that the present study does not take into account the energy demand profile of the companies, but even so, the algorithm assists in determining the economy from the appropriate shutdown of loads at certain times of the day. The results of this work can be used by companies together with specialized consultancies for better decision making. The consulting firms themselves could use the system as presented here.

Main contribution of the proposed system is to help the energy customers to obtain costs reduction of energy bill. The system allows identify load as loads with non-priority so them can be temporarily disconnected in order to maintain energy consumption within the limits established in contracts with the energy concessionaire. This initiative is important as the demand management for customers of the energy free market is still little explored.

The paper is organized as follows: Section II presents the general concept of demand response; Section III explain the concept of demand response to free consumers within the Brazilian energy market; Section IV presents the demand response program developed in this paper; in section V the results of this work are discussed; in section VI the main conclusions are drawn.

2. Demand Response Concept

The demand response takes place when the consumer makes an adjustment in their consumption profile in response to some stimulus. That is, the demand response can be defined as the payment of incentives designed to induce a lower consumption of electricity at times when prices are high or when system reliability is impaired. A demand response policy can result in three general types of consumer responses: The first, known as load shedding, occurs by reducing electricity consumption during peak periods of the system, when prices are higher, without the consumption pattern of other periods is changed. This measure results in a loss of momentary comfort for the consumer. An example of this type of response is when the thermostat settings of heaters or air conditioners are changed temporarily [5]. A second type of response, called load shifting, is when consumers respond to high prices by shifting consumption at peak times to off peak times. An example would be the change of some residential activities (e.g. washing machines, dryers or pool pumps) to off-peak hours [5]. The third form of response is when the consumer uses his own generation, in which case the consumer must have distributed generation. From local generation consumers get little, if any, change in the pattern of electric power consumption. However, the generation will be providing more capacity for the system, since the system sees that the consumer has reduced its consumption of electrical energy [5].

The demand curve of consumers who are not subject to any demand response program (DR) is a vertical straight line. That is, demand is inelastic. When consumers somehow feel the short-term price changes, the demand curve becomes a straight inclined line, that is, demand is elastic. The different demand curves can be observed in Figure 1 [6].

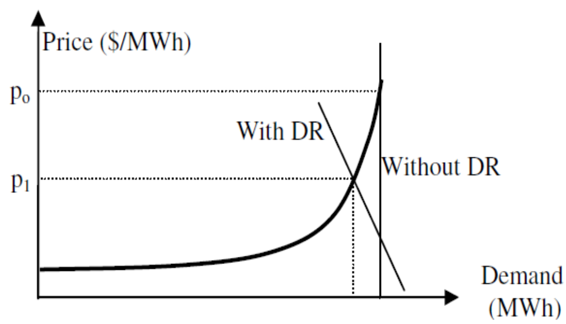

Figure 1. Simplified effect of DR on short-term electricity prices [6].

The demand response causes investments in new transmission lines and generation units to be postponed. When demand response programs act, the lines are not overloaded. In other words, the program provides more capacity for the system [7,8].

3. Demand Response Applied to the ACL

The Brazilian free energy market has a natural incentive of demand response due to the use of the PLD to compare the value differences established in the contract and consumption. The demand response in this context can be obtained through the load shedding or load shifting models. Load shedding is usually observed in commercial consumers and load shifting in industrial consumers.

In practical terms, when the consumer has more energy contracted than consumption for a certain hour of the day, it is said that the consumer has sufficiency of energy contracts at that time, which is valued to the PLD and credited to the consumer. If the consumer has less energy contracted in relation to the consumption of energy at a given time, it is said that this consumer is lacking in energy contracts, in which case the difference will be valued to the PLD and the amount must be paid by the consumer. All accounting and financial operations involving this methodology are the responsibility of the CCEE.

The mechanism of hourly determination of contractual differences means that a particular consumer can choose to reduce its consumption so that in a purposeful way might exists excess of energy as established in contract, resulting in a balance receivable by CCEE in order to reduce its energy bill power. In order this action might be successful, the consumer must map which loads are non-priority and what are the impacts of disconnecting those loads at certain times of the day.

4. Demand Management Program

Based on the aforementioned mechanism, this work proposes the implementation of a demand response program that seeks to optimize the financial result of a free consumer by cutting non-priority loads subject to a criterion that is a function of the energy contract price in the market free and spot price. There are two main parameters that should be used as a reference in a demand response program for a free consumer. These are: contracted demand with the distributor (DC) and price of energy contracted in the free market (PC). Based on these two factors and on pre-established criterion the program must make the decision to cut or not part of the load at a given instant of time. The criterion that can be pre-established refer to the definition of the loads that can be considered non-priority for the operation of the company on certain days when it is necessary to cut certain loads, and thus, be able to save energy considering the valuation in the PLD.

In the case of the demand contracted with the distributor, the decision is made based on the rule established by the National Electric Energy Agency (ANEEL) that if the measured instantaneous demand exceeds 5% of the contracted demand, that consumer will pay a higher tariff called of exceeding demand. Thus, if the program identifies an increase of more than 5% in DC, there should be a cut in the load (some loads must be temporarily disconnected) so that the consumer is not penalized in relation to the PC, criteria should be established observing the behavior of the short-term market energy price (PMC) to determine if a load-cutting action will be required. If the PC is higher than the PMC, there will be no need to cut the load. However, when the PMC is higher than the PC at any given time, part of the load must be cut off to have the power margin to be consumed in accordance with the contract. If the energy saved is large, there may be a margin of energy to be settled in the short-term market, allowing a positive financial result to be credited to the consumer included in the demand response program. The definition of non-priority load sets depends on each consumer. In the case of a university, for example, it is possible to list as non-priority and cuttable loads: set of elevators, escalators, set of air conditioners, part of the lighting of common areas, etc. The concept used to define non-priority loads is that they are loads that can be cut without generating activity and discomfort. Figure 2 shows a flowchart of a consumer for which, within a finite set of **N** loads, three sets of loads were defined as capable of acting in the demand response program. In this specific case, the cut-off criterion for the PMC was defined as follows, and may vary from consumer to consumer:

If PMC ≤ PC: there is no load cut;

If PC < PMC ≤ PC + 25%: there is a cut off of load 1;

If PC + 25% < PMC ≤ PC + 50%: there is a cut off of loads 1 e 2;

If PMC > PC + 50%: there is a cut off of loads 1, 2, 3.

Since the order of priority is:

Load N > Load N-1 > … > Load 3 > Load 2 > Load 1

That is, the first N-1 loads are of high priority and cannot be switched off.

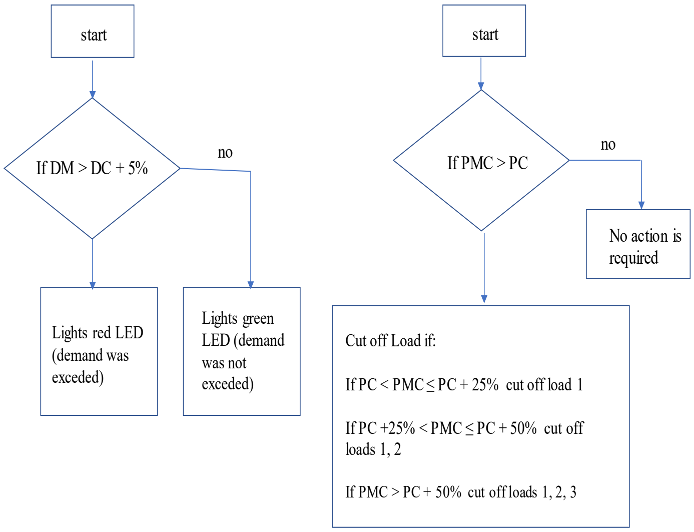

Figure 2. Flowchart for demand management program implementation [5].

The criteria for cutting the load must be defined in a specific way for each consumer according to their load pattern. To determine the economy of the consumer that participates in the demand response program, the calculation methodology, defined in (1) [9], was used. That is, the financial economy is the sum of the period of 1 to ***n*** hours of the difference between PMC and PC, when there is the intervention of the demand management program, multiplied by the demand [9].

$$VE = \sum_{i=1}^{n} \frac{(PMC - PC) * DR}{1000} \quad (1)$$

Where:

VE is the economy due to the demand response in a month basis, in R$;

PMC is the price of energy in the short-term market, in R$/MWh;

PC is the contracted energy price, in R$/MWh;

DR s the reduced demand due to the demand response action, in kW;

n corresponds with the hours of the month.

When PC > PMC, there is no load cut and DR will be zero, not contributing to the sum. The value of *n* varies according to the number of days of the months of a given period considered in the analysis. In the case of Brazil, in the Southeast region, the value of n is 673 for a month of 28 days with the end of summer (February), 720 for a month, considering months of 30 days (April, June, September and November), 744 for a 31-day month (January, March, May, July and August) and 743 for a 31-day month with start of summer season (October). The calculation of the number of hours is determined by multiplying the number of days of the month by 24h/day, and at the begin of the summer season must be subtracted one hour in the month, and at the end of the summer season one hour in the month is added.

It is also possible to determine the hourly economy, in R$, from the action of a given load cut off by using (2) [9].

$$VE_{horaN} = \frac{(PMC_{horaN} - PC) * DR_{horaN}}{1000} \quad (2)$$

Where:

VEhoraN is the economy due to the demand response in a month, in R$ during an hour N;

PMChoraN is the price of energy in the short-term market, in R$/MWh during an hour N;

PC is the contracted energy price, in R$/MWh;

DRhoraN is the reduced demand due to the demand response action, in kW during an hour N;

n are the hours of the month.

4.1. LabVIEW Implementation

Virtual instrumentation is a powerful tool for automation designers using conventional computers and specific hardware instead of traditional instrumentation. LabVIEW is software that allows the user to design programs for instrumentation, automation and process control, using a friendly interface. The CompactDAQ platform was used in this project and basically consists of a console that works in conjunction with easily configurable analog/digital input and output modules [10]. Spot energy prices are published weekly in a specific CCEE worksheet, prices that are inserted in an algorithm elaborated in LabVIEW, so that, from the date informed by the computer is able to find the corresponding spot price in the spreadsheet, providing to the management program demand updated values constantly. Details of the implementation of the algorithm can be seen in [9,11]. Figure 3 shows the spreadsheet provided by CCEE in Excel (CSV format), and Figure 4 shows the worksheet already incorporated in the LabVIEW environment which is used for calculations made by the elaborated algorithm. The import of the pricing information released by CCEE is performed through a routine that identifies the month, start date and end date information of each of the lines of the CSV file. This information is read by the program and stored in an array as shown in figure 4.

For the main demand management routine, the data of DC, PC, PCM and measured demand (DM) are used. The DC and PC variables are obtained through the signed agreement and must be informed by the user. The PCM variable is obtained through the spreadsheet provided by CCEE and the spot price verification algorithm. However, to obtain the DM it is necessary to make the acquisition of data of the demand, being necessary the use of an acquisition module of specific data for such function. That is, it is necessary to make the voltage and current measurement, or make the direct measurement through a wattmeter to inform the measured demand to the demand manager.

With the variables in hand, the algorithm presented in the flowchart of Figure 2 is implemented. The DM variable is compared to the DC variable and if DM is 5% greater than DC, a time interval is triggered to ensure that the demand is exceeded. If there is no such confirmation time, there may be undue load cuts as there may be increased demand for a short time due to activation of heavy loads. After the confirmation time is counted, the program checks the PMC (short-term market energy price) and the PC (free market contracted energy price).

	A	B	C	D	E	F	G	H	I	J	K
1	Year	Mounth	Week	Start Data	Final Data	Heavy	Medium	Light	Heavy	Medium	Light
2	2017	9	1	26/08/2017	01/09/2017	452,85	452,85	442,35	452,85	452,85	442,35
3	2017	9	2	02/09/2017	08/09/2017	499,38	499,38	488,05	499,38	499,38	488,05
4	2017	9	3	09/09/2017	15/09/2017	533,82	533,82	533,82	533,82	533,82	533,82
5	2017	9	4	16/09/2017	22/09/2017	533,82	533,82	533,82	533,82	533,82	533,82
6	2017	9	5	23/09/2017	29/09/2017	533,82	533,82	533,82	533,82	533,82	533,82
7	2017	10	1	30/09/2017	06/10/2017	533,82	533,82	533,82	533,82	533,82	533,82
8	2017	10	2	07/10/2017	13/10/2017	533,82	533,82	533,82	533,82	533,82	533,82

Figure 3. PLD sheet released by CCEE [5].

array

Year	Mounth	Week	Start	Final	Heavy	Medium	Light	Heavy	Medium	Light
2017	9	1	26/08/	01/09/	452,85	452,85	442,35	452,85	452,85	442,35
2017	9	2	02/09/	08/09/	499,38	499,38	488,05	499,38	499,38	488,05
2017	9	3	09/09/	15/09/	533,82	533,82	533,82	533,82	533,82	533,82
2017	9	4	16/09/	22/09/	533,82	533,82	533,82	533,82	533,82	533,82
2017	9	5	23/09/	29/09/	533,82	533,82	533,82	533,82	533,82	533,82
2017	10	1	30/09/	06/10/	533,82	533,82	533,82	533,82	533,82	533,82
2017	10	2	07/10/	13/10/	533,82	533,82	533,82	533,82	533,82	533,82

file path (dialog if empty)

D:\prices.csv

Figure 4. Importation of Short-Term Price Information (PLD).

According to the flowchart conditions of Figure 2, the result of the comparison can lead to turn off one, two, or three loads. To facilitate the implementation of this algorithm was used the MathScript tool, which allows the elaboration of programming in a similar way to Matlab. To cut only one load, the established condition for this is that PCM is between PC and PC + 25%. If the condition, however, indicates that the PCM is between PC + 25 and PC + 50%, two loads will be turned off. Three loads are cut off when the PCM value is above PC + 50%. It is important to emphasize that the criteria used for the disconnection of loads must be studied and must be according to the needs of the customer, such as the loads that must be disconnected and the adopted criteria of values between PC and PCM.

With the load-cutting information provided after processing in MathScript, the load-cutting information is decoded to be used as a digital signal. The cutoff indication occurs through signaling in the program itself and through digital signals through a specific module, and in this algorithm, each digital output represents a load. That is, when a digital signal is triggered, it indicates the cut of that load. Figure 5 shows the demand management program, while Figure 6 illustrates the experimental apparatus assembled for conducting the tests.

The apparatus of Figure 6 consists of obtaining instant consumer demand measurement through the CompactDAQ for processing in LabVIEW according to the algorithm implemented. Based on the algorithm, it will be determined whether any load set should be cut. In case of cut-off, the load-disconnection operation takes place through CompactDAQ.

In the case of load cut due to exceeded demand, a delay time (Elapsed Time in figure 7) was inserted in the algorithm to ensure that the loads are cut only if the demand is at least 10 seconds above the contracted demand plus 5% (Figure 7). That is, the LabVIEW program identifies the ultrapassing of load, but will act to cut the load only if this condition is maintained for 10 seconds.

The purpose of this mechanism is to ensure that instant demand peaks, such as for example, when a motor starts, will cause the demand manager to act.

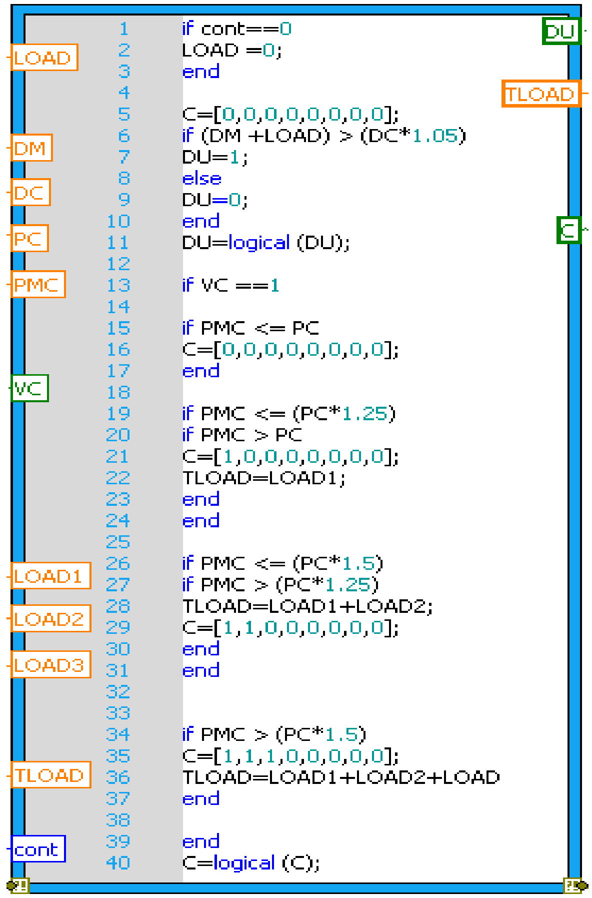

Figure 5. LabVIEW Demand Management Program [9].

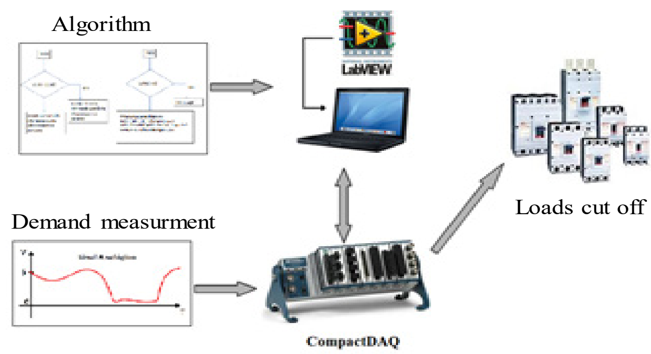

Figure 6. Illustrative pilot set-up to implement the Demand Management Program [9].

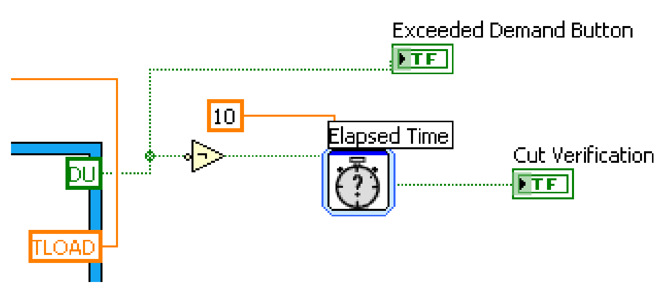

Figure 7. Delay time for load cutting action.

Also included in the program were the hourly savings in R$, savings that comes from the action of that load cut in accordance with (2) as described above. This is illustrated in figure 8.

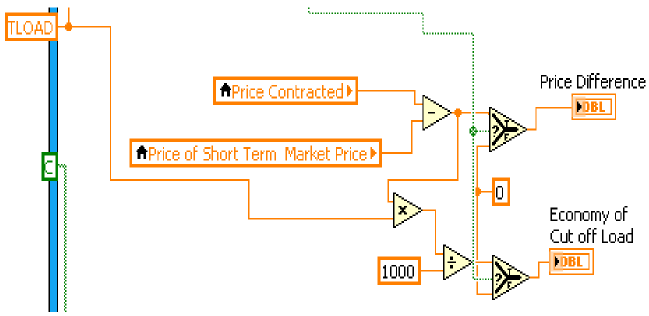

Figure 8. Hourly economy calculation included in the algorithm.

The complete LabVIEW program integrating all parts is illustrated in Figure 9.

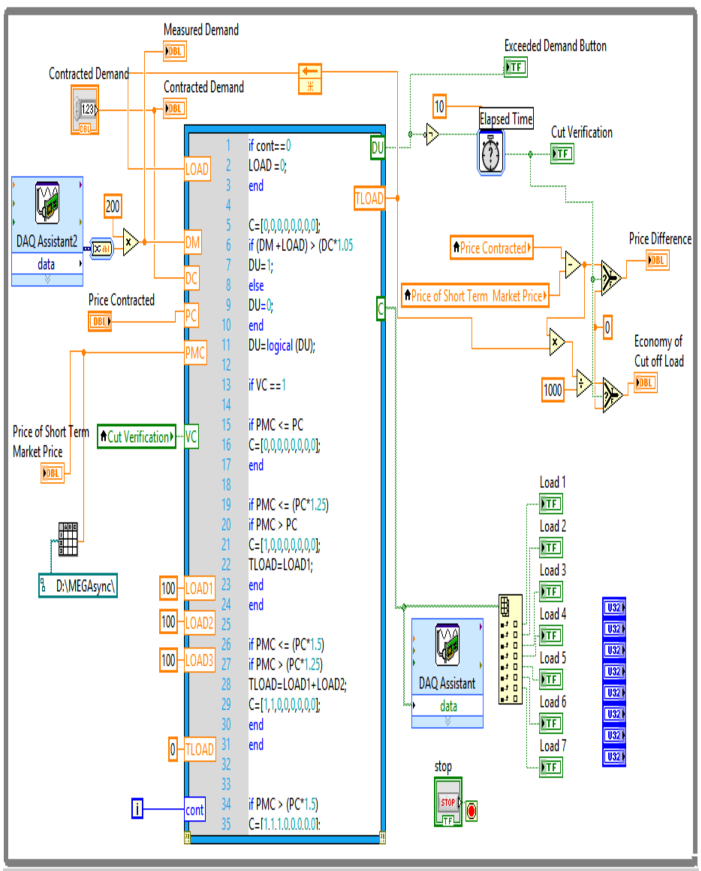

Figure 9. Complete LabVIEW algorithm of the demand management program.

4.2. Graphical Interface

In the graphical interface environment of LabVIEW an initial graphical interface was developed, shown in Figure 10, with the information of Measured Demand (kW), Contracted Demand (kW), Contract Value (R$/MWh), Short Term Price R$/MWh) and Hourly Economy (R$/h) obtained with the demand response manager. All these items are presented in the program in a simple numeric display.

In this graphical interface was inserted a button that will indicate when the instantaneous demand exceeds 5% of the value of the contracted demand, since after this limit of tolerance the consumer will pay a fine to exceed the demand. This criterion is valid for all types of consumers, whether captive or free, within or outside a demand response program. The aim of this indicator is to alert the consumer to the fine for exceeding demand, thus avoiding financial losses.

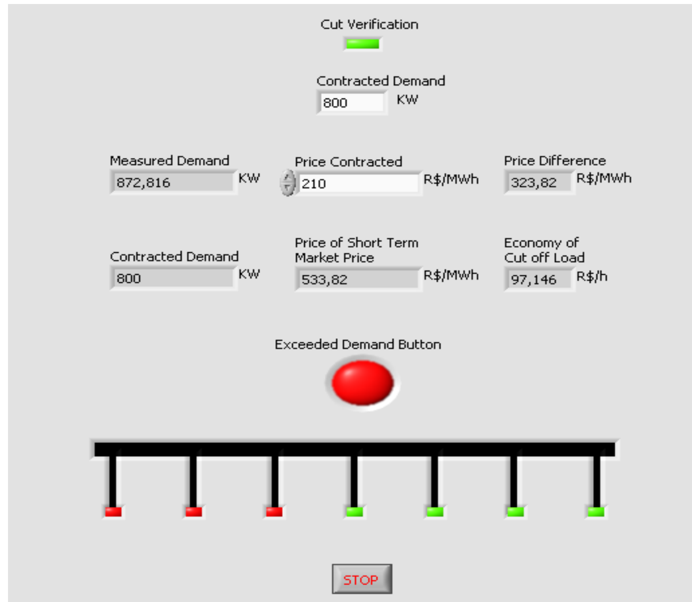

Figure 10. Graphical demand manager interface in LabVIEW [9].

Still in the graphic interface elaborated (Figure 10), there is a representation of the set of seven loads, which will be cut or re-connected, according to their order of priority. In the figure, the loads are represented by LEDs, with green LEDs representing active loads (priority), and in the red color representing loads that must be switched off in accordance with the established load-cutting criteria.

5. Test and Results

An experimental apparatus was developed that simulates the physical action of the demand response program for a consumer. As previously mentioned, a CompactDAQ was used as well as the NI-9219 and NI-9401 modules used to obtain the input and output variables, respectively, as shown in Figure 11. In this system, the input voltage on the NI module 9219, for verification purposes, represents the measured instantaneous demand. The voltage is measured and a constant conversion factor was applied to convert this information into demand values in kW.

In a practical situation, this information would be provided to the demand manager by the CT (current transformer) and TP (power transformer) of the measuring cabin equipment. A set of LEDs were connected to the output module, where each LED, as already mentioned, represents a load set. In the experiment, the LEDs lit (green LEDs) to indicate that the charging set is on. When the program sends the signal to turn off a certain LED, in practice, this action would correspond to the shutdown of that load. Figure 12 shows in more detail the highlight number 2 of figure 11, where the LEDs indicate the loads that must remain connected and the loads that must be disconnected according to the management algorithm.

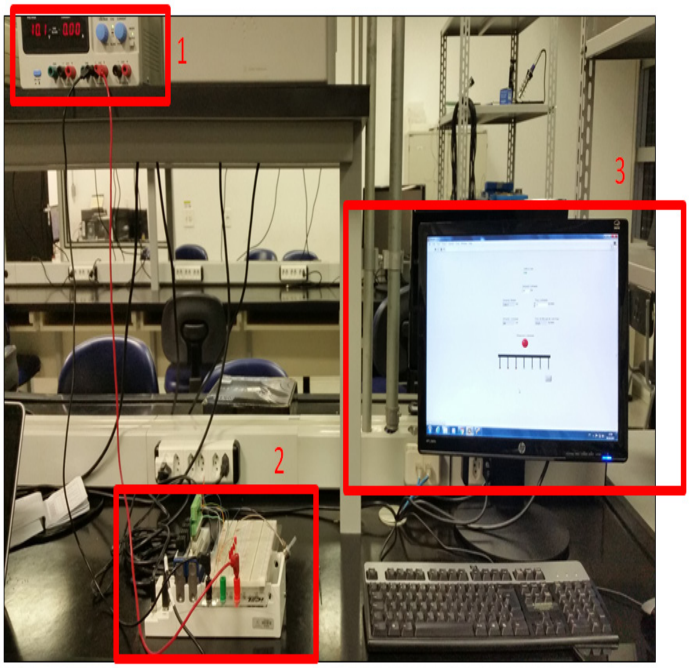

Figure 11. Experimental set-up used.

The results using the CompactDAQ were effective since, given an input signal corresponding to the measured demand, the CompactDAQ assembly was able to operate through a digital output signal that determined which output points should remain on or off. With respect to the input signal, in the experiment represented by a 10 V DC voltage source, it was obtained through a voltage divider with a potentiometer used to change the voltage.

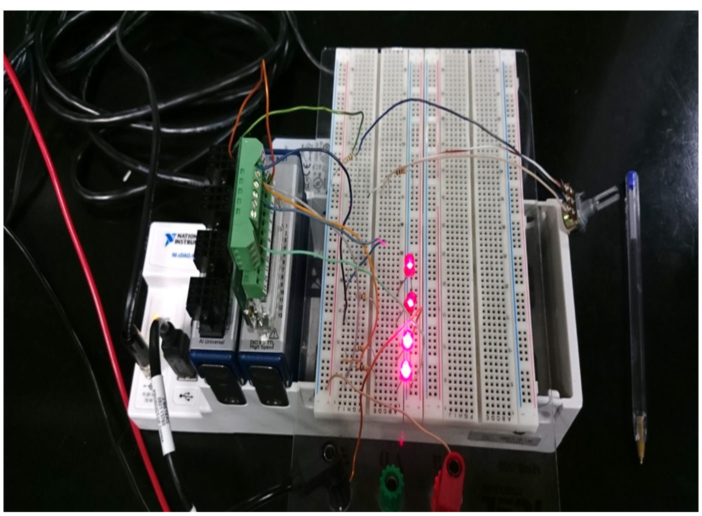

Figure 12. Experimental Circuit in operation.

In a practical system it would be equivalent to the output of the TC or TP of the meter, with corresponding corrections of that meter's constants. The output module used provides the digital signal of which ports should be switched on or off. In practice, this would be equivalent to signaling which relays/circuit breakers should be on or off at any given time, and each load set should be in a different electrical installation. To complement the experiment and identify quantitatively what could be the economy provided by the proposed demand management program, we verified the results that could be obtained at the Santo André campus of UFABC. Tests were carried out considering the period from January to September 2017, considering that contracted campus demand is 1.400 kW, energy contract price of R$ 210.00/MWh and considering the cut criterion presented in the methodology of this work. Table 1 shows the results obtained.

Table 1. Results obtained with the Demand Response algorithm

Months	*Monthly Average PLD (R$/MWh)*	*Total Economy (R$)*
janeiro-17	121,44	0,00
fevereiro-17	128,43	0,00
março-17	216,24	1.201,87
abril-17	371,47	35.976,24
maio-17	411,49	49.873,24
junho-17	124,7	0,00
julho-17	280,81	11.977,75
agosto-17	505,95	67.049,14
setembro-17	521,83	67.626,36
	Total (R$)	**233.704,60**

By the analysis of table 1, it is possible to observe that the program of Demand Response did not result in improvement of results in the months of January, February and June. These months were times when the energy price in the short term (PLD) was lower than the contract price (R$ 210.0/MWh). The results are significant for all those months in which the PLD is higher than the energy contract price (R$ 210/MWh). In the analyzed period, from January to September, a potential savings of R$ 233.704,60 from the proposed Demand Response Program was observed, according to the values presented in table 1.

The low PLD moments happen when the electrical system is in favorable conjuncture conditions, for example, when the levels of reservoirs are within the one planned by the National System Operator (ONS) and the rains are above the historical average. When the electrical system is in unfavorable condition of rainfall and reservoir levels, the PLD rises significantly and it is at that moment that the Demand Response Program becomes interesting and creates opportunities for the consumer to reduce the energy bill with the cut load and sale of excess of energy contracted. The savings opportunities increase as the average monthly PLD increases.

6. Conclusions

A tool for intelligent demand management was developed with the purpose of using the Demand Response concept to reduce a consumer's electricity bill in the free market. Tests were applied to the Santo André campus of UFABC. The program implementation was performed in LabVIEW and the tests were performed using the CompactDAQ hardware. The tests were enough to verify all the operation of the program in LabVIEW. Authors believe that the system developed is a novelty. The system allows the temporary disconnection of non-priority loads contributing to reduce energy consumption and consequently reducing the energy bill of the users of the free energy market.

It was verified how much the campus could economize with the demand response program based on the months of January to September 2017. As results for this period, a reduction potential of R$ 233.704,60 was observed, referring only to the demand response implemented through the Demand Management Program. It is important to emphasize that the results obtained are preliminary, and, therefore, more tests are required with the application of the developed tool. It is also important to highlight that the scenario is an example of the use of the system developed to verify both the software and the implemented hardware. Thus, the loads chosen by the authors as non-priority loads were disconnected, and, therefore, the results are representative of this scenario. Thus, the key conclusion of this paper in light of the results obtained is that, Intelligent Demand Management, by observing hourly price variations can result in an excellent opportunity to reduce free energy consumer costs and relief to the electrical system. It is hoped, therefore, that the system developed in LabVIEW can assist companies and consultants with regard to decision-making in regard to obtaining savings by migrating to the ACL.

Acknowledgments

The authors thank the Federal University of ABC for the support given to this work.

References

[1] CCEE – Câmara de Comercialização de Energia Elétrica, “General operations overview at CCEE (In Portuguese)”, São Paulo, 2013, in: www.ccee.org.br/StaticFile/Visao_Geral_das_Operacoes_CCEE_2013.pdf, accessed at: 09/30/2017.
[2] ABRACEEL – Brazilian Association of Electric Energy Traders, “Booklet: Free Energy Market (In Portuguese)”, in: www.abraceel.com.br/archives/files/Abraceel_Cartilha_MercadoLivre_V9.pdf. Accessed at:10/07/2017.
[3] Rodrigues Flávia, “Energy Contracting Programming Considering Distributed Generation in the New Model of the Brazilian Electricity Sector (In Portuguese)”, PhD Thesis, UFRJ, Rio de Janeiro, 2006.
[4] Luciano Macedo Freire, “Electric Energy Markets, International Experience and the Brazilian Model of Energy Trading (In Portuguese)”, in:http://www.abraceel.com.br/zpublisher/paginas/Download_file.asp?nome=...%20%C2%B7%20Arquivo%20PDF, accessed in: 03/16/2016.
[5] CCEE – Câmara de Comercialização de Energia Elétrica, “Free Consumers in the scope of CCEE (In Portuguese)”, in: www.ccee.org.br/search/query/redirect.jsp?qid=259786&did=3193776&pos=1&idx=1&fid=&pdfq=%22consumidores%20livres%20treinamento%22, accessed at: 10/14/2017.
[6] Albadi, M. H.; El-Saadany, E. F., “Demand Response in Electricity Markets: An Overview”, Power Engineering Society General Meeting, IEEE, 2007. https://ieeexplore.ieee.org/abstract/document/4275494.
[7] Chakrabarti, B.; Bullen, D., Edwards, C., Callaghan, C., “Demand Response in the New Zealand Electricity Market”, Transmission and Distribution Conference and Exposition (T&D), IEEE PES, 2012. https://ieeexplore.ieee.org/abstract/document/6281718.
[8] Jidong, L., Zehui, Z., Li, Z., Xueshan, H., “Evaluating Short Term Benefits of Demand Response”, Electric Utility Deregulation and Restructuring and Power Technologies (DRPT), 4th International Conference on. 2011. https://ieeexplore.ieee.org/document/5994079.
[9] Souza, R. V. X., “Migration Study of the Santo André Campus of UFABC for the Free Electric Power Market and LabVIEW Development of an Intelligent Demand Manager (In Portuguese)”, Master Dissertation, Federal University of ABC - UFABC, Santo André, Brazil, 2017.
[10] NATIONAL INSTRUMENTS, “Getting Started with LabVIEW”, in: www.ni.com/pdf/manuals/373427f.pdf, accessed at: 03/12/2017.
[11] Souza, R. V. X., Silva, A. S., Munoz, R.R., “Development of an Intelligent Energy Demand Response Program for a Brazilian Free Consumer of Energy”, in: VII Brazilian Symposium on Electrical Systems - SBSE, Niteroi – RJ, 2018. https://ieeexplore.ieee.org/document/8395579.

Advances in Science, Technology and Engineering Systems Journal Vol. 4, No. 2, 91-101 (2019)

www.astesj.com

Special Issue on Advancement in Engineering and Computer Science

ASTESJ

ISSN: 2415-6698

A Systematic Mapping Study of Cloud, Fog, and Edge/Mobile Devices Management, Hierarchy Models and Business Models

Isaac Odun-Ayo[1,*], Rowland Goddy-Worlu[1], Victor Geteloma [1], Emanuel Grant[2]

[1]*Department of Computer and Information Sciences, Covenant University, 112233, Nigeria*

[2]*School of Electrical Engineering & Computer Science, University of North Dakota, 58202, USA.*

A R T I C L E I N F O

Article history:
Received: 10 January, 2019
Accepted: 22 February, 2019
Online: 15 March, 2019

Keywords:
Cloud computing
Fog computing
Edge computing

A B S T R A C T

Cloud computing is an exceptional paradigm, which is facilitating the developments and utilization of resources over the internet. Fog computing operates at the edge of the network saving bandwidth, by not sending all information to the cloud, while edge computing does processing of data at the edge of the cloud. Edge computing reduces the distance data must travel on the network. The unique relationship between cloud, fog and edge computing makes research in these areas mandatory. Deciding on a specific area of research as regards these subjects could be a bulky procedure for a scientist. Therefore, reviews and paper studies for recognizing potential research gaps are required. A systematic mapping study is utilized in giving a summary of the conducted research in a particular study area. The objective of this paper is to conduct systematic mapping studies on cloud, fog, edge/mobile devices management, hierarchy models and business models. The results showed that publications that discussed process in relations to the field of study is 14.04% out of the 114 papers included. Also method contributed 24.56%, model had 42.98% and tool contributed 18.42%. Furthermore, evaluation research in terms of the field of study was 27.5% out of 120 papers included. Also, validation was discussed in 17.5% of the papers, solution was 32.5%, philosophical was 5.83%, experience was 15.83% and opinion was 0.83%. The clearly highlighted gaps ought to inspire more enthusiasm for additional research by both researchers and industry practitioners.

1. Introduction

The Cloud is a parallel and appropriated computing system comprising of interconnected and virtualized computers that are powerfully displayed as a unified computing resource, which is dependent on service level approvals set up through dealings between service providers and users [1]. Cloud computing is basically interconnected computers and applications used to deliver services over the Internet. When systems are connected in this manner, device management also becomes paramount. Cloud computing is presently delivering services at all layers hence, there is everything as a service, but there are three primary services in the cloud which are Software-as-a-Service (SaaS), Platform-as-a-Service (PaaS) and Infrastructure-as-a-Service (IaaS). In SaaS, major cloud service provider (CSP) like Salesforce.com offer custom-built applications for users on the internet, hence the user do not need to bother about installation and license. In PaaS, the user develops and deploys his application through the infrastructure made available by the CSP. In IaaS, the user utilized resources on the CSP infrastructure on a pay as you go basis. The CSPs have massive data centers with state of the art system; hence, the user can start up without the cost of infrastructure. Although the CSPs strive in providing effective and trustworthy services on the cloud, there are also issues of trust [2]. The effectiveness of cloud computing becomes very evident as services improve and expand regularly, due to the fundamental applications running on the cloud [3,4]. In addition, there are four cloud computing models namely the private, public, community and hybrid models. Private clouds provide organizations infrastructures that are hosted on premises or off premises making use of in house staff. Private clouds are considered more secure. Public clouds provide massive elastic, on-demand pool of resources to the users through the CSP

*Corresponding Author: Isaac Odun-Ayo, Contact No. +234 802 88 29456, Email: isaac.odun-ayo@covenantuniversity.edu.ng

https://dx.doi.org/10.25046/aj040212

infrastructure. Community cloud make services available to institutions that share infrastructure but operate independently. Hybrid clouds provide the potential to host core applications on private cloud and auxiliary applications on public clouds. However, due to the process of virtualization and multitenancy on the cloud, there are concerns about security [5,6].

Fog and edge computers carry out storage and processing at the edge of the cloud. This saves bandwidth and makes usage simple. However, there are technologies that must be used to monitor these applications data and services operating within and at the edge of cloud computing. Edge computing is characterized by proximity to end users, zone geographical distribution, and support for high mobility and value addition for customer IoT services [7]. Mobile edge computing aims at reducing both network latency and resource demand by shifting computing and storage capacities from the Internet cloud to the mobile edge [8]. In [9], the cloud system is described with a 3-layer hierarchy, the cloud computing infrastructure layer, the edge computing or mobile clouds, which are utilized in vertically integrated applications where a part of the processing and analytics happens on the edge device while the cloud is used for coordination and data retrieval [10]. The service measurement index framework discussed in [11] is a business model that provides an understanding of CSP rankings, and has 7 major characteristics namely: accountability, agility, assurance, financial, performance, security and privacy and usability [11].

Systematic mapping studies provides a platform for categorizing research using a scheme and structure indicating the frequency of research in such an area and the results are presented visually on a map. Systematic mapping requires less effort: yet provides a more coarse-grained overview in the area of study [12]. This enables the coverage of the research field to be determined. The systematic process in this work was accomplished using three facets: the topic, contribution and research facets. The topic facet extracts key consideration from the scope of study. The contribution facet deals with method or mode of the work, while the research facet considers the nature of research such as evaluation or opinion. While the goal of this study is to conduct a systematic mapping study, the rest of the paper is organized as follows: Section II examines the related work. Section III examines the materials and methods, Section IV presents the results and discussion and Section V is the conclusion and suggestion for future work.

2. Related Work

In [13], the authors explored the developing stage of a systematic mapping study by identifying the software designs present at the requirement engineering stage of the project, and providing a comprehension of the roles played by these patterns based on basic parameters required in the development process. A protocol was developed for the study with basic steps to enable the replication of their work by the research community, which results in confirming the validation of the research. For this paper, ACM DL, IEEEXplore, SCOPUS, and Web of Science digital libraries were utilized, and the guidelines laid down in [12] were adhered to.

In [14], the authors dwelled on describing the protocol for a systematic map, in relation to domain-specific languages (DSL). The authors focused on channeling their work on the advanced apprehension of the DSL domain of research, while emphasizing on trending researches and subsequent expectations, and utilizing the requirements for conducting a systematic review, all within the interval of July 2013 to October 2014.

The authors in [15] analyzed the utilization of concept maps in Computer Science, which resulted in a systematic map focused on gathering and analyzing previous articles on concept maps. This resulted in a thorough examination of concept maps, with emphasis on learning and teaching supports. Also, the searching process involved the utilization of backward snowballing and manual methods, and search strings applied on SCOPUS, ScienceDirect, Compedex, ACM DL, and IEEExplore digital libraries.

In [16], the researchers examined how games related methods are implemented in software engineering, and how these methods assist specified software engineering knowledge domains. Based on publications from 1974 to 2016, the authors utilized 156 primary studies, which were centered on using and evaluating games in software engineering education. The mapping procedure was done in line with the guidelines provided in [12].

In [17], the authors did a mapping of power system model by providing a summary of power system models and its subsequent usage by European organizations in terms of analysis of their modeling features and identification of modeling gaps. 228 surveys were sent out to power experts for data extraction, while 82 questionnaires were eventually completed and utilized for the mapping.

In [18], a mapping study of domain-specific languages was conducted with a primary interest in the type of contribution and research, and the area of focus. By exploring reputable articles from 2006 to 2012, a mapping study was conducted by defining research questions, conducting the search, and extracting the data.

In [19], the authors focused on searching studies on "legal theory" and "legal concepts". The selected studies were grouped on contributions in terms of language, tool, method, and model. The other steps include identification of the used legal theories in legal core ontologies building process, identification of focus with a clear recommendation on the use of two ontologies, and analyzing each highlighted research for conclusive findings about legal and ontological research.

In [20], the researchers gave a summary of an empirical research in software cloud-based testing in the process of building a classification scheme. The authors examined functional and non-functional testing techniques, their applications, and their peculiarities. Sixty-nine (69) primary studies out of seventy-five (75) research articles were utilized for a rigorous statistical analysis, and an eventual quantitative result. Most articles utilized a singular experiment approach for evaluating their expected result.

In [21], the authors presented a comprehensive review of knowledge management in organization with a focus on the potential role of Information Technology (IT) in the process. They further discussed several important issues bordering on the process of managing knowledge and the role of IT in propelling and assisting these processes. Also, emphasis was made on the need to support in creating, storing, transferring and applying knowledge in organizations.

In [22], the authors discussed the usefulness and limitations of systematic literature review in information system and social sciences. They are of the opinion that the general stand that systematic literature review provide a holistic and superior approach to literature review is not only questionable but also unacceptable. In their argument and justification of this, they concluded that caution and restrains should be exercised when choosing systematic literature review as it could undermine critical engagement with literature and the scholarly nature of academic work.

In [23], the authors discussed the lessons learned from utilizing a systematic literature review process on software engineering domain. The authors summarized the review process, highlighted the reviews of other authors and finally extracted and discussed findings as regards applying this practice to software engineering domain.

In [24], the researchers opined that research reviews must pay close attention to rigorous methodology that is required of primary researcher. The author further conceptualized the research review as a scientific enquiry involving five stages that parallel those primary research, which includes: formulating the problem, collecting data, evaluating the data points, analyzing and interpreting the data, and lastly, presenting the results. All the functions; sources of variance and the other potential treats to validity with each stage are discussed.

In [25], the authors provided useful insights to researchers for carrying out literature review. They suggested synthesizing trends and patterns while preparing to write literature review, among which includes: the purpose and voice before beginning to write must be considered, then consider how to reassemble the notes as well as create a topical outline that traces the argument in the literature review. All of these provides the guidelines for developing a thorough and coherent literature review.

In [26], the researchers assessed the effectiveness of a systematic literature review, which recommends evidence-based software engineering methods for aggregating evidence. The authors utilized manually searched Journals (10) and conference proceedings (4). Of the twenty (20) significant articles considered, eight (8) articles focused on research trends rather than evaluating the technique utilized, and seven (7) systematic literature reviews focused on estimating the cost. The quality of systematic literature reviews was fair with only three scoring less than 2 out of 4.

In [27], the authors have an opinion that the evaluation of the approaches of systematic mapping, as carried out by researchers, is needed in identifying the improved guidelines that are centered on the experiences from existing systematic maps and literature reviews. In the affirmative, the authors carried out a systematic mapping study and considered a few practices of the systematic review guidelines. They discovered that amongst the extensive number of studies carried out, various guidelines were utilized and integrated, leading to multiple methods of conducting systematic mapping studies.

In [28], the authors stressed the importance of literature review in scientific enquiry and the need to avoid standing on the shoulders of dwarf literature search, which remains a point of concern for enhancing a productive literature review. The authors further discussed the difficulties of literature search in the ever-increasing dynamic setting of data frameworks, and proffer solutions on how these difficulties can be dealt with.

In [29], the authors presented the systematic mapping study of high-performance computing and the cloud which based their work on the concepts of [27]. This study provided six classes of studies in the areas of architecture, virtualization, application, optimization, design and implementation, and performances in relation to the focus of study. The selected studies were applied on the contribution facet such tool, method, and model. In addition, the selected studies were used on the research facet which dealt with evaluation, validation and solution research.

In [30], the researchers examined the systematic mapping study of cloud resources management and scalability in brokering, scheduling, capacity planning and elasticity. The classification scheme in relation to resource management, discussed scalability, brokering, scheduling, capacity planning, elasticity, and resource sharing. The selected studies were applied on the contribution facet such metric, tool, method, and model. In addition, the selected studies were applied to the types of research.

3. Materials and Methods

The systematic mapping study is a useful tool for both researchers and practitioners alike. A mapping study provides a visual representation of scope of work in a particular discipline. This study was carried out utilizing the guidelines on systematic mapping studies, as seen in [12]. Systematic mapping study involves replicating a process for deducing and interpreting accessible materials, in line with a research objective [31]. This important process (Figure 1) involves defining the research question and outlining the scope of the review. Next is screening the articles to select the important ones and key wording the abstract of the articles, with the goal of creating a classification scheme. Finally, the last step involves extracting the data, which ultimately leads to creating the systematic map. At every stage of the process there was an outcome which was refined for better overall output of the systematic map.

3.1. Definition of Research Questions

The goal of a systematic map is to provide more insight into the quantity and type of work being conducted in a particular discipline. It may also be necessary to know the places where such work were published. These issues help in determining the appropriate research questions to apply to the study in this paper.

The research questions are:

RQ 1: What areas are addressed and what number of articles are covered in the highlighted areas of the research topic?

RQ 2: What sets of articles are published in the highlighted areas and what are their evaluations and originality?

3.2. Conduct of Research for Primary Studies

For the purpose of getting papers for this study, four (4) major digital libraries based on their impact factor of conferences and journal publication were utilized. Table 1 contains the digital libraries and their corresponding uniform resource locator (URL).

Table 1: Electronic databases used for the systematic mapping study

Electronic Databases	URL
ACM	http://dl.acm.org/
IEEE	http://ieeexplore.ieee.org/xplore
SCIENCE DIRECT	http://www.sciencedirect.com/
SPRINGER	http;//www.springerlink.com/

The search string was designed based on population, outcome and intervention of the papers. The keywords used in the research was gotten from all parts of the structure of this study's title; the search string is as follows:

(TITLE (cloud) AND KEY (cloud) AND (TITLE-ABS-KEY) (fog) OR TITLE-ABS-KEY (edge and mobile) OR TITLE-ABS-KEY ("devices management") AND (KEY (Models) OR TITLE (models)

The searches were performed on the electronic database, which involves utilizing the designed search string above on document metadata to guarantee the inclusion of significant articles. For this study, findings from relevant databases relating to cloud computing and computer science were utilized, and a total of 120 papers were relevant to be included out of an underlying pursuit comprising of 1339 papers. This study covered the period 2001 – 2018. The list of primary studies utilized for this work is at the Appendix.

3.3. Screening of Papers for Inclusion and Exclusion

The importance of selection criteria is identifying and incorporating all papers relevant to the study. This was a vital aspect of the study. It was essential to use the inclusion and exclusion criteria to eliminate irrelevant articles as regards to cloud, fog, and edge/models device management. In addition, the criteria was utilized in removing all materials not providing answers to the research question. Some abstract usually mention only one aspect of the focus of study without further details and such papers are also excluded. This study also excluded panel discussions, editorials, prefaces, presentation slides, summaries and tutorials. It was pertinent to consider articles that had the main focus and able to also provide some secondary details. The main focus of this study was devices management and models as it relates to cloud, fog, and computing. Therefore, the inclusion and exclusion process was done using details depicted in Table 2.

Table 2: Inclusion and exclusion criteria

Inclusion criteria	Exclusion criteria
The abstract explicitly mentions cloud, fog, edge, mobile devices management, hierarchy models and business models. Furthermore, discussions in this area are meant to achieve cloud management.	The paper lies outside the area of cloud computing as it identifies with cloud management. The paper does not contribute to issues of management in the cloud.

3.4. Keywording of Abstracts

Keyword of abstracts is an important process in systematic mapping, used to design the classification scheme for the study and involves the following stages as shown in Figure 1.

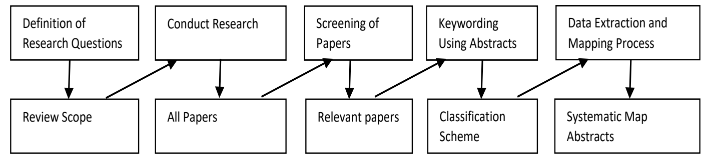

Figure 1: The systematic mapping process [27]

Key wording was useful in decreasing the required time for designing a classification scheme for cloud management and model studies. Also, key wording ensured that only the significant papers were considered in the scheme. The abstracts were studied in order to extract concepts and keywords relating to the focus of this study. Therefore, keywords from different publications were combined together to give satisfactory knowledge about the nature of the contributing research. This was eventually utilized in determining the facts or categories of the study.

A cluster of keywords were finally used in this paper to determine the categories and the eventual systematic map. In this paper, the three categories focused on topics based on all aspect of the title of the study. The second facets discussed the types of contributions in relation to metric, tool, method, process and model [12]. The third facet concentrated on research types such as evaluation and validation.

3.5. Research type Facts with Category and Description

A study of this nature will be inadequate without all the categories outlined. The following is the classification of research methods, which was utilized for the third facet, as listed in [32]:

1. **Validation of research:** The utilized methods are unique but not yet executed, either in form of an application or experiments.
2. **Evaluation research:** The methods have been executed and analyzed with a proof of concept. Outcomes are examined in terms of advantages and disadvantages.
3. **Solution proposal:** The method offers an essential solution to a problem; the benefits and application of such results are also outlined.
4. **Philosophical papers:** The papers discuss techniques that provide new methods of solving a problem in relation to concepts and framework.
5. **Opinion papers:** The research papers do not apply any known methods, but simply expressed the opinion of individuals.
6. **Experience papers:** This paper relates the personal experience of the researcher. It offers insight into how something was done

These categories were considered adequate and sufficient to be used in the classification scheme of this study, as to research facet. The papers included in this study were all examined based on the various research categories.

3.6. Data Extraction and Mapping Studies

Relevant articles were sorted into a classification scheme at the key wording stage. This next step allowed data extraction from the primary studies. The method of extracting data shaped the nature of the classification scheme. The procedure for extracting data was achieved on Microsoft Excel tables. The Excel tables contained the various groups of the classification scheme. The frequency of publications in each category was extracted to different tables. The frequency of publications in each category was combined into a table either contenting the topic/contribution category or the topic/research category. The analysis was focused on presenting the frequencies of articles based on the entries made into the various Excel tables. The essence was to identify which aspect of device management and models as it relates to cloud, fog and edge/mobile computing were given more emphasis in this study This enabled the determination of gaps and made it easy to identify areas for further research.

Based on the results extracted to the Excel tables, bubble plots were subsequently utilized in presenting the frequency of the articles using a map. The map included a two x-y scatter plot with bubbles at the crossing point of the classifications. The size of the bubble coordinates corresponds to the quantity of articles in such combined categories. There were two quadrants based on the three facets under consideration. Each quadrant provided different visualized maps on the basis of the intersection of the topic category with either the contribution or research category. The different facets could be considered simultaneously, providing an overview of the results of the study.

4. Results and Discussion

The analysis of the result is meant to present the frequencies of publication in each category, and to identify which category has been emphasized in past research [12]. The essence of this was the identification of gaps and the possibility of researching further. From the analysis, gaps were identified by using the systematic map, which showed topic areas where there was dearth of study, and indicated the areas that were explored as regards articles. In this systematic study, high-level categories was utilized in assessing the primary studies, which was used to create the systematic map.

4.1. Topic and Contribution Facet

The topics extracted at the classification scheme in this field of study comprise of the following:

1. Architecture
2. Application
3. Implementation
4. Networking
5. Mobile computing
6. Embedded systems

The list of primary studies used for checking the topics against the types of contributions is at Table 3. The systematic map is shown at Figure 2. The contribution facet shows the type of contribution to the field of study. The results showed that publications that discussed process in relations to the field of study was 14.04% out of the 114 papers included. In addition, method contributed 24.56%, model had 42.98% and tool contributed 18.42%. There were no contributions at all from metric.

Models discussion contributed 42.98% of the papers reviewed. In relation to the topics, model had 5.22% in terms of architecture, 12.28% in terms of application, and 3.51% in the area of implementation, 10.53% in the area of networking, 3.51% in the aspect of mobile computing and 7.89% on embedded system. Other aspects of topic and contribution aspect are reflected in Figure 2.

4.2. Type and Research Facet

The list of primary studies used for examining the topics against the types of research is at Table 4. On the x-axis of the right quadrant of Figure 2 are the results of the types of research conducted with respect to the field of study. The result indicated that evaluation research in terms of the field of study was 27.5% out of 120 primary studies. Also, validation was discussed in 17.5% of the papers, solution in 32.5%, philosophical in 5.83%, experience in 15.83% and opinion in 0.83%.

Solution proposal constituted 32.5% of the papers examined in this field of study in relation to the topics. Solution proposal had 1.67% in terms of architecture, 8.33% in terms of applications, 5% in relation to implementation, 11.67% with respect to networking, 3.33% in terms of mobile computing and 2.5% in terms of embedded system. Other aspects of research and topic contribution is as shown in Figure 2.

4.3. Major Findings

From Figure 2,

a. It can be identified from the visual map that there were more publications on implementations and mobile networking that discussed metric with 26%, more publication on applications that examined model with 12.28%, more papers on architecture that discussed method with 6.14% and more work on embedded systems examining process at 6.14%.

b. Similarly, on the left quadrant of Figure 2, there were more articles on mobile computing that discussed evaluation research with 9.17%, more publications on application that examined validation research with 5%, more work on network in terms of solution proposal at 11.67%, more publication on mobile computing in terms of philosophical paper with 3.33%, more materials on application in term of experience papers and only one opinion paper related to embedded system.

c. On the other hand, this study had shown that there were no discussions at all relating to metric in this field of study. There were no papers on architecture in terms of tool. There were no articles on implementation and networking in terms of process. In addition, there was no work on architecture, application, and networking in the area of philosophical papers.

d. Furthermore, publications on application topic as it related to tool, mobile networking and implementations

Table 3: Primary studies for topic and contribution facet

Contribution Facet / Topic	Metric	Tool	Model	Method	Process
Architecture			30, 37, 80, 92, 93, 95,	18, 42, 60, 77, 84, 90, 116,	4, 8,
Application		28,	25, 36, 39, 38, 45, 48, 54, 57, 71, 78, 82, 85, 115, 119,	5, 11, 14, 86, 94,	105, 108,
Implementation		13, 19, 26, 101, 118, 120	50, 55, 87, 100,	2, 43, 46,	
Networking		22, 24, 29, 31, 33,	7, 9, 12, 15, 16, 91, 96, 98, 103, 104,106, 112,	20, 41, 47, 70, 79, 83,	
Mobile computing		3, 6, 10, 23, 109, 110,	27, 32, 34, 35	2, 73, 75, 76, 89, 99	44, 53, 56, 58, 71
Embedded Systems		49, 61, 62,	1, 64, 65, 66, 67, 68, 74, 115, 119	81	17, 21, 51, 52, 97, 113, 114,
Percentage	**0.0%**	**18.42%**	**42.98%**	**24.56%**	**14.04%**

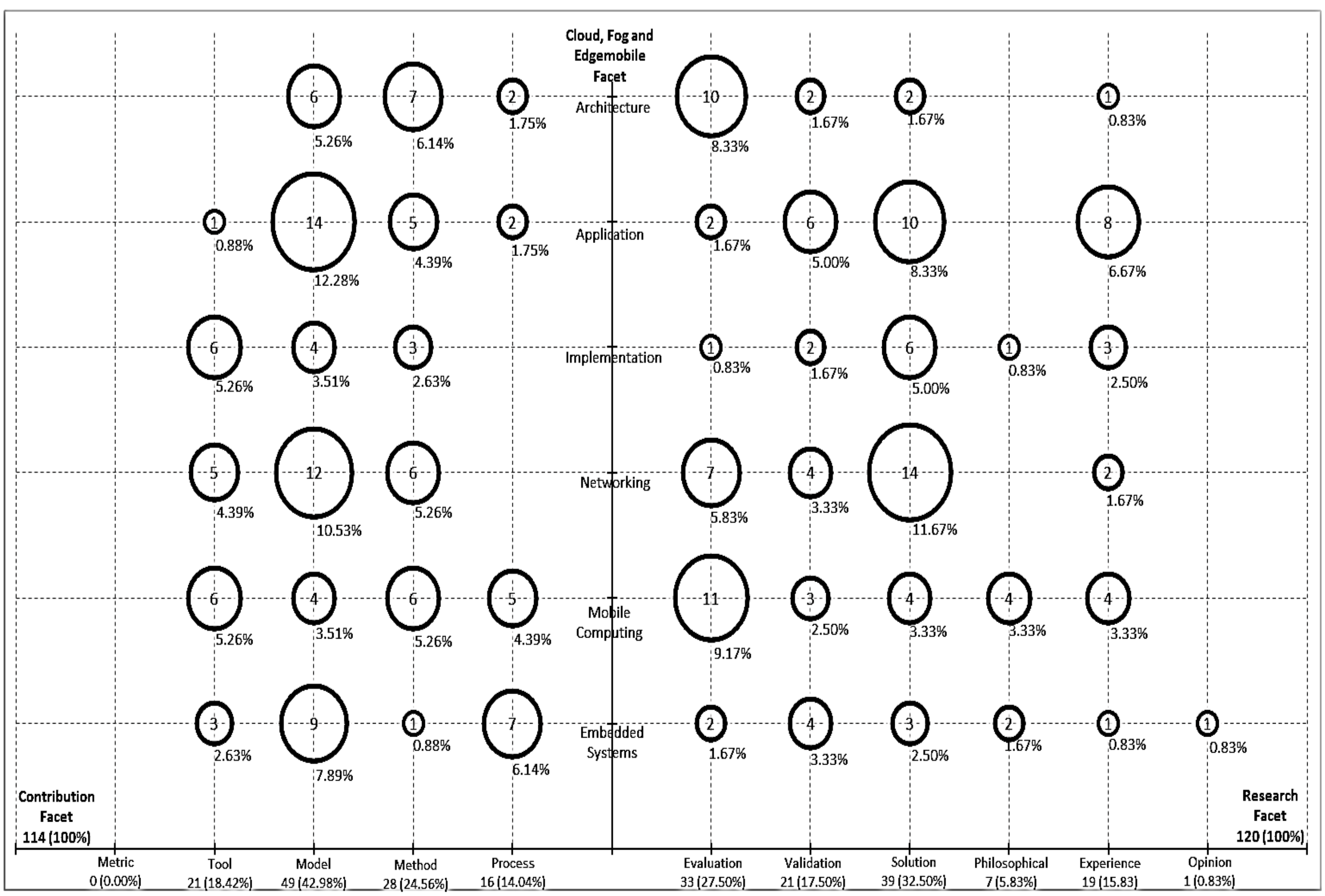

Figure 2: Systematic map of cloud fog, and edge/mobile devices management, hierarchy and business models

Table 4: Primary studies for topic and research facets

Research Facet / Topic	Evaluation	Validation	Solution	Philosophical	Experience	Opinion
Architecture	4, 8, 37, 42, 60, 80, 84, 90, 95, 116	18, 30	92, 93		77	
Application	78, 102	11, 14, 59, 63, 105, 108	5, 36, 39, 38,48, 54, 82, 85, 115, 119		25, 28, 45, 57, 69, 71, 86, 94	
Implementation	2	13, 87	19, 26, 43, 46, 118, 120	101	50, 55, 100	
Networking	7, 20, 22, 24, 29, 31, 33	41, 47, 88, 91	9, 12, 15, 16, 49, 61, 62, 70, 104,106, 112, 96, 98, 103		79, 83	
Mobile computing	3, 6, 10, 23, 34, 35, 75, 99, 111, 113, 114	76, 89, 107	40, 44, 73, 117	53, 56, 58, 72	27, 32, 109, 110	
Embedded Systems	1, 65	17, 21, 51, 52	64, 81, 97	66, 67	74	68
Percentage	**27.50%**	**17.50%**	**32.50%**	**5.83%**	**15.83%**	**0.83%**

in terms of model, embedded systems were the least having, 0.88%, 3.51%, 0.88% and 1.75% respectively.

e. In terms of the topic and research types, implementation topic in relation to evaluation research, implementation and architecture in relation to solution proposals, implementation with respect to philosophical paper, architecture and embedded systems in terms of experience papers had the least publications with 0.83%, 1.67%, 0.83% and 0.83% respectively.

From the foregoing, the visual appeal of a systematic map assists in summarizing and offering researchers with the likelihood of stimulating interest in the results.

The different categories combined together makes the bubble plot more useful. It is imperative to state that the creation of a systematic map in the absence of a successive systematic review is valuable in itself. This is because the systematic map enables the identification of research gaps and shortage of publication in this field of study. This paper provided six classes of studies namely architecture, application, implementation, networking, mobile computing and embedded systems, which could be discussed as regards to either tool, model, method, metric and process or evaluation, validation, solution, philosophical and opinion research. The few aforementioned areas, along these lines, are suggested for additional research, and the rundown of primary studies would likewise help meaning researchers.

5. Conclusion

Cloud computing is providing opportunities in different areas of human life. More areas of cloud research are opening up on a regular basis. This has led to increasing studies and consequent publications in cloud computing. There are volumes of research effort that is useful both to the cloud users and cloud providers alike. The aspect of devices management and models in relation to cloud, fog, edge and mobile computing has continued to receive attention. Despite the large quantity of publications in this field of study, the systematic map has shown that there are shortage of publications in this field of study. The visual representation provided by the systematic map enhances decision on areas of further research. This systematic mapping study has been able to identify some areas where there were less emphasis on the topic, based on the categories used in the scheme. This paper has therefore contributed to knowledge by highlighting the different aspects of the study with gaps, and recommending them for further studies. Also, further research could be carried out to validate this study or resolve contradictory issues. In summary, this study created a systematic map that could be advantageous to the cloud community, and will assist researchers in uncovering the critical gaps that were not previously explored.

Conflict of Interest

The authors declare no conflict of interest.

Acknowledgment

We acknowledge the support and sponsorship provided by Covenant University through the Centre for Research, Innovation, and Discovery (CUCRID).

References

[1] R. Buyya, J. Broberg, and A. Goscinski, "Cloud computing principles and paradigms," John Wiley and Son, 2011, pp. 4-10.

[2] I. Odun-Ayo, S. Misra, N. Omoregbe, E. Onibere, Y. Bulama, and R. Damaševičius, "Cloud-based security driven human resource management system," Frontiers in Artificial Intelligence and Applications. 295, pp. 96 – 106, 2017. doi:10.3233/978-1-61499-773-3-96

[3] I. Odun-Ayo, M. Ananya, F. Agono, and R. Goddy-Worlu, "Cloud computing architecture: A critical analysis," In IEEE Proceedings of the 2018 18th International Conference on Computational Science and Its Applications (ICCSA 2018), pp. 1-7 doi: 10.1109/ICCSA.2018.8439638

[4] I. Odun-Ayo, B. Odede, and R. Ahuja, "Cloud applications management- Issues and developments," Lecture Notes in Computer Science (including

subseries Lecture Notes in Artificial Intelligence and Lecture Notes in Bioinformatics), Vol.10963, pp. 683-694, 2018, Berlin, Germany: Springer.
[5] I. Odun-Ayo, S. Misra, O. Abayomi-Alli, and O. Ajayi, "Cloud multi-tenancy: Issues and developments," UCC '17 Companion, Companion Proceedings of the10th International Conference on Utility and Cloud Computing. pp. 209 – 214, 2017.
[6] I. Odun-Ayo, N. Omoregbe, M. Odusami, and O. Ajayi, "Cloud ownership and reliability - Issues and developments," Lecture Notes in Computer Science (including subseries Lecture Notes in Artificial Intelligence and Lecture Notes in Bioinformatics), Vol. 10658, pp. 231-240, 2017, Berlin, Germany: Springer.
[7] S. K. Datta and C. Bonnet, "An Edge computing Architecture integrating virtual IOT Devices," EURECO Sophia Antipolis, France.
[8] T. M. Beck and M. Maier, "Mobile Edge computing challenges for future Virtual Networking Embedding Algorithms," IARIA, 2014.
[9] J. Wenke and M. Jiangbo, "A Reference Model of cloud operating and open source software implementation mapping," 18th IEEE international Work Shop on enables Technologies: Infrastructures for collaborations Enterprises, 2009.
[10] P. Varshney and Y. Simmhan, "Demonstrating Fog computing: Characterizing Architectures, Applications and Abstractions," arxiv: 1702.06331v1 [cs.Dc] 21 Feb. 2017.
[11] G. Baranwal and D. P. Vidyarthi, "A cloud service selection model using improved ranked voting method", Concurring and Computation: Practice and Experience," Wileyonhinelibrary.com, 2008.
[12] K. Petersen, R. Feldt, S. Mujtaba and M. Matisson, "Systematic Mapping Studies In Software Engineering", EASE'08 Proceedings of the 12th international conference on Evaluation and Assessment in Software Engineering, Italy — June 26 - 27, 2008, , pp. 68-77
[13] J.L. Barros-Justo, A.L. Cravero-Leal, F. B. Benitti, and R. Capilla-Sevilla, "Systematic mapping protocol: the impact of using software patterns during requirements engineering activities in real-world settings," Cornell University Library, 2017. arXiv:1701.05747v1 [cs.SE].
[14] T. Kosar, S. Bohra, and M. A. Mernik, "Protocol of a systematic mapping study for domain-specific languages," Journal of Information and Software Technology 21(C). pp. 77-91, 2016.
[15] V. Santos, E. F. Souza, K. R. Felizardo, and N. L. Vijaykumar, "Analyzing the Use of Concept Maps in Computer Science: A Systematic Mapping Study," Informatics in Education, 16(2) pp. 257–288, 2017. doi:10.15388/infedu.2017.13
[16] M. Souza, L. Veado, R. T. Moreira, E. Figueiredo, and H. Costa, "A systematic mapping study on game-related methods for software engineering education," Information and Software Technology 95, pp. 201-218, 2018.
[17] C. R. Fernandez-Blanco, F. Careri, K. Kavvadias, I. Hidalgo Gonzalez, A. Zucker, and E. Peteves, "Systematic mapping of power system models: Expert survey," EUR 28875 EN, Publications Office of the European Union, Luxembourg, 2017, ISBN 978-92-79-76462-2, doi:10.2760/422399, JRC109123.
[18] M. Mernik, "Domain-specific languages: A systematic mapping study," International Conference on Current Trends in Theory and Practice of Informatics, Lecture Notes in Computer Science, Vol. 10139, pp. 464-472, 2017, Berlin, Germany: Springer.
[19] C. Griffo, J. P. A. Almeida, and G. Guizzardi, "A systematic mapping of the literature on legal core ontologies," In Brazilian Conference on Ontologies, ONTOBRAS 15, 2015, CEUR Workshop Proceedings.
[20] A. Ahmad, P. Brereton, and P. Andras, "A systematic mapping study of empirical studies on software cloud testing methods," In IEEE International Conference on Software Quality, Reliability and Security Companion, pp. 555-562, 2017.
[21] M. Alavi, and D. E. Leidner, "Knowledge management and knowledge management systems: Conceptual foundations and research issues," MIS Quarterly, pp. 107-136, 2001.
[22] S. K. Boell, and D. Cecez-Kecmanovic, "On being 'Systematic' in literature reviews," In Formulating Research Methods for Information Systems, Palgrave Macmillan, London, pp. 48-78, 2015.
[23] P. Brereton, B. A. Kitchenham, D. Budgen, M. Turner, and M. Khalil, "Lessons from applying the systematic literature review process within the software engineering domain," Journal of Systems and Software, vol. 80, no. 4, pp. 571-583, 2007.
[24] H. M. Cooper, "Scientific guidelines for conducting integrative research reviews," Review of educational research, vol. 52, no.2, pp. 291-302, 1982.
[25] J. L. Galvan, and M. C. Galvan, "Writing literature reviews: A guide for students of the social and behavioral sciences," Routledge, 2017.
[26] B. Kitchenham, O. P. Brereton, D. Budgen, M. Turner, J. Bailey, and S. Linkman, "Systematic literature reviews in software engineering–a systematic literature review," Information and Software Technology, vol. 51, no. 1, pp. 7-15, 2009.
[27] K. Petersen, S. Vakkalanka, and L. Kuzniarz, "Guidelines for conducting systematic mapping studies in software engineering: An update," Information and Software Technology, vol. 64, pp. 1-18, 2015.
[28] J. Vom Brocke, A. Simons, K. Riemer, B. Niehaves, R. Plattfaut, and A. Cleven, "Standing on the Shoulders of Giants: Challenges and Recommendations of Literature Search in Information Systems Research," CAIS, vol. 37, no. 9, 2015
[29] I. Odun-Ayo, R. Goddy-Worlu, O. Ajayi and E. Grant, "A Systematic Mapping Study of High Performance Computing and the Cloud". ARPN Journal of Engineering and Applied Sciences, vol. 13, Issue 24, pp. 9886-9700, 1 Dec 2018.
[30] I. Odun-Ayo, O. Ajayi, R. Goddy-Worlu and J. Yahaya, "A Systematic Mapping Study of Cloud Resources Management and Scalability in Brokering, Scheduling, Capacity Planning and Elasticity". Asian Journal of Scientific Research, vol. 12, pp. 151-166, 2019.
[31] A. C. Muhammed and A. B. Muhammed, "A systematic Mapping study of software architectures for cloud based systems," Software System section, IT University of Copenhagen, 2014.
[32] R. Wieringa, N. A. Maiden, N. R. Mead and C. Rolland, "Requirement engineering paper classification and evaluation criteria. A proposal and a discussion," Requirement Engineering, vol. 11, pp. 102-107, 2006.

Appendix: List of primary studies

[1] Al-Jaroodi, J., Mohamed, N., Jawhar, I., Mahmoud, S. CoTWare: A Cloud of Things Middleware (2017) Proceedings - IEEE 37th International Conference on Distributed Computing Systems Workshops, ICDCSW 2017, art. no. 7979819, pp. 214-219.
[2] Al-Joboury, I.M., Al-Hemiary, E.H. F2CDM: Internet of things for healthcare network based fog-to-cloud and data-in-motion using MQTT protocol (2017) Lecture Notes in Computer Science (including subseries Lecture Notes in Artificial Intelligence and Lecture Notes in Bioinformatics), 10542 LNCS, pp. 368-379.
[3] Alonso-Monsalve, S., García-Carballeira, F., Calderón, A. A heterogeneous mobile cloud computing model for hybrid clouds (2018) Future Generation Computer Systems, . Article in Press.
[4] Alsaffar, A.A., Pham, H.P., Hong, C.-S., Huh, E.-N., Aazam, M. An Architecture of IoT Service Delegation and Resource Allocation Based on Collaboration between Fog and Cloud Computing (2016) Mobile Information Systems, 2016, art. no. 6123234, .
[5] Anantula, P.R., Someswar, G.M. Protecting data in cloud environment from intruders using fog computing mechanism and control flows (2018) Proceedings of the 2nd International Conference on Communication and Electronics Systems, ICCES 2017, 2018-January, pp. 176-182.
[6] Arfat, Y., Aqib, M., Mehmood, R., Albeshri, A., Katib, I., Albogami, N., Alzahrani, A. Enabling Smarter Societies through Mobile Big Data Fogs and Clouds (2017) Procedia Computer Science, 109, pp. 1128-1133.
[7] Arun, S.H., Sharma, S.K., Chaurasia, S., Kumar, R. Detection and analysis of fog/low cloud using Ceilometer and INSAT-3D satellite data over Delhi Earth Station, New Delhi (2017) 38th Asian Conference on Remote Sensing - Space Applications: Touching Human Lives, ACRS 2017, 2017-October, .
[8] Bhatia, M., Sood, S.K. Exploring Temporal Analytics in Fog-Cloud Architecture for Smart Office HealthCare (2018) Mobile Networks and Applications, pp. 1-19. Article in Press.
[9] Bruschi, R., Davoli, F., Lago, P., Lombardo, A., Lombardo, C., Rametta, C., Schembra, G. An SDN/NFV platform for personal cloud services (2017) IEEE Transactions on Network and Service Management, 14 (4), pp. 1143-1156.
[10] Bruschi, R., Lago, P., Lombardo, C. In-Network Programmability for Next-generation Personal Cloud Service Support (INPUT) (2016) Procedia Computer Science, 97, pp. 114-117.
[11] Byrne, J., Svorobej, S., Giannoutakis, K.M., Tzovaras, D., Byrne, P.J., Östberg, P.-O., Gourinovitch, A., Lynn, T. A review of cloud computing simulation platforms & related environments (2017) CLOSER 2017 - Proceedings of the 7th International Conference on Cloud Computing and Services Science, pp. 651-663.
[12] Chaudhary, D., Bhushan, K., Gupta, B.B. Survey on DDoS attacks and defense mechanisms in cloud and fog computing (2018) International Journal of E-Services and Mobile Applications, 10 (3), pp. 61-83.
[13] Chaudhary, R., Kumar, N., Zeadally, S. Network Service Chaining in Fog and Cloud Computing for the 5G Environment: Data Management and

Security Challenges (2017) IEEE Communications Magazine, 55 (11), art. no. 8114560, pp. 114-122.

[14] Chen, F., Li, H., Liu, J., Li, B., Xu, K., Hu, Y. Migrating big video data to cloud: a peer-assisted approach for VoD (2017) Peer-to-Peer Networking and Applications, pp. 1-15. Article in Press.

[15] Deepali, Bhushan, K. DDoS attack defense framework for cloud using fog computing (2018) RTEICT 2017 - 2nd IEEE International Conference on Recent Trends in Electronics, Information and Communication Technology, Proceedings, 2018-January, pp. 534-538.

[16] Deng, R., Lu, R., Lai, C., Luan, T.H., Liang, H. Optimal Workload Allocation in Fog-Cloud Computing Toward Balanced Delay and Power Consumption (2016) IEEE Internet of Things Journal, 3 (6), art. no. 7467406, pp. 1171-1181.

[17] Desirena Lopez, H.J., Siller, M., Huerta, I. Internet of vehicles: Cloud and fog computing approaches (2017) Proceedings - 2017 IEEE International Conference on Service Operations and Logistics, and Informatics, SOLI 2017, 2017-January, pp. 211-216.

[18] Dixit, A., Yadav, A.K., Kumar, S. An efficient architecture and algorithm for server provisioning in Cloud computing using clustering approach (2017) Proceedings of the 5th International Conference on System Modeling and Advancement in Research Trends, SMART 2016, art. no. 7894532, pp. 260-266.

[19] Elkhatib, Y., Porter, B., Ribeiro, H.B., Zhani, M.F., Qadir, J., Riviere, E. On using micro-clouds to deliver the fog (2017) IEEE Internet Computing, 21 (2), art. no. 7867723, pp. 8-15.

[20] El-Latif, A.A.A., Abd-El-Atty, B., Hossain, M.S., Elmougy, S., Ghoneim, A. Secure quantum steganography protocol for fog cloud internet of things (2018) IEEE Access, 6, pp. 10332-10340.

[21] Elmisery, A.M., Rho, S., Aborizka, M. A new computing environment for collective privacy protection from constrained healthcare devices to IoT cloud services (2017) Cluster Computing, pp. 1-28. Article in Press.

[22] Elmisery, A.M., Sertovic, M. Privacy enhanced cloud-based recommendation service for implicit discovery of relevant support groups in healthcare social networks (2017) International Journal of Grid and High Performance Computing, 9 (1), pp. 75-91.

[23] Elmroth, E., Leitner, P., Schulte, S., Venugopal, S. Connecting Fog and Cloud Computing (2017) IEEE Cloud Computing, 4 (2), art. no. 7912269, pp. 22-25.

[24] Escamilla-Ambrosio, P.J., Rodríguez-Mota, A., Aguirre-Anaya, E., Acosta-Bermejo, R., Salinas-Rosales, M. Distributing computing in the internet of things: Cloud, fog and edge computing overview (2018) Studies in Computational Intelligence, 731, pp. 87-115.

[25] Farris, I., Militano, L., Nitti, M., Atzori, L., Iera, A. MIFaaS: A Mobile-IoT-Federation-as-a-Service Model for dynamic cooperation of IoT Cloud Providers (2017) Future Generation Computer Systems, 70, pp. 126-137.

[26] Farris, I., Girau, R., Militano, L., Nitti, M., Atzori, L., Iera, A., Morabito, G. Social Virtual Objects in the Edge Cloud (2015) IEEE Cloud Computing, 2 (6), art. no. 7397053, pp. 20-28.

[27] Farris, I., Militano, L., Nitti, M., Atzori, L., Iera, A. Federated edge-assisted mobile clouds for service provisioning in heterogeneous IoT environments (2015) IEEE World Forum on Internet of Things, WF-IoT 2015 - Proceedings, art. no. 7389120, pp. 591-596.

[28] Fernandez, E.B., Yoshioka, N., Washizaki, H., Syed, M.H. Modeling and security in cloud ecosystems (2016) Future Internet, 8 (2), art. no. 13, .

[29] Goleva, R., Stainov, R., Kletnikov, N., Achkoski, J., Mirtchev, S., Ganchev, I., Savov, A. Performance Analysis of End-to-End Sensor-to-Cloud Personal Living Platform (2017) Procedia Computer Science, 113, pp. 615-620.

[30] Gupta, R., Garg, R. Mobile Applications Modelling and Security Handling in Cloud-Centric Internet of Things (2015) Proceedings - 2015 2nd IEEE International Conference on Advances in Computing and Communication Engineering, ICACCE 2015, art. no. 7306695, pp. 285-290.

[31] Hajibaba, M., Gorgin, S. A review on modern distributed computing paradigms: Cloud computing, jungle computing and fog computing (2014) Journal of Computing and Information Technology, 22 (2), pp. 69-84.

[32] Hajji, W., Tso, F.P. Understanding the performance of low power raspberry pi cloud for big data (2016) Electronics (Switzerland), 5 (2), art. no. 29, .

[33] Hani, Q.B., Ditcher, J.P. Stand-Out Segmentation Access Control for Cloud Outsourced Data (2017) Proceedings - 2017 IEEE 1st International Conference on Edge Computing, EDGE 2017, art. no. 8029278, pp. 210-215.

[34] Hasan, R., Hossain, M., Khan, R. Aura: An incentive-driven ad-hoc IoT cloud framework for proximal mobile computation offloading (2017) Future Generation Computer Systems, . Article in Press.

[35] Hong, H.-J. From cloud computing to fog computing: Unleash the power of edge and end devices (2017) Proceedings of the International Conference on Cloud Computing Technology and Science, CloudCom, 2017-December, pp. 331-334.

[36] Huang, C.-Y., Xu, K. Reliable realtime streaming in vehicular cloud-fog computing networks (2016) 2016 IEEE/CIC International Conference on Communications in China, ICCC 2016, art. no. 7636838, .

[37] Hung, S.-C., Hsu, H., Lien, S.-Y., Chen, K.-C. Architecture harmonization between cloud radio access networks and fog networks (2015) IEEE Access, 3, art. no. 07359093, pp. 3019-3034.

[38] Jalali, F., Hinton, K., Ayre, R., Alpcan, T., Tucker, R.S. Fog computing may help to save energy in cloud computing (2016) IEEE Journal on Selected Areas in Communications, 34 (5), art. no. 7439752, pp. 1728-1739.

[39] Jayalath, C., Stephen, J.J., Eugster, P. Atmosphere: A universal cross-cloud communication infrastructure (2013) Lecture Notes in Computer Science (including subseries Lecture Notes in Artificial Intelligence and Lecture Notes in Bioinformatics), 8275 LNCS, pp. 163-182.

[40] Kanapram, D., Lamanna, G., Repetto, M. Exploring the trade-off between performance and energy consumption in cloud infrastructures (2017) 2017 2nd International Conference on Fog and Mobile Edge Computing, FMEC 2017, art. no. 7946418, pp. 121-126.

[41] Khalid, A., Shahbaz, M. Adaptive deadline-aware scheme (ADAS) for data migration between cloud and fog layers (2018) KSII Transactions on Internet and Information Systems, 12 (3), pp. 1002-1015.

[42] Khalid, A., Shahbaz, M. Service architecture models for fog computing: A remedy for latency issues in data access from clouds (2017) KSII Transactions on Internet and Information Systems, 11 (5), pp. 2310-2345.

[43] Kim, O.T.T., Dang Tri, N., Nguyen, V.D., Tran, N.H., Hong, C.S. A shared parking model in vehicular network using fog and cloud environment (2015) 17th Asia-Pacific Network Operations and Management Symposium: Managing a Very Connected World, APNOMS 2015, art. no. 7275447, pp. 321-326.

[44] Kirkham, T., Armstrong, D., Djemame, K., Jiang, M. Risk driven Smart Home resource management using cloud services (2014) Future Generation Computer Systems, 38, pp. 13-22.

[45] Kirkman, S.S., Newman, R. Bridging the Cloud Trust Gap: Using ORCON Policy to Manage Consumer Trust between Different Clouds (2017) Proceedings - 2017 IEEE 1st International Conference on Edge Computing, EDGE 2017, art. no. 8029260, pp. 82-89.

[46] Kitanov, S., Janevski, T. Energy efficiency of 5G mobile networks in hybrid Fog and Cloud Computing environment (2016) CEUR Workshop Proceedings, 1746, pp. 41-46.

[47] Krishnan, Y.N., Bhagwat, C.N., Utpat, A.P. Fog computing - Network based cloud computing (2015) 2nd International Conference on Electronics and Communication Systems, ICECS 2015, art. no. 7124902, pp. 250-251.

[48] Kumar, R., Rajalakshmi, S. Mobile cloud computing: Standard approach to protecting and securing of mobile cloud ecosystems Computer Sciences and Applications, CSA 2013, art. no. 6835687, pp. 663-669.

[49] Liang, Y., Wang, T., Bhuiyan, M.Z.A., Liu, A. Research on coupling reliability problem in sensor-cloud system (2017) Lecture Notes in Computer Science (including subseries Lecture Notes in Artificial Intelligence and Lecture Notes in Bioinformatics), 10658 LNCS, pp. 468-478.

[50] Lin, Y., Shen, H. CloudFog: Leveraging Fog to Extend Cloud Gaming for Thin-Client MMOG with High Quality of Service (2017) IEEE Transactions on Parallel and Distributed Systems, 28 (2), art. no. 7465785, pp. 431-445.

[51] Lin, Y., Shen, H. Cloud fog: Towards high quality of experience in cloud gaming (2015) Proceedings of the International Conference on Parallel Processing, 2015-December, art. no. 7349605, pp. 500-509.

[52] Lin, Y., Shen, H. Leveraging Fog to Extend Cloud Gaming for Thin-Client MMOG with High Quality of Experience (2015) Proceedings - International Conference on Distributed Computing Systems, 2015-July, art. no. 7164961, pp. 734-735.

[53] Lobo, F.L., Lima, M., Oliveira, H., Harrington, J., El-Khatib, K. SoLVE: A localization system framework for VANets using the cloud and fog computing (2017) DIVANet 2017 - Proceedings of the 6th ACM Symposium on Development and Analysis of Intelligent Vehicular Networks and Applications, Co-located with MSWiM 2017, pp. 17-22.

[54] Lubamba, C., Bagula, A. Cyber-healthcare cloud computing interoperability using the HL7-CDA standard (2017) Proceedings - IEEE Symposium on Computers and Communications, art. no. 8024513, pp. 105-110.

[55] Macías-Macías, M., García-Orellana, C.J., González-Velasco, H., Gallardo-Caballero, R. Independent component analysis for cloud screening of meteosat images (2003) Lecture Notes in Computer Science (including subseries Lecture Notes in Artificial Intelligence and Lecture Notes in Bioinformatics), 2687, pp. 551-558.

[56] Macías-Macías, M., García-Orellana, C.J., González-Velasco, H.M., Gallardo-Caballero, R., Serrano-Pérez, A. A comparison of PCA and GA selected features for cloud field classification (2002) Lecture Notes in Artificial Intelligence (Subseries of Lecture Notes in Computer Science), 2527, pp. 42-49.
[57] Mahmoud, M.M.E., Rodrigues, J.J.P.C., Saleem, K., Al-Muhtadi, J., Kumar, N., Korotaev, V. Towards energy-aware fog-enabled cloud of things for healthcare (2018) Computers and Electrical Engineering, 67, pp. 58-69.
[58] Makitalo, N., Ometov, A., Kannisto, J., Andreev, S., Koucheryavy, Y., Mikkonen, T. Safe and Secure Execution at the Network Edge: A Framework for Coordinating Cloud, Fog, and Edge (2018) IEEE Software, . Article in Press.
[59] Manasrah, A.M., Aldomi, A., Gupta, B.B. An optimized service broker routing policy based on differential evolution algorithm in fog/cloud environment (2017) Cluster Computing, pp. 1-15. Article in Press.
[60] Masip-Bruin, X., Marin-Tordera, E., Jukan, A., Ren, G.-J. Managing resources continuity from the edge to the cloud: Architecture and performance (2018) Future Generation Computer Systems, 79, pp. 777-785.
[61] Masip-Bruin, X., Marin-Tordera, E., Gomez, A., Barbosa, V., Alonso, A. Will it be cloud or will it be fog? F2C, A novel flagship computing paradigm for highly demanding services (2017) FTC 2016 - Proceedings of Future Technologies Conference, art. no. 7821744, pp. 1129-1136.
[62] Meng, X., Wang, W., Zhang, Z. Delay-Constrained Hybrid Computation Offloading with Cloud and Fog Computing (2017) IEEE Access, 5, art. no. 8023966, pp. 21355-21367.
[63] Mo, Y., Peng, M., Xiang, H., Sun, Y., Ji, X. Resource allocation in cloud radio access networks with device-to-device communications (2017) IEEE Access, 5, art. no. 7855644, pp. 1250-1262.
[64] Mohamed, N., Al-Jaroodi, J., Jawhar, I., Lazarova-Molnar, S., Mahmoud, S. SmartCityWare: A service-oriented middleware for cloud and fog enabled smart city services (2017) IEEE Access, 5, art. no. 7990214, pp. 17576-17588.
[65] Mohamed, N., Lazarova-Molnar, S., Jawhar, I., Al-Jaroodi, J. Towards Service-Oriented Middleware for Fog and Cloud Integrated Cyber Physical Systems (2017) Proceedings - IEEE 37th International Conference on Distributed Computing Systems Workshops, ICDCSW 2017, art. no. 7979797, pp. 67-74.
[66] Mohamed, N., Lazarova-Molnar, S., Al-Jaroodi, J. Cloud of things: Optimizing smart city services (2017) 2017 7th International Conference on Modeling, Simulation, and Applied Optimization, ICMSAO 2017, art. no. 7934875, .
[67] Mohan, N., Zhou, P., Govindaraj, K., Kangasharju, J. Managing data in computational edge clouds (2017) MECOMM 2017 - Proceedings of the 2017 Workshop on Mobile Edge Communications, Part of SIGCOMM 2017, pp. 19-24.
[68] Mohan, N., Kangasharju, J. Edge-Fog cloud: A distributed cloud for Internet of Things computations (2017) 2016 Cloudification of the Internet of Things, CIoT 2016, art. no. 7872914, .
[69] Mueller, H., Gogouvitis, S.V., Seitz, A., Bruegge, B. Seamless computing for industrial systems spanning cloud and edge (2017) Proceedings - 2017 International Conference on High Performance Computing and Simulation, HPCS 2017, art. no. 8035079, pp. 209-216.
[70] Mueller, H., Gogouvitis, S.V., Haitof, H., Seitz, A., Bruegge, B. Poster abstract: Continuous computing from cloud to edge (2016) Proceedings - 1st IEEE/ACM Symposium on Edge Computing, SEC 2016, art. no. 7774685, pp. 97-98.
[71] Munir, A., Kansakar, P., Khan, S.U. IFCIoT: Integrated Fog Cloud IoT: A novel architectural paradigm for the future Internet of Things (2017) IEEE Consumer Electronics Magazine, 6 (3), art. no. 7948854, pp. 74-82.
[72] Nan, Y., Li, W., Bao, W., Delicato, F.C., Pires, P.F., Zomaya, A.Y. A dynamic tradeoff data processing framework for delay-sensitive applications in Cloud of Things systems (2018) Journal of Parallel and Distributed Computing, 112, pp. 53-66.
[73] Nan, Y., Li, W., Bao, W., Delicato, F.C., Pires, P.F., Dou, Y., Zomaya, A.Y. Adaptive Energy-Aware Computation Offloading for Cloud of Things Systems (2017) IEEE Access, 5, art. no. 8081765, pp. 23947-23957.
[74] Okafor, K.C., Ugwoke, F.N., Obayi, A.A. Evaluation of virtualized osmotic cloud network using discrete event Branch-And-Bound heuristics (2018) 2017 IEEE 3rd International Conference on Electro-Technology for National Development, NIGERCON 2017, 2018-January, pp. 425-437.
[75] Osanaiye, O., Chen, S., Yan, Z., Lu, R., Choo, K.-K.R., Dlodlo, M. From Cloud to Fog Computing: A Review and a Conceptual Live VM Migration Framework (2017) IEEE Access, 5, art. no. 7896564, pp. 8284-8300.
[76] Ostberg, P.-O., Byrne, J., Casari, P., Eardley, P., Anta, A.F., Forsman, J., Kennedy, J., Le Duc, T., Marino, M.N., Loomba, R., Pena, M.A.L., Veiga, J.L., Lynn, T., Mancuso, V., Svorobej, S., Torneus, A., Wesner, S., Willis, P., Domaschka, J. Reliable capacity provisioning for distributed cloud/edge/fog computing applications (2017) EuCNC 2017 - European Conference on Networks and Communications, art. no. 7980667, .
[77] Pahl, C., Helmer, S., Miori, L., Sanin, J., Lee, B. A container-based edge cloud PaaS architecture based on raspberry Pi clusters (2016) Proceedings - 2016 4th International Conference on Future Internet of Things and Cloud Workshops, W-FiCloud 2016, art. no. 7592710, pp. 117-124.
[78] Pham, X.-Q., Man, N.D., Tri, N.D.T., Thai, N.Q., Huh, E.-N. A cost- and performance-effective approach for task scheduling based on collaboration between cloud and fog computing (2017) International Journal of Distributed Sensor Networks, 13 (11), .
[79] Pradilla, J.V., Palau, C.E. Micro Virtual Machines (MicroVMs) for Cloud-assisted Cyber-Physical Systems (CPS) (2016) Internet of Things: Principles and Paradigms, pp. 125-142.
[80] Ramirez, W., Masip-Bruin, X., Marin-Tordera, E., Souza, V.B.C., Jukan, A., Ren, G.-J., Gonzalez de Dios, O. Evaluating the benefits of combined and continuous Fog-to-Cloud architectures (2017) Computer Communications, 113, pp. 43-52.
[81] Renner, T., Kliem, A., Kao, O. The Device Cloud - Applying Cloud Computing Concepts to the Internet of Things (2014) Proceedings - 2014 IEEE International Conference on Ubiquitous Intelligence and Computing, 2014 IEEE International Conference on Autonomic and Trusted Computing, 2014 IEEE International Conference on Scalable Computing and Communications and Associated Symposia/Workshops, UIC-ATC-ScalCom 2014, art. no. 7306981, pp. 396-401.
[82] Seo, D.B., Jeon, Y.-B., Lee, S.-H., Lee, K.-H. Cloud computing for ubiquitous computing on M2M and IoT environment mobile application (2016) Cluster Computing, 19 (2), pp. 1001-1013.
[83] Shah-Mansouri, H., Wong, V.W.S. Hierarchical Fog-Cloud Computing for IoT Systems: A Computation Offloading Game (2018) IEEE Internet of Things Journal, . Article in Press.
[84] Sharma, P.K., Chen, M.-Y., Park, J.H. A Software Defined Fog Node Based Distributed Blockchain Cloud Architecture for IoT (2018) IEEE Access, 6, art. no. 8053750, pp. 115-124.
[85] Sharma, S.K., Wang, X. Live Data Analytics with Collaborative Edge and Cloud Processing in Wireless IoT Networks (2017) IEEE Access, 5, art. no. 7882669, pp. 4621-4635.
[86] Shekhar, S., Gokhale, A. Dynamic resource management across cloud-edge resources for performance-sensitive applications (2017) Proceedings - 2017 17th IEEE/ACM International Symposium on Cluster, Cloud and Grid Computing, CCGRID 2017, art. no. 7973763, pp. 707-710.
[87] Shekhar, S., Gokhale, A. Poster abstract: Enabling IoT applications via dynamic cloud-edge resource management (2017) Proceedings - 2017 IEEE/ACM 2nd International Conference on Internet-of-Things Design and Implementation, IoTDI 2017 (part of CPS Week), pp. 331-332.
[88] Shen, S., Huang, L., Zhou, H., Yu, S., Fan, E., Cao, Q. Multistage Signaling Game-Based Optimal Detection Strategies for Suppressing Malware Diffusion in Fog-Cloud-Based IoT Networks (2018) IEEE Internet of Things Journal, 5 (2), pp. 1043-1054.
[89] Shirazi, S.N., Gouglidis, A., Farshad, A., Hutchison, D. The extended cloud: Review and analysis of mobile edge computing and fog from a security and resilience perspective (2017) IEEE Journal on Selected Areas in Communications, 35 (11), art. no. 8060526, pp. 2586-2595.
[90] Shroff, G.Enterprise cloud computing: Technology, architecture, applications (2010) Enterprise Cloud Computing: Technology, Architecture, Applications, 9780521760959, pp. 1-273.
[91] Simonet, A., Lebre, A., Orgerie, A.-C. Deploying distributed cloud infrastructures: Who and at what cost? (2016) Proceedings - 2016 IEEE International Conference on Cloud Engineering Workshops, IC2EW 2016, art. no. 7527837, pp. 178-183.
[92] Sinaeepourfard, A., Garcia, J., Masip-Bruin, X., Marin-Tordera, E. A Novel Architecture for Efficient Fog to Cloud Data Management in Smart Cities (2017) Proceedings - International Conference on Distributed Computing Systems, art. no. 7980258, pp. 2622-2623.
[93] Singh, H., Bonev, B., Petkov, P., Patil, S. Cloud attenuation model at millimeter frequency bands (2018) 2017 International Conference on Infocom Technologies and Unmanned Systems: Trends and Future Directions, ICTUS 2017, 2018-January, pp. 175-180.
[94] Siravenha, A.C., Sousa, D., Bispo, A., Pelaes, E. Evaluating inpainting methods to the satellite images clouds and shadows removing (2011) Communications in Computer and Information Science, 260 CCIS, pp. 56-65.
[95] Souza, V.B., Masip-Bruin, X., Marín-Tordera, E., Sànchez-Lópex, S., Garcia, J., Ren, G.J., Jukan, A., Juan Ferrer, A. Towards a proper service

placement in combined Fog-to-Cloud (F2C) architectures (2018) Future Generation Computer Systems, 87, pp. 1-15.

[96] Souza, V.B., Masip-Bruin, X., Marin-Tordera, E., Ramirez, W., Sanchez-Lopez, S. Proactive vs reactive failure recovery assessment in combined Fog-to-Cloud (F2C) systems (2017) IEEE International Workshop on Computer Aided Modeling and Design of Communication Links and Networks, CAMAD, 2017-June, art. no. 8031528,

[97] Souza, V.B.C., Ramirez, W., Masip-Bruin, X., Marin-Tordera, E., Ren, G., Tashakor, G. Handling service allocation in combined Fog-cloud scenarios (2016) 2016 IEEE International Conference on Communications, ICC 2016, art. no. 7511465, .

[98] Srinivas, K.K., Ramana, T.V. Severe cause of cloud attenuation and rain attenuation on space communication link at millimetre band and differentiation between rain attenuation and cloud attenuation (2017) Proceedings - 7th IEEE International Advanced Computing Conference, IACC 2017, art. no. 7976797, pp. 255-259.

[99] Stankova, E.N., Korkhov, V.V., Kulabukhova, N.V., Vasilenko, A.Y., Holod, I.I. Computational environment for numerical modeling of the results of cloud seeding (2016) Lecture Notes in Computer Science (including subseries Lecture Notes in Artificial Intelligence and Lecture Notes in Bioinformatics), 9788, pp. 454-462.

[100] Syed, M.H., Fernandez, E.B. Cloud ecosystems support for internet of things and DevOps using patterns (2016) Proceedings - 2016 IEEE 1st International Conference on Internet-of-Things Design and Implementation, IoTDI 2016, art. no. 7471379, pp. 301-304.

[101] Taherkordi, A., Eliassen, F. Poster abstract: Data-centric IoT services provisioning in Fog-Cloud computing systems (2017) Proceedings - 2017 IEEE/ACM 2nd International Conference on Internet-of-Things Design and Implementation, IoTDI 2017 (part of CPS Week), pp. 317-318.

[102] Tang, C., Wei, X., Xiao, S., Chen, W., Fang, W., Zhang, W., Hao, M. A Mobile Cloud Based Scheduling Strategy for Industrial Internet of Things (2018) IEEE Access, 6, pp. 7262-7275.

[103] Tao, M., Ota, K., Dong, M. Foud: Integrating Fog and Cloud for 5G-Enabled V2G Networks (2017) IEEE Network, 31 (2), art. no. 7884943, pp. 8-13.

[104] Teerapittayanon, S., McDanel, B., Kung, H.T. Distributed Deep Neural Networks over the Cloud, the Edge and End Devices (2017) Proceedings - International Conference on Distributed Computing Systems, art. no. 7979979, pp. 328-339.

[105] Tinini, R.I., Reis, L.C.M., Batista, D.M., Figueiredo, G.B., Tornatore, M., Mukherjee, B. Optimal Placement of Virtualized BBU Processing in Hybrid Cloud-Fog RAN over TWDM-PON (2018) 2017 IEEE Global Communications Conference, GLOBECOM 2017 - Proceedings, 2018-January, pp. 1-6.

[106] Truong, H.-L., Narendra, N.C., Lin, K.-J. Notes on ensembles of IoT, network functions and clouds for service-oriented computing and applications (2018) Service Oriented Computing and Applications, 12 (1), .

[107] Tseng, F.-H., Cho, H.-H., Chang, K.-D., Li, J.-C., Shih, T.K. Application-oriented offloading in heterogeneous networks for mobile cloud computing (2018) Enterprise Information Systems, 12 (4), pp. 398-413.

[108] Van Kempen, A., Crivat, T., Trubert, B., Roy, D., Pierre, G. MEC-ConPaaS: An Experimental Single-Board Based Mobile Edge Cloud (2017) Proceedings - 5th IEEE International Conference on Mobile Cloud Computing, Services, and Engineering, MobileCloud 2017, art. no. 7944867, pp. 17-24.

[109] Varghese, B., Buyya, R. Next generation cloud computing: New trends and research directions (2018) Future Generation Computer Systems, 79, pp. 849-861.

[110] Wang, H., Wang, Z., Domingo-Ferrer, J. Anonymous and secure aggregation scheme in fog-based public cloud computing (2018) Future Generation Computer Systems, 78, pp. 712-719.

[111] Wang, J., Yang, Y., Zhang, G., Yu, S. Climatic trend of cloud amount related to the aerosol characteristics in Beijing during (2010) Acta Meteorologica Sinica, 24 (6), pp. 762-775.

[112] Wang, L., Xie, W., Li, L., Pei, J. A thin cloud and fog removal method for remote sensing multi-spectral images (2013) Shenzhen Daxue Xuebao (Ligong Ban)/Journal of Shenzhen University Science and Engineering, 30 (6), pp. 592-597.

[113] Wang, S., Urgaonkar, R., He, T., Chan, K., Zafer, M., Leung, K.K. Dynamic Service Placement for Mobile Micro-Clouds with Predicted Future Costs (2017) IEEE Transactions on Parallel and Distributed Systems, 28 (4), pp. 1002-1016.

[114] Wang, T., Li, Y., Chen, Y., Tian, H., Cai, Y., Jia, W., Wang, B. Fog-based evaluation approach for trustworthy communication in sensor-cloud system (2017) IEEE Communications Letters, 21 (11), art. no. 8010796, pp. 2532-2535.

[115] Wang, T., Zeng, J., Bhuiyan, M.Z.A., Tian, H., Cai, Y., Chen, Y., Zhong, B. Trajectory Privacy Preservation Based on a Fog Structure for Cloud Location Services (2017) IEEE Access, 5, art. no. 7918561, pp. 7692-7701.

[116] 2016) IEEE Workshop on Local and Metropolitan Area Networks, 2016-August, art. no. 7548853, .

[117] Yannuzzi, M., Milito, R., Serral-Gracia, R., Montero, D., Nemirovsky, M. Key ingredients in an IoT recipe: Fog Computing, Cloud computing, and more Fog Computing(2014) 2014 IEEE 19th International Workshop on Computer Aided Modeling and Design of Communication Links and Networks, CAMAD 2014, art. no. 7033259, pp. 325-329.

[118] Zeng, J., Wang, T., Jia, W., Peng, S., Wang, G. A Survey on Sensor-Cloud (2017) Jisuanji Yanjiu yu Fazhan/Computer Research and Development, 54 (5), pp. 925-939.

[119] Zeng, J., Wang, T., Lai, Y., Liang, J., Chen, H. Data Delivery from WSNs to Cloud Based on a Fog Structure (2017) Proceedings - 2016 International Conference on Advanced Cloud and Big Data, CBD 2016, art. no. 7815194, pp. 104-109.

[120] Zhao, W., Liu, J., Hara, T. Optimal Replica Distribution in Edge-Node-Assisted Cloud-P2P Platforms for Real-Time Streaming (2018) IEEE Transactions on Vehicular Technology, . Article in Press.

Advances in Science, Technology and Engineering Systems Journal Vol. 4, No. 2, 102-106 (2019)

www.astesj.com

ASTESJ

ISSN: 2415-6698

Design and Analysis of 32-bit Parallel Prefix Adders for Low Power VLSI Applications

Samraj Daphni*, Kasinadar Sundari Vijula Grace

Electronics and Communication Engineering, Noorul Islam Centre for Higher Education, 629180, India

A R T I C L E I N F O

Article history:
Received: 26 January, 2019
Accepted: 27 February, 2019
Online: 15 March, 2019

Keywords:
Parallel Prefix Adder
Ladner Fischer Adder
Power Gating Technique
Carry Generation Stage
Carry Look ahead Adder

A B S T R A C T

The basic processes like addition, subtraction can be done using various types of binary adders with dissimilar addition times (delay), area and power consumption in any digital processing applications. To minimize the Power Delay Product (PDP) of Digital Signal Processing (DSP) processors is necessary for high performance in Very Large Scale Integration (VLSI) applications. In this paper, a 32–bit various Parallel Prefix adders design is proposed and compared the performance results on the aspects of area, delay and power. Implementation (Simulation and Synthesis) results really achieve significant improvement in power and power-delay product when compared with the previous bit adders which is used in processors. To reduce the power, here apply the energy recovery logic like power gating technique for all three adders. All the simulations and synthesis results can be noted using Xilinx ISE 14.2i tool.

1. Introduction

Generally, the basic processes such as addition, subtraction, division that can be done by using different types of binary adders in any digital based processors and control systems [1]. The adder performance which is used in the device is only measured the high speed and accuracy of a processor or system. Previously the processors are used 32 bit carry adders like Ripple Carry Adder (RCA), Carry Propagate Adder (CPA), and Carry Look ahead Adders (CLA) with different addition times (delay), area and power consumption [2]. How fast the carry reaches for every single bit position, from which the delay of any binary adder is calculated. Henceforth, the carry chain which generates the carry bit is the major challenge in binary adder design. But the above existing 32 bit basic carry adders having high delay value in higher order bits because each level of adder has to wait for the previous carry result [3]. Due to the above problem of 32 bit basic existing carry adders, in today’s world of technology, PPA is well suitable designed adder for high speed addition process with less delay in VLSI technology [4]. Also the PPA is one of the most popular designs and provides good negotiation amongst area, speed and power [5]. The low order PPA is designed at earlier like 8 bit and 16 bit. This paper is designed as follows, in second section: describes briefly about PPA, in third section: explains the design of 32 bit proposed Parallel Prefix (Kogge Stone Adder, Brent kung Adder, Ladner Fischer Adder), in fourth section: it expresses the simulation results (waveform and reports) of 32 bit PPA which we have designed in the previous section with the performance aspects (delay, area and power). The last section is concluded that Kogge Stone Adder performance is best among other adders with low power and less delay from the above analyzed results of 32 bit PPA.

*Samraj Daphni, W/O. Mr. D. Thavasumony, North Midalakkadu, Palappallam Post, Kanyakumari District – 629159, Tamil Nadu, India, +91 8675857541 & daphnithavasumony@gmail.com

2. Parallel Pefix Adder

Now a days, to avoid the higher delay problem of existing carry adders the PPA is used which is simply the modified design form of CLA. The Prefix adders can be designed in many different ways based on the different requirements and the production of carries [6]. Recently, use the tree structure form of adders to raise the speed of addition function in any kind of processors. PPA are fastest adders with tree structure based and used for high performance arithmetic processes in successive industries and DSP laboratories [7].

The PPA’s are also called as logarithmic delay adders because the delay value is established using logarithmic functions [8]. Addition in PPA can be processed using three main actions such as Pre-computation (P and G signal generation), Prefix-computation (carry signals group generation), Post-computation (Sum signal generation) [9].

2.1. Pre – Computation

In the pre-processing stage, propagate functions and generate functions are calculated depends upon the given input signals [10]. The propagate functions are carried out by the equation (1).

$$P[j] = X[j] \oplus Y[j] \quad (1)$$

It is stated that X and Y are the input signals that composed by XOR logic gate. The generate functions are carried out by the equation (2).

$$G[j] = X[j] \cdot B[j] \quad (2)$$

It is stated that X and Y are the input signals that composed by AND logic gate. Since the above equations (1) and (2) are done in parallel, it does not increasing a significant calculation of area consumption and delay fully depends upon the bit size which is desired at the input [11].

2.2. Prefix – Computation

This prefix computation stage, calculates the carry signal groups directly, which uses the input and values which measured from the first stage. Carry signals generation uses the more than two inputs for which the delay is automatically increased in this process [12]. The carry propagation function and carry generation function [13] is measured by the equations (3) and (4).

$$\text{Carry } P = P[j] \cdot P[j+1] \quad (3)$$

$$\text{Carry } G = (G[j] \cdot P[j+1]) + G[j+1] \quad (4)$$

2.3. Post – Computation

In this stage, the sum result is generated by an Ex-OR operation that uses the values of carry generation stage (prefix-computation). The last sum operation is calculated by the equation (5)

$$S[j+1] = P[j+1] \oplus C[j] \quad (5)$$

Where C is the last carry signal and P is the propagate function [14].

3. Design and analysis of proposed 32 bit various PPA

To overcome high delay problem of existing carry adders this work proposed the design of 32-bit various PPA for less delay and low power VLSI applications. This proposed system consists of two modules: The first module is to design of 32 bit PPA like KSA, BKA, and LFA. The second module is to analyses the performance comparison of PPA on the basis of area, delay and power.

In this section, analyse the different technologies of adders to design in the form of parallel prefix, apart from the RCA topology, such as Kogge-Stone, Brent-Kung, and Ladner-Fisher PPA. The important aim is to examine the trade-off between area consumption delay and power consumption in the particular PPA depends upon the design performance. All the designs are using a power gating technique to reduce the power consumption [15].

3.1. Kogge Stone Adder (KSA)

Normally, the KSA attains the key role with fast addition operation and it reflects like prefix form of Carry Look ahead Adder (CLA). Also this type of PPA entirely decreases the delay time in design to generate the carry signals [16]. Henceforth this KSA is popularly used in DSP (Digital Signal Processing) laboratory and Control system industries for fast arithmetic function.

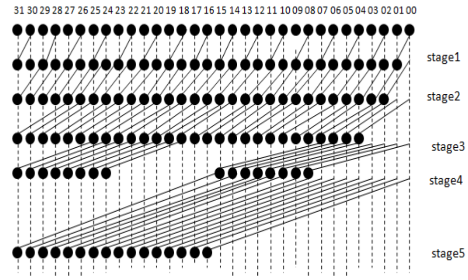

Figure 1: 32 bit Kogge Stone Adder design

The structure of 32-bit KSA design is exposed in Figure 1. This design can be divided into 5 stages [17]. The calculation of Propagate and Generate signals using full adders with carry input that process included in first and second stage. The generation of carry signals which used the values of Propagate and Generate that process included in third and fourth stage. The calculation of sum bits based on the P and carry generation values that is included in the fifth stage [18]. This 32 bit design of KSA is coded by VHDL and viewed the test bench waveform and analyzed the performance and noted the results.

3.2. Brent Kung Adder (BKA)

The BKA calculates the prefixes based on the bit groups. Initially calculate the prefixes values for 2 bit groups. These 2 bit prefix values are used to find the prefix values for the 4 bit groups, that are used to calculate the prefix values for 8 bit groups and so on [19]. Then these prefixes values are used to measure the carry out of the particular bit stage. These carries will be used along with the Group Propagate of the next stage to calculate the Sum bit of that stage [20]. Brent Kung Tree will be using (2log2N-1) stages for any bit design.

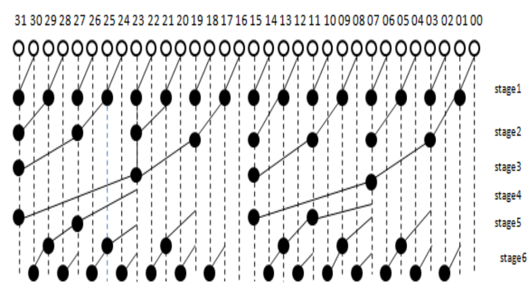

Figure 2: 32 bit Brent Kung Adder design

The structure of 32-bit BKA design is given in Figure 2. Hence the designing of 32- bit adder takes the number of stages will be 9. The fan-out for every bit stage is limited to 2. The above diagram shows the fan out being reduced and the loading on the advance stages being reduced [21]. This 32 bit design of BKA is coded by VHDL and viewed the test bench waveform and analysed the performance and noted the results.

3.3. Ladner Fischer Adder (LFA)

The LFA tree structures are a family of tree networks between Brent Kung and Sklansky tree. It is very close like to Sklansky PPA, but it calculates the prefix values for odd number bits after that again uses another stage which ripple into the even locations [22]. At higher order bits, to get improved in speeds the cells must still be properly sized or grouped.

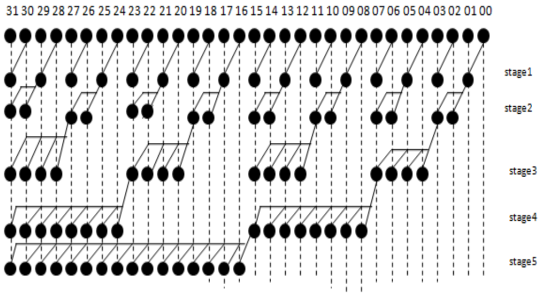

Figure 3: 32 bit Ladner Fischer Adder design

The structure of 32-bit LFA design is exposed in Figure 3. The Ladner Fischer adder is used for high performance arithmetic operation with complicate designs. The LFA consists of black cells and gray cells with 5 stages for 32 bit design. Each black cell encloses only one OR logic gate and two AND logic gates. Each gray cell contains only one AND logic gate [23]. This 32 bit design of LFA is coded by VHDL and viewed the test bench waveform and analysed the performance and noted the results.

4. Simulation results of proposed 32 bit PPA

In this simulation section, took all three types of 32 bit parallel prefix adders (KS, BK, LF) that are discussed above. All the PPA's are designed on VHDL (Very high speed Hardware Description Language) / Verilog project navigator 14.2i is used for synthesis (Xilinx version) [24]. Simulation results are verified on the basis of area, power and delay. In addition to that the waveforms and the comparison results for all three parallel prefix adders are given.

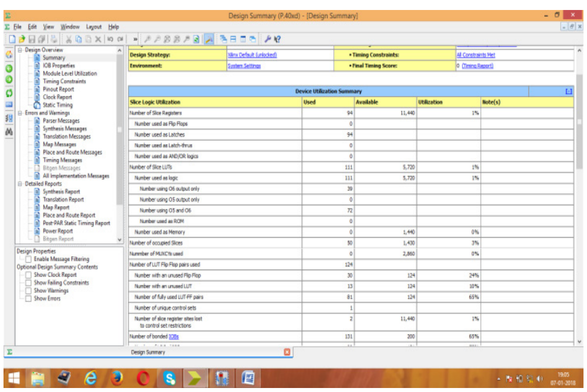

Figure 4: Area Consumption report for KSA

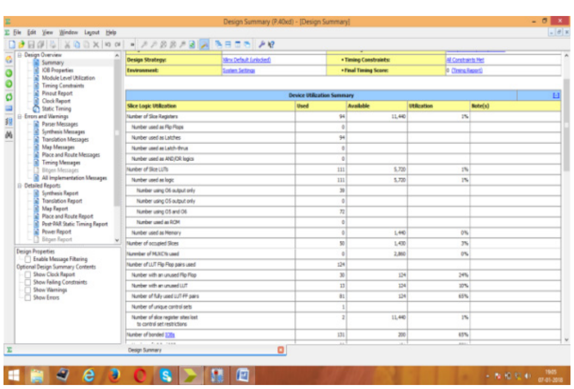

Figure 5: Power Analyzer report for KSA

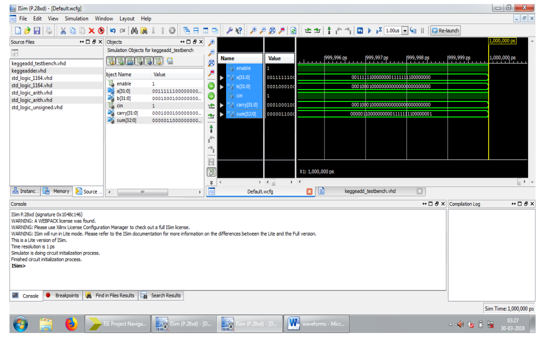

Figure 6: Test bench waveform results of KSA

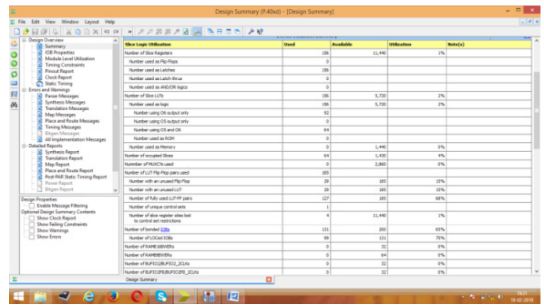

Figure 7: Area Consumption report for BKA

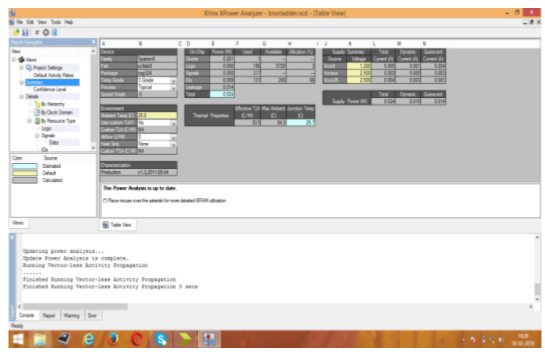

Figure 8: Power Analyzer report for KSA

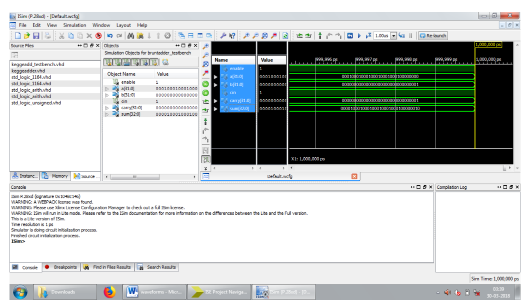

Figure 9: Test bench waveform results of BKA

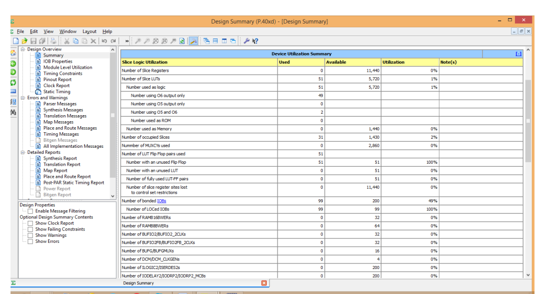

Figure 10: Area Consumption report for LFA

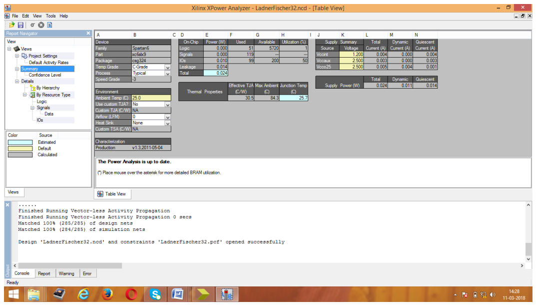

Figure 11: Power Analyzer report for KSA

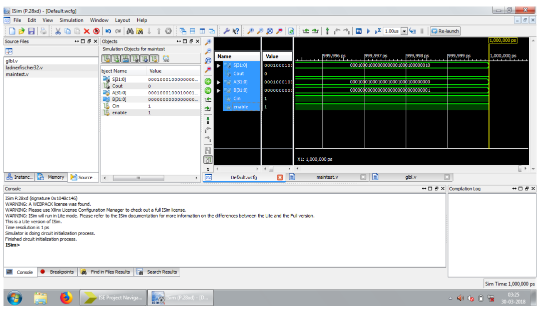

Figure 12: Test bench waveform results of LFA

Area consumption, power analysis, and the test bench waveform of KSA are shown in figures 4, 5, and 6 respectively. Area consumption, power analysis, and the test bench waveform of BKA are shown in figures 7, 8, and 9 respectively. Also the area consumption, power analysis, and the test bench waveform of LFA are shown in figures 10, 11, and 12 respectively.

From the above figures, the comparison results of all three PPA on the aspects of area, delay and power is given in table I. From the analysis, LFA is better due to the less area consumption but the power utilization is more compared to other adders. Normally PPA's have less delay in any processors while doing addition. Accordance with low power application, KSA is more suitable due to less power utilization in any digital based processors.

Table 1: Comparison results of area, delay and power for various types of PPA

Adder Types	LUT's Used	Delay(ns)	Power (mW)
Kogge Stone Adder	189	6.483	21
Brent kung Adder	156	6.489	24
Ladner Fischer Adder	51	21.879	24

Conclusion

In this paper, an efficient 32 bit Parallel Prefix adders like KSA, BKA, LFA is designed. This proposed 32 bit adder addition operation offers a great advantage in reducing delay. For low power VLSI applications, also the designed adders are compared on the basis of power, area consumption, and delay. The synthesis results reveal that among the proposed adders, KSA is achieved some saving of power-delay product due to less power utilization. But the area delay product is little increased, compared to other adders due to high area consumption. For decreasing the complexity at all performance aspects, further optimization techniques can be achieved on the performance parameters that will be the future work of the paper.

References

[1] P. Patronik, S. J. Piestrak, "Design of RNS Reverse Converters with Constant Shifting to Residue Datapath Channels" Journal of Signal Processing Systems, 2017. https://doi.org / 10.1007/s11265-017-1238-6

[2] D. Kunjan, Shinde, S. Badiger, "Analysis and comparative study of 8-bit adder for embedded application" International Conference on Control, Instrumentation, Communication and Computational Technologies (ICCICCT), 2015. https://doi.org /10.1109/iccicct.2015.7475290

[3] S. Gedam, Pravin Zode, and Pradnya Zode, "FPGA implementation of hybrid Han-Carlson adder" in 2nd International Conference on Devices Circuits and Systems (ICDCS), 2014. https://doi.org/10.1109/icdcsyst.2014.6926185

[4] H. Moqadasi, M. B. Ghazvani-Ghoushchi, "A new parallel prefix adder structure with efficient critical delay path and gradded bits efficiency in CMOS 90nm technology" in 23rd Iranian Conference on Electrical Engineering (ICEE), 2015. https://doi.org /10.1109/iraniancee.2015.7146426

[5] P. Kumar and M. Kiran, "Design of optimal fast adder" in International Conference on Advanced Computing and Communication Systems, 2013. https://doi.org /10.1109/icaccs.2013.6938692

[6] A. Zarandi, A. Molahosseini, M. Hosseinzadeh, S. Sorouri, S. Antão, and L. Sousa, "Reverse Converter Design via Parallel-Prefix Adders: Novel Components, Methodology, and Implementations" IEEE transactions on very large scale integration (VLSI) systems, 2014. https://doi.org/10.1109/tvlsi.2014.2305392

[7] Saxena and Pallavi, "Design of low power and high speed Carry Select Adder using Brent Kung adder" in International Conference on VLSI Systems Architecture Technology and Applications (VLSI-SATA), 2015. https://doi.org/10.1109/vlsi-sata.2015.7050465

[8] N. Shanil Mohamed, T. Y. Siby, "16-bit Velocious Fault Lenient Parallel Prefix Adder" in International Conference on Electronics, Communication and Computational Engineering (ICECCE), 2014. https://doi.org/10.1109/icecce.2014.7086612

[9] S. A. H. Ejtahed, M. B. Ghaznavi-Ghoushchi, "Design and Implementation of a Power and Area Optimized Reconfigurable Superset Parallel Prefix Adder" in 24th Iranian Conference on Electrical Engineering (ICEE), 2016. https://doi.org/10.1109/iraniancee.2016.7585787

[10] I. Marouf, M. M. Asad, A. Bakhuraibah and Q. Abu Al-Haija, "Cost Analysis Study of Variable Parallel Prefix Adders Using Altera Cyclone IV FPGA Kit" in International Conference on Electrical and Computing Technologies and Applications (ICECTA), 2017. https://doi.org/10.1109/icecta.2017.8252011

[11] S. Arthireena, G. Shanmugavadivel, "Efficient Sign Detection using Parallel Prefix Adder" in International Conference on Electrical, Instrumentation and Communication Engineering (ICEICE), 2017. https://doi.org/10.1109/iceice.2017.8191852

[12] S. Daphni, K. S. Vijula Grace, "A review analysis of parallel prefix adders for better performance in VLSI applications" in Proceedings of 2017 IEEE International Conference on Circuits and Systems (ICCS), 2017. https://doi.org/10.1109/ICCS1.2017.8325971

[13] F. Liu, Q. Tan, G. Chen, "Formal proof of prefix adders" Mathematical and Computer Modelling, ELSEVIER, 2010. https://doi.org/10.1016/j.mcm.2010.02.008

[14] S. K. Yezerla, B. Rajendra Naik, "Design and Estimation of delay, power and area for Parallel prefix adders" in Proceedings of RAECS UIET Panjab University Chandigarh., 2014. https://doi.org/10.1109/raecs.2014.6799654

[15] A. E. Shapiro, F. Atallah, K. Kim, J. Jeong, J. Fischer, E. G. Friedman, "Adaptive power gating of 32-bit Kogge Stone adder" INTEGRATION, the VLSI journal, ELSEVIER, 2015. https://doi.org/10.1016/j.vlsi.2015.12.001

[16] M. Ozer, M. Eren Çelik, Y. Tukel, A. Bozbey, "Design of RSFQ wave pipelined Kogge–Stone Adder and developing custom compound gates" Cryogenics, ELSEVIER, 2014. https://doi.org/10.1016/j.cryogenics.2014.05.007

[17] P. Chaitanya kumari, R. Nagendra, "Design of 32 bit Parallel Prefix Adders" IOSR Journal of Electronics and Communication Engineering (IOSR-JECE), 2013. https://doi.org/10.9790/2834-610106

[18] C. Shilpa, K. D. Shinde, H. V. Nithin, "Design, Implementation and Comparative Analysis of Kogge Stone Adder using CMOS and GDI design: A VLSI Based Approach" in 8th International Conference on Computational Intelligence and Communication Networks, 2016. https://doi.org/10.1109/cicn.2016.117

[19] N. Poornima, V. S. Kanchana Bhaaskaran, "Area Efficient Hybrid Parallel Prefix Adders" in 2nd International Conference on Nano materials and Technologies (CNT), ELSEVIER, 2014. https://doi.org/10.1016/j.mspro.2015.06.069

[20] L. Hars, "Applications of Fast Truncated Multiplication in Cryptography" EURASIP Journal on Embedded Systems, 2007. https://doi.org/10.1155/2007/61721

[21] J. Thomas, R. Pushpangadan, S. Jinesh, “Comparative Study of Performance Vedic Multiplier on The Basis of Adders Used” IEEE International WIE Conference on Electrical and Compter Engineering (WIECON-ECE), 2015. https://doi.org/10.1109/wiecon-ece.2015.7443929

[22] A. Baliga, "Design of High Speed Adders Using CMOS and Transmission Gates in Submicron Technology: A Comparative Study" in Fourth International Conference on Emerging Trends in Engineering & Technology, Nov 2011. https://doi.org/ 10.1109/icetet.2011.25

[23] S. Baba Fariddin, E. Vargil Vijay, “Design of Efficient 16-Bit Parallel Prefix Ladner Fischer Adder” International Journal of Computer Applications, 2013. https://doi.org/ 10.5120/13943-1784

[24] M. Macedo, L. Soares, B. Silveira, C. M. Diniz, Eduardo A. C. da Costa, "Exploring the use of parallel prefix adder topologies into approximate adder circuits” in 24th IEEE International Conference on Electronics, Circuits and Systems (ICECS), 2017. https://doi.org/10.1109/icecs.2017.8292078

Advances in Science, Technology and Engineering Systems Journal Vol. 4, No. 2, 107-111 (2019)

www.astesj.com

Special Issue on Advancement in Engineering and Computer Science

ASTESJ

ISSN: 2415-6698

Deep Feature Representation for Face Sketch Recognition

Weiguo Wan[1], Hyo Jong Lee [1, 2, *]

[1]*Division of Computer Science and Engineering, Chonbuk National University, 54896, Korea*

[2]*Center for Advanced Image and Information Technology, Chonbuk National University, 54896, Korea*

A R T I C L E I N F O

Article history:
Received: 07 January, 2019
Accepted: 28 February, 2019
Online: 15 March, 2019

Keywords:
Face sketch recognition
Face sketch synthesis
VGG-Face network

A B S T R A C T

Face sketch recognition aims at matching face sketch images to face photo images. The main challenge lies in modality discrepancy between face photo and sketch images. In this work, we propose a new facial sketch-to-photo recognition approach by adopting VGG-Face deep learning network, with which face images can be represented by compact and highly discriminative feature vectors. Different from existing VGG-Face based methods which directly match face sketches to photos, we firstly transform the gallery photos to sketches for decreasing the modality difference. Experimental results on multiple face photo-sketch datasets indicate the superiority of our method.

1. Introduction

Face sketch to photo recognition is a key branch of face recognition to address the lack of face photos, which has wide application in forensics [1]. If crime happened, and only incomplete information is obtained about the suspect because of the bad quality of monitoring videos, face sketches which drawn by the artists with the description of witnesses are used to identity the possible suspect. The police can shrink the range of suspects by searching the law enforcement face databases or surveillance cameras with the drawn face sketch images [2].

Face sketch to photo recognition approaches can be mainly classified into common space projection approaches and local feature descriptor approaches. Common space projection approaches attempt to transform facial images from various modalities to common subspace where the modality difference is reduced. After that, facial photos and sketches could be directly identified in the common space. Lin et al. [3] translated heterogeneous features to common feature space with common discriminant feature extraction (CDFE). In [4], Lei et al. proposed a subspace learning framework named coupled spectral regression (CSR) for heterogeneous face recognition. Then, they improved the CSR algorithm through learning a mapping from all modalities to all samples [5]. In [6], Sharma et al. employed partial least squares (PLS) algorithm to project heterogeneous facial images into common subspace. Mignon et al. [7] proposed to learn a discriminative latent space by using cross modal metric learning (CMML) method. In [8], Kan et al. suggested a multiple view analysis algorithm, with which the dependencies from intra-view and inter-view can be utilized to obtain a discriminant subspace for heterogeneous face recognition. However, the space projection based methods may lose the underlying information of the source images and lead to degradation of the recognition effect.

Local feature representation approaches aim at extracting robust and modality-invariant face feature representations from the heterogeneous face images. In [9], Klare et al. put forward a face sketch recognition approach with a local feature discriminant analysis (LFDA) framework which taking advantage of multiscale local binary pattern (MLBP) [10] and scale invariant feature transform (SIFT) [11]. In [12], Zhang et al. suggested a coupled information theoretic encoding based local face descriptor for face sketch to photo recognition. And later, the coupled information theoretic encoding algorithm was modified to the random forests by using various sampling methods. Galoogahi et al. [13] put forward a facial feature descriptor named local radon binary pattern (LRBP) for face sketch recognition, which firstly projects the face images into the radon space and then encodes them with the local binary patterns (LBP). In addition, a local face descriptor based on histogram of averaged oriented gradients (HAOG) is suggested by Galoogahi et al. to decrease the modality difference [14]. In [15], Lei et al. put forward a heterogeneous face

*Corresponding Author: Hyo Jong Lee, hlee@chonbuk.ac.kr

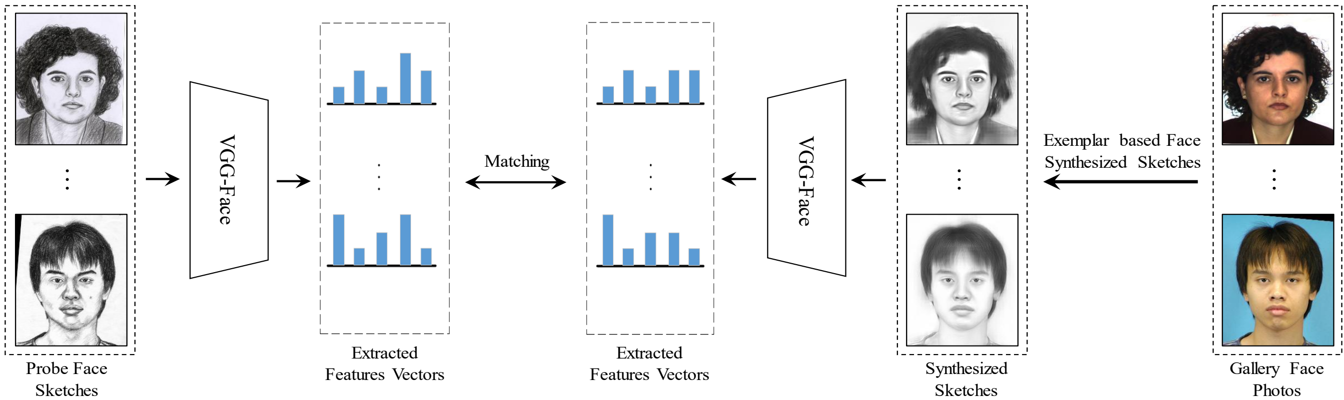

Figure 1. The illustration of the proposed face sketch recognition approach.

recognition method based on discriminant image filter learning. Alex et al. [16] suggested a local difference of Gaussian binary pattern algorithm for heterogeneous face recognition. However, when extracting the face feature representation, the local feature descriptor based approaches lose the sight of the holistic spatial structure of face, which is important for face sketch recognition.

Moreover, because of the huge differences between the face photo and sketch images, it is difficult for traditional homogeneous face recognition approaches to achieve good performance by directly matching the sketches to photos. In this paper, we transform the photo images into sketch images by adopting an exemplar-based sketch generation approach to decrease the modality difference between face photo and sketch images. In [17], Parkhi et al. presented a deep learning network, namely VGG-Face, which is able to map a face images to a compact space where distances can be used for measuring the face similarity. Peng et al. [18] mentioned that it can be adopted for face sketch recognition. Motivated by its efficient performance, we adopt it to extract the discrimination face feature representation in this paper. With the VGG-Face network, the feature vectors which represent the corresponding face images can be obtained. The illustration of the proposed approach is showed in Figure 1.

2. Related Works

2.1. Exemplar-based Sketch Generation

The exemplar-based face sketch generation approach needs a group of training dataset which contains some face photo-sketch pairs. First, each test photo **T** is divided into several image patches with overlapping between adjacent patches. Then, for each test photo patch **t**, several number of closest photo patches are chose from the training photo images which are cut image patches with the same approach. At the same time, we can get *K* corresponding sketch candidate patches with the obtained photo patches. Finally, the sketch patches are generated by combining the *K* candidate sketch patches with the corresponding weighting coefficients. The sketch generation operation can be represented as follow:

$$\min_{w} \| \mathbf{t} - \mathbf{X} \cdot \mathbf{w} \|_2^2, \ \ s.t. \mathbf{1}^T \mathbf{w} = 1 \quad (1)$$

where **X is** the *K* selected photo patches from training data. **w** is the weighting vector to combine candidate sketch patches.

Then we can obtain the target sketch patch ***s*** by:

$$\mathbf{s} = \mathbf{Y} \cdot \mathbf{w} \quad (2)$$

where **Y** represents the corresponding sketch patches of the test photo patch **t**.

2.2. VGG-Face Networks

The VGG-Face networks [17] are built on the basis of VGG-Very-Deep-16 convolutional neural network (CNN) architecture. The VGG-Face networks consist of a series of convolutional, pool, and fully-connected layers. The first eight blocks are convolutional layers and the remaining three blocks are fully-connected layers. For each convolutional layers, a ReLU activation layer is followed. The output dimensions of the first two fully-connected layers are 4096 and the output dimension of final fully-connected layer is 2622. The filters of convolutional layers are with size of 3×3 while the pool layers perform subsampling with a factor of two. Figure 2 displays the framework of the VGG-Face model.

In the proposed method, a pretrained VGG-Face model with 37 basic layers is utilized to extract deep face features. The pretrained model is trained on a big face dataset which has 982,803 images from 2622 subjects. The pretrained VGG-Face model only can recognize the people in the training dataset, however, we are able to extract face features from its bottleneck layers for any face images by forwarding the face images through the whole networks. The extracted features are highly discriminative, compact, and interoperable encodings of the input face images. When the face features are obtained from the bottleneck layers of the VGG-Face model, the sketch to photo matching can be performed based on these obtained face features. In this paper, the MatConvNet toolbox, which provides the pretrained implementation of the VGG-Face model, is utilized to extract deep face features.

3. The Proposed Method

In this paper, we presented a new facial sketch-to-photo recognition approach with the VGG-Face network and face sketch generation. The proposed method mainly consists of face image preprocessing, face sketch synthesis, and face sketch recognition three steps, which will be described later.

3.1. Face Image Preprocessing

Face photo and sketch images vary in properties, e.g. varying resolution, pose, and deformation. We firstly normalized all the

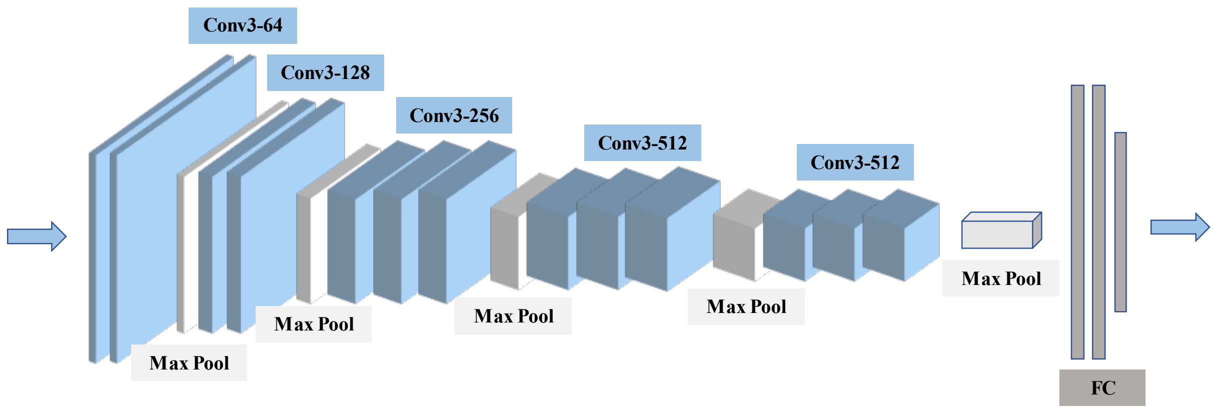

Figure 2. The VGG-Face CNN architecture.

sketch and photo images by fixing the coordinates of eyes centers. The common-used Dlib library was used to detect eyes position, and then translation, rotation, and scaling operations are conducted to align face images based on the detected eyes coordinates. Figure 3 shows some samples of original and preprocessed face photo and sketch images.

3.2. Face Photo to Sketch Synthesis

Assuming there are M geometrically aligned training photo-sketch pairs. We first divide these photo images and sketch images in training data into patches. Then, we reshape every patch to a vector. For each patch position, the searching area is extended c pixel around the patch. Thus, we can obtain $(2c+1)^2$ patches in the searching area for each patch position. We will obtain $(2c+1)^2M$ face photo and sketch patches from the training data, respectively. We employ the random sampling algorithm for selecting K face photo patches $\mathbf{U}^{(i,j)} \in \mathbf{R}^{2p^2 \times K}$ and sketch patches $\mathbf{V}^{(i,j)} \in \mathbf{R}^{2p^2 \times K}$ from training data. (i, j) is the patch position at the m-th row and the n-th column. Each image patch can be reshaped to a d-dimensional column vector.

For each test photo patch $\mathbf{t}_1^{(i,j)}$, we can compute the reconstruction weight by using equation (3):

$$\min_{\mathbf{w}^{(i,j)}} \| \mathbf{t}_1^{(i,j)} - \mathbf{U}^{(i,j)}\mathbf{w}^{(i,j)} \|_2^2 + \lambda \| \mathbf{d}^{(i,j)} \odot \mathbf{w}^{(i,j)} \|, s.t. \mathbf{1}^T \mathbf{w}^{(i,j)} = 1 \quad (3)$$

where $\mathbf{d}^{(i,j)} \in \mathrm{R}^{K \times 1}$ represents the L2 distance of the test photo patch $\mathbf{t}_1^{(i,j)}$ and the selected photo patches $\mathbf{U}^{(i,j)}$ from training data, $\mathbf{w}^{(i,j)} \in \mathrm{R}^{K \times 1}$ represents the weighting coefficients of the test photo patch $\mathbf{t}_1^{(i,j)}$.

Equation (3) has the closed-form solution:

$$\begin{aligned} \mathbf{w}'^{(i,j)} &= (\mathrm{C}^{i,j} + \lambda \mathrm{diag}(\mathbf{d}^{(i,j)})) \backslash \mathbf{1} \\ \mathbf{w}^{(i,j)} &= \mathbf{w}'^{(i,j)} / \mathbf{1}^T \mathbf{w}'^{(i,j)} \end{aligned} \quad (4)$$

where $\mathbf{1}$ represent a column vector, its elements all are 1. $\mathrm{C}^{i,j} = (\mathbf{U}^{(i,j)} - \mathbf{1}\mathbf{t}_1^{(i,j)^T})(\mathbf{U}^{(i,j)} - \mathbf{1}\mathbf{t}_1^{(i,j)^T})^T$ is the covariance matrix, $\mathrm{diag}(\mathbf{d}^{(i,j)})$ is a diagonal matrix which is extended from $\mathbf{d}^{(i,j)}$.

By linearly combining K selected sketch patches of the training data and the weighting coefficients $\mathbf{w}^{(i,j)}$, the result sketch block $\mathbf{s}^{(i,j)}$ could be generated:

Figure 3. Facial photo-sketch examples in CUFS dataset and CUFSF dataset.

$$\mathbf{s}^{(i,j)} = \mathbf{V}^{(i,j)}\mathbf{w}^{(i,j)} \quad (5)$$

We can generate the final target sketch with overlapping area averaged when get all the target sketch patches,. Fig. 3 shows some generated examples with the exemplar-based face sketch generation. From Figure 3, we can observe that the modality difference between the sketch image and the transformed sketch image smaller than the photo image.

3.3. Face Sketch Recognition with VGG-Face Network

After the photo images are generated to sketch images, the VGG-Face network was adopted to get the facial feature vectors of synthesized sketch images. We then call the synthesized sketch images gallery, and the test face sketch images probe.

We extract the face features by utilizing the VGG-face networks which is provided by the MatConvNet toolbox. The VGG-face architecture is composed of several convolution layers with 3×3 filters, several pooling layers with a factor of 2, and 3 fully-connected layers. In VGG deep networks, the early layers are

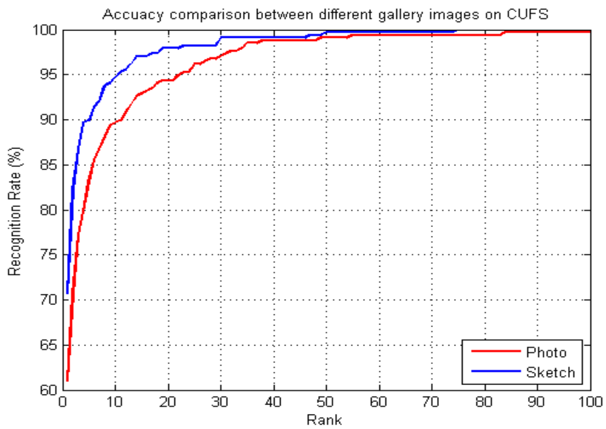

Figure 4. Performance comparison by using different gallery images.

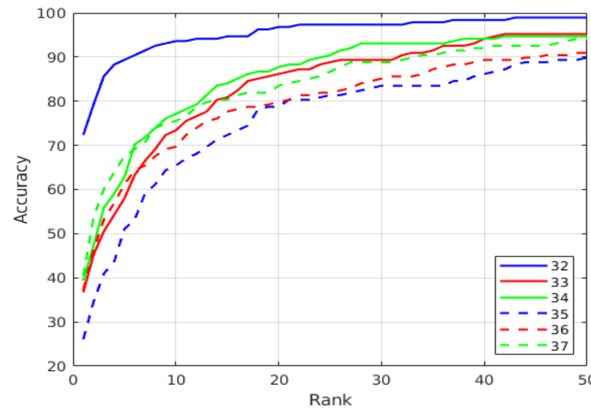

Figure 5. Performance comparison by different VGG-Face layers.

the low-level representation for input images such as edge and corner, the intermediate layers represent mid-level features like parts, and the high-level representations exist in the last layers. In order to find the optimum high-discrimination face features for face sketch-to-photo recognition, we selected activation maps from 32nd layer to 37th layer as the deep feature representation. The performance comparison results, which will be analyzed in the experiment section, indicated that the 32nd layer obtains the highest recognition accuracy. In this case, each face image was represented by a 25,088-dimension deep feature vector.

By using the well-trained VGG-Face network model, we can map all the sketch images in gallery into 25,088-dimension feature vectors. And a same length feature vector can be obtained by using the pre-trained network for each input probe image. We use the squared Euclidean distance of the face feature vectors to calculate the facial similarities. Face images from the different subjects have large distances while facial images of the same person have small distances. Hence, the face sketch recognition can be regarded as a nearest neighbor classification problem. The illustration of the proposed face sketch recognition method is shown in Figure 1.

4. Experiments and Results

4.1. Datasets

Two public available datasets are adopted to assess the recognition effect of the proposed approach: the CUHK dataset (CUFS) and the CUFSF dataset [19]. The CUFS dataset is composed of facial images from 3 datasets: the CUHK student dataset (188 subjects), the AR dataset (123 subjects), and the XM2VTS dataset (295 subjects). The CUFSF dataset has 1194 subjects of FERET dataset. In CUFS and CUFSF datasets, there are one photo image and one sketch image for each subject. All the face photo and sketch images are normalized and cut to with size of 250×200. The first two rows of Figure 3 shows the examples of photo-sketch pairs from these two datasets. The first three columns are face images of CUFS and the final column are face images of CUFSF. The first row are the original face sketches and the second row are the face photos. The final row are the generated sketches.

4.2. Experiments

First. we evaluated the recognition effect between adopting face photo images as gallery and adopting the generated sketch images as gallery. Figure 4 shown the comparison results, from it we can see that using the synthesized sketch images as gallery obtained better recognition performance. The results indicated that modality difference of the face photo and sketch images was narrowed down after synthesizing face photos to sketches.

We extracted last several layers from the VGG-face networks as the deep face features for recognition. To compare the performance by different layers, the experiment on CUHK student sub-dataset was conducted with same distance measurement. The result shown in Figure 5 indicated that the 32nd layer obtains the highest recognition accuracy. Thus, the feature vectors extracted from 32nd layer were set as the face representation in this paper.

Three existing approaches are compared to assess the recognition effect of the proposed approach, namely the HOG based approach, the DCP based approach [20] and the Light-CNN based approach [21]. Figure 6 (a) and (b) shown the comparison results on the CUFS and CUFSF datasets. Table 1 shown the rank-1, rank-5 and rank-10 recognition accuracies on CUFS and CUFSF datasets. From them, it can be seen that the proposed approach achieves the best recognition performance, compared to other methods. For the CUFS dataset, even though it is easy for other approaches to obtain high recognition performance, but our approach is the quickest one achieving 100% accuracy. The CUFSF dataset is more difficult due to the face photo images are taken under various illumination conditions. In addition, the face sketches exist shape deformation compared with the photos in CUFSF dataset. But the proposed approach still achieves the best recognition accuracy. In summary, the proposed face sketch to photo recognition approach is effective and practical.

5. Conclusions

In this paper, we presented a face sketch-to-photo recognition approach based on deep feature representation. The face photos were synthesized to face sketches to decrease the modality gap of the face photo images and sketch images. After that, the VGG-Face network was employed to extract feature representation for each face image. With the extracted face features, the face similarity can be measured directly. Experimental results on the CUFS and CUFSF datasets indicated the superiority of the proposed approach. The proposed approach in this paper is our preliminary research and only the pre-trained VGG-Face network was adopted. In the future, we plan to develop high-performance networks for face photo to sketch recognition.

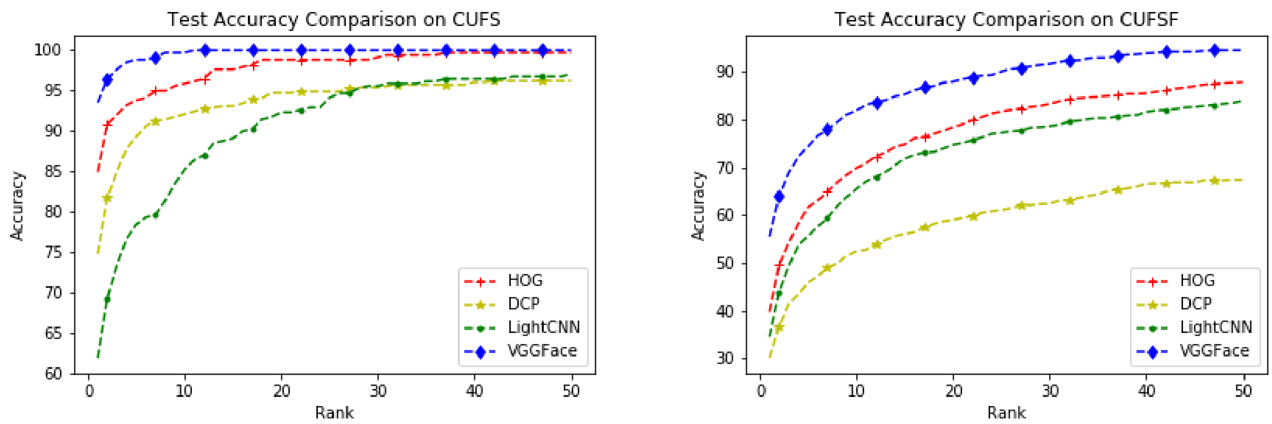

(a) (b)

Figure 6. The comparison of recognition accuracies by different approaches on the CUFS and CUFSF datasets.

Table 1. Recognition accuracy (%) by different methods.

Methods		HOG	DCP	LightCNN	Proposed
CUFS	Rank-1	84.91	74.75	61.83	**93.49**
	Rank-5	93.79	89.27	78.40	**98.81**
	Rank-10	95.86	92.08	85.21	**99.70**
CUFSF	Rank-1	39.72	30.08	34.53	**55.51**
	Rank-5	61.65	45.87	55.61	**74.36**
	Rank-10	69.81	52.43	6.546	**81.89**

Conflict of Interest

The authors declare no conflict of interest.

Acknowledgment

This research was supported by "Research Base Construction Fund Support Program" funded by Chonbuk National University in 2018. This research was also supported by the MSIP (Ministry of Science, ICT and Future Planning), Korea, under the ITRC (Information Technology Research Center) support program (IITP-2018-2015-0-00378) supervised by the IITP (Institute for Information & communications Technology Promotion). This research was also supported by Basic Science Research Program through the National Research Foundation of Korea (NRF) funded by the Ministry of Education (GR 2016R1D1A3B0393 1911).

References

[1] M. Zhang, J. Li, N. Wang, and X. Gao, "Recognition of facial sketch styles," *Neurocomput.*, vol. 149, pp. 1188-1197, 2015.

[2] N. Wang, X. Gao, L. Sun, et al., "Anchored Neighborhood Index for Face Sketch Synthesis," *IEEE Trans. Circuits Syst. Video Technol*, 2017.

[3] D. Lin and X. Tang, "Inter-modality face recognition," *in Proc. 9th Eur. Conf. Comput. Vis.*, 2006, pp. 13–26.

[4] Z. Lei and S. Li, "Coupled spectral regression for matching heterogeneous faces," *IEEE Conf. Comput. Vis. Pattern Recog.*, 2009, pp. 1123–1128.

[5] Z. Lei, C. Zhou, D. Yi, A. Jain, and S. Li, "An improved coupled spectral regression for heterogeneous face recognition," *in Proc. Int. Conf. Biomed.*, 2012, pp. 7–12.

[6] A. . Sharma and D. Jacobs, "Bypass synthesis: PLS for face recognition with pose, low-resolution and sketch," *in Proc. IEEE Conf. Comput. Vis. Pattern Recog.*, 2011, pp. 593–600.

[7] A. Mignon and F. Jurie, "CMML: A new metric learning approach for cross modal matching," *in Proc. Asian Conf. Comput. Vis.*, 2012.

[8] M. Kan, S. Shan, H. Zhang, S. Lao, and X. Chen, "Multi-view discriminant analysis," *in Proc. 12th Eur. Conf. Comput. Vis.*, 2012, pp. 808–821.

[9] B. Klare, Z. Li, and A. Jain, "Matching forensic sketches to mug shot photos," *IEEE Trans. Pattern Anal. Mach. Intell.*, vol. 33, no. 3, pp. 639–646, Mar. 2011.

[10] T. Ojala, M. Pietik€ainen, and T. M€aenp€a€a, "Multiresolution grayscale and rotation invariant texture classification with local binary patterns," *IEEE Trans. Pattern Anal. Mach. Intell.*, vol. 24, no. 7, pp. 971–987, Jul. 2002

[11] D. Lowe, "Distinctive image features from scale-invariant keypoints," *Int. J. Comput. Vis.*, vol. 60, no. 2, pp. 91–110, 2004.

[12] W. Zhang, X. Wang, and X. Tang, "Coupled information-theoretic encoding for face photo-sketch recognition," *in Proc. IEEE Conf. Comput. Vis. Pattern Recog.*, 2011, pp. 513–520.

[13] H. Galoogahi and T. Sim, "Face sketch recognition by local radon binary pattern," *in Proc. 19th IEEE Int. Conf. Image Process.*, 2012, pp. 1837–1840.

[14] H. Galoogahi and T. Sim, "Inter-modality face sketch recognition," *in Proc. IEEE Int. Conf. Multimedia Expo*, 2012, pp. 224–229.

[15] Z. Lei, D. Yi, and S. Li, "Discriminant image filter learning for face recognition with local binary pattern like representation," *in Proc. IEEE Conf. Comput. Vis. Pattern Recog.*, 2012, pp. 2512–2517.

[16] A. Alex, V. Asari, and A. Mathew, "Local difference of gaussian binary pattern: Robust features for face sketch recognition," *in Proc. IEEE Int. Conf. Syst. Man Cybern.*, 2013, pp. 1211–1216.

[17] O. M. Parkhi, V. Andrea, and Z. Andrew, "Deep face recognition," British Machine Vision Conference, vol. 1, no. 3, 2015.

[18] C. Peng, X. Gao, N. Wang N, et al., "Face recognition from multiple stylistic sketches: Scenarios, datasets, and evaluation," *Pattern Recognition*, 2018, 84: 262-272.

[19] Wang X, Tang X. Face photo-sketch synthesis and recognition. *IEEE Transactions on Pattern Analysis and Machine Intelligence*, 2009, 31(11): 1955-1967.

[20] Ding, C, Choi J, Tao D, Davis L S. Multi-directional multi-level dual-cross patterns for robust face recognition. *IEEE Trans Pattern Anal Mach Intell*, 2016, 38:518-531.

[21] Wu X, He R, Sun Z, Tan T. A light CNN for deep face representation with noisy labels. *IEEE Trans Inf Forensics Security*, 2018, 13:2884-2896.

Advances in Science, Technology and Engineering Systems Journal Vol. 4, No. 2, 112-118 (2019)

www.astesj.com

ASTESJ

ISSN: 2415-6698

A Fuzzy PID-Based Cascade Control for Continuous Material Weighing Conveyor

Trinh Luong Mien*

Department of cybernetics, Faculty of electrical and electronic engineering, University of transport and communications, No.03, Caugiay, Langthuong, Dongda, Hanoi, Vietnam

A R T I C L E I N F O

Article history:
Received: 20 January, 2019
Accepted: 12 March, 2019
Online: 16 March, 2019

Keywords:
PID
Fuzzy
PLC
Conveyor
Weigh feeder

A B S T R A C T

This article presents a nonlinear model of the continuous weighing conveyor system as considering the delay time of material transport, and then given a novel two-loop control strategy based on PID combined with fuzzy logic: inner velocity control loop and outer mass flowrate control loop. Then, two designed controllers for the velocity and mass flowrate control loops are simulated and evaluated in MATLAB. After that, experimental setup of real-time weighing conveyor system is built in the UTC's laboratory. Finally, these controllers are installed into PLC to control the material mass flowrate following on the reference input. The simulation and experimental results show that the proposed fuzzy-PID algorithm is right and able to improve the material mass flowrate control quality in industrial continuous weighing conveyor system using PLC controller.

1. Introduction

The continuous material weighing conveyor is an automatic weighing machinery, used to weigh the particulate materials in the form of a continuous stream. These weighing conveyors are used for continuous transport of the solid particulate materials in industries, such as: mining and quarrying, building materials, beverage and food processing, power generation, agricultural, pharmaceutical. These weighing conveyors may be incorporated into the conveying line to obtain a mass feed rate in a continuous process or totalized mass material delivered. The mass flow rate of material is deduced from two distinct measurements: the velocity of the conveyor and the average linear density of the material (mass per length) contained within the weigh length (the length of a conveyor section installed weigh frame with load cell sensor [1]). Consequently, the weighing conveyor performance depends not only on the conveyor velocity control loop, but also on the material mass flow control loop.

The weight feeder system is presented in [2] with a dedicated controller to control material at a specified rate, and then it is applied in many fields, such as processing industry [3], cement industry [4] and so on. Sato and Kameoka [5] proposed the generalized minimum variance control method to minimize the variance of discharged material. Then, Sato [6] applied the generalized predictive control to improve the quality of the weight control conveyor. Recent studies [7-9] focus on applying modern control techniques, such as combining PID with PSO algorithm to achieve optimal PID parameters, close to industrial weighing process. The studies [10,11] present fuzzy logic-based control method that mimics PID control rules or use fuzzy logic to adjust PID parameter to overcome some nonlinear characteristic of weighing conveyor.

The majority of these studies [2-11] only mention the conveyor velocity control loop with acceptable control quality but have not consider to the fact that output mass flow control of the conveyor must be attached according to the production technology trajectory (for material mass flow control problem). Moreover, the only-velocity-control-loop can cause large mass difference when conveyor runs at high velocity, or when hopper's material varies greatly (source of input materials).

This article presents a novel cascade control strategy for the continuous weighing conveyor based on PID control and fuzzy logic with two-loop-control-structure: inner-velocity-control-loop and outer-mass-flowrate-control-loop. The PID parameters are synthesized based on the identified velocity control object. Then, the fuzzy logic block was developed to adjust the PID parameters of the material mass flowrate control loop according to the input reference, based on the output error and the output error differential. The parameters of this controller can be assigned directly to PLC instructions to stabilize the material mass flowrate according to the input reference. The rest of this article is organized as follow. Section 2 introduces the structure and operation principle of the weighing conveyor. Section 3 deals with the design of controllers for material weighing conveyor. Section 4 presents

* *Trinh Luong Mien, Tel: +84 904 684 595. Email: mientl@utc.edu.vn*

the experimental setup of the real-time weight system. And then, the experimental results are discussed in section 5. Finally, section 6 presents conclusions.

2. Structure and operation principle of the weighing conveyor

2.1. Description of continuous weighing conveyor

Figure 1 describes the basic components of a continuous weighing conveyor, are built to test the research result in this article, including: (1)-material hopper, (2)-weighing table, (3) loadcell, (4)-conveyor motor, (5)- loadcell signal amplifier, (6)- PLC controller, (7,8)-power converter, (9)-DC source, (10)- control panel, (11)-PLC cable, (12)-PC for monitoring.

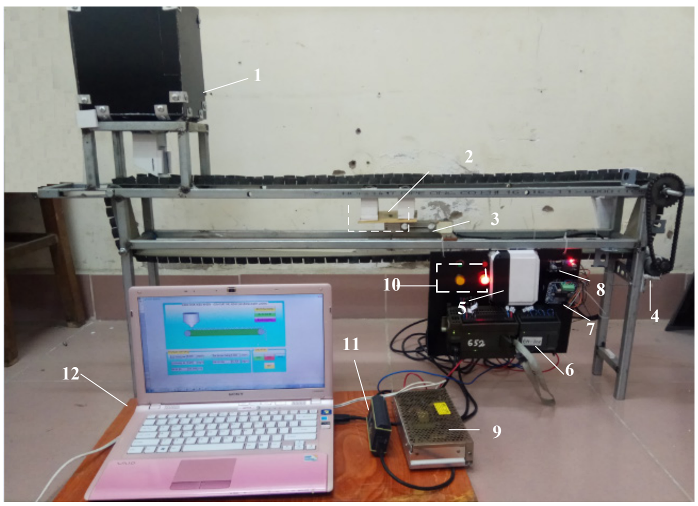

Figure 1. Structure of continuous weighing conveyor

This weighing conveyor system has the follows basic parameters: conveyor length 1000[mm], conveyor velocity 0.2[m/s], material's mass flowrate 1.0[kg/s], weighing table length 100[mm], roller diameter Ø26[mm]. Conveyor drive by EXCEM DC motor with capacity 400[W], power require 24[V], maximum velocity 3000[rpm]. Measure the density of material on conveyor using a weighing table, putting on OBU loadcell with power supply 10[V], capacity 10[kg], rated output 2±10%[mV/V]. The velocity of conveyor is measured by LPD3806 rotary encoder with a DC operating voltage of 5-24[V], resolution 100[pulse/rotation].

2.2. Weighing conveyor block diagram

Material mass flowrate on weighing conveyor is determined by simultaneously measuring two parameters: conveyor velocity (v [m/s]) and material density (γ [kg/m]). The control of material mass flowrate on conveyor following on reference input is done by adjusting conveyor velocity, as shown in Figure 2.

Types of solid grain materials (grain coal, small rocks, cement concrete, corn grain, rice and so on) contain in hopper, are spread evenly on weighing conveyor to ensure uniformity in the density of materials on weighing table.

Where: EN- conveyor velocity measuring encoder, LC- material density on weighing table weight measuring loadcell, KD- weight measuring signal amplifier, HS- gearbox, DC- electric motor, BD- power converter for motor, PLC- controller (ADC- analog/digital converter, HSC- high velocity counter, PWM- pulse width modulation, ALQ- algorithm of material mass flowrate control).

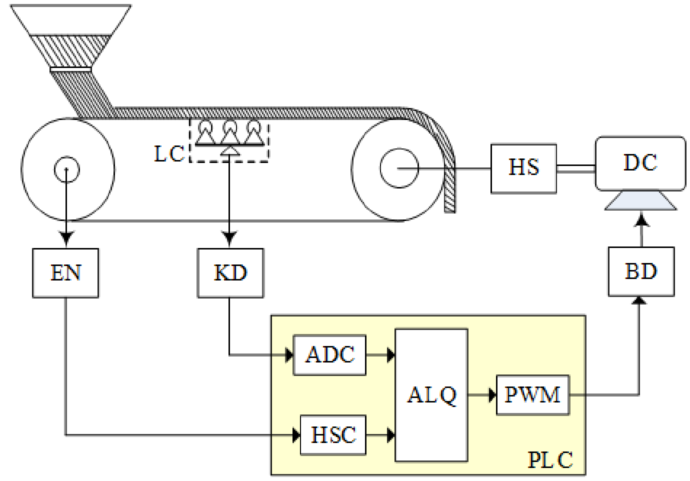

Figure 2. Schematic view of the weighing conveyor

2.3. Calculation of the material mass flowrate on conveyor

Conveyor velocity is determined by counting the numbers of pulses of the encoder attached to conveyor spindle (the conveyor always rotates follow the shaft and has no sliding phenomenon)

$$v = \frac{\pi D}{N_m T_p} p \tag{1}$$

Here: N_m[pulse]- encoder pulses on a rotation (encoder resolution); T_p[s]- pulse counting cycle; D[m]- conveyor roller diameter mounted coaxially with EN; p[pulse]- counted pulses.

Material density is proportional to the weight of material on the weighing table measured by loadcell [11]:

$$\gamma = \frac{q_w}{L_w} = \frac{q_w}{L_A/2 + L_B + L_C/2} \tag{2}$$

Here: q_w[kg]- material weight on weighing table measured by loadcell; L_w[m]- converted weighing table length, L_B[m]- conveyor length between two rollers on weighing table, L_A[m]- conveyor length between two rollers on feeding side, L_B[m]- conveyer length between two rollers on exiting side.

The following analysis makes the simplifying assumption that any section of conveyor and the bulk material it carries is fully supported by the two closest rollers. This being the case, the full weight of product distributed on the conveyor and indeed the weight of the conveyor in the region L_B of Figure 3.

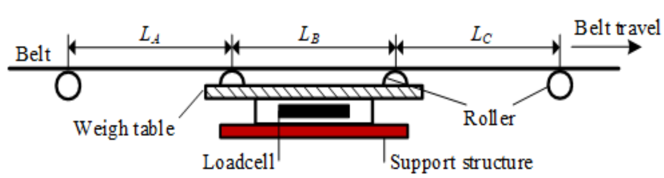

Figure 3. Schematic representation of the belt weigher

Momentary material mass flowrate on the conveyor equals to multiplication of material density and conveyor velocity, according to the following formula as:

$$q_m = \gamma \times v = \frac{\pi D}{L_w N_m T_p} q_w \times p \tag{3}$$

The mass flowrate of material (mass per time) is determined by multiplying the linear density (mass per length) by the velocity of the material (length per time). The velocity of the material is obtained by measuring the velocity of the conveyor and making the assumption that the material moves at the same velocity. However, care has to be taken to ensure that this is the case. The most common way of measuring conveyor velocity is through determination of the revolutions of a wheel in contact with the clean side of the conveyor.

The actual average mass flowrate on conveyor is determined by taking the instantaneous mass flowrate integration with the integral time constant T_q[s], according to the following formula:

$$q = \frac{1}{T_q}\int_0^{T_q} q_m dt = \frac{1}{T_q}\int_0^{T_q} (\gamma \times v) dt \tag{4}$$

3. Design of controllers for material weighing conveyor

3.1. Structure block diagram of material flowrate control system

Structure block diagram of the material mass flowrate control system on the conveyor consists of two control loops: the inner conveyor velocity control loop and the outer mass flowrate control loop, as shown in Figure 4.

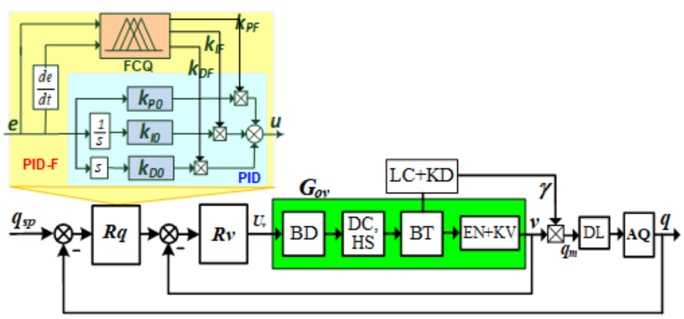

Figure 4. Structure block diagram of the weighing conveyor control system

Here: R_q- mass flowrate controller, R_v- conveyor velocity controller, BT- conveyor, DL- delay block when considering the time delay of the material transport on the conveyor, AQ- average mass flowrate calculation block, q_{sp}- flow set point, U_v- conveyor velocity control signal, G_{ov}- conveyor velocity control object, including BD converter based on MOSFET, motor and gearbox DC+HS, conveyor BT, encoder measuring and calculating conveyor velocity EN+KV.

Mass flowrate controller *Rq* is designed based on the principle of PID control law with the parameters k_{PF}, k_{IF}, k_{DF} that are adjusted online by fuzzy calculating block FCQ based on initial parameters k_{P0}, k_{I0}, k_{D0} synthesized according to traditional methods.

3.2. Identify the object of the conveyor velocity control loop

Experimental diagram to identify the control object of the loop to control the conveyor velocity as shown Figure 5.

The laptop/PC (with monitoring interface based on Wincc) communicates with PLC controller. Pulse width modulation mode setting time: $T_{PWM}=1ms$. To achieve the conveyor velocity characteristic, we do the following: on the computer, setting the velocity value $v_{sp}=0.2m/s$; at this time, the PLC outputs feed the control pulse with time $T_{ON}=T_{PWM}$, corresponding to the control signal $U_v=100\%$. This pulse is sent to the BD power converter to fully open the MOSFET supply U_{dm} for the DC motor and therefore the BT conveyor operates. Conveyor velocity is determined by counting number of pulses at PLC input (connected to the encoder). The characteristic of conveyor velocity is collected on the WinCC interface on the computer, as shown in Figure 6.

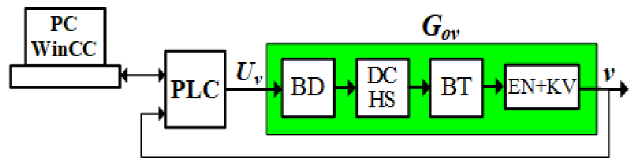

Figure 5. Block diagram for identifying object of velocity control loop

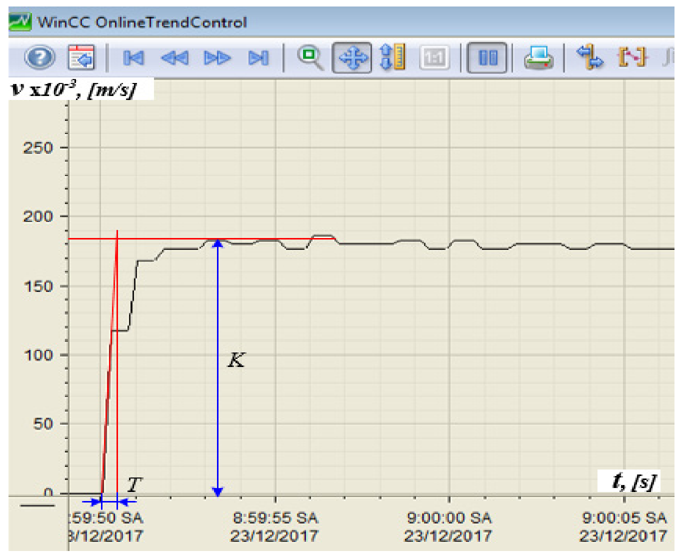

Figure 6. Response of the conveyor velocity control loop

Based on the characteristic type of the velocity loop control object, allow to approximate this control object as the first order inertia object, with the transfer function as follow:

$$G_{ov}(s) = \frac{k_v}{T_v s + 1} \tag{5}$$

Here: k_v là gain coefficient; T_v inertial time.

From graph on Figure 6, to determine T_v, drawing the tangent to the characteristic, the inertial time T_v can specify: $T_v=0.5[s]$.

Gain coefficient k is determine as follow:

$$k_v = \frac{\Delta v}{\Delta U_v} = \frac{0.185}{1} = 0.185[\text{m/s}] \tag{6}$$

Thus the transfer function of the velocity loop control object, in approximate form, as follow:

$$G_{ov}(s) = \frac{k_v}{T_v s + 1} = \frac{0.185}{0.5s + 1} \tag{7}$$

3.3. Design of the conveyor velocity controller

The block diagram of the conveyor velocity control loop is shown in Figure 7.

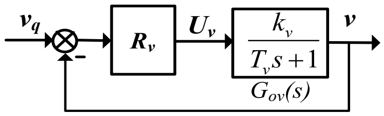

Figure 7. Block diagram of velocity control loop

Applying the module optimal method for the conveyor velocity control object, the velocity controller is determining as the integral control law (I) with the transfer function:

$$R_v(s) = \frac{k_I^v}{s} = \frac{5.4}{s} \tag{8}$$

3.4. Design of the material mass flowrate controller

The approximate transfer function of the conveyor velocity control loop takes the form as:

$$G_{kv}(s) \approx \frac{1}{2T_v s+1} = \frac{1}{s+1} \tag{9}$$

The block diagram of the material mass flowrate control loop on the conveyor, with the assumption of constant material density, taking into account the delay time of material transport on the conveyor, as shown in Figure 8.

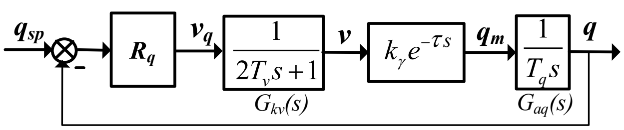

Figure 8. Block diagram of mass-flow control loop

In this diagram the parameters are as follows: $k_\gamma = 0.5$[kg/m] is the coefficient of calculating the material mass flowrate when the velocity is in a steady state; $\tau = 1$[s] is the time of material transport delay on the conveyor; $G_{aq}(s) = 1/(T_q s)$ is the transfer function of the material mass flowrate average calculation block, $T_q = 1$[s].

The control object of the material mass flowrate control loop has the equivalent transfer function as follows:

$$G_{oq}(s) = \frac{k_\gamma e^{-\tau s}}{T_q s(2T_v s+1)} \tag{10}$$

Applying symmetrical optimum (SO) method to the mass flowrate control object, the mass flowrate controller is determined as proportional - integral - differential control law (PID-SO) with the transfer function as follows:

$$R_v(s) = k_{P0} + \frac{k_{I0}}{s} + k_{D0}s = 1.25 + \frac{0.25}{s} + s \tag{11}$$

3.5. Design of the fuzzy calculation block for the seft-tunning parameters of the mass flowrate PID controller

The FCQ fuzzy calculation block has two inputs: the error of the material mass flowrate EQ and the deviation differential of the material mass flowrate DEQ, corresponding to the signal $e = q_{sp} - q$ and the deviation differential signal de/dt. The FCQ block has three outputs, proportional coefficient-PQ, integral coefficient-IQ, the differential coefficient - DQ, corresponding to the three output values are k_{PF}, k_{IF}, k_{DF}. With the above structure, the coefficients of the PID controller in combination with the fuzzy calculation block (PID-F) are determined as follows:

$$k_P^* = k_{P0}k_{PF},\; k_I^* = k_{I0}k_{IF},\; k_D^* = k_{D0}k_{DF} \tag{12}$$

Using the membership functions of triangles, implementing the input variables by 5 fuzzy sets {NB (Negative Big), NS (Negative Small), ZE (ZEro), PS (Positive Small), PB (Positive Big)} and output variables are equal to 5 fuzzy sets {SM (SMall), ME (MEdium), BI (BIg), QB (Quite Big), VB (Very Big)}. The physical value range of the input variables and the output variables are as follows: $EQ \in [-1.0, 1.0]$, $DEQ \in [-10.0, 10.0]$, $PQ \in [0, 1.0]$, $IQ \in [0, 0.01]$, $DQ \in [0, 0.5]$. Based on the weight conveyor operation experience, the characteristic of the material mass flowrate control process and the PID control principle to improve the control quality for the system, the fuzzy rule table for FCQ is built as Table 1. Using the Max-Min inferential law and defuzzification according to the centroid point method, the output clear values of FCQ block k_{PF}, k_{IF}, k_{DF} are defined.

Table 1. Fuzzy rules of the FCQ block

PQ IQ DQ		**EQ**				
		NB	**NS**	**ZE**	**PS**	**PB**
DEQ	**NB**	SM	SM	SM	SM	SM
	NS	SM	ME	SM	SM	SM
	ZE	SM	SM	BI	BI	QB
	PS	SM	SM	BI	QB	VB
	PB	SM	SM	QB	VB	VB

3.6. Simulation of the mass flowrate control system on MATLAB

Building the material mass flowrate control system on Matlab with the $\mathbf{R_v}$ controller according to (8), the $\mathbf{R_q}$ controller has been re-calibrated with the toolbox PID Tuner so that the control quality meets the requirements, Figure 9 shows the step response of this system. The $\mathbf{R_q}$ controller parameters, after adjusting by toolbox PID Tuner as follows:

$$k_{P0} = 0.486, k_{I0} = 0.001, k_{D0} = 0.101 \tag{13}$$

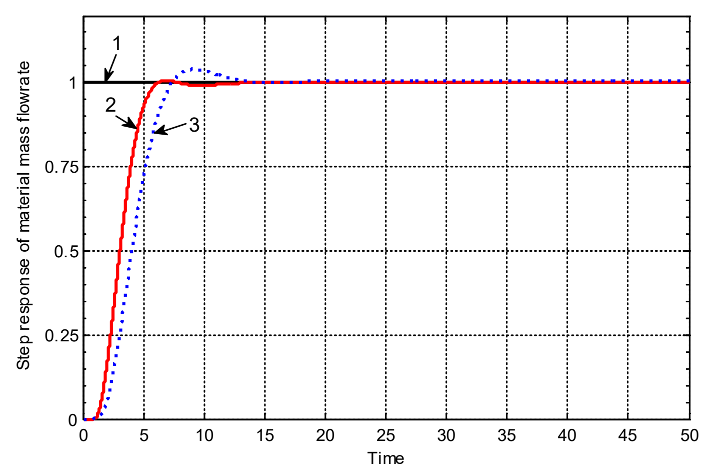

Figure 9. Step response of the weight control system: 1- reference input, 2- controller PID-F, 3- controller PID

Simulation results show that the PID controller combined with self-tuning parameters (PID-F) gives better control quality than the traditional PID controller: quick response, reduced overshoot, small steady state error, reduced the impact of noise (the level of material in the hopper).

Table 2. Quality Improvement of PID-F controller and others

Controller / Index	PID-F	PID-SO
Rise time	Small, ~5.1s	Large, ~7.1s
Steady time	Small, ~6.2s	Large, ~11.8s
Overshoot	Very small, 0.2%	Large, ~11.5%
Steady error	Eliminate, or very small	Small

4. Experimental setup of the real-time weight system

4.1. Hardware wiring diagram

In this experimental system, PLC programmable logic controller Siemens S7-200 is used to install PID algorithm for velocity control loop and PID-F algorithm for the mass flowrate control loop. The equipment of the system is shown in Figure 1. The complete system is shown in Figure 10.

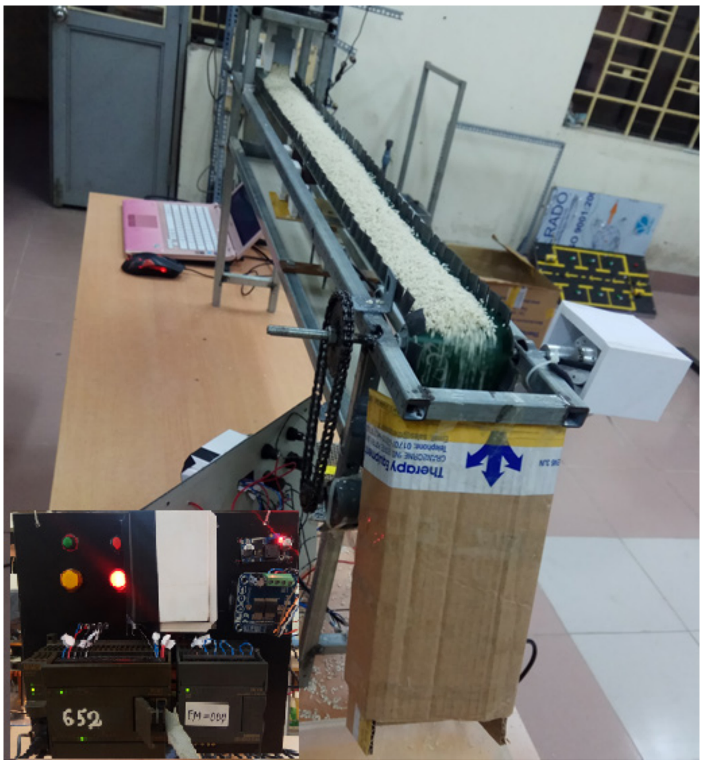

Figure 10. Experimental setup of the weighing conveyor

4.2. Algorithm for controlling material mass flowrate

The general algorithm to control the material mass flowrate for continuous weight conveyor system is shown in Figure 11.

After initializing the initial values for the system, the main program in turn calls subroutines: calculating conveyor velocity, calculating the mass of the material, calculating the material mass flowrate, calculating the error of the material mass flowrate and its deviation differential. Then the main program calls the subroutine to execute the $\mathbf{R_q}$, $\mathbf{R_v}$ controller algorithms. Finally, the main program calls the PLC's pulse calculation function to send to the BD converter, thereby controlling the motor velocity and thus meeting the required material mass flowrate.

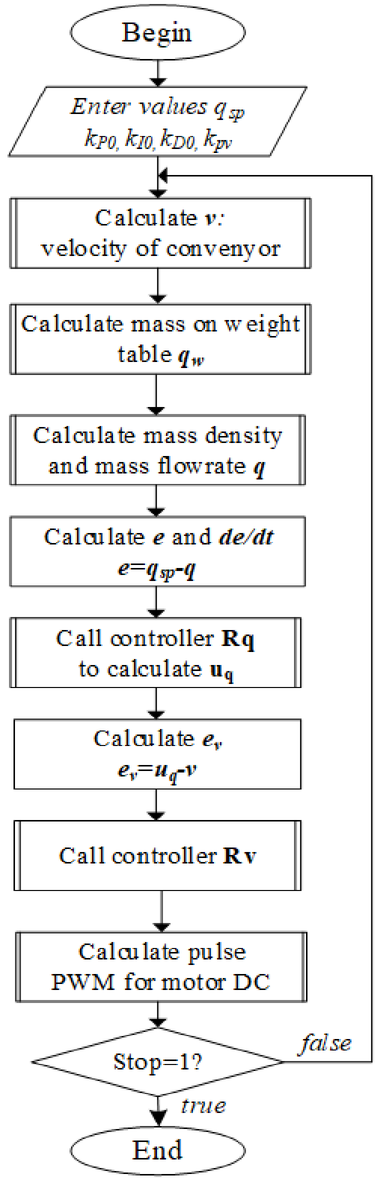

Figure 11. General algorithm for controlling mass flowrate

The algorithm for programming material mass flowrate controller R_q on PLC is shown in Figure 12.

The algorithm to program the conveyor velocity controller R_v on PLC is shown in Figure 13.

5. Experimental results

The experimental setup is shown in Figure 1, 10. In this study, the PLC S7-200 and expansion module analog EM235 are used. The laptop is communicated with PLC S7-200 through the PC Adapter USB cable to download the user program (control algorithm) into PLC S7-200 station. The output channel (PWM) from the PLC is supplied to the driver (BD) of the conveyor's motor. The conveyor's velocity measured by the encoder LPD3806 is fed back to the PLC via the high velocity counter input channel. The mass of materials moving on the conveyor measured by the loadcell OBU is fed back to the analog input channel of the EM235 module, after having amplified by the KD amplifier device.

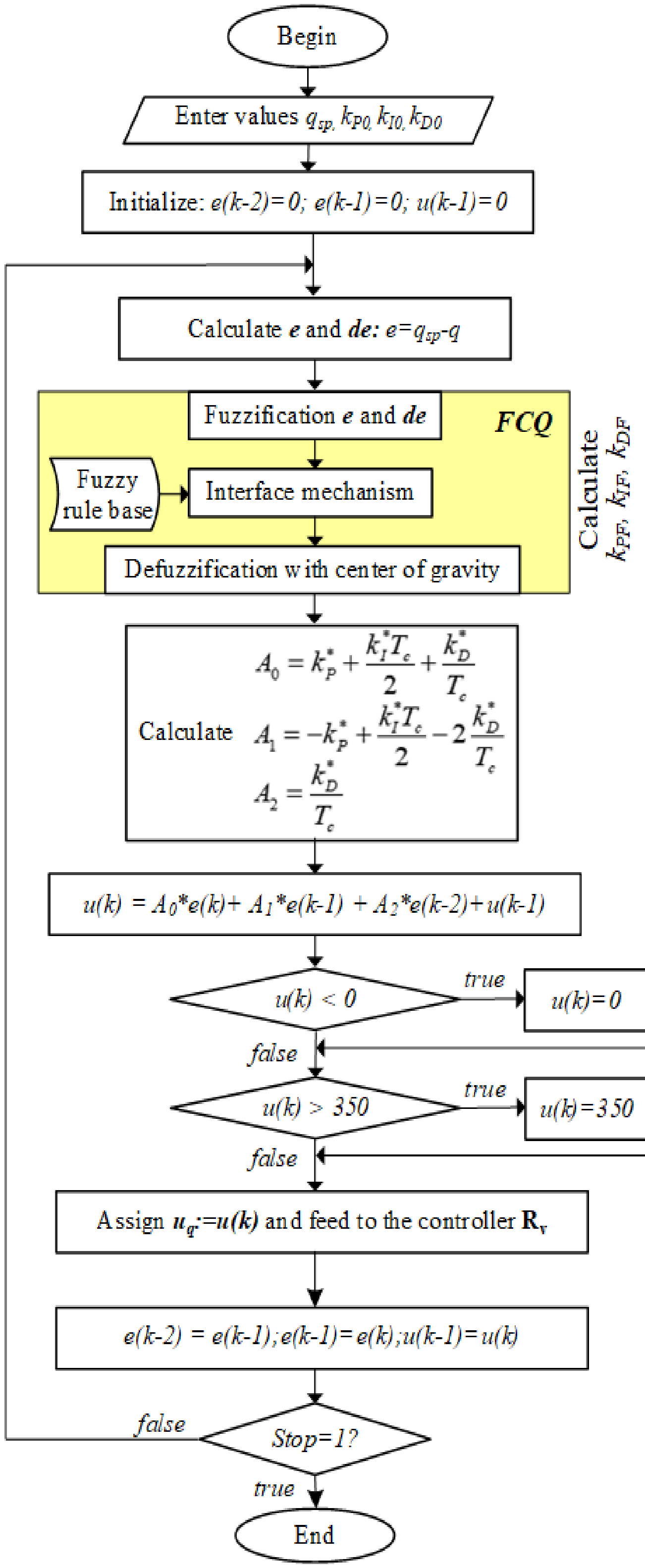

Figure 12. Algorithm of the controller R_q

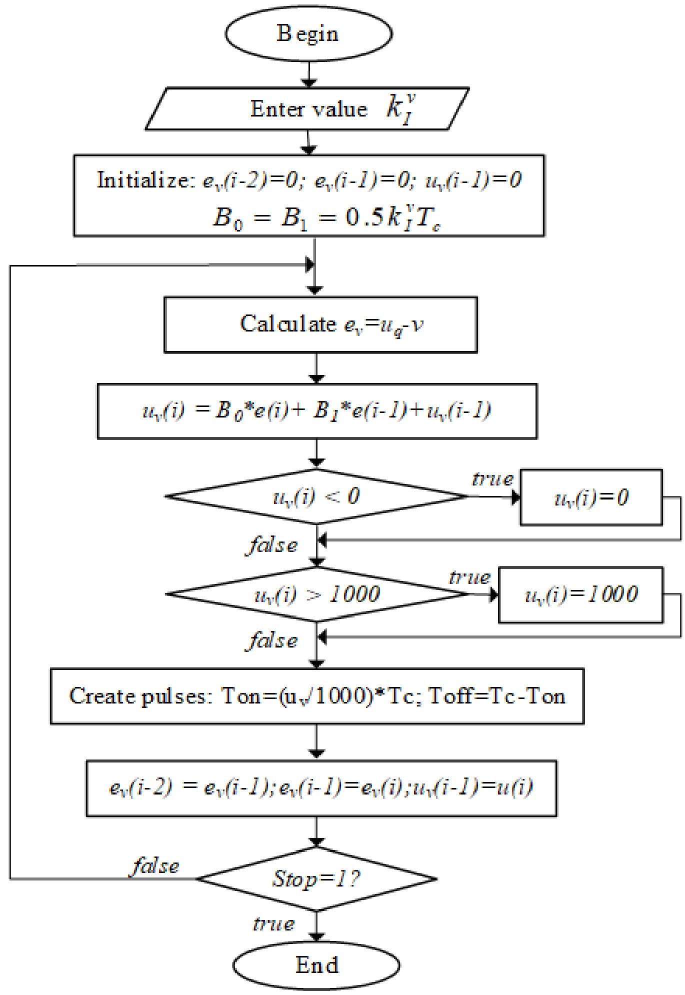

Figure 13. Algorithm of the controller R_v

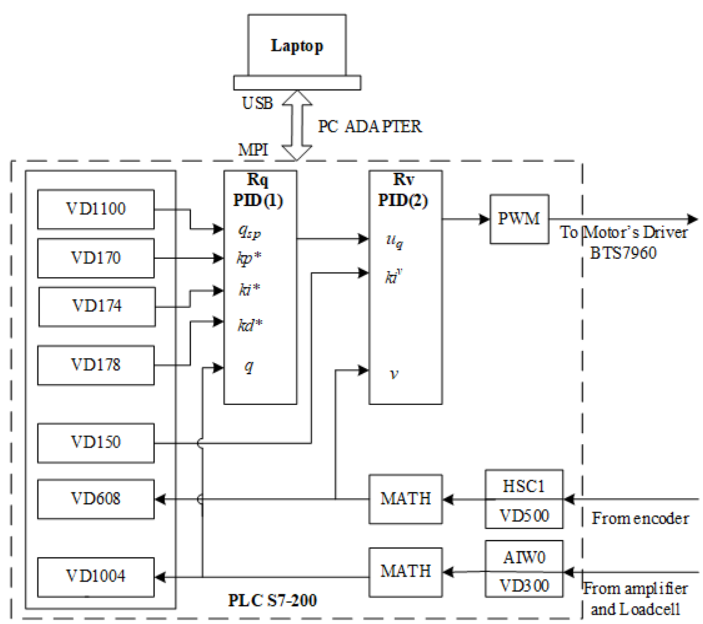

Figure 14. PID algorithms organization in PLC

The PID algorithms for the velocity control loop and the mass flowrate control loop are organized in PLC S7-200, as shown in Figure 14. The fuzzy logic calculation algorithm for adjusting PID parameters of the mass flowrate control loop is also programmed with the separate subroutine on this PLC.

The screen for monitoring the weighing conveyor was built on WinCC, as described in Figure 15.

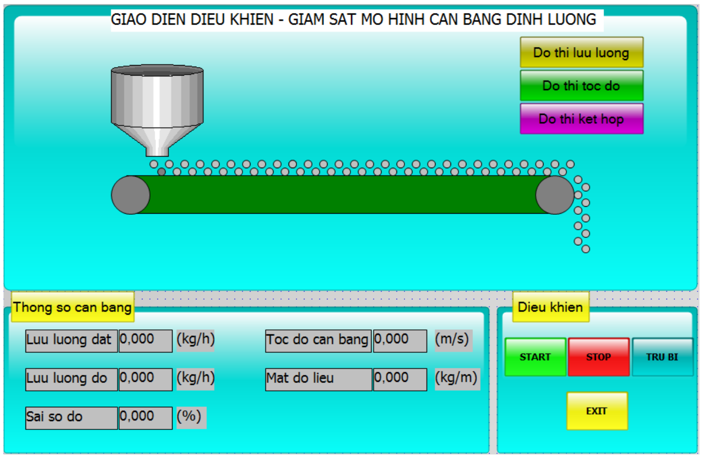

Figure 15. Screen for monitoring the weighing conveyor

This experiment was carried out with the materials - rice. The tests were done at the material's mass flowrate $q_{sp}=80$[kg/h], and $q_{sp}=100$[kg/h].

The experimental results with algorithm PID combined fuzzy calculating block (PID-F) to adjust the PID's parameters are shown as Figure 16-17.

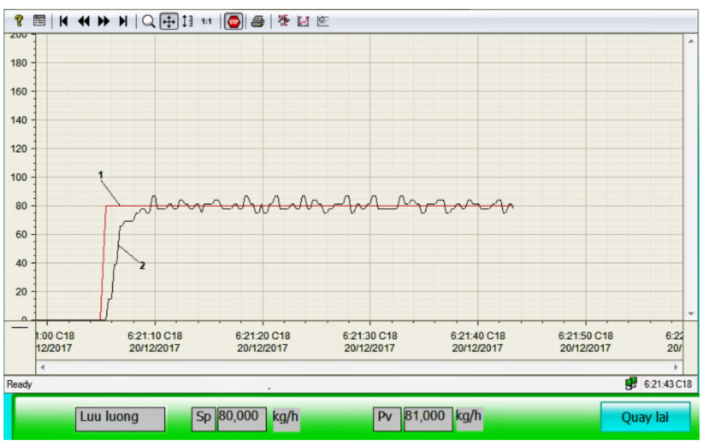

Figure 16. Real-time response of the material mass flowrate as using PLC with PID-F algorithm at $q_{sp}=80$[kg/h]: 1- reference, 2- response

Figure 17. Real-time response of the material's mass flowrate as using PLC with PID-F algorithm at $q_{sp}=100$[kg/h]: 1- reference, 2- response

From the real-time response of the material's mass flowrate, shows that the control object of the mass flowrate loop exits delay time with the constant delay time approximate 1 second; rising time about 5 second; after about 6.5 second, the steady state is reached; then, mass flowrate is small oscillated around the input reference. This oscillation is caused by noise measurement of the material's mass on the conveyor by loadcell combined with the no-filter amplifier circuit.

6. Conclusion

In this article, a nonlinear model of the weighing conveyor system is developed as considering the delay time of material transport on conveyor. This is more suitable for the actual weighing process in industries. And then, a novel two-control-loop strategy is applied for controlling the material mass flowrate on conveyor. The integral control algorithm-based inner control loop is designed for the conveyor velocity object which is identified from the experimental device system at UTC's laboratory. The outer control loop is developed for the material mass-flowrate object based on PID controller combined self-tuning parameters by the fuzzy logic calculation block. Thereafter, the proposed control strategy is verified and evaluated by simulation on MATLAB and performed experimentally on the physical equipment system at UTC's laboratory. The experimental results show that PLC controller is capable of performing the proposed control strategy with reasonable cost, but bring better control quality, thanks to the application of advanced control techniques.

Future research focuses on improving quality of controller or/and combined with IMC, GA, GPC algorithms, as considering disturbance and applying for other materials with different density and changing parameters of the object in real time.

Conflict of interest

The authors declare no conflict of interest.

References

[1] Allgeier T., Anthony J., "A Guide to Dynamic Weighing for Industry", The Institute of Measurement and Control, 2010.
[2] Hopkins M., "Loss in weight feeder systems", Measurement + Control, 39(8), 237–240, 2006.
[3] Heinrici H., "Continuous weighing and feeding systems - an integral component in process engineering", Aufbereit Tech, 41 (8), 376–383, 2000.
[4] Haefner H., "Advanced weigh feeder system for optimization of the kiln system", World Cement, 27(6), 19–27, 1996.
[5] Sato T., Kameoka K., "Self-tuning control of a weigh feeder", Transactions of the Society of Instrument and Control Engineers, 43(6), 522–524, 2007.
[6] Sato T., Design of a GPC-based PID controller for controlling a weigh feeder, Control Engineering Practice, 18, 105–113, 2010.
[7] Howimanporn S., Thanok S., Chookaew S., Sootkaneung W., "Speed control technique for conveyor using PSO based PID with programmable logic controller", System Integration, 2016 IEEE/SICE International Symposium on, 670-675, 2016.
[8] Lakshmi K.V. and Srinivas P., "Optimal tuning of PID controller using Particle Swarm Optimization", in Proceedings of the International Conference on Electrical, Electronics, Signals, Communication and Optimization, Visakhapatnam, India, pp.1-5, 2015.
[9] Palma L.B., Coito F.V., Ferreira B.G. and Gil P.S., "PSO based online optimization for DC motor speed control", in Proceedings of the 9th International Conference on Compatibility and Power Electronics (CPE), Costa da Caparica, Portugal, pp.301-306, 2015.
[10] Yanan Zhao and Emmanuel G. Collins, "Fuzzy PI Control Design for an Industrial Weigh Belt Feeder", IEEE transactions on fuzzy systems, vol. 11, no. 3, pp.311-319, June 2003.
[11] Xu-hui Chen, Md Lutfar Rahman, Yin Zhang, "Adaptive Fuzzy PID speed control of DC belt conveyor system", 17th IEEE/ACIS International Conference on Software Engineering, Artificial Intelligence, Networking and Parallel/Distributed Computing, 2016.

Advances in Science, Technology and Engineering Systems Journal Vol. 4, No. 2, 119-126 (2019)

www.astesj.com

Special Issue on Recent Advances in Engineering Systems

ASTESJ

ISSN: 2415-6698

Assessment of Coordinated Multipoint Transmission Modes for Indoor and Outdoor Users at 28 GHz in Urban Macrocellular Environment

Muhammad Usman Sheikh[*,1,2], Ritayan Biswas[1],Jukka Lempiainen[1], Riku Jantti[2]

[1]*Tampere University, Faculty of Information Technology and Communication Sciences, Finland.*

[2]*Aalto University, Department of Communications and Networking, Finland.*

A R T I C L E I N F O

Article history:
Received: 04 December, 2018
Accepted: 03 March, 2019
Online: 16 March, 2019

Keywords:
CoMP
mmWave propagation
Macro cellular
3D ray tracing
Performance analysis

A B S T R A C T

The aim of this article is to analyze and evaluate the performance of Coordinated Multipoint (CoMP) transmission approach at a frequency of 28 GHz using three dimensional ray tracing simulations in an urban macrocellular environment. The new performance metric introduced in this article is the relative power usage. Other performance metrics examined in this article are received power, the Signal to Interference plus Noise Ratio (SINR), user throughput, relative throughput gain, and the percentage of overlapping area with multiple cells. Indoor and outdoor users are separately analyzed for few key performance indicators. Different cases of coordinated multipoint transmission i.e. intra-node and inter-node coordination is analyzed. The post analysis of the acquired simulation data shows that the use of CoMP functionality is more beneficial for the cell edge users compared with the other users in terms of improving the user's experience. The throughput gain as well as the transmission overhead of the CoMP approach increases with the increase in number CoMP ports. Inter-node CoMP is much more power efficient and beneficial in comparison with the intra-node CoMP case.

1. Introduction

This article is an extension of the research work originally presented at Vehicular Technology Conference (VTC Spring 2018) [1]. In reference [1], the performance of Coordinated Multipoint Transmission (CoMP) was studied, and the performance metrics considered for the analysis were Signal to Interference plus Noise Ratio (SINR), throughput, and relative throughput gain. Whereas in this article the performance of CoMP transmission for the indoor and for the outdoor users is separately analyzed. Additional performance metrics included in this article are received signal strength, the percentage of carriers within the overlapping zone of 3 dB, 5 dB, and 7 dB, and relative power usage.

Cellular systems have evolved enormously since its inception. Current cellular technologies such as Long Term Evolution (LTE) and LTE-Advanced (LTE-A) are capable of providing data rates and capacity which are significantly higher than preceding technologies. However, the Fifth Generation (5G) of mobile communication has use cases, which have the requirement of thousand times more capacity in comparison with today's standards. This requirement is driven by bandwidth hungry applications, and those applications require high data rates. These applications may include uncompressed high definition video streaming, analyzing huge data sets for real time monitoring, and artificial intelligence applications to name a few. Additionally, the Cisco network index (VNI) report estimates that by the year 2020 there will be approximately 1.6 billion connected devices [2]. This indicates a huge increase in the number of connected devices and the amount of data utilized by these devices and applications. Therefore, in order to fulfill these requirements, different capacity enhancement solutions are needed. Several technologies such as network densification [3], heterogeneous networks, multi Carrier Aggregation (CA), Inter Cell Interference Coordination (ICIC), Enhanced ICIC (eICIC) [4], Coordinating Multipoint (CoMP) transmission and Millimeter wave (mmWave) communications [5-8] have been proposed for enhancing the capacity of cellular systems.

Traditionally, the cellular communication utilizes the microwave frequency band (sub 4 GHz frequency range) of the electromagnetic spectrum. Different operating frequency bands have been allocated for different mobile technologies. The mmWave frequency band, which lies in the range of 30 GHz – 300

[*] Muhammad Usman Sheikh, Email: muhammad.sheikh@tut.fi

GHz has the abundance of unused free spectrum. The large unlicensed bandwidth present at the mmWave frequencies can support huge data rates which is required in case of 5G technology. The mmWaves have certain attributes such as high path loss, high Building Penetration Loss (BPL) and adverse propagation properties which make them suitable only for short range communications. However, the frequency band of 28 GHz experiences less rain attenuation and absorption [6] compared with other mmWave frequency bands. This enables the 28 GHz band to be considered as a preferred band for cellular operators for future cellular communications. Additionally, the higher penetration and path loss can be coup with large antenna arrays with high directivity. This can be achieved due to the short wavelength of mmWaves which enables the utilization of large antenna arrays at both the transmitter and receiver side [6].

Generally, a single transmission point/cell serves a user in traditional wireless communications. However, in 3rd Generation Partnership Project (3GPP) release 10 the concept of coordinating multipoint transmission (CoMP) is introduced as a part of LTE-Advance technology, and that enables the user to receive signals from multiple transmission points. The coordination between different transmission points is based on the geographical location and the spatial separation. CoMP helps to improve the quality and the strength of the received signal [9-10]. Furthermore, the coordination can occur between the cells of the same base station or different base stations [9]. Coordinated Multipoint transmission can be categorized into following three categories, (1) Dynamic Point Selection (DPS) [11], (2) Joint Transmission (JT), and (3) Coordinated Beamforming/ Scheduling (CB/CS) [12]. A key drawback of CoMP is the huge quantity of data that is transferred between the coordinating transmission points.

2. Background Theory

2.1. Millimeter Waves

5G is expected to provide extremely high data rates for end users/devices. Researchers envision a thousand-fold increase in the data rate in 5G in comparison with the present technologies such as LTE-A. Higher data rates are can be achieved by increasing the bandwidth of the system. Traditional cellular communications utilize a part of the frequency band between 700 MHz and 4 GHz, that have limited bandwidth and is already occupied by the mobile operators.

The spectrum between 30 GHz and 300 GHz constitute the millimeter wave band. The wavelength of millimeter waves is in an order of few millimeters. The underutilization of the mmWave spectrum is due to the adverse conditions that affect the propagation [6]. Rain absorption, high penetration loss, low diffraction around the obstacles and a higher path loss are some of the key unfavorable factors that affect the propagation at millimeter wave frequencies. Additionally, in urban or dense urban city type environment, the communication links with only non-line-of-sight (NLOS) paths have a great challenge. As the signal attenuates more quickly at mmWave due to various adverse factors mentioned before in this article. Due to un-favorable propagation characteristics, the mmWave was envisioned as a solution for only short-range communications, particularly at the 60 GHz frequency [14].

Large unlicensed bandwidth (up to continuous 7 GHz) present at the 60 GHz band is of the primary reason for attraction, as this available bandwidth can be used for the future cellular communications system for providing enormous high data rates. The size of the bandwidth available at 60 GHz band is comparable to the bandwidth assigned for Ultra Wideband (UWB) purposes [15]. In addition the 60 GHz band is less restricted in terms of power limits. Additionally, 60 GHz frequency band utilizes greater power in comparison with Wireless Local Area Network (WLAN) and Wireless personal Area Network (WPAN). This is due to the 60 GHz frequency band regulation that allows the use of higher power. Therefore, the higher power can compensate for the greater path loss up to some extend at 60 GHz band [14]. This enables the 60 GHz frequency band to be a viable operating frequency for future wireless communications. However, there are other factors like high path loss, high rain attenuation and higher atmospheric absorption attributed to 60 GHz band; therefore, we have focused on 28 GHz band in this article.

In the sub-6 GHz frequency band, most of the spectrum is licensed and has given by the government for various purposes. It has resulted in a shortage of free available spectrum in sub-6 GHz band. Nevertheless, the un-utilized 28 GHz frequency band can help in alleviating the problem of capacity crunch by offering large free bandwidth [6]. However, there are some drawbacks of using mmWave frequency band. Based on the fundamental laws of physics, the frequency is inversely proportional to the pathloss and that results in the limited coverage at the 28 GHz frequency [16]. Absorption in the atmosphere due to the presence of rain, fog and mist also affects coverage at mmWave frequencies. Operation at mmWave frequencies and advancement in the semi-conductor technology has enabled to place a large number of antenna elements in a small cross-section, and it results in high directivity gain [6]. An antenna array with a large number of antennas can be utilized at both the transmitting and receiving sides due to the relatively small wavelength of mmWave. Additionally, electrically steerable antennas are also practical due to the development of CMOS RF circuits and that helps in improving the communication range [6].

2.2. Coordinated Multipoint (CoMP) Transmission

The 3GPP introduced coordinating multipoint technology as part of its Release 11 for LTE-Advanced systems [4]. The CoMP technology helps in establishing coordination among the multiple sectors of the same or different macro cellular base station. The coordinated communication is established by either selecting the sectors from the same macro site or from different macro sites. Intra-site coordination means two or more sectors/cells from the same macro site provide communication to the user. In inter-site CoMP, two or more sectors from different macro sites coordinate to provide the signal to the user. The coordinated transmission helps in alleviating the interference from adjoining cells and that helps in improving the spectral efficiency of the cell. The improvement in the quality of the signal (at the cell edge) occurs as the interfering signal coming from the other port is converted into a meaningful signal in the joint transmission technique. The cell-edge uses experience a poor quality of the signal as the received signal strength from multiple base stations are in a close range in terms of power. The utilization of the CoMP technology helps in improving the throughput, not only for the cell edge users only but also for the other users [17-18].

In traditional cellular macro-sites, a single sector/cell establishes a communication link to a particular user in the downlink direction. Here, a cell corresponds to a transmission point. However, LTE Release 11 aims to provide support for coordinated transmission both on the uplink and downlink channel. CoMP overcomes the hindrance arising from the interference that is caused by neighboring cells [19]. CoMP can be classified into different categories. The categorization of CoMP depends on the presence of a backhaul connection between the transmission points that are coordinating. Scheduling also has a major impact on the CoMP subcategories [11]. The three sub-categories of the CoMP technology are 1) Dynamic Point Selection (DPS) [11], (2) Joint Transmission (JT) [19-20], and (3) Coordinated Beamforming or Coordinated Scheduling (CB/CS).

In case of DPS, a single transmission point from multiple coordinating TPs is selected during every transmission time interval. The user equipment reports the Channel State Information (CSI), the identity of the favorable transmission point and other essential information such as the resources required to the central node. In DPS, after the selection of the transmission point, the data is transmitted to UE only from the selected transmission point, and other coordinating transmission points stays in mute mode during the transmission [19]. Utilizing the joint transmission type CoMP technique helps in providing channel diversity. The simultaneous transmission of identical data from different TPs helps in achieving the channel diversity. However, a suitable combining technique must be utilized at the receiver to combine the data coming from different transmission points. The joint transmission technique can be either coherent or non-coherent [19]. The signals are precoded simultaneously in coherent transmission. However, in non-coherent transmission, the precoding of the signals are performed separately at different transmission ports. The user throughput can be improved by using a joint scheduler that utilizes the available resources in more efficiently in different load condition. However, the increase in the number of TPs increase the complexity of the joint transmission technique. In coordinated scheduling and coordinated beamforming, only the CSI is transmitted from various TPs. However, only one TP is used for the actual data transmission [20]. The interference can be eliminated by utilizing one of the CoMP techniques mentioned above. It is essential to strike a balance between the performance gain and the network upgradation cost [21]. As stated above, the increase in the number of coordinating transmission ports increases the complexity of the coordinating system. A major drawback of the CoMP technology is that there is a large amount of information exchange among the coordinating TPs. Consequently, CoMP operation requires higher channel estimation and strict synchronization among the coordinating TPs. The authors in [20] and [21] demonstrate that the spectral efficiency of the system is improved by utilizing the CoMP technique. CoMP transmission help in mitigating the interference in some cases, and provide spatial diversity.

2.3. Proposed Performance Metric

In the current Information and Communication Technology (ICT) industry there is a dire need to design energy or power efficient systems. Power efficiency can be achieved by having energy efficient architectures, energy efficient resource management, and by utilizing energy efficient radio technologies [22-23]. Utilizing simultaneous connections in addition to deploying small cells help in increasing the coverage of the network. In order to compute the consumption of power at a site, a power consumption model is presented at [24] and [25] and is given as:

$$P_{BS} = P_{const} + P_{load} * F, \tag{1}$$

In equation (7), P_{BS} is the total power consumption of the base station, P_{const} is the load-independent power consumption factor, P_{load} is the load-dependent power consumption factor and F is the load factor. For the BS operating at full load i.e. 100 %, the load factor F is equal to 1. The load-independent and load-dependent factors included in this study of this article are presented in Table .

Table 1. Parameters of power consumption model.

Parameter	Unit	Value
Transmit power per transmission port	dBm	46
Power consumption of DSP unit	W	100
Power Amplifier (PA) efficiency	%	45
Consumption of tranceiver's power	W	100
Consumption of rectifier's power	W	100
Consumption of fiber optic unit power	W	7.5

The relative power usage (P_{Rel}) in [%] is defined as follows:

$$P_{Rel} = \left(\frac{P_U - P_{Ref}}{P_{Ref}}\right) * 100\,, \tag{2}$$

In equation (8), P_U and P_{Ref} is the power usage of the case under consideration and power usage of the reference case, respectively. The power usage of the reference case (P_{ref}) and considered case (P_U) is computed as given in equation (9) and (10), respectively. In equation (9), T_{ref} is the time of the reference case and is defined as the time required for sending the reference amount of data (D_{Ref}) with a data rate of reference case (R_{Ref}) as given equation (11). Whereas, in equation (10), T_{Rel} is the relative amount of time needed to transmit the reference data (D_{Ref}) and is defined as a ratio of T_U and T_{Ref} as expressed in equation (12), where T_U is the time of the considered case and is defined in equation (13) as the time required for sending the reference amount of data (D_{Ref}) with a data rate of case under consideration (R_U).

$$P_{ref} = P_{BS}T_{ref} \tag{3}$$

$$P_U = P_{BS}T_{Rel} \tag{4}$$

$$T_{Ref} = D_{Ref}/R_{Ref} \tag{5}$$

$$T_{Rel} = T_U/T_{Ref} \tag{6}$$

$$T_U = D_{Ref}/R_U \tag{7}$$

Details of the other performance metric i.e. area spectral efficiency, and relative capacity gain can be found at [1].

3. Simulation Environment, Cases and Parameters

3.1. Simulation Environment

A three-dimensional ray tracing simulator called "sAGA" is developed by the authors using a MATLAB platform for the simulation purpose. An 'Image Theory' based ray tracing algorithm is to find the propagation paths between the transmitter and the receiver. A tracing simulator requires 3D building data to accurately determine the paths between the transmitter and the receiver. For this study work, a Krunuuhaka region from Helsinki is considered. The two-dimensional map of considered area is shown in Figure 1. This type of environment illustrates an urban

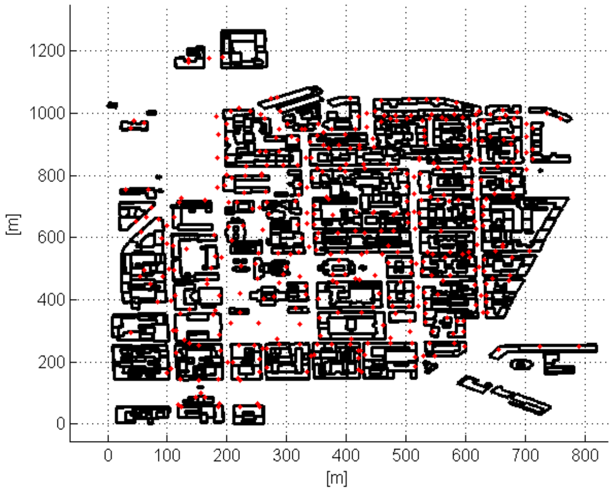

Figure 1. Simulation area.

macro cellular environment. It is assumed that users are located both in indoor and outdoor locations. For indoor users, it is assumed that there are no walls inside the indoor environment. However, BPL and ceiling penetration loss are considered for indoor users. For the outer wall with the 40 cm thickness, the wall penetration loss is 26.5 dB at 28 GHz frequency [13]. As a fairly large number of miniature antenna elements can be placed inside a small area at 28 GHz, therefore, an additional gain of 16 dB is assumed in our analysis. The basis of this additional gain is the assumption that a large array of an antenna can provide additional diversity gain, beamforming gain and combining gain.

There are ten base stations with three sectors. The height of the antenna is set at 30 m for all cells. The illustration of the antenna locations of the antennas is given in Figure 3. The users (850) were placed in the environment with approximately 85% of the users located indoors and the remaining 15% located outdoors. The indoor users are located on different floors. A floor height of 3 meters was considered for the indoor environment. The locations of users on different levels of the building are elucidated in Table.

Table 2 . User distribution.

	Number	Percentage
Total RX points	850	100
Outdoor	128	15.06
Indoor	722	84.94
Ground floor	269	31.65
Second floor	259	30.47
Fifth floor	160	18.82
Seventh floor	34	4

A. Simulation cases

Cellular networks are generally deployed with the macro layer to provide the coverage and the basic capacity to the network, and such networks are called homogeneous networks. Therefore, for the research work of this article, only homogeneous scenarios with only macro sites are considered. The simulation cases considered for this work are presented below.

3-sector site (Reference case): The reference case illustrates a case with the macro site, where only one cell (acting as the serving cell) provides connection to the user. A serving cell is selected on the basis of the strength of the received signal. In order to restrict the interference from the neighboring cells, a downtilt of 9° was considered for all the sectors, as the sites are located fairly close to each other

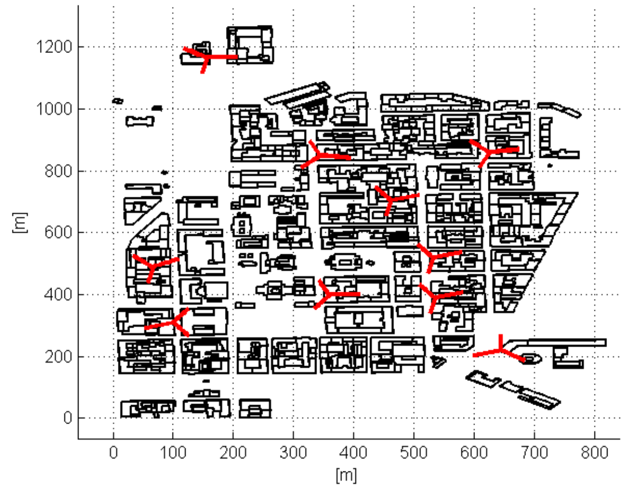

Figure 2. Three-sector site plan.

Intra-Node 2 TP: The same macro base station provides coordinated transmission by virtue of utilizing two Transmission Points (TPs). In this context, a TP represents a single sector/cell. The utilization of the same macro cellular site eliminates the requirement for a backhaul link between the coordinating cells.

Intra-Node 3 TP: In this case there is a coordinated transmission from the 3 cells of the same macro site.

Inter-Node 2 TP: This case represents a scenario where the coordinated transmission is provided from two sectors from different macro sites. As a result, a backhaul link is necessary in such a scenario.

Inter-Node 3 TP: This scenario illustrates the coordinated transmission from three cells belongs to different sites.

Inter-Node 4 TP: It involves transmission from four cells which may belong to different sites.

The antenna radiation pattern is obtained using an extended version of the 3GPP antenna model. The key parameters utilized for the antenna modeling are summarized in Table 3.

Table 3: Antenna model parameters

$HPBW_H$	$HPBW_V$	FBR_H	SLL_V	A_M
65°	6.2°	30 dB	-18 dB	18.23 dBi

Other simulation parameters are provided in Table 4.

Table 4. General simulation parameters

Parameters	Unit	Value
Frequency	GHz	28
System bandwidth	MHz	20
TX power	dBm	46
Number of cells	No.	30
Antenna height	m	30
Building penetration loss	dB	26.5
UE noise figure	dB	8

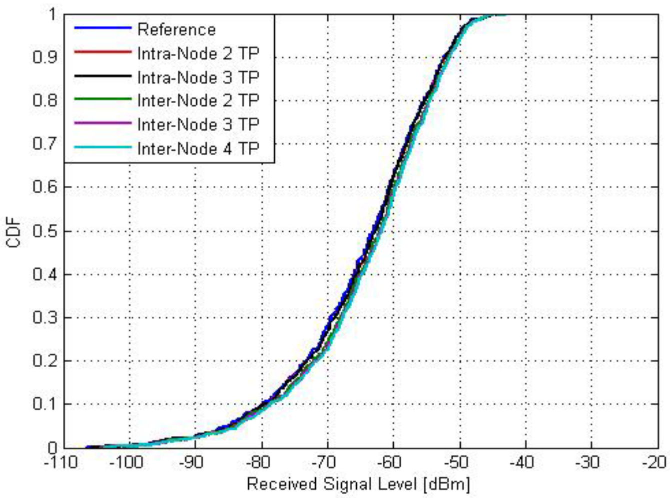

(a)

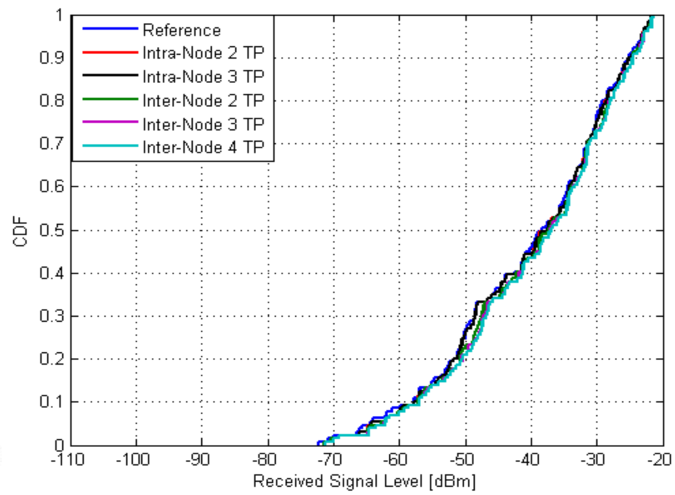

(b)

Figure 3. Received signal level, (a) CDF plot of indoor users, (b) CDF plot of outdoor users.

4. Simulation Results and Discussions

The first metric considered for the analysis is the received signal strength. Indoor and outdoor users are separately analyzed in this paper. Figure 3 (a) shows the CDF plots of received signal level in [dBm] for different considered cases for indoor users. It can be seen in Figure 3 (a) that almost identical received signal levels were obtained by reference cases and other coordinated multipoint transmission cases. Mean received level of -64.85 dBm is obtained with reference case, and with marginal improvement the received signal strength of -64.57 dBm and -64.56 dBm is achieved with two and three points intra-node CoMP transmission, respectively. Similarly, the maximum mean received signal strength of -63.59 dBm is acquired with four points inter-node CoMP case, and that is again not significantly better compared with the reference case. The Figure 3 (b) shows the CDF plots of received signal level in [dBm] for outdoor users. It is clearly evident that outdoor users have stronger signal strength compared with indoor users, as the indoor signal experiences the building penetration loss. Mean RX level of -40.46 dBm is obtained with the reference case for outdoor users, and mean received signal strength of -39.37 dBm is acquired with four points inter-node CoMP case.

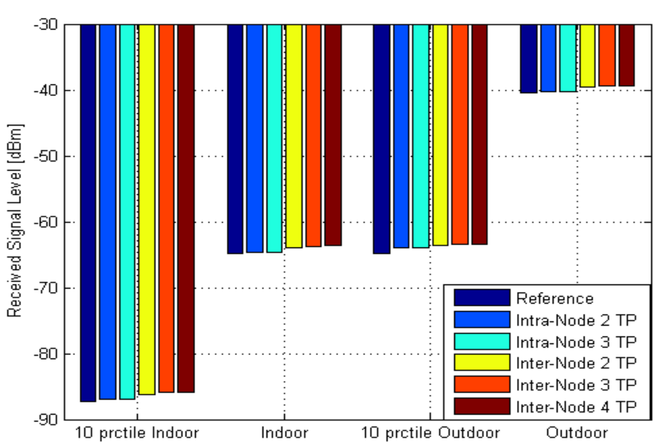

Figure 4: Bar plot of mean received signal levels.

The performance of the users within the 10^{th} of the sample data are more critical and crucial. Therefore, we have separately targeted the cell edge users (10^{th} percentile data) for our later analysis and comparison of performance. Therefore, we have separately targeted the cell edge users (10^{th} percentile data) for our later analysis and comparison of performance. Figure shows the bar plot of mean received signal level for indoor and outdoor users considering the 10^{th} percentile users and the whole data set. It is interesting to see that mean received signal of indoor users considering the whole data set is almost identical to the signal levels of outdoor users within the 10^{th} percentile of data. Only received signal level does not tell about the actual user experience, and in order to have more deep understanding of user experience, a quality metric i.e. SINR needs to be analyzed along with signal strength.

Figure 5 (a) and figure 5 (b) shows the CDF plots of the SINR of indoor users and outdoor users for different considered cases, respectively. The reference case considered in this article offers a mean SINR of about 7.1 dB and 8.37 dB in the targeted area for indoor and outdoor users, respectively. It can be seen in figures 5 (a) and 5 (b) that the CoMP functionality has improved the SINR compared with the reference case, and the inter-node CoMP deployment is found more beneficial compared with intra-node CoMP performance. In case of intra-node CoMP deployment, it was found that increasing the number of joint transmission points (cells) from two to three shows no significant improvement in SINR, which is due to large spatial separation between the sectors of the same site. For indoor users, the mean SINR of about 9.12 dB and 9.7 dB is achieved with two and three points intra-node CoMP functionality, respectively. However, in case of inter-node CoMP functionality the gain in improving the received SINR enhances with the increase in number of joint transmission points. For indoor users, the mean SINR of 12.83 dB, 16.72 dB, and 19.30 dB is acquired from 2-, 3-, and 4-point joint inter-node CoMP transmission, respectively. A higher mean SINR values are achieved in outdoor environment, and similarly the CoMP technique improves the SINR of outdoor users as well. A mean SINR of 25.6 dB attained with 4-point joint inter-node CoMP transmission for outdoor users.

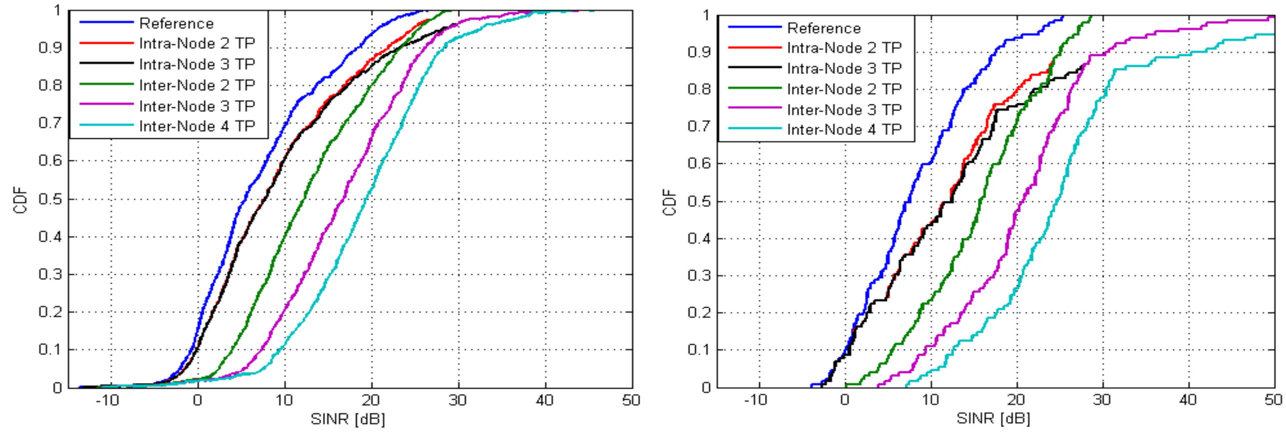

(a) (b)

Figure 5. Signal to interference plus noise ratio, (a) CDF plot of indoor users, (b) CDF plot of outdoor users.

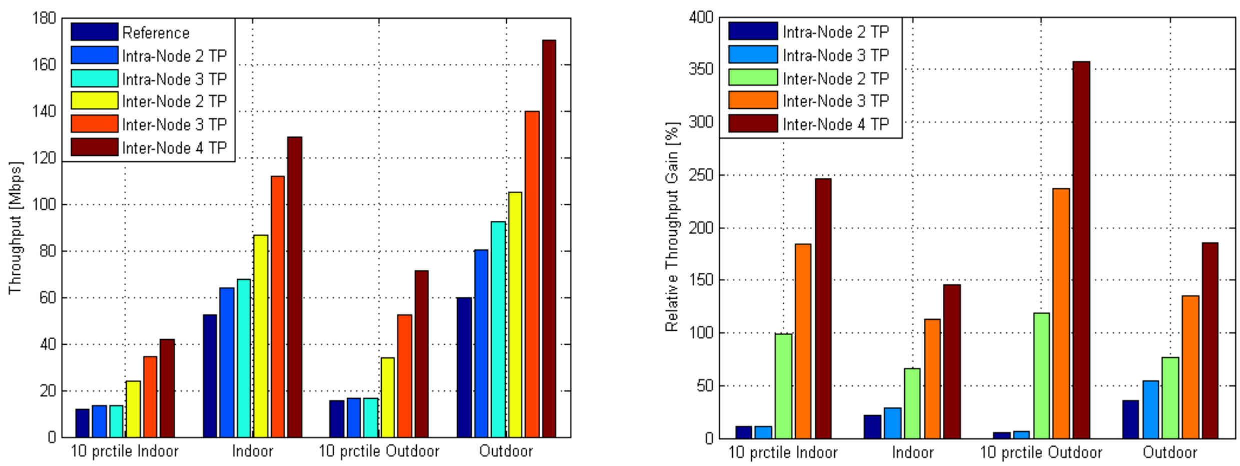

(a) (b)

Figure 6. Throughput, (a) Mean user throughput, and (b) Relative throughput gain.

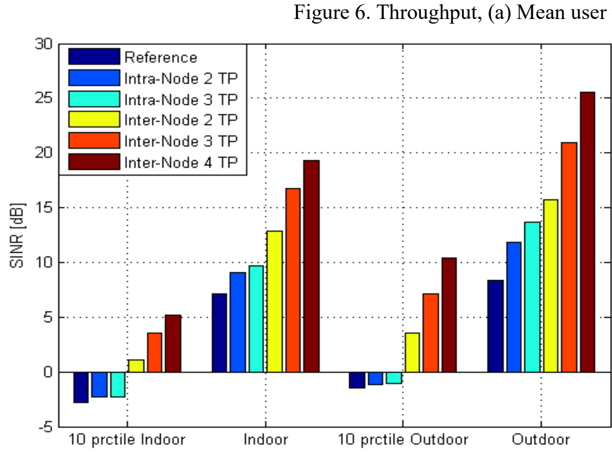

Figure 7. Bar plot of SINR.

As stated earlier, that the users within 10th percentile data are vital and figure (5) shows the bar plot of mean SINR for indoor and outdoor users considering the 10th percentile users and the whole data set. Considering the SINR results presented in 5 (a) and 5 (b) it can be said that the CoMP deployment has improved the SINR of the cell edge users by considerable margin. The mean SINR of indoor cell edge users is improved from -2.84 dB to -2.28 dB, and that means a gain of just 0.56 dB. Again, no additional sign of improvement is witnessed by increasing a number of TPs from two to three for intra-node CoMP transmission. However, the inter-node CoMP deployment improves the indoor user experience in downlink direction and provides a gain of 3.96, 6.42, and 7.98 dB by 2, 3, and 4 points inter-node joint transmission, respectively. Considering only 10th data, even higher gains are achieved in an outdoor environment and a gain of 4.99, 8.6, and 11.8 dB is provided by 2, 3, and 4 points inter-node joint transmission, respectively compared with the reference case. It shows the potential of CoMP deployment in improving the user quality at the cell edge.

The Figure 6 (a) shows the mean throughput of the users for different considered cases for indoor and outdoor environment, whereas the Figure 6 (b) shows the relative throughput gain of different CoMP cases with respect to the reference case. The "10th prctile" in Figure depicts the throughput of the users in the lower 10 percentile users' throughput distribution. In 6 (a), although the increase in the absolute value of throughput (capacity) by CoMP is small at cell edge level, however the relative capacity gain coming from CoMP functionality is higher for cell edge users compared with overall cell users as shown in 6 (b). It is also learned from the results presented in Figure that the intra-node CoMP deployment is less efficient for cell edge users, and does not provide any significant gain i.e. around 11.01 – 11.4 % for indoor users, and 5.8 – 6.1 % for outdoor users, respectively. However, inter-node CoMP deployment can offer the maximum relative capacity gain of about 98.2 %, 183.7 %, and 246.6 % with

2, 3, and 4 points joint scheduling and joint transmission for indoor users. Similarly, for outdoor users in the lower 10 percentiles, CoMP offered relative capacity gain of about 118.6 %, 237 %, and 357 % with 2, 3, and 4 points inter-node CoMP transmission.Table shows the results of the overlapping zone with 3 dB, 5 dB, and 7 dB window for different considered cases. The information about the number of available servers (carriers) within the window of certain dBs is commonly used by mobile operators to evaluate the design and performance of the network, and is also used as a metric of network quality during the planning process. The percentage of the area with the single server within the window of certain dBs shows the clear dominance area. However, an overlapping between the cells is required to support the handover between them. An area overlapped by multiple servers is affected by higher interference, and is called as "polluted" area with multiple servers; therefore the SINR is directly related to carrier overlapping. In Table it can be seen that the cell dominance i.e. single server area improves with CoMP functionality. With 5 dB window, the reference case has 67.48 % of clear cell dominance area which is then extended to 75.64 % with intra-node 2 point transmission. It can be also seen that no additional improvement is brought to cell dominance area with intra-node 3-point transmission, and therefore there was no additional improvement in SINR results with intra-node 3-point transmission, which were earlier presented in figure (7). However, for the cases of inter-node CoMP deployment, the cell dominance area continued to improve with the additional number of coordinated points. For the case of 5 dB window the inter-node 3 point CoMP transmission provides cell dominance area of 97.55 %, which is then further improved to 100 % with inter-node 4 point CoMP transmission. Similarly, the statistics of the overlapping zone with 3 dB and 7 dB for different cases can be found at Table . Interestingly, the results presented in Table show that on one hand CoMP extends the cell dominance area, on the other hand it diminishes the handover area with small difference of levels between the available servers, and it will help in avoiding the ping-pong effect during the handover procedure.

Figure shows the relative power usage of different considered CoMP cases with respect to the reference case using 10th percentile users' data and all users' data set. In case of a reference case, a user is connected with only one transmission point, whereas in CoMP the user is connected with multiple transmission ports, therefore utilizes the radio and power resources of multiple sources. The relative power usage of 0 % means a same power is required in the considered case as used in the reference case, and a 100 % relative power usage means twice the power is required in case under consideration with respect to the reference case.

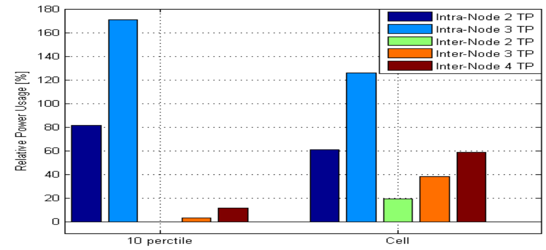

It is already established from the SINR and throughput results presented in figure (8) and Figure that the CoMP transmission improves the SINR of the user which in turn improves the user throughput. However, the Figure shows that intra-node CoMP transmission is not power efficient solution. It is learned from relative power usage results presented in Figure that while using two point and three point intra-node CoMP transmission, 81.2 % and 170.1 % relative additional power is required in comparison with the reference case considering cell edge users. Similarly, 61 % and 125.5 % relative additional power is required in comparison with the reference case considering whole cell data. On the other hand, inter-node CoMP techniques are quite much power efficient and work better for serving cell edge users. Two-point inter-node CoMP transmission is even more power efficient compared with reference case, and three point and 4-point inter-node CoMP has a relative power usage of only 3.2 % and 11.2 %, respectively for 10th percentile data. The summary of the results considering the whole data set is given in Table 6.

5. Conclusion

It is learned from the results presented in this article that the coordinated multipoint transmission and joint scheduling technique help in alleviating the problem of bad coverage and poor signal quality for the users located at the cell edge. It was found that CoMP is more beneficial for the cell edge users in comparison with the users located near the base station. The conventional case of 3-sector site was used as a reference case to compute the relative throughput gain for different CoMP configurations. The findings of this article revealed that utilizing two TPs in CoMP mode from the same base station provides the relative throughput of 10.32 % for the cell edge users. However, significant gain is not witnessed by utilizing three cells from the same base over two TPs from the same base station. Utilization of two, three and four TPs from different coordinating base stations yields a mean relative throughput gain of 100.5 %, 190.5 % and

Table 5. Results of overlapping zone.

Case	Single server 3dB (%)	Two servers 3dB (%)	≥Three servers 3dB (%)	Single server 5dB (%)	Two servers 5dB (%)	≥Three servers 5dB (%)	Single server 7dB (%)	Two servers 7dB (%)	≥Three servers 7dB (%)
Reference	80.65	16.32	3.03	67.48	23.43	9.09	55.59	29.84	14.57
Intra-Node 2 TP	85.78	12.47	1.75	75.64	18.18	6.18	65.04	24.13	10.84
Intra-Node 3 TP	85.78	12.47	1.75	75.64	18.18	6.18	65.04	24.13	10.84
Inter-Node 2 TP	100.0	0	0	97.55	2.21	0.23	90.68	7.69	1.63
Inter-Node 3 TP	100.0	0	0	100.0	0	0	99.53	0.47	0
Inter-Node 4 TP	100.0	0	0	100.0	0	0	100.0	0	0

Table 6 Results summary

Case	Mean RX Level [dBm]	Mean SINR [dB]	Relative SINR Gain [dB]	Mean Cell Spectral Eff. [bps/Hz]	Mean Throughput [Mbps]	Relative Throughput Gain [%]	Relative Power Usage [%]
Reference	-61.19	7.29	0	2.66	53.38	0	0
2Point Intra	-60.91	9.53	2.24	3.31	66.34	24.27	60.94
3Point Intra	-60.90	10.30	3.01	3.55	71.00	33.0	125.57
2Point Inter	-60.29	13.26	5.97	4.47	89.40	67.47	19.43
3Point Inter	-60.04	17.36	10.07	5.79	115.85	117.0	38.25
4Point Inter	-59.95	20.24	12.95	6.73	134.76	152.42	58.46

260 %, respectively, for the cell edge users. Similarly, over the whole cell area the coordinated multipoint transmission from 2, 3, and 4 TPs from different nodes can offer the mean relative throughput gain of 67.5 %, 117 %, and 152.5 %, respectively.

It was also found that utilizing two TPs and three TPs intra-node CoMP transmission requires 81.2 % and 170.1 % relative additional power in comparison with the traditional single point transmission considering only cell edge users. Whereas the inter-node CoMP transmission is found much more power efficient compared with single point transmission and intra-node Three TPs and four TPs inter-node CoMP has additional 3.2 % and 11.2 % power usage in comparison with single point transmission.

It was also revealed through simulation results that CoMP deployment clearly improves the cell dominance area, and shrinks the cell border area which is overlapped by multiple servers. The results presented in this paper show the potential of CoMP transmission in overcoming the problem of cell edge users. It is learned that intra-node CoMP solution is not a power efficient technique. However, inter-node CoMP does not only improves the user experience i.e. SINR and throughput; rather it is also power efficient to use inter-node coordinated multipoint transmission. The simulation results given in this research article have been collected for an urban area of Helsinki city with the certain simulation parameters and assumptions. Therefore, performance results can vary depending upon simulation environment, setup, modeling errors and impairment, and system parameters.

References

[1] M. U. Sheikh, R. Biswas and J. Lempiaeinen, "Performance Evaluation of Coordinated Multipoint Transmission at 28 GHz Frequency Using 3D Ray Tracing," 2018 IEEE 87th Vehicular Technology Conference (VTC Spring), Porto, 2018, pp. 1-6.

[2] Cisco white paper, Visual Networking Index, Feb. 2016.

[3] M. U. Sheikh, J. Lempiäinen and H. Ahnlund, "Advanced Antenna Techniques and Higher Order Sectorization with Novel Network Tessellation for Enhancing Macro Cell Capacity in DC-HSDPA Network", International Journal of Wireless & Mobile Networks. vol. 5, no.5, pp. 65–84.

[4] 3GPP, TS 36.300 "E-UTRA and E-UTRAN Overall description: Stage 2" (Release 11), V11.5.0, April. 2013.

[5] H. Zhao , R. Mayzus , S. Sun , M. Samimi , J. K. Schulz , Y. Azar , K. Wang , G.N. Wong , F. Gutierrez Jr. and S.T. Rappaport , "28 GHz Millimeter Wave Cellular Communication Measurements for Reflection and Penetration Loss in and Around Buildings in New York City", Proc. IEEE Int. Conf. Commun. , pp.1 -6 , 2013.

[6] T. S. Rappaport , J. N. Murdock and F. Gutierrez , "State of the art in 60 GHz Integrated Circuits & Systems for Wireless Communications" , Proc. IEEE , vol. 99 , pp.1390 -1436 , 2011.

[7] Z. Pi, and F. Khan, "An introduction to Millileter-wave Mobile Broadband Systems", IEEE Communications Magazine, vol. 49, no. 6, pp. 101-107, June 2011.

[8] S. K. Yong and C.-C. Chong, "An overview of Multigigabit wireless through millimetre wave technology: potentials and technical challenges," EURASIP journal on wireless communications and networking, 2007.

[9] T. Abe, Y. Kishiyama, Y. Kakura, and D. Imamura, "Radio Interface Technologies for Cooperative Transmission in 3GPP LTE-Advanced", IEICE Transaction on Communications., vol. E94-B, no. 12, pp. 3202-3210, Dec. 2011.

[10] D. Lee, H. Seo, B. Clerckx, E. Hardouin, D. Mazzarese, S. Nagata, K. Sayana, "Coordinated multipoint transmission and reception in LTE-advanced: deployment scenarios and operational challenges," IEEE Communications Magazine, vol.50, no.2, pp.148-155, February 2012.

[11] 3GPP TR36.814 V2.0.1 : "Evolved Universal Terrestrial Radio Access (E-UTRA): Further Advancements for E-UTRA Physical Layer Aspects", March 2010.

[12] R. Irmer, H. Droste, P. Marsch, M. Grieger, G. Fettweis, S. Brueck, H. P. Mayer, L. Thiele, V. Jungnickel, "Coordinated multipoint: Concepts, performance, and field trial results," IEEE Communications Magazine, vol.49, no.2, pp.102-111, February 2011.

[13] B. G. Choi, W. H. Jeong, K. S. Kim, "Characteristics Analysis of Reflection and Transmission According to Building Materials in the MillimeterWave Band", Recent Advances on Electroscience and Computers, pp. 154-158, 2015.

[14] S. K. Yong and C.-C. Chong, "An overview of Multigigabit wireless through millimetre wave technology: potentials and technical challenges," EURASIP journal on wireless communications and networking, 2007.

[15] ETSI, Accessed on 21/03/2016: http://www.etsi.org/technologies-clusters/technologies/radio/ultra-wide-band

[16] Digi International, Accessed on 21/03/2016: http://www.digi.com/technology/rf- articles/rf-basics.

[17] 3GPP, TR 36.819 "Coordinated Multi-Point Operation for LTE Physical Layer Aspects."

[18] K. M. Karakayli, G. J. Foschini, and R. A. Valenzuela, "Network Coordination for Spectrally Efficient Communications in Cellular Systems," IEEE Wireless Communication, vol. 13, no. 4, pp. 56–61, Aug 2006.

[19] J. Lee, Y. Kim, H. Lee, B. L. Ng, D. Mazzarese, J. Liu, W. Xiao, Y. Zhou, "Coordinated multipoint transmission and reception in LTE-advanced systems," IEEE Communications Magazine, vol.50, no.11, pp.44-50, November 2012.

[20] D. Lee, H. Seo, B. Clerckx, E. Hardouin, D. Mazzarese, S. Nagata, K. Sayana, "Coordinated multipoint transmission and reception in LTE-advanced: deployment scenarios and operational challenges," IEEE Communications Magazine, vol.50, no.2, pp.148-155, February 2012.

[21] R. Irmer, H. Droste, P. Marsch, M. Grieger, G. Fettweis, S. Brueck, H. P. Mayer, L. Thiele, V. Jungnickel, "Coordinated multipoint: Concepts, performance, and field trial results," IEEE Communications Magazine, vol.49, no.2, pp.102-111, February 2011.

[22] Su, X. , Sun, E. , Li, M. , Yu, F. and Zhang, Y. (2013) A Survey on Energy Efficiency in Cellular Networks. Communications and Network, 5, 654-660. doi: 10.4236/cn.2013.53B2117.

[23] O. Adigun, and C. Politis, "Energy Efficiency Analysis for MIMO Transmission Schemes in LTE," Computer Aided Modeling and Design of Communication Links and Networks (CAMAD), 2011 IEEE 16th International Workshop on, Kyoto, 10-11 June 2011, pp. 77-81.

[24] S.F. Yunas, J. Niemela, M. Valkama, T. Isotalo, "Techno-economical analysis and comparison of legacy and ultra-dense small cell networks," in Local Computer Networks Workshops (LCN Workshops), 2014 IEEE 39th Conference on , vol., no., pp.768-776, 8-11 Sept. 2014.

[25] M. U. Sheikh, J. Sae, and J. Lempiäinen, "In Preparation Towards Future Cellular Network: The Detailed Analysis of Macro and Micro Site Densifcation and Sector Densification", Journal of Telecommunication Systems. vol. 65, no.4, pp. 621–636, August 2017.

Advances in Science, Technology and Engineering Systems Journal Vol. 4, No. 2, 127-133 (2019)

www.astesj.com

Special Issue on Advancement in Engineering and Computer Science

ASTESJ

ISSN: 2415-6698

Automatic Stitching of Medical Images Using Feature Based Approach

Kyi Pyar Win[1,*], Yuttana Kitjaidure[1], Kazuhiko Hamamoto [2]

[1]*King Mongkut's Institute of Technology Ladkrabang, Electronic Department, Faculty of Engineering, 10520, Thailand*

[2]*Tokai University, School of Information and Telecommunication Engineering, 143-0001, Tokyo, Japan*

A R T I C L E I N F O

Article history:
Received: 06 February, 2019
Accepted: 07 March, 2019
Online: 19 March, 2019

Keywords:
Biomedical images
Feature based approach
Image stitching
ORB features
Panorama

A B S T R A C T

Image stitching is a process of creating a panoramic image by combining multiple images that have overlapping regions of the same scene. It is a challenging topic in image processing, multimedia, and medical applications. The proposed system can be applied in medical applications for scoliosis operations and other long limb operations. The problem of the traditional x-ray machine is the narrow view. So, it can't produce the large view of body x-ray image in a single frame. Therefore, this problem is solved by combining two or more x-ray images into a panorama one. This paper proposes a system which automatically stitches the x-ray images and produced a panorama x-ray image. The proposed stitching method is based on feature based approach, ORB (Oriented FAST and Rotated BRIEF). In feature detection stage, Oriented FAST approach is used. In feature description stage, Rotated BRIEF approach is applied. The two important criterias for determining the stitching performance are stitched image quality and processing time. Therefore, the aim of my proposed system is to produce a panorama x-ray image with high resolution and low processing time based on feature extraction approach. We compared our proposed method with three different features detectors. SIFT, SURF, and Harris corner detectors were tested and measured the rate of correct features detection and computation time. Finally, we measured the quality of result images that produced by stitching system of different feature based methods. According to the experimental results, ORB approach can produce high quality panorama image with least processing time.

1. Introduction

Image mosaicing or stitching is creating a panorama image by stitching or mosaicing many images that have overlapping points of the same view. A panorama is a large view of a scenery. It can be obtained by merging many pictures that have overlapping parts of the same scene. Image stitching is very popular in many applications such as construction of large view map, stitching arial images or satellite images and mosaicing radiography images in medical applications. In medical applications, it is needed to view the whole body x-ray images. The large view of x-ray images helps the surgeons to diagnose a disease for example long leg alignment operation, scoliosis patients etc. The traditional x-ray machine cannot produce large view x-ray image. Therefore, our proposed system can be applied in medical applications to view a panorama x-ray image.

Image stitching methods can be divided into two groups. They are direct method and feature based. Direct based method minimizes pixel to pixel mismatching, pixel based approach [1]. Feature based methods find distinctive features and then matched each other between two input images. The robust detectors can extract important characteristics (for example robust in translation, scale, noise and rotation). There has been great progress in medical images stitching system using features based approach. They are SIFT (Scale Invariant Feature Transform) [2], SURF (Speedup Robust Feature detector) [3], HARRIS detector [4] [5], Principal Component Analysis SIFT (PCA-SIFT) [6], and FAST (Features from Accelerated Segment Test). A good feature detector can be choose depending on the nature of the problem. Two main stages in feature based methods are the registration stage and the stitching stage.

The aim of this paper is to develop high quality image stitching system with low processing time. The proposed system contains five main stages. They are preprocessing, feature detection and

[*] Corresponding Author: Kyi Pyar Win, 1 Soi, Chalong Krung, Ladkrabang, Bangkok, Thailand, +66-6-17430344, kyipyarwin5@gmail.com, 60601169@kmitl.ac.th

https://dx.doi.org/10.25046/aj040217

description, feature matching, Homography estimation and images stitching. This paper is an extension of work originally presented in 2018 International Conference on Intelligent Informatics and Biomedical Sciences [7].

The rest of this paper comprise of five parts. Part 2 presents the background of research work. Part 3 contains the briefly reviews of three features detection approaches. In Part 4, the proposed image stitching methodology is discussed. In Part 5, the results of proposed system are explained. Finally, Part 6 discusses the conclusion and the future works.

2. Background

Recently there has been done many researches works in image stitching using feature based approaches. Many researchers tried to develop the feature based methods that can detect reliable and repeatable features than traditional methods. But there still a great challenge in image stitching. There are many features detectors that were used in images stitching such as SIFT, SURF, Harris etc. Harris corners fail in image scaling and SIFT is the longest processing time [8].

According to the literatures, there are mainly two methods for image stitching. They are direct based approach and feature based method. Direct methods calculate the camera parameters by minimizing an error function based on the intensity difference of the overlapped region. Transformation matrix is calculated based on intensity difference. Direct based methods give accurate registration, but they fail in image scaling, illumination change and noise. Compared to feature based method, it requires a good initial estimation to achieve transformation matrix which is a major weak point of this method.

Feature based method detects different features, for example edges, points, corners, lines, or other shapes and calculates the relationship between these features. Compared to direct method, it is strong to light change, scale, affine transformation, noise, and orientation of the image. It takes care of locality around detected features to describe that feature as feature descriptor. In feature based method, all main features in an image pair are compared with that of every feature in other image by using the descriptors [9].

There are many feature detector methods exist that are used in medical images stitching system. Feature based approach is suitable for any movement of scene happened in image because of its robustness. This method is very faster, and it has the capability to identify a panorama image by detecting the neighbor correlation between two images. But, feature based techniques rely on accurate recognition of image features.

By using direct based approach, there had been done researched for medical images stitching. Among them, cross correlation was mostly applied because it can be developed using the FFT (Fast Fourier Transform) for stitching two images of the same size. But the weak point is high in costs [10].

There has been great progress in image stitching using feature based approaches. SIFT, SURF, and Harris detectors were mostly used [11]. Gong was presented an image stitching method. In feature extraction, SURF detector was used. The weak point is that it can't detect correct features in image with noise [4] [5]. Singla presented images stitching using x-ray images by combining SIFT and SURF [12]. RANSAC (Random Sample Consensus) algorithm was used to select the correct features points but high in computation complexity. Adel et al. [13] compared many feature based detectors. They showed that ORB was the fastest in processing time compared with other detectors.

Many researchers have been proposed the medical images stitching using feature based approach, but ORB method has not been applied yet. Therefore, this research work is the first work of biomedical images stitching using ORB feature based approach. The proposed system used ORB method in feature detection and description. The correct features points were chosen by using RANSAC algorithm. Homography matrix was estimated by applying the four feature pairs. As a final, the system mosaiced the two x-ray images together using Homography matrix. In blending stage, weight average method was used to eliminate the seam. The proposed system can be used in medical applications to help for surgeons to diagnose the diseases and to save time.

3. Feature Detection and Description

3.1. SIFT

SIFT (Scale Invariant Feature Transform) is an algorithm for local feature extraction and descriptor representation. The SIFT features are robust in image scale and rotation [3]. In SIFT algorithm, there are three major stages. These stages are key point or interest points detection, orientation assignment, and key point descriptor. Key point detection used difference of Gaussian function (DOG) to detect feature points which are invariant to scale and rotation. In orientation assignment stage, one or more orientations are assigned to each key point. In key point descriptor stage, a vector descriptor is developed for each key point.

3.2. SURF

Bay et al. developed the SURF algorithm [1]. SIFT and SURF algorithms process a little different way in detecting features. SIFT creates an image pyramids and then filters each layer with Gaussians by increasing sigma values and taking the difference. SURF makes a stack without down sampling. By using integral images, SURF filters the stack using a box filter approximation of second order Gaussian partial derivatives. Integral images allow the computation of rectangular box filters in near constant time [6].

3.3. Harris

Harris and Stephens presented a corner detector, which is called Harris detector [14]. This detector is widely used to detect feature points and corners. To find the corners in the input image, Harris method takes look at the average intensity which is directional. The intensity change in the small specific area called window around an interested point. The point where the average intensity strongly high changes as compared to the previous one direction is called as a corner point.

4. Methodology

The proposed methodology of x-ray images stitching is shown in Figure 1. There are five main stages in our proposed system. They are preprocessing, feature extraction and description, feature matching, Homography estimation and images blending. Our proposed system accepted input x-ray images that have overlapped regions and recognized overlapped areas of the images by extracting the ORB features of those images and stitched them automatically to generate the final large view image. In our proposed system, there are two main components, namely overlapped area searching and stitching the images using the searched overlapped area. By using ORB features, the system can find the overlapped areas of the images efficiently. Moreover, the system can stitch the images to produce the seamless high resolution image with low processing time.

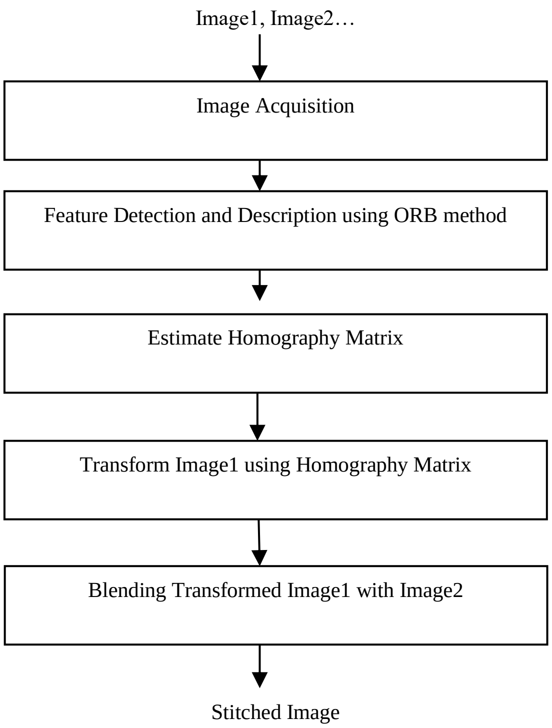

Figure 1. Proposed Images Stitching System Using ORB Feature Based Approach.

4.1. Image Preprocessing

The preprocessing step is an essential step in image processing. First, the original DICOM format is converted into JPEG format to reduce the image size. We used 100 x-ray images with 50 pairs of overlapped images as the input images. It is required about 15-30% of overlapped regions to be stitched. The samples of the input x-ray images are illustrated in Figure 2.

4.2. Features Extraction and Description

Our proposed images stitching system used ORB feature based approach. ORB approach is a combination of Oriented FAST detector and Rotated BRIEF descriptor. Oriented FAST is used to detect feature points and Rotation BRIEF is used to generate descriptors. The speed of FAST and BRIEF are very fast, so ORB has advantages in speed. The good point of this algorithm is fast and having rotational invariance and reducing sensitivity to noise. Figure 3 and Figure 4 show the extracted ORB features of input x-ray images.

4.2.1. Oriented FAST Detector

Both FAST algorithm and BRIEF algorithm do not have scale invariance. FAST detector can detect the features that are translation and rotation invariance, insensitive to noise and high reliability. But the feature points do not have information about direction. Therefore, ORB algorithm uses the Oriented FAST algorithm to detect the feature points which has direction information. Using intensity centroid method, it can calculate the direction of the corner and produce features with direction information.

$$m_{pq} = \sum_{x,y} x^p y^q I(x,y)$$

From Equation 2, we can know the center of gravity or centroid.

$$C = \left(\frac{m_{10}}{m_{00}}, \frac{m_{01}}{m_{00}}\right) \quad (2)$$

The orientation of the vector from corner to center of gravity can be calculated by using Equation 3.

$$\theta = \arctan\ 2(m_{01}, m_{10}) \quad (3)$$

4.2.2. Rotated BRIEF Descriptor

BRIEF produces binary descriptors by binary coding method. The binary descriptor is simple and storage space is smaller than SIFT and SURF.

$$\tau(\mathrm{p}; \mathrm{x}, \mathrm{y}) = \begin{cases} 1 \text{ if } & \mathrm{p(x)} < \mathrm{p(y)} \\ 0 & \text{otherwise} \end{cases} \quad (4)$$

Where p(x) is the pixel intensity at that point. The feature descriptor is defined as follows:

$$f_n(P) = \sum_{1 \le i \le n} 2^{i-1} \tau(P; Xi, Yi) \quad (5)$$

n BRIEF pairs (a1, b1), ……., (an, bn) can be written as a matrix S as follows:

$$S = \begin{bmatrix} a_1 & \cdots & a_n \\ b_1 & \cdots & b_n \end{bmatrix}$$

A rotated version of $\boldsymbol{S_\theta}$ can be computed by using Equation 6.

$$\boldsymbol{S_\theta} = \boldsymbol{R_\theta S} \quad (6)$$

Where, S_θ is the test position for the binary pixel after rotation. θ is the rotation angle, R_θ is the rotation matrix of the main direction.

4.3. Features Matching

After detecting the ORB features, the next stage is features matching. In this step, hamming distance is applied to find the matched features. The results of features matching stage are shown in Figure 5 and Figure 6.

4.4. Compute Homography Matrix

After features matching, the next stage is Homography estimation. The RANSAC (Random Sample Consensus) algorithm is used to eliminate the wrong matched features and to compute the Homography matrix. The matching relationship of the images are found by using transformed Homography matrix.

4.4 RANSAC (Random Sample Consensus) Algorithm

RANSAC algorithm has three stages. In the first step, it chooses four random feature pairs. Second, it produces the Homography matrix for those selected feature pairs. In the third stage, it calculates an error measure pairs using Homog matrix.

4.4.1. Homography Estimation from Point Correspondences

For two images that have a correspondence between 4 points, homography matrix can be expressed as below:

$$\begin{bmatrix} x_i' \\ y_i' \\ 1 \end{bmatrix} \cong \begin{bmatrix} a & b & c \\ d & e & f \\ h & i & 1 \end{bmatrix} \begin{bmatrix} x_i \\ y_i \\ 1 \end{bmatrix}$$

It is required 2 linear equations and 8 unknowns for each correspondence. Therefore, it is needed 8 linear equations for 4 correspondences. Two linear equations can be calculated by Equation 7 and 8.

$$ax_i + by_i + c - x_i'(hx_i + ky_i + 1) = 0 \tag{7}$$

$$dx_i + ey_i + f - y_i'(hx_i + ky_i + 1) = 0 \tag{8}$$

In these equations, x_i' and y_i' are coordinates of changed stitched image.

(1) (2)

(3) (4)

Figure 2. The example input images that used in our proposed system.

4.5. Images Blending

The final stage of images stitching is images blending. The aim of this step is to adjust the pixels intensity and to eliminate the visible seams. In this stage, the weighted average method is applied. Figure 7 and Figure 8 show the result images of our proposed system.

Figure 3. The result of features extraction from two knee x-ray images.

Figure 4. The result of features extraction from two leg x-ray images.

Figure 5. The result of features matching stage from the two knee x-ray images.

Figure 6. The result of features matching from the two leg x-ray images.

Figure 7. Final knee stitched image.

5. Results

The proposed system is the automatic images stitching system using medical x-ray images. Our proposed images stitching system is based on feature based approach. In feature detection and description, ORB method was used. The good point of ORB approach is rotation invariant, robust in noise and speed in processing time. We compared our proposed method with three different detectors, SIFT, SURF and Harris. According to the experiments, we can prove that our proposed method is the best in processing time and performance accuracy compared with three features detector methods. We examined the accuracy of our proposed method using 100 x-ray images. Our input samples consist of spine, lower limb and upper limb x-ray images. As the inputs images, our proposed system needs two overlapped x-ray images to be stitched. It is needed about 15-30% of overlapping regions to be stitched. The sample dataset was received from Department of Medicine, Aung Hospital, Lashio in Myanmar. Our proposed system can be used in medical applications such as scoliosis operations. The tested equipment to run for our proposed method is a computer with Core i7 CPU 2GHz and RAM 4GB. Table 1 and 2 describe the comparison of features extraction performance that tested with SIFT, SURF, Harris and ORB. Table 3 shows the comparison of quality measurement of the ORB method and other feature based image stitching methods using MSE and PSNR values. According to this table, images stitching using ORB method has lager PSNR value and smaller MSE value compared with other feature based methods. From experimental results, ORB can detect correct features points with lowest processing time. Therefore, ORB method is suitable for real time applications.

Figure 8. Final leg mosaiced image.

Table 1. The comparison of features extraction performance (SIFT, SURF, Harris and ORB) for Figure 2 (1) and (2).

Methods	Image Pixels	Features 1	Features 2	Time(s)	Matched features
SIFT	1295 x1224 1477 x1297	3295	1043	8.201892	211
SURF	1295 x1224 1477 x1297	459	873	0.682011	145
Harris	1295 x1224 1477 x1297	4321	2639	0.7356092	399
ORB	1295 x1224 1477 x1297	11	24	0.013491	4

Table 2. The comparison of features extraction performance (SIFT, SURF, Harris and ORB) for Figure 2 (3) and (4).

Methods	Image Pixels	Features 1	Features 2	Time(s)	Matched features
SIFT	1521 x1601 1521 x1275	1369	869	10.391036	304
SURF	1521 x1601 1521 x1275	287	172	0.876134	132
Harris	1521 x1601 1521 x1275	3922	2977	1.837210	457
ORB	1521 x1601 1521 x1275	56	43	0.018932	32

Table 3. Quality measurement of the resultant image that produced by ORB method and other feature based image mosaicing methods.

Methods	MSE	PSNR	Average Processing Time(s)
Image Stitching Using ORB	139.23	26.89	0.013491
Image Stitching Using SIFT	146.47	26.51	8.012932
Image Stitching Using SURF	186.75	25.91	0.65411
Image Stitching Using Harris	216.31	23.67	0.75314

6. Conclusion and Future Work

In this paper, we proposed automatic images stitching system using feature based approach. In features detection and matching, ORB features were used. The proposed method was tested with 100 x-ray images with 50 overlapping pairs. The main goal of our proposed system is to develop a high quality images stitching system with low processing time. The contribution of our proposed system is that it is the first work of medical images stitching system using ORB approach. The proposed system was compared with other feature based images stitching algorithms, SIFT, SURF and Harris. The final image quality measured between the ORB algorithms and other feature based methods were computed using MSE and PSNR values. Experimental results show that the ORB algorithm can produce high quality seamless image mosaic of medical images with low processing time.

Our proposed method tends to be extended for 3D image stitching, 2D images stitching with moving objects and using hybrid of feature based with direct based approaches to get better results as a future work.

Conflict of Interest

The authors declare no conflict of interest.

Acknowledgment

The authors highly appreciate the Asian University Network (AUN/SEED-Net) for their financial support to contribute this research. Moreover, we also thank 'Aung' Hospital, Lashio, Myanmar, for the x-ray images used in this study.

References

[1] Niu Jing, Yang Fan and Shi Lingyi, "Improved method of automatic image stitching based on SURF," First International Symposium on Future Information and Communication Technologies for Ubiquitous HealthCare (Ubi-HealthTech), Jinhua, pp. 1-5, 2013. https://doi.org/ 10.1109/Ubi-HealthTech.2013.6708059

[2] Cansin Yildiz, "An Implementation on Recognizing Panoramas", Department of computer engineering, Bilkent University, Ankara, Turkey, 2005. https://www.cs.bilkent.edu.tr/

[3] Matthew Brown and David Lowe, "Automatic Panoramic Image Stitching using Invariant Features", International Journal of Computer Vision, Department of Computer Science, University of British Columbia, Vancouver, Canada, 2007. https://doi.org/10.1007/s11263-006-0002-3

[4] Jun Hui Gong, Jun Hua Zhang, Zhen Zhou An, Wei Wei Zhao and Hui-Min Liu, "An approach for X-ray image mosaicing based on Speeded-Up Robust Features," International Conference on Wavelet Active Media Technology and Information Processing (ICWAMTIP), Chengdu,pp.432.435,2012.https://doi.org/10.1109/ICWAMTIP.2012.6413530

[5] R. Botan, K. F. Coco and K. S. Komati, "Implementation of an Image Stitching Algorithm to a Low-Cost Digital Microscope," 30th SIBGRAPI Conference on Graphics, Patterns and Images (SIBGRAPI), Niteroi, pp. 285-291, 2017. https://doi.org/ 10.1109/ICIHT.2017.7899142

[6] Luo Juan and Oubong Gwun, "A comparison of SIFT, PCA-SIFT and SURF," 2009 International Journal of Image Processing (IJIP), pp. 143-152, 2009. https:// http://www.cscjournals.org/

[7] K. PyarWin and Y. Kitjaidure, "Biomedical Images Stitching using ORB Feature Based Approach," 2018 International Conference on Intelligent Informatics and Biomedical Sciences (ICIIBMS), Bangkok, 2018, pp. 221-225. https://doi.org/ 10.1109/ICIIBMS.2018.8549931

[8] Chakrasali A. and Manjunatha P. "Automatic Image Mosaicing Using Discrete Cosine Transform", Proceedings of International Conference on VLSI, Communication, Advanced Devices, Signals & Systems and Networking, Lecture Notes in Electrical Engineering, Vol 258, Springer, India, 2013. https://doi.org/10.1007/978-81-322-1524-0_35

[9] Samsudin, S., Adwan, S., Arof, H. et al. J, "Development of Automated Image Stitching System for Radiographic Images", Journal of Digital Imaging, Volume 26, Issue 2, pp. 361-370, April 2013. https://doi.org/10.1007/s10278-012-9483-5

[10] M. Dawood, C. Cappelle, M. E. El Najjar, M. Khalil and D. Pomorski, "Harris, SIFT and SURF features comparison for vehicle localization based on virtual 3D model and camera," 3rd International Conference on Image Processing Theory, Tools and Applications (IPTA), Istanbul, pp. 307-312, 2012. https://doi.org/ 10.1109/IPTA.2012.6469511

[11] Singla, Savita and Reecha Sharma. "Medical Image Stitching Using Hybrid of Sift & Surf Techniques." International Journal of Advanced Research in Electronics and Communication Engineering (IJARECE) Volume 3, Issue 8, August 2014. https://www.citeseerx.ist.psu.edu/

[12] Ebtsam Adel, Mohammed Elmogy and Hazem Elbakry "Image Stitching System Based on ORB Feature-Based Technique and Compensation Blending", International Journal of Advanced Computer Science and Applications, Vol. 6, No. 9, pp. 55-62, 2015. https://www. citeseerx.ist.psu.edu/

[13] S. Adwan and R. Majed, "A development of an augmented registration approach towards Scoliosis's radiographic images stitching method,". International Conference on Informatics, Health & Technology (ICIHT), Riyadh, pp. 1-6, 2017. https://doi.org/10.1109/ICIHT.2017.7899142

[14] Chia Yen Chen, "Image Stitching Comparisons and New Techniques", computer science department, University of Auckland, 1998. https://doi.org/10.1007/3-540-48375-6_73

[15] David Lowe, "Distinctive Image Features from Scale-Invariant Key points", Computer Science Department, University of Columbia, International Journal

of Computer Vision, Vol.60, No.2, 2004. https://doi.org/10.1023/B:VISI.0000029664.99615.94

[16] Yang Fan; He Yan; Deng Zhen Sheng and Yan Ang, “Improvement of automated image stitching system for DR X-ray images”, Computer in Biology and Medicine, Vol 71, pp. 108-114, 2016. https://doi.org/10.1016/j.compbiomed.2016.01.026

[17] B. Baheti, U. Baid and S. N. Talbar, "A novel approach for Automatic Image Stitching of spinal cord MRI images using SIFT," International Conference on Pervasive Computing (ICPC), pp. 1-5, June 2015. https://doi.org/ 10.1109/PERVASIVE.2015.7087071

[18] G. Wang, Z. Zhai, B. Xu and Y. Cheng, "A parallel method for aerial image stitching using ORB feature points," IEEE/ACIS 16th International Conference on Computer and Information Science (ICIS), pp. 769-773, 2017. https://doi.org/ 10.1109/ICIS.2017.7960096

[19] A. Pandey and U. C. Pati, "A novel technique for mosaicing of medical images”, Annual IEEE India Conference (INDICON), pp. 1-5, June 2014. https://doi.org/ 10.1109/INDICON.2014.7030465

[20] E. Rublee, V. Rabaud, K. Konolige and G. Bradski, "ORB: An efficient alternative to SIFT or SURF,” International Conference on Computer Vision, Barcelona, pp. 2564-2571, 2011. https://doi.org/ 10.1109/ICCV.2011.6126544

[21] Hassaballah M., Abdelmgeid A.A. and Alshazly H.A. Image Feature Detectors and Descriptors. Studies in Computational Intelligence, SCI vol 630. Springer, 2016.

Advances in Science, Technology and Engineering Systems Journal Vol. 4, No. 2, 134-139 (2019)

www.astesj.com

ASTESJ

ISSN: 2415-6698

Sentiment Analysis of Regional Head Candidate's Electability from the National Mass Media Perspective Using the Text Mining Algorithm

Ahmad Zainul Hamdi[1], Ahmad Hanif Asyhar[*,2], Yuniar Farida[2], Nurissaidah Ulinnuha[2], Dian Candra Rini Novitasari[2], Ahmad Zaenal Arifin[3]

[1]*Religious Studies Department, UIN Sunan Ampel Surabaya, Indonesia*

[2]*Mathematics Department, UIN Sunan Ampel Surabaya, Indonesia*

[3]*Mathematics Department, Universitas PGRI Ronggolawe, Indonesia*

A R T I C L E I N F O

Article history:
Received: 08 January 2019
Accepted: 08 March 2019
Online: 20 March 2019

Keywords:
Sentiment analysis
Text mining
East Java regional head election

A B S T R A C T

Mass media plays an important role in leading public opinion, including in the election of regional head candidates. The tendency of mass media coverage can be used as a parameter to measure the strength of each regional head candidate. To analyze the tendency of media opinion, sentiment analysis is needed. In this study, text mining techniques were used to analyze opinion sentiments of a regional head election in East Java from the national media perspective. The researcher used the Support Vector Machine algorithm to build a sentiment analysis model. News documents about candidates for the regional head in East Java 2018 were taken from national mass media samples, namely JPNN, Kompas, Detik and Republika. From the test results, the model built on Khoffifah's data as a candidate for regional head number one has a value of precision, recall and AUC of 0.927, 0.931 and 0.902, respectively. Furthermore, the model built on Gus Ipul's data as a candidate for regional head number two has a value of precision, recall, and AUC of 0.940, 0.948 and 0.890 respectively. The models built on both data shows good performance with accurate estimation results. Based on the data obtained, the national media tends to have alignments to the regional head candidate number two namely Gus Ipul.

1. Introduction

The development of the internet in this globalization era is growing rapidly, the internet plays an important role in various scientific disciplines, such as science, psychology, sociology, marketing, communication, and politics too [1]. Human needs on the internet and information are always developing, causing rapid technological advancements. Most people use the internet to access media, both online and social media. Online mass media such as jpnn.com, kompas.com, detik.com, republika.co.id, and others are online media that continue to grow along with the rapid growth of people who are aware of information flows.

Recognized or not, opinions from national or local media can also lead to public opinion. Opinion in online media or social media plays a very large role in influencing habits or behavior towards the election of the head of state, regional head, or people's representatives both at the central and regional levels [2]–[5]. Online media is very accessible compared to print media because now everything is in your hands.

In 2018 is a political year in several regions including East Java province. In 2018, it will also be the end of the term of office of the Governor of East Java, so that regional head election needs to be held for the period 2018-2023. The East Java regional head election is also in the spotlight for the people of Indonesia in addition to the DKI Jakarta regional head election and also West Java and Central Java regional head elections because the election in these regions become political barometer in this country. The two Governor candidates are Khofifah and Gus Ipul.

The DKI Jakarta regional head election left an impression on how the votes for the pair Ahok and Djarot had to drop dramatically only due to religious sentiment and the issue of

*Corresponding Author: Ahmad Hanif Asyhar, UIN Sunan Ampel Surabaya, Indonesia, +62 82233250005, hanif@uinsby.ac.id

money politics on a few days before the voting. Here the role of media greatly influences candidates. The DKI Jakarta regional head election that has just finished raises an important note, namely the strong pulling of public opinion through the media. On national online media news in the pre-implementation and implementation of the DKI Jakarta regional head election, there were various opinions and responses with positive and negative sentiments. The problems that arise when analyzing all the results of sentiment and the classification of social media news or national online media manually, it takes a lot of time and effort in its implementation. From these problems, an opinion classification system is needed in the form of sentiment text on national mass media to predict the strength of the pair governor and deputy candidate early quickly and accurately [6]. Media news that available online can be used as a data source to predict the results of political elections. The influence of media opinion that has a major impact on public opinion, as happened in the case of elections in DKI Jakarta, needs to be considered in order to make predictions on the electability of governor elections.

To analyze media opinion, sentiment analysis is needed [7]. Sentiment analysis is a branch of learning science in the text mining domain that studies analysis of the opinion, sentiment, emotion, attitude, an evaluation which is poured into textual form [7]. The use of sentiment analysis techniques is often used for product reviews, reputation management, analysis of a topic and so on[2]. Research that analyzes mathematically or computationally about online media sentiments about the election is rarely found. This is because the collection of news data through online media requires extra hard work compared to twitter data collection that can be easily accessed via the Twitter API.

There are two main problems in this study. The first problem is because of the lack of negative data on media data, there will be an imbalance class. The problem obstacle is that there are so many features on news data that feature selection will be needed before going into sentiment analysis. In this research, by considering this problem, the classification of news sentiment in online mass media will be applied in politics, in a case study of regional head elections in East Java in 2018.

2. Related Works

In recent years, sentiment classification has become a principle problem in sentiment analysis research. Sentiment classification aims to determine the polarity of sentiment documents. The sentiment classification mostly focuses on English. Moreover, research focuses on film reviews, products, and others. In Mullen's research and also the research conducted by Wilson and the team [8], the supervised learning method was applied in the classification of film reviews. In the research conducted by Cui and the team [9], as well as the research conducted by Dave and the team [10], the sentiment classification was applied to product reviews. Sentiment research on Indonesian-language documents, especially in news article documents, was not found. In addition, sentiment analysis of documents is a problem because of the many ways opinions are developed in one document. News articles present a bigger challenge because news writers usually avoid overt attitude indicators. However, despite real neutrality, news articles can still bear polarity if they describe events that are objectively positive or negative.

Today, sentiment analysis of the textual data is one of the interesting topics. Many researchers are working on the automated techniques of extraction and analysis of a huge amount of user-generated data, which is available in social media and online mass media. In [11], the authors proposed a way to get the pre-labeled data from Twitter which can be used to train an SVM classifier. They used the Twitter hashtags to judge the polarity of the tweet. To analyze the accuracy of the proposed technique, a test study on the classifier was conducted which showed the result with the accuracy of 85%. Support Vector Machine (SVM) method resulted in a relatively higher accuracy compared to other machine learning methods but was greatly influenced by the number of data sets, training data, testing data and the number of positive data and the negative. In this study, it was explained that the use of the SVM method successfully classifies documents. This is indicated by the high level of accuracy of the method used. Similarly, Priyavrat's research concluded that the Support Vector Machine (SVM) method also has a better level of accuracy compared to other machine learning methods, namely Naive Bayes, Decision Tree and Neural Network [12]. Based on some of the studies that have already been conducted, in this sentiment analysis study, the classification method that will be used is SVM. This is because the SVM method proved to be more resilient to noisy data that is relatively high compared to other methods.

3. Proposed System

In this study, sentiment classification will be carried out with text mining processing. The construction of the sentiment model uses the machine learning method, Support Vector Machine (SVM). There are two additional processes that aim to improve the performance of the SVM algorithm. The first process is to select features with the information gain method. Feature selection is very important because the news text domain has several tens of thousands of features. The second process is boosting to deal with class imbalances. The classification of data with unbalanced class divisions can cause a significant decrease in performance. The method used in the second process is adaptive boosting. The best SVM model is not only tested through kernel selection but also involves feature selection and boosting. This aims to determine whether feature selection and boosting can improve the performance of models in sentiment classification.

3.1. Text Mining

Text mining is mining data in the form of text where data sources are usually obtained from documents. The purpose of text mining is to get useful information from a set of documents. The specific tasks of text mining include categorizing text and grouping text (text clustering). Based on the irregularity of the text data structure, the process of text mining requires several initial stages which in essence is to prepare so that the text can be changed to be more structured. Text mining can be considered as a two-stage process that begins with the application of structures to text data sources and continues with the extraction of relevant information and knowledge from structured text data using the same techniques and tools like data mining. Therefore, it is not surprising that text mining and data mining will be at the same architectural level. The stages of text mining are shown in Figure 1.

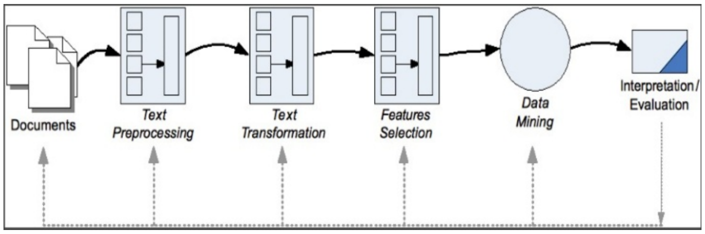

Figure 1: Text mining stages [13]

The stages are (1) Document collection (2) Preparation (3) Text Transformation (4) Feature Selection (5) Mining Data Process (6) Interpretation/Evaluation [13]. In the text transformation stage, several studies have applied a combination of TF and IDF combinations, namely multiplying local and global weights (TF-IDF) [14], [15]. The TF-IDF method combines two concepts, namely the frequency of occurrence of a word in a document and the inverse frequency of the document containing the word. The IDF formula is shown by equation 1, while the TF-IDF formula is indicated by Equation 2.

$$idf = \log\left(\frac{N}{df}\right) \tag{1}$$

$$w(t,d) = tf(t,d) * idf \tag{2}$$

where *tf (t, d)* is the appearance of the word *t* in document *d, N* is the number of documents in the collection of document, and *df* is the number of documents containing term *t*.

3.2. Feature Selection

In general, sentiment analysis becomes more difficult when the volume of text increases, due to the complex relationship between words and phrases. This is mostly because the text domain has several tens of thousands of features. Feature selection can make classification more effective by reducing the amount of data analyzed, as well as identifying features that are suitable for consideration in the process of making learning algorithms so that they can run in a faster and more efficient way.

Information gain is often superior to other feature selection methods [16]. Information gain measures how much information is present and the absence of a role word to make correct classification decisions in any class. Information gain is one filter approach that is successful in classifying text.

3.3. Support Vector Machine

Classification is the process of finding a model from a set of data [17], [18]. The purpose of classification is to make a decision by predicting a case based on the results of the classification obtained [19]. In the classification process, there are two processes carried out, namely the training process and the testing process. The classification method used is Support Vector Machine classification. The advantage of using SVM compared to other classification algorithms such as K-Means or Naive Bayes is that SVM finds decision boundaries that maximize the distance from the closest data points of all classes. SVM not only finds the limits of decisions but also finds the most optimal decision limits.

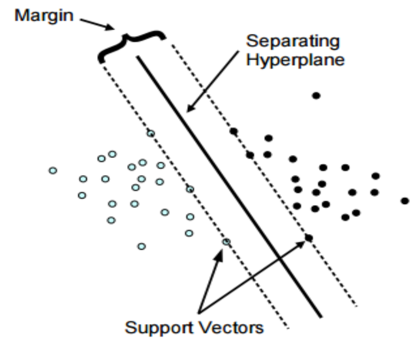

Figure 2: Illustration SVM[20]

In the illustration, there are several data points that touch the highest margin line. These data points are referred to as support vectors. The data used in the SVM method is denoted by $x_i \in R^d$ and the label is denoted by $y_i \in \{1,2\}$ to $i = 1,2,...,l$ where l is the amount of data.

There are several kernel functions [21] that will be tested in this study, they are:

(1) The function of Linear Kernel

The linear Kernel function is defined as:

$$k(x_i, x_i) = x_i^T x_i \tag{3}$$

(2) The function of the Polynomial Kernel

Polynomial Kernel functions with degrees of *d*, where *r* and *d* are parameters defined as follows:

$$k(x_i, x_j) = (\gamma x_i^T x_j + r)^a, \gamma > 0 \tag{4}$$

(3) Kernel Radial base Function (RBF) function

The function of the RBF Kernel is also called the Kernel-Gaussian function. The RBF Kernel function is defined as

$$k(x_i, x_j) = \exp(-\gamma \|x_i - x_j\|^2 \tag{5}$$

where γ is a positive parameter to set distance.

(4) The function of the Sigmoid Kernel

The function of the sigmoid kernel is defined as follows:

$$k(x_i, x_j) = \tanh(\gamma x_i, x_j + r) \tag{6}$$

where $\tanh(a) = 2\sigma(a) - 1$ and $\sigma(a) = \frac{1}{1+\exp(a)}$

3.4. Boosting Algorithm

Boosting algorithm is an iterative algorithm that gives different weights to the distribution of training data in each iteration. Each boosting iteration adds weight to examples of classification errors and decreases the weight in the correct classification example, so it can change the distribution of training data effectively [22]. The Boost algorithm (adaptive boosting) is an algorithm that builds strong classifiers by combining a number of simple (weak) classifiers. The first model was built according to the classification method used. Each instance in the training dataset is weighted and the weight is updated based on the accuracy of the entire model and whether an instance is correctly classified or not. Subsequent models are trained and added until minimum accuracy is reached or no further improvement is possible. Each model is given a weight based on its skills and this weight is used when combining predictions from all models in the new data.

3.5. Analysis Method

There are two analyzes used in analyzing sentiments results. The first is the accuracy of model analysis, and the second is an analysis of patterns of media trends based on news topics.

3.5.1. Evaluation method

The accuracy of the model analysis can be seen from the value of precision and recall resulting from the confusion matrix. The more precision and recall values are close to 100, it indicates the more accurate this model in analyzing news sentiments, and vice versa. To find out the strength of the model in overcoming imbalance data, Area Under Curve (AUC) measurements were carried out. If the AUC value closer to 1, indicates a good model performance in classifying data [23] and vice versa. This study will evaluate the performance of SVM model through the accuracy based on precision, recall and AUC by doing: 1) testing four SVM kernels namely linear, polynomial, RBF and sigmoid, 2) setting the number of features used in classification through the feature selection process and 3) adding the boosting process and vice versa into the construction of the model.

3.5.2. News Topic Analysis

Analysis of news topics will be shown by graphs compiled of word patterns in the news. The more words appear together in one document, the stronger the pattern of relationships will be. Based on the graph, media trends can be analyzed against two pairs East Java regional head candidates, namely Khofifah–Emil and Gus Ipul–Puti.

4. Result and Discussion

4.1. Data Presentation

The news data relating to the candidates for governor of East Java 2018 is taken from the period of January 1, 2018, to June 26, 2018. To obtain these data, carried out by accessing directly the data on news portals available online with national media samples, namely JPNN, Kompas, Detik and Republika. To find data relating to candidate governor with number one, Khofifah Indar Parawansa, the keyword "khalifah" was used. From the process of collecting data in the four national media, there were 998 data obtained.

Title	Content	Polarity	Tanggal	Resource
Kakek Detektif, Penebar	Akun Twitter @KakekDetektif menyita perhatian publik lan	NEGATIF	25/06/2018	detik.com
Ini Cagub Jatim yang Kuasai	Calon Gubernur Saifullah Yusuf dan Cawagub Puti Guntur Sc	NEGATIF	25/06/2018	detik.com
Debat Pilgub Jatim Terakhir	Sekjen DPP PDI Perjuangan (PDIP) Hasto Kristiyanto menga	NEGATIF	23/06/2018	detik.com
Hadiri Doa Bersama Guyub	Cagub Cawagub Jatim Khofifah Indar Parawansa-Emil Dard	POSITIF	26/06/2018	detik.com
Pilkada Rasa Pilpres, AHY: P	Partai Demokrat (PD) menargetkan perolehan suara melar	POSITIF	26/06/2018	detik.com

Figure 3: Sample data for Khofifah

To find data relating to candidate governor number two, Saifullah Yusuf, the keyword "gus ipul" was used. From the data collection process in the four national media, 1082 data were obtained.

Title	Content	Polarity	Tanggal	Resource
Debat Langsung Panas, Khofifah	Debat terakhir cagub Jatim berlangsung cukup seru. D	NEGATIF	23/06/2018	detik.com
Poltracking: Khofifah-Emil Unggu	Poltracking Indonesia melakukan survei elektabilitas p	NEGATIF	23/06/2018	detik.com
Survei RTK: Khofifah-Emil Unggul	Roda Tiga Konsultan merilis hasil survei terhadap elek	NEGATIF	22/06/2018	detik.com
Survei SMRC: Khofifah-Emil Ungg	Saiful Mujani Research and Consulting (SMRC) melaku	NEGATIF	22/06/2018	detik.com
Hadiri Doa Bersama Guyub Ruku	Cagub Cawagub Jatim Khofifah Indar Parawansa-Emil	POSITIF	26/06/2018	detik.com

Figure 4: Sample data for Saifullah Yusuf

4.2. Data Processing

The data obtained is labeled according to its tendency, whether it is positive sentiment or negative sentiment. Not all data was taken to construct the sentiment classification model. This is because the number of documents with positive sentiments is much greater than the number of documents provided with negative sentiments with a ratio of 52:1. Therefore document retrieval from positive sentiments is randomly around 30% of the positive sentiment document database with a ratio of 14:1 to the number of documents negative sentiment. Table 3 shows the ratio of the overall data and sample data to Khofifah and Gus Ipul database documents. It can be noted that all negative news population data are all sampled to build a classification model.

Table 1: Sentiment ratio of overall data and sample data

Database	Positive Population	Negative Population	Positive samples	Negative Samples
khofifah	949	49	344	49
gus ipul	1059	23	320	23

The next step is pre-processing text, at this stage carried out of cleansing, folding case, stopword removal. After that, the tokenization and weighting of the tokenization data were carried out to partition the documents in the form of sentences. This is done so that the words in the news document can be given weights for each word. The word weighting method used is TF-IDF which is a development of the TF method. After TF shooting, the weight of each word is also multiplied by the IDF or the number of occurrences of the word in the relevant document. The less often a word appears in a document, the greater IDF value generated.

After the word weighting is carried out, then the data is analyzed. To analyze data, two different scenarios were carried out, namely SVM without combination (pure SVM) and SVM method combined with the selection of information gain feature. The comparative process is carried out on the value of precision and recall generated when not using the feature selection method, and when using the feature selection method. Total features tested with feature selection in the system included 500, 1000, 2000 and 3000 features where the total features of Khofifah's data were 4764 features, and Gus Ipul's data were 4381 features

4.3. Implementation of Text Mining Algorithm

Comparison of SVM performance as an algorithm used in text mining with four different kernels namely linear, polynomial, RBF and sigmoid as shown in table 6. Based on the results of sentiment classification, it can be observed that in Khofifah's data, the best SVM model is in a linear kernel using feature selection with as many as 500 features The model also has the fastest execution time among other kernel models. Whereas in Gus Ipul's data, the best SVM model is in the RBF kernel that uses feature selection with 500 features. Even though it has good performance, the model has the slowest execution time among other kernel models. Even though in the polynomial kernel, feature selection does not affect SVM performance, both in Khofifah's data and Gus Ipul's data, the best performance is obtained when boosting and selection features with as many as 500 features. This shows that boosting and feature selection can improve the SVM method classification performance.

Table 2: Comparison of SVM performance with four different kernels

Can-didate	**Type of Boosting**	**Kernel**	**N attri-butes**	**Presisi**	***Recall***	**AUC**	**Time (s)**
Khofifah	with *boosting*	Linear	500	0,927	0,931	0,902	0,58
	with *boosting*	Polino-mial	4764	0,893	0,878	0,505	1,73
	with *boosting*	RBF	500	0,930	0,934	0,899	3,12
	with *boosting*	Sigmoid	500	500	0,863	0,885	1,65
Gus Ipul	with *boosting*	Linear	500	0,931	0,942	0,793	0,71
	-	Polino-mial	-	0,870	0,933	0,500	0,33
	with *boosting*	RBF	500	0,940	0,948	0,890	3,43
	with *boosting*	Sigmoid	3000	0,940	0,936	0,865	1,07

4.4. Evaluation of the Text Mining Model

Model evaluation was carried out by looking at the value of precision, recall, and AUC. The more value of precision, recall, and AUC is close to 1, the model is getting closer to the best performance. The best performance of the model in Khofifah's data achieved a precision value of 0.927, recall of 0.931 and AUC of 0.902 using SVM linear kernel. Whereas in Gus Ipul's data, the best performance of the model reached a precision value of 0.940, recall of 0.948 and AUC of 0.890 using the RBF kernel. Precision, recall and AUC scores above 0.8 in both the Khofifah and Gus Ipul data indicates that the SVM model that is enhanced by feature selection and boosting can work well in classifying news sentiment data. From collecting news documents to building SVM models, various problems were found that made this research work not optimally, such as data imbalance, inappropriate polarity sentiment reading, and document sentiment not reflected in all sentences.

4.5. Results of National media Trends

Relationships that exist in the data of two candidates for the regional head in the four major national media in Indonesia namely JPNN, Kompas, Detik and Republika are visualized in figure 5. The names of the pair Gus Ipul – Puti are more frequently mentioned that the names of the pair Khofifah – Emil. It means that Gus Ipul is more dominant in the four online media. In addition, the name "Sukarno" which is the grandfather of Puti is also often referred to. This is one of the things that can strengthen the electability of the pair Gus Ipul and Puti. In addition, the names "megawati" and "pdip" are also often referred to as the main supporters of the pair Gus Ipul and Puti. There is also the name "risma" which when called is almost always related to Gus Ipul and Puti. This shows that Risma was one of the leaders who supported Gus Ipul and Puti.

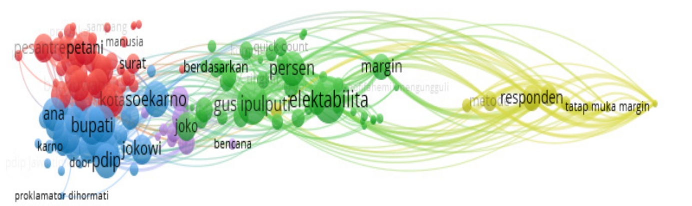

Figure 5: The results of the Khofifah-Gus Ipul data visualization on all four media

Even so, in the majority of the news in the four online media, it was said that according to the survey institute, the electability of the pair Khofifah and Emil Dardak was still superior to Gus Ipul and Puti. In addition, in some news also stated that Khofifah and Emil had a target to gain a lot of votes from undecided voters. This is also supported by the fact that the pair Khofifah and Emil are considered as representations across generations x and y because of Khofifah's experience and the youth spirit brought by Emil. This is certainly one of the hallmarks of Khofifah and Emil in gaining the voice of undecided voters, the majority of which are from the younger generation. It was also stated that the way Khofifah-Emil campaign directly touched the lowest layer of voters. This makes the relationship and political identification between Khofifah-Emil and voters direct.

4.6. Discussion

Based on the news gathered from four major national media in Indonesia, namely in JPNN, Kompas, Detik and Republika, the number of positive news sentiments of Gus Ipul is more than the number of positive sentiments of Khofifah with a ratio of 53 %: 47%. Negative news sentiment on Gus Ipul tends to be less than

Khofifah with a ratio of 32 %: 68%. From all the data obtained, it can be concluded that the number two governor candidate, Gus Ipul is superior to the national online media sentiment version rather than the number one candidate governor, Khofifah. This conclusion can be obtained based on the fact that: (1) candidate number two governor gets more attention from national media coverage with more evidence of data that mentions governor candidate number two, (2) percentage of news with positive sentiment towards Gus Ipul – Puti is more than Khofifah – Emil and the percentage of negative sentiment towards Gus Ipul – Puti is less than Khofifah – Emil.

5. Conclusion

Text mining method is a method that can be used to classify text documents, especially the classification of news document sentiments. To obtain an optimal architecture model and an accurate estimation, an experiment is performed. Model evaluation was carried out by looking at the value of precision, recall, and AUC. The best performance of the model in Khofifah's data reached a precision value of 0.927, recall of 0.931 and AUC of 0.902 using a linear kernel. Whereas in the Gus Ipul's data, the best performance of the model reached a precision value of 0.940, recall of 0.948 and AUC of 0.890 using the RBF kernel. The values of precision, recall, and AUC obtained in both Gus Ipul and Khofifah's data are above 0.8, which indicates that the model has a good performance in classifying news sentiments. Based on the data obtained and processed from the four media, both JPNN, Kompas, Detik and Republika, the media more often mentioned the pair Gus Ipul and Puti than the Khofifah-Emil pair.

Acknowledgment

Our gratitude goes to UIN Sunan Ampel Surabaya for giving a research grant in 2018.

References

[1] T. Peng, L. Zhang, and Z. Zhong, "Mapping the landscape of Internet Studies: Text mining of social science journal articles 2000–2009," 2013.
[2] M. M. Mostafa, "More than words: Social networks' text mining for consumer brand sentiments," *Expert Syst. Appl.*, vol. 40, no. 10, pp. 4241–4251, 2013.
[3] X. Bai, "Predicting consumer sentiments from online text," *Decis. Support Syst.*, vol. 50, no. 4, pp. 732–742, 2011.
[4] M. Eirinaki, S. Pisal, and J. Singh, "Journal of Computer and System Sciences Feature-based opinion mining and ranking," *J. Comput. Syst. Sci.*, vol. 78, no. 4, pp. 1175–1184, 2012.
[5] H. Savigny, "Public Opinion, Political Communication and the Internet," *Politics*, vol. 22, no. 1, pp. 1–8, 2002.
[6] A. R. T. Lestari, R. S. Perdana, and M. A. Fauzi, "Analisis Sentimen Tentang Opini Pilkada Dki 2017 Pada Dokumen Twitter Berbahasa Indonesia Menggunakan Näive Bayes dan Pembobotan Emoji," *J. Pengemb. Teknol. Inf. dan Ilmu Komput.*, vol. 1, no. 12, pp. 1718–1724, 2017.
[7] B. Liu, *Sentiment Sentiment Analysis Analysis and and Opinion Opinion Mining Mining*. 2012.
[8] P. Hoffmann, "Recognizing Contextual Polarity in Phrase-Level Sentiment Analysis."
[9] M. Cui, hang., Mittal, Vibhu., Datar, "Comparative Experiments on Sentiment Classification for Online Product Reviews," *J. Comput. Sccience*, pp. 1265–1270, 2006.
[10] K. Dave, S. Lawrence, and D. M. Pennock, "Mining the Peanut Gallery: Opinion Extraction and Semantic Classification of Product Reviews," *Proc. 12th Int. Conf. World Wide Web (WWW '03)*, pp. 519–528, 2003.
[11] W. A. Zgheib and A. M. Barbar, "A Study using Support Vector Machines to Classify the Sentiments of Tweets."
[12] A. J. Singh, "Sentiment Analysis : A Comparative Study of Supervised Machine Learning Algorithms Using Rapid miner," vol. 5, no. Xi, pp. 80–89, 2017.
[13] B. Susanto, *Text Mining*. Surabaya: Graha Ilmu, 2015.
[14] R. Intan, A. Defeng, J. T. Informatika, F. T. Industri, U. Kristen, and P. Surabaya, "Hard : Subject-Based Search Engine Menggunakan Tf-Idf Dan Jaccard ' S Coefficient," pp. 61–72.
[15] A. F. Hidayatullah *et al.*, "Analisis sentimen dan klasifikasi kategori terhadap tokoh publik pada twitter," vol. 2014, no. semnasIF, pp. 115–122, 2014.
[16] A. K. Uysal, "An improved Global feature Selection Schene for Text Classification.," *Expert Syst. With Appl*, vol. 43, pp. 82–92, 2016.
[17] Suyanto, *Data mining Untuk Klasifikasi dan Klasterisasi Data*. Bandung: Informatika, 2017.
[18] D. K. S. Putra, *Media dan Politik*. Surabya: Graha Ilmu, 2012.
[19] R. Primartha, *Belajar Machine Learning Teori dan Praktik*. Bandung: Informatika, 2018.
[20] Muthu krishnan, "Understanding Support vector Machines using Python," 2018.
[21] C. Hsu and C. Lin, "A Comparison of Methods for Multiclass Support Vector Machines," vol. 13, no. 2, pp. 415–425, 2002.
[22] P. Harrington, *Machine Learning in Action*. New York: Manning Publication Co, 2012.
[23] F. Shabani, L. Kumar, and M. Ahmadi, "Assessing Accuracy Methods of Species Distribution Models: AUC, Specificity, Sensitivity and the True Skill Statistic," *Glob. J. Hum. Soc. Sci.*, vol. 18, no. 1, 2018.

Advances in Science, Technology and Engineering Systems Journal Vol. 4, No. 2, 140-152 (2019)

www.astesj.com

Special Issue on Advancement in Engineering and Computer Science

ASTESJ

ISSN: 2415-6698

Educational Domain Management Knowledge Content Identification and Knowledge Updating Method, Based on Enterprise Management Information Interactions

Jurij Tekutov[*, 1, 2, 4], Saulius Gudas[3], Vitalijus Denisovas[2, 4], Julija Smirnova[1]

[1]*Klaipeda State University of Applied Sciences, Faculty of Technology, Information Technologies Department, Bijunu St. 10, LT-91223 Klaipeda, Lithuania*

[2]*Klaipeda University, Faculty of Marine Technologies and Natural Sciences, Informatics and Statistics Department, Bijunu St. 17, LT-91225 Klaipeda, Lithuania*

[3]*Vilnius University, Faculty of Mathematics and Informatics, Institute of Data Science and Digital Technologies, LT-04812 Vilnius, Lithuania*

[4]*Lithuania Business University of Applied Sciences, Informatics Department, Turgaus St. 21, LT-91249 Klaipeda, Lithuania*

ARTICLE INFO

Article history:
Received: 29 December, 2018
Accepted: 04 March, 2019
Online: 20 March, 2019

Keywords:
The Detailed Value Chain Model
The Elementary Management Cycle
Educational domain knowledge content

ABSTRACT

The aim of this paper is to develop the educational domain management knowledge content identification and knowledge updating method, based on formal descriptions of enterprise management information interactions. This is very important because the progress of modern science leads to the emergence of new factual or conceptual knowledge. There is a need for proper methods that allow, first, to study and make decisions regarding the relevance of the content, and then take practical steps on the content and possibly of the corresponding structure adaptation. The authors suggest a systematic solution for this problem. The hierarchical Detailed Value Chain Model and Elementary Management Cycle model of educational domain knowledge content identification and updating is formally described, computerized process measures are proposed. The paper provides a method for updating the knowledge of the analyzed domain, referred to as "enterprise domain", based on enterprise modelling in terms of management information interactions. A method, whose formal DVCM and EMC descriptions are provided in BPMN notation, was designed, allowing to develop a two-level (granular) model for describing knowledge of educational domain management information interactions. In implementing this model and its algorithms in technological terms, a subsystem of enterprise knowledge has been created in a knowledge-based CASE system (computerized knowledge-based IS engineering), performing the function of a domain knowledge database.

1. Introduction

This paper is an extension of work originally presented in 2018 2nd International Symposium on Multidisciplinary Studies and Innovative Technologies (ISMSIT) [1].

Meeting modern, constantly evolving educational enterprise needs requires enterprise integration with information technologies and computerized information systems (IS) that would be able to adapt to organizations' enterprise changes. In the context of this paper enterprise is understood as a educational institution.

Among different IS development approaches one of the most promising is model-driven approach, which aims to utilize formal domain knowledge to perform, adjust and manage and engineering process. One of the earliest stages of IS development life-cycle is enterprise modelling, which becomes especially important in applying model-driven IS development methodology (MDE – Model Driven Engineering) and its methods [2]. The aim of enterprise modelling is to create an enterprise model of an

[*]Jurij Tekutov, Email: jurij.tekutov@yahoo.com

organization, which would help to deal with issues of an analysed domain. The concept of Model Driven Architecture (MDA) defines IS development process as a three-level model (CIM – the Computation Independent Model, PIM – the Platform Independent Model, PSM – the Platform Specific Model) interaction, whose purpose is to directly link enterprise modelling and further stages of IS analysis, design and implementation. Thus, from enterprise modelling professionals' point of view MDA concept [3, 4] should be thought of as an effort to integrate enterprise modelling methods with full life-cycle Computer-Aided Systems Engineering (CASE) technologies characterized by the bottom-up approach, i.e. from engineering methods to enterprise modelling methods for IS engineering needs. Hence, modern IS development methodologies pay increasingly more attention not only (and not as much) to software and IS engineering methods, but rather organizations' enterprise modelling issues, i.e. domain knowledge mapping.

IS engineering methods (IS life-cycle stage models) based on intra-enterprise engineering, the basis of which is subject area (domain) pattern model, are called knowledge-based methods [5]. The purpose of MDE-based computerized IS engineering enterprise model is to systematize and formalize knowledge on a certain analysed domain (subject area). IS engineering methods are emerging that seek to integrate knowledge about operational functions, processes, rules in CASE systems and use them in intellectualizing IS development process. There have also been attempts to apply domain knowledge content creation and updating methods [6] from similar areas, such as e-learning, Business Intelligence systems [7, 8], business rule modelling [9].

The analysis of IS engineering stages (1. traditional IS engineering, 2. computerised software engineering, 3. computerised IS engineering (including enterprise modelling), 4. knowledge-based IS engineering) reveals the key features of the variations in the IS engineering process (methods, knowledge sources, software types). Hence, it enables to define the key characteristics of the knowledge-based IS engineering methodology and the composition of the basic components. In traditional computerized IS engineering a system is created empirically, by first collecting, analysing and specifying consumer needs. Works linked to knowledge-based IS development allow to take software development to a higher level of abstraction, partly automate these processes and use the models in other systems. Business activity modelling, the improvement of knowledge formalization and the application of the conceptual modelling in developing the IS are the key things for the further development of the IS engineering methods. In knowledge-based computerized IS engineering a system is created using an enterprise knowledge base and domain knowledge stored in it. It is believed that the main characteristic of knowledge-based IS engineering is a subsystem of domain knowledge, which is based on an organization's enterprise model and is designed to acquire knowledge on a computerized domain. Such knowledge acquisition subsystem should perform the functions of a storage of domain knowledge, required for the creation of IS project models. The following structure for a subsystem was proposed: enterprise model and enterprise metamodel (formalized enterprise management knowledge structure).

Domain knowledge acquisition subsystem should become the essential component of a knowledge-based CASE measure, intellectualizing the whole process of IS development. The creation of such subsystem is one of the most urgent scientific problems addressed in this paper. The development of knowledge-based IS engineering methods requires an internal approach to business process modelling, which should be based on the internal business process logic – the causal links between business processes, i.e. necessary and sufficient components of activity elements and interactions between them (the activity goals of material processes, information processes and structural information units). Therefore, the above-mentioned diagram shows the managerial information exchange (in proposed modified Value Chain Model).

In our previous works it was proposed that the development of these systems should be performed by focusing on Value Chain Model (VCM) [10], since computerization involves enterprise management functions and processes, as well as interactions between organization's functional areas, which are revealed by the VCM. In computerizing enterprise, a research of informational interactions between enterprise management functions and processes is performed, requiring further decomposition of value chain elements, i.e. further VCM modification is performed [11], a Detailed Value Chain Model (DVCM) is created. Hence, knowledge-based IS development is based on knowledge on enterprise management, which defines fundamental attributes of enterprise management information interactions. In previous work [12] was shown the enterprise management information interaction is specified as an Elementary Management Cycle (EMC), linking enterprise management function and process by a feedback loop. The novelty of the work is the application of the expanded VCM and the EMC to manage operational knowledge; after defining the assessment criteria, such management model allows to objectively assess and constantly improve the knowledge content of the subject area.

This paper elaborates a proposed domain management knowledge modelling method, which is based on formal DVCM and EMC descriptions presented in a BPMN notation. Educational domain has been chosen intentionally, on the basis of methodological terms. In academic field IS development typically starts with enterprise management function analysis, in which enterprise management information interactions are important. The analysed higher education study domain is multivariate, dynamic and requires constant knowledge content updating. Only by actualizing study programme structure and knowledge content in a timely manner is it possible to properly take into account changing needs and requirements from all stakeholders.

This paper is devoted to the actual topic of modern university management. Improving the quality of higher education and the corresponding management approaches are very important. The authors propose to apply the proven methods of enterprise management. This is a very promising decision, because, firstly, such business-oriented models have proven their effectiveness, and then such models are focused on practical solutions.

Previous works. One of the pioneers of analysing study programme development as an IS engineering process were MOCURIS – Modern Curriculum Development in Information Systems at Master Level project promoters, who offered in their works a model study programme design method [13]. They have introduced the notion of study programme engineering, defined study programme architecture and by analyzing a study programme as a system of courses and modules, they have applied the standard IS engineering process to develop a Master‘s study programme. Using this method, a large IS-related Master's programme specification document was created, which would act as a guideline for developers of certain programmes, courses and modules. However, already in the project fundamental flaws of this method became evident. Such programme development process could only be effectively implemented by the authors, meanwhile, the resultant artefact (textual specifications document) because of its technicality, complexity and size was unsuitable to perform the main function of requirement specification which is to ensure communication of all process participants and coordinate their work. After analysing requirement identification, localization and specification (granularity) issues, it was found that these limitations are inherent in traditional non-automated requirement engineering processes. Therefore, other researchers (including the authors of this paper) have suggested to automate this process by creating a study programme requirement engineering system on the basis of CASE measures [14]. With a direct involvement of the authors, such a system has been created and applied for the development of new study programmes [15, 16]. However, in a fast changing environment timely study programme modernization, quality assurance and knowledge content updating become especially relevant. It all requires effective feedback from all stakeholders. To solve the issues mentioned in this paper, a DVCM has been used, ensuring constant information feedback, which sends descriptive data (attributes) to the enterprise management function and retrieves management decisions to direct enterprise process. The method is implemented by creating an enterprise knowledge database in IS engineering CASE system, which is designed on the basis of a computerized educational domain enterprise model.

The creation of knowledge content specification includes the collection of domain knowledge, its preparation and analysis, verification and validation. In this paper domain knowledge is understood as a dynamic set of knowledge attributes, described according to requirements as a system of facts, principles and theories related to a specific professional activity. In other words, knowledge attribute set is an expression of a domain in current context. Enterprise modelling can be assigned to requirement collection and analysis stage. Then enterprise models are transformed into requirement specification for the system being

Figure 1. Concept map of enterprise modelling techniques (languages, notations) (using *Mindjet MindManager Pro*^{TM} tool)

developed. Systems (for example, domain knowledge content) and separate component specifications are produced during IS engineering process. The most important step in every effective domain knowledge management process is the writing down of the requirements identified during the selection. It helps to ensure accurate communication and management of the requirements during their development. Documents are an understandable form for requirement recording. These documents provide a basis for context identification and requirement collection, yet are not very useful in supplementing and modifying requirement information.

The main aim of this paper is to develop the educational domain management knowledge content identification and knowledge updating method, based on formal descriptions of enterprise management information interactions.

The remainder of the paper is structured as follows: Section 2 reviews domain modelling methods in terms of knowledge content modelling. Section 3 introduces the created educational domain management knowledge modelling method, based on enterprise management information interactions. The application of a Detailed Value Chain and Elementary Management Cycle model for knowledge content description and updating is demonstrated. The created educational domain management knowledge content identification and knowledge updating computerized process model are laid out in Section 4.

2. The Analysis of Current Domain Modelling Methods in Terms of Knowledge Content Modelling

Due to the fact that many new enterprise modelling approaches, methodologies and methods were recently created, a separate research area has occurred, called enterprise modelling.

Therefore, there is a need to systematize the variety of these methods in order to select the most convenient way of modelling management activities. To facilitate this selection a concept map of different enterprise modelling techniques (languages, notations) [17-23] was designed (Figure 1).

Enterprise models are divided into the following categories: business process models, data flow models, data models, business objective models, control flow models, management process models, knowledge management processes [24]. Widely known enterprise modelling methods are structural-functional modelling (Data Flow Diagrams or DFD), business process modelling languages, BPMN (Business Process Modeling) notation, IDEF (Integration of computer aided manufacturing DEFinition) set of standards and enterprise modelling language UEML (Unified Enterprise Modelling Language), and business architecture modelling language UPDM (The Unified Profile for DoDAF/MODAF). Well known enterprise modelling methodologies and standards are CIMOSA, GERA, EPC, DoDAF, MODAF, MDA [23]. However, amongst them one can rarely find those that would model enterprise in terms of management, i.e. performance management information components and their interactions.

When comparing modern enterprise modelling methods (languages, notations), it is becoming clearer that enterprise modelling needs to have capable methodologies because it has to be ensured that all necessary structures can be modelled. For this purpose, the above mentioned concept map can be used, that shows primary and systematized information and provides references to all other required sources of domain modelling methodologies. When analysing known enterprise modelling methods (notations, languages) in terms of domain management, it is becoming clearer that only a few methods can actually evaluate management information interactions that are necessary to manage domain from a theoretical perspective.

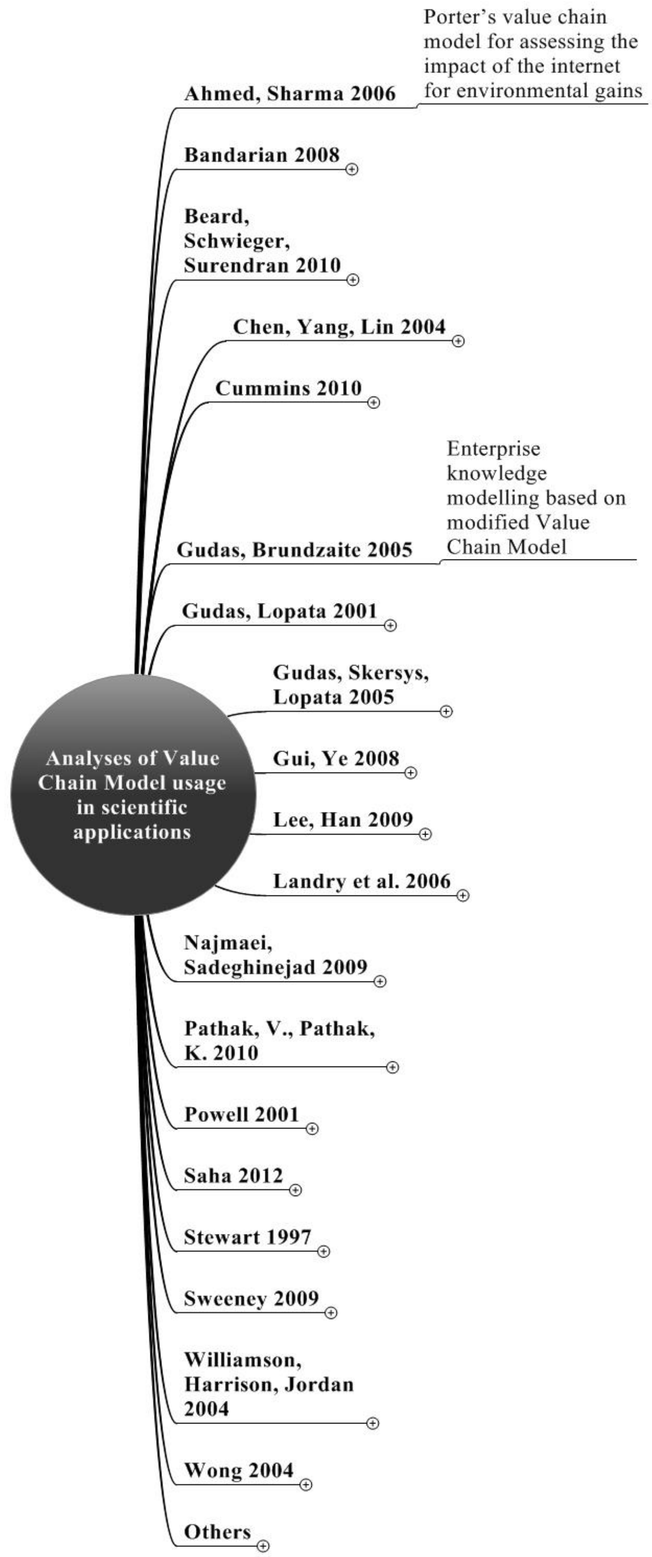

Figure 2. Conceptual map of Value Chain Model in scientific applications

In organizational management practice Value Chain Model (herein referred to as VCM), created by Porter, is popular and has been used in many works (Figure 2) [26-42].

The concept map (Fig. 2) illustrates examples of the application of VCM in scientific research (other examples of the analysis can be accessed by clicking on the plus sign in the concept map in Mindjet MindManager[TM] environment): Porter's value chain model for assessing the impact of the internet for environmental gains [26]; Enterprise knowledge modelling based on modified Value Chain Model [40]; others.

The structured DVCM is used to identify the information transactions between Management Functions and Enterprise Processes. Detailed Value Chain Model (DVCM) embodies a procedural approach to enterprise consisting of: primary activities (operational processes) and support activities (operational functions). The formal description of DVCM is as follows:

$$DVCM = \{(Fi)x(Pj)\} \tag{1}$$

Where: (F1,…, Fi,…., Fn) – a set of Enterprise Management Functions, (P1,…, Pj,…., Pm) – a set of Enterprise Processes, x – relationship between a set of Management Functions {F} and a set of Enterprise Processes {P} (management information transactions $(Fi \times Pj)$.

The interrelationship between primary and secondary business processes explored in Gudas, Lopata [43] identified a different nature of these 2 enterprise activities: secondary processes possess informational nature and are referred to as enterprise (management) Functions; while primary processes are concrete (non-informational) and are named enterprise (material) Processes. This paper presents more detailed content of Function Fi since it defines a sequence of definite types of interacting information activities directed to control Process Pj.

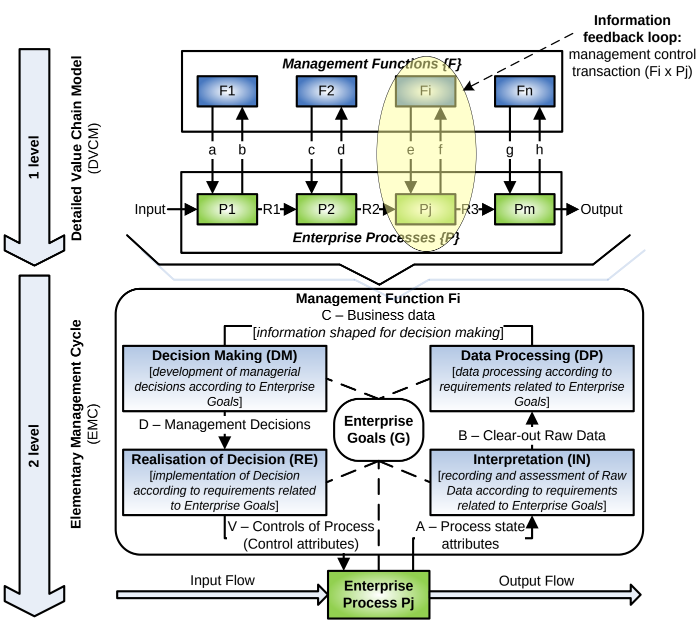

Figure 3. The formalized model of the interaction between the Function Fi and Process Pj (Elementary Management Cycle – EMC) in modified (structured) DVCM

In brief, the concept of EMC is a formalized description of the Enterprise management control as the interaction between the Function and the Process – as two core components of enterprise from the control point of view. On the basis of these findings, the Value Chain Model is modified. The decomposition of the information interactions $(Fi \times Pj)$ in the DVCM between the Management Function Fi and Enterprise Process Pj is defined as Elementary Management Cycle (EMC) on the lower level in Figure 3. The interaction between the core elements a Function and a Process is formally assumed as a Control Process with the Feedback Loop between the Function Fi and the Process Pj. The two levels of granularity: 1) the Detailed VCM (DVCM) and 2) the Elementary Management Cycle (EMC).

A detailed model of the informational interactions between the Function Fi and Process Pj can be defined by:

$$EMC(Fi, Pj) = \begin{pmatrix} Pj(A,G) \rightarrow IN(A,B,G) \rightarrow P(B,C,G) \rightarrow \\ M(C,D,G) \rightarrow RE(D,V,G) \rightarrow Pj(V,G) \end{pmatrix} \tag{2}$$

Where A – state attributes of the process Pj, needed in terms of G; B – systemized (interpreted) primary data, needed for the enterprise management function Fi in terms of G; C – enterprise data, formed by data processing DP, prepared for decision making DM and needed in terms of G; D – goal-congruent management decision formed by the decision making process DM; V – goal-congruent effects of management on the process Pj, formed by the realization process RE.

The expanded DVCM and EMC was printed in the general format [15, 16]. As proposed in works [44, 45], the Elementary Management Cycle (EMC) is the basic construct of Enterprise Management modelling, it refines the components of management (control) cycle as well as content of management information transformations. The mandatory steps (Interpretation – IN, Data Processing – DP, Decision Making – DM, Realisation of Decision – RE) of the EMC are defined as information transferring processes focused on the control of the content of the Management Functions Fi. The Management Function Fi consists of a sequence of definite types of goal-driven information transformation activities (steps of EMC) aimed to control a state of an Enterprise Process Pj. For example, in the structure of an EMC: Pj (A, G), Pj (V, G) – Technological Process (managed object), its input (I) and output (O) are Material Flows. Material Flows are defined by state attributes of a specific Process Pj, which are necessary to perform a specific enterprise management Function Fi in combination with enterprise Goals (G).

Based on this general model, the authors have proposed a specialised model for particular problem domain.

3. Educational Domain Management Knowledge Modelling Method, Based on Enterprise Management Information Interactions

Educational domain management knowledge modelling method, based on enterprise management information interactions, was created in order to identify the discrepancy between the existing knowledge model and the actual domain knowledge model. The resulting method is designed to create a two-level (granular) knowledge description model for the analyzed educational domain management information interactions, to form current knowledge and domain knowledge models and to perform the analysis of knowledge models. The computerisation of the organisational activities involves an examination of the information interactions between the management functions and the business processes, which requires the decomposition of the value chain elements, i.e. the VCM is modified and a Detailed Value Chain Model (DVCM) is created. Thus, the knowledge-based IS development is performed based on that business management knowledge which defines the key features of business management information interactions. A business management information interaction is specified as an Elementary Management Cycle (EMC), which links the business management function and the business process through a feedback circuit. A two-level subject area management knowledge model was selected. The two levels of knowledge description are:

1. First level of detail – DVCM that identifies information interactions.

2. Second level of detail – a detailed model of each management information interaction by applying EMC.

Such model is believed to be sufficient in all cases of activity knowledge modelling. The decomposition of the organisational system business management functions and the business processes can be continued up to the required level of detail of the business management function.

Paper comprise known approaches to create educational domain content knowledge models updated existing. Model is created on to levels that combines DVCM and EMC model presenting the transformation of the existing and the domain knowledge models on the basis of management information interactions", BPMN notation (Figure 4).

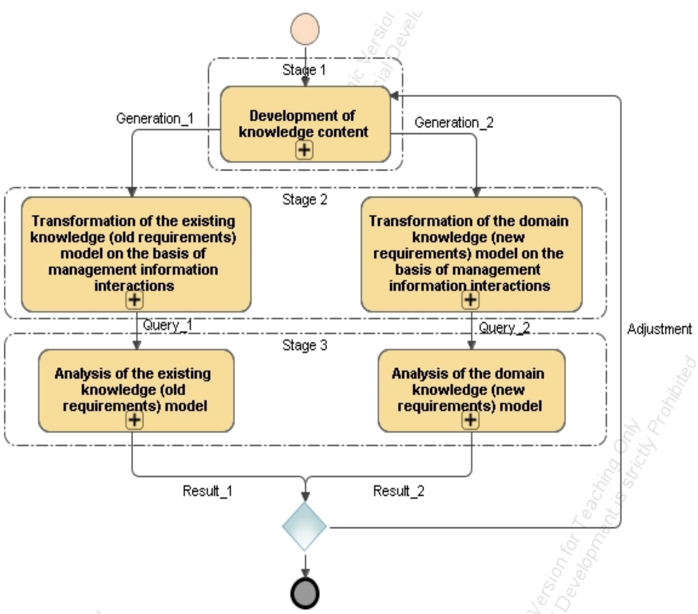

Figure 4. A principal scheme of educational domain management knowledge modelling method (BPMN notation)

Development of knowledge content (Figure 5) involves structural, functional, quality and other requirements.

The method is elaborated in a specific domain – higher education study programme design and updating. In terms of the current domain (for example, programme structure), the smallest structural component is a study module. Module composition is described in terms of attributes. To establish a system hierarchy, modules are combined into study blocks (subject groups). Main blocks are defined in the general requirements for study programmes (component_1 in Fig. 5). Functional (study content) requirements are defined by the purpose, stage and objectives of a study programme that are defined in regulatory documents and derived from other requirement sources (component_2 in Fig. 5).

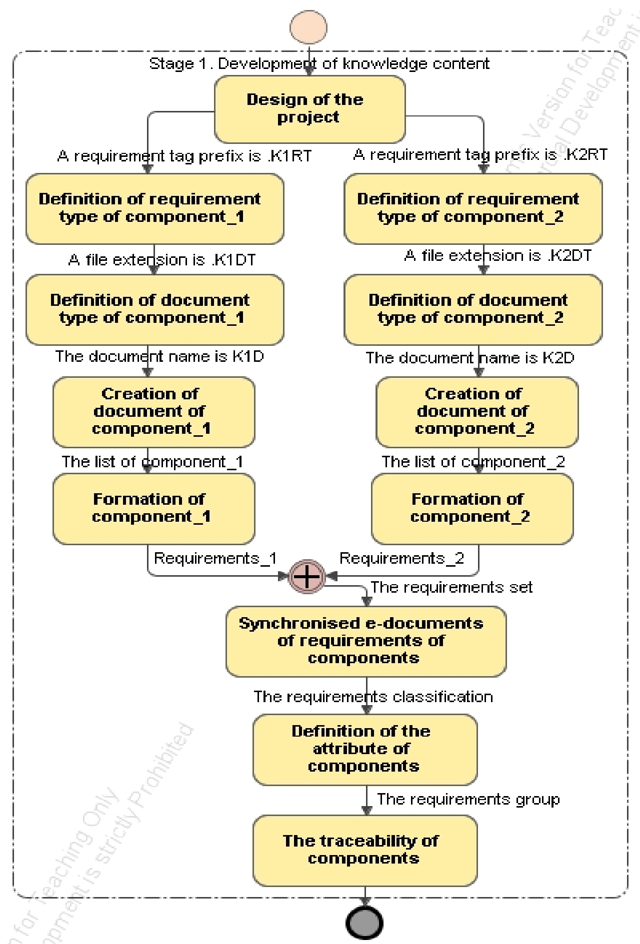

Figure 5. Part of the method (Stage 1 "Development of knowledge content", BPMN notation, using *MagicDraw*™ tool)

Designing a knowledge base on the basis of DVCM and EMC. Management knowledge model based on DVCM and EMC is created in two stages (Figure 6):

1. On the basis of the Detailed Value Chain Model (DVCM) identifying management Functions and their information resources.

2. Each intersection between management Function and Process is modelled in detail as the managed process by creating their Elementary Management Cycle (EMC) models.

1st stage of designing a management knowledge model and a knowledge base. Designing a knowledge base on the basis of the Detailed Value Chain Model (DVCM) requires to evaluate not only DVCM structure, but also all the informational attributes (data) of interactions between management Functions and Processes:

1. Analyze the general case of the Detailed Value Chain Model (DVCM) which is the formalized DVCM structure.

2. Verify that management Function hierarchy exists.

3. Verify that Process hierarchy exists.

4. Verify that data (information attributes) related to each intersection between a management Function and a Process exists.

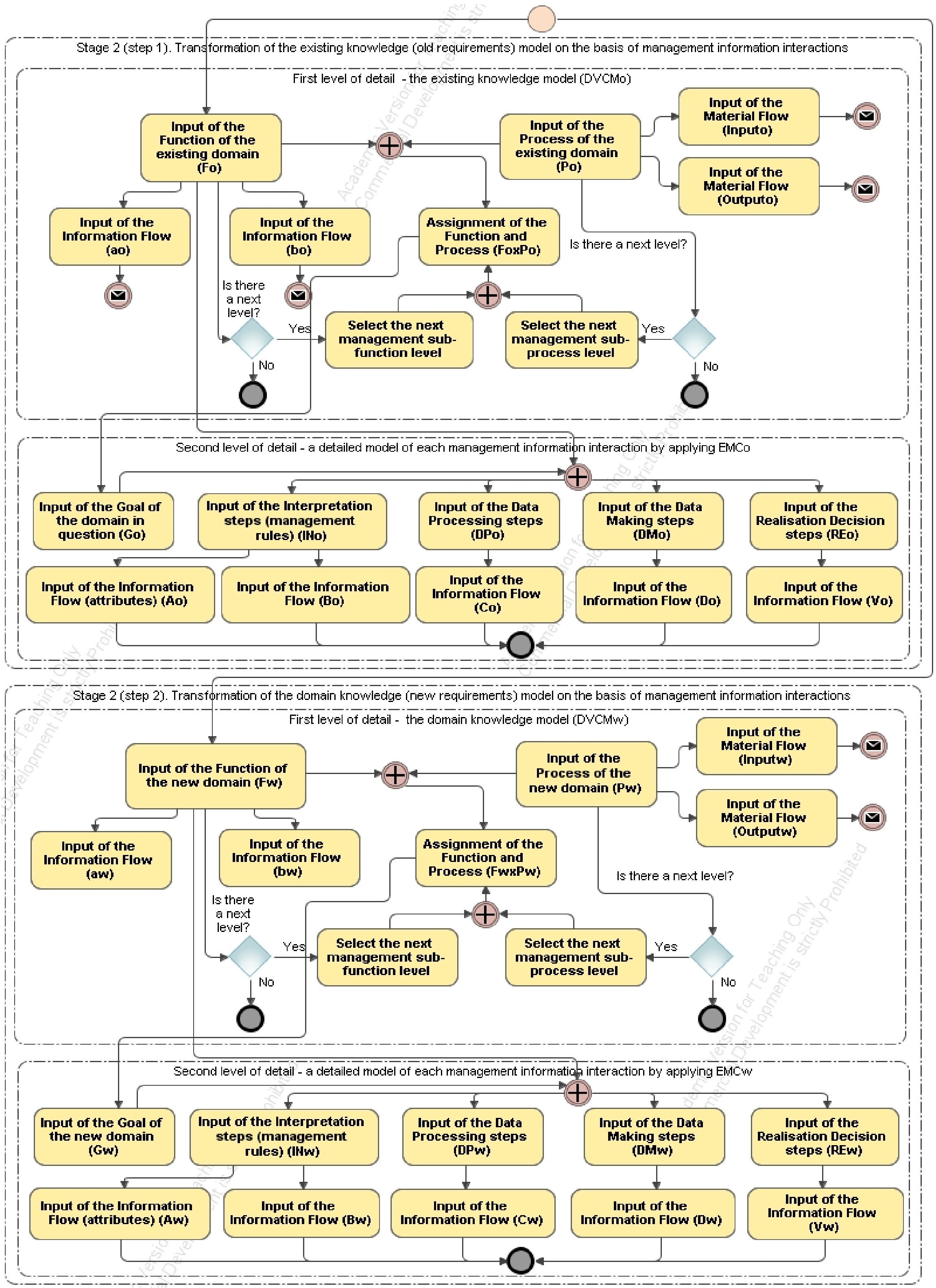

Figure 6. Part of the method (Stage 2 "Transformation of the existing and the domain knowledge models on the basis of management information interactions", BPMN notation)

2nd stage of designing a management knowledge model and a knowledge base. The resulting management knowledge model does not assess the internal structure (informational transformations performed by the enterprise management Function itself) of management Functions, i.e. information interactions between the structural parts (components) of a management Function. Next, the internal structure of each management Function is modelled on the basis of Elementary Management Cycle (EMC) description:

1. Select a specific management Function and Process pair (intersection) identified with DVCM, that will further be modelled as a managed process (formally described EMC).

2. Create an Elementary Management Cycle (EMC) model of the selected management Function and Process intersection by identifying (naming) all EMC components: IN, DA, SP and RE processes, related goals G, information flows between EMC components.

3. Illustrate DVCM and EMC through domain entity class model.

4. Develop a prototype of a knowledge base.

When requirements documents are created and linked together while the requirements themselves are kept in the Knowledge Base (KB), an opportunity appears to automate requirements analysis by using computerized systems (Figure 7). Within the selected CASE tool (IBM Rational RequisitePro^{TM}) special visual environments (so called views) for knowledge analysis are selected. It is possible to review knowledge (requirements) presented in different views in parallel by using various matrices or hierarchical structures (trees) where requirements with their attributes and/or traceability links between different requirement types are represented. For example, one of the problems of requirement analysis is the determination of requirements attributes.

When applying the visual environment of Attribute Matrix, it is possible to comfortably revise all the requirements of a particular type and attributes related to them. When analyzing a current domain (for example, study programme), the following actions with the matrix are performed: the establishment and editing of a requirement title, text, attributes and traceability links; the saving of matrix query; matrix printing. Filtering and sorting functions can also be applied to analyze requirements, thus maximizing the informational value of each requirement. By choosing one or several attributes and/or traceability signs (indicators), it is possible to perform requirement filtering and sorting, therefore, selecting the necessary requirements or forming new categories of them. In particular, it is used to design the architecture of a study programme and it's structural components (study blocks and modules).

Modification of a structured Value Chain Model to identify educational domain knowledge content. To reflect these needs the authors have proposed a new problem domain life cycle model, which is based on modified VCM. This specialised model is presented in Figure 8.

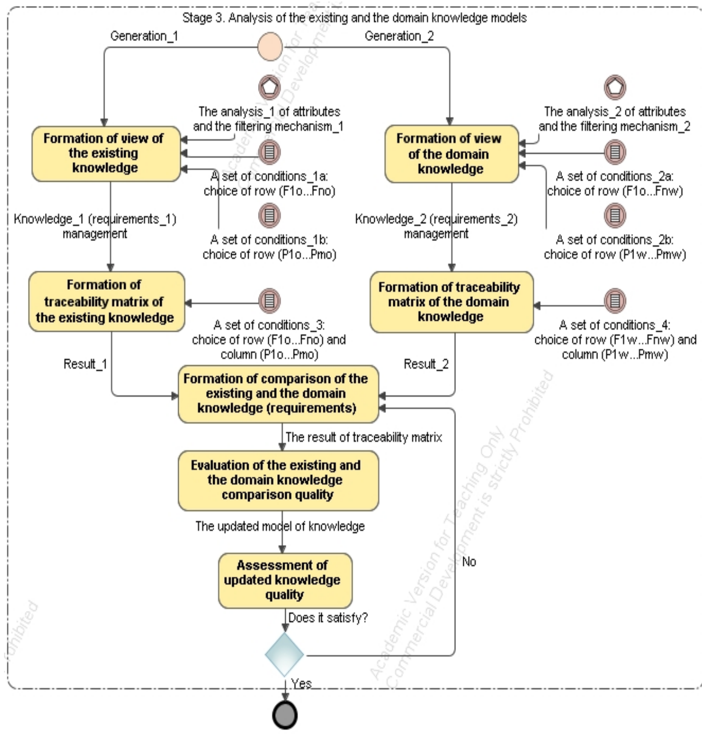

Figure 7. Part of the method (Stage 3 "Analysis of the existing and the domain knowledge models", BPMN notation)

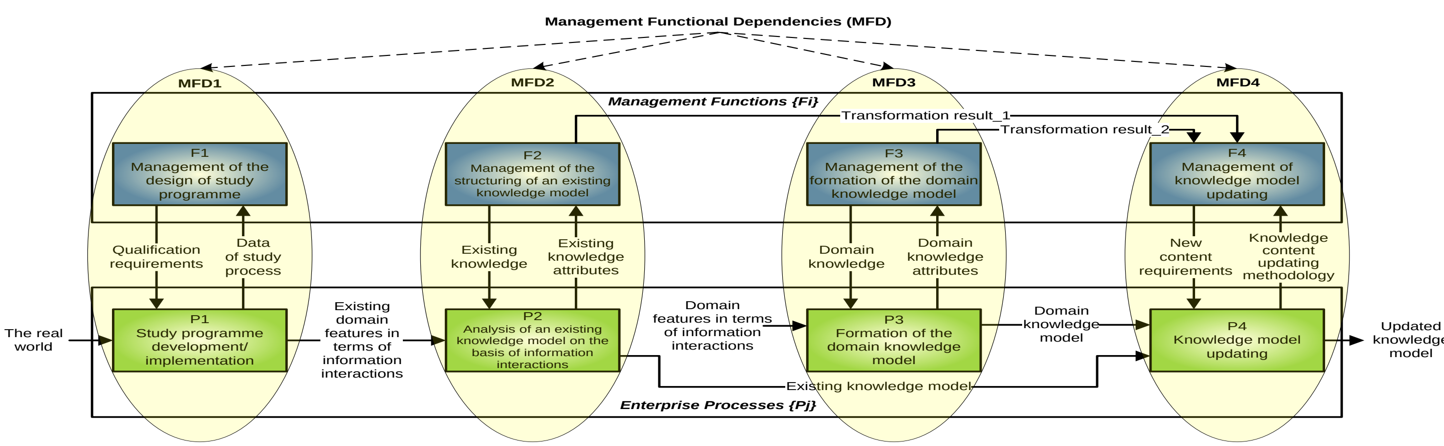

Figure 8. Informational model of educational domain knowledge content identification process

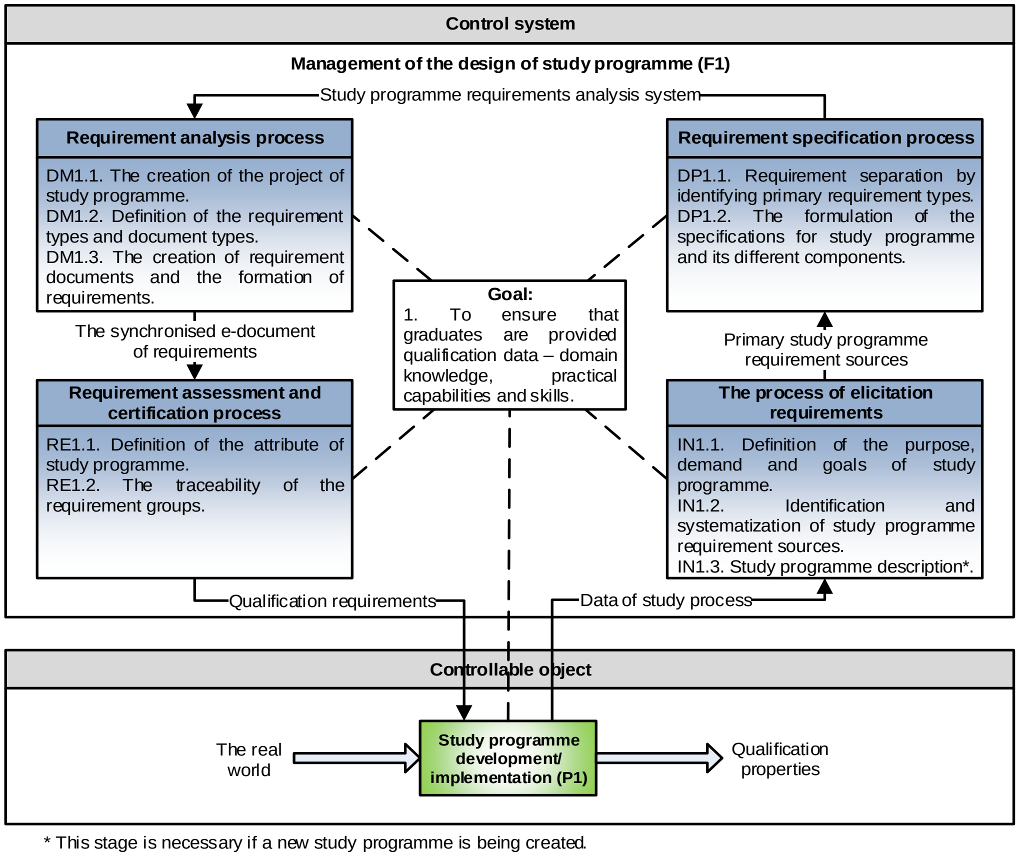

Figure 9. The Formalised Model of the Interaction between the *Function F1 = "Management of the design of study programme"* and the *Process P1 = "Study programme development/ implementation"*

Each interaction between management Function Fi and Process Pj $(Fi \times Pj)$ identified with DVCM is seen as a managed process that implements a specific Management Functional Dependence (MFD).

For example, the formalised model of the interaction between the Function F1 = "Management of the design of study programme" and the Process P1 = "Study programme development/ implementation" (see Fig. 8) is presented in Figure 9.

It is important to mention that any specific EMC does not end, it continues with each new domain process cycle. Thus, the current domain is developed based upon the spiral principle with the renewal of the quality in general. In particular, the steps (rules) and the attributes (data) of the transformation of current domain management information were identified.

4. Educational Domain Management Knowledge Content Identification and Knowledge Updating Computerized Process Model

This section provides a principal scheme of knowledge content identification and educational domain knowledge updating model, on the basis of which a knowledge-based specification is performed. A particular enterprise Management Functional Dependency is the aggregate of the necessary information interactions among specific enterprise management Function components, specified by a particular Elementary Management Cycle.

Construction of a principal scheme of knowledge content identification and domain knowledge updating model. A principal knowledge content identification and domain knowledge updating model scheme is provided in Figure 10.

When analysing the principal knowledge model scheme, it can be stated that management Function model, in this case, becomes a scenario that defines mandatory information interactions, necessary to computerize all tasks that constitute management Function.

The identification of the existing (old) knowledge which are documented before and the new subject area knowledge related with problem domain is presented in two upper DVCM in Figure 11.

Mapping and comparison of the old and the new knowledge allow to construct a modified DVCM producing a set of updated knowledge.

A technique of knowledge analysis is used for comparison between $DVCM^{o}$ and $DVCM^{w}$. Comparison of these two (($DVCM^{o}$ and $DVCM^{w}$) domain models allow to identify the changes of problem domain content (i.e. identify the actual changes of knowledge about domain) and to construct a derivative new Detailed VCM ($DVCM^{N}$) encompassing all actual domain knowledge components. Afterwards the $DVCM^{N}$ is used for identification of new knowledge requirements. Traceability Matrix shows the relation of two knowledge sets (Figure 12).

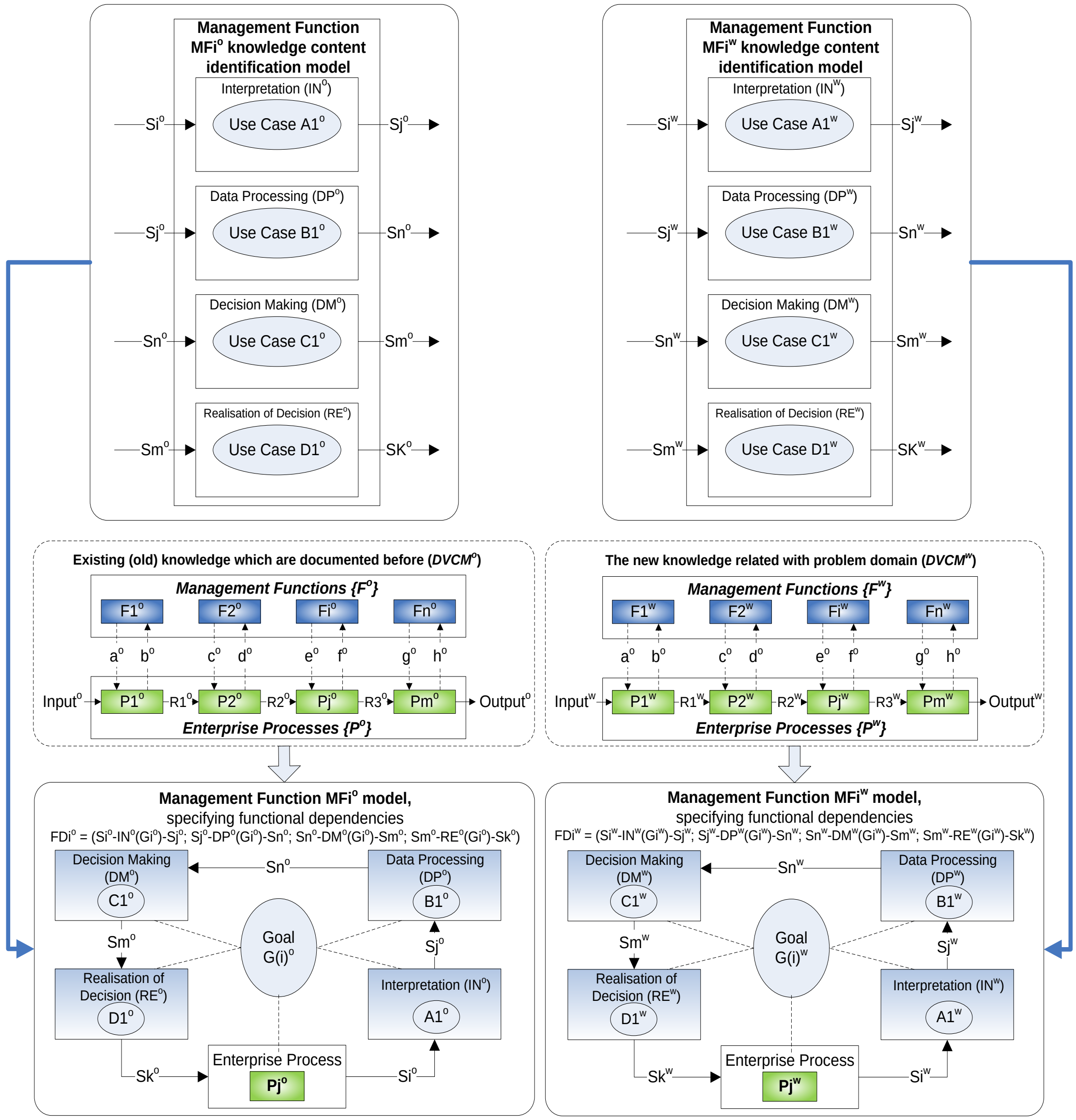

Figure 10. A principal scheme of knowledge content identification and domain knowledge updating model (based on enterprise management function)

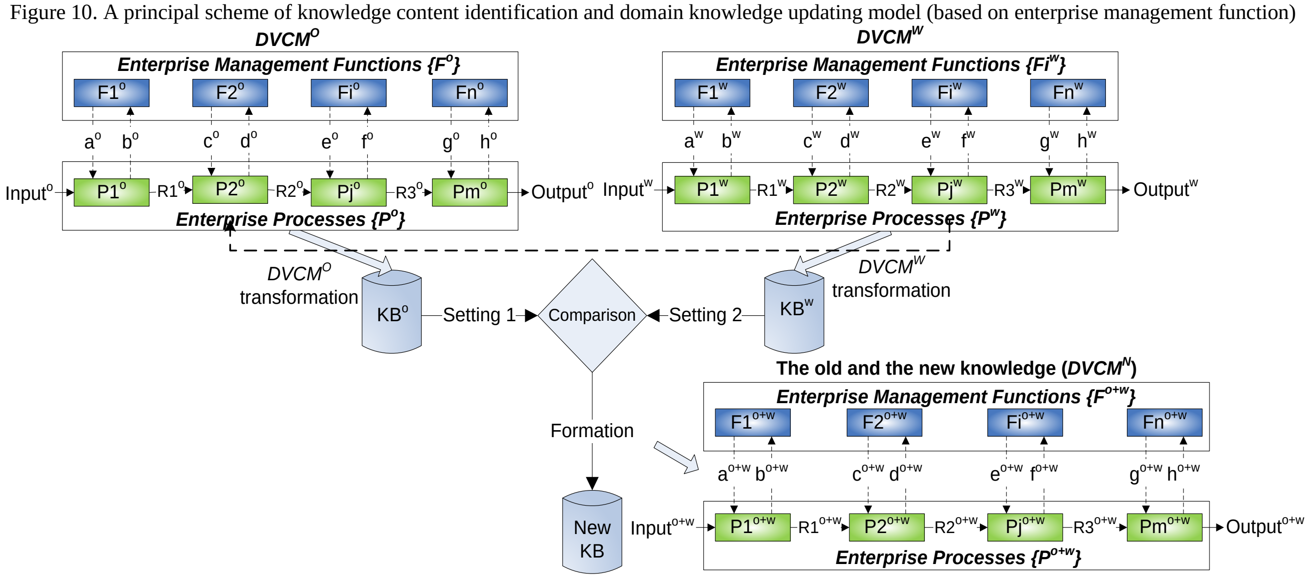

Figure 11. The identification of the existing and the new knowledge (here: *DVCM°* – the old knowledge; *DVCMʷ* – the new knowledge; *DVCMᴺ* – the renewed domain content model))

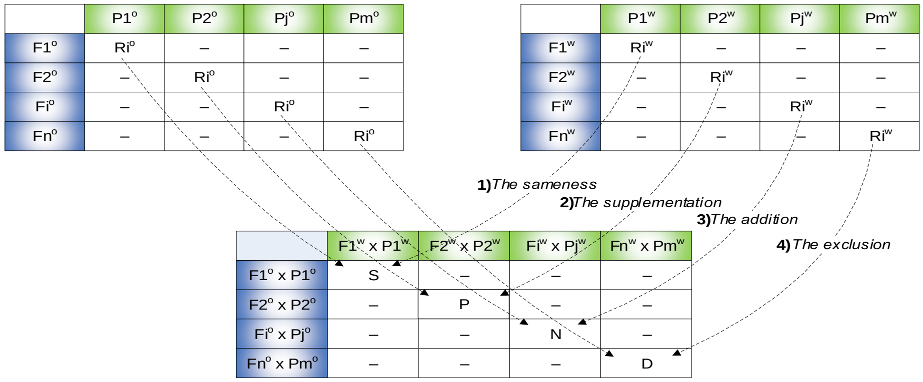

Figure 12. The relations between existing (old) and the new knowledge (requirements) (where $R_1^o, R_2^o, \ldots, R_i^o$, $R_1^w, R_2^w, \ldots, R_i^w$ – the existing and new managed process results)

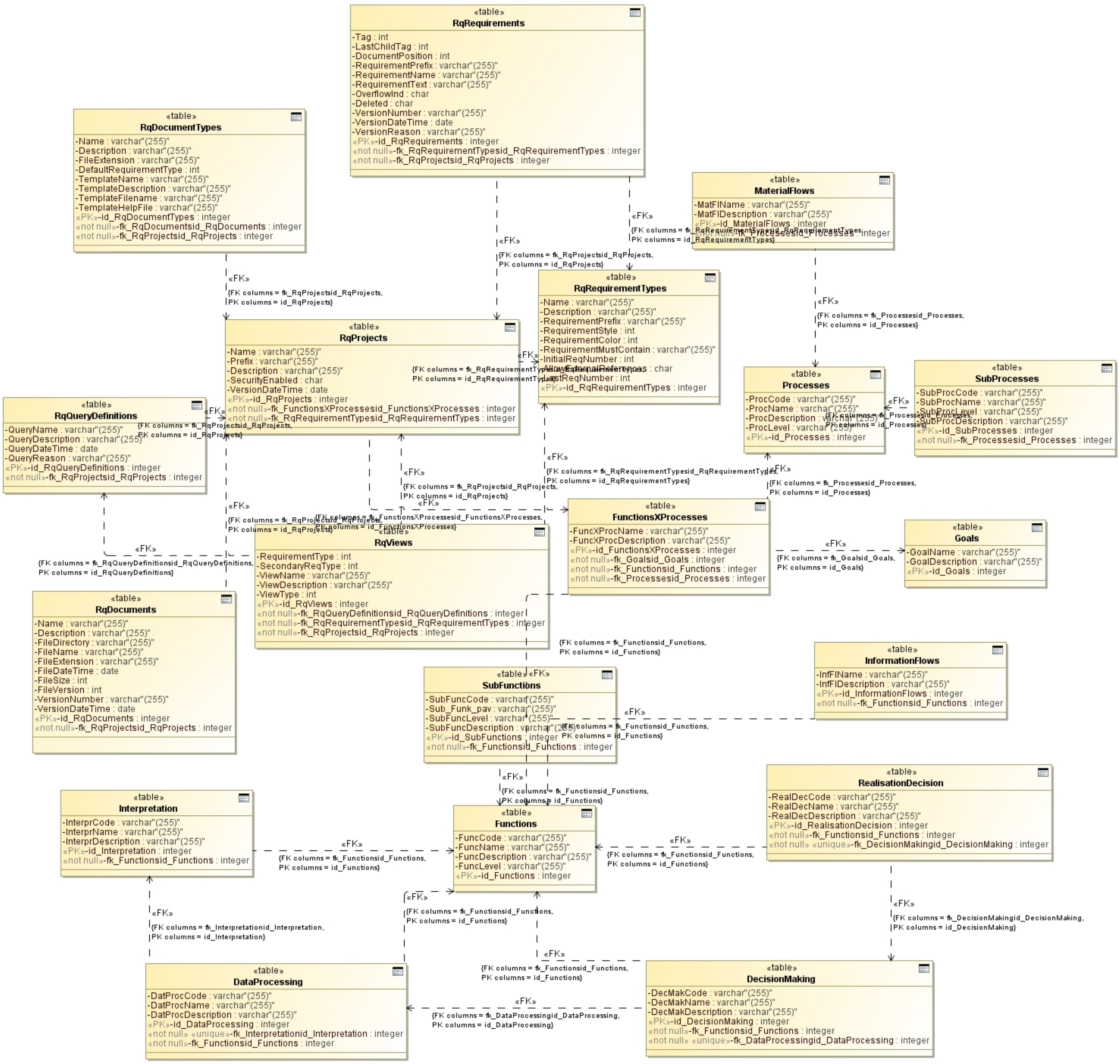

Figure 13. Subject area entity class model (physical data model)

There are several situations that can be identified: 1) the sameness of knowledge (equal requirements, knowledge remains unchanged, denoted by S); 2) the supplementation of existing knowledge with lacking new subject area knowledge (current knowledge only partially covers new requirements and should be supplemented, denoted by P); 3) the addition (inclusion) of new domain knowledge (denoted by N); 4) the exclusion of present knowledge from the current domain (no longer meets subject area requirements, competency becomes less important, denoted by D).

Implementation of the knowledge repository. Implementation of the knowledge repository of proposed model for current domain requirement improvement and knowledge content updating. Subject area entity class model (physical data model) is presented in Figure 13 (using MagicDraw™ CASE tool). The solution is implemented by extending the requirement management system by knowledge-based components.

Requirement management is performed on the basis of IBM Rational RequisitePro™ tool, meanwhile, the structure of a knowledge base is based on Detailed Value Chain and Elementary Management Cycle.

Subject area entity class model of the knowledge repository specifies DVCM and EMC elements which can be a function (consisting of information activities: Interpretation, Data Processing, Decision Making and Decision Realization), a process, a material flow, etc. Thus, the current domain parameters derived from DVCM and EMC together with requirements are stored in the knowledge databases and can be used for solving specific problems of expected application areas.

5. Conclusions

After conducting theoretical and experimental research, the following scientific and practical conclusions were drawn:

After analysing domain modelling methodologies and methods (languages, notations), it was found that a knowledge based enterprise modelling method for identifying organization's operational objectives, as well as the informational interaction between a controlled object and a controlling system forming control feedback, can be based on a Detailed Value Chain Model.

The Detailed Value Chain Model (DVCM) is defined as a problem domain content model. The peculiarity of the DVCM is refinement of the Management Functions {Fi} and Processes {Pj} as an obligatory component types of problem domain knowledge content. Management Functions (F) possess information transformations; while Enterprise Processes (P) are concrete material transformations.

The educational domain management knowledge modelling method was designed, allowing to create a two-level (granular) model for describing knowledge of domain management information interactions: the highest level Detailed Value Chain Model is further elaborated into a set of Elementary Management Cycle models; the chosen hierarchical structure allows to create new structural knowledge models and to update existing ones.

The work goes beyond formal presentation; the method is applied in a specific domain, which requires constant knowledge content updating – higher education study programme construction and updating. The flexibility of the proposed solutions should be noted – the possibility to integrate the created domain knowledge base into a study programme requirement management system, by identifying knowledge management processes and implementing a knowledge subsystem in an existing CASE system environment. Its approval provided results relevant and useful for the members, employees and professionals of academic community in higher education institutions, working on improving existing study programs and seeking to ensure their quality.

Conflict of Interest

The authors declare no conflict of interest.

Important note of applied research

This paper contributes to the applied scientific research at Klaipeda State University of Applied Sciences “Application of Enterprise Management Models in Knowledge-based Information Systems Engineering”. Area: sustainable environmental development; Field: Innovative Technologies; Branch (topic): Smart Information Technology, TMV-027.

References

[1] J. Tekutov, V. Denisovas, S. Gudas, and J. Smirnova, “The Refinement of Curricula Content Based on a Problem Domain Model,” ISMSIT 2018: 2nd International Symposium on Multidisciplinary Studies and Innovative Technologies. Kızılcahamam / Ankara / Turkey, October 19-21, 2018, p. 689–694, 2018.

[2] B. Trask, and A. Roman, “Introduction to Model Driven Development with Examples using Eclipse Frameworks,” ACM Conference on Object-Oriented Programming, Systems, Languages and Applications, Orlando, 2009.

[3] L.C. Christensen, B.W. Johansen, N. Midjo, J. Onarheim, T.G. Syvertsen, and T. Totland, “Enterprise modelling – practices and perspectives,” http://www.idi.ntnu.no/grupper/su/publ/pdf/asme95.pdf. 1995.

[4] S. Gudas, “Knowledge-Based Enterprise Framework: A Management Control View, New Research on Knowledge Management Models and Method,” http://www.intechopen.com/books/new-research-on-knowledge-management-models-and-methods/knowledge-based-enterprise-framework-a-management-control-view. 2012.

[5] S. Gudas, Information systems engineering theory. Vilnius: Vilnius University Press, pp. 25-65, 2012.

[6] A. Caplinskas, “Curricula engineering: application of systems engineering methods to the development of university curricula,” Information technology and control, vol. 22, no. 1, pp. 53–58, 2002.

[7] J. Hagerty, R.L. Sallam, and J. Richardson, “Magic Quadrant for Business Intelligence Platforms,” Gartner Inc., http://www.gartner.com/technology/reprints.do?id=1-1982NPD&ct=120208&st=sb. 2012.

[8] D. Henschen, “BI and Information Management Trends,” InformationWeek, http://www.umsl.edu/~sauterv/DSS/research-2012-bi-and-information-management_9951311.pdf2011. 2011.

[9] A. Andreescu, and M. Mircea, “Managing Knowledge as Business Rules,” Informatica Economică, vol. 13, no. 4, pp. 63–74, 2009.

[10] M.E. Porter, Competitive Advantage: Creating and Sustaining Superior Performance, 1998.

[11] S. Gudas, and A. Lopata, “The enterprise model based on identification of information resources,” Information Sciences, vol. 19, pp. 43–50, 2001.

[12] S. Gudas, “Enterprise knowledge modelling: domains and aspects,” Technological and Economic Development of Economy, vol. 15, no. 2, pp. 281–293, 2009.

[13] A. Caplinskas, and O. Vasilecas, “Modern curricula in information systems: a case study,” Information technology and control, vol. 22, no. 1, pp. 59–63, 2002.

[14] V. Denisovas, S. Gudas, and J. Tekutov, “Study program requirements engineering method and information system,” Information Sciences, vol. 53, pp. 106–126, 2010.

[15] J. Tekutov, S. Gudas, V. Denisovas, and J. Tekutova, “The Study Programme Requirements Enhancement Based on a Problem Domain Model,” INTEL-EDU 2012: 3rd International Workshop on Intelligent Educational Systems and Technology-enhanced Learning, pp. 108–120, 2012.

[16] J. Tekutov, S. Gudas, and V. Denisovas, “The Refinement of Study Program Content Based on a Problem Domain Model,” Transformations in Business & Economics, vol. 11, no. 1 (25), pp. 199–212, 2012.

[17] A. Bolt, M. de Leoni, and W.M.P. van der Aalst, “Process variant comparison: Using event logs to detect differences in behavior and business rules,” Information Systems, vol. 74, p. 53–66, 2018.

[18] J. Henderson, and N. Venkatraman, “Strategic alignment: A model for organization transformation via information technology,” pp. 3223–3290, 1990.

[19] K. Mertins, and R. Jochem, “Architectures, methods and tools for enterprise engineering,” International Journal of Production Economics, vol. 98, no. 2, pp. 179–188, 2005.

[20] C.A. Millette, “Status of department of defense architecture framework (DoDAF) implementation within the aeronautical systems center (ASC),” Air force institute of technology, http://www.stormingmedia.us/11/1134/A113434.html. 2005.

[21] OMG consortium, “Business modelling specifications,” http://www.omg.org/spec/. 2009.

[22] A.-W. Scheer, and K. Schneider, “ARIS – Architecture of Integrated Information Systems,” Handbook on Architectures of Information Systems, Part Three, pp. 605–623, 2006.

[23] I. Wowczko, “Skills and Vacancy Analysis with Data Mining Techniques,” Informatics, vol. 2, p. 31–49, 2015.

[24] G.M. Giaglis, “A Taxonomy of Business Process Modelling and Information Systems Modelling Techniques,” International Journal of Flexible Manufacturing Systems, vol. 13, no. 2, pp. 209–228, 2001.

[25] A. Morkevičius, and S. Gudas, “Enterprise Knowledge Based Software Requirements Elicitation,” Information technology and Control, vol. 40, no. 3, pp. 181–190, 2011.

[26] N.U. Ahmed, and S.K. Sharma, “Porter’s value chain model for assessing the impact of the internet for environmental gains,” Management and Enterprise Development, vol. 3, no. 3, pp. 278–295, 2006.

[27] R. Bandarian, “Exploiting value chain process concepts in research organisations,” International Journal of Value Chain Management, vol. 2, no. 3, pp. 400–416, 2008.

[28] D. Beard, D. Schwieger, and K. Surendran, “A Value Chain Approach for Attracting, Educating, and Transitioning Students to the IT Profession,” Information Systems Education Journal, vol. 8, no. 7, pp. 1–12, 2010.

[29] Y-L. Chen, T.-C. Yang, and Z-S. Lin, “A study on the modelling of Knowledge value chain,” Knowledge Management, pp. 1–12, 2004.

[30] F. Cummins, “Value Chain Modelling: Linking Customer Value to Business Process Design and 2010 Automation,” Cutter IT Journal, vol. 23, no. 2, pp. 23–30, 2010.

[31] S. Gudas, and R. Brundzaitė, “Enterprise knowledge modelling based on modified value chain model,” Information Sciences, vol. 35, pp. 179–192, 2005.

[32] S. Gudas, A. Lopata, and T. Skersys, “Approach to enterprise modelling for information systems engineering,” Informatics, vol. 16, no. 2, pp. 175–192, 2005.

[33] S. Gui, and Z. Ye, “The Research of Value Chain Operation Model in E-Commerce,” International Seminar on Business and Information Management, pp. 238–241, 2008.

[34] M.C. Lee, and M.W. Han, “Knowledge Value Chain Model Implemented for Supply Chain Management Performance,” Fifth International Joint Conference on INC, IMS and IDC, pp. 606–611, 2009.

[35] R. Landry, N. Amara, A. Pablos-Mendes, R. Shademani, and I. Gold, “The knowledge-value chain: a conceptual framework for knowledge translation in health,” Bulletin of the World Health Organization, vol. 84, no. 8, pp. 597–602, 2006.

[36] A. Najmaei, and Z. Sadeghinejad, “Competitive Strategic Alliances Through Knowledge Value Chain,” International Review of Business Research Papers, vol. 5, no. 3, p. 297–310, 2009.

[37] V. Pathak, and K. Pathak, “Reconfiguring the higher education value chain,” Management in Education, vol. 24, no. 4, pp. 166–171, 2010.

[38] A. Saha, “Mapping of Porter’s value chain activities into business functional units,” Management Innovation eXchange, http://www.managementexchange.com/hack/mapping-porter%E2%80%99s-value-chain-activities-business-functional-units. 2012.

[39] G. Stewart, “Supply-chain operations reference model (SCOR): the first cross-industry framework for integrated supply-chain management,” Logistics Information Management, vol. 10, no. 2, p. 62–67, 1997.

[40] E. Sweeney, “Supply Chain Management and the Value Chain. Supply Chain Perspectives,” Journal of the National Institute for Transport and Logistics, vol. 10, no. 2, p. 13–15, 2009.

[41] E. A. Williamson, D. K. Harrison, and M. Jordan, “Information Systems Development Within Supply Chain Management,” International Journal of Information Management, vol. 24, no. 4, p. 375–385, 2004.

[42] H.K. Wong, “Knowledge Value Chain: Implementation of New Product Development System in a Winery,” The Electronic Journal of Knowledge Management, vol. 2, no. 1, pp. 109–122, 2004.

[43] S. Gudas, and A. Lopata, “Towards internal modelling of the information systems application domain,” Informatica, vol. 27, no. 1, p. 1–29, 2016.

[44] J. Tekutov, “Model of Domain Knowledge Content Updating Based on Management Information Interactions” PhD dissertation, Dept. of Informatics, Vilnius Univ., 2013.

[45] J. Tekutov, S. Gudas, and V. Denisovas, “The Formation of Requirements Engineering Processes Based on a Problem Domain Model,” Proceedings in Conference of Informatics and Management Sciences (ICTIC-2018). Zilina, Slovak Republic, vol. 7, no. 1, p. 93–97, 2018.

Advances in Science, Technology and Engineering Systems Journal Vol. 4, No. 2, 153-161 (2019)
www.astesj.com
Special Issue on Recent Advances in Engineering Systems
ASTESJ
ISSN: 2415-6698

Frequency-Based Design of Electric System for Off-shore Wind Power Plant (OWPP)

Uttam S. Satpute[*,1], Diwakar R. Joshi[2], Shruti Gunaga[3]

[1]Department of Electrical and Electronics Engineering, VDIT Haliyal, Karnataka, 581329, India

[2]Department of Electrical and Electronics Engineering, GIT Belagavi, Karnataka, 590008, India

[3]Department of Electrical and Electronics Engineering, Oxford College of Engineering, Bangalore 560068, India

A R T I C L E I N F O

Article history:
Received: 08 January, 2019
Accepted: 25 February, 2019
Online: 20 March, 2019

Keywords:
Optimum Frequency
Offshore wind power plant
Optimization

A B S T R A C T

The paper presents a novel concept of design of electric system for Off-shore Wind Power Plant (OWPP) based on frequency. In the literature, a new transmission system i.e. Fractional Frequency Transmission System (FFTS) has been proposed as an economic alternative to High Voltage AC (HVAC) and High Voltage DC (HVDC) for power transmission from Off-shore Wind Farm (OWF) to on-shore grid. In the FFTS power transmission is proposed at 1/3rd of conventional frequency (50Hz). The choice of this frequency (50/3Hz) for FFTS is not based on any mathematical analysis and seems to be a compromise. Since, frequency is one of the prominent parameter that reflects on the project economy, the paper explores on the choice of operational frequency for electric system in view of reduction in the investment cost. The existence of optimum frequency is realized based on the finding that, the costs of power system components are frequency-dependent and they imbibe the trade-off in their costs. The paper presents a comprehensive methodology to compute the most economical operational frequency for electric system by optimization of frequency-based cost model of the system using Genetic Algorithm (GA). The proposed methodology is applied to 160MW OWF (Horns-Rev) as a case study. For off-shore distances of 50km, 100km, 150km and 200km, the optimum operational frequencies are obtained as 52Hz, 32Hz, 22Hz and 16Hz respectively. The proposed methodology for the design of electric system based on frequency results in significant saving in the investment cost for moderate transmission distance. Hence it is concluded that, the work presented in this paper gives a new dimension for planning and cost effective design of electric system for OWPP. Further, it promotes the investor for deployment of OWF which leads to reduction in air pollution and global warming which are major concerns of the world today in the endeavor.

1. Introduction

This paper is an extension of original paper entitled, "Optimum Frequency-Based Design of Off-shore Wind Power Plant (OWPP)", presented in 2017 IEEE PES Asia Pacific Power and Energy Engineering Conference (APPEEC), India [1]. In the present paper, the author has made an attempt to address all the comments, queries and issues raised during the publication of the previous original paper. To avoid de-linking, a brief introduction to the theme of the paper has been presented from the original work.

Harvesting energy from wind has become one of the major contributions to the energy sector across the globe. Due to policy instability as well as specific issues linked to land acquisition for wind power projects on land; deployment of wind project offshore has been increased in the recent times. High-stable offshore wind potential, large installation space, no visual effects, closeness of major load centers and technological advancement in the wind industry has supplemented its growth. Globally offshore installation has been progressed with an average growth rate of 30% per annum during 2010-2017, reaching to a total installed capacity of 18GW at the end of 2017 [2]. Opportunities for further scaling up are humongous. An ambitious target of 40GW by 2020

* Uttam S. Satpute, Email: uttamsatpute@gmail.com

https://dx.doi.org/10.25046/aj040220

has been reported.

Huge initial investment is one of prominent slog in the path of offshore development. Highly evolved tower construction, offshore substation, seabed lying of submarine cable and high maintenance cost are some of reasons for heavy investment. And it is the major hindrance for offshore deployment. Presently, the Levelized Cost of Energy (LCOE) is more than \$5-6 millions per MWh, and it warrants for the technological changes to reduce the investment, and make OWPP economically feasible [3].

In the OWPP, among the split-up, electrical infrastructure cost shares significant portion in the total project cost. It includes the cost of inter-farm distribution network which collects the power from the wind turbines and the cost of main transmission network which exports the power from the off-shore substation to on-shore grid. In broader perceptive, the paper exploits on opportunities to reduce the electrical infrastructure cost for OWPP.

In respect of this, a new transmission system i.e. Fractional Frequency Transmission System (FFTS) has been proposed in the literature as an economic alternative to HVAC and HVDC [4]. FFTS is also named as Low Frequency AC (LFAC) by some researchers. In the LFAC, power transmission is proposed at 1/3rd of the nominal frequency (50/60Hz), and at the grid-side, frequency converter is employed to transform fractional frequency (50/3Hz) to nominal frequency (50Hz). In the LFAC, due to low frequency operation charging current requirement of the cable is less and that increases its power transmission capacity, and unlike HVDC it requires only one converter at the grid-side are main attributes for its cost reduction [4].

The technical and economic viability of LFAC over HVDC and conventional HVAC has been investigated by many researchers [4]-[9]. It is stated that, LFAC has economic and performance advantages over conventional HVAC and HVDC and it has a future trend.

The fundamental quest on the choice 50/3 Hz frequency for LFAC has initiated this paper. Literature states that, single-phase 50/3Hz system is already in-use for supplying electric power to traction in German and in LFAC cyclo-converter can be employed for frequency transformation which is less costly compared to other converters [9]. After a careful perusal of the literature, it is revealed that, the choice of 50/3Hz frequency for LFAC seems to be a compromise, and it is not based on any rigorous mathematical analysis. The choice of frequency for power transmission is very important, because it reflects on the project economy. The original paper has dealt with the choice of operational frequency for electric system integrating OWF to on-shore grid, in view of reduction in the investment cost. Thus, a novel thought of optimum frequency-based design of OWPP had been proposed in the previous work.

In the original work, the reviewers and the panel of judges had raised the following major issues,

The first major issue was related to the methodology adopted for the computation of optimum frequency. In the previous work, optimum operational frequency was computed through optimization of the frequency-based cost model of the electric system. Genetic Algorithm (GA) was used for the optimization. Since the cost model was of single-variable (frequency), the reviewer raised the question on the applicability of GA for the optimization of a simple-single-variable model as it is applied for the case of complex system. In the present work, operating voltage of the electric system is added as another variable for enhancing optimization of the system. Furthermore, in the previous work, cost model of the system had been developed by adding frequency-based cost models of various power system components involved in the system. These cost models of the components were developed separately in the sequence. Firstly the components were designed and then from the design parameters the costs were computed for different frequencies and then from the frequency-based cost curves their cost models were derived using curve fitting techniques. The reviewer suggested combining these processes into a single execution, which is incorporated in the present work. The paper presents a newer computational structure for the computation of the optimum frequency in a single execution.

The second major issue was related to validation of the designs and cost models of the components. Design and frequency-based cost model of the transformer developed in the original paper has been validated with the models available in the literature.

The third major issue was in respect of generation of fractional frequency from the wind turbine generator. In the original work, optimization was performed on Fractional Frequency Wind Power System (FFWPS). Reference [10] has proposed this configuration for integrating OWF to on-shore grid. It eliminates individual power converter in the wind turbine and proposes speed control from single large power converter (cyclo-converter). Since the generator required in this configuration would be bulky as it has to generate low frequency power, it demands for modification in the wind turbine generator. The reviewer had questioned the implications on the design and verification with wind turbine manufacturers. Reference [10] has validated FFWPS for its practical implementation because it reduces the cost of wind turbine generator in twofold; firstly it reduces the gear ratio and secondly it eliminates the power converter. So, in the present paper, FFWPS is considered for the optimization process.

The paper is organized as follows. The structure of FFWPS and the concept of optimum operational frequency are presented in Section 2. Section 3 presents the development of frequency-based cost model of FFWPS. Section 4 presents the development of computation structure for the optimization of the developed model. Section 5 presents the rating of components of FFWPS for application of the developed methodology. The results are discussed in the Section 6 and finally Section 7 concludes the paper.

2. System model (FFWPS) and the concept of optimum frequency

Fractional Frequency Wind Power System (FFWPS) is one of the electric system configuration proposed in the literature for integrating OWF to on-shore grid [10]. Figure 1 shows the structure of this system.

In FFWPS, the entire electric system including generator, inter-farm distribution network and main power transmission network operates at 50/3Hz frequency. Frequency converter at the grid-side transforms frequency from 50/3Hz to 50Hz and the power is injected onto the grid. FFWPS eliminates the full scale power converter in the wind turbine and proposes rotor speed control from the single large power converter (cycloconverter). Due to elimination of individual power converter the cost is reduced but there is a 3% loss in the energy yield [11]. Reference [13] has discussed synchronization scheme for FFWPS and shown safe and reliable integration of offshore wind farm to onshore grid. From the literature it is revealed that, FFWPS is technically and economically suitable configuration to transmit electrical power from off-shore wind farms to the power grid.

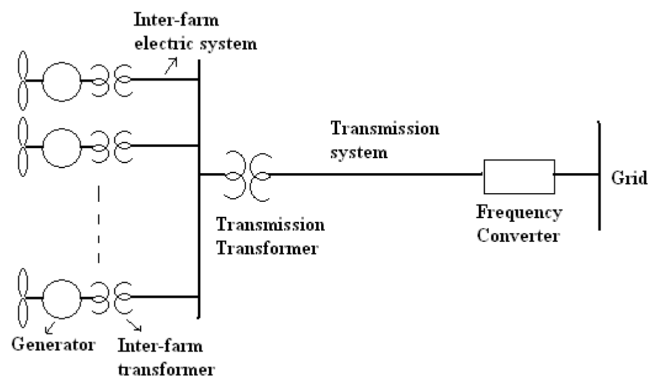

Figure 1: Structure of Fractional Frequency Wind Power System (FFWPS)

In this paper, the study on FFWPS is extended from the perspective of its operational frequency. The operational frequency of FFWPS is 50/3 Hz, but as discussed in the previous section, the choice of 50/3 Hz frequency for FFWPS seems to be compromise rather than based on any formal mathematical analysis. The paper particularly, deals with the choice of frequency (economically-optimal) for FFWPS based on the criterion of minimum investment cost.

The existence of optimum frequency for FFWPS is realized based on the finding that, the cost of power system components (generator, transformer, submarine cable, and compensator) varies with the frequency and they imbibe a tradeoff in their costs. Specifically, the cost of generator and transformer varies in inverse proportion to frequency. Because, the size of magnetic system (no. of turns/ core area) decreases with increase in frequency and hence cost decreases. Whereas, the cost of submarine cable network varies in direct proportion to frequency. Because, as the frequency increases, the charging current requirement of the cable increases, and for the same active current, the size of the conductor increases with increase in frequency and hence the cost increases.

So it is found that there is tradeoff in two broad categories of cost;

- Sum of cost of generators and transformers
- Sum of cost of submarine cable networks

Figure 2 shows the typical variation of these two costs with respect to frequency. The system cost, which is sum of these two costs, will be parabolic in nature with respect to frequency. The point of inflection on the system cost curve corresponds to the optimum point.

The X and Y co-ordinates of the optimum point corresponds to optimum operational frequency and the optimum cost respectively. The cost of generator and transformer are independent of off-shore distance, but the cost of transmission system depends upon the off-shore distance. So the point of inflection and hence the optimum cost and optimum frequency changes with the distance. Hence it is realized that, for the given power rating and off-shore distance of FFWPS, the system investment cost is a function of frequency and it get optimized (minimized) at certain economically-optimum frequency.

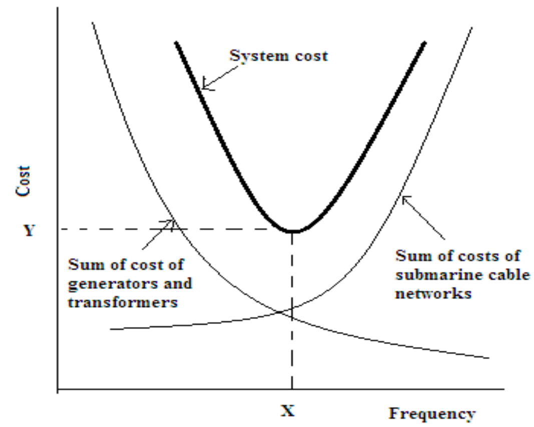

Figure 2 Show the concept of optimum frequency

3. Development of mathematical model

It is evident from the former discussion that, for a given FFWPS, the optimum operational frequency can be determined by optimizing its system cost. It represents an optimization problem. The system cost is sum of the cost of generators, inter-farm transformers, inter-farm electric system and transmission system. Mathematically, it is described as below,

The objective function is defined as,

$$\min\ C(f) \tag{1}$$

where,

$$C(f) = N * C_{gen}(f) + N * C_{itran}(f) + C_{ttran}(f) + C_{in-elec-system}(f) + C_{trans-system}(f) \tag{2}$$

Subject to,

$$1 \le f \le 100$$

where,

N- no. of wind turbines in the farm, $C_{gen}(f)$-cost of generator, $C_{itran}(f)$- cost of inter-farm transformer, $C_{ttran}(f)$- cost of transmission transformer, $C_{in-elec-system}(f)$- cost of inter-farm electric system, $C_{trans-system}(f)$- cost of transmission system.

The cost of frequency-converter which is independent of frequency, and the cost of other equipments simply act as an offset, so they are not included.

The cost of generator, inter-farm transformer, transmission transformer, inter-farms electric system and transmission system are estimated as follows.

3.1 Estimating Generator cost

The cost of the generator is estimated from its design parameters. Since the design parameters and hence the cost are subjective to design constants (variables).To obtain economy, the generator-cost is optimized in terms of its design variables. Specific magnetic loading (B_{av}), specific electric loading (ac), width of ventilating duct (w_{ds}), width of stack length (w_{ss}), slot pitch (y_s), current density (δ) and Short Circuit Ratio (SCR) are selected as design variable with appropriate bonds. Copper and iron are major elements in the generator. So the cost of generator is estimated by considering only the cost of copper and iron. Mathematically it is described as below,

The objective function is defined as,

$$\min \quad C_{gen}(B_{av}, ac, w_{ds}, w_{ss}, y_s, \delta, SCR) \tag{3}$$

where,

$$C_{gen} = C_{ig} + C_{cg} \tag{4}$$

Subject to,

$$0.52 \leq B_{av} \leq 0.65$$
$$20000 \leq ac \leq 40000$$
$$8 \leq w_{ds} \leq 10$$
$$40 \leq w_{ss} \leq 80$$
$$10 \leq y_s \leq 50$$
$$3 \leq \delta \leq 5$$
$$1 \leq SCR \leq 1.5$$

where,

C_{gen} – cost of generator, C_{ig} – iron cost, C_{cg} – copper cost.

Cost of iron and copper is estimated from the volume of iron and copper, which are calculated from the main dimensions, number and size of stator slots, depth of stator core, dimension of rotor pole, depth of rotor core and number of stator and rotor turns.

3.2 Estimating Inter-farm transformer cost

The cost of the transformer is estimated from its design parameters. Since the design parameters and hence the cost are subjective to design constants (variables). To obtain economy, the transformer-cost is optimized in terms of its design variables. A constant (K), as defined in Equation (6) is selected as design variable.

$$k = 4.44 * f * \left(\frac{\varphi}{AT}\right) * 10^3 \tag{6}$$

Cost of copper and iron are only considered for estimating the cost of transformer. Mathematically it is defined as below,

The objective function is defined as,

$$\min \quad C_{itran}(k) \tag{7}$$

where,

$$C_{itran} = C_{it} + C_{ct} \tag{8}$$

Subject to,

$$0.1 \leq k \leq 1$$

where,

C_{itran}– transformer cost (M €), C_{it} - iron cost (M €), C_{ct} - copper cost (M €).

Cost of iron and copper is estimated from the volume of iron and copper, which in-turn are calculated from the core area, primary and secondary turns and width and height of core.

3.3 Estimating Transmission transformer cost

The cost of transmission transformer is estimated as similar to inter-farm transmission transformer (discussed above).

3.4 Estimating Inter-farm electric system cost

The inter-farm electric system includes the interconnection of wind turbines in the farm by submarine cables. The cost of inter-farm electric system is estimated as per by Equation (9). It includes only the cost of copper core. As per the standard practice, size of the core is assumed 50% more than the actual requirement.

$$C_{trans-system} = 3 * \frac{1.5 * I}{\delta} * L * S_c * D_c \tag{9}$$

where,

I – net current to be carried by the cable/phase (amps) , δ – current density (amp/m^2), L – length of the cable (m), S_c- specific cost of copper (/kg), D_c –density of copper (kg/m^3).

The net current is calculated by adding the active current and the charging current as per Equations (10)-(12).

$$I = \sqrt{(I_a{}^2 + I_c{}^2)} \tag{10}$$

$$I_a = \frac{P}{(\sqrt{3} * V * \cos\emptyset)} \tag{11}$$

$$I_c = \left(\frac{V}{\sqrt{3}}\right) * 2 * \pi * f * C \tag{12}$$

where,

I_a – active current /phase(amps), I_c – charging current/phase(amps), P – 3-phase power (W), V – line-to line voltage (V), $\cos\varphi$ – power factor of load, f – frequency (Hz), C – Capacitance of the cable (F).

3.5 Estimating Transmission system cost

The transmission system exports power from local off-shore grid to on-shore grid by submarine cable. Its cost is estimated as similar to inter-farm electric system (discussed above).

4. Implementation of mathematical model

The mathematical model developed in the previous section, describes the requirement of optimization of system cost model to determine optimum operational frequency. Further, to achieve overall economy, it demands for optimal design of generator and transformers. To implement this, a computational structure with two-stage optimization is developed as shown in the Figure 3. In the first-stage (stage-I), the cost of generator, inter-farm transformer and the transmission transformer are optimized in terms of their design variables, whereas, the system cost is optimized in terms of frequency in the second-stage (stage-II).

This unique feature ensures over-all optimization of the problem. Genetic Algorithm (GA) is used for all the optimizations.

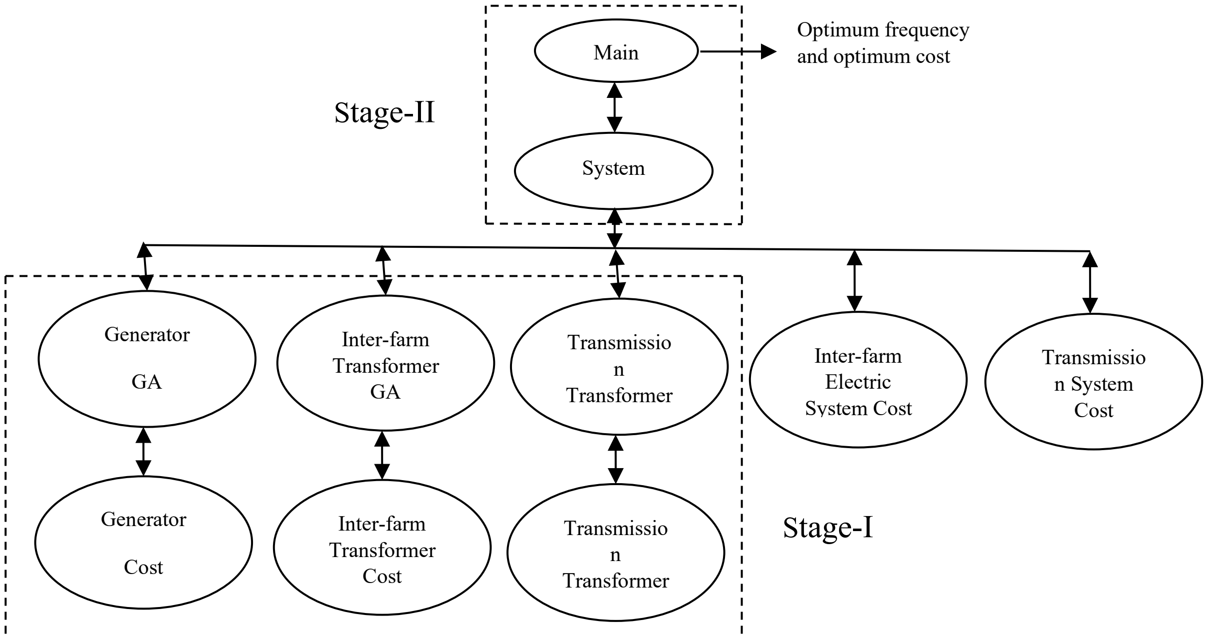

Figure 3: Computational structure of optimization

Figure 4 depicts the process of computation of optimum operational frequency. For simplification, working of Main-GA is only presented. The size of population (fre_pop_max)) for variables (frequency and voltage) and maximum generation limit (gen_max) are set to 50 and 100 respectively. The main core of the algorithm is the evaluation of fitness values (system costs). Initially the population for frequency and voltage is generated randomly. Then, the fitness values are evaluated for each of the population by adding the cost of power system components, which are computed from the executions of respective subroutines. The population is improvised through reproduction, crossover and mutation process and the iteration of generation is continued till the maximum generation count is reached.

Then finally, the minimum fitness value of the last generation which corresponds to the optimum cost is evaluated. The population corresponding to the optimum cost is the optimum frequency.

This methodology of computation of optimum frequency through single-execution effectively addresses all the issues raised by the reviewers in the original paper.

Table 1: Rating of various components of OWPP

Component	**Rating**
Generator	EESG: 2MVA, 690V, 35rpm
Inter-farm transformer	3-phase, core type: 2MVA, 0.69/33kV.
Inter-farm electric system	Submarine cable: 33kV,100km
Transmission Transformer	3-phase core type: 160MVA, 33/150kV
Transmission system	Submarine cable: 160MW,150kV, varying length

5. Results and discussions

Based on the computational structure and the flow chart presented in the previous section, code is written in MATLAB-7.The ratings of power system components are initialized as per the prototype FFWPS. The code is executed under different scenarios to obtain the following results.

6.1 Validation of the generator and transformer design

Electrically Excited Synchronous Generator (EESG) of 2MVA, 690V, 35 rpm is designed using Genetic Algorithm for different frequencies. Table 2 in Appendix, shows the design and performance parameters. Similarly, Table 3 in Appendix shows the design and performance parameters of 3-phase, core type, 2MVA, 0.69/33kV transformer designed using Genetic Algorithm. It can be seen that, core and copper volume for generator and transformer increases with decrease in frequency and hence the cost increases, it complies with the fundamental fact that, the size of the magnetic system increases with decrease in frequency. Since only the cost of iron and copper are taken into account in estimating the cost, the figures given in the tables do not reflect the real costs. Further, since the feasibility of frequency-based design of electric system is evaluated in comparison to LFAC and HVAC, only qualitative variation in the cost with respect to frequency is needed.

6.2 Verifying the existence of optimum frequency

It was postulated in the Section 2 that, the system cost is parabolic in nature w.r.t. frequency and the co-ordinates of the optimum point corresponds to the optimum cost and the optimum operational frequency. To investigate this phenomenon, prototype FFWPS with 50km off-shore distance is considered. The cost of power system components and the system cost are estimated for different frequencies. Table 4 gives the variation in the costs w.r.t. frequency. It can be seen that, the cost of generator, inter-farm transformer and transmission transformer decreases with increase

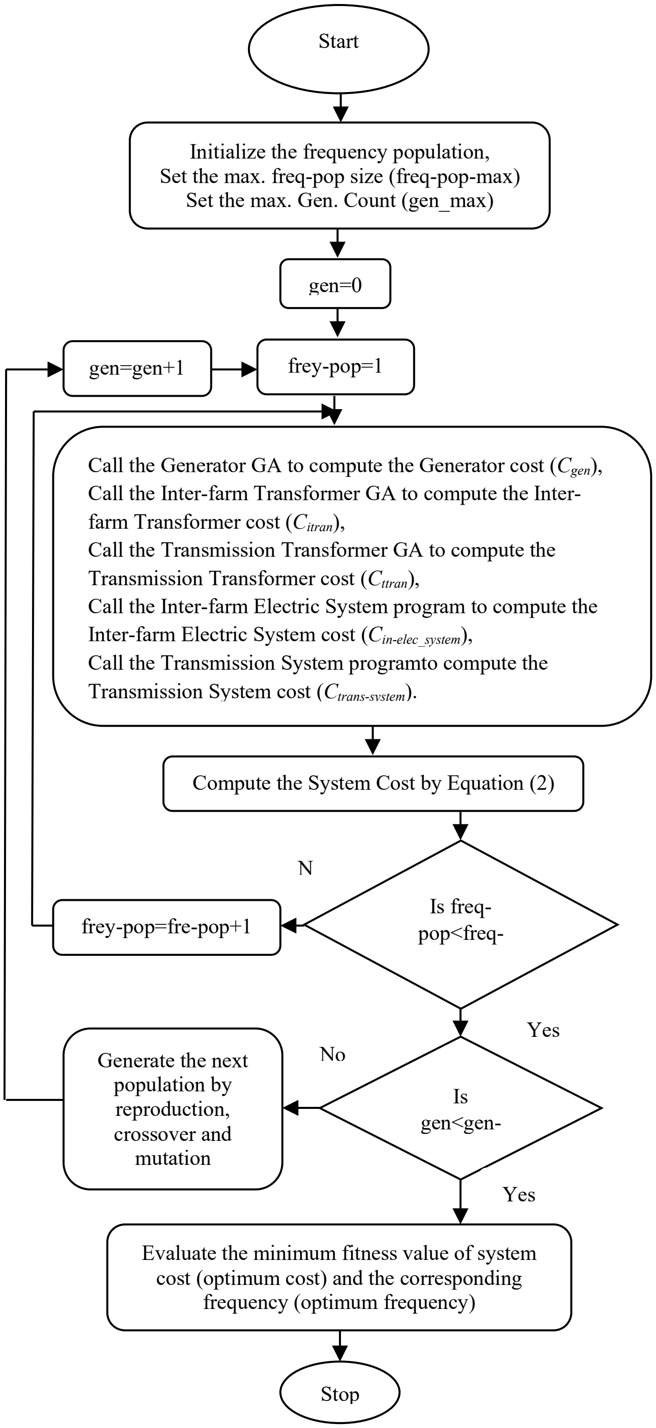

Figure 4: Flow chart showing working of computational structure

in frequency, whereas the cost of inter-farm electric system and transmission system increases with increase in frequency. It can also be seen that, the system cost decreases initially up-to certain optimum frequency (indicated by shading) and then increases with the frequency. Figure 5 shows the system cost w.r.t. frequency. It can be seen that, the cost of FFWPS is parabolic in nature and their lies an optimum operational frequency where the system cost is minimum. For 50km transmission length, the optimum operational frequency is obtained as 52Hz and the corresponding optimum cost is 64.73M€. If the system is operated at 50/3Hz, the system cost will be 78.43M€. Thus the result clearly indicates that, if the FFWPS is operated at optimum operational frequency rather than operating at 50/3Hz, substantial amount of saving can be achieved. Figure 6 shows the savings for different frequencies. It can be seen that; the saving is maximum (17.47%) at the optimum operational frequency. Thus it is verified that, for the given FFWPS, there exist an optimal operational frequency.

Table 4: Variation in the cost of various power system components w.r.t. frequency

(1)	(2)	(3)	(4)	(5)	(6)	(7)
50/3	21.31	8.12	19	0.78	29.21	78.43
20	18.25	6.75	19.14	0.68	29.31	74.14
30	13.39	4.58	19.7	0.52	29.7	67.89
40	10.75	3.5	20.45	0.42	30.25	65.37
52	9.22	2.84	21.38	0.35	30.94	64.73
60	8.2	2.43	22.46	0.31	31.77	65.18
70	7.56	2.11	23.68	0.28	32.72	66.34
80	6.99	1.86	25.01	0.26	33.78	67.9
90	6.51	1.68	26.43	0.24	34.95	69.8
100	6.05	1.59	27.94	0.22	36.21	72.01

(1)- Frequency (Hz), (2)- Generator cost (M€), (3)- Inter-farm transformer cost (M€), (4)- Inter-farm electric system cost (M€), Transmission transformer cost (M€), (5)- Transmission system cost (M€), (7)- System cost (M€)

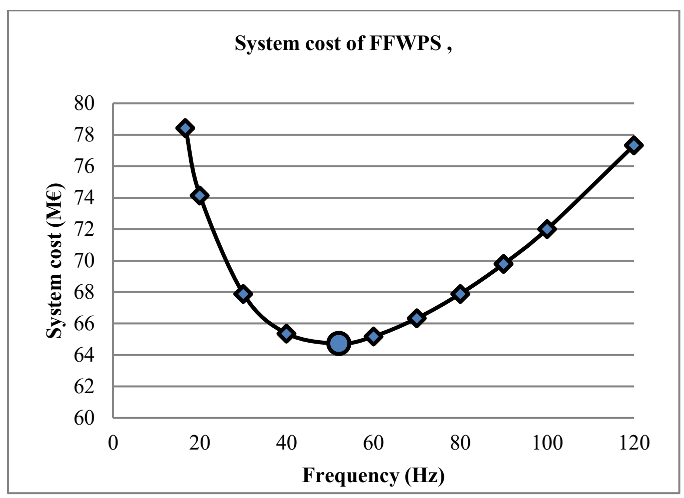

Figure 5: Variation in cost of FFWPS v/s frequency (off-shore distance 50km)

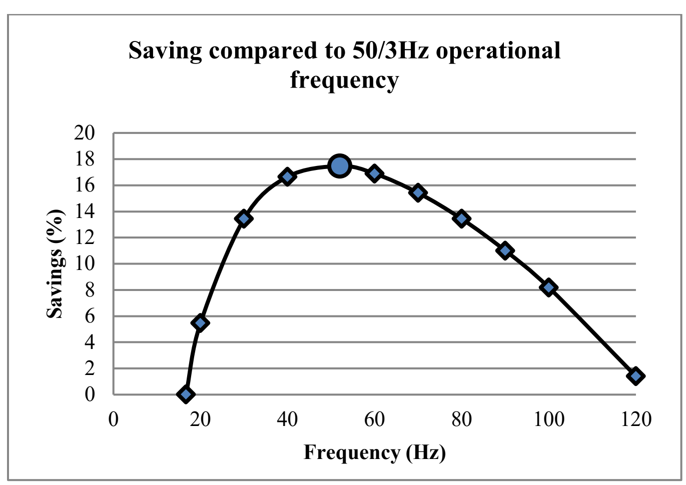

Figure 6: Saving with optimum design in comparison to LFAC (off-shore distance 50km)

Further, since the optimum operational frequency depends upon the off-shore distance. With the aid of **Main-GA,** optimum operational frequencies for different transmission lengths are obtained as shown in the Figure 7. It can be seen that, the optimum operational frequency decreases with increase in the transmission length. It complies with the fact that, HVAC (50 Hz) is economical for short distance transmission and HVDC (0 Hz) is for long distance.

5.1. Feasibility of optimum frequency-based design

As stated earlier, the main objective of paper is to enhance the project economy by reducing its electric infrastructural cost through its operation at optimum frequency. To investigate this, savings accrued from optimum frequency-based design, in comparison to conventional HVAC (50Hz) and LFAC (50/3Hz) are estimated as shown in the Figure 8 for different transmission lengths.

The saving is expressed as percentage of the cost of system under comparison. It can be seen that, compared to LFAC, optimum frequency-based system gives substantial amount of saving in the investment cost up-to 150km (approx.). Whereas, compared to HVAC, the saving is substantial beyond 80km (approx.). So, when it is question of choice of system, the results indicates that, HVAC is undoubtedly better up-to 80km distance, but beyond that and up-to 150km, optimum frequency-based system is a promising choice. The results suggest that, for the given FFWPS, optimum frequency-based system is feasible for the off-shore distance in the range of 80-150 km, and for this range the operational frequency is 20 to 40 Hz.

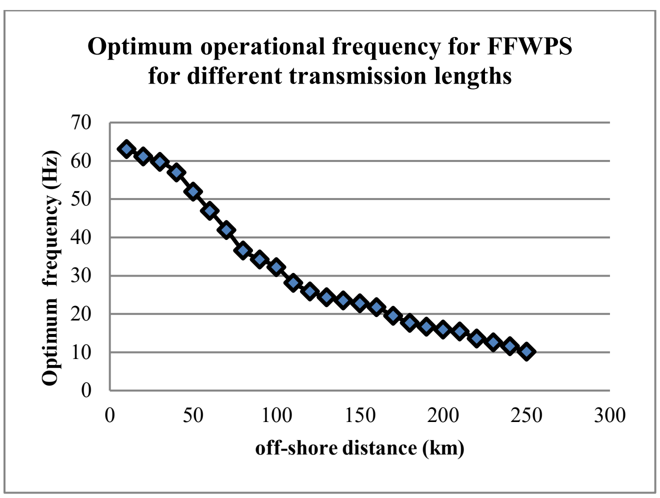

Figure 7: Optimum operational frequencies for FFWPS for different off-shore distances

6.2 Consideration of optimum operating voltage

The savings shown in the Figure 8 are obtained with fixed operating voltages i.e. 33kV for inter-farm electric system and 150kV for transmission system. But the savings can be enhanced enormously if the operating voltages are selected appropriately. The basic thumb rule recommends for the selection of highest possible operating voltages. Even-though, higher operating voltage reduces the cost of inter-farm electric system and transmission system, but on contrary, they increase the cost of inter-farm transformer and transmission transformer.

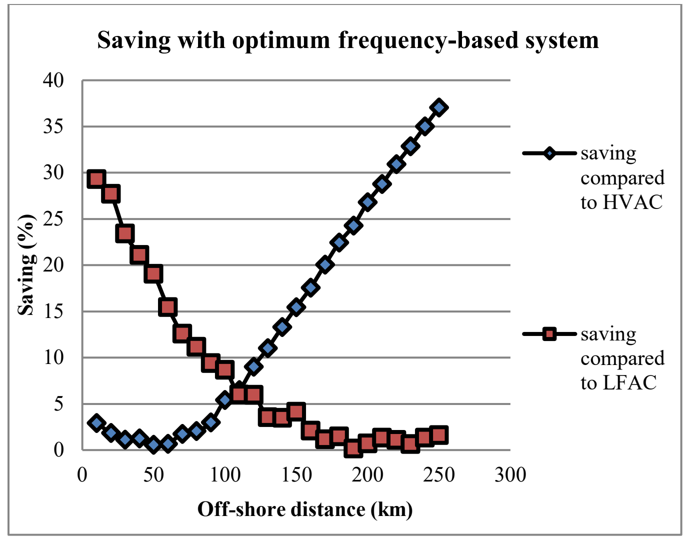

Figure 8: Saving with optimum frequency-based system

So there is trade-off in the costs and it demands for optimum selection of operating voltages.

To address this issue, the operating voltages of inter-farm electric system and transmission system are initialized as variables in the optimization (Main-GA) along with frequency. This leads to an idea of optimum frequency-voltage-based design of FFWPS. Figure 9 shows the saving accrued from this system compared to HVAC and LFAC. For HVAC and LFAC system the operating voltages are kept fixed as before.

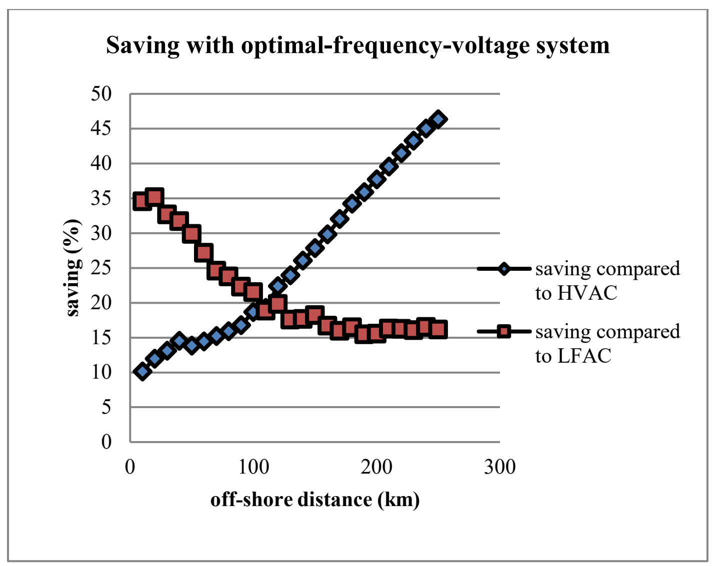

Figure 9: Saving with optimum-frequency-voltage system

It can be seen that the savings are augmented by optimum selection of operating voltages along with optimum choice of operational frequency.

Thus the results reveal that, there exits an optimum operational frequency and if the electric system is designed and operated at the optimum frequency rather at the standard conventional frequencies, substantial amount of saving in the investment can be achieved.

6. Conclusions

The paper has extended the work on optimum frequency-based design of electric system for OWPP. It deals with the computation of most economical operational frequency so that the electrical infrastructural cost is minimal. The paper has presented a newer methodology for the optimal design of electric system through optimization of frequency-based cost model of the system in a single execution. The developed methodology is applied to a prototype FFWPS and shown that the investment cost can be reduced significantly if the system is designed and operated at the optimum frequency. Further, the paper effectively addresses all the issues of the original paper. It is concluded that, the proposed optimal design for electric system is economically competitive compared to HVAC and LFAC for moderate transmission distance. The work carried out in this paper provides a new dimension for economical design of electric system. It also helps in motivating the investors for deployment of OWF to dovetail the energy gap between generation and demand. Further it also indirectly addresses the problem of environment pollution and global warming which are the major concerns of world today in the endeavor. Nevertheless in the proposed design, power system components such as generator, transformer and compensation units need to be redesigned for the operation at nonconventional frequencies. But for large size wind farms (>1000MW), it will not be major paramount because the required generators and transformers can be manufactured cheaply in mass. In the present paper only investment cost is considered for the optimal design but in the future work operational cost can also be added in the optimization to get better results. Further, the study can be extended to other configurations of electric system.

References

[1] Uttam S. Stpute, D.R. Joshi, "Optimum Frequency-Based Design of Off-shore Wind Power Plant (OWPP)", proc. of 2017 IEEE PES Asia-Pacific Power and Energy Engineering Conference (APPEEC), Bengaluru, India, Nov. 2017.

[2] 'Global Wind Energy Council (GWEC) global 2015 report', available at : http://www.gwec.net/global, visited on: 25th August 2018.

[3] Yuan-Kang Wu, Li Wang, Yong-Qing Huang, Shu-Wei Liu, "Overview of Important State-of-the-art Technologies in Off-shore Wind Energy System," International Journal of Smart Grid and Clean Energy, vol. 2, no. 2, pp. 64-67, May 2013.

[4] X. Wang, "The fractional frequency transmission system," in Proc. IEEE 5th Annu. Conf. Jpn. Power Energy, Tokyo, Japan, Jul. 1994,pp 53-58.

[5] X. Wang and X. Wang, "Feasibility study of fractional frequency transmission system," IEEE Trans. Power Syst., vol. 11, no. 2, pp. 962-967, May 1996.

[6] X. Wang, C. Cao, and Z. Zhou, "Experiment on fractional frequency transmission system," IEEE Trans. Power Syst., vol. 21, no. 1, pp. 372-377, Feb. 2006.

[7] U. Satpute, S. Jangamshetty, and D. Joshi, "Feasibility study of fractional frequency transmission system," in Proc. Joint Int. Conf. Power Electron. Drives Energy Syst., New Delhi, India, Dec. 2010, pp. 1-6.

[8] X. Wang, "Fractional frequency transmission system and its applications on wind power and renewable resource integration into system," Power Elect. Eng., vol. 2, no. 1, pp. 12-14, 2008.

[9] W. Fischer, R. Braun and I. Erlich, "Low frequency high voltage offshore grid for transmission of renewable power", proc. of 3rd IEEE PES Innovative SmartGrid Technologies Europe, Berlin, Oct. 2012.

[10] X. Wang, "Fractional frequency wind power system," Mod. Elect. Power, vol. 24, no. 1, p. 1, 2007

[11] Z. Song, X. Wang, Y. Teng, L. Ning, and Y. Meng, "Optimum control study for fractional frequency wind power system," in Proc. Asia-Pac. Power Energy Eng. Conf. Shanghai, China, Mar. 2012, pp. 1-5.

[12] O. Gomis-Bellmunt, A. Junyent-Ferr´e, A. Sumper, and S. Galceran-Arellano, "Maximum generation power evaluation of variable frequency offshore wind farms when connected to a single power converter," Appl.Energy, vol. 87, no. 10, pp. 3103–3109, Oct. 2010.

[13] Xifan Wang, Xiaohui Wei, and YongqingMeng, "Experiment on grid-connection process of wind turbines in fractional frequency wind power system," IEEE Trans. On Energy Conversion, vol. 30, no. 1, pp. 22-31, March 2015.

Appendix

Table 2: Design and performance parameters of 2MVA, 690V, Salient pole Synchronous Generator

Design and performance parameters	5Hz	10Hz	50/3Hz	20Hz	25Hz	30Hz	35Hz	40Hz	45Hz	50Hz
Optimal Cost (M €)	0.7355	0.4152	0.2661	0.2291	0.1935	0.1689	0.1490	0.1360	0.1258	0.1166
Stator Bore Diameter (m)	3.9244	4.5426	5.2074	5.5080	5.8600	6.2130	6.4700	6.7840	6.9900	7.2640
Stator Length (m)	0.8219	0.6205	0.4674	0.4220	0.3760	0.3370	0.3080	0.2842	0.2649	0.2481
Poles	18	34	58	70	86	104	120	138	154	172
Turns/pole	51	56	66	69	72	77	80	85	86	88
Flux/pole (wb)	0.3655	0.1668	0.0849	0.0677	0.0519	0.0404	0.0334	0.0275	0.0242	0.0213
Volume of stator iron (m^3)	1.8363	0.8836	0.4656	0.3753	0.2871	0.2267	0.1791	0.1484	0.1259	0.1060
Volume of stator copper (m^3)	0.2026	0.1624	0.1482	0.1426	0.1363	0.1345	0.1320	0.1329	0.1281	0.1258
Volume of rotor iron (m^3)	3.3626	1.8963	1.1727	0.9993	0.8236	0.6951	0.6032	0.5330	0.4825	0.4446
Volume of rotor copper (m^3)	0.2841	0.2210	0.1982	0.1805	0.1720	0.1681	0.1571	0.1527	0.1520	0.1430
Loss (MW)	0.4197	0.2839	0.2289	0.2118	0.1833	0.1739	0.1632	0.1585	0.1539	0.1485
Efficiency (%)	79.400	85.100	87.910	88.840	89.670	90.170	90.690	90.940	91.230	91.540
Stator temp rise (^{0}c)	196.05	141.89	107.00	98.210	88.720	77.610	75.970	68.350	66.194	64.250
Rotor temp rise (^{0}c)	236.32	214.99	190.32	188.73	174.63	164.77	160.75	159.32	144.42	144.54

Table 3: Design and performance parameters of 2MVA, 0.69/33kV, 3-phase core type transformer

Design and performance parameters	5Hz	10Hz	50/3Hz	20Hz	25Hz	30Hz	35Hz	40Hz	45Hz	50Hz
Optimal Cost (M €)	0.2350	0.1447	0.0999	0.0838	0.0678	0.0571	0.0496	0.0434	0.0391	0.0354
Constant (k)	0.1150	0.1524	0.3353	0.3556	0.3830	0.4064	0.4350	0.4427	0.4669	0.4801
Core area (m^2)	0.1544	0.1023	0.1351	0.1194	0.1029	0.0910	0.0835	0.0743	0.0697	0.0645
Primary turns	77	60	28	25	25	24	24	21	21	21
Secondary turns	3705	2795	1275	1200	1100	1050	975	950	900	875
Width of transformer (m)	1.9492	1.5867	1.8230	1.7138	1.5907	1.4960	1.4328	1.3521	1.3092	1.2594
Height of transformer (m)	1.3875	1.1294	1.2977	1.2199	1.1323	1.0648	1.0199	0.9624	0.9319	0.8965
Volume of core (m^3)	6970	3760	5700	4730	3790	3150	2770	2330	2110	1880
Volume of copper (m^3)	6180	4230	439	400	359	338	317	309	269	266
Loss (MW)	0.1258	0.0831	0.0717	0.0614	0.0549	0.0513	0.0431	0.0469	0.0407	0.0395
Efficiency (%)	92.7658	95.066	95.858	96.311	96.661	96.895	97.380	97.153	97.519	97.500
Regulation (%)	4.5138	3.4294	19.519	21.298	26.561	32.104	21.080	49.623	38.329	47.159
No-load current as % of full load current (%)	7.2447	5.9768	11.522	12.000	11.134	10.882	12.368	9.8491	10.792	10.386

ASTES

Advances in Science, Technology and Engineering Systems Journal
Vol. 4, No. 2, 162-169 (2019)
www.astesj.com
Special Issue on Advancement in Engineering and Computer Science

ASTES Journal
ISSN: 2415-6698

Feature Selection for Musical Genre Classification Using a Genetic Algorithm

Abba Suganda Girsang[1], Andi Setiadi Manalu[1], Ko-Wei Huang[*,2],

[1]*Computer Science Department, BINUS Graduate Program-Master of Computer Science Bina Nusantara University Jakarta, Indonesia 11480*

[2]*Department of Electrical Engineering, National Kaohsiung University of Science and Technology, Kaohsiung City, Taiwan*

ARTICLEINFO

Article history:
Received: 11 January, 2019
Accepted: 13 March, 2019
Online: 23 March, 2019

Keywords:
Music genre classification
Feature extraction
Genetic algorithm
Machine learning
Low-level features

ABSTRACT

Music genre classification is an important multimedia research domain, including aspects of music piece representation, distances between genres, and categorization of music databases. The objective of this study was to develop a model for automatic classification of musical genres from audio data by using features from low-level time and frequency domains. These features can highlight the differences between different genres. In the model, feature selection is performed using a genetic algorithm (GA), and the resulting dataset is classified using the k-nearest neighbor (KNN), naive Bayes classifier (NBC), and support vector machine (SVM) learning methods. Tenfold cross-validation is used to obtain the optimal f-measure value. In this study, the data were obtained from the GTZAN genre collection datasets. In the performance evaluation, it was found that the GA-based feature selection strategy can improve the F-measure rate from 5% to 20% for the KNN, NBC, and SVM-based algorithms. In addition, the proposed SVM-GA algorithm can exactly better than other comparison algorithms.

1 Introduction

Music genre classification is used to categorize musical data into suitable categories based on shared characteristics. In the modern era, numerous musical genres are appreciated, such as blues, classical, country, disco, hip-hop, jazz, metal, pop, reggae, and rock. New technologies and globalization have been beneficial for the evolution of music, leading to the emergence of world music. These developments have increased research interest in music information retrieval (MIR), a field of automatic music management including music recommendation [1], music mood classification [2], and musical instrument classification [3]. As musical genres are most commonly used to manage music databases, a previous study investigated the extraction of audio features and techniques for classifying musical genres [4, 5, 6, 7]. However, genre classification has remained a challenge[8, 9], as it requires systems that are capable of performing automatic grouping [10] and querying retrieving data from large a music data set [8]. The identification of commonalities between genres requires feature extraction [11]. In the case of audio files, combinations of relevant features are used for modeling the musical genre [4]. These features may include timbral texture, rhythmic content, and pitch content [12]. Musical genres have been modeled using different features including short-term Mel-frequency cepstral coefficients (MFCCs) [13, 14], and Daubechies wavelet coefficient histograms (DWCHs), depending on the required application. Features are selected to improve performance and accuracy [15]. Achieving optimal feature selection and extracting appropriate features and dimensions of the features reduction are very challenging tasks [16, 17]. There are many different approaches that have been proposed to classify music genre, such as data mining [18, 19], deep learning strategy [20, 21, 22, 23, 24], and machine learning stretegies such as hidden Markov model, AdaBoost, and support vector machine [25, 26, 27, 28, 29, 30, 31, 32, 33, 34].

In addition to the above, musical genre classification problems can be solved with constant evolutionary algorithms [35]. Among them, a genetic algorithm (GA) based optimization has become a widely used approach for optimizing the selection of relevant features [36, 37, 38, 39, 40].

*Corresponding Author: Ko-Wei Huang, Department of Electrical Engineering, National Kaohsiung University of Science and Technology, Kaohsiung City, Taiwan Contact No & elone.huang@nkust.edu.tw

https://dx.doi.org/10.25046/aj040221

Among the several methods developed for musical genre classification, the performance of classification algorithms has become the benchmark [41]. In this paper, we propose a model for musical genre classification using low-level time and frequency-domain features for short and mid-term feature extraction. In this model, feature extraction is performed using a GA, and musical genre classification is conducted using a range of machine learning algorithms, including the K-Nearest Neighbor (KNN) [42], Nave Bayes Classifier (NBC) [43], and the Support Vector Machine (SVM) [25] were used for music genre classification. In the performance evaluation, it was found that the GA-based feature selection strategy can improve the F-measure rate from 5% to 20% for the KNN, NBC and SVM-based algorithms. In addition, the proposed support vector machine genetic algorithm (SVM-GA) algorithm can exactly better than other comparison algorithms

The remainder of this paper is organized as follows. Section 2 provides background information and discusses related studies. The proposed algorithm is presented in Section 3, and its performance is evaluated in Section 4. Finally, the conclusions and future research are presented in Section 5.

2 Literature review

The primary challenge in genre identification is selecting features for extraction from audio data [8]. Audio data comprise a series of samples that together represent an audio signal. Classification cannot simply be applied to the audio samples. In previous studies, audio analysis has been prominently performed by extracting numerical values for representative features. In music signals, these features correspond to primary dimensions such as pitch, rhythm, harmony, melody, timbre, and spatial location. Low-level features, such as temporal, energy, and spectral features, are some of the most prominently used features in sound signal analysis. In audio signal analysis, low-level features are generally extracted from the time and frequency domains [44]. Moreover, 11 sets of low-level time- and frequency-domain features are prominently used.

2.1 Time-domain audio features

In general, time-domain features are directly extracted from samples of audio signals. The features include short-term energy, short-term zero-crossing rate, and entropy. These features provide a simple approach to analyzing audio signals, and combining these features with sophisticated frequency-domain features is generally essential.

(1) Energy: The sum of squares of signal values, normalized by the respective frame length.

(2) Zero-Crossing Rate: The rate at which the sign of the signal changes within a particular frame.

(3) Entropy of Energy: The entropy of the normalized energies of subframes, which can be interpreted as a measure of abrupt changes in the signal.

2.2 Frequency-domain audio features

The discrete Fourier transform (DFT) is extensively used in audio signal analysis, because it provides a convenient representation of the frequency content distribution of a signal as a sound spectrum. Numerous audio features are based on the DFT of a signal. These are termed frequency-domain (or spectral) audio features.

(1) Spectral Centroid: The center of gravity of a spectrum.

(2) Spectral Spread: The second central moment of a spectrum.

(3) Spectral Entropy: The entropy of the normalized spectral energies for a set of sub-frames.

(4) Spectral Flux: The squared difference between normalized magnitudes of the spectra of two successive frames.

(5) Spectral Rolloff: The frequency below which 90% of the magnitude distribution of a spectrum is concentrated.

(6) MFCCs: MFCCs are used to capture short-term, spectral-based features. The logarithm of the amplitude spectrum based on a short-time Fourier transform is derived for each frame. Frequency bins are then grouped and smoothed using Mel-frequency scaling to ensure that they agree with predetermined concepts. MFCCs are generated by decorrelating Mel-spectral vectors by using a discrete cosine transform.

(7) Chroma Vector: A chroma vector is a 12-element representation of spectral energy, wherein bins represent 12 equal-tempered pitch classes of Western music (semitone spacing).

(8) Harmonic: Harmonic features represent beats, and the harmonic ratio and fundamental frequency are two harmonic features.

Although studies have been conducted on music genre classification, the most accurate results have been achieved using the GTZAN dataset. A comprehensive set of features was proposed for the direct modeling of music signals [4]. When these features were employed for genre classification by using KNNs and Gaussian Mixture models (GMMs), an accuracy rate of 61% was achieved. A novel feature extraction method was proposed for musical genre classification, wherein DWCHs are combined with machine learning classification algorithms, including SVMs and linear discriminant analysis [14]. An accuracy of 78.5% was obtained with this method. Feature integration methods and late information fusion were examined in a previous study [12], by using majority voting for classification of all short-time features. A novel feature integration technique using an autoregressive (AR) model was proposed. This approach was reported to exhibit superior performance to that obtained by the use of mean variance features. Another study [45] addressed musical genre classification from a multilinear perspective. Multiscale spectro-temporal modulation features were extracted on the basis of an auditory cortical processing model, which provided an accuracy of 78.2%. Nonnegative matrix factorization was used to obtain a novel description of the timbre of musical sounds[13]. A spectrogram was factorized, which provided a characteristic spectral analysis. Gaussian Mixture Models were then applied, to achieve a reported accuracy of 74%. An ensemble approach [37], involving the use of multiple feature vectors and time and space decomposition strategies was also reported in a previous study. In the study, time decomposition was performed using feature vectors, which were extracted from music segments obtained from the beginning, middle, and end of the original signal. The study also employed four machine learning algorithms, namely NBC, decision trees, SVMs, and multilayer perceptron (MLP) neural nets, which provided a maximum accuracy of 65.06%. In an alternative approach [46], a method based on the classification accuracy of an SVM classifier was proposed for selecting training instances. These instances comprised feature vectors representing short-term, low-level characteristics in an audio signal. This method was reported to provide an accuracy of 59.6%. An invariance of MFCCs to musical key and tempo was explored in a previous study[47]. The study indicated that MFCCs encode both timbral and key information. An accuracy of 69.3% was achieved by applying GMMs. The acoustic signal feature can be derived using a mathematical model that represents the acoustic signal [39]. In this approach, features were selected using a GA. Classification was then performed by generating an adjusted KNN classifier. The reported accuracy was 67.6%. In a previous study, a subspace cluster analysis process was used to automate the construction of a classification tree[48]. Experimental results validated the tree-building algorithm, and the study provided a new research direction for automatic genre classification. Several machine learning algorithms were employed, such as KNNs, J48, logistic regression (LOG), LibSVM with a radial basis function kernel, MLP neural networks, and sequential minimal optimization (SMO) SVM with a polynomial kernel. This method was reported to achieve an accuracy of 72.9%. Another study[49] proposed automatic musical genre classification by using spectral, time-domain, tonal, rhythmic, sound effect, and high-level descriptors. An analysis was conducted using KNNs, an SVM, and a GMM, with a resulting accuracy of 79.7%.

3 Methods

3.1 Feature extraction

Feature extraction is a crucial step in audio analysis, because it is also required in other pattern recognition and machine learning tasks. Extraction is performed in the following two steps: short- and mid-term processes. In short-term feature extraction, the input signal is divided into brief windows (or frames), and the number of features is computed for each frame, generating a sequence of short-term feature vectors from the entire signal. In mid-term extraction, statistical analysis is generally applied to these short-term feature sequences to obtain the signal. Several statistics, including mean, median, standard deviation, standard deviation by mean, max, and min, are derived for each short-term feature sequence. The data are then normalized to avoid the introduction of anomalies and minimize redundancy

3.2 Machine learning methods (naive Bayes classifier (NBC), K-nearest neighbor (KNN), support vector machine (SVM)) combined with genetic algorithm (GA)

Fig. 1 shows the system design. GA optimization is combined with the KNN, NBC, and SVM learning methods. The fitness function uses the largest f-measure value derived using machine learning, and is evaluated using 10-fold cross-validation. The system then derives the maximum fitness.

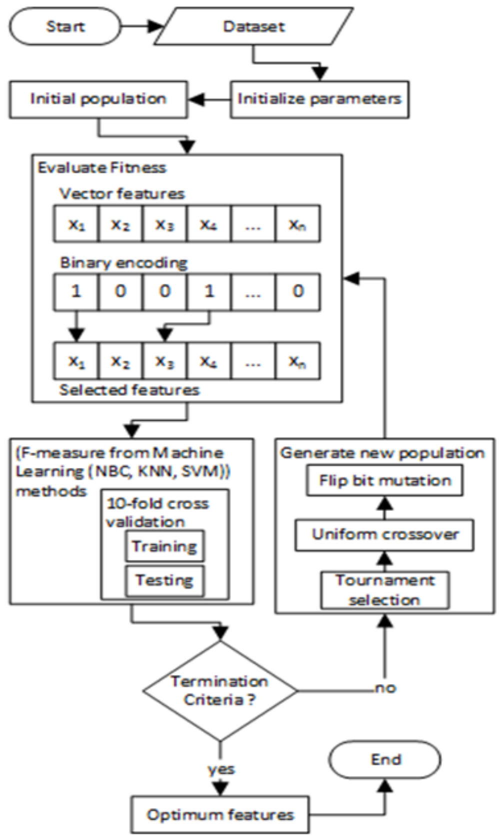

Figure 1: Machine learning methods (NBC, KNN, SVM) combined with GA

(1) The dataset is a feature vector containing normalized data. All necessary parameters are initialized. The initial population is generated and encoded in binary $\{0,1\}$. Individual solutions are randomly generated to form the initial population $P = \{S_1, S_2, S_3, \cdots, S_n\}$; $S_1 = S_2 = S_3 = \cdots = S_n = \{G_1, G_2, G_3, \cdots, G_n\}$. Here S is a solution and G_n represents features, where $G_n \in \{0,1\}$; feature labeled 0 are not used, whereas those labeled 1 are used.

(2) The fitness of each solution (S) is evaluated using the highest f-measure value for musical genre classification conducted through the KNN, NBC, and SVM learning methods, following the 10-fold cross-validation method. The highest fitness value indicates the optimal classification result.

(3) After all fitness values are obtained, tournament selection is used to select parents. This prominently used method probabilistically selects genomes for recombination; the selection is based on fitness. The algorithm

randomly selects genomes from the population to compete in tournaments of user-selected size T. The genome with the highest fitness value in each tournament is selected for recombination.

(4) A uniform crossover is primarily used for problems, wherein elements in the genome are independent of each other. In this case, the locations of genes relative to each other in the genome do not influence fitness. The probability of crossover per gene is set by the user. The uniform crossover process generates a solution in the (t+1)th generation by randomly selecting genes from each of the winners, corresponding to the relevant locations.

(5) A matrix of 1s and 0s is generated, and mutation is applied individually to each element. The probability of mutation per gene is set by the user. The selected values are interchanged such that 1s become 0s (and vice versa).

(6) Crossover and mutation then generate a new population (solution), whose fitness value is reevaluated.

(7) The process is stopped when the required criteria are satisfied; otherwise, the fitness is reevaluated.

(8) The GA then identifies the optimal solution, which in this case is a set of optimal features.

3.3 Evaluation

For the proposed method, selected audio files were used as validation data in this study. Each file was tested through cross-validation for ensuring its allocation to the accurate class. The result was presented in a confusion matrix summarizing accurately and inaccurately classified cases. The f-measure value was calculated from the matrix to determine the optimal classification. The harmonic mean of precision and recall was used as the f-measure value, with the highest f-measure value indicating the most accurate classification.

4 Experimental results

4.1 Environment setting

The data used in this study comprised instrumental music files from the GTZAN genre collection datasets[4]. The data were obtained from the following source:[1]. The dataset comprised 1000 30-s music files in an audio format at a sampling rate of 22050 Hz in 16-bit mono. Samples were classified into the following 10 musical genres: blues, classical, country, disco, hip-hop, jazz, metal, pop, reggae, and rock. The raw data were obtained from audio data files. The data were preprocessed by converting the data files into a numerical form before the execution of feature extraction. A total of 11 sets of low-level time- and frequency-domain features were extracted.

All experiments were performed over 15 independent runs and conducted using MATLAB 2016b with the parallel toolbox. The experiments were conducted on a standard laptop with an Intel i5-3320M 2.60-GHz CPU and 4-GB RAM.

4.2 Without feature selection

4.2.1 Experimental results obtained using KNN

As presented in Table 1, the KNN method performed data execution in less than 1 second in all experiments, with the F-measure mean (Fmean) time being 0.87s and a standard deviation (Fsd) time of 0.03s, yielding an Fmean of 66.2%. The difference between the best F-measure (Fbest) and the worst F-measure (Fworst) was not significant, at 1.4%. Moreover, the Fsd value was negligible, at 0.5%. For classification, the f-measure range was 65.5% to 66.9%. In the results shown, the performance of KNN is less than 70%, but very quickly classifies the music data, owing to the fact that KNN does not need the training process..

[1] http://marsyasweb.appspot.com/download/data_sets

Table 1: Results obtained by KNN without feature selection

Fbest		Fworst		Fmean		Fsd	
Value	time(s)	Value	time(s)	Value	time(s)	Value	time(s)
66.9%	0.67	65.5%	0.83	66.2%	0.83	0.5%	0.03

Table 2: Results Obtained by NBC without Feature Selection

Fbest		Fworst		Fmean		Fsd	
Value	time(s)	Value	time(s)	Value	time(s)	Value	time(s)
59.1%	9.07	56.8%	8.90	58.0%	8.93	0.6%	0.08

Table 3: Results Obtained by SVM without Feature Selection

Fbest		Fworst		Fmean		Fsd	
Value	time(s)	Value	time(s)	Value	time(s)	Value	time(s)
77.0%	14.37	75.3%	12.36	76.2%	13.16	0.005%	1.69

4.2.2 Experimental results obtained using NBC

Table 2 shows the NBC results. The Fmean time for data execution was 8.93s, with an Fsd time of 0.08s for each experiment and an Fmean of 58%. The difference between Fbest and Fworst was not significant, at 2.3%. Fsd was also very small, at 0.6%. For classification, the f-measure range was approximately 56.8% to 59.1%. In the results show, the performance of NBA is less than 60% and even slower than the KNN.

4.2.3 Experimental results obtained using SVM

Table 3 shows the SVM results. For all experiments, the Fmean and Fsd times for data execution were 13.16 and 1.69 s, respectively, with an Fmean of 0.762 (76.2%). The difference between Fbest and Fworst was 0.017 (1.7%), which was nonsignificant. Moreover, the Fsd value was 0.005 (0.5%), which was negligible. The f-measure range for classification was 0.7530.770 (75.3%77.0%).

4.3 With GA feature selection

4.3.1 Parameter Setting

The previous result shows that KNN is the best algorithm for F-measure and computation times. Thus, in this section we will try to import the GA-based feature selection strategy into these three algorithms. The basic parameter settings of all experiments are listed in Table 4. All experimental results are collected from 15 independent runs, each of 100 iterations.

Table 4: GA parameter settings

Parameter	Setting
iteration	100
population	15
crossover rate	90%
mutation rate	1%
selection operator	tournament
crossover operator	uniform
tournament size	2
Number of features	204

4.3.2 Experimental results obtained using KNNGA

From Table 5, it can be seen that KNN-GA required less than 5s for data execution in each experiment. The Fmean time of 4.74 s and Fsd time of 0.43 s gave an Fmean of 71.3%. The difference between Fbest and Fworst was not significant, at 1.2%. Fsd was also very small, at 0.3%. For classification, the approximate f-measure range was 70.8% to 72%. . In summary, we found that the GA-based feature selection will improve the 5% F-measure rates with the KNN approach.

4.3.3 Experimental results obtained using NBCGA

From Table 6 it can be seen that, for data execution, the NBC-GA required a fairly long Fmean time of 61.46 s. With the Fsd time of 8.50 s for each experiment, this gave an Fmean of 66.8%. The difference between Fbest and Fworst was not significant, at 0.9%. The Fsd was also insignificant, at 0.3%. The f-measure range for classification was approximately 66.4% to 67.3%. In summary, we found that the GA-based feature selection will improve the 10% F-measure rates with the NBC approach.

4.3.4 Experimental results obtained using SVMGA

As can be seen from Table 7, SVM-GA required a fairly long Fmean time for data execution, of 125.614s. With an Fsd time of 44.29s from each experiment, the Fmean was 79.5%. The difference between Fbest and Fworst was not significant, at 1.1%. The Fsd was also very small, at 0.3%. The f-measure range for classification was approximately 79.0% to 80.1%. In summary, we found that the GA-based feature selection will improve about the 3-5% F-measure rates with the SVM approaches.

4.3.5 Convergence Rates of KNN-GA, NBC-GA, and SVM-GA

The graphs in Figs 2, 3, and 4 reach steady state because they include a stop criterion at the 100th iteration when the process ended.

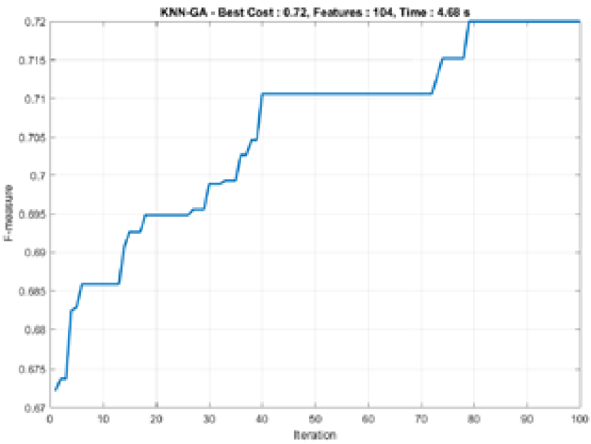

Figure 2: Convergence rates of KNN with Genetic Algorithm

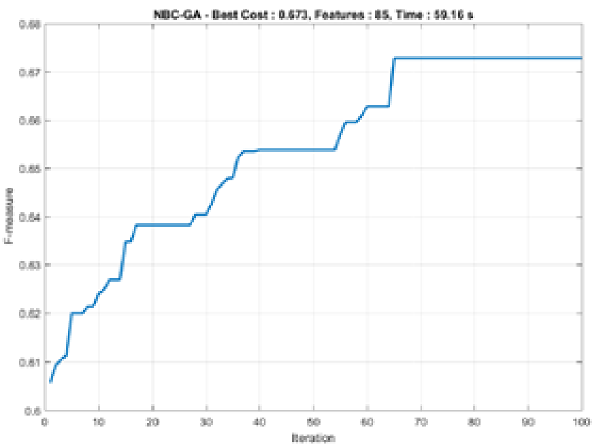

Figure 3: Convergence rates of NBC with Genetic Algorithm

Table 5: Results Obtained by KNN with Feature Selection

Fbest		Fworst		Fmean		Fsd	
Value	time(s)	Value	time(s)	Value	time(s)	Value	time(s)
72.0%	4.68	70.8%	4.66	71.3%	4.74	0.003%	0.43

Table 6: Results Obtained by NBC with Feature Selection

Fbest		Fworst		Fmean		Fsd	
Value	time(s)	Value	time(s)	Value	time(s)	Value	time(s)
67.3%	59.16	66.4%	57.52	66.8%	61.46	0.3%	8.50

Table 7: Results Obtained by SVM with Feature Selection

Fbest		Fworst		Fmean		Fsd	
Value	time(s)	Value	time(s)	Value	time(s)	Value	time(s)
80.1%	121.19	79.0%	123.46	79.5%	141.05	0.3%	44.29

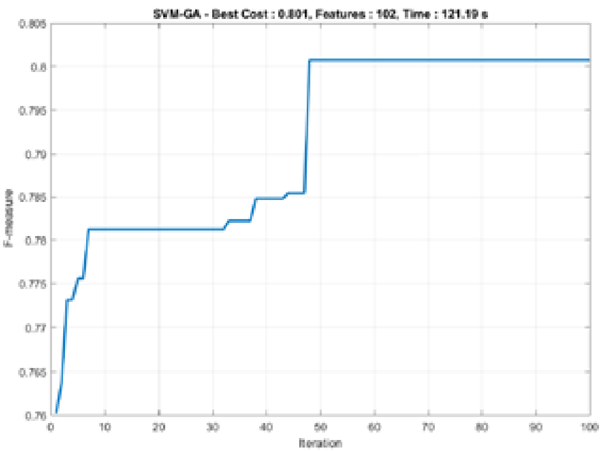

Figure 4: Convergence rates of SVM with Genetic Algorithm

4.4 Comparison of F-measure values

The performance is assessed based on Eq. 1.

$$\Delta F_M = \left(\frac{F_{new} - F_{orig}}{F_{orig}} \right) \times 100\% \tag{1}$$

Here, ΔF_M denotes the improvement of the F-measure values, Δt_{avg} denotes the improvement of computation time, F_{new} denotes the F-measure values of the KNN, NBA, and SVM algorithm performing the genetic algorithm feature selection, and F_{orig} denotes the KNN, NBA, and SVM algorithms without performing any feature selection strategy, and t_{avg} is the computation time in seconds.

Table 8 shows that the average increase in the Fmean value was approximately 7.24% for KNN-GA, approximately 13.27% for NBC-GA, and 4.23% for SVM-GA. However, in order to perform the feature selection strategy, the computation time was increased to between 500% and 871%. In summary, the feature selection increases the quality of the solution, but with a massive increase in computation time, especially with SVM-GA, which requires spending more than 10 times the computation time..

4.5 Comparison of results in this study with those in previous studies

Previous results showed the ability of a GA to improve the quality of result classification by reducing features. The existing algorithm performs poor quality classification (approximate Fmean 59%66%). Moreover, by feature selection using the GA, the quality classification can be improved until Fmean is 67%80%. In this section, we compare the proposed algorithm with other algorithms to verify the performance or proposed algorithms. Table 9 compares the accuracy of different methods with our proposed algorithms, KNN-GA, NBA-GA, and SVM-GA, using the highest measure achieved by each. All studies used the same GTZAN Genre Collection Data Sets [4]. The KNN-GA method from the current study produced an Fbest value of 72%, which is better than the comparison algorithms of [4, 39, 47, 48]. The NBC-GA method produced an Fbest value of 67.3%, which exceeded that reported in [4]. The SVM-GA method produced an Fbest value of 80.1%, which exceeded previous studies. In summary, the GA combined with the SVM method can obtain a better solution than other algorithms.

5 Conclusions and Future work

In this study, automatic musical genre classification was conducted by combining GA optimization with three machine learning methods. This approach entails using low-level time- and frequency-domain features. The features are extracted using short- and mid-term processes. The optimal classification accuracy levels achieved in the study were determined to be comparable to those achieved by other state-of-the-art musical genre classification algorithms. However, the feature selection strategy will consume a massive amount of computation time. As part of our future research, we aim to investigate three aspects: 1) applying other meta-heuristic methods such as particle swarm optimization (PSO) to select low-level features; 2) combining deep-learning techniques such as CNN with a meta-heuristic algorithm to improve the accuracy of classification results; and 3) decreasing the computation time by using feature reduction mechanisms to make the algorithm perform more effectively.

Table 8: Comparison of f-measure values

Measure	KNN-GA		NBA-GA		SVM-GA	
	ΔF_M	$\Delta\ t_{avg}$	ΔF_M	$\Delta\ t_{avg}$	ΔF_M	$\Delta\ t_{avg}$
Fbest	7.08	598	12.18	552	3.87	743
Fworst	7.49	461	14.46	546	4.68	898
Fmean	7.15	444	13.17	588	4.15	971
Average	7.24	501	13.27	562	4.23	871

Table 9: Comparison with previous studies

Algorithm	Feature Selection	Accuracy
Tzanetakis et al. [4]	none	61.0%
Li et al. [14]	none	78.5%
Holzapfel et al. [13]	none	74.0%
Panagakis et al. [45]	none	78.2%
Li et al. [47]	none	69.3%
Karkavitsas et al. [39]	Hybrid GA	67.6%
Ariyaratne et al. [48]	none	71.3%
Martins de Sousa et al. [49]	none	79.7%
KNN-GA	GA	**72.0%**
NBA-GA	GA	**67.3%**
SVM-GA	GA	**80.1%**

6 Acknowledgement

This work was supported in part by the Ministry of Science and Technology, Taiwan, R.O.C., under grants MOST 107-2218-E-992-303-.

References

[1] Markus Schedl. The lfm-1b dataset for music retrieval and recommendation. In *Proceedings of the 2016 ACM on International Conference on Multimedia Retrieval*, pages 103–110. ACM, 2016.

[2] Xiao Hu, Kahyun Choi, and J Stephen Downie. A framework for evaluating multimodal music mood classification. *Journal of the Association for Information Science and Technology*, 68(2):273–285, 2017.

[3] DG Bhalke, CB Rama Rao, and Dattatraya S Bormane. Automatic musical instrument classification using fractional fourier transform based-mfcc features and counter propagation neural network. *Journal of Intelligent Information Systems*, 46(3):425–446, 2016.

[4] G. Tzanetakis and P. Cook. Musical genre classification of audio signals. *IEEE Transactions on Speech and Audio Processing*, 10(5):293–302, 2002.

[5] R Hillewaere. Computational models for folk music classification. *Vrije Universiteit Brussel*, 2013.

[6] Débora C Corrêa and Francisco Ap Rodrigues. A survey on symbolic data-based music genre classification. *Expert Systems with Applications*, 60:190–210, 2016.

[7] Izaro Goienetxea, José María Martínez-Otzeta, Basilio Sierra, and Iñigo Mendialdua. Towards the use of similarity distances to music genre classification: A comparative study. *PloS one*, 13(2):e0191417, 2018.

[8] Z. Fu, G. Lu, K. M. Ting, and D. Zhang. A survey of audio-based music classification and annotation. *IEEE Transactions on Multimedia*, 13(2):303–319, 2011.

[9] Marius Kaminskas and Francesco Ricci. Contextual music information retrieval and recommendation: State of the art and challenges. *Computer Science Review*, 6(2):89–119, 2012.

[10] N. Scaringella, G. Zoia, and D. Mlynek. Automatic genre classification of music content: a survey. *IEEE Signal Processing Magazine*, 23(2):133–141, 2006.

[11] Dalibor Mitrovi, Matthias Zeppelzauer, and Christian Breiteneder. Features for content-based audio retrieval. volume 78, pages 71–150. Elsevier, 2010.

[12] A. Meng, P. Ahrendt, and J. Larsen. Improving music genre classification by short time feature integration. In *Proceedings. (ICASSP '05). IEEE International Conference on Acoustics, Speech, and Signal Processing, 2005.*, volume 5, pages v/497–v/500 Vol. 5, 2005.

[13] A. Holzapfel and Y. Stylianou. Musical genre classification using nonnegative matrix factorization-based features. *IEEE Transactions on Audio, Speech, and Language Processing*, 16(2):424–434, 2008.

[14] Tao Li, Mitsunori Ogihara, and Qi Li. A comparative study on content-based music genre classification. In *Proceedings of the 26th Annual International ACM SIGIR Conference on Research and Development in Informaion Retrieval*, pages 282–289, 2003.

[15] Girish Chandrashekar and Ferat Sahin. A survey on feature selection methods. *Computers & Electrical Engineering*, 40(1):16 – 28, 2014.

[16] I. Vatolkin, W. Theimer, and G. Rudolph. Design and comparison of different evolution strategies for feature selection and consolidation in music classification. In *2009 IEEE Congress on Evolutionary Computation*, pages 174–181, 2009.

[17] Babu Kaji Baniya, Joonwhoan Lee, and Ze-Nian Li. Audio feature reduction and analysis for automatic music genre classification. In *2014 IEEE International Conference on Systems, Man, and Cybernetics (SMC)*, pages 457–462. IEEE, 2014.

[18] Mangesh M Panchwagh and Vijay D Katkar. Music genre classification using data mining algorithm. In *2016 Conference on Advances in Signal Processing (CASP)*, pages 49–53. IEEE, 2016.

[19] Nimesh Ramesh Prabhu, James Andro-Vasko, Doina Bein, and Wolfgang Bein. Music genre classification using data mining and machine learning. In *Information Technology-New Generations*, pages 397–403. Springer, 2018.

[20] Arjun Raj Rajanna, Kamelia Aryafar, Ali Shokoufandeh, and Raymond Ptucha. Deep neural networks: A case study for music genre classification. In *2015 IEEE 14th International Conference on Machine Learning and Applications (ICMLA)*, pages 655–660. IEEE, 2015.

[21] Il-Young Jeong and Kyogu Lee. Learning temporal features using a deep neural network and its application to music genre classification. In *Ismir*, pages 434–440, 2016.

[22] Sergio Oramas, Oriol Nieto, Francesco Barbieri, and Xavier Serra. Multi-label music genre classification from audio, text, and images using deep features. *arXiv preprint arXiv:1707.04916*, 2017.

[23] Yandre MG Costa, Luiz S Oliveira, and Carlos N Silla Jr. An evaluation of convolutional neural networks for music classification using spectrograms. *Applied soft computing*, 52:28–38, 2017.

[24] L Rafael Aguiar, MG Yandre Costa, and N Carlos Silla. Exploring data augmentation to improve music genre classification with convnets. In *2018 International Joint Conference on Neural Networks (IJCNN)*, pages 1–8. IEEE, 2018.

[25] Thorsten Joachims. Text categorization with support vector machines: Learning with many relevant features. In *European conference on machine learning*, pages 137–142. Springer, 1998.

[26] Wei Chai and Barry Vercoe. Folk music classification using hidden markov models. In *Proceedings of international conference on artificial intelligence*, volume 6. sn, 2001.

[27] Guodong Guo and Stan Z Li. Content-based audio classification and retrieval by support vector machines. *IEEE transactions on Neural Networks*, 14(1):209–215, 2003.

[28] Changsheng Xu, Namunu Chinthaka Maddage, and Xi Shao. Automatic music classification and summarization. *IEEE transactions on speech and audio processing*, 13(3):441–450, 2005.

[29] Alexios Kotsifakos, Evangelos E Kotsifakos, Panagiotis Papapetrou, and Vassilis Athitsos. Genre classification of symbolic music with smbgt. In *Proceedings of the 6th international conference on PErvasive technologies related to assistive environments*, page 44. ACM, 2013.

[30] Kamelia Aryafar, Sina Jafarpour, and Ali Shokoufandeh. Automatic musical genre classification using sparsity-eager support vector machines. In *Proceedings of the 21st International Conference on Pattern Recognition (ICPR2012)*, pages 1526–1529. IEEE, 2012.

[31] Loris Nanni, Yandre MG Costa, Alessandra Lumini, Moo Young Kim, and Seung Ryul Baek. Combining visual and acoustic features for music genre classification. *Expert Systems with Applications*, 45:108–117, 2016.

[32] AB Mutiara, R Refianti, and NRA Mukarromah. Musical genre classification using support vector machines and audio features. *TELKOMNIKA TELKOMNIKA (Telecommunication, Computing, Electronics and Control)*, 14:1024–1034, 2016.

[33] Hareesh Bahuleyan. Music genre classification using machine learning techniques. *arXiv preprint arXiv:1804.01149*, 2018.

[34] Aldona Rosner and Bozena Kostek. Automatic music genre classification based on musical instrument track separation. *Journal of Intelligent Information Systems*, 50(2):363–384, 2018.

[35] B. Xue, M. Zhang, W. N. Browne, and X. Yao. A survey on evolutionary computation approaches to feature selection. *IEEE Transactions on Evolutionary Computation*, 20(4):606–626, 2016.

[36] Il-Seok Oh, Jin-Seon Lee, and Byung-Ro Moon. Hybrid genetic algorithms for feature selection. *IEEE Transactions on Pattern Analysis and Machine Intelligence*, 26(11):1424–1437, 2004.

[37] C. N. Silla Jr., A. L. Koerich, and C. A. A. Kaestner. Feature selection in automatic music genre classification. In *2008 Tenth IEEE International Symposium on Multimedia*, pages 39–44, 2008.

[38] Dragan Matic. A genetic algorithm for composing music. volume 20, pages 157–177, 2010.

[39] George V. Karkavitsas and George A. Tsihrintzis. Automatic music genre classification using hybrid genetic algorithms. In *Intelligent Interactive Multimedia Systems and Services*, pages 323–335, 2011.

[40] Chih-Fong Tsai, William Eberle, and Chi-Yuan Chu. Genetic algorithms in feature and instance selection. *Knowledge-Based Systems*, 39:240 – 247, 2013.

[41] Bob L. Sturm. Classification accuracy is not enough. *Journal of Intelligent Information Systems*, 41(3):371–406, 2013.

[42] Muhammad Atif Tahir, Ahmed Bouridane, and Fatih Kurugollu. Simultaneous feature selection and feature weighting using hybrid tabu search/k-nearest neighbor classifier. *Pattern Recognition Letters*, 28(4):438–446, 2007.

[43] Jingnian Chen, Houkuan Huang, Shengfeng Tian, and Youli Qu. Feature selection for text classification with naïve bayes. *Expert Systems with Applications*, 36(3):5432–5435, 2009.

[44] Theodoros Giannakopoulos and Aggelos Pikrakis. *Introduction to Audio Analysis: A MATLAB Approach*. Academic Press, 1st edition, 2014.

[45] I. Panagakis, E. Benetos, and C. Kotropoulos. Music genre classification: a multilinear approach. In JP Bello, E Chew, and D Turnbull, editors, *International Symposium Music Information Retrieval*, pages 583 – 588, 2008.

[46] M. Lopes, F. Gouyon, A. L. Koerich, and L. E. S. Oliveira. Selection of training instances for music genre classification. In *2010 20th International Conference on Pattern Recognition*, pages 4569–4572, 2010.

[47] Tom L. H. Li and Antoni B. Chan. Genre classification and the invariance of mfcc features to key and tempo. In *Advances in Multimedia Modeling*, pages 317–327, 2011.

[48] H. B. Ariyaratne and D. Zhang. A novel automatic hierachical approach to music genre classification. In *2012 IEEE International Conference on Multimedia and Expo Workshops*, pages 564–569, 2012.

[49] J. Martins de Sousa, E. Torres Pereira, and L. Ribeiro Veloso. A robust music genre classification approach for global and regional music datasets evaluation. In *2016 IEEE International Conference on Digital Signal Processing (DSP)*, pages 109–113, 2016.

Advances in Science, Technology and Engineering Systems Journal Vol. 4, No. 2, 170-175 (2019)

www.astesj.com

Special Issue on Recent Advances in Engineering Systems

ASTESJ

ISSN: 2415-6698

Development & Implementation of Smart Vehicle Over Speeding Detector using IoT

Mohammad Ahmar Khan[1], Sarfraz Fayaz Khan [2], Taher Alawi Taher Barham BaOmar [1], Abdul Rahman Mohammed Aqeel Ba Omar[1]

[1]*Department of Management Information System, College of Commerce and Business Administration, Dhofar University, 211, Salalah, Sultanate of Oman*

[2]*Department of Information & Communication Technology, Algonquin College, K2G1V, Ottawa, Canada*

ARTICLE INFO

Article history:
Received: 06 January, 2019
Accepted: 28 February, 2019
Online: 25 March, 2019

Keywords:
Over speeding
Internet of Thing
Vehicle Over Speed Detection
Smart Vehicle

ABSTRACT

Nowadays over speeding is one of the most common traffic violations. Generally, over speeding is the result of restless and bad behavior of drivers. As the accident rates are increasing it is important to develop and implement a system which can automatically detect and report over speeding to the traffic control authorities as early as possible. Nearly all the roads are marked with speed limits depending upon the size of moving vehicles and heaviness of traffic, but some drivers habitually ignore this speed limit. The advancement in technology has replaced most of the manual or semi-automatic systems with an automated system. To add on to various systems in place, this research is making the use of Internet of Things to detect and report over speeding of the vehicle on which the device has been preinstalled. IoT is a technique to integrate various devices to exchange data among themselves. This research proposes the design, development and functioning of a smart device that helps in automatically detect and report to competitive authority, when so ever the subject vehicle exceeds the speed limit. The device has been developed based on the Global Positioning System (GPS) Technology using Raspberry Pi hardware and Android OS and has been practically tested on real time basis by installing it in a car.

1. Introduction

One of the main causes for accidents all over the world is rash driving. The traffic has increased in many folds but the system of monitoring the speed has been compromised. Rash driving causes severe risk not only to the driver & passenger but also to general public. Despite the fact that rash driving is a serious issue its present detection methods by patrol officers lacks efficiency [1].

Speed increase multiplies the hazard of accident and the risk of injury during the accidents [2]. At greater speed the vehicle needs a larger distance to stop. The need of hour is to develop a system that will detect and report the over speed of vehicles. The other factors like conditions of weather and driving at night also impact the manual system.

Daily death toll of India due to road accidents is greater than 4 times the yearly death toll from terrorism [3]. 1,39,671, people lost their lives on roads of India during 2014 that is 382 deaths every day. If 57,844 people lost their lives due to over speed nearly 6,969 Indians died because of speed driving post consumption of alcohol in 2014. The below figure shows the deaths caused due to accidents in roads

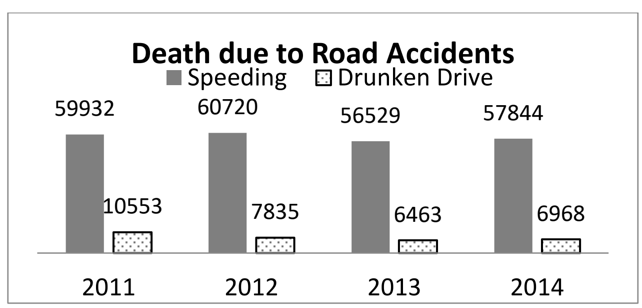

Figure 1: Deaths caused due to accidents in roads
Source: [3]

From the above figure it's evident that over speeding is the major cause of death on road accidents from 2011 to 2014. Over speed was responsible for 41 percent of deaths in accidents while dangerous or careless driving claimed 32 percent of deaths in accidents [4]. Mechanical defects in vehicles and bad weather conditions are other causes for deaths in accidents. Maharashtra and Tamil Nadu has reported several numbers of deaths due to over

*Dr. Mohammad Ahmar Khan, Dept. of MIS, CCBA, Dhofar University, PO Box 2509, PC 211, Sultanate of Oman +96898188243 mkhan@du.edu.om

https://dx.doi.org/10.25046/aj040222

speed of vehicles. The below figure shows the fatal road accidents by causes in 2015

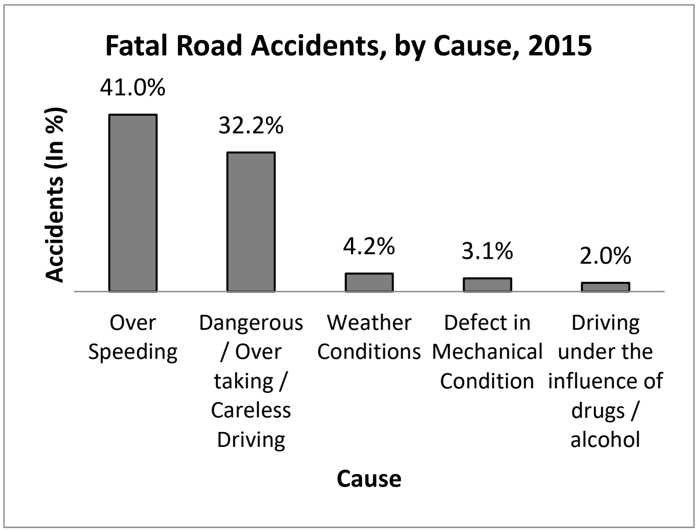

Figure 2: Fatal Road BY Cause in 2015
Source: National Crime Boards Bureau

In [5] the author has mentioned that a vehicle travelling on greater speed will have greater influence during the accident and may cause more number of injuries. Within the driver's fault category during 2016 accidents caused and killed individuals due to over speed accounted for greater number of 2,68,342 out of 4,03,599 accidents and 73,897 deaths out of 1,21,126 deaths respectively.

The author in [6] has stated that the over speed issue necessitates to develop a new way for managing the traffic system to avoid road accidents. This can be handled through real time traffic management using internet of things. Internet of things is a network which handles the physical devices through internet and this network offers rapid, exact and precise results. Internet of things system is designed to store entire database in PC and this storage is performed mainly through internet. Further this database is used accordingly as their applications and needs.

In [7] the author has mentioned that Internet of things system enhances the components to be accessed from far distanced which mainly reduces the work of humans or their interferences and this makes it much economical. Internet of things is linking various devices of application to each other through internet and this is possible because of sensors which support to transmit vast number of data location.

Internet of things connects the real world objects to virtual globe [8]. It comprises to a globe where living beings and physical objects as well as virtual environments and data, communicate with each other. Internet of Things based intelligent transportation systems are designed to assist the vision of Smart city which targets at using the powerful and advanced communications techniques for the administration of the citizens and the city. Internet of Things plays an essential part in the management of traffic enhancing the effectiveness of data transmission, developing the conditions of traffic, efficiency of management, reducing the costs of management and traffic safety.

Internet of Things is a global network linking the entire smart objects together [9]. The benefits of using internet of things in managing traffic are control of traffic, detection of human proximity, avoidance of theft, emergency response, avoidance of accident and autonomous vehicles. Similarly, the drawbacks of internet of things in managing traffic are network failure and security.

In [10] the authors had stated that enabling internet in every vehicle on the road can pave way for whole vehicle automation and traffic. The internet of things concept can be expanded to entire transport modes making an essential difference in the way that interaction exists between various modes of transport.

Thus it can be inferred that internet of things is an effective way for management of traffic and makes the road travel good for everybody in future.

2. Literature Review

The present modern human civilization era the traffic medium plays an essential part in the economic growth of the country [11]. Nowadays a control system is capable to manage such circumstances but not that much efficiently because it needs feedback from humans. A system is needed which must provide continuous update of satellite so that it can manage the traffic smoothly. This will be carried out using IoT using the transmission control protocol/internet protocol. A centralized server must be framed which many of the humans will view after entire analysis of traffic. Relying upon the traffic intensity the diversion path and waiting time will be determined.

In [12] the authors had presented a traffic and vehicle monitoring system based on Internet of Things. Traffic in urban regions and modern cities is making huge risk and is a main concern for the administration and public system. The circumstances namely traffic jams and accidents have become similar because of exponential development in vehicles on road. While human mistakes are one of the major reasons for these issues and lack of appropriate steps and adaptive control system of traffic is another reason. Security for vehicles is also essential. Even in this latent technical globe hackers are handling to break the aspects of security incorporated in modern vehicles. Several technologies namely Bluetooth, Radio Frequency Identification, GSM-GPS and Zigbee based systems were developed but they have restrictions in terms of usage and operation. IOT is a technology that links different objects and is developing at a rapid rate. This system is capable of resolving issues such as congestion in traffic, spotting of vehicle, early warnings considering traffic jams, emergency and VIP clearance of vehicles.

In [13], the researcher presented in their research that urban mobility is one of the unprecedented barriers to be handled in the management of a large city in the contemporary world. This research examines the every developing Urban population around the world and explains about the traffic systems in densely populated cities. Further an advanced system of traffic management is proposed and implemented using IoT (internet of things). The system is assisted by a circuit embedded in the vehicle which runs using radio frequency identification with clustered systems. The system functionalities involves effective light control of traffic, identification of parking space and security mechanism of antitheft. The suggested architecture and process with big data analytics including Hadoop is presented and supervised learning methods are suggested that would support in deciding the roads standard, evaluating overall flow of traffic and examining the vehicles traffic path.

The authors in [14] proposed an intelligent traffic management based on internet of things. The congestion of traffic is a big problem in several big cities of India and the lights of traffic are use basically to manage the vehicle flow. Signal failure, huge number of vehicles, bad enforcement of law and poor management of traffic results in congestion of traffic. One of the main problems with the cities in India is that the existing infrastructure is not expanded much so there have only one choice available which manages traffic better. The traffic control system effectiveness relies on its capability to react on conditions of real time traffic. However conventional system of traffic control is not capable to perform this whatever the density of traffic low or high the signals are timed and performed according to that time. This result in increased congestion in traffic along the roads which outcome in pollution of air. This research proposed a smart traffic management system based on IoT to assist the traffic officers decision making.

In [15] the authors proposed a new method for managing the traffic system which utilizes an IoT (internet of things) concept. An intelligent traffic controller is framed with tools namely Pi-Camera, Raspberry Pi, IR sensors and Radio Frequency Identification. Raspberry Pi is the major tool which is employed to manage entire acts like a controller. The traffic density will be determined with the support of IR sensors and in order to provide zero traffic for emergency vehicles radio frequency identification technique is used. This study propose two modes of system control that is manual with introversion of human and automatic without any introversion of human.

In [16] the authors developed a smart traffic management system for control of traffic using automated electronic and mechanical devices. In the present smart city context particularly in the market and industrial zones the scenario of traffic is congested every time specifically at business hours peak time. Due to increasing development of vehicles and population in metropolitan and smart cities people faces huge issues at the main traffic points of business. It not only affects the delays in travelling but also contributes to pollution in environment as well as health risks due to pollution caused by fuels in vehicles. To resolve such problems several radiant urban communities are implementing smart control structures that run on traffic automation standards with hindrance of previously mentioned problems. In this research an enhanced traffic monitoring and control structure has been suggested that runs rapid transmission of information and their corresponding action. The simulation is undertaken using NS2 simulator which motivates the outputs in terms of good performance to manage the delay and hinder any accident due to profound congestion to a large extent.

In [17] the authors developed an internet of things based controller of traffic light in smart city. Nowadays the congestion of traffic has become a major issue in rapidly developing Indian cities which develops the air pollution. The vehicular density as well as consumption of fluid and this necessitates a new way for managing the traffic system. This has been handled through real time traffic density management using internet of things/ an intelligent traffic management system has been designed to manage the traffic system which involves components comprising of IR sensor, Raspberry Pi and display of LCD. Raspberry Pi is the major tool which is employed to manage the entire multitasking performance and IR sensor is employed to supervise the traffic density. The corresponding information is made feasible on site to show the status of traffic so that people will get early update and avoids traffic jams.

3. Design of the System

The study intends to propose, develop and install the Over Speeding Detector device for vehicle with the use of Internet of Things. The vehicles are fitted with over speeding detector device which has the capability for sharing information, recording and storing the data about the speed of vehicle. The following diagram shows the system architecture:

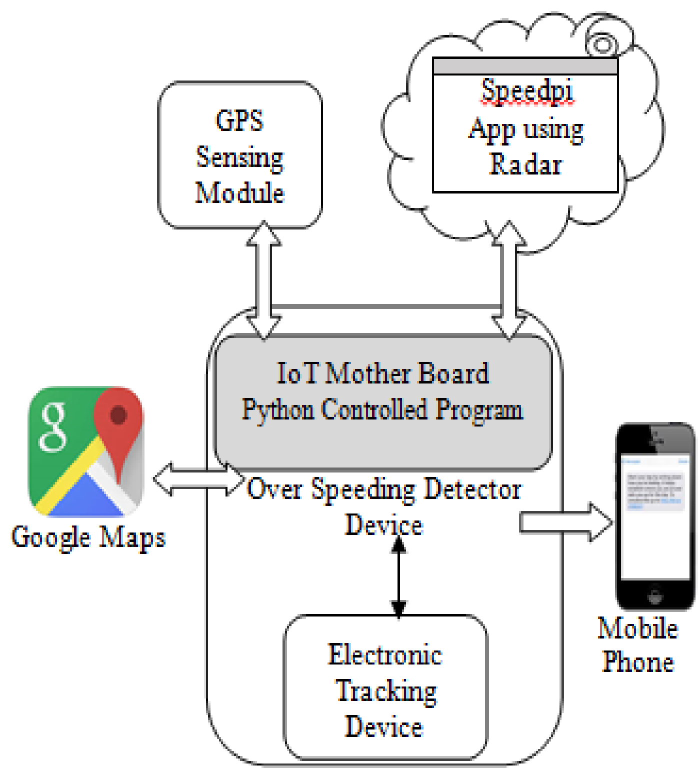

Figure 3: System Architecture
Source: Author

Google Maps:

The Google Maps Road Apps permits to plot GPS coordinates to geometry of the road and also to identify the vehicle's speed limits on the road segments. The following are services exposed for Google Maps Apps:

i. Snap to Roads: It returns the best-fit geometry of the road for a provided GPS coordinates set.
ii. Nearest Roads: It returns individual road divisions for a provided GPS coordinates set.
iii. Speed Limits: It returns the positioned speed limit for the road segment.

GPS Sensing Module:

GPS is a constellation of 24 or more satellites flying 20,350 km above the surface of the Earth. Each one circles the planet twice a day in one of six orbits to provide continuous, worldwide coverage.

GPS Working

i. GPS satellites broadcast radio signals providing their locations, status, and precise time (t1) from on-board atomic clocks.
ii. The GPS radio signals travel through space at the speed of light (c), more than 299,792 km/second.
iii. A GPS device receives the radio signals, noting their exact time of arrival (t2), and uses these to calculate its distance from each satellite in view.
   To calculate its distance from a satellite, a GPS device applies this formula to the satellite's signal: distance = rate x time, where rate is (c) and time is how long the signal traveled through space.
   The signal's travel time is the difference between the time broadcast by the satellite (t1) and the time the signal is received (t2).
iv. Once a GPS device knows its distance from at least four satellites, it can use geometry to determine its location on Earth in three dimensions.

Some GPS applications have the option to set speed limit warning. Generally, the longer the journey and the more measurements that are taken result in a more accurate, overall speed reading.

While some may argue that the speed returned by a GPS receiver is higher than the speedometer in the vehicle, most modern GPS receivers can collect speedometer readings using the OBDII port. This provides a method of verifying the vehicle's speed.

The GPS receiver, fitted with a cellular modem, transmits data to Speed limiter mother board by internal connection normally every minute however it can be more frequent if required. The data is processed on the Speed limiter motherboard.

4. Working of the Over Speed Detecting Device

The system works to determine if a vehicle is exceeding the speed limit based solely on the vehicle's speed? That's where the magic of big data comes in.

The GPS sends the speed calculated based on the aforesaid formula and this speed is send to a program inside the mother board.

The mother board actually works in two parts one a web server and second a continuously running program to monitor the incoming data from the GPS.

The Web Server contains a self-hosted web page which has a simple user interface for input. The input are

i. Mobile number for which the high speed alter should be sent.
ii. Speed Limit in km per hour (kmph) as integer input this will be the check value for the speed limiter.
iii. A save button will be displayed

Figure 4: Screen Shot of SpeedPi
Source: Author

The monitor program performs seven actions,

i. Watch for the Speed data from the GPS.
ii. Based on circumference of the wheel calculate the Revolutions per second and convert it to speed. This data can be get from the OBD port if available.
iii. Cross validate the GPS speed data and calculated data.
iv. Check the GPS speed data against the speed limit value entered in the web application.
v. If GPS speed limit crosses the speed limit data then, the program activates another small routine / method which triggers the cellular modem board present alongside the speed limiter motherboard and sends out an SMS to the mobile number entered and stored via web application.
vi. The application continuously send SMS till the speed limit gets below the speed limit mentioned via application.
vii. Once the speed goes below speed limit then the application stops sending SMS and once again starts monitoring the GPS data.

The self-hosted web application can be accessed from any mobile or PC browser.

The speed limiter itself works as a Wi-Fi access point. The mobile or PC can be connected to the speed limiter Wi-Fi network. Then open any browser and type the provided URI in instruction set above. You can see the web application, enter the relevant data and press save.

Then the application captures the data and saves it in a file inside the speed limiter mother board.

The monitor application uses the data stored as file to validate the speed limit as well as mobile number to send SMS.

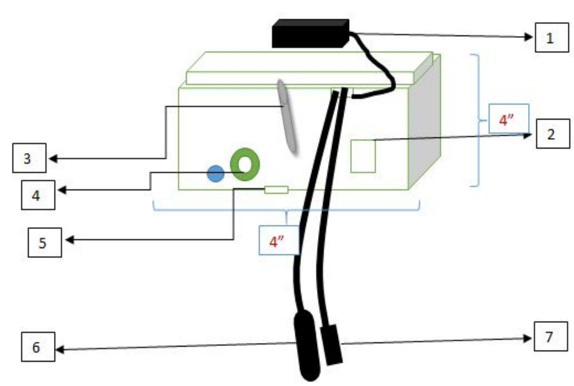

Figure 5: Device Block Diagram
Source: Author

5. Installation and Implementation

1 - GPS receiver	2 - Space for light indication
3 - Mobile Unit Antenna	4 - Mobile unit hard reset button
5 - SIM slot	6 - 12 volts min 2 amp DC power input slot
7 - 05 volts 2 amp DC power input slot	

The implementation steps used in detecting the over speed of smart vehicle with the use of IoT is described below with the results:

Step 1: The first step is to insert a valid SIM card with optimal cash balance of SMS in the provided slot.

Step 2: The GPS antenna is placed (a black square concealed piece) in the automobile dashboard or stick it to bonnet (hoop) outside or top of the automobile, it can be affixed to metal because of internal magnet.

Step 3: Power up the Processing Unit and GPS unit with respective 5 volts 2 amperes and 12 volts 2 amperes from the automobile charging unit or utilizing battery with enough amperage.

Step 4: Make a long press for 2 to 3 seconds after powering up the Green button. Item no 4 in reference diagram. This is too difficult and reset the mobile unit.

Step 5: Wait for 4 to 5 seconds to acquire the mobile phone tower and satellite for fixing.

Step 6: A blue button will flash continuously for every two seconds, when viewed and the blue light and one red light can be seen blinking continuously. This mean everything is better to go.

Step 7: Now on the wireless connection a mobile phone is taken and browse for mobile application named SpeedPi, choose it and enter the Raspberry password.

Step 8: Now open the URL in the cell phone and type http://192.168.0.10:8080/Index where a web page can be viewed and the relevant details are entered into it. Care must be taken that they must enter only integers in alert cell number and speed limit any space or characters which will hinder application from performing properly. Then the details are entered and press save a message named OK will be shown.

Step 9: Start the vehicle and enjoy the ride, whenever the limit of speed is crossed an SMS will be send to the cell number entered through the mobile application i.e. SpeedPi

6. Troubleshooting and Maintenance

i. Check the power connections for appropriate amperes using a multi meter.
ii. After finishing step 5 see inside through the spaced provided.

No red light	Check the power
Blinking blue light with blinking green light and static red light	Power off and on the instrument and long press the green button for two to three seconds
No blinking blue	Satellite is not fixed place the instrument in open air
Two blinking blue lights one static red light	Normal works perfect

iii. SMS is not going
   a. Check SIM is correctly inserted in the slot
   b. Check for SMS balance
   c. Check for validity of SIM card
   d. Redo step two (ii) of troubleshooting.
   e. Check for the proper number entered through application
   f. Check for the valid speed limit entered through application

iv. Application is not opening in mobile.
   a. Check for Wi-Fi connection restart the instrument and wait for few seconds and check the availability of Access point **SpeedPi**
   b. Remember to enter proper password **Raspberry**
   c. Ping IP 192.168.0.10 and check for reply.

7. Conclusion

Road accident is a major cause of accidental deaths. Among all the causes of road accidents, over speeding is leading the trail. Several efforts have been made to provide well organized and consistent ways of check and safely handle over speeding. There are many existing approaches but at times they are ineffective. The strategy for this research is to produce a much easily operable and reliable device. Since Over Speeding Detector device is based on radio frequency, the data related to the vehicle is obtained and hence tracking will become easier. Thus it can be concluded that Internet of Things is used in as one of the technology for decreasing the overspeed of vehicle and this technique can be established on roads in future which can be easily transferable.

Figure 6: Device Photograph
Source: Author

Conflict of Interest

The authors declare no conflict of interest.

Acknowledgment

This research was funded and supported by The Research Council (TRC), Sultanate of Oman, we express our thanks and regards to them along with our serving university, Dhofar University, Salalah, Sultanate of Oman. We will also like to express our very sincere thanks to the two reviewers "anonymous", for their insights.

References

[1] Jain, M., Kumar, P., Singh, P., Arora, C. N., & Sharma, A. (2015). Detection of Over Speeding Vehicles on Highways. International Journal of Computer Science and Mobile Computing, 4(4), 613-619.

[2] Deshpande, S., Bhole, V., Dudhade, P., Gourkar, N., & Darade, S. (2017). Implementing a system to detect over speeding & inform authorities in case of any violations, International Research Journal of Engineering and Technology (IRJET), Volume 04, Issue: 04, pp 2445-2449.

[3] Goenka V (2015), How Information Technology can make Indian Roads & Highways Better and Safer!, Available at https://vinitgoenka.wordpress.com/2015/09/25/how-information-technology-can-make-indian-roads-highways-better-and-safer/, accessed on 27th October 2018.

[4] Scroll (2018), Three killed every 10 minutes: Road accident deaths in India up 9% in 4 years, Available at https://scroll.in/article/826264/three-killed-every-10-minutes-road-accident-deaths-in-india-up-9-in-4-years, accessed on 27th October 2018.

[5] Malik Y S (2017), Road Accidents in India-2016, Available at http://www.indiaenvironmentportal.org.in/files/file/Road%20accidents%20in%20India%202016.pdf, accessed on 27th October 2018.

[6] Thakur T T, Naik A, Vatari S and Gogate M (2016), "Real Time Traffic Management using Internet of Things" International Conference on Communication and Signal Processing, pp.6-8.

[7] Sheela. S, Shivaram. K.R, Sunil Gowda.R , Shrinidhi.L, Sahana.S and Pavithra H S (2016), "Innovative Technology for Smart Roads by Using IOT Devices" International Journal of Innovative Research in Science, Engineering and Technology,pp.1-4 Vol. 5, Special Issue 10.

[8] Chandana, K. K, Sundaram M, D'sa C, Swamy M N and Navya K (2017), A Smart Traffic Management System for Congestion Control and Warnings Using Internet of Things (IoT), Saudi Journal of Engineering and Technology, UAE,

[9] Dandala, T. T., Krishnamurthy, V., & Alwan, R. (2017), Internet of Vehicles (IoV) for traffic management. In Computer, Communication and Signal Processing (ICCCSP), 2017 International Conference on (pp. 1-4). IEEE.

[10] Barth, M., Boriboonsomsin, K., & Wu, G. (2013), The potential role of vehicle automation in reducing traffic-related energy and emissions. In 2nd IEEE International Conference on Connected Vehicles and Expo (ICCVE),pp. 604-605.

[11] Thakur T and Gogate M (2015), Traffic Controlling and Monitoring using Internet of Things, International Journal of Latest Trends in Engineering and Technology, Volume 6, Issue 2, pp 240-246.

[12] Bharath Kumar Perumalla and M. Sunil Babu (2015), An Intelligent Traffic and Vehcile Monitring System using Internet of Things Architecture, International Journal of Science and Research, Volume 5, Issue 11, pp 853-856

[13] Lakshminarasimhan M (2016), IoT Based Traffic Management System, Available at https://www.researchgate.net/publication/310036684_IoT_Based_Traffic_Management_System, accessed on 26th October 2018.

[14] Sonali P. Kshisagar, Priyanka H. Mantala, Gayatri D. Parjane and Kalyani G. Teke, Intelligent Traffic Management based on IoT, International Journal if Computer Application, Volume 157, Issue 2, pp 26-28

[15] Vijetha H and Nataraj K R (2017), IOT Based Intelligent Traffic Control System, International Journal for Research in Applied Science and Engineering Technology, Volume 5, Issue 5, pp 707-710.

[16] Rath M (2018), Smart Traffic Management System for Traffic Control using Automated Mechanical and Electronic Devices, IOP Publishing Private Limited.

[17] Sharma S, Giradkar V, Sanap A and Sarolkar S (2018), IOT based Traffic Light Controller in Smart City, International Journal of Advanced Research in Electrical, Electronics and Instrumentation Engineering, Volume 7, Issue 1, pp 117-123.

Advances in Science, Technology and Engineering Systems Journal Vol. 4, No. 2, 176-182 (2019)

www.astesj.com

ASTESJ

ISSN: 2415-6698

Multiple Social Metrics Based Routing Protocol in Opportunistic Mobile Social Networks

Halikul Lenando[1], Mohamad Alrfaay [2,*], Haithem Ben Chikha [2]

[1]*Faculty of Computer Science and Information Technology, Department of Computer Systems & Communication Technologies, Universiti Malaysia Sarawak, 94300, Malaysia*

[2]*College of Computer and Information Sciences, Computer Engineering and networks, Jouf University, 72388, Saudi Arabia*

A R T I C L E I N F O

Article history:
Received: 15 February, 2019
Accepted: 14 March, 2019
Online: 25 March, 2019

Keywords:
Mobile social network
Social-based routing
Social features
Similarity
Centrality
Social activeness

A B S T R A C T

In Opportunistic Mobile social networks (OMSNs), the social characteristics and behavior of humans carrying mobile devices are exploited to improve information provision and data routing in the network. Social-based routing algorithms attempt to exploit users' social features such as similarity, centrality and betweenness, singularly or combined, to select a suitable relay node among neighbors. However, when combining multiple social metrics to enhance routing performance in opportunistic mobile social networks, most existing algorithms ignore considering the correlation and the mutual impacts among these social metrics. In this paper, we propose a social-based routing approach called Multi Social Metrics (MSM) to enhance data routing in OMSN. In MSM, three social metrics, namely degree centrality, social similarity, and social activeness are exploited, also the mutual impacts among them are considered for performance enhancement. Using real dataset traces, simulation results show the efficiency of MSM by comparing it with other benchmark schemes. Empirical results show that MSM scheme decreases the overhead ratio and the average hop count while achieving competitive delivery ratio and average latency in OMSN.

1. Introduction

Delay Tolerant Networks (DTN) [1] is a special subclass of Ad Hoc network where an established connection between sender and receiver prior sending data is not exist or guaranteed. The connectivity in DTN is intermittent and the links between nodes are broken frequently. Data delivery in such a network is a challengeable issue; Opportunistic networks (OppNets) is a paradigm of DTN uses store-carry-forward [2] mechanism to tackle with this challenge, where message is stored in node's buffer and carried while moving until there is an opportunity to forward it to a candidate relay. This process continues until the delivery of the message.

The wide proliferation of mobile devices leads to the emergence of the Opportunistic Mobile Social network (OMSN). In this communication form, social properties of human beings and networking technology such as, Bluetooth and Wi-Fi are combined to enable people to share information through wireless network [3]. Because of the relative stability of social characteristics and behavior of people carrying the mobile devices compared to communication links and dynamic topologies they are exploited to make data routing in OMSN more efficient [4] [5] [6][7].

In opportunistic networking paradigm, messages are forwarded neighbors. on the basis of communication opportunity with the current So, selecting the suitable relay nodes play a key role for efficient data routing process .Social-based routing algorithms utilize social metrics deduced from the mobile users' social relationships and interconnecting to form an effective message forwarding decision when routing data in OMSN [8]. Various Social features such as similarity, centrality, and friendship are defined and utilized in the literature to design social based routing schemes [9].

Social based routing algorithms exploit social metrics either singularly [10] [11] where one social feature such as similarity or centrality is exploited, or multiple social metrics are combined to form a utility function used to select the next relay [12]. Exploiting multiple social metrics to form the forwarding strategy is strong trend in social-based routing in OMSN. However, when exploiting multiple social metrics we believe that it is important to consider

* Mohamad Alrfaay, College of Computer and Information Sciences, Computer Engineering and networks Department, Jouf University, 72388, Saudi Arabia, 00966534429170, mhrifai@ju.edu.sa

the interrelations and the mutual impacts among the exploited social features and not utilize them separately.

In this paper, we propose a social-based routing scheme that exploits multiple social properties namely, social activity, centrality, and similarity, and we also consider the mutual impacts and interrelation between these social metrics to ensure efficient forwarding decision in OMSN. The rest of the paper structure is organized as follows. In section 2, related works are discussed with motivation for our proposed scheme. Section 3 presents an overview of our proposed protocol and the social metrics that are exploited to form the forwarding decision. Experimental simulation results and performance evaluation are presented in Section 4. Section 5 concludes this paper.

2. Related works and motivation

Data routing in OMSN is one of the key challengeable issues that derive tremendous interest in the research community where several routing strategies have been proposed [2] [13] [14]. These schemes aim to tackle with the intermittent and dynamic topology of the opportunistic networks and to develop efficient routing protocols with higher delivery ratio and lower delivery overhead and end-to-end delay. Flooding and flooding-based schemes like Epidemic [15] is the straightforward routing schemes in the opportunistic networks, where replicas overwhelm the network in the sake of delivering data to destinations. However, these schemes exhaust the network and the node's resources because of the high rate of message replication.

Prediction and probability based routing schemes like PRoPHET [16] protocol depend on the contact history between nodes to predict the future encounter. Each node calculates and maintains the encounter probability with other peers, where this probability is increased with every meeting and decreases if nodes do not meet over time. In these schemes, pervious interactions are the key factor to form the forwarding decision while other factors such as social relations and behavior patterns are not considered.

Social characteristics of mobile users and the related social properties provided by Socially Aware Networking (SNA) [17] are exploited widely in the literature to improve routing performance in OMSN [18] . The common goal of the social-based schemes is to make more accurate forwarding decision by selecting a relay which has the largest probability to encounter the destination by exploiting social properties. Different social metrics, such as similarity, activity, and popularity are defined to reflect the social relation and ties among mobile nodes [3]. These metrics are exploited to design efficient social-based routing protocols in OMSN [19] . In [10], a fuzzy routing-forwarding algorithm (FCNS) was proposed to exploit node similarity. This scheme considers the similarity among social attributes and the nodes' mobility history, and also it uses feedback mechanism for more stable forwarding of message in the network.

Exploiting multiple social metrics such as, similarity, betweenness and popularity for efficient routing is strong trend in the research community. In Bubble Rap [20] , similarity and community structure are exploited. In this algorithm, communities with different sizes are formed. Nodes belong to these communities have different levels of ranking of two types; global denotes node's popularity in the entire network and local for node's popularity inside the community. A node is selected as a relay if it has higher global ranking until a node in the destination's community is encountered. Then, local ranking is examined to forward messages to nodes that have higher local ranking until reaching the destination.

Xia et al. [12] consider multiple social characteristics to design multi-dimensional routing protocol for socially-aware networking. Three social factors are utilized in this work. The first one is physical proximity which indicates the contacting ability when two nodes within their communication rang. The second one is user interests, it reflects the users' preferences, and finally social relationship which reflects the social ties and relationships with other peers such as friendship and family relations. Utility function is composed based on these factors and messages are forwarded to nodes that have the highest utility value when nodes encounter.

Rahim et al. [21] proposed a social-based routing protocol for data dissemination in Vehicular Social Networks (VSNs).The proposed protocol, named Social-Acquaintance based Routing Protocol (SARP), exploits multiple social metrics; community acquaintance, social activeness, and degree centrality. Each node maintains and updates the values of these metrics and a priority value is calculated based on them. When a message carrying node encounters another node, messages will be forwarded if the encountered node has higher priority value than the relay.

Social properties such as popularity, similarity and similarity describe the social behavior of a mobile user in a network, and the interactions among different users in the network and their social behaviors are interrelated. Therefore, for efficient data routing and information provision in OMSN, the correlation and the mutual impacts among the exploited social features should be considered. Therefore, unlike the other above-mentioned methods, in this paper, we propose a social based routing scheme called MSM that considers the mutual impact of the social metrics. Three social metrics namely social activity, centrality, similarity and their mutual correlations are exploited to form a utility function used for the selection of the best relay for forwarding a message in OMSN. We present the details of the proposed protocol in the next section.

3. Proposed routing protocol

MSM is a social based routing protocol. It utilizes three social metrics; social activity, social similarity, and social centrality. These three metrics are combined together in conjunction with the correlation among them in order to make more precise forwarding decision.

Social activity, similarity, and centrality are common social metrics in the Mobile Social Network (MSN) [18] [22]. In the next subsections, we define these metrics and we present the way how we evaluate them.

3.1. Social Activity

The opportunistic network has a dynamic topology, so the current neighbors of each node change frequently. Node that has higher rate of meeting new peers is considered socially active node. For example, if there are two nodes N1 and N2 , and at time t1: the neighbors of node N1 are: N2, N4, N3 and N7 , while the neighbor of node N2 are: N1, N4, N5 and N9 . Then at time t2 where t2> t1, N1 has the neighbors: N3, N4, N5 and N7, while the neighbors of N2 are: N8, N12, N6 and N9. In this example, node N2 is more socially active than node N1 because it has more new peers at t2 i.e. N8, N12 and N6, while N1 has only one new neighbor: N5.

The social activity of a node is calculated as follows [20]:

$$Act(Ni) = 1 - (Nib^{tl} \cap Nib^{tp}) / (Nib^{tl} \cup Nib^{tp}) \quad (1)$$

where *tl* represents the time of the last change in the neighbors of Ni and *tp* denotes the time of the previous change in the neighbors of Ni . Nib^{tl} , Nib^{tp} are the set of the current neighbors of Ni at *tl* and *tp* , respectively.

3.2. Social similarity

From the social science, people tend to build clusters inside their social networks with peers have common social characteristics, behaviors, or friends. People belongs to a cluster may meet each other more frequently than others, and hence the probability of the future meeting is high [3].

The similarity between two nodes Ni and Nj based on the common neighbors is computed as:

$$SimNb_{i,j} = Nb_i \cap Nb_j \quad (2)$$

where Nb_i and Nb_j are the current neighbors of nodes Ni and Nj respectively [5].

3.3. Degree centrality

It is an indicator of the social importance (popularity) of a node in the social network. Node gets higher popularity when it encounters more other nodes in the network. So, the increasing in degree centrality results in higher probability to deliver messages.

Degree centrality of a node N_i calculate as follows [6] :

$$DC(Ni) = \Sigma_{i=1,N} En(i,k) , \quad (3)$$

where En (i,k) =1 if there is a direct connection between N_i and N_k. N denotes the number of the nodes in the network.

3.4. Forwarding policy

In our work, social activity, degree centrality, and social similarity are combined to make the forwarding decision when routing messages in OMSN. An encounter node will be selected as a relay in two cases: first, if it is more socially active than the current node, and it has a similarity with the destination and its similarity is more than the current relay node. We put this condition because there is a probability that a node has higher social activity (meet more new people frequently) but it is socially far from the destination. So that, forwarding message to such a node is an unwise decision. Applying this condition leads to select relays that are more socially closer to the destination and hence the probability to encounter the destination is higher. The second case; the relay has higher centrality metric than the current node and it has contacted with the destination before and if it has a similarity with the destination.

We define a utility function U_{Ni} of a node N_j as following:

$$U_{Ni} = SimF_{i,j} \times Act(N_j) + CenF_{i,j} \times DC(N_j) \quad (4)$$

The factors $SimF_{i,j}$ and $CenF_{i,j}$ are used to strict the selection of the relay to the nodes that are socially closer to the destination. Act (N_j) is calculated based on (1) and DC(N_j) is calculated based on (3) .

According to similarity metric, a node will be selected as a relay only if it has a similarity with the destination and if it has higher similarity value than the current node. So that, the value of the similarity factor simF is:

$$SimF = 1 : \Delta sim_{i,j} = SimNb_{j,d} - SimNb_{i,d} > 0 \quad (5)$$

$$SimF = 0 : \Delta sim_{i,j} = SimNb_{j,d} - SimNb_{i,d} \leq 0 \quad (6)$$

While for centrality metric the relay will be chosen only if it encountered the destination previously and it has a similarity with the destination. So, the value of the centrality factor cenF is:

$$cenF = 1: SimNbj,d > 0 \text{ and } Encj,d \neq 0 \quad (7)$$

$$cenF = 0: SimNbj,d \leq 0 \text{ or } Encj,d \neq 0 \quad (8)$$

here similarities are calculated based on (2).

When a node N_i encounters another node N_j , each node calculates the values of Act (N_i), Act (N_j), $SimNb_{i,d}$, $SimNb_{j,d}$, , and $Enc_{j,d}$ metrics for each message stored in their buffers. Then based on these values, each node evaluates SimF, cenF. Finally, the utility of the two nodes U_{Ni} , U_{Nj} is calculated. If and only if the utility of the encountered node U_{Nj} is greater than the current node U_{Ni}, the message will be forwarded to the encountered node, else the current node continues carrying the message.

Algorithm 1 shows the pseudo code of the forwarding process in MSM.

Algorithm 1: Pseudo-code of forwarding process in MSM

```
Node_i encounter Node_j
For each message in Node_i buffer
compute Act(N_i), Act(N_j), SimNb_j,d , SimNb_i,d , Enc j,d
Compute SimF, CenF
Compute U_Nj, U_Ni
If U_Ni > U_Nj
  forward message to Node_j
End if
End for
```

Regarding the time complexity of Algorithm 1, each node computes the social metrics values for all of its buffered messages, therefore the complexity is proportional to the number of the buffered messages (M). So, the complexity of Algorithm1 is O(M).

4. Performance evaluations

4.1. Data set

Traces of real datasets are used to do our experiments and to evaluate the efficiency of MSM. INFOCOM05 and INFOCOM06 datasets were used for evaluation. These datasets is widely used in the literature [12] [23] and available at the website of CRAWDAD project (http://crawdad.org/cambridge/haggle).

INFOCOM05 dataset is conducted during the IEEE INFOCOM 2005 conference in Miami where 41 iMotes devices with wireless range of around 30 meters using Bluetooth technology for communication. The experiment where carried by attendees for 3 to 4 days. In INFOCOM06 dataset, 78 mobile iMotes are used. Bluetooth encounters between 78 short range nodes are traced and stored.

4.2. Simulation setup

We use Opportunistic Network Environment (ONE) [24] simulator to do the experiments. We compare MSM with three benchmark routing protocols: Epidemic which is flooding-based routing protocol, PRoPHET which is prediction-based routing protocol and Bubble Rap which is social-based routing protocol. Simulator settings are as follows:

The Broadcast type is Bluetooth interface with the transmit speed of 2 Mbps for all the nodes. The message event generator in ONE simulator generates one new message in every 30 to 40 seconds. Message size is 124 KB. We vary the simulation end time from 4hours (14400 seconds) to 40 hours (144000 seconds) by 4 hours step for INFOCOM06 dataset, and from 4hours (14400 seconds) to approximately 70 Hours (254150 seconds) for INFOCOM05 dataset. Also, we change message TTL value as follows: (10m, 30m, 1h, 4h, 8h, 16h, 20h, 1d, 1d&4h, 1d&8h, 1.5d, 1.6d) where m stands for minutes, h for hours and d for days.

Simulation setup settings are given in Table 1.

Table 1: Simulation Settings

Simulation Time(seconds	(INFOCOM05):14400 to 254150 (INFOCOM06):14400 to 144000 with 4hours step
Interface	Bluetooth Interface
Number of nodes	41 short range devices in (INFOCOM05) 78 short range devices in (INFOCOM06)
Transmit Speed	250 k (2 Mbps)
Mobility	Real trace data (INFOCOM05, INFOCOM06)
Buffer Size	5 MB
Protocols	MSM, Epidemic , PRoPHET, BubbleRap
Message Size	128 KB
Event Interval	30 to 40 seconds
Message TTL	10m, 30m, 1h, 4h, 8h, 16h, 20h, 1d, 1d&4h, 1d&8h, 1.5d, 1.6d

In each experiment, we compare the performance of protocols MSM, Epidemic, PRoPHET and Bubble Rap based on the following metrics:

Successful Delivery ratio: it is the ratio between the number of delivered messages and the total number of created messages. The ideal value of the successful delivery ratio is (1.0) when all created messages are delivered to their destinations.

Overhead Ratio: it is the additional bytes are sent for successfully delivering a message to a destination.

Average Latency: it is the average of the time elapsed between message creation and delivery.

Average Hop Count: it is the average of the number of hops that messages must take in order to reach the destination.

4.3. Experiments and results

In this work, we carried out a comparison between the proposed MSM and Epidemic, PRoPHET and Bubble Rap in terms of delivery ratio, overhead ratio, average latency and average hop count respectively. Figures 1, 2, 3, and 4 show the evaluation of the protocols' performance over the experiment time for the both datasets. We aim to study the achievement of our protocol against the benchmark protocols over the time of the experiment. For this purpose, we fixed the messages TTL to 600m (10 Hours) and the buffer size to 5MB and change the simulation end time from 14400s (4 Hours) to 144000s (1.6Day) for INFOCOM06 dataset, and from 14400s (4 Hours) to 254150s (2.9 Day) for INFOCOM05 dataset with 4 Hours step.

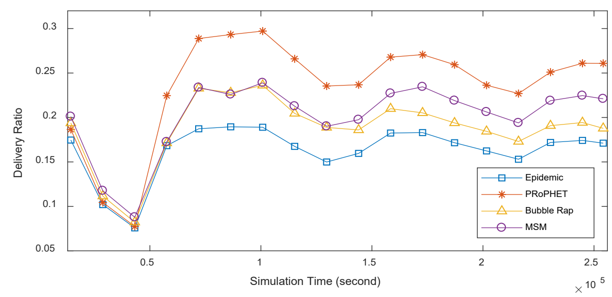

Figure 1. (a) Delivery ratio over Time (INFOCOM05)

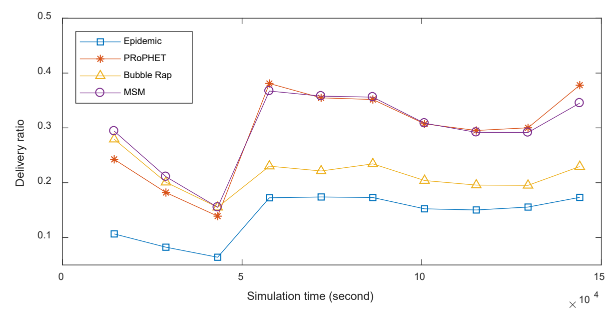

Figure 1. (b) Delivery ratio over Time (INFOCOM06)

Figure 1 depicts the successful delivery ratio over the time. From these results, it is clearly shown that MSM outperforms both Epidemic and Bubble Rap and has close achievement compared to PRoPHET over the experiment time. This is because MSM exploits three social metrics to make forwarding decision, so it forwards messages to nodes that are socially closer to the destination. In addition, considering the correlation between the different social metrics, where social similarity adjusts social activity and similarity and contact history adjust centrality, makes the forwarding decision more accurate. Therefore, the selected relays in MSM have higher probability to encounter the destination and the delivered data amount will be higher. This results in increasing the delivery ratio in the network.

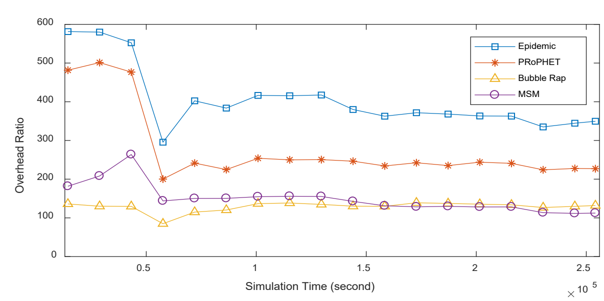

Figure 2. (a) Overhead ratio over Time (INFOCOM05)

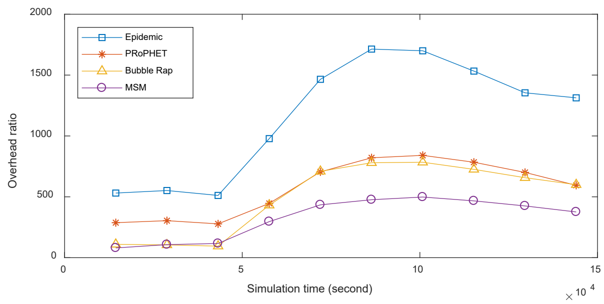

Figure 2. (b) Overhead ratio over Time (INFOCOM06)

Figure 2 shows that MSM is able to significantly control the overhead in OMSN with high delivery rates as shown in Figure 1. MSM achieves a higher reduction in delivery overhead in INFOCOM06 experiment than INFOCOM05. This is because INFOCOM06 has higher number of mobile nodes, so the exploiting of the social information has more impact on the routing performance.

Compared to Bubble Rap, MSM has almost similar performance at the beginning of the experiment (First 8 Hours) in INFOCOM06 experiment where the overhead ratio is the lowest compared to Epidemic and PRoPHET. Then, for the proceeding in the experiment time, MSM outperforms all the other protocols with high reduction in the overhead ratio. In fact, the gain is about (36%, 39%, and 70%) by comparing with Bubble Rap, PRoPHET, and Epidemic, respectively. Gain is thanks to exploitation of social information by MSM in an effective way, i.e., social metrics including the activity, the centrality, the similarity and their mutual impacts that allow the selection of the relay, which is socially closer to the destination. This decreases the forwardings in the network while increases the delivered messages. Consequently, the overhead ratio (relayed-delivered/ delivered) will be decreased.

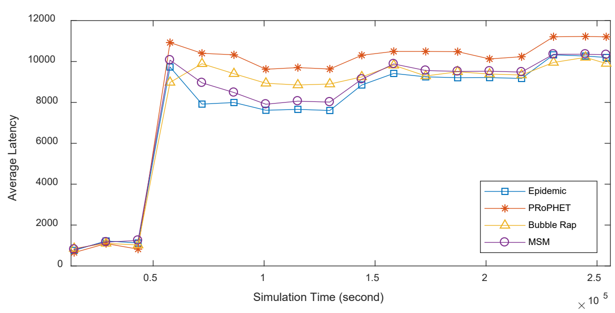

Figure 3. (a) Average latency over Time (INFOCOM05)

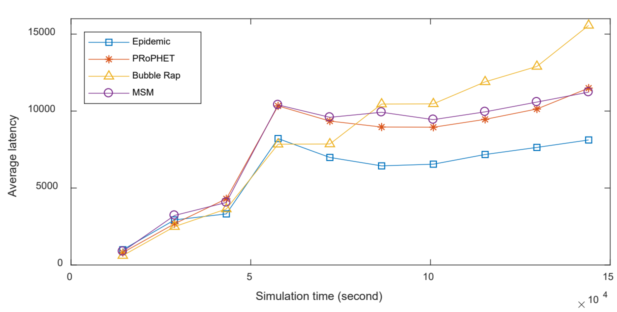

Figure 3. (b) Average latency over Time (INFOCOM06)

Figures 3 shows the performance evaluation in term of average latency. Epidemic has the best achievement regarding this metric because it is a flooding-based scheme. However, in INFOCOM05 experiment, MSM has, on average, lower average latency compared with Bubble Rap and PRoPHET Protocols and has very close achievement compared to Epidemic. In INFOCOM06 experiment, MSM almost has similar average latency compared to PRoPHET and it outperforms Bubble Rap at the end of the experiment.

In Figure 4, it is clear that MSM outperforms all other protocols in term of average hop counts. Exploiting three social metrics and considering the mutual impacts among them enables MSM to decrease the number of forwardings in the network. Selecting the next forwarder in MSM is based on the strength of the social relationship with the destination, so a lower number of mobile nodes will contribute in the forwarding process, this results in decreasing the average hop count and help to preserve the network and nodes resources.

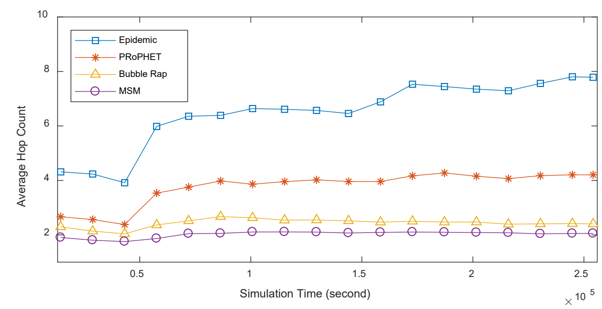

Figure 4. (a) Average hop count over Time (INFOCOM05)

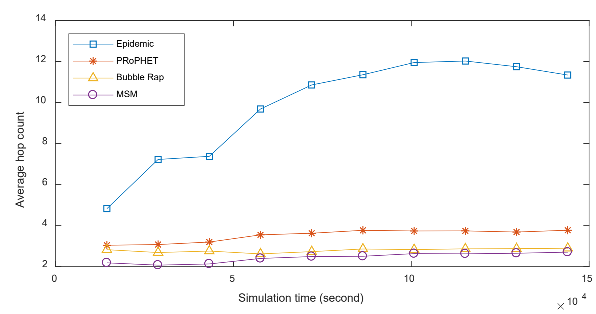

Figure 4. (b) Average hop count over Time (INFOCOM06)

We also investigate the efficiency of MSM for different TTL values. In fact, we evaluate the performance by changing the TTL from value low vale 10 minutes to high value 1.6 days. In Figures 5, 6, 7 and 8, we plot the varying of delivery ratio, overhead ratio, average latency and average hop count versus TTL value for both datasets.

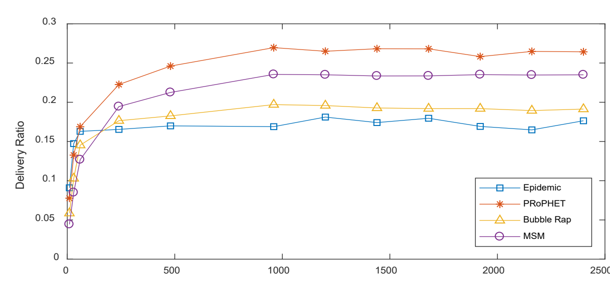

Figure 5. (a) Delivery ratio vs. TTL (INFOCOM05)

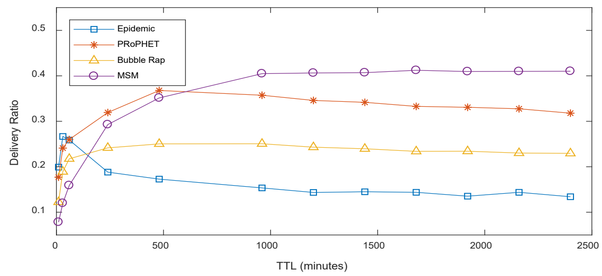

Figure 5. (b) Delivery ratio vs. TTL (INFOCOM06)

It is shown in Figure5 (a) and (b) that all routing scheme have low delivery ratio in low TTL values scenarios (10m-1h). This is due to the high dropping ratio of messages as a result of expired TTL. Increasing TTL causes rising up the delivery ratio until reach a plateau where increasing TTL values decrease slightly the delivery ratio.

For very low TTL values (i.e., 10, 30 and 60 minutes), MSM has a low number of delivered messages since it straitens the selection of relay nodes based on the social metrics. This results in a very low number of delivered messages hence low delivery ratio. However, with increasing TTL value, MSM achieves better delivery ratio and outperforms all other schemes except PRoPHET in INFOCOM05 and all other schemes INFOCOM06 when TTL is higher than 8 hours. This is because MSM forwards messages to nodes having tight social relations with destinations, which increases the probability of delivering the message.

Figure 6 shows the overhead ratio vs. the TTL value. The results show that MSM provide significant gain comparing to all other schemes and for all TTL values for both datasets. It reduces the overhead in the network by applying a strict relay selection strategy, where social activity, similarity and similarity metrics are exploited to select the next message's forwarder. The objective of this forwarding method of MSM is to reduce the number of forwardings in the network and also forward messages to nodes that are more socially closer to the destination and therefore have a have high probability to deliver messages.

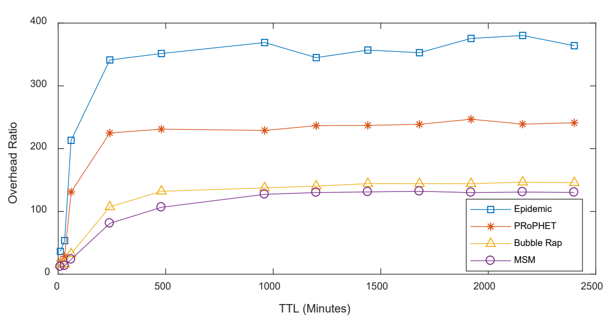

Figure 6. (a) Overhead ratio vs. TTL (INFOCOM05)

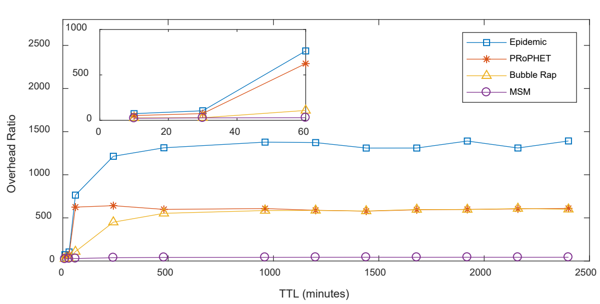

Figure 6. (b) Overhead ratio vs. TTL (INFOCOM06)

Average latency of MSM in comparison with Epidemic, PRoPHET and Bubble Rap with respect to TTL value is given in figures 7. (a) and (b). It is shown in this figure that MSM achieves a close performance compared to the other protocols and has lower average latency than PRoPHET in INFOCOM05 experiment while it outperforms both PRoPHET and Bubble Rap in INFOCOM06 and its superiority becomes higher as TTL value increases. This is because MSM selects relays that have stronger social ties with the destination, which means that they will deliver messages in a shorter end-to-end delay. Therefore, the average latency of MSM is lower. Compared to Epidemic, MSM achieves higher average latency because Epidemic is a flooding-based approach so it has the lowest end-to-end delay compared to other protocols in OMSN.

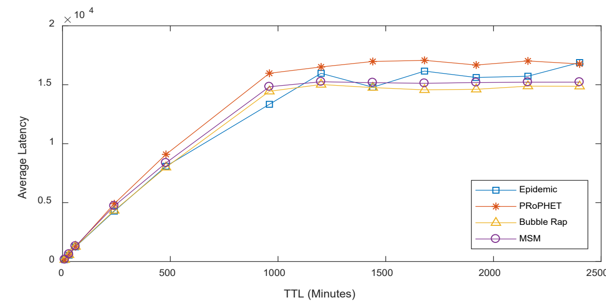

Figure 7. (a) Average latency vs. TTL (INFOCOM05)

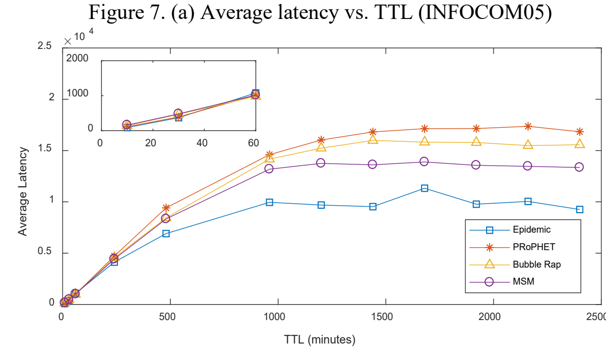

Figure 7. (b) Average latency vs. TTL (INFOCOM06)

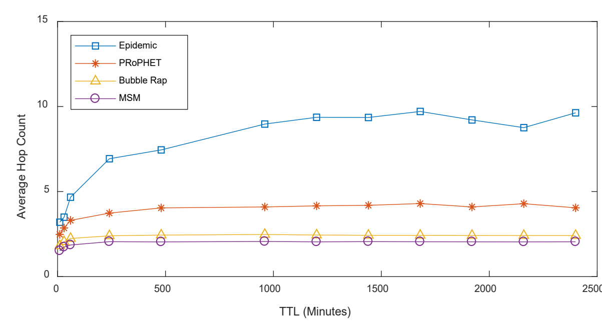

Figure 8.(a) Average hop count vs. TTL(INFOCOM05)

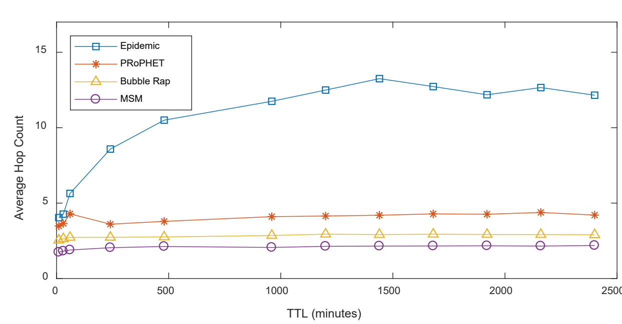

Figure 8.(b) Average hop count vs. TTL (INFOCOM06)

Figure 8 depicts the achievements of MSM, Epidemic, PRoPHET and Bubble Rap in term of average hop counts metric. From this results, it is clear that MSM has the lowest average hop counts, so it decreases network and node overhead in OMSN. The reason is that MSM decreases the number of nodes participating in messages forwarding by selecting as a relay only node which has better social relation with destination based on the three social metrics, i.e., activity, similarity and centrality.

5. Conclusion

In this paper, we have presented a social-based routing scheme exploiting three social metrics; activity, centrality and similarity. The protocol, namely, Multi Social Metrics routing protocol (MSM), exploit the social metrics and their mutual impacts to improve routing performance in OMSN, and precisely we focused on controlling node and network overhead in OMSN by decreasing delivery overhead and average hop counts. Real mobility traces are used to evaluate our proposal where simulation results are carried out by ONE simulator to show the efficiency of the proposed protocol. We compared MSM performance with three widely well-known routing protocols in OMSN; Epidemic, PRoPHET, and Bubble Rap. The results show that MSM outperforms theses protocols in terms of overhead ratio, average hop count and has competitive for delivery ratio and average latency. This routing scheme and its forwarding strategy can be applied in any mobile social network scenarios such as conference or university campus.

Conflict of Interest

The authors declare no conflict of interest.

References

[1] KHABBAZ, Maurice J., ASSI, Chadi M., and FAWAZ, Wissam F.,, "Disruption-tolerant networking: A comprehensive survey on recent developments and persisting challenges," IEEE Communications Surveys & Tutorials, vol. 14, no. 2, pp. 607--640, 2012. https://doi.org/10.1109/SURV.2011.041911.00093

[2] Zhu, Konglin and Li, Wenzhong and Fu, Xiaoming and Zhang, Lin, "Data routing strategies in opportunistic mobile social networks: Taxonomy and open challenges," Computer Networks, vol. 93, pp. 183--198, 2015. https://doi.org/10.1016/j.comnet.2015.10.018

[3] Daly, Elizabeth M and Haahr, Mads, "Social Network Analysis for Information Flow in Disconnected Delay-Tolerant MANET" IEEE Transactions on Mobile Computing, vol. 8,no. 2, pp. 606--621, 2009. https://doi.org/10.1109/TMC.2008.161

[4] Boldrini, Chiara and Conti, Marco and Passarella, Andrea, "Exploiting users' social relations to forward data in opportunistic networks: The HiBOp solution," Pervasive and Mobile Computing, vol. 4, no. 5, pp. 633--657, 2008. https://doi.org/10.1016/j.pmcj.2008.04.003

[5] Guan, Jianfeng and Chu, Qi and You, Ilsun, "The social relationship based adaptive multi-spray-and-wait routing algorithm for disruption tolerant network," Mobile Information Systems, vol. 2017, 2017. https://doi.org/10.1155/2017/1819495

[6] Halikul Lenando and Mohamad Alrfaay, "EpSoc: Social-based epidemic-based routing protocol in opportunistic mobile social network," Mobile Information Systems, vol. 2018, p. 8, 2018. https://doi.org/10.1155/2018/6462826

[7] Wang, Tong and Tang, MengBo and Song, Houbing and Cao, Y and Khan, Zaheer, "Opportunistic protocol based on social probability and resources efficiency for the intelligent and connected transportation system," Computer Networks, vol. 149, pp. 173--186, 2019. https://doi.org/10.1016/j.comnet.2018.11.034

[8] Pirozmand, Poria and Wu, Guowei and Jedari, Behrouz and Xia, Feng, "Human mobility in opportunistic networks: Characteristics, models and prediction methods," Journal of Network and Computer Applications, pp. 45--58, 2014. https://doi.org/10.1016/j.jnca.2014.03.007

[9] Ahmed, Manzoor and Li, Yong and Waqas, Muhammad and Sheraz, Muhammad and Jin, Depeng and Han, Zhu, "A Survey on socially aware device-to-device communications," IEEE Communications Surveys & Tutorials, vol. 20, no. 3, pp. 2169--2197, 2018. https://doi.org/10.1109/COMST.2018.2820069

[10] Liu, K.; Chen, Z.; Wu, J.; Wang, L., "FCNS: A fuzzy routing-forwarding algorithm exploiting comprehensive node similarity in opportunistic social networks," Symmetry 2018, 10, 338. https://doi.org/10.3390/sym10080338

[11] Asl, Sepideh Tahouri and Derakhshanfard, Nahideh, "SFQ: Social Features Based Quota Routing in Mobile Social Networks," Wireless Personal Communications, vol. 104, no. 3, pp. 1109--1120, 2019. https://doi.org/10.1007/s1127

[12] Xia, Feng and Liu, Li and Jedari, Behrouz and Das, Sajal K, "PIS: A multi-dimensional routing protocol for socially-aware networking," IEEE Transactions on Mobile Computing, no. 11, pp. 2825--2836, 2016. https://doi.org/10.1109/TMC.2016.2517649

[13] Sobin, CC and Raychoudhury, Vaskar and Marfia, Gustavo and Singla, Ankita, "A survey of routing and data dissemination in delay tolerant networks," Journal of Network and Computer Applications, vol. 67, pp. 128--146, 2016. https://doi.org/10.1016/j.jnca.2016.01.002

[14] N. Chakchouk, "A survey on opportunistic routing in wireless communication networks," IEEE Communications Surveys & Tutorials, vol. 17, no. 4, pp. 2214--2241, 2015. https://doi.org/10.1109/COMST.2015.2411335

[15] Amin Vahdat , David Becker, "Epidemic Routing for Partially-Connected Ad Hoc Networks," Duke University, Technical Report CS-200006, 2000.

[16] Lindgren, Anders and Doria, Avri and Schelen, Olov, "Probabilistic routing in intermittently connected networks," Springer, pp. 239--254, 2004. https://doi.org/10.1007/978-3-540-27767-5_24

[17] Xia, Feng and Liu, Li and Li, Jie and Ma, Jianhua and Vasilakos, Athanasios V, "Socially Aware Networking: A Survey," IEEE Systems Journal, vol. 9, no. 3, pp. 904--921, 2015. https://doi.org/10.1109/JSYST.2013.2281262

[18] Zhu, Ying and Xu, Bin and Shi, Xinghua and Wang, Yu, "A survey of social-based routing in delay tolerant networks: Positive and negative social effects," IEEE Communications Surveys & Tutorials, vol. 15, no. 1, pp. 387--401, 2013. https://doi.org/10.1109/SURV.2012.032612.00004

[19] Roy, Animesh and Acharya, Tamaghna and DasBit, Sipra, "Quality of service in delay tolerant networks: A survey," Computer Networks, vol 130, pp. 121-133, 2018. https://doi.org/10.1016/j.comnet.2017.11.010

[20] Hui, Pan and Crowcroft, Jon and Yoneki, Eiko, "Bubble rap: Social-based forwarding in delay-tolerant networks," IEEE Transactions on Mobile Computing, vol. 10, no. 11, pp. 1576-1589, 2011. https://doi.org/10.1109/TMC.2010.246

[21] Rahim, Azizur and Qiu, Tie and Ning, Zhaolong and Wang, Jinzhong and Ullah, Noor and Tolba, Amr and Xia, Feng, "Social acquaintance based routing in Vehicular Social Networks," Future Generation Computer Systems, vol. 93, pp. 751-760, 2017. https://doi.org/10.1016/j.future.2017.07.059

[22] Wang, Yufeng and Vasilakos, Athanasios V and Jin, Qun and Ma, Jianhua, "Survey on mobile social networking in proximity (MSNP): approaches, challenges and architecture," Wireless networks, vol. 20, no. 6, pp. 1295--1311, 2014. https://doi.org/10.1007/s11276-013-0677-7

[23] Yao, Lin and Man, Yanmao and Huang, Zhong and Deng, Jing and Wang, Xin, "Secure routing based on social similarity in opportunistic networks," IEEE Transactions on Wireless Communications, vol. 15, no. 1, pp. 594--605, 2016. https://doi.org/10.1109/TWC.2015.2476466

[24] Ari Keränen, Jörg Ott , Teemu Kärkkäinen, "The ONE simulator for DTN protocol evaluation," in Simutools '09 Proceedings of the 2nd International Conference on Simulation Tools and Techniques, Brussels, Belgium, 2009. https://doi.org/10.4108/ICST.SIMUTOOLS2009.5674

Advances in Science, Technology and Engineering Systems Journal
Vol. 4, No. 2, 183-189 (2019)
www.astesj.com
Special Issue on Advancement in Engineering and Computer Science

ASTES Journal
ISSN: 2415-6698

Effects of Educational Support Robots using Sympathy Expression Method with Body Movement and Facial Expression on the Learners in Short- and Long-term Experiments

Yuhei Tanizaki*,1, Felix Jimenez[2], Tomohiro Yoshikawa[1], Takeshi Furuhashi[1], Masayoshi Kanoh[3]

[1]Graduate School of Engineering, Nagoya University, 464-8603, Japan

[2]Information Science and Technology, Aichi Prefectural University, 480-1198, Japan

[3]Engineering, Chukyo University, 466-8666, Japan

ARTICLEINFO

Article history:
Received: 19 January, 2019
Accepted: 08 March, 2019
Online: 28 March, 2019

Keywords:
Educational-Support Robot
Sympathy Expression Method
Body Motion

ABSTRACT

Recently, educational-support robots have been attracting increasing attention as studying-support gadgets. Previous studies used the sympathy expression method in which the robot expressed emotions in sympathy with the learners; however, the robots considered in those studies expressed only facial emotions. Presently, there is no study that uses body movements together with facial expressions in the sympathy expression method. Thus, in this paper, we examine the effects of two types of robots that have different method of expressing emotions on learners in two experiments.

1 Introduction

Recent developments in robotics have prompted an increase in educational-support robots that assist in studying. For instance, a robot supports students at school [1] or helps them to learn the English language[2]. Koizumi introduced the robot as a "watching over" in situations where children learn while discussing the programming that controls the assembly and motion of the car robot by the Lego block [3]. Our research focus on educational support robots to learn with people. The serious problem that these robots face is that the learner gets tired of the robot because they find the behavior of the robots to be monotonous [4], [5]. To address this problem, previous researches developed a sympathy expression method that allows a robot to express emotions sympathetic to learners [6]. Through the subject experiments, the previous research reported that the robot using empathy expression method reduced the monotonicity of learning and reduced tiredness. However, sympathy expression method has been studied only for a robot that expresses emotions by changing facial expressions. In the area of human-robot interactions, conventional research stated that body motions of robots are useful in the interactions between humans and robots as well as in expressing emotions [7]. Thus, sympathy expression method using both facial expression change and body motion may be better than one based only on facial expression change. This paper reported the Experiment1 to measure the short-term impression and the Experiment2 to measure studying effects and long-term impression.

2 Sympathy expression method

The sympathy expression method is based on Russell's circumplex model of affect (shown in Fig.1). This method can be used to express emotions in the circumplex model using the correct answer vector $\vec{A}$ and the incorrect answer vector $\vec{B}$; thus, the learners believe that the robot sympathizes with them. If learner correctly answers the question, the robot expresses emotions using $\vec{A}$; in contrast, the robot expresses emotions using $\vec{B}$ for incorrect answer. $\vec{A}$ moves in the area $0 \leq L_A \leq 1.0$ and $-90° \leq \theta_A \leq 90°$. $\vec{B}$ moves in the area $-1.0 \leq L_B \leq 0$ and $-90° \leq \theta_B \leq 90°$. $L\cos\theta$ refers to the axis of "Pleasure-Displeasure." $L\sin\theta$ refers to the axis of

*Yuhei Tanizaki, Room #309, Building No.3, Furo-cho, Chikusa-ku, Nagoya, Aichi, +81-52-789-2793 & tanizaki@cmplx.cse.nagoya-u.ac.jp

https://dx.doi.org/10.25046/aj040224

"Arousing-Sleep." The emotion vectors move as follows [6].

if (learners solve the problem correctly)
$L_A \leftarrow L_A + 0.2$
$L_B \leftarrow L_B + 0.2$
else
$L_A \leftarrow L_A - 0.2$
$L_B \leftarrow L_B - 0.2$
if (the time of answer < reference time)

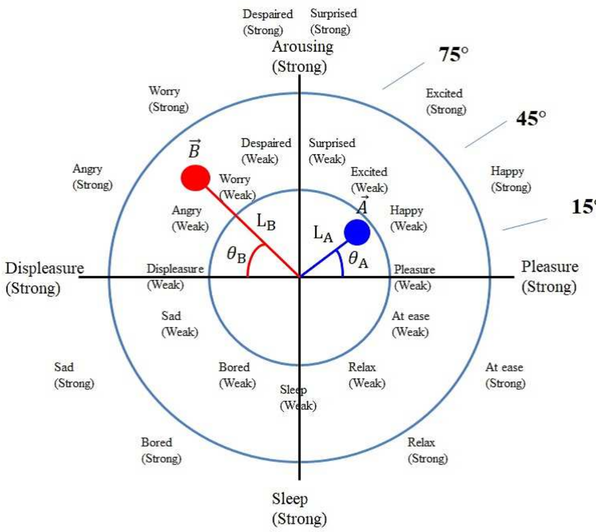

Figure 1: Sympathy expression method

if (learners solve the problem correctly)
$\theta_A \leftarrow \theta_A + 15$
else
$\theta_B \leftarrow \theta_B + 15$
else
if (learners solve the problem correctly)
$\theta_A \leftarrow \theta_A - 15$
else
$\theta_B \leftarrow \theta_B - 15$

In these experiments, the reference time is decided by the answer time in the earlier question. In the 1st question of studying, reference time is decided by the average answer time before studying. However, in first studying, reference time is 60. All robots utilized in these experiments were assumed to have the same sympathy expression method to enable a fair comparison.

3 Robot

3.1 Overview

In this study, we used a tablet robot ,"Tabot", whose head consists of tablets. as shown in Fig. 2. Tabot can express a lot of facial expressions by expressing the agent on the screen of the tablet.. It has 14 degrees of freedom: the neck has 3 degrees of freedom, the arms have 10 degrees of freedom, and the legs have 1 degree of freedom. So, it can do many body motions. It can express many emotions by combination of body motions and facial expressions. In these experiments, 2 Tabots were utilized for reducing the effects of the shape of robot.

Figure 2: The Tabot used in the experiment

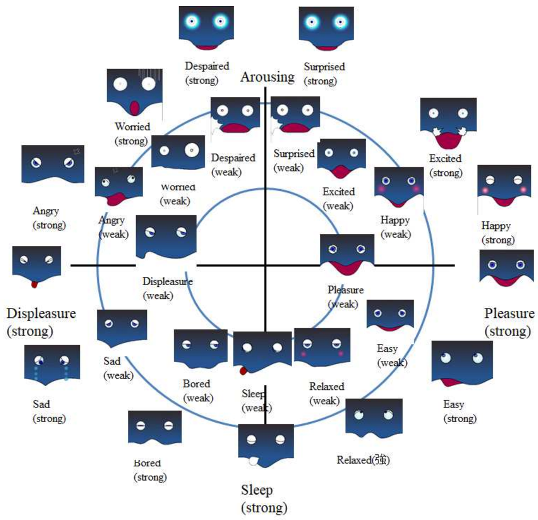

Figure 3: Facial expression

3.2 Facial expressions and body motions

The face displayed in its tablet and the changes in Tabot's facial expressions were developed based on a specific design. Two types of facial expressions were used to express the emotions corresponding to each emotion in the circumplex model. Fig. 3 shows example of facial expression of the Tabot. Conversely, Tabot's body motions were created on the basis of [8] and [9], which discussed the relation between human emotion and physical activity. Two types of body motions can be used to express each emotion and the corresponding emotions in the circumplex model. The body motions and facial expressions that expressed the same emotions were combined. We implemented facial expression as well as a combination of facial expressions and body motions such that emotions can be communicated precisely to the learners. Fig. 4 shows example of combination of facial expression and body motion of the Tabot.

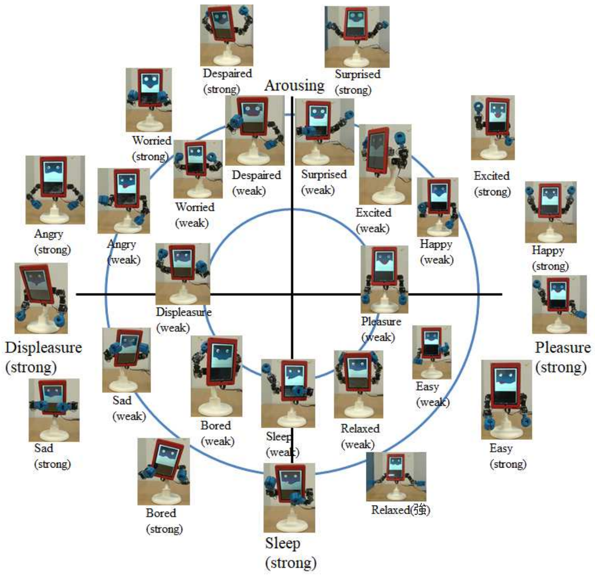

Figure 4: Combination of facial expression and body motion

4 Experiment 1

4.1 Method

The subjects learned with the robot comprising the sympathy expression method and a studying system. When a subject answered a question, the studying system displayed a correct or a incorrect response. Subjects learned by answering the questions displayed in the studying system. 4 university students and 8 graduate students in the science stream were gathered for this experiment. The participants had never used a Tabot previously. The twelve learners used two types of robots. The first type of robot was called "Robot-Facial-Group", which expressed emotions using only facial expressions. The second type of robot was called "Robot-Combination-Group", which used both facial expressions and body motions. The robots were used in a random manner. The subjects answered 20 questions in each group.

The upper side of Tabot's tablet displayed facial expressions. The lower side of the robot's tablet displayed studying systems. Tabot expressed emotions when the studying system gave either a correct or a incorrect response.

4.2 Overview of the studying system

We used the studying system (Fig. 5) for math questions called "Synthetic Personality Inventory 2 (SPI2)." SPI2 is used as a recruitment test for employment. Moreover, it uses junior high school level math questions. Therefore, university students do not require knowledge for SPI2.

Subjects first log in with an account number. Fig. 5(a) shows a menu of the study contents (i.e.,math questions). The column used for choosing the number of questions is shown under the study items. When a learner selected "20," 20 questions were shown randomly. Subsequently, repeating the same selection would display different twenty questions that could be repeated until all 100 questions are displayed. Thus, it enables learners to answer all the questions within the chosen study item. When a subject selected a study content and the number of questions, the studying screen (Fig. 5(b)) appeared and the studying process began. The subject answered the question from the selection list. Subsequently, the system displayed whether it was the correct answer as shown in Fig. 5(c). When the subject selected "Next" as shown in Fig. 5(c), the system moved on to the next question. When the subject selected "Result" as shown in Fig. 5(c), or solved all the questions, the system moved on to the results page (Fig. 5(d)), which presented the number of correct answers. When the subject selected "Study again," the menu of the studying items was displayed (Fig. 5(a)). When the subject selected "Study incorrect answers," the study page presented questions that were answered incorrectly (Fig. 5(b)).

4.3 Evaluation criterion

Impression evaluation used the rating scale method, which is a quantitative evaluation of impressions as shown in Fig.6. The rating scale method has 14 questions; it uses a range of values, e.g, "Friendly - Friendless," "Emotional - Intelligent," "Be pleased with me - Be not pleased with me," and "Enjoying studying - Not enjoying studying". The scores of the rating scale method range from 1 to 7. In Fig. 6, the left score is 7, and the right score is 1. In each group, subjects answered this questionnaire at the end of studying. Furthermore, subjects answered a questionnaire on the general comments about impressions. We defined the sum of scores of all questions as the score of good impressions. We conducted paired t-test for impression evaluation.

4.4 Result

Fig. 7 indicates the average impression score in two groups. This graph indicates the score of the Robot-Combination-Group is better than that of the Robot-Facial-Group. The result of paired t-test showed that the good impression score of the Robot-Combination-Group is significantly different from that of the Robot-Facial-Group. These results show that the robot that expresses emotions using both body motions and facial expressions can give learners a better impression than the one that expresses emotions using facial expressions only.

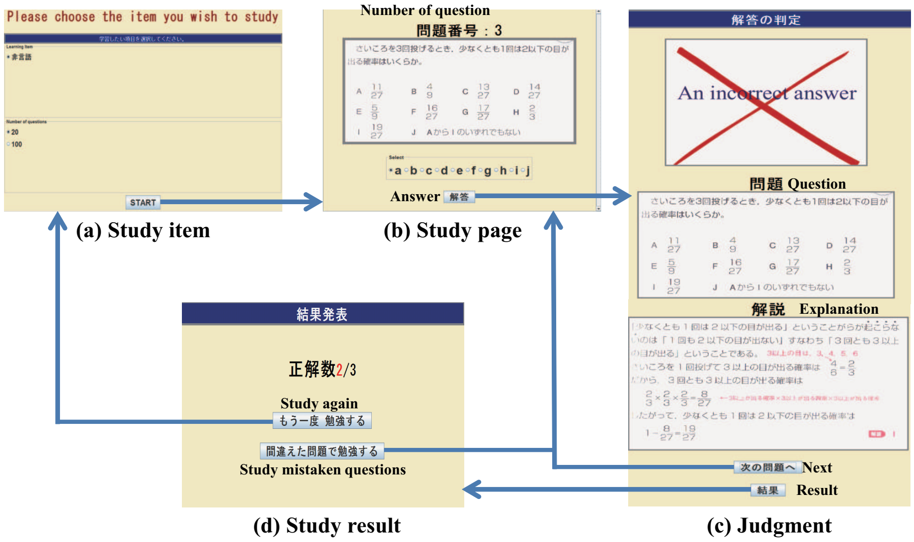

Figure 5: studying system

4.5 Discussion

The result of the experiment indicate that the sympathy expression method that expresses emotions using both body motions and facial expressions can give learners a better impression than a method that expresses emotions using facial expressions only. In the general comments column, somebody stated, “It was difficult for me to look at the robot’s facial expressions.” This implies that it is possible for some learners to not notice that the facial expression of the robot was changing because they concentrated on the questions of the studying system. Therefore, the impression made by the Robot-Combination-Group was quite different from that made by the Robot-Facial-Group.

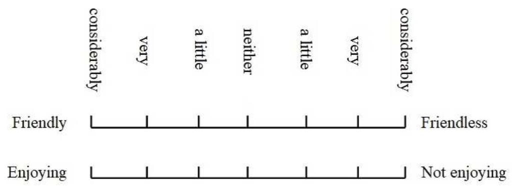

Figure 6: Examples of the rating scale method

5 Experiment 2

5.1 Method

The subjects learned with a robot comprising a sympathy expression method and a studying system. When a subject answers question, the studying system shows a correct or incorrect judgment. Subjects learned by answering the questions which were displayed by the studying system.

20 university students who had never studied with Tabot previously were gathered for this experiment. 20 subjects were divided into two groups of 10 students each; “Robot-Facial-Group” and “Robot-Combination-Group.” The subjects in Robot-Facial-Group studied with Tabot, which expresses only facial expressions. The subjects in Robot-Combination-Group studied with Tabot, which expresses a combination of facial expressions and body motions. These subjects were instructed in math by the studying system for 40 minutes, 2 or 3 times a week, for 1 month. Thus, they studied 12 times in a month. During the studying of 1st and 12th time, subjects used studying system on their own to measure their ability before and after studying. These are the pre-test and the post-test scores. From the 2nd time to 11th time, subjects learned using the studying system with the Tabot.

The upper side of Tabot’s tablet showed facial expressions. The lower side of Tabot’s tablet showed the studying system. Tabot expressed emotions when the studying system gave a correct or an incorrect response.

The robot and studying system used in this experiment is the same as those used in Experiment1.

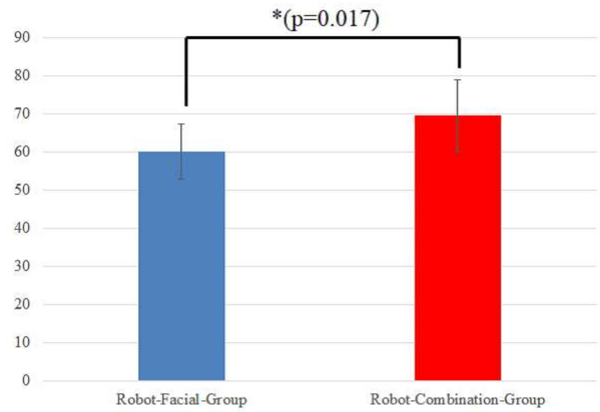

Figure 7: Impression score in experiment1

5.2 Evaluation criterion

Studying effect was calculated based on the improvement score got by difference of the pre-test score and post-test score. Each of these scores was calculated by

100 questions shown by the studying system. Impression evaluation was calculated in rating scale method, that is same as Experiment1. In all groups, subjects answered the questionnaire after the 11th studying. We defined the sum of scores of all questions as the score of good impressions. We conducted a Welch's t-test to improve the studying effect and the impression evaluation. To admit a significant difference based on the fact that p values is 5%, we adjusted the significance level (p = 0.025) using the Bonferroni method.

5.3 Result

5.3.1 Improvement score

Fig. 8 indicates the pre-test average score and the post-test average score in two groups. Fig. 9 indicates the average improvement score in two groups. Fig.9 indicates that the score of the Robot-Facial-Group is higher than the score of the Robot-Combination-Group. We conducted Welch's t-test to compare the studying effects. The results show that there was no significant difference in the improvement score between the two groups.

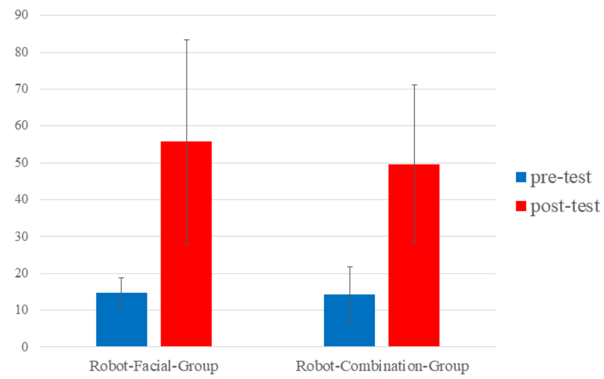

Figure 8: Score of pre- and post-test

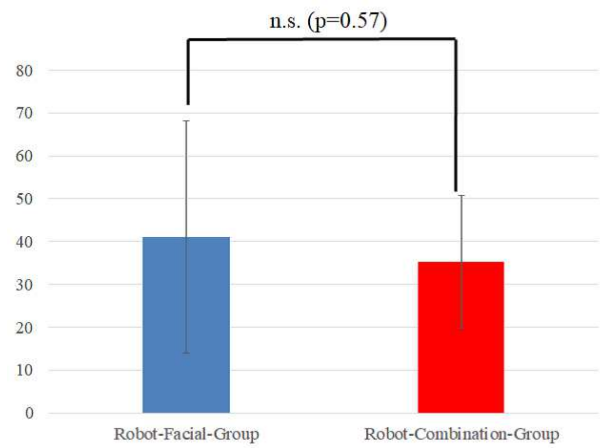

Figure 9: Improvement score

5.3.2 Questionnaire

Fig. 10 shows the average impression score in two groups. This graph shows that the average impression score of the Robot-Combination-Group is higher than that of Robot-Facial-Group. We conducted Welch's t-test to compare the impression scores. The results showed there was no significant difference in the impression score between the two groups.

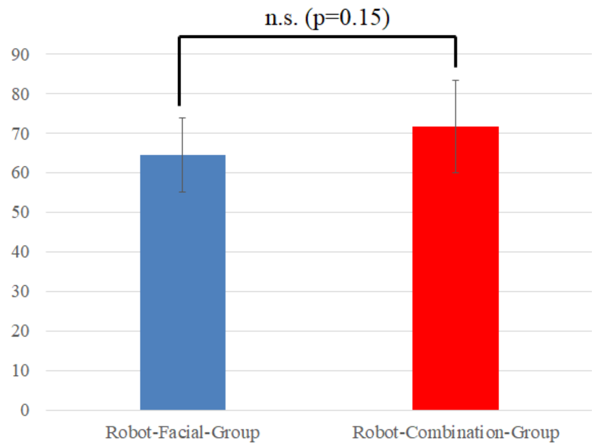

Figure 10: Impression score in Experiment2

5.4 Discussion

The result of studying effect indicates that it is higher in Robot-Facial-Group than in Robot-Combination-Group. Table.1 shows the number of answering questions in Robot-Facial-Group. Table.2 shows the number of answering questions in Robot-Combination-Group. The average number of answering questions is shown in Fig. 11. The answering questions were defined as the number of answered questions in each studying session. The average number of answering questions shows that its number was higher in Robot-Facial-Group than in Robot-Combination-Group. The time to express emotion by body motion is longer than the time to express emotions by facial expression change. Thus, the fact that the robot cannot move to the next problem while expressing emotion produced the difference in the average number of answers between the two groups. Moreover, we determined that the studying time in Robot-Combination-Group was shorter than that in Robot-Facial-Group. We believe that it is possible that the studying effect can be influenced by the number of answering questions.

In contrast, the result of the questionnaire shows that the robot in the Robot-Combination-Group gave a better impression than that in the Robot-Facial-Group. Therefore, the body motion of the robot manifested emotion efficiently as reported in conventional research [7]. Therefore, we believe that learners felt the more sympathy from the robot expressing emotions using body motions than from the robot expressing emotions using facial expressions only.

However, in this experiment, we could not find significant difference in the impression score between the two groups. Thus, we calculated the percentage of the expressed emotions. Fig. 12 shows the percentage of emotions expressed in the Robot-Combination-Group. It shows that only three types of emotion out of 28 were often expressed by robots in the Robot-Combination-Group. Therefore, learners may feel that robots in this group always expressed the same emotion. Therefore, robots that expressed emotions using body motions and facial expressions did not show any significant difference compared to the robots that expressed emotions using facial expressions only.

Table 1: The number of answering questions in Robot-Facial-Group

No.	2nd	3rd	4th	5th	6th	7th	8th	9th	10th	11th
1	36	29	41	48	52	51	50	59	61	70
2	26	23	18	25	38	41	39	39	38	38
3	20	14	25	24	27	30	36	26	27	38
4	21	24	25	21	19	20	31	27	33	44
5	25	32	29	36	29	38	46	53	70	80
6	24	26	22	21	31	29	31	36	39	41
7	31	31	29	38	38	40	50	72	79	93
8	16	18	20	17	18	14	22	23	14	30
9	38	31	36	36	33	36	51	40	36	45
10	24	33	31	30	40	39	41	55	53	69

Table 2: The number of answering questions in Robot-Combination-Group

No.	2nd	3rd	4th	5th	6th	7th	8th	9th	10th	11th
1	24	32	39	26	32	37	38	47	40	43
2	19	18	20	15	27	28	30	40	45	54
3	25	25	25	29	30	35	40	43	36	37
4	22	18	24	23	32	33	30	38	43	41
5	21	23	27	24	30	26	32	28	36	40
6	18	19	17	27	22	17	23	30	35	26
7	17	17	24	26	20	28	29	29	34	41
8	23	28	26	29	47	38	52	51	63	66
9	17	18	23	30	40	28	38	37	47	46
10	24	23	28	23	38	39	49	59	81	83

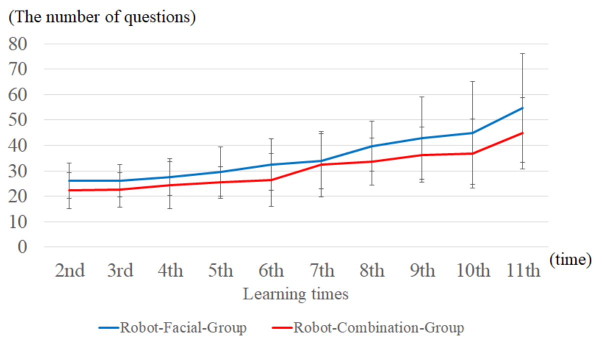

Figure 11: The average number of answering questions

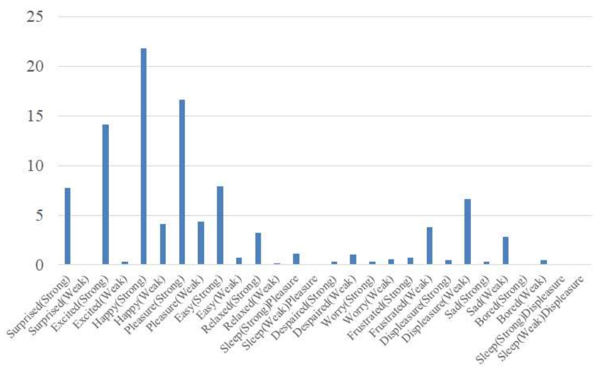

Figure 12: The percentage of expressed emotion

6 Conclusion

This paper examined the effects of sympathy expression method using body motion and facial expression in short-term and long-term experiments. We used "Tabot", a tablet-type robot that has a tablet head. Tabot has a sympathy expression method. In the experiment we performed, we used two types of' Tabot; robots that express emotions using facial expressions only and those that use a combination of body motions and facial expressions to express emotions. The results of Experiment1 suggest that the robot that expressed emotions using body motions and facial expressions prompted more impression to the learners than the robot that expressed emotions using facial expressions only. The results of Experiment2 suggest that robots that express emotions using facial expressions can better prompt learners to improve their studying effect than those that express emotions using the combination of body motions and facial expressions. Moreover, we determined that the robots that express emotions using facial expressions and body motions prompted more impression to the learners than those that express emotions using facial expressions only. However, robot that express emotions using body motions and facial expressions has issues relating to the time of expressing emotions and the kind of emotions they expressed.

In the future, we plan to improve the algorithm for sympathy expression in a way that solves the problem of time of expressing emotions and the kind of emotions expressed by the robot.

Acknowledgment This work was supported by MEXT KAKENHI (Grant-in-Aid for Scientific Research (B), No.16H02889)

References

[1] T. Kanda, T. Hirano, D. Eaton and H. Ishiguro, "Interactive robots as social partners and peer tutors for children: A field trial," Hum-Comout. Interact., vol.10, no. 1, pp. 61–84, 2004

[2] O.H. Kwon, S.Y. Koo, Y.G. Kim, and D.S. Kwon, "Telepresence robot system for English tutoring," IEEE Workshop on Advanced Robotics and its Social Impacts, pp. 152–155, 2010

[3] S. Koizumi, T. Kanda, and T. Miyashita, "Collaborative studying Experiment with Social Robot (in Japanese)," Journal of the Robotics Society of Japan, vol. .29, no. 10, pp. 902–906, 2011

[4] T. Kanda, T. Hirono, E. Daniel and H. Ishiguro, "Participation of Interactive Humanoid Robots in Human Society: Application to Foreign Language Education," Journal of the Robotics Society of Japan, vol. .22, no. 5, pp. 636–647, 2004

[5] F. Jimenez, M. Kanoh, T. Yoshikawa, T. Furuhashi, "Effects of Collaborative studying with Robots That prompts Constructive Interaction," Proceedings of IEEE International Conference on Systems, Man and Cybernetics, pp. 2983–2988, 2014

[6] F. Jimenez, T. Yoshikawa, T. Furuhashi and M. Kanoh, "Effects of Collaborative studying with Robots using Model of Emotional Expressions," journal of Japan Society for Fuzzy Theory and Intelligent Informatics, vol. 28, no. 4, pp. 700–704, 2016

[7] T. Kanda, M. Imai, T. Ono, H. Ishiguro, "Numerical Analysis of Body Movements on Human-Robot Interaction," IPSJ Journal, Japan, Vol.44, No.11, pp.2699-2709,2003

[8] Y. Toyama and L. Ford, "US-Japan Body Talk augmented New version Gestures · Facial expressions · Gesture's dictionary," Sanseido, Japan, 2016

[9] D. Morris and Y. Toyama, "Body talk New style version World gesture dictionary," Sanseido, Japan, 2016

Advances in Science, Technology and Engineering Systems Journal Vol. 4, No. 2, 190-196 (2019)

www.astesj.com

Special Issue on Recent Advances in Engineering Systems

ASTESJ

ISSN: 2415-6698

Nonlinear Analytic Modeling for Novel Linear Variable Reluctance Motors

Aymen Lachheb[*,1], Jalel Khediri[2], Lilia El Amraoui[1]

[1]*SEICT, LR18ES44, Enicarthage, 2035, Tunisia*

[2]*SIME, University of Tunis, 1008, Tunisia*

A R T I C L E I N F O

Article history:
Received: 05 January, 2019
Accepted: 03 March, 2019
Online: 26 March, 2019

Keywords:
Linear motor
Analytic modeling
Finite elements method
Fourier series

A B S T R A C T

In this paper, an analytical modeling is proposed to compute the static and dynamic characteristics of linear variable reluctance motors with taking account of the saturation and the non-linearity of the magnetic circuit. The proposed model is based on the Fourier series expression of the phase flux in which the variation of the linkage flux with phase current is defined by arc tangent function. Then, an analytical expression for the co-energy and electromagnetic forces are derivative. The effectiveness of the proposed method is proved in terms of accuracy by comparing the computed results obtained by the two dimensional finite elements method with analytic model. Subsequently, the proposed modeling approach is simple and provides accurate representation of linear variable reluctance motor, as confirmed by the compared results.

1. Introduction

Linear variable reluctance motor (LVRM) becomes one of the most promising candidates for direct drive systems [1] and it will be more attractive because of its higher developed force and its immense efficiency which make it more competitive with conventional rotary motor [2]. Furthermore, the LVRM is highly robust with low cost manufacturing, this allows linear motors to be used in the numerical control of machine tools and in robotics applications. Hence, a drive system with LVRM has gained a great interest for several industrial application [3].

However, the LVRMs operate with a high magnetic flux density in order to produce a maximum of power, which causes a saturation in the magnetic circuit. In addition, the characteristic of LVRM is strongly dependent on the state of the magnetic circuit, which is depending on the supplying current of windings and the position of translator relative to the stator teeth [4]. Then, the performance of LVRM is strongly influenced by the saturation of magnetic circuit for high levels of flux density, this phenomenon is repeated periodically as long as the translator move out from the unaligned position to reach the aligned position. In fact, the magnetic non–linearity makes the study of this motor more difficult.

Therefore, to predict the static and the dynamic performance of the motor precisely requires a correct representation of magnetic quantities, it is necessary to elaborate an analytical model, which takes account of the saturation effects in the magnetic circuits during the operation of this motor.

Several modeling technique has been proposed recently for studying the static and dynamic performances of the linear motor, finite element method (FEM) is one of popular approach adopted for the non-linear magnetic analysis of electrical machines [5], but it requires high computer performance and the calculation time needed to solve the equations governing the motor operation is quite long. For this reason, that we find many research works are adopting the analytic modeling to determine the characteristics of the variable reluctance motor [6].

Recently several research works have dealt with modeling and simulation of switched reluctance motor, some models are based on the expression of the inductance on the other hand, some model is based on the expression of the flux linkage [7, 8].

In reference [9], a nonlinear model is proposed which takes into account the magnetic saturation, a nonlinear representation of the phase inductance has been used to predict the characteristics for variable witched reluctance motor.

The authors in [10] propose an alternative approach for variable reluctance motor is based on the decomposition of flux linkage into vector functions of rotor position and current.

This paper presents a novel analytical modeling for LVRM based on the flux linkage expression, taking account the non-linearity of the magnetic circuit.

[*]Aymen Lachheb, aymen.lachheb@enicarthage.rnu.tn

https://dx.doi.org/10.25046/aj040225

Then, the flux linkage expression is described by a Fourier series in which the three first components are considered, the coefficients of the terms in the Fourier series are determined by the characteristic of the flux as function of current obtained from the finite element analysis at the aligned, unaligned and middle position. Then, the effectiveness of the developed model is proved by 2D FEM results.

2. The structure and principal of LVRM

The motor investigated in this study is a three phases linear variable reluctance motor. A cross section of the machine is presented in Figure 1, which show the overall structure of the motor. It has a two salient construction parts the stator and the translator. The coils are concentrated around the poles of the stator and the translator has no windings, the three phase windings are designed by A, B and C. Therefore, each phase of this motor is composed of two poles and each pole has two coils in series.

Firstly, we consider that the poles of the phase A are aligned with the stator teeth, when current passed through the winding of phase B , a pull force is produced that tends to align the translator with stator poles which corresponds to a position with minimum reluctance.

In order to ensure a regular movement, each phase winding is energized by a available current at a suitable translator position. It means that the phases excitation is done by order from phase to the next phase as the translator moves from a shifted position to an aligned position.

For continuous motion the excitation sequence is A, B, C then A, B, C. Similarly, motion in the opposite direction can be produced by using the excitation sequence A, C, B, A, C, B.

2.1. Electric model for LVRM

For a variable reluctance actuator, the electrical model refers to a phase winding, can be described by a voltage equation.

Based on the Faraday's and Ohm's laws, the voltage supply the phase winding is given as:

$$U = RI + \frac{d\phi(x,I)}{dt} \tag{1}$$

Where, I is the current passing through a phase coils, R is the resistance per phase, x the position of translator and ϕ is the flux linkage of a phase.

2.2. Force equation

The force developed by a LVRM is relative to the rate of varaition of co-energy as long as the translator changes its position from one position to another. It can be defined as:

$$F_e(I,x) = \frac{\partial W_c(x,I)}{\partial x} \tag{2}$$

Where F_e is the instantaneous electromagnetic force and W_c is the co-energy. The latter can be expressed in terms of the flux linkage, as follows.

$$W_c = \int_0^I \phi(x,I)dI \tag{3}$$

The expression of the co-energy can be substitute in equation (2), which yields:

$$F_e(I,x) = \frac{\partial w_c}{\partial x} = \int_0^I \frac{\partial\phi(x,I)}{\partial x}dI \tag{4}$$

2.3. Mechanical equation

Before describing in detail the developed model, it is useful to present the equation governing the mechanical behavior of the linear motor.

The mechanical equation governing the linear motor operation can be given as:

$$m\,a = F_e - F_l - \xi\frac{dx}{dt} - f_0 \sin g(v) \tag{5}$$

Where m is the mass of the mobile, a is the acceleration, F_e is the developed force, F_l is the load force and ξ is the friction coefficient [11].

3. Finite Element Design of LVRM

The developed finite element model is performed according to the geometric parameters of the motor presented in table I.

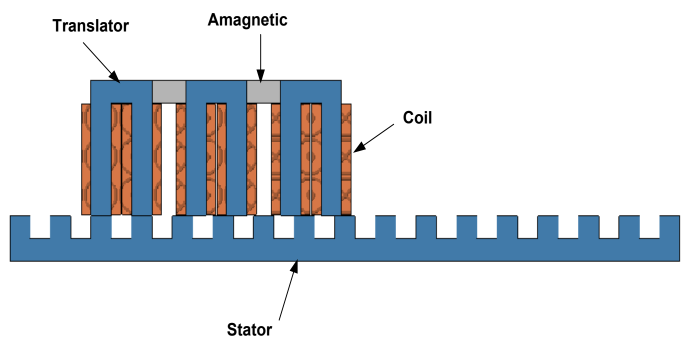

Figure 1. Single sided variable reluctance motor

To achieve a regular operation in step mode, the teeth and the slot widths are chosen equal.

$$\text{Hence } W_{tp} = W_{ts} = 30\text{mm} \tag{6}$$

The pole and slot widths are related to the pole pitch by the following equation:

$$\lambda = W_{ts} + W_{tp} \tag{7}$$

Where W_{ts} is the translator slot width, W_{tp} is the translator pole width and λ is the pole pitch.

The operation of the variable reluctance motor is based on the principle that the phases are powered independently and only one phase pole must be aligned with the stator poles. Then, to impose a regular step during the operation, a non-magnetic separation between different phases is necessary.

The translator is composed by three similar module separated by a non-magnetic material whose width is determinate by :

$$S = S_0 + k\lambda \tag{8}$$

With $0 < S_0 < \delta$ and $k = \{0,1,2,3\}$

The mechanical step δ_m is correlated to the pole pitch and the phases number N by the following equation (9):

$$\delta_m = |S_0 - W_{ts}| = \frac{\lambda}{N} \tag{9}$$

The yoke thickness of the stator and the translator are choosing equal to the slot width.

$$Y_{sy} = Y_{ty} = W_{ts} \tag{10}$$

Table 1: Specific geometry of designed motor

Parameters	Value(mm)
Stator pole width	30
Stator slots width	30
Stator yocke thikness	30
Translator pole width	30
Translator slots width	30
Translator yocke thikness	30
Separation	50
No of turns of wdg/phase	350
Section of copper	0.5
Air gap length	0.5

The 2D finite elements results obtained by the developed model are used to elaborate a surface response of the thrust force and flux linkage according to the translator positions and different supplying current level Figure 2 and Figure 3.

The simulation results are performed during a mechanical cycle where the moving part translates from the initial aligned position (x=0) to the next aligned position (x=0.06m) going through the unaligned position (x=0.03m).

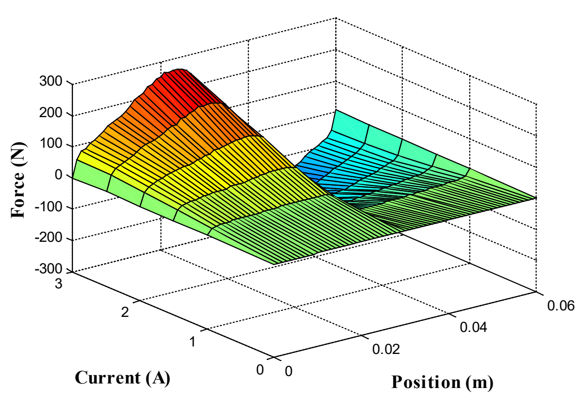

Figure 2 . Force as function of position for different current level

In order to develop a high force, the variable reluctance motor operates in saturation part of the B-H curve of the magnetic material, so it has a nonlinear behavior. The origin of this non linearity is mainly due to the non-linearity of the material used for the construction of magnetic circuits and the salient structure of the studied motor [12].

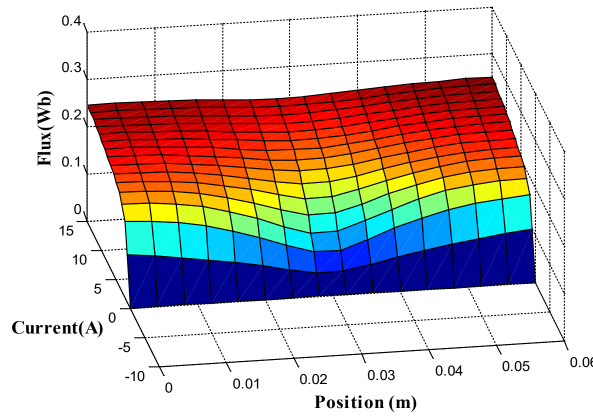

Figure 3 . Flux according to the translator position for different current

To avoid the problem of inaccuracies of the numerical method and in order to achieve a precise model of LVRM, it is recommended to use a methodology that permits to take account the nonlinearity of the magnetic characteristic of the used material while minimizing the simulation time. There are two main analytic modelling of LVRM used in previous work: the flux based model and the inductance based model [13, 14, 15].

In this study, the flux-based model is adopted to determine the static and the dynamic performances of the proposed motor. The proposed model for LVRM can be divided into two parts: a electrical and a mechanical part, they are realized as follows.

4. Analytical Modelling Approach for LVRM

In literature, there are two types of modelling, the linear model and the nonlinear model. Several research studies have adopted either the linear model [13] or the nonlinear model to predict the performance of a variable reluctance motor. The basic concept of this modeling consists of dividing the static flux linkage characteristics into two areas such as the unsaturated region and the saturated region as shown in Figure4. From the flux linkage characteristics, the two analytical models of the LVRM are defined as follows.

In the unsaturated region, when the phase current is lower than the saturation current $I_j \leq I_{sat}$, the LVRM is defined by a linear model. In the other hand, in the saturated region, when $I_j \geq I_{sat}$, the LVRM performances can be defined by a nonlinear model.

In the both models the flux linkage is represented by Fourier series and assumed has a cosine function of the position x although. However, in the nonlinear model a great harmonic order in Fourier series is used to give a satisfactory result. Then, it is possible to add another higher harmonics in the proposed model when more accuracy is needed [4].

4.1. Nonlinear Flux Based Model of LVRM

The modeling of variable reluctance machines is more complex than those of alternative current machines because of its highly nonlinear operation. The flux in each phase has a nonlinear

$2\pi/3$.

Consequently, an analytical model for the flux based on Fourier series representation is developed in this part.

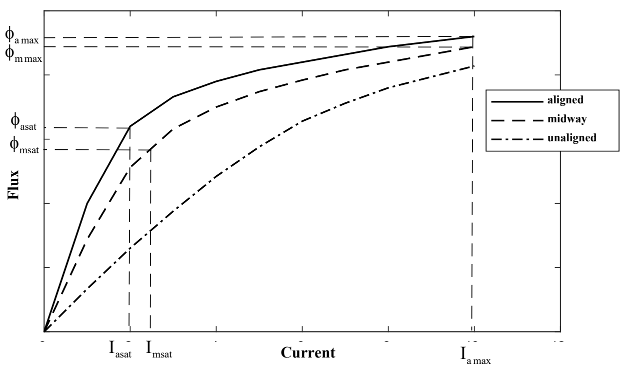

Figure 4. Flux current characteristic for three positions

Considering the first three components in Fourier series [7]. The flux in each phase can be represented as:

$$\begin{cases} \phi_j(x,I) = \sum_{k=0}^{n} \phi_k(I)\cos(k\frac{2\pi}{\lambda}x - (j-1)\frac{2\pi}{3}) \\ 0 < k < n \quad \text{and } j = 1,\ 2,\ 3 \end{cases} \tag{11}$$

Where n is the number of terms included in the Fourier series and j is the phase index.

Considering the first three components of the Fourier series in Equation (11), the flux expression become:

$$\begin{aligned} \phi_j(x,I) &= \phi_0(I) + \phi_1(I)\cos(\frac{2\pi}{\lambda}x - (j-1)\frac{2\pi}{3}) \\ &+ \phi_2(I)\cos(\frac{4\pi}{\lambda}x - (j-1)\frac{2\pi}{3}) \end{aligned} \tag{12}$$

Where ϕ_0, ϕ_1, ϕ_2 are the first three terms of Fourier series.

The developed model is written in a matrix form as:

$$\phi_j(x,I) = \begin{bmatrix} \phi_0(I) & \phi_1(I) & \phi_2(I) \end{bmatrix} \begin{bmatrix} 1 \\ \cos(\frac{2\pi}{\lambda}x - (j-1)\frac{2\pi}{3}) \\ \cos(\frac{4\pi}{\lambda}x - (j-1)\frac{2\pi}{3}) \end{bmatrix} \tag{13}$$

The matrix model of flux is developed by considering three important positions, the aligned position (x=0), the midway position (x=15mm) and the unaligned position (x=30mm).

$$\begin{cases} \begin{bmatrix} \phi_{al} \\ \phi_m \\ \phi_{un} \end{bmatrix} = \begin{bmatrix} 1 & 1 & 1 \\ 1 & \cos(\frac{2\pi}{\lambda}15) & \cos(\frac{4\pi}{\lambda}15) \\ 1 & \cos(\frac{2\pi}{\lambda}30) & \cos(\frac{2\pi}{\lambda}30) \end{bmatrix} \begin{bmatrix} \phi_0(I) \\ \phi_1(I) \\ \phi_2(I) \end{bmatrix} \\ \begin{bmatrix} \phi_{al} \\ \phi_m \\ \phi_{un} \end{bmatrix} = \begin{bmatrix} 1 & 1 & 1 \\ 1 & 0 & -1 \\ 1 & -1 & 1 \end{bmatrix} \begin{bmatrix} \phi_0(I) \\ \phi_1(I) \\ \phi_2(I) \end{bmatrix} \end{cases} \tag{14}$$

With ϕ_{al}, ϕ_m and ϕ_{un} are the flux values for the aligned, intermediate and unaligned positions respectively.

Hence,

$$\begin{bmatrix} \phi_0(I) \\ \phi_1(I) \\ \phi_2(I) \end{bmatrix} = \begin{bmatrix} 1 & 1 & 1 \\ 1 & 0 & -1 \\ 1 & -1 & 1 \end{bmatrix}^{-1} \begin{bmatrix} \phi_{al} \\ \phi_m \\ \phi_{un} \end{bmatrix} \tag{15}$$

The three coefficients ϕ_0, ϕ_1, ϕ_2 can be computed based on the flux in three positions as follow.

$$\phi_0 = \frac{1}{2}\left[\frac{1}{2}(\phi_{al} + \phi_{un}) + \phi_m\right] \tag{16}$$

$$\phi_1 = \frac{1}{2}(\phi_{al} - \phi_{un}) \tag{17}$$

$$\phi_2 = \frac{1}{2}\left[\frac{1}{2}(\phi_{al} + \phi_{un}) - \phi_m\right] \tag{18}$$

The flux at the aligned and the midway position is determined by an arctangent function.

$$\phi_{al} = \frac{\tan^{-1}(\alpha_1 I)}{\alpha_2} \tag{19}$$

$$\phi_m = \frac{\tan^{-1}(\beta_1 I)}{\beta_2} \tag{20}$$

Where α_1, α_2, β_1 and β_2 are constants that can be calculated by following the steps below:

- Define two points $\phi_{a\,max}$ and ϕ_{asat} on the flux curve relative to the aligned position.

The value of the flux $\phi_{a\,max}$ corresponds to the maximum current I_{max} (maximum current), whereas ϕ_{asat} it corresponds to the current I_{asat} (Saturation current).

-The constant α_1 can be determined by using the relation below:

$$\frac{\phi_{a\,max}}{\phi_{asat}} = \frac{\tan^{-1}(\alpha_1 I_{max})}{\tan^{-1}(\alpha_1 I_{asat})} \tag{21}$$

Where $\phi_{a\,max}$ is the maximum flux linkage at the aligned position, ϕ_{asat} is the saturated flux, I_{max} is the maximum current and I_{sat} is the saturated current.

-The constant α_2 can be determined as follow:

$$\alpha_2 = \frac{\phi_{sat}}{\tan^{-1}(\alpha_1 I_{sat})} \tag{22}$$

-The coefficient β_1 and β_2 can be calculated in the same way as α_1 and α_2 by using the suitable data obtained from the flux curve in the midway position.

-Since the saturation effect does not exist in unaligned position, therefore the flux linkage can be approximated by a linear equation.

$$\phi_{un} = L_{un} I \tag{23}$$

Where, L_{un} represent the phase inductance at the unaligned position.

4.2. Computation of Electromagnetic Force

The developed electromagnetic force is proportional to the square of current if the motor is unsaturated (L_a and L_{un}=cte), when the current increase and exceeds the saturation current then the electromagnetic force is no longer proportional to only the square of current it can be derived from the co-energy expression.

The flux depends to the translator position and the phase current. Then, the partial derivative of the flux with translator position can be written as:

$$\begin{aligned}\frac{\partial \phi_j}{\partial x} &= -\frac{2\pi}{\lambda}\phi_1 \sin\left[\frac{2\pi x}{\lambda} - (j-1)\frac{2\pi}{3}\right] \\ &-\frac{4\pi}{\lambda}\phi_2 \sin\left[\frac{4\pi}{\lambda} - (j-1)\frac{2\pi}{3}\right]\end{aligned} \tag{24}$$

From equation (4), the developed force by one phase of the LVRM is described as:

$$\begin{aligned}F_e &= \int_0^I \left[-\frac{2\pi}{\lambda}\phi_1 \sin(\frac{2\pi}{\lambda}x) - \frac{4\pi}{\lambda}\phi_2 \sin(\frac{4\pi}{\lambda}x)\right] dI \\ &= -\frac{2\pi}{\lambda}\sin(\frac{2\pi}{\lambda}x)\int_0^I \phi_1 dI - \frac{4\pi}{\lambda}\sin(\frac{4\pi}{\lambda}x)\int_0^I \phi_2 dI\end{aligned} \tag{25}$$

By substituting the equations (17) and (18) into equation (25), the expression of the force become.

$$\begin{aligned}F_e &= -\frac{2\pi}{\lambda}\sin(\frac{2\pi}{\lambda}x)\left[\frac{1}{2}\int_0^I \phi_{al} dI - \frac{1}{2}\int_0^I \phi_{un} dI\right] \\ &-\frac{4\pi}{\lambda}\sin(\frac{4\pi}{\lambda}x)\left[\frac{1}{2}\int_0^I \phi_{al} dI + \frac{1}{2}\int_0^I \phi_{un} dI - \int_0^I \phi_m dI\right]\end{aligned} \tag{26}$$

Where

$$\begin{cases}\int_0^I \phi_{al} dI = \int_0^I \frac{\tan^{-1}(\alpha_1 I)}{\alpha_2} dI = \frac{1}{\alpha_1\alpha_2}\left[(\alpha_1 I)\tan^{-1}(\alpha_1 I) - \frac{1}{2}\ln\left|1+(\alpha_1 I)^2\right|\right] \\ \int_0^I \phi_m dI = \int_0^I \frac{\tan^{-1}(\beta_1 I)}{\beta_2} dI = \frac{1}{\beta_1\beta_2}\left[(\beta_1 I)\tan^{-1}(\beta_1 I) - \frac{1}{2}\ln\left|1+(\beta_1 I)^2\right|\right] \\ \int_0^I \phi_{un} dI = \int_0^I L_{un} I dI = \frac{1}{2}L_{opp} I^2\end{cases} \tag{27}$$

5. LVRM Performances Prediction

To validate the model developed, we conducted simulation tests by developing a program designed around the Matlab/Simulink environment and adopting the following parameters:

U=24V, ξ =65Nsm^{-1}, $R = 8\Omega$, $\alpha_1 = 0.75$, $\alpha_2 = 6.55$, $\beta_1 = -0.54$, $\beta_2 = -6.59$, m=20Kg and L_{un}=0.5H.

In this section, the analytic model presented previously is simulated to predict the static and the dynamic performances of the LVRM. Subsequently, the obtained results are presented.

5.1. Static performances

The simulations results shown in this part are obtained basing on the analytical modeling approach described in part 3.

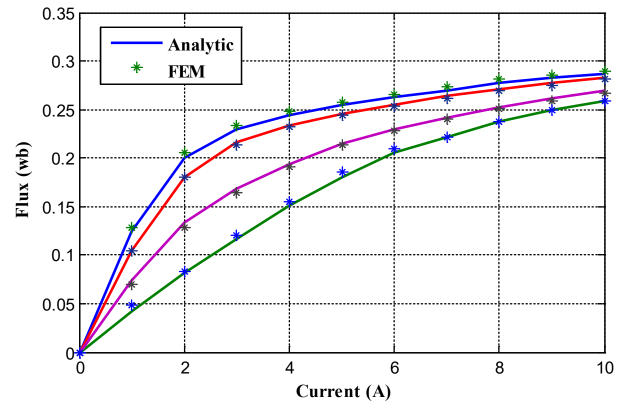

Figure 5 . Comparison between the calculated flux linkage and the FEM

Figure 5 shows a comparison of flux linkage/current characteristics for the designed motor of the analytic model with the result obtained by finite elements method (FEM). The comparison is made at four positions from aligned to completely unaligned position, it shows that the calculated flux is in good agreement with the computed FEM results.

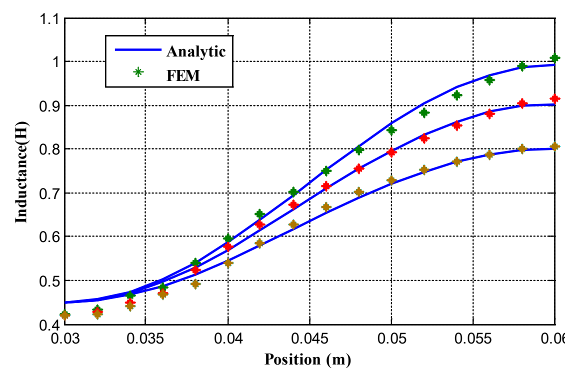

Figure 6 . Inductance as function of position for three current level

Figure 6 show the comparison of the computed magnetizing curves of the LVRM obtained by the proposed model and 2D Finite Element Method (FEM). Each curve of inductance is calculated under the condition that the phase A is excited by a selected current at different translator position. In addition, it is found that the obtained magnetizing curves from 2D FEM almost agree with those from the proposed model, only a slight difference in unaligned position is observed between the results obtained by both methods, due mainly to the assumption of non-existence of saturation at the unaligned position.

The phase inductance varies considerably at the aligned position with the current phase because of the magnetic saturation effect but the inductance at the unaligned position does not very much mainly because of the large reluctance that characterizes huge air gap in the flux path.

The accuracy of the proposed model can be enhanced by the appropriate choice of the number of Fourier terms. Thus, the observed mismatch can be improved by adding another Fourier term in the proposed model.

We can observe from Figure 6 that on the aligned position the values of the inductance vary considerably depending on the current level as the current increases the inductance decrease due to the saturation effect of the magnetic circuit and the inductance is constant at the unaligned position independent of the current value the effect of saturation is negligible.

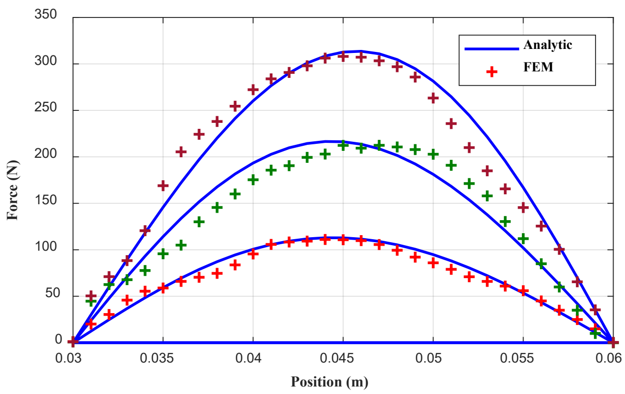

Figure 7 . Static force curve comparison for three current level

The comparative results of static force computed by the 2D FEM and calculated by an analytic model are shown in Figure 7, the comparison is done under the single phase operation at three different supplying currents from 1 A to 3A.

It can be observed from Figure 7, that the profile of the calculated force waveform relatively agrees well with that of the analytic one. Therefore, the validity of the proposed modelling approach is verified.

The developed model is validated from the above static behavior of the motor, so it will be possible to predict the dynamic performance of the motor by the proposed analytic modeling. In the following section, a non-linear dynamic performances analysis of LVRM are described.

5.2. Non-linear dynamic performances analysis :

In order to examine the validity of the proposed model in dynamic operating conditions, the analytical representation of flux is used to define the dynamic model by substituting this expression in the voltage equation. Then, the given model is implemented in Matlab Simulink to establish the dynamic performances of the LVRM and the obtained results has been compared with the FEM results. Therefore, a dynamic analysis based on the analytical model explained in this section.

For the variable reluctance motors, the flux linkage varies as a function of current and position, the phase voltage differential equation for active phase is given by.

$$U_j = RI_j + \frac{\partial \phi_j(x,I)}{\partial I}\frac{dI}{dt} + \frac{\partial \phi_j(x,I)}{\partial x}\frac{dx}{dt} \qquad (27)$$

Incorporating the flux expression (13) into equation (27), yields,

$$U_j = R_j I_j + \frac{\partial \phi_j}{\partial x} v + \begin{bmatrix} \frac{\partial \phi_0}{\partial I} + \frac{\partial \phi_1}{\partial I}\cos\left(\frac{2\pi x}{\lambda} - (j-1)\frac{2\pi}{3}\right) \\ + \frac{\partial \phi_2}{\partial I}\cos\left(\frac{2\pi x}{\lambda} - (j-1)\frac{2\pi}{3}\right) \end{bmatrix} \frac{dI}{dt} \qquad (28)$$

Therefore, the derivative of current can be obtained by calculating the partial derivative of the flux with translator position and the partial derivative of the flux with excitation current as:

$$\frac{dI}{dt} = \frac{U_j - R_j I_j - \frac{\partial \phi_j}{\partial x} v}{\begin{bmatrix} \frac{\partial \phi_0}{\partial I} + \frac{\partial \phi_1}{\partial I}\cos\left(\frac{2\pi x}{\lambda} - (j-1)\frac{2\pi}{3}\right) \\ + \frac{\partial \phi_2}{\partial I}\cos\left(\frac{2\pi x}{\lambda} - (j-1)\frac{2\pi}{3}\right) \end{bmatrix}} \qquad (29)$$

Where

$$\frac{\partial \phi_0}{\partial I} = \frac{1}{4}\left(\frac{\partial \phi_{al}}{\partial I} + \frac{\partial \phi_{un}}{\partial I}\right) + \frac{1}{2}\frac{\partial \phi_m}{\partial I} \qquad (30)$$

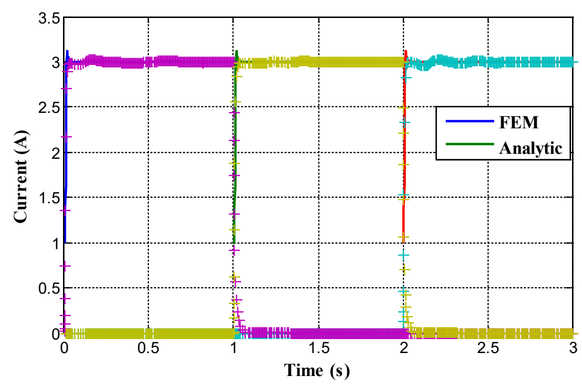

Figure 8 . Comparison of the computed and FEM phase current

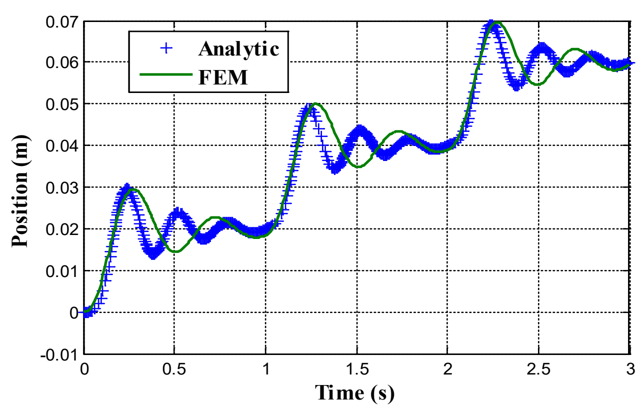

Figure 9 . Comparison of dynamic response of the motor

Figure 8 and Figure 9 present the comparison of the dynamic behavior of the motor. The superposition of these results shows that the dynamic response obtained by both methods admits the same response time with same over shoot, but slight difference noted for the number of oscillations between them. A rather good correlation in the results between the proposed model and FEM is observed.

6. Conclusion

In this paper, a novel non-linear model for a variable reluctance linear motor has been presented and compared with 2D FEM analysis results. This model based on the Fourier series analytical representation of flux linkage taking into consideration the effect of nonlinearity which has been neglected in some work describes its static characteristics. The model requires the motor flux characteristics obtained by finite element analysis.

The validity of the proposed model has been verified by the comparisons with results obtained from 2D FEM analysis. Furthermore, the accuracy of the proposed approach in dynamic conditions has been demonstrated. The developed model proves to be adapted for various uses with different machine configurations.

The developed model is motivated by the accurate performance prediction. In fact, it will be used to elaborate a control strategy for this motor.

Conflict of Interest

The authors declare no conflict of interest.

References

[1] I .Mahmoud, H .Rehaoulia, "Design and modeling of open loop components for a biomedical application" International transactions On Electrical Energy Systems, 2016. https://**doi**.org/10.1002/etep.2204

[2] F .Daldaban, N .Ustkouncu, "A novel linear switched reluctance motor for railway transportation systems". Energy Conversion and Management,465-469,2009. http://dx.**doi**.org/10.1016/j.enconman.2009.10.009

[3] F R .Salmasi, B. Fahmi, "Modeling switched reluctance machines by decomposition of double magnetic saliencies". IEEE Transactions On Magnetics, Vol 40, No.3, 2004. https://ieeexplore.ieee.org/document/1298927

[4] A. Khalil, I. Hussain, "Fourier series generalized geometry based analytical model of switched reluctance machines". IEEE Transactions On Industry Applications, Vol 43, No.3, 2007.

[5] A .Lachheb, L .El Amraoui, J. Khediri, "Finite element modelling of linear motor for automatic sliding door application". International journal of advanced computer science and applications, Vol.7 No.8, 2016.

[6] B .Fahimi, G .Suresh, J .Mahdavi, M. Ehsani, "A new approach to model switched reluctance motor drive application to dynamic performance prediction control and design". IEEE Powers Electronics, 1998.

[7] D. A. Andrade, R. Krishnan, "Characterization of switched reluctance machines using fourier series approach". 36th Conference Industry Applications, USA,2001. https://ieeexplore.ieee.org/document/955391

[8] H .Gao, F.R .Salmasi, M. Ehsani "Inductance model based sensorless control of the switched reluctance motor drive at low speed". IEEE Transactions On Power Electronics, Vol.19, No.4, 2004.

[9] H.P .Chi, R.L .Lin, J. F. Chen, "Simplified flux linkage model for switched reluctance motors" IE Proc Electr Power Applications, 152 (3), 2005.

[10] P. Lobato, S .Rafael, J. Pires, "Flux linkage characteristics models for switched reluctance machines". IECON 2010 - 36th Annual Conference on IEEE Industrial Electronics Society 2010.

[11] W. Zaafrane, J. Khedhiri, H. Rehaoulia, "Low-cost linear switched reluctance motor velocity and position control". Journal of Circuits Systems and Computers, 2016.

[12] M. Alrifai, M. Zribi, R. Krishnan , M .Rayan, "Nonlinear Speed Control of Switched Reluctance Motor Drives Taking into Account Mutual Inductance". Hindawi Journal of Control Science and Engineering, 2007.

[13] S. Buja, M. I. Valla, "Control characteristics of the SRM drives operation in the linear region". IEEE Transactions on Industrial Electronics, Vol.38 No.5, 1991.

[14] Z. Zhu, Y. Sun, Y. Yuan, "Decoupling control for fual winding Bearingless switched reluctance motor based on improved inverse system method". Hindawi Journal Mathematical Problems in Engineering, 2017.

[15] S.Husain, A.Hossain, "Modeling simulation and control of switched reluctance motor drives" IEEE Transactions On Industrial Electronics, Vol 52, No.6, 2005.

[16] S .Mir, I .Husain, M. E .Elbuluk, "Switched reluctance motor modeling with on-line parameter identification" IEEE Transactions On Industry Application, Vol.34, No.4, 1998.

[17] J .Fang, Y. Ren, "Decoupling control of magnetically suspended rotor system in control moment gyros based on an inverse system method". IEEE/ASME Transactions on Mechatronics 2012; Vol. 17, No. 6, pp. 1133–1144, 2012.

[18] Siadatan A, Torkaman H, Afjei E, "Septic segment switched reluctance machine design modeling and manufacturing". International Transactions on Electrical Energy Systems, 2016.

[19] J .Faiz, K M .Zadeh, "Design optimization of switched reluctance machines for starter generator of hybrid electric vehicle by genetic algorithm". European Transactions on electrical power 2009.

Advances in Science, Technology and Engineering Systems Journal Vol. 4, No. 2, 197-202 (2019)

www.astesj.com

ASTESJ

ISSN: 2415-6698

Computational and Technological Models of Cognitive Monitoring Systems

Alexander Vodyaho[1], Evgeniy Postnikov[2], Osipov Vasiliy[3], Nataly Zhukova[3], Michael Chervontsev[2], Nikolai Klimov[*,4]

[1]*Saint Petersburg Electrotechnical University, Saint-Petersburg, 197022, Russia*

[2]*Research and Engineering Center of Saint Petersburg Electro-Technical University, Saint-Petersburg, 197022, Russia*

[3]*Saint Petersburg Institute for Informatics and Automation of the Russian Academy of Sciences, Saint-Petersburg, 197022, Russia*

[4]*Saint Petersburg National Research University of Information Technologies, Mechanics & Optics, Saint-Petersburg, 197022, Russia*

A R T I C L E I N F O

Article history:
Received: 21 January, 2019
Accepted: 13 March, 2019
Online: 26 March, 2019

Keywords:
Cognitive monitoring,
Computational models synthesis

A B S T R A C T

The approach to the construction of promising cognitive monitoring systems is considered. Based on the analysis of known solutions, the problem of automatic synthesis of computational models of cognitive monitoring is posed. In the synthesis of models, it is proposed to reduce them to relatively finite operational automata. An example of a synthesized model of cognitive monitoring is given.

1. Introduction

Monitoring systems (MS) is one of the important subclasses of information systems (IS). Nowadays one can observe an increasing of interest to this class of IS because of a high relevance of these IS in practice. Due to increasing amount of observable objects, their complexity and variability of it's properties, existing MS very often are not able to solve the challenges they face. Many creative tasks of monitoring are solved only with the participation of a person. Significant time and material resources are spent. Among such difficult creative tasks are the following: constructing models of objects and situations, assessing their state and the impact of external and internal factors on possible scenarios for the development of of events, synthesis and implementation of monitoring programs and others. Solution of these problems can be provided prospective cognitive monitoring systems (CMS).

The CMSs should allow machine control of the monitoring processes of the target objects. Such management should be carried out proceeding from solved applied problems. CMSs form a separate subclass of cognitive systems (CS). For CMSs the input data are received from observed objects. Data can include target information and measurement results of object state parameters. The tasks to be solved include obtaining data, processing them, managing the collection of data about objects.

CMSs are intelligent IS that are able to perceive information about the state of the external world and their own state. These systems must bind the observed events and form their space-time models. On the basis of these models, management of monitoring itself should also be carried out. Ability to work at these models allows CMSs, in contrast to traditional management systems, realize content adaptive processing of information streams received from observable objects. Content adaptive is the processing of the semantic content of information flows taking into account the observed context, which is determined by monitoring conditions, set goals. Such processing allows identify information elements in data streams, to establish relations between them. The resulting coupled structures can be considered as models of real world objects, reflecting the states of these objects and their variation in space and time. In the process of IS operation, the constant reconstruction of these models is carried out. It should be noted that CMS can realize cognitive behavior, and can solve specific application tasks, which can relate to a variety of subject domains.

The article suggests an approach to the construction of promising cognitive monitoring systems. This approach develops the existing theoretical and methodological apparatus of cognitive monitoring from the standpoint of implementing such systems. In the second section of the article, an analysis of modern CS, the models, methods and architectural solutions used in them is carried out. In the third section, the problem of synthesis of computational models of CS is formulated. The fourth section proposes a method for their synthesis. In the final section, an example of synthesis is considered.

2. Analysis of modern CS and their capabilities

The principles of CS organization are investigated already throughout not less than thirty years and the considerable experience of creation of such systems is accumulated.

[*]Corresponding Author: Nikolai Klimov, Email: hocico16@gmail.com

https://dx.doi.org/10.25046/aj040226

Some models, methods and architectures of CS have been proposed in research [1, 2, 3, 4]. In the early CS, such formalisms as cognitive maps were widely used, in which factors (elements of the system) and relations between them were determined [5, 6]. In later systems, mechanisms for working with situation patterns and fusion mechanisms [7 - 10] were applied. In accordance with the existing approaches to creation of CS models of information representation and working methods with them are classified according to the types of cognitive architectures. There are three main types of cognitive architectures — symbolic, emergent and hybrid [7]. The first type is characterized by the use of production and graph models of knowledge, for the second type - the use of associative neural network methods, as well as other competitive models and methods. Hybrid architectures involve the sharing of knowledge models and neural network methods. Examples of systems are given in15.

The well-known are such CS as SOAR [11], ICARUS [12], ACT-R [13], which position themselves as IS with cognitive architecture. A detailed overview of IS with cognitive architecture is given in [14].

The first approach to constructing the CS has been developing for a long time. Early work done in this direction was of an experimental nature. They can only partially simulate the intellectual activity of man through the reproduction of individual heuristic algorithms. Now, the attention of research teams working in this direction is mainly focused on the study of static cognitive structures. The questions of constructing and using dynamic cognitive structures are practically not being researched [15 - 21].

In a significant part of modern CSs try to use the neural networks. However, so far the possibilities of usage the big neural networks are significantly limited due to high requirements for computing resources and imperfect architectures these networks.

In practice, engineers prefer to use symbolic and hybrid CSs. In all cases the architectural issues of the creation and maintenance of the CS remain, notably the issues of the accumulation and use of architectural knowledge, the development of flexible architectures, as well as mechanisms for self-monitoring and self-adjustment of such systems.

The main difficulty in using readymade cognitive models, methods and architectures for solving monitoring and management tasks is that they do not provide for controlled reorganization under changing monitoring conditions. In particular, content adaptation is not provided for data processing, adaptation to changing monitoring and control requirements, and monitoring environment capabilities.

Some works are known, in which some issues of creating the CS in the interests of solving problems in the field of monitoring and management are considered, but their number is very limited. In addition, almost all of them are focused on solving particular problems for specific subject domains. For example, in [22], we consider possible ways of realizing cognitive possibilities in the field of transport.

In general, the analysis of the state of modern CMSs has shown that they are rather scattered, a general approach to the construction of CS has not been formed to date, and existing solutions are poorly applicable for the construction of CMSs.

From the point of view of creating CMS, an approach focused on working with models of objects and monitoring processes5 is of considerable interest. Nowadays this approach finds practical implementation. The idea of the model-oriented approach is based on the methods of automatic synthesis [23]. The created apparatus determines the theoretical basis of CM and provides a sufficiently powerful methodical apparatus. It allows build agile systems.

Agility is achieved due to an informed choice of the values of dozens of tuning parameters and their timely correction. There are separate implementations of systems, which were tuned by IT specialists. For practical usage of this the approach, it is necessary to have a tool to develop models that determine how to implement and configure CMS in practice. First of all it is computational models of these systems.

The CMS can be considered as the domain specific CS.

The system of models which describes, both structure, and behavior of a target system is the basis for functioning of CSM. CSM has to solve rather wide class of tasks, in particular: i) automatic creation of models, ii) check of relevance of models, iii) presentations to stakeholders information about target system status in the required form; iv) to solve problems of optimization of target system structure and target system business of processes and many other problems.

The following main requirements are imposed to CSM: i) CSM must have all properties of CS, ii) models can be used for describing both target system dynamic structure and dynamic business processes; iii) models can describe multilevel systems and parallel processes; iv) procedures of automatic creation of models (model synthesis) must be available; v) models must be suitable for describing target system in time.

Different approaches to creation of models can be used/ First of all following approaches are used: i) ontology, ii) Petri nets and graph models, iii) neural networks iv) automata models.

Table 1: Advantages and disadvantages of different approaches

N	Technology	Advantages	Disadvantages
1	Ontologies	Can describe dynamic structures Logical inference is available	Problems with description of target system behavior and problems with synthesis
2	Petri nets and graph models	Can describe target system behavior. Algorithm of process mining are available	Problems with description of multilevel structures
3	Neural networks	High speed of operation	Problems with description of multilevel structures and problems with synthesis
4	Automata models	Enough good speed of operation. Algorithm of synthesis are available	Problems with description of parallel processes.

One can effectively use ontologies for the description a structural component of a target system, there is a good query language but for describing of target system behavior they are not very good.

Petri nets and graph models (work flow graphs) can be effectively for business processes modeling. They can describe parallelism and can be automatically generated from log files. These models are widely used within Process Mining [24]. This approach is rather good for describing target system behavior but not for working with multilevel structures. Neural networks show very good performance but there are problems with synthesis and working with multilevel structures. Automata models are used relatively seldom for CS realization but have a number of advantages, in particular, they can work with multilevel structures and can be generated automatically.

Advantages and disadvantages described above approaches are presented in the table 1.

Thus, it is apparent that one model can't solve all problems and a multimodel approach is to be used. Nowadays primary interest for CMS practical implementation is the solution of 2 problems: i) development of multimodel for target system description and ii) solving the problem of describing multilevel structures i.e. with the help of automata models.

3. The problem of synthesis of a computational model

In a broad sense, a computation model determines the behavior of the system as a whole, based on the behavior of its individual parts. The construction of the computation model involves the definition of the set of permissible operations used for computations, as well as the relative costs of their application. The computation model allows to characterize the necessary resources - the execution time, the amount of memory, as well as the limitations of algorithms or hardware8. The main purpose of the computational model is to ensure the possibility of efficient use of available resources in solving problems of CM. When evaluating computational models, parameters of the generated models of cognitive monitoring can also be taken into account.

Then a computational model can be defined as B(R,E,T)=F(u(E), v(T),g(R)), where u(E) - is the function of monitoring subtasks distribution among the elements of target systems E, v(T) is a function of technologies definition T, which are used for monitoring problems solving, g(R) - is the function of requirements for technologies of monitoring problems forming which are defined by monitoring formal models R. So, for building a computational models of CMS 3 models are to be determined: the formal model of monitoring, monitoring environment model and the technological model. These models determine the conditions for constructing computational models, their structure and parameters. The position of computational model in a general CM model system is shown in the fig. 1.

The CM formal models can be defined in the frames of general CM theory [25]. The CM process model can be presented as a system of correlated cognitive functions {Fi}, FiF, which allow build models of real world objects.

The model of the monitoring environment can be presented as a set of elements {E}, EiE. Monitoring environment as a rule is multilevel distributed media with permanently changing parameters. Monitoring systems in this case can have several levels. The levels are defined by types of used hardware. Monitoring hardware can be located inside the objects of a target system such as local servers, clusters etc.

The CM technological model is defined as a set of technological stacks {Ti}, TiT. Each stack Ti includes the set of technologies {Tj}, TjTi which are similar mentioned above but they have different parameters {Tj} TjTi. The example of technological model, which supports 3 stacks (T1, T2, T3}, is presented in the fig.1. In each stack N technologies are defined. For CM process realization one can use different technological solutions depending on the monitoring environment and goal. So we have the following dependency T(R,E).

Generally, the problem of CM model synthesis can be formulated in the following way. It is necessary to find an effective computational model Bo for which Wopt - extremum of the key indicator of efficiency (minimum of amount of resources which are necessary for CM procedure realization)Wopt (B0)=extrv W(M(Bv)), in case of restrictions for auxiliary indices of efficiency M(Bv) which are defined by the parameters of CM models to be formed: M(By) =F(R(Bv),E(Bv),T(Bv)), M(Bv)DM, R(Bv)DR E(Bv)ER,T(Bv)TR, where A is a set of variants of CM models organization, DM is the area of admissible parameter values of CM models, DR is the area of admissiblevariotions of requirements to parameter values of CM models, DE are restrictions defined by the CM environment, DTis the set of available technologies. The main CS model parameters are accuracy, reliability, completeness, etc.

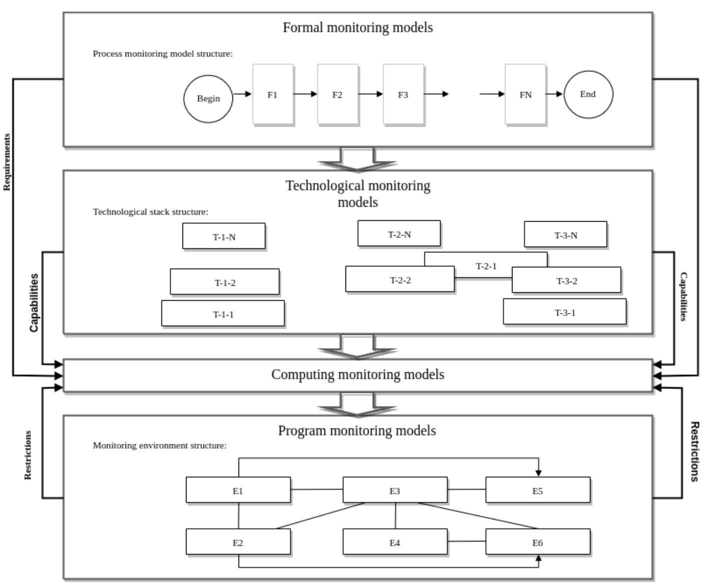

4. Synthesis of the CM computational model

According to the given above definition of the CM Computational model it can be presented in the form of three dimensional structure: $A = \{ai,j,k\}$, $ai,j,k \in \{0,1\}$In this case *i-th* dimension reflects realized CM functions, *j-th* dimension describes components of monitoring environment and *k-th* dimension defines components of technological stack. In this matrix an elementai,j,k is equal to 1 if *i-th* cognitive function is realized on *j-th* component using *k-th* technology. Matrix projections on two dimension space $j \times k$ i.e. on the monitoring environment space and technological components stack for defined element *i* is shown in the fig 2a.

In order to synthesize such structures, it is proposed to use relatively finite operational automata (FOA)[26]. The synthesis scheme of the computational model is shown in Fig. 2b). In accordance with[27], each automate FOA_r in *r*-th moment of the time is described by a set of ten parameters:

$$FOA_r = \{\underline{da_r}, \underline{db_r}, \underline{dc_r}, F_r^b, F_r^c, DA(\underline{db_{r-1}}), \dots\}$$
$$\{\dots, DB(\underline{db_{r-1}}), DC(\underline{db_{r-1}}), FB(\underline{db_{r-1}}), FC(\underline{db_{r-1}})\}$$

, where $\underline{da_r}$- vector of input data; $\underline{db_r}$- vector of internal state parameters;$\underline{dc_r}$ - vector of exit state parameters. FunctionsF_r^b of transitions of an automate from one internal state to another and functionsF_r^c are written in the form:$\underline{db_{r+1}} = F_r^b(\underline{da_r}, \underline{db_r})$,$\underline{dc_r} = F_r^c(\underline{da_r}, \underline{db_r})$. States $\underline{da_r}$, $\underline{db_r}$, $\underline{dc_r}$, and functions F_r^b, F_r^c, characterizing the automaton at the rth moment of time, must satisfy certain conditions:$\underline{da_r} \in DA(\underline{db_{r-1}})$, $\underline{db_r} \in DB(\underline{db_{r-1}})$, $\underline{dc} \in DC(\underline{db_{r-1}})$,$\underline{F_r^b} \in FB(\underline{db_{r-1}})$, $\underline{F_r^c} \in FC(\underline{db_{r-1}})$, where $DA(\underline{db_{r-1}})$, $DB(\underline{db_{r-1}})$, $DC(\underline{db_{r-1}})$, $FB(\underline{db_{r-1}})$, $FC(\underline{db_{r-1}})$- allowable sets of states and functions of the automate defined with respect to *r-1* time. The transition from the $FOAr$ to the $FOAr + 1$ automate by $r + 1$ moment can be written as:$F_r^b: FOA_r, \underline{da_r} \rightarrow FOA_{r+1}$

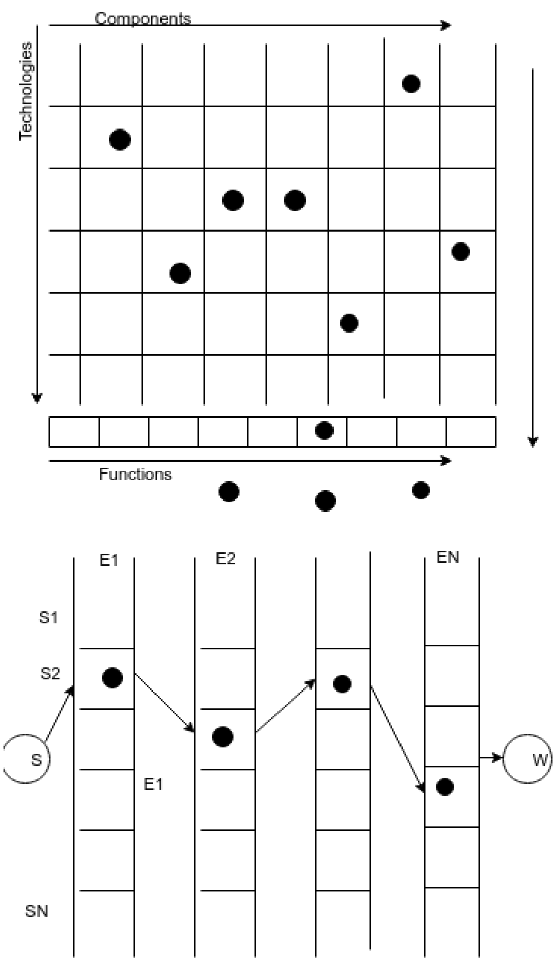

It is envisaged to build your machine for each of the functions. As a result, the computational model at time r will be described by a family of automata:$FFOA = \{FOA(F1), FOA(F2), \dots, FOA(FN)\}$. FOA for different functions can be constructed in any order.

During synthesis of FOA for i -*th* functions can take into account other previously synthesized automata, then there is a dependence $FFOA_r(FFOA_{r-1})$. This approach is justified when certain functions can be expressed through other functions, i.e. $F_k = G(F_i)$,$i \in \{1..N\}$. In this case, one can speak of a system of interconnected automata.

5. An example of a CM model

CM and control systems can be used in many subject domains including the "smart house" systems. These systems can be divided into three subclasses: centralized, bus and mixed.

Each smart house system consists of various modules, for example: supply module, security module, security module, management module. The supply module may include the following submodules: a power supply submodule, a water supply submodule, a submodule of equipment and household appliances. The security module can include an alarm submodule, a submodule of video surveillance, a submodule of fire alarm. The control module, as a rule, consists of a submodule of access control and access control, a fire suppression module, a climate control submodule and lighting control.

The domain description of the smart house system includes the following main components: automated functions, data processing tasks and procedures, users, information elements and relationships between them, characteristics of information elements and procedures for data processing, relationships between information elements and procedures.

Thus, the domain model is represented in the form: $M =< F, H, P, O, R >$, where F is the set of automatized functions, H is the set of tasks (procedures) for data processing, P is the set of users, O is the set of objects and automation processes, R is the set of relations (relationships) between the components $\{F, H, P, O, V\}$, V is the complete set of informational elements of the domain.

Systems of the smart house class can be implemented in the form of CM and management systems. Various modules of such a system can act as automated monitoring units (fire alarm, burglar alarm and power consumption) capable of adjusting control actions as a result of analyzing and processing incoming data and constructing an environment model and a monitoring model based on this data. Information from monitoring units can also be processed at the central control point of the system from which the subsystems also receive control actions.

As one of the monitoring subsystems, consider the fire monitoring module. This subsystem consists of modules for monitoring fire alarm and control module (fire suppression module). The behavior of the fire alarm module at each point in time is set by the monitoring environment model, at each time formed on the basis of data coming from groups of fire sensors (smoke and heat detectors), as well as historical indications. The control action can consist in forming a notification of a sensor failure, generating a pre-fire notification and sending control commands to the fire suppression subsystem in accordance with a predetermined algorithm.

Definition of a set of automation objects: a group of smoke detectors, a group of thermal detectors, a group of address points, a peripheral microcontroller of a substation, a group of fire extinguishing elements (relays, etc.), a central controller of a substation.

Definition of a set of automated functions: monitoring of detector malfunction, monitoring of room temperature, monitoring of optical density of the environment, start-up of the fire-extinguishing system, stopping of the fire-extinguishing system, generation of an alarm notification on the fact of sensor failure detection.

Definition of a set of data processing procedures: collection of information about the failure from the central controller, rotation of obsolete (irrelevant) data, archiving of fault notifications, aggregation of historical data for the subsequent analysis of the current situation on the gradient.

Definition of a set of users of the system: the administrator (owner), the module of the central database.

Definition of a set of information elements of the fire alarm system: device identifier, status identifier, event identifier, event date, event time, event data storage time, event response event, system response date, system response time.

Consider the possible scenario of cognitive monitoring and management of the fire alarm and firefighting system:

The monitoring system periodically poll groups of sensors and stores the readings. In real time, the derivatives are calculated from the changes in the readings. Data processing occurs on several levels:

1. At the level of the peripheral controller, the data undergoes preliminary filtration and purification, the malfunction of specific sensors is analyzed;
2. At the central controller level, data from the peripheral controller is stored and the fire is analyzed for the gradient;
3. At the level of the fire control and fire control subsystem, decisions are made on the control effect;
4. At the level of the general monitoring system, high-level notifications from the fire alarm subsystem are aggregated, an administrator is notified.

The monitoring procedure is adjusted in real time depending on the internal and external input data:

1. If a defective detector is detected, it can be excluded from the list of the system elements being polled; If a possible fire on a gradient is detected, the frequency of polling of sensors in the area of the alleged incident is increased;
2. According to indications from adjacent subsystems (volume and presence sensors, climate control systems), thresholds for fire alarm elements can be adjusted.

Consider the synthesis of a computational model of a fire system at the level of the central and peripheral controllers. The state machine for the peripheral controller is described by the following sets:

1. Set of Input Data $DA(\underline{db_{r-1}})$- integer values of optical density of sensors;
2. Set of internal state $DB(\underline{db_{r-1}})$- the indicator of serviceability of fire loop elements, the frequency of polling of the elements of the fire loop;
3. Set of output state$DC(\underline{db_{r-1}})$- aggregated indicators of sensors, fault messages;
4. Set of transition functions between internal states F_r^b - making a decision about the condition of the sensor.

The state machine for the central controller is described by the following sets:

1. Set of Input Data $DA(\underline{db_{r-1}})$- aggregated readings from peripheral controllers, data from adjacent climate control subsystems and firefighters;
1. Set of internal state $DB(\underline{db_{r-1}})$- a fire indicator by a gradient in a particular area;
2. Set of output state$DC(\underline{db_{r-1}})$- notification of malfunctions in the system, warnings and fires;
3. Set of transition functions between internal statesF_r^b - making a decision on a fire by a gradient.

With the help of control actions, the load can be redistributed at different levels of the system: in the case of a fault diagnosis, the central controller decides on reducing the frequency of polling the problem sensor by the peripheral controller; In the diagnosis of the premozharnoy situation, the frequency of the poll, on the contrary, a decision is made to increase the frequency of polling the target and adjacent sensors.

Consider the synthesis of the computational model of the subsystem of fire alarm and fire extinguishing in the "smart house". Set of input parameters$DA(\underline{db_{r-1}})$ in the system - numerical values of the optical density and temperature obtained from the sensors. Set of internal states of the monitoring system $DB(\underline{db_{r-1}})$ is set by the polling rate of each sensor, as well as by one of the operating modes of the system: Normal, Pre-fire, Sensor Fault, Fire. As a computational model, the derivative of the change in the readings of the sensors P.

In the "Normal" state, the load on the central and peripheral controllers polling the sensors is distributed evenly, the polling period of each sensor is t1. The transition to the "Pre-fire" state is determined by the excess of the derivative P of the admissible value P1. In this case, a redistribution of the computational load occurs: the frequency of polling of the target and adjacent sensors to t2 increases. Also, the technological models and functions used are changed: instead of the derivative P, the received sensor observations begin to be compared with a certain threshold value R1. The transition to the "Fire" state passes when the fire hypothesis is confirmed, at which the value of the observation begins to exceed the threshold value R1. Polling of sensors in the prospective area of the fire is stopped, and the computing resources are transferred to the control subsystem, activating the fire suppression algorithm in this area.

The CMS of the fire situation in the smart house has a number of advantages over the classical systems of fire alarm and fire extinguishing:

1. On the basis of a real time model of the monitoring environment, it is possible to quickly recognize the dysfunctional parts of the system (fire detectors) for the purpose of their subsequent replacement, as well as the formation of premonitory notifications based on the calculation of the derived values of the sensor readings;

It allows in real time to change the composition of the monitored monitoring environment and to generate control actions more localized.

Conclusion

Usage of CMSs allows solve a problem of managing distributed IS with a very big number of elements and variable structure i.e. allows build IS with higher levels of complexity. CMSs assume operation on the model level. The key problem of CM is on the fly generation of target IS model. In suggested article the problem of model generation from data is discussed. This is only the first step which allows build rather simple CMS. The next step to be done is looking for methods of model synthesis methods on the base not only raw data but knowledge, including knowledge from the external ontologies.

References

[1] M. Glodek, F.Honold, T. Geier, G. Krell, F. Nothdurft, S. Reuter, F. Schüssel, T. Hörnle, K. Dietmayer, W. Minker, S. Biundo, M. Weber, G. Palm, F. Schwenker Fusion paradigms in cognitive technical systems for human–computer interaction Journal Neurocomputing archive Volume 161 Issue C, August 2015 Pages 17-37

[2] Osipov V., Vodyaho A, Zhukova N., Glebovsky P. Multilevel Automatic Synthesis of Behavioral Programs for Smart Devices, Control, Artificial Intelligence, Robotics & Optimization (ICCAIRO), 2017

[3] Madl, T., Chen, K., Montaldi, D., and Trappl, R. (2015). Computational cognitive models of spatial memory in navigation space: a review. Neural Netw. 65, 18–43. doi:10.1016/j.neunet.2015.01.002

[4] Zagoruiko, NG Cognitive analysis of data. - Academic publishing house "GEO", 2012. - 203 p.

[5] Axelrod, R. The cognitive mapping approach to decision making.// In: Structure of Decision. The Cognitive Maps of Political Elites, R. Axelrod (ed.), (3-18), ISBN: 069107578-6, Princeton University Press, Princeton. 1976.

[6] Avdeeva Z.K. Comparative analysis of selective cognitive maps by the degree of formalization // Cognitive analysis and management of the development of situations (CASC'2009): Proceedings of the International Conference (November 17-19, 2009, Moscow). Moscow: IPP RAS, 2009. P.11-22.

[7] Duch W., Oentaryo R., Pasquier M., Cognitive architectures: where do we go from here? Proceedings of the Second Conferenceon AGI, 2008.

[8] Gardner K. M., Rush A., Crist M. K., Teegarden B. Cognitive Patterns: Problem-Solving Frameworks for Object Technology. Robert K Konitzer. Zurich, Switzerland. 2011. 166 p.

[9] Glodek M., Honold F., Geier T., Krell G., Nothdurft F., Reuter S., Schüssel F., Hörnle T., Dietmayer K., Minker W., Biundo S., Weber M., Palma G., Schwenker F. Fusion paradigms in cognitive technical systems for human–computer interaction. Neurocomputing 161. 2015. p. 17–37

[10] Perlovsky L. I. Cognitive high level information fusion Information Sciences 177 (2007) 2099–2118

[11] Laird J., Rosenbloom P., Newell A., Soar: an architecture for general intelligence, Artificial Intelligence 33. (1987).

[12] P.Langley, An adaptive architecture for physical agents, in: Proceedings of the 2005 IEEE/WIC/ACM International Conference on Intelligent Agent Technology, 2005.

[13] Anderson J. R., Lebiere C. The newell test for a theory of cognition, Behavioral and BrainSciences 26 (2003).

[14] I. N. Rozenberg Cognitive Transport Management. TheStateCounsellor, No. 2, 2015. From 47-52

[15] Osipov V.Y. Development of Information Processing Processes in Associative Intelligent Machines // Mechatronics, Automation, Control, No. 6, 2014, pp. 8-13.

[16] Osipov V.Y. A recurrent neural network with layer structure in the form of a double helix // Information Technologies, No. 7, 2014, pp. 56-60.

[17] Osipov V.Y. Associative intelligent machine with three signal systems // Information-control systems, No. 5, 2014, P. 12-17.

[18] Osipov V.Y. Limits of memory of recurrent neural networks with erasure of outdated information // Scientific Bulletin of Novosibirsk State Technical University, No. 3 (56), 2014, P. 115-122.

[19] Neyrodynamic Systems Of Multiagent Modeling Based On The Modern Theory Of Catastropes Nechaev Y.I. Neurocomputers: development, application. 2017. No. 1. P. 16-29.

[20] Neurodynamic modeling of nonlinear nonstationary systems based on the modern theory of catastrophes Nechaev Y.I., Lav N.S. Neurocomputers: development, application. 2017. № 3. P. 3-16.

[21] Concept of neural networks under the functioning of self-organizing systemsS Nechaev Y.I. In the collection: Proceedings of the XI International Conference on Nonequilibrium Processes in Nozzles and Jets (NPNJ'2016) Moscow Aviation Institute (National Research University). 2016. P. 445-447.

[22] Osipov V. Yu. Automatic Synthesis of Action Programs for Intelligent Robot // Programming and Computer Software. 2016. Vol. 42. No. 3. pp. 155 -160.

[23] Encyclopedia of Management. URL: http://www.enotes.com/management-encyclopedia/management-thought

[24] Wil van der Aalst. Process Mining Data Science in Action Second Edition (DOI 10.1007/978-3-662-49851-4) Springer-Verlag Berlin Heidelberg 2016. 467 p.

[25] Osipov V. Sintez rezultativnyih programm upravleniya informatsionno-vyichislitelnyimi resursami [Syntesis of resultive programs for information and computing resources managment] Priboryi i sistemyi upravleniya. 1998. #12. S.24-27

Advances in Science, Technology and Engineering Systems Journal Vol. 4, No. 2, 203-210 (2019)

www.astesj.com

ASTESJ

ISSN: 2415-6698

Parallel Hybrid Testing Tool for Applications Developed by Using MPI + OpenACC Dual-Programming Model

Ahmed Mohammed Alghamdi*, Fathy Elbouraey Eassa

Department of Computer Science, King Abdul-Aziz University, Jeddah, Saudi Arabia

A R T I C L E I N F O

Article history:
Received: 24 January, 2019
Accepted: 21 March, 2019
Online: 26 March, 2019

Keywords:
Software Testing
Hybrid Testing Tool
OpenACC
MPI
Dual-programming Model

A B S T R A C T

Building massively parallel applications has become increasingly important with coming Exascale related technologies. For building these applications, a combination of programming models is needed to increase the system's parallelism. One of these combinations is the dual-programming model (MPI+X) which has many structures that increase parallelism in heterogeneous systems that include CPUs and GPUs. MPI + OpenACC programming model has many advantages and features that increase parallelism with respect heterogeneous architecture and support different platform with more performance, productivity, and programmability.

The main problem in building systems with different programming models that it is a hard job for programmers and it is more error-prone, which is not easy to test. Also, testing parallel applications is a difficult task, because of the non-determined behavior of the parallel application. Even after detecting the errors and modifying the source code, it is not easy to determine whether the errors have been corrected or remain hidden. Furthermore, integrating two different programming models inside the same application makes it even more difficult to test. Also, the misusage of OpenACC can lead to several run-time errors that compilers cannot detect, and the programmers will not know about them.

To solve this problem, we proposed a parallel hybrid testing tool for detecting run-time errors for systems implemented in C++ and MPI + OpenACC. The hybrid techniques combine static and dynamic testing techniques for detecting real and potential run-time errors by analyzing the source code and during run time. Using parallel hybrid techniques will enhance the testing time and cover a wide range of errors. Also, we propose a new assertion language for helping in detecting potential run-time errors. Finally, to the best of our knowledge, identifying and classifying OpenACC errors has not been done before, and there is no parallel testing tool designed to test applications programmed by using the dual-programming model MPI + OpenACC or the single-programming models OpenACC.

1. Introduction

In recent years, building massively-parallel supercomputing systems based on heterogeneous architecture have been one of the top research topics. Therefore, creating parallel programs becomes increasingly important, but there is a lack of parallel programming languages, and the majority of traditional programming languages cannot support parallelism efficiently. As a result, programming models have been created to add parallelism to the programming languages. Programming models are sets of instructions, operations, and constructs used to support parallelism.

*Ahmed Mohammed Alghamdi, Email: amalghamdi@uj.edu.sa

Today, there are various programming models which have different features and created for different purposes; including message passing, such as MPI [1] and shared memory parallelism, such as OpenMP [2]. Also, some programming models support heterogeneous systems, which consisting of a Graphics Processing Unit (GPU) coupled with a traditional CPU. Heterogeneous parallel programming models are CUDA [3] and OpenCL [4], which are low-level programming model and OpenACC [5] as a high-level heterogeneous programming model.

Testing parallel applications is a difficult task because parallel errors are hard to detect due to the non-determined behavior of the parallel application. Even after detecting the errors and modifying

https://dx.doi.org/10.25046/aj040227

the source code, it is not easy to determine whether the errors have been corrected or hidden. Integrating two different programming models inside the same application even make it more difficult to test. Despite the available testing tools that detect static and dynamic errors, still, there is a shortage in such a testing tool that detects run-time errors in systems implemented in the high-level programming model.

The rest of this paper is structured as follows. Section 2 describes the research objectives, while Section 3 briefly gives an overview of some programming models and some run-time errors. The related work will be discussed in Section 4, the proposed architecture in Section 5, a discussion will be in Section 6 and finally the conclusion with future work in Section 7.

2. Research Objectives

This research aims to develop a parallel hybrid testing tool for systems implemented in MPI + OpenACC dual programming model with C++ programming language. The hybrid techniques combine static and dynamic testing techniques for detecting real and potential run-time errors by analyzing the source code and during run-time. Using parallel hybrid techniques will enhance the testing time and cover a wide range of errors. The following are the primary objectives of our research:

2.1. Provide new static testing techniques for detecting real and potential run-time errors for systems implemented in dual programming model (OpenACC and MPI) and C++ programming language.

These techniques are analyzing the source code before compilation for detecting static errors. Some run-time errors can also be detected from the source code, such as send-send deadlocks in Figure 2 B. These errors should be sent to developers to solve them because they will occur definitely in run-time. Also, potential run-time errors are errors that might or might not be occurred after compilation and during run-time. The reasons cause these potential errors can be detected from the source code before compilation by using static testing. However, if these errors have not been detected, it will become run-time errors. As a result, the developers should be warned about these errors and consider them; also our tool will instrument these errors by using assertion language.

The source code will include a combination of the program implemented in C++ and dual programming model source codes, which leads to one big size source code including a considerable number of statements. These static testing techniques will decrease the time of detecting run-time errors after the compilation, which will speed up the system testing time. These techniques also will allow us to correct or inform developers by providing them with a list of potential errors that in some cases in the running time these errors might happen.

The following example in Figure 1 shows a potential run-time error, when process_1 first receive request from any process beside process_0, there is no problem. However, if process_1 receives from process_0 first, the statement REC_FROM (P_0) will never, and the process_1 will be waiting. In that case, from the source code we discover that, somehow, this will cause a run-time error (Deadlock). This situation called a potential deadlock.

Also, Figure 2 shows an example of a real run-time error called (deadlock), which happened because of Process_0 block and waiting for receiving from Process_1, which also block and waiting for receiving from Process_0. Similarly, this also happened between Process_2 and Process_3.

Process_0 (P_0)	Process_1 (P_1)	Process 2 (P_2)	Process 3 (P_3)
SEND_TO (P_1)	REC_FROM (ANY)	SEND_TO (P_1)	SEND_TO (P_1)
	REC_FROM (P_0)	REC_FROM (P_3)	

Figure 1: Potential Deadlock caused by Wildcard Receive

Process_0 (P_0)	Process_1 (P_1)
REC_FROM (P_1)	REC_FROM (P_0)
SEND_TO (P_1)	SEND_TO (P_0)

(A) Receive - Receive Deadlock

Process_2 (P_2)	Process_3 (P_3)
SEND_TO (P_3)	SEND_TO (P_2)
REC_FROM (P_3)	REC_FROM (P_2)

(B) Send - Send Deadlock

Figure 2: Real Deadlocks caused by two different reasons

2.2. Providing a new assertion language for helping in detecting potential run-time errors.

This assertion language will be used to specify the properties of the programs under test and to verify that the developers' assumptions of the program remain valid during the program run-time. During testing, assertion statements help for the recording of some information, testing the correctness of statements, and monitor the values of variables. To do this, the dynamic tester will automatically insert assertion statements into the code, then provides a method for capturing, organizing, and analyzing assertions output. This will help to increase the error detection capability of a test by using the instrumentation technique. The instrumentation approach based on the idea that the tested part of a program can be specified regarding assertion or values that must be assumed by variables at specific critical points in the program, which can cause run-time errors [6].

Usually, assertion statements start with comment symbol of the programming language, such as "//" in C++, before each assert statements. The main reason behind this is reducing the compiled code that will be delivered to the customers because any statement starts with the comment symbol will be ignored during the compilation. In other words, the assert statements are in the source code but not in the compiled code, which will be delivered to the customers.

2.3. Provide new parallel dynamic testing techniques for detecting run-time errors for systems implemented in dual programming model (OpenACC and MPI) and C++ programming language.

These techniques will use the provided assertion language for detecting errors that happened during run-time, by instrumenting and analyzing the system during run-time. This is challenging because different factors and complicated scenarios can cause these errors. Also, testing parallel programs is a difficult task because of the nature of such programs and their behavior. This will add more work on the testing tool for covering every possible scenario of the test cases and data. As a result, detecting parallel run-time errors is more difficult. Furthermore, these dynamic techniques are sensitive to the execution environment and can affect the system execution time.

2.4. Integrated the provided techniques for developing a parallel hybrid testing tool for systems implemented in dual programming model (OpenACC and MPI) and C++ programming language.

Our proposed architecture will integrate static and dynamic testing techniques for creating a new hybrid testing tool for parallel systems. This allows us to take advantages of both previously mentioned techniques for detecting some of the dynamic errors from the source code by using the static testing techniques, which will enhance the system execution time. Also, our system will work in parallel to detect run-time errors, by creating testing threads depending on the number of the application threads. Intra-process and Inter-process run-time detections will be included in our tool. The inter-process detector will be responsible for detecting run-time errors that happened within the process, and the Intra-process detector for detecting errors happened between processes each other.

3. Background

In this section, the main components involved in our research will be displayed and discussed. This will include the programming models that will be used in our research and describing why they have been chosen. Also, some run-time errors and testing techniques will also be described and discussed in this section.

3.1. OpenACC

In November 2011, OpenACC stands for open accelerators, was released for the first time in the International Conference for High-Performance Computing, Networking, Storage and Analysis [7]. OpenACC is a directive-based open standard developed by Cray, CAPS, NVIDIA and PGI. They design OpenACC to create simple high-level parallel programming model for heterogeneous CPU/GPU systems, that compatible with FORTRAN, C, and C++ programming languages. Also, OpenACC Standard Organization defines OpenACC as "a user-driven directive-based performance-portable parallel programming model designed for scientists and engineers interested in porting their codes to a wide variety of heterogeneous HPC hardware platforms and architectures with significantly less programming effort than required with a low-level model." [5]. The latest version of OpenACC was released in November 2017. OpenACC has several features and advantages comparing with other heterogeneous parallel programming models including:

- Portability: Unlike programming model like CUDA works only on NVIDIA GPU accelerators, OpenACC is portable across different type of GPU accelerators, hardware, platforms, and operating systems.[8]
- OpenACC is compatible with various compilers and gives flexibility to the compiler implementations.
- High-level programming model, which makes targeting accelerators easier, by hiding low-level details. For generation low-level GPU programs, OpenACC relies on the compiler using the programmer codes. [9]
- Better performance with less programming effort, which gives the ability to add GPU codes to existing programs with less effort. This will lead to reduce the programmer workload and improve programmer productivity and achieving better performance than OpenCL and CUDA. [10]
- OpenACC allows users to specify three levels of parallelism by using three clauses:
  - Gangs: Coarse-Grained Parallelism
  - Workers: Medium-grained Parallelism
  - Vector: Fine-Grained Parallelism

OpenACC has both a strong and significant impact on the HPC society as well as other scientific communities. Jeffrey Vetter (HPC luminary and Joint Professor Georgia Institute of Technology) wrote: “OpenACC represents a major development for the scientific community. Programming models for open science by definition need to be flexible, open and portable across multiple platforms. OpenACC is well-designed to fill this need.” [5].

3.2. Message Passing Interface (MPI)

Message Passing Interface (MPI) [1] is a message-passing library interface specification. In May 1994, the first official version of MPI was released. MPI is a message-passing parallel programming model that moves data from a process address space to another process by using cooperative operations on each process. The MPI aims to establish a standard for writing message-passing programs to be portable, efficient, and flexible. Also, MPI is a specification, not a language or implementation, and all MPI operations are expressed as functions, subroutine or methods for programming languages including FORTRAN, C, and C++. MPI has several implementations including open source implementations, such as Open MPI [11] and MPICH [12]; and commercial implementations, such as IBM Spectrum MPI [13] and Intel MPI [14]. MPI has several features and advantages including:

- **Standard**: MPI is the only message passing library that can be considered a standard. It has been supported on virtually all HPC platforms. Also, all previous message passing libraries have been replaced by MPI.
- **Portability:** MPI can be implemented on several platforms, hardware, systems, and programming languages. Also, MPI can work correctly with several programming models and work with heterogeneous networks.
- **Availability:** Various versions of MPI implementations from different vendors and organization are available as open source and commercial implementations.
- **Functionality:** On MPI version 3.1 there are over 430 routines has been defined including the majority of the previous versions of MPI.

The new MPI standardization version 4.0 [1] is in progress, which aims to add new techniques, approaches, or concepts to the MPI standard that will help MPI address the need of current and next-generation applications and architectures. The new version will extend to better support hybrid programming models including hybrid MPI+X concerns and support for fault tolerance in MPI applications.

3.3. Dual-Level Programming Model: MPI + OpenACC

Integrating more than one programming model can enhance parallelism, performance, and the ability to work with heterogeneous platforms. Also, this combination will help in moving to Exascale systems, which need more powerful programming models that support massively-parallel supercomputing systems. Hybrid programming models can be classified as:

- Single-Level Programming Model: MPI
- Dual-Level Programming Model: MPI + X
- Tri-Level Programming Model: MPI + X + Y

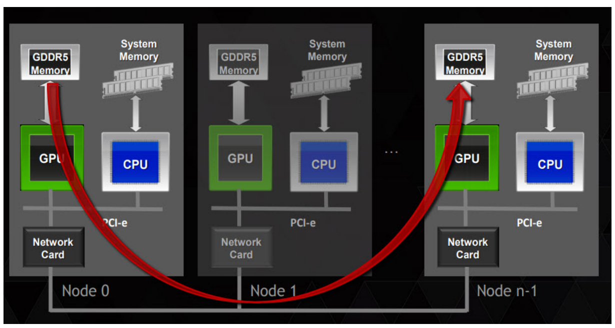

Figure 3: Multi GPU Programming with MPI and OpenACC [15]

In order to write portable and scalable applications for heterogeneous architecture, the dual-programming model MPI + OpenACC can be practical. It inherits the advantages, such as high performance, scalability, and portability from MPI and programmability and portability from OpenACC [16]. However, this dual-programming model might introduce different types of run-time errors, which have different behaviors and causes. Also, some complexities and inefficiencies might happen including redundant data movement and excessive synchronization between the models, which need to be considered and take care of, but it is better than using CUDA or OpenCL, which is more complicated and harder to program, resulting in lower productivity.

3.4. Common Run-Time Errors

There are several types of run-time errors that happened after compilation and cannot be detected by the compilers, which cause the program not to meet the user requirements. These errors even sometimes have similar names, but they are different in the reasons that cause the run-time error or the error behavior. For example, deadlock in MPI has different causes and behaviors comparing with OpenACC deadlocks. Also, run-time errors in the dual-programming model are different. Also, some run-time errors happened specifically in a particular programming model. By investigating the documents of the latest version of OpenACC 2.7 [17], we found that OpenACC has a repetitive run-time error that if a variable is not present on the current device, this will lead to run-time error. This case happened in non-shared memory devices for different OpenACC clauses.

Similarly, if the data is not present, a run-time error is issued in some routines. Furthermore, detecting such errors is not easy to do, and to detect them in applications developed by dual-programming model even more complicated. In the following, some popular run-time errors will be displayed and discussed in general with some examples.

3.4.1. Deadlock

A deadlock is a situation in which a program is in a waiting state for an indefinite amount of time. In other words, one or more threads in a group are blocked forever without consuming CPU cycles. The deadlock has two types including resource and communication deadlock. Resource deadlock is the situation where a thread waits for another thread resource to proceed.

Similarly, the communication deadlock occurs when some threads wait for some messages, but they never receive these messages [18–20]. The reasons that cause deadlock are different depending on the used programming models, systems nature and behavior. Once the deadlock occurs, it is not difficult to detect, but in some cases, it is difficult to detect them before it happened as they occur under specific interleaving. Finally, deadlocks in any system could be potential or real deadlocks.

3.4.2. Livelock

Livelock is similar to deadlock, except that livelock is a situation that happened when two or more processes change their state continuously in response to changes in the other processes. In other words, it occurs when one or more threads continuously change their states (and hence consume CPU cycles) in response to changes in states of the other threads without doing any useful work. As a result, none of the processes will make any progress and will not complete [21,22]. In a livelock, the thread might not be blocked forever, and it is hard to distinguish between livelock and long-running process. Also, livelock can lead to performance and power consumption problems because of the useless busy-wait cycles.

3.4.3. Race Condition

A race condition is a situation that might be occurred due to executing processes by multiple threads and where the sequence of execution for the threads makes a difference in the result of the concurrent execution. The execution timing and order will affect the program's correctness [20,23]. Some researchers do not differentiate between data race and race condition, which will be explained in the data race definition.

3.4.4. Data Race

A data race happened when there are two memory accesses in the program where they both are performed concurrently by two threads or target the same location [23, 24]. For example, at least one read and one write may happen at the same memory location, at the same time. The relation between data race and race condition, the race condition is a data race that causes an error. However, data race does not always lead to a race condition.

3.4.5. Mismatching

Mismatching is a situation that happened in arguments of one call, which can be detected locally and are sometimes even detected by the compiler. Mismatching can be caused by several forms including wrong type or number of arguments, arguments involving more than one call, or in collective calls. Developers need to make special attention when comparing matched pairs of derived data types. Some examples of mismatching that occurred in MPI as the following [23]:

- To send two (MPI INT, MPI DOUBLE) and to receive one (MPI INT, MPI DOUBLE, MPI INT, MPI DOUBLE
- To send one (MPI INT, MPI DOUBLE) and to receive one (MPI INT, MPI DOUBLE, MPI INT, MPI DOUBLE) (a so-called partial receive).

3.5. Testing Techniques

There are many techniques used in software testing, which include static, dynamic, as well as other techniques. Static testing is the process of analyzing the source code before compilation phase for detecting static errors. It handles the application source code only without launching it, which give us the ability to analyze the code in details and have full coverage. In contrast, the static analysis of parallel application is complicated due to the unpredicted program behavior, which is parallel application nature. However, it will be beneficial to use static analysis for detecting potential run-time errors and some real run-time errors that are obvious from the source code, such as some types of deadlocks and race condition.

Dynamic testing is the process of analyzing the system during run-time for detecting dynamic (run-time) errors. It demands to launch programs, sensitive to the execution environment, and slow down the speed of application execution. It is useful to use dynamic analysis in the parallel application, which gives the flexibility to monitor and detect each thread of the parallel application. However, it is difficult to cover the whole parallel code with tests, and after correcting the errors, it cannot be confirmed that errors are corrected or hidden.

Finally, it is the error types and behaviors that determine which techniques will be used, because static analysis and others cannot detect dynamic techniques cannot detect some errors. As a result, in our research, a hybrid technique will be used for different purposes and reasons. Furthermore, this hybrid technology will be working in parallel to detect parallel run-time errors and analyzing the application's threads.

4. Related Works

Many studies have been done in software testing for HPC and parallel software. These researches are varied, for different purposes and scopes. These variations include testing tools or detection for a specific type of errors or a different type of errors. Some studies focus on using static testing techniques [25–28] to detect errors by analyzing the source code and find real as well as potential run-time errors [29,30]; dynamic testing techniques [31,32] to detect errors after execution and at run-time; or hybrid testing techniques [33–35]. Also, detecting errors in programming models also varied from the testing tool for single level programming model to the tri-level programming model. Even in the same classification of programming model the variation between testing the programming models themselves, because each programming model has a different error to detect as discussed earlier in Section 3.4.

For detecting a specific type of errors, there are many types of research worked on detecting deadlock, livelock and race condition by using different techniques. In deadlock detection, there are many tools and studies that are using static or dynamic testing techniques to detect deadlocks including resource and communication deadlocks. UNDEAD [19] is a deadlock detection and prevention, which helps to defeats deadlocks in production software with enhancing run-time performance and memory overheads. More deadlock detection can be found in [19,36] . Regarding detecting data race, a hybrid test-driven approach has been introduced in [35] to detect data race in task-parallel programs. Also, many data race detection approaches in [28,37]. Finally, some livelock detection techniques have been proposed in [21,22].

Regarding testing the programming model, many approaches have been introduced to test and detect errors in parallel software. Many studies have been done in a single level programming models such as MPI, OpenMP, CUDA and OpenCL. While some studies focus on dual-level programming models including MPI + X hybrid programming models, which include homogeneous and heterogeneous systems. One popular combination is MPI + OpenMP, which appears in [33,38,39]. Some of these studies focus on dynamic testing, while some of them in regression testing, which is the process of analyzing the system after the maintenance phase.

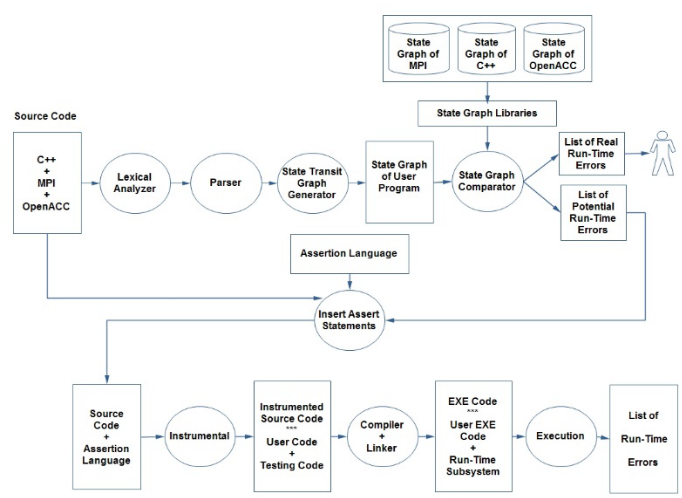

Figure 4: Our Proposed Architecture

Regarding open source testing tools, ARCHER [37] is a data race detector for an OpenMP program that combines static and dynamic techniques to identify data race in large OpenMP applications. Also, AutomaDeD [42] (Automata-based Debugging for Dissimilar Parallel Tasks) is a tool that detects MPI errors by comparing the similarities and dissimilarities between tasks. MEMCHEKER [11] allows finding hard-to-catch memory errors in MPI application such as overwriting of memory regions used in non-blocking communication and one-sided communication. Furthermore, MUST [32] detects run-time errors in MPI and report them to the developers, including MPI deadlock detection, data type matching, and detection of communication buffer overlaps.

Testing OpenACC has limited studies in testing and detecting static and dynamic errors. There are some researches regarding related OpenACC testing. In [43], they evaluate three commercial OpenACC compilers by creating a validation suite that contains 140 test case for OpenACC 2.0. They also check conformance, correctness, and completeness of specific compilers for the OpenACC 2.0 new features. This test suite has been built on the same concept as the first OpenACC 1.0 validation test suite in [44], which three commercial compilers were evaluated including CAPS, PGI and CRAY. Similarly, this OpenACC test suite was published in [45] for OpenACC version 2.5, which is the past version, to validate and verify compilers' implementations of OpenACC features.

Recently, another testing of the OpenACC application was published in [46], which considered detecting numerical differences that can be occurred due to computational differences in different OpenACC directives. They proposed a solution for that by generating code from the compiler to run each computes region on both the host CPU and the GPU. Then, the values computed on the host and GPU are compared, using OpenACC data directives and clauses to decide what data to compare.

Despite the efforts that have been done in creating and proposing software testing tools for parallel application, still, there is a lot to be done primarily for OpenACC and for dual-programming models for heterogeneous systems. Finally, in our best knowledge, there is not a parallel testing tool built to test applications programmed by using the dual-programming model MPI + OpenACC.

5. Proposed Architecture

We propose a parallel hybrid testing tool for the dual-programming model (MPI + OpenACC) and C++ programming language as shown in Figure 4. This architecture has the flexibility to detect potential run-time errors and report them to the developer, detect them automatically by using assertion language and execute them to get a list of run-time errors, or detecting dynamic errors. This architecture uses hybrid testing techniques including static and dynamic testing. The static testing part is shown in Figure 5 while the dynamic part in Figure 6.

The source code includes C++ programming language and MPI + OpenACC as dual-programming models. The part that displayed in Figure 5 is responsible for detecting real and potential run-time errors by using static testing. This part produces a list of potential run-time errors for the developer.

Also, this list could be an input to the assertion process that these potential errors will be automatically detected and avoided during the dynamic testing part. Also, any real run-time errors also will be addressed to the developed with warning messages, as these errors must be corrected because they will defiantly occur during run-time. Also, these real run-time errors that been discovered from the source code can be automatically corrected before the process move to the dynamic testing part, which reduces the testing time and enhances the testing performance. The static part of the architecture includes:

- **Lexical analyzer:** This will take the source code that includes C++, MPI, and OpenACC as an input. This analyzer will understand the source code because it has all the information related to the programming language and the determined programming models. This information includes keywords, reserved words, operators, variable and constant definitions. Then, it will convert the application source code into tokens and allocate them into tables of tokens. The output of this analyzer will be a token table, which includes token names and their respective type.
- **Parser:** This Part is responsible for analyzing the syntax of the input source code and confirming the rule of a formal grammar. This process will produce a structural representation of the input (Parser Tree) that shows the syntax relation to each other, checking for correct syntax in the process.
- **State transit graph generator:** This part will generate a state graph for the user program, which includes C++, MPI, and OpenACC. This state graph will be represented by any suitable data structure such as a matrix or linked list.

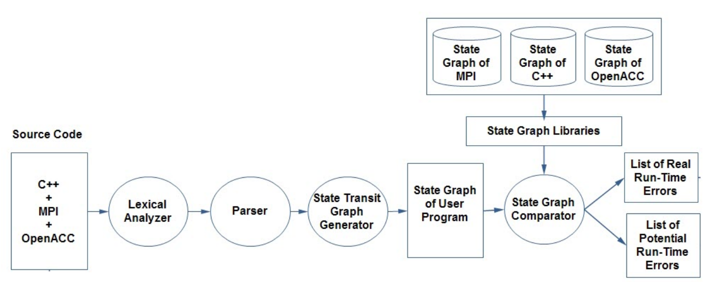

Figure 5: Static Part of the Proposed Architecture

The dynamic testing part of the proposed architecture is shown in Figure 6, which takes the source code and the assertion language as an input and move them to the instrumental. The instrumental depending on the semantics of the assertion language will produce code in the targeted programming language. The instrumental consist of four modules including; a lexical analyzer, parser, semantic, and code translator. The instrumental will produce an instrumented source code as an output. The instrumented source code includes the user codes and the testing codes both of them wrote in the user code programming language. Two methods can do instrumentation. Firstly by adding the testing codes, assertion statements, to the source code which leads to bigger code size as it will have user code and testing code. The second method is by adding the assert statements as calling of API functions, and these functions will test the part of the code that needs to be tested. This method leads to a smaller code size that any testing needed a call statement will be written, and the function will do the test. It is noticeable when we have the same testing code for several parts of the user code, in the previous method this testing code will be repeated many times, while in this method it will be only written once and called multiple times.

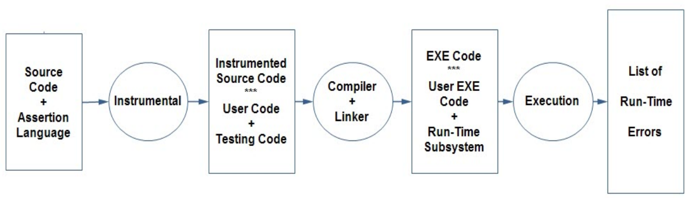

Figure 6: Dynamic Part of the Proposed Architecture

Further investigation of the instrumentation will be considered in our future progress. The resulted instrumented code will be compiled and linked, which results in EXE codes including user executable code and run-time subsystems. Finally, these EXE codes will be executed and provide a list of run-time errors.

6. Discussion

There are many tools, and researches have been done to detect a run-time error that occurs in parallel systems, which used MPI, CUDA, and OpenMP programming models. However, even though OpenACC can work in heterogeneous architecture, hardware, and platforms, as well as used by non-computer science specialist, which easily can have several errors. There is not a research or testing tool that detects OpenACC run-time errors. Also, OpenACC becomes increasingly used in different research fields as well as one of the main programming models targeting Exascale systems. Recently, OpenACC has been used in five of 13 applications to accelerate performance in the top supercomputer in the world Summit. Also, three of the top five HPC applications are using OpenACC as well. Therefore, this increased in using OpenACC will come with more errors that need to be detected.

In our tool, we consider having hybrid testing techniques including static and dynamic testing. This combination takes the advantages of two testing techniques, reduces disadvantages, and reduces the testing time. The first part of the hybrid technique is a static testing technique which analyses the source code before compilation to detect static errors. Some of the run-time errors can also be detected from the source code and should be sent to developers to solve them because they will occur definitely at run-time. In addition, potential run-time errors are errors that might or might not be occurred after compilation and during run-time based on the execution behavior. The reasons that cause these potential errors can be detected from the source code before compilation by using static testing. However, if these errors have not been detected, it will become run-time errors. As a result, the developers should be warned to these errors and consider them.

The second part of the hybrid technique is a dynamic testing technique that is detecting errors that happened during run-time, by instrumenting and analyzing the system during run-time. This is challenging because different factors and complicated scenarios can cause these errors. In addition, testing parallel programs is a difficult task because of the nature of such programs and their behavior. This will add more work to the testing tool for covering every possible scenario of the test cases and data. Furthermore, these dynamic techniques are sensitive to the execution environment and can affect the system execution time. Finally, it is the run-time errors type and behavior that determines which techniques will be used, because static analysis and others cannot detect dynamic techniques cannot detect some errors.

7. Conclusion and Future Works

High-performance computing has become increasingly important, and the Exascale supercomputers will be feasible by 2020; therefore, building massively parallel supercomputing systems based on a heterogeneous architecture has become even more important to increase parallelism. Using hybrid programming models for creating parallel systems has several advantages and benefits, but mixing parallel models within the same application leads to more complex codes. Testing such complex applications is a difficult task and needs new techniques for detecting run-time errors.

We proposed a parallel hybrid testing tool for detecting run-time errors for systems implemented in C++ and MPI + OpenACC. This proposed solution integrates static and dynamic testing techniques for building a new hybrid testing tool for parallel systems. This allows us to take advantages of both previously mentioned techniques for detecting some of the dynamic errors from the source code by using the static testing techniques, which will enhance the system execution time. Also, our system will work in parallel to detect run-time errors, by creating testing threads depending on the number of the application threads.

In our future work, we will identify and classify the OpenACC run-time errors and study their behavior and causes to be our guide in building our testing tool. Also, we will implement our architecture and evaluate its ability to detect OpenACC run-time errors and also we will identify and address the run-time errors that resulted from the dual-programming model MPI + OpenACC. Our experiments will be conducted in AZIZ supercomputer, which is one of the top ten supercomputers in the Kingdom of Saudi Arabia. On June 2016, AZIZ was ranked No. 359 among the Top 500 supercomputers in the world.

Conflict of Interest

The authors declare no conflict of interest.

Acknowledgment

This work was funded by the Deanship of Scientific Research (DSR), King Abdulaziz University, Jeddah, under grant No. (DG1440 - 12 - 611). The authors, therefore, acknowledge with thanks DSR technical and financial support.

References

[1] Message Passing Interface Forum, "MPI Forum," 2017. [Online]. Available: http://mpi-forum.org/docs/.
[2] OpenMP Architecture Review Board, "About OpenMP," *OpenMP ARB Corporation*, 2018. [Online]. Available: https://www.openmp.org/about/about-us/.
[3] NVIDIA Corporation, "About CUDA," 2015. [Online]. Available: https://developer.nvidia.com/about-cuda.
[4] Khronos Group, "About OpenCL," *Khronos Group*, 2017. [Online]. Available: https://www.khronos.org/opencl/.
[5] OpenACC-standard.org, "About OpenACC," *OpenACC Organization*, 2017. [Online]. Available: https://www.openacc.org/about.
[6] F. E. Eassa, L. J. Osterweil, and M. Z. Abdel-mageed, "AIDA: a dynamic analyser for Ada programs," *Inf. Softw. Technol.*, vol. 36, no. 2, pp. 107–117, 1994.
[7] SC11, "the International Conference for High Performance Computing, Networking, Storage and Analysis," 2011. [Online]. Available: http://sc11.supercomputing.org/.
[8] A. Fu, D. Lin, and R. Miller, "Introduction to OpenACC," 2016.
[9] M. Daga, Z. S. Tschirhart, and C. Freitag, "Exploring Parallel Programming Models for Heterogeneous Computing Systems," in *2015 IEEE International Symposium on Workload Characterization*, 2015, pp. 98–107.
[10] J. A. Herdman, W. P. Gaudin, O. Perks, D. A. Beckingsale, A. C. Mallinson, and S. A. Jarvis, "Achieving portability and performance through OpenACC," *Proc. WACCPD 2014 1st Work. Accel. Program. Using Dir. - Held Conjunction with SC 2014 Int. Conf. High Perform. Comput. Networking, Storage Anal.*, no. July 2013, pp. 19–26, 2015.
[11] The Open MPI Organization, "Open MPI: Open Source High Performance Computing," 2018. [Online]. Available: https://www.open-mpi.org/.
[12] MPICH Organization, "MPICH," 2018. [Online]. Available: http://www.mpich.org/.
[13] IBM Systems, "IBM Spectrum MPI," 2018. [Online]. Available: https://www.ibm.com/us-en/marketplace/spectrum-mpi.
[14] Intel Developer Zone, "Intel MPI Library," 2018. [Online]. Available: https://software.intel.com/en-us/intel-mpi-library.
[15] J. Kraus and P. Messmer, "Multi GPU programming with MPI," in *GPU Technology Conference*, 2014.
[16] J. Kim, S. Lee, and J. S. Vetter, "IMPACC: A Tightly Integrated MPI+OpenACC Framework Exploiting Shared Memory Parallelism," in *Proceedings of the 25th ACM International Symposium on High-Performance Parallel and Distributed Computing - HPDC '16*, 2016, pp. 189–201.
[17] OpenACC Standards, "The OpenACC Application Programming Interface version 2.7," 2018.
[18] K. Shankari and N. G. B. Amma, "Clasp: Detecting potential deadlocks and its removal by iterative method," in *IC-GET 2015 - Proceedings of 2015 Online International Conference on Green Engineering and Technologies*, 2016.
[19] J. Zhou, S. Silvestro, H. Liu, Y. Cai, and T. Liu, "UNDEAD : Detecting and Preventing Deadlocks in Production Software," in *Proceedings of the 32nd IEEE/ACM International Conference on Automated Software Engineering*, 2017, pp. 729–740.
[20] J. F. Münchhalfen, T. Hilbrich, J. Protze, C. Terboven, and M. S. Müller, "Classification of common errors in OpenMP applications," *Lect. Notes Comput. Sci. (including Subser. Lect. Notes Artif. Intell. Lect. Notes Bioinformatics)*, vol. 8766, pp. 58–72, 2014.
[21] M. K. Ganai, "Dynamic Livelock Analysis of Multi-threaded Programs," in *Runtime Verification*, 2013, pp. 3–18.
[22] Y. Lin and S. S. Kulkarni, "Automatic Repair for Multi-threaded Programs with Deadlock / Livelock using Maximum Satisfiability," *ISSTA Int. Symp. Softw. Test. Anal.*, pp. 237–247, 2014.
[23] B. Krammer and M. M. Resch, "Runtime Checking of MPI Applications with MARMOT," in *Performance Computing*, 2006, vol. 33, pp. 1–8.
[24] M. Cao, "Efficient , Practical Dynamic Program Analyses for Concurrency Correctness," The Ohio State University, 2017.
[25] E. Saillard, P. Carribault, and D. Barthou, "MPI Thread-Level Checking for MPI+OpenMP Applications," in *EuroPar*, vol. 9233, 2015, pp. 31–42.
[26] N. Ng and N. Yoshida, "Static deadlock detection for concurrent Go by global session graph synthesis," *CC 2016 Proc. 25th Int. Conf. Compil. Constr.*, vol. 1, no. 212, pp. 174–184, 2016.
[27] A. Santhiar and A. Kanade, "Static deadlock detection for asynchronous C# programs," in *Proceedings of the 38th ACM SIGPLAN Conference on Programming Language Design and Implementation - PLDI 2017*, 2017, pp. 292–305.
[28] P. Chatarasi, J. Shirako, M. Kong, and V. Sarkar, "An Extended Polyhedral Model for SPMD Programs and Its Use in Static Data Race Detection," 2017, pp. 106–120.
[29] J. Jaeger, E. Saillard, P. Carribault, and D. Barthou, "Correctness Analysis of MPI-3 Non-Blocking Communications in PARCOACH," in *Proceedings of the 22nd European MPI Users' Group Meeting on ZZZ - EuroMPI '15*, 2015, pp. 1–2.
[30] A. T. Do-Mai, T. D. Diep, and N. Thoai, "Race condition and deadlock detection for large-scale applications," in *Proceedings - 15th International Symposium on Parallel and Distributed Computing, ISPDC 2016*, 2017, pp. 319–326.
[31] Y. Cai and Q. Lu, "Dynamic Testing for Deadlocks via Constraints," *IEEE Trans. Softw. Eng.*, vol. 42, no. 9, pp. 825–842, 2016.
[32] RWTH Aachen University, "MUST: MPI Runtime Error Detection Tool," 2018.
[33] E. Saillard, "Static / Dynamic Analyses for Validation and Improvements of Multi-Model HPC Applications . To cite this version : HAL Id : tel-01228072 DOCTEUR DE L ' UNIVERSITÉ DE BORDEAUX Analyse statique / dynamique pour la validation et l ' amélioration des applicat," University of Bordeaux, 2015.
[34] Y. Huang, "An Analyzer for Message Passing Programs," Brigham Young University, 2016.
[35] R. Surendran, "Debugging, Repair, and Synthesis of Task-Parallel Programs," RICE UNIVERSITY, 2017.
[36] V. Forejt, S. Joshi, D. Kroening, G. Narayanaswamy, and S. Sharma, "Precise Predictive Analysis for Discovering Communication Deadlocks in MPI Programs," *ACM Trans. Program. Lang. Syst.*, vol. 39, no. 4, pp. 1–27, Aug. 2017.
[37] Lawrence Livermore National Laboratory, University of Utah, and RWTH Aachen University, "ARCHER," *GitHub*, 2018. [Online]. Available: https://github.com/PRUNERS/archer.
[38] B. Klemme, "Software Testing of Parallel Programming Frameworks," University of New Mexico, 2016.
[39] H. Ma, L. Wang, and K. Krishnamoorthy, "Detecting Thread-Safety Violations in Hybrid OpenMP/MPI Programs," in *2015 IEEE International Conference on Cluster Computing*, 2015, pp. 460–463.
[40] Allinea Software Ltd, "ALLINEA DDT," *ARM HPC Tools*, 2018. [Online]. Available: https://www.arm.com/products/development-tools/hpc-tools/cross-platform/forge/ddt.
[41] R. W. S. Inc., "TotalView for HPC," 2018. [Online]. Available: https://www.roguewave.com/products-services/totalview.
[42] G. Bronevetsky, I. Laguna, S. Bagchi, B. R. de Supinski, D. H. Ahn, and M. Schulz, "AutomaDeD: Automata-based debugging for dissimilar parallel tasks," in *IFIP International Conference on Dependable Systems & Networks (DSN)*, 2010, pp. 231–240.
[43] J. Yang, "A VALIDATION SUITE FOR HIGH-LEVEL DIRECTIVE-BASED PROGRAMMING MODEL FOR ACCELERATORS A VALIDATION SUITE FOR HIGH-LEVEL DIRECTIVE-BASED PROGRAMMING MODEL FOR," University of Houston, 2015.
[44] C. Wang, R. Xu, S. Chandrasekaran, B. Chapman, and O. Hernandez, "A validation testsuite for OpenACC 1.0," in *Proceedings of the International Parallel and Distributed Processing Symposium, IPDPS*, 2014, pp. 1407–1416.
[45] K. Friedline, S. Chandrasekaran, M. G. Lopez, and O. Hernandez, "OpenACC 2.5 Validation Testsuite Targeting Multiple Architectures," 2017, pp. 557–575.
[46] K. Ahmad and M. Wolfe, "Automatic Testing of OpenACC Applications," in *4th International Workshop on Accelerator Programming Using Directives*, vol. 10732, 2018, pp. 145–159.

Advances in Science, Technology and Engineering Systems Journal Vol. 4, No. 2, 211-220 (2019)

www.astesj.com

Special Issue on Advancement in Engineering and Computer Science

ASTESJ

ISSN: 2415-6698

A Critical Analysis of Topics in Software Architecture and Design

Janet Bishung, Ooreofe Koyejo, Adaugo Okezie, Boma Edosomwan, Sylvester Ani, Abisola Ibrahim, Austin Olushola, Isaac Odun-Ayo*

Department of Computer and Information Sciences, Covenant University, Ogun State, Nigeria

A R T I C L E I N F O

Article history:
Received: 20 January, 2019
Accepted: 07 March, 2019
Online: 27 March, 2019

Keywords:
Software Architecture
Software Design
Service Oriented Architecture
Design Patterns

A B S T R A C T

Software architecture and design is an important component in the software engineering field. This aspect of software engineering covers the functional and non-functional requirements of any system being proposed to be developed, while software architecture deals with non-functional requirements, software design entails the functional requirements.

The objective of this paper is to critically analyze current topics in Software architecture and design. The method of analysis involved the use of inclusion and exclusion criteria of papers published in journals and conferences. These papers were accessed from digital libraries like ScienceDirect, and IEEE explore*, with a quantitative approach of analysis been imbibed. From the analysis, the result showed that, of 35 papers used in analysis, 34.3% discussed stakeholders' involvement and decisions in software design. 17.1% for design quality, 20% examined software reuse while 11.4% discussed software evaluation and 8.6% of papers reviewed discussed software management, evolution and software development life cycle each which should be more focused as it is the fundamentals of software design and architecture. From the analysis derived, stakeholder's involvement and decision in software design is an integral part in software building for effective use. Thereby making researchers dwell more on the topic. The least discussed topics was due to the expectations of researchers. Expecting readers to have a fore knowledge of the fundamentals of design which includes software management, evolution and software development life cycle.*

1. Introduction

Software Architecture gives the high-level description of a software and the discipline of creating the structures and systems [1]. It gives blueprint for the system, laying out tasks to be executed in a logical manner through the design [2]. It is the fundamental structural choices made vis a vis the business needs of the organization which may be costly to change once implemented [3]. Although there are no standard procedures to follow in software architecture that can address all issues of concern in general software development, certain factors should be of utmost non-negotiable fundamentals in software development, to ensure standardization thereby avoiding incessant collapse of systems witnessed in the early years of software developments [4]. Among the factors that will be enumerated briefly is the factor of proper documentation. This facilitates communication among stakeholders, captures decisions about the structures of the task and the design options – focusing on the decisions that must be right from the onset, otherwise, the imminent collapse of such system will be devastating– [5]. Since software architecture is largely driven by the required or expected functionalities, the current insight to software architecture is that required functionalities should reflect or incorporate all the quality attributes which include fault-tolerance, reliability, backward compatibility, extensibility, availability, maintainability, usability, security amongst others. Stakeholders concerns should reflect these quality attributes at both non-functional and functional stages without recourse to extra cost.

Software design envisions and defines software solutions to problem sets. It involves a sequence of steps that describe all aspects of the software in development [6]. Here, solutions to the problem the software is to solve are expressed in a logical sequence with details of their relationships. It begins with describing the total components to be built, then refine them to every detail. It is

*Isaac Odun-Ayo, Covenant University, +2348028829456
isaac.odunayo@covenantuniversity.edu.ng

the physical expression of all the processes that create solutions according to stakeholders' expectations. The designs are taken within the confines of fundamental principles which ensure designs are traceable to requirement analysis, uniformity, integration, structured for change etc. This ensures standardization while addressing the business objectives and stakeholders' needs [7]. In general, software development is dependent on time and cost and the design option should reflect these critical factors.

Software Design addresses all the expected required functionalities of the business objectives. This includes specifications of services, components, integration, data models and algorithms. Meanwhile, Software Architecture addresses design standard ensuring that it aligns with stated strategy as it pertains to business and technology of an organization. This includes considerations such as compliance, technology standards and operational efficiency. An architecture designed is intended to prevent repetitive mistakes in design or inconsistency with other aspects of the organization. It could be said that architecture is global optimization of software and design is local optimization [8]. In general, software architecture provides standardization upon which software designs are tailored.

Software architecture and software design are extremely important for a software project. So, here are brief points highlighting benefits of software architecture & design; solid foundation for software project, scalability of platform, increase performance, identification of area of cost savings, vision implementation, increase quality, better code maintainability, prioritization of goals, higher adaptability, faster platform, risk management and enable quicker changes among many others [9].

This study is aimed at helping researchers to have an in-depth knowledge of the fundamental as well as critical topics involved in software architecture and design of proposed and existing systems. It would also help in uncovering the critical gaps in which many researchers were not able to explore thereby improving knowledge as regards software architecture and design. The objective of this paper is to conduct a critical analysis on current topics in Software architecture and design. Published papers and articles on the topics discussed in the paper were reviewed with the percentages of each topic in relation to others were calculated.

Other parts of the paper are organized as follows: Section 2 gives review of some related work done, Section 3 gives a highlight on software architectural styles, Section 4 discusses Software Oriented Architecture, Section 5 is a discussion on Design Patterns; section 6 presents the results and discussion of the major topics selected for analysis from literatures. Section 7 gives a conclusion of the paper with recommendations for future work.

2. Related Work

In [10], the importance of software architecture as a vital aspect of software development was examined. The paper explored two important components, software evolution and re-usability. These are very critical component that helps curb the huge expenses involved in the development of software. Software architecture that can be evolved and reused should be in high demand, as software evolution and reuse are more likely to receive higher pay-off. [11] considers the fact that researchers cannot overlook the year's technology as well as the fact that software architecture employs fully detailed explorations of notations, techniques, analysis, tools and creation methods. There exist an intersection and interrelationship of software architecture with the study of software design, domain-specific design, program analysis, software families, specific classes of components and component-based reuse. The comparative analysis of software evolution methods in [12] explains the systematic comparison between architecture models and evolution methods centering its base on the scenario-based approach of software architecture.

The review on the successes and failure for software architecture in [13], gives insight into software architecture development and management process. It assesses previous literature and experiences to identify the factors that cause success and failure for software architecture and classifying these factors into subgroups as indicated by practitioners. [14] proposed a different methodology as a guide for practitioners supporting software architecture and design in an agile environment. Highlights of phases in software design process were covered, tools and techniques were proposed to implement those phases. Architectural design decisions and knowledge in [15], examine the essence of reusable architectural knowledge and the importance of documenting quality attributes along with the decisions captured during architectural design.

In [16], the concept of sustainability was introduced for software design. It was essential in integrating it into the existing catalog of design quality attributes. This was because design is a key factor in software development and this has been noted by many researchers. The information produced during software design tends to evaporate progressively due to certain conditions like software evolution. [17] considered all developed software need to meet required and specified quality standards as requested by users or stakeholders, quality being a major issue in software systems today. To achieve the quality requirements, different analysis approach was explored and a critical evaluation of the software system was carried out. This was to analyze the architecture, thereby verifying that quality requirements have been duly addressed in the design.

From an in-depth review of System Development Methodologies (SDMs) conducted by [18], a list of the important features in each methodology was made. Despite several SDMs, most of them share similar activities which include well known and practiced requirements-analysis, design, codification-test and implementation, all put together in project management. Four stages in the evolution of SDMs were reported which include pre-methodologies, rigor-oriented methodologies, agile-oriented methodologies and emergent service-oriented methodologies. Well-recognized SDMs in software engineering include Rational Unified Process, Microsoft Solutions Framework and Model-based (system) architecting and software engineering.

The software architecture chosen in the development of a software product is dependent on the software requirements and constraints. A Design Association Theory (DAT) to show the causal relationship of why a design should exist was proposed by [19] for associating design concerns, design problems and design solutions. DAT proposes a five-step association-based design review process, which includes the extraction of requirements, extraction of design, construction of causal relationship between design elements and design solutions, discovery of potential design issues and verification and confirmation of design issues with architects. In documenting design decisions and design reasoning for objective evaluation, architects also utilize DAT. The DAT model helps designers and reviewers in associating architectural knowledge.

3. Software Architectural Styles

Architectural Styles are principles which shapes an application. It is more of an abstract framework of a system in the area of its organization. There are six major types of architectural styles. Namely:

3.1 Dataflow Architecture

In this, all software systems are categorized as lists of shifts on chronological set of input data, where data and operations are independent of each other. When data enters this system, it flows through the modules one at a time until they are assigned to some final destination [20]. Its aim is to achieve the qualities of reuse and immovability and is suitable for applications involving series of independent data computations on orderly defined input and output. There are three execution sequences between modules that the data flow architecture uses; Batch sequential, Pipe and filter or non-sequential pipeline mode and the Process control [20].

3.2 Data-centered Architecture

Data is centralized in this form of architecture and accessed frequently by other components that modify data. Its main purpose is achieving integrality of data. It contains different components that communicate using shared data repositories. The components access a shared data structure and are independent, meaning, they interact only through the data store. The flow of control sums the types of Data-centered architecture into two types; The repository and the blackboard architecture style. This form of architecture is mostly used in information system [20].

3.3 Hierarchical architecture

This views the whole system as a hierarchy structure whereby software systems are decomposed into subsystems at different levels in the hierarchy. It is mostly used in designing system software such as network protocols and operating systems. [20].

3.4 Interaction oriented architecture

The main aim of the interaction-oriented architecture is to separate users' interaction from data abstraction and business data processing. It divides the system into three major partitions: Data module (which provides the data abstraction and all business logic.), Control module (Which identifies the flow of control and system configuration actions) and the View presentation module (This is responsible for the visual or audio presentation of data output. It has two major styles: Model-View-Controller (MVC) and The Presentation-Abstraction-Control (PAC) [20].

3.5 Component based architecture

It is an architecture that decomposes software designs into functional components with their own methods, events and properties. These components become loosely coupled and reusable to provide modular programs that can be tailored to fit any need. [21]

3.6 Distributed architecture

This is a form of architecture that sits in the middle of a system and manages or supports the different components of that distributed system. Its aim is transparency, reliability, and availability. It hides the way in which resources are accessed and the differences in data platform, the resource location, different technologies from users, failures and resource recovery and a host of others. [20]. It is the most widely used form of architecture as it aligns with the technological advancement of the 21st century. Software development has improved greatly with the introduction of the internet. Software is now been distributed, components been reused, as well as introduction of concurrency and simultaneous change in the modification of data. These are the major advantages of the distributed architecture which has made it a common form of architecture in time past. [20]. There are different types of Distributed Architecture;

3.6.1 Broker Architecture: Mostly used to coordinate and enable the communication between registered servers and clients more like a software bus [20].

3.6.2 Client-server Architecture: Is commonly used by search engines, web servers, mail servers, it is mostly based on the functionality of the clients that is, requesting services of other components. The Service Oriented Architecture is a major sub-division of this. It supports business-driven Information Technology (IT) approach in which an application consists of software services and software service consumers. It has the ability to develop new functions rapidly which makes it mostly used along with its basic features which would be explained in the next section. [22]

Service Oriented Architecture would be further discussed due to its relevance in the current IT revolution. It is a known fact that cloud computing has come to stay and due to the integration ability of Service Oriented Architecture it has become a yardstick in the cloud computing revolution as their technologies have become more like bridges to the cloud.

4. Service Oriented Architecture (SOA)

SOA is a software architecture and design styles that entails the use of services as its main building component [23]. A service (as a software component), is a technique that allows access to several capabilities. SOA is now a mainstream software development mechanism. Despite the introduction of new architectural variants like cloud computing or micro-services [24], SOA is still widely used. This is due to its support for fast building applications using assembling of Internet-accessible services, allowing software organizations to hasten the development of distributed applications as well as a result time-to-market. After all this, a service is simply a distinct unit of performance that specifies a business function. This simply means it relies on Web Services for its implementation [24].

SOA carries out two core functions. Which are creating broad architectural models that explain application goals, including the approaches that help meet the goals. The second function is it defines the implementation specifications, which is mostly integrated to the Web Services Description Language (WSDL) and the Simple Object Access Protocol (SOAP) specifications [25].

4.1 Major Principles of SOA

The major principles of SOA are [26]:

i. Regulate Service Contract - In this, there must be a form of description that explains what the service is about. This makes it easier for the client applications to understand what the service is meant to do.

ii. Loose Coupling –It entails components having little or no dependency on each other. This is a major characteristic of web services that emphasizes that there should be less dependency between web services and the client initiating this web service. Therefore, if any service functionality changes at any point in time, it should not hinder the client application from working.

iii. Service Abstraction - In this, service is ought to encapsulate its procedures and not expose how it executes its functionality. Explaining to the client application what it does and not how it does it for security purposes.

iv. Service Re-usability - Logic is separated into services with the aim of increasing reuse capability. In any technology, re-usability is a major issue as no one would want to spend time and effort writing the same codes again for multiple applications that require them.

v. Service Autonomy -The service knows everything about the application or system and what functionality it offers so it has complete control over the source code it encompasses.

vi. Service Statelessness - Superlatively, services ought to be stateless. Meaning they should not withhold any form of information from one state to the other.

vii. Service Discoverability - Services can be identified in a service registry. A service registry is a resource that allows controlled access to data for the controlling of SOA.

viii. Service Composability - It splits big issues into little ones. It is to be noted that not all functions should be embedded in an application and moved into one single service. Instead the service should be split into modules each having separate business functionalities.

ix. Service Interoperability - Services should accept and make use of various standards allowing different subscribers to use their various service.

For the implementation of SOA to be a success, you would need a productive SOA method that explains the plans, discoveries, procedures and the selected goals [26].

The integration platform for SOA plays a crucial role in the merging of existing application to cloud services. With SOA, components were split into services that became re-usable and easy to use among several systems. This is similar to the system means used in the automotive industry, where different layouts/systems share the same components e.g. engines. Cloud computing is re-vamping the IT world as we know it. The IT systems are utilized by users and companies. In the automotive industry, owners do not need to buy their own vehicles but can use car-sharing services. These service providers show the cars to several drivers. Comparably, in IT, a cloud service provider acts as a middle man and merges several clouds. Existing IT systems that require combination with new cloud-based solutions or inter-mediated are resolved using cloud service providers [37].

Cloud computing is re-modelling the IT industry and how its services are utilized, just like how petrol is soon going extinct in the automotive industry. Electric cars are now in use even as we use petroleum-based cars. As IT companies continue to make use of more cloud technologies the SOA technologies will continue to serve as bridges to the cloud.

Micro-service-based software architecture is the re-industrialized application of the SOA model. The components are developed as services using Application Programming Interfaces (API), just like the SOA would require. An API broker serves as a mediator to access components, ensuring SOA security and governance practices are followed.

SOA principles have taken us to the cloud and aides the most improved version of cloud software development techniques in use today. [27]

4.2 Advantages of SOA [28]

- Services can be reused in multiple applications independent of their interactions with other services.
- Due to service in-dependency, services can be easily updated or maintained without having to worry about other services.
- SOA-based applications are more reliable since they are small independent services that are easier to test and debug.
- Multiple instances of a single service can run on different servers at the same time.
- It improves Software Quality.

4.3 Disadvantages of SOA [28]

- Every time a service interacts with another service, complete validation of every input parameter takes place. This increases the response time and machine load, and thereby reduces the overall performance.
- There would be high investment cost as implementation of SOA requires a large upfront investment by means of technology, development, and human resource.

5. Design Patterns

Software design could be considered the most important aspect of software development as well as the most difficult process in a software development life cycle. Over the years, based on experience, programmers have embodied and recommended demonstrated results to fulfill the persistent issues that arise during design. Accordingly, the experience-based clarifications are composed and acknowledged as a consistent model for designs patterns [29]. Various design patterns have been presented and classified either as a sanctioned or a variation key to take care of design issues. The current programmed systems for design pattern(s) options help fledgling programmers to choose the more proper pattern(s) from the rundown of relevant examples, to tackle an issue during the design period of software that is been developed. [29]

In software engineering, a design pattern is a general repeatable result for an ordinarily happening issue in programming structure [30]. Design patterns are used to ensure reuse of software design solutions in the early phases of software development, especially in the requirements engineering phase. Patterns do not provide visible solutions, but they present the concepts from which solutions are derived [31]. Design patterns have been introduced for defining good practices in software design [33]. Design patterns can be used in requirements engineering as patterns exist for core activities of a process. Design patterns are not pure inventions like a light bulb or a car. They are derived patterns that software engineers and architects found, that could be standardized to be used to solve similar problems categorized across three major areas; creational, structural and behavioral. When we determine the proper structure design for a task or issue, it helps us avoid changes that would require budgetary expenses, untenable, multiple and inefficient codes as the system scales up [32].

5.1 Classification and Selection of Design Patterns

The intrigue and involvement of programmers are utilized to present recent arrangement plans for the association of design patterns of specific concerns like object-oriented development and real-time applications [30]. The outline of current efforts describes the number of important categories of design patterns which relies upon the sort and multifaceted nature of target issues. For instance, [33] introduced three important classifications namely behavioral, creational, and structural in the setting of object-oriented advancement to solve recurring issues. In a specific circumstance of working applications, [30] introduced a catalog of thirty-four patterns, which are divided into five categories based on their relevance. In this paper, we would consider the object-oriented advancement categories.

A. Creational Design Patterns

Creational design patterns manage object creation systems attempting to make questions in a way that suits the circumstance. The essential type of object creation could result in design issues or added intricacy to the design. Creational design patterns take care of this issue by controlling this object creation [30]. These patterns can be further divided into class-creation patterns and object-creation patterns. Class-creation patterns use legacy viably in the instantiating of procedures while object-creation designs use assignment adequately to take care of business [35]. Creational design patterns are singleton, abstract factory, prototype, factory method, builder and object pool [31].

B. Structural patterns

Structural Design Patterns are used to ease a design by recognizing a straightforward method to acknowledge relationships [30]. These design patterns are tied in with sorting out various classes and object to frame bigger structures and give new usefulness [35].

C. Behavioral patterns

Behavioral design patterns are design patterns that identify basic correspondence designs among object and understands the patterns. By doing so, these patterns increment adaptability in doing this correspondence [30]. Behavioral patterns are about identifying basic correspondence designs among object and understanding the patterns that exist among them [35].

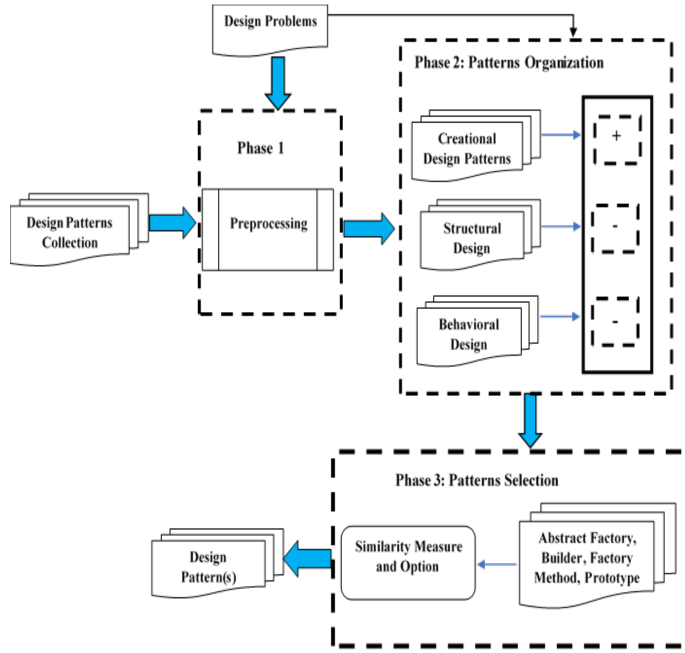

Figure 1: Diagrammatic Representation of Design Patterns Classification and Selection [34].

5.2 Design Pattern Topics

Six research design pattern topics concluded by [36] includes; pattern usage, quality evaluation, pattern mining, pattern specification, pattern development and miscellaneous issues.

i. Pattern development: This involves any advancements in design pattern research such as:
   a. Proposing a new model or new model language
   b. Reviewing model variants, composing models or elaborating a specific model, model evolution.
   c. Arranging current design patterns into distinct areas.
ii. Pattern usage: this relates to the commitment of utilizing patterns in the software development process. They are characterized into two primary groups:
   a. Pattern utilization
   b. Pattern application
iii. Pattern mining: this includes discovering examples of the pattern in the code or design of a system. It can be characterized into two major classes:
   a. Introduction
   b. Evaluation
iv. Quality Evaluation: the quality and effect of a design pattern on a system after applying it, is one important concern developers have. This can be characterized into two major classes:
   a. Pattern evaluation
   b. Application evaluation
v. Pattern specification: it includes utilizing distinctive strategies and notation of representing the patterns. The two main groups are:

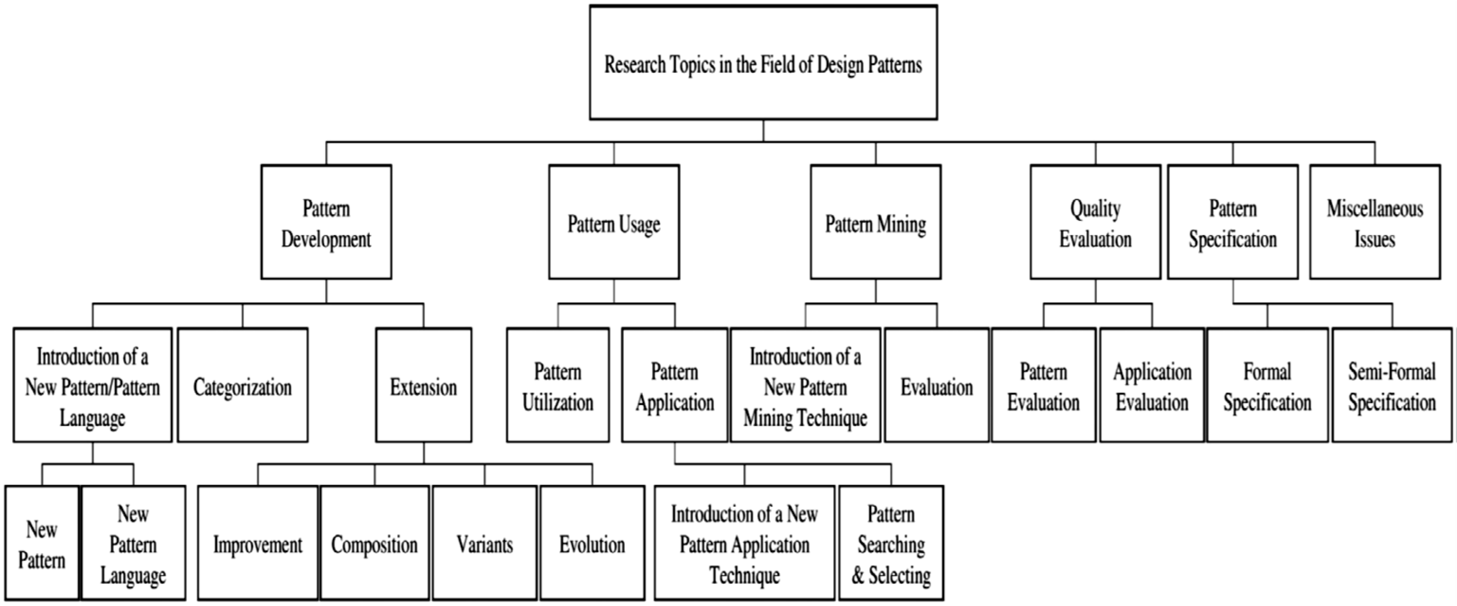

Figure 2: Design Pattern Research Tree [36]

a. Formal specification schemes
b. Semi-formal specification schemes

vi. Miscellaneous issues: this includes other issues that cannot fit into any of the previous classifications' issues such as re-factoring, code smells and anti-patterns. A major challenge of design patterns as discussed in [34,38, 39] is the searching and selection of design patterns before employing a right pattern into the system.

5.3 Pros and Cons of Design Patterns

It is worthy of note that there are very many design patterns available and a lack of understanding of these patterns pose problems for designers in software development especially for the novice [37]. Some of the pros and cons of the design patterns include:

Pros: [40]

- Easy to adapt and very flexible to predictable changes in business needs.
- Easy to test unit and validate individual components.
- Can provide organization and structure when business requirements become very complicated.

Cons: [40]

- Beginner engineers may not understand them, and these can cause a huge delay in development.
- Oftentimes used improperly without a realistic understanding of how the software is likely to change.
- It can add memory and processing overhead, sometimes it is not appropriate for applications such as low-level systems programming or certain embedded systems.

Design pattern, in general, enhances the nature of a product framework by giving a demonstrated solution for repeating design issues [41]. Also, the application of patterns brings about increment in quality and profitability of the software development process [31].

6. Results and Discussion

Table 1 shows several topics in software architecture and design alongside relevant work from several authors. Only one facet was used in this analysis, which are topics that relate to the subject (software architecture and design) discussed by these important authors. These topics were selected using inclusion and exclusion criteria. The essence of the selection criteria was to locate and add all papers that are necessary for the analysis. The inclusion and exclusion criteria were used to eliminate publications that were not significant to the study. It was observed that these topics were the most discussed and they also cut across academics and industry practice. The papers used for this review were access online from digital libraries like ScienceDirect, and IEEE explore. The authors and title of publications are listed in no particular order.

6.1. Software Evolution

Software evolution is the process of developing a software product, employing software engineering principles and methods. It follows the initial development of software and required maintenance. Updates are done till the desired software product is developed, thereby satisfying the (user) expected requirements [42]. This process implements changes to the original software, until the desired software is accomplished. Of the 35 papers used in this analysis, 8.6% of them reported on software evolution. From table 1, the findings show that software evolution though an integral part of software development was not substantially discussed by majority of the literature reviewed during the course of this study. This implies that there may be a decrease in research of software evolution.

6.2. Software Reuse

Software reuse involves creating new software systems from existing software frameworks rather than building software systems from beginning. This simple yet powerful methodology of software development was introduced in 1968 and now widely

Table 1: analysis of software architecture and design topics

Authors	Software Evolution	Software Reuse	Software Management	SDLC	Software Evaluation	Stakeholder Involvement/ Decision Making	Design Quality
Mekni, M., Buddhavarapu, G., Chinthapatla, S. and Gangula, M. (2018) "Software Architectural Design in Agile Environments"	-	-	-	x	x	-	-
Robillard, M.P. (2016) "Sustainable Software development"	-	-	x	-	-	-	x
I. Lytra, G. Engelbrecht, D. Schall and U. Zdun (2015) "Reusable Architectural Decision Models for Quality-driven Decision Support: A Case Study from a Smart Cities Software Ecosystem"	-	x	-	-	-	-	x
A. Ramirez, J. R. Romero and S. Ventura (2018) "Interactive multi-objective evolutionary optimization of software architectures"	-	-	-	-	-	-	-
O. Sievi-Korte, S. Beecham and I. Richardson (2018) "Challenges and recommended practices for software architecting in global software development"	-	-	x	-	-	-	-
N. Hamalainen, J. Markkula, T. Ylimaki and M. Sakkinen (2006) "Success and Failure Factors for Software Architecture"	-	-	x	-	x	-	-
A. Alhar, R. Mazamal and F. Azam (2016) "A Comparative Analysis of Software Architecture Evaluation Methods"	-	-	-	-	x	-	-
David Garlan. (2000) "software architecture"	-	-	-	-	-	-	-
R.Kazman, C.H Lung, (1997) "An approach to software architecture analysis for evolution and reusability"	x	x	-	-	-	-	-
Smrithi Rekha V and Henry Muccini, (2018) "Group decision-making in software architecture: A study on industrial practices"	-	-	-	-	-	x	-
Hans van Vliet and Antony Tang, (2016) "Decision making in software architecture"	-	-	-	-	-	x	-
R.Kazman, C.-H. Lung, s. Bot, and K. kalaichelvan (1997) "An approach to software architecture analysis for evolution and reusability"	x	x	-	-	-	-	-
M.Shaw, and P.Clements(2006) "The golden age of software architecture: a comprehensive survey."	-	-	-	-	-	x	-
H.V. Mohammad, A. Bavar, N.M. Khashayar, and D. Negin(2009)	-	-	-	-	-	-	-
I. Dobrica, and E. Niemela (2002) "A survey on software architecture analysis methods"	-	-	-	-	-	-	-
L. Tan, Y. Lin and H. Ye, (2012). "Quality Oriented Software Product Line Architecture Design,"	-	-	-	-	-	-	x
T. Mens, J. Magee and B. Rumpe(2010). "Evolving Software Architecture Descriptions of Critical System"	x	-	-	-	-	-	-
P. Abrahamsson, M. Ali Babar and P. Kruchen(2010). "Agility and Architecture: Can They Coexist"	-	-	-	x	-	x	-
A.Tang and M. F. Lau (2014) "Software architecture review by association"	-	-	-	-	-	x	-
H.Vlieta and A.Tang(2016) "Decision making in software architecture"	-	-	-	-	-	x	x
P.Y. Reyes-Delgado, M. Mora,H. A. Duran-Limon, L. C. Rodríguez-Martínez,R. V. O'Connorn and R. Mendoza-Gonzalez,(2016)	-	-	-	-	-	-	-
W. Hasselbring (2018) "Software Architecture: Past, Present, Future"	-	x	-	-	-	x	x
S. Orlov and A. Vishnyakov (2017) "Decision Making for the Software Architecture Structure Based on the Criteria Importance Theory"	-	-	-	-	-	x	-
Nitin Upadhyay (2016) "SDMF: Systematic Decision-making Framework for Evaluation of Software Architecture"	-	-	-	-	-	x	-
T. Kim, S. Yeong-Tae, L. Chung and Dung T. Huynh (2015). "Architecture Analysis: A Dynamic Slicing Approach"	-	-	-	-	-	-	-

M. Razavian, B. Paech and A. Tang (2018). "Empirical Research for Software Architecture Decision Making: An Analysis"	-	-	-	-	-	x	-
E. J. Eichwald, E. C. Lustgraaf, & B. Wetzel, (1999). "Transfer of the White Graft Reaction"	-	-	-	-	-	-	-
C. Manteuffel, P. Avgeriou and R. Hamberg (2018) "An exploratory case study on reusing architecture decisions in software-intensive system projects"	-	x	-	-	-	x	-
P.Bengtsson, (1999). "Software Architecture-Design and Evaluation."	-	-	-	-	-	-	-
A. Sharma, M. Kumar and S. Agarwal (2015) "A Complete Survey on Software Architectural Styles and Patterns"	-	-	-	x	-	-	-
M. Ozkaya and M. A. Kose (2018) "SAwUML – UML-based, contractual software architectures and their formal analysis using SPIN"	-	-	-	-	-	-	x
G. Vazquezab, J. Andres, D. Pacec and M Campoab (2014) "Reusing design experiences to materialize software architectures into object-oriented designs"	-	-	-	-	-	-	-
B. Jalendar, A. Govardhan and R. Emchand (2012) "Desiging code level reusable software components"	-	x	-	-	-	-	-
B. Kitchenham, S. Charters (2007) "Guidelines for performing systematic literature reviews in software engineering"	-	x	-	-	-	-	-

adopted all over the world [43]. Only 20% of the papers reviewed, showed software reuse as a major aspect of modern software development**.** More literatures reviewed discussed this subject as indicated in table 1 above, this implies that research still goes on in this area with respect to software architecture and design, as well as in the aspect of software development.

6.3. Software Management

Software management refers to the art and science of leading and planning software projects. From the analysis carried out, software management covers 8.6% of the relationship between software architecture and design and other parameters considered. Like software evolution, the aspect of software management was not widely discussed in literatures reviewed. Substantial research is therefore made in software architecture and design in this area.

6.4. Software Development Life cycle

Software Development Life Cycle (SDLC) gives a description of the development process of a system from the initial study until the time it is updated or replaced. There are six steps that make up the SDLC [44]. The major function of the SDLC is to neatly lay out the process of system development. Despite being a popular and well-discussed topic in practice and theory. 8.6% of the reviewed papers discussed the topic. Unlike other topics, this is a major aspect of software, from the reviewed literature there was no substantial amount of discussion made in this aspect**.**

6.5. Software Evaluation

Comprehensively, non-systematic checklists can be applied to a program in the software evaluation process [45]. In recent times, software assessment using theory-based approaches which incorporates relevant criteria derived from psychological, linguistic and pedagogical models of language learning and teaching has been proposed. 11.4% of the 35 articles reviewed, discussed the importance of software evaluation in developed systems. There has been current research going on in the aspect of software evaluation, hence making it one of the major discussed topics from table 1 above.

6.6. Stakeholder Involvement/ Decision Making

The nature of the design problem also determines the form of decision that will be made. As reported in [46], a structured design problem makes the decision-making process better and easier. In this analysis, 34.3% of the articles reviewed, considered stakeholder involvement and in some cases, decision-making as a factor in software architecture and design, making it the most emphasized topic. This had the highest number of literatures discussing the topic, this implies that currently, more researchers are gearing towards this aspect during the course of their research to emphasize the need of stakeholders' involvement during software development.

6.7. Design Quality

If the quality of a design is not considered properly, it could lead to a negative impact on the product being developed [47]. The quality of any software is dependent on how well it conforms with the design plan of that product, it determines if the product would deliver the requirements desired properly and efficiently. 17.1% of the papers used for analysis discussed this topic, either directly or by evaluation of some design quality factors like quality attributes or design decisions. Also, this was among the topics discussed substantially in the selected literatures, which makes design quality a high recommended aspect of software architecture and design both in terms of academics as regards research and also in the industry.

From the results, the most discussed topics gotten from the analysis of selected literatures were stakeholder involvement and design, software reuse, design quality and software evaluation while the least discussed topics include software management, software evolution and software development life cycle.

7. Conclusion

Software architecture and design is an important component in the software engineering field. For success in the software engineering field both the architecture and design of software must be considered. Hence, various fundamental topics as regards software architecture and design have been analyzed.

The objective of this paper was to critically analyze current topics in software architecture and design. The method of analysis adopted was the collection of published papers and articles on the topics discussed in the paper and the percentages of each fundamental topic was calculated. From the analysis, the result showed that, of 35 papers used in analysis, 34.3% discussed stakeholders' involvement and decisions, 17.1% for design quality, 20% examined software reuse while 11.4% discussed software evaluation and 8.6% of papers reviewed discussed software management, evolution and software development life cycle each.

From the analysis, it can confidently be concluded that aspects of software architecture and design such as software evolution, management, re-usability and building software which are fault tolerant, reliable, backward compatible, maintainable and secured are under-discussed. Several authors addressed various aspects of software architecture and design, but there are no standard procedures to follow that addresses all issues of concern in general software developments. As earlier stated, some factors should be non-negotiable in software development to ensure standardization thereby reducing incessant collapse of systems witnessed in the early years of software developments. This research stressed the significance and rigorous work involved in the development of software and outlined major factors that should be considered.

Therefore, it is important to note that a critical and rigorous analysis of software architecture and design is required to overcome the overall failure or crash of software in software development process and to also identify relevant gaps in the architecture and design styles or methods. Software architecture and design as an ever-growing field of software engineering, calls for further analysis to test and validate principles as they evolve. This study would help other researchers in the quest of knowing more about software development and the need to research further on the least discussed topics which are software management, software evolution and software development life cycle (SDLC).

Conflict of Interest

The authors declare no conflict of interest.

References

[1] C. Paul, F. Bachmann, L. Bass, D. Garlan, J. Ivers, R. Little, P. Merson, R. Nord, J. Stafford, (2010). "Documenting Software Architectures: Views and Beyond", Second Edition. Boston: Addison-Wesley. ISBN 978-0-321-55268-6, pp. 592.

[2] D. E. Perry, A. L. Wolf, (1992). "Foundations for the study of software architecture". ACM SIGSOFT Software Engineering Notes. 17 (4): CiteSeerX 10.1.1.40.5174. doi:10.1145/141874.141884, pp. 40.

[3] "SoftwareArchitecture".(2018), https://www.sei.cmu.edu/educationoutreach/courses/course.cfm?coursecode=p34. Retrieved 2018-07-23.

[4] B. Len, P. Clements and R. Kazman, (2012). "Software Architecture in Practice", Third Edition. Boston: Addison-Wesley. ISBN 978-0-321-81573-6.

[5] M. Fowler, (2003). "Design – Who needs an architect?". IEEE Software. 20 (5): 11–44. doi:10.1109/MS.2003.1231144

[6] F. Peter and D. Hart, (2004). "A Science of design for software-intensive systems". Communications of the ACM. 47 (8): 19–21 [20]. doi:10.1145/1012037.1012054.

[7] A. Davis, (2004)" Principles of Software Development", McGraw-Hill, Inc. New York, NY, USA, ISBN:0-07-015840-1.

[8] J. Spacey, (2017) "Software Design Vs Software Architecture.", https://simplicable.com/new/software-design-vs-software-architecture , Retrieved 2018-07-23.

[9] E. Novoseltseva, (2016). "https://apiumtech.com/blog/15-benefits-of-software-architecture/", Retrieved 2018-07-23.

[10] R.Kazman, C.-H. Lung, s. Bot, and k. kalaichelvan, (1997) " an approach to software architecture analysis for evolution and reusability", center for advanced studies conference, pp. 144-154.

[11] M.Shaw, and P. Clements, (2006)" the golden age of software architecture: a comprehensive survey.", institute for software research international school of computer science. Camegie mellon university, Pittsburgh, PA,0740-7459/06/.

[12] A.Alhar, M. Liaqat and F.Azam, (2016). "A Comparative Analysis of Software Architecture Evaluation Methods" Journal of Software Vol 11, No. 9. DOI:10.17706/JSW.11.9.934-942.

[13] N. Hämäläinen, J. Markkula, T. Ylimäki and M. Sakkinen, (2006)"Success and Failure Factors for Software Architecture". Available: https://jyx.jyu.fi/bitstream/handle/123456789/41384/Article_Success_and_Failure_Factors_for_SA.pdf;sequence=1 , Retrieved: 2018-08-21.

[14] M. Mekni, G. Buddhavarapu, S. Chinthapatla and M. Gangula, (2018) "Software Architectural Design in Agile Environments," Journal of Computer and Communications, 6, pp. 171-189. Available: https://doi.org/10.4236/jcc.2018.61018 .

[15] I. Lytra, G. Engelbrecht, D. Schall and U. Zdun, (2015) "Reusable Architectural Decision Models for Quality-driven Decision Support: A Case Study from a Smart Cities Software Ecosystem". Available: https://eprints.cs.univie.ac.at/4330/1/paper.pdf . Retrieved: 2018-08-21.

[16] M. P. Robillard (2016). "Sustainable Software development,". Available: https://www.cs.mcgill.ca/~martin/papers/fse2016.pdf . Retrieved: 2018-08-21.

[17] l. Dobrica, and E. Niemela, (2002) "a survey on software architecture analysis methods", IEEE Transactions on software engineering, vol 28, no. 7. Available: https://www.researchgate.net/publication/3188246. Retrieved: 2018-07-23.

[18] Antony Tang and Man F. Lau, (2014) "Software architecture review by association", Journal of Systems and Software", Volume 88, pp 87-101, ISSN 0164-1212.

[19] P.Y. Reyes-Delgado, M. Mora, Hector A. Duran-Limon, L. C. Rodríguez-Martínez, R. V. O'Connor and R. Mendoza-Gonzalez, (2016) "The strengths and weaknesses of software architecture design in the RUP, MSF, MBASE and RUP-SOA methodologies: A conceptual review, Computer Standards & Interfaces", Volume 47, pp 24-41, ISSN 0920-5489.

[20] "Software architecture and design tutorial," Tutorialpoints, 2019.[Online]. Available: https://www.tutorialspoint.com/software_architecture_design/index.htm. Retrieved:27-Feb-2019.

[21] R. J. de Paula, V. Falvo and E. Y. Nakagawa (2016), "Architectural Patterns and Styles" [Online]. Available:https://edisciplinas.usp.br/pluginfile.php/977101/course/section/268862/S4-%20Architectural%20Patterns%20and%20Styles.pdf.

[22] S. Boyd, M. D'Adamo, C. Horne, N. Kelly, D. Ryan and N. Tsang (2013), "SOFTWARE ARCHITECTURAL STYLES" SENG 403-W2013 Paper Project (Group4) [Online]. Available:http://kremer.cpsc.ucalgary.ca/courses/seng403/W2013/papers/04ArchitectureStyles.pdf

[23] D. Ameller, X. Burgués, D.Costal,C.Farré, X. Franch, (2018) "Non-functional requirements in model-driven development of service-oriented architectures"Science of Computer Programming,Volume 168, Pp 18-37.

[24] G.Rodríguez, J. A. Díaz-Pace and Á.Soria (2018) "Information Systems A case-based reasoning approach to reuse quality-driven designs in service-oriented architectures", Information Systems Volume 77, pp 167-189.

[25] "What is service-oriented architecture (SOA)? - Definition from WhatIs.com," SearchMicroservices, 2014. [Online]. Available: https://searchmicroservices.techtarget.com/definition/service-oriented-architecture-SOA. Retrieved: 13-Dec-2018.

[26] "SOA (Service Oriented Architecture) Principles," Meet Guru99 - Free Training Tutorials & Video for IT Courses, 2018. [Online]. Available: https://www.guru99.com/soa-principles.html. Retrieved: 13-Dec-2018.

[27] S. Pulparambil and Y. Baghdadi (2018) "Service oriented architecture maturity models: A systematic literature review", Computer Standards & Interfaces, Volume 61, pp. 65-76.

[28] "Advantages and Disadvantages of Service-oriented Architecture (SOA)" Techspirited, 2018. [Online]. Available: https://techspirited.com/advantages-disadvantages-of-service-oriented-architecture-soa. Retrieved:27-Feb-2019.

[29] S. Hussain, J. Keung, and A. A. Khan, (2017). "Software design patterns classification and selection using text categorization approach". Applied Soft Computing Journal, vol.58, pp. 225–244. http://doi.org/10.1016/j.asoc.2017.04.043

[30] "Design Patterns and Refactoring", (2018). [Online]. Available: https://sourcemaking.com/design_patterns. Retrieved: 13- Dec- 2018.

[31] J.L. Barros-Justo, B.V.B. Fabiane, L.C. Ania, (2018) "Software patterns and requirements engineering activities in real-world settings: A systematic mapping study", Computer Standards & Interfaces 58, pp. 23-42.

[32] J.O. Coplien, N.B. Harrison, (2005) "Organizational Patterns of Agile Software Development", Pearson Prentice Hall, ISBN-13: 978-0131467408.

[33] E. Gamma, R. Helm, R. Johnson and J.Vlissides , (1995) " Design Patterns: Elements of Reusable Object-oriented Software". Boston: Addison-Wesley Longman Publishing Co., Inc.

[34] S. Hussain, J. Keung, M. K. Sohail, A. A. Khan, and M. Ilahi (2019). "Automated framework for classification and selection of software design patterns". Applied Soft Computing Journal, vol.75, pp.1–20. http://doi.org/10.1016/j.asoc.2018.10.049

[35] "Design Patterns | Set 1 (Introduction) - GeeksforGeeks", GeeksforGeeks, (2018). [Online]. Available: https://www.geeksforgeeks.org/design-patterns-set-1-introduction/. Retrieved: 13- Dec- 2018.

[36] B. Bafandeh Mayvan, A. Rasoolzadegan and Z. G. Yazdi (2017) "The state of the art on design patterns: A systematic mapping of the literature", Journal of Systems and Software, Volume 125, pp. 93-118.

[37] J. Kress, B. Maier, H. Normann, D. Schmeidel, G. Schmutz, B.Trops, C. Utschig-Utschig and T. Winterberg. (2014). "SOA and Cloud Computing", https://www.oracle.com/technetwork/articles/soa/ind-soa-cloud-2190513.html Retrieved: 2018-01-09

[38] A. Birukou, (2010) A survey of existing approaches for pattern search and selection, in: Proceeding of PLoP DISI - University of Trento, Italy, ACM 978-1-4503-0259-3.

[39] P. Velasco-Elizondo, R. Marín-Piña, S. Vazquez-Reyes, A. Mora-Soto and J. Mejia, (2016), Knowledge representation and information extraction for analyzing architectural patterns, Sci. Comput. Program. Vol. 121 pp. 176–189.

[40] 2018. [Online]. Available: https://www.quora.com/What-are-some-pros-and-cons-of-using-Design-Patterns-to-describe-your-business-model. Retrieved: 2018-12- 13.

[41] D. K. Kim, L. Lu, and B. Lee, (2017). "Design pattern-based model transformation supported by QVT". Journal of Systems and Software, vol.125, pp.289–308. http://doi.org/10.1016/j.jss.2016.12.019

[42] Tutorials.point. "Software engineering overview" available:https://www.tutorialspoint.com/software_engineering/software_engineering_overview.html, Retrieved: 2018-12-13

[43] C.W. Krueger, (1992) "Software reuse", School of Computer Science, G'arnegie Mellon University, Pittsburgh, Pennsylvania. Available: https://dl.acm.org/citation.cfm?doid=130844.130856

[44] En.wikibooks.org, (2012) "Computer Revolution". [Online]. Available: https://en.wikibooks.org/wiki/The_Computer_Revolution/MIS/SDLC. Retrieved: 2018-11-2.

[45] IGI Global, (2012) "Software Evaluation". [Online]. Available: https://www.igi-global.com/dictionary/software-evaluation/27677 Retrieved: 2018-11-3.

[46] C. Zannier, M. Chiasson and F. Maurer, (2007) A model of design decision making based on empirical results of interviews with software designers. Inf. Softw. Technol. Vol. 49 (6), pp. 637–653.

[47] L. Tan, Y. Lin and H. Ye, (2012). "Quality Oriented Software Product Line Architecture Design," Journal of Software Engineering and Applications, vol. 5, pp. 472-476, [Online]. Available: http://www.SciRP.org/journal/jsea

[48] A. Ramírez, J. R. Romero and S. Ventura, (2018)" Interactive multi-objective evolutionary optimization of software architectures" Information Sciences, Vol 463–464, pp 92-109 Available: www.elsevier.com/locate/ins

[49] O. Sievi-Korte, S. Beecham and I. Richardson, (2018)"Challenges and recommended practices for software architecting in global software development" Information and Software Technology, In press, Available: www.elsevier.com/locate/infsof

[50] D. Garlan, (2000), "software architecture", School of Computer Science, Carnegie Mellon University, 5000 Forbes Avenue, Pittsburgh, PA.

[51] S. B. chung-Horng Lung, (1997) "An Approach to software Architecture Analysis for Evolution and Reusability," in Centre for Advanced Studies Conference, Toronto, Canada.

[52] V. S. Rekha and H. Muccini, (2018) "Group decision-making in software architecture: A study on industrial practices", Information and Software Technology, Vol. 101, pp. 51-63, ISSN 0950-5849.

[53] M. Unterkalmsteiner, T. Gorschek, R. Feldt and E.riks Klotins, (2015) Assessing requirements engineering and software test alignment—Five case studies, Journal of Systems and Software, Vol. 109, pp. 62-77, ISSN 0164-1212.

[54] H. Vlieta and A.Tang (2016)."Decision making in software architecture", Science Direct-Journal of Systems and Software,Vol 117,pp. 638-644, https://doi.org/10.1016/j.jss.2016.01.017 .

[55] A. Tang and M. F. Lau (2014). "Software architecture review by association", Journal of Systems and Software, Vol 88, pp.87-101, https://doi.org/10.1016/j.jss.2013.09.044 .

[56] T. Mens, J. Magee and B. Rumpe (2010). "Evolving Software Architecture Descriptions of Critical System", IEEE Computer Society, vol 43, pp. 42-48. DOI: 10.1109/mc.2010.136

[57] P. Abrahamsson, M. Ali Babar and P. Kruchen (2010). "Agility and Architecture: Can They Coexist", IEEE Computer Society, pp16-22.

[58] S. Orlov and A. Vishnyakov (2017). "Decision Making for the Software Architecture Structure Based on the Criteria Importance Theory", Procedia Computer Science, Vol 104, pp. 27-34, ISSN 1877-0509.

[59] Nitin Upadhyay (2016). "SDMF: Systematic Decision-making Framework for Evaluation of Software Architecture", Procedia Computer Science, Vol 91, pp. 599-608, ISSN 1877-0509.

[60] T. Kim, S. Yeong-Tae, L. Chung and D. T. Huynh (2015). Architecture Analysis: A Dynamic Slicing Approach. Dept. of Computer Science University of Texas at Dallas https://doi.org/10.1017/CBO9781107415324.004

[61] M. Razavian, B. Paech and A. Tang (2018). "Empirical Research for Software Architecture Decision Making: An Analysis", Journal of Systems and Software, ISSN 0164-1212.

[62] C. Manteuffel, P. Avgeriou and R. Hamberg (2018). "An exploratory case study on reusing architecture decisions in software-intensive system projects", Journal of Systems and Software, Vol 144, pp. 60-83, ISSN 0164-1212

[63] E. J. Eichwald, E. C. Lustgraaf, & B. Wetzel, (1999). Transfer of the White Graft Reaction. Proceedings of the Society for Experimental Biology and Medicine, vol. 126(3), pp. 619–620. https://doi.org/10.3181/00379727-126-32521

[64] P.Bengtsson, (1999). Software Architecture-Design and Evaluation.University of Karlskrona PerOlof Bengtsson Department of Software Engineering and Computer Science. https://pdfs.semanticscholar.org/6c1c/a7056fbb2ee1f82f04c3ae2b7b7e16f41c6c.pdf

[65] A. Sharma, M. Kumar and S. Agarwal,(2015) "A Complete Survey on Software Architectural Styles and Patterns," Procedia Computer Science, Vol. 70, pp. 16-28 https://doi.org/10.1016/j.procs.2015.10.019

[66] M. Ozkaya and M. A. Kose, (2018) "SAwUML – UML-based, contractual software architectures and their formal analysis using SPIN,"Computer Languages, Systems & Structures,Vol 54, pp. 71-94, https://doi.org/10.1016/j.cl.2018.04.005

[67] G. Vazquezab, J. Andres, D. Pacec and M. Campoab, (2014), "Reusing design experiences to materialize software architectures into object-oriented designs,"Information Sciences Vol. 259, pp. 396-411 https://doi.org/10.1016/j.ins.2010.03.013

[68] B. Jalendar, A. Govardhan and R. Emchand, (2012) "Desiging code level reusable software components", International Journal of Software Engineering & Applications, Vol. 3, n. 1, pp. 219-229.

[69] B. Kitchenham and S. Charters, (2007) "Guidelines for performing systematic literature reviews in software engineering", EBSE,Software Engineering Group, School of Computer Science and Mathematics, Keele University, Keele, Staffs, ST5 5BG, UK and Department of Computer Science, University of Durham, Durham, UK .

[70] W. Hasselbring (2018). "Software Architecture: Past, Present, Future in: Gruhn V., Striemer R. (eds) The Essence of Software Engineering". Springer, Cham. https://doi.org/10.1007/978-3-319-73897-0_1]

Advances in Science, Technology and Engineering Systems Journal Vol. 4, No. 2, 221-227 (2019)

www.astesj.com

Special Issue on Advancement in Engineering and Computer Science

ASTESJ

ISSN: 2415-6698

Virtualization in Cloud Environment: Bandwidth Management

Isaac Odun-Ayo*, Blessing Idoko, Temidayo Abayomi-Zannu

Department of Computer and Information Sciences, Covenant University, Ota, 112233, Nigeria

A R T I C L E I N F O

Article history:
Received: 22 January, 2019
Accepted: 20 March, 2019
Online: 27 March, 2019

Keywords:
Cloud computing
Virtualization
Bandwidth Management
Applications
Hypervisor
Virtual Machines

A B S T R A C T

Cloud computing recently emerged as an interesting model that enables computing and other related internet activities to take place anywhere, anytime. Cloud service providers centralize all servers, networks, and applications to allow their users' access at any time and from any location. Cloud computing uses already existing resources like server, CPU and storage memory but runs on a new technology known as virtualization. The core idea of virtualization is to create several virtual versions of one single computing device or resource. This enables many user operating systems to work on such a single underlying piece of device. Network bandwidth is one of the critical resources in a cloud environment. Bandwidth management involves the use of techniques, technologies, tools, and policies to help avoid network congestion and ensure optimal use of the subscribed bandwidth resources while also being a bedrock of any subscription-based access network. Bandwidth management is being utilized by organizations to allow them to efficiently utilize their subscribed bandwidth resources. Bandwidth management deals with the measurement and control of packets or traffic on a network link in order to refrain from overburdening or overloading the link which can lead to poor performance and network congestion. In this paper, the highest development with respect to virtualization in cloud computing is presented. This study review papers available on cloud computing and relevant published literature in multiple areas like conferences, journals etc. This paper examined present mechanisms that enable cloud service providers to distribute bandwidth more effectively. This paper is therefore a study of virtualization in cloud computing, and the identification of bandwidth management mechanisms in the cloud environment. This will benefit forthcoming cloud providers and even cloud users..

1. Introduction

This paper expands upon the findings of the research carried out in the 2017 international conference on next-generation computing and information systems [1]. It expands on cloud bandwidth management, its mechanisms, and challenges. Cloud computing means "almost anything can be accessed" [2]. This allows for ubiquitous, convenient, on-demand network access to customizable computing resources e.g. storage, networks, servers, services, applications etc. that service providers could quickly render with minimal intervention. Cloud computing is powerfully changing the manner in which organizations and enterprises perform IT-related activities. Cloud computing features like elasticity, scalability, multi-tenancy, resource pooling, lower initial investment, easy management, faster deployment, location independent, device independent, reliability, and security make it attractive to business owners and IT users [3],[4]. Cloud computing model permits outsourcing of computational resources in a way that is more effective. The huge computing power and storage size of cloud resources permit day-to-day internet users to perform their tasks on pay-as-you-go terms. Cloud data centers will keep expanding, as their client base becomes larger.

In general, the Cloud massive network is built using an approach known as virtualization which permits the installation of different applications and operating systems unto physical hardware. It creates a different layer for the operating system (OS) to seat on, thereby separating the OS from the physical hardware and the core OS. Virtualization is done on the physical hardware by installing a hypervisor. A Hypervisor is a common technique used for the implementation of Virtualization. It permits for different operating systems to be installed on the same hardware. Though the operating systems coexist on the same physical hardware, they behave as each OS have its dedicated resources. Some of the types of Hypervisors include VMware ESX, KVM, Xen, and Hyper-V. Another emerging approach for implementing

*Isaac Odun-Ayo, Covenant University, +2348028829456
isaac.odunayo@covenantuniversity.edu.ng

virtualization is containerization commonly known as Container-based virtualization or operating system virtualization [5].

Cloud data centers normally have mechanisms for planning how their resources like computing space, memory, and bandwidth are released to the users. Bandwidth is required to distribute resources across different cloud networkS. It is very important to maintain cloud bandwidth to meet up with the increasing request from cloud resources across data centers. On a cloud network, the bandwidth size requested by a customer is usually not assured [2].

For a satisfactory performance and fair usage of the network, bandwidth management is used to achieve this with the implementation and creation of network policies which ensures that the sufficient amount of bandwidth being required is readily available for those time-sensitive and mission-critical applications. It also avoids opposition between lower priority traffic and the critical applications for the limited network. With cloud tenants making greater use of cloud networking infrastructure in a shared manner, there is an increased desire and a growing concern on how to arrange, reserve and monitor the bandwidth in the cloud computing environment [6], [7].

Generally, bandwidth management involves the use of techniques, technologies, tools, and policies put together by an organization in order to ensure optimal utilization of the available bandwidth [8]. The reason for a network bandwidth management is to ensure the accurate bandwidth size is available and assigned to the accurate users and application at the right location and time [9]. Generally, without an active plan for ensuring bandwidth management, the available bandwidth regardless of its size can never be sufficient for the ever-increasing request of the users [10]. Also, Malicious Cloud Bandwidth Consumption (MCBC) which attack is a new type of attack that aims to consume the bandwidth maliciously causing the financial burden to the cloud service host can be mitigated or avoided when utilizing bandwidth management [11].

Different operating systems (Oss) are running simultaneously on a physical server is a process known as Virtualization and is carried out utilizing a hypervisor or virtual machine manager (VMM). The physical network resources require sufficient bandwidth to assign to the virtual machines (VMs) and optimal bandwidth allocation to VMs is very critical especially in today's cloud data centers with massive networked VMs. Bandwidth management poses a significant tension especially within a cloud-computing environment that permits the idea of VMs to have specific aims like load balancing and failure tolerance. High latency and a sharp drop in network speed are expected if there is no sufficient bandwidth after VM-migration. Every initiated data transfer that must take place over the internet requires bandwidth. For example, server to VMs data transmission over the internet requires bandwidth; this is one reason why network administrators must ensure accurate bandwidth management.

The objective of this study is to analyze bandwidth management in a cloud-based computing and virtualization environment. Various area of virtualization and cloud computing will be discussed. This research will impart to the knowledge of cloud-based bandwidth allocation approaches and management. The remaining section of the research is as follows. Section 2 examines related work. Section 3 discusses virtualization in a cloud environment and bandwidth management mechanisms. Section 4 concludes the paper and suggests future work.

2. Related work

In [12] the author suggested a solution in Bandwidth Management on Cloud Computing Network, to distribute available bandwidth according to user priorities and actual demand of data transfer to-from the cloud is proposed. Three key metrics: throughput, response time and utilization for monitoring and analyzing the network performance were presented. In [13], the authors proposed an approach that will only permit the guaranteed bandwidth size when providing the requested service. It also discussed how Linux kernel module called Linux TC can be used to manage the allocation of network bandwidth. In [14], the authors proposed having a formal definition for cloud-based applications that are free and open to all. The authors built a Cloud Resources Allocation Model named CRAM4FOSS for these free and opened applications. According to the authors, the proposed solution is to accurately certify the stability of allocating Cloud resources. In [15], the authors discussed the idea of an open source virtualization. Several other virtualization ideas are addressed and afterward, analysis of two open sources IaaS systems was presented. [16] discussed the idea of skewness to strengthen the manipulation of servers. [17] proposed an approach to introduce separation of VMM concept instead of kernels separation concept since it will enable suitable separation of cloud VMs. In [18], the authors concentrated on the idea of VM migration for cloud providers and reviewed VM placements in data centers alongside its limitations and advantages were conducted. 1n [19], the authors focused on virtualization and its application in radiology. In [20], the authors highlighted how virtualization affects information security. In [21], the authors proposed a modular kind of the bandwidth manager that could rapidly adapt to unexpected changes that can be induced by the rates of dirty inactive applications or due to network congestion. The authors' goal is to optimize bandwidth consumption and latency during live VM migration. [22] proposed a combined algorithm for optimal allocation which enables network bandwidth and VMs to minimize the cost affiliated with the users. A decision is made by the algorithm to restrain network bandwidth and VMs from some specified cloud providers. [23] Argued on the importance of stability and fair bandwidth allocation. The authors proposed a method to prevent interference between the underlying hardware and VMs. In [24], the authors proposed an algorithm for dynamic bandwidth shaping while still maintaining the limitations on network resources. In [25], "Towards a Tenant Demand-aware bandwidth allocation strategy in the cloud data center" is discussed. The authors propose a strategy to handle the issue of over bandwidth subscription cloud datacenter. The main functions of the proposed system involve bandwidth prediction, bandwidth pre-allocation, and bandwidth gathering. In [26], the authors developed SpongeNet; which is a bandwidth allocation proposal that's made up of three determinants. Component one is to provide an accurate, flexible and simple way for users' requirements definition. Component two is an algorithm for merging policies to handle multiple goals. Component three is to guarantee fairness between dedicated and non-dedicated bandwidth users. In [27], the authors proposed a framework for predicting resource management to overcome the drawbacks of the reactive cloud resource management approach. In [28], the authors discussed the current trend and development in cloud computing and open source software. The authors found out that Open Source Software (OSS) like OpenStack provides the most comprehensive infrastructure in cloud computing and open source software.

3. Virtualization in Cloud Environment and Bandwidth Management

3.1. Virtual Machines and Containers Technology

A. Concept of Virtual Machines

The infrastructure layer is the host of the virtual machines (VMs) within the cloud network. It is a component within cloud computing. The core concept of virtualization is to separate OS from the underlying hardware, it divides a physical hardware machine such as a server into multiple virtual machines. This makes it possible to run all types of operating like Linux, Unix, Mac OS, and Windows on a host or physical machine, that is the coexistence of different operating systems on the same physical machine. Bandwidth size that closely matches the actual task and needs of each VM can be assigned. It allows for maximum utilization of the host machine. Hypervisors also knew as Virtual Machine Managers (VMSs) are used to create and control VMs. The virtual machine is then tied to the hypervisors and not directly to the physical hardware. There are two types of hypervisors. Type-1 hypervisors remove an extra layer between the underlying host hardware and the virtual machines because it executes directly on physical hardware without a base OS and acts as the operating system on the hardware. Here, physical hardware without a base OS can be known as a bare-metal. Type-2 hypervisors are hosted hypervisors since the installation is done on top of the existing OS on the physical hardware. These hypervisors execute as applications and the host machine won't need to be set up separately for setting up the virtual machines. Figure 2 depicts the Type-1 hypervisor and Figure 3 depict the Type-2 hypervisor [29].

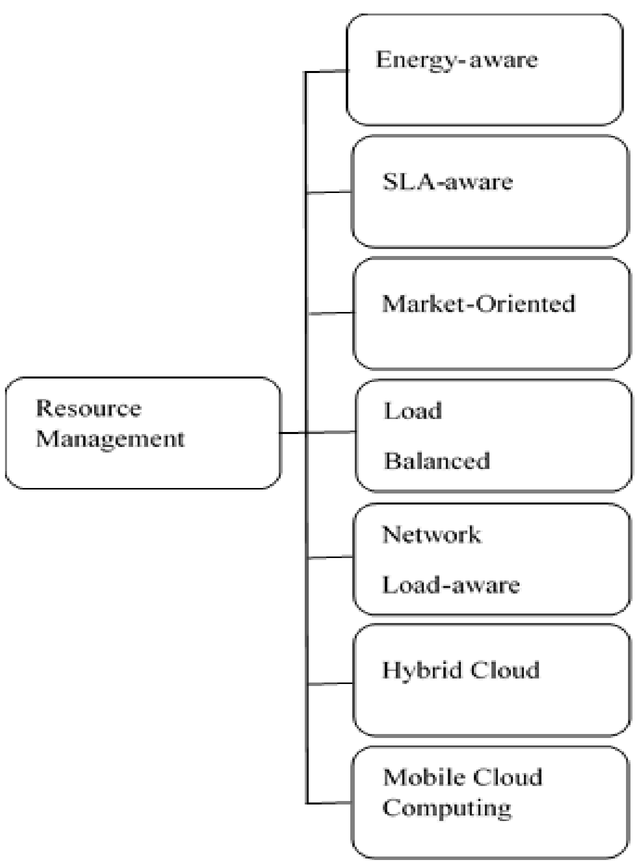

Figure 1: Classification of Resource Management Techniques [32]

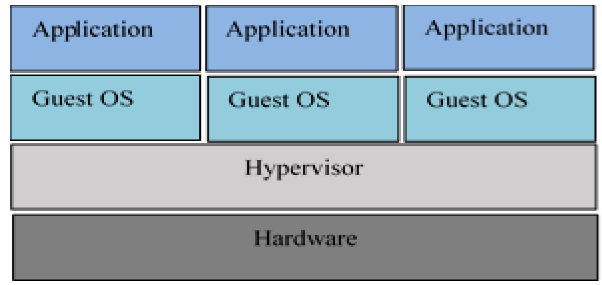

Figure 2: Type-1 Hypervisor [29]

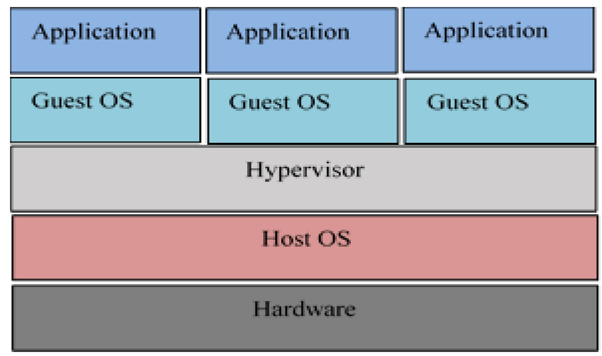

Figure 3: Type-2 Hypervisor [29]

B. Concept of Containers

Containerization is known as a virtualization technique which occurs within the OS level instead of the hardware level. Containers allow for easy migration between platforms and hosts compared to virtual machines and share a single OS kernel within an isolated environment [30]. This creates isolation confines within the application area instead of the server area which makes sure that if an error occurs within the single container, it won't affect the whole server or VM but only that individual container. Container technology is continuously evolving and guarantees an easy to deploy, streamlined and secure means of enacting certain infrastructure requirements while offering offer an alternative to VMs and mitigates the compatibility issues between applications which exists within the same OS [31].

Cloud containers are trending within the IT world and are modeled to virtualize just one application. Linux is the only server OS that supports cloud containers presently and Hyper-V containers are to be integrated to Microsoft Azure after being introduced by Microsoft [1].

C. Characteristics, Application, Benefits of Virtualization

In [1] it is highlighted the following characteristics of virtualization and its application areas as follows:

- Partitioning: This is a key feature in virtualization, used to logically divide a physical hardware resource for the installation of different/several operating systems.
- Isolation: Virtual machines coexist on the same physical hardware but each virtual machine exists separately from the core physical hardware and other virtual machines. With this feature, if there is a breakdown/downtime on one VM, the other active VMs will not be affected. Also, there is no data-sharing between VMs.

- Encapsulation: The encapsulated process maybe a business service and VMs can be stored and labeled as a file for identifying its service type. This averts the issue of hindrance amongst the applications. Storage, memory, networks, application, operating systems, and hardware are some of the application areas of virtualization. Here, to separate a software implies placing that software in a separate virtual machine space or in a container so that it does not coexist with other operating systems.

Virtualization of hosts or physical machines provides the following benefits [1]:

- Functional Execution Isolation: The hypervisor is assigned the responsibility of maintaining protection between the VMs and applications deployed on multiple VMs. Privileges may be given to users in their VM without violating the host integrity or isolation.
- Enhance Reliability: Hypervisors provides greater reliability of hosted virtualized applications due to their live migration capabilities enabling them to be independent and reliable.
- Customized Environment: Virtualization permits for the creation of customized space for a dedicated user, upon request for a customized and dedicated environment can be created and provided to handle a specific need.
- Testing and Debugging Parallel applications: Testing parallel applications can leverage virtualized environments, as a fully distributed system could be emulated inside a single physical host.
- Easier Management: Custom-made run-time environment can be migrated, started-up, shut down in a considerably variable way which depends upon the requirements of the person that is responsible for the essential hardware.
- Ability to coexist with legacy applications.
- VMs help to preserve binary compatibility in the run-time environment for legacy applications.

3.2. Resource Management Techniques

Cloud Resource management involves the procurement and release of cloud resources like physical hardware, storage space, virtual memory, and network bandwidth. Cloud resources can be physical or virtual components of limited availability. Resource management in virtualization environment and cloud computing is very critical. [32] used SLA-awareness, load balancing, energy efficiency etc. in the classification of resource management techniques, also depicted in figure 1.

- Energy-aware RM techniques: This involves minimizing the energy consumption by merging workload on a few numbers of physical servers. Virtual machines (VMs) on physical hardware with less load are migrated to other hardware that can accommodate more workload. This less loaded and idle hardware is then switched off to reduce the power expenses incurred by service providers and decreases Carbon dioxide (CO_2) emission. [33] Presented a centralized control system for the allocation and management of all the concerned cloud resources. Resource Management (RM) choices are done hourly in order to reduce the subsequent effects. The choices can be based on the shutdown of the server, VM migration between multiple servers and powering up of the server.
- Load-balanced RM techniques: This is an important feature of the system in any computing environment. It is made use of in order to explain the idea of distributing the workload or traffic request between many resources and can maximize the performance of available bandwidth. Operations are moved amongst the physical machines after the load balancing algorithm have been applied and the system efficiently balances the load amongst the cloud resources while the usage by each server is examined. Once there is an overload of server resources, it migrates some of these workloads to an underutilized server but in a situation whereby both are underutilized, one server gets all the workload transferred to itself while the other server will be left unutilized or on standby. If hypothetically speaking that the workload migration failed, the server itself can be scaled down or up accordingly.
- SLA-aware RM techniques: Cloud-based Service Providers (CSPs) must strongly discourage the issue of violations, maintaining regular check during service provisioning to users. A service level agreement (SLA) is signed between the CSPs and customers which includes information such as the price, penalty clause that is enforced in an event of agreement violation and required a level of service(s). Authors in [34] proposed algorithms for capacity allocation in the hope of guaranteed SLA and handle fluctuating workloads which interfaces with the resource controllers that are geographically distributed while redirecting the network traffic load whenever congestion is observed. An application can also execute on different workloads and VMs equally allocated on the VMs if necessary. A workload analyst is utilized in order to predict future workload necessities throughout the workloads fluctuation and the capacity is altered on the premise of resultant predictions. Additionally, SLA violations can be mitigated by making sure that the response time is low when inter-VM communications are ongoing but if there is a higher response time, the VM is carried/moved to another physical machine.
- Market-oriented RM techniques: This involves solutions that are beneficial to cloud service providers and market-oriented. [35] Presented an RM technique where a SaaS service provider employs an IaaS service provider to serve its clients. Clients pay to the SaaS service provider for the services received and depending on the satisfaction level shown by the clients, a one-of-a-kind optimal function is utilized to calculate the amount that the user has to pay. According to [36], each cloud server has a dynamic voltage/frequency scaling (DVFS) module and it is assumed that a server cannot be switched on or off, also there is a common cost of VM migration

- Network load aware RM: This technique reduces high network traffic that can degrade the overall network performance. It allows service providers to choose a data center that could fulfill the interests of the clients. A user sends a request to the service provider and resources are assigned using an adaptive resource allocation algorithm. These algorithms achieve this by selecting a data center either based on the distance between the user or based on the distance between the data center. After the data center is chosen, the work is allocated to one of the servers thanks to the VM.
- RM techniques for the hybrid/federated cloud: In this technique, private cloud users are offered the benefit of utilizing the resources in a public cloud environment whenever there are insufficient resources to handle the needs of it, in-house users. To address the issue of decision-making on when to use public cloud resource, the authors in [37] presented a solution that is rule-based for hybrid clouds. Users' requests are divided into two which are the critical data/tasks request that is granted higher precedence and secondary data/tasks request that are granted lower priority. The critical data/tasks are hosted on the private clouds for security while the task with low priority can utilize the resources of both private and public cloud. When the resources of the private cloud are exhausted, the public cloud resources would be utilized.
- RM techniques for mobile clouds: Here, an energy efficient solution is presented to solve the problem of energy which is a major challenge in mobile systems. The authors in [38] proposed a technique to reduce the total power consumption. All the mobile devices primary job is to move the workload to one of the available servers in order to reduce the overall energy consumption.

3.3. Cloud Bandwidth Allocation Mechanisms

According to [2], bandwidth mechanisms used by Cloud providers in allocating bandwidth resource and ensuring load balancing include:

- Fair-Share Bandwidth allocation: In this approach, the specific time interval is set for the flow of the defined data size between the host machine and virtual machines. The Throughput and Network weight are used to ensure fairness during the data flows. When the calculated fair share values reach the random acceptable values, the packets are transferred otherwise they are dropped.
- Transmission Control Protocol (TCP): Here, packets are divided into segments and assigned a sequence number each to specify the order of the data. Transmission takes place at a specific time interval. An acknowledgment is received for every successful transmission otherwise, retransmission takes place. This approach is connection oriented and for end-to-end congestion controls.
- Bandwidth Capping: in this approach, a specific bandwidth limit is set for the VM when transmission of data is happening simultaneously.
- Secondnet: This approach guarantees the assignment of network bandwidth amongst every VM pair and the communication patterns between multiple pair of the VM can vary due to the time as well as the data received/transferred amongst them.
- Netshare: Utilized in big data centers and function as a central system for allocating bandwidth in a virtual cloud network. It lessens the tasks in data centers. Each Cloud customer is connected to various cloud network resources. Division of the network into slices is done and each of the slices is assigned bandwidth via the link connecting it to the cloud network.
- Approximate Fairness- Quantized Congestion Notification (AF-QCN): This is a congestion control approach for data centers, delivered via a switch. The network bandwidth is shared among the transmitter's connection to the VM.

3.4. Bandwidth Management Benefits

In [39] the author highlighted the following benefits using the Zscaler Bandwidth Control solution:

- Prioritization of business applications: It limits the possible impact of bandwidth-intensive applications like streaming media, file sharing, and social media business applications. Bandwidth constraints and policies are checked and reconfigured to meet user requirement
- Deliver a better user experience: features like segmentation of network traffic and retransmission provide a faster Internet connection and avoid loss of packet after a successful data transmission.
- Reduce costs and simplify IT: Eliminate the need to install and manage additional hardware in-house and prevent bottlenecks due to the enforced cloud policies.

In [26] the author highlighted the following benefits:

- Work-conservation
- Guarantees bandwidth
- Practical enforcement
- Fairness between tenants
- Applicability to different contexts
- Easy deployment
- Precise and flexible requirement expression
- Efficient bandwidth saving

In [25] the author presented the following benefits:

- Provides dynamic network management
- Improves network efficiency
- Easy integration.

3.5. Cloud Bandwidth Management Challenges

According to [40], as VMs scale bigger, utilizing more memory, higher bandwidth, the need to maintain optimal performance and health management tools become difficult for the existing management software. These tools require multiple information about the different features of each VM, the underlying host storage infrastructure, machine, and networking. Supporting these tools and coordinating the activities of a large number of simultaneous users with management privileges require a secure connection in real-time with a high level of consistency and must be backward compatible. Scaling the bandwidth of the ever-increasing hundreds of VMs means improving the existing code for optimal performance. Since users are getting used to virtualization and migrating every one of their in-house server workloads/applications to virtual environments, the need to scale bandwidth capacity will continuously get bigger for the predictable future. The management software needed to scale bandwidth to reach the level of the users' needs is highly challenging. [9] Presented the following challenges in the utilization of bandwidth and can become a problem for the existing management tools:

- The absence of administrative support
- Uncontrolled users' downloads
- Virus attacks
- Higher demand compared to available bandwidth
- Unreliable Internet service provider
- Technical breakdowns
- Different user bandwidth requirements
- Too many network users

4. Conclusion

Cloud computing enables many organizations store, compute and retrieve/access their application from any location over the internet. This has shifts management core concern of maintaining in-house hardware resources and reduced the cost incurred. The concept of VMs-migration in cloud computing requires that the right bandwidth size must be made available on the host or physical machine. For example, when a VM is unable to serve its users request due to a technical failure on the host machine, the VM is moved to another physical machine to provide the needed services. VMs-migrated enables better management and optimization of the data centers and host machines. This paper focused on Cloud bandwidth management. An analysis of the concept of VM-migration and bandwidth management approaches was done. In conclusion, with the increasing number of cloud users and data centers, further research work for enhancing the bandwidth allocation approaches and management is required. This will further enhance the resource-sharing feature of the VMs.

Conflict of Interest

The authors declare no conflict of interest.

Acknowledgment

We acknowledge the support and sponsorship provided by Covenant University through the Centre for Research, Innovation, and Discovery (CUCRID).

References

[1] I. Odun-Ayo, O. Ajayi, and C. Okereke, "Virtualization in Cloud Computing: Developments and Trends," in 2017 International Conference on Next Generation Computing and Information Systems (ICNGCIS), 2017, pp. 24–28. https://doi.org/10.1109/ICNGCIS.2017.10

[2] K. Chandrakanth and S. Gayathri, "Examining Bandwidth Provisioning on Cloud Computing and Resource Sharing Via Web," Int. J. Eng. Sci. Adv. Technol. [IJESAT], vol. 2, no. 5, pp. 1372–1376, 2012.

[3] M. Peter, and G. Timothy, "The NIST Definition of Cloud Computing," NIST Special Publication pp. 800-145, 2011. https://doi.org/10.6028/NIST.SP.800-145

[4] M. Ahmed, A. Sina, R. Chowdhury, M. Ahmed, and M. H. Rafee, "An Advanced Survey on Cloud Computing and State-of-the-art Research Issues," vol. 9, no. 1, pp. 201–207, 2012.

[5] Y. Al-dhuraibi, F. Paraiso, N. Djarallah, P. Merle, and C. Computing, "Elasticity in Cloud Computing : State of the Art and To cite this version : Elasticity in Cloud Computing : State of the Art and Research Challenges," 2018.

[6] C. T. Yang, J. C. Liu, R. Ranjan, W. C. Shih, and C. H. Lin, "On construction of heuristic QoS bandwidth management in clouds," Concurr. Comput. Pract. Exp., vol. 25, no. 18, pp. 2540–2560, Dec. 2013. https://doi.org/10.1002/cpe.3090

[7] A. Amaro, W. Peng, and S. McClellan, "A survey of cloud bandwidth control mechanisms," in 2016 International Conference on Information and Communication Technology Convergence (ICTC), 2016, pp. 493–498. https://doi.org/10.1109/ICTC.2016.7763520

[8] G. Hong, J. Martin, and J. Westall, "Adaptive bandwidth binning for bandwidth management," Comput. Networks, vol. 150, pp. 150–169, 2019. https://doi.org/10.1016/j.comnet.2018.12.019

[9] C. Technology, "Bandwidth management in universities in Zimbabwe : Towards a responsible user base through effective policy implementation Lockias Chitanana Midlands State University, Zimbabwe," vol. 8, no. 2, pp. 62–76, 2012.

[10] Y. Liu, V. Xhagjika, V. Vlassov, and A. Al Shishtawy, "BwMan: Bandwidth Manager for Elastic Services in the Cloud," in 2014 IEEE International Symposium on Parallel and Distributed Processing with Applications, 2014, pp. 217–224. https://doi.org/10.1109/ISPA.2014.37

[11] M. Chidananda, A. Manjunatha, A. Jaiswal, and B. Madhu, "Detecting Malicious Cloud Bandwidth Consumption using Machine Learning," Int. J. Eng. Technol., vol. 8, no. 5, pp. 2199–2205, Oct. 2016. https://doi.org/10.21817/ijet/2016/v8i5/160805210

[12] E. Randa, I. Mohammed, A. Babiker, and A. N. Mustafa, "Bandwidth Management on Cloud Computing Network," vol. 17, no. 2, pp. 18–21, 2015. https://doi.org/10.9790/0661-17221821

[13] G. F. Anastasi, M. Coppola, P. Dazzi, and M. Distefano, "QoS Guarantees for Network Bandwidth in Private Clouds," Procedia - Procedia Comput. Sci., vol. 97, pp. 4–13, 2016. https://doi.org/10.1016/j.procs.2016.08.275

[14] S. Jlassi, A. Mammar, I. Abbassi, and M. Graiet, "Towards correct cloud resource allocation in FOSS applications," Futur. Gener. Comput. Syst., vol. 91, pp. 392–406, 2019. https://doi.org/10.1016/j.future.2018.08.030

[15] A. Kovari and P. Dukan, "KVM & OpenVZ virtualization based IaaS Open Source Cloud Virtualization Platforms : OpenNode, Proxmox VE," pp. 335–339, 2012.

[16] Z. Xiao, W. Song, and Q. Chen, "Dynamic Resource Allocation using Virtual Machines for Cloud Computing Environment, IEEE Transaction On Parallel And Distributed Systems," pp. 1–11, 2013.

[17] J. McDermott, B. Montrose, M. Li, J. Kirby, and M. Kang, "The Xenon Separation VMM: Secure Virtualization Infrastructure for Military Clouds", Naval Research Laboratory Center for High Assurance Computer Systems, Washington. https://doi.org/0.1109/MILCOM.2012.6415673

[18] M. Masdari, S. Shahab, and V. Ahmadi, "An overview of virtual machine placement schemes in cloud computing", Journal of Network and Computer Applications, vol. 66, pp. 106–127, 2016. https://doi.org/0.1016/j.jnca.2016.01.011

[19] R.P. Patel, "Cloud computing and virtualization technology in radiology", Clinical Radiology, vol. 67, pp. 1095 -1100, 2012.

[20] L. Shing-Han, C. David, C. Shih-Chih, P.S. Chen, L. Wen-Hui and C. Cho, "Effects of virtualization on information security", Computer Standards & Interfaces, vol. 42, pp. 8, 2015. https://doi.org/10.1016/j.csi.2015.03.001

[21] E. Baccarelli, D. Amendola, and N. Cordeschi, "Minimum-energy bandwidth management for QoS live migration of virtual machines," Comput. Networks, vol. 93, pp. 1–22, 2015. https://doi.org/10.1016/j.comnet.2015.10.006

[22] J. Chase, R. Kaewpuang, W. Yonggang, and D. Niyato, “Joint Virtual Machine and Bandwidth Allocation in Software Defined Network (SDN) and Cloud Computing Environments,” pp. 2969–2974, 2014.

[23] H. Tan, L. Huang, Z. He, Y. Lu, and X. He, “Journal of Network and Computer Applications DMVL : An I / O bandwidth dynamic allocation method for virtual networks,” J. Netw. Comput. Appl., vol. 39, pp. 104–116, 2014. https://doi.org/10.1016/j.jnca.2013.05.010

[24] X. Chen and S. Mcclellan, “Improving Bandwidth Allocation in Cloud Computing,” no. August, 2016.

[25] J. Cao, Z. Ma, J. Xie, X. Zhu, F. Dong, and B. Liu, “Towards tenant demand-aware bandwidth allocation strategy in cloud datacenter,” Futur. Gener. Comput. Syst., 2017. https://doi.org/10.1016/j.future.2017.06.005

[26] J. P. D. Comput, H. Yu, J. Yang, H. Wang, and H. Zhang, “Towards predictable performance via two-layer bandwidth allocation,” J. Parallel Distrib. Comput., vol. 126, pp. 34–47, 2019. https://doi.org/10.1016/j.jpdc.2018.11.013

[27] M. Balaji, C. Aswani, and G. S. V. R. K. Rao, “Predictive Cloud resource management framework for enterprise workloads,” J. King Saud Univ. - Comput. Inf. Sci., vol. 30, no. 3, pp. 404–415, 2018. https://doi.org/10.1016/j.jksuci.2016.10.005

[28] I. Odun-ayo, A. Falade, and V. Samuel, “Cloud Computing and Open Source Software : Issues and Developments “ C,” vol. I, pp. 140-145, 2018.

[29] S. C. Mondesire, A. Angelopoulou, S. Sirigampola, and B. Goldiez, “Simulation Modelling Practice and Theory Combining virtualization and containerization to support interactive games and simulations on the cloud,” Simul. Model. Pract. Theory, no. August, pp. 1–12, 2018.

[30] V. Chang et al., “Journal of Network and Computer Applications,” vol. 77, no. May 2016, pp. 87–105, 2017. https://doi.org/10.1016/j.jnca.2016.10.008

[31] U. Agreement, R. Issued, B. Internet, T. Advisory, G. Technical, and W. Group, “Port Blocking,” no. August 2013.

[32] S. Mustafa, B. Nazir, A. Hayat, R. Khan, and S. A. Madani, “Resource management in cloud computing : Taxonomy, prospects, and challenges q”, Comput. Electr. Eng., vol. 47, pp. 186–203, 2015. https://doi.org/10.1016/j.compeleceng.2015.07.021

[33] D. Ardagna, B. Panicucci, M. Trubian, and L. Zhang, “Energy-aware autonomic resource allocation in multitier virtualized environments,” IEEE Trans Serv Comput; vol. 5, pp. 2–19, 2012.

[34] D. Ardagna, S. Casolari, M. Colajanni, and B. Panicucci, “Dual time-scale distributed capacity allocation and load redirect algorithms for cloud systems.” J Parallel Distrib Comput; vol 72, pp. 796–808, 2012.

[35] L. Chunlin, and L. Layuan, “Multi-Layer RM in cloud computing. J Network Syst Manage”, 2013. http://dx.doi.org/10.1007/s10922-012-9261-1

[36] S. Ali, S. Jing, S. Kun, “Profit-aware DVFS enabled RM of IaaS cloud. Int J Comput Sci Issues (IJCSI)”, vol. 10 pp. 237–47, 2013.

[37] R.K. Grewal, and P.K. Pateriya, “A rule-based approach for effective resource provisioning in hybrid cloud environment. Adv Intell Syst Comput”, vol. 203, pp. 41–57, 2013.

[38] Y. Ge, Y. Zhang, Q. Qiu, and Y. Lu, “A game theoretic resource allocation for overall energy minimization in mobile cloud computing system, In: Proceedings of the 2012 ACM/IEEE international symposium on low power electronics and design ISLPED”, vol. 12,. pp. 279–84, 2012.

[39] D. Sheet, “Zscaler Bandwidth Control.”

[40] X. Xu, Q. Zhang, S. Maneas, S. Sotiriadis, and C. Gavan, “Simulation Modelling Practice and Theory VMSAGE : A virtual machine scheduling algorithm based on the gravitational effect for green Cloud computing,” Simul. Model. Pract. Theory, no. June, pp. 1–17, 2018. https://doi.org/10.1016/j.simpat.2018.10.006

Advances in Science, Technology and Engineering Systems Journal Vol. 4, No. 2, 228-236 (2019)

www.astesj.com

Special Issue on Advancement in Engineering and Computer Science

ASTESJ

ISSN: 2415-6698

Cloud Service Level Agreements and Resource Management

Isaac Odun-Ayo*, Blessing Udemezue, Abiodun Kilanko

Department of Computer and Information Sciences, Covenant University, 112233, Nigeria

A R T I C L E I N F O

Article history:
Received: 22 January, 2019
Accepted: 24 March, 2019
Online: 27 March, 2019

Keywords:
Cloud Computing
Cloud Providers
Resource Management
Service Level Agreements

A B S T R A C T

Cloud computing is a technical "as-a-service" usage model utilizing virtualization. Virtual machines are the core of cloud computing that runs as independent machine grouped into different networks within the hypervisor. Practically done by deployment of clouds computing hosts enterprise servers in virtual machines on an array of high-end servers. Managing cloud resources has to do with controlling and limiting access to the pool of available resources. This brings about the conception of an agreement between the resource services cloud providers and the customers otherwise known as Service Level Agreement, in other to restrict access to provisioned resources. Resource provisioning is a flexible on-demand pay-as-you-go package that is negotiated; and signed based on SLAs between customers and cloud providers. SLAs enable cloud providers to evade costly SLA consequences payable when there are violations, optimizing the performance of customers' applications and professionally manage resources to reduce cost. These documents are the agreements called Service Level Agreements (SLAs). SLAs outline the expectations which are: terms, conditions, and services of the clients from their service providers regarding availability, redundancy, uptime, cost, and penalties in cases of violations. These ensure clients' confidence in the services offered. Managing resource is an on-going major issue in cloud computing. Considering the limitation of resources, it poses a challenge for cloud service providers to make provision for all resources as needed. This paper seeks a solution to problems that relates to the present trends and developments of what cloud Service Level Agreements are and it ensures so by reviewing current literature. Thus, this research is a study of cloud Service Level Agreements, cloud resource management and their challenges. This paper has made provision to act as guidance for future research and it is anticipated to be beneficiary to potential cloud end users and cloud service providers.

1. Introduction

This paper is an extension of work originally presented in 2018 International Conference on Next Generation Computing and Information Systems [1]. This expands on resource management on Cloud computing and its challenges. Cloud computing makes provision for services by cloud service providers to simplify computing, storage and applications development by an end user using the Internet. Cloud computing is a computing method that enables ubiquitous service which is accessible to a mutual group of computerised resources. . Cloud computing is not limited to networks, services, storage and applications which can be swiftly made provision for and made available with minimal supervision involved [2].

In a cloud environment, resource management is challenging because of the scalability of present data centers, the heterogeneity in types of resources, the interconnection amongst these resources, the inconsistency and irregularity of the load, and the variety of aim of varied end users [3]. Cloud computing and management of resource provisioning are actualized at:

a. Infrastructure-as-a-Service (IaaS) - resources not limited to physical machines, virtual machines, and storage devices are offered as a service to customers.

b. Platform-as-a-Service (PaaS) - offers pre-installed software to customers for application development and testing.

c. Software-as-a-Service (SaaS) - offers a service instance with customizable interfaces to many customers in a cost-efficient manner [2].

Cloud resources management and cloud services are made available based on established Service Level Agreement (SLA) indicated and contracted between Cloud service providers and their end users describing the relations of what is agreed, which

*Isaac Odun-Ayo, Covenant University, +2348028829456
isaac.odunayo@covenantuniversity.edu.ng

https://dx.doi.org/10.25046/aj040230

also does not exclude non-functional requests, such as quality of service (QoS). In [4], the authors discussed that cloud end users prefer to choose a cloud service appropriate for them from the major service providers that can offer services with adequate quality of service guaranteed.

Lock manager is an independent algorithm that runs on cloud for one manager per server. Algorithm is a set of steps used to solve computing problems such as consistency in maintaining distributed files in cloud computing. There are many client requests made to different servers, requesting for granting simultaneous access to the same file. These requests run independently of each other and pool resources with one another to maintain uniformity of the files in the cloud. This algorithm contributes solution to the major concerns for availability and scalability of file resources [5]. Making the provisioning of resource management flexible and reliable and SLAs are very important to Cloud providers and their clients. Flexible and dependable provision of resource management and SLA agreements in SaaS, PaaS and IaaS are important to the Cloud providers and their clients. This enables cloud providers to evade exorbitant SLA penalties billed for infringements, to professionally manage resources, and lessen charge while elevating the performance of clients' applications. To assure SLA of customer applications, cloud providers need refined resource and monitoring of SLA approaches to accomplish sufficient data for the management procedure [6].

Cloud computing makes use of the concept of virtualization and multi-tenancy to provide service for their end users. Enterprises can migrate some of their applications and utilize services based on appropriate agreements. Cloud computing is made up of four types of deployment: the public, private, community and hybrid clouds. Organizations own private cloud. The amenities can either be in-house or off and the management is by a third party. Private clouds are often perceived to be more secure. Service providers that offer their services with a cost to cloud users majorly own public clouds. Public cloud make use of big data centres most times across many geographical locations. They are perceived to be less secure. Community cloud are run by some firms that have shared mutual interest. The management could be a community or a third party. The combination of either private, community or public cloud is known to be Hybrid cloud. Hybrid computing is cloud utilizes on the benefits of the different cloud types.

Service Level Agreement (SLA) is an official agreement between service providers and clients to assure consumers the quality service expectancy can be realised [6], Service Level Agreement lifecycle involves six phases: ascertain the cloud service providers, outline the Service Level Agreement, institute an agreement, observe likely SLA violators, end SLA and implement consequences [6]. Service Level Agreements are used to officially define the services that offered, the Quality of Service anticipated from cloud provider, duties of both parties involve and possible fines [7]. According to [8], Service Level Agreements ought to comprise of five simple matters. They are: set of services that are made available by the cloud service providers; an explicit and imminent evidence terms of services offered; set of Quality of Service metrics for assessing service delivery points; a way of monitoring these metrics; and means of make a decision during disagreements that may arise as a result of failure in meeting the Service Level Agreement terms. It is imperative for cloud end users to delight in the resources and service assured by the cloud service provider, as the cloud service provider should gain optimally from the resources being provided [9].

The aim of this paper discusses cloud service computing, SLA and resource management. The paper discusses SLA in depth, looks at issues that relate to cloud computing and resource management from the industry perspective. The remaining paper is as follows. Section 2 studies related work. Section 3 converses Service Level Agreement in terms of resource management. Section 4 concludes the paper.

2. Related Works

Managing resources for cloud computing environments is an active field in research. We now present relevant work in Service Level Agreement, resource monitoring and management, framework, method, and model.

In [9], the authors presented dynamic data-centred virtual reality method that prevents Service Level Agreement defilements in combined cloud settings. This research offered an architecture that enables the release of end users resources without problems or violation of the Service Level Agreement. This achieved was through the use of several cloud service providers consumed by end users. SLA in Cloud Computing was offered in [10]; whereby the authors scrutinized SLAs between end users and cloud service providers. A Web Service Level Agreement structure was projected, applied, and confirmed. In [8], a structure for dialoguing SLA of Cloud-based Services was offered. The framework decides the best appropriate cloud service provider for cloud end users. These writers as well emphasised the significant characters of cloud dealers for optimal resource consumption by the cloud end user. The role of supremacy and other Service Level Agreement concerns in cloud environment were made known in [11]. The work untaken, includes main characteristics to be well thought-out when drafting up cloud service legal contracts in cloud computing. The problem of cloud domination was also evaluated with an understanding to determine right ways of handling information with least consequences. In [12], the writers proposed a method that concurrently provided for Quality of Service observing and resource optimal usage in cloud data centres. These authors offered a methodology which gathered user workloads into groups and used these groups to avert Service Level Agreement violation and at the time make better resource consumption, thus profiting both the cloud consumers and cloud providers.

In [2][13], the authors presented a resource monitoring framework which is push-pull technique for Cloud computing environments. This method is established in addition to dominant push and pull methodology monitoring method in Grids to Cloud computing with the aim to create a capable monitoring framework to be able to share resources in Clouds. In [14], the authors defined cloud federalism as being able to bring together services from different cloud vendors to provide a solution; an example is Cloud Burst. According to [15], on resource management, performing live migration is a recent feature concept within Cloud systems for active fault tolerance by flawless movement of Virtual Machines from waning hardware to unwavering hardware with the consumer not being aware of any change in a virtualized environment. Resource consolidation and management can be performed though the use of virtualization technologies. With the use of hypervisors contained by a cluster environment, it enables the consolidation of some standalone physical machines into a virtualized environment, therefore needing fewer physical resources when compared to a system without virtualization capabilities. Nonetheless, this improvement is still inadequate. Big Cloud deployments have need of physical machines in thousands and megawatts of power.

Data-driven models can be used to manage resource cloud complex systems. The author in [16] discussed his dissertation and argued the advancements in machine learning for the management and optimization of today's resource systems through arising insights from the performance and utilization data these systems create. In other to bring to reality the vision of model-based resource management, there is need for the key challenges data-driven models raise to be dealt with such as uncertainty in predictions, cost of training, generalizability from benchmark datasets to real-world systems datasets, and interpretability of the models. Challenges of data-driven models includes:

a. Robust modelling procedures being able to work with noisy data, and to develop methods for model uncertainty estimates [17].

b. Data-driven model has to incorporate domain knowledge into the modelling process in order to increase the model accuracy and trust in the modelling results [17].

c. Transforming or migrating data from a relational schema to schema-less is difficult to accomplish due to data modeling challenges [18].

In [2], the authors designed a run-time monitoring framework name LoM2HiS to perform monitoring fixated towards increasing the scalability and practice in distributed and parallel environments. The run-time system observer target is to observe the services established on the negotiated and contracted Service Level Agreements by mapping rules; Cloud Service Provider's (CSP) clients request the provision of a contracted service; and the run-time monitor loads the service Service Level Agreement from the decided Service Level Agreement depository. Infrastructure resources are based on the service provisioning that represents hosts and network resources in a data center that host Cloud computing services. The design of this run-time monitor framework is aimed at being highly scalable.

There is a practice of dynamically allocating and de-allocating resources on physical machines in the public cloud environments [16]. As all kind businesses move to cloud, this leads to increase in varied workloads running in the Cloud; and each has diverse performance requirements and financial trade-offs [19]. According to [16], there are varied collection of Virtual Machine (VM) cloud providers, and the main problem of accurately and economically selecting the best VM for a specified workload resources is addressed. Considering the speed of growth in Cloud computing, some VM management platform solutions including OpenStack [13] has come into play.

Apache VCL in [20] is an open-source system for flexible resource providing and reserving of computation resources for different applications in a data center by the use of simplified web interface. In [16], the author discussed about Manjrasoft Aneka a service platform to build and deploy distributed applications on Clouds that makes provision for many applications for the transparency, exploiting distributed resources; and Service Level Agreement focused on allocating resource that distinguishes requested services based on their available resources and hence provides for consumers' needs.

3. Cloud Computing SLA and Resource Management

3.1. Service Level Agreement Concepts

1) National Institute of Standards and Technology (NIST)

The NIST describes cloud computing synopsis and recommendations in its publication [21], viewed from a viewpoint of cloud service provider. Based on this report, a usual profit-making cloud service level agreement has to consist of:

a. These agreements which should clearly include an agreement addressed to the consumer regarding constant availability of service, resolution of dispute steps, preservation of data, and legal protection of consumers' private information.
b. Cloud service provider has limitation of service offered due to effects of natural disasters that are beyond the control of cloud providers', outages in service, and updates. Cloud service providers are nonetheless obligated to provide realistic warning to their end users.
c. The anticipations from cloud consumers, which consist of receiving of terms and conditions including a fee for used services.

This NIST's point of view to Service Level Agreement is quite inflexible and baised in support of the Cloud providers. For a case in point, it does not take into contemplation choice for consumers to converse on the amendment to service level agreements with service cloud providers if the default SLA terms do not address all of the consumers' needs. The report also appeals consumers to know that Service Level Agreements may change at the providers' choice with practical reasons ahead of time notification. In order to be ready to transfer workloads to alternate cloud service providers in case of changes that might be undesirable. This though is not an easy activity, because of vendor lock-in and lack of standardization that could enable interoperability between cloud providers is still an on-going issue in cloud computing.

3.2. Service Level Agreement Levels

Some of the important levels related with cloud Service Level Agreements discussed:

a. Facility Level: The cloud service provider delivers on Service Level Agreement that covers the data centre services needed to conserve the client generated data and/or applications. These consist of things including electrical power, onsite generator, and refrigerating device. Service Level Agreements do assure high availability, fault tolerance, and data replication services.
b. Platform Level: There is need for physical servers, virtualization infrastructure, and network associated hardware possessed by the cloud provider and consumed by the cloud clients. Service Level Agreement at this level would contain information regarding physical security for the rejection of illegal accessibility to the building, facility, and computing resource. Checking background and analysing the character of staff should be carried out before employment by cloud service providers. [22] Every end user has control over his or her applications and some resources, while the CSP has complete control over the platform.
c. Operating System Level: A cloud service provider typically would convey certain volume of services managed to their clients. This additional service authorizes

the cloud provider to assure that the Operating System is properly continuous in operation so that it is reliably available. Service Level Agreements would enclose information regarding updates on security, system patches, confidentiality, or encryption, user authorization, and audit trails log files.

d. Application Level: This level provides safety against problems that associated with application level data. At this point, the cloud provider ensures the readiness, stability, and performance of their cloud user software which they are hosting. This is sometimes difficult to assure specifically in Infrastructure-as-a-Service and Platforma-as-a-Service whereby the end-user is only responsible for the application they put on the cloud.

3.3. Cloud Provider Service Level Agreement

The usual Service Level Agreement of cloud service providers include:

a. Service Assurance: This metric states the service level which a provider is obligated to over a contracted time frame.
b. Service Assurance Time Period: This explains the period of a service assurance ought to take place. The duration can be billed per month, or as contracted upon by mutual parties.
c. Service Assurance Granularity: This outlines the measure of resources for cloud providers to specify services assurance. For instance, the granularity can be as per service, per data centre, per instance, or per transaction basis. In relation to time of the assured service it can be fixed if granularity of service assurance is fine–grained. Service guarantee granularity can also be set up as accumulative of the considered resources such as contacts.
d. Service Guarantee: Oversights are occurrences which are not included in the service guarantee metric calculations. The oversight usually will contain mismanagement of the system by a consumer or an interruption connected with the programmed care.
e. Service Recognition: Is the account attributed to the customer or geared in the direction of forthcoming expenses if the service guarantee does not get realised. The total can be an inclusive or regulated acknowledgement of the consumer reimbursement for an overestimated service.
f. The Service Violation Measurement and Reporting: This explains how and who processes and informs of the violation of service assured respectively. The users typically do this but cloud service provider could also perform this role. In certain instances, a regulating service-monitoring third party could be assigned this.

3.4. Service Level Agreement Benefits and Challenges

2) **Service Level Agreement Benefits**

It is important to have comprehensive contract between the client and cloud provider to guarantee trust and confidence on both sides. The following are a number of the benefits of having a cloud Service Level Agreement [11]:

a. SLA supports solid understanding of cloud service and responsibilities of all stakeholders involved.
b. SLA assists the consumer to realise their understanding.
c. SLA emboldens clarity, accountability, and trustworthiness.
d. Make available information on team performance, capabilities, and staffing judgment.
e. SLA sees to the establishment of reassuring and communal functioning.

3) **Service Level Agreement Challenges**

All single agreement has certain challenges that requires both parties to deal with. These challenges include:

a. Service Level Agreements are difficult to achieve in cloud computing for the reason that some infrastructure and circumstances such as network and force majeure are beyond the control of both the cloud service provider and consumer, therefore challenging to draft a Service Level Agreement.
b. In circumstances where multi-tenancy is in use, Service Level Agreements relating to service separation and high obtainability may be challenging to for the cloud service provider for assurance.
c. Regarding cloud Software-as-a-Service model, Service Level Agreements are challenging to achieve due to the fact that it is almost impossible for the cloud service provider to assess all potential user software/application with diverse system configuration ahead of time.
d. It is challenging to come to an agreement on a cloud Service Level Agreement that is covering security. Distributed Denial of Service (DDoS), keystroke timing and side-channel attacks have been identified as some of the greatest common attacks in cloud environment [15] and continue to be a continuous challenge. As a result of the dynamic and always changing nature of these attacks, a cloud service provider can only at best give a general security-based Service Level Agreement and may not be capable of guaranteeing it.
e. In distributed and multi-cloud application deployment, Service Level Agreements are challenging to agree on as the several providers apply various standards. These standards are often proprietary and unable to interoperate therefore single Service Level Agreement for all parties concerned may be difficult to realise.

3.5. Resource Management and Challenges

4) **Resource Management Models**

Cloud provides a working tool towards achieving high efficiency in resource management and low cost service provisioning [2]. Sophisticated monitoring techniques are needed to cope with resources and the enforcement of SLAs by Cloud providers. Presently, most Cloud providers offer multi-tenant software as a service where provisioning of an application instance is made available to many customers. This has presented problems to monitor especially on the problem of how to ensure Service Level Agreements for diverse customers. The implementation of any application may affect the presentation of the others when Cloud providers make use of sharing resource for provisioning customer applications as a result of different economic reasons. Monitoring a Cloud environment can move to large number of nodes in a data center or distributed within geographical locations which is not a minor undertaking considering that the Cloud provider makes sure the monitoring processes does not make weak the performance of the applications being provisioned. In [23] [24] the authors discussed about ant colony algorithm, a job programmed algorithm of cloud computing. Considering the cloud computing architecture and the that of ant colony algorithm analysis, managing cloud computing resources is intended to have varied rights management for its users, be it admins. It involves inspecting and the application status of host VM, monitor the task application and task performance scheduling, and the submission of computed tasks.

Sharing resources in cloud computing technology is established on virtualization of physical machines in order to attain most importantly security and performance separation. Virtual machines do share resources of physical machines when they are operational. These virtual machines provide individual customer services, and are shared among customers. It is quite challenging to effectively handle shared resources in order to decrease cost and achieve high utilization. According to [25], Autonomic resource management makes sure that Cloud providers serves huge number of demands without breaking terms of the SLA. With dynamism it manages the resources though the use of VM migration and consolidation. The upcoming computing paradigm is projected to be *utility computing;* that is, making computing services available when users require them, that is making computing services to become commodity utilities, just as internet, electric power, fuel, and telephone.

In [16], the authors pointed out that workload resource requirements are impervious, and during various points at production, it is tough finding out the resources critical for utmost performance. It has been difficult for hosted computing services like AWS Lambda for the load handled as black box functionality. It is understood that the performance detected may be due to primary environmental implementation, the allocation policies, issues performance isolation, or non-linear dependency of performance on resources accessibility. Monitoring resources expended while running task might aid in ascertaining resources for the utilization for that run, but will not indicate performance impacts in controlled set ups, or changed hardware or software.

The author Singh in [24], presented resource allocation model that evaluates users' request centered on resource requirements and resources that are available in order to get least run time. Information on resource represent if resources are available and configured. The resource allocation proposed algorithm assigns resource to negotiate the requirements for minimal run time. Client needs varies and heterogeneous therefore it is considerable to allocate using optimal solution. Availability of resource decides the allocation decision and performance, which brings about pool of various resources. Workload linked with the computing power available of the central processing unit is considered as below demand and present consumption of resources. In uncertain cloud environment, manage resources efficiently; allocation issue executed with swarm optimization tactic made better, the likelihood to look for best appropriate resource for task with least run time possible. Swarm practice is built on nature motivated and artificial intelligence system which involves of self-sufficient agent with combined activities with the use of decentralized system[24] [26].

These authors in [27] presented Ant Colony Optimization (ACO) based energy aware solution to address the problem of allocating resource. This proposed Energy Aware Resource Allocation EARA methodology aims to optimize the allocating of resources so as to make energy efficiency better in the cloud infrastructure while meeting up to the QoS requirements of the end users. The allocation of resources to jobs is based on their QoS requirements. EARA uses ACO at two levels which are: the level where ACO allocates virtual machines resources to jobs, and the level where ACO allocates physical machines resources to Virtual Machines. EARA is handled from the cloud service provider's and end users' point of view. This reduces: the overall energy consumption for the benefit of cloud service provider, and the overall execution cost and entire time of execution for the clients' satisfaction. Benefits of ant colony algorithm includes [28]:

a. Making use of decentralized approach to provide good solution to its single point of failure
b. Collecting information faster
c. Reduces load on networks.

Challenges of ant colony algorithm includes [28]:

a. Dispatching a lot of ants which result to network overloads.
b. Some operating parameters are not taken into consideration which might result to poor performance.
c. Points of initiating ants and the number of ants are not established.

In [29], the authors Zhang and Li proposed a user utility oriented queuing model to handle task scheduling in cloud environment. These authors modelled task scheduling as an M/M/1 queuing system, classified the utility into time utility and cost utility, and built a linear programming model to maximize total utility for time utility and cost utility. They also proposed a utility oriented algorithm to make the most of the total utility. They described the randomness of tasks with the $M/M/1$ model of queuing theory. This utility model involves one server, some schedulers, and some computing resources. When users' tasks are submitted, the server analyzes and schedules the tasks to different schedulers, and adds them to local task queue of the corresponding scheduler. This model can reschedule remaining tasks dynamically to get the maximised utility. Finally, every scheduler schedules its local tasks to obtainable computing resources. The main aim of utility computing is to make provision for the computing resources, which includes: computational power, storage capacity and services to its users while charging them for their usage [30]. In [31], the authors stated that utility computing makes provision for services and computing resources to customers, such as storage, applications, and computing power. This utility computing model services is the foundation of the shift to on demand computing, software as a service and cloud computing models. Benefits of utility computing:

a. The end user have no need to buy all the hardware, software and licenses needed in order to conduct business with cloud service provides.
b. Companies have the option to subscribe to a single service and use the same suite of software throughout the whole client organization.
c. It provides compatibility of all the computers in large companies.
d. It offers unlimited storage capacity

Disadvantages of utility computing:

a. Reliability issue. This means the service could be halted from the utility computing organization for any reason such as a financial trouble or equipment problems.
b. There are many servers across various administrative domains

Some utility computing driving factors [30]:

a. Virtualization enables the abstraction of computing resources so that a physical machine can function as a set of multiple logical virtual machines.
b. Resource pricing in other to develop a pricing standard that can gainfully support economy based utility computing paradigm.
c. Standardization and commoditization are important use of utility services. Standardized information technology services facilitate transparent use of services and make services ideal candidate for utility computing. The commoditization of hardware and software applications such as office suites is increasing with the acceptance of the open standards.
d. Resource allocation and scheduling handle user requests to satisfy user quality of service and maximize profit. A scheduler determines the resources based on what is required of a job which is a user request, performs the resource allocation, and then maps the resources to that job.
e. Service Level Agreement defines service constraints required by the end users. Cloud service providers know how users value their service requests, hence it provides feedback mechanisms to encourage and discourage a service request.

In [32], the author Kim proposed a resource management model that CloudStack supports. CloudStack is an effective resource model that enables scalability, multi-tenant, and it is a cloud computing software that manages the creation and deployment of cloud infrastructure. The system manager is unable to monitor VMs computing resources, but increases visibility into resource allocation and can look up the status of Virtual Machines such as if it is on or off at the console of cloud management. Comprehensive information regarding the status of the Virtual Machine chosen by the system manager can be monitored; examples are the central processing unit use rate, disk, and network activities. The main aim of this management model for resource is to evaluate unprocessed data, then report the statistical information about the Virtual Machine usage volume for the computing resources contained by the resources constraint. What this resource management model specifically does is that:

a. It enables system manager to look into the statistical analysis and the status from the log analysis framework from communication among VMs.
b. It aids system manager in generation of rules for the present constraint of obtainable computing resources gotten from the log analysis framework. An instance is when users make request and create Virtual Machines using a quad core central processing unit, the system manager has the choice of scaling down from a quad core to a dual core for the sum of central processing units constructed on the statistical report from the log analysis framework.
c. Based on firewall policy, it provides the chance to enable the system manager to script enabling the cloud management console to automatically, measure the virtual machines upward or downward.
d. Enables the system manager to produce policies during emergencies for service stability of the virtual machines.

5) Resource Management Challenges

Traditional resource management methods are not enough for cloud computing because they are on virtualization technology with distributed nature [33]. Considering the growth in Cloud computing, it has challenges for managing resource because of heterogeneity in hardware capabilities, per request service model, pay-as-you-use model and assurance to satisfy quality of service. Managing resources dynamically will reduce the resource controversy, scarcity of resources, fragmentation of resource, and overflow / underflow problems. To circumvent these difficulties resources should be adjusted with dynamism to manage resources efficiently in the cloud architecture [34].

There are challenges in the capacity to monitor resource and to manage SLAs in cloud computing, they include [2]:

a. Distributed Application Execution – NetLogger is a distributed system that monitors in order to observe and collect information of computer networks. In [2], the authors discussed ChaosMon, an application that monitors and displays performance information for parallel and distributed systems. This monitoring system is aimed to support application developers to enable them specify performance metrics and to also observe them visually in order to identify, evaluate, and comprehend performance logjams. This system is a distributed monitoring that has a centralized control.
b. Enforcement of the Agreed SLA – Enforcing SLAs is challenging and it involves complex processes whereby both parties might have to keep going back and forth until a mutual agreement is achieved. Implementation of different technologies poses challenges to evaluate Service Level Agreement documents, multifaceted deployment procedures, and scalability concerns. Ensuring uninterrupted monitoring and dynamic resource provision can be employed to put into effect agreed SLA.
c. Energy Management - Managing the consumption of energy is becoming challenging. Statistics and report show unchecked energy consumption might be a key problem in few years' time. According to [14], Stanford University made known that there is an annual increase of 56% in the consumption of electricity in data centers between 2005 and 2010.
d. Multi-Tenancy Application – This provision is becoming standard amongst Cloud providers to cost efficiently provide their sole instant application to numerous consumers. The technology approach is still challenging in its realization. In [2], the authors discussed proposed SLAs that is multi-tenant oriented in monitoring performance, in detection, and to schedule architecture with their clients. The writers aimed towards separating and guaranteeing optimized performance of each client in the Cloud space. This is complex and challenging to manage such resource because the cloud provider is making provision for every tenant with the same

application instance whereby the Service Level Agreements for the applications are contacted on per tenant basis. In situations like this, the workload of some tenants' applications will affect the unusual resource consumptions by other tenants considering the Cloud hardware, and all tenants share software resources. To solve this issue, a dynamic SLA mechanism architecture is designed, which monitors application grades, discerns what is not normal, and dynamically schedules shared resources to make sure of tenants' SLAs and optimize system performance.

e. High Availability - This is the server's availability for use for its intended purpose. High availability main objective is to ensure a system continues to function regardless of the failure of any components. This can be achieved through redundancy and elimination of single point of failure [14].

f. The Scalability of the Monitoring Mechanism - Key factors of cloud computing includes scalability of resource and application provisioning on-demand in a pay-as-you-go method. Cloud environments measure thousands of computing devices in large-scale environments; hence, the need for scalable monitoring tools. In [35], the authors proposed some methods to handle the challenges in setting up virtualized datacenter management systems that are scalable. The plan is to strategise a high performance and strong management tool that will be able to scale from some hosts to a large-scale Cloud datacenter. These authors indicated how they came about a scalability management tool by noting these challenges:
   a. Performance / Fairness;
   b. Security;
   c. Robustness;
   d. Availability; and
   e. Backward compatibility.

3.6. Trending Practices in Cloud Resource Management

Daily growing attributes and advancements in cloud computing are promising the future and luring organizations and stakeholders towards the use of cloud computing. This fast growth of cloud computing is in need of stricter security and large quantity of resources like memory, process and storage to meet the Service Level Agreement standards. The trending practices include:

a. Live Migration – The use of live migration of virtual machines is an indispensable attribute of virtualization, enabling a seamlessly and transparent migrating of virtual machines from a source host to another destination host, even though the VM is still running without interrupting VMs [36]. Cloud live migration is on the increase in cloud computing with the aim to gain the cloud benefits from non-cloud situated applications. Live migration is a recent concept within cloud computing that is utilized during practical fault tolerance for instance by faultlessly moving Virtual Machines away from faulty hardware to stable hardware without the consumer noting any adjustment in a virtualized space. This is so because in the use of live migration, the end user is unaware there is only a delay of 60 mini seconds to 300 mini seconds [15]. Virtual Machine live migration can be performed via static migration or Dynamic migration. In order to fulfill Service Level Agreement, static Virtual Machine migration is used as required resources gets carefully chosen as per requirement in SLA, but in dynamic Virtual Machine provisioning, the resources change dynamically to handle unforeseen workload changes [37]. Major benefit for live VM migration includes [36]:
   a. Load balancing, the moving of over-loaded servers to light-loaded servers in order to release congested hosts.

   c. Proactive fault tolerance and online maintenance

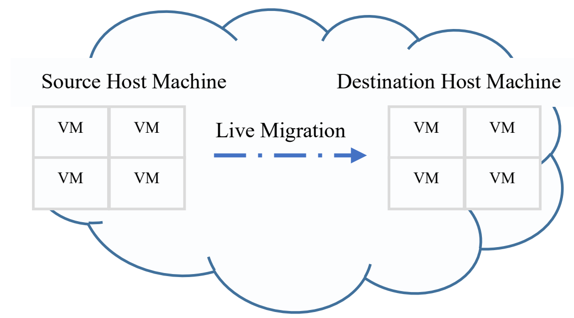

Figure 1: Live Migration [27]

b. Power Saving in Green Computing - the authors in [38] discussed a proposed resource-utilization- aware energy saving server consolidation algorithm for the provision of improved utilization of resources as it reduces the total number of virtual machines during live migrations. Experimental results demonstrated its ability to reduce the consumption of energy and violations in Service Level Agreement in cloud data center. In [39], the authors describes green data center as a depository of a competent management of the system with a reduced amount of power consumed environment. The power consumption by an average data center can be so enormous that it can serve as a power source for approximately 25,000 private homes. In [40], Jena presented an optimization algorithm that arrange job with the aim of achieving an optimized energy usage and overall computation time using Clonal Selection Algorithm (CSA). Dynamic Voltage Frequency Scaling (DVFS) technique designed to reduce the usage of cloud resources by managing the power voltage as well as the regularity of the processor without ruining the performance. In [41], the authors presented an optimization framework of two modules that run concurrently: the Datacenter Energy Controller that reduces the use of datacenter energy without degrading the Quality-of-Service (QoS) and; the Green Energy Controller that brings about renewable sources. This Green Energy Controller computes the anticipated energy budget for the datacenter by the use of the lithium-ion battery as an added energy reserve or the grid of both banks in which the Hybrid Electric Systems can drain. For cloud providers to make their services become green computing, they have to spend in renewable energy sources to generate power from renewable sources of energy, like wind, solar, or hydroelectricity [42]. Merging resources can advance utilization and make provision for increase in space, power and cooling capacity within the same facility environment. Energy preserving approaches includes [43]:

a. Nano Data Center is a distributed computing platform that makes provision for computing and storage services and adopts a managed peer-to-peer model to form a distributed data center infrastructure.
b. Reduction of Central Processing Unit Power Dissipation adapts free cooling so that power dissipation reduces.
c. Server Consolidation is the migration of server roles from various underutilized physical servers to VMs for the reduction of hardware and energy consumption.
d. Energy Saving Strategy of System Software is a dynamic energy usage, so the operating system can dynamically manipulate the system unit for obtaining the minimal power consumption without degrading already assigned the task or any job in performance.
e. Live Migration of Virtual Machine is about the movement of a running Virtual Machine from one host to another.

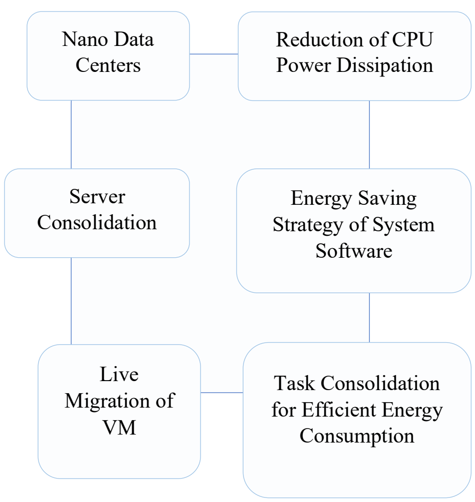

Figure 2: Energy Preserving Approaches [34]

3.7. Resource Grid Architecture Management

In [34], the authors proposed a Resource Grid Architecture for Multi Cloud Environment (RGA) for allocation and management of the resources with dynamism in virtual manner. Resource Management in Single Cloud Architecture is an ongoing area in research and RGA for Multi Cloud Environment is a current practice that has high scalability to manage resource at single cloud environments. This architecture presents a resource layer with logical resource grid and the usages of the VMs to project the resources in contrast to physical systems of a cloud. Experimentations have showed that their Resource Grid Architecture can efficiently manage the resources against numerous clouds and support the green computing. Logically, RGA is grouped into four layers to manage resource efficiently:

a. Cloud Layer - This layer investigates the assigned resources to cloud application in order to keep log of record for resource usage and directs the information to cloud Resource Prediction Unit for hot spot detection and cold spot detection. Local Resource Manager is a component that verifies the resource allocation and utilization only at cloud level and is a proxy of Global Resource Manager.
b. Network Layer - This layer supports high-speed commutation among cloud and is the backbone for the experimented architecture for the reason that intra cloud communication is very much in demand in the implementation for resource sharing and process sharing.
c. Virtual Machine Layer - This layer is a separate group of virtual machine for sole cloud architecture to accomplish the operational feasibility. Each group of virtual machine is a set of virtual machines for physical system representation and are constantly accessible to resource grid layer monitoring and resource mapping.
d. Resource Grid Layer – This layer is an assembly of management modules of this architecture such as Global Resource Manager; these modules are interwoven for the monitoring, analyzing, allocating and tracking of resource information of multiple clouds at a centralized virtual location.

4. Conclusion

Cloud computing makes provision for scalable, on demand, elastic, multi-tenant and virtualization of services to customers on the Internet through cloud service providers. The types of service are the SaaS which provides applications with customizable interfaces, PaaS provides platform for application development and testing, and IaaS which makes provision of storages and computing infrastructure to users and extends to physical machines, virtual machines. These services provided are based on the service level agreements between the cloud service providers and the client. The service level agreement stipulates the terms of the services makes provision for mutually beneficial transaction between the parties. This paper presented a survey of recent developmental trends and issues in resource management in cloud computing. Cloud computing is aimed at providing the best resource to its users. Many researchers are focused on request allocation and resource management for Cloud Computing. All-encompassing use of learning empowers systems to be dynamic in handling workloads and execution environments. This paper documented techniques for creating scheduling and resource allocation choices for cloud computing and the datacenters. This paper concluded with a review of resource management on Cloud computing and cloud SLAs.

Conflict of Interest

The authors declare no conflict of interest.

Acknowledgment

We acknowledge the support and sponsorship provided by Covenant University through the Centre for Research, Innovation, and Discovery (CUCRID).

References

[1] I. Odun-ayo, A. Olasupo, and N. Omoregbe, "Cloud Service Level Agreements – Issues and Development," Int. Conf. Next Gener. Comput. Inf. Syst., pp. 1–6, 2017.
[2] V. C. Emeakaroha and R. N. Calheiros, "Achieving Flexible SLA and Resource Management in Clouds," Achiev. Fed. self-manageable cloud infrastructures theory Pract., pp. 266–287, 2012.
[3] N. M. Gonzalez, T. C. M. de B. Carvalho, and C. C. Miers, "Cloud resource management: towards efficient execution of large-scale scientific applications and workflows on complex infrastructures," J. Cloud Comput. Adv. Syst. Appl., vol. 6, no. 1, 2017.
[4] I. Odun-ayo, O. Ajayi, and A. Falade, "Cloud Computing and Quality of Service : Issues and Developments," Proc. Int. MultiConference Eng. Comput. Sci., vol. I, pp. 179–184, 2018.
[5] A. Koci and B. Cico, "ADLMCC-Asymmetric Distributed Lock Management In Cloud," Int. J. Inf. Technol. Secur., vol. 10, 2018.
[6] L. Wu, S. K. Garg, and R. Buyya, "Journal of Computer and System Sciences SLA-based admission control for a Software-as-a-Service provider in Cloud computing environments," J. Comput. Syst. Sci., vol. 78, no. 5, pp. 1280–1299, 2012.
[7] K. Buck, D. Hanf, and D. Harper, "Cloud SLA Considerations for the Government Consumer," Syst. Eng. Cloud Comput. Ser., pp. 1–65, 2015.
[8] R. El-awadi and M. Abu-rizka, "A Framework for Negotiating Service Level Agreement of Cloud-based Services," Int. Conf. Commun. Manag. Inf. Technol., no. 65, pp. 940–949, 2015.
[9] F. Faniyi, R. Bahsoon, and G. Theodoropoulos, "A dynamic data-driven simulation approach for preventing service level agreement violations in cloud federation," Int. Conf. Comput. Sci. ICCS, pp. 1167–1176, 2012.
[10] S. B. Dash, H. Saini, T. C. Panda, A. Mishra, and A. B. N. Access, "Service Level Agreement Assurance in Cloud Computing : A Trust Issue," Int. J. Comput. Sci. Inf. Technol., vol. 5, no. 3, pp. 2899–2906, 2014.
[11] M. Cochran and P. D. Witman, "Governance and Service Level Agreement Issues in A Cloud Computing Environment," J. Inf. Technol. Manag., vol. XXII, no. 2, 2011.
[12] Olasupo O. Ayayi, F. A. Oladeji, and C. O. Uwadia, "Multi-Class Load Balancing Scheme for QoS and Energy Conservation in Cloud Computing," West African J. Ind. Acad. Res., vol. 17, pp. 28–36, 2016.
[13] Y. Jiang, H. Sun, J. Ding, and Y. Liu, "A Data Transmission Method for Resource Monitoring under Cloud Computing Environment," Int. J. Grid Distrib. Comput., vol. 8, no. 2, pp. 15–24, 2015.
[14] O. Ajayi and F. . Oladeji, "An overview of resource management challenges in cloud computing," UNILAG Annu. Res. Conf. Fair, vol. 2–3, pp. 554–560, 2015.
[15] A. J. Younge, G. Von Laszewski, L. Wang, S. Lopez-alarcon, and W. Carithers, "Efficient Resource Management for Cloud Computing Environments," Int. Conf. Green Comput. IEEE , 2010.
[16] N. Yadwadkar, "Machine Learning for Automatic Resource Management in the Datacenter and the Cloud," Ph.D. Diss. Dept. Electr. Eng. Comput. Sci. Electr. Eng. Comput. Sci. Univ. California, Berkeley, U.S. Accessed Jan. 6, 2019. Available http//digitalassets.lib.berkeley.edu/etd/ucb/text/Yadwadka, 2018.
[17] A. Ostfeld, "Data-Driven Modelling : Some Past Experiences and New Approaches approaches," J. Hydroinformatics, vol. 10, no. 1, 2008.
[18] A. Schram and K. M. Anderson, "MySQL to NoSQL Data Modeling Challenges in Supporting Scalability," Proc. 3rd Annu. Conf. Syst. Program. Appl. Softw. Humanit., pp. 191–202, 2012.
[19] C. Reiss, G. R. Ganger, R. H. Katz, and M. A. Kozuch, "Heterogeneity and Dynamicity of Clouds at Scale : Google Trace Analysis," Proc. Third ACM Symp. Cloud Comput., 2012.
[20] G. Blanchard, G. Lee, and C. Scott, "Generalizing from Several Related Classification Tasks to a New Unlabeled Sample," Proc. 24th Int. Conf. Neural Inf. Process. Syst., pp. 2178–2186, 2011.
[21] L. Badger, R. Patt-corner, J. Voas, L. Badger, R. Patt-corner, and J. Voas, "Cloud Computing Synopsis and Recommendations," Natl. Inst. Stand. Technol. Spec. Publ. 800-146, 2012.
[22] I. Odun-ayo, N. Omoregbe, and B. Udemezue, "Cloud and Mobile Computing – Issues and Developments," Proc. World Congr. Eng. Comput. Sci., vol. I, 2018.
[23] F. G. Fang, "Study on Resource Management Based on Cloud Computing," MATEC Web Conf., vol. 63, 2016.
[24] H. Singh, "Efficient Resource Management Technique for Performance Improvement in Cloud Computing," Indian J. Comput. Sci. Eng., vol. 8, no. 1, pp. 33–39, 2017.
[25] R. Buyya, S. K. Garg, and R. N. Calheiros, "SLA-Oriented Resource Provisioning for Cloud Computing : Challenges, Architecture, and Solutions," Int. Conf. Cloud Serv. Comput., 2011.
[26] E. Pacini, C. Mateos, and C. García Garino, "Distributed job scheduling based on Swarm Intelligence: A survey," Comput. Electr. Eng., vol. 40, no. 1, pp. 252–269, 2014.
[27] K. Ashok, K. Rajesh, and S. Anju, "Energy aware resource allocation for clouds using two level ant colony optimization," Comput. Informatics, vol. 37, pp. 76–108, 2018.
[28] B. Ghutke, "Pros and Cons of Load Balancing Algorithms for Cloud Computing," Int. Conf. Inf. Syst. Comput. Networks, 2014.
[29] Z. Zhang and Y. Li, "User utility oriented queuing model for resource allocation in cloud environment," J. Electr. Comput. Eng., vol. 2015, pp. 1–8, 2015.
[30] I. Chana and T. Kaur, "Delivering IT as A Utility- A Systematic Review," Int. J. Found. Comput. Sci. Technol. (IJFCST)., vol. 3, no. 3, 2013.
[31] S. Mawia, I. Omer, and A. B. A. Mustafa, "Comparative study between Cluster, Grid, Utility, Cloud and Autonomic computing," IOSR J. Electr. Electron. Eng., vol. 9, no. 6, pp. 61–67, 2014.
[32] A. Kim, J. Lee, and M. Kim, "Resource management model based on cloud computing environment," Int. J. Distrib. Sens. Networks, vol. 12, no. 11, 2016.
[33] S. Parikh, N. Patel, and H. B. Prajapati, "Resource Management in Cloud Computing : Classification and Taxonomy," Comput. Res. Repos., 2017.
[34] C. Aruna and R. Prasad, "Resource Grid Architecture for Multi Cloud Resource Management in Cloud Computing," Emerg. ICT Bridg. Futur. - Proc. 49th Annu. Conv. Comput. Soc. India, vol. 1, pp. 631–640, 2015.
[35] S. Vijayaraghavan and K. Govil, "Challenges in Building Scalable Virtualized Datacenter Management," ACM SIGOPS Oper. Syst. Rev., vol. 44, no. 4, pp. 95–102, 2012.
[36] M. Noshy, A. Ibrahim, and H. A. Ali, "Optimization of live virtual machine migration in cloud computing : A survey and future directions," J. Netw. Comput. Appl., vol. 110, no. March, pp. 1–11, 2018.
[37] S. B. Rathod and K. R. Vuyyuru, "Secure Live VM Migration in Cloud Computing : A Survey," Int. J. Comput. Appl., vol. 103, no. April 2016, 2014.
[38] B. Saha, "Green Computing : Current Research Trends," Int. J. Comput. Sci. Eng., vol. 6, no. June, pp. 3–6, 2018.
[39] S. Sharma and G. Sharma, "A Review on Secure and Energy Efficient Approaches for Green Computing," Int. J. Comput. Appl., vol. 136, no. May, 2016.
[40] R. K. Jena, "Energy Efficient Task Scheduling in Cloud Environment," 4th Int. Conf. Power Energy Syst. Eng., vol. 141, pp. 222–227, 2017.
[41] A. Pahlevan, R. Maurizio, G. D. V. Pablo, B. Davide, and A. David, "Joint computing and electric systems optimization for green datacenters Handbook of Hardware / Software Codesign Soonhoi Ha and Jürgen Teich," Jt. Comput. Electr. Syst. Optim. Green Datacenters. Ha S., Teich J. Handb. Hardware/Software Codesign. Springer, Dordr., no. November, 2016.
[42] M. K. Aery, "Green Computing : A Study on Future Computing and Energy Saving Technology," An Int. J. Eng. Sci., vol. 25, no. November 2017, 2018.
[43] A. D. Borah, D. Muchahary, and S. K. Singh, "Power Saving Strategies in Green Cloud Computing Systems," Int. J. Grid Distrib. Comput., vol. 8, no. February, pp. 299–306, 2015.

Advances in Science, Technology and Engineering Systems Journal Vol. 4, No. 2, 237-243 (2019)

www.astesj.com

Special Issue on Advancement in Engineering and Computer Science

ASTESJ

ISSN: 2415-6698

Application of The Half-Sweep Egsor Iteration for Two-Point Boundary Value Problems of Fractional Order

Rostang Rahman[1,*], Nur Afza Mat Ali[1], Jumat Sulaiman[1], Fatihah Anas Muhiddin[2]

[1]*Mathematics with Economics Programme, Faculty of Science and Natural Resources, Universiti Malaysia Sabah, 88400 Kota Kinabalu, Sabah, Malaysia*

[2]*Faculty of Computing and Mathematical Sciences, Universiti Teknologi MARA Sabah, 88997 Kota Kinabalu, Sabah, Malaysia*

A R T I C L E I N F O

Article history:
Received: 03 January, 2019
Accepted: 07 March, 2019
Online: 29 March, 2019

Keywords:
4HSEGSOR
Caputo's fractional operator
Finite difference method
Two-point boundary value problem

A B S T R A C T

The point of this study is to explore and elucidating the performance of the four-point Half-Sweep EGSOR (4HSEGSOR) iterative method to solve fractional two-point boundary value problems by using Caputo's fractional operator and family of finite differences (FD) schemes. To apply the iterative methods, linear system needs to be constructed via the discretization process with fractional order to get the approximation equation of the linear fractional two point boundary value problem by using the Caputo's derivative operator. Then the generated linear system has been solved using the proposed 4HSEGSOR iterative method. In the addition, the formulation and application of the 4HSEGSOR method to solve the problems are also presented. Three numerical examples and comparison are used to illustrate with tested FSSOR and HSSOR methods. The numerical results reveals the effectiveness of 4HSEGSOR method compared with tested iterative methods.

1. Introduction

This paper inspired from numerous researchers in science and engineering where there have been discuss the steady-state problems which refer to Fractional Boundary Value problems (FBVPs) since this problem become more attractive in the recent years in many applications such as mathematics, engineering, economy, and other fields [1,2]. Since the rapid growth of computer technology, the numerical techniques are used to solve the large size problem. Following that, there are many researcher have been proposed numerical methods to solve the FBVPs such as Fix et al [3] applied the Least Squares Finite-element methods, Li et al [4] applied the Reproducing Kernel method, Odibat et al [5] applied the Modified Homotopy Perturbation method, and Diethelm et al [6] applied the Extrapolation method. For instance, Sunarto et al [7] started the study on the finite different method to solve the unsteady-state problems using application of the SOR method. In addition, Sunarto et al [8] extended the study with the application of the full-sweep AOR iteration concept to the same problem. Furthermore, this study extend the study to steady-state problems and focus to two-point Fractional BVPs. The problem will be solved numerically and represented as follows [9]:

$$d(x)\frac{\partial^\beta v(x)}{\partial x^\beta}+a(x)\frac{\partial^2 v(x)}{\partial x^2}+b(x)\frac{\partial v(x)}{\partial x}+c(x)v(x)=F(x),\ x\in[\gamma,\mu] \qquad (1)$$

with the Dirichlet boundary conditions,

$$u(\gamma)=\gamma_0, \qquad u(\mu)=\mu_1.$$

where $a(x)$, $b(x)$, $c(x)$ and $d(x)$ are known functions or constants respectively. Then the derivative term of fractional order is $\frac{\partial^\beta v(x)}{\partial x^\beta}$ and the parameter β represent fractional order with the range in this study consider as $1\le\beta\le 2$. To get the approximate solution of two-point FBVPs must be discretized to form an approximation equations. Based on the family of FD schemes and Caputo's fractional derivative operator, the approximation equations use to construct a linear system at each point.

For solving the linear systems which have large and sparse, there are several concept iterative methods from previous researchers have been discussed [10,11]. Other than that, Rahman et al. [12] studied the numerical solution of two-point FBVPs based on the iterative method where SOR method has been used

*Corresponding Author: Rostang Rahman, Mathematics with Economics Programme, Faculty of Science and Natural Resources, Universiti Malaysia Sabah, 88400 Kota Kinabalu, Sabah, Malaysia, Contact No:+60 14 654 1569, rostang054@gmail.com

and AGE method in studied Rahman et al. [13]. From the studied, this paper focus to expand the iterative method to the half-sweep scheme. The idea come from Abdullah (1991) who initiated of Half-sweep iteration which is ones of the common utilized use iterative techniques to solve any linear systems. Following that, in this paper proposed 4HSEGSOR iterative method as linear solver to increase the iteration convergence rate so as to solve the two-point FBVPs on the Caputo's FD approximation equation. To demonstrate the capability of the 4HSEGSOR method, the implementation of the Half-Sweep SOR (HSSOR) iterative method also considered as comparison method in this study and Full-Sweep SOR (FSSOR) iterative methods react as a control method.

After that, the approximation equation will be construct for the problem (1) based on the HS second-order Caputo's fractional operator via fractional derivative theory. Therefore, let discuss some definitions that can be applied to construct the approximation equation towards problem (1) by using the Caputo's fractional derivative operator.

Definition 1 [14]. The definition of fractional integral operator for Riemann-Liouville, ${}^{*}J^{\beta}$ of order $-\beta$ given by:

$$ {}^{*}J^{\beta}F(x)=\frac{1}{\Gamma(\beta)}\int_{0}^{x}(x-t)^{\beta-1}F(t)dt,\quad \beta>0,\quad x>0 \tag{2}$$

Definition 2 [14]. The definition of Caputo's fractional derivative operator, D^{β} of order $-\beta$ given by:

$$ D^{\beta}F(x)=\frac{1}{\Gamma(m-\beta)}\int_{0}^{x}\frac{F^{(m)}(t)}{(x-t)^{b-m+1}}dt,\quad \beta>0 \tag{3}$$

Where parameter β refer to $m-1<\beta\le m,\ m\in N,$ and $x>0$.

Definition 3 [15]. The function of Gamma denoted by $\Gamma(\beta)$ is a generalization of factorial function for complex argument with positive real part it is defined as:

$$ \Gamma(\beta)=\int_{0}^{\infty}x^{t-1}e^{-x}dx \tag{4}$$

To solve the problem (1) as mentioned in early section, we get numerical approximations by using fd scheme via the Caputo's derivative definition with Dirichlet boundary conditions and fractional derivative operator. In addition to that, the existence and uniqueness of the solution for the problem (1) can be referred and discussed by Diethelm in 2002 in the study Analysis of Fractional Differential Equations [16].

Theorem 4 (existence) [16]. Assume that $D:=\left[0,x^{*}\right]\times\left[x_0^{(0)}-\eta,\ x_0^{(0)}+\gamma\right]$ with some $x^{*}>0$ and let the function $F:D\to\mathbb{R}$ be continuous. Furthermore, define $x:=\min\left\{x^{*},\left(h\Gamma(\beta+1)/\|f\|_{\infty}\right)^{1/\beta}\right\}$. Then there exists a function $v:[0,x]\to\mathbb{R}$ solving the initial value problem (1).

Theorem 5 (uniqueness) [16]. Assume that $D:=\left[0,x^{*}\right]\times\left[x_0^{(0)}-h,\ x_0^{(0)}+h\right]$ with the $x^{*}>0$. Besides that, let the function $F:D\to\mathbb{R}$ be bounded on D and fulfill a Lipschitz condition the second variable.

Before solving the problem (1), the solution domain of the problem has been confined to the finite domain $a\gamma\le x\le\mu$, with $1\le\beta\le 2$ whereas the parameter β refers to the fractional order derivative. In order to solve the problem (1), let consider the Caputo's fractional derivative of order β as:

$$ \frac{d^{\beta}v(x_i)}{dx^{\beta}}=\frac{1}{\Gamma(2-\beta)}\int_{0}^{x_n}\frac{dv^{2}(s)}{dx^{2}}\left(x_n-s\right)^{1-\beta}ds \tag{5}$$

2. Half-sweep Approximation Equation

Before discretizing problem (1), let the solution domain of the problem be partitioned consistently to facilitate in discretizing process. In order to discretize, we consider some positive integers N which is the number of subintervals $\left[\gamma,\mu\right]$ and then the length of grid size are defined as.

$$ h=\Delta x=\frac{\gamma-\eta}{N} \tag{6}$$

and

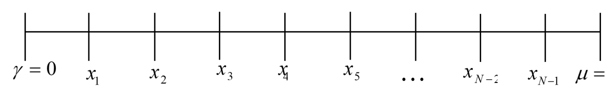

Figure 1: The distribution of interior node points over the finite grid network.

From the Figure 1, we develop the consistently grid network of the solution domain where the polar grid of the solution domain will be shown as $x_i=\gamma+ih,\ i=0,1,2,\ldots,N$ and the values of function $v(x)$ at point x_i are given as $v(x_i)=v_i$. As mentioned in Section 1, the half-sweep concept is imposed to improve the convergence rate. Here the different values of h from the current point to next point between full-sweep and half-sweep is shown in Figures 2 which is Figure 2(a) shows the implementation of the full-sweep iteration which all interior nodes are considered one by one point in which its distance for each point is h. However, for half-sweep iteration with its distance $2h$ can be seen in Figure 2(b).

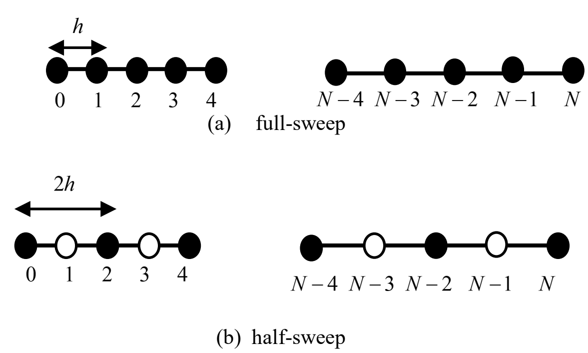

Figure 2: The distribution of uniform grid network

After that, to obtain the approximation equation of problem (1), now the equation (5) will be consider to derive based on the formulation of Caputo's fractional derivative operator which can be gotten by a straightforward quadrature formula as follows.

$$\begin{aligned}\frac{d^\beta v(x_i)}{dx^\beta} &= \frac{1}{\Gamma(2-\beta)}\int_0^{x_n}\frac{dv^2(s)}{dx^2}\left(x_n-s\right)^{1-\beta}ds \\ &= \frac{1}{\Gamma(2-\beta)}\sum_{j=0}^{i-1}\int_{jh}^{(j+1)h}\left(\frac{v_{i-j+1}-2v_{i-j}+v_{i-j-1}}{h^2}\right)\left(x_nh-s\right)^{1-\beta}\partial s \\ &= \frac{1}{\Gamma(2-\alpha)}\sum_{j=0}^{i-1}\left(\frac{v_{i-j+1}-2v_{i-j}+v_{i-j-1}}{h^2}\right)x\int_{jh}^{(j+1)h}\left(x_nh-s\right)^{1-\beta}ds \\ &= \frac{h^{-\beta}}{\Gamma(3-\beta)}\sum_{j=0}^{i-1}\left(v_{i-j+1}-2v_{i-j}+v_{i-j-1}\right)\left((j+1)^{2-\beta}-j^{2-\beta}\right)\end{aligned} \tag{6}$$

Then the discrete approximation of equation (6) can be given as

$$\frac{d^\beta v(x_i)}{dx^\beta} = \sigma_{\beta,h}\sum_{j=0}^{i-1}g_j^\beta\left(v_{i-j+1}-2v_{i-j}+v_{i-j-1}\right)+O(h) \tag{7a}$$

Where can be define by

$$\sigma_{\beta,h} = \frac{h^{-\beta}}{\Gamma(3-\beta)} \tag{7b}$$

and

$$g_j^\beta = \left(i+1\right)^{1-\beta}-i^{1-\beta}. \tag{7c}$$

However, this study don't use the operator (7) which is shown as the full-sweep Caputo's fractional derivative since this study focus to the half-sweep concept. Refer to the study of Sonarto et al [17] over the problem, we have propose the half-sweep concept to the Caputo's fractional derivative operator based on the operator (7) as follows:

$$\frac{\partial^\beta v(x)}{\partial x^\beta} \cong \sigma_{\beta,k}\sum_{j=0}^{N}g_j^\beta(v_{i-j+2}-2v_{i-j}+v_{i-j-2}) \tag{8a}$$

where we have the following expressions

$$\sigma_{\beta,h} = \frac{2h^{-\beta}}{\Gamma(3-\beta)} \tag{8b}$$

and

$$g_j^\beta = \left(\frac{i}{2}+1\right)^{2-\beta}-\frac{i}{2}^{2-\beta}. \tag{8c}$$

As mentioned in Section 1, using the second-order and first-order half-sweep central difference discretization scheme and half-sweep Caputo's fractional derivative operator (8), the second-order Half-Sweep Caputo's fd approximation equation for problem (1) given as:

$$\begin{aligned}&d_i\sigma_{\beta,h}\sum_{j=0}^{j-2}g_\beta^j(v_{i-j+2}-2v_{i-j}+v_{i-j-2})+a_i\left(\frac{v_{i+2}-2v_i+v_{i-2}}{4h^2}\right) \\ &+b_i\left(\frac{v_{i+2}-v_{i-2}}{4h}\right)+c_i(v_i)=F_i\end{aligned} \tag{9}$$

Now, the approximation (9) is known as the half-sweep FD approximation equation it means that the value for each point considers at $i=2,\ 4,\ 6,\ \ldots,\ N-2$ refer to the figure 2(b) which show the distribution of grid network. By simplifying (9), the approximation equation can be written as:

$$a_i^* v_{i-2}+b_i^* v_i+c_i^* v_{i+2}-R_i=F_i, \qquad i=2,4,6 \tag{10}$$

Let us define

$$\left.\begin{aligned}&\lambda_i=\mathrm{d}_i\sigma_{\beta,h}, \quad a_i^*=\alpha_i-\mu_i-\lambda_i, \quad b_i^*=c_i-2\alpha_i+2\lambda_i, \\ &c_i^*=\alpha_i+\mu_i-\lambda_i, \quad R_i=\lambda_i\sum_{j=1}^{j-2}g_j^\beta(u_{i-j+2}-2u_{i-j}+u_{i-j-2})\end{aligned}\right\} \tag{11}$$

Again, besides the values of $i=2,4,$ and 6, the simplify of approximation equation (9) should be appeared for $i=8,10,12,\ldots,N-2$. To simplify the approximation equation, the second-order Half-Sweep Caputo's FD approximation equation can be expressed as follows:

$$R_i^*+p_iv_{i-6}+q_iv_{i-4}+r_iv_{i-2}+s_iv_i+z_iv_{i+2}=F_i, \quad i=8,10,12,\ldots,N-2 \tag{12}$$

where

$$\left.\begin{aligned}&q=\lambda_ig_2^\beta-2\lambda_ig_4^\beta, \quad p=\lambda_ig_4^\beta, \quad r=a_i^*-2\lambda_ig_2^\beta+\lambda_ig_4^\beta, \\ &s=b_i^*+\lambda_ig_2^\beta, \quad R_i^*=\lambda_i\sum_{j=6}^{j-2}g_j^\beta(u_{i-j+2}-2u_{i-j}+u_{i-j-2}), \quad z=c_i^*.\end{aligned}\right\} \tag{13}$$

According to equations (10) and (12), the linear system can be constructed in matrix form to facilitate in solving system of second-order half-sweep Caputo's approximation equations. As a result, the system of linear equations in the form can be given as:

$$A\underline{v}=\underline{f} \tag{14}$$

where can be define,

$$A=\begin{bmatrix} s_2 & z_2 & 0 & 0 & 0 & 0 & 0 \\ r_4 & s_4 & z_4 & 0 & 0 & 0 & 0 \\ q_6 & r_6 & s_6 & z_6 & 0 & 0 & 0 \\ p_8 & q_8 & r_8 & s_8 & z_8 & 0 & 0 \\ 0 & \ddots & \ddots & \ddots & \ddots & \ddots & 0 \\ 0 & 0 & p_{N-4} & q_{N-4} & r_{N-4} & s_{N-4} & z_{N-4} \\ 0 & 0 & 0 & p_{N-2} & q_{N-2} & r_{N-2} & s_{N-2}\end{bmatrix}_{\left(\frac{N}{2}-1\right)\times\left(\frac{N}{2}-1\right)} \tag{15}$$

and

$$\underline{v}=\left[v_2 \quad v_4 \quad v_6 \quad \cdots \quad v_{N-4} \quad v_{N-2}\right]^T \tag{16}$$

and

$$\underline{F}=\begin{bmatrix} F_2+p_2v_2 \\ F_4+q_4v_4 \\ F_6+r_6v_6 \\ F_8+R_i \\ \vdots \\ F_{N-4}+R_{N-4} \\ F_{N-2}+R_{N-2}-z_{N-2}v_N\end{bmatrix} \tag{17}$$

3. Iterative Method

From previous discussion in Section 2 and refer to the linear system equation (14), the formulation of 4HSEGSOR iterative method will be discussed in this section to test the examples than record the numerical results of linear system. Based on the characteristics of the coefficient matrix A, it's showed the matrix have parse and large-scale. Following to the characteristics, the iterative methods are suitable option to solve the linear system [10]. Besides to improve the consequence rate of iterative method for solving the linear system numerically, there are iterative methods have been proposed from previous researchers such as Jacobi, GS, and SOR methods. However, this study considers the application of 4HSEGSOR method as linear solver as mentioned in early this section.

Particularly, the 4HSEGSOR method is essentially the extension to half-sweep concept for the Four-point Explicit Group SOR (4EGSOR) iterative method which is combination between EG method developed by Evans [18] and SOR method developed by Young [10]. From previous study, Saudi and Sulaiman [19] have been discuss the explicit group to apply into the robot path planning and elucidated the EGSOR iterative method using Nine-Point Laplacian [20] in order to improve the consequence rate of iterative method in the study.

The aim of EGSOR method is to reduce the computational time of the convergence rate by uses small constant size groups strategy based on mesh point and weighted parameter "ω" with its range value given as $\omega \in [1,2)$. However, the main propose of the half-sweep iteration concept in this study is to reduce the computational complexities during iteration process. Following to that, the linear system was divided into several completed small group of four points ($p=4$) start with $i=8,16,24,\ldots,N-8$. However, for the first three points $i=2,4,$ and 6 can be treated as ungroup case [21]. Since this paper deals with application 4HSEGSOR iterative method for solving the linear system (14), it can be stated as:

$$\begin{bmatrix} v_i \\ v_{i+2} \\ v_{i+4} \\ v_{i+6} \end{bmatrix} = (1-\omega)\begin{bmatrix} v_i \\ v_{i+2} \\ v_{i+4} \\ v_{i+6} \end{bmatrix} + \omega \begin{bmatrix} s_i & z_i & 0 & 0 \\ r_{i+2} & s_{i+2} & z_{i+2} & 0 \\ q_{i+4} & r_{i+4} & s_{i+4} & z_{i+4} \\ p_{i+6} & q_{i+6} & r_{i+6} & s_{i+6} \end{bmatrix}^{-1} \begin{bmatrix} S_2 \\ S_4 \\ S_6 \\ S_8 \end{bmatrix}, \tag{18}$$

for $i=8,16,24,\ldots,N-8$. To show the illustration, implementation of the 4HSEGSOR iterative method can be shown in Figure 3. Again the first three points, $i=2,4,$ and 6 can be stated as ungroup case in which these point can be used to construct the 3-point HSEGSOR method.

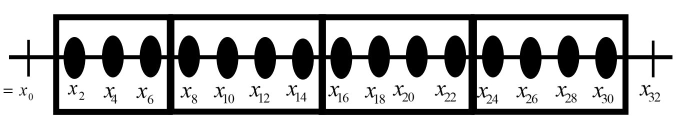

Figure 3: Implementation of the half-sweep 4EGSOR iterative method at solution domain m=32.

Based on Figure 3, Algorithm 1 is the implementation of 4HSEGSOR method that be summarized where the optimum values for the parameters, "ω" depends on the minimum number of iterations from several executions. The tolerance error set as $\varepsilon = 10^{-10}$.

Algorithm 1: 4HSEGSOR iteration

i. Set the value of parameters, $\underline{v}^{(0)} \leftarrow 0, \varepsilon \leftarrow 10^{-10}$
ii. Calculate the coefficient matrix, A.
iii. Calculate the vector, $\underline{F}$.
iv. Calculate the value of $\underline{v}^{(k+1)}$
  a) For $i=2$ calculate an ungroup cases.
  b) For $i=8, 16, 24, \ldots, N-8$, calculate again equation (10).
v. Perform the convergence test, $\left|\underline{v}^{(k+1)} - \underline{v}^{(k)}\right| \le \varepsilon = 10^{-10}$. If yes, move to step (vi). Otherwise repeat the step (iv).
vi. Display approximate solution.

4. Numerical Experiment

This paper demonstrates three examples of numerical experiments for the comparison of two-point FBVPs where the exact solution for each example already given at $\beta = 1.50$. Besides that, this paper considers others two different values to analyse the performance of Caputo's Fractional operator in which $\beta = 1.25$ and $\beta = 1.75$ refer to Section 1 the range parameter "β" is $1 \le \beta \le 2$. Other than that, three different iterative methods will be implemented such as FSSOR, HSSOR and 4HSEGSOR methods. Beyond that point, considered such as number of iterations (K), computational time measured in second (s) and maximum absolute error (error) as measurement parameters in the numerical experiments need to be recorded while the convergence test considered the tolerance error which is fixed as $\varepsilon = 10^{-10}$. The following are three examples of numerical experiments for problem (1).

Example 1

By considering the fractional two point BVP below [22]

$$\frac{\partial^\beta v(x)}{\partial x^\beta} + \frac{\partial^2 v(x)}{\partial x^2} + v(x) = x^2 + x + \frac{4}{\sqrt{\pi}}\sqrt{x} + 3, \qquad 0 \le x \le 1 \tag{19}$$

With the subject boundary condition as $v(0)=1,$ and $v(1)=3$, and the exact solution for the problem given by $v(x) = x^2 + x + 1$ when the value of $\beta = 1.50$.

Example 2

By considering the fractional two-point BVP below [23]

$$\frac{\partial^2 v(x)}{\partial x^2} + \frac{\partial^\beta v(x)}{\partial x^\beta} + v(x) = \frac{15}{4}x^{0.5} + \frac{15}{8}\sqrt{\pi}x + x^{2.5} + 1, \qquad 0 \le x \le 1 \tag{20}$$

With the subject boundary condition as $v(0)=1,$ and $v(1)=2$, and the exact solution for the problem given by $v(x) = x^{2.5} + 1$ when the value of $\beta = 1.50$.

Example 3

By considering the fractional two-point BVP below [23]

$$a\frac{\partial^\beta v(x)}{\partial x^\beta} + b\frac{\partial^2 v(x)}{\partial x^2} + cv(x) = 4\sqrt{\frac{x}{\pi}} + x^2 + 2, \qquad 0 \le x \le 1 \tag{21}$$

With the subject boundary condition as $v(0)=0,$ and $v(1)=1$, and the exact solution for the problem given by $v(x) = x^2$ when the value of $\beta = 1.50$.

The implementation for the numerical experiments consider the C programing language as a tools. Following to that, all the

Table 1. Numerical results on iterative methods for problem 1.

M	Method	$\beta=1.25$			$\beta=1.50$			$\beta=1.75$		
		K	Time	Max Error	K	Time	Max Error	K	Time	Max Error
128	FSSOR	751	0.10	2.1230e-02	769	0.13	1.3915e-05	1130	0.12	1.7118e-02
	HSSOR	385	0.02	2.1242e-02	320	0.01	1.3887e-05	385	0.01	1.7188e-02
	HS4EGSOR	132	0.01	2.1242e-02	114	0.01	1.3889e-05	125	0.01	1.7188e-02
256	FSSOR	1483	0.78	2.1228e-02	2051	0.77	1.3924e-05	3547	1.25	1.7081e-02
	HSSOR	765	0.08	2.1230e-02	769	0.09	1.3915e-05	1130	0.10	1.7118e-02
	HS4EGSOR	264	0.02	2.1230e-02	239	0.03	1.3917e-05	285	0.04	1.7118e-02
512	FSSOR	2975	5.62	2.1229e-02	5603	10.68	1.3912e-05	11600	15.90	1.7063e-02
	HSSOR	1522	0.83	2.1228e-02	2130	1.14	1.3922e-05	3525	1.88	1.7082e-02
	HS4EGSOR	512	0.20	2.1228e-02	551	0.19	1.3929e-05	691	0.25	1.7082e-02
1024	FSSOR	6020	33.26	2.1230e-02	15229	58.89	1.3862e-05	11600	199.24	1.7054e-02
	HSSOR	2975	6.25	2.1229e-02	5603	11.70	1.3912e-05	5700	24.29	1.7063e-02
	HS4EGSOR	1005	1.34	2.1229e-02	1309	1.77	1.3933e-05	1883	2.49	1.7063e-02
2048	FSSOR	11785	439.15	2.1230e-02	41071	1281.11	1.3708e-05	123730	1717.04	1.7048e-2
	HSSOR	6020	49.89	2.1230e-02	15229	125.68	1.3862e-05	38179	313.63	1.7054e-02
	HS4EGSOR	1973	10.25	2.1230e-02	3189	16.57	1.3928e-05	5465	28.20	1.7054e-02

Table 2. Numerical results on iterative methods for problem 2.

M	Method	$\beta=1.25$			$\beta=1.50$			$\beta=1.75$		
		K	Time	Max Error	K	Time	Max Error	K	Time	Max Error
128	FSSOR	759	0.02	3.2817e-05	769	0.04	8.8991e-04	1110	0.03	3.2013e-02
	HSSOR	382	0.01	3.1865e-02	320	0.01	1.7051e-03	385	0.01	3.2604e-02
	HS4EGSOR	129	0.01	3.1865e-02	112	0.01	1.7051e-03	125	0.01	3.2604e-02
256	FSSOR	1493	0.16	3.3317e-02	2039	0.24	4.6070e-04	3384	0.40	3.1690e-02
	HSSOR	741	0.03	3.2822e-02	769	0.05	8.8708e-04	1110	0.05	3.2010e-02
	HS4EGSOR	259	0.02	3.2822e-02	239	0.02	8.8708e-04	281	0.03	3.2010e-02
512	FSSOR	2826	1.25	3.3570e-02	5478	2.39	2.4094e-04	11330	4.93	3.1521e-02
	HSSOR	1493	0.29	3.3317e-02	2039	0.37	4.6019e-04	3384	0.60	3.1690e-02
	HS4EGSOR	492	0.09	3.3317e-02	541	0.10	4.6019e-04	693	0.15	3.1690e-02
1024	FSSOR	5813	9.88	3.3699e-02	14856	25.44	1.2919e-04	37258	63.29	3.1433e-02
	HSSOR	2826	1.91	3.3570e-02	5478	3.61	2.4085e-04	11330	7.51	3.1521e-02
	HS4EGSOR	1004	0.70	3.3570e-02	1283	0.90	2.4087e-04	1845	1.27	3.1521e-02
2048	FSSOR	11427	77.53	3.3764e-02	40209	271.72	7.2583e-05	121355	820.21	3.1387e-02
	HSSOR	5806	15.14	3.3699e-02	14856	38.43	1.2917e-04	37258	96.54	3.1433e-02
	HS4EGSOR	1975	5.30	3.3699e-02	3121	8.34	1.2924e-04	5349	14.32	3.1433e-02

results of numerical experiments have been recorded based on the iterative methods which are FSSOR, HSSOR and 4HSEGSOR methods in Tables 1, 2, and 3 with three different values of β as mentioned in early section. For the grid sizes have used at five different values where the values of m = 128, 256, 512, 1024, and 2048.

5. Discussions of result

Through numerical experiments results from Tables 1, 2, and 3 by imposing the comparison between HSSOR and 4HSEGSOR iterative methods with FSSOR method react as control method as discuss in Section 1 with three different values of parameter $\beta=1.25,\ 1.50,\ \text{and}\ 1.75$, it is conspicuously that number of iterations at Table 1 for HSSOR and 4HSEGSOR iterative method have declined. The result showed the number of iterations when the parameter set to $\beta=1.50$, at size 128 declined from 769 for FSOR to 320 for HSSOR. Again, the number of iterations declined from 320 to 114 for 4HSEGSOR. It's the same situation for another size the number of iteration has declined. To show more clearly, the percentage of number iterations declined approximately by 82.20% –83.31%, 85.18% – 92.24%, and 83.77% – 95.58% which corresponds to the HSSOR iterative method. For execution time, the result showed 4HSEGSOR method reduce the computational complexity. The execution time when the

Table 3. numerical results on iterative methods for problem 3.

M	Method	$\beta = 1.25$			$\beta = 1.50$			$\beta = 1.75$		
		K	Time	Max Error	K	Time	Max Error	K	Time	Max Error
128	FSSOR	712	0.04	2.1230e-02	768	0.07	1.3915e-05	1031	0.06	1.7118e-02
	HSSOR	385	0.01	2.1242e-02	319	0.01	1.3889e-05	378	0.01	1.7188e-02
	HS4EGSOR	126	0.00	2.1242e-02	107	0.00	1.3888e-05	115	0.00	1.7188e-02
256	FSSOR	1397	0.32	2.1228e-02	1988	0.51	1.3926e-05	3272	0.72	1.7081e-02
	HSSOR	712	0.02	2.1230e-02	768	0.06	1.3915e-05	1031	0.04	1.7118e-02
	HS4EGSOR	243	0.02	2.1230e-02	218	0.02	1.3916e-05	247	0.02	1.7118e-02
512	FSSOR	2789	2.44	2.1229e-02	5128	4.34	1.3919e-05	10600	12.24	1.7063e-02
	HSSOR	1397	0.17	2.1228e-02	1988	0.24	1.3926e-05	3272	0.39	1.7082e-02
	HS4EGSOR	473	0.10	2.1228e-02	474	0.10	1.3931e-05	578	0.11	1.7082e-02
1024	FSSOR	5489	19.7	2.1230e-02	13970	54.84	1.3863e-05	34573	136.42	1.7054e-02
	HSSOR	2789	1.24	2.1229e-02	7230	3.18	1.3899e-05	11331	4.95	1.7063e-02
	HS4EGSOR	910	0.66	2.1230e-02	1097	0.79	1.3937e-05	1563	1.19	1.7063e-02
2048	FSSOR	10845	165.55	2.1230e-02	37307	598.82	1.3708e-05	111085	1531.67	1.7048e-02
	HSSOR	5489	9.40	2.1230e-02	13970	23.85	1.3863e-05	34573	59.15	1.7054e-02
	HS4EGSOR	1892	5.28	2.1230e-02	2643	7.28	1.3931e-05	4729	13.02	1.7054e-02

parameter set to $\beta = 1.50$, a size 128 declined from 0.13 seconds for FSOR to 0.01 seconds for HSSOR. But, the number of iterations remain same from 0.01 seconds to 0.01 for 4HSEGSOR. It's the same situation for another size the execution time has reduce. To show more clearly, the percentage of execution time reduced about 90.00% – 97.67%, 92.31% – 98.71%, and 91.67% –98.75% corresponds to the HSSOR method. From the elucidating result for Table 1, the effectiveness 4HSEGSOR can be conform better compare to HSSOR.

In fact, Table 2 show that the numerical experiments for number of iterations HSSOR and 4HSEGSOR iterative method have declined. However, the result showed the number of iterations 4HSEGSOR drastically declined compare with HSSOR. It can be show when the parameter set to $\beta = 1.50$, the number of iteration declined from 5478 for FSOR to 541 for 4HSEGSOR meanwhile for HSSOR just to 2039 from 5478. It's the same situation for another size the number of iteration has drastically declined. To show more clearly, the percentage of number iterations declined approximately by 82.73%–83.00%, 85.44–92.24% and 88.74%–95.60% respectively as compared with the HSSOR method. Also for execution time, the result showed 4HSEGSOR method reduce the computational complexity. The execution time at size 2048 declined from 77.53 seconds for FSOR to 15.14 seconds for HSSOR. Again, the execution time declined from 15.14 seconds to 5.30 seconds for 4HSEGSOR. It's the same situation for another size the execution time has reduce. To show more clearly, the percentage of execution time reduced about 50.00%–93.16%, 75.00%–96.93%, and 66.67%–98.25% respectively than the HSSOR method. From the elucidating result for Table 2, the effectiveness 4HSEGSOR can be conform more better compare to HSSOR.

Lastly, from the numerical results in Table 3 show that the number of iterations for the 4HSEGSOR iterative method have declined. The result showed the number of iterations at size 512 declined from 2789 for FSOR to 1397 for HSSOR. Again, the number of iterations declined from 1937 to 473 for 4HSEGSOR. It's the same situation for another size the number of iteration has declined. To show more clearly, the percentage of number iterations declined approximately by 82.30%–83.42%, 86.07%–92.92% and 88.85%–95.74% respectively as compared with the HSSOR method. Also, implementations of computational time for the result showed 4HSEGSOR method reduce the computational complexity. The execution time at size 512 declined from 2.44 seconds for FSOR to 0.17 seconds for HSSOR. Again, the number of iterations declined from 0.17 seconds to 0.10 for 4HSEGSOR. It's the same situation for another size the execution time has reduce. To show more clearly, the percentage of execution time reduced about 93.75% - 100.00%, 96.08%–100.00% and 97.22%–100.00% respectively than the HSSOR method.

6. Conclusion

For the conclusion, this study success the numerical experiments of the application 4HSEGSOR iteration to solve the linear system generated by the steady-state problems which is two-point FBVPs. The family FD scheme and Caputo's fractional derivative operator was applied to construct the linear system. From the linear system, the iterative methods success to applied to get the approximation solution. From the numerical results recorded in Tables 1, 2, and 3 by imposing the comparison between HSSOR and HS4EGSOR iterative methods with FSSOR method react as control method, clearly the results promising two improvements in the number of iterations (K) and execution time (s). According to the numerical results are recorded, it can be showed that the HS4EGSOR method is superior and it has required a much lesser number of iterations and computational time to solve the problems.

Acknowledgment

The authors acknowledge the research grant scheme (GUG0227-1/2018) from Universiti Malaysia Sabah, Malaysia for the completion of this article.

References

[1] C. Kou, and X. Zhang, "Solutions of the fractional differential equations with constant coefficients." IEEE. Eighth ACIS International Conference on Vol. 3, pp. 1056-1059, 2007.

[2] D. Matignon, "Stability results for fractional differential equations with applications to control processing." In Comp eng in systems appl., Vol. 2, pp. 963-968, 1996.

[3] G. J. Fix, and J. P. Roof, "Least squares finite-element solution of a fractional order two-point boundary value problem." Computers & Mathematics with Applications., 48(7-8), 1017-1033, 2004.

[4] X. Li, H. Li, and B. Wu, "A new numerical method for variable order fractional functional differential equations." Applied Mathematics Letters., 68, 80-86, 2017.

[5] Z. Odibat, and S. Momani, "Modified homotopy perturbation method: application to quadratic Riccati differential equation of fractional order." Chaos, Solitons & Fractals., 36(1), 167-174, 2008.

[6] K. Diethelm, & G. Walz, "Numerical solution of fractional order differential equations by extrapolation." *Numerical Algorithms.*, *16*(3-4), 231-253, 1997.

[7] A. Sunarto, J. Sulaiman, and A.Saudi, "Application of The Full-Sweep AOR Iteration Concept for Space-Fractional Diffusion Equation." IOP Publishing, In Journal of Physics., 710(1), 012019, 2016.

[8] A. Sunarto, J. Sulaiman, and A.Saudi, "SOR method for implicit finite difference solution of time-fractional diffusion equation." In Proceedings of the 11th Seminar on Science and Technology., pp. 132-139, 2013.

[9] S. Alkan, K. Yildirim, and A. Secer, "An efficient algorithm for solving fractional differential equations with boundary conditions." Open Physics., 14(1), 6-14, 2016.

[10] Young, D.M., 1971. Iterative solution of large Linear Systems, Academic Press, London, England, Pages:570.

[11] W. Hackbusch, Iterative Solution of Large Sparse Systems of Equations, Springer-Verlag, New York, 1995.

[12] R. Rahman, N. A. M. Ali, J. Sulaiman, and F. A. Muhiddin, "Caputo's finite difference solution of fractional two-point boundary value problems using SOR iteration." In American Institute of Physics Conference Series, 2013(2), 2018.

[13] R. Rahman, N. A. M. Ali, J. Sulaiman, and F. A. Muhiddin, "Caputo's Finite Difference Solution of Fractional Two-Point BVPs Using AGE Iteration." In Journal of Physics: Conference Series, IOP Publishing, vol. 1123, no. 1, p. 012044. 2018.

[14] I. Podlubny, "Fractional differential equations: an introduction to fractional derivatives, fractional differential equations, to methods of their solution and some of their applications" Academic press, New York, USA., Pages 340, 1999b.

[15] B. R. Sontakke, and A. S. Shaikh, "Properties of Caputo operator and its applications to linear fractional differential equations." International Journal of Engineering Research and Applications 5, 5(22-29), 2015.

[16] Diethelm, K., & Ford, N. J. Analysis of fractional differential equations. Journal of Mathematical Analysis and Applications, 265(2), 229-248, 2002.

[17] A. Sunarto, J. Sulaiman, and A. Saudi, "August. Solving the time fractional diffusion equations by the Half-Sweep SOR iterative method." IEEE. In Advanced Informatics: Concept, Theory and Application (ICAICTA), International Conference of pp. 272-277, 2014.

[18] D. J. Evans, "Group explicit iterative methods for solving large linear systems." International Journal of Computer Mathematics., 17(1), 81-108, 1985.

[19] A. Saudi, and J. Sulaiman, "Block Iterative Method for Robot Path Planning." In The 2nd Seminar on Engineering and Information Technology (SEIT2009), Kota Kinabalu, Malaysia. 2009.

[20] A. Saudi, and J. Sulaiman, "Robot path planning via EGSOR iterative method using Nine-Point Laplacian." In 2012 Third International Conference on Intelligent Systems Modelling and Simulation, pp. 61-66. IEEE, 2012.

[21] D. J. Evans, and A. R. Abdullah, "A new explicit method for the diffusion-convention equation." Computers & mathematics with applications., 11(1-3), 145-154, 1985.

[22] A. El-Ajou, O. A. Arqub, and S. Momani, "Solving fractional two-point boundary value problems using continuous analytic method." Ain Shams Engineering Journal., 4(3), 539-547, 2013.

[23] A. Pedas, and E. Tamme, "Piecewise polynomial collocation for linear boundary value problems of fractional differential equations." Journal of Computational and Applied Mathematics., 236(13), 3349-3359, 2012.

[24] H. Azizi, "Chebyshev Finite Difference Method for Fractional Boundary Value Problems." Journal of Mathematical Extension., 9, 57-71, 2015.

Advances in Science, Technology and Engineering Systems Journal Vol. 4, No. 2, 244-250 (2019)

www.astesj.com

ASTESJ

ISSN: 2415-6698

Designing IT Blue Print Academic System on Higher Education with Togaf

Holilah[1], Abba Suganda Girsang[1,*], Melva Hermayanty Saragih [2]

[1]*Department of Computer Science, BINUS Graduate Program-Master of Computer Science, Bina Nusantara University, Jakarta,11480, Indonesia*

[2]*Management Department, BINUS Business School Undergraduate Program, Bina Nusantara University, Jakarta, 11480 Indonesia*

A R T I C L E I N F O

Article history:
Received: 16 January, 2019
Accepted: 08 March, 2019
Online: 29 March, 2019

Keywords :
College
Blueprint
Togaf Adm
Enterprise architecture

A B S T R A C T

STIE XYZ is one of the universities of economics that has not been optimal in the use of information technology. IT implementation is applied when there are urgent and sudden needs. So it is not planned carefully according to the development needs of this educational institution. Therefore many patchy applications are created. As the consequence, it affects the quality of service for all stake holder include students, lectures and all staffs. This study aims to provide solutions to existing problems by designing an output or blueprint that can be used as a foundation for the development of a better academic system in support of business process STIE XYZ. The blueprint is designed by using framework TOGAF and ADM framework. The solution is built by creating artifacts of each core architecture in TOGAF (business, data, application and technology architecture). This research focuses on new admissions services, study plan cards, lectures, study cards, graduation, and finance. The results show some recommendations to build based on each architecture.

1. Introduction

The development of information technology is increasingly fast, of course, can affect various aspects and elements, includes education sector. STIE XYZ is one of the universities that applies education in the field of economics. Currently this university does not use the information technology optimally. The non-optimal causes a variety of important problems. Some of new student registration processes are still manual. Desktop-based applications and the common constraints that students have to queue to register the courses and is validated manually by each student's academic supervisor, which totally usually takes 10 minutes / student. The card exam which is the required document to take the exam has to be validated manually to the financial system. And many things which disruptive the teaching and learning process. In short, the use of information technology is still very minimal and affects the bad service for all stakeholders. However, there are several important things that encourage information technology needs in organizations, such as decision-making that is not based on information, available information is not relevant, existing information is not utilized by management, information is not timely, too much inaccurate information, the redundant data, and the existence of data that is not flexible.

During this time the university tried to solve problems one by one if they appeared. However this approach causes the system not being integrated. Therefore, solving with comprehensive system should be performed in this school. The restoration system is started blue print IT in this university which cover all of the system such as business architecture, data architecture, application architecture, technology architecture. The IT blueprint provides current and desired explanations and documentation, and will describe the basic architecture and target architecture so that it will create harmony between business strategy and information technology [1] [2] [3]. The main contribution of this research is to build IT blueprint in university XYZ to improve the quality system process using framework TOGAF

2. Related Work

Many frameworks are created by the different purpose. Some researchers uses the Zachman, TOGAF, FEA, and Gartner for design blueprint IT [4] [5]. Girsang et al use ITIL for improve system service on financial company [6] and software company [7], also uses COBIT for maturity in government office [8] and so forth. The method used in this study is the Open Group Architecture Framework (TOGAF), a framework developed by the Open Group Architecture that was first introduced in 1995, and used to develop enterprise architecture with detailed methods and tools to

*Abba Suganda Girsang, Email: gandagirsang@yahoo.com

https://dx.doi.org/10.25046/aj040232

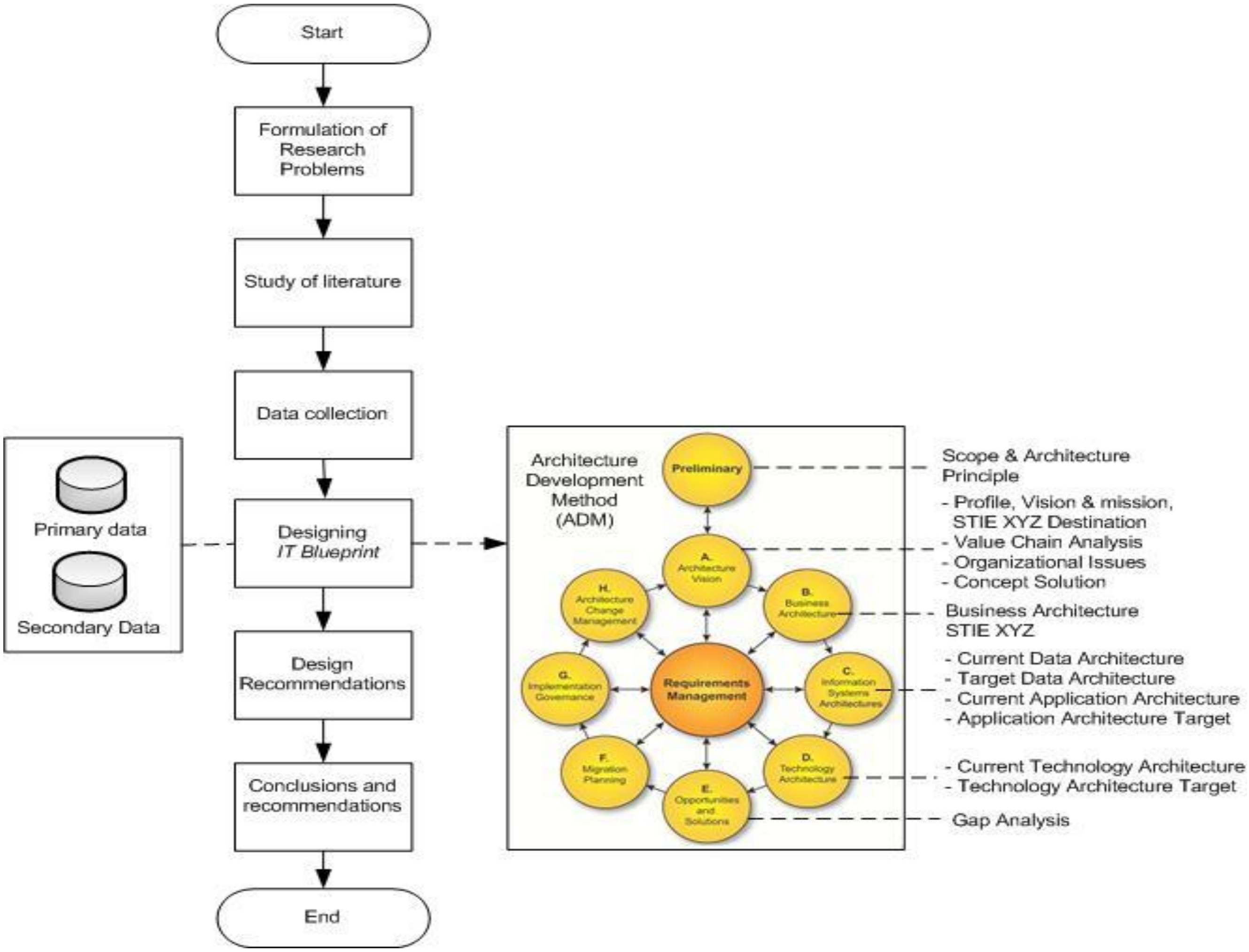

Figure 1: Conceptual Model

implement it that distinguishes. Another enterprise architecture framework and the advantages of using the TOGAF Framework are because of its flexible and Open Source nature [9] [10] [11]. TOGAF has some advantages. TOGAF provides detailed methods on how to build, manage and implement architecture and enterprise information systems called the Architectural Development Method (ADM) [9]. Architectural Development Method (ADM) is a generic method that contains a series of activities used in modeling the development of corporate architecture. This method can also be used as a guide or tool for planning, designing, developing and implementing information system architectures for organizations [12] [13].

3. Research Method

The method used in this research uses TOGAF framework to create a blueprint design of academic system on STIE XYZ. Figure 1 shows the conceptual model of the research phase.

Explanation of the figure 1 concept model is describe as follows.
1. Formulation of research problems, which generate research questions about the problems studied.

2. Study the literature by studying various documents, theories or references related to the TOGAF framework. Study the literature either online or done through books, journals and previous research results.

3. Data collection is the stage of collecting data required both primary and secondary data.

4. Designing IT Blueprint is an activity to perform data processing to compose the vision of architecture, business architecture, information system and technology as well as opportunities and solutions using TOGAF ADM framework.

5. Furthermore provide recommendations in the form of blueprint system design as a solution of some problems that exist in STIE XYZ.

6. And the last stage of research methodology in this study is the conclusion and suggestions from the research that has been done.

4. Results And Analysis

The scope of this study does not take all phases in TOGAF ADM, only Preliminary phase, Architecture Vision phase, Business Architecture phase, Information Architecture phase, Phase Technology Architecture, Opportunities and Solution phase will be discussed in this research. The steps of this study can be seen in Figure 2 of the following TOGAF ADM.

4.1. Preliminary Phase

Preliminary phase is the preparation step in the design of enterprise architecture. This stage defines the enterprise architecture to be created such as the determination of the framework and methodology used, the scope of enterprise and the general architectural principles used

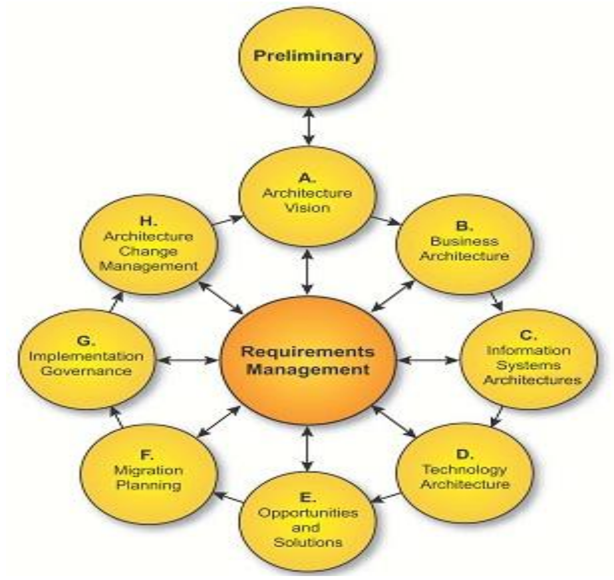

Figure 2: TOGAF ADM Cycle

Determination of Framework and Methodology. In the design of enterprise architecture, TOGAF ADM divides enterprise architecture into 3 parts of business architecture, information system architecture (consists data architecture and application architecture), and technology architecture [14].

Enterprise Scope. The design of STIE XYZ blueprint refers to several business activities including:

a. Academic Activities, is the main activity in STIE XYZ including new admissions, filling of study plan cards, lecture process, process of study cards, graduation and alumni, and financial administration services
b. Non-Academic Activities, including tax training, English training and computer training for students as well as a place for lecturers to update their knowledge.
c. Supporting Activities, is a supporting activity on the implementation of academic and non academic activities. Supporting activities include human resources management, quality assurance, research and community service, facilities and infrastructure management, cooperation management.

General Principles of Architecture. The principles of general architecture are the principles derived from the TOGAF framework and confirmed at the management level to obtain principles relevant to STIE XYZ. The STYLE XYZ architecture principles are as follows [12] :

a. The Principle of Business Architecture is the guarantee of business continuity and the system can keep running despite interruption, in this case demands the system to always operate so that the application and infrastructure must have high level of availability.
b. Architecture Principle Data, data is a valuable asset for the enterprise and needs to be well managed, and can assist in decision making process. Like any other asset, data must be well managed. Data management is needed to ensure that data location is known, data accuracy is reliable, and can be accessed easily, and data security must be protected from unauthorized access, in accordance with standardized processing and data security.
c. The Principles of Application Architecture is that the application must be easy to use and can run on multiple platforms. Existing or established applications must have a common look and feel and take into account the ergonomic needs. Dependency on the platform will cause great loss and effort to repair in case of failure.
d. Principle of Architecture Technology, is the interoperability that hardware and software must conform to established standards and support interoperability for data, applications, and technology. In addition to interoperability, technology must also ensure the availability of systems and data so that it can serve the needs, and utilization of existing infrastructure can be used optimally.

4.2. Phase Architecture Vision

The resulting vision architecture documents include Stakeholder Map Matrix, Value Chain Diagram, Solution Concept Diagram, with the following details [15] .

Stakeholder Map Matrix. Table 1 shows the stakeholder matrix from the observation and analysis of the organizational structure of the task and authority of each section in STIE XYZ [15] .

Table 1: Stakeholder Map Matrix

Stakeholder	Involvement	Concerns
Vice Chairman I	Have a high level of policy / direction related to vision and mission, and how to translate it into an effective business process and IT architecture and promote performance.	-Document -Related Policy
Study program	The main key in the management and preparation of lecture schedules, as well as until the release / graduation	-Document Policy of Study Program
Student Affairs and Academic Section (BAAK)	Assisting academic management and implementation, academic services.	- Academic calendar - Academic rules and policies
Academic Information System Section (SIAK)	Assisting the provision and management of information systems, databases and recapitulation	- Academic information systems, databases, data recaps and information
Finance Administration	The main key in the management of financial administration	- Financial documents - Financial policy
General and Household Administration Section	Assist the management of Finance administration and related management of facilities and infrastructure.	-Document of Adm. General -Facilities and infrastructure

Value Chain Diagram. One of the core architecture TOGAF is business architecture. Value Chain is a good tool to see the comprehensive program of one company. Taylor in his research

[16] uses the value chain to enhance quality the supply chain management (SCM). Porter (1985) described the value chain for buyer is a starting point for understanding what is valuable to a customer is a starting point for understanding what is valuable to a customer. It can be described as a series of actions a buyer (customers) [17].The value chain is controlled by vision mission of a company and consists some program to achieve the target of vision mission. This diagram shows a series of main activities and activities that STIE XYZ undertakes to achieve the organization's vision and mission, shown in Figure 3 [18].

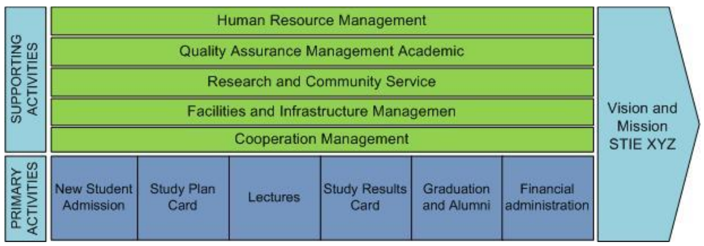

Figure 3: Value Chain STIE XYZ

4.3. Business Architecture Phase

The resulting artifacts include functional decomposition diagrams, Business Interaction Matrix, Organization / Actor Catalog, and business process diagrams described as follows [1] :

Functional Decomposition Diagram . Functional decomposition diagrams describe the organizational hierarchy based on the main activity, where each business function consists of smaller main operational activities. The functional decomposition diagram is shown in Figure 4 [18]

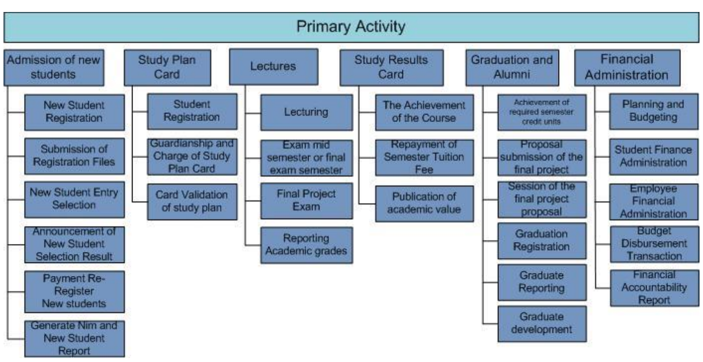

Figure 4: Functional decomposition of the main activity diagram

Business Interaction Matrix. The purpose of this matrix is to describe the interaction relationships between organizations and business functions throughout the organization. Understanding the business interactions of an organization is important because it helps to know the value chains throughout the organization. Table 2 describes the Business Interaction Matrix [1].

Business Process Diagrams. At this stage, the analysis of business functions in STIE XYZ, with observations and interviews with the new student admissions department, academic and financial departments, is processed by using a notation of Business Process Modeling Notation (BPMN) [18]. The business processes modeled in this study include business processes in the new admission process, the process of filling out study plan cards and printing study results.

Table 2: Business Interaction Matrix

Consuming Business Service	Financial Services	New Admissions Service	Study Plan Card Service	Lecture Service	Study card service	Graduation Service
Financial Services		financial information of the new academic year	Enable KRS access that has re-registered	student data information is active, non active and leave	Publication of study result card	
New Admissions Service	Data of new students in the new academic					
Study Plan Card Service	Provide active student data				subject data already in contract	
Lecture Service	Provide lecturer attendance data					
Study card service			Data on the value of the courses in the student contract			Data of academic value of courses that have been taken
Graduatio\n Service	Data of students who have passed the					

- New Student Admission Business Process, consisting of 8 business processes.
- Plan for Business Card Process Filling Process, which consists of 6 business processes.
- The Study Results of Print Business Process Cards, consisting of 4 business processes.

Because of the limited space available, there is only one example of business process modeling manifested in every part of STIE XYZ from all business processes that have been successfully modeled as shown in Figure 5 of the new student admissions business process.

4.4. Information Architecture Phase

Information system architecture stage aims to look at information systems that have been applied in STIE XYZ and information systems expected to the fore. In the information system architecture there are two stages dianataranya data architecture and application architecture.

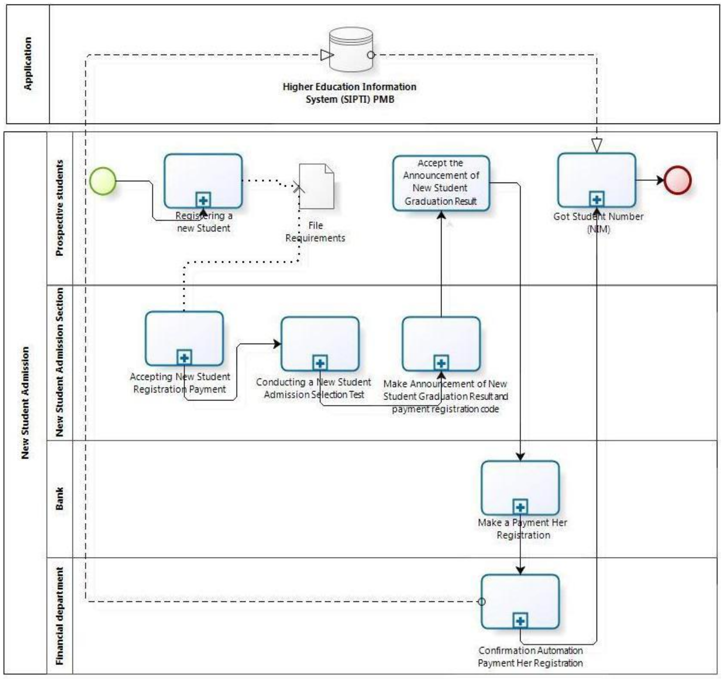

Figure 5: Business Process of New Student Admission

Architecture Currently. To find out the current data architecture and application architecture needs to identify the data requirement for STIE XYZ business activity and application inventory through interview and inventory result then stored in Information Resource Catalog (IRC) which contains description of application, manager and user of application. Here Matrix application that shows the quality of application services in STIE XYZ. It is used to identify non-functional requirements, this matrix is denoted by CRUD. CRUD consists of four roles: Create, Read, Update, Delete. Application Matrix can be seen in table 3 [21].

Target Architecture. The target archetype is done by creating a concept model through the class diagram of the data that has been identified in the previous stage, the data entity is a class on the class diagram [22] .

4.5. Phase of technology architecture.

The technology architecture stage is the stage in documenting the basic organization of information technology systems that include hardware, software, and communication technology, and identification of current technology and the creation of target architectures needed by STIE XYZ [23].

Current Architecture. Hardware identification includes 50 computer program units, 9 laptop units, 7 multifunction copier units, 4 inkjet printer units, 2 laserjet printer units, 3 switch units, 1 router unit, 3 access point units, 1 scanner unit, 1 network attach unit storage (NAS), 6 units of external hard drives. While identification for existing software is a Windows-based operating system, for database management there are Microsoft Excel, Microsoft Access and DBMS / DBF, and general-purpose applications.

Table 3: Application Matrix

Module / DB-Entity	New Admissions	Data of Prospective Students	Lecture Service	Card Services	Graduation Service	Financial Administration Services
Campus Information	CRUD	R	R	R	R	R
Data of Prospective Students	CRUD					R
Student Data		R		R		R
Lecturer Data		CRUD	RUD	R		
Course Data		CRUD		R		RU
Course Values Data		R		CRUD		RU
Graduate Data					CCRUD	R
Financial Data	R	R	R	R		CRUD

Target Architecture. This stage is the mapping phase between the systems used with the proposed technology. The purpose of this mapping is to see the relationship between recommended applications and the architecture used. Figure 6 shows that component interchange and user interfaces will be mapped to web portals in the application landscape, data management components will be mapped to the DBMS in the application landscape, Location & Directory components will be mapped to profile management users in landscape applications, business applications will be mapped to systems found in the application landscape [24] .

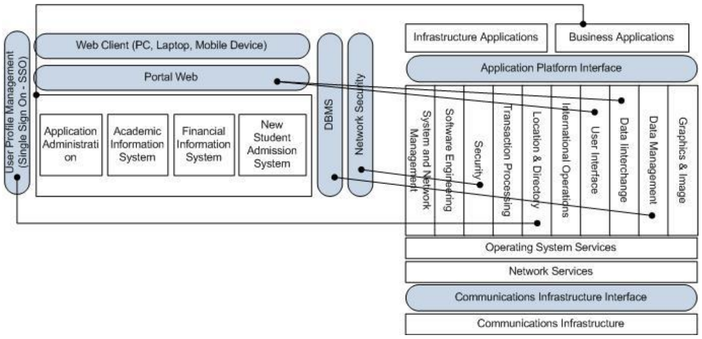

Figure 6: Application Perspective

This stage describes the location where the application is implemented and identifies the technology and application where the business interaction occurs. This diagram also shows the location of the environment for applications and data to support STIE XYZ business activities. Here figure 7 Environments and Location Diagram in STIE XYZ.

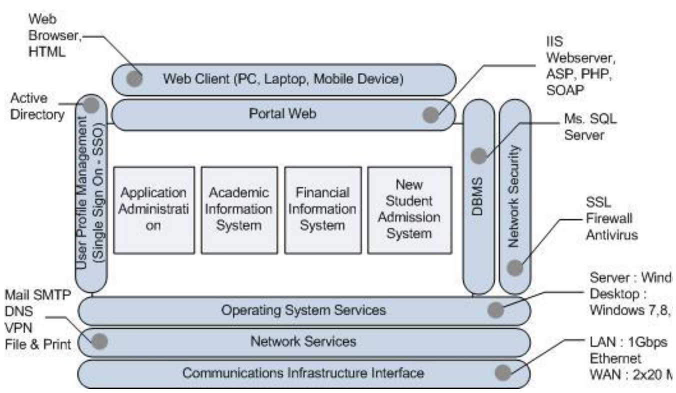

Figure 7: Environments and Location Diagram

3.6 *Opportunities and Solution*

his stage aims to perform gap analysis that occurs between the current condition and the target conditions of information system architecture and technology architecture. The result of this stage is the application that needs to be integrated the module (partially replaced), replaced (replaced), the application needs to be added function (upgrade). Application analysis gap can be seen in table 4.

Table 4: Application Gap Analysis

Target Application	**Current Application**			
	PMB SIPTI	**Academic SIPTI**	**Finance SIPTI**	**Payroll Application**
New Admissions System	R			
Academic Information System		U		
Financial Information System			U	R

5. Conclusion

Based on the results and discussion, it can be concluded from this study that: 1) this study focuses on modeling corporate architecture in business activities at STIE XYZ in the scope of business modeling, information and technology; 2) Some latest information technology architecture in STIE XYZ can still be used but need to improve to optimize academic system services. 3) blueprint design using TOGAF ADM has been able to provide integrated information technology and recommendations to optimize services at STIE XYZ which focuses on new student admission services, study plan cards, lectures, study cards, graduation, and finance.

In order for the design of this IT Blueprint to be implemented properly, it is deemed necessary to develop human resources for managing information technology at STIE XYZ.

References

[1] Monalita Rahayu, Murahartawaty, and R. Hanafi," Designing Business Architecture for academic function at institute XYZ Using TOGAF ADM Framework Case Study of Academic Information System (SIAKAD)", *Journal of Systems & Industrial Engineering*,Vols.3, No.1, pp.33-39, January 2016.

[2] F. Bustamante, W. Fuertes, P. Diaz, and T. Toulqueridis, "Methodology for Management of Information Security in In-dustrial Control Systems: A Proof of Concept aligned with Enterprise Objectives.," 2017.

[3] E. Putro, A. N. Hidayanto, H. Prabowo, and others, "The alignment factors of business-IT on enterprise architecture: A systematic literature review," in *2017 International Conference on Information Management and Technology (ICIMTech)*, 2017, pp. 215-219

[4] Setiawan, E. B. "Selection of EA Framework", *2009 SNATI*, Yogyakarta, Indonesia, June, 2009, pp. BB115.

[5] E. Gunawan and I. Sutedja, "Using Enterprise Architecture with the Open Group Architecture Forum to Design Information Technology Plan Gap Analysis at Bank Pengkreditan Rakyat (BPR)," in *2018 International Conference on Information Management and Technology (ICIMTech)*, 2018, pp. 388–393.

[6] D. Handoko and A. S. Girsang, "Service Desk Implementation with Information Technology Infrastructure Library Framework (Study Case Financial Company)," in *Journal of Physics: Conference Series*, 2018, vol. 1090, no. 1, p. 12059.

[7] A. S. Girsang, Y. Kuncoro, M. H. Saragih, and A. N. Fajar, "Implementation helpdesk system using information technology infrastructure library framework on software company," in *IOP Conference Series: Materials Science and Engineering*, 2018, vol. 420, no. 1, p. 12106

[8] A. Ekanata and A. S. Girsang, "Assessment of capability level and IT governance improvement based on COBIT and ITIL framework at communication center ministry of foreign affairs," in *2017 International Conference on ICT for Smart Society, ICISS 2017*, 2018, vol. 2018-Janua.

[9] The Open Group, "*TOGAF Version 9 The Open Group Architecture Framework (TOGAF)*", The Open Group, 2009.

[10] Rahman Rosyidi, Purwadi, "Designing Architecture Development of Academic Information System Using TOGAF (Case Study: STIMIK AMIKOM Purwakerto)", *Journal of Telematics*, Vols. 7, No. 1, pp. 50-65, February 2014

[11] Yunis Roni, K. S. "Designing Enterprise Architecture Model with TOGAF Architecture Development Method", *2009 SNATI*, Yogyakarta, Indonesia, pp. E25, June 2009**.**

[12] Yunis Roni, Kridanto S., Erwin S.P., "Development of Enterprise Architecture Model for Higher Education", *JUTI*, Vol. 8, No. 1, pp. 9-18, January 2010.

[13] David T. Bourgeois, P., "Information Systems for Business and Beyond Creative Commons Attribution*", Creative Commons Attribution, Taylor Foundation*, February 2014.

[14] Saputro, Setyo Wahyu., "Designing Architecture Management System Research Activities and Community Service on STMIK Banjarbaru Using TOGAF Framework", *Journal of Bianglala Informatics*, Vol. 4, No. 1, pp. 2338-9761, March 2016.

[15] Anggrainingsih Rini, Abdul Aziz, Umi Salamah, and Sari Widya Sihwi, "Architectural Preparation Vision and Business Architecture As Stages of Enterprise Architecture Design University of Sebelas Maret UNS With TOGAF Framework", *Jurnal ITSMART*, Vol. 2, No. 2, pp. 2301-7201, December 2013.

[16] D. H. Taylor, "Value chain analysis: an approach to supply chain improvement in agri-food chains," *Int. J. Phys. Distrib. Logist. Manag.*, vol. 35, no. 10, pp. 744–761, 2005.

[17] M. E. Porter, *Competitive advantage: Creating and sustaining superior performance*. simon and schuster, 2008.

[18] Hadi Widiyanto, Rosidi Abidarin, Lutfi Emha, "Analysis of Enterprise Architecture Modeling To Support Academic Information Systems With Togaf (The Open Group Architecture Framework) (Case Study AMIK AMIKOM Surakarta)", Duta.com, Vol. 5 No. 1, pp. 2086-9436, September 2013.

[19] Ginanjar, Andika Desta, Muraharwaty, Ridha Hanafi, "Design Of Data Architecture For Academic Functions at Institut XYZ Using TOGAF ADM Framework Case Study Academic Information System (SIAKAD)", e-proceeding of Engineering, Vol. 2, No. 2, pp. 5400-5407, August 2015.

[20] Ali Ramadhani, Moch.,"Modeling Business Process Academic System Using Approach Business Process Modeling Notation (BPMN) case study Institution of Higher Education XYZ", Journal of information, Vol. VII, No. 2, pp.84-93, November 2015.

[21] Suseno Endra, "Modeling of Enterprise Architecture Architecture Using TOGAF Method (Case Study of Nahdlatul Ulama University Cirebon)", Jurnal Cloud Information, Vol. 1, No.1, pp. 2527-5224.

[22] Eloranta, Lauri and kalio, Eero., "A Notation Evaluation of BPMN and UML Activity Diagrams", 2006.

[23] Minoli,D., "Enterprise architecture A to Z : frameworks, business process modeling, SOA, and infrastructure technology", CRC Press Taylor & Francis Group, 2008.

[24] Kasenda, M.G., Eko Nugroho, Selo Sulistyo, "Strategic Design of Information Technology in the Public Sector Using the Framework The Open Group Architecture Framework (TOGAF)", National Seminar on Indonesian Information System, September 2014.

Advances in Science, Technology and Engineering Systems Journal Vol. 4, No. 2, 251-259 (2019)

www.astesj.com

Special Issue on Recent Advances in Engineering Systems

ASTESJ

ISSN: 2415-6698

A New Model of Supplier's Selection for Sustainable Supply Chain Management

Oussama El Mariouli*, Abdellah Abouabdellah

Systems Engineering Laboratory, MOSIL, ENSA, University Ibn Tofail, Kenitra, Morocco

A R T I C L E I N F O

Article history:
Received: 17 December, 2018
Accepted: 04 March, 2019
Online: 03 April, 2019

Keywords:
Supply Chain
Criteria
Sustainable development
Supplier selection

A B S T R A C T

In the last years, industrial company began to understand the central role that plays sustainable supplier selection (SSS) process for obtaining a sustainable supply chain (SSC). This paper proposes a new multi-criterion decision-making (MCDM) model for managers, which makes it possible to select the best suppliers who respect the sustainable development (SD) concept for a SSC. We start our paper by selecting the most recent economic, environmental and social criterion used in researches. After, we develop a new model mathematic that take into consideration the SD criteria in sustainable supplier rank and selection. Finally, we present a case study for testing our model.

1. Introduction

Recently, most industrial companies adopt the strategy of integrating the SD policy into their supply chain (SC), from downstream (purchase) upstream (distribution) to remain competitive and open up to new international markets, this approach starts with the selection of suppliers who respect SD's dimensions: SSS is central to the management of an SSC [1,2].

The new strategic direction of companies towards the SD concept, has required new economic, environmental and social criteria instead of conventional criteria (quality, cost and lead time) in purchasing decisions, therefore the process of supplier selection is has become a complex and multi-criteria decision that depends on several qualitative and quantitative criteria.

In this paper, we develop a new multi-objective mathematical model that allows measuring the index of supplier's sustainability for chooses the best between them. Our research methodology is articulated around two phases of realization, which we will detail them below:

- The first phase is the identification of recent SD criteria used to measure supplier performance;
- Last Phase present the equation that measures and rank sustainable supplier performance.

2. Literature Review

This section has four subsections. The first part presents a brief overview of the SSC management. The second part presents work on selection criteria. The last part presents the different vendor selection models found in the literature search and the last section presents the methods and approaches used in ranking the best SS.

2.1. Sustainable supply chain management

In the last 10 years, the SSC has become an important topic in the businesses and academies [3]. The role of the SSCM is to manage flows, information and cooperation among organizations throughout the supply network, taking into account economic, environmental and social criteria [4].

2.2. Supplier selection criteria

In the literature, we noticed that the selection criteria of suppliers change with the globalization and the appearance of the new concept such as Just-a-temp.

The first selection criteria for suppliers were made by Dickson (1966); he conducted a survey of 274 Canadian and American companies that are members of the National Association of Purchasing Managers (NAMP), and identified 23 criteria used by companies in the 1960s to select their suppliers [5].

The study by Weber and al. (1991) showed that these criteria remained the same until the 1990s, but the importance and the coefficient relative to each of the criteria are changed [6].

The study by Larson (1993) showed that the quality and the total cost of the product purchased are the most important criteria in the selection of suppliers [7].

The study by Vonderembse and al. (1995) out of 268 US companies, NAPM member has defined 10 important criteria used

*Oussama El Mariouli, Email: oussama.el.mariouli@gmail.com

https://dx.doi.org/10.25046/aj040233

for the choice of suppliers; it has shown that these companies specify the performance and the quality of the product in the selection of the suppliers [8].

The study by Verma and al. (1998) on 323 US companies showed 4 criteria (quality, price, delay and flexibility) for the selection of suppliers [9].

The study by Katsikeas and al. (2004) out of 237 British companies showed that the choice of suppliers is based on 4 criteria (reliability of the delays, price competitiveness, service offered and technological capacity) [10].

The study by Aguezzoul and Ladet (2006) showed that the QCD triptych (quality, cost and delay) was the most used in the selection of suppliers [11].

The Baumann study (2011) defined 15 indicators to measure the sustainable development of the supply chain [12].

The study by Boukherroub and al (2013), inspired by Baumann (2011), defines 7 criteria for sustainable development because of their relevance in the scientific literature and international standards [13].

The study of Ouzlem and al. (2015) proposed a list formed by 8 main criteria and 31 ecological subscribers [14].

The study of Caron and al. (2016) identify 8 principles and 27 criteria of SD using in mineral exploration industry [15].

The study of Song and al. (2017) used 10 criteria to SSS for solar air-conditioner manufacturer [16].

The study of Vasiljević and all. (2018) proposed 20 criteria used to evaluate the supplier in automotive industry [17].

The study of Sureeyatanapas and al. (2018) proposed 39 supplier selection criteria [18]. The study of Memari and al. (2019) presented the top 10 economic, environmental and social criteria for SSS [19].

In the second section, we will give a new list of recent criteria used for the supplier selection in a context of sustainable development.

2.3. Selection of suppliers

Supplier selection is one of the most crucial decisions made by managers in organizations [20]. The decision has become multi-criteria and very complex, it depends on qualitative and quantitative factors at the same time. Several research and literature reviews [21-23, 11] presented different methods and approaches for help buyers make the decision to select the best supplier. The table (Table1) presents the different methods of selection and evaluation of suppliers found in the literature.

In the literature, we find several recent researches that study the problem of the selection of suppliers. We can notice that:

- Most of this research does not include the three sustainable development dimensions in the supplier selection process; it focused only on green supplier problem [24-30].
- Most methods developed are complex to use.
- AHP is the most used method in the literature, but this method has the disadvantage of uncertainty of judgment.

In this study, our model developed has as originality:

- Integration of SD criteria most used in literature and internationals standards in the supplier selection process.
- Simple to apply and can be used in any industrial enterprise.

Table 1: Methods of selection and evaluation of suppliers

<table>
<tr><th colspan="2">Supplier selection method</th><th>Disadvantage</th></tr>
<tr><td rowspan="4">Artificial intelligence</td><td>CBR (Case Based Reasoning system)</td><td rowspan="4">- The collection and processing of supplier data by experts take a lot of time.</td></tr>
<tr><td>ES (Expert System).</td></tr>
<tr><td>NN (Neural Network)</td></tr>
<tr><td>FST (Fuzzy Sets Theory)</td></tr>
<tr><td rowspan="2">Statistical / Probabilistic Models</td><td>CA (Cluster Analysis)</td><td rowspan="2">- Absence of optimal solution
- Difficulty of analysis
- Absence of the possibility of adding mathematical constraints in the model</td></tr>
<tr><td>FA (Factor Analysis)</td></tr>
<tr><td rowspan="9">Model of mathematical programming</td><td>DEA (Data Envelopment Analysis)</td><td rowspan="9">- Difficulty of dealing with subjective criteria
- Absence of optimal solution
- Difficulty analyzing the result obtained from the method</td></tr>
<tr><td>GP (Goal Programming) or multi-objective programming</td></tr>
<tr><td>MOP (Multi Objectifs Pprogramming)</td></tr>
<tr><td>AHP (Analytic Hierarchy Process)</td></tr>
<tr><td>FST (Fuzzy Sets Theory)</td></tr>
<tr><td>ANP (Analytic Network Process)</td></tr>
<tr><td>TOPSIS (Technique for the Order Performance by Similarity to Ideal Solution)</td></tr>
<tr><td>MAUT (Multiple Attribute Utility Theory)</td></tr>
<tr><td>TCO (Total Cost Ownership)</td></tr>
<tr><td>The categorical method</td><td>It relies on the experience and expertise of the buyer</td><td>- A subjective method
- Absence of the relative importance of each criterion</td></tr>
<tr><td>Hybrid models</td><td>It represents the combination of two or more methods of evaluation</td><td>- Computational complexity</td></tr>
</table>

3. Methodology

3.1. Determining criteria for measuring sustainable supplier performance

This paper aims to provide a broad synthetic analysis of an area that has experienced rapid growth in knowledge [40]. The data collected for this paper will help to identify the SD criteria that are cited in the various published research to define a useful theoretical overview to better understand SS phenomena.

The literature review follows a systematic methodology (Briner and Denyer 2012) to reduce the number of articles published and focuses on leading journals that publish SS research [41]. In our initial library research on relevant documents. we did an analysis of the different databases "ScienceDirect, Springer, Emerald, Taylor Francis, Inderscience, GoogleShooler ..." by the combination of keywords "procurement, supply chain, sustainable development, performance, indicators, supplier's selection, review of the literature, criteria, economiec, social, environment", These words were carefully chosen to ensure that as many relevant articles as possible could be included.

In the literature, we identified the first study of supplier selection criteria was in 1966 (Dickson 1966), we followed the documents until 2018. Also we searched at international standards such as SCOR, GRI, OECD sustainable toolkit [31] and ISO 26000...

We have observed an increase in the work published from the year 1966 to the beginning of 2018.

The filtration process was carried out in three steps. In the first step, we found an initial list of 168 criteria that are related to SD, after we chose 34 criteria that are most relevant in the literature and finally, we defined 28 criteria that are related to the SSS process (fig.1).

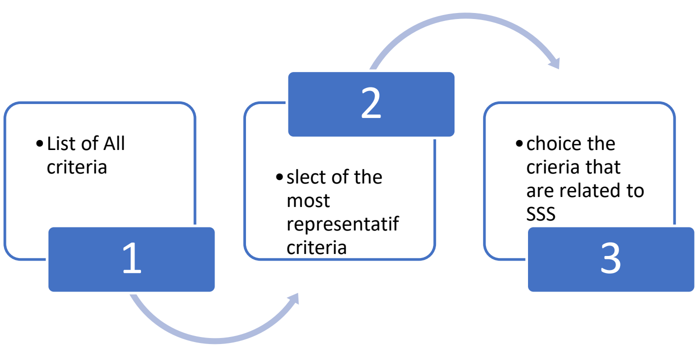

Figure 1: Follow-up methodology

A review of the literature and a database search were carried out to build a common list of SD criteria for the SS process and in international standards, as a result:

Economic criteria

The traditional model of supplier selection depended on economic criteria (quality, cost and time), but with increasing concern about environmental and social issues, other criteria are added in the purchasing decision. The economic criteria found in the literature for the selection of suppliers are:

- Innovation capacity (C_1): Is the ability to bring new solutions or to improve an existing solution in order to be competitive.
- Production capacity (C_2): The ability to meet customer needs.
- Technical and technological capacity (C_3): The use of new techniques and technologies in production.
- Cost (C_4): This is the cost associated with purchasing the raw material or component provided.
- Deadlines (C_5): This is the time needed to respond to an expressed need.
- Reliability (C_6): Customer satisfaction in terms of product choice, quality or lead time.
- Financial (C_7): Costs related to the design and/or development of products.
- Flexibility (C_8): Is the ability to respond to situations and likely disruptions.
- Delivery (C_9): Transport of goods and assurance of their delivery to the destination.
- Quality (C_{10}): It is defined by standards such as ISO to satisfy expressed needs.
- Reactivity (C_{11}): It is the ability to respond quickly to increasingly diverse needs in the global market.
- Customer references (C_{12}): It is the development of references, testimonials and customer success.

Environmental criteria

Environmental criteria are aimed at making choices of products and services that minimize the exploitation and consumption of natural resources, avoid the production of waste and reduce the risk of contamination of the living environments arising from consumer habits and the whole Activities related to their life cycle. The environmental criteria found in the literature for the selection of suppliers are:

- Waste (C_{13}): This is the waste from manufacturing.
- Emission (C_{14}): These are the various gases and substances emitted from the manufacture and transport of products.
- Environmental label (C_{15}): Quality labels to establish that if a product or actor has a reduced impact on the environment.
- Pollution (C_{16}): Pollution emitted in air, soil and water due to production.
- Program (C_{17}): These are the different programs and management policy for the protection of the environment.
- Recycling (C_{18}): The reuse of raw materials.

- Compliance with rules (C_{19}): Respect for environmental and social requirements.
- Use of resources (C_{20}): Materials used in the component supplied and the energy consumption during the manufacture of the product.
- Toxic or dangerous substances (C_{21}): The use of hazardous materials in the manufacture of products.

Social criteria

Social criteria support the ethical management of staff at CS suppliers, equity and encourage the responsibility of suppliers. Social criteria are little discussed in the literature; research in the literature has resulted in:

- Human rights (C_{22}): Are represented by the absence of forced labor and child labor, freedom of association and non-discrimination.
- Jobs and wealth (C_{23}): Improving the standard of living by ensuring full employment and stable employment.
- Training, support and education (C_{24}): All continuing training to ensure the development of human resources.
- Occupational health and safety (C_{25}): This is the protection of workers against the risks and adaptation of the working environment to the physiological and psychological needs of workers.
- Working conditions (C_{26}): Improvement of wages and respect for working time, rest periods, prayer periods, holidays, disciplinary practices and dismissals, maternity protection issues and such as access to drinking water, canteens and access to medical services.

3.2. Proposed mathematical model for measuring supplier sustainability index

We consider a manger that would like to select the best supplier who respects the three dimensions of SD. The following mathematical model allows decision-makers to choose the most sustainable supplier:

Parameter

N_{ns}	Number of new solution
N_{is}	Number of improved solution
Q_s	Quantity served
Q_d	Quantity requested
N_{nt}	Number of techniques and technologies in production renewed
C_{ost}	Cost associated with the purchase of the raw material or component provides (USD)
N_d	Number of days needed to respond to a expressed need
N_{cs}	Number of satisfied customers
N_{tc}	Total number of customers
C_{cd}	Costs related to product design and / or development (USD)
I_{fl}	Index ability to react to situations and likely disturbances
C_{ostd}	Cost of transporting goods to destination (USD)
N_s	Number of quality standards
I_{re}	Index of ability to respond very quickly to increasingly diverse needs in the global market
N_{gt}	Number of good testimonials
N_{tt}	Total number of testimonials
I_{wm}	Waste quantity index of product manufacturing
I_{egs}	Quantity index of the different gases and substances emitted from the manufacture and transport of products
I_{ql}	Quality Label Index
I_{pe}	Pollution index of air, soil and water due to production
I_{pp}	Index of different programs and management policy for the protection of the environment
I_{rm}	Index of reuse of raw materials
I_{rr}	Index of compliance with environmental and social requirements
I_{ur}	Index of quantity of materials (lead, chromium, coal ...) and energy (gas, water, electricity ...) used during the production of the product
I_{tds}	Quantity index of hazardous or toxic materials in the product
I_{hr}	Index of respect for human rights
I_{jw}	Improvement index for the standard of living of employers
I_{tse}	Index of continuing education to ensure the development of human resources
N_{wa}	Number of employees injured
N_{tw}	Total number of employees
I_{cw}	Index of respect for working conditions
I_{eco}	Index of economic dimension

I_{env} Index of environmental dimension

I_{soc} Index of social dimension

W_i Weight associated with the criterion C_i

W_{eco} Weight associated with the economic dimension

W_{env} Weight associated with the environmental dimension

W_{soc} Weight associated with the social dimension

Objective function

In this paper, the objective function is the index of sustainability supplier. It is represented by set of SD criteria having a value limited between 1 and 0. We use the ratio for facilitating the aggregation of the different elements in the objective.

The following equations represent the calculation of the set of SD criteria:

$$C_1 = \frac{N_{ns} + N_{is}}{N_{ns} + N_{is} + 1} \quad (1)$$

$$C_3 = \frac{Q_S}{Q_D} \quad (2)$$

$$C_3 = \frac{N_{nt}}{N_{nt} + 1} \quad (3)$$

$$C_4 = \frac{1}{C_{ost}} \quad (4)$$

$$C_5 = \frac{1}{N_d} \quad (5)$$

$$C_6 = \frac{N_{cs}}{N_{tc}} \quad (6)$$

$$C_7 = \frac{C_{cd}}{C_{cd} + 1} \quad (7)$$

$$C_8 = \frac{1}{I_{fl}} \quad (8)$$

$$C_9 = \frac{1}{C_{ostd}} \quad (9)$$

$$C_{10} = \frac{N_s}{N_s + 1} \quad (10)$$

$$C_{11} = \frac{1}{I_{re}} \;,\; I_{re} = \begin{cases} 1 \text{ if Good} \\ 2 \text{ if Average} \end{cases} \quad (11)$$

$$C_{12} = \frac{N_{gt}}{N_{tt}} \quad (12)$$

$$C_{13} = \frac{1}{I_{wm}} \;,\; I_{wm} = \begin{cases} 1 \text{ if Little} \\ 2 \text{ if Average} \end{cases} \quad (13)$$

$$C_{14} = \frac{1}{I_{egs}} \;,\; I_{egs} = \begin{cases} 1 \text{ if Little} \\ 2 \text{ if Average} \end{cases} \quad (14)$$

$$C_{15} = I_{ql} \,,\, I_{ql} = \begin{cases} 1 \text{ if the product has a quality label} \\ 0 \text{ if not} \end{cases} \quad (15)$$

$$C_{16} = \frac{1}{I_{pe}} \;,\; I_{pe} = \begin{cases} 1 \text{ if Little} \\ 2 \text{ if Average} \\ 3 \text{ if Much} \end{cases} \quad (16)$$

$$C_{17} = \frac{1}{I_{pp}} \;,\; I_{pp} = \begin{cases} 1 \text{ if Beaucoup} \\ 2 \text{ if Average} \\ 3 \text{ if Little} \end{cases} \quad (17)$$

$$C_{18} = I_{rm} \;,\; I_{rm} = \begin{cases} 1 \text{ if Recyclable} \\ 0 \text{ if No} \end{cases} \quad (18)$$

$$C_{19} = \frac{1}{I_{rr}} \;,\; I_{rr} = \begin{cases} 1 \text{ if Much} \\ 2 \text{ if Average} \\ 3 \text{ if Little} \end{cases} \quad (19)$$

$$C_{20} = \frac{1}{I_{ur}} \quad , \quad I_{ur} = \begin{cases} 1 \text{ if Little} \\ 2 \text{ if Average} \\ 3 \text{ if Much} \end{cases} \tag{20}$$

$$C_{21} = I_{tds} \quad , \quad I_{rm} = \begin{cases} 1 \text{ if Recyclable} \\ 0 \text{ if No} \end{cases} \tag{21}$$

$$C_{22} = \frac{1}{I_{hr}} \quad , \quad I_{hr} = \begin{cases} 1 \text{ if Good} \\ 2 \text{ if Average} \end{cases} \tag{22}$$

$$C_{23} = \frac{1}{I_{jw}} \quad , \quad I_{jw} = \begin{cases} 1 \text{ if Good} \\ 2 \text{ if Average} \end{cases} \tag{23}$$

$$C_{24} = \frac{1}{I_{tse}} \quad , \quad I_{tse} = \begin{cases} 1 \text{ if Much} \\ 2 \text{ if Average} \end{cases} \tag{24}$$

$$C_{25} = \frac{N_{wa}}{N_{tw}} \tag{25}$$

$$C_{26} = \frac{1}{I_{cw}} \quad , \quad I_{cw} = \begin{cases} 1 \text{ if Good} \\ 2 \text{ if Average} \end{cases} \tag{26}$$

After obtaining the criteria values, decision makers are asked to assign weights to the chosen criteria. Each criteria value is multiplied by its weight. We obtain three value represents economic, environmental and social indicator, respectively as follows:

$$I_{eco} = \frac{\sum_{i=1}^{12} W_i C_i}{12} \qquad i = \{1,2,\ldots,12\} \tag{27}$$

$$I_{env} = \frac{\sum_{i=13}^{21} W_i C_i}{9} \qquad i = \{13,14,\ldots,21\} \tag{28}$$

$$I_{soc} = \frac{\sum_{i=22}^{26} W_i C_i}{5} \qquad i = \{22,23,\ldots,26\} \tag{29}$$

In the end, the decision-makers are asked to choose the weights of the three dimensions of sustainable development according to their policy followed by the company, then each value of SD dimension indicator obtained by equation (27) to (29) are multiplied by these weight.

The sustainability performance score of the supplier is given by the following maximum function:

$$\text{Max } P = \frac{W_{eco} I_{eco} + W_{env} I_{env} + W_{soc} I_{soc}}{3} \tag{30}$$

The MaxP equation represents the function of the developed model. The maximum value of the equation (30) is one.

Constraints:

- The sum of the weights in each dimension must not exceed the value 1.

$$Q_S \le Q_D \tag{31}$$

- The sum of the weights in each dimension must not exceed the value 1.

$$\sum_{i=1}^{12} W_i = 1 \tag{32}$$

$$\sum_{i=13}^{21} W_i = 1 \tag{33}$$

$$\sum_{i=22}^{26} W_i = 1 \tag{34}$$

$$W_{eco} + W_{env} + W_{soc} = 1 \tag{35}$$

- The sum of the weights of the dimensions of SD is equal to 1.

$$0 \le C_i \le 1 \qquad \forall i = \{1,2,\ldots,26\} \tag{36}$$

4. Data analysis

A company X decides to choose the best supplier among five suppliers. Managers have chosen the weights of each criterion in such a way that: the sum of the weights of the criteria of each dimension is equal to one.

All criteria value under each of the three pillars are multiplied by their respective weights and aggregated as indicated by Equations (27) to (29). The result is three index

Table 2: Index of environmental, economic and social dimensions

Dimension	Criteria	Weight	Supplier1	Supplier2	Supplier3	Supplier4	Supplier5
Economic	C_1	0,101	0,500	0,600	0,700	0,800	0,900
	C_2	0,079	0,200	0,400	0,600	0,800	1,000
	C_3	0,106	0,500	0,600	0,700	0,800	0,900
	C_4	0,115	0,910	0,920	0,930	0,940	0,950
	C_5	0,095	0,167	0,200	0,250	0,333	0,500
	C_6	0,098	0,500	0,600	0,700	0,800	0,900
	C_7	0,061	0,917	0,929	0,941	0,950	0,980
	C_8	0,053	0,333	0,500	0,500	1,000	1,000
	C_9	0,051	0,005	0,006	0,007	0,010	0,011
	C_{10}	0,082	0,710	0,770	0,790	0,870	0,920
	C_{11}	0,079	0,500	0,500	1,000	1,000	1,000
	C_{12}	0,080	0,850	0,880	0,900	0,980	1,000
	I_{eco}		0,528376	0,595915	0,691638	0,701738	0,858031
Environment	C_{13}	0,112	0,333	0,500	0,500	1,000	1,000
	C_{14}	0,115	0,333	0,333	0,500	0,500	1,000
	C_{15}	0,133	0,000	0,000	1,000	1,000	1,000
	C_{16}	0,137	0,333	0,333	0,500	0,500	1,000
	C_{17}	0,130	0,333	0,333	0,500	0,500	1,000
	C_{18}	0,074	0,000	0,000	1,000	1,000	1,000
	C_{19}	0,154	0,333	0,333	0,500	0,500	0,500
	C_{20}	0, 074	0,333	0,333	0,333	0,333	0,500
	C_{21}	0, 071	0	0	0	1,000	1,000
	I_{env}		0,240426	0,25913	0,555642	0,682642	0,886
Social	C_{22}	0,232	0,333	0,333	0,500	0,500	1,000
	C_{23}	0,129	0,333	0,333	0,500	0,500	1,000
	C_{24}	0,198	0,333	0,333	0,500	0,500	1,000
	C_{25}	0,191	0,200	0,240	0,250	0,290	0,300
	C_{26}	0,250	0,5	0,5	1,000	1,000	1,000
	I_{soc}		0,349347	0,356987	0,57725	0,58489	0,8663

values representing the environmental, economic and social dimensions, respectively (Table2).

The enterprise X choice the scenario of weigh dimension like as:

$$W_{eco} = W_{env} = W_{soc} = \frac{1}{3}$$

The final sustainable performance indices of suppliers were used to rank the suppliers in the X enterprise (Table3), supplier5 is identified as the best sustainable supplier with MaxP=0,29 (Fig2).

5. Conclusion

With the appearance of the new sustainable development concept in the last 20 years, industrial company have begun to

Table 3: The sustainable performance indices of the supplier

	I_{eco}	I_{env}	I_{soc}	sustainable performance	Rank
Supplier1	0,528376	0,240426	0,349347	0,12423878	5
Supplier2	0,595915	0,25913	0,356987	0,13467022	4
Supplier3	0,691638	0,555642	0,57725	0,20272556	3
Supplier4	0,701738	0,682642	0,58489	0,21880778	2
Supplier5	0,858031	0,886	0,8663	0,29003678	1

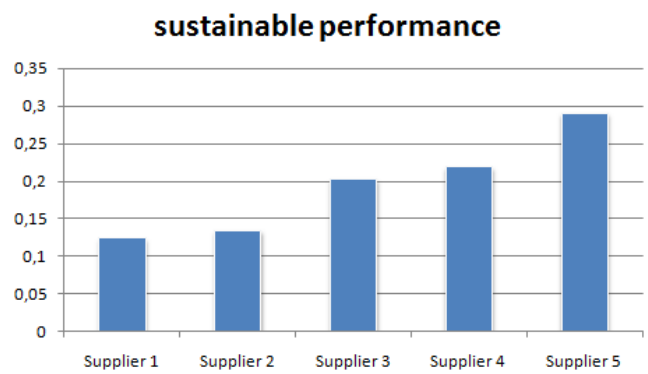

Figure 2: Sustainable performance of the supplier

integrate environmental and social concerns into the management of their activities in order to protect the company's durability and open up new markets. The process of integrating SD into the company starts with the selection of suppliers. In this paper, we have given a list that includes all the relevant criteria in the literature for the selection of suppliers. These criteria influence the functioning of all the other services of the company (transport, stock, production, etc.). In the last, we have presented an easy-to-use mathematical model for managers to measure vendor performance. Our developed model is simple to apply and can be used in any industrial enterprise to select the best sustainable supplier.

References

[1] Atefeh Amindousta, Shamsuddin Ahmeda, Ali Saghafiniab, Ardeshir Bahreininejada, Sustainable supplier selection: A ranking model based on fuzzy inference system, Applied Soft Computing 12 (2012) 1668–1677.

[2] Buyuközkan, G., Çifci, G., 2011. A novel fuzzy multi-criteria decision framework for sustainable supplier selection with incomplete information. Comput. Ind. 62, 164–174.

[3] X. Zhou, et al., Type-2 fuzzy multi-objective DEA model: An application to sustainable supplier evaluation, Appl. Soft Comput. J. (2016), http://dx.doi.org/10.1016/j.asoc.2016.04.038.

[4] Fallahpour, A., Udoncy Olugu, E., Nurmaya Musa, S., Yew Wong, K., Noori, S., A decision support model for sustainable supplier selection in sustainable supply chain management, Computers & Industrial Engineering (2017), doi: http://dx.doi.org/10.1016/j.cie.2017.01.005.

[5] Dickson, G. W. (1966). An analysis of vendor selection systems and decisions. Journal of Purchasing, 2 (1), 28-41.

[6] Weber, C. A., Current, J. R., & W. C. Benton (1991). Vendor selection criteria and methods. European Journal of Operational Research, 50, 2-18.

[7] Larson, P. D. (1993). Buyer-Supplier co-operation, product quality and total cost. International Journal of Physical Distribution & Logistics Management, 24 (6), 4-10.

[8] Vonderembse, M., Tracey, M., Tan, C. L., & E. J. Bardi (1995). Current purchasing practices and JIT: some of effects on inbound logistics. International Journal of Physical Distribution & Logistics Management, 25 (3), 33-48.

[9] Verma, R., & M. E. Pullma (1998). An analysis of the supplier selection process. International Journal of Management Science, 26 (6), 739-750.

[10] Katsikeas, C. S., Paparoidamis, N. G., & E. Katsikea (2004). Supply source selection criteria: the impact of supplier performance on distributor performance. Indutrial Marketing Management.

[11] Aicha Aguezzoul, Pierre Ladet. S_election et _evaluation des fournisseurs : Crit_eres et m_ethodes. Revue fran_caise de gestion industrielle, Paris-La-D_efense : Association fran_caise de gestion industrielle ; Montrouge : Centrale des revues, 2006, 2, pp.5-27.

[12] Emilie Baumann. Modèles d'évaluation des performances économique, environnementale et sociale dans les chaines logistiques. Gestion et management. INSA de Lyon, (2011).

[13] Tasseda Boukherroub. Int_egration des objectifs du d_eveloppement durable dans la gestion strat_egique et tactique de la chaine logistique. Gestion et management. INSA de Lyon, 2013.

[14] Ozlem Gurel, A. Z. Acar, I. Onden, I. Gumus (2015). Determinants of the green supplier selection. Procedia - Social and Behavioral Sciences 181 (2015) 131 – 139.

[15] Joanie Caron, Suzanne Durand, Hugo Asselin, (2016). Principles and criteria of sustainable development for the mineral exploration industry. Journal of Cleaner Production 119 (2016) 215-222.

[16] Wenyan Song, Zhitao X, Hu-Chen Liu, (2017). Developing sustainable supplier selection criteria for solar air-conditioner manufacturer: An integrated approach. Renewable and Sustainable Energy Reviews 79 (2017) 1461–1471.

[17] Marko Vasiljević, Hamed Fazlollahtabar, Željko Stevića, Slavko Vesković, (2018). A ROUGH MULTICRITERIA APPROACH FOR EVALUATION OF THE SUPPLIER CRITERIA IN AUTOMOTIVE INDUSTRY. Decision Making: Applications in Management and Engineering Vol. 1, Number 1, 2018, pp. 82-96. ISSN: 2560-6018. DOI: 10.31181/dmame180182v.

[18] Panitas Sureeyatanapas, Kawinpob Sriwattananusart, Thanawath Niyamosothath, Weerapat Setsomboon, Sirawadee Arunyanart, Supplier selection towards uncertain and unavailable information: an extension of TOPSIS method, Operations Research Perspectives (2018), doi: 10.1016/j.orp.2018.01.005.

[19] Ashkan Memaria, Ahmad Dargib, Mohammad Reza Akbari Jokara, Robiah Ahmadc, Abd. Rahman Abdul Rahimc, (2019). Sustainable supplier selection: A multi-criteria intuitionistic fuzzy TOPSIS Method. Journal of Manufacturing Systems 50 (2019) 9–24.

[20] Chunguang Bai, Joseph Sarkis, (2010). Integrating sustainability into supplier selection with grey system and rough set methodologies. Int. J. Production Economics 124 (2010) 252–264.

[21] Hacer Guner Goren, A Decision Framework for Sustainable Supplier Selection and Order Allocation with Lost Sales, Journal of Cleaner Production (2018), doi: 10.1016/j.jclepro.2018.02.211.

[22] Konrad Zimmer, Magnus Fröhling & Frank Schultmann (2015): Sustainable supplier management – a review of models supporting sustainable supplier selection, monitoring and development, International Journal of Production Research, DOI: 10.1080/00207543.2015.1079340.

[23] Ilgin MA, et al. Use of MCDM techniques in environmentally conscious manufacturing and product recovery: State of the art. J Manuf Syst (2015), http://dx.doi.org/10.1016/j.jmsy.2015.04.010.

[24] Babbar C, Amin SH. A multi-objective mathematical model integrating environmental concerns for supplier selection and order allocation based on fuzzy QFD in beverages industry. Expert Syst Appl 2018;92:27 – 38

[25] Jain, Vipul, Kumar Sameer, Kumar Amit, Chandra Charu. An integrated buyer initiated decision-making process for green supplier selection. J Manuf Syst 2016;41:256 – 65.

[26] Kannan D, Govindan K, Rajendran S. Fuzzy Axiomatic Design approach based green supplier selection: a case study from Singapore. J Clean Prod 2015;96:194 – 208.

[27] Ghayebloo S, Tarokh MJ, Venkatadri U, Diallo C. Developing a bi-objective model of the closed-loop supply chain network with green supplier selection and disassembly of products: the impact of parts reliability and product greenness on the recovery network. J Manuf Syst 2015;36:76 – 86.

[28] Govindan K, Rajendran S, Sarkis J, Murugesan P. Multi criteria decision making approaches for green supplier evaluation and selection: a literature review. J Clean Prod 2015;98:66 – 83.

[29] Banaeian, N., Mobli, H., Fahimnia, B., Nielsen, I.E., and Omid, M. (2018). Green supplier selection using fuzzy group decision making methods: A case study from the agri-food industry. Computers & Operations Research 89, 337-347.

[30] Keshavarz Ghorabaee, M., Zavadskas, E.K., Amiri, M., and Esmaeili, A. (2016). Multi-criteria evaluation of green suppliers using an extended WASPAS method with interval type-2 fuzzy sets. Journal of Cleaner Production 137, 213-229

[31] OECD Sustainable Manufacturing Toolkit. Avalable online: http://www.oecd.org/sti/inno/ 48101937.pdf (accessed on 25 December 2014).

ASTES

Advances in Science, Technology and Engineering Systems Journal
Vol. 4, No. 2, 260-269 (2019)
www.astesj.com
Special Issue on Advancement in Engineering and Computer Science

ASTES Journal
ISSN: 2415-6698

Effects of Different Activation Functions for Unsupervised Convolutional LSTM Spatiotemporal Learning

Nelly Elsayed[*,1], Anthony Maida[2], Magdy Bayoumi[3]

[1,2]*School of Computing and Informatics, University of Louisiana at Lafayette, 70503, Louisiana, USA*

[3]*Department of Electrical Engineering, University of Louisiana at Lafayette, 70504, Louisiana, USA*

ARTICLEINFO

Article history:
Received:03 February, 2019
Accepted: 26 March, 2019
Online: 10 April, 2019

Keywords:
Convolution LSTM
Activation function
Video prediction
Moving MNIST
Prediction

ABSTRACT

Convolutional LSTMs are widely used for spatiotemporal prediction. We study the effect of using different activation functions for two types of units within convolutional LSTM modules, namely gate units and non-gate units. The research provides guidance for choosing the best activation function to use in convolutional LSTMs for video prediction. Moreover, this paper studies the behavior of the gate activation and unit activation functions for spatiotemporal training. Our methodology studies the different non-linear activation functions used deep learning APIs (such as Keras and Tensorflow) using the moving MNIST dataset which is a baseline for video prediction problems. Our new results indicate that: 1) the convolutional LSTM gate activations are responsible for learning the movement trajectory within a video frame sequence; and, 2) the non-gate units are responsible for learning the precise shape and characteristics of each object within the video sequence.

1 Introduction

Problems in video prediction (spatiotemporal prediction) are important in both research and industry. Examples include human action recognition [1], spread of infections, medical predictions [2], weather forecast prediction [3], and autonomous car video prediction systems [4, 5].

Spatiotemporal (e.g. video) datasets are challenging to predict due to the spatial and temporal information which the datasets carry through time. In sequence prediction problems, the prediction at the current step depends primarily on the previous history. Making a near future prediction requires an computational tool that is able to discover both the long and short-term dependencies in the data. Initially, recurrent neural networks (RNN) [6] were proposed to model data which was sequential in nature. However, straightforward RNNs have major drawbacks. RNNs suffer from the vanishing/exploding gradient problem which prevents them from learning long-term data dependencies [7–9]. There are several gate-based RNN models that attempt to solve this classic problem. These include the long short-term memory unit (LSTM) [7], peephole LSTM [10], gated recurrent unit (GRU) [10], and minimal recurrent unit (MRU) [11].

This paper studies the LSTM architecture as an attractive architecture architecture to perform spatiotemporal (video) prediction. In addition, Gref et al. [12] empirically showed that the LSTM is the most efficient recurrent architecture to solve for speech recognition, handwriting recognition, and polyphonic music modeling [12]. The LSTM has the highest number of gates compared with other gated units [9–11]. Furthermore, the choice of the activation function for gate and non-gate units within the LSTM has an essential effect on the the LSTM's function [12].

This work studies gate activations and non-gate activations within the LSTM architecture. In most APIs the gate activations and non-gate activations are known as recurrent activations and unit activations, respectively. To solve image and video related problems, different convolution-based models are used such as in Kalchbrenner et al [13], Elsayed et al. [5], Lotter et al. [4], Finn at al. [14], and Wang et al. [15]. However, the most widely used architecture for video prediction to-date is the convolution LSTM. Hence, we performed our experiments on a convolution-based LSTM (convolutional LSTM) network model [4]. We studied the effect of different gate activation and unit activation

*Corresponding Author: Nelly Elsayed, School of Computing and Informatics& nel.elsayed@gmail.com

https://dx.doi.org/10.25046/aj040234

functions through the learning process of the convolutional LSTM architecture [3]. Our experiments use the convolutional LSTM found in the Keras deep learning framework [16]. Training was performed on the moving MNIST dataset as the most commonly used benchmark for video prediction problems [17].

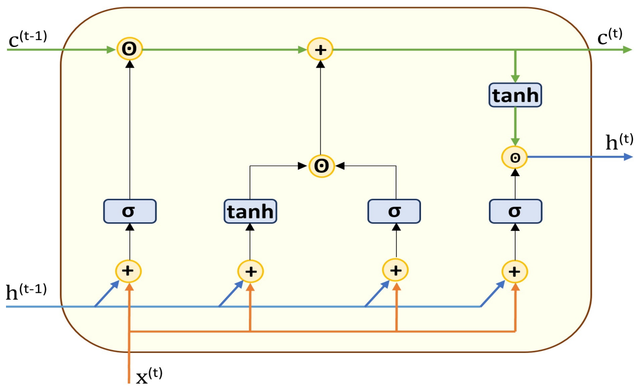

Figure 1: The unrolled LSTM architecture. The memory-state and output lines are time-evolving and labelled c and h, respectively. The CEC is indicated by the plus sign on the c line. The level of description is coarse enough so that this could either depict a standard LSTM or a convolutional LSTM.

In our empirical study, we worked with a model than what was needed for optimal prediction. Specifically, it had fewer parameters. This reduction allows us to more clearly see the effect of gate and unit activations on the convLSTM model without contamination by influences of other high-effect parameters. For example, it avoids saturation effects on the model accuracy which helps to see changes in activation function effects [18]. Our study compares different activation functions on a simple convolutional LSTM model for spatiotemporal (video) prediction task. We investigated the responsibilities of the convolutional LSTM gates and unit activations over the training process. Furthermore, we found the most appropriate function to be applied for the gates and for the unit activation for solving video prediction problem.

2 Convolutional LSTM

The LSTM [7] is the first gate-based recurrent neural network. As noted earlier, it was motivated by the need to mitigate the vanishing gradient problem and did so by using the principle underlying a constant error carousel (CEC) [7] to improve the learning of long-term dependencies. This was implemented by adding a memory-state line to the architecture (Figure 1). This memory-state line can retain (remember) the recurrent values over arbitrary time intervals. Gres et al. [8] added a forget gate to the LSTM cell to allow information to be removed from (forgotten) the memory-state line. This gate was trainable so that the module could learn when stored information was no longer needed. Gers et al. [10] improved the design by adding so-called peephole connections from the memory cell to the LSTM gates. The peephole connections enable the memory line to exert control over the activation of all three of the gates. This helps the LSTM block to avoid vanishing gradients and also helps learning of precise timing in conjunction with Constant Error Carousel (CEC) [8]. The CEC is the key ingredient mitigate the vanishing gradient problem.

LSTMs are used in several application areas including speech recognition [19,20], language modeling [21], sentiment analysis [22], music composition [23], signal analysis [24], human action recognition [1], image caption generation [25], and video prediction [3,4,17,26].

The convolutional LSTM (convLSTM) was introduced in 2015 by Shi et al [3] for weather precipitation forecast prediction task. This is an enhancement to the LSTM discussed previously. The crucial change is that the data within the module takes the form of a multichannel 2D feature map (image stack). The convLSTM improves predicted video on data sets of evolving precipitation maps compared to the non-convolutional LSTM. Apparently, it captures spatiotemporal correlations better than non-the standard variant [3,17].

An unrolled convLSTM module in Figure 1 can be either standard or convolutional because it does not make the relevant internal operations and weights explicit. Like the standard LSTM, the architecture has three gates indicated by the activation functions labeled σ. These are the forget, input, and output gates [9]. There are two non-gate units which are labeled with tanh activation functions. The convLSTM gates (input, forget, and output) have the ability to multiplicatively attenuate the outputs of tanh units and the value on the $c^{(t-1)}$ line. The forget gate attenuates information deemed unnecessary from the previous cell memory state $c^{(t-1)}$. $h^{(t-1)}$ is the convLSTM cell output at time $t-1$, and $h^{(t)}$ is the output of the convLSTM cell at time t. $x^{(t)}$ is the current video frame target at time t. $c^{(t-1)}$ and $c^{(t)}$ are the memory cell states at consecutive times.

The following equations calculate all of the gate and the unit values based on the Gers et al. [8] LSTM combined the convolutional model of Shi et al. [3]. These operations should be compared with Figure 2.

$$i^{(t)} = \sigma(W_{xi} * x^{(t)} + U_{hi} * h^{(t-1)} + b_i) \tag{1a}$$
$$g^{(t)} = tanh(W_{xg} * x^{(t)} + U_{hg} * h^{(t-1)} + b_g) \tag{1b}$$
$$f^{(t)} = \sigma(W_{xf} * x^{(t)} + U_{hf} * h^{(t-1)} + b_f) \tag{1c}$$
$$o^{(t)} = \sigma(W_{xo} * x^{(t)} + U_{ho} * h^{(t-1)} + b_o) \tag{1d}$$
$$c^{(t)} = f^{(t)} \odot c^{(t-1)} + i^{(t)} \odot g^{(t)} \tag{1e}$$
$$h^{(t)} = tanh(c^{(t)}) \odot o^{(t)} \tag{1f}$$

The the input, forget, and output gate activations s are denoted $i^{(t)}$, $f^{(t)}$, and $o^{(t)}$. σ denotes logsig. The gates have activation values falling in the interval $[0,1]$ where 1 means completely open and 0 means completely closed. $g^{(t)}$, is the current input. $c^{(t)}$ represents the current memory module state. $h^{(t)}$ represents the current output. b_i, b_g, b_f, and b_o are biases for the respective gate. W's and U's are the feedforward and

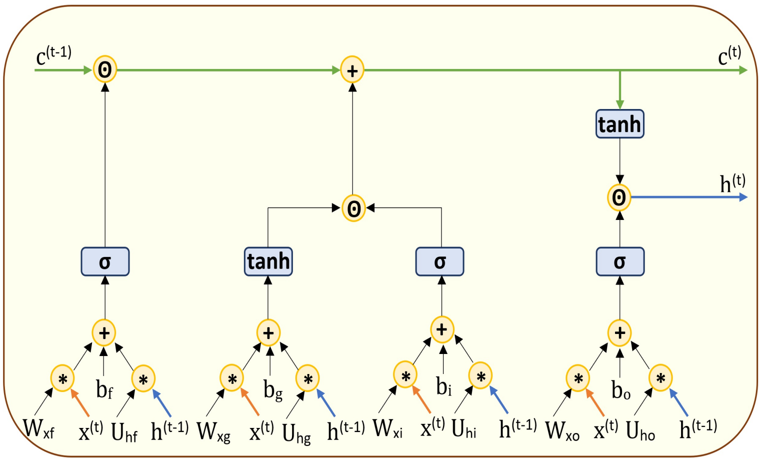

Figure 2: The unrolled convLSTM architecture at the arithmetic operation level. This rendering makes convolution operations and weights explicit and should be compared with Equation Set 1.

recurrent weights, respectively. "⊙" denotes element-wise multiplication, and "∗" denotes the convolution operator.

Figure 2 shows the arithmetic operational level of the convLSTM architecture where the convLSTM components and their corresponding weights are shown explicitly.

3 Activation Functions

As explained earlier, gate units usually have sigmoid (range $[0,1]$) activation functions and non-gated units usually have *tanh* activation functions. This paper studies the effects of using different activation functions for these units. This section reviews the most common activation functions used. All of the functions discussed are nonlinear.

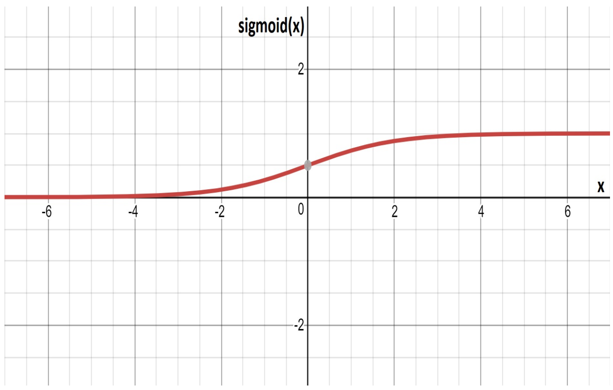

Figure 3: The curve of the logsig (σ) function.

3.1 Logsig Function

The logistic sigmoid (logsig) function [27] is shown in Figure 3. It is given by the following equation:

$$f(x) = \sigma(x) = \frac{e^x}{e^x + 1} = \frac{1}{1 + e^{-x}}, \qquad (2)$$

The logsig is commonly denoted by $\sigma(x)$, where $x \in (-\infty, \infty)$ and $\sigma(x) \in (0,1)$. The logsig is historically common in network models because it intuitively represents the firing rate of a biological neuron. The logsig is still used in recurrent models for gating purposes. The input value is usually known because it appears in the feedforward sweep of the network. Because of this, its derivative can be computed efficiently as shown in (3).

$$f'(x) = \sigma'(x) = f(x)(1 - f(x)) \qquad (3)$$

3.2 Hard-Sigmoid Function

The hard-sigmoid (hardSig) function is considered a noisy activation function. HardSig approximates logsig function by taking the first-order Taylor expansion around zero and clipping the result according to function's range $[0,1]$. Hardsig appears in Figure 4 and is calculated as follows:

$$hardSig(x) = \max(\min(0.25x + 0.5, 1), 0) \qquad (4)$$

This function allows a crisp decision for the gradient during function saturation phase to be either fully on or fully off. In the non-saturation range near zero, hardSig is linear. This helps avoid vanishing gradients [28].

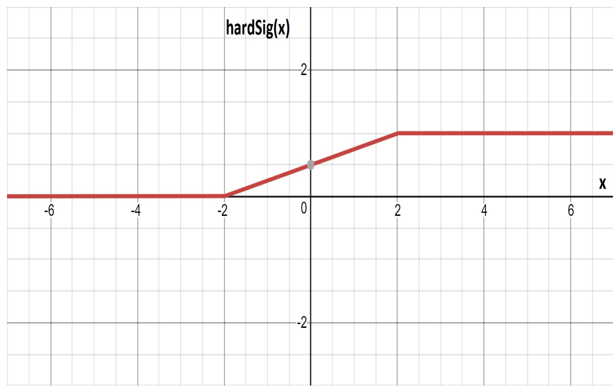

Figure 4: The curve of the hardSig function.

3.3 Hyperbolic Tangent Function

tanh is a saturating activation function. It is typically used as the recurrent activation function in RNNs [6].

In some cases, tanh is considered as cheaper for gradient evaluation in comparison to the logsig function. The function graph appears in Figure 5 and is specified by (5):

$$\tanh(x) = \frac{\sinh(x)}{\cosh(x)} = \frac{e^x - e^{-x}}{e^x + e^{-x}} = \frac{e^{2x} - 1}{e^{2x} + 1} \quad (5)$$

$$tanh'(x) = 1 - tanh^2(x) \quad (6)$$

A convenient property of the tanh activation function is that calculating its first derivative from a known input value is easy as seen in Eqn. (6).

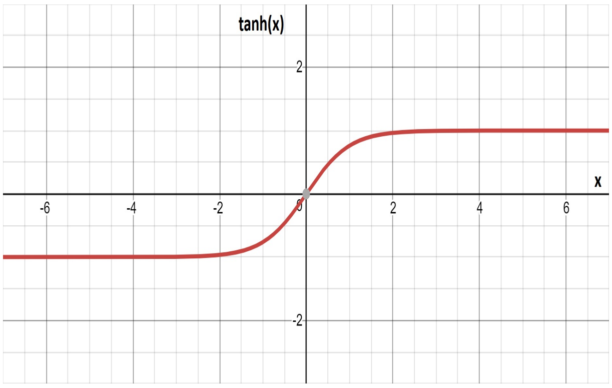

Figure 5: The curve of the Hyperbolic Tangent function.

3.4 SoftSign Function

The SoftSign function was introduced in [29]. Its grahp is given in Figure 6 and is specified by:

$$SoftSign(x) = \frac{x}{1 + |\, x \,|} \quad (7)$$

The SoftSign function range is $(-1, 1)$ and the function domain is $x \in (-\infty, \infty)$. The first derivative of SoftSign also can be evaluated simply as the following:

$$SoftSign'(x) = \frac{x}{(1 + |\, x \,|)^2} \quad (8)$$

SoftSign is an alternative function to hyperbolic *tanh*. In comparison to *tanh*, it does not saturate as quickly, improving its robustness to vanishing gradients.

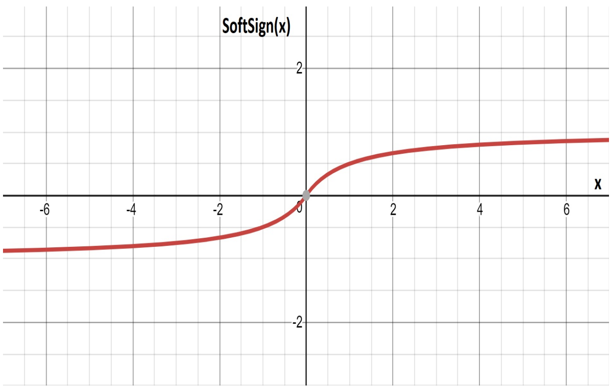

Figure 6: Curve of the SoftSign function.

3.5 ReLU Function

The rectified linear unit (ReLU) is very efficient compared to other activation functions. It was proposed in [30]. For $x \geq 0$ it is the identity function and appears in Figure 7. ReLU is defined by:

$$ReLU(x) = max(x, 0) \quad (9)$$

Its has domain $x \in (-\infty, \infty)$ and range $[0, \infty)$.

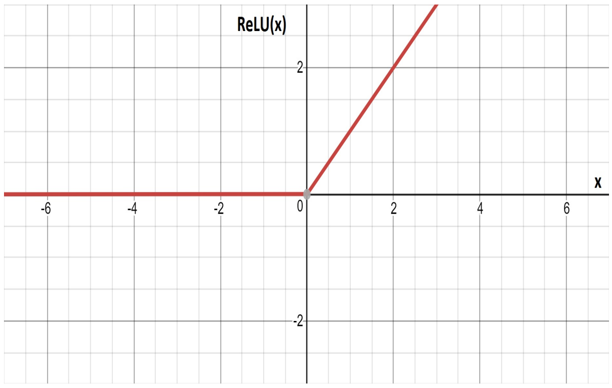

Figure 7: The curve of the ReLU function.

3.6 SoftPlus Function

The SoftPlus function (Figure 8) was proposed in [31]. It modifies the ReLU by applying a smoothing effect [29] and is defined:

$$SoftPlus(x) = \ln(1 + e^x) \quad (10)$$

with $x \in (-\infty, \infty)$ and range $(0, \infty)$. Its derivative is:

$$SoftPlus'(x) = \frac{1}{1 + e^x} \quad (11)$$

Like the SoftSign function, the SoftPlus function is used only in specific applications.

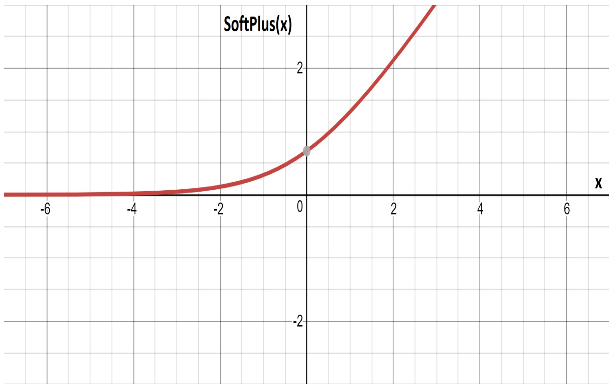

Figure 8: The curve of the SoftPlus function.

3.7 ELU Function

The exponential linear unit (ELU) was introduced in [32] to avoid a zero derivative for negative input values. The ELU achieved better classification accuracy than ReLUs [32] and is defined by:

$$ELU(x) = \begin{cases} \alpha(e^x - 1), & \text{if } x < 0 \\ x \quad , & \text{otherwise} \end{cases} \quad (12)$$

Its domain and range is $(-\infty,\infty)$. Assuming that $\alpha = 1$, its graph is shown in Figure 9 .

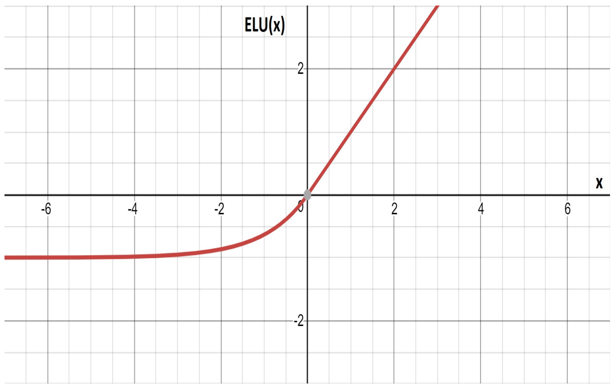

Figure 9: The curve of the ELU function.

3.8 SELU Function

The scaled exponential linear unit (SELU) an ELU function modified with two hyperparameters. Its definition follows:

$$SELU(x) = \lambda \begin{cases} \alpha(e^x - 1) \quad , & \text{if } x < 0 \\ x \, , & \text{otherwise} \end{cases} \tag{13}$$

Its domain is the same as the ELU function, but its range is limited to $-(\lambda\alpha,\infty)$. λ and α are hyperparameters that depend on the mean and variance of the training data. If the data is normalized to $\mu = 0$ and $\sigma = 1$, then $\lambda = 1.0507$ and $\alpha = 1.6732$ whose graph appears in Figure 10.

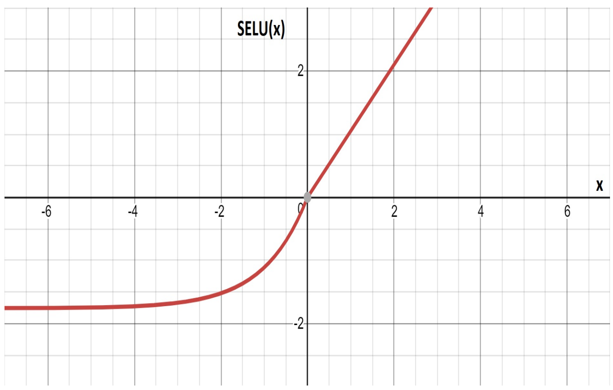

Figure 10: The curve of the SELU function.

The first derivative of SELU is calculated as shown below:

$$SELU'(x) = \lambda \begin{cases} \alpha e^x \quad , & \text{if } x < 0 \\ 1 \, , & \text{otherwise} \end{cases} \tag{14}$$

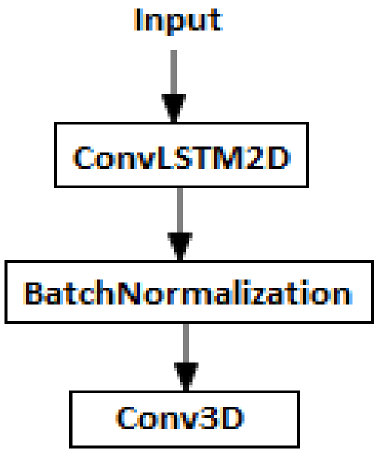

Figure 11: The model architecture used in our experiments.

4 Experiments and Results

This section the results of comparing different activation functions for both the gate units and non-gate units. We chose the functions described in the previous section. They are commonly available in deep learning frameworks. We explore the question of which activation function is best as a gate activation and which is best as a unit activation for convolutional LSTMs in an unsupervised context. Moreover, we want to understand the differential behavior of the gate and non-gate units as a result of training.

We calculated several measures: training loss, validation loss, elapsed training time, and appearance of the predicted video frames compared with ground truth. We did our experiment and analysis on the moving MNIST [17] as explained in the introduction. The moving MNIST dataset consists of 10,000 different video sequences. Each sequence has a length of 20 frames. Each frame is 64×64 pixels and contains two randomly selected handwritten digits from the standard 28×28 MNIST dataset. The two digits move randomly within the frame [17].

4.1 Framework

Our framework uses Shi's et al. [3] convLSTM. Because we had limits on our computing power, our test were serendipitously performed using a small model with insufficient learning capacity for fully accurate predictions. However, this did let us more clearly see the effects of the activation function manipulations. The reduced capacity models helped us avoid ceiling effects so that we could see differential performances in the activation functions.

The model is implemented using the Keras API [16] and appears in Figure 11. It consists of three layers. The first layer is a convLSTM with 40 size 3x3 kernels. The next layer is batch normalization. Finally, we used $3 \times 3 \times 3$ kernel to get the video output shape. Table 1 provides details of the model parameters.

The Adam optimizer [33] was used with initial learning rate $r = 0.001$, $\beta_1 = 0.9$, $\beta_2 = 0.999$. The cost

Table 1: Description of the proposed model architecture used in this study.

Layer (type)	Output Shape	Param Number
ConvLSTM2D	(None, None, 64, 64, 10)	4000
Batch Normalization	(None, None, 64, 64, 10)	40
Conv3D	(None, None, 64, 64, 1)	271
Total params	4,311	
Trainable params	4,291	
Non-trainable params	20	

function was MSE [34].

Each input was a 20-frame video randomly sampled from moving MNIST [17]. As previously mentioned, the amount of input data is $10,000$ videos each of length 20 frames. We used $9,500$ for training and 500 for validating.

The task is proposed for sequence to sequence video prediction. A sequence of five future frames were predicted using the previous five frame sequence. Because of the reduced learning capacity mentioned at the beginning of this section, the trained network could predict only the two temporally closed frames clearly and the rest were unclear because of the reduced learning capacity in the model.

We used an Intel(R) Core $i7-7820HK$, 32GB RAM, and a GeForce GTX 1080 GPU. Training was for ten epochs in each experiment. In each epoch, we fit 475 batches where each batch size was set to 20 for our model experiments. All parameters were held constant over all experiments except for the recurrent activation function that was being tested.

4.2 Results

Our results pertain to the relative performance of varied activation functions for gate and non-gate units.

4.2.1 Results for Gate Activation Functions

For a fair comparison of different gate activation functions, we only changed the gate activation functions and preserved the remaining parameters with the same initializations and values during each experiment. The gate effects were studied collectively because we used the default convolutional LSTM module in found in the Keras API. The API allowed us to change all the gate functions at once (not each gate separately) for setting up an experiment.

For this experiment, the gate activation functions apply to all three gates gates described in Eqns 1a, 1c, and 1d. Accordingly, only functions with range $(0,1)$ are eligible. Thus, this experiment only compared the logsig and hardSig functions.

Table 2 shows the performance results, including average elapsed training time (in minutes), MSE loss (Loss-MSE) for training, validation loss (Val-loss-MSE), percent accuracy (Accuracy) for $n = 3$, and the standard error (SE) for training loss ($n = 3$). The elapsed training time using the hardSig activation is higher than the logsig function by about ten percent. We are not sure why this happens. In Table 2, both logsig and hardSig have nearly exactly the same MSE and MAE.

Figure 12 shows the training and validation loss for the logsig and hardSig activation functions. From the figure, one can also see that the loss average difference between the training and validation runs using the hardSig function is smaller than the logsig function.

We also examined the differences between the accuracy of both training and validation runs using the logsig versus hardSig functions. The average ($n = 3$ for all data points) accuracy values for each function appear in Figure 13. Blue represents training and yellow represents validation accuracy. Both logsig and hardSig functions have similar validation and training accuracy It is also temporally time. The hardSig shows a more comparable accuracy among the training and validation curves. Moreover, hardSig curve does not contain frequent validation accuracy drops down as in logsig curve.

Figure 14 visually shows the prediction results for both the sigmoid and hardSig gate activations of the model. The first row shows ground truth. The two rows below show predictions using the logsig versus hardSig gate activation functions. Both logsig and hardSig are comparable. From the figure, both functions show that the model attempts to learn the digit movement trajectories as shown in each of the prediction frames. The 'double exposure' appearance indicates that the prediction retains the object's previous location within the predicted frame. Despite the double exposure look, digit shape is preserved. Moreover, the hardSig function shows better prediction accuracy than the sigmoid. This agrees with the Gulcehre et al. [28] theory stating that noisy activation functions are better than their non-noisy counterparts.

This experiment suggests the gate activation functions of the convolutional LSTM play a role learning the movement trajectories.

4.2.2 Results for Non-gate Activations

Our second experiment analyzes which activation function is best to use for non-gate units (input-update and output activation) as seen in Eqns. 1b and 1f. We applied the same setup and initialization as in the first experiment except that we retained all the convLSTM parameters. Only the set of possible unit activation functions were manipulated. Gate activations were

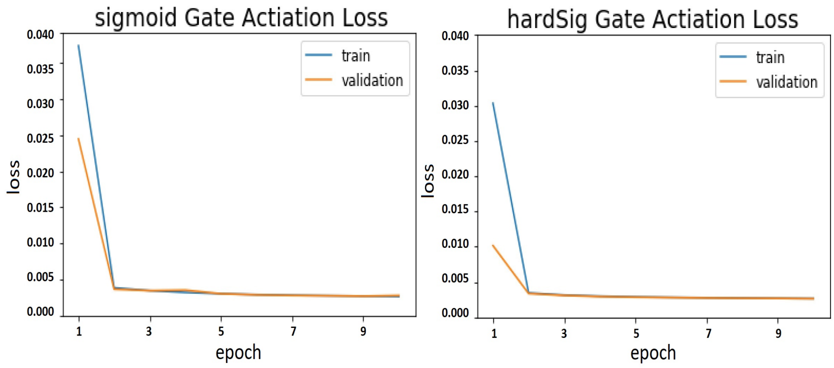

Figure 12: Training and validation loss for each gate activation function over each training epoch. In the left figure, all three gate units used the logsig activation. In the right figure, all three gate units used the hardSig activation function.

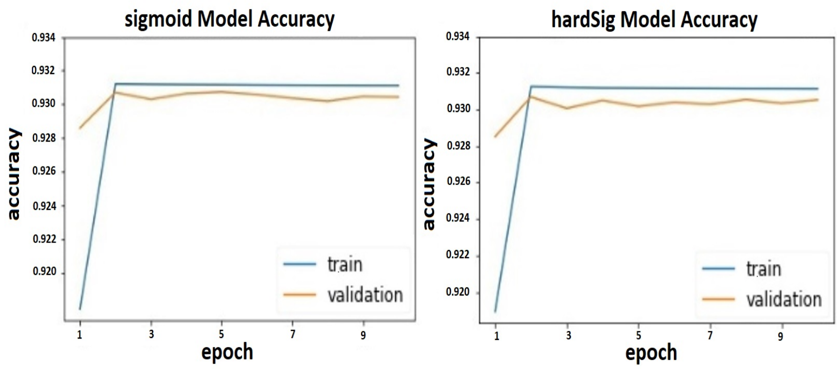

Figure 13: Training and validation accuracy for each gate activation function over each training epoch.

Table 2: Gate Activation Effect on the ConvLSTM Training Process.

Activation function	Training Results					
	Time (Minutes)	*Loss (MSE)*	*Val-loss (MSE)*	*Mean Absolute* **Error (MAE)**	*Accuracy (Percentage)*	*SE (Loss)*
sigmoid	20.2	0.00433	0.00510	0.01726	0.92979	0.0000498
hardSig	22.5	0.00420	0.00525	0.01699	0.92999	0.0000147

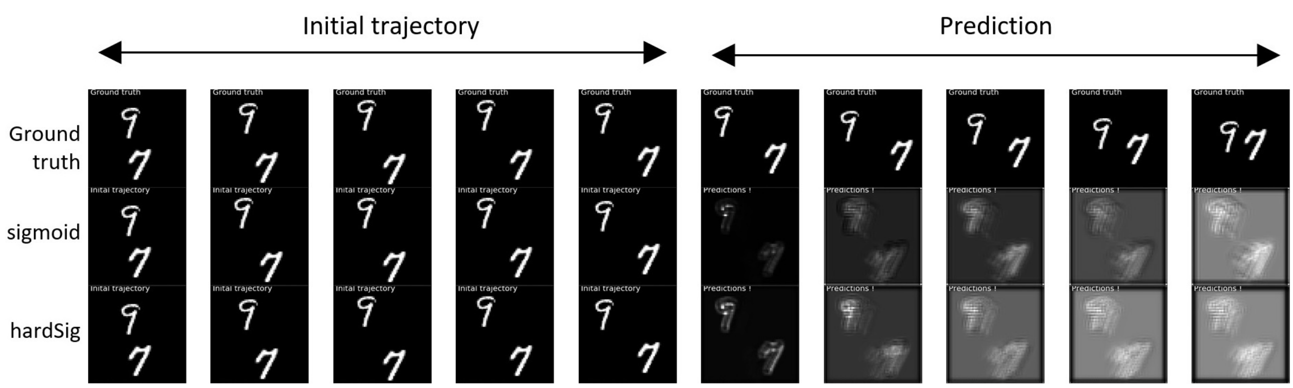

Figure 14: The history and predicted frames using logsig and hardSig as gate activations. Except for the 'double exposure effect,' the predicted shape is preserved.

Table 3: The Non-Gate Unit Effect on Training.

Activation function	Training Results					
	Time (Minutes)	*Loss (MSE)*	*Val-loss (MSE)*	*Mean Absolute* Error (MAE)	*Accuracy (Percentage)*	*SE (Loss)*
sigmoid	24.5	0.00367	0.00387	0.02597	0.93058	0.0000438
tanh	23.9	0.00423	0.00537	0.01751	0.93003	0.0000607
hardSig	25.3	0.00347	0.00386	0.02401	0.93076	0.0000300
softSign	23.9	0.00431	0.00442	0.01777	0.92972	0.0001690
softPlus	24.2	0.00342	0.00308	0.02044	0.93073	0.0000400
ReLU	23.7	0.00424	0.00451	0.01911	0.93015	0.0000723
ELU	23.6	0.00453	0.00555	0.01760	0.93001	0.0001431
SELU	26.5	0.00392	0.00407	0.01784	0.93031	0.0001984

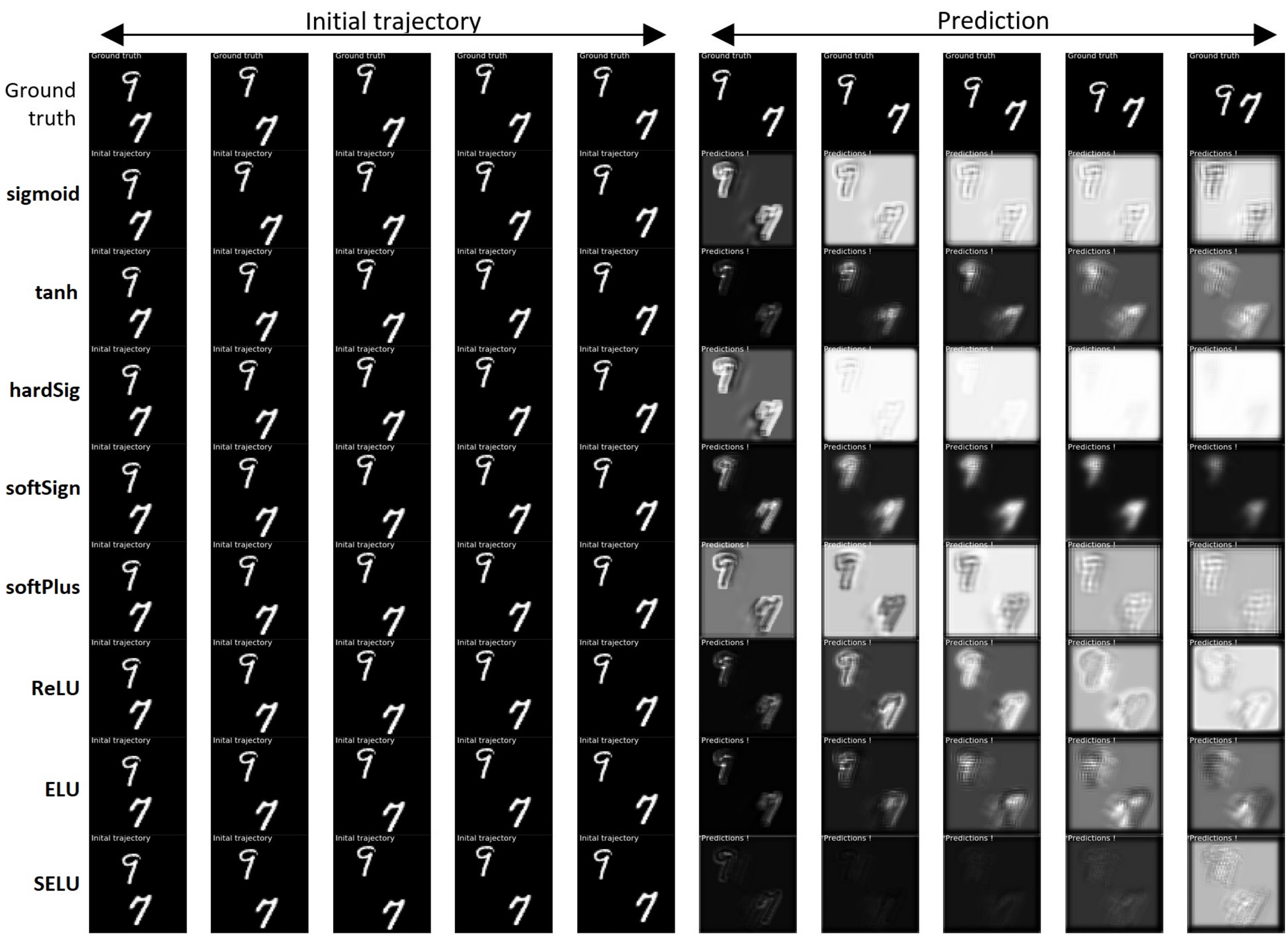

Figure 15: The initial trajectory and predicted frames for each non-gate unit activation function. Although there is shape distortion, the movement directions seem to be preserved.

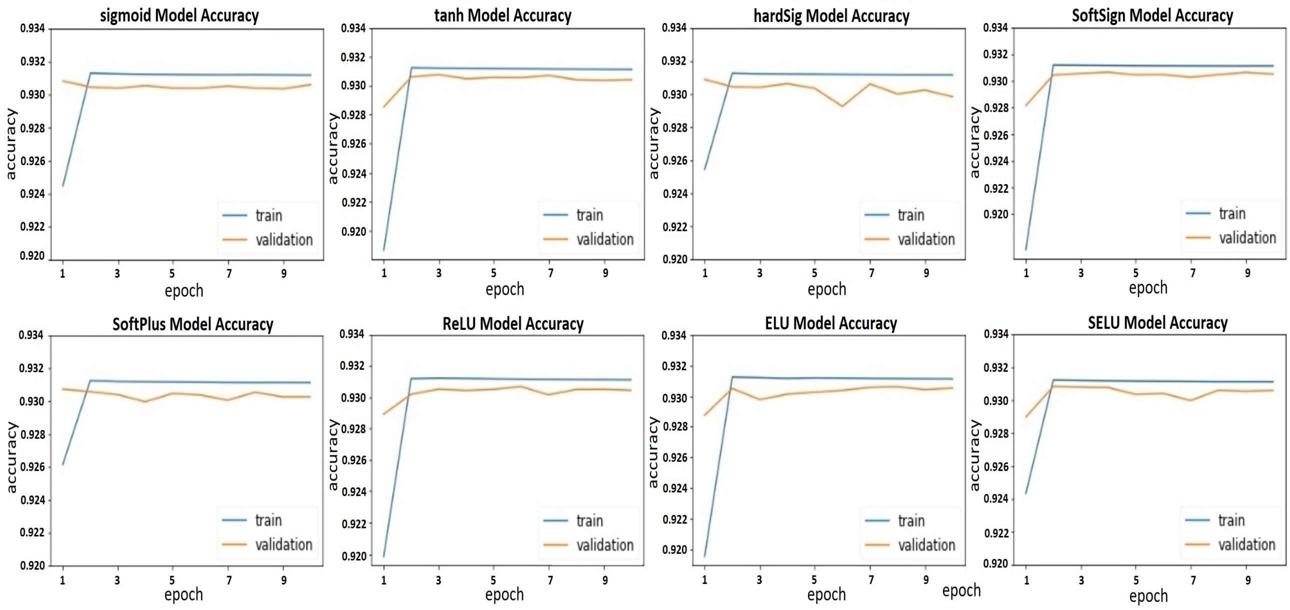

Figure 16: Training and validation accuracy non-gate unit activations. All tested functions are shown for each training epoch.

always set to hardSig. This happens to be the default recurrent activation in the Keras convLSTM API.

There is no restriction on the range of the unit activation function selection compared to the gate activation. Therefore, we tested all eight of the functions from Section 3. Table 3 shows average training time, training loss, validation loss, validation mean absolute error, training accuracy, and standard error of training loss ($n = 3$). The units of training and validation loss are MSE.

Table 3 shows that the elapsed training time of the functions is overall about the same and the highest training time (SELU) is about two minutes longer than the rest. Loss was calculated using MSE and is about the same for all tested functions.

Accuracy of the training and validation tests appears in Figure 16 where the hardSig has the lowest validation accuracy because the accuracy degraded over time. In addition, it has a significant average difference between both the training and validation accuracy curves. For the SoftPlus, SELU, ReLU, and ELU diagrams, there is a notable unstable validation accuracy compared to the training accuracy. However, the most stable validation accuracy for the other tested functions is found when the activation was sigmoid, tanh, or the softSign function. However, the average difference between training and validation accuracies for logsig is higher than the tanh and softSign.

The predicted videos as compared with ground truth for the non-gate unit functions is shown in Figure 15. The lowest visual accuracy occurs when the SELU function is used. The hardSig, logsig, ReLU, and softPlus functions show roughly the same visual prediction results. These functions were unable to maintain, the object's outline, the background, or object's color. The ELU function could not retain the digit outline through time. The softSign function was able to maintain the shape of the objects but it maintained the object's location with reducing their actual sizes. It also suppressed object movement. The tanh preserved the object shape and movement.

In important insight can be seen by looking at the differential visual prediction results in Figure 15. Although changing the non-gate activation functions changes the shape distortion, the predicted movement accuracy seems to be the same across the different activation functions. This indicates that non-gate units play more of a role in predicted shape than in predicting movement direction. In contrast, we saw the opposite pattern with the gate activation functions.

As seen in Figures 14 and 15, prediction accuracy should be improved for practical applications. The intent of our work was to study differential activation function effects. Prediction accuracy can be improved by enhancing the model architecture by increasing the number of the convolutional LSTM layers and adding regularization techniques such as dropout [35]. Further improvements can be obtained by adding more channels to each layer, increasing the number of training epochs, adjusting the input batch size, and adjusting the hyper-parameters. Moreover, using an information flow propagation transfer algorithm (such as predictive coding [4, 36, 37]) to data between the multilayered hierarchy could significantly increase the prediction performance.

5 Conclusion

We found that the choice of gate unit activation function, when used in the convLSTM video prediction problem, affects acquisition of the digit's movement trajectory throughout the video frame sequence. The role of the non-gate unit activation is to enhance the object's shape and determine its details. Only activation functions with range [0, 1] are eligible as a gate activation functions. The convLSTM exhibited the best prediction performance when the gate activation used the hardSig function and it had the best prediction visual results. In addition, the relation between training and validation accuracies was stable. The model also obtained better predictions when the tanh function was used as the non-gate activation. The tanh has similar training loss and training time to the other functions examined in our experiments.

References

[1] M. Baccouche, F. Mamalet, C. Wolf, C. Garcia, and A. Baskurt, "Sequential deep learning for human action recognition," in *International Workshop on Human Behavior Understanding*, pp. 29–39, Springer, 2011.

[2] T. Pham, T. Tran, D. Phung, and S. Venkatesh, "Deepcare: A deep dynamic memory model for predictive medicine," in *Pacific-Asia Conference on Knowledge Discovery and Data Mining*, pp. 30–41, Springer, 2016.

[3] X. Shi, Z. Chen, H. Wang, D.-Y. Yeung, W.-K. Wong, and W.-c. Woo, "Convolutional *LSTM* network: A machine learning approach for precipitation nowcasting," in *Advances in neural information processing systems*, pp. 802–810, 2015.

[4] W. Lotter, G. Kreiman, and D. Cox, "Deep predictive coding networks for video prediction and unsupervised learning," *arXiv preprint arXiv:1605.08104*, 2016.

[5] N. Elsayed, A. S. Maida, and M. Bayoumi, "Reduced-gate convolutional LSTM using predictive coding for spatiotemporal prediction," *arXiv preprint arXiv:1810.07251*, 2018.

[6] L. Medsker and L. Jain, "Recurrent neural networks," *Design and Applications*, vol. 5, 2001.

[7] S. Hochreiter and J. Schmidhuber, "Long short-term memory," *Neural computation*, vol. 9, no. 8, pp. 1735–1780, 1997.

[8] F. A. Gers, J. Schmidhuber, and F. Cummins, "Learning to forget: Continual prediction with LSTM," *Neural Computation*, 2000.

[9] I. Goodfellow, Y. Bengio, and A. Courville, *Deep Learning*. MIT Press, 2016. `http://www.deeplearningbook.org`.

[10] F. A. Gers, N. N. Schraudolph, and J. Schmidhuber, "Learning precise timing with LSTM recurrent networks," *Journal of machine learning research*, vol. 3, no. Aug, pp. 115–143, 2002.

[11] G.-B. Zhou, J. Wu, C.-L. Zhang, and Z.-H. Zhou, "Minimal gated unit for recurrent neural networks," *International Journal of Automation and Computing*, vol. 13, no. 3, pp. 226–234, 2016.

[12] K. Greff, R. K. Srivastava, J. Koutnik, B. R. Steunebrink, and J. Schmidhuber, "LSTM: A search space odyssey," *IEEE Transactions on Neural Networks and Learning Systems*, vol. 28, pp. 2222–2232, Oct 2017.

[13] N. Kalchbrenner, A. v. d. Oord, K. Simonyan, I. Danihelka, O. Vinyals, A. Graves, and K. Kavukcuoglu, "Video pixel networks," *arXiv preprint arXiv:1610.00527*, 2016.

[14] C. Finn, I. Goodfellow, and S. Levine, "Unsupervised learning for physical interaction through video prediction," in *Advances in neural information processing systems*, pp. 64–72, 2016.

[15] Y. Wang, M. Long, J. Wang, Z. Gao, and S. Y. Philip, "PredRNN: Recurrent neural networks for predictive learning using spatiotemporal LSTMs," in *Advances in Neural Information Processing Systems*, pp. 879–888, 2017.

[16] K. T. P. D. L. library, "Keras documentation," 2018.

[17] N. Srivastava, E. Mansimov, and R. Salakhudinov, "Unsupervised learning of video representations using LSTMs," in *International conference on machine learning*, pp. 843–852, 2015.

[18] N. Elsayed, A. S. Maida, and M. Bayoumi, "Empirical activation function effects on unsupervised convolutional LSTM learning," in *2018 IEEE 30th International Conference on Tools with Artificial Intelligence (ICTAI)*, pp. 336–343, IEEE, 2018.

[19] A. Graves, N. Jaitly, and A.-r. Mohamed, "Hybrid speech recognition with deep bidirectional LSTM," in *Automatic Speech Recognition and Understanding (ASRU), 2013 IEEE Workshop on*, pp. 273–278, IEEE, 2013.

[20] A. Graves and N. Jaitly, "Towards end-to-end speech recognition with recurrent neural networks," in *International Conference on Machine Learning*, pp. 1764–1772, 2014.

[21] M. Sundermeyer, R. Schlüter, and H. Ney, "LSTM neural networks for language modeling," in *Thirteenth annual conference of the international speech communication association*, 2012.

[22] S. Ruder, P. Ghaffari, and J. G. Breslin, "A hierarchical model of reviews for aspect-based sentiment analysis," *arXiv preprint arXiv:1609.02745*, 2016.

[23] D. Eck and J. Schmidhuber, "A first look at music composition using LSTM recurrent neural networks," *Istituto Dalle Molle Di Studi Sull Intelligenza Artificiale*, vol. 103, 2002.

[24] F. Ordóñez and D. Roggen, "Deep convolutional and LSTM recurrent neural networks for multimodal wearable activity recognition," *Sensors*, vol. 16, no. 1, p. 115, 2016.

[25] O. Vinyals, A. Toshev, S. Bengio, and D. Erhan, "Show and tell: A neural image caption generator," in *Proceedings of the IEEE conference on computer vision and pattern recognition*, pp. 3156–3164, 2015.

[26] S. Bengio, O. Vinyals, N. Jaitly, and N. Shazeer, "Scheduled sampling for sequence prediction with recurrent neural networks," in *Advances in Neural Information Processing Systems*, pp. 1171–1179, 2015.

[27] M. Schtickzelle, "Pierre-François Verhulst (1804-1849). La première découverte de la fonction logistique," *Population (French edition)*, pp. 541–556, 1981.

[28] C. Gulcehre, M. Moczulski, M. Denil, and Y. Bengio, "Noisy activation functions," in *International Conference on Machine Learning*, pp. 3059–3068, 2016.

[29] J. Bergstra, G. Desjardins, P. Lamblin, and Y. Bengio, "Quadratic polynomials learn better image features," *Technical report, 1337*, 2009.

[30] Y. W. Teh and G. E. Hinton, "Rate-coded restricted Boltzmann machines for face recognition," in *Advances in neural information processing systems*, pp. 908–914, 2001.

[31] C. Dugas, Y. Bengio, F. Bélisle, C. Nadeau, and R. Garcia, "Incorporating second-order functional knowledge for better option pricing," in *Advances in neural information processing systems*, pp. 472–478, 2001.

[32] D.-A. Clevert, T. Unterthiner, and S. Hochreiter, "Fast and accurate deep network learning by exponential linear units (ELUS)," *arXiv preprint arXiv:1511.07289*, 2015.

[33] D. P. Kingma and J. Ba, "Adam: A method for stochastic optimization," *arXiv preprint arXiv:1412.6980*, 2014.

[34] Z. Wang and A. C. Bovik, "A universal image quality index," *IEEE signal processing letters*, vol. 9, no. 3, pp. 81–84, 2002.

[35] N. Srivastava, G. Hinton, A. Krizhevsky, I. Sutskever, and R. Salakhutdinov, "Dropout: a simple way to prevent neural networks from overfitting," *The Journal of Machine Learning Research*, vol. 15, no. 1, pp. 1929–1958, 2014.

[36] J. M. Kilner, K. J. Friston, and C. D. Frith, "Predictive coding: an account of the mirror neuron system," *Cognitive processing*, vol. 8, no. 3, pp. 159–166, 2007.

[37] R. P. Rao and D. H. Ballard, "Predictive coding in the visual cortex: a functional interpretation of some extra-classical receptive-field effects," *Nature neuroscience*, vol. 2, no. 1, p. 79, 1999.

ASTES

Advances in Science, Technology and Engineering Systems Journal
Vol. 4, No. 2, 270-279 (2019)
www.astesj.com
Special Issue on Recent Advances in Engineering Systems

ASTES Journal
ISSN: 2415-6698

Enabling the Edge - A method for dynamic virtualizable connections for 5G deployments

James Robert Pogge*,1, Stephen lucien Scott[2]

[1]*Electronics Computer Engineering Dept, Tennessee Technological University, 38505, USA*

[2]*Computer Science Dept, Tennessee Technological University, 38505, USA*

ARTICLEINFO

Article history:
Received: 20 December, 2018
Accepted: 25 March, 2019
Online: 10 April, 2019

Keywords:
5G
Terabit
Edge routing

ABSTRACT

The telecommunications industry continues to move forward with plans for 5G service with rates including 6Gb/s followed by upgrade paths promising 20Gb/s. Despite advances in wireless technology associated with 5G roll-outs, there remains the problem of providing sufficient back-haul throughput and efficient handling of hand-off services within the relatively small projected cell boundaries that can handle the higher frequencies required for these data rates. Dense network discussions include proposals for macrocell centric groupings that directly support multiple micro-cells to create a larger service area. The two-tiered approach presents additional complexities when considering the dynamic nature of mobile wireless networks. The added delays of multi-tier hand-offs compound the already heavily burdened throughput capability of the back-haul service towers. The 5G enabled network should easily allow legacy technology 4G and 3G connectivity without sacrificing usable bandwidth by dedicating limited back-haul ports to legacy technology. The presented methodology is a hybrid distributed optical switch embedded directly within the micro-cell towers that simplify hand-off and allows for dynamic allocation of bandwidth on demand. Simulation results and a test-bed optical network interface suggests that bandwidth on demand topology is possible combined with software-defined dynamic routing in a flat plane topology. The solution uses already available technology found in high-speed Internet backbone distributions.

1 Introduction

Large scale deployments of 5th generation (5G) enabled towers to require ever-increasing access to bandwidth to provide near real-time service to connected customers, [1]. At the high frequencies projected for 5G deployments 56-60GHz, the effects of propagation fade and multi-path issues in dense urban environments become more prevalent. [2]. [3]. The pre-rollout solutions being tested now trend toward a network model of multisector closely spaced cell towers, [4] , [5]. The emerging deployment model is classified as an ultra-dense network, [6], one that is tightly spaced clusters of overlapped minicells. The emerging 5G topologies include multiple backhaul proposals using millimeter wave macro cells as shown in figure 1, a centralized aggregated service portal with fiber access switch to the Internet [7]. These macrocells use millimeter-wave wireless modems within the higher capacity 28-100 GHz proposed RF bands. The bandwidth requirements of the microcells stress the limit even for 60 GHz channels. High-density RF modulation directly from the macro tower to the microcell service cluster using OFDM (Orthogonal Frequency Division Multiplexing) is necessary to deliver promised service to multiple wireless customers while maintaining regulatory requirements for supporting legacy 3G and 4G LTE access, [7].

In existing cell networks such as those found in 4G Long Term Evolution(LTE) base stations, the moderate backhaul requirements are provided through the proper arrangement of high-speed network switches, [8], typically a series of aggregated gigabit Ethernet. In high-density networks of this type, the switch latency

*Corresponding Author: James Robert Pogge, Kingstom, TN USA, (865) 335-4164 & jrpogge42@students.tntech.edu

https://dx.doi.org/10.25046/aj040235

and density of data are limited by existing centralized 10G switches. The high volume of traffic times makes 5G promised real-time data streams difficult to achieve. Consider that the proposed 5G service rates of nominally 5Gb/s to the projected 20 Gb/s service require high bandwidth when each sector microcell should service 10 or more customers to meet market expectations.

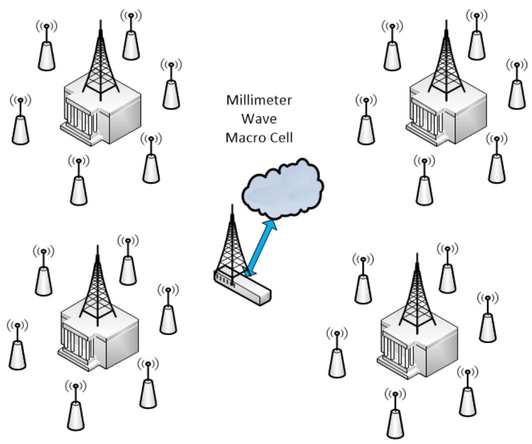

Figure 1: Millimeter wave Macrocell Backhaul

In a dense urban environment that demand load can change dynamically, [8]. In the latest industry projection for data usage requirements, the demographic shift of post-millennials shows that tablets are gaining in favor. Video phone calls are displacing texting and traditional voice calls especially in urban work environments. The current trends suggest that the majority connection will use a significant portion of the advertised 6Gb/s connections, [8]. Despite Multiple Input, Multiple Output (MIMO) radios covering the last connection in the microcell, the service to individual users is determined by the underlying switch topology under stress in high-density population centers and not the carrying capacity of the local radio modem, [9]. Additionally, the cost of a multi-tiered TCP/IP switch network in smaller area ultra-dense networks due to the propagation limits of the proposed RF bands implies that following the existing 4G aggregated network model becomes prohibitively expensive. [10], [11].

In this paper, the authors propose a dynamically reconfigurable network interface that allows bandwidth allocation to be resolved on the fly and shared equally with adjacently connected towers. The backhaul demand is accomplished through a virtualizable plane parallel optical topology that relies on the use of available fiber optic technology originally intended for long distance backhaul Internet applications. The proposed solution includes emerging flex-net transceivers located directly in the minicell sector 5G radios eliminating the need for expensive aggregated switches. The individual sectored wireless links gain direct access to the entire optical bandwidth of the backhaul network as required without upgrading micro cell towers. All of the microcell sector RF modems are serviced directly through a locally centrally managed sector scheduler node. This proposal includes a method for (SDN) software-defined network bandwidth allocation, use scheduling, and access control. Service scalability is handled through user-specified virtual networks connections that coexist with existing allocated fiber traffic. New connection and microcell commissioning can be achieved entirely without interference to existing network traffic flow or pathway allocations.

This paper introduces the concept of virtualizable ports or service interconnects by utilizing existing technology previously reserved for the highest speed terabit optical Internet backbone. The goal of this work is a presentation of a truly programmable SDN 5G solution. The result is a near flat network topology capable of accessing maximum available bandwidth on demand while maintaining system scalability. The embedded optical switch in the sector modem edge device is direct to fiber routing switch eliminating the need for a more traditional centralized layered network switch distribution approach.

2 Legacy Network Model

Typically in a switch based topology, increased access to bandwidth is limited by the availability of existing ports or pathways through the aggregated layered switches. In abnormal traffic situations breakdown occurs when the number of allocated switch ports exceed the expected number of users in a given sector. In the use case of a special event, such as a conference or sporting event where unusual traffic is concentrated in a smaller area, this requires the installation of additional switch devices installed specifically for the event along with increased numbers of temporary microcell sites. Additionally, connection delays in adjacent macrocell sectors are introduced as routing paths are arranged to handle the increased load. In ultra-dense networks, as expected the probability of achieving a successful connection to the user network decreases as the number of active nodes increase. Mitigating this effect requires dynamic allocation of bandwidth to the microcell. Responding to the increased demand during peak usage times is altered when unusual circumstances occur within the service area demographics.

The switch fabric connecting the tower to adjacent towers and subsequently the backhaul Internet connection must exceed the expected number of active end-user nodes without interfering with existing service connections. The probability that more than one node $(N+1)$ attempts to access the network port simultaneously is expressed in Equation 1the probability (p) of access success is directly affected by the number of users attempting to connect. Which naturally implies that increased activity will adversely affect available bandwidth as the number of endpoint nodes (users) increases. The backhaul bandwidth is further reduced as the shared bandwidth of each microcell connection is assigned. Additionally, adjacent sectors need reliable access to backhaul bandwidth to help take up the slack of the system and ensure timely hand-offs.

$$\sum_{i=1}^{N+1} \binom{N}{i} p^i (1-p)^{N-i} \tag{1}$$

In legacy network switch based systems, during expected normal use cases, the majority of the backup capacity resources allocated to a sector remain under-utilized. The common base station design solution found in the majority of installations is to use additional routers and sector servers to increase the number of available sub-nets in the system. In low demand situations, these additional ports are fixed to the macrocell sector and are unused. These ports cannot be easily transferred to adjacent sectors or towers.

The underlying issue is that even with the use of millimeter backhaul the availability of routing ports in traditional network switches remains relatively static. New pathways to the centralized service center must be re-commissioned affecting the entire network. In most legacy systems prudent cost reductions require that only predicted network traffic load patterns are considered when designing the microcell distribution. If the base station is operating under stress, the result is an overall reduction in system performance. The solution lies in finding a methodology that both increases bandwidth and allows simple dynamic allocation and access to the increased bandwidth.

3 Edge Network Model

The most reliable 5G base station distribution model to date, which has been demonstrated in-situ, requires less than 1km between sector clusters. In most cases, urban models for high population centers suggest a 200-meter cell spacing. [3], [4]. The propagation models used in this proposal follow the (ETSI) European Standards Organization study [4] for an urban propagation model demonstrated in Equation 2 which models high density urban wireless networks. Highly dense urban models suffer from dense user traffic, propagation blocking obstacles, and multiple overlapping microcells. The maximum expected intra-base station spacing lies within the proposed 5km macrocell placement limit [4]. This limit also falls well below the threshold for significant optical dispersion interference between the closely packed optical channels required within the photonic switches. This suggested 5km limit also eliminates the need for optical amplifiers or repeaters between the microcells and the optical macrocell. Microcells are projected for 500m spacing however the ultra dense urban environment may make 200m more likely. The proposed networking topology model and router definitions used in this study reflect this limitation.

$$PL_{UMa-LOS} = \begin{cases} PL_1 & 10m \le d_{2D} \le d'_{BP} \\ PL_2 & d'_{BP} \le d_{2D} \le 5km \end{cases} \tag{2}$$

The test model follows the ITU specification [12], for channel allocation. The number of occupied channels in the fiber connection between stations contains a finite number of substreams covering N sector nodes in the system. This implies that there is a probability p that K active nodes are accessing the network at any given instance. In high traffic demand areas, this load changes dynamically and is expressed in Equation 3.

$$\binom{N}{K} p^K (1-p)^{N-K} \tag{3}$$

Consider that the majority of network traffic lies in simple data transfers such as email and web browsing requests, or similar nonstreaming operations. The emerging 5G network proposals offer much higher data rates to provide more advanced services. These services have near real-time prioritized packets, such as (VOIP) voice over IP and video streaming. In these use cases, the network path must stable to allow a steady non-blocking stream regardless of sector load. In most cases, the system designer builds the edge server to a predicted load model with approximately 20% overhead to handle additional network demands. Over-designing a sector results in increased power consumption, installation and maintenance costs for a given cell tower.

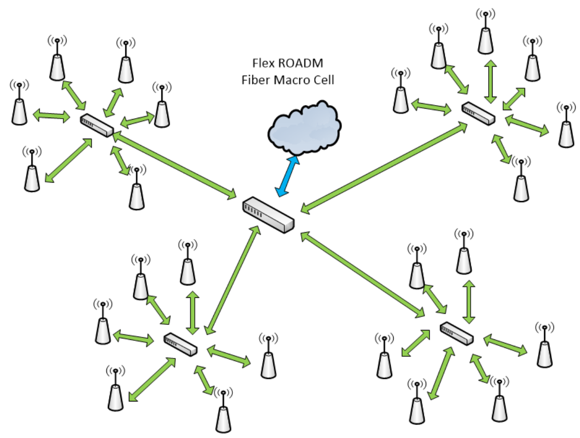

Figure 2: Flex Fiber ROADM Switched Backhaul Macrocell

Edge networking is a method that moves the control and access to the network directly to the end user node, at the edge. The optical network model proposed moves network access to the point of use. In traditional networks, multiple paths to a macrocell require fixed switch port allocations. In contrast, using the extreme bandwidth afforded by tunable laser transceivers and multiple wavelength selectable photonics switches allows the system manager to dynamically allocate bandwidth to meet the needs of the base station. When load demand increases, unused bandwidth can be allocated dynamically, without changing or adding existing equipment. Pathways to the Wide Area Network (WAN), are replaced with user selectable optical wavelength channels virtualizing port connections within the network. The photonic user reconfigurable switch embedded in each NIC allows all microcells to be interconnected and any backhaul pathway on demand, as in Figure 2 using the proposed solution model.

In the proposed solution the edge network wireless interface and the available capacity of the sector radio modem are finite and represents the only limitation to the system architecture. Predicting 5G deployment is difficult, the base station location remains static, while the connection load and bandwidth demand are intrinsically dynamic. In switch based topologies, priority signals with high data rate connections experience interference with the routing requirements of new connection requests. The radio hand-off and other management traffic requirements use much smaller packets in the transport model and can be handled in a secondary network designated for command and control. In edge networking, parallel network pathways are common to alleviate traffic congestion. An increase in the number of users and therefore required connections sharing backhaul access pathways cut into available port bandwidth, even for simple management tasks. The result is an increase in asynchronous packet collisions on the central network access ports that are simultaneously attempting to stream high-speed data and handle the dynamically changing handoff management packets. The wide-ranging user access data rates necessary to provide efficient, reliable 5G level service requires a new methodology. Bandwidth allocation for the requested service and the number of network connections need to be either commissioned or placed back in the service pool on the fly without interfering with ongoing network traffic.

4 Plane Parallel Optical Network Topology

The concept of a "plane parallel" network is based on open and free connectivity between all attached nodes within a computer cluster topology. This concept can be easily adapted to data delivery services found in cell tower networks. The optical network topology further introduces the concept of virtualizable interconnects or ports made up of assigned combined optical and temporal data streams. This access flexibility enables the system administrator to create connections or ports on demand within the available optical bandwidth, which on a single fiber is currently in excess of 14Tb/s [13]. The underlying concept is to separate the optical wavelengths into service channels to parallelize the number of active networks within the system. Current research involves methods for managing high-speed data streams in optical systems. However, these methods are more of an adaptation of existing switch technology involving aggregated lower tiered switch networks. Once an optical pathway is set it remains relatively static to service the Internet backbone pathway, [14], [15].

The proposed optical backhaul uses extreme bandwidth networking interfaces to create a plane parallel network topology that allows multiple networks to reside on the same backbone without interference with adjacent traffic and increased delays. The proposed solution allows the sector control system to quickly establish and bring up additional sub-networks and assign service temporal data streams as required. The newly assigned virtualized interconnections allow system administrators to handle increased data loads and temporary high throughput services within the plane parallel topology. All access is direct to the optical network without reassigning existing pathways or switching through other physical ports as within a tiered switch system. Redundancy and resiliency are provided through access to multiple fibers. Optical networks have direct scalability intrinsic to this methodology through the use of redundant fiber bundles.

Networks and sub-clusters can be commissioned and decommissioned on the fly as opposed to required downtime through manipulation of the physical switch port and cable swaps between the installed macrocells. The basis for this plane parallel system is the use of photonic (ROADM) Re-configurable Optical Add Drop Multiplexer optical switch device and wavelength tunable transceiver lasers. These photonic interfaces are embedded directly within each network interface controller (NIC) located at the microcell sector interface. The central traffic management software can program any ROADM device to switch any frequency to a specific fiber. Using the ITU channel specification, the single fiber can handle 72 200Gb/s wavelengths simultaneously. The ROADM device allows one or more of these wavelengths to pass through reducing unnecessary traffic at the end node. A single fiber can easily handle multiple macro cells at the proposed full capacity of the 5G microcells. Legacy protocols are all supported through a required new socket layer control interface that can encapsulate existing protocols delivered to the NIC. Pre-assigned management and service data streams are located on separate wavelength networks within the optical interface. Service requests are handled as a task-oriented or process assignment which allows individual control of both the node service commissions and separation of parallel sub-networks providing requested services.

The centralized system scheduler-management application utilizes a common management network to respond to service requests from sector modems. Since all nodes are simultaneously available on the parallel fiber interface, a method is provided to handle handoff and assignment to active data streams that utilize a process ID addressing scheme rather than the common physical address used in existing network protocols. Service to the user is assigned a process ID, in email text legacy phone services these packets transmitted in the backhaul with the process or service connection ID and the IP addressing is decoded at the sector micro cell interface. If multiple users are streaming video this process ID can be parallelized to send the live video, or conference meeting stream to multiple users without establishing separate connections.

4.1 Optical Network Topology

The proposed network takes advantage of the extreme bandwidth availability using existing optical network interface equipment. A closed loop testbed was built to verify simulation models for both physical transmission of highly dense optical signals and the proposed transceiver modem used in the proposed NIC. Since this application is intended for use in a large scale distributed edge computing environment, one that can contain more than 10K connected nodes or devices, it is assumed that the maximum distance between any node is within a 1 km boundary to avoid dispersion effects found in long haul optical networks. In this configuration, any of the issues associated with optical dispersion and ICI (inter-channel interference) have negligible effects within this application.

The outstanding challenge involved with 5G backhaul bandwidth allocation is handling the dynamic increase in high-speed streaming services combined with the relatively short distance between handoff nodes. The number of users and the type of service requested is dynamically changing. It would be a waste of the proposed system's available bandwidth to simply assign optical channels of equal capacity to each microcell sector. The handoff from one radio to another is as simple as enabling an otherwise blocked temporal substream in the new radio already present on the optical interface, verifying the connection and dropping or blocking the stream on the previous radio. The proposed solution simulation example utilizes 50Gb/s tunable transceivers although 10Gb/s work just as well. The ROADM optical switches are embedded in each network interface card to allow a contention-less, colorless and bidirectional connection directly to one or more backbone fibers making up the plane parallel network distribution. Ideally, scalability of services requires adding fiber transceivers to the NIC interfaces in the microcell node using one or more of the dark fibers in the macrocell bundle. Telecom fiber installations typically include 12 to 24 fiber pairs for future use.

4.2 Flex Grid at the Edge

The use of ROADM based photonic switches flexible grid capability does not limit nor relegate the available channel spacing to one fixed size, rather the scheduler-manager application can assign varied channels boundaries within available requested optical range as needed to fill the optical boundaries. See Figure 3, which illustrates the flexible distribution of optical channels allocated. The impact of this optical boundary flexibility is that existing optical backhaul networks with fixed optical bandwidth boundaries can easily coexist with the addition of flexible channel allocation. Temporary ad-hoc networks commissioned for short term use can be combined into a larger channel if needed by a macrocell. Higher capacity channels can be assigned in a specific sector during peak usage hours and reassigned as the demand changes throughout the system.

The entire proposed network topology shares one or more common bidirectional fibers linking the sector modem at the edge thus bypassing the traditional distributed layered switch topology found in most 4G and legacy networks. The proposed method achieves a high-end user count with a flexible ratio of streaming (large packets) to service and management (small packet) distribution. Secondary transport methods evaluated varied between more common TCP/IP, and RDMA (Remote Direct Memory Access) favored by streaming clients. RDMA has significantly lower response latency because it systematically bypasses the processor core software by using the transport layer stack writing to memory directly. RDMA has an advantage in streaming services because large data files can be downloaded directly to the macrocell buffer to be distributed at a lower rate, freeing up the bandwidth to service other requests.

Proposed 5G market strategies favor streaming applications, and therefore the proposed solution will focus on the challenges of higher speed data and streaming packets. The optical router to radio interface will assume a 40Gb/s - 50Gb/s Ethernet connection assigned to one or more optical channels on a single fiber. The simulation of the control system assumes a minimum of four separate fibers available to each macrocell microcell cluster. Integrated multiplexing photonic switches allow for any four fibers to any four fibers multiplexing switch at the edge, controlled electronically by the sector node. The backhaul access can easily be scaled up to a 16-by-16 switch in future deployments. Similar networks have been proposed in HPC (high-performance computing) platforms [16, 13]. The embedded optical switch proposed allows the system to select one or more optical fiber pathways to adjacent towers or directly to the centralized backhaul Internet connection or data telecommunication center. Handoff communications are handled by the local towers rather than a centralized data center.

4.2.1 Available Optical Bandwidth Potential

The ROADM devices coupled with wavelength tunable lasers offer a "flexible" wavelength grid mapping capability that is completely user programmable. Acknowledging that this system proposed must exist in legacy networks, we will follow the ITU 694 wavelength channel assignment grid [12]. The ITU G694 specification currently has a defined maximum channel capacity of 100 GHz bandwidth each within the L band (1500 nm), made up of 72 optical channels of 100 GHz each from 190 THz to 194 THz [12]. Each 100 GHz channel has a standard capacity of 200 Gb/s each, using the common PAM (pulse amplitude modulation) 2 bit per Hz method. The data rates used in this study reflect this to illustrate the system viability using lower density modulation techniques. Emerging transceivers are demonstrating QAM 16, QAM 64 and OFDM over fiber, [13]. The term "flex grid" suggests that each available optical channel can be broken up into sub-channels as long as the highest density channel boundaries remain static. Sub-optical channels are chosen such that the entire boundary is filled leaving no unused assigned space. A simple example is that of a single 100 GHz channel. The highest bandwidth under ITU, which can be subdivided into any combination equal to 100 GHz. Example, a single 50GHz channel, a single 25 GHz channel and the remaining can be a second 25 GHz channel or two 12.5 GHz channels as needed. The scheduler manager makes this allocation based on the type of service (data rate) and the number of expected users (nodes) on the microcell sector radio. The ROADM device is programmable electro-optically allowing these boundaries to be assigned. The optical wavelength and bandwidth representing the allocated sub-network channel to pass either upstream or downstream along the fiber. Figure 3, illustrates the existing boundaries within the ITU grid [12], and the flexible boundary assignments within each ROADM switch NIC device. It is important to note that ROADM devices have been demonstrated operating outside of the ITU assigned channel grid constraints and can have a completely user programmable boundary for channel allocation, [17]. In the test bed for legacy network compatibility the ITU grid boundary definitions are used.

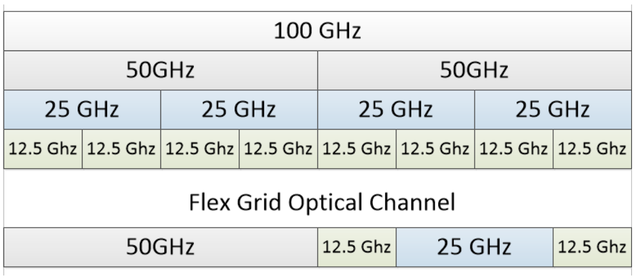

Figure 3: Single channel 100 GHz band divisions

Optical-Temporal data distribution is a method where the optical channels exist in a parallel plane. Each subsequent optical channel is broken up into temporal streams to accommodate varying bandwidth requirements filling otherwise empty space. The proposed solution provides that each assigned optical channel has the ability to further allocate the available bandwidth with a subset of temporal data-streams. Since most individual user connections cannot fully utilize 200 GB/s and promised 5G service is no more than 5 GB/s, the wide optical bands are filled with multiple data streams separated by time. A TDMA based set of temporal sub-data streams are included in the proposed solution shown in Figure 4. This hybrid optical channel/temporal data stream method allows the management controller to fully utilize the extreme bandwidth of the fiber, without using de-aggregation fixed port network switches. This arrangement is desired because the bulk of the connections will be asynchronous and flexible in size. Connection assignments are made using a single data stream or can be combined into compound streams when higher throughput is required by the service requested.

Table 1: Single fiber sub-channel data capacity

Optical Bandwidth	Modulation Density	Channels Available	TDMA Streams	Stream Bit Rate
100 GHz	200 Gb/s	72	2304	6.25 Gb/s
50 GHz	100 Gb/s	144	4068	3.125 Gb/s
25 GHz	50Gb/s	288	9216	1.56 Gb/s
12.5 Ghz	25 G/s	576	18432	781 Mb/s

Once a connection has established the wavelength and temporal stream assigned to the connection are given a unique connection ID code used as a compact routing header. The resulting connection assignment serves as a virtual port and is defined as a specific optical channel with one or more temporal data stream. The routing pathway is therefore further defined as Fiber 1...n, ITU channel wavelength 1...n, and temporal data stream 1 + n + m. One or more end user can share a single optical channel and temporal stream using the assigned connection ID code in the proposed socket header as a delivery method.

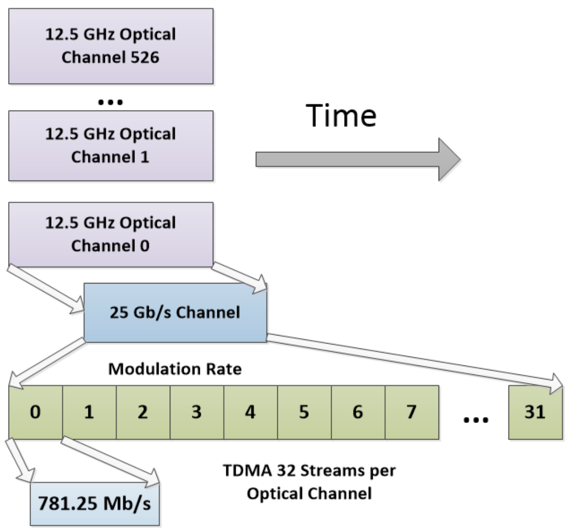

Figure 4: Parallel Optical Temporal Streams

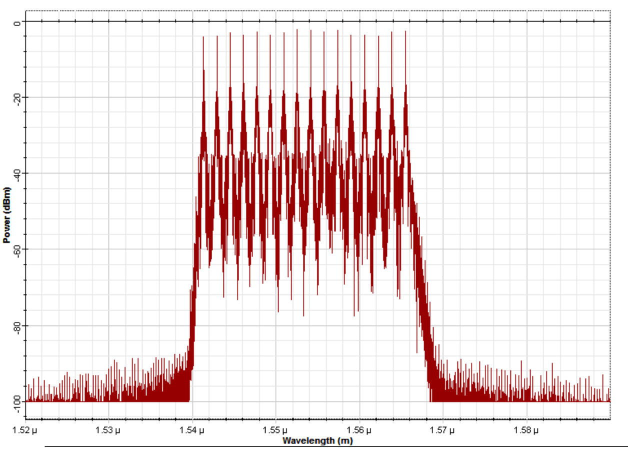

Figure 5: Parallel Optical Wavelengts

The sub-data streams are assigned by the scheduler-manager software when a connection is commissioned for a specific service or process. A channel request packet is sent to the scheduler manager node for increasing or relinquishing assigned bandwidth back to a common resource allocation pool. The number of temporal sub-streams assigned is entirely up to the schedule manager. In the example application, each ITU designated optical channel has been assigned 32 temporal data slots within each optical transport band. A single base station can supply 9,216 1.56 GB/s data streams using a 50 Gb/s laser transceiver on a single fiber. Individual connection capacity is calculated using existing radios modulation capability coupled with the assigned bandwidth of the optical channel. In the test bed, example channel capacity is limited to a simple optical PAM modulation signal and using existing ITU defined channel boundaries. Simulation indicates that the multiple wavelengths can easily coexist at these channel boundaries. Figure 5, shows a simulation of 16 ITU sub channels all using 40 Gb/s lasers over a single 1 km fiber. A breakdown of an available channel using the suggested 32 sub-temporal data slots is shown in Table 1. This table contains the channel capacity for each of the assigned optical bands and temporal sub-channel count and the number of supported streams and capacity of each. A single fiber with 72 100 GHz optical channels can contain up to 14.4 TB/s capacity using this method. The backhaul quad fiber integrated edge switch has a capacity for 57.6 Tb/s.

The proposed photonic NIC contains packet buffers in the physical layer with intrinsic transceiver buffer load and unload times dependent on buffer size and memory access speed. The use of temporal data slots allows the system to synchronize the projected arrival time of the next data slot to match the physical load time of the buffers used. In most cases using temporal sub-channels allows for data buffers to be loaded or unloaded while waiting for the next available data slot, thus limiting transmission gaps within the optical channel.

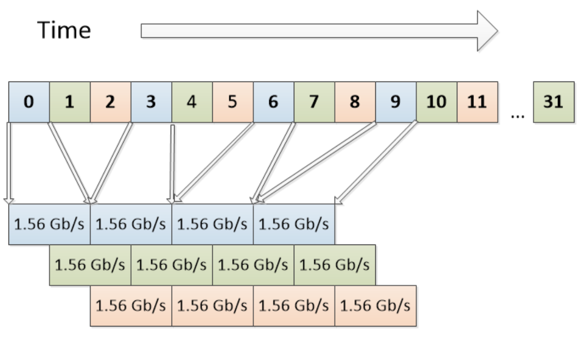

Figure 6: Aggregated staggered Temporal Data Stream

The chart in Figure 6 shows a typical scheduler assignment that uses four lower rate temporal data streams of 1.56 Gb/s each to be combined as a single 6.25 Gb/s virtualized port. In this example, the assigned multiple temporal slots are staggered to match the buffer fill times. The result is an effective zero buffer wait state for the physical transceiver buffers. In high bandwidth transmission non-aggregated packets that make up the bulk of networking traffic leave behind large gaps in the available transmit times. The temporarily assigned optical channel and sub-data stream act as virtualized connections at the socket layer. In the proposed network a commissioned modem tunes the laser and the ROADM receiver filter to a specific optical frequency and the electronics receiver uses the frame-sync timing signal from the command and control stream to synchronize the radio transceiver. The majority of packet buffering is handled directly at the edge as data is loaded into the physical layer buffer of the 5G radio modem.

4.2.2 Switch Scalability Model

The proposed 5G 5Gb/s use case can be realized using this distributed aggregation model using an optical transceiver with 25 Gb/s capacity shared across 32 temporal substreams. This transport data rate closely matches the proposed 5G maximum data rate and fits within the existing boundary of the existing ITU grid. As an example, in a single fiber network, consisting of eight sector 5G radio modems this represents non-blocking capacity for over 2000 individual 6 Gb/s data streams on a single fiber. A quad fiber ROADM switch increases this capacity per base station to 8000 non-interfering streams. Assuming the average expected end-user node typically requires around 1 Gb/s the number of available connections can be increased to 32K. The entire network capacity shares the plane parallel bandwidth assignment boundaries and an updated boundary map is distributed as a management packet on the control network. This allows all connected macrocells and microcells to know where a service stream is located within the optical/temporal channel assignment. Consider a 5G urban network with 6 Gb/s service capability and a projected average of 200 active connections at any one time per macrocell spaced at 1km. Using a shared fiber backbone connection 40 microcells spaced a maximum distance of 200 m from the macrocell can be serviced using only four shared fibers. The quad-optical switch proposed allows any sector radios access to the four backhaul fibers. The central scheduler manager handles the subnetwork assignments from the resource pool. When a connection is dropped, the channel allocation is demapped and returned to the resource pool. All connection requests use the single command and control optical network.

In this macrocell configuration, each of the four backbone fibers has a full spectrum carrying capacity of 14.5 Tb/s based on the ITU 100 GHz grid model. A single 16 sector microcell utilizing a quad fiber has direct access to 57.6 Tb/s of backhaul bandwidth. This translates to 9216 connection single temporal data streams each carrying 6.25 Gb/s covering the basic 6 Gb/s desired service with overhead for control messaging, from table 1. If 20 Gb/s connections are required, there are two compromise solutions using the standard ITU grid. Three temporal data streams can be combined for 18.75 Gb/s on 3072 virtualized connections or four data streams can be combined for 2304 25Gb/s connections. The user programmable flexibility of the optical and temporal data assignments suggests that any combination up to the optical switch's maximum capacity for an assigned channel can be commissioned on the fly. The bandwidth allocation and connection commissioning are handled by the central scheduler manager node as required. Channel and sub-net assignments are negotiated by the requesting node for the type of service desired without impacting the other ongoing connections.

4.2.3 Test bed model

A testbed modem was used for the study using a two-channel transceiver with a functioning block diagram as shown in Figure 7 . The test bed consists of two (SPF+), Small Form-factor Pluggable, 10 G Tunable Lasers, and a pair of ROADM photonics devices. The testbed was used to verify that two adjacent dense packed optical channels can co-exist using a commercially available ROADM device [18], on the same fiber.

Measurements were made with adjacent lasers at full data rates and through separate photonics filters assigned before transmission. Inter-channel interference was measured on adjacent channels using a 20GS/s oscilloscope and found to be well below 100db specified by the ITU grid flex switch manufacturer, captured in Figure 8. Individual grid assigned optical wavelength channels can be duplicated as long as they are not located on the same fiber.

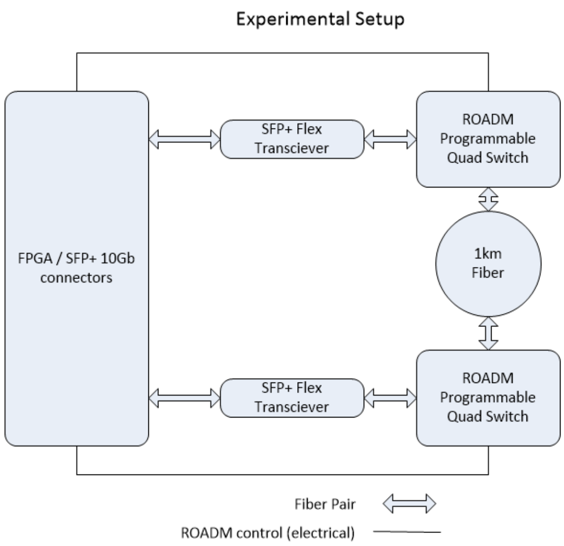

Figure 7: Experiment Schematic

Consider an extremely large control system, one defined as having more than 10K device connections. Distributive control is easily realized using this proposed topology. Lower bandwidth connections such as voice traffic, email or Internet browsing are assigned much smaller subdivided optical-temporal data streams. In most applications, these assigned data streams contain more capacity within the sub-channels then their existing counterpart high bandwidth switch based ports.

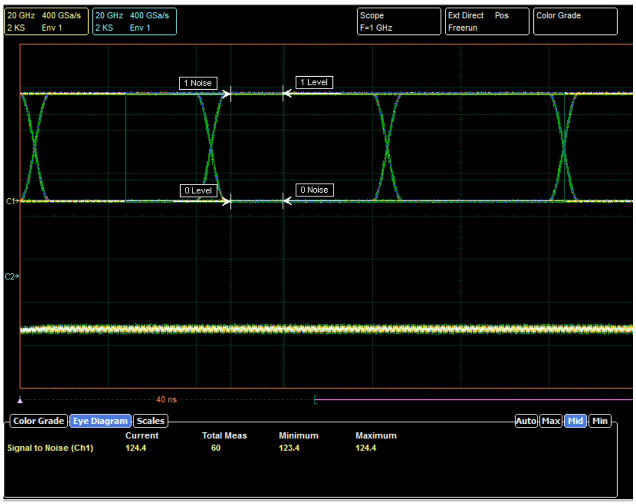

Figure 8: 10G received eye pattern with less than 100 db SNR

Advanced modulation techniques can increase the bandwidth of existing ITU channels or a custom optical channel distribution can be used in a homogeneous configuration. Specifically, one that does not have to conform to any industry-wide standards for channel spacing and center frequencies, such as a singularly connected private network. A recently demonstrated 400 Gb/s 64 QAM modulator [19], could increase the number of available 5 Gb/s links for a base station with a single fiber to just over 4500 service sub-nets, with a 500m separation limit. The bit rate limitation is due to the optical distortion effects common in higher order modulation methods.

4.2.4 Dynamic Port Assignments

A control access channel connection is maintained such that all available resources and radios can request service from the scheduler manager from a shared local network management channel. This same control path is shared by adjacent towers to facilitate handing off sub-nets instructing the new radio to switch the optical signal to the new sector. The process of bandwidth allocation and commissioning of system resources is independent of ongoing connections. In most applications, one or more optical-temporal streams are assigned as default command and control pathways for the desired service. The only one universally available command access network is permanently assigned to all macrocells and microcell NIC cards to facilitate a fallback command and management network path. During registration and commissioning the original transceiver MAC (media access controller) address, specific to the physical NIC in the sector radio, is used to identify the requesting device. Once commissioned all data transfers are sent with the process connection node ID code assigned during commissioning. The highest physical layer of the optical modem selects the optical channel and captures the assigned temporal streams and checks each transfer with the process ID, to repackage and route the data to the end user. The control management system can directly access any assigned device by using the commissioned user node ID registered in the resource pool data base. During task and process communications, all network traffic after this uses the assigned optical temporal data paths and connection ID codes to distribute packets to their intended recipients.

4.2.5 Simulation Results

Performance of the proposed topology is limited to the latency in the photonics switching and modulation technique used. There are no multi-tier network switch buffers to fill, as are found in non-blocking switches. There is however a delay exists when an edge NIC is waiting for the next periodic arrival of the assigned temporal data stream.

During commissioning, the scheduler Manager uses the database of resources coupled with the requested data rate to match the temporal streams to the service NIC buffer fill and flush times. This temporal assignment mitigates extraneous delays and creates a near zero wait state delivery schedule. The total latency is defined by the stream availability delay and the electronic to optical conversion delay and modeled in Equation 4. Where total latency is the slot arrival time T_{slot}, added the data transfer propagation delay, $\frac{P_{length}}{D_{rate}}$ and finally electro-optical delay transforming the electronic signal to optical T_{e-o}. In the hybrid optical edge switch, there is no tiered switch induced latency. Ideally, the arrival time of the next available temporal data stream should match the time to fill the transceiver buffer. This method hands-off large stream buffering to the microcell sector radio rather than the shared network switching topology.

$$T_{total} = T_{slot} + \frac{P_{length}}{D_{rate}} + T_{e-o} \tag{4}$$

Throughput is dependent on a number of active links and their respectively assigned optical bandwidths. It is therefore defined by the average of the sum of the through-puts of all the subchannel links N_{link} as in Equation 5, where T_{e-o} represents the electronic to optical conversion delay.

$$Throughput_{avg} = \frac{\sum_{i=1}^{n} Throughput_{perlink} * i}{N_{link}} \tag{5}$$

In this study, the single pathway latency for a delivered packet was both simulated and measured in the test bed to determine the average delivery latency. The size of the packet used was a range of test packet sizes from 16 bytes (management request or acknowledge) and large scale streaming 16K packets and found to center around 4 uS in the 40Gb transceiver, and 3.5 uS in the 50Gb/s Ethernet over Infiniband transceiver as shown in Figure 9. The simulation used NS-3 with a custom model generated using the measured latency from the testbed, There is a slight increase in latency as the packet size is maximized due to the last point buffer fill times piling up during transmission. In most cases the entire receive buffer is available long before the next packet arrives when simulating a 6 Gb/s 5G user link.

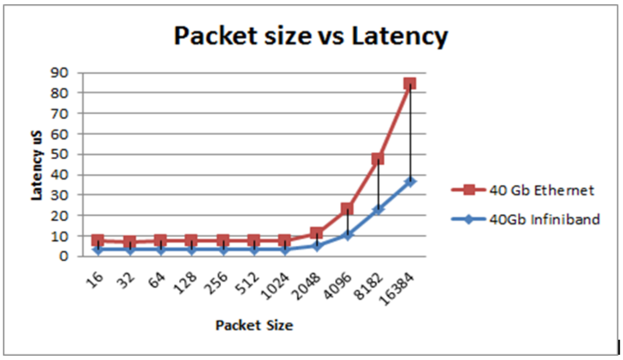

Figure 9: Transport latency vs. packet size

As the network load approached the maximum throughput of the assigned channels, the latency increased, primarily due to occasional loss of synchronization with the assigned data stream. This can be remedied by either increasing the staggered delay assigned slot or the size of the fill buffer in the transmitter-receiver interface. The lower network loads from 1 to 85% capacity remain reasonably static as shown in Figure 10. The temporal data streams are continuous, so it follows that the increase in latency at the higher packet sizes is due to the encapsulating of the segmented packets within the new socket structure. This effect was caused by the legacy TCP/IP protocols, including Ethernet ARP (address resolution protocol) included within the network stack. The optical transport header making up the outside layer using the process ID code to identify the packet at the destination, replacing the physical addressing used in the legacy protocols. Jumbo frames were not used in the study, so the limitation of 1500 bytes [20], remained requiring the transmission of several smaller packets when larger block sizes where transmitted.

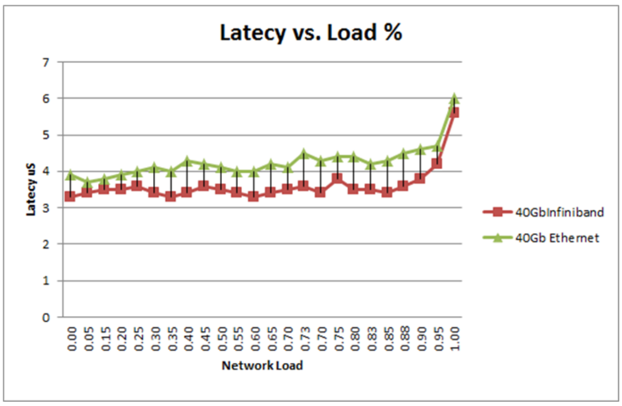

Figure 10: Transport latency vs. network load

5 Conclusion

The purpose of this study was to explore an alternative approach to the issue of bandwidth availability in 5G macrocells. The proposed approach was to use emerging technology for terabit networking and apply it as a (FTTC) fiber to the curb solution. There are three key issues addressed.

- Reconfiguration of the bandwidth to match dynamic loads.
- Reduce system costs while providing scalability.
- Provide a method for de-aggreagating 200 Gb/s streams directly to 6Gb/s streams without tiered switch network.

Simulations followed by testbed experiments show that the emerging ROADM photonics technology can be adapted to allow the network designer to provide a complete software-defined distribution network that is dynamically reconfigurable on the fly. The existing commercial hardware meets this constraint. Direct optical access requires replacing the Ethernet physical layer in the TCP/IP stack with a new layer that provides a bridge between the terabit optical interface and the 5G microcell sector modem 10G Ethernet NIC. Scalability requires a swap out of the SFP photonics transceiver device in the NIC to 40Gb/s model to support the expected 20Gb/s 5G service model. A prototype interface was tested and acted as a proof of concept for this work, which met the requirements of the 6Gb/s service model using a ROADM module [18] and an SFP+ 10 Gb transceiver through 500m of fiber. Certainly, within the confines of existing legacy optical network standards [12], it has been shown that it is possible to provide adequate 6Gb/s data streams co-existing on a single fiber without blocking or interference with legacy 4G and 3G traffic. Additional efforts are needed to fully refine and test a new physical (SDN) software-defined networking protocol layer to be applied to a fully expanded testbed that models an entire 5G macrocell. Future efforts will focus on the command and management protocol necessary for full deployment of this concept.

Conflict of Interest The authors declare no conflict of interest.

Acknowledgment The authors would like to thank Optiwave Inc, and Infinera Inc. for simulation software and flexgrid photonics technical information.

References

[1] T.S. Rappaport, S. Hu, R. Mayzus et al.,*Millimeter Wave Mobile Communications for 5G Cellular. It will Work, IEEE Access Vol1, pp 335-349, May 2013.*

[2] N. Bitar, *SDN and potential applicability to access net- works*, in Optical Fiber Communication Conf. and Exhibition OFC 2014, paper Th1G.4.piling

[3] M. Coldry, J-E Berg, L. Manholm, C. Larsson, J. Hasryd, *Non Line of Sight small cell backhauling sing microwave technology, IEEE Wireless Commun. Mag , Vol 51 No. 9, pp. 78-84, 2013.*

[4] ETSI. New ETSI Group on Millimetre Wave Transmission Starts Work. Technical report.

[5] C. Dehos, J.L. Gonzales. A. D. Dmoenico, D. Ktennas L.Dussopt, *Millimeter Wave Access and Backhauling: The solution to the Exponential Data Traffic Increase in 5G Mobile Communications Systems, IEEE Trans Wireless Commun. Mag , Vol 52 No. 9, pp. 88-95, Sep 2014.*

[6] X. Ge, S. Tu, G. Mao, C.X. Wang, T. Han,*5G Ultra-Dense Cellular Networks, IEEE Wireless Communications, 2016.*

[7] S. Hur, T. Kim, D.J. Love, J.V. Krogmeier, T.A. Thomas, A. Ghosh, *Millimeter Wave Access and Beamforming for Wireless Backhaul and Access in Small Cellular Networks, IEEE Trans Wireless Communications, Vol 61 No. 10, pp. 4391-4403, Oct 2013.*

[8] CISCO. Global Visual Networking Index: Globile mobile data traffic report forcast update, 2015-2020 (2015) White Paper

[9] S.F. Yumas, M. Valkama, J. Niemela, ,*Spectral and Energy Efficiency of Ultra Dense Networks under Different Deploymenmt Strategies, IEEE Commun. Mag , Vol 53 No. 1, pp. 90-100, 2015.*

[10] Intel Case study: Rethinking small cell business model(2012), Intel White paper

[11] J. Robson. Small cell backhaul: an analysis of small cell backhaul requirements and comparison of solution, Cambridge Broadband Networks Limited(2012) White Paper

[12] International Telecommunications Union *Spectral grids for WDM applications: DWDM frequency grid*, REC G.694.1 201202 I 2012

[13] N. Terzenidis, P. Maniotis, and N. Pleros, *Bringing OptoBoards to HPC- scale environments: An OptoHPC simulation engine, in Proc. 1st Int. Workshop Adv. Interconnect Solutions Technol. Emerging Comput. Syst., 2016, Art. no. 6.*

[14] X. Li, K. Kanonakis, N. Cvijetic, A. Tanaka, C. Qiao, and T. Wang, *Joint bandwidth provisioning and cache management for video distribution in software-defined passive optical networks, in Optical Fiber Communication Conf. and Exhibition (OFC), San Francisco, CA, Mar. 2014, paper Tu3F.5.*

[15] V. Lpez, O. Gonzlez de Dios, L. M. Contreras, J. Foster, H. Silva, L. Blair, J. Marsella, T. Szyrkowiec, A. Autenrieth, C. Liou, A. Sasdasivarao, S. Syed, J. Sun, B. Rao, F. Zhang, and J. P. Fernndez-Palacios, *Demonstration of SDN orches- tration in optical multi-vendor scenarios, in Optical Fiber Communication Conf. and Exhibition (OFC), Los Angeles, CA, 2015.*

[16] Y. Matsuoka et al. *20-Gb/s/ch high-speed low-power 1-Tb/s multilayer optical printed circuit board with lens-integrated optical devices and CMOS IC, IEEE Photon. Technol. Lett., vol. 23, no. 18, pp. 13521354, Sep. 2011.*

[17] Infinera The Next Generation of Coherent Optical, Advance Coherent toolkit for Super Channels (2016), Infinera White paper

[18] SANTEC 4 Channel Mux / Demux Module MDM-15 (2018), SANTEC data sheet

[19] G. Wei-Lu T. Sakamoto, T. Kawanishi, *Flexible high order QAM transmitter using tandem IQ modulators for generating 16/32/36/64-QAM with balanced complexity in electronics and optics, OSA Optics express Vol 21, No 5, pp. 6213-6223 Nov 2013.*

[20] M. Mathis, J. Semke, J. Mahdavi, T Ott *The Macroscopic Behavior of the TCP Congestion Avoidance Algorithm CCR ACM SIGCOM (1997) vol 27 No. 3 ISSN 0146-4833*

Advances in Science, Technology and Engineering Systems Journal Vol. 4, No. 2, 280-287 (2019)

www.astesj.com

ASTESJ

ISSN: 2415-6698

Estimation of Software Development Project Success using Fuzzy Logics

Andro Majid, Djoko Budiyanto Setyohadi*, Suyoto

Magister Teknik Informatika, Universitas Atma Jaya Yogyakarta, Yogyakarta, Indonesia, 55281

A R T I C L E I N F O

Article history:
Received: 08 February, 2019
Accepted: 26 March, 2019
Online: 08 April, 2019

Keywords:
Fuzzy Logic
Software development
Project success

A B S T R A C T

To date, software development is vital since software is a critical element in information technology. Requirements gathering, planning, estimation, estimation, development, collaboration, testing, and deployment. The problem is when it is delivered, so it reduces the risk of the problem which could happen is important. Threat prediction should be made. It will be aimed at both the threat and control of the risks which appear when the software development is performed. Fuzzy logic is one powerful method for solving management risk problems. Since the risk management of software development influence directly to the success of software development, this study proposes that fuzzy logic for risk management problems in software development. The case study of software development projects is divided into the category of medium and small. Based on the research program, the development environment, and the Constraint Program. Each of these indicators has sub-classes and factors that explain the indicators in detail from a technical point of view.

1. Introduction

Software development has several steps, namely requirement gathering, planning & estimation, development, collaboration, testing and deployment, and the processes of software development face many problems on each step [1]. However, at each of these stages, it has its general issues. The gathering requirement has a problem where when there is an error it will produce bad software because gathering requirements describe the needs of the client. Poor planning & estimation will have an impact on the estimate of time and costs that do not fit eventually resulting in software that is of poor quality because it affects the stages of development and testing that produce many bugs. Deployment has frequent problems with software and environmental platforms that need adjustment, while collaboration has issues in human resource management [2].

Planning & estimation has a very vital role in the stage of software development. Overly optimistic estimates can lead to errors so that software development will go out of time and increase costs, but excessive estimation can also lead to the use of human resources that are not by needs, ultimately offering too much development costs [3]. This condition can cause losses to the developer and client. Risk management is needed to identify risks of failure; it useful to minimize the risks that can be detrimental to software development [4].

Risk management is a systematic process for identifying, analyzing and controlling risks in a project. Management helps identify threats to project planning and estimation (such as time, resource use, costs, etc.) [5]. By knowing and predicting threats that will occur, the project manager can determine the right steps to avoid threats that might happen or control the risks that arise [6]. The stages of software risk management consist of identification, analysis, prioritization, management, resolution, and risk monitoring. Based on studies that have been carried out the application of risk management increases the success rate of software development projects and the swelling of project costs is only 5 percent of the initial estimate [7].

In the studies that have been conducted, many methods can be used for risk management in software such as Software Risk Management, Bayesian Network, Fuzzy Logic. SERIM has been applied as a method for risk management in developing software with risk results on software development that can be calculated by predicting risks on technical, cost, schedule aspects [8]. The Bayesian Network application is applied to several studies with the results of more real risks based on the risk probability of the elements used. Fuzzy logic is one of the methods most often used to solve management risk problems [9]. Previous research show, fuzzy produces the best estimation results compared to another approach [3].

Based on the problems described, this study proposes the use of fuzzy logic to solve risk management problems at PT. Mindo Small Business Solutions (MINDO) in the software development process. Based on the risks can be used to determine the success rate of software development projects. Fuzzy logic is selected because it has several advantages including being very flexible, having tolerance for incorrect data and can work with conventional

*Djoko Budiyanto Seyohadi, Universitas Atma Jaya Yogyakarta, Jl. Babarsari 44 Yogyakarta, Indonesia 55281, Email: djoko.bdy@gmail.com

control techniques [10]. Fuzzy logic works by recognizing the value of uncertain parameters which are then connected with the rules that produce a conclusion where experts make these rules. Therefore fuzzy logic is very flexible according to the case needed [11] [12]. In fuzzy logic, there are various inference methods such as Mamdani, Tsukamoto, and Sugeno. In this study the inference engine used was Tsukamoto. Research that has been carried out the Tsukamoto inference engine has a better performance compared to Sugeno and Mamdani [13]. Fuzzy logic will be used to determine the risks in software development projects at MINDO on technical risks, costs and time. With the existence of risk management, it will help project managers in making measurable decisions to increase success and efficiency in software development.

There are several studies which are used as literature reviews of this study as study material. Research used as a literature review is a study that has a relationship to the topic of research related to risk management in software development. Ezghari and Zahi (2018) proposed effort estimation using a consistent fuzzy analogy-based method [3]. They said that software effort estimation is one of the most critical activities in software project development because it is crucial to optimal planning and important for controlling software resources. Based on the research fuzzy analogy based method has a promising approach that provides a strong qualification of uncertainty in effort estimation of a new software development project. The experiment's result shows that the proposed model has good performance higher 50% accuracy. Kumar and Yadwa (2015) investigated risk assessment and estimation using the probabilistic model. Indicators to determine software development risk are Product Engineering, Development Environment and Program Constraint. Each of the indicators has a subclass that defines the technical detail [9]. The model used on the research is based on the Bayesian Belief Network. Each of the factors from indicators uses as input then the Bayes model is used to process that has output result probability of risk from the software development project. From the experiment result from the risk of software development project easy to estimate based on the probability value. Fan and Yu (2004) proposed software development management risk using Bayesian network-based probability techniques [14]. The proposed model is built on a mathematical model that provides an analysis of the effectiveness of resource use. The model is used to monitor software development projects by predicting project risks and sources of risk. The results of the analysis are used to assist project managers in making decisions in adjusting the allocation of resources dynamically. Besides the advantages of the proposed model is to provide support for decision making in uncertain conditions. Arun Kumar et al. introduced risk assessment in software development project based on fuzzy reinforcement paradigm [15]. Software risk prioritization is an essential role in determining the plan will be successful. This research proposed a hybridizing fuzzy multi-criteria decision-making approach for the development of an assessment framework to identify and rank software development project risks that aid to decision making during the production phase. From the experiment, the result shows that fuzzy is useful and accurate to solve the problem.

2. Research Method

This chapter contains proposed research methodology from data collection, data processing and proposed fuzzy model for software development project success by identifying the risks. All of the steps can be seen in Figure 1.

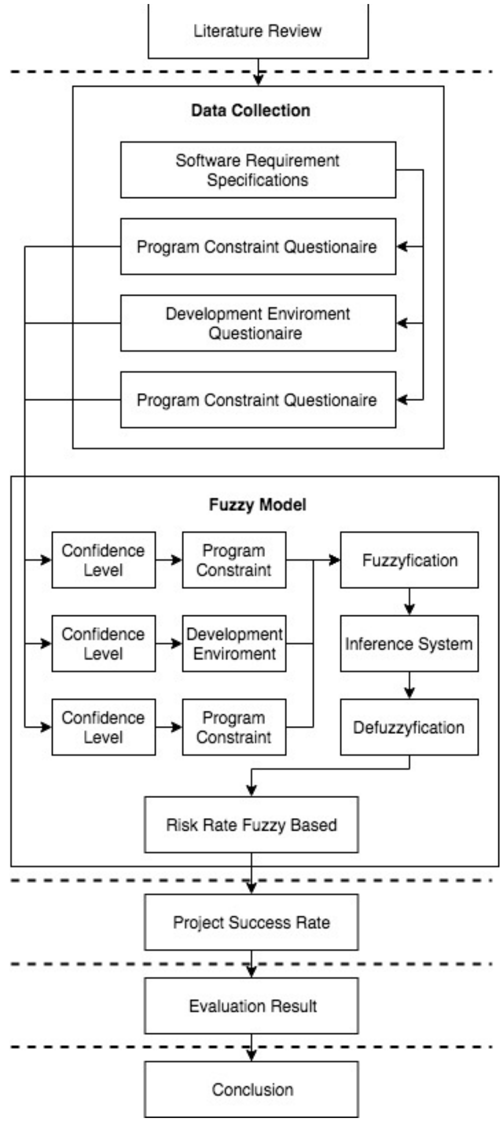

Figure. 1. Research Methodology.

2.1. Research Methodology

Research methodology initialized from the literature review as the research reference based on the same case of software risk management. Software risk management research contains a different method such as a probabilistic model and the fuzzy-based model. Data collection stage consist of review the software specifications requirements. The result of the review is the questionnaire based on each stakeholder based on the project production domain. The fuzzy model proposed in this research start by calculating the confidence value of the questionnaire by the software risk indicators. The result of the confidence level used as input of fuzzy logic that starts from fuzzification, inference system, and defuzzification. The output of the fuzzy model is project risk rate from high, medium and low. Based on the risk output successful rate of a software development project can be identified. Evaluation result will review all aspect from input, process, and output to get the conclusion of the research.

2.2. Data Collection

There are many risk indicators for software development projects [16] [17]. The primary indicator matrix of software development risk is Product Engineering, Development Environment, Program Constraint [14] [18]. The indicators are further divided into sub-classes with various factors.

The dataset in this study are the results of a questionnaire based on the risk parameters of a project. The survey consists of questions that will be filled by project stakeholders. The quiz consists of issues related to the current project especially factors in software development. Furthermore, the answer represents the level of each of the elements.

Questionnaire answers were obtained from respondents consisting of front-end developer staff, backend developer staff, project managers and expert analysts. The answer given by the respondent is the result of a review of the specifications of the request given by the prospective client. The results of the survey are subjective judgments based on the experience of each respondent.

1) Product Engineering Indicators

In the product engineering indicator, there are three respondents. They consist of front end developer staff, backend developers and project managers. In this aspect, the questionnaire is taken based on stakeholders related to the aspect of production directly. Product Engineering risk indicators have nine questions as listed in Table 1. Questions on Product Engineering indicators are connected to the production process starting from software requirements, implementation to integration and testing

Table 1: Product engineering questionnaire result

Factor	Resp. 1	Resp.2	Resp.3	Avg
Requirement Stability	0.70	0.75	0.75	0.73
Requirement Clarity	0.75	0.75	0.75	0.75
Requirement Dependence	0.50	0.60	0.60	0.57
Requirement Complexity	0.50	0.40	0.40	0.43
Reuse Level	0.70	0.75	0.75	0.73
Interfacing Level	0.75	0.75	0.75	0.75
No. of Programming Language	0.40	0.40	0.40	0.40
Product Stability	0.80	0.75	0.75	0.77
Difficult Level to Implement Security	0.75	0.70	0.70	0.72

2) Development Environment Indicators

In the development environment indicator, the questionnaire was filled by stakeholders at the managerial level including the project manager and expert analyst. Project managers are included in the Development Environment questionnaire because they are included in managerial level stakeholders. The project manager is a manager who is responsible for the production or supervision process at the staff level. Indicator Development Environment, which is listed in Table 2, is a factor that affects the production of software from a managerial point of view and management of human resources.

3) Program Constraint Indicators

On the Program Constraint indicator, the questionnaire is filled by stakeholders with managerial level. Expert analysts have the task of translating client requirements into technical matters related to software development. Also, the expert analyst also controls every aspect of software development. The Program Constraint Indicator has coverage on factors related to human resources; the listing of the related factor is shown in Table 3.

Table 2: Development enviroment questionaire result

Factor	Resp. 3	Resp. 4	Avg
Experience on The Development Process	0.85	0.80	0.825
Development Infrastructure Availability	0.90	0.90	0.90
Development Software Availability	0.90	0.90	0.90
Project Manager Experience Level	0.85	0.85	0.85
Project Dependence Level	0.80	0.80	0.80
Maturity Level	0.80	0.80	0.80
Motivational Level	0.80	0.80	0.80
Effective Role of Organization	0.75	0.70	0.725
Team Focus	0.70	0.70	0.70
Turnover	0.70	0.70	0.70

Table 3: Program constraint questionnaire result

Factor	Resp. 3	Resp. 4	Avg
Team Knowledge Level	0.85	0.85	0.85
Team Experience Level	0.85	0.80	0.825
Team Size	0.70	0.75	0.725
Project Size	0.75	0.75	0.75
Financial Feasibility	0.9	0.90	0.90
External Dependence Level	0.6	0.60	0.60
Client Experience	0.7	0.75	0.725
Client Participation Level	0.8	0.85	0.825

4) Confidence Level of Risk Indicators

The value of level confidence is obtained from experts who analyze software risk indicators. Confirmation of value is given to reduce indicators that have a small effect on the final results of estimating the success of software development. The confidence value is given by an expert on each indicator based on subjectivity with a range of values between 0 and 1. The detailed of the value of each factor is listed in Table 4, the higher the value of the indicator, the more the impact on estimating the success of software development.

2.3. Software Success Estimation Model based on Fuzzy Logics

The method developed by the researcher is the Tsukamoto fuzzy method with the steps represented in Figure 2.

1) Input survey data use the factor of software development risk indicator.

2) Calculate the confidence interval of each indicators using the formula of each indicator as listed below.

$$\text{Indicator}[x] = \begin{cases} 0; \; x < 0.8 \\ x; \; x \geq 0.8 \end{cases} \tag{1}$$

3) Indicators that cross the threshold will be used as fuzzy inputs.

Table 4: Confidence level of risk indicators

No	Factor	Confidence Level
1	Requirement Stability	0.65
2	Requirement Clarity	0.90
3	Requirement Dependence	0.60
4	Requirement Complexity	0.85
5	Reuse Level	0.70
6	Interfacing Level	0.65
7	No. of Programming Language	0.80
8	Product Stability	0.60
9	Difficult Level to Implement Security	0.70
10	Experience on The Development Process	0.85
11	Development Infrastructure Availability	0.60
12	Development Software Availability	0.90
13	Project Manager Experience Level	0.60
14	Project Dependence Level	0.50
15	Maturity Level	0.60
16	Motivational Level	0.60
17	Effective Role of the Organization	0.60
18	Team Focus	0.80
19	Turnover	0.60
20	Team Knowledge Level	0.85
21	Team Experience Level	0.75
22	Team Size	0.75
23	Project Size	0.75
24	Financial Feasibility	0.90
25	External Dependence Level	0.70
26	Client Experience	0.60
27	Client Participation Level	0.75

4) Fuzzy logic process steps:

a. Fuzzyfication input using each input (product Engineering, Development Enviroment, Program Constraint) as listed below:

$$\mu LOW[x] = \begin{cases} 1; & x \le 0 \\ (0.33 - x)/(0.33 - 0); & 0 \le x \le 0.33 \\ 0; & x \ge 0.33 \end{cases} \quad (2)$$

$$\mu MEDIUM[x] = \begin{cases} 0; & x \le 0.14 \\ (x - 0)/(0.14 - 0); & 0 \le x \le 0.14 \\ 0.1; & 0.14 \le x \le 0.43 \\ (0.54 - x)/(0.54 - 0.43); & 0.46 \le x \le 0.54 \\ 0; & x \ge 0.54 \end{cases} \quad (3)$$

$$\mu HIGH[x] = \begin{cases} 0; & x \le 0.63 \\ (x - 0.63)/(0.96 - 0.63); & 0.96 \le x \le 0.63 \\ 0.63; & x \ge 0.96 \end{cases} \quad (4)$$

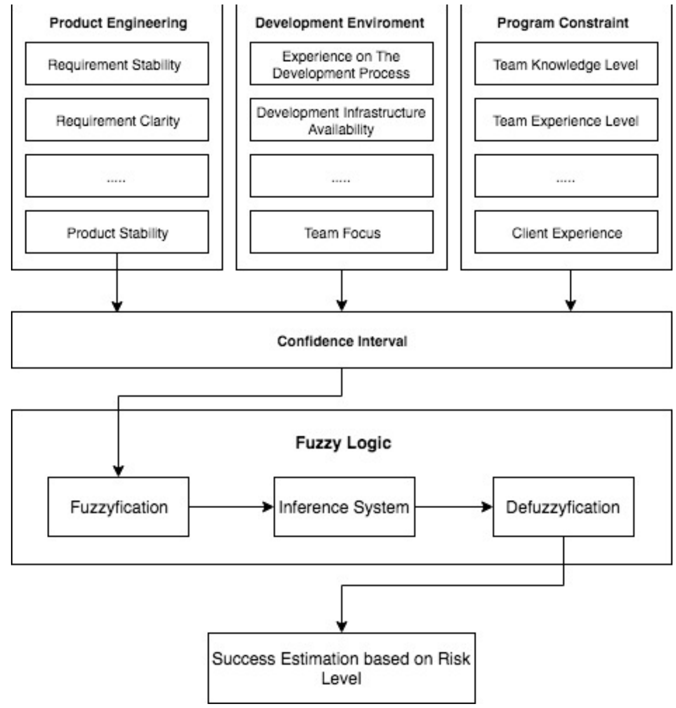

Figure. 2. Fuzzy Logic Model Software Risk.

b. Fuzzy inference system is used for calculating input based on the rule, and The rule is shown in Table 5.

Table 5: Fuzzy rule

Rule No	Rule IF	Then (Risk)
1	Indicator$_1$ = LOW AND Indicator$_2$ = LOW AND Indicator$_3$ AND, ….. AND Indicator$_n$ = LOW	HIGH
2	Indicator$_1$ = LOW AND Indicator$_2$ AND Indicator$_3$ = MEDIUM AND, ….. AND Indicator$_n$ = MEDIUM	MEDIUM
3	Indicator$_1$ = HIGH AND Indicator$_2$ = HIGH AND Indicator$_3$ =HIGH AND, ….. AND Indicator$_n$ = LOW	LOW

c. Defuzzification

Final Result of the fuzzy *output* (z) obtain using an average of the inference system from the formula as shown below:

$$z = \frac{\alpha_1 z_1 + \alpha_2 z_2}{\alpha_1 + \alpha_2} \quad (5)$$

5) Risk output based on the defuzzification.

Based on the risk output will be used to determine the success of the software development project. Fuzzy output risk is HIGH, MEDIUM and LOW.

3. Results and Analysis

This chapter describes the results of the research in the form of data collection and detail explaining the proposed risk management model with fuzzy logic. Data were collected from questionnaires that had been filled by stakeholders at PT Mindo Small Business Solutions which contained the factors of software development projects. Then explained the results of the calculation of the data with fuzzy logic with the output level of risk from various factors of software development. From the predictions that have been made then a discussion of strategies in risk mitigation can be done to increase the success of software development projects at PT Mindo Small Business Solutions

Data collected is in the form of data related to the project to be carried out and questionnaires based on project-related data. Project related data is a software specification needed by the client. While the survey is the result of a review by stakeholders based on the specifications of the software.

3.1. Processing Questionnaires Data

The initial stage in processing data is calculating the average value of the questionnaire given by all respondents. The results of the average value of each factor can be seen in table 6.

Table 6. Questionnaires average data values

Factor	**Average**
Requirement Stability	0.73
Requirement Clarity	0.75
Requirement Dependence	0.57
Requirement Complexity	0.43
Reuse Level	0.73
Interfacing Level	0.75
No. of Programming Language	0.40
Product Stability	0.77
Difficult Level to Implement Security	0.72
Experience on The Development Process	0.82
Development Infrastructure Availability	0.90
Development Software Availability	0.90
Project Manager Experience Level	0.85
Project Dependence Level	0.80
Maturity Level	0.80
Motivational Level	0.80
Effective Role of Organization	0.725
Team Focus	0.70
Turnover	0.70
Team Knowledge Level	0.85
Team Experience Level	0.825
Team Size	0.725
Project Size	0.75
Financial Feasibility	0.90
External Dependence Level	0.60
Client Experience	0.725
Client Participation Level	0.825

The average results of each factor in table 6, from the average value of each of these factors, will be selected using the interval confidence formula to obtain indicators that have a significant effect on the estimation of the success of software development in this study. Indicators that do not exceed the threshold in the confidence formula of the interval are eliminated. Final indicator obtained from the confidence interval formula shown in Table 7.

Table 7. Indicator confidence interval values

Indicator	Factor	Confidence Level
Product Engineering	Requirement Clarity	0.90
	Requirement Complexity	0.85
	No. of Programming Language	0.80
Development Environment	Experience on The Development Process	0.85
	Development Software Availability	0.90
	Team Focus	0.80
Program Constraint	Team Knowledge Level	0.85
	Financial Feasibility	0.90

Based on the indicator selection process in table 6 it is selected eight indicators used. The eight indicators are used as input attributes on fuzzy logic in the next process. These results are used as a matrix of software development risk indicators shown in Table 8.

Table 8. Software risk indicator metrics

Factor	**Average**
Requirement Clarity	0.75
Requirement Complexity	0.43
No. of Programming Language	0.40
Experience on The Development Process	0.82
Development Software Availability	0.90
Team Focus	0.70
Team Knowledge Level	0.85
Financial Feasibility	0.90

Software risk indicator matrix above is used as input from the fuzzy model proposed in this study. The input of the model consists of indicators of Product Engineering, Development Environment and the program constraints.

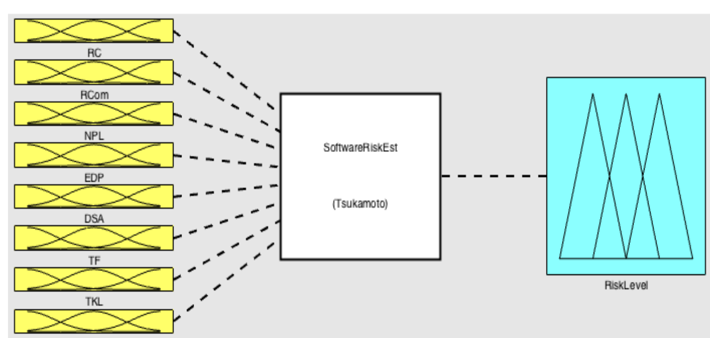

Figure. 3. Fuzzy Logic Scheme.

3.2. Fuzzification

The process of fuzzy logic is started by fuzzification input. Input on fuzzy logic consists of Requirement Clarity (RC), Requirement Complexity (RCom), No. Programming Language (NPL), Experience on The Development Process (EDP), Development Software Availability (DSA), Team Focus (TF), Team Knowledge Level (TKL) and Financial Feasibility (FF). The results of these inputs will produce output in the form of risk. Input, process and output schemes can be seen in Figure 3.

1) Requirement Clarity (RC = 0.75)

- Membership function fuzzy LOW:

$$\mu\text{LOW}[x] = \begin{cases} 1; & x \le 0 \\ (0.33 - x)/(0.33 - 0); & 0 \le x \le 0.33 \\ 0; & x \ge 0.33 \end{cases}$$

$$\mathbf{x \ge 0.33, \text{then } x=0}$$

- Membership function fuzzy MEDIUM:

$$\mu\text{MEDIUM}[x] = \begin{cases} 0; & x \le 0.14 \\ (x - 0)/(0.14 - 0); & 0 \le x \le 0.14 \\ 0.1; & 0.14 \le x \le 0.43 \\ (0.54 - x)/(0.54 - 0.43); & 0.46 \le x \le 0.54 \\ 0; & x \ge 0.54 \end{cases}$$

$$\mathbf{x \ge 0.54, \text{then } x = 0}$$

- Membership function fuzzy HIGH:

$$\mu\text{HIGH}[x] = \begin{cases} 0; & x \le 0.63 \\ \dfrac{x — 0.63}{0.96 - 0.63}; & 0.96 \le x \le 0.63 \\ 0.63; & x \ge 0.96 \end{cases}$$

$$\mathbf{0.96 \le x \le 0.63, \text{then}}$$

$$\mu\text{HIGH}[x] = \frac{x — 0.63}{0.93 - 0.63} = \frac{0.75 — 0.63}{0.93 - 0.63} = 0.4$$

Continued calculation for all indicators from Requirement Clarity (RC=0.75), Requirement Complexity (RCom=0.43), No. Programming Language (NPL=0.40), Experience on The Development Process (EDP=0.825), Development Software Availability (DSA=0.9), Team Focus (TF=0.7), Team Knowledge Level (TKL=0.85) and Financial Feasibility (FF=0.9) resumed in Table 9 below:

3.3. Fuzzy Inference System

The process of inference system is to convert fuzzy inputs into fuzzy (z) output by following the rules (IF-THEN Rules) based on the fuzzy knowledge base that has been made by experts on table 5. The process of the inference machine is explained according to the following steps from the 1st Rule to the 3125th Rule.

3.4. Defuzzification

After the inference system process that produces output from every rule (Z_1, Z_2 …., Z_{28}). Then the defuzzification stage is carried out, which is used to change the fuzzy output from the inference engine to a firm value using the appropriate membership function. Membership fuzzification can be seen in Figure 4.

Based on the range of linguistic sets on the input variables, the parameters of PE, DE and PC are entered in the "HIGH" set category as shown in Table 10.

Table 9: Range fuzzyfication

	LOW	MEDIUM	HIGH
RC	0	0	0.40
RCom	0	0.1	0
NPL	0	0.1	0
EDP	0	0	0.65
DSA	0	0	0.90
TF	0	0	0.23
TKL	0	0	0.73
FF	0	0	0.90

Table 10. Range fuzzyfication

Parameter	Linguistic Categorization
RC	HIGH
RCom	MEDIUM
NPL	MEDIUM
EDP	HIGH
DSA	HIGH
TF	HIGH
TKL	HIGH
FF	HIGH

From the linguistic input rule use in this case are:

Inference System Rule Number 2984:

IF RC = HIGH AND RCom = HIGH AND NPL = HIGH AND EDP = HIGH AND DSA = HIGH AND TF = HIGH AND TKL = HIGH AND FF = HIGH THEN RISK = LOW

$$\alpha_{28} = 0.1$$
$$Z_{28} = 0.7355$$

Then,

$$z = \frac{(\alpha_{28} Z_{28})}{\alpha_{28}}$$

$$z = \frac{(0.1 \times 0.7355)}{0.1}$$

$$z = \frac{0.07355}{0.1}$$

$$z = 0.7355$$

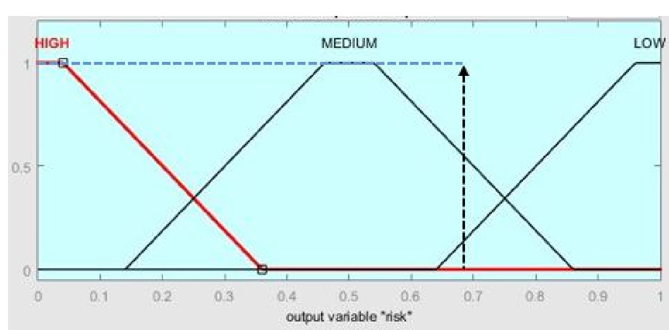

Figure. 4. Risk Output Membership Function.

Based on the fuzzy calculation of risk value from inputRequirement Clarity (RC), Requirement Complexity (RCom), No. Programming Language (NPL), Experience on The Development Process (EDP), Development Software Availability (DSA), Team Focus (TF), Team Knowledge Level (TKL) and Financial Feasibility (FF) generated risk output in the software development project amount 0.7355, the value is entered in the fuzzy variable output set then the value is included in the risk set "MEDIUM" and "LOW".

3.5. Experimental Results

Fuzzy process calculation starts with the input software risk factor. The risk factors have a value between 0 to 1 with a range of linguistic variables 0 to 0.33 LOW, 0.34 to 0.64 MEDIUM and 0.65 to 1 HIGH.

There are 27 software risk indicators. The indicator is used as a basis in taking questionnaire questions to stakeholders of software development projects. From these 27 indicators, selection indicators are conducted which have an important influence on the process of estimating the success of software development projects. Indicator selection is made with a confidence interval value to produce eight indicators that are considered necessary by the expert. The indicator used are Requirement Clarity (RC), Requirement Complexity (RCom), No. Programming Language (NPL), Experience on The Development Process (EDP), Development Software Availability (DSA), Team Focus (TF), Team Knowledge Level (TKL) and Financial Feasibility (FF).

The process starts with the input indicator risk fuzzification (RC, RCom, NPL, EDP, DSA, TF, TKL, FF) then the process is continued with engine inference and defuzzification. From the process of risk output in software development projects in the case described is 0.7355, the value is categorized on the "MEDIUM" and "LOW" risk sets. Compared with an expert assessment of risk in the development project, this project has a risk level of 0.85 categorized into the "LOW" risk sets, so the performance of fuzzy logic has an accuracy of 85%. Based on the risk output project has been categorized as a low risk, so the chance success of the project is high. From the input stage which consists of Product Engineering, Development Environment and Constraint Program, Product Engineering has the smallest value so that stakeholders of software project development can anticipate the factors that exist in Product Engineering indicators to overcome risks and improve the success of software development projects at PT. Mindo Small Business Solutions.

Results of experiments will be compared to the state of the art research with risk management cases in the software development project. The result shows that our approach is promising since accuracy is improved. Comparison to research is shown in table 11.

Table 11: Comparison with the previous reserach

Method	Accuracy	Research
Fuzzy analogy based method	72%	[3]
Bayesian Belief Network	90%	[9]
Bayesian network-based probability techniques	82%	[14]
Fuzzy Logic	85%	This Research

4. Conclusion

Planning & estimation has a very vital role in the stage of software development. Risk management is a systematic process for identifying, analyzing and controlling risks in a project. Risk management helps identify threats to project planning and estimation. This study proposes the use of fuzzy logic to determine software development project success at PT. Mindo Small Business Solutions Based on the research that has been done the conclusions obtained are risk management to assess software development project success using fuzzy logic has been successfully applied at PT. Mindo Small Business Solutions on a software development project with a case study of making a website-based polling and website-based mobile data collection system in real time on a national scale. In risk management indicators of the software used are Product Engineering, Development Environment and Constraint Program. Each of these indicators has sub-classes and factors that explain the indicators in detail from a technical point of view.

Based on the value of indicator used as fuzzy input are Requirement Clarity (RC=0.75) categorized as HIGH, Requirement Complexity (RCom=0.43) categorized as MEDIUM, No. Programming Language (NPL=0.40) categorized as MEDIUM, Experience on The Development Process (EDP=0.825) classified as HIGH, Development Software Availability (DSA=0.9) categorized as HIGH, Team Focus (TF=0.7) categorized as HIGH, Team Knowledge Level (TKL=0.85) categorized as HIGH and Financial Feasibility (FF=0.9) categorized as HIGH fuzzy input set. The output of fuzzy logic produces a risk output of 0.7355 which is included in the set of risk outputs "MEDIUM" and "LOW." So it can be concluded that the case studies on software development projects that are being worked on have risks that categorized of medium and small risk. With these risks, the project to be worked on has the possibility of high success.

Although having a small risk, the software development project stakeholders must be able to anticipate risks by looking at the value of sub-factors in the software risk indicator. The amount of these sub-factors can also be used as a basis in making decisions to reduce risk and increase the success of software development projects at PT. Mindo Small Business Solutions. This research conducted 85% of accuracy. The suggestions for further research are is that we can use decision support in addition to fuzzy logic such as the neural network, Nearest Neighbor, ANFIS and others.

References

[1] Mall Rajib, Fundamentals of software engineering.: PHI Learning Pvt. Ltd, 2018.

[2] Chawan and Jijnasa Pati, "Software risk management," International Journal of Computer Science and Mobile Computing, vol. 2.5, pp. 60-66, 2013.

[3] Soufiane Ezghari and Azeddine Zahi, "Uncertainty Management In Software Erroft Estimation Using a Consistent Fuzzy Analogy-Based Method," Applied Soft Computing, pp. 540-557, 2018.

[4] Bijan Elahi, "Chapter 15: Software Risk Management," in Safety Management for Medical Devices., 2018, pp. 127-149.

[5] Rory Burke, Project management: planning and control techniques. New Jersey, 2013.

[6] Michael Dedolph, "The Neglected Management Activity: Software Risk Management," Bell Labs Technical Journal, vol. 8(3), pp. 91-95, 2003.

[7] Fairley, Richard E. "Software risk management." IEEE Software 3 (2005): 101.

[8] Wen-Ming, and Sun-Jen Huang Han, "An empirical analysis of risk components and performance on software projects," Journal of Systems and Software , vol. 80.1, pp. 42-50., 2007.

[9] Chandan Kumar and Dilip Kumar Yadav, "A Probabilistic Software Risk Assessment and Estimation Model for Software Projects," Eleventh International Multi-Conference on Information Processing, pp. 353-361, 2015.

[10] Clerence W De Silva , Intelligent control: fuzzy logic applications.: CRC Press, 2018.

[11] Freerk Lootsma, Fuzzy logic for planning and decision making.: Springer Science & Business Media, 2013.

[12] Ali Idri, Azeddine Zahi, and Alain Abran, "Software cost estimation by fuzzy analogy for Web hypermedia applications," in Proceedings of the International Conference on Software Process and Product Measurement, 2006.

[13] Aep Saepullah, "Comparative Analysis of Mamdani, Sugeno And Tsukamoto Method of Fuzzy Inference System for Air Conditioner Energy Saving," Journal of Intelligent System, 2015.

[14] Chin-Feng, and Yuan-Chang Yu Fan, "BBN-Based Software Risk Management," Journal of Systems and Software , vol. 73(2), pp. 193-203, 2004.

[15] Arun Kumar Sangaiah, Oluwarotimi Williams Samuel, Xiong Li, Mohamed Abdel Basset, and Haoxiang Wang, "Towards an efficient risk assessment in software projects–Fuzzy reinforcement paradigm," Computers & Electrical Engineering, 2018.

[16] Kwan-sik Na, James Simpson, Xiaotong Li, Tushar Singh, and Ki-Yoon Kim, "Software development risk and project performance measurement: Evidence in Korea," The Joirnal of Systems and Software, 2007.

[17] Mohd Sadiq and Mohd Sahid, "A systematic approach for the estimation of software risk and cost using esrcTool," CSI Transactions ICT, 2013.

[18] Shareeful Islam, "Software development risk management model: a goal driven approach," Foundations of Software Engineering, 2009.

Advances in Science, Technology and Engineering Systems Journal Vol. 4, No. 2, 288-298 (2019)
www.astesj.com
ASTESJ
ISSN: 2415-6698

ITSM Software Ranking for Small Medium Enterprises Based on ITIL V3 Quick Win Criteria using Fuzzy SIR Method

Husni Teja Sukmana[1], Luh Kesuma Wardhani[1], Sarah Khairunnisa[1], Kyung Oh Lee[2,*], Risa Wati[3]

[1]UIN Syarif Hidayatullah Jakarta, Information Technology, Saints and Technology Faculty, 15412, Indonesia

[2]Sun Moon University, Computer Engineering, 31460, South Korea

[3]Universitas Bina Sarana Informatika, Jakarta 12450, Indonesia

A R T I C L E I N F O

Article history:
Received: 11 February, 2019
Accepted: 03 April, 2019
Online: 08 April, 2019

Keywords:
IT Service Management
IT Infrastructure Library
ITIL Quick-Win Criteria
Small Medium Enterprises (SMEs)
Fuzzy SIR

A B S T R A C T

There are various software related to the implementation of IT Service Management (ITSM) for a company, including those that are open source and commercial. An input is needed for companies in determining what software to choose from various software, especially for small and medium enterprises (SMEs) that have limited human and financial resources. In this study, we have contributed in evaluating open source ITSM software (including OTRS, ITOP, and SDP) that are suitable for use by small and medium-sized companies. In the evaluation process, we evaluated various appropriate criteria, so that we finally chose the quick-win criteria from ITIL V3 (one of the best practices that are widely used in ITSM). The method used for training is Fuzzy SIR (Superiority and Inferiority Ranking) with assessment criteria for data taken in the form of quantitative data from experts who have used and had certificates in the field of ITSM. The results showed that OTRS was the best software with a value of 0.86, SDP was in second place with a value of 0.77, and ITOP was in the last place with a value of 0.04.

1. Introduction

The use of the IT Service Management (ITSM) framework has been widely used in order to increase the value of a service delivered by the company to its stakeholders. ITSM provides a framework to structure IT operations that enables organizations to provide quality of IT services to meet business needs and adhere to service level agreements (SLAs) [1]. Various ITSM frameworks has been developed to provide guidelines and best practice to help manager improve IT operations. ITSM Framework can be divided into two, first made by the vendor, among others, includes: MOF 4.1 (Microsoft), ITUP (IBM) and the framework created by organizations and communities, including ITIL which was pioneered by the ITSM Forum (ITSMF), CMMI-SVC by Software Engineering Institute (SEI), COBIT from ISACA, and International Organization for Standardization (ISO) published standards related ITSM such as ISO 20000-1 [2]. Among the various frameworks, ITIL is the most influential and popular to be used today. To support this statement, in 2017 itSMF conducted a survey about ITSM which mention in [3], where among the surveyed frameworks (ITIL, ISO/IEC 20000, DevOps, Service Integration and Mgt, and Lean), ITIL is the most widely adopted framework for respondents.

To support the implementation of ITSM, many service providers have made applications based on the ITSM framework and ITIL V3 best practices. Even The ITSM software industry is one of the fastest growing sectors in the computer software industry which now includes hundreds of ITSM software solutions in the market [4]. Based on report from Gartner, some of these software includes: Samanage Service Desk, SolarWind Web Help Desk, Freshservice, Zendesk, Manage Engine Service Desk Plus, Spiceworks, and JIRA Service Desk. In addition, several companies also developed open source ITSM software including: Combodo ITOP, OTRS, CITSMART, Project Open, OCS Inventory NG, and I-DOIT. Each software has its advantages and disadvantages. For this reason, a method is needed to determine

*Corresponding Author: Kyung Oh Lee, Dept. Computer Engineering, Sun Moon University, leeko2002@naver.com

https://dx.doi.org/10.25046/aj040237

which application is suitable for use by a company, especially for small and medium enterprises (SMEs). So that the investment spent on the implementation of the application is in line with the results that will be obtained.

Research related to ITSM software rankings has been carried out by [1], [2], [5], [6]. Each of these studies differs from three sides, first related to the software to be ranked, secondly related to the criteria taken, and the third difference based on the method of decision making taken. The chosen method varies from the use of AHP [2], Fuzzy TOPSIS, [1] and Fuzzy SIR [5]. In terms of software selection, there are studies that prioritize open source software ranking [2], [6] and there are two studies that do not list the types of software studied [1], [5]. The fundamental difference from these studies is from the selection of criteria. Research by [1], [5] used all the criteria from ITIL V.3, while [2] employed criteria from the side of ITIL V.3 service operation. Research [6] has tried to see larger criteria with organizational, financial, end-user risk and technical risk aspects.

The use of these criteria is important, especially related to the type of company that will implement this software. Companies that do have services in the IT field such as telecommunications companies should use full ITSM criteria, while small and medium enterprises for the initial stages of implementation can adequately use several important processes in ITIL V.3. Small-Medium Enterprises (SMEs) are businesses that maintain revenues, assets, or a number of employees below a certain threshold. SMEs play a significant role in emerging economies. Based on report from SMEs create 80% of the new jobs in emerging economies[7], [8]. According to the website[9], there are 3 main problems commonly faced by SMEs including: difficulty in hiring staff, high manpower costs, and increasing business competition. So that certain processes need to be chosen to guarantee the implementation of ITSM in accordance with the capacities of these SMEs.

In this study, we looked for different perspectives from previous studies related to the selection of criteria for small and medium enterprises, which we then got 9 criteria for quick win processes from ITIL V.3 which will be used as ranking criteria. To rank this software, the author used the Fuzzy Superiority and Inferiority Ranking (Fuzzy SIR) method. This method was originally developed by Xiaozhan Xu in 2001 in [10].

2. Related Works

2.1. The Evaluation Methods

In this research, the author used the Fuzzy SIR (Superiority and Inferiority Ranking) method based on [5] which was initially developed by Xiaozhan Xu in 2001 [10]. Based on the research from [12], it explained the differences between several MCDM methods. Analytical Hierarchy Process (AHP) [11] and fuzzy models methods can only handle ordinal data. Neither provides preference structures for decision making, a technique that can mimic the decision-makers' mindset in describing the nature of the criteria. ELECTRE III [12] only provides a single preference structure without other options for criteria of a different nature.

In contrast, the SIR method [10] can process both cardinal and ordinal data. It also provides six different preference structures and incorporates outranking rationale to deal with the "poor" true-criteria preference structure. Therefore, the SIR method provides more information to represent decision-making preferences for each decision criterion. Table 1 shows a comparison of several MCDM methods.

Table 1. Comparison of MCDM Methods

Characteristic	AHP	ELECTRE III	Fuzzy Evaluation System	PROMETHEE	SIR METHOD
Handle real data?	No	Yes	No	Yes	Yes
Different weight between criteria?	Yes	Yes	No	No	Yes
Provide multi preferences structure?	No	No	No	Yes	Yes
Best choice?	No	No	No	No	Yes

According to the research of [13], some of the advantages of the SIR method include:

1. Providing scientific methods for alternative selection processes.
2. Provide a user-friendly and multi-criteria decision-making model for practitioners.
3. Improve the alternative selection process where all factors that affect performance will be considered.
4. Avoid common traps of other decision-making models in the alternative selection, such as oversimplifying decision criteria.

The SIR technique is an easy to understand logical model. This methodology enables all leaders to consider consistently and can improve precision and unwavering quality in the determination procedure. Thus, in general execution can be improved by choosing fitting software [13]. As per the examination from [5] which was cited from [14], one of the restrictions of conventional procedure for Superiority and Inferiority Ranking (SIR) is utilizing fresh qualities in the assessment procedure. A few criteria are hard to gauge by fresh qualities, so amid the assessment, these criteria are frequently ignored. In any case, in numerous genuine cases, the human inclination show is dubious, and chiefs unfit to relegate fresh qualities for their decisions. Leaders face trouble to deal with vulnerabilities of genuine world in the customary MCDM approach and lean toward interim decisions than in pointing out their decisions in fresh qualities. Consequently, fluffy SIR is an appropriate strategy to take care of positioning issues [15]. Along these lines, this investigation has built up the conventional SIR strategy under dubious conditions.

2.2. ITSM Selection Criteria

Several studies have tried to compare ITSM software including by [1], [2], [5], [16]–[19]. These studies have the same purpose, namely, to evaluate and rank software based on ITSM criteria. The differences in each of these studies are in the selection of criteria, the software to be evaluated, the selection of evaluation methods and the object objectives that will utilize the results of the evaluation.

For example studies [1] and [5] used overall criteria from ITIL V.3, starting from service strategic, service design, service transition, service operation, and coupled with continual service improvement. This research also adds several nonfunctional criteria, including portability, platforms, security, etc. While [18], [19] use four main criteria in the form of risk factors, for example for financial risk, there are two attributes, namely new business opportunity and switching costs. The organizational risk in the form of training, user investment, top management support, end-user risk in the form of functionality, usability, quality, and usefulness. Technical risk uses attribute maturity, interoperability, communication support, documentation, security, and technical environment.

In previous studied [2], the author have evaluated some ITSM software by using only service operation criteria, which consist of request fulfillment, incident management, problem management and event management. The purpose of this study is to help new companies or organizations want to use the ITSM concept in determining what software should be selected from the many open source software on the market. We assume that they do not need to apply all the criteria because usually these companies fall into the category of small and medium enterprises, where they are usually constrained by a shortage of IT experts, funds and some of them are not making IT their main business.

More detailed information related to the use of criteria, software that will be evaluated and evaluation methods from previous studies can be seen in the Table 2. Our research uses different criteria from previous research, which we call the quick win criteria. These criteria are taken from companies where they have just tried to implement IT Service Management.

Table 2 Tools Selecting Criteria

Journal	Criteria	Method	Tools
[1], [5]	46 criteria (function and non-functional)	Fuzzy TOPSIS [1] Fuzzy SIR [5]	ITSM Tools 1-5
[18], [19]	1. Financial 2. Organization 3. End user 4. Technical	Multiple *attribute decision making* (MADM)	ITOP, IDOIT, OTRS
[17]	1. Product Functionality 2. Requirements for Free and Open Source Project 3. Specifications 4. User friendliness	Multiple-criteria decision-making (MCDM)	Zenos, Nagios
[2]	ITSM Service Operation 1. Request Fulfillment 2. Incident management 3. Problem Management 4. Event Management	Analytical Hierarchy Process (AHP)	ITOP, IDOIT, OTRS
[16]		Multiple Criteria Decision Analysis (MCDA)	

3. Research Method

3.1. Research stages

The overall research stages can be seen in Figure 1, which consist of 5 steps.

a. First, we conducted a literature study. This phase aims to analyze existing problems related to ITSM by comparing similar literature studies. After obtaining references, the author searches for the information needed in this research to be used in the preparation of the theoretical foundation and method determination.

b. Second, we made planning for identified the alternative software, identify ITSM criteria for SMEs, and finding the selection method.

c. Third, we collect the data by making questionnaires for getting the weight of rules and alternatives.

d. Fourth, conducting the evaluation calculation by using Fuzzy SIR method.

e. Fifth, evaluating, analyzing the result and end with a summary

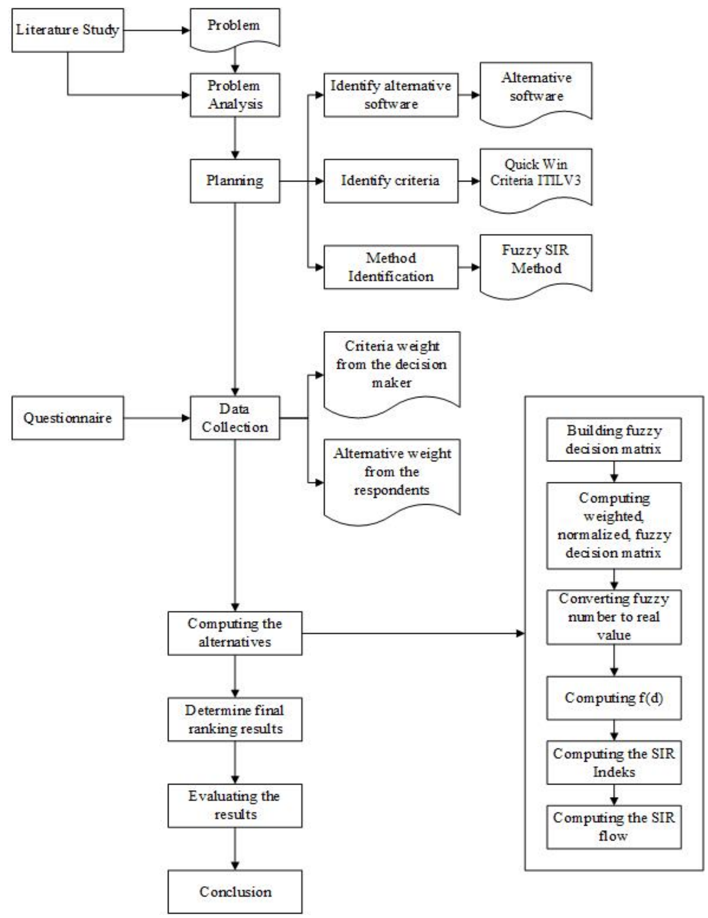

Figure 1 Research Flow

3.2. Research sample and location

We used a quantitative approach by disseminating data for two purposes, first to determine the weight of each of the quick win (decision maker) criteria. Respondents were selected as five ITSM experts who had participated in ITIL V3 training, had ITIL V3 certificates, and the companies where they worked had implemented ITIL V3 best practices in Indonesia. Second, the alternative weight questionnaire uses ten respondents, who have worked using ITSM software. We did an online survey using the Google Forms application. This questionnaire link is then distributed to the appropriate respondents through social media such as WhatsApp and LinkedIn.

3.3. ITSM Software Evaluation Method

In evaluating software ratings, the author uses the Fuzzy SIR method. Fuzzy SIR method is a modification of classic SIR method. Classic SIR method uses crisp value in evaluation process. For ITSM software ranking case, the criteria were gained from expert who involved in this area. However, criteria from human preferences are sometimes uncertain, therefore not all criteria from expert in ITSM can be measured using crisp value [1]. Fuzzy logic, due to its nature can process criteria with uncertain value. Modifying Fuzzy logic and SIR become the best solution for ITSM software ranking.

In their research, [5] using Triangle Fuzzy Number (TFN) for fuzzy SIR calculations because of its ease of use in performing calculations. Also, it has been displayed that modelling with triangular fuzzy numbers is an effective way to formulate decision problems when the available information is subjective and inaccurate. In [20]–[22] triangular membership function shows better performance concerning the steady-state behavior compare to gaussian fuzzy number. In this research, we follow the step how to calculate the Fuzzy SIR by using equation 1-20 which mentioned in [5]

4. Quick Win Selection Criteria

In identifying ITSM software selection criteria, the authors conducted a literature study on several books, research journal, and global survey from itSMF to determine what criteria would be used in this study. In this research, the generated criteria will lead to processes that exist in ITIL V3. Based on research conducted by [1] and [5], both of the research uses 46 criteria to rank the ITSM software, which are grouped into functional criteria and non-functional criteria. Functional criteria are determined based on ITIL V3 which consists of 5 main criteria. This main criterion is taken based on the 5 phases in the ITIL V3 lifecycle, namely: Service Strategy, Service Design, Service Transition, Service Operation, and Continual Service Improvement. Then, for the sub categories it is taken from the functional process of each phase. Meanwhile, the non-functional criteria consist of 4 main criteria, namely: Quality, Technical, Vendor, and Implementation.

Based on research conducted by [2], the criteria used for ranking are determined based on ITIL V3 at the service operation process. These criteria include: Event Management, Incident Management, Problem Management, and Request Fulfillment. The approach to criteria in service operations process was chosen because many new organizations wanted to implement ITSM and almost all started from service operations.

According to the book entitled "ITIL V3: Where to Start & How To Achieve Quick Wins" written by [23] –an IT Management Consultant from Pink Elephant–, to implement ITIL is not an easy thing and sometimes can take several years or more. Therefore, a plan is needed to achieve "quick win". Pink Elephant recommends starting with what are called with 'Customer Fulfillment' process, such as Incident Management, Service Level Management and Change Management, which has daily interaction and visibility with the business. Some suggested processes include: Incident Management, Service Desk, Change Management, Service Catalog Management, Problem Management and Service Assets & Configuration Management (SACM).

Based on the global survey results which is cite by [3] in 2016, there are 5 sub-process in ITIL V3 Life Cycle that widely used by organizations in implementing ITSM, among others, include: Service Desk, Incident Management, Problem Management, Change Management, and Service Level Management. The percentage of the survey can be seen in the Figure 3 below.

According to the survey results which is cited by [3], that there are 3 processes in ITIL V3 which is the most widely used by companies including: Service Operations, Service Transitions, and Service Design. Therefore, based on previous literature studies, the criteria used in this study will be taken from the three processes mentioned before as a quick-win criteria that will be implemented in Small-Medium Enterprises (SMEs). Summary of criteria can be seen in the Table 3 below.

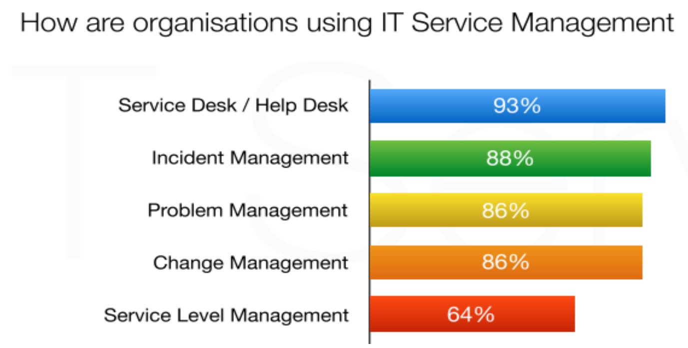

Figure 2 How are organizations using IT Service Management. Source: [3]

Table 3. Quick Win Criteria in ITIL V3

No	Criteria	Main Phase in ITIL V3
C1	Service Desk	Service Operation Function
C2	Event Management	Service Operation Process
C3	Incident Management	Service Operation Process
C4	Problem Management	Service Operation Process
C5	Request Fulfilment	Service Operation Process
C6	Change Management	Service Transition Process
C7	Service Catalogue Management	Service Design Process
C8	Service Asset and Configuration Management	Service Transition Process
C9	Service Level Management	Service Design Process

5. Fuzzy SIR implementation in Quick Win Criteria

This section describes the implementation of experiments conducted by the author, starting from the stage of problem analysis, collecting primary data, determining criteria and weighting criteria, determining alternatives and calculations using the Fuzzy SIR method.

5.1. Problem Analysis

To support the implementation of ITSM in a company, appropriate ITSM software is needed. Currently available various kinds of software, ranging from software that is available for free (open source) to paid software. For companies that are large and stable, purchasing paid software may not be too problematic. Also for companies that have made IT as a service that is inseparable from other services, such as the banking industry, purchasing paid software can help transfer risk both in terms of integration into existing systems, or cases of problems or bugs in the system that occur. However, with quite expensive costs, Small Medium Enterprises (SMEs) that will implement ITSM may be more suitable to try ITSM implementation using open source software.

The question is how Small Medium Enterprises (SMEs) who want to implement ITSM can choose the appropriate open source software? What criteria are appropriate to evaluate ITSM software ratings? Which ITSM open source software ranks best? Therefore, this research was built to answer these questions.

5.2. Planning

In this phase, there are 3 things done by the author, including: identify alternative software, identify criteria, and method identification. In identifying alternative software, the author conducted a literature study on ITSM software that is widely used today. Based on the research from [1] and [5], the software ranking is applied to a local company in Iran engaged in IT services to analyse 6 software, namely: ITSM I, ITSM II, ITSM III, ITSM IV , ITSM V, and ITSM VI. Whereas based on the research [2], there are 3 open source software that were studied using the AHP method, namely: OTRS, ITOP, and IDOIT. The reason for choosing this three software is because the three software are the most widely used ITSM software. According to ITSM daily report, there are 6 best ITSM software solutions including: ITOP, OTRS, CITSMART, Project Open, OCS Inventory NG, and I-doit. In addition, there are some of the best commercial software alternatives including: ManageEngine Service Desk Plus, Freshservice, and Samanage. Therefore, the author also made further observations. According to research conducted by Garther, Manage Engine Service Desk Plus is one of the best ITSM software based on user reviews. Manage Engine Service Desk Plus gets a 4.3 rating of a maximum of 5. Therefore, the author decided to conduct ITSM software selection research on 3 software, namely: OTRS, ITOP, and Manage Engine Service Desk Plus (SDP). The criteria used for software ranking can be seen in Table 3. Whereas for software ranking method is fuzzy SIR which was discussed earlier in the section 3.3.

Table 4. Criteria measurement scale

Linguistic Variable	Description
Not Important (NI)	Activities in the process have no effect on the service.
Less Important (LI)	Activities in the process have less influence on the service.
Enough (E)	Activities in the process have an effect on the service.
Important (I)	Activities in the process affect the service.
Very Important (VI)	Activities in the process greatly affect the service.

Table 5. Software measurement scale

Linguistic Variable	Description
Very Bad (VB)	1. Not able to minimize the adverse effects that will occur. 2. Not able to prevent when an incident occurs
Bad (B)	1. Does not explain the relationship between events that occur in software infrastructure. 2. Cannot detect incidents or instructions (notifications).
Average (A)	1. Able to provide and examine incidents that occur. 2. Need settings, so that it is rather difficult for users.
Good (G)	1. Good processing, because of the detail and complexity. 2. There is an escalation process.
Very Good (VG)	1. In its use, it is easier for users. 2. The request process can be done by an external or service desk. 3. Able to manage incidents (minimize adverse effects). 4. Able to diagnose the cause of the incident. 5. Able to provide requests for services from users

5.3. Data Collection

At this stage, the author collects primary data that will be processed using a predetermined method. Before conducting data collection, the writer first determines the measurement scale, where in this study the author uses a Likert scale. Explanation of the measurement scale used can be seen below.

1. Criteria measurement scale

The weight of the criteria used in this study is the weight obtained from the decision maker that has been determined previously in section 3.2. The weighting of these criteria aims to find out what criteria are most influential in this study. The weight of each criterion that has been given by the decision maker is summarized in the Appendix 1.

2. Software measurement scale

The weight of alternative software is used to rank which alternative software is best based on quick win criteria in ITIL V3. The weight of each alternative software that has been given by the decision maker is summarized in the Appendix 1. This section describes the implementation of experiments conducted by the author, starting from the stage of problem analysis, collecting primary data, determining criteria and weighting criteria, determining alternatives and calculations using the Fuzzy SIR method.

5.4. Computing the Alternatives

In calculating of software ratings, the author uses the Fuzzy SIR method.

1. Building Fuzzy Decision Matrix

At this stage, the weight of the alternative software that has been obtained from the results of the questionnaire from the respondent will be changed into a Triangular Fuzzy Number (TFN). The use of Triangular Fuzzy Number (TFN) is due to its simplicity and is useful in promoting representation and information processing.

Before forming a fuzzy decision matrix, the writer first determines the Triangular Fuzzy Number (TFN) scale for each rating weight. In applying the TFN scale there are three points in each value, namely: Lower (*l*), Median (*m*), and Upper (*u*) to calculate the value of uncertainty in the assessment given.

a. Criteria measurement scale

Table 6 TFN scale for measuring criteria

Scale	Linguistic Variable	Fuzzy Number	Membership Function
1	Not Important (NI)	(0.00, 0.00, 0.25)	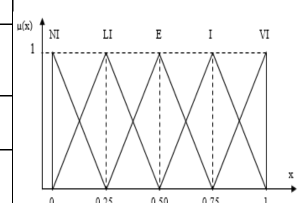
2	Less Important (LI)	(0.00, 0.25, 0.50)	
3	Enough (E)	(0.25, 0.50, 0.75)	
4	Important (I)	(0.50, 0.75, 1.00)	
5	Very Important (VI)	(0.75, 1.00, 1.00)	

b. Software measurement scale

Table 7 TFN scale for software measurement

Scale	Linguistic Variable	Fuzzy Number	Membership Function
1	Very Bad (VB)	(0.00, 0.00, 0.25)	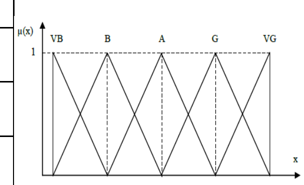
2	Bad (B)	(0.00, 0.25, 0.50)	
3	Average (A)	(0.25, 0.50, 0.75)	
4	Good (G)	(0.50, 0.75, 1.00)	
5	Very Good (VG)	(0.75, 1.00, 1.00)	

After determining the weight of the fuzzy value, the author changes the value of the linguistic variable in the questionnaire (Appendix 1) into a triangular fuzzy number according to the equation (7) where the fuzzy value (*l, m, u*) used can be seen in the Table 6. To be processed at the next stage, the data must be aggregated first. Therefore, the author uses the equation (8) as the aggregation procedure.

2. Computing Weighted, Normalized Fuzzy Decision Matrix

At this stage, we will multiply the triangular fuzzy number by weighting the criteria determined by the decision maker. The results can be seen in Appendix 2.

3. Converting fuzzy numbers to real values

The equation (10) is used for the defuzzification process.

4. Computing *f*(*d*)

In the research [5], using Gaussian criterion because it is the best nonlinear function. Nonlinear functions are more universal than linear. Therefore, the author uses the equation (11) in calculating *f*(*d*).

5. Computing the SIR Index

The SIR index consists of 2, namely: Superiority Index and inferiority index. Equation (12) and (13) used in this process of calculating the SIR index. Superiority and inferiority indices will form two types of matrices, namely Superiority and Inferiority matrices as can be seen below.

a. *Superiority Matrix*

$$S = \begin{bmatrix} 0.44386 & 0.10913 & 0 & 0.16724 & 0 & 0.18920 & 0.03077 & 0.06025 & 0.13334 \\ 0 & 0 & 0.00404 & 0 & 0.00422 & 0.01272 & 0.06020 & 0 & 0 \\ 0.37831 & 0 & 0.29623 & 0.16724 & 0 & 0 & 0 & 0.00245 & 0.18450 \end{bmatrix}$$

b. *Inferiority Matrix*

$$I = \begin{bmatrix} 0 & 0 & 0.17381 & 0 & 0.00211 & 0 & 0.00404 & 0 & 0.00450 \\ 0.81718 & 0.05457 & 0.12646 & 0.33448 & 0 & 0.06275 & 0 & 0.04089 & 0.31334 \\ 0 & 0.05457 & 0 & 0 & 0.00211 & 0.13918 & 0.08693 & 0 & 0 \end{bmatrix}$$

6. Computing the SIR *Flow*

In calculating SIR flow, an aggregation function is needed. For that, equation (16) and (17) used in this study. The results can be seen in the table below.

Table 8 S-flow dan I-flow Matrix

Software	S-flow	I-flow
OTRS	0.957322829	0.151767908
ITOP	0.065921576	1.497607927
SDP	0.876659551	0.250528121

6. ITSM S/W Evaluation Result

Alternative ranking of ITSM software is determined by superiority flow and inferiority flow. Superiority Flow $\varphi^{>}(A_i)$ measures how A_i is globally superior to all the others, and Inferiority flow $\varphi^{<}(A_i)$ measures how A_i is globally inferior to all the others. Therefore, the higher S-flow $\varphi^{>}(A_i)$ and the lower I-flow $\varphi^{<}(A_i)$, the better alternative A_i is.

Based on Table 8, we obtain two complete ratings from the alternatives as follows:

$$R_{>} = \text{OTRS} \rightarrow \text{SDP} \rightarrow \text{ITOP}$$

$$R_{<} = \text{OTRS} \rightarrow \text{SDP} \rightarrow \text{ITOP}$$

Information:

$$R_{>} = S - \text{ranking}$$

$$R_{<} = I - \text{ranking}$$

The two complete ranks are different complete rankings. The two complete ratings are then combined into partial rankings $R = \{P, I, R\} = R_{>} \cap R_{<}$

$$R \cap R = R_{>} \cap R_{<} = \text{OTRS} \rightarrow \text{SDP} \rightarrow \text{ITOP}$$

The results of the partial ranking, as described above, cannot yet be used to determine the final ranking of this study. To get a complete ranking, several synthesis streams can be used to determine ratings. In this study, n-flow will be used $\varphi_n(A_i)$ (like net flow in the PROMETHEE method) and r-flow $\varphi_r(A_i)$ (like the relative flow in the TOPSIS method). Of the two synthesis streams, one of them can be used to determine the final ranking. For this reason, the equation is used (19) and (20) in doing the final ranking. The table below shows the process of calculating n-flow and r-flow.

Table 9. Calculation of n-flow

Software	n-flow	Result
OTRS	0.957322829 – 0.151767908	0.805554921
ITOP	0.065921576 – 1.497607927	-1.431686351
SDP	0.876659551 – 0.250528121	0.62613143

Table 10. Calculation of r-flow

Software	r-flow	Result
OTRS	$\frac{0.957322829}{(0.957322829 + 0.151767908)}$	0.863160062
ITOP	$\frac{0.065921576}{(0.065921576 + 1.497607927)}$	0.042162029
SDP	$\frac{0.876659551}{(0.876659551 + 0.250528121)}$	0.777740542

As we can see from the two tables above (Table 9 and 10), that the value of n-flow $\varphi_n(A_i)$ not only has a positive value but can also be negative. While, the value of r-flow $\varphi_r(A_i)$ always positive between 0 and 1. The following are tables and graphs based on the final results of ITSM software ratings.

Table 11 Final results of software ranking

Software	n-flow	r-flow
OTRS	0.805554921	0.863160062
ITOP	-1.431686351	0.042162029
SDP	0.62613143	0.777740542

From both data, it can be concluded as follows:

$$R_n = \text{OTRS} \rightarrow \text{SDP} \rightarrow \text{ITOP}$$

$$R_r = \text{OTRS} \rightarrow \text{SDP} \rightarrow \text{ITOP}$$

OTRS software still ranks first from the results of ITSM software ranking analysis based on ITIL V3 quick-win process criteria.

From the results of the ranking (see Table 11), can be seen that OTRS software is superior to ITOP and SDP software with n-flow values (0.80) and r-flow (0.86). This result shows that OTRS is the best software when viewed from the ITIL V3 criteria in the service operation process. Whereas in the second position there is SDP software with n-flow value (0.62) and r-flow (0.77). ITOP software is ranked last with n-flow values (-1.43) and n-flow (0.04).

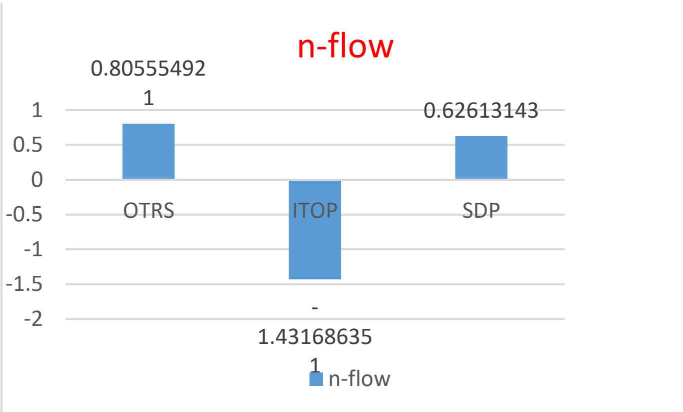

Figure 3. The n-flow graph

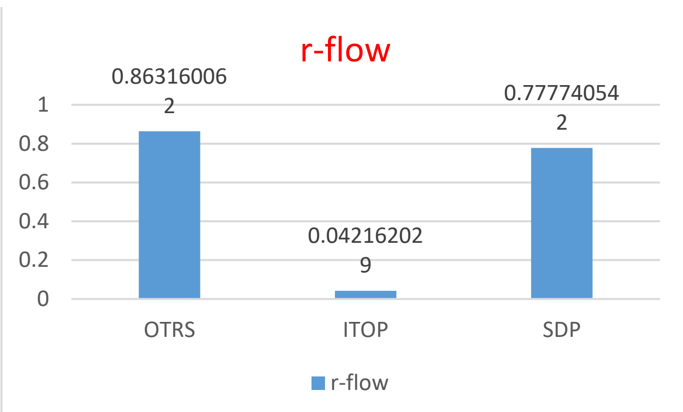

Figure 4 The r-flow graph

7. Conclusion and Future Work

Based on the results of research that has been done, the author uses the fuzzy SIR (Superiority and Inferiority Ranking) method in ITSM software ratings. The ITSM software that was evaluated in this study included: OTRS, ITOP, and Service Desk Plus (SDP). The evaluation was done by using some criteria which taken from ITIL V.3 that widely used by companies including: Service Operations, Service Transitions, and Service Design. We use 9 criteria based on that quick win, namely: Service Desk, Event Management, Incident Management, Problem Management, Request Fulfilment, Change Management, Service Catalogue Management, Service Asset and Configuration Management and Service Level Management.

The OTRS software shows a value of 0.86, while ITOP software has a value of 0.04, then the Service Desk Plus (SDP) software has a value of 0.77. So, the final software ranking shows that OTRS software is the best software that meets the ITIL V3 criteria in the service operation process, SDP software is in second place, and ITOP software is in the last position.

In order to improve the results of better research, the authors suggest the addition of criteria in ranking alternative software. The criteria used can be adjusted to the needs of the company so that the ranking of alternative software can better meet the needs of users (in this case Small-Medium Enterprises (SMEs)) to improve their company performance for the better. In addition, this research can be developed into an application to facilitate the decision maker in determining ITSM software that is in accordance with the vision and mission of the company.

Conflict of Interest

The authors declare no conflict of interest.

Acknowledgment

This work was supported by The Research-Based National Publication Program, The Center of Research and Publication, Syarif Hidayatullah State Islamic University Jakarta, Indonesia

References

[1] S. Rouhani and A. Z. Ravasan, “A Fuzzy TOPSIS based Approach for ITSM Software Selection,” *Int. J. It/bus. Alignment Gov.*, vol. 5, no. 2, pp. 1–26, 2014, https://10.4018/ijitbag.2014070101.
[2] H. T. Sukmana, L. K. Wardhani, R. Argantone, and K. Lee, “The Evaluation of ITSM Open Source Software for Small Medium Organizations Based on ITIL v.3 Criteria using AHP Method,” *Int. J. Control Autom.*, vol. 10, no. 7, pp. 203–216, 2017, https://10.14257/ijca.2017.10.7.17.
[3] J. Wulf, T. J. Winkler, and W. Brenner, “Measuring IT Service Management Capability: Scale Development and Empirical Validation,” in *12th International Conference on Wirtschaftsinformatik*, 2015, pp. 630–644.
[4] E. Hubbert, P. O’Neill, and B. Echols, “Market Overview: IT Service Management Support Tools,” Cambridge, 2010.
[5] S. Rouhani, “A fuzzy superiority and inferiority ranking based approach for IT service management software selection,” *Kybernetes*, vol. 46, no. 4, pp. 728–746, 2017, https://10.1108/K-05-2016-0116.
[6] M. Mora, “An Initial Classification of Open Source Software Tools for Supporting the IT Service Management Processes by Using Formal Concept Analysis,” pp. 1–5, 2010.
[7] D. Yazdanfar and P. Öhman, “Firm-level determinants of job creation by SMEs: Swedish empirical evidence,” *J. Small Bus. Enterp. Dev.*, vol. 22, no. 4, pp. 666–679, 2015.
[8] I. Mandl and S. Ledermaier, “SMEs and job creation in Europe,” in *European Born Globals*, Routledge, 2017, pp. 22–35.
[9] Y. Sudaryo and D. Permatasari, “Strategy Development Micro Small And Medium Business Performance In Small And Medium Enerprises (Smes) Cibaduyut Shoe Bandung,” *Int. J. Sci. Technol. Res.*, vol. 6, no. 3, pp. 102–105, 2017.
[10] Xiaozhan Xu, “The SIR method: A superiority and inferiority ranking method for multiple criteria decision making.” European Journal of Operational Research, China, pp. 587–602, 2001.
[11] R. W. Saaty, “The Analytic Hierarchy Process-What It is and How It is Used,” *Math Model.*, vol. 9, no. 3–5, pp. 161–176, 1987.
[12] B. Roy, “ELECTRE III: Un algorithme de classements fondé sur une représentation floue des préférences en présence de critères multiples,” *Cah. du CERO*, vol. 20, no. 1, pp. 3–24, 1978.
[13] C. M. Tam, T. K. L. Tong, and Y. W. Wong, “Selection of Concrete Pump Using the Superiority and Inferiority Ranking Method,” *J. Constr. Eng. Manag.*, vol. 130, no. 6, pp. 827–834, 2004, https://10.1061/(ASCE)0733-9364(2004)130:6(827).
[14] M. Daugdeviren and I. Yüksel, “Developing a fuzzy analytic hierarchy process (AHP) model for behavior-based safety management,” *Inf. Sci. (Ny).*, vol. 178, no. 6, pp. 1717–1733, 2008, https://https://doi.org/10.1016/j.ins.2007.10.016.
[15] J. Chai, J. N. K. Liu, and Z. Xu, “A New Rule-Based SIR Approach To Supplier Selection Under Intuitionistic Fuzzy Environments,” *Int. J. Uncertainty, Fuzziness Knowledge-Based Syst.*, vol. 20, no. 03, pp. 451–471, 2012, https://10.1142/S0218488512500237.
[16] N. Encantado Faria and M. Mira da Silva, “Selecting a Software Tool for ITIL using a Multiple Criteria Decision Analysis Approach,” in *Designing Digitalization (ISD2018 Proceedings)*, 2018.
[17] L. Kralik, R. Senkerik, and R. Jasek, “Comparison of MCDM methods with

users' evaluation," *Iber. Conf. Inf. Syst. Technol. Cist.*, vol. 2016–July, 2016, https://10.1109/CISTI.2016.7521387.

[18] M. Mora, J. Gomez, R. V O\textquoterightConnor, and O. Gelman, "A Risk-based MADM Model for Selecting Free-Libre Open Source Software Tools in the Domain of IT Service Management," in *16th Symposium on Decision Technology and Intelligent Information Systems*, 2016, no. August.

[19] M. Mora, J. Marx Gómez, R. V O 'connor, and O. Gelman, "'An MADM risk-based evaluation- selection model of free-libre open source software tools A MADM Risk-based Evaluation-Selection Model of Free- Libre Open Source Software Tools," *Int. J. Technol. Policy Manag.*, vol. 16, no. 4, 2016, https://10.1504/IJTPM.2016.081665.

[20] O. A. M. Ali, A. Y. Ali, and B. S. Sumait, "Comparison between the Effects of Different Types of Membership Functions on Fuzzy Logic Controller Performance," *Int. J. Emerg. Eng. Res. Technol.*, vol. 3, no. 3, pp. 76–83, 2015.

[21] P. Harliana and R. Rahim, "Comparative Analysis of Membership Function on Mamdani Fuzzy Inference System for Decision Making," *J. Phys. Conf. Ser.*, vol. 930, no. 1, 2017, https://10.1088/1742-6596/930/1/012029.

[22] J. Gayathri Monicka, D. N.O.Guna Sekhar, and K. Ramash Kumar, "Performance Evaluation of Membership Functions on Fuzzy Logic Controlled AC Voltage Controller for Speed Control of Induction Motor Drive," *Int. J. Comput. Appl.*, vol. 13, no. 5, pp. 8–12, 2011, https://10.5120/1778-2451.

[23] G. Case, "ITIL V3: Where To Start & How To Achieve Quick Wins," *Consultant*, pp. 1–7, 2007.

APPENDIX 1 Questionnaire Data

1. The weight of the criteria from the decision maker (DM).

	DM	C1	C2	C3	C4	C5	C6	C7	C8	C9
1	DM1	5	4	5	4	5	4	5	4	4
2	DM2	5	5	5	3	5	5	5	5	5
3	DM3	5	4	4	4	3	5	5	3	5
4	DM4	5	5	5	5	3	5	4	3	5
5	DM5	5	4	4	5	2	4	4	4	5

2. The alternatives weight from the respondent

[redacted]		Respondent														
		1			2			3			4			5		
NO	Quick Win Process	OTRS	ITOP	SDP	OTRS	ITOP	SDP	OTRS	ITOP	SDP	OTRS	ITOP	SDP	OTRS	ITOP	SDP
1	Service Desk	4	2	3	4	3	3	3	4	4	4	4	4	4	4	3
2	Event Management	3	2	3	4	3	2	3	3	4	4	4	4	4	4	3
3	Incident Management	4	2	3	4	4	3	3	4	4	3	3	4	4	4	3
4	Problem Management	4	2	3	5	3	3	3	3	4	3	3	4	4	4	3
5	Request Fulfillment	3	3	2	3	3	4	3	4	4	3	3	4	4	4	3
6	Change Management	3	3	2	4	4	3	3	3	4	3	3	3	4	4	3
7	Service Catalog Management	3	3	2	3	3	3	3	4	4	3	4	3	4	4	3
8	Service Asset and Configuration Management	2	2	2	5	3	2	3	3	4	4	4	4	4	4	3
9	Service Level Management	3	2	3	4	2	3	3	4	4	3	4	4	4	4	3
	USER?	NO	YES	YES	YES	YES	YES	NO	NO	YES	YES	YES	YES	YES	YES	NO

Continue…

[redacted]		Respondent														
		6			7			8			9			10		
NO	Quick Win Process	OTRS	ITOP	SDP	OTRS	ITOP	SDP	OTRS	ITOP	SDP	OTRS	ITOP	SDP	OTRS	ITOP	SDP
1	Service Desk	4	3	5	3	2	4	5	3	4	4	4	4	5	4	5
2	Event Management	3	3	3	3	3	4	4	4	4	4	4	4	4	5	4
3	Incident Management	3	3	4	2	3	4	4	4	5	4	4	4	4	5	5
4	Problem Management	3	2	4	3	2	3	3	3	4	3	3	3	4	4	4
5	Request Fulfillment	5	3	3	3	3	4	4	5	4	4	4	4	4	5	4
6	Change Management	4	3	2	3	3	4	4	3	4	4	4	4	5	3	5
7	Service Catalog Management	3	4	3	3	3	4	4	3	4	4	4	3	4	3	5
8	Service Asset and Configuration Management	4	3	4	3	3	3	4	4	4	4	4	4	4	3	4
9	Service Level Management	4	3	4	3	3	4	4	4	4	3	4	4	5	3	4
	USER?	NO	NO	YES	NO	NO	YES	YES	YES	YES	YES	YES	NO	YES	NO	YES

APPENDIX 2 Fuzzy Decision Matrix

1. Fuzzy Decision Matrix

	C1			C2			C3			C4		
OTRS	*l*	*m*	*u*	*l*	*m*	*u*	*l*	*m*	*u*	*l*	*m*	*u*
R1	0.50	0.75	1.00	0.25	0.50	0.75	0.50	0.75	1.00	0.50	0.75	1.00
R2	0.50	0.75	1.00	0.50	0.75	1.00	0.50	0.75	1.00	0.75	1.00	1.00
R3	0.25	0.50	0.75	0.25	0.50	0.75	0.25	0.50	0.75	0.25	0.50	0.75
R4	0.50	0.75	1.00	0.50	0.75	1.00	0.25	0.50	0.75	0.25	0.50	0.75
R5	0.50	0.75	1.00	0.50	0.75	1.00	0.50	0.75	1.00	0.50	0.75	1.00
R6	0.50	0.75	1.00	0.25	0.50	0.75	0.25	0.50	0.75	0.25	0.50	0.75
R7	0.25	0.50	0.75	0.25	0.50	0.75	0.00	0.25	0.50	0.25	0.50	0.75
R8	0.75	1.00	1.00	0.50	0.75	1.00	0.50	0.75	1.00	0.25	0.50	0.75
R9	0.50	0.75	1.00	0.50	0.75	1.00	0.50	0.75	1.00	0.25	0.50	0.75
R10	0.75	1.00	1.00	0.50	0.75	1.00	0.50	0.75	1.00	0.50	0.75	1.00
ITOP	*l*	*m*	*u*	*l*	*m*	*u*	*l*	*m*	*u*	*l*	*m*	*u*
R1	0.00	0.25	0.50	0.00	0.25	0.50	0.00	0.25	0.50	0.00	0.25	0.50
R2	0.25	0.50	0.75	0.25	0.50	0.75	0.50	0.75	1.00	0.25	0.50	0.75
R3	0.50	0.75	1.00	0.25	0.50	0.75	0.50	0.75	1.00	0.25	0.50	0.75
R4	0.50	0.75	1.00	0.50	0.75	1.00	0.25	0.50	0.75	0.25	0.50	0.75
R5	0.50	0.75	1.00	0.50	0.75	1.00	0.50	0.75	1.00	0.50	0.75	1.00
R6	0.25	0.50	0.75	0.25	0.50	0.75	0.25	0.50	0.75	0.00	0.25	0.50
R7	0.00	0.25	0.50	0.25	0.50	0.75	0.25	0.50	0.75	0.00	0.25	0.50
R8	0.25	0.50	0.75	0.50	0.75	1.00	0.50	0.75	1.00	0.25	0.50	0.75
R9	0.50	0.75	1.00	0.50	0.75	1.00	0.50	0.75	1.00	0.25	0.50	0.75
R10	0.50	0.75	1.00	0.75	1.00	1.00	0.75	1.00	1.00	0.50	0.75	1.00
SDP	*l*	*m*	*u*	*l*	*m*	*u*	*l*	*m*	*u*	*l*	*m*	*u*
R1	0.25	0.50	0.75	0.25	0.50	0.75	0.25	0.50	0.75	0.25	0.50	0.75
R2	0.25	0.50	0.75	0.00	0.25	0.50	0.25	0.50	0.75	0.25	0.50	0.75
R3	0.50	0.75	1.00	0.50	0.75	1.00	0.50	0.75	1.00	0.50	0.75	1.00
R4	0.50	0.75	1.00	0.50	0.75	1.00	0.50	0.75	1.00	0.50	0.75	1.00
R5	0.25	0.50	0.75	0.25	0.50	0.75	0.25	0.50	0.75	0.25	0.50	0.75
R6	0.75	1.00	1.00	0.25	0.50	0.75	0.50	0.75	1.00	0.50	0.75	1.00
R7	0.50	0.75	1.00	0.50	0.75	1.00	0.50	0.75	1.00	0.25	0.50	0.75
R8	0.50	0.75	1.00	0.50	0.75	1.00	0.75	1.00	1.00	0.50	0.75	1.00
R9	0.50	0.75	1.00	0.50	0.75	1.00	0.50	0.75	1.00	0.25	0.50	0.75
R10	0.75	1.00	1.00	0.50	0.75	1.00	0.75	1.00	1.00	0.50	0.75	1.00

Continue…

C5			C6			C7			C8			C9		
l	*m*	*u*	*l*	*m*	*u*	*l*	*m*	*u*	*l*	*m*	*u*	*l*	*m*	*u*
0.25	0.50	0.75	0.25	0.50	0.75	0.25	0.50	0.75	0.00	0.25	0.50	0.25	0.50	0.75
0.25	0.50	0.75	0.50	0.75	1.00	0.25	0.50	0.75	0.75	1.00	1.00	0.50	0.75	1.00
0.25	0.50	0.75	0.25	0.50	0.75	0.25	0.50	0.75	0.25	0.50	0.75	0.25	0.50	0.75
0.25	0.50	0.75	0.25	0.50	0.75	0.25	0.50	0.75	0.50	0.75	1.00	0.25	0.50	0.75
0.50	0.75	1.00	0.50	0.75	1.00	0.50	0.75	1.00	0.50	0.75	1.00	0.50	0.75	1.00
0.75	1.00	1.00	0.50	0.75	1.00	0.25	0.50	0.75	0.50	0.75	1.00	0.50	0.75	1.00
0.25	0.50	0.75	0.25	0.50	0.75	0.25	0.50	0.75	0.25	0.50	0.75	0.25	0.50	0.75
0.50	0.75	1.00	0.50	0.75	1.00	0.50	0.75	1.00	0.50	0.75	1.00	0.50	0.75	1.00
0.50	0.75	1.00	0.50	0.75	1.00	0.50	0.75	1.00	0.50	0.75	1.00	0.25	0.50	0.75
0.50	0.75	1.00	0.75	1.00	1.00	0.50	0.75	1.00	0.50	0.75	1.00	0.75	1.00	1.00
l	*m*	*u*	*l*	*m*	*u*	*l*	*m*	*u*	*l*	*m*	*u*	*l*	*m*	*u*
0.25	0.50	0.75	0.25	0.50	0.75	0.25	0.50	0.75	0.00	0.25	0.50	0.00	0.25	0.50
0.25	0.50	0.75	0.50	0.75	1.00	0.25	0.50	0.75	0.25	0.50	0.75	0.00	0.25	0.50
0.50	0.75	1.00	0.25	0.50	0.75	0.50	0.75	1.00	0.25	0.50	0.75	0.50	0.75	1.00
0.25	0.50	0.75	0.25	0.50	0.75	0.50	0.75	1.00	0.50	0.75	1.00	0.50	0.75	1.00
0.50	0.75	1.00	0.50	0.75	1.00	0.50	0.75	1.00	0.50	0.75	1.00	0.50	0.75	1.00
0.25	0.50	0.75	0.25	0.50	0.75	0.50	0.75	1.00	0.25	0.50	0.75	0.25	0.50	0.75
0.25	0.50	0.75	0.25	0.50	0.75	0.25	0.50	0.75	0.25	0.50	0.75	0.25	0.50	0.75
0.75	1.00	1.00	0.25	0.50	0.75	0.25	0.50	0.75	0.50	0.75	1.00	0.50	0.75	1.00
0.50	0.75	1.00	0.50	0.75	1.00	0.50	0.75	1.00	0.50	0.75	1.00	0.50	0.75	1.00
0.75	1.00	1.00	0.25	0.50	0.75	0.25	0.50	0.75	0.25	0.50	0.75	0.25	0.50	0.75
l	*m*	*u*	*l*	*m*	*u*	*l*	*m*	*u*	*l*	*m*	*u*	*l*	*m*	*u*
0.00	0.25	0.50	0.00	0.25	0.50	0.00	0.25	0.50	0.00	0.25	0.50	0.25	0.50	0.75
0.50	0.75	1.00	0.25	0.50	0.75	0.25	0.50	0.75	0.00	0.25	0.50	0.25	0.50	0.75
0.50	0.75	1.00	0.50	0.75	1.00	0.50	0.75	1.00	0.50	0.75	1.00	0.50	0.75	1.00
0.50	0.75	1.00	0.25	0.50	0.75	0.25	0.50	0.75	0.50	0.75	1.00	0.50	0.75	1.00
0.25	0.50	0.75	0.25	0.50	0.75	0.25	0.50	0.75	0.25	0.50	0.75	0.25	0.50	0.75
0.25	0.50	0.75	0.00	0.25	0.50	0.25	0.50	0.75	0.50	0.75	1.00	0.50	0.75	1.00
0.50	0.75	1.00	0.50	0.75	1.00	0.50	0.75	1.00	0.25	0.50	0.75	0.50	0.75	1.00

0.50	0.75	1.00	0.50	0.75	1.00	0.50	0.75	1.00	0.50	0.75	1.00	0.50	0.75	1.00
0.50	0.75	1.00	0.50	0.75	1.00	0.25	0.50	0.75	0.50	0.75	1.00	0.50	0.75	1.00
0.50	0.75	1.00	0.75	1.00	1.00	0.75	1.00	1.00	0.50	0.75	1.00	0.50	0.75	1.00

2. Aggregated Fuzzy Decision Matrix

	C1			C2			C3			C4		
	l	*m*	*u*	*l*	*m*	*u*	*l*	*m*	*u*	*l*	*m*	*u*
OTRS	0.25	0.75	1.00	0.25	0.65	1.00	0.00	0.63	1.00	0.25	0.63	1.00
ITOP	0.00	0.58	1.00	0.00	0.63	1.00	0.00	0.65	1.00	0.00	0.48	1.00
SDP	0.25	0.73	1.00	0.00	0.63	1.00	0.25	0.73	1.00	0.25	0.63	1.00

Continue…

C5			C6			C7			C8			C9		
l	*m*	*u*	*l*	*m*	*u*	*l*	*m*	*u*	*l*	*m*	*u*	*l*	*m*	*u*
0.25	0.65	1.00	0.25	0.68	1.00	0.25	0.60	1.00	0.00	0.68	1.00	0.25	0.65	1.00
0.25	0.68	1.00	0.25	0.58	1.00	0.25	0.63	1.00	0.00	0.58	1.00	0.00	0.58	1.00
0.00	0.65	1.00	0.00	0.60	1.00	0.00	0.60	1.00	0.00	0.60	1.00	0.25	0.68	1.00

3. Weighted, Normalized Fuzzy Decision Matrix

	C1			C2			C3			C4		
	l	*m*	*u*	*l*	*m*	*u*	*l*	*m*	*u*	*l*	*m*	*u*
OTRS	0.19	0.75	1.00	0.13	0.55	1.00	0.00	0.56	1.00	0.06	0.50	1.00
ITOP	0.00	0.58	1.00	0.00	0.53	1.00	0.00	0.59	1.00	0.00	0.38	1.00
SDP	0.19	0.73	1.00	0.00	0.53	1.00	0.13	0.65	1.00	0.06	0.50	1.00

Continue…

C5			C6			C7			C8			C9		
l	*m*	*u*	*l*	*m*	*u*	*l*	*m*	*u*	*l*	*m*	*u*	*l*	*m*	*u*
0.00	0.42	1.00	0.13	0.61	1.00	0.13	0.54	1.00	0.00	0.47	1.00	0.13	0.62	1.00
0.00	0.44	1.00	0.13	0.52	1.00	0.13	0.56	1.00	0.00	0.40	1.00	0.00	0.55	1.00
0.00	0.42	1.00	0.00	0.54	1.00	0.00	0.54	1.00	0.00	0.42	1.00	0.13	0.64	1.00

Advances in Science, Technology and Engineering Systems Journal Vol. 4, No. 2, 299-304 (2019)

www.astesj.com

Special Issue on Advancement in Engineering and Computer Science

ASTESJ

ISSN: 2415-6698

Conversion of 2D to 3D Technique for Monocular Images using Papilio One

Priya Arokia*, Anupama Patil

E&TC department, DYPIEMR, Pune, 411 044, India

ARTICLE INFO

Article history:
Received: 26 December, 2018
Accepted: 24 March, 2019
Online: 10 April, 2019

Keywords:
Monocular image
Depth
Scenic feature

ABSTRACT

A 3D image adds realism in viewing experience and can assist in simplifying the graphical displays. A Third dimension supplement to the input can improve pattern recognition, and can be used for 3D scene reconstruction and robot navigation. Recently popularity of 3D hardware is also increased which makes it a hot topic. The production of content as 3D is not matching with its need so there is scope of improvement of these 3D contents. Monocular cues give profundity data when seeing a scene with one eye. When a spectator moves, the evident relative movement of a few stationary articles against a foundation gives indicates about their relative separation. Depth estimation from monocular cues is a difficult task because single image lacks prior information like depth information, motion information etc. In Depth using scene features depth is estimated by exploring the features like shape, edges, color, texture and as well as an analysis of the environment of the scene that are of interest with respect to the target. Different objects have different hue and value and hence color is useful for depth estimation. Shape and texture provides disparity which is used to estimate depth. The main problem in converting a 2 dimensional to 3 dimensional images using single image is that it lacks information required for reconstruction in 3D data. While doing conversion by taking different cues or combination of multiple cues from scene conversion has been done e.g. structure form shape, motion, defocus etc. But such methods work for restricted scenarios not for global scenes. For instance, outdoor algorithms worked poor for indoor algorithms. Here we have implemented automatic conversion of 2 dimensional to 3 dimensional images using monocular image which can convert global images in visually comfortable 3D image.

1. Introduction

In this era 3D supporting hardware's are increasing, but the demand of content in 3D and its availability does not go hand in hand. Still 3D contents are surpassed by the 2D contents. So there is a requirement of 3D data and obvious many researchers are already working on this to close this gap in the future. One solution of direct taking 3D using multi-view method is available but it is costly and already there is large amount of 2D data is available; it will be costly to create newly 3D contents. To work on this problem, there should be the technique which convert large amount of 2D available data into 3D. The converted data should have comfortable visual quality and should not time consuming.

The available 2D data is a monocular data, which is taken from using only single view. The main problem in conversion of 2 dimension to 3 dimension using single image is that it lacks information required for reconstruction in 3D data. As discussed earlier in 2 dimension to 3 dimension conversion two approaches are available i.e. automatic and semi-automatic. Semiautomatic method gives good results but this method is time consuming and costly. Real time implementation of automatic method is preferable as semi-automatic method requires human intervention and is also known as a most trustable tool in extracting the depth from a particular scene. Disparity-pixels extracting algorithm and the camera quality determines the accuracy of the results.

2D image depth estimation is usually done in steps. A monochromatic-picture is oulined by depth where a distant separation from a camera is demonstrated by a low intensity and neaby separation is shown by a high power. i.e. it deals with luminance intensity [1]. Thus depth map, as afunction of the image co-ordinates, presents the depth in corresspondence to the camera position of a point in the visualscene. Estimating depth from a single picture or video quite exciting. As depth is an

*Priya Arokia,VIIT Research scholar,9923240728,Email: prinnu@yahoo.com

important cue of a scene which is lost in image acquisition. Because of this reason and several application needs this information, hence various methods are proposed to extract depth.

Depth Image Based Rendering (DIBR) needs a flow of mono-scopic images and a subsequent flow of depth map images that gives details of per pixel depth. Knowing the depth of each point in an input picture, rendering of any close-by perspective into a sample picture can be done by anticipating the pixels of the first picture to their appropriate 3-D areas and re-anticipating them onto the world-picture-plane. In this manner, DIBR grants the formation of novel pictures, utilizing data from the depth maps, as though they were caught with a camera from various perspectives. A favorable position of the DIBR approach is the higher capability with which coding of the depth maps can be done, than two scenes of common pictures, consequently lessening the transfer speed required for transmission. Rendering an image /video has been well realized and there are also very many algorithms available for producing quality and standard images.

In the left image the closer objects to the camera are located in the right while in the right image they are located in the left. The objects farther away from the camera appears in the same place in both the images. The object displacement in the two images is the disparity. The higher depth is indicated by a smaller disparity and a lower depth by a higher disparity. This is why pixel matching between the two images is essential. Output classification into dense and sparse is done on the stereo correspondence algorithms. An optimum mix of speed and accuracy is obtained by applying method of segments & edges.

Real time applications like robotics require dense output. Since our focus was oriented towards algorithms for real time application, the focus was on 'dense stereo correspondense'. According to [2] dense matching algorithms are divided as local and global matching. The local one is either area based or feature based. Since the disparity is determined chiefly by the intensity values of a particular window, area-based local method applies variable windows. The window size, depending on the output can be changed such that a dense output is obtained to suit most of the real time applications. The feature extraction on which the feature based methods rely on provides a sparse output. However, they are quite fast. The accurate global methods, also called the energy based methods are rather very slow and computanionally expensive.

The object/features mapped in both right and left images is assumed to have the same intensity and the algorithms would be implemented. The illumination effects on the objects, with different view points of the cameras, may at times create a diffrence in the intensity values and invalidate these assumptions. Although the two cameras under consideration are completely tuned and both the images are simltaneously captured, stereo vision normally fails in non-ideal lighting. The reason is that the orientation or the pose of the cameras with respect to the light source may result in the variation of the light intensity of the captured images from the respective view points.

Pixel matching is then the whole idea. For this matching the pixels in the left images are to be looked for in the right images. The search becomes difficult if by chance the variations are both in the x and the Y co-ordinates, since the images are captured by to cameras from two different view points.. Image rectification, nothing but the process of horizontally aligning the epipolar lines of the two cameras is deployed to avoid this. Unidirectional alignment is done by means of linear transformations like rotate, skew and translate.

Authors have proposed an automatic 2D to 3D conversion algorithm rooted on multiple depth indications. Three distintive methods were considered for depth generation and consequently 2-D scene one depth generation method was carriedout [3]. The limitation of this method is latency. A few researchers have presented automatic pathway of learning the 3-D scene structure. In this pathway, an easier algorithm is recommended that learns the scene depth from a huge store of image + depth pairs. The produced anaglyph images provides a decent 3-D perception. However, they are notabsolutely devoid of distortions.

As image or video is having its attributes at a pixel level that are learned by a point transformation, it is applied to a monocular image.. The limitation of this system is cannot apply same transformation to images with potentially different global 3D scene structure.The same authors have also presented method to automatically convert a monoscopic video into stereo for 3D visualization. They are taking plausible automatically extracted depth maps at every frame and presented a framework using temporal information for improved and time-coherent depth when multiple frames are available. They have mixed indoor and outdoor images; hence indoor images work poor for outdoor images and vice-versa. This system is complex.

Guttmann proposed semi-automatic user defined strokes corresponding to a rough estimate of the depth values are defined for the image of interest in the scene[4]. This particular system finds the depth values for the rest of the image, and produces a depth map in order to create stereoscopic 3D image pairs. This can be further extended to automatic method.

This paper proposes the use of image rectification after the calibration of the camera.

The remainder of this brief is arranged as follows. Section II provides the process block diagram and its explanation. Section III presents the simulation results, Section IV subjective analysis and Section V draws the conclusion.

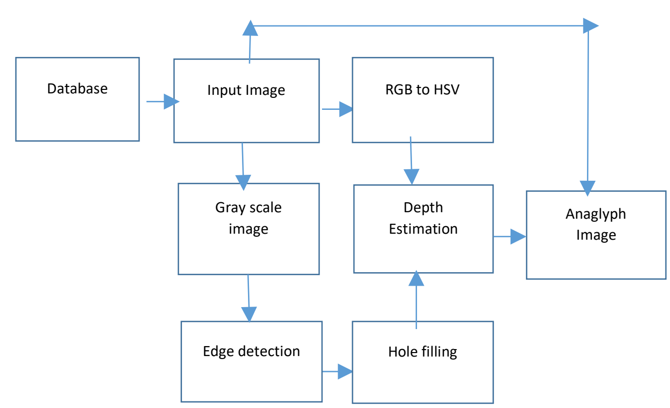

Figure 1.Block diagram of process

2. Process Block Diagram

2.1. Process flow

In 2D-to-3D conversion, input is a RGB monocular color image. Bit depth gives number of bits per pixel and here bit depth should be 24 as the input expected is a RGB image. As an input one can give image of file formats JPEG, BMP and PNG. Figure 1 is the block diagram of the whole process.

The input image is taken from database. Four datasets are used i.e. Make3D dataset [5], NYU dataset [6], Middlebury dataset [7] and our own dataset. Make3D dataset is of outdoor images. It consists of 534 images, each is having 1704X272 dimensions.

The NYU-depth v2 dataset is involved video grouping from assortment scenes taken indoor captured by both RGB and Depth cameras of Microsoft Kinect. This dataset consists of indoor scenes like basements, bedrooms, bathrooms, bookstores, cafe, classroom, dining rooms, kitchens, living rooms, offices etc. Middlebury dataset is one of the well-known dataset, which comprised of stereo images of various scenes along with its ground truth. We also have created indoor dataset of 22 images each image is of 4608X3456 using Sony Device [8]. Input image is given from one of this dataset. For computational efficiency original input images are re-sized.

2.2. RGB to HSV Conversion

The Papilio one is an expandable development board having a "Xilinx Spartan 3E FPGA chip", which is powerful and is in open-source. The whole conversion process happens in Papilio one.

The conversion process of RGB to HSV is shown in Figure 2. 2D query image is given from PC through MATLAB to Papilio one and the development board is used for conversion.From HSV value (V) attribute is considered here to estimate depth and hence a color model from RGB to HSV conversion is done.

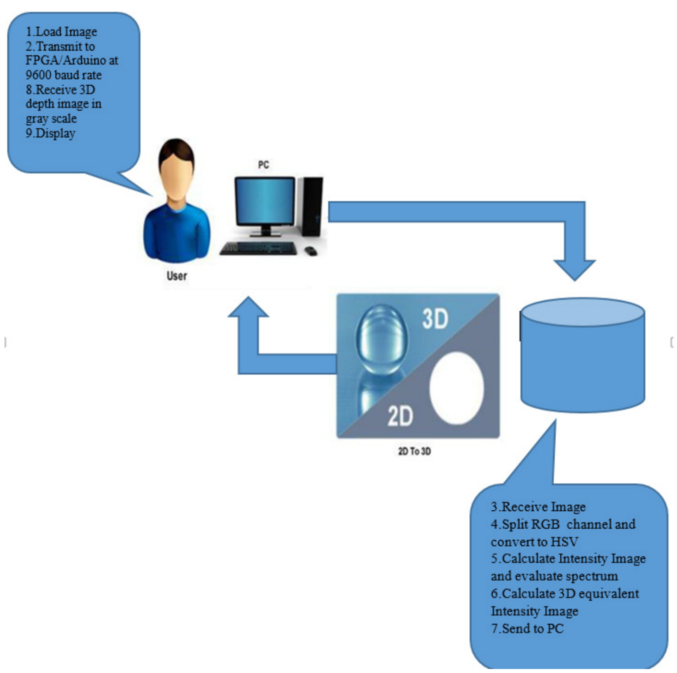

Figure 2. Block diagram of process

Since Papilio One is used for conversion and it has memory constraint ,instead of whole image being sent at a time to the kit, serially pixels are sent to Papilio One for computation one row after another. HSV image is then generated in MATLAB from these processed pixels.

2.3. Edge detection

As per Figure 1 the next step is to detect the edge. Here the input images are converted to gray scale for proper edge detection. Edge detection is the technique of identifying those points in the digitized image which causes a drastic change in the splendor of the image or that causes discontinuities. The edges are identified by rapid change in frequency. The objective is to capture these much needed rapid variations in the properties of the world. Edge detection is done by applying masks on the input which transforms the image into output image highlighting the sharp edges in the object. There are several masks available like Canny, Prewitt, Sobel, Roberts etc. which extracts the sharpness in the images.

The Canny detection is a popular edge detection method. It basically locates the maxima of gradient-I in the neighborhood. Gaussian channel derivative is used to compute the gradient. All the four steps [9] are used to detect the edges of the image. The strategy utilizes two edges, to distinguish solid and frail edges, and incorporates the powerless edges in the yield just on the off chance that they are associated with solid edges. Gaussian channel is connected to evacuate any clamor show in a picture, and more inclined to identify genuine powerless edges [10].

Object should be detected properly, because if it is not then the next operation of hole filling will not be performed properly. Morphological dilation operation is added before the hole-filling to improve the object detection. Pixels are added to the object boundaries during dilation and the number of pixels added is a function of the shape & size of the structuring elements deployed for processing the image.

2.4. Hole filling and depth estimation

The images under go morphological operations viz., dilation and after dilation operation, the detected objects are filled using MATLAB imfill function. For this filling operation first labeling is done using `bwlabel' function which generates a matrix same size as that of the input matrix containing labels for all connected objects in the input matrix.

The input "n" can either be a four connected or eight connected objects with a default value of eight. The pixels with 0 labelling coressponds to the background and the labelling from 1 through 8 coressponds to each of the coneected objects. The ouput gives the number of the connected objects in the iput image. Along with bwlabel function n is used to return vectors of indices for the pixels that make up a specific object. Then that specific object is cropped for filling new depth values using `imcrop' function. This function creates an interactive crop image. From that cropped object maximum and minimum values are calculated. For the same coordinates, values of V (intensity) retrieved from FPGA are stored in array. From the array maximum and minimum values of V are searched to calculate the range. 255/range = multiValue. So for the same coordinates the new value which gives depth is calculated using following equation:

$$val=((imgHSV(yy,xx,3))-minVal)*multiVal \quad (1)$$

where, val is new depth value of depth, (imgHSV(yy,xx,3) gives values of V for that particular pixel, minVal is minimum value from array and multivalue .

2.5. Anaglyph Image Generation

So far depth map image is estimated, now using this depth map and 2D input image anaglyph image is generated. The anaglyph image is generated by using the difference value of each pixel from the depth map. Each pixel is shifted by the corresponding difference value in an input image. The parallax is given by

$$parallax(x,y)=C[1-depth(x,y)]/128 \quad (2)$$

where C is the maximum parallax. Anaglyph image is got by shifting each pixel to the right by parallax(x,y)/2.

Algorithm:

- Load input 2D image from database.
- Send input images pixel serially to FPGA to perform RGB to HSV conversion.
- Display HSV image on PC.
- Convert input image to grayscale image.
- Perform Canny edge detection on grayscale image.
- Display edge detection output.
- Perform dilation operation on edge detection output.
- Perform hole filling operation.
- Label images for object detection.
- Crop the detected objects.
- From the HSV image get the values of V for the same coordinates of the object.
- Assign depth value to new pixel using equation 1 and display.
- Generate anaglyph images and display.

3. Simulation Results

The algorithms we used work only for restricted scenario since cues are not considered. Proposed algorithm is tested for indoor image database, outdoor images database and database created by our own. Figure 3 is the output of various stages of proposed block diagram.

Input is from Make3D dataset of 500X 500 resolution. The first dataset used is a Make3D dataset made up of out-door images which has the depth fields that are acquired by a laser finder. For computational efficiency, the images are resized and the resolutions of the Make3D images are 1704 x 2272. All the stages of the block diagram are given as the output. Figure 3 (f) gives the 3d output which has to be viewed by the 3d glasses.

Figure 4 is the output of various stages and Input is from Middlebury dataset of 300X 259 resolution an in-door image, for computational efficiency, the images are re-sized. Figure 4 (f) gives the 3d output which has to be viewed by the 3d glasses.

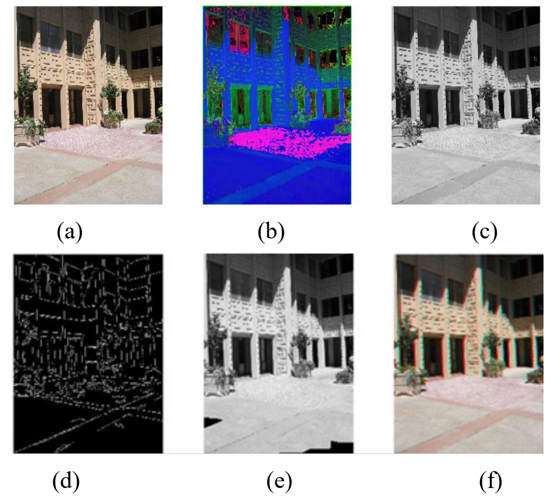

Figure 3: (a) Query (b) HSV (c) Grayscale (d) Edge Detected (e) Depth (f) Anaglyph .

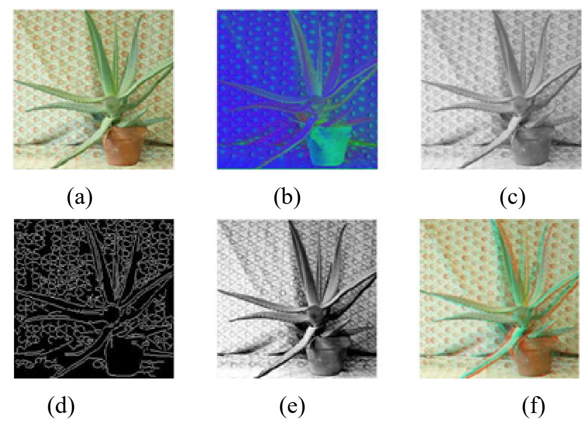

Figure 4: (a) Query (b) HSV (c) Grayscale (d) Edge Detected (e) Depth (f) Anaglyph.

We continued the experiment with our own database with dataset of 300 X 225 resolution, indoor images. The quality of the output was good as that of the Middlebury.

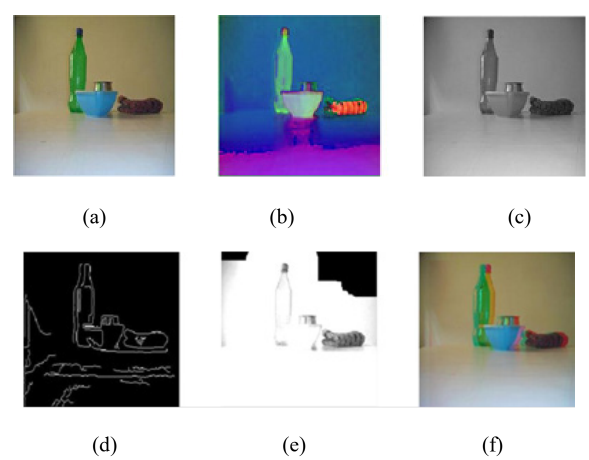

Figure 5: (a) Query (b) HSV (c) Grayscale (d) Edge Detected (e) Depth (f) Anaglyph

Following is the analysis of the images in terms of computing time efficiency of Make 3D dataset. The algorithm was executed in MATLAB and in FPGA and the table shows the time taken of the images for execution.

Table 1: Analysis of Images from Make3D Dataset

Size of input image	Execution time	
	MATLAB	FPGA
100*100	1.08ms	15min 26s
200*200	1.76ms	1hr 00min
300*300	9.05ms	2hr 26min
400*400	37.41ms	4hr 06min
500*500	122.65ms	-
600*600	274.75ms	-
700*700	505.38ms	-
800*800	888.00ms	-
900*900	1451.07ms	-
1000*1000	2196.97ms	-

The time taken by MATLAB to execute the complete process using a single core processor is in milliseconds and for FPGA the time taken is exponentially increasing with increase in the size of the input image. For any real time processing MATLAB would give a time efficient output and the future scope is to extend this algorithm work for multi-core processors.

4. Subjective analysis

Various objective quality metrics like MSE and PSNR are available. This can be used for objective analysis of 2D but not suitable for the 2-D to 3-D contents [11]. The generated depth-map is a pseudo-depth map and is not a real depth-map. So to evaluate the visual quality of output of proposed algorithm it is compared with other algorithms [12]. Figure 6 shows the form shared with people to mark the quality of the images shared with them to analyze. It shows the credit score in percentage depending on the visual perception of the viewer.

Figure 7 shows the subjective analysis of people. For subjective analysis survey from 50 people with normal or correct-to-normal visual acuity and stereo acuity for visual comfort of output. We have shown them output of our algorithm and for the same images output of other two methods. Images are taken from standard dataset.

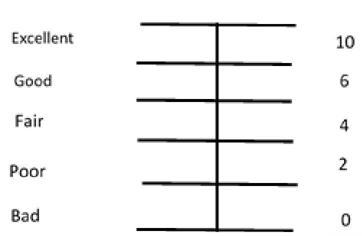

Figure 6: Rating scales used for assessment

Table 2 shows subjective evaluation, where M1 is our method, M2 is global method and M3 is Make3d algorithm. People has given good scale to our algorithm while excellent scale to other to algorithms. The scale on which people has given rating is shown in Figure 6. From the survey its found that they felt proposed methods output good, while of other two method's excellent. The subjective analysis also shows that proposed algorithm provides comfortable viewing experience.

Table 2: Sample Analysis of Images from Make3D Dataset

viewer count	Image1			Image 2			Image 3			Image 4		
	M 1	M 2	M 3	M 1	M 2	M 3	M 1	M2	M 3	M 1	M2	M 3
1	8	10	10	8	10	10	8	10	8	6	10	8
2	6	10	10	6	10	10	8	10	10	6	10	10
3	8	10	10	6	10	10	8	10	8	6	10	8
4	8	10	10	8	10	10	8	10	10	8	10	10
5	8	10	10	8	10	10	8	10	10	6	10	10
6	8	10	10	8	10	10	8	10	8	8	10	8
7	8	10	10	8	10	10	8	10	8	8	10	10
8	8	10	10	8	10	10	8	10	8	8	10	10
9	8	10	10	8	10	10	8	10	8	8	10	8
10	10	8	8	10	8	8	8	10	8	8	10	8
total	80	98	98	80	98	98	80	100	86	72	100	90

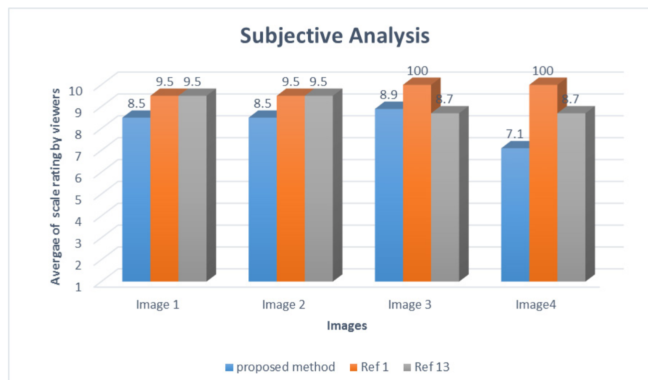

Figure 7: Graph of Subjective Analysis

(a) (b) (c)

Figure 8: output images (a) proposed method (b) global method (c) Make3d

5. Conclusion

In current scenario, 2D-to-3D conversion is a very active research area as it gives more lifelike viewing experience and hence its popularity is increasing. As there are many hardware available which support 3D and hence there is an urgent need of 3D contents. Though there are distinct methods introduced by researchers but these method works for restricted scenes.

In this paper 2D-to-3D image conversion was implemented which can take global image as an input. The work comes under automatic approach of conversion, in which algorithm itself does the whole conversion. Using RGB to HSV conversion along with simple MATLAB operations 2D image is converted into 3D. The method was tested on three distinct standard databases and on our own database. For output analysis subjective evaluation was done on 10 people for visual comfort of implemented systems output with the output of other two methods. People rated output as good from scaling range as visual comfort.

The work can be further extended by working on video. Here conversion from RGB to HSV step is implemented on starter kit of FPGA; it may be possible to implement whole system on a computational efficient FPGA.

Conflict of Interest

The authors declare no conflict of interest.

Acknowledgment

The authors hereby express their gratitude to Dr. D Y. Patil Institute of Engineering, Research and Management, Akurdi for facilitating this research. We are highly privileged to have got the much needed support and assistance from almost each and every people of the institution for the successful outcome of this work. Special thanks, to all the teaching staffs of the institution, for their constant encouragement and guidance which has helped us in successfully completing this work. .

References

[1] R. Phan and D. Androutsos " Literature survey on recent methods for 2d to 3d video conversion" Multimedia Image and Video Processing, Second Edition, pages 691to716, 2012.

[2] J. Konrad, Meng Wang, P. Ishwar, Chen Wu, and D. Mukharjee. "Learning-based, automatic 2d-to-3d image and video conversion". Image Processing, IEEE Transactions on, 22(9):3485-3496, 2013. https://doi:10.1109 / TIP. 2013.2270375.

[3] Pan Ji, Lianghao Wang, Dong-Xiao Li, and Ming Zhang. "An automatic 2d to 3d conversion algorithm using multi-depth cues", In Audio, Language and Image Processing (ICALIP), 2012 International Conference on, pages 546-550, 2012.

[4] M. Guttmann, L. Wolf, and D. Cohen-Or. "Semiautomatic stereo extraction from video footage" Computer Vision, 2009 IEEE 12th International Conference on, pages 136-142, 2009.

[5] Make3D, Convert your still image into 3D model, (2015, June 20). http://make3d.cs.cornell.edu/data.html.

[6] NYU Depth Dataset V2, (2016, Jan 11) , https://cs.nyu.edu/ ~ silberman / datasets /nyu_depth_v2.html

[7] Middlebury Stereo Datasets, (2013, Nov 14), http:// vision.middlebury.edu /stereo/data/

[8] Welcome to Sony Support , (2015, Dec 24), https:// www.sony.co.uk /electronics /support

[9] Zhao Xu1, Xu Baojie, Wu Guoxin1 "Canny edge detection based on Open CV" 2017 IEEE 13th International Conference on Electronic Measurement & Instruments ICEMI', pages 53-56, 2017.

[10] Janusz Konrad, Meng Wang, and Prakash Ishwar," 2D-to-3D Image Conversion by Learning Depth from Examples", Computer Vision and Pattern Recognition Workshops (CVPRW), 2012 IEEE Computer Society Conference, 2012. https://doi.org/ 10.1109/CVPRW.2012.6238903.

[11] Mani B. Fard, Mani B. Fard, Ulug Bayazit, Ulug Bayazit, "Automatic 2D-to-3D video conversion by monocular depth cues fusion and utilizing human face landmarks", Proc. SPIE 9067, Sixth International Conference on Machine Vision (ICMV 2013), 90670B, 2013. https://doi.org/10.1117/12.2049802.

[12] Saxena, A. and Min Sun and Ng, A.Y. Make3D:" Learning 3D Scene Structure from a Single Still Image". Pattern Analysis and Machine Intelligence, IEEE Transactions, pages 824-840,2009.https://doi.org/ 10.1109/TPAMI.2008.132.

ASTES

Advances in Science, Technology and Engineering Systems Journal
Vol. 4, No. 2, 305-313 (2019)
www.astesj.com
Special Issue on Advancement in Engineering and Computer Science

ASTES Journal
ISSN: 2415-6698

Noise Cancellation Algorithm Based on Air- and Bone-Conducted Speech Signals by Considering an Unscented Transformation Method

Hisako Orimoto*, Akira ikuta

Prefectural University of Hiroshima, Faculty of Management and Information System, 734-8338, Japan

ARTICLEINFO

Article history:
Received: 22 February, 2019
Accepted: 10 April, 2019
Online: 12 April, 2019

Keywords:
Noise Cancellation
Speech Signal
Air- and Bone-conducted
UT Method

ABSTRACT

Noise control is essential when applying speech recognition in noisy environments such as factories. In this study, a signal processing for noise cancellation is proposed by using a noise-insensitive bone-conducted speech signal together with an air-conducted speech signal. The speech signal is generally expressed by a nonlinear model. The extended Kalman filter is very famous as a state estimation method for nonlinear systems. However, this filter needs a linearized approximation model for the nonlinear systems. By using the sample point called Sigma point, the unscented Kalman filter (UKF) can be applied to the nonlinear system model without linear approximation. In this study, new type method is proposed based on the UKF. Although UKF considers Gaussian noise, an extended UKF considering non-Gaussian noise is proposed. A noise cancellation method is derived by use of air- and bone-conducted speech signals. The validity of this method is investigated by using both conducted speech signals measured in a noisy real environment.

1 Introduction

Recently, speech recognition systems are used in car navigation systems and smart speakers etc.. However, speech recognition can not be performed effectively in circumstances with heavy noises. Therefore, some countermeasures against surrounding noise are indispensable in such situations.

Kalman filter has been applied to many noisy circumstances as a noise cancellation method for speech signal [1],[2],[3]. This filter assumes a linear model subject to white and Gaussian noise as the system equation and the observation equation [4],[5]. Though, the extended Kalman filter (EKF) [6] can be applied to nonlinear systems, linear approximation models of nonlinear systems are required. Therefore, many improvements are necessary for the noise cancellation method to apply it to actual speech signal processing. From the above viewpoint, in our preciously reported study, a noise cancellation method was proposed by using air- and bone-conducted speech signals in the situation contaminated by non-Gaussian and non-white noises [7].

However, since the calculation of the expansion coefficients in the previous algorithm was very complicated, a simplified method is required.

On the other hand, the unscented Kalman filter (UKF) by use of unscented transformation (UT) method can be applied to nonlinear system[9]. The UT method is a technique for calculating the statistics of a random variable that has been nonlinearly transformed. The set of samples on so-called sigma points(σ-points) are chosen so that they capture the specific properties of the underlying distribution. Therefore, this method can be applied to arbitrary nonlinear systems. In our previous study, a noise cancellation method based on only air conducted speech signal has been proposed by applying the UT method [8].

In this study, a new noise cancellation algorithm based on air- and bone-conducted speech signals is proposed by considering the UT method. The relationship between air-conducted speech signal and backgrand noise is expressed as an additive model based on the additive property of sound pressure. However, propagation mechanism of bone-conducted speech signal is complicated and has to be considered as an unknown system in general. Therefore, a system model including unknown parameters is introduced in this study. More specifically, the sample points obtained by using the UT method are introduced. The noise cancellation algorithm is derived by use of an expansion expression of Bayes' theorem. This method can be considered non-Gaussian properties of noises and nonlinear correlation information between the speech signal and observation. Furthermore, the validity of the proposed method is experimentally confirmed by applying it to real speech signal with noises.

*Corresponding Author: Hisako Orimoto, Address, +81 82 251 9804 & orimoto@pu-hiroshima.ac.jp

https://dx.doi.org/10.25046/aj040239

2 Theory

2.1 Modeling of Air- and Bone-Conducted Speech Signals

We consider the original speech signal x_k, observed air-conducted speech signal y_k and bone-conducted speech signal z_k at discrete time k. The observation y_k is contaminated by a surrounding noise v_k. According to the additive property of sound pressure, the following relationship can be established.

$$y_k = x_k + v_k, \tag{1}$$

where the mean and variance of v_k are known. In order to derive the propagation model of the bone-conducted speech signal, the correlation information between x_k and z_k is required.However, it is difficult to obtain prior information on the unknown speech signal x_k. In this study, a new adaptive algorithm for noise cancellation is proposed by introducing a propagation model with unknown parameters between x_k and z_k as the bone-conducted speech signal model for z_k:

$$z_k = a_k x_k + b_k w_k, \tag{2}$$

where w_k is a random noise ($mean: 0, variance 1$) and a_k and b_k are unknown parameters.

2.2 Estimation Method Combined Bayes' Theorem with UT Method

The conditional joint probability distribution of the specific signal x_k and the unknown parameters a_k and b_k is expressed by using expansion expression of Bayes' theorem[10]. To simplify the derivation process of the estimation algorithm, σ-points and the weighting coefficients are introduced in expansion coefficients.

The conditional probability distribution of x_k, a_k and b_k is expressed as

$$\begin{aligned}
&P(x_k, a_k, b_k | Y_k, Z_k) \\
&= P_0(x_k|Y_{k-1}, Z_{k-1}) P_0(a_k|Y_{k-1}, Z_{k-1}) P_0(b_k|Y_{k-1}, Z_{k-1}) \\
&\quad \textstyle\sum_{l=0}^{\infty}\sum_{m=0}^{\infty}\sum_{n=0}^{\infty}\sum_{s=0}^{\infty}\sum_{t=0}^{\infty} A_{lmnst} \\
&\quad \varphi_l^{(1)}(x_k)\varphi_m^{(2)}(a_k)\varphi_n^{(3)}(b_k)\varphi_s^{(4)}(y_k)\varphi_t^{(5)}(z_k) \\
&\quad / \textstyle\sum_{s=0}^{\infty}\sum_{t=0}^{\infty} A_{000st}\varphi_s^{(4)}(y_k)\varphi_t^{(5)}(z_k),
\end{aligned} \tag{3}$$

with

$$A_{lmnst} \equiv \left\langle \varphi_l^{(1)}(x_k)\varphi_m^{(2)}(a_k)\varphi_n^{(3)}(b_k)\varphi_s^{(4)}(y_k)\varphi_t^{(5)}(z_k) | Y_{k-1}, Z_{k-1} \right\rangle, \tag{4}$$

where $Y_k (= \{y_1, y_2, ..., y_k\})$ and $Z_k (= \{z_1, z_2, ..., z_k\})$ are sets of air- and bone-conducted speech signal data up to time k. The above five functions $\varphi_l^{(1)}(x_k), \varphi_m^{(2)}(a_k)$, $\varphi_n^{(3)}(b_k), \varphi_s^{(4)}(y_k)$ and $\varphi_t^{(5)}(z_K)$ are orthonormal polynomials of degrees l, m, n, s and t with weighting functions $P_0(x_k \mid Y_{k-1}, Z_{k-1}), P_0(a_k \mid Y_{k-1}, Z_{k-1}), P_0(b_k \mid Y_{k-1}, Z_{k-1}), P_0(y_k \mid Y_{k-1}, Z_{k-1}), P_0(z_k \mid Y_{k-1}, Z_{k-1})$, which can be chosen as the probability functions describing the dominant part of the fluctuation. As the examples of standard probability functions, Gaussian distribution is adopted:

$$\begin{cases}
P_0(x_k \mid Y_{k-1}, Z_{k-1}) = N(x_k; x_k^*, \Gamma_{x_k}), \\
P_0(a_k \mid Y_{k-1}, Z_{k-1}) = N(a_k; a_k^*, \Gamma_{a_k}), \\
P_0(b_k \mid Y_{k-1}, Z_{k-1}) = N(b_k; b_k^*, \Gamma_{b_k}). \\
P_0(y_k \mid Y_{k-1}, Z_{k-1}) = N(y_k; y_k^*, \Omega_k), \\
P_0(z_k \mid Y_{k-1}, Z_{k-1}) = N(z_k; z_k^*, \Phi_k),
\end{cases} \tag{5}$$

with

$$N(x; \mu, \Gamma) = \frac{1}{\sqrt{2\pi\Gamma}} e^{\left\{-\frac{(x-\mu)^2}{2\Gamma}\right\}},$$

$$\begin{aligned}
x_k^* &\equiv \langle x_k \mid Y_{k-1}, Z_{k-1} \rangle, \\
\Gamma_{x_k} &\equiv \left\langle (x_k - x_k^*)^2 \mid Y_{k-1}, Z_{k-1} \right\rangle, \\
a_k^* &\equiv \langle a_k \mid Y_{k-1}, Z_{k-1} \rangle, \\
\Gamma_{a_k} &\equiv \left\langle (a_k - a_k^*)^2 \mid Y_{k-1}, Z_{k-1} \right\rangle, \\
b_k^* &\equiv \langle b_k \mid Y_{k-1}, Z_{k-1} \rangle, \\
\Gamma_{b_k} &\equiv \left\langle (b_k - b_k^*)^2 \mid Y_{k-1}, Z_{k-1} \right\rangle, \\
y_k^* &\equiv \langle y_k \mid Y_{k-1}, Z_{k-1} \rangle, \\
\Omega_k &\equiv \left\langle (y_k - y_k^*)^2 \mid Y_{k-1}, Z_{k-1} \right\rangle, \\
z_k^* &\equiv \langle z_k \mid Y_{k-1}, Z_{k-1} \rangle, \\
\Phi_k &\equiv \left\langle (z_k - z_k^*)^2 \mid Y_{k-1}, Z_{k-1} \right\rangle.
\end{aligned} \tag{6}$$

The orthonormal polynomials[11] with five weighting probability distributions in Eq. (5) are then specified as

$$\varphi_l^{(1)}(x_k) = \frac{1}{\sqrt{l!}} H_l\left(\frac{x_k - x_k^*}{\sqrt{\Gamma_{x_k}}}\right), \tag{7}$$

$$\varphi_m^{(2)}(a_k) = \frac{1}{\sqrt{m!}} H_m\left(\frac{a_k - a_k^*}{\sqrt{\Gamma_{a_k}}}\right), \tag{8}$$

$$\varphi_n^{(3)}(b_k) = \frac{1}{\sqrt{n!}} H_n\left(\frac{b_k - b_k^*}{\sqrt{\Gamma_{\beta_k}}}\right), \tag{9}$$

$$\varphi_s^{(4)}(y_k) = \frac{1}{\sqrt{s!}} H_s\left(\frac{y_k - y_k^*}{\sqrt{\Omega_k}}\right), \tag{10}$$

$$\varphi_t^{(5)}(z_k) = \frac{1}{\sqrt{t!}} H_t\left(\frac{z_k - z_k^*}{\sqrt{\Phi_k}}\right). \tag{11}$$

The estimates for mean and variance (i.e., conditional mean and variance) of x_k, a_k, b_k, which are the first and second order statistics, can be expressed as follows:

$$\begin{aligned}
\hat{x}_k &\equiv \langle x_k \mid Y_k, Z_k \rangle \\
&= \frac{\sum_{l=0}^{1}\sum_{s=0}^{\infty}\sum_{t=0}^{\infty} A_{l00st} c_{1l} \varphi_s^{(4)}(y_k)\varphi_t^{(5)}(z_k)}{\sum_{s=0}^{\infty}\sum_{t=0}^{\infty} A_{000st}\varphi_s^{(4)}(y_k)\varphi_t^{(5)}(z_k)},
\end{aligned} \tag{12}$$

$$\begin{aligned}
\hat{a}_k &\equiv \langle a_k \mid Y_k, Z_k \rangle \\
&= \frac{\sum_{m=0}^{1}\sum_{s=0}^{\infty}\sum_{t=0}^{\infty} A_{0m0st} d_{1m} \varphi_s^{(4)}(y_k)\varphi_t^{(5)}(z_k)}{\sum_{s=0}^{\infty}\sum_{t=0}^{\infty} A_{000st}\varphi_s^{(4)}(y_k)\varphi_t^{(5)}(z_k)},
\end{aligned} \tag{13}$$

$$\begin{aligned}
\hat{b}_k &\equiv \langle b_k \mid Y_k, Z_k\rangle \\
&= \frac{\sum_{n=0}^{1}\sum_{s=0}^{\infty}\sum_{t=0}^{\infty} A_{00nst} e_{1n} \varphi_s^{(4)}(y_k)\varphi_t^{(5)}(z_k)}{\sum_{s=0}^{\infty}\sum_{t=0}^{\infty} A_{000st}\varphi_s^{(4)}(y_k)\varphi_t^{(5)}(z_k)}, \quad (14)\\
P_{x_k} &\equiv \left\langle (x_k - \hat{x}_k)^2 \mid Y_k, Z_k\right\rangle \\
&= \frac{\sum_{l=0}^{2}\sum_{s=0}^{\infty}\sum_{t=0}^{\infty} A_{l00st} c_{2l} \varphi_s^{(4)}(y_k)\varphi_t^{(5)}(z_k)}{\sum_{s=0}^{\infty}\sum_{t=0}^{\infty} A_{000st}\varphi_s^{(4)}(y_k)\varphi_t^{(5)}(z_k)}, \quad (15)\\
P_{a_k} &\equiv \left\langle (a_k - \hat{a}_k)^2 \mid Y_k, Z_k\right\rangle \\
&= \frac{\sum_{m=0}^{2}\sum_{s=0}^{\infty}\sum_{t=0}^{\infty} A_{0m0st} d_{2m} \varphi_s^{(4)}(y_k)\varphi_t^{(5)}(z_k)}{\sum_{s=0}^{\infty}\sum_{t=0}^{\infty} A_{000st}\varphi_s^{(4)}(y_k)\varphi_t^{(5)}(z_k)}, \quad (16)\\
P_{b_k} &\equiv \left\langle (b_k - \hat{b}_k)^2 \mid Y_k, Z_k\right\rangle \\
&= \frac{\sum_{n=0}^{2}\sum_{s=0}^{\infty}\sum_{t=0}^{\infty} A_{00nst} e_{2n} \varphi_s^{(4)}(y_k)\varphi_t^{(5)}(z_k)}{\sum_{s=0}^{\infty}\sum_{t=0}^{\infty} A_{000st}\varphi_s^{(4)}(y_k)\varphi_t^{(5)}(z_k)}. \quad (17)
\end{aligned}$$

Where coefficients are appropriate constant satisfying the following equality:

$$\begin{aligned}
x_k &= \textstyle\sum_{l=0}^{1} c_{1l}\varphi_l^{(1)}(x_k),\ (x_k - \hat{x}_k)^2 = \sum_{l=0}^{2} c_{2l}\varphi_l^{(1)}(x_k),\\
a_k &= \textstyle\sum_{m=0}^{1} d_{1m}\varphi_m^{(2)}(a_k),\ (a_k - \hat{a}_k)^2 = \sum_{m=0}^{2} d_{2m}\varphi_m^{(2)}(a_k),\\
b_k &= \textstyle\sum_{n=0}^{1} e_{1n}\varphi_n^{(2)}(b_k),\ (b_k - \hat{b}_k)^2 = \sum_{n=0}^{2} e_{2n}\varphi_n^{(3)}(b_k). \quad (18)
\end{aligned}$$

By using the UT method, the expansion coefficients defined by (4) can be realized for arbitrary nonlinear systems. When the UT method is applied to approximate the means and variances of x_k, a_k, b_k, y_k and z_k, the σ-points $x_k^{*(i)}$, $a_k^{*(i)}$, $b_k^{*(i)}$, $y_k^{*(i)}$ and $z_k^{*(i)}$ are obtained as sample points, as follows:

$$\begin{aligned}
x_k^{*(0)} &= x_k^*,\\
x_k^{*(1)} &= x_k^* + \sqrt{(1+\lambda)\Gamma_{x_k}},\ x_k^{*(2)} = x_k^* - \sqrt{(1+\lambda)\Gamma_{x_k}},\\
a_k^{*(0)} &= a_k^*,\\
a_k^{*(1)} &= a_k^* + \sqrt{(1+\lambda)\Gamma_{a_k}},\ a_k^{*(2)} = a_k^* - \sqrt{(1+\lambda)\Gamma_{a_k}},\\
b_k^{*(0)} &= b_k^*,\\
b_k^{*(1)} &= b_k^* + \sqrt{(1+\lambda)\Gamma_{b_k}},\ b_k^{*(2)} = b_k^* - \sqrt{(1+\lambda)\Gamma_{b_k}},\\
y_k^{*(0)} &= y_k^*,\\
y_k^{*(1)} &= y_k^* + \sqrt{(1+\lambda)\Omega_k},\ y_k^{*(2)} = y_k^* - \sqrt{(1+\lambda)\Omega_k},\\
z_k^{*(0)} &= z_k^*,\\
z_k^{*(1)} &= z_k^* + \sqrt{(1+\lambda)\Phi_k},\ z_k^{*(2)} = z_k^* - \sqrt{(1+\lambda)\Phi_k}, \quad (19)
\end{aligned}$$

The σ-points are decided so as to obtain the approximately same mean and variance as original variables. Where λ is a regulation parameter. The weights to be used are obtained as follows:

$$\begin{aligned}
W^{(0)} &= \frac{\lambda}{(1+\lambda)},\\
W^{(1)} &= \frac{1}{2(1+\lambda)},\\
W^{(2)} &= \frac{1}{2(1+\lambda)}. \quad (20)
\end{aligned}$$

Here, the weighing coefficients $W^{(i)}$ have to satisfy the normalization constraint.

$$\textstyle\sum_{i=0}^{2} W^{(i)} = 1. \quad (21)$$

Each expansion coefficient A_{lmnst} defined by (4) is obtained specifically by substituting σ-points $x_k^{*(i)}$, $a_k^{*(i)}$, $b_k^{*(i)}$, $y_k^{*(i)}$ and $z_k^{*(i)}$ into the conditional expectation of x_k, y_k and z_k.

$$\begin{aligned}
A_{10010} &= \tfrac{1}{\sqrt{\Gamma_{x_k}}\sqrt{\Omega_k}} \textstyle\sum_{i=0}^{2} W^{(i)}(x_k^{*(i)} - x_k^*)(y_k^{*(i)} - y_k^*),\\
A_{10020} &= \tfrac{1}{\sqrt{2}\sqrt{\Gamma_{x_k}}\Omega_k} \textstyle\sum_{i=0}^{2} W^{(i)}(x_k^{*(i)} - x_k^*)\left\{(y_k^{*(i)} - y_k^*)^2 - \Omega_k\right\},\\
A_{20010} &= \tfrac{1}{\sqrt{2}\Gamma_{x_k}\sqrt{\Omega_k}} \textstyle\sum_{i=0}^{2} W^{(i)}\left\{(x_k^{*(i)} - x_k^*)^2 - \Gamma_{x_k}\right\}(y_k^{*(i)} - y_k^*),\\
A_{20020} &= \tfrac{1}{2\Gamma_{x_k}\Omega_k} \textstyle\sum_{i=0}^{2} W^{(i)}\left\{(x_k^{*(i)} - x_k^*)^2 - \Gamma_{x_k}\right\}\\
&\qquad \cdot\left\{(y_k^{*(i)} - y_k^*)^2 - \Omega_k\right\},\\
A_{10001} &= \tfrac{1}{\sqrt{\Gamma_{x_k}}\sqrt{\Phi_k}} \textstyle\sum_{i=0}^{2} W^{(i)}(x_k^{*(i)} - x_k^*)(z_k^{*(i)} - z_k^*),\\
A_{10002} &= \tfrac{1}{\sqrt{2}\sqrt{\Gamma_{x_k}}\Phi_k} \textstyle\sum_{i=0}^{2} W^{(i)}(x_k^{*(i)} - x_k^*)\left\{(z_k^{*(i)} - z_k^*)^2 - \Phi_k\right\},\\
A_{20001} &= \tfrac{1}{\sqrt{2}\Gamma_{x_k}\sqrt{\Phi_k}} \textstyle\sum_{i=0}^{2} W^{(i)}\left\{(x_k^{*(i)} - x_k^*)^2 - \Gamma_{x_k}\right\}(z_k^{*(i)} - z_k^*),\\
A_{20002} &= \tfrac{1}{2\Gamma_{x_k}\Phi_k} \textstyle\sum_{i=0}^{2} W^{(i)}\left\{(x_k^{*(i)} - x_k^*)^2 - \Gamma_{x_k}\right\}\left\{(z_k^{*(i)} - z_k^*)^2 - \Phi_k\right\},\\
A_{10011} &= \tfrac{1}{\sqrt{\Gamma_{x_k}}\sqrt{\Omega_k}\sqrt{\Phi_k}} \textstyle\sum_{i=0}^{2} W^{(i)}(x_k^{*(i)} - x_k^*)(y_k^{*(i)} - y_k^*)(z_k^{*(i)} - z_k^*),\\
A_{20011} &= \tfrac{1}{\sqrt{2}\Gamma_{x_k}\sqrt{\Omega_k}\sqrt{\Phi_k}} \textstyle\sum_{i=0}^{2} W^{(i)}\left\{(x_k^{*(i)} - x_k^*)^2 - \Gamma_{x_k}\right\}\\
&\qquad \cdot(y_k^{*(i)} - y_k^*)(z_k^{*(i)} - z_k^*),\\
A_{10021} &= \tfrac{1}{\sqrt{2}\sqrt{\Gamma_{x_k}}\Omega_k\sqrt{\Phi_k}} \textstyle\sum_{i=0}^{2} W^{(i)}(x_k^{*(i)} - x_k^*)\\
&\qquad \cdot\left\{(y_k^{*(i)} - y_k^*)^2 - \Omega_k\right\}(z_k^{*(i)} - z_k^*),\\
A_{10012} &= \tfrac{1}{\sqrt{2}\sqrt{\Gamma_{x_k}}\sqrt{\Omega_k}\Phi_k} \textstyle\sum_{i=0}^{2} W^{(i)}(x_k^{*(i)} - x_k^*)\\
&\qquad \cdot(y_k^{*(i)} - y_k^*)\left\{(z_k^{*(i)} - z_k^*)^2 - \Phi_k\right\},\\
A_{20012} &= \tfrac{1}{2\Gamma_{x_k}\sqrt{\Omega_k}\Phi_k} \textstyle\sum_{i=0}^{2} W^{(i)}\left\{(x_k^{*(i)} - x_k^*)^2 - \Gamma_{x_k}\right\}\\
&\qquad \cdot(y_k^{*(i)} - y_k^*)\left\{(z_k^{*(i)} - z_k^*)^2 - \Phi_k\right\},\\
A_{10022} &= \tfrac{1}{2\sqrt{\Gamma_{x_k}}\Omega_k\Phi_k} \textstyle\sum_{i=0}^{2} W^{(i)}(x_k^{*(i)} - x_k^*)\\
&\qquad \cdot\left\{(y_k^{*(i)} - y_k^*)^2 - \Omega_k\right\}\left\{(z_k^{*(i)} - z_k^*)^2 - \Phi_k\right\},\\
A_{20021} &= \tfrac{1}{2\Gamma_{x_k}\Omega_k\sqrt{\Phi_k}} \textstyle\sum_{i=0}^{2} W^{(i)}\left\{(x_k^{*(i)} - x_k^*)^2 - \Gamma_{x_k}\right\}\\
&\qquad \cdot\left\{(y_k^{*(i)} - y_k^*)^2 - \Omega_k\right\}(z_k^{*(i)} - z_k^*),\\
A_{20022} &= \tfrac{1}{2\sqrt{2}\Gamma_{x_k}\Omega_k\Phi_k} \textstyle\sum_{i=0}^{2} W^{(i)}\left\{(x_k^{*(i)} - x_k^*)^2 - \Gamma_{x_k}\right\}\\
&\qquad \cdot\left\{(y_k^{*(i)} - y_k^*)^2 - \Omega_k\right\}\left\{(z_k^{*(i)} - z_k^*)^2 - \Phi_k\right\}, \quad (22)
\end{aligned}$$

with

$A_{00000} = 1, A_{10000} = A_{00010} = A_{00001} = A_{20000} = A_{00020} = A_{00002} = 0.$

Furthermore, expansion coefficients of a_k, y_k and z_k are expressed as follows:

$$A_{01010} = \frac{1}{\sqrt{\Gamma_{a_k}}\sqrt{\Omega_k}} \sum_{i=0}^{2} w^{(i)}(a_k^{*(i)} - a_k^*)(y_k^{*(i)} - y_k^*),$$
$$A_{01020} = \frac{1}{\sqrt{2}\sqrt{\Gamma_{a_k}}\Omega_k} \sum_{i=0}^{2} w^{(i)}(a_k^{*(i)} - a_k^*)\left\{(y_k^{*(i)} - y_k^*)^2 - \Omega_k\right\},$$
$$A_{02010} = \frac{1}{\sqrt{2}\Gamma_{a_k}\sqrt{\Omega_k}} \sum_{i=0}^{2} w^{(i)}\left\{(a_k^{*(i)} - a_k^*)^2 - \Gamma_{a_k}\right\}(y_k^{*(i)} - y_k^*),$$
$$A_{02020} = \frac{1}{2\Gamma_{a_k}\Omega_k} \sum_{i=0}^{2} w^{(i)}\left\{(a_k^{*(i)} - a_k^*)^2 - \Gamma_{a_k}\right\} \cdot\left\{(y_k^{*(i)} - y_k^*)^2 - \Omega_k\right\},$$
$$A_{01001} = \frac{1}{\sqrt{\Gamma_{a_k}}\sqrt{\Phi_k}} \sum_{i=0}^{2} w^{(i)}(a_k^{*(i)} - a_k^*)(z_k^{*(i)} - z_k^*),$$
$$A_{01002} = \frac{1}{\sqrt{2}\sqrt{\Gamma_{a_k}}\Phi_k} \sum_{i=0}^{2} w^{(i)}(a_k^{*(i)} - a_k^*)\left\{(z_k^{*(i)} - z_k^*)^2 - \Phi_k\right\},$$
$$A_{02001} = \frac{1}{\sqrt{2}\Gamma_{a_k}\sqrt{\Phi_k}} \sum_{i=0}^{2} w^{(i)}\left\{(a_k^{*(i)} - a_k^*)^2 - \Gamma_{a_k}\right\}(z_k^{*(i)} - z_k^*),$$
$$A_{02002} = \frac{1}{2\Gamma_{a_k}\Phi_k} \sum_{i=0}^{2} w^{(i)}\left\{(a_k^{*(i)} - a_k^*)^2 - \Gamma_{a_k}\right\} \cdot\left\{(z_k^{*(i)} - z_k^*)^2 - \Phi_k\right\},$$
$$A_{01011} = \frac{1}{\sqrt{\Gamma_{a_k}}\sqrt{\Omega_k}\sqrt{\Phi_k}} \sum_{i=0}^{2} w^{(i)}(a_k^{*(i)} - a_k^*)(y_k^{*(i)} - y_k^*)(z_k^{*(i)} - z_k^*),$$
$$A_{02011} = \frac{1}{\sqrt{2}\Gamma_{a_k}\sqrt{\Omega_k}\sqrt{\Phi_k}} \sum_{i=0}^{2} w^{(i)}\left\{(a_k^{*(i)} - a_k^*)^2 - \Gamma_{a_k}\right\} \cdot(y_k^{*(i)} - y_k^*)(z_k^{*(i)} - z_k^*),$$
$$A_{01021} = \frac{1}{\sqrt{2}\sqrt{\Gamma_{a_k}}\Omega_k\sqrt{\Phi_k}} \sum_{i=0}^{2} w^{(i)}(a_k^{*(i)} - a_k^*) \cdot\left\{(y_k^{*(i)} - y_k^*)^2 - \Omega_k\right\}(z_k^{*(i)} - z_k^*),$$
$$A_{01012} = \frac{1}{\sqrt{2}\sqrt{\Gamma_{a_k}}\sqrt{\Omega_k}\Phi_k} \sum_{i=0}^{2} w^{(i)}(a_k^{*(i)} - a_k^*)(y_k^{*(i)} - y_k^*) \cdot\left\{(z_k^{*(i)} - z_k^*)^2 - \Phi_k\right\},$$
$$A_{02012} = \frac{1}{2\Gamma_{a_k}\sqrt{\Omega_k}\Phi_k} \sum_{i=0}^{2} w^{(i)}\left\{(a_k^{*(i)} - a_k^*)^2 - \Gamma_{a_k}\right\} \cdot(y_k^{*(i)} - y_k^*)\left\{(z_k^{*(i)} - z_k^*)^2 - \Phi_k\right\},$$
$$A_{01022} = \frac{1}{2\sqrt{\Gamma_{a_k}}\Omega_k\Phi_k} \sum_{i=0}^{2} w^{(i)}(a_k^{*(i)} - a_k^*) \cdot\left\{(y_k^{*(i)} - y_k^*)^2 - \Omega_k\right\}\left\{(z_k^{*(i)} - z_k^*)^2 - \Phi_k\right\},$$
$$A_{02021} = \frac{1}{2\Gamma_{a_k}\Omega_k\sqrt{\Phi_k}} \sum_{i=0}^{2} w^{(i)}\left\{(a_k^{*(i)} - a_k^*)^2 - \Gamma_{a_k}\right\} \cdot\left\{(y_k^{*(i)} - y_k^*)^2 - \Omega_k\right\}(z_k^{*(i)} - z_k^*),$$
$$A_{02022} = \frac{1}{2\sqrt{2}\Gamma_{a_k}\Omega_k\Phi_k} \sum_{i=0}^{2} w^{(i)}\left\{(a_k^{*(i)} - a_k^*)^2 - \Gamma_{a_k}\right\} \cdot\left\{(y_k^{*(i)} - y_k^*)^2 - \Omega_k\right\}\left\{(z_k^{*(i)} - z_k^*)^2 - \Phi_k\right\}. \tag{23}$$

The expansion coefficients of b_k, y_k and z_k ($A_{00110}, A_{00120}, A_{00210}, A_{00220}, A_{00101}, A_{00102}, A_{00201}, A_{00202}, A_{00111}, A_{00211}, A_{00121}, A_{00112}, A_{00212}, A_{00122}, A_{00221}, A_{00222}$) are calculated through the same manners.

After substituting (1) (2) into the definition of four parameters y_k^*, Ω_k, z_k^* and Φ_k in (6), the following expressions can be derived.

$$y_k^* = x_k^* + \langle v_k \rangle, \tag{24}$$
$$\Omega_k = \Gamma_{x_k} + \left\langle (v_k - \langle v_k \rangle)^2 \right\rangle, \tag{25}$$

$$z_k^* = a_k^* x_k^*, \tag{26}$$
$$\Phi_k = (\Gamma_{a_k} + a_k^{*2})(\Gamma_{x_k} + x_k^{*2}) + (\Gamma_{b_k} + b_k^{*2})\left\langle w_k^2 \right\rangle - a_k^{*2} x_k^{*2}. \tag{27}$$

In order to derive the predicted values of the speech signal x_k and the unknown parameters a_k, b_k, the time transition of the speech signal x_k is expressed as follows.

$$x_{k+1} = F x_k + G u_k, \tag{28}$$

where, u_k is a random input with mean 0 and variance 1. Parameters F and G are calculated from time correlation information of x_k and x_{k+1}:

$$F = \frac{\langle x_{k+1} x_k \rangle}{\langle x_k \rangle^2}, \quad G = \sqrt{(1 - F^2)\left\langle x_k^2 \right\rangle}. \tag{29}$$

Therefore, x_{k+1}^* and $\Gamma_{x_{k+1}}$ can be expressed as follows:

$$x_{k+1}^* = F\hat{x}_k + G\langle u_k \rangle, \tag{30}$$
$$\Gamma_{x_{k+1}} = F^2 P_{x_k} + G^2\left\langle (u_k - \langle u_k \rangle)^2 \right\rangle, \tag{31}$$

Since the parameters a_k and b_k are constants, time transition models are introduced for the recursive estimation.

$$a_{k+1} = a_k, b_{k+1} = b_k. \tag{32}$$

By using these relationships, the predictions are given as follows,

$$a_{k+1}^* = \hat{a}_k, \quad \Gamma_{a_{k+1}} = P_{a_k}, \tag{33}$$
$$b_{k+1}^* = \hat{b}_k, \quad \Gamma_{b_{k+1}} = P_{b_k}. \tag{34}$$

The state estimation algorithm with expansion coefficient A_{lmnst} reflecting linear and nonlinear correlation information among variables and statistics of non-Gaussian noise is completed.

3 Experiment

In order to confirm the validity of the proposed noise cancellation algorithm, we compared it with the method using only the air-conducted speech signal. The compared method was derived by considering the following conditional probability distribution.

$$\begin{aligned} &P(x_k, a_k, b_k | Y_k) \\ &= P_0(x_k|Y_{k-1})P_0(a_k|Y_{k-1})P_0(b_k|Y_{k-1}) \\ &\quad \sum_{l=0}^{\infty}\sum_{m=0}^{\infty}\sum_{n=0}^{\infty}\sum_{s=0}^{\infty} A_{lmns} \\ &\quad \varphi_l^{(1)}(x_k)\varphi_m^{(2)}(a_k)\varphi_n^{(3)}(b_k)\varphi_s^{(4)}(y_k) \\ &\quad / \sum_{s=0}^{\infty}\sum_{t=0}^{\infty} A_{000s}\varphi_s^{(4)}(y_k). \end{aligned} \tag{35}$$

Based on (35), the estimates of mean and variance of x_k are derived as follow:

$$\hat{x}_k \equiv \langle x_k \mid Y_k \rangle = \frac{\sum_{l=0}^{1}\sum_{s=0}^{\infty} A_{l00s} c_{1l} \varphi_s^{(4)}(y_k)}{\sum_{s=0}^{\infty} A_{000s}\varphi_s^{(4)}(y_k)}, \tag{36}$$
$$P_{x_k} \equiv \left\langle (x_k - \hat{x}_k)^2 \mid Y_k \right\rangle = \frac{\sum_{l=0}^{2}\sum_{s=0}^{\infty} A_{l00s} c_{2l} \varphi_s^{(4)}(y_k)}{\sum_{s=0}^{\infty} A_{000s}\varphi_s^{(4)}(y_k)}. \tag{37}$$

Male and female speech signals were used in the experiment. The speech signal data were measured in the anechoic chamber in the acoustic laboratory. The observed speech signal are contaminated with the white noise, the pink noise and the machine noise respectively. The spectra of these noises are shown in Figures 1-3. Furthermore, the observation data of air-conduced speech signal were created by mixing noises with speech signal on a computer.

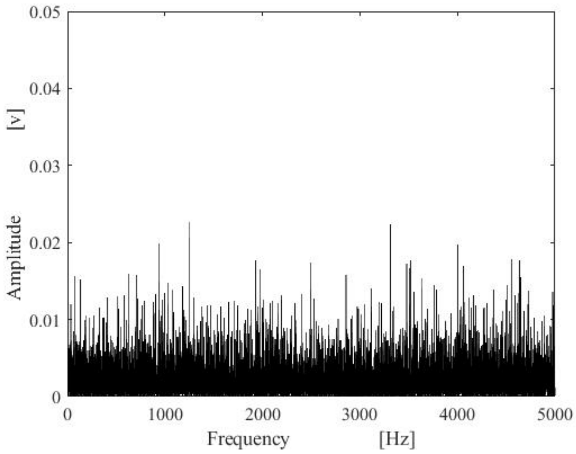

Figure 1: Spectrum of white noise.

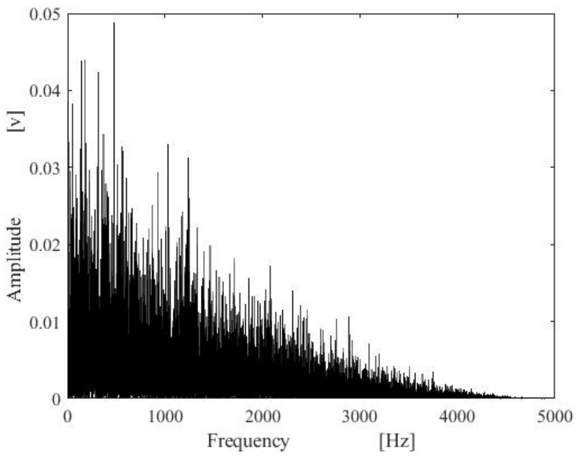

Figure 2: Spectrum of pink noise.

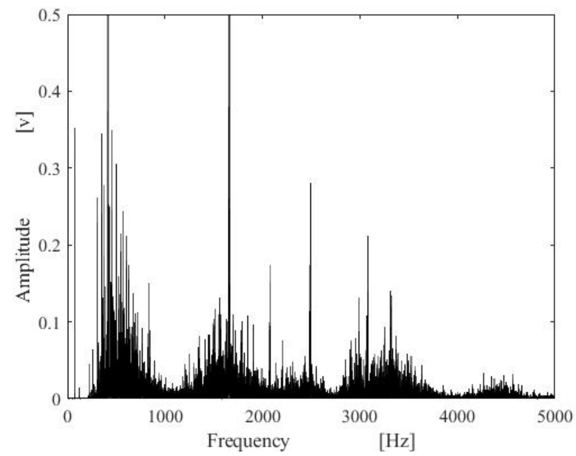

Figure 3: Spectrum of machine noise.

Table 1 shows the specifications of the personal computer for signal processing in the experiment. The signal processing time for speech signal of about 3.5 seconds in length was from 0.5 to 0.8 seconds.

Table 1: The specifications of the personal computer.

	Specification
PC	Dell Vostro 3650
CPU	Intel Core i7-6700 @ 3.40GHz
MEMORY	8.00G
OS	Win 10 Pro 64bit

As an evaluation method of estimation result, the Root Mean Square Error (RMSE) and Performance Evaluation Index (PEI) are adopted.

$$RMSE = \sqrt{\frac{\Sigma(x_k - \hat{x}_k)^2}{N}}, \quad (38)$$

$$PEI = 10\log_{10}\frac{\Sigma x_k^2}{\Sigma(x_k - \hat{x}_k)^2} \quad [dB]. \quad (39)$$

As the RMS Error is smaller value, the better estimation result is obtained. On the other hand, the larger the PEI is, the better the estimation is. Table 2 and Table 3 show the results for the male speech signal and a female speech signal respectively. In the cases of lower noises, almost the same estimation results are obtained in the proposed method and the compared method. On the other hand, in the case of higher noises, the proposed method obtains better results than the compared method. Furthermore, in comparison with our previous method [7] with complicated algorithm, almost the same accurate estimation results are obtained as the proposed method. Therefore, the superiority of the proposed method adopting the simplified algorithm could be confirmed.

Table 2: Comparisons of RMSE and PEI for a male speech signal.

(a) white noise

	Proposed method		Compared method	
S/N	RMSE	PEI	RMSE	PEI
1/1	0.0160	6.8438	0.0163	6.7057
1/2	0.0225	3.8693	0.0269	2.3286
1/3	0.0267	2.4111	0.0450	-2.1282
1/4	0.0330	0.5615	0.0838	-7.5301
1/5	0.0480	-2.6982	0.1338	-11.6004

(b) pink noise

	Proposed method		Compared method	
S/N	RMSE	PEI	RMSE	PEI
1/1	0.0192	5.2693	0.0207	4.6124
1/2	0.0281	1.9414	0.0345	0.1846
1/3	0.0322	0.7773	0.0626	-4.9946
1/4	0.0419	-1.5062	0.0823	-7.3776
1/5	0.0669	-5.5803	0.1334	-11.5703

(c) machine noise

	Proposed method		Compared method	
S/N	RMSE	PEI	RMSE	PEI
1/1	0.0238	3.4024	0.0272	2.2381
1/2	0.0313	1.0116	0.0489	-2.8538
1/3	0.0399	-1.0931	0.0767	-6.7613
1/4	0.0586	-4.4310	0.1080	-9.7397
1/5	0.0686	-5.8003	0.1409	-12.0497

Some of the waveform summarized in Tables 2 and 3 are shown in Figures 4-23. Figures 4 and 14 show the original speech signals of male and female, respectively. Figures 5, 8, 11, 15, 18 and 21 show the speech signals contaminated by noises with amplitude of 3 times larger than the original signals. The estimated results by using of proposed method are shown in Figures 6, 9, 12, 16, 19 and 22. On the other hand, the comparison results are shown in Figures 7, 10, 13, 17, 20 and 23. In the cases of contaminated by white noise and pink noise, the better results are obtained by the proposed method than the compared method.

Table 3: Comparisons of RMSE and PEI for a female speech signal.

(a) white noise

	Proposed method		Compared method	
S/N	RMSE	PEI	RMSE	PEI
1/1	0.0134	4.8382	0.0104	7.0371
1/2	0.0159	3.3213	0.0160	3.2779
1/3	0.0180	2.2390	0.0195	1.5406
1/4	0.0198	1.4447	0.0273	-1.3608
1/5	0.0260	-0.9548	0.0457	-5.8342

(b) pink noise

	Proposed method		Compared method	
S/N	RMSE	PEI	RMSE	PEI
1/1	0.0136	4.656	0.0128	5.2366
1/2	0.0176	2.4293	0.0211	0.8777
1/3	0.0231	0.0790	0.0271	-1.297
1/4	0.0241	-0.2875	0.0374	-4.1092
1/5	0.0264	-1.0874	0.0510	-6.8009

(c) machine noise

	Proposed method		Compared method	
S/N	RMSE	PEI	RMSE	PEI
1/1	0.0147	3.9846	0.0168	2.8276
1/2	0.0207	1.0503	0.0237	-0.1545
1/3	0.0293	-1.9655	0.0499	-6.6083
1/4	0.0456	-5.8243	0.0553	-7.5024
1/5	0.0425	-5.2075	0.0660	-9.0326

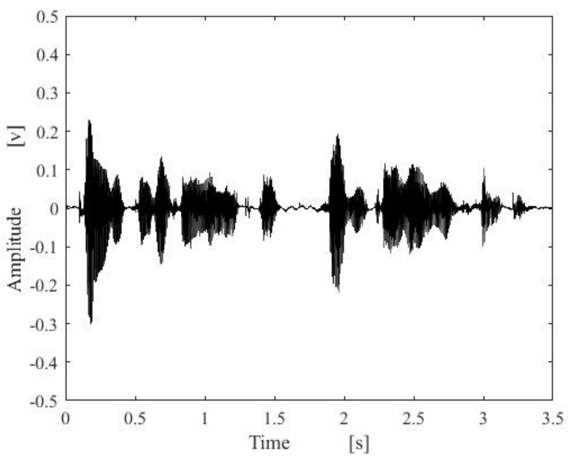

Figure 4: Original male speech signal

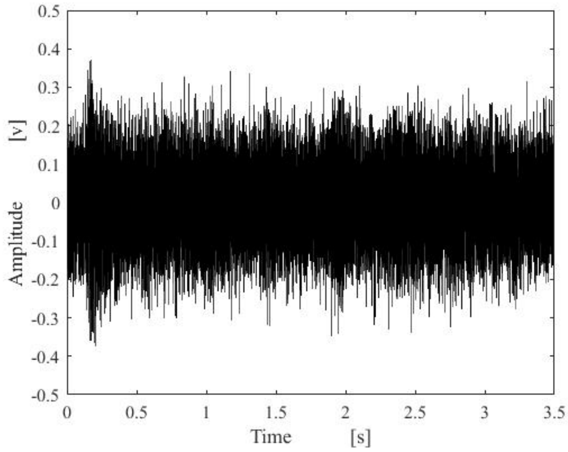

Figure 5: Male speech signal containing a white noise

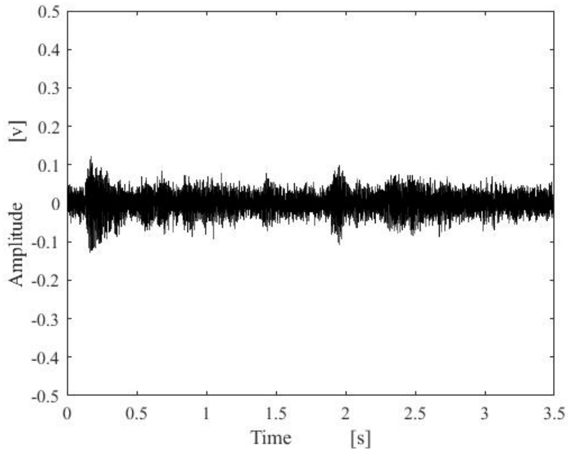

Figure 6: Estimated results by using proposed method.

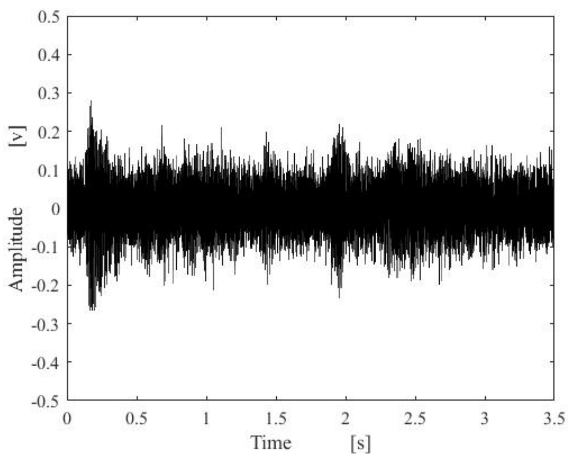

Figure 7: Estimated results by using compared method.

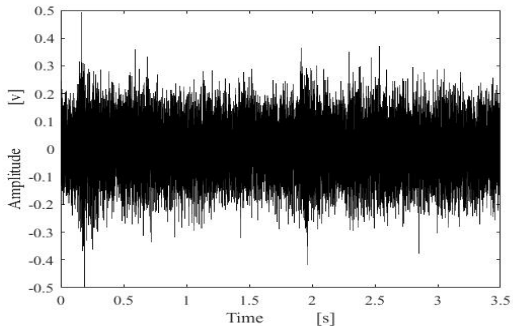

Figure 8: Male speech signal containing a pink noise

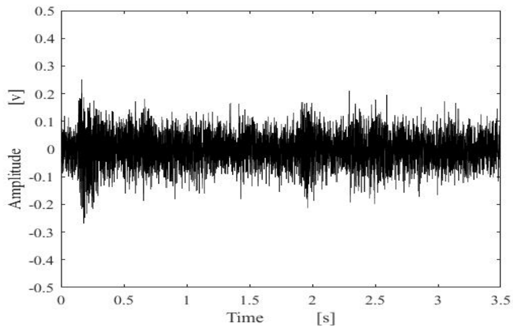

Figure 9: Estimated results by using proposed method.

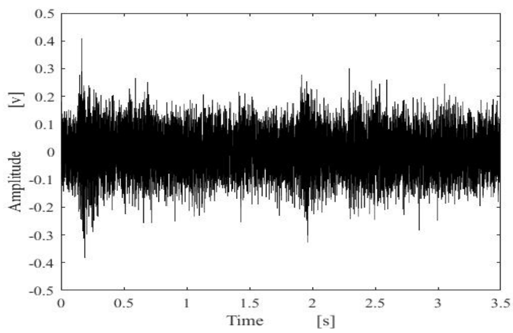

Figure 10: Estimated results by using compared method.

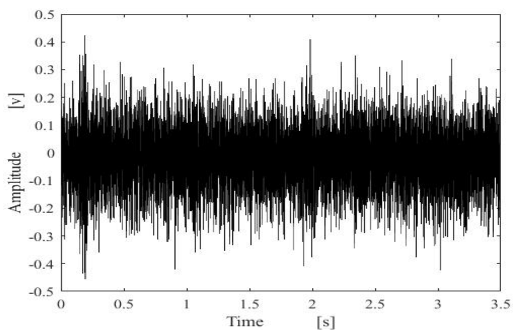

Figure 11: Male speech signal containing a machine noise

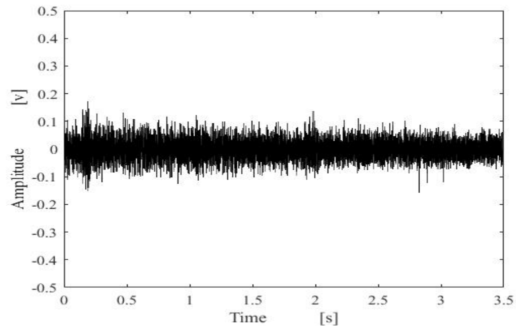

Figure 12: Estimated results by using proposed method.

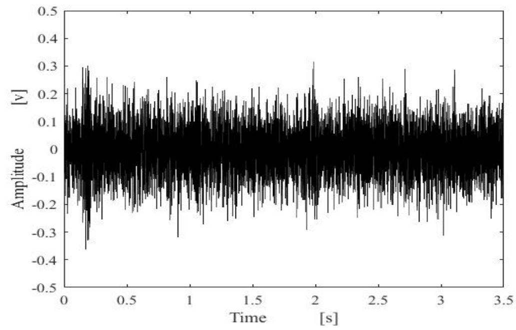

Figure 13: Estimated results by using compared method.

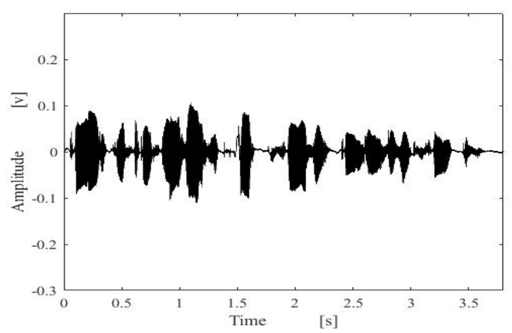

Figure 14: Original female speech signal

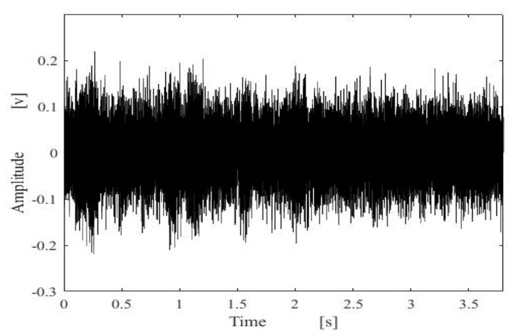

Figure 15: Female speech signal containing a white noise

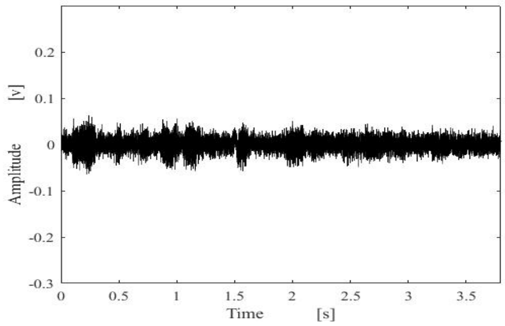

Figure 16: Estimated results by using proposed method.

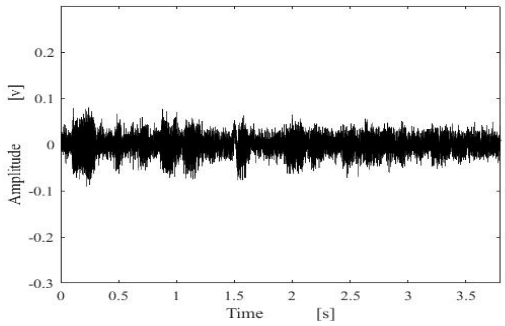

Figure 17: Estimated results by using compared method.

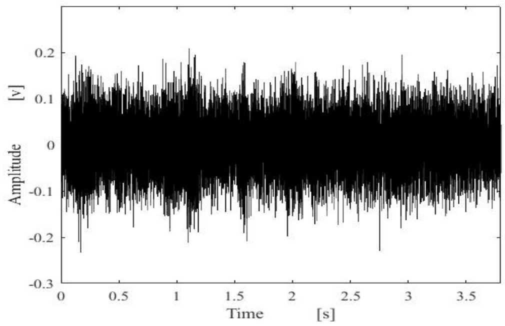

Figure 18: Female speech signal containing a pink noise

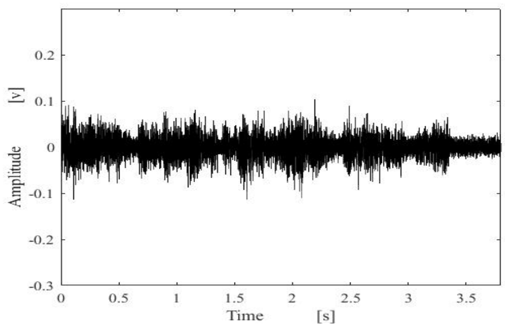

Figure 19: Estimated results by using proposed method.

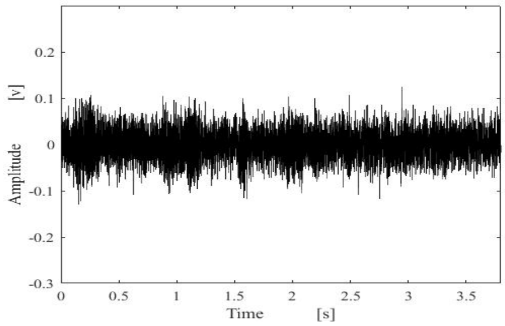

Figure 20: Estimated results by using compared method.

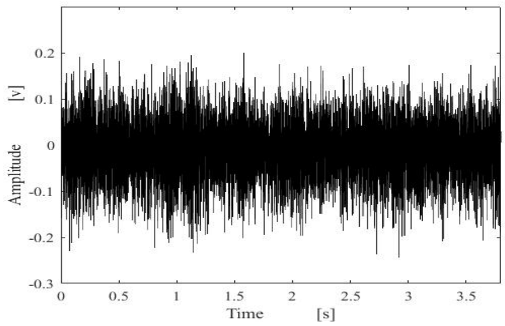

Figure 21: Female speech signal containing a machine noise

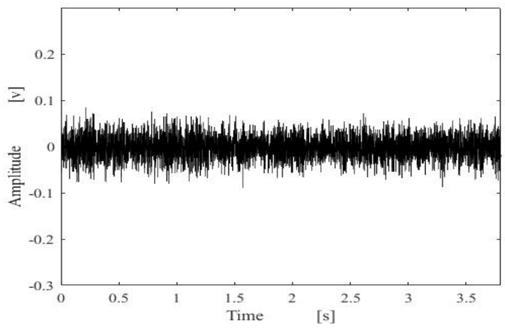

Figure 22: Estimated results by using proposed method.

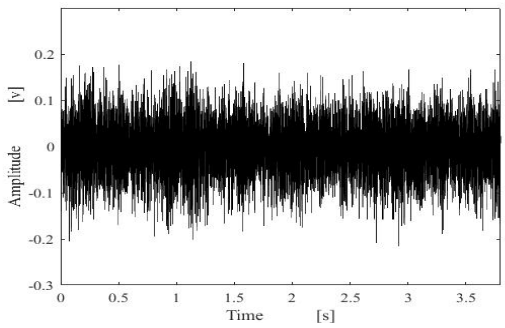

Figure 23: Estimated results by using compared method.

4 Conclusion

In this paper, a new method to suppress noise for speech signal has been proposed, which is applicable to actual environment with non-Gaussian and non-white noises. The aim of the proposed method is to improve the accuracy of estimation by using air- and bone-conducted speech signals.

The proposed method considered σ-points of not only x_k but also unknown parameter a_k, b_k and observation values y_k, z_k. Moreover, this study has proposed a method including the higher order correlation information between σ-points. Our algorithm has been realized by utilizing the Bayes' theorem as the fundamental principle of estimation and UT method using σ-points. Application of our algorithm has been made to real speech signal contaminated by noises. It has been revealed by experiments that better estimation results could be obtained by the proposed algorithm as compared with the method without using bone-conducted speech signal. However, we have not tried to apply the proposed algorithm to real speech recognition by use of a voice recognition software. Therefore, by applying the algorithm to speech recognition system, the effectiveness of the theory has to be confirmed experimentally.

The proposed approach is quite different from those traditional standard techniques. However, we are still in an early stage of development, and a number of practical problems are yet to be investigated in the future. These include: (i) Introduction of a realistic nonlinear model expressing the actual propagation characteristics of bone-conducted speech signal instead of the simple model in (2). (ii) Consideration of higher order expansion coefficients A_{lmnst} $(l, m, n, s, t \geqq 3)$, in the estimation algorithm. (iii) Selection of an optimal point to put the sensor to measure the bone-conducted speech signal.

References

[1] M. Gabrea, E. Grivel, and M. Najim, "A single microphone Kalman filter-based noise canceller", IEEE Signal Process. Lett., 6 (3), 55-57, 1999.

[2] W. Kim, and H. Ko, gNoise variance estimation for Kalman filtering of noisy speech", IEICE Trans. Inf. and Syst., E84-D (1), 155-160, 2001.

[3] N. Tanabe, T. Furukawa, and S. Tsuji, "Robust noise suppression algorithm with the Kalman filter theory for white and colored disturbance", IEICE Trans. Fundamentals, E91-A (3), 818-829, 2008.

[4] R. E. Kalman, "A new approach to linear filtering and prediction problems", Trans. ASME, Series, D, J. Basic Engineering, 82 (1), 35-45, 1960.

[5] R. E. Kalman and R. S. Buch, "New results in linear filtering and prediction theory", Trans. ASME Series D, J. Basic Engineering, 83 (1), 95-108, 1961.

[6] H. J. Kushner, "Approximations to optimal nonlinear filter", IEEE Trans. on Automatic Control, 12 (5), 546-556, 1967.

[7] A.Ikuta, H.Orimoto and G. Gallagher, "Noise suppression method by jointly using bone- and air-conducted speech signals", Noise Control Engr. J. 66 (6), 472-488, 2018.

[8] H.Orimoto and A.Ikuta, "Signal processing for Noise cancellation method of speech signal by using an extension type UKF", Proceedings of SIGNAL PROCESSING algorithms, architectures, arrangements, and applications (SPA), 304-309, 2018.

[9] James V. Candy, Bayesian Signal Processing Classical, Modern, and Particle Filtering Methods, Wiley-IEEE Press, 2009.

[10] M. Ohta and H. Yamada, "New Methodological Trials of Dynamical State Estimation for the Noise and Vibration Environmental System", Acustica, 55 (4), 199-212, 1984.

[11] M. Ohta and T. Koizumi, "General statistical treatment of the response of a non-linear rectifying device to a stationary random input", IEEE Trans. Inf. Theory, 14 (4), 595-598, (1968).

ASTES

Advances in Science, Technology and Engineering Systems Journal
Vol. 4, No. 2, 314-318 (2019)
www.astesj.com

ASTES Journal
ISSN: 2415-6698

Acquiring Energy from the Harmful Radiation Emitted by Compact Fluorescent Lamps

Mohamed Zied Chaari*, Harb Aljabri, Rashid AL-Rahimi, Mohamed Abdelfatah

FAB LAB, Qatar Scientific Club, 9769, Doha–Qatar

A R T I C L E I N F O

Article history:
Received: 31 October, 2018
Accepted: 29 March, 2019
Online: 14 April, 2019

Keywords:
Compact fluorescent lamp
RF to DC converter
Electromagnetic pollution
Flat wound planar coil

A B S T R A C T

The purpose of this work is to present new technology in acquiring energy from the compact fluorescent lamp (CFL) and store it in a super-capacitor to operate the emergency exit lights. Many studies show energy-efficient light bulbs may emit harmful radiation. This type of lamp emits high levels of radiation, causing migraine headaches, fatigue, and other health problems. The proposed system is based on the magnetic near-field coupling between the flat wound induction coil and the compact fluorescent lamp. CFL bulbs emit excessive dirty energy, the most of this energy will energize the super-capacitor and then in emergency lighting batteries through DC/DC step-up converter. So the proposed electronic device show a new technology to harvest the radiation generated by the bulb and charging batteries and secondly reduce the electromagnetic radiation inside a home, offices, and protect our children from radiation. The primary objective of the device is to reduce electromagnetic pollution at home and offices and re-generate energy from harmful radiation. The results are satisfactory and advantages of using technology to recycle electromagnet radiation to charge a battery, use at a critical time like an emergency light system. Besides, we can use it for many other applications. This purpose of this working is an extension of work initially presented in 2017 Ninth International Conference on Advanced Computational Intelligence (ICACI).

1 Introduction

Many studies from world health organization approve that the compact fluorescent light bulb (CFL) produce electromagnetic pollution. These unsafe radiate products directly from light and distributed in all our bedroom, meeting room, and offices [1,2,3,4] the nearer your seat to the bulbs the greater your electromagnetic exposure. The electromagnetic radiation generated is not the same amount of energy, as the bulb power increases the radiation increases too, as shown in Figure 1. The research paper has focused on how much power can acquire from this harmful radiation. Electromagnetic radiation energy harvesting represents a promising solution in charging the super-capacitor from free energy around us, and we start making electromagnetic pollution recycle system [5,6,7]. In this work, we focus on the possibility to reuse radiation for charging the battery of emergency exit lights. In particular, we propose to exploit a near-field magnet coupling to acquire maximum radiation. Experimental studies have demonstrated that lamp emits a relatively intense electromagnetic field in the frequency range from 26 kHz to 28 kHz [8,9,10,11,12].

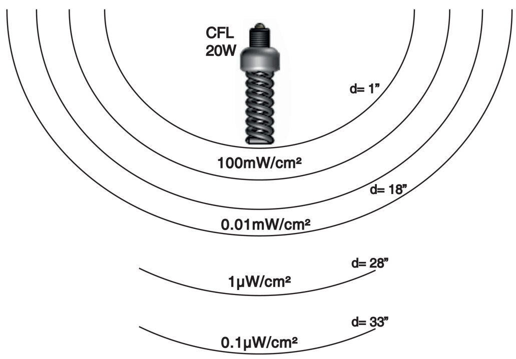

Figure 1: Shows that the field strength very high near the CFL lamp

The device consists of a flat wound planar coil (resonant inductive coupling), a voltage multiplier, a super-

*Corresponding Author:Doha-Qatar, chaari_zied@ieee.org

https://dx.doi.org/10.25046/aj040240

capacitor, and DC/DC adjustable step-up power to energize the emergency exit light, as shown in Figure 2. This research is organized as follows: in Section 2: We present the simulation and design of the flat planar coil. Section 3: Architecture of the proposed harvester Circuit. Section 4: Presents the results and verification. Finally, Section 5: Conclusions.

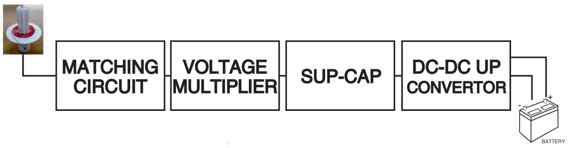

Figure 2: Block diagram of CFL energy harvesting device

2 Simulation and design of the flat planar coil

This present section shows the conceptions and characterization of planar inductor. The planar coil is mostly used in high-frequency applications and designed as tracks on solid support [13,14,15,16]. The proposed Coil shown in Figure 3, was optimized by evolving the form of the flat spiral coils. In this section, the design of the flat wound coil is described, and coil specifications for the effective permeability are introduced. The variables that parameterize the form of the coil are the wire thickness (t), inside diameter (d), outside diameter (D), number of turns (N), the average radius of the coil in inches (R) and width of the loop in inches (W). In the following section, the fabrication process is present in detail. Characteristic properties of the type of coil are high magnetic leakage and parasitic capacitance highly. This formula applies at low frequencies using copper wire.
Where:
L= Inductance of coil in Henry (H);
W= width of winding area (cm);
a= average radius (cm);
N= Number of winding ;

L=(21.5*N2*2*a)/(1+2.72*(W/2a))

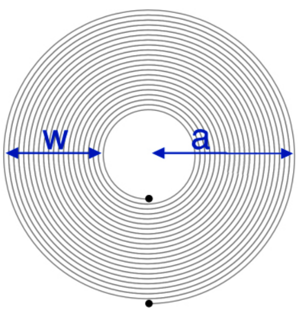

Figure 3: Flat wound planar induction coil

The actual fabrication process will make on plastic diameter approximately 90 mm. With the current mask design, one level contains only one coil, as shown in figure 4.

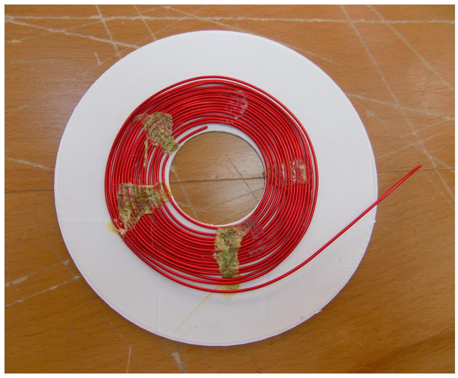

Figure 4: Top view (with dimensions) of planar inductor

It is interesting to note that the Pout increases with the increase of the area diameter and the number of turns (N) of the planar coil. This will can be used to select an adequate output power. Since the device is an inductor, in practice, the resistance to the electromagnetic coil can be neglected compared to the reactance. The inside diameter of the flat coil must be the same as the CFL diameter with average tolerance. Thus, we can fix the CF light inside the induction coil, as shown in figure 5.

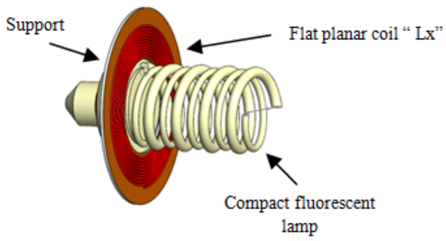

Figure 5: 3D design of the inductive coupling method

2.1 Analysis of a resonant coupled system

There are two ways to measure the H field in the axis direction of the planar induction coil and the radial direction of the coil; it can be seen in Figures 6 and 7, respectively.

Figure 6: Magnetic field measurement in the axis direction of the flat coil

Figure 7: Magnetic field measurement in the radial direction of the flat coil

2.2 Validation of the resonant inductive coupling

The position of the planar coil is most important compared with the position of CFL and the quantity of energy and efficiency changes. The testing is done, and we conclude that when the planar coil at 90° to CFL the energy I maximum, it can be seen in Figure 8. It is encouraging to note that the radiation recovered from the CFL is higher and maximum when the axis of the planar induction coil is in the direction of the axis of the lamps at 90° (near filed coupling) as shown in figure 9. During the test phase, we will use the magnetic field in the direction of the axis of the coil in our measure of construction and testing.

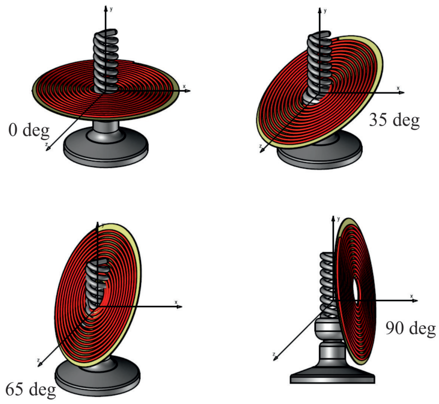

Figure 8: Testing different angles of resonant inductive coupling

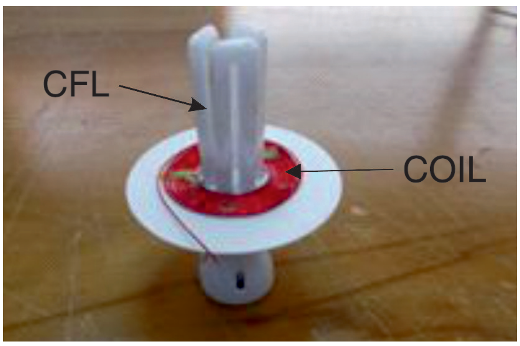

Figure 9: A real photograph of our test phase

After the construction phase of the flat wound planar induction coil coupled in the axis direction of the CFL (90°), we will study the electronic circuit board which can convert the harmful radiation energy to DC power.

3 Architecture of the proposed circuit

The corresponding architecture of the proposed harvester circuit demonstrated in Figure 10. It consists of a resonant inductive coupling, supercapacitor and DC/DC step-up convector connected to the battery of the emergency exit lamp.

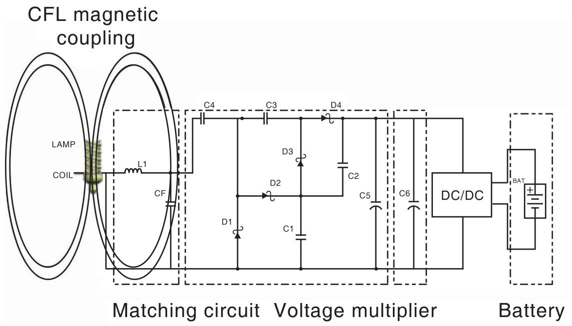

Figure 10: The schematic of a harvest and charging circuit

The components which are used to make harvesting circuit, as shown in the Table 1.

Table 1: Proposed harvester circuit components

Components Name	Components Value
Harvesting Coil Lxl	1 Henry
Diode D1,D2,D3,D4	HSMS 2820
Capacitor C1,C2,C3,C4	56 pF
Sup-Cap	5.1V/400F
DC/DC converter	5.1V/5.7V

The resonator circuit consists of a flat induction coil is coupled with the compact fluorescent lamp (near-field coupling). All reported measurements prove that electromagnetic radiation emissions from CF lamp have a peak at about 26.74 kHz, more precisely, the spectrum of the signal received in the case of coupling between the flat coil and the fluorescent lamp (20W) has been used as adjustable impedance matching circuit at 26.74 kHz [17]. The maximum amount of energy is extracted from the coil when the capacitor is a conjugate match to the source, as shown in Figure 11.

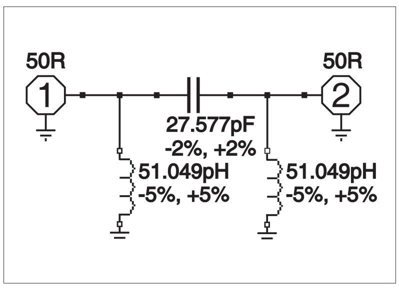

Figure 11: Matching network circuit

Voltage doubler rectify low Alternate Current (AC) collected from the resonator circuit to DC voltage [18,19,20,21,22,23]. It uses a series of capacitors and Schottky diodes to step up and rectify power concurrently. The energy is stored in a super-capacitor and energizing the battery of emergency exit lights. The picture below shows the final prototype used voltage multiplier with the output capacitor, as presented in the photograph 12.

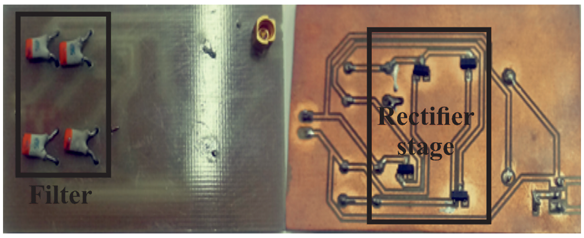

Figure 12: Picture of PCB rectifier circuit

4 Results and Verification

The hardware configuration of the CFL energy harvesting device is mainly on the inductive coupling method. The complete circuit diagram of the project can be divided into two different sections: Resonant inductive coupling, converter section (Rectifier). The flat receiver coil will have connected to a converter circuit through four stages. The first stage is a compensating network to maximize the induced current at the secondary stage by a matching circuit. The second part is a two-stage voltage doubler design with all the stage capacitors being the same value. The third stage is a super-capacitor for storing energy. The last step is A DC-to-DC power step up, as shown in Figure 13.

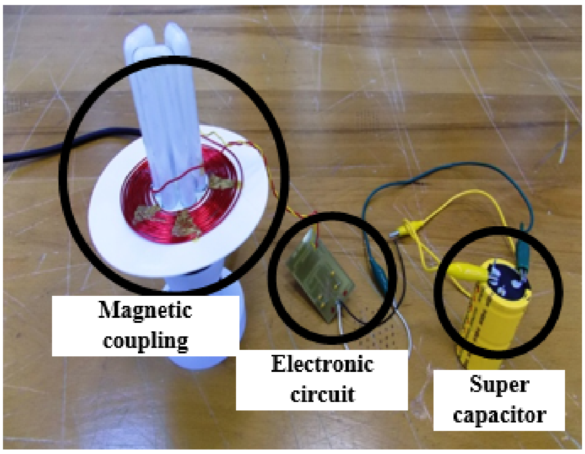

Figure 13: Previous project device

The DC voltage generated by the voltage multiplier will start charging the super-capacitor (5.1V /400F). The battery charging time depends on the range of storage capacity. Table 2 shows the necessary time to charge super-capacitor from CF lamp 20W.

Generally, charging time changes according to the storage capacity of Sup-cap. When the value of ability gets essential, the time of charging gets necessary too. The above table shows us that to charge a Sup-cap of 400F, we need a minimum of 15 days while the fluorescent is working 24h/24h, and a minimum of 5 days to charge a 400.0F Sup-cap. This phase demonstrated that the sup-cap is an excellent low-temperature charger which is, so safe device to be used in our office and home-owners. There are many applications of the proposed idea such as: charging the battery of the emergency exit lights, smoke detector battery or alarm system. Finally, measurements of the DC power generated by coupling between harvesting circuit (Sup-Cap 5.1V /400F) with a 20W CF lamp as illustrated in Figure 14.

Table 2: Charging time for super capacitor with CFL (20W)

Charging Time (Hour)	Charging a capacitor (Volts)
0	0V
1	0.3V
10	0.8V
24	1.35V
48	1.89V
72	3.45V
360	5.05V

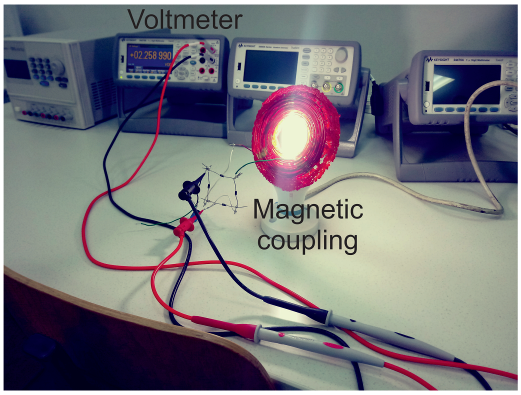

Figure 14: Conceptual view of radio-frequency (RF) energy harvesting

5 Conclusion

The concept of applying harvesting energy from the compact fluorescent lights application has been explored in this work. In this paper, we approved the announcement of the world health organization, that the compact fluorescent light bulbs are a popular choice for businesses and home looking for ways to reduce their electricity bills. High power density recovered when the planar coil in 90 degrees with the lamp. The coupling between the proposed harvester circuit and the CFL for energizing emergency exit light is presented and approved. The measured results of the spectrum of the power acquired by electromagnetic coupling. Only with one geometry type of lamp. In the next work, we will test more examples of light according to the geometry design.

References

[1] Masamitsu, Emily (May 2007). "The Best Compact Fluorescent Light Bulbs: PM Lab Test". Popular Mechanics. Archived from the original on April 26, 2007.

[2] S. Safari, M. Kazemi, H. Dehghan, H. A. Yousefi, and B. Mahaki, "Evaluation of ultraviolet radiation emitted from compact fluorescent lamps," Journal of Health System Research, vol. 9, no. 11, pp. 11771183, 2013.

[3] Abernathy. A, P. Cumbie," Mercury accumulation by largemouth bass (Micropterus salmoides) in recently impounded reservoirs. Bull", Environ. Contam. Toxicol. 17, pp. 595-602.

[4] Kane, Raymond; Sell, Heinz ," Revolution in Lamps: A Chronicle of 50 Years of Progress (Second ed.)". The Fairmont Press, Inc. pp. 189190. ISBN 978-0-88173-378-5, (2001). "Philips Tornado Asian Compact Fluorescent". Lamptech.co.uk. Retrieved 18 June 2013.

[5] Marks, A.M. Device for conversion of light power to electric power. U.S. Patent 4 445 050, 1984.

[6] Flaviu Pop, Clio Munteanu and Adina Rcan, "The assessment of human exposure to radiated fields from different types of lighting", International Conference on Modern Power Systems, pp. 6-9 June 2017.

[7] W.G. Fano, "RF emissions of compact fluorescent lights", Interference Technology, 2012.

[8] Flaviu Pop; Clin Munteanu; Adina Rcan and Silvan Pruu," The assessment of human exposure to radiated fields from different types of lighting", International Conference on Modern Power Systems (MPS), June 2017.

[9] Khodijah Mohamed; Hussain Shareef and Azah Mohamed, ''Analysis of harmonic emission from dimmable compact fluorescent lamps", July 2011.

[10] Sam Aerts; Gnter Vermeeren; Carolina Calderon; Bla Vali; Matthias Van den Bossche and Leen Verloo, ''Exposure to electric and magnetic fields at intermediate frequencies of household appliances", March 2017.

[11] E. coca, V. Popa, and G. Buta, " compact fluorescent lamps l electromagnetic compatibility measurements and performance evaluation",2011 IEEE EURO ,Portugal.pp.1-4.2011.

[12] P. kar, T. G. Palanivelu and B. Revathi, ''effective tests and measurements meclianisms or emi level identification in fluorescent lamp operation", European Journal of Scientific Research, vol. 34, pp. 495-505, 2009.

[13] S. Bsan, S.Sahoo, R. Kumar and . K. Panda, ''Wireless energy transmission to piezoelectric component by flat spiral coil antenna-like structure", IEEE International conference Sustainable Energy Technologies, Kandy, pp. 1-4, 2010.

[14] Kraus J. D., Fleisch D. A.: Electromagnetics with applications, Edition, McGraw-Hill, 1998.

[15] A. Rida, L.Yang and M.M. Tentzeris, RFID-enabled sensor design and application, Boston : Artech House, 2010.

[16] M.Kovama; N.Nago , R.Imai, M.shikida, H.Honda , M. Sato, "Evaluation of Magnetic Beads Agitation Performance Operated by Multi-Layered Flat Coils", International Solid-State Sensors, Actuators and Micro-systems Conference, pp. 2385-2388, 2007.

[17] Myung-Eun Song; Yongke Yan; Sreenivasulu Gollapudi; Mirza Bichurin; Vladimir Petrov; Mohan Sangh, Design of Metglas/polyvinylidene fluoride magnetoelectric laminates for energy harvesting from power cords, 2016 IEEE SENSORS, 30 Oct.-3 Nov. 2016.

[18] Gadalla, M .. M. Abdel-Rahman, and A. Shamim, "Design. optimization and fabrication of a 28.3 THz nanorectenna for infrared detection and rectification11 , Scientific reports, 2014.

[19] Yang. X, Jiang. C, Elsherbeni, A.Z, Yang. F and Wang. Y, "A novel compact printed rectenna for data communication systems", IEEE Trans. Antennas Propag, pp. 2532-2539, 2013.

[20] A. I. Petrariu and V. Popa, "The role of impedance matching for power transfer efficiency in HF RFID systems", 2015 9th International Symposium on Advanced Topics in Electrical Engineering, Bucharest, pp. 386-391, 2015.

[21] Sasaki, Susumu, Tanaka, Koji, Maki, Ken-ichiro, "Microwave Power Transmission Technologies for Solar Power Satellites", Proceedings of the IEEE Vol. IO I, pp. 1438-1447, June 2013.

[22] Rault, Tifenn, Bouabdallah, Abdelmadjid, hallal, Yacine, "Multi-hop wireless charging optimization in Low-Power Networks", IEEE Global Communications Conference, 2013.

[23] Sellali. Mehdi; A. Betka ; S. Drid ; A. Djerdir ; M. Tiar ; S. Abdedaim, Implementation of new adaptive power-split management strategy in a battery-supercapacitor electric vehicle, International Conference on Electrical Sciences and Technologies in Maghreb (CISTEM), Oct. 2018.

Advances in Science, Technology and Engineering Systems Journal
Vol. 4, No. 2, 319-332 (2019)
www.astesj.com
Special Issue on Recent Advances in Engineering Systems

ASTES Journal
ISSN: 2415-6698

An Innovative EPC Architecture based on Not Only Stack for beyond 5G Mobile Networks

Binwei Wu[1], Lu Ge[*,2], Jie Zeng[2], Xiangyun Zheng[1], Youxi Tang[1], Xin Su[2]

[1] *National Key Laboratory of Science and Technology on Communication, University of Electronic Science and Technology of China, 610054, China*

[2] *Beijing National Research Center for Information Science and Technology (BNRist), Tsinghua University, 100062, China*

ARTICLEINFO

Article history:
Received: 14 December, 2018
Accepted: 02 April, 2019
Online: 18 April, 2019

Keywords:
EPC
Network architecture
Not only Stack framework
Virtualization
Beyond 5G (B5G) networks

ABSTRACT

The traditional long-term evolved (LTE) network architecture faces major challenges due to the rapid development of mobile intelligent applications. Evolved packet core (EPC) network, as the core network of the LTE system, faces the same problem as well. In this paper, we propose an innovative EPC architecture, i.e., Not only stack (NOS)-EPC, in which we redesign the control paradigm based on the NOS framework. NOS-EPC contains the user plane (U-plane), the control plane (C-plane), the management plane (M-plane), and the global network view (GNV). By using NOS framework, distributed control paradigm is turned into a centralized manner which simplifies the signaling flows, reducing the procedure latency and overheads. The operation of NOS-EPC is expounded by four main EMM procedures, including initial attachment, service request, handover, and detachment. Through comparison to LTE/EPC, and software-defined networking(SDN)-EPC, we elaborate the advantages of NOS-EPC on operating expense (OPEX), scalability, flexibility, signaling overheads, and user traffic transmission capability. The simulation results confirm that the proposed NOS-EPC takes advantages on the procedure latency and signalling overheads compared to the other EPC solutions, e.g., LTE/EPC and SDN-EPC.

1 Introduction

Current cellular network (i.e., LTE/EPC) is built as a hardware-based, closed, and inflexible architecture. It faces major challenges due to the rapid development of mobile intelligent applications. It is anticipated that the new generation cellular network, e.g., beyond 5G (B5G) network [1], achieves over 100 and 1000 times enhancement on the aspects of capacity and transmission rate. Advanced wireless techniques are developed to relieve the burdens on the air interface of the cellular network, e.g., massive multiple-input-multiple-output (MIMO), non-orthogonal multiple access (NOMA). However, if we simply rely on these air interface-related techniques, severe challenges in B5G cannot be completely solved since various scenarios pose different requirements. For example, the ultra-reliable low-latency communication (uRLLC) scenarios mainly appeal to the reliability and latency of transmission, while the machine-to-machine (M2M) considers more about the massive volumes of connections. Thus, advanced network means and flexible network elements (NEs) design need to be applied to improve the system performance on the network level.

Considerable works have been done to improve the system performance. One of the most effective ways is the virtualization [2]. Several mainstream virtualization solutions have been proposed, such as network function virtualization (NFV), software-defined networking (SDN), cloud computing [3]. Among these solutions, NFV and SDN are promising approaches [4]. The NFV technique decouples the NEs from the underlay physical infrastructures. NE-special hardware is replaced with the commodity servers, which largely decreases the procure cost. Moreover, NEs could migrate among multiple commodity servers as software

[*]Corresponding Author: Lu Ge, Beijing National Research Center for Information Science and Technology (BNRist), Tsinghua University, 100062, China, l_ge@mail.tsinghua.edu.cn

https://dx.doi.org/10.25046/aj040241

instances. Thus, operators could remotely schedule the resources according to dynamic workloads, decreasing the operational cost. SDN is another promising solution which separates the control plane and data plane. Most SDN-based architectures consist of a distributed data plane and a centralized control plane. The control functions in LTE/EPC are packaged as SDN applications. The SDN controller schedules the network resources in a centralized manner, which improves the programmability of the system.

However, SDN and NFV are originally intended for wired transmission networks. The direct integration of SDN and NFV into cellular networks lead to degeneration of performance improvement. There are several fundamental differences between the cellular network and conventional wired networks. First, in the cellular networks, NEs have more complicated functions compared to the wired network. The control functions include mobility management, traffic engineering, QoS guarantee, etc. The user functions include packet forwarding, integrity checking, etc. On the one hand, existing SDN protocols (e.g., OpenFlow) cannot deliver so many services. What's more, a centralized SDN controller usually results in severe network congestion since it could not support so many services at the same time. Second, the protocol stacks in the cellular networks are tightly coupled. In the wired network, the routing table loosely decouples the routing function and data forwarding function. However, in the cellular network, it is difficult to decouple the control plane and user plane without changing the current protocol stacks. Additionally, each protocol entity in the cellular network maintains complex states (i.e. registered, idle, and connected) that involves a mass of signaling interactions, while the wired network works in a stateless manner.

Therefore, in order to improve the performance of virtualization techniques in the cellular network, it is necessary to redesign the control paradigms in LTE/EPC. In our previous work, we proposed an innovative EPC architecture based on the NOS, i.e., NOS-EPC[5]. The NOS-EPC simplifies the signaling flows in LTE/EPC, reducing procedure latency and signaling overheads. In this paper, we conduct the research in a more comprehensive manner. The main contributions are summarized as follows:

- We propose an innovative EPC architecture based on NOS framework. We detail its evolution from a conventional LTE/EPC. The main components of NOS-EPC are elaborated.

- We use four main EMM procedures to illustrate how NOS-EPC works. The EMM procedures include initial attachment, service request, handover, and detachment. Additionally, we elaborate on how to incorporate new services in NOS-EPC to address the flexibility of NOS-EPC.

- We show advantages of NOS-EPC through comparisons among LTE/EPC, SDN-EPC, and NOS-EPC. We emphasize the features of NOS-EPC on operating expense (OPEX), scalability, flexibility, signaling overheads and user traffic transmission capability.

- We evaluate the performance of NOS-EPC through NS3 simulations. The simulations show that the proposed NOS-EPC could improve system performance significantly, compared to traditional LTE/EPC and SDN-EPC.

The rest of paper is organized as follows. In Section II, we review the current works on the architecture of the cellular network. In Sections III, we describe the structure of our proposed NOS-EPC. Section IV details how the NOS-EPC works, using four main EMM procedures. Then, in Section V, a comprehensive comparison between LTE/EPC, SDN-EPC, and the proposed NOS-EPC is given. We conduct NS3 simulations in Section VI, which evaluates the performance of the proposed NOS-EPC. We conclude the paper in Section VII.

2 Background and related works

The architecture of the cellular network is a hot topic in the past few decades. The current LTE/EPC could not satisfy the strict requirements of 5G and B5G [3]. Considerable efforts have been made to investigate the disadvantages of the current LTE/EPC system.

First, in the LTE system, NEs are built on the dedicated hardware, which raises CAPEX and OPEX. Second, NEs in LTE are highly integrated. In order to deliver a particular service, NEs needs to cooperate with each other which motivates unnecessary singling overheads. Moreover, highly-integrated NE design makes it hard to incorporate emerging applications. Third, diverse protocols are designed for different NEs. Heterogeneous protocols result in extra cost during traffic/signaling transmission.

In order to overcome above-mentioned challenges, some researches focus on the optimization of network architecture. Most works use virtualization techniques (e.g., NFV, SDN) to enhance network programmability. In these architectures, NEs are instantiated as packages on the SDN controllers or the software instances hosted on the VMs[6, 7, 8, 9]. The authors of [6] present an SDN-based architecture, named MobileFlow, to validate the feasibility of using SDN in the cellular network. [7] proposes a cloud-based architecture, i.e., CONCERT, which coordinates physical resources as virtual resources. The authors of [8] present an SDN-based 5G cellular system, i.e., SoftAir, in which a unified U/C-plane interface is designed based on OpenFlow. Another high-level cloudlet-based architecture is proposed in [9]. The authors address the seamlessness and low end-to-end latency between UEs and its Avatar.

EPC, as a part of the cellular system, has also been extensively studied [10, 11, 12, 13]. The authors of [10] propose a programmable mobile core network with an OpenFlow-enable data plane. The control function is implemented with an OpenFlow Controller that cooperates with MME. [11] presents a number of different options which are associated with the implementation of EPC over a cloud infrastructure and providing it "as a Service". In [12], the authors detail an OpenFlow-based protocol to enhance network flexibility and programmability. A much more detailed analysis is given in [13], in which authors evaluate the network performance, considering five commonly used procedures.

Some other works conduct the optimization from the aspects of a particular service. [14] investigates an SDN/NFV-based platform in order to improve the performance of video broadcasting service. The improvement owes to the orchestrator in the core network, which is in charge of flow operations like replication and transcoding. [15] designs a 5G user plane function component (UPF) based on SDN to support network slicing, reducing the latency and improving the throughput. [16] focuses on PDN data transmission, in which the authors analyze the cost incurred by different virtualization schemes. In [17], the authors propose an SDN-enabled EPC to carry out inter-domains handover, which uses OpenFlow (OF)-enabled switches as the main forwarding nodes.

It is noticed that the above-mentioned researches do not change the control patterns and interfaces in traditional LTE/EPC. The problems brought by the ossified protocol stack in LTE/EPC still exist. Thus, some researchers focus on the redesign of traditional paradigms in LTE. In [18], C-plane of RAN was reconstructed via data-signaling separation in the air interface. The control coverage and the data coverage are separately controlled according to the on-demand network. A virtualized RAN based on NOS is proposed in [19], which is aimed to optimize flexibility and sustainability. Meanwhile, signaling overheads and service response time are reduced.

The redesign of control paradigms in RAN motivates us to conduct similar methods to LTE/EPC. [20] only focuses on the reconstruction of S/P-GW in EPC. In this paper, we consider the whole region of the EPC/LTE network. We reconstruct the control paradigm based on NOS framework to decrease the signaling overheads and latency.

3 An innovative NOS-based EPC architecture for the mobile network

Unlike the mainstream virtualization techniques like SDN and NFV, the NOS focuses on the redesign of the paradigm of the cellular network [19]. It offers a mechanism that can help to build a virtualized cellular network architecture. In this architecture, network resources can be dynamically allocated and configured to improve the efficiency of utilization. Signaling interactions can be optimized to shorten the procedure duration and decrease the network overheads.

3.1 An Innovative EPC based on NOS framework

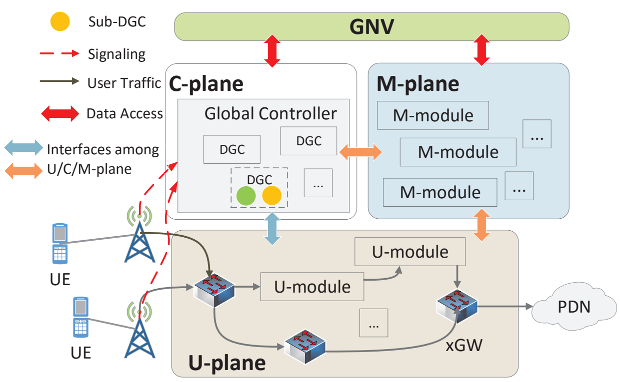

Figure 1: The architecture of the NOS-EPC

The essential methodology of NOS framework is breaking the boundary of protocol entities into different functions, and reconstructing the paradigm of the cellular network in the level of functions. The NOS framework decomposes the functions of NEs into the user plane (U-plane), the control plane (C-plane) and the management plane (M-plane). Data sources which are originally distributed among different NEs are now gathered into a logically centralized GNV. We redesign the network architecture by using NOS framework. The proposed NOS-based architecture is shown in Figure 1. It consists of U-plane, C-plane, M-plane, and GNV. The details of C/U/M plane and GNV are illustrated as followings.

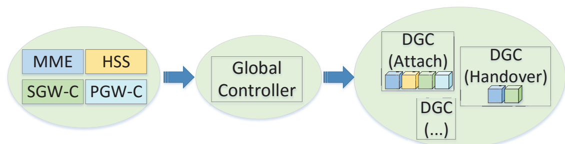

Figure 2: The generations of the DGCs

The U-plane is built in a distributed manner. In the U-plane, the user functions (i.e. GTP encapsulations, rules installations) of the service gateway (SGW) and PGW are merged into the xGW. U-plane modules (U-modules) for emerging services are introduced. Each U-modules is a processing element. The user traffic is routed among these U-modules under the control of C/M plane.

In the C-plane, the traditional control functions are logically centralized into an entity named as GC. The GC is decomposed into multiple modules, denoted as distributed-GCs (DGCs). The splitting of DGCs is conducted according to LTE EMM procedures. Figure 2 demonstrates the process of the generations of these DGCs. The circles with different colors represent the functions in different traditional NEs. SGW-C and PGW-C stand for the collections of control functions in SGW and PGW, respectively. Moreover, the DGCs could be further split up into sub-DGCs in order to decrease its complexity. In order to cover a wide area, copies of DGCs and sub-DGCs are scattered in different clouds/cloudlets. The states and correlated information of DGCs/sub-DGCs are collected into GNV.

The M-plane is designed for the management and administration of multitudinous DGCs/sub-DGCs and U-modules. Its responsibilities could be categorized into resource management, orchestration, scheduling, interpretation and diagnostic, each of which is implemented as M-plane modules (M-modules). The resource management module is in charge of resource allocation for the NOS-EPC components, such as DGCs/sub-DGC and U-models. These modules (DGCs/sub-DGC and U-models) are instantiated as software applications and hosted in VMs. Thus, the resource management module is used to manage the resources for these components, i.e., create/migrate/delete VMs, etc. DGCs/sub-DGCs and U-modules are orchestrated by the orchestration modules to deliver services. The interpreter modules provide unified Application Programming Interfaces (APIs) for the network operators, reducing the cost of the maintenance and upgrades. The diagnostic modules could automatically detect the system performance issues, providing a decision basis for the scheduling modules or network operators.

GNV contains all the information of users and system. It is logically centralized and could be deployed in a distributed manner with the purpose of reducing the access loads. GNV fully decouples the U/C planes and make the modules in C/U/M planes into stateless. Supported by a logically centralized data source, control functions, and management are easy to be realized. Moreover, global optimization is more convenient to be carried out in NOS-EPC since global network information (view) is provided. From the perspective of implementation, GNV is essentially a distributed database which stores the system/user information. Modules in different plane use the data in GNV as a basis to carry out their jobs. Thus, the performance of NOS-EPC highly depends on the reading/writing speed of GNV. Fortunately, there are plenty of mature techniques in the field of distributed databases. Some of them have already been brought into the commercial market for decades[21, 22].

Unlike the traditional EPC, a unified communication protocol is employed for the interactions among the modules in C/U/M planes. Transaction operations are introduced in the C/M planes to ensure integrity. The multicast and concurrent multipath transfer (CMT) are used.

3.2 Implementation and virtualization of NOS-EPC

The deployments of the physical infrastructures and logical elements in Section 3.1 are discussed in this section. The infrastructures used in NOS-EPC could provide a platform, capable of hosting 5G functions. The infrastructures are classified as commodity servers and switches/routers. All the logical elements (DGCs/sub-DGCs, U/M-modules, and GNV) are hosted within virtual machines (VMs) instantiated on commodity servers. In order to cover a huge area, duplications of NEs (i.e., GNV, sub-DGCs) are installed on different sites. Since the network state, user information, and session information are stored in GNV, it is convenient for the M-models to balance the workloads among multiple duplications.

Ephemeral states of the VMs (i.e. resource utilization, workloads) are synced into GNV. The sync is performed periodically or triggered by events, controlled by M-modules. The placements of logical modules and the associations between modules (DGC/sub-DGC, U/M-modules) and users are dynamically optimized. Switches/routers in the NOS-EPC are extended, similar to OpenvSwitches. Flows including control flows and user flows are identified by FLOW_IDs. The Switches/routers route the user flows according to the flow tables. Flow tables could be dynamically configured by DGCs/subDGCs or M-modules through open APIs.

4 The operations of NOS-EPC

In this section, we illustrate the operations of the NOS-EPC. An unambiguous view of the C/M plane is demonstrated through several user cases. We mainly focus on the initial attachment, detachment, service request, and X2 handover procedure in NOS-EPC. Moreover, to emphasize the flexibility of the proposed NOS-EPC, an example of how to incorporate an emerging application is also demonstrated.

4.1 Initial attachment

4.1.1 Initial attachment procedure in LTE

Initial attachment is the first control procedure for users to access into the LTE network. It is triggered by the attach request sent by the user. The procedure can be divided into five sub-phases according to their different specific purposes which shows as below:

Phase 1: *Mobile equipment identity acquisition (MEIA)*. In this phase, the user equipment submits its equipment identity and the other equipment-related information such as supported secure algorithms and integrity protection algorithms to the network.

Phase 2: *Authorization*. In this phase, users and networks identify each other and verify the integrity protection algorithms through the negotiation.

Phase 3: *NAS secure setup*. In this phase, users and networks confirm the security mechanism with each other to ensure the safety and reliability of exchanging of NAS messages.

Phase 4: *Location update*. In this phase, the users are registered in the network and MME gets the user information related to the service type.

Phase 5: *Default EPS bearer setup*. In this phase, the network assigns corresponding resources to establish communication bearers for the users. These bearers allow users to use some basic services.

The details of the messages exchanging during the procedure vary depending on the circumstances. For simplicity, we assume that neither the user nor network has the context about the last attachment. The signaling interactions during the initial attachment in LTE/EPC are shown in Figure 3 [23].

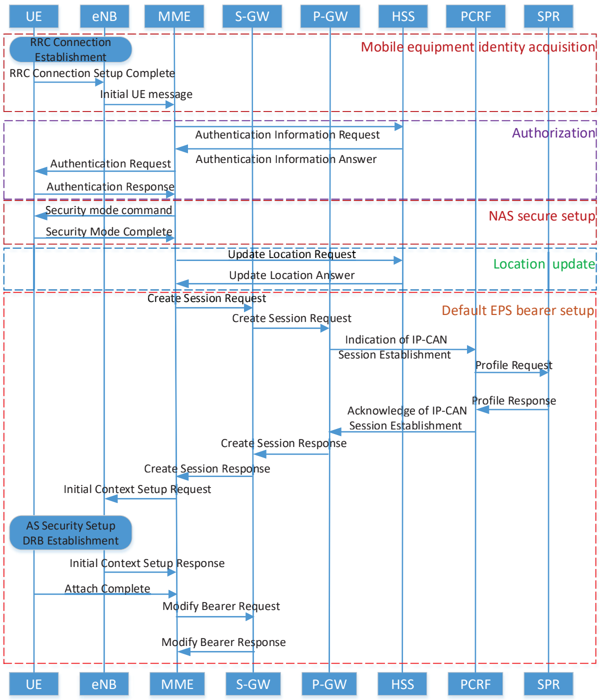

Figure 3: The initial attachment procedure in the LTE/EPC

4.1.2 Initial attachment in NOS-EPC

There are 4 types of sub-DGCs (named as InitialCtrl, AuthCtrl, SecuCtrl, and BearerSetup) involved during the initial attachment procedure in NOS-EPC. The InitialCtrl, AuthCtrl, and SecuCtrl cover the former three phases (i.e., MEIA, Authorization, and NAS secure setup). The BearerSetup covers the latter two phases. The resources (i.e. VMs' CPU and memory) and the dependencies for the DGCs/sub-DGCs are managed by the M-models, which ensures that the user signaling is processed with a right order.

The M-modules allocate the resources (i.e. VMs CPU and memory) for the above sub-DGCs. Dependencies among DGCs/sub-DGCs are determined by the orchestration module, which ensures that user signaling is processed with a right order. In traditional LTE/EPC, the functions related to mobile equipment identity acquisition and NAS security setup phases are centralized in the MME. Therefore, InitialCtrl and SecuCtrl simply play the roles of MME during the procedure. The modifications are focused on the other phases. We mainly details the operations of AuthCtrl and BearerSetup.

MEIA and NAS security setup phases. In traditional LTE/EPC, the functions related to MEIA and NAS security setup phase are located in the MME. We separate these functions from the MME and organize them into the InitialCtrl and SecuCtrl, respectively. The signaling interactions associated with InitialCtrl and SecuCtrl are plotted in Figure 4. In order to maintain the compatibility with traditional LTE/EPC, signaling contexts in NOS-EPC keep unchanged.

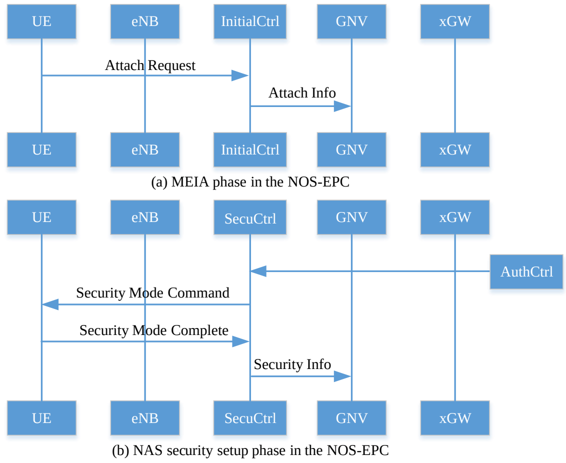

Figure 4: MEIA and NAS security setup phase in the NOS-EPC

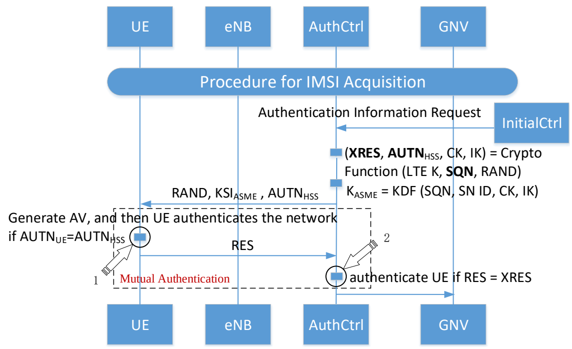

Figure 5: Authentication phase in the NOS-EPC

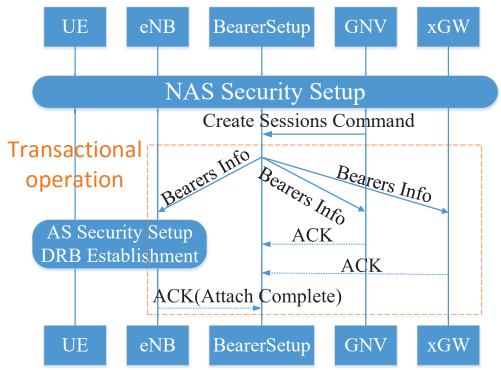

Figure 6: The default bearer setup phase in the NOS-EPC

The authentication phase. In the NOS-EPC, the authentication functions originally dispersed in the MME and HSS are centralized into AuthCtrl. The authentication process in LTE consists of two steps: authentication vector (AV) acquisition and mutual authentication. AV is a quadruple, containing XRES, AUTN, K_{ASME}, RAND. The AuthCtrl generates the AV with two steps, similar to HHS. First, the AuthCtrl calculates XRES, $AUTN_{HSS}$ with a random value RAND.

Next, it uses the key derivation function (KDF) to derive K_{ASME}. During the mutual authentication, UEs authenticate the network with RAND and $AUTN_{HSS}$ (the circle marked with 1 in Figure 5). A RES is then produced if the network has been authenticated (i.e., $AUTN_{HSS}$=$AUTN_{UE}$, where $AUTN_{UE}$ is calculated with RAND and $AUTN_{HSS}$). The network authenticates the UEs by comparing RES and XRES (the circle marked with 2 in Figure 5). In the end, the results are synced to GNV for the records. The details of the signaling interactions for authorization in NOS-EPC are shown in Figure 5.

The location update and default EPS bearer setup. The functions involved in these two phases are originally distributed among HSS, MME, S-GW, P-GW, PCRF, and SPR. In the NOS-EPC, they are reorganized into the BearerSetup. A create session command would be sent by the GNV to the sub-DGCs (BearerSetup). The create session command contains all the necessary information to establish a bearer, including the information in the traditional "update location answer", "profile response" and so on. Once the BearerSetup receives the signaling, it carries out the bearer establishment algorithm, producing the bearer contexts. Then the bearer contexts are disseminated to the U-plane (UE, eNB, xGW) simultaneously. The bearer contexts for different entities are heterogeneous. The signaling interactions involved by BearerSetup in NOS-EPC are shown in Figure 6. The results (bearer context) of the sub-DGCs (BearerSetup) would be updated to the GNV to ensure the completeness.

4.2 Service request

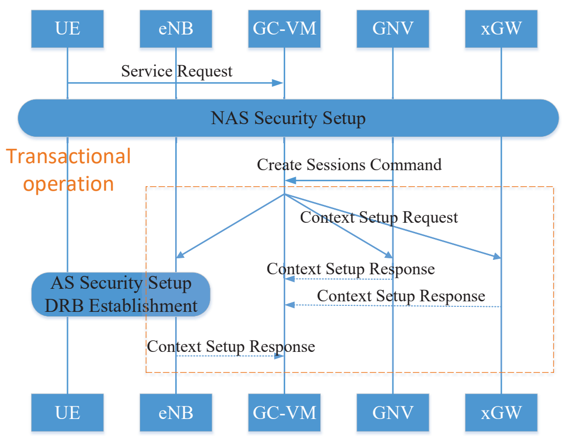

Figure 7: The service request procedure in the NOS-EPC

The service request could be trigged by UEs (uplink transmission) or network (downlink transmission). In this paper, we emphasis the procedure trigged by UEs in Figure 7. The procedure is executed when UEs wants to use a service from the Internet or the PDN networks.

We first focus on the signalling flows during the service request procedure. The main purpose is to setup a data forwarding path between the UE and its destination. The procedure is initiated when a service request message is sent to BearerSetup. Once BearerSetup receives the service request messages, it performs an integrity check on NAS-MAC. If the authentication check is passed, BearerSetup obtains the user-service-related information from GNV, including the UE subscription levels, requested service types, overall network congestions. According to these information, BearerSetup setups the forwarding path by distributing the context setup requests. The context setup requests include the IDs (i.e., TEIDs, bearer IDs), which identify the traffic channels for different UEs among NEs.

The establishment of data forwarding path involves resource allocation, e.g., routing scheduling, QoS mechanism, etc. On the aspect of route scheduling, efforts can be made to improve the capacity of U-plane. Since SDN and NFV technique are used, NOS-EPC is highly programmable. Adaptive routing strategies can be adopted to reduce the congestions by configuring the flow tables. Examples can be found in [24, 25], in which operators jointly optimize task routing and cloud selection to improve the system cost. Meanwhile, the implementation is more convenient in NOS-EPC owing to GNV, which has a global view of the network. BearerSetup can direct the traffic by configuring the flow table in the U-plane, bypassing the congestion links and improving the transmission capacity [26]. Other than routing strategy, advanced resource allocation algorithms or framework like [14, 15] can be migrated into NOS-EPC directly.

Resource allocation is another main concern since QoS mechanisms need to be incorporated to support multiple services with different QoS requirement. To support the legacy of LTE/EPC, conventional QoS mechanisms are fully migrated to NOS-EPC. In order to assign network resources to the traffic of each UE and manage them properly, BearerSetup acquires the subscriptions of UEs and services from GNV through create session command. BearerSetup first classifies user traffic into different service data flows (SDFs). Each SDF contains the flows with the same QoS parameters, e.g., QCI. Different QoS parameters are meant for different priorities of traffic flow which is shown in Table 1. BearerSetup appends QoS rules into Contest setup requests. The enforcement of QoS rules on NEs in the U-plane is the same as the cases in LTE/EPC, which is detailed in [23].

4.3 X2 Handover

4.3.1 Handover in LTE/EPC

X2 handover allows a UE to move from a serving cell to a neighbor cell and reestablish a new radio resource connection(RRC)[27]. Before the handover, the UE collects measurement reports about the signal strength and the quality of adjacent cells, and sends them to the source eNodeB(SeNB). SeNB determines whether the UE initiates handover to a target eNodeB(TeNB) or not. Three phases of handover are successively carried out.

Table 1: The procedure duration in different architectures

QCI	Resource Type	Priority	Packet delay budget	Packet error loss rate	Example services
1	GBR	2	100 ms	10^{-2}	Conversational voice
2		4	150 ms	10^{-3}	Conversational video (live streaming)
3		3	50 ms	10^{-3}	Real time gaming
4		5	300 ms	10^{-6}	Non-conversational video (buffered streaming)
5	Non-GBR	1	100 ms	10^{-6}	IMS signalling
6		6	300 ms	10^{-6}	Video (buffered streaming)
7		7	100 ms	10^{-3}	Video (live streaming)
8		8	300 ms	10^{-6}	Video (buffered streaming)
9		9			

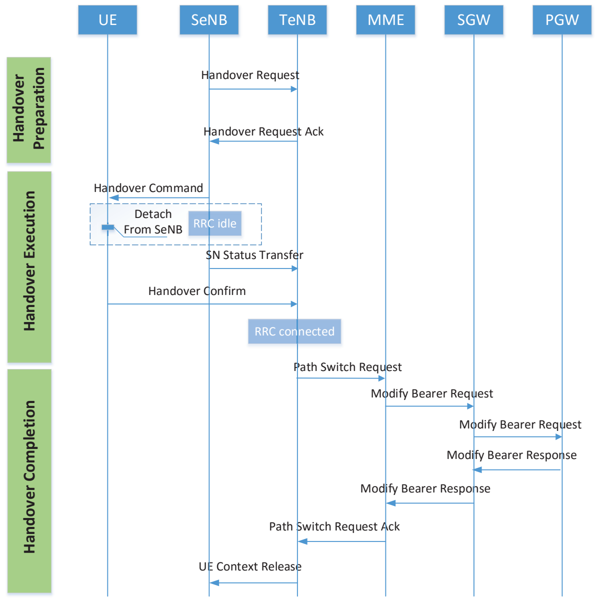

Figure 8: The signaling flow for X2 handover in LTE/EPC

Phase 1: Handover preparation. SeNB forwards the UE context along with S1 TEID to TeNB, assisting with the uplink from TeNB to SGW. The SeNB TEID is sent to TeNB to establish the X2 transport bearer, through which TeNB receives downlink packets while UE attempts to attach TeNB.

Phase 2: Handover execution. SeNB informs the UE to perform handover by sending a message related to TeNB. The message includes cells radio network temporary identity, access stratum security algorithm, *etc*. The UE detaches from SeNB and access TeNB, in the meantime the RRC connection is required to be reconfigured.

Phase 3: Handover completion. When the UE has been connected to the target cell, TeNB is obligated to inform MME to modify the bearer path accordingly. TeNB transmits its TEID to SGW and PGW via MME. The response has to double back. SGW sends the downlink packets to TeNB through the newly established downlink bearer.

Consider the latency during the handover procedure in LTE/EPC. The latency could be presented in (1).

$$D^{\mathrm{LTE}} = 5D_{\mathrm{X2}} + 2D_{\mathrm{RRC}} + 2D_{\mathrm{S1}} + 2D_{\mathrm{S11}} + 2D_{\mathrm{S5/8}} \quad (1)$$

where D_{X2}, D_{RRC}, D_{S1}, D_{S11}, and $D_{\mathrm{S5/8}}$ are the latency motivated by X2, RRC, S1, S11, and S5/8, respectively. It is noticed that (1) assume successful transmission at first attempt. The actual delay values can be higher if some steps require re-transmissions.

4.3.2 Handover in NOS-EPC

In NOS-EPC, the control functions are converged into GC-VMs. We use eNB-U represents eNB that exclusively retains user functions. The handover-related GC-VMs control the handover procedure, which is shown in Figure 9.

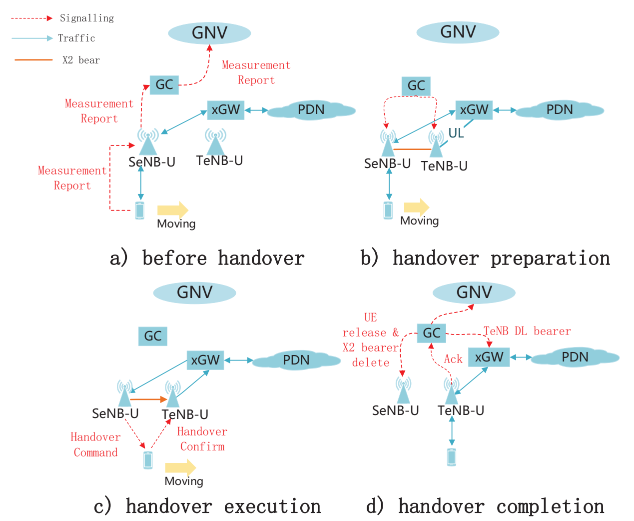

Figure 9: The Handover procedure in NOS-EPC

Initially, an UE reports its measurement to the network. Next, GC-VM accesses users' information from GNV and makes the handover decision. The decision determines when and where to perform the handover procedure. Also, it points out which target cell the UE is about to attach.

Phase 1: Handover preparation. When the TeNB is determined, GC-VM pass the handover execution information to SeNB. Also, GC-VM dispatches TEID of SeNB and xGW to the TeNB. The former TEID is for X2 transport downlink bearer setup. The latter one is for the establishment of an xGW uplink bearer. The setup of X2 transport downlink bearer ensures that the data could be buffered in target base station during the handover execution.

Phase 2: Handover execution. Once receiving the handover command from GC-VM, the UE obtains the information (e.g., access stratum keys) for attaching to the TeNB. There are no packet transmissions until it successfully accesses to TeNB. Packets from PDN are temporarily stored in the TeNB. The state of non-access stratum layer on UE remains unchanged during the handover execution. The radio link connection is inactive. Then, TeNB connects to the UE with access stratum security algorithms.

Phase 3: Completion. Once the UE connects to the TeNB, it informs the GC-VM that the handover procedure is completed. Then, GC-VM instructs SeNB to release the UE context and delete the previous tunnel (i.e., the tunnel between xGW and SeNB). Meanwhile, GC-VM distributes TeNB's TEID to xGW, which helps to establish the downlink bearer from xGW to TeNB. Also, the instantaneous location and the context of UE are updated to GNV.

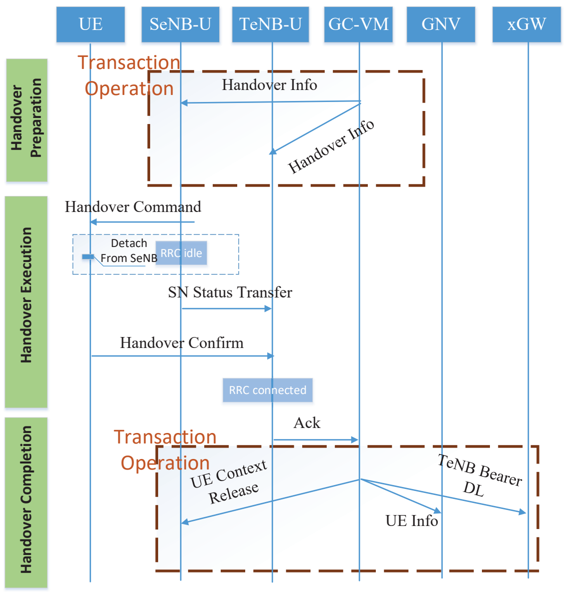

Figure 10: The Signaling flow for X2 handover in NOS-EPC

Consider the latency during the handover procedure in LTE/NOS-EPC. The latency could be presented in (2)

$$D^{\text{NOE-EPC}} = 2D_{\text{TO}} + 2D_{\text{RRC}} + D_{\text{X2}} + D_{\text{CU}} \tag{2}$$

where D_{RRC} and D_{X2} are the latency motivated by RRC and X2. D_{TO} is the latency incurred by transaction operation. D_{CU} is latency between eNB and GC. The actual delay values can be higher if some steps require re-transmissions.

4.4 detach

In the detach procedure, the UE is detached/detaches from the network he attached to. After this procedure, the network resources associated with the UE are completely released.

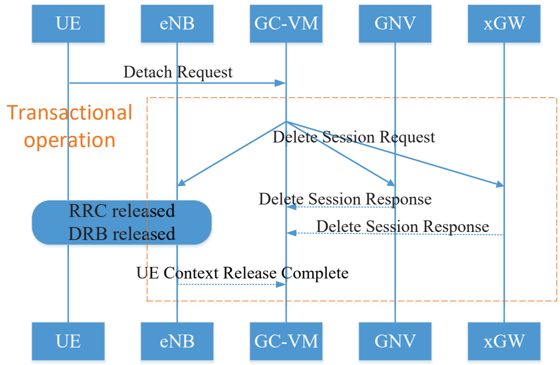

Figure 11: The detach procedure in NOS-EPC

The detach procedure in NOS-EPC is shown in Figure 11. It is an inverse operation of initial attachment. We assume that the detach procedure is triggered by the UE. Initially, the UE sends the detach request to the GC-VMs. The detach request mainly contains the GUTI and detach type of UE. Once the GC receives the detach request, it dispenses the delete session requests to eNB, GNV, and xGW simultaneously. The requests send to different NEs are heterogeneous, e.g., the request sent to eNB contains the 'detach accept' to the UE. These NEs (i.e., eNB, GNV, and xGW) delete the local context about UEs, i.e., network resources and return the response messages to GC-VM.

4.5 The Incorporation of new applications/services in NOS-EPC

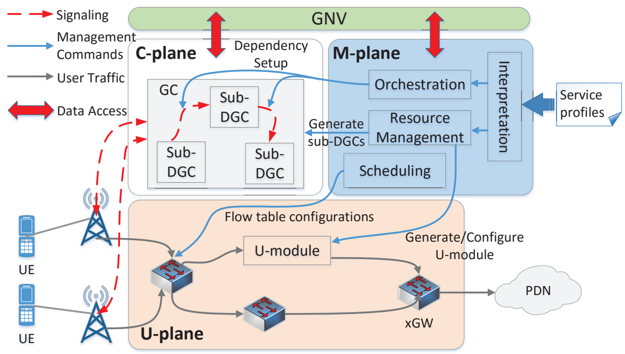

Figure 12: The integration of innovative applications in NOS-EPC

The process of integrating a new application/service in NOS-EPC is shown in Figure 12. First, the service provider submits the profiles into the M-plane through the interpretation module. The profiles contain the functions and the requirements of the new application/service. The interpretation module is essentially a man-machine interface, which analyzes the profiles and generates a series of commands. The control functions are constructed as DGCs/sub-DGCs. The user functions are constructed as U-plane modules. The dependency among modules is configured into NE's flow tables. The meta information (e.g., traffic template) are synced into the GNV.

5 The comparisons between NOS-EPC and the other EPC solutions

In this section, we compare our solutions with the traditional EPC and the SDN-based EPC in order to analyze the pros and cons of our NOS-EPC. Firstly, we brief the architectures of traditional EPC and SDN-based EPC.

Table 2: Comparisons between different architectures

	LTE	SDN-EPC	NOS-EPC
OPEX	High	Med	Low
Scalability	Low	Low	High
Flexility	Low	Med	High
Overheads	Med	High	Low
Capability	Low	High	High

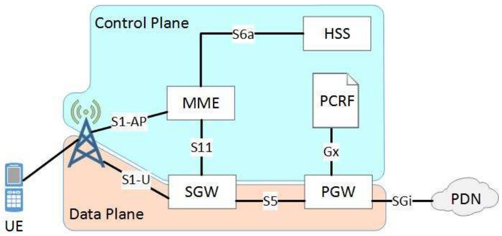

Figure 13: The architecture of the traditional LTE/EPC

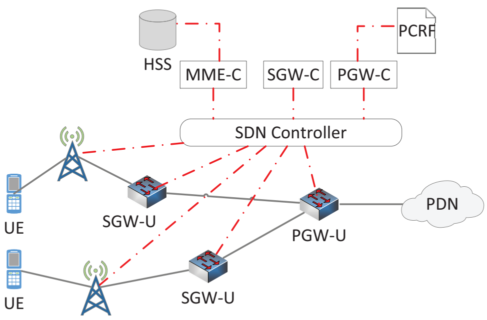

Figure 14: The architecture of the EPC based on SDN

The architecture of traditional LTE/EPC is shown in Figure 13. The details could be referred to [28]. The SDN-based architecture is shown in the Figure 14. In SDN-EPC, the control plane and data plane are decoupled by an SDN controller (i.e. floodlight). NEs (i.e. MME, SGW-C, SGW-P) in the control plane are implemented as SDN applications. The functions in the data plane are achieved with the extended SDN+ switches. The architecture of SDN-EPC could be referred to [29].

Table 2 compares these three architectures, covering OPEX, flexibility, scalability, signaling overheads, and user traffic transmission capability. We detail the comparisons as followings.

OPEX: The NEs (i.e. MME, SGW, PGW, HSS, SPR) in the traditional EPC are deployed on dedicated hardware. The special-designed hardware for different NEs increases the cost of procurement. The NOS-EPC and the control plane of SDN-EPC apply the virtualization technique. Commercial servers are used, which means the OPEX could be reduced.

Flexibility: Flexibility refers to the ability of adaption. In the traditional EPC, any modifications require considerations for the entire system because of the distributed control. The control paradigms in SDN-EPC are not changed compared with traditional LTE network. Therefore, the SDN-EPC has the exact same problems. On the other hand, in our NOS-EPC architecture, innovative services could be easily incorporated, as we described earlier. Thus, the flexibility of the proposed NOS-EPC is more superior.

Scalability: In order to improve the capabilities of the traditional EPC, operators usually need to replace the NEs with more powerful appliances. The replacements need to be accomplished locally and manually. Moreover, the traditional EPC typically scale vertically [29], which means the enhancements could not target at specific services. SDN-EPCs have similar issues. However, it would be easier in the SDN-EPC due to virtualization. Unfortunately, the SDN-EPC introduces bottleneck nodes (SDN controllers) between the control plane and the user plane. The scalability would be largely affected by the capacity of bottleneck nodes. Although some advanced techniques are proposed to deploy SDN in a large-scale network, there are still some problems need to be solved so far [30].

In the NOS-EPC, the 'logical centralized' GNV can be deployed as distributed databases, which has been widely used in the commercial market [21]. Supported by GNV, it is quite convenient to enhance system capacity by deploying replicas of modules and DGCs. Moreover, system enhancements can be accomplished remotely and automatically due to the existence of M-plane and GNV. Horizontally scaling of the EPC could be achieved through the duplications of the related DGCs/sub-DGCs or U/M-modules. The access loads on GNV could be relieved by distributed deployment (distributed databases).

Distinct from the SDN-base architecture, in NOS-EPC, the capacity of the connections between different planes (U/C/M plane) would not be limited by a single node (or host/server). The diagnosis modules and the scheduling modules would automatically route the traffic to bypass the congestion links.

Signaling overheads: The distributed control in the traditional EPC or SDN-EPC contributes the coordination signaling and complicated handshakes among NEs. Additionally, in SDN-EPC, more signaling and handshakes are needed due to the separations of PGW and SGW. On the other hand, in our proposed NOS-EPC, the logic for a particular LTE procedure or service is encapsulated into DGCs/sub-DGCs. The signaling overheads introduced by cooperation and handshakes are cutoff. The performance of the NOS-EPC would be considerably improved.

Moreover, in LTE, the signaling is delivered layer by layer. For example in the handover procedure, the signaling is successively enforced to MME, SGW and PGW when TeNB establishes bearers between

SGW/PGW. However, in the NOS-EPC, signaling interactions among NEs is no longer constrained by layers. Thus, signaling overheads and handshakes are significantly cut down. In fact, LTE/EPC requires 12 signaling interactions during the handover. However, in NOS-EPC, only 9 interactions are required.

Transmission capability: In the EPC, packet loss is typically unacceptable. In traditional EPC, more resources (i.e. bandwidth, links, etc.) need to be provisioned to ensure the reliability. In dynamic network surroundings, performance degradation due to congestion is inevitable even with more resources. In SDN-EPC and NOS-EPC, the traffic routes could be optimized globally. A proper control can improve the average link utilization from 30%∼40% to nearly 100% [31].

There are some costs for our NOS-EPC as well. The replacements of dedicated hardware with commodity servers lead to consistent degradation (nearly 7% degradation [32]) on the aspect of the processing capacity. Second, the deployments of GNV need to be further investigated.

6 Performance evaluations

In this section, we evaluate the performance of the NOS-EPC. We mainly concentrate on the performance of C-plane in different architectures (traditional EPC/EPC, SDN-EPC, and NOS-EPC). We compare the network efficiency on procedure durations (i.e., latency) and signaling overheads. The comparisons highlight the superiority of NOS-EPC on the aspects of procedure performance and network efficiency. The results also suggest that the NOS can help to build a promising cellular network. The comparisons are conducted with NS3.

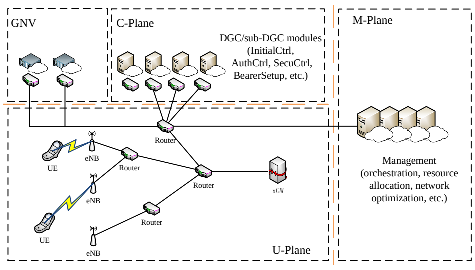

Figure 15: Simulation setting for NOS-EPC.

In the simulations, we use Cost266 as the network topology of NOS-EPC [33]. We assume that nodes in Cost266 are equipped with computation resources. We deploy sub-DGCs/DGC (e.g., InitialCtrl, SecuCtrl, Authctrl, and BearerSetup), U/M modules, and GNV as NS3 applications on separate nodes. eNBs are added which connects the nodes in Cost266. We deploy eNBs in a line with different cell size (R_{cell}), connecting the nodes in Cost266. A complete NOS-EPC is then built as Figure 15. The bandwidth of links between the nodes is uniformly configured as 1Gbps.

UEs in Figure 15 are also implemented with nodes in NS3. In this paper, we mainly focus on the latency and signaling overheads motivated by initial attachment, service request, handover, and detach procedure. Thus, we set that each UE attaches to the EPC with an average interval equalling 250 ms. Once an initial attachment procedure is triggered, the following procedures (service request, detach) are sequentially invoked. The handover procedure is initialized when UE moves out of the current eNB's coverage. We change the number of UEs to vary workloads of EPC. In the simulations, UEs move on a line with different speed (V_{UE}). The parameters for the simulations are summarized in Table 3.

We carry out the simulations in both static scenarios (without UE mobility) and dynamic scenarios (with UE mobility). In static scenarios, we rule out the influences brought by UE mobility and address the performance of initial attachment, service request, and detach. In dynamic scenarios, we focus on the influences under different cell size and UE velocity.

We first evaluate the performance in a static environment ($V_{\text{UE}} = 0$). Table 4 shows the procedure duration in different architectures. The percentages in parentheses tell the ratios using the traditional EPC as the baseline. The variances of the duration in the table indicate the jitters of the procedure duration. From the points of average duration and jitters, the NOS-EPC takes advantages. Compared with the traditional EPC, the NOS-EPC could decrease the procedure duration by nearly 42.5%. On the other hand, the SDN-EPC shows its degradation about 27.5%. The average procedure duration is mainly affected by the number of interactions among different NEs. The number of interactions in different architectures is shown in Table 5. In this table, each transaction operation is viewed as an interaction. It could be seen that NOS-EPC decreases the signaling overheads by at least 25% compared to LTE/EPC. On the other hand, the SDN-EPC suffers from redundant signaling overheads due to its crude U/M decoupling.

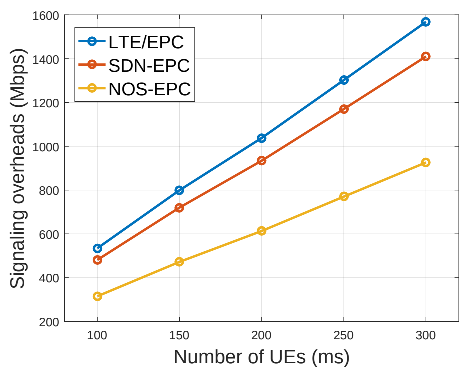

Figure 16: The signaling overheads in different architectures.

Figure 16 shows the signaling overheads in different architectures, which coincides with the conclusions implied by Table 5. It proves that our NOS-EPC could sufficiently decrease the signaling overheads. The reductions in NOS-EPC could be as much as 35% com-

Table 3: Simulation parameters

Description	Values
UE number	100∼300
Average interval of initial attachment	25 ms
UE velocity (V_{UE})	0 ∼ 40 m/s
Cell size (R_{cell})	150 ∼ 400 m
Link bandwidth	1 Gbps

Table 4: The procedure duration in different architectures

	Number of users	Average duration (ns)	Variance
LTE EPC	100	160047.06(=1)	0.25
	150	160047.10(=1)	0.40
	200	160047.12(=1)	0.45
	250	160047.15(=1)	0.59
	300	160047.19(=1)	0.77
SDN-EPC	100	204055.07(∼+27.50%)	0.26
	150	204055.11(∼+27.50%)	0.50
	200	204055.15(∼+27.50%)	0.71
	250	204055.17(∼+27.50%)	0.79
	300	204055.21(∼+27.50%)	0.97
NOS-EPC (Proposed)	100	92028.02 (∼-42.50%)	0.08
	150	92028.03 (∼-42.50%)	0.11
	200	92028.04 (∼-42.50%)	0.15
	250	92028.05 (∼-42.50%)	0.18
	300	92028.07 (∼-42.50%)	0.24

Table 5: The number of interactions in different architectures

	Initial attach	Detach	Service request	Handover
LTE EPC	19	6	6	12
SDN EPC	23	10	10	16
NOS-EPC	10	3	3	6

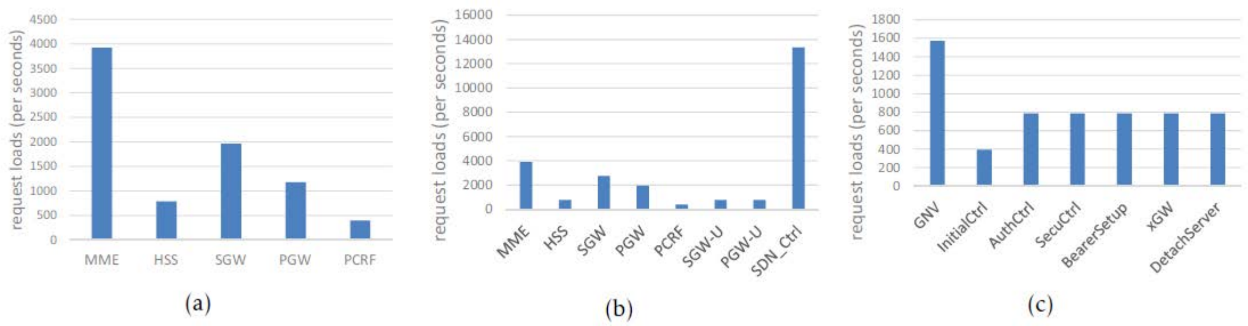

Figure 17: The request loads on the NEs in different architectures. The loads are measured in the simulations with 10 UEs. (a) shows the loads on the NEs in traditional EPC. (b) shows the loads of the NEs in SDN-EPC including the SDN controllers. (c) shows the cases in NOS-EPC. The strings in x label denote the name of sub-DGCs in the C-plane.

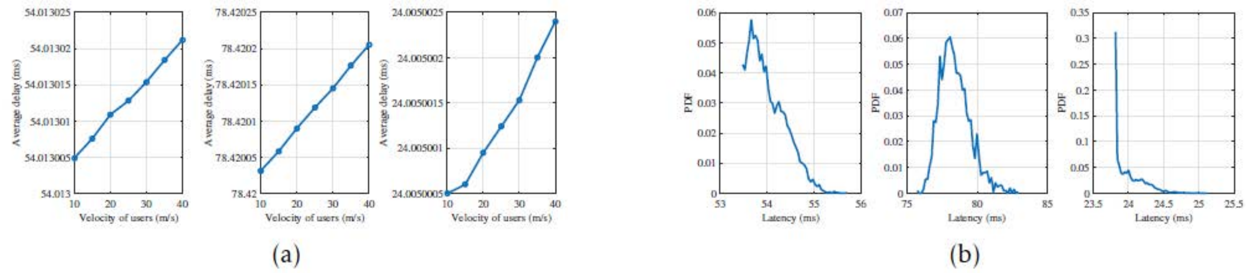

Figure 18: The handover latency in different architectures. (a) The handover latency with different UE velocity when $R_{\mathrm{cell}} = 150m$. (b) The probability distribution function (PDF) of handover latency with $V_{\mathrm{UE}} = 40m/s$ and $R_{\mathrm{cell}} = 150m$.

pared with traditional EPC. The signaling overheads also influences the jitters. The queue delays (as random variables) become significant as the overheads increases. Therefore, the jitters of transmissions become larger.

Figure 17 shows the request loads for different NEs in three architectures with $V_{\mathrm{UE}} = 0$. In traditional EPC, the pressure on the MME is the heaviest. In the SDN-EPC, the bottleneck node (SDN controller) has the highest request loads. Other than GNV, the distribution of request loads in NOS-EPC is nearly balanced. The heavy loads on GNV could be relieved if the GNV is deployed in a distributed manner. The requests loads on different NEs imply the scalability of different EPCs. The SDN controller and MME would become the bottlenecks in SDN-EPC and traditional EPC, respectively. In the NOS-EPC, things become less tricky due to virtualization and nature of the architecture. The distributions of loads on different NEs also affect the duration. A congested path would largely increase the variance of the latency [34]. With a heavy loaded SDN controller, the jitters in NOS-EPC are more significant. The results are agreed with prior results (jitters) in Table 4.

In order to emphasis NOS-EPC performance in a dynamic environment, we evaluate the performance of NOS-EPC. We vary V_{UE} and R_{cell} in the range of $5 \sim 40$m/s and $150 \sim 400$m, respectively.

Figure 18(a) plots the tendency of handover latency with different UE velocity. It shows that the average handover delay stays about 54.01ms, 78.42ms, and 24.00ms in LTE/EPC, SDN-EPC, and NOS-EPC, respectively. The delay slightly increases with the UE velocity since a higher V_{UE} results in higher congestion in EPC. The proposed architecture (NOS-EPC) reduces the delay by nearly 55.5% compared to the LTE/EPC. The benefit is owing to the redesigns of the control paradigm. Redundant signaling interactions are cut off due to the centralized control. On the other hand, SDN-EPC has the longest handover delay. The reason is that more signaling overheads are required due to the sync between SGW(or PGW) and SGW-U(or PGW-U).

Figure 18(b) compares the latency distributions of handover procedure in different architectures. The left graph is for the handover procedure in LTE/EPC. The middle one represents the case in SDN-EPC and the right graph is the case in NOS-EPC. The shapes of the curves in Figure 18(b) tells the probability distributions of the handover procedure. Moreover, the peaks of the curves describe the number of network backlogs. When the network suffers severe congestion (backlogs), the queue delay on NEs increases, shifting the peaks to the rightwards. Vice Versa. Therefore, the procedure in NOS-EPC causes fewer network backlogs than the other network architectures.

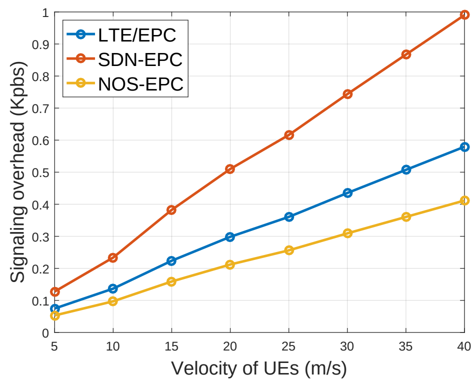

Figure 19: The signaling overheads brought by a single UE with different V_{UE}. We set $R_{\mathrm{cell}} = 150m$.

Figure 19 shows the relationships between the signaling overheads and V_{UE}. As V_{UE} increases, the handover procedure is invoked more frequently, which increases the signaling overheads. Compared with LTE/EPC, the proposed NOS-EPC could always cut off the signaling overheads by nearly 28.8%. In NOS-EPC, the overall information elements in handover signaling decrease from 373 bytes to 265 bytes. The SDN-EPC take more signaling overheads compared to LTE/EPC and SDN-EPC since it requires additional signaling to sync the U/C plane, e.g., PGW and PGW-U, SGW and SGW-U.

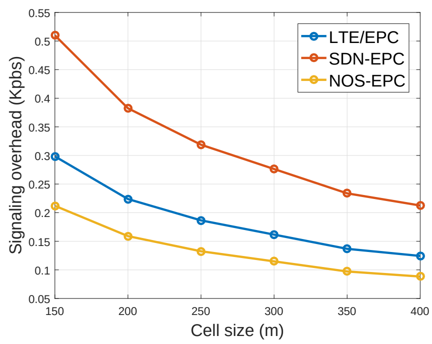

Figure 20: The signaling overheads brought by a single UE with different R_{cell}. We set $V_{\mathrm{UE}} = 10m/s$.

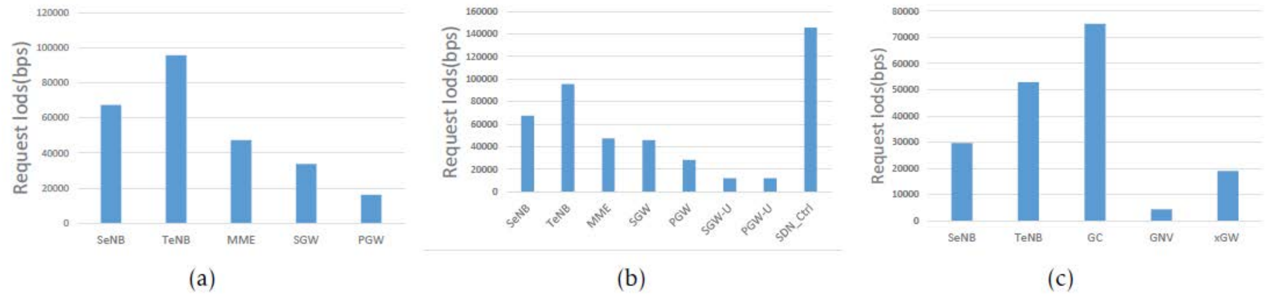

Figure 21: The request load brought by handover in different architectures. The loads are measured in the simulations with 2000 UEs. (a) shows the loads on the NEs in traditional EPC. (b) shows the loads on the NEs in SDN-EPC including the SDN controllers. (c) shows the cases in NOS-EPC.

Figure 20 plots the relationships between the signaling overheads and R_{cell}. A small-size cell requires frequent handovers. As R_{cell} increases from 200m to 400m, the handover times decrease by nearly 54.4%. Therefore, when R_{cell} increases, signaling overheads decreases. Coincided with former analysis, the overheads in NOS-EPC decrease by nearly 28.8% compared to LTE/EPC. Meanwhile, SDN-EPC performs the worst owing to a roughly decouple between U-plane and C-plane.

Figure 21 shows the overheads on NEs in different architectures. Similar to the static scenarios, the proposed NOS-EPC shows relatively balanced distributions. In LTE/EPC and SDN-EPC, MME and SDN controller are the bottlenecks which would significantly degenerate the system performance. The heavy load on these NEs would result in additional network cost, such as packet loss, workload expiration, etc. On the other hand, the load in NOS-EPC is nearly balanced. Moreover, supported by GNV, the capacity of NEs could be easily enhanced by the duplication of NE instances.

7 Conclusion

In this paper, we proposed an innovative EPC architecture based on NOS framework, which consists of the U-plane, C-plane, M-plane, and GNV. We describe the operation of the NOS-EPC with four common EPS mobility management(EMM) procedures, i.e., initial attachment, service request, handover and detach. We detail the comparison among conventional LTE/EPC, SDN-EPC, and the proposed NOS-EPC on OPEX, scalability, flexibility, signaling overheads, and transmission capability. Compared to the conventional LTE/EPC, the proposed NOS-EPC takes advantages since we loosely decouple the U/C/M plane through GNV. C/M plane is carefully designed to deliver a centralized control. The GNV is deployed in a distributed manner. Thus, no bottleneck node exists in the proposed architecture compared to the SDN-EPC. The simulations verify that compared with LTE/EPC and SDN-EPC, NOS-PEC could significantly decrease the signaling overheads (by at least 35%) and procedure duration (by at least 42%). Moreover, we conduct the simulations to evaluate the workload on different NEs. The results show that the load distribution in NOS-EPC is nearly balanced. On the other hand, LTE/EPC and SDN-EPC suffer from severe congestion on MME and SDN controller, which decreases the performance on scalability. The advantages on the scalability, programmability and the improvements of the procedure duration, signaling overheads, and loads distribution mean that the NOS-EPC is a promising solution for the B5G network. In the future work, we will focus on the division granularity of the GC modules and GNV, which can be further optimized to enhance the performances of the network. Moreover, a testbed for NOS-EPC evaluation would be developed.

Acknowledgment This work is supported by the National S&T Major Project(No.2018ZX03001004).

References

[1] S. Sekander, H. Tabassum, and E. Hossain, “Multi-Tier Drone Architecture for 5G/B5G Cellular Networks: Challenges, Trends, and Prospects,” IEEE Communications Magazine, 56(3), 96-103, March 2018.

[2] S. Abdelwahab, B. Hamdaoui, M. Guizani, and T. Znati, “Network function virtualization in 5G,” IEEE Communications Magazine, 54(4), 84-91, April 2016.

[3] E. J. Kitindi, S. Fu, Y. Jia, A. Kabir, and Y. Wang, “Wireless Network Virtualization with SDN and C-RAN for 5G Networks: Requirements, Opportunities, and Challenges,” IEEE Access, 19099-19115, May 2017.

[4] Q. Duan, N. Ansari, and M. Toy, “Software-defined network virtualization: an architectural framework for integrating SDN and NFV for service provisioning in future networks,” IEEE Network, 30(5), 10-16, Sep. 2016.

[5] B. Wu, L. Ge, J. Zeng, X. Zheng, Y. Kuang, X. Su, and J. Wang, “An Innovative EPC with Not Only Stack for beyond 5G Mobile Networks,” 2018 IEEE 87th Vehicular Technology Conference (VTC Spring), 1-5, June 2018.

[6] K. Pentikousis, Y. Wang, and W. Hu, “Mobileflow: Toward software-defined mobile networks,” IEEE Communications Magazine, 51(7), 44-53, Jul. 2013.

[7] J. Liu, T. Zhao, S. Zhou, Y. Cheng, and Z. Niu, “CONCERT: a cloud-based architecture for next-generation cellular systems,” IEEE Wireless Communications, 21(6), 14-22, Dec. 2014.

[8] I. F. Akyildiz, P. Wang, and S.-C. Lin, “SoftAir: A software defined networking architecture for 5G wireless systems,” Computer Networks, 85, 1-18, 2015.

[9] X. Sun and N. Ansari, "Green cloudlet network: A distributed green mobile cloud network," IEEE Network, 31(1), 64-70, Jan. 2017.

[10] S. Shanmugalingam and P. Bertin, "Programmable Mobile Core Network," 2014 IEEE Symposium on Computers and Communications (ISCC), 1-7, June 2014.

[11] T. Taleb, M. Corici, C. Parada, A. Jamakovic, S. Ruffino, G. Karagiannis, and T. Magedanz, "EASE: EPC as a service to ease mobile core network deployment over cloud," IEEE Network, 29(2), 78-88, March 2015.

[12] M. R. Sama, S. B. H. Said, K. Guillouard, and L. Suciu, "Enabling network programmability in LTE/EPC architecture using OpenFlow," 2014 12th International Symposium on Modeling and Optimization in Mobile, Ad Hoc, and Wireless Networks (WiOpt), 389-396, May 2014.

[13] V. Nguyen and Y. Kim, "Proposal and evaluation of SDN based mobile packet core networks," EURASIP Journal on Wireless Communications and Networking,2015(1), 172-190, 2015.

[14] V. D'Amico, A. Lombardo, M. Melita, C. Rametta, and G. Schembra, "An SDN/NFV telco operator platform for video broadcasting," IEEE Communications Magazine, 54(10), 122-128, Oct. 2016.

[15] J. Costa-Requena, A. Poutanen, S. Vural, G. Kamel, C. Clark, and S. K. Roy, "SDN-Based UPF for Mobile Backhaul Network Slicing," 2018 European Conference on Networks and Communications (EuCNC), 48-53, June 2018.

[16] X. An, W. Kiess, J. Varga, J. Prade, H. Morper, and K. Hoffmann, "SDN-based vs. software-only EPC gateways: A cost analysis," 2016 IEEE NetSoft Conference and Workshops (NetSoft), 146-150, June 2016.

[17] E. B. Hamza and S. Kimura, "A Scalable SDN-EPC Architecture Based on OpenFlow-Enabled Switches to Support Inter-domain Handover," 2016 10th International Conference on Innovative Mobile and Internet Services in Ubiquitous Computing (IMIS), 272-277, July 2016.

[18] S. Zhou, T. Zhao, Z. Niu, and S. Zhou, "Software-defined hypercellular architecture for green and elastic wireless access," IEEE Communications Magazine, 54(1), 12-19, Jan. 2016.

[19] J. Zeng, X. Su, J. Gong, L. Rong, and J. Wang, "5G virtualized radio access network approach based on NO Stack framework," Communications (ICC), 2017 IEEE International Conference on, 1-5, IEEE, 2017.

[20] A. Basta, W. Kellerer, M. Hoffmann, K. Hoffmann, and E. Schmidt, "A Virtual SDN-Enabled LTE EPC Architecture: A Case Study for S-/P-Gateways Functions," 2013 IEEE SDN for Future Networks and Services (SDN4FNS), 1-7, Nov. 2013.

[21] G. DeCandia, D. Hastorun, M. Jampani, G. Kakulapati, A. Lakshman, A. Pilchin, S. Sivasubramanian, P. Vosshall, and W. Vogels, "Dynamo: Amazon's Highly Available Key-value Store," SIGOPS Oper. Syst. Rev., 41(6), 205-220, Oct. 2007.

[22] J. C. Corbett, J. Dean, M. Epstein, A. Fikes, C. Frost, J. J. Furman, S. Ghemawat, A. Gubarev, C. Heiser, P. Hochschild, W. Hsieh, S. Kanthak, E. Kogan, H. Li, A. Lloyd, S. Melnik, D. Mwaura, D. Nagle, S. Quinlan, R. Rao, L. Rolig, Y. Saito, M. Szymaniak, C. Taylor, R. Wang, and D. Woodford, "Spanner: Google&Rsquo;s Globally Distributed Database," ACM Trans. Comput. Syst., 31(2), 8:1-8:22, Aug. 2013.

[23] Netmanias, "EMM Procedure 1. Initial Attach - Part 2. Call Flow of Initial Attach." `https://www.netmanias.com/en/?m=view&id=techdocs&no=6102/`. Accessed Jan. 16, 2014.

[24] A. Ceselli, M. Premoli, and S. Secci, "Mobile Edge Cloud Network Design Optimization," IEEE/ACM Trans. Netw., 25(3), 1818-1831, June 2017.

[25] B. Yang, W. K. Chai, Z. Xu, K. V. Katsaros, and G. Pavlou, "Cost-Efficient NFV-Enabled Mobile Edge-Cloud for Low Latency Mobile Applications," IEEE Transactions on Network and Service Management, 15(1), 475-488, March 2018.

[26] J. Hansen, D. E. Lucani, J. Krigslund, M. Medard, and F. H. P. Fitzek, "Network coded software defined networking: enabling 5G transmission and storage networks," IEEE Communications Magazine, 53(9), 100-107, Sep. 2015.

[27] 3GPP TS 36.420 V14.0.1, "X2 general aspects and principles (Release 14)," 1, 0-14, 2017.

[28] U. Barth, "3GPP Long-Term evolution/system architecture evolution overview," Alcatel White Paper, 2006.

[29] A. Jain, N. Sadagopan, S. K. Lohani, and M. Vutukuru, "A comparison of SDN and NFV for re-designing the LTE packet core," Network Function Virtualization and Software Defined Networks (NFV-SDN), IEEE Conference on, 74-80, IEEE, 2016.

[30] T. Huang, F. R. Yu, C. Zhang, J. Liu, J. Zhang, and Y. Liu, "A Survey on Large-Scale Software Defined Networking (SDN) Testbeds: Approaches and Challenges," IEEE Communications Surveys Tutorials, 19(2), 891-917, Secondquarter 2017.

[31] S. Jain, A. Kumar, S. Mandal, J. Ong, L. Poutievski, A. Singh, S. Venkata, J. Wanderer, J. Zhou, M. Zhu, J. Zolla, U. Hölzle, S. Stuart, and A. Vahdat, "B4: Experience with a globally-deployed software defined WAN," SIGCOMM Comput. Commun. Rev., 43(4), 3-14, Aug. 2013.

[32] D. Lake, G. Foster, S. Vural, Y. Rahulan, B. H. Oh, N. Wang, and R. Tafazolli, "Virtualising and orchestrating a 5G evolved packet core network," 2017 IEEE Conference on Network Softwarization (NetSoft), 1-5, Jul. 2017.

[33] S. Orlowski, R. Wess?ly, M. Piro, and A. Tomaszewski, "SNDlib 1.0 Survivable Network Design Library," Networks, 55(3), 276-286.

[34] D. E. Comer, Computer networks and Internets. Prentice Hall Press, 2008.

Advances in Science, Technology and Engineering Systems Journal Vol. 4, No. 2, 333-339 (2019)

www.astesj.com

Special Issue on Advanced Electrical and Communication Technologies

ASTESJ
ISSN: 2415-6698

Optimization of Statcom in a Nouakchott Power System

Ethmane Isselem Arbih Mahmoud[*,1], Mohamed Maaroufi[1], Abdel Kader Mahmoud[2], Ahmed Yahfdhou[3]

[1,2]*EREEC, MSI, University UM5, 765, Rabat-Agdal, Morocco*

[2]*LRAER, FST, University El-Assrya, 5000, Nouakchott, Mauritania*

[3]*LASES, FST, UCAD, Dakar, Senegal*

A R T I C L E I N F O

Article history:
Received:11 March, 2019
Accepted:11 April, 2019
Online: 17 April, 2019

Keywords:
STATCOM
Optimization
PSS/E and MATLAB

A B S T R A C T

STATCOM a shunt connected Flexible Alternative Current Systems (FACTS) device using for fast control of voltage and reactive power control in the power grid. To optimize Nouakchott power system at 2030 year, we anticipate both generation and demand grow. A set of nonlinear equations are solved through Newton Raphson method and programmed in PSS/E and MATLAB. The results will be analyzed for two situations, without STATCOM and with STATCOM connected to the grid. The found results show the degree of performance and capacity of STATCOM to reduce the power mismatches, improve the voltage at buses and reduce the harmonics in Nouakchott power system. The impact of the renewable energies to improve transient stability of system will be considered. In the end, the power system is optimized at 2030 year by integration the STATCOM device. It will be generating or absorb reactive power to stabilize the system voltage at 1 pu. That means enhances transits active power thereby providing additional capacity to consumers.

1. Introduction

Electrical networks supply energy between the production site and the customer site, with a required power, a voltage and frequency. According to the standards, the voltage drop in the network is limited to ± 5%. The power plants of Nouakchott consist of multi-sources that supply several loads, located in seven different places in town making a loop of 33 KV. It should be noted that the frequency varies continuously. Variations ± 5% of the nominal frequency affect the stability of network and may lead to load shedding. The voltage level must remain within an authorized range at any point in the network. This will be in all foreseeable production and consumption situations. The proposed goal for this work is to find a solution for load shedding. In this case, we proposed an analysis for both the current and projected production system. That allows us to meet the domestic demand of the Nouakchott 33 KV network. This analysis allows us to reach and maintain the voltage profile in stability margin for the network manager. Before that we modelize the electrical network by its transit capabilities. And analysis its simulation results programmed in MATLAB and PSS/E. The growths of distributed renewable generation (solar, wind, etc) are creating challenges for the power grid stability [1-3]. The intermittence problem of these energies makes us always to seek to solve it. To synchronize renewable energy with conventional energy, to make our system more efficient, it requires a delicate control procedure: frequency, phase sequences, phase angles and magnitudes of all the four independent sources should match exactly. A real time monitoring circuitry is necessary which should turn on and off the sources when the loads reach preset values. Another goal is to optimize Nouakchott power system. The STATCOM device (Static Var Compensator) is a technique for achieving this goal [4, 5]. Per comparison with other types of FACTS (Table 5), STATCOM has been chosen. Thus, to realize predetermined goals, we take the following four steps:

- First step, the single line schematic of the Nouakchott 33 KV loop network is given (Figure 1).
- Secondly, the lines data and voltages (Table 1).

Thirdly generation and load grow are given from 2020 to 2030 years (Tables 2 and 4).

- Thirdly, a mathematical model of power flow equations are solved by Newton Raphson (NR) method, programmed on MATLAB software and PSS/E simulator for two situations

[*]Ethmane Isselem Arbih Mahmoud, EETFP-NDB, (+222) 47403369, ethmaneisselemarbih1966@gmail.com

(without STATCOM and with STATCOM device) [6-11]. The results of simulations will be following by discussions.

- Last step, a conclusion of the work.

For insertion of the STATCOM device, it is sought a stable power system, even during a disturbance (out limit voltage drop or frequency) to provide the demand power [12, 13]. We notice that FACTS devices are defined by IEEE as "power electronic based controllers and other static equipment which can regulate the power flow and transmission voltage through rapid control action". Nowadays power system control is based on FACTS devices. STATCOM a shunt connected FACTS device using to rapid voltage and reactive power control, also to reduce harmonics in power system (Table 5). This is realized while keeping constant the frequency to the margin limit of stability and alternators speed rotation also the voltage magnitude in the various network buses [14, 15].

2. Structure of System

2.1. One line diagram of Nouakchott Power Grid

The One –line diagram (Figure.1), represents the 33 KV loop (part of the network). The lines data and initials voltage at each bus, the values of generated and load grow are given in Tables 1 and 2 respectively. The system include eleven(11) transmissions lines, two renewable plants (one wind power ,one solar plant), two thermal plants and 1 Dual fuel plant)and five(5) loads connected at buses 2,4,5,6 and 7 respectively. The active and reactive powers generated are given in MW and MVAR respectively. The voltage at each bus (i) is given in KV. The load bus is characterized by its active power P and reactive power Q. Therefore, (P, Q) are specified, while (V) is to be calculated. In this context, it is proposed for the North bus (1), to be a slack bus. Finally, it should also be noted that a bus is numbered (i) and it is connected to (k) other buses such as those shown in Figure 1[16].

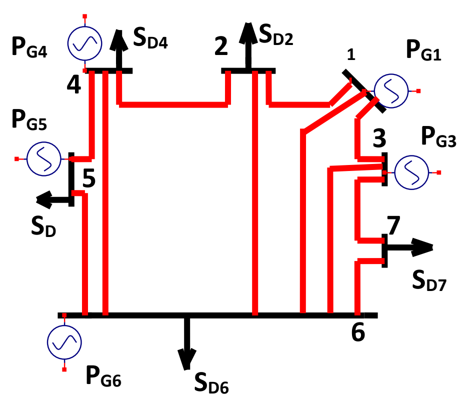

Figure 1: Simplified One Line Diagram; of Nouakchott System

Table 1 present, the active resistances(R), the lines reactances values(X), bus voltage (V), the lengths of each line (L), at each bus (i) connected to the bus (k).

2.2. Given Data of System

Table 4 are presented the simulation results for PSS/E simulator, case before insertion of STATCOM, we can notice the profile of voltage magnitudes and the voltage angles. The results show that the values of voltage magnitude are below the range of the stability for all system except the slack bus. In blue color the buses were connected the renewable plants (3, 5 and 7 buses).

Table 1: Lines Data and Bus Voltage of Figure 1

N	i	k	R(Ω)	X(Ω)	V(KV)	L(km)
1	1	2	0,122	0,167	33	6,27
2	1	3	0,067	0,092	33	3,47
3	1	6	0,024	0,037	33	20
4	2	4	0,027	0,037	33	13,98
5	2	6	0,032	0,044	33	16,8
6	3	6	0,061	0,08	33	15
7	3	7	0,141	0,193	33	7,25
8	4	5	0,17	0,232	33	8,72
9	4	6	0,127	0,173	33	4,51
10	5	6	0,101	0,15	33	5,66
11	6	7	0,232	0,31	33	11,87

Table 2: Generation Data at 2020 to 2030 Years [16]

	2020		2025		2030	
N	MW	MVAR	MW	MVAR	MW	MVAR
1	180	87,17	270	130,68	360	174,24
3	15	7,26	15	7,26	15	7,26
4	36	17,42	36	17,42	36	17,42
5	30	14,52	70	33,88	60	29,4
6	137	66,34	199,7	96,67	217,2	105,15
7	0	0	50	24,2	50	24,2

Table 3: Load Grow at 2020 to 2030 Years [16]

N	2020		2025		2030	
	MW	MVAR	MW	MVAR	MW	MVAR
2	27,68	15,8	142,55	81,37	734,142	419,05
4	11,71	6,36	60,3	32,3	310,5	166,34
5	1,34	1,138	6,9	5,86	35,53	30,179
6	9,4	1,17	48,4	6,02	249,31	36,8
7	13,49	7,18	69,48	36,97	357,86	190,39

Table 4: Simulation Results of NR without STATCOM

N	Remarque	Vpu	δ(°)
1	Slack	1	0
2	PQ	0,8	-5,6
3	PV	0,93	-1,8
4	PQ	0,75	-7,3
5	PV	0,78	-6,5
6	PV	0,8	-5,8
7	PQ	0,83	-4,6

3. Mathematical Modelisation of STATCOM

The Static Synchronous Compensator (STATCOM) device is a shunt connected FACTS to the buses. It uses the forcing electronic power commutation (GTO, IGBT and IGCT). A STATCOM controls reactive power source can improve the transient stability of systems. This provides voltage support by generating or absorbing reactive power at the point of common

Table 5: Comparison of FACTS systems in terms of technical efficiency [17, 18]

Problem	FACTS Systems					
	Shunt		Series		Hybrid	
	SVC	STATCOM	SSSC	TCSC	IPFC	UPFC
Control of the voltage (static state)	++	++	++	+	+	+
Control of the voltage (dynamic state)	++	++	++	+	+	+
Static stability	++	++	-	-	-	+
Dynamic Stability	++	++	-	-	-	+
Damping of power oscillation	++	++	++	++	+	++
Transitional stability	+	++	-	++	+	++
Power flow (static condition)	+	+	++	++	++	++
Limitation of the fault current	-	-	-	-	+	+

++: Very Good +: Sufficient -: Inappropriate

Table 6: comparison of the two numerical methods NR and GS

Elements of comparison	Comparison between the methods of N.R and G.S
iterations Number	Is greater for G-S than (16) compared to (4) for N-R
convergence Time	For G-S is 0.05seconds and 0.22seconds for N-R
Preference of resolution method	N-R with polar coordinates, G-S with rectangular form.
Other Precision Items	With broader systems larger for N-R than G-S.
Indifferent with slack bus choice	for N-R and for G-S is critical choice
Complex by the Jacobian matrix	The G-S resolution is simpler than N-R

coupling without the need of large external or capacitor banks. The basic voltage source converter diagram is shown in Figure 2.

The Table 5 corresponds to the best choice of STATCOM to optimize the system performance.

3.1. Power Flow Equations of STATCOM Connected to i^{th} bus

Power flow equation of system with STATCOM connected at bus (i) in Figure 1 and is treated as reactive power source:

$$P_i = P_{Gi} + P_{STCi} - P_{Di} \quad (1)$$

$$Q_i = Q_{Gi} - Q_{STCi} - Q_{Di} \quad (2)$$

Hence P_{STCi} – is a STATCOM's active power at bus (i) and Q_{STCi} - is a STATCOM's reactive power at bus (i), Pi – is injected active power at bus (i), Qi – is injected reactive power at bus (i), P_{Di} – is active power demand at bus (i) and Q_{Di} – is a reactive power demand at bus (i), P_{Gi} – is a generator's active power at bus (i), Q_{Gi} – is a generator's reactive power at bus (i).

Equations (1) and (2) represent a case where STATCOM generate reactive power at bus (i) if for reactive power absorption, the signs of Q_{STCi} will be reversed (positive).

The solution of nonlinear power flow equations (1) and (2) is numerical methods. However, the adopted method in this work is the Newton-Raphson (NR). The specifications of this method, its faster rate of convergence and accuracy, when compared with others methods as Gauss-Seidel (GS), coupled NR, decoupled NR or Gauss method. We notice this comparison of NR with Gauss Seidel: NR indifferent for choice of slack bus while GS is critical, the resolution of NR with polar coordinates while GS is with rectangular form, the number of iterations is less for NR (4 iterations) compared with GS (16 iterations), with broader systems larger for NR than GS. So the convergence time is lees for GS (0.05 seconds) than NR (0.22 seconds) and the GS resolution is simpler than NR (see Table 6).

In the Table 6 below is given the comparison of the two best numerical methods. These two are important indicators to analyze the quality of the studied network. And also demonstrates the optimal choice of NR method for our work.

3.2. Modeling of STATCOM

So below is presented the basic schematic and Thevenin's equivalent circuit of STATCOM respectively, the fundamental frequency operation of the switched mode voltage source inverter and its transformer (Figure 2).

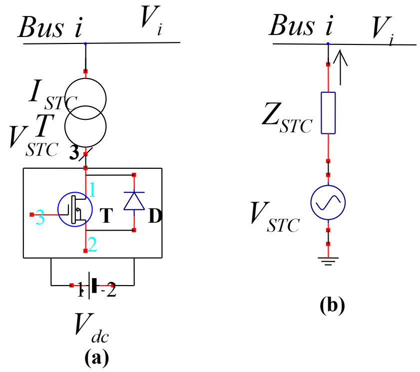

Figure 2: (a) Basic Schematic; (b) Equivalent Circuit [17, 18]

We define STACOM voltage by the equation (3):

$$V_{STC} = V_i + Z_{SC} I_{STC} \tag{3}$$

Hence V_{STC} - is a STATCOM's voltage, I_{STC} - is STATCOM's current, Z_{SC} - is transformer's impedance.

The voltages constraints of STATCOM and at bus (i) are given in equation (4)

$$\begin{aligned} V_{STC(\min)} \le V_{STC} \le V_{STC(\max)} \\ V_{i(\min)} \le V_i \le V_{i(\max)} \end{aligned} \tag{4}$$

Where V_{STC} (min) and V_{STC} (max) are minimum and maximum STATCOM's voltages, V_i (min) and V_i (max) are minimum and maximum voltages values at bus (i).

Equation (3) is transformed into a power flow expression for STATCOM and power injected at bus (i) by equations (5) and (6) respectively:

$$S_{STC} = V_{STC} I^*_{STC} = V_{STC} V^*_{STC} Y^*_{SC} - V_{STC} Y^*_{SC} V_i \tag{5}$$

$$S_i = V_i I^*_{STC} = V_i V^*_i Y^*_{SC} - V_i Y^*_{SC} V^*_{STC} \tag{6}$$

Hence S_{STC} – is a STATCOM's apparent power, I^*_{STC} - is a STATCOM's complex conjugate current, V^*_{STC} - is a STATCOM's complex conjugate voltage, Y^*_{SC} - is a complex conjugate of short-circuit admittance.

The voltages in rectangular coordinates system are expressed as equations (7) and (8) respectively:

$$V_i = e_i + jf_i \tag{7}$$

$$V_{STC} = e_{STC} + jf_{STC} \tag{8}$$

Where e_i – is a active component of voltage at bus (i), f_i - is a imaginary component of voltage at bus (i), e_{STC} – is a active component of STATCOM's voltage, f_{STC} – is a imaginary component of STATCOM's voltage.

The STATCOM's voltage magnitude and angle are expressed as equations (9) and (10) respectively:

$$\begin{aligned} |V_{STC}| = \left(e^2_{STC} + f^2_{STC}\right)^{\frac{1}{2}} \\ |V_i| = \left(e^2_i + f^2_i\right)^{\frac{1}{2}} \end{aligned} \tag{9}$$

$$\begin{aligned} \delta_{STC} = \tan^{-1}\left(\frac{f_{STC}}{e_{STC}}\right) \\ \delta_i = \tan^{-1}\left(\frac{f_i}{e_i}\right) \end{aligned} \tag{10}$$

The active and reactive power components for the STATCOM and bus (i) on the basis of equations (7) to (10) are respectively expressed by equations (11) to (14):

$$P_{STC} = G_{SC}\left\{\left(e^2_{STC} + f^2_{STC}\right) - \left(e_{STC} e_i + f_{STC} f_i\right)\right\} + B_{SC}\left(e_{STC} f_i - e_{STC} f_i\right) \tag{11}$$

$$Q_{STC} = G_{SC}\left(e_{STC} f_i - f_{STC} e_i\right) + B_{SC}\left\{\left(e_{STC} e_i + f_{STC} f_i\right) - \left(e^2_{STC} + f^2_{STC}\right)\right\} \tag{12}$$

$$P_i = G_{SC}\left\{\left(e^2_i + f^2_i\right) - \left(e_i e_{STC} + f_i f_{STC}\right)\right\} + B_{SC}\left(e_i f_{STC} - e_i f_{STC}\right) \tag{13}$$

$$Q_i = G_{SC}\left(e_i f_{STC} - f_i e_{STC}\right) + B_{SC}\left\{\left(e_i e_{STC} + f_i f_{STC}\right) - \left(e^2_i + f^2_i\right)\right\} \tag{14}$$

Where P_{STC} – is a STATCOM's active power, Q_{STC} - is a STATCOM's reactive power, G_{SC} - is a short-circuit conductance, B_{SC} – is a short-circuit susceptance.

The Newton-Raphson set of linearized equations for power flow equations (5), (6), (11) and (12) obtained taken into consideration the modeling of shunt-connected STATCOM at bus (i) is given by equation (15):

$$\begin{bmatrix} \Delta P_i \\ \Delta Q_i \\ \Delta P_{STC} \\ \Delta Q_{STC} \end{bmatrix} = \begin{bmatrix} \frac{\partial P_i}{\partial e_i} & \frac{\partial P_i}{\partial f_i} & \frac{\partial P_i}{\partial e_{STC}} & \frac{\partial P_i}{\partial f_{STC}} \\ \frac{\partial Q_i}{\partial e_i} & \frac{\partial Q_i}{\partial f_i} & \frac{\partial Q_i}{\partial e_{STC}} & \frac{\partial Q_i}{\partial f_{STC}} \\ \frac{\partial P_{STC}}{\partial e_i} & \frac{\partial P_{STC}}{\partial f_i} & \frac{\partial P_{STC}}{\partial e_{STC}} & \frac{\partial P_{STC}}{\partial f_{STC}} \\ \frac{\partial Q_{STC}}{\partial e_i} & \frac{\partial Q_{STC}}{\partial f_i} & \frac{\partial Q_{STC}}{\partial e_{STC}} & \frac{\partial Q_{STC}}{\partial f_{STC}} \end{bmatrix} \begin{bmatrix} \Delta e_i \\ \Delta f_i \\ \Delta e_{STC} \\ \Delta f_{STC} \end{bmatrix} \tag{15}$$

The partial derivatives of the Jacobian matrix are defined as following: (expression (16))

4. Simulations Results

The Table 7 below presents the simulation results of NR with STATCOM. Also presents the best locations at buses.

Table 7: Results of NR with STATCOM

N°	Vpu	δ(°)
1	1	0
2	0,97	-11,1
3	0,99	-3,9
4	0,95	-13
5	1,01	-14,1
6	0,97	-11,1
7	0,98	-9,8

$$\begin{cases}
\frac{\partial P_i}{\partial e_i} = G_{SC}(2e_i - e_{STC}) + B_{SC} f_{STC} \\
\frac{\partial P_i}{\partial f_i} = G_{SC}(2f_i - f_{STC}) - B_{SC} e_{STC} \\
\frac{\partial P_i}{\partial e_{STC}} = -G_{SC} e_i - B_{SC} f_i \\
\frac{\partial P_i}{\partial f_{STC}} = -G_{SC} f_i + B_{SC} e_i \\
\frac{\partial Q_i}{\partial e_i} = G_{SC} f_{STC} + B_{SC}(e_{STC} - 2e_i) \\
\frac{\partial Q_i}{\partial f_i} = G_{SC} e_{STC} + B_{SC}(f_{STC} - 2f_i) \\
\frac{\partial Q_i}{\partial e_{STC}} = -G_{SC} f_i + B_{SC} e_i \\
\frac{\partial Q_i}{\partial f_i} = G_{SC} e_i + B_{SC} f_{STC} \\
\frac{\partial P_{STC}}{\partial e_i} = -G_{SC} e_{STC} - B_{SC} f_{STC} \\
\frac{\partial P_{STC}}{\partial f_{STC}} = -G_{SC} f_{STC} + B_{STC} e_{STC} \\
\frac{\partial Q_{STC}}{\partial e_i} = -G_{SC} f_{STC} + B_{SC} e_{STC} \\
\frac{\partial Q_{STC}}{\partial f_i} = G_{SC} e_{STC} + B_{SC} f_{STC} \\
\frac{\partial Q_{STC}}{\partial e_{STC}} = G_{SC} f_i + B_{SC}(e_i - 2e_{STC}) \\
\frac{\partial Q_{STC}}{\partial f_{STC}} = -G_{SC} e_i + B_{SC}(f_i - 2f_{STC})
\end{cases} \quad (16)$$

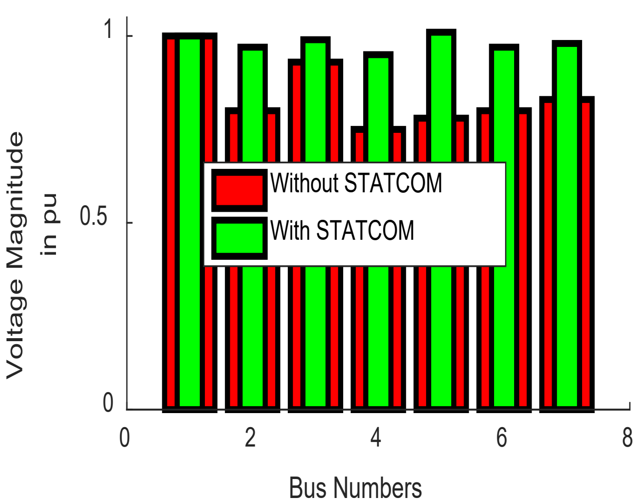

Figure 3: (a) Voltage magnitude as a function of bus numbers

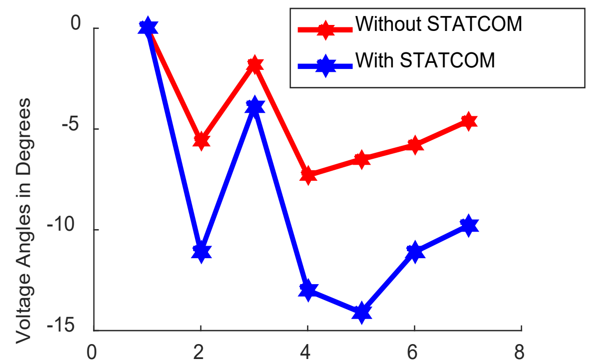

Figure 3 (b): Voltage angle as a function of bus numbers

The voltage magnitude and their phase angle before and after insertion of STATCOM are shown in the figure 3(a) and (b) respectively. It demonstrates the improved values at the following buses: the voltage magnitude for the bus 2 at 0, 80 (value out stability margin) to 0, 97 pu and their angle at -5, 6 to -11, 1 degree. Bus 3 at 0, 93 to 0,99pu and their angle at -1, 8 to -3, 9 degrees. The bus 4 at 0, 75 to 0,95pu and their angle at -7, 3 to -13 degree. The bus 5 at 0, 78 to 1,01pu and their angle at -6, 5 to -14, 1 degree. The bus 6 at 0, 8 to 0,97pu and their angle at -5, 8 to -11, 1 degree. The bus 7 at 0, 83 to 0, 98 pu and their angle at -4, 6 to -9, 8 degrees.

In the Table 8 below is given the simulation results of total power mismatch.

Table 8: Total Power Mismatch

Case	Active Power Losses (MW)	Reactive Power Losses (MVAR)
Without STATCOM	305.7	419
With STATCOM	262.9	360.3

From the Figure 4(a) and (b) below, the power mismatch was reduced at 305, 7 MW to 262, 9 MW for active power losses and 419 MVAR to 360, 3 MVAR for reactive power losses, thereby improving the active power transmission lines.

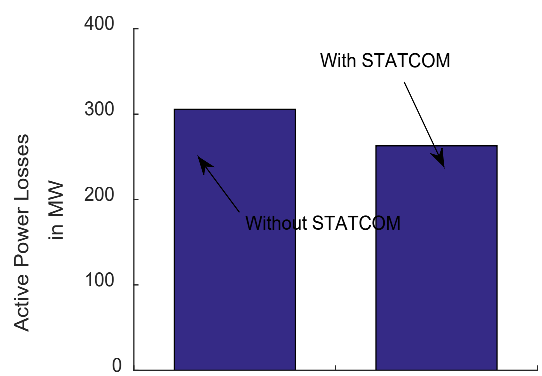

Figure 4: (a) Active Power Losses;

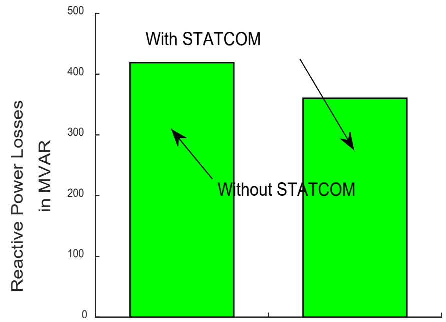

Figure 4 (b): Reactive Power Losses

Table 9: Reached Tolerance in 4 Iterations

N	Without STATCOM		With STATCOM	
It.	ΔV(V)	Δδ(°)	ΔV(V)	Δδ(°)
0	0.18	0.096	0.053	0.249
1	0.06	0.027	0.037	35E-4
2	0.005	0.025	0.001	12E-5
3	4E-5	0	0	0
4	0	0	0	0

From the Figure.7 so below demonstrates the comparison of the voltage errors variation (a) and the delta angle (b) with and without STATCOM connected to the system as a function of iteration numbers.

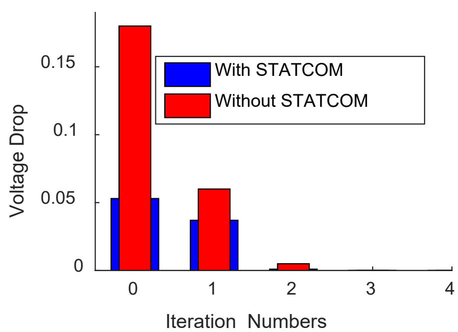

(a)

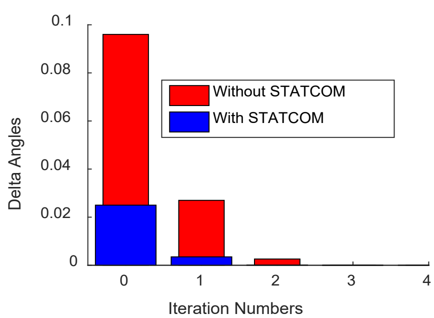

(b)

Figure 5: (a) Voltage drops function of iterations numbers; (b) Voltage angle function of iterations numbers

5. Conclusions

The simulation results of load flow program on PSS/E Simulator using the NR method have been done.

The main information obtained is the stability exceeding limits at all buses voltage of system except the slack bus (Table 4).

After insertion of STATCOM the voltage for all buses has been improved to the stability limit (Table 7).

The voltages at buses (5, 3 and 7) where connected the renewable plants have improved in limit of stability after insertion of STATCOM

The power mismatch was being reduced after insertion of STATCOM (Table 8).

The novelty is that the studied network presents four different sources in Figure 1. This network undergoes very common load shedding. The cause of these load shedding can be due to the load growth at the nodes. But it can be caused by the presence of clouds or when there is no wind to turn the blades, or non-rainy periods in the Sahel countries. In order to remedy this situation of load shedding, STATCOM has been proposed as a solution.

The STATCOM will replace also the conventional system compensation of reactive power (as shunt capacitor or series capacitor…).

The expected disturbances and the poor power quality problems of the studied power system, at 2030 year, were solved by integration of STATCOM that is able generate or absorb reactive power and maintain the voltage at 1pu. The following areas are proposed or put in mind:

Other FACTS controller can also be incorporated along the STATCOM and their effect on the system can be studied [17, 18].

Optimal location of STATCOM can be found out using Genetic Algorithm and fuzzy logic.

Economic Assessment of FACTS devices versus other methods can be studied.

Conflict of Interest

The authors of the manuscript declare no conflict of interest.

Acknowledgment

The author likes greatly thank National Electrical Company of Mauritania (SOMELEC) for providing all system data. I also like to thank the General chair of ISAECT2018, Nabil SRIFI, for extended paper to special issue of Advances in Science, Technology and Engineering Systems Journal (ASTESJ) and all reviewers for their corrections and comments.

References

[1] E. Catz, "Evolutions Techniques du Système de transport et de distribution d'électricité" J3eA, 5(1), pp.01-07, 2006. https://doi.org/: 10.1051/J3ea :20060025.
[2] N. Cherkaoui, T. Haidi, A. Belfqih, F. El Mariami, J. Boukherouaa "A Comparison Study of Reactive Power Control Strategies in Wind Farms with SVC and STATCOM" IJECE, 8(6), pp. 4836~4846. 2018. DOI: 10.11591/ijece.v8i6.pp4836-4846.
[3] R.M. Marco, D.Z. Cruz, Desta, S. F. Fitiwi, S.J. Santos, Silvio, J. P. S. Mariano, P.S. João, "Prospects of a Meshed Electrical Distribution System Featuring Large-Scale Variable Renewable Power " Energies, pp. 01-18, 2018. https/doi.org/: 10.3390/en11123399.

[4] R.A. Jokojeje, I.A, Adejumobi, O.I, Adebisi, Mufutau, "Reactive Power Compensation in Nigeria Electricity Grid Using Static Synchronous Compensator (STATCOM)" IOSR-JEEE, **10**(2), pp. 08-20, 2015. https://doi.org/: 10.9790/1676-10114657.

[5] Z. Rahman, A. Tiwari., "Enhancement of Voltage Profile by Using Static Synchronous Compensator (Statcom) in Power System Networks" S-JPSET, **8**(2), pp. 01–16, 2006. https://doi.org/: 10.18090/samriddhi.v8i2.714410.

[6] N. Mancer, B. Mahdad, K. Srairi., "Multi Objective Optimal Reactive Power Flow Based STATCOM Using Three Variant of PSO" IJEE, **2**(2), pp. 01-07, 2012. https://doi.org/: 10.5923/j.ijee.20120202.01

[7] N. Z. M. Ali, I. Musirin, H. Mohamad, "Effect of SVC Installation on Loss and Voltage in Power System Congestion Management" ijeecs, **14**(1), pp. 428-435, 2019.

[8] T.T. Nguyen, R. Gianto, "Application of Optimization Method for Control Coordination of PSSs and FACTS Devices to Enhance Small-Disturbance Stability," Proc. IEEE PES 2005/2006 T&D Conference and Exposition, 2006.

[9] A.K. Sahoo, S.S. Dash, T. Thyagarajan. "Modeling of STATCOM and UPFC for Power System Steady State Operation and Control". IET-UK ICTES 2007.

[10] R.S. Joel, "Application of FACTS devices for power system transient stability enhancement," Master of sciences, Joma Kenyatta University of agriculture and technology, 2016.

[11] W. C. B. Vicente, "Modélisation des réseaux de distribution sous incertitudes," Thèse de doctorat, Université de Grenoble, 2006.

[12] A. Ahmedi, "Participation des parcs de production éolienne au réglage de la tension et de la puissance réactive dans les réseaux électriques, " Thèse de doctorat, Ecole centrale de Lille, Thèse de doctorat, 2010.

[13] Z. Cabrane, "Gestion et supervision d'un système d'alimentation photovoltaïque avec stockage d'énergie hybride, batteries-supercondensateurs. Application au véhicule solaire, " thèse de doctorat, Université Mohamed V- Agdal, 2017.

[14] G.W. Stagg, A. H. El-Abiad, Computer methods in power systems analysis, Mc Grew Hill international book company: New-York, 1968.

[15] J.G. John, D. William, JR. Stevenson, Power system analysis, Mc Grew Hill, New-York, 1994.

[16] P. Jean, Plan directeur de production et transport de l'énergie électrique en Mauritanie entre 2011-2030, GOPA-International Energy Consultants GmbH Leopoldsweg2, 61348 Bad Homburg, Allemagne ,2011.

[17] J. Wiley, FACTS, Modeling and Simulation in Powers Networks, The Atrium, Southern Gate, Chichester, West Sussex PO19 8SQ, England, 2004.

[18] E. Acha, FACTS modeling and simulation in power networks, John Wiley and Sons, LTD, 2004.

Advances in Science, Technology and Engineering Systems Journal Vol. 4, No. 2, 340-350 (2019)

www.astesj.com

Special Issue on Advancement in Engineering and Computer Science

ASTESJ

ISSN: 2415-6698

Hybrid Technique for Enhancing Underwater Image in blurry conditions

Chrispin Jiji[*,1], Nagaraj Ramrao[2]

[1] *Kalasalingam Academy of Research and Education, Krishnankoil-626126, Tamilnadu, India*

[2] *Department of ECE, The Oxford College of Engineering, Bengaluru-560068, Karnataka, India*

A R T I C L E I N F O

Article history:
Received:03 March, 2019
Accepted:10 April, 2019
Online: 17 April, 2019

Keywords:
Image Restoration
Image Enhancement
Color Adjustment
Hybrid Technique

A B S T R A C T

Enhancing underwater visualization using hybrid technique is generally employed into oceanic production. Through growing oceanic learning, undersea processing has drawn extra importance owing towards necessary task of picture towards attaining data. Although, suitable to reality of dust-like constituent and beam reduction, undersea descriptions continually experience small contrast and color alteration. In this paper, we estimate submerged beam transmission progression also intend an effectual means to defeat the backscatter trouble. Our scheme generally includes three steps; first, we reconstruct the picture using adaptive regularization. Second, we separate the reconstructed picture with weighted decomposition; third, we exploit color adjustment along with dehazed process via gradient guided filter towards holding dual mechanisms independently; at last, re-establish fine effect, we use hybrid technique for enhancing the picture. The tentative outcome illustrates that our proposed process extensively get better quality of unclear submerged descriptions. In common, our proposed method verified as well-performed and effectual than existing technique.

1. Introduction

In the modern years, scientists and researchers have exposed their main concern in capturing the aquatic life beneath the water. Although the statement that 70% of the globe encloses water includes enormous energy, abundant mineral assets and biological resources. The living beneath the water is still not as much look at. Conversely, challenges related by capturing descriptions beneath the water have been complex to defeat, owing to carry-over haze and color cast. The muddy nature of water suitable to process element such as mineral deposits, sand and plankton, showed a huge difficulty in undersea look at region. These elements set up lack of clarity in undersea descriptions which spoils the clearness and ocular analysis of the picture and in turn, inappropriate for any advance use. Researchers have finished that the spreading and absorption property of beam underneath are the chief basis for this deformation [1]. While water is roughly 800 times denser than air, so when beam penetrate from air to water, it come across reflection fact at the surface owing to which only unfair measure of beam go through water. Afterwards the beam undergoes spreading cause when it strikes and element and minerals suspend in water. Scattering diverges the beam in dissimilar directions which diminish the measure of beam falling on the object captured underneath. The end effect of spreading outcome is that the undersea captured descriptions are dim in look [2]. A further problem is causal to lack of clarity of picture that the water molecules take up certain measure of beam when beam hit on them. Because the mass of water is larger than air, it employs dissimilar absorption possessions for diverse beam wavelengths, so the color of undersea descriptions is typically deformed. Generally, red part vanishes first as of its highest wavelength, where blue beam, by small wavelength, convey the greatest path beneath water. Therefore, undersea descriptions are often dominated via blue color. In common, color cast and beam scattering reason deviate color along with contrast degradation into descriptions attained undersea as shown in Figure 1.

In contrast, our system uses dual phases specifically Adaptive Regularization for restoration and Hybrid technique intended for improving its quality. In this work we suggested for merging the thought mainly dictionary knowledge by structural cluster along with picture restoring functions.

Our advance establishes novel regularization to beat a superior stability among local and non-local strength. Generally, our algorithm interprets learning through local and non-local similarity give inference of each picture elements. The restored picture decomposes into dissimilar elements for signifying their

[*]Chrispin Jiji, 8951627124 & chrispinjij@gmail.com

https://dx.doi.org/10.25046/aj040243

basic depiction, later uses diverse development for every part individually along with hybrid technique introduced for rebuilding enhanced picture. The projected process is close towards or even slightly superior to the state-of-the-arts. Tentative results exposed that projected process extensively outperforms many important process in existing arts.

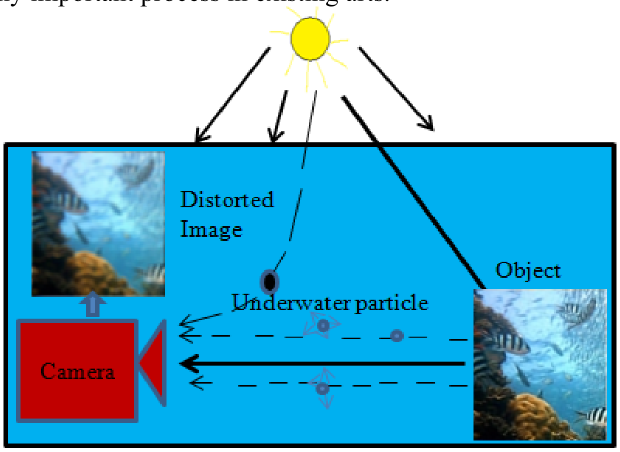

Figure 1: Underwater Imaging System

The summary of this work described as follow. Section 2 portray existing art. Section 3 projects hybrid technique using gradient guided filter for enhancing undersea descriptions. Section 4 illustrates numerical experiments. At last, Section 5 concludes this work.

2. Existing art

Enhancement system for undersea degradation typically explore the undersea optical form and balance bad possessions caused by water along with elements, or simply via undersea processing process for enhancing unclear imagery. State-of-arts are generally considered meant for single image enhancement, since multi-images may limit performance choice, slow down the processing speed. Instinctively, handling this concern well, undersea optical form must consider and investigated at first. Among different undersea imaging methods, the representation method [3], give a complete undersea optical form, within which beam transmission path, beam reduction relation of dissimilar color channel, vertical as well as horizontal deepness of undersea surroundings, non-natural beam possessions and etc are in use. This process is entirely with real form and meet outstanding for a few undersea problems, conversely, its evaluation procedure is difficult and time overwhelming, which is hard to meet, but it gives a full-scale study of undersea surroundings. Fusion-based method, which combines processing outcome by color correction system and histogram equalization method, it also makes a superior outcome for several submerged environments, though, it merely uses scheme of image processing as well as ignoring submarine features, hence ending results undergo more or less fog, data defeat as well as over-enhancement difficulty. To explain these problems well, both processes combined and projected a new method. Semi-inverse approach in [4] employed towards perceiving foggy region and then expected atmospheric rate in plain areas. At last, they meet enhanced picture using a simple weighted fusion.

For few picture, particularly scenes underneath, mist exposure using semi-inverse system will be unsuccessful suitable to the small dissimilarity among true and the inverse picture. This means if hazy region exposure not succeeds and obtains a bad performance. To solve this problem, a simple fusion-based dehazed method using a dissimilar descriptions also resultant from true picture [5], [6]. The primary picture estimate white balance process, and the next input picture through a simple linear change for enhancing contrast of hazy picture. At last, the pixel-fusion scheme uses three weight maps for combining that imagery for enhancing visibility of foggy picture also extended fusion-based scheme [7]. Fusion-based dehazed procedure is easy, speedy as well as meets alike result as the DCP scheme in [8] and [9]. But it is not succeeding when the picture includes inhomogeneous haze. The cause is that this process did not take into account the deepness data of a hazy picture. The dual descriptions attained by gamma correction by various scales for sandstorm enhancement [10]. The enhanced fusion-based approach using various descriptions uses single picture dehazed scheme in [11]. Fusion approach is new and efficient intended for single picture defogging. The primary picture is for enhancing dissimilarity; in addition, later picture mainly for compensating color deformation as well as decrease halo effect plus noise. While above techniques are fast as well as simple, they cannot make excellent picture. Amusingly, the multi-scale progression can be approximated with well-organized and visually satisfying single-scale process [12]. HR fusion in [13] has to be measured as a possible balance, useful to our process when high resolution is required.

The algorithm [14] are effective methods with low computational complexity also great performance, which stretch histograms of picture for improving the dynamic range compress the display area towards enhancing dissimilarity, but these methods often cause over-enhancement, amplify the noise and show poor effect on color correction. Owing towards the drawbacks of single image processing, some relatively complicated methods are proposed. Meanwhile, [15] proposes a retinex-based approach to deal with undersea issues, however, performance of this system is not distinct, color cast as well as contrast degradation still exist. The system may guess a uniform [16, 17] or an extra reasonable non-uniform [18] background-radiance. Enhancement technique eliminates the colour cast [19, 20] with overall white balancing.
This work is extensive to the effort primarily obtained through ICCIC [21]. Moreover, the projected work is for Enhancing Underwater Image in blurry conditions using hybrid technique. Revised outcome much improves lighting plus color cast trouble during submerged descriptions. Excellence process not essential to resolve substantial type of corrupted representation, other than fairly enhances dissimilarity also gets superior picture excellence as individual illustration view. Experimental results show good performance meant for underneath representation.

2.1. Motivation

Underwater distorted descriptions typically to explore optical model also compensating bad effects caused by underwater element uses processing scheme to restore performance of distorted images. The state-of-arts are mostly designed for single-image enhancement, since multi-images may limit performance range and slow down processing speed. Towards handling this problem well, initially we considered Image re-establishment process. The physical system of ocular imaging, reverse

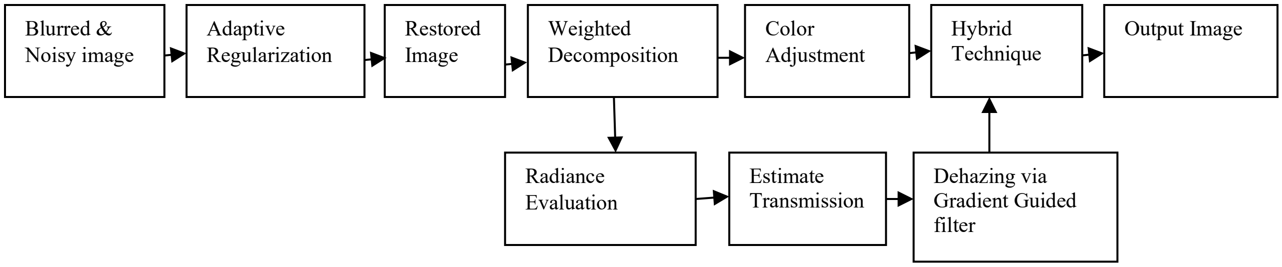

Figure 2: Block diagram of Proposed Method

degradation process and balance distortion to get clear imagery but it has small visibility and color cast problem. Image enhancement process do not get the source of picture degradation into account, but mainly use targeted version to get better dissimilarity, detail, and ocular possessions. It provides complete undersea ocular form, where the illuminated transmission path, beam reduction of dissimilar color path taken into concern totally based on physical model and achieves excellent for some underwater backscatter issues. However, its evaluation development is difficult and time-consuming, but it gives full-scale analysis of undersea situation. To enhance dissimilarity, visibility, color spread of restored imagery, fusion-based model which boost picture by fusing several input imageries have received much attention. The processing results by color constancy and dehazed algorithm, generates good results. However, it only uses technique of image processing and so its results suffer from more or less haze, information failure as well as over-enhancement problem.

In order to solve this issue well, we proposed a Hybrid Technique for Enhancing Underwater Image in blurry conditions by joining dehazed technique via gradient guided filter with color balance of the restored imagery.

3. Proposed Method

As depicted in Figure 2 our new scheme primarily to Enhance Undersea picture in blurry conditions using hybrid technique. Initially, we recreate the picture using adaptive regularization. Secondly, we split reconstructed picture using weighted decomposition. Thirdly, improve contrast and texture information using Dehazing via gradient guided filter. Here we estimate global radiance by obtaining average rate vector as brightest rate, transmission map evaluation mainly for enhancing texture feature. Fourth, a color adjustment towards enhancing color. At last, we used hybrid technique for obtaining better picture by computing the mechanisms of dual weights in addition to efficient.

3.1. Adaptive Regularization for Restoration

For an image $d \in P^{HXW}$, we believe patch based depiction $d_m = Pd \in P^N$, $m = 1,2,.....N$ where P indicates a parameter to extract patch d_m as of d. Suppose a known dictionary φ_m meant for d_m, we get $d_m = \varphi_m \alpha_m$ entails α_m as sparse depiction of d. In particular, restoration describes

$$D = \left(\sum_{i=1}^{N} P_i^T P_i\right)^{-1} \left(\sum_i P_i^T d_i\right) \tag{1}$$

The iterative shrinkage key towards l1-estimation is widely used in previous art. Since the evaluation of $\hat{d}$ get simplified by convergence, trained by a novel dictionary. At present let us include adaptive regularization term [22, 23]. For every patch d_m k-nearest-neighbors patch signify $d_m^{(1)},.....d_m^{(k)}$. The weighted guess is representing

$$d_i^{\wedge} = \sum_{t=1}^{k} w_{m,t} D_i^{(t)}, w_{m,t} = \exp\left(-\left\|D_m - D_m^{(t)}\right\| / h\right) \tag{2}$$

where h stands for constant to manage the window. Since (2) local form by picture roughly considered with

$$D_L(d) = \sum_{m=1}^{M} \left\| d_m - a_{k_m}^T \chi_m \right\|_2^2 \tag{3}$$

In matrix type (3) represents

$$D_L(d) = \sum_{m=1}^{M} \left\| (I - V) d_m \right\|_2^2 = \left\| (I - V) \varphi\alpha \right\|_2^2 \tag{4}$$

where I specify identity matrix and

$$V(m,n) = \begin{cases} a_i, if\ d_n \text{ is an element of } \chi_m, a_m \in a_{k_m} \\ 0, \text{ otherwise} \end{cases} \tag{5}$$

It follows from (2) that the nonlocal similarity in a picture roughly considered through

$$D_{NL}(d) = \sum_{m=1}^{M} \left\| d_m - \sum_{t=1}^{k} w_{m,t} d_m^{(t)} \right\|_2^2 \tag{6}$$

which can be written more efficiently in a matrix type as

$$D_{NL}(d) = \sum_{m=1}^{M} \left\| (I - W) d_m \right\|_2^2 = \left\| (I - W) \varphi\alpha \right\|_2^2 \tag{7}$$

Where I stands for the identity and

$$W(m,l) = \begin{cases} b_i^l, if\ d_m^l \text{ is an element of } \beta_m, b_m^l \in b_m \\ 0, \text{ otherwise} \end{cases} \tag{8}$$

Joining (4) and (7), we have the next novel regularization as

$$\hat{\alpha} = \arg\min\left\{ \left\| d - H\varphi\alpha \right\|_2^2 + \sum_{m=1}^{M}\sum_{n=1}^{N} \lambda_{mn} \left|\alpha_{m,n}\right| \right\} + \gamma \left\| (I - V)\varphi\alpha \right\|_2^2 + \eta \left\| (I - W)\varphi\alpha \right\|_2^2 \tag{9}$$

where a novel regularization factor η manage stability among local variation with nonlocal strength. The nonlocal regularization term not only imposes nonlocal similarity however as well not directly assist the evaluation of signal variance essential with λ_{mn} as $\lambda_{mn} = \frac{2\sqrt{2}\sigma_w^2}{\left|\hat{\sigma}_{m,n}\right| + \varepsilon}$ where $\sigma_{m,n}$ and σ_w signifies the variance of signal and noise correspondingly.

3.2. Weighted Decomposition

Weighted decomposition used to separate imagery into various parts and then perform several schemes according to their characteristics. Techniques like wavelet transform and weighted decomposition are most well-liked process. Former scheme is time consuming and cannot take out the characteristics. Later on initiate a weighted decomposition means, which divide true picture into dual part, one conveys the illuminant part as another states the reflectance part of picture as:

$$I_c(d) = I_c^R(d) + I_c^I(d) \tag{10}$$

where $c \in \{r, g, b\}$ signifies every color part of picture, $I_c^R(d)$ denotes reflectance part and $I_c^I(d)$ represents illumination part.

$$I_c^R(d) = \Upsilon . I_c(d) \tag{11}$$

$$I_c^I(d) = (1 - \Upsilon) . I_c(d) \tag{12}$$

where Υ denotes weighted factor which improve the dissimilarity of reflectance part for removing backscatter as

$$\Upsilon = \xi . \frac{I_c(d)}{I_c^{\max}} \tag{13}$$

Where $I_c^{\max}$ denotes maximal pel rate of color, ξ signify a direct cause by resolving reflectance weight, $\xi \in (0,1)$, if $\xi = 0$, the entire picture treated as illuminate part, while $\xi = 1$, the entire picture is denoted by reflectance part.

The backscatter outcome simply exists with illuminate part, whereas reflectance part simply experiences as of color deformation.

3.3. Radiance Evaluation

To approximate background beam, a supreme approach is to select a picture element, while color deformation and dissimilarity degradation are distance dependent. Though, in this system, scenes are vivid than surrounding beams, may perhaps an unwanted collection outcome. To get precise outcome, we exploit a hierarchical searching means using quad-tree subdivision [24]. Initially, the picture broken up into four identical rectangular areas, after that used for all area by estimating mean rate subtracted from standard deviation as

$$Score_l = \frac{1}{3N} \sum_{c \in \{r,g,b\}} \sum_{d=1}^{N} I_l^c(d) - \frac{1}{3} \sum_{c \in \{r,g,b\}} \sqrt[2]{\frac{\sum_{d=1}^{N} \left(I_l^c(d) - \bar{I}_l^c \right)^2}{N}} \tag{14}$$

Where $l = 1, 2, 3, 4$ stand for four image areas, N denotes the picture element number contained by the area, $I_l^c(d)$ signifies picture element of d rate c section in l area, $\bar{I}_l^c$ represents mean picture element rate of c part in l area. Later, we choose the area by least variance, as well as split into quadrant areas. This procedure continues until the size is smaller than threshold. The average rate attained as surrounding beam and considered as brightest rate with the complete representation.

3.4. Estimate Transmission

The transmission rate cannot be selected randomly; dissimilarity improvement with data defeat lessening must chose keen on concern. First, dissimilarity improvement cost task, E_c, with data loss cost task E_i reduce dual function concurrently, while dissimilarity improvement cost as negative summation of C_{MSE} of every color channels, furthermore data defeat cost as summation of square of reduced picture elements as

$$E_c = -\sum_{c \in \{r,g,b\}} \sum_{d=1}^{N} \frac{\left(J_c^T(d) - \bar{J}_c^T \right)^2}{N} = -\sum_{c \in \{r,g,b\}} \sum_{d=1}^{N} \frac{\left(I_c^T(d) - \bar{I}_c^T \right)^2}{N . t(d)^2} \tag{15}$$

$$E_i = -\sum_{c \in \{r,g,b\}} \sum_{d=1}^{N} \left\{ \left(\min\left\{0, J_c^T(d)\right\} \right)^2 + \left(\max\left\{0, J_c^T(d) - 255\right\} \right)^2 \right\} \tag{16}$$

At last, for every local region the best transmission rate $t(d)$ is approximated by reducing the later task as,

$$E = E_c + \gamma . E_i \tag{17}$$

where γ denotes weighted factor to organize the control of data loss cost.

3.5. Dehazing via Gradient Guided Filter

The Guided filter in [25] refine transmission map but cannot signify fine next to a few boundaries. While there might be a few halos in the descriptions. The halos decrease the visual excellence of the resultant descriptions. Hence Gradient guided filtering is an effectual and process transmission map, use input picture as guidance can have executed by linear system as

$$(L + \lambda . U) . t = \lambda . \tilde{t} \tag{18}$$

where L represents matting Laplacian matrix, U denotes identity matrix, and λ signify regularization factor. The Laplacian matrix represents

$$L_{ij} = |\omega|\left(\delta_{ij} - W_{ij}\right) \quad (19)$$

where $|\omega|$ stands for number of picture elements in a block, δ_{ij} denotes Kronecker delta, and W_{ij} represents gradient guided filter [26] kernel weight as:

$$W_{ij} = \frac{\left(\chi\left(D^{'}\right)+\varepsilon\right)}{mn}\sum_{p}^{m}\sum_{p}^{n}\frac{1}{\chi\left(D^{'}\right)+\varepsilon} \quad (20)$$

where $\chi\left(D^{'}\right)=\sigma_{G,1}\left(D^{'}\right)\sigma_{G,\xi_1}\left(D^{'}\right)$, ξ_1 denotes dimension of filter and D signify guidance picture.

To reach a precise transmission map as well as fine points, the advanced diffusion map split up into smooth and detailed part as

$$t = t_{smooth} + t_{\det ail} \quad (21)$$

where t_{smooth} signify smooth part of transmission map while $t_{\det ail}$ denotes detailed part. For smooth part, we obtain Gaussian low-pass filter as effective smoothing filter, and denoted as:

$$G(d,b) = \frac{1}{2\pi\sigma^2}.e^{\frac{\left(d^2+b^2\right)}{2\sigma^2}} \quad (22)$$

where σ denotes scale factor of Gaussian blur. Therefore, the smooth and detailed part can estimate as

$$t_{smooth} = t * G \quad (23)$$

$$t_{\det ail} = t - t_{smooth} \quad (24)$$

Following, the improved transmission map evaluated as:

$$t_{enhanced} = t_{smooth} + \alpha.t_{\det ail} \quad (25)$$

where α represents the enhancement factor to manage the improved measure of detailed part.

3.6. Color Adjustment

The reflectance part returns the texture and fine points of submerged picture, and only undergoes color deformation caused with energy absorption underneath. Simplest color adjustment [27] is an outstanding means for confirming vast stability among adjustment concert in addition to data loss. The energy absorption in undersea causes color distortion. To overcome this problem, simplest color balance scheme for only extend the picture element of color means whereas conserve data as much as probable with physically set dissimilar truncation relation of color channel, so their histograms are capable towards maximum range [0,255]. For quick stretch, apply an affine transform function on each color channel for mapping picture element from 0 to 255. Though, only some unusual pels previously map most and least standards, for improving color act with small picture element by peak and least rates prior to affine transform task. In fact, this procedure source extra or less white and black area may seem to be not natural. In general, this algorithm not focuses for proper color allotment, but give color adjustment with contrast to some degree.

3.7. Hybrid Technique

A hybrid technique mainly combines dual imagery to generate clear representation. The vital task is mainly for computing weight maps of descriptions furthermore joins them mutually by luminance, saliency along with exposedness weight map for deriving normalized weighted maps [28].

Luminance weight map [29] represents luminance factor of every picture part, created with computing STD among color channels along with luminant rate, where luminant rate l represents:

$$l = \alpha.r + \beta.g + \gamma.b \quad (26)$$

where $\alpha+\beta+\gamma=1$, each denotes weight constraint of color part.

It is capable for exactly reflect luminant measure of picture and illustrate better improvement; it confirms negative possessions on contrast and colourfulness. Headed for avoiding these, introduces successive weight maps.

Saliency weight-map [30], reflects salient things and points, intends to highlight this discerning submerged sight. Main drawback is for overestimating important area, as a result exposedness weight-map exploits to assure precision as well as defend middle color in picture.

Exposedness weight-map [30], assess significance of exposed picture elements. It protects local dissimilarity be non-exaggerated or non-understated. In general, picture element rates close to average rate are likely to have superior look. Gaussian-modelled remoteness to average rate represents

$$W_E = e^{-\frac{\left(I(d)-\bar{I}\right)}{2\sigma^2}} \quad (27)$$

where σ denotes standard deviation, $I(d)$ signify pel rate set at location d and $\bar{I}$ represent mean rate. As a result, the entire weight maps proficient for generating fine look for output imagery. The normalized weight map is simply computes:

$$W_{norm} = \sum_{k=1}^{K} W_k \quad (28)$$

where W_k specify the kth weight map.

The last free backscatter and color deformation picture be derived as:

$$R_c = \sum_{n=1}^{N} W_{norm}^{n}.J_c^{n} \quad (29)$$

where R_c denotes color part of fused image, J_c^n signifies color part of n[th] input. To get enhanced output, we basically exploit a multi-scale pyramid decomposition system for achieving fusion technique. The joint development represents

$$R_c^l = \sum_{n=1}^{N} G^l\left\{W_{norm}^{n}\right\}.L^l\left\{J_c^{n}\right\} \quad (30)$$

where $L^l\left\{J_c^n\right\}$ denotes Laplacian pyramid of color part of n^{th} input representation, $G^l\left\{W_{norm}^n\right\}$ is n^{th} stabilized weight map and l represents pyramid stages. While this scheme achieves quite rapid with the enhanced output image can make excellent result.

4. Experimental Results and Analysis

The projected technique evaluates the state-of-art processes; by imagery composed as of representational undersea test imagery and dissimilar metrics utilized to compare enhancement performances of these processes.

4.1. Qualitative Evaluations

To verify the effectiveness adaptive regularizations, we primarily use reconstruction outcome taking place in picture *seer* with projected technique in Figure 2. Adaptive regularization shows improved results to remove ringing artifacts near boundaries. The projected technique in Figure 3 composed of adaptive regularization to reconstruct the imagery, weighted decomposition process to separate illuminant and reflecting part. The illuminant part is to improve contrast and texture details using dehazing via gradient guided filter. The reflecting part is to enhance color using color adjustment. Finally, Hybrid technique used to enhance the result. As of Figure 4 weights of dual mechanisms applies a proficient technique for attaining excellence picture. In order to represent different features, we used numerous weight map process to compute the descriptions of true imagery and then join to obtain normalized weight maps. Evaluation of a projected scheme with existing technique shown in Figure 5. The scheme in [21] better reconstructs the picture but fails to enhance its visibility. The scheme in [14] fails to correct and enhance visibility of degraded picture, amplify noise as well as show poor effect on color adjustment. The process in [15] over-enhance distorted picture, which causes severe, color distortion along with noise amplification, thus integral performance of enhanced picture is worse. The scheme [30] gets good result, not only correcting the color casting but also enhancing the contrast for removing haze. Though, dissimilarity is overstretched in [24], a few picture elements reduced using over-flow or under-flow. The over-enhancement problem in [25] for test images and some information loss exist as well as in boundary effect due to guided filter introduced. Our projected technique is close towards or even somewhat improved than state of the arts. The RGB color space of dissimilar patch dimension in Figure 6 attains fewer pel map result. Moreover, RGB color space in Figure 7 of original imagery with improved results that all the pels of original picture maps into RGB color space gather in left corner, where is large green rate and small blue and red rate, and other method make more or less stretch of the pixel mapping results. The mapping outcome of our scheme is most excellent and it maps the largest area in the RGB color space, which means it has the best integral dynamic compression range. However, many mapping pixels of our method mapped the boundary, i.e., dark region and brightest region, it indicates that there is information loss of our method.

4.2. Quantitative Evaluations

The submerged quality metrics for evaluating and analyzing excellence of underneath imagery, including gray mean, standard deviation, mean gradient etc. The gray mean rate of an image reflects integral intensity, and higher the gray mean is, higher the intensity is, while standard deviation of a picture reflects high frequency part of a picture, which relates picture contrast, higher the standard deviation is, higher the contrast is as well as greater color data. Meanwhile, [31] show that a picture shows good integral quality when gray mean among 100 and 200 and its standard deviation among 35 and 80 after they analyzed and statistic a large measure of imagery. Mean gradient reflects speed of the changes of minor details in picture; it can represent the features of texture transform and the degree of clearness well. Table 1 review metric outcome for reconstruction used for different patch dimension also patch by small dimension offer better result. Following, Table 2 achieves best results in [15], μ_{RG} and $\boldsymbol{\mu_{YB}}$ which are close to zero. The largest $\boldsymbol{\sigma_{RG}}$ in [25], largest $\boldsymbol{\sigma_{YB}}$ in original imagery. Overall, our method obtains the highest score after computing the PSNR, SSIM, UICM, UIConM and UIQM value, lowest score in SSIM. Consequently, projected system is better than existing system giving enhanced outcome.

$$Mean = \frac{1}{UV}\sum_{u=1}^{U}\sum_{v=1}^{V}E(u,v) \tag{31}$$

$$\sigma^2 = \frac{1}{UV}\sum_{u=1}^{U}\sum_{v=1}^{V}\left\{E(u,v)-Mean\right\}^2 \tag{32}$$

$$AG = \frac{1}{UV}\sum_{u=1}^{U}\sum_{v=1}^{V}\sqrt{\frac{\left[E(u,v)-E(u+1,v)\right]^2+\left[E(u,v)-E(u,v+1)\right]^2}{2}} \tag{33}$$

Where σ^2 denotes standard deviation, *Mean* represents mean picture element, *AG* represents mean gradient and *UV* signify amount of picture elements. Efficient metric UIQM composed of three independent measurements [32-34] as described below.

a) Undersea Image Colorfulness Measurement (UICM)

The performance of color correction used for evaluating performance of undersea picture improvement progression, with red-green (rg) along with yellow-blue (yb) color parts are used:

$$rg = r - g \tag{34}$$

$$yb = \frac{r+g}{2} - b \tag{35}$$

Considering that submerged picture often suffers heavy noise, the asymmetric alpha-trimmed statistical standards [35] used for measuring submerged picture colorfulness,

$$\mu_{rg} = \frac{1}{N-T_L-T_r}\sum_{x=T_L}^{N-T_r} Intensity_{rg}(x) \tag{36}$$

where N signify total number of pels in the rg part and all pels sorted as $x_1 < x_2 < ..... < x_N, T_L = \alpha_L N$ and $T_r = \alpha_r N$ are the amount of least and most picture element to be reduced as of sorted order $x_1 < x_2 < ..... < x_N$. The average rate μ_{rg} corresponds to chrominance gray, and average rate close towards nil in rg-yb color part imply superior for balancing color. Further, the second-order statistic variance is defined by:

$$\sigma_{rg}^2 = \frac{1}{N}\sum_{x=1}^{N}\left(Intensity_{rg}\left(x\right)-\mu_{rg}\right)^2 \qquad (37)$$

σ_{rg}^2 represents the pixel activity. The first and second order statistic information μ_{yb} and σ_{yb}^2 of the yellow-blue part be computing in similar way. The whole, colorfulness coefficient parameter is expressed as

$$UICM = -0.0268.\sqrt[2]{\mu_{rg}^2+\mu_{yb}^2} + 0.1586.\sqrt[2]{\sigma_{rg}^2+\sigma_{yb}^2} \qquad (38)$$

b) Undersea Image Sharpness Measurement (UISM)
Sharpness reflects details and edges of an image, and fine captured images are likely to show better sharpness. For more efficient, enhancement measure estimation (EME) as

$$EME = \frac{2}{s.t}\sum_{K=1}^{s}\sum_{L=1}^{t}\log\left(\frac{I_{\max,K,L}}{I_{\min,K,L}}\right) \qquad (39)$$

where picture divided by $s.t$ blocks, and obtain the maximal and minimal pel values in each block, $\frac{I_{\max,K.L}}{I_{\min,K,L}}$ indicates comparative dissimilarity relation in every block. Then the undersea image sharpness measure (UISM) can be written as:

$$UISM = \sum_{c=1}^{3}\lambda_c.EME\left(grayscale\ \text{edge}_c\right) \qquad (40)$$

where λ_c stands for weight coefficient of each color part.

c) Undersea Image Contrast Measurement (UICM)
Intended for submerged descriptions, dissimilarity Distortion is usually happened with backscattering. The contrast performance be measured by:

$$\log AMEE = \frac{1}{s.t}\sum_{K=1}^{s}\sum_{L=1}^{t}\frac{I_{\max,K,L}-I_{\min,K,L}}{I_{\max,K,L}+I_{\min,K,L}}.\log\left(\frac{I_{\max,K,L}-I_{\min,K,L}}{I_{\max,K,L}+I_{\min,K,L}}\right) \qquad (41)$$

and submerged picture contrast measure be written as:

$$UIConM = \log AMEE\left(\mathrm{I}ntensity\right) \qquad (42)$$

d) Undersea Image Quality Measurement (UIQM)
Undersea descriptions modelled as linear superposition of absorbed as well as spreaded part. Meanwhile, absorption and scattering by dusk-like particles causes color casting, sharpness attenuation with dissimilarity distortion. Consequently, logical use of linear form to create entire UIQM as:

$$UIQM = \alpha.UICM + \beta.UISM + \gamma.UIConM \qquad (43)$$

where α , β , and γ signifies weight coefficients to organize each measure as well as balance their values.

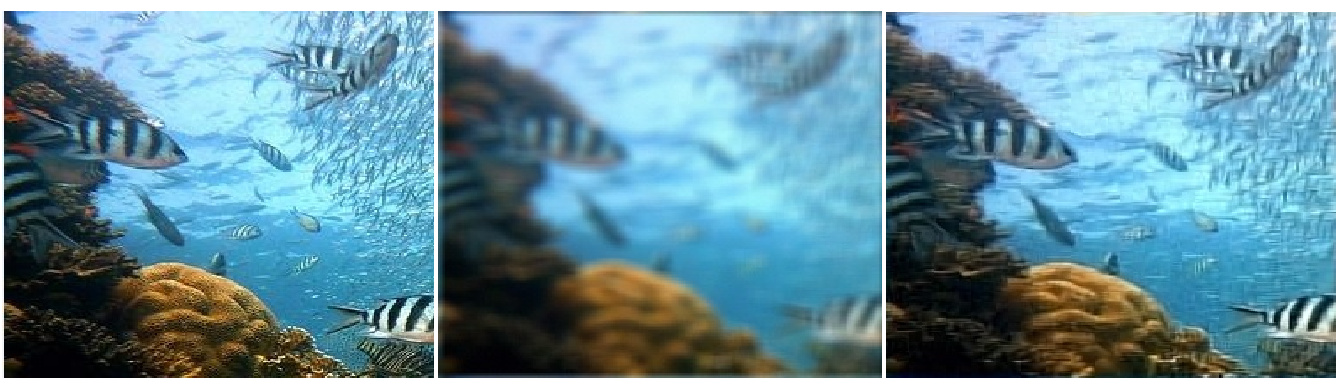

a) True Picture b) Blurred c) Restored Picture

a) Reconstructed Image b) Reflectance c) Color Balance f) Final Output

d) Illuminance e) Dehazing viagradient guided filter

Figure 3: Results on the process of Proposed Method

a) Luminance weight 1 b) Saliency weight 1 c) Exposedness weight 1 d) Normalized weight 1

e) Luminance weight 2 f) Saliency weight 2 g) Exposedness weight 2 h) Normalized weight 2

a) [21] b) [14] c) [30] d) [24]

e) [15] f) [25] g) Ours

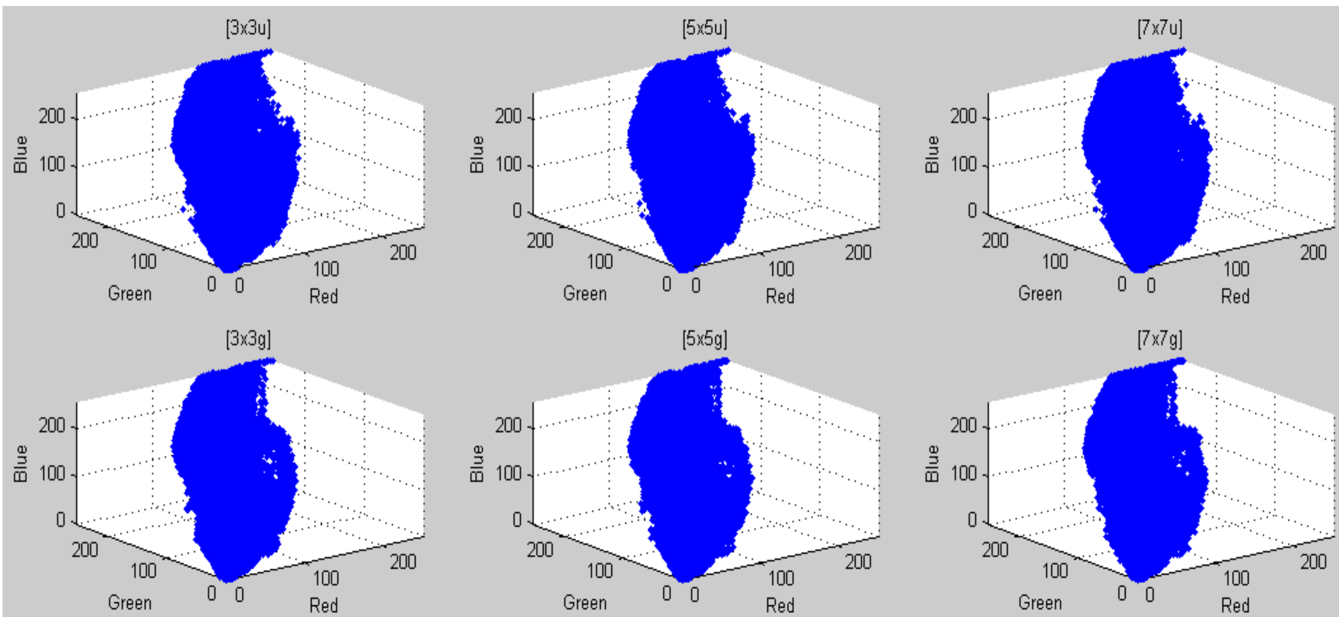

Figure 6: RGB color space mapping reconstruction results on seer image

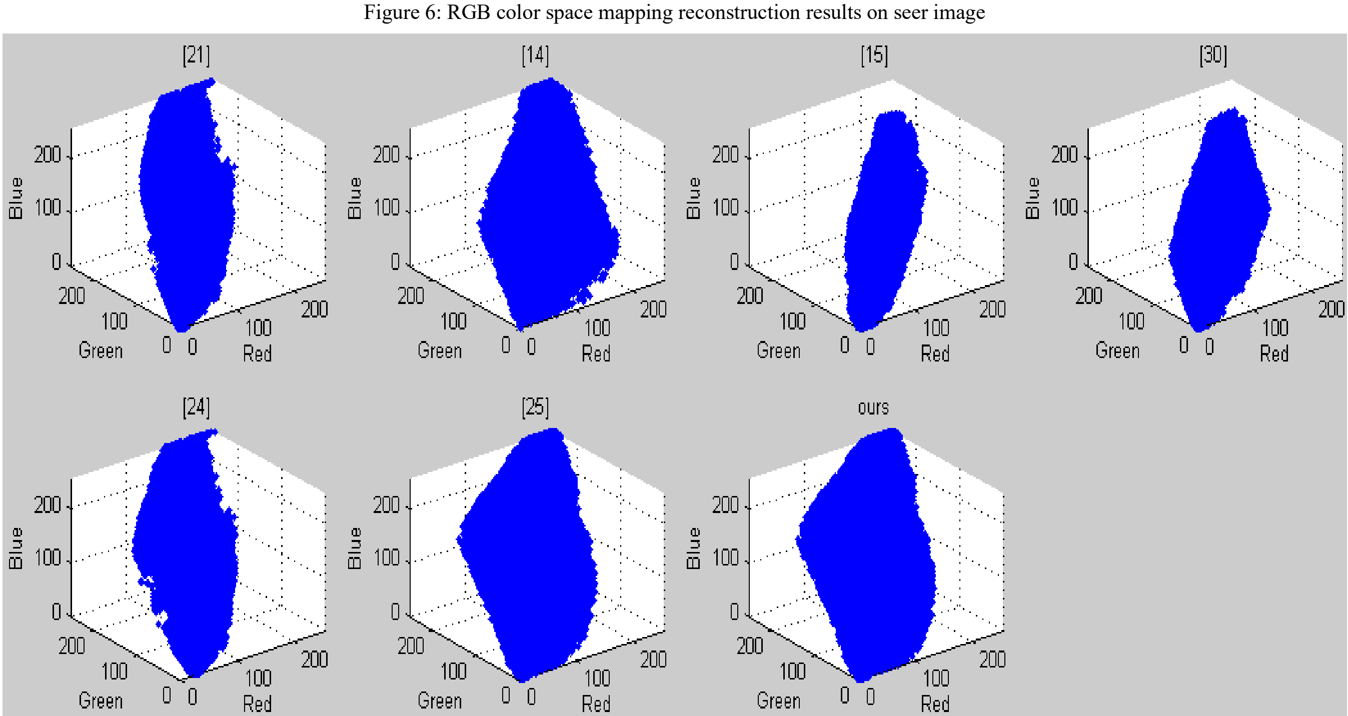

Figure 7: RGB color space mapping Enhancement results on seer image

Table 1: Reconstruction metric results of seer image

	Uniform blur			Gaussian blur		
	7x7	**5x5**	**3x3**	**7x7**	**5x5**	**3x3**
Mean	127.33	127.35	127.36	127.35	127.37	127.37
SD	71.266	71.184	71.136	70.148	70.065	70.027
AG	9.767	8.910	8.476	6.721	6.262	6.129
PSNR	26.16	26.28	26.35	23.96	24.04	24.05
RMSE	17.827	17.469	17.270	13.689	13.320	13.169
SSIM	0.741	0.754	0.756	0.618	0.623	0.622
μ_{RG}	-45.531	-45.543	-45.558	-45.535	-45.538	-45.537
μ_{YB}	27.93	27.92	27.906	27.734	27.73	27.729
σ_{RG}	-41.214	-41.311	-41.352	-41.272	-41.326	-41.34
σ_{YB}	27.004	27.038	27.052	26.892	26.91	26.918
UICM	-45.531	-45.543	-45.558	-45.535	-45.538	-45.537
UIConM	0.745	0.737	0.736	0.716	0.704	0.704
UISM	7.059	6.890	6.906	6.512	6.276	6.244
UIQM	3.467	3.388	3.389	3.199	3.0891	3.080

Table 2: Enhancement metric results of seer image

	Original	**[21]**	**[14]**	**[30]**	**[24]**	**[15]**	**[25]**	**Ours**
Mean	127.39	127.34	129.26	104.05	128.99	103.41	136.21	**136.21**
SD	66.272	71.236	68.047	56.586	70.056	64.509	82.112	**83.494**
AG	3.790	9.226	**15.819**	11.89	9.326	8.660	12.212	12.517
PSNR	21.53	24.10	27.670	28.483	16.557	28.073	30.004	**30.013**
RMSE	21.369	13.717	10.544	9.602	37.900	10.022	8.059	**8.052**
SSIM	0.466	0.619	0.724	0.786	0.839	0.765	0.841	**0.842**
μ_{RG}	-45.685	-45.533	-4.937	-24.524	-33.344	**-0.960**	-37.795	-37.801
μ_{YB}	-41.664	-41.224	-13.078	-25.712	-36.852	**-1.732**	-35.456	-35.472
σ_{RG}	27.789	27.93	22.343	23.581	33.732	11.964	**29.896**	29.888
σ_{YB}	**27.155**	27.016	20.332	22.625	30.378	9.647	26.214	26.226
UICM	4.505	4.516	-4.937	4.223	-33.344	-0.960	4.917	**4.917**
UIConM	0.621	0.741	0.836	0.827	0.790	0.872	0.480	**1.0318**
UISM	5.771	7.005	**7.132**	7.055	7.003	6.911	7.013	6.997
UIQM	2.637	3.434	4.957	4.3512	3.952	5.132	2.723	**4.689**

5. Conclusion and Future Work

This work is mainly for Enhancing undersea representation in blurry conditions using Hybrid technique. Our scheme composed with Adaptive regularization for recreation, weighted decomposition procedure to separate recreated imagery into color change along with dehazed schemes separately, then multi-scale fusion technique towards enhancing picture. The strong with effective Hybrid technique which incorporate the description of all fused imagery into resultant outcome constitute backbone of projected scheme. In fact, the projected scheme generally beats other methods in terms of qualitative as well as quantitative evaluations. Our technique confirms excellent act for undersea imagery, but border effect cause data loss. Meantime, our technique does not outperform some of the state-of-art system and even direct over improvement for precise cases. The challenging work for future would be to find out a well-organized means to about vertical deepness and optimize the transmission deepness of undersea imagery more precise, at last build up absolute, effective and well-organized system.

Conflict of Interest

The authors declare no conflict of interest.

Acknowledgment

The authors thank the reviewers for their thorough and helpful remarks.

References

[1]. Ruo W, Yaf W, Jun Z, Xianp F. "Review on Underwater Image Restoration and Enhancement Algorithms", 7th Intern Confrnc on Intrnt Multimedia Comput and Serv ACM, 2015.

[2]. Schetni R, Cors S. “Underwater Image Processing: State of the Art of Restoration and Image Enhancement Methods”, EURASIP Jrn Advn sgnl Pr, Jan 2010.
[3]. John C, Yin C.C. Underwater Image Enhancement by Wavelength Compensation and Dehazing, IEEE Transc Img Pr-2012.
[4]. C. Ancut, Hermns, and Beka, “A Fast Semi Inverse Approach to Detect and Remove the Haze from a Single Image',' *Comp Vis*: Springer, Nov2011
[5]. O. Ancu, C. Anc, and Bekae,” Effective Single Image Dehazing by Fusion," *Procd IEEE Intr. Confr. Img Proc*, Sep-2010.
[6]. Ancut and Ancut C, ``Single Image Dehazing by Multi-Scale Fusion," *IEEE Transct Img Proc*, Aug-2013.
[7]. C. O. Ancu, T. Habe, and Bekae, “Enhancing Underwater Images and Videos by Fusion," *Proce. IEEE Confrn. Comp. Visn. Pattrn Recogn,* Jun. 2012.
[8]. K. Hem, Jia S, and Xiao T, “Single Image Haze Removal using Dark Channel Prior,”, *IEEE Transc. Patrn Analy. Macnn*, Dec. 2011.
[9]. Raan F, “Single Image Dehazing”, *ACM -Transc Graphic*, Aug- 2008.
[10]. Xue F, Yu H, Del Z, Xia P and Xing D, “A Fusion-based Enhancing Approach for Single Sandstorm Image”, *IEEE Intrn. Wrkshp Mult S/gl Proc*, Sept-2014.
[11]. Fan G, Jin T and Zix C, “Fusion Strategy for Single Image Dehazing”, *Intrn. Jrn. Dig. Contt Techl. App*, Jan. 2013.
[12]. C. O. Ancuti, C. Ancuti, C. De Vleeschouwer, and A. C. Bovik, “Single-scale fusion: An effective approach to merging images,” *IEEE Trans. Image Process.*, vol. 26, no. 1, pp. 65–78, Jan. 2017.
[13]. H. Lu, Y. Li, S. Nakashima, H. Kim, and S. Serikawa, “Underwater image super-resolution by descattering and fusion,” *IEEE Access*, vol. 5,pp. 670–679, 2017.
[14]. Zuiderv K., “Contrast limited adaptive histogram equalization”, pub book Graphcs gem IV, 1994.
[15]. Fu X, Zhug P, Huang Y, Yin L, Xia P and Xing D, “A Retinex-based Enhancing Approach for Single Underwater Image”, Img Procd IEEE Intrl Confr, 2014.
[16]. Emb S., Chi L., Cava A, “Underwater image and video dehazing with pure haze region segmentation”, Comp Vis and Im Unde, 2018.
[17]. Peng Y, Cos P,”Underwater image restoration based on image blurriness and light absorption”,IEEE Tran on Im Pro, 2017.
[18]. Li C, Cava, “Background light estimation for depth-dependent underwater image restoration”,IEEE Intl Conf on Ima Processg, 2018.
[19]. AncuC., Ancut., D Vlee, Bekt, P, “Color balance and fusion for underwater image enhancement” IEEE Transa Imge Pro, 2018.
[20]. Ber D., Trei T., Avid S, “Diving into haze-lines: Color restoration of underwater images”, Brith Mach Visn Confer, 2017
[21]. Chrispin jiji and Nagaraj Ramro “Deblurring Underwater Image Degradations based on Adaptive Regularization” IEEE Inter Conf on Computat Intelli and Comput Rese, 2017
[22]. Weis D, Guang S, Xi L, Lei Z and Xiaol, “Image Reconstruction with Locally Adaptive Sparsity and Nonlocal Robust Regularization”, S/gl Procg: Imag Comn, Nov-2012.
[23]. Dong, Zhan, Gua S and Xiaoli, "Image Deblurring and Super Resolution by Adaptive Sparse Domain Selection and Adaptive Regularization", IEEE Transa Ime Proces, July 2011.
[24]. Kwa K, Wo J , You S “Optimized Contrast Enhancement for Real Time Image and Video Dehazing”, Jrn Visu Commn Img Repr, Feb-2013.
[25]. Zhang, “Removing backscatter to enhance the visibility of underwater objects”,msc dissertn, Nanyang Univ, 2016
[26]. F Ko, Weih C, Changy W, Zhengg L, “Gradient Domain Guided Image Filtering”, *IEEE Transc Img Proceg*, 2015.
[27]. Cod. Ancut , Cosm Chri , Philip, “Color Balance and Fusion for Underwater Image Enhancement”, IEEE Tra Img Procg, Jan 2018
[28]. C.Anc, Ancu Cod, T Hab, Phil B,”Fusion-based Underwater Image Enhancement by Weight Map Techniques”,IC3-2018,Chap *in* Adv in Intell Sys and Comp, Jan 2019.
[29]. Ancti, Habr T and Phil B. Fusion-based Restoration of the Underwater Images”, Intrn Confrn Img Proc, Sep-2011.
[30]. Ancti C, Ancu O, Haer “Enhancing Underwater Images and Videos by Fusion”, Compr Visn Patn Recogn , Jun-2012.
[31]. Jobson D, Rahman Z, Woodel “The Sstatistics of Visual Representation”, Procd SPE- 2002.
[32]. Panet K, Ga C and Agai S,“Human-Visual-System-Inspired Underwater Image Quality Measures”, Jr of Ocen E-2016.
[33]. Cha Y, Ric M, Andr C, “An Online Platform for Underwater Image Quality Evaluation”, Intl Confr on Patn, CPR 2018
[34]. Priya S and Sim, “Quality measure technique for Underwater images using Artificial neural network” Jon of Eng and Appl Sc, 2018
[35]. Bedr and Watt, “Alpha-Trimmed means and their relationship to Median Filters,” IEEE Transc Acost. Spch Sigl Proc, 1984.

Advances in Science, Technology and Engineering Systems Journal Vol. 4, No. 2, 351-356 (2019)

www.astesj.com

Special Issue on Advancement in Engineering and Computer Science

ASTESJ

ISSN: 2415-6698

Location Prediction based on Variable-order Markov Model with Time Feature and User's Spatio-temporal Rule

Ying Xia*[1], Yu Gong[1], Xu Zhang[1], Hae-young Bae[2]

[1]*School of Computer Science and Technology, Chongqing University of Posts and Telecommunications, 400065, China*

[2]*Department of Computer Engineering, Inha University, 22212, South Korea*

A R T I C L E I N F O

Article history:
Received: 28 January, 2019
Accepted: 05 April, 2019
Online: 24 April, 2019

Keywords:
Location prediction
Active grid
Variable-order Markov model
Time feature
Spatio-temporal rule

A B S T R A C T

Location-based service has been widely used in modern life. It brings a lot of convenience to our lives. Improving the accuracy of location prediction can provide better location-based service. We propose a location prediction method based on the variable-order Markov model with time feature and user's spatio-temporal rule. First, the user's trajectory data needs to be abstracted, and then the useful stay points in the user's trajectory are extracted. The location prediction is performed by scoring each candidate area, and the score is composed of scores in time and space dimensions. Finally, for the possible zero frequency problem, it is solved by mining the spatio-temporal rule of the user. Experiments using the actual data set GeoLife show that the proposed method improves the prediction accuracy.

1. Introduction

With the popularity of mobile location devices, the acquisition of location information is becoming more and more easier. Location-based services have become common services in our lives. It is necessary for us to mine location data and use the acquired knowledge to extend location services or improve service quality. Location prediction is an important research point in the field of location data mining, which can provide us with better recommendation services, social networking services and so on.

This paper is an extension of work originally presented in conference name [1].

Markov chain is a set of discrete random variables with Markov and the probability of each event depends only on the previous event. The Markov process is named after the Russian mathematician Andrey Markov. In this process, the future state is only related to the current state and has nothing to do with the past. Markov chain is divided into continuous Markov chain and discrete Markov chain. In discrete state-space, discrete time random process is called discrete Markov chain, and continuous time random process is called continuous Markov chain. [2]

Markov chain is a common statistical model, which is widely used in various kinds of prediction. It has the advantages of simplicity and efficiency, and is a good representation of time series data. Therefore, it can also be used for location prediction.

In literature [3], a location prediction method based on adaptive higher-order Markov model was proposed, which significantly improves the accuracy of location prediction. The difference between a higher-order Markov model and a Markov model is that the future state depends on the current state of the model and the past k-1 state of the model, not just the current state. However, it does not solve the problem of not finding current state in the history data, which is called the zero frequency problem. Literature [4] used variable-order Markov model for location prediction. It is based on high-order Markov model and makes the best use of history data. The zero frequency problem is also solved by an approach called escaped rule. Moreover, we found that many people have a regular life activity. By analyzing these people' history data, certain rules can be mined in time and space. These rules can be used in location predication. In the literature [5], the author not only considered the influence of user space factors on location prediction, but also considered the time factor, which further improved the accuracy of location prediction. This lets us notice the importance of time factor in location predication. Literature [6] provided a method for location prediction by using space-time rules, which is not only simple, but also can obtain good prediction results. These studies gave us a lot of inspiration.

*Corresponding Author: Ying Xia, Email: xiaying@cqupt.edu.cn

With lots of studies, a location predication method based on variable-order Markov model with time feature and user's spatio-temporal rule was proposed. It included the preprocessing of data, the construction of variable-order Markov model with time feature and the analysis of the time and spatial rules of users. First, data preprocessing makes the location data more suitable for location prediction. Since time and spatial factors both have impact on location predication, a variable-order Markov model with time feature is constructed for location predication. Finally, for the case that the variable-order Markov model cannot be used to perform the prediction, the prediction is made by analyzing users' time and spatial rules.

2. Data preprocessing

Before predicting the location, location data needs to be preprocessed, which includes three steps, that is, data cleansing, location information abstraction and stay point extraction.

2.1. Data cleaning

The purpose of data cleansing is to make the data more real, regular, and easy to handle. First, you need to modify the irregular data to make it more regular. Second, data not in research range needs to be deleted. In this study, Beijing was chosen as the research object so the range of location data control is between east longitude 115.25 ° to 117.3 ° and north latitude 39.26° to 41.03°. If not, it is regarded as data that is not in this range. Finally, incomplete or unreal data are cleaned up.

2.2. Location information abstraction

Location data is usually obtained by mobile device. And it is mainly composed of coordinate location data. The data are very detailed and it is difficult for us to analyze them. Location data needs to be abstracted into area data to perform conventional mining. The abstraction of location data also helps decrease computational complexity. In literature [7], the idea of building active grid was proposed. We use this method to abstract the location data:

- First, the user's activity range is set in a large rectangular area and the edge is parallel to the longitude and latitude lines.
- Then, the rectangular area is divided into a square grid. And the user's location point is mapped to the grid.
- Finally, active grid is connected based on time passage. This is user's active grid sequence.

The raw location data is composed of points. This is original trajectory data. $\{p_1,p_2...p_i...p_n\}$. P_i is the location point in the trajectory data. After the abstraction, the original user location sequence $\{p_1,p_2...p_n\}$ is converted to active grid sequence $\{z_1,z_2...z_i...z_n\}$. z_i is the grid in the abstract trajectory data.

2.3. Stay points extraction.

The stay points of moving objects are important points or areas such as shopping centers, workplaces, places of residence and so on. These points should be emphasized in location-based services. Therefore, the stay points in the trajectory need to be extracted. And there are many ways to extract stay points. The method of considering time and space factors is not only simple but also effective. It is based on the principle that a place is a stop point when you stay longer than the set time. The extraction method includes the following steps:

- Set the time value *t*, which is the standard of residence time.
- Search the area with residence time exceeding t in the trajectory data. The residence time is calculated by the difference between the maximum residence time and the minimum residence time.
- The stay points by time chronological order constitutes the new track.

The trajectory data composed of residence points are extracted by the above method. Algorithm 1 is the pseudocode used for the residence point extraction.

Algorithm 1 Stay points extraction

```
Input: User's historical data d_data  and stay time threshold t
Output: User's stay points s_area
The maximum time value to stay in the area time_max
The Minimum time value to stay in the area time_min
Sort the data of d_data by time
for each area of  d_data do
    stay time = time_max -time_min
    if stay time > t
      The area  add to the stay area s_ area
end for
return s_ area
```

3. Location Prediction

The method of location prediction includes constructing variable-order Markov model with time feature and analysis of user's time and spatial rules. It's named location prediction based on variable-order Markov model with time feature and user's spatio-temporal rule (VMTST).

3.1. Variable-order Markov Model with Time Feature construction and prediction methods

Variable-order Markov model is an improved model based on high-order Markov model. It makes use of the excellent prediction ability of the high-order Markov model and further realizes the automatic selection of high-order Markov model order. Time feature are also important for location prediction. Thus, time feature and variable-order Markov model are combined, and the scoring method is used to achieve the location predication. The method is as follows:

- Extract the historical track data composed of user's stay points.

- Search history tracks based on the user's current track. If the matching historical trajectory information is found, the transition probability of the next grid in these trajectories is calculated. It is called *P*.

- If the matching track information is not searched, some active grids must be removed and then new current track is created. The earliest active grids need to be removed because the earlier an active grid arrives, the less impact it will have on its future location. This process requires multiple executions until matching trajectory data is found.

  For example, Figure 1 shows the user's historical trajectory. If the user's current trajectory (Z_2-Z_3), all historical trajectory data containing (Z_2-Z_3) are searched. Z_4 after calculation is the highest region with transition probability. Region Z_4 is the predicated result. But if the user's current trajectory is (Z_4-Z_5-Z_6). The current trajectory is not found in history data. Z_4 is the earliest region and has the least influence on location predication, so Z_4 region should be deleted and search it again from the historical track.

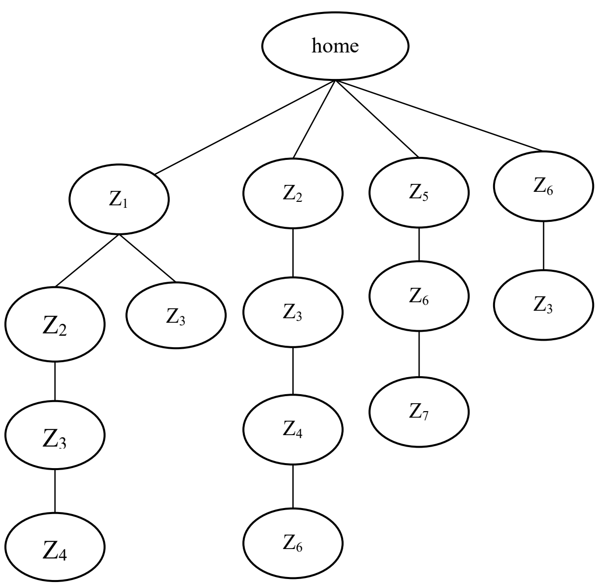

Figure 1: User's historical trajectory

- For each candidate region, their scores are composed of spatial accessibility scores and time feature scores. The scoring formula is as follows:

$$Score = W_1 * P + W_2 * S \tag{1}$$

W_1 and W_2 are the weights which are possible to reach spatial scores and time characteristic scores in the total scores.

Time information includes two parts: date and time. Therefore, the score of time feature *S* is composed of two parts: the periodic coefficient of the date and the similarity score of time.

$$S = C * Si \tag{2}$$

Si is the similarity score of time. Clustering and normalization idea is used here. It is obtained by the following formula.

$$Si = 1 - t/12 \tag{3}$$

$$t = th - tn \tag{4}$$

th is the hourly portion of historian data record.

tn is the hour component of current status.

C is the periodic coefficient of date. It is divided into workdays and holidays. It is calculated by the following rules:

If record date and forecast date are workdays, it means the location data is regular. Thus, the value of *C* is greater than 1.

If historical date and forecast date are holidays, it means the location data is irregular. Thus, the value of *C* is less than 1.

In other cases, *C* is 1 .

- The zone with the highest score is used as the predicting outcomes.

The location prediction algorithm of variable-order Markov model with time feature is as follows:

Algorithm 2 Construction of the variable-order Markov model with time feature

---

Input: users historical data *h_data*,users current trajectary *c_try*

Output: users next area *n_zone*

The weight of the space in the total score W_1

The weight of the time in the total score W_2

while Search from historical data (*h_data*) with user's current trajectory(*c_try)* return false

    c_try = remove the earliest zone from the user's current trajectory

    if the number of areas in user's current trajectory ==1

        break

Calculate the transition probability *P* of each next areas in the matched trajectory

for each area of next areas **do**

    Calculate the time similarity score *Si* and date coefficient *C* for this area

    Time feature score for this area *S* = *C***Si*

    Score for this area *score* = W_1**P*+W_2**S*

end for

Search for the highest scored area *n_zone* in the next area of historical data

return *n_zone*

3.2. Analyze Spatio-temporal Rule of Moving Objects

When users have less historical data, it is difficult to search matching historical track information. Location predication is done by analyzing the user's time and spatial rules. Spatio-temporal rule mainly refers to the regularity of users' time and spatial positions at different times. The following methods are used to analyze the spatio-temporal rule of users:

- The time interval is set to t.
- In the user's historical data, count the number of occurrence of user in each interval and each active grid. The region with the maximum number is the hot spot region during this time period.
- Set the numbered ID for each time period in time order.
- The result of spatio-temporal rule is composed of ID, hot region.

During this period, the more time periods are divided, the better the prediction effect is, but the more time is needed for calculation. It is easy to understand that the more active grids are present, the more likely they are to become a mobile destination for users. Therefore, hot spot active grids with the maximum number of occurrences are the prediction area based on spatio-temporal rule. Algorithm 3 describes this process.

In the location prediction, the user's current activity time matches the ID in the spatio-temporal rule. Next ID hotspot region is searched in the spatio-temporal rule, which is considered a place where users may arrive in the future. This process is algorithm 4.

Algorithm 3 Analysis of user's spatio-temporal rule

Input: users historical data *h_data*, time period *t*
Output: users spatio-temporal rule result *s_t_result*
Dividing the time period according to the value of *t*
for each time period **do**
    Set a number for each time period *t_ID*
    Calculate the area with the most user arrivals during this time period *max_area*
    t_ID and *max_area* added to the spatio-temporal rule result *s_t_result*
end for
return *s_t_result*

Algorithm 4 Location prediction using user's spatio-temporal rule

Input: users spatio-temporal rule result *s_t_result*
    recording time of the user's current trajectory *r_time*
Output: location prediction area obtained by users spatio-temporal rule *next_area*
Get the number of the *r_time* named *n_ID*
for each number in the time period **do**
    if *n_ID* = number in the time period
        get the hot area of the next time period *hot_area*
        next_area=hot_area
return *next_area*

4. Experiment

4.1. Experimental design

In order to verify the effectiveness of the proposed prediction method, experiments were performed using the GeoLife [8] trajectory data set. This data set includes trajectory data of 182 users over five years. It has about 18,670 tracks, including longitude, latitude, time and other information. And it records track data like users' work, entertainment and sports as well as other outdoor activities.

After data cleansing, extract the user's ID, longitude, latitude, date, time and other attributes. The experiment data set is shown in table 1. 10% data is randomly selected for test data and the rest are training data. Experimental research area is east longitude 115.25° to 117.3° and latitude 39.26° to 41.03°. The size of grid unit is 100m*100m, the limit time of residence time point t is 10 min and the time interval selected for the analysis of users' spatio-temporal rule is 2 hours.

Contrast model:

MM: High order Markov location predication model.

VOMM: Location prediction model proposed in literature[4] uses variable-order Markov model for location prediction and escaped rules to solve the zero frequency problem.

VMSTPM: The location prediction model is proposed in literature [1]. This method uses the variable-order Markov model for location prediction and also uses spatio-temporal rule to solve the zero frequency problem.

Table 1: Sample of Data

ID	latitude	longitude	date	time
10	39.921695	116.472345	2007-08-04	03:30:34
10	39.961675	116.472315	2007-08-04	03:30:36
10	39.924583	116.472290	2007-08-04	03:30:38
10	39.921572	116.472290	2007-08-04	03:30:39
10	39.921565	116.475588	2007-08-04	03:30:40
10	39.921577	116.472210	2007-08-04	03:30:41
10	39.921570	116.472300	2007-08-04	03:30:42
10	39.921576	116.475588	2007-08-04	03:30:44
10	39.921580	116.472290	2007-08-04	03:30:46
10	39.921576	116.472321	2007-08-04	03:30:50

4.2. Evaluation Factors

Prediction accuracy and recall rate were used as evaluation indexes in the experiment. The formula is as follows:

$$Precision = \frac{accurate}{accurate+wrong} \quad (5)$$

$$Recall = \frac{accurate+wrong}{total} \quad (6)$$

Table 2: The value of W_1 and W_2 in different situation

	case 1	case 2	case 3	case 4	case 5	case 6	case 7	case 8	case 9
W_1	0.1	0.2	0.3	0.4	0.5	0.6	0.7	0.8	0.9
W_2	0.9	0.8	0.7	0.6	0.5	0.4	0.3	0.2	0.1

Table 3: The value of C_1 and C_2 in different situations

	case 1	case 2	case 3	case 4	case 5	case 6	case 7	case 8	case 9
C1	1.1	1.2	1.3	1.4	1.5	1.6	1.7	1.8	1.9
C2	0.9	0.8	0.7	0.6	0.5	0.4	0.3	0.2	0.1

In the above equations, accurate indicate the number of correct predictions, wrong indicate the number of incorrect predictions total indicate the number of all testing trajectories.

4.3. Analysis of Experimental Results

First, the coefficients in the candidate region scoring formula were tested by experiments and prediction accuracy was used as the evaluation index. The experiment selected nine different values, as shown in table 2. From table 2, we can see that the prediction accuracy is the highest when W_1 and W_2 are 0.3 and 0.7. It proves the importance of time feature to location prediction. Thus, when the weight of time feature is great, the prediction accuracy is higher.

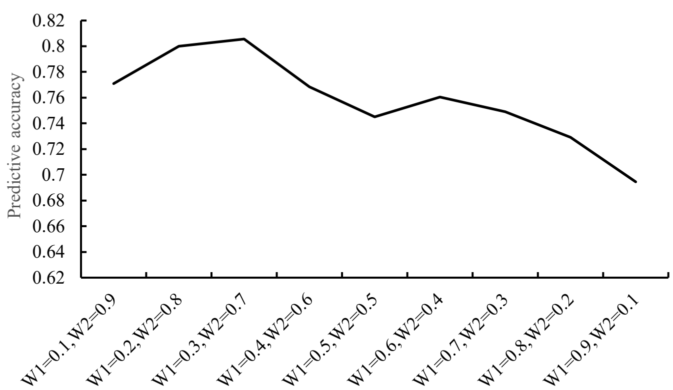

Figure 2: Prediction precision of W_1 and W_2 in different situations

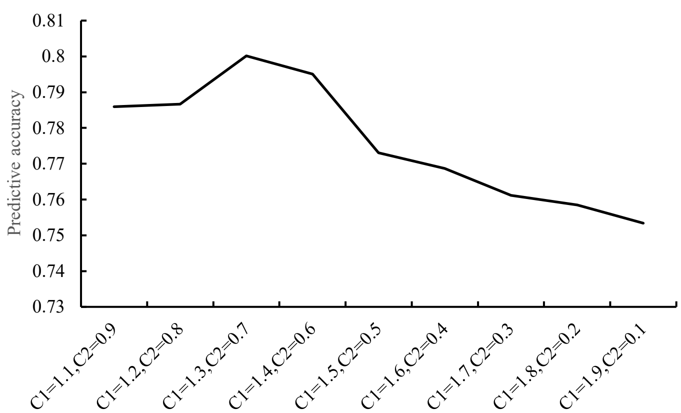

Figure 3: Prediction precision of C_1 and C_2 in different situations

Besides, the period coefficient value of the date obtained the best value by experiments. The value of C is C_1 when record date and prediction date are both workdays. And the value of C is C_2 when both historical date and prediction date are holidays. C_1 and C_2 take the values in table 3. It can be seen from figure 3 that the prediction outcome is best when C_1 is 1.3 and C_2 is 0.7. Therefore, other experiments were performed with these values.

Then, lots of prediction experiments were performed to verify the prediction outcome of the model. The prediction outcome is shown in figure 4. And VMTST at different orders showed more accurate prediction result. The best prediction result is obtained in the second order, which is about 30% higher than the original high-order Markov model and about 20% higher than the VOMM model. In figure 5, we can see that VMTST model is more stable in higher-order predictions. Therefore, it is better to use the current state and a history state for location prediction. This will get the optimum result. These results show that VMTST model has good predictive performance.

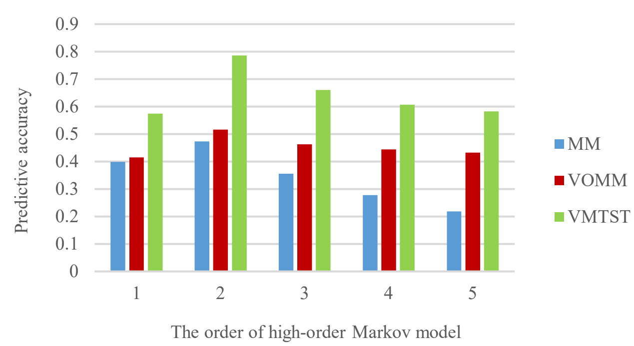

Figure 4: Prediction precision with different orders

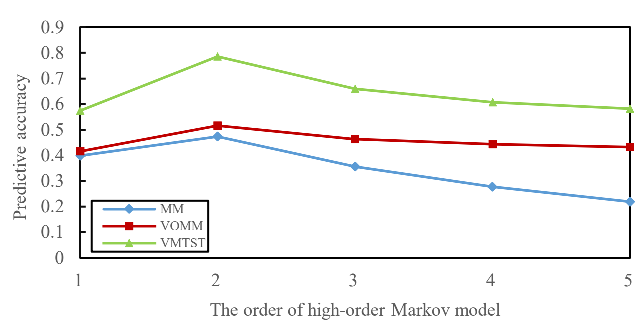

Figure 5: Prediction precision with different models

Experiments were conducted to verify the importance of time in prediction. The prediction accuracy is still used as the evaluation index in the experiment. And the results are shown in figure 6. It can be seen that the prediction accuracy of VMTST is higher than that of VMSTPM with different orders, which proves that time feature is a very important factor in location prediction.

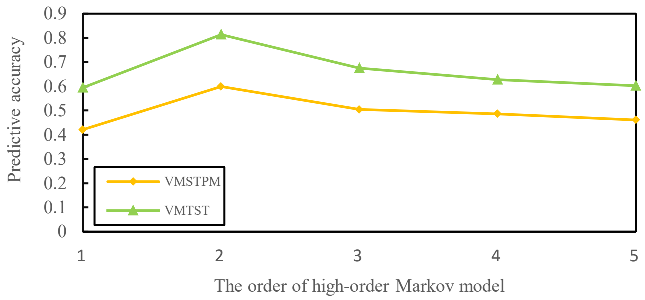

Figure 6: Prediction precision of VMSTPM and VMTST

The figure 7 is the comparison of recall rates of three models. As you can see, the recall rate of VMTST is 1.0, which is higher than high order Markov model. This means that it is effective to solve the zero frequency problem by using the user's spatio-temporal rule. However, the recall rate of VOMM model is also 1.0, which means VOMM model also solves the zero frequency problem. More experiments are required to verify the performance of VMTST.

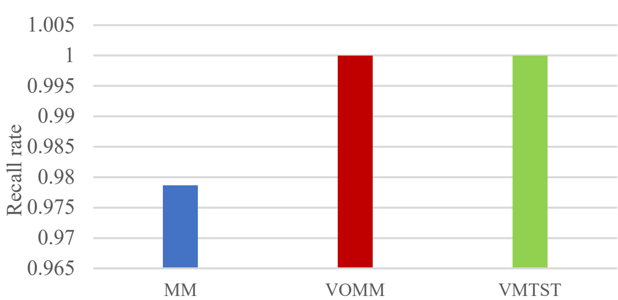

Figure 7: Recall rate of different models

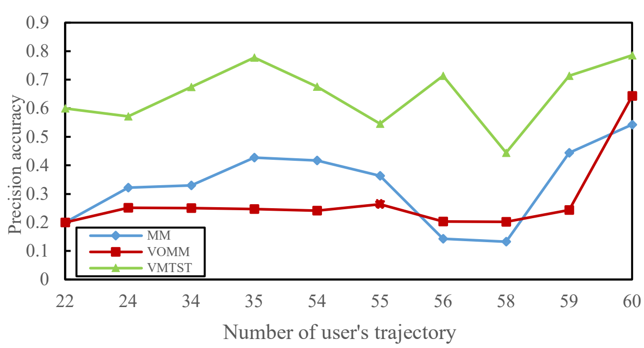

Figure 8: Prediction precision of users with fewer trajectory

The above experiments show that the spatio-temporal rule can solve the zero frequency problem. But, it is necessary to verify the performance of spatial and temporal laws in predicting accuracy through experiments. The experiment selected 10 users with less historical data. Therefore, it is easier to generate zero frequency problem. And it can be seen from the experimental results in figure 8 that when the trajectory quantity is small, the prediction accuracy of VMTST model is still higher than other models. Therefore, the spatio-temporal rule of users is more suitable to solve the problem of zero frequency.

5. Conclusion

A location prediction method was proposed in this paper, including preprocessing of location data, construction of variable-order Markov model with time feature and analysis of user's spatio-temporal rule. The preprocessing of position data makes the research scope fixed and the track data easier to analyze and process. Variable-order Markov model is an improved model of high-order Markov and it has higher location prediction accuracy. The time features are added to the variable-order Markov model to further increase the prediction accuracy. The problem of zero frequency can be solved by analyzing the spatio-temporal rule of users. Finally, lots of experiments were carried out using the actual trajectory data set.

By summing up the experiments, we can conclude that VMTST model improves the prediction accuracy. Time features are very important for location prediction. And the spatio-temporal rule can solve the problem of zero frequency, and be also more suitable.

In the future, we will look for new methods to mine the spatio-temporal rule of users so as to get the higher prediction accuracy. Also we will study the application of location prediction method in practice.

References

[1] Y. Xia, Y. Gong, X. Zhang and H. Y. Bae, "Location Prediction Based on Variable-order Markov Model and User's Spatio-temporal Rule" in International Conference on Information and Communication Technology Convergence, Korea, 2018. https://doi.org/10.1109/ICTC.2018.8539593

[2] P. A. Gagniuc, Markov Chains: From Theory to Implementation and Experimentation, John Wiley & Sons, 2017.

[3] M. Q. Lü, L. Chen, G. C. Chen, "Position Prediction Based on Adaptive Multi-Order Markov Model" Journal of Computer Research and Development, 47(10), 1764-1770, 2010

[4] J. Yang, J. Xu, M. Xu, N. Zheng, Y. Chen, "Predicting next location using a variable order Markov model." ACM Sigspatial International Workshop on Geostreaming, USA, 2014. https://doi.org/10.1145/2676552.2676557

[5] X. Li, C. Yu, L. Ju, J. Qin, Y. Zhang, L. Dou, S. Y. Qing, "Position Prediction System Based on Spatio-Temporal Regularity of Object Mobility" Information Systems, 75, 43-55, 2018. https://doi.org/10.1016/j.is.2018.02.004

[6] H. M. Wong, S. V. Tseng, C. C. J. Tseng. "Long-Term User Location Prediction Using Deep Learning and Periodic Pattern Mining." in International Conference on Advanced Data Mining and Applications, 2017. https://doi.org/10.1007/978-3-319-69179-4_41

[7] F. Giannotti, M. Nanni, F. Pinelli, "Trajectory pattern mining." in Acm Sigkdd International Conference on Knowledge Discovery & Data Mining ACM, 2007. https://doi.org/10.1145/1281192.1281230

[8] Y Zheng, X Xie, W. Y. Ma, "GeoLife: A Collaborative Social Networking Service among User, location and trajectory" IEEE Data Eng, 33(2), 32-39, 2010

Advances in Science, Technology and Engineering Systems Journal Vol. 4, No. 2, 357-369 (2019)

www.astesj.com

Special Issue on Advancement in Engineering and Computer Science

ASTESJ

ISSN: 2415-6698

Computer Security as an Engineering Practice: A System Engineering Discussion

Robert M. Beswick*

Mission Design and Navigation Section, NASA, Jet Propulsion Laboratory, California Institute of Technology 91109 USA

A R T I C L E I N F O

Article history:
Received: 29 June 2018
Accepted: 03 April 2019
Online: 24 April 2019

Keywords:
Computer Security Engineering
Security Fault Tolerance
Ground Data System
Defense in Depth
Defense in Breadth
Least Privilege
Vulnerability Removal
Absolute Security
Sterility in Implementation
Time Based Security
Communications Security
Operations Security
Complementary Intersection

A B S T R A C T

We examine design principles from more than 20 years of experience in the implementation and protection of mission critical flight systems used by the Mission Design and Navigation Section at NASA's Jet Propulsion Laboratory. Spacecraft navigation has rigorous requirements for completeness and accuracy, often under critical and uncompromising time pressure. Fault tolerant and robust design in the ground data system is crucial for the numerous space missions we support, from the Cassini *orbital tour of Saturn to the Mars rover* Curiosity. *This begins with the examination of principles learned from fault tolerant design to protect against random failures, and continues to the consideration of computer security engineering as a derivative effort to protect against the promotion of malicious failures. Examples for best practice of reliable system design from aviation and computer industries are considered and security fault tolerance principles are derived from such efforts. Computer security design approaches are examined, both as abstract postulates (starting from cornerstone principles with the concepts of Confidentiality, Integrity, and Availability) and from implementation. Strategic design principles including* defense in depth, defense in breadth, least privilege, *and* vulnerability removal *are target points for the design. Additionally, we consider trust in the system over time from its sterile implementation, viewed against the backdrop of Time Based Security. The system design is assessed from external access data flows, through internal host security mechanisms, and finally to user access controls. Throughout this process we evaluate a* complementary intersection – *a balance between protecting the system and its ease of use by engineers. Finally, future improvements to secure system architecture are considered.*

1. Introduction

This paper examines approaches used in the process of securing the computer systems employed by the Navigation Ground Data System. This text is meant to serve as a discussion about best practices in computer security engineering. It is based on twenty years of the author's practical, "in the trenches", field experience on systems involved in this effort. These systems comprise a multi-mission network that encompasses the navigation elements of more than forty current and previous interplanetary flight missions here at the Jet Propulsion Laboratory. This paper does not seek to be a prescriptive document (do this one thing, buy this product, etc.), but instead seeks to examine a process of how secure systems are designed – i.e., what general security principles we have found valuable [1].

Few systems require as much resiliency or have as much risk of causing negative (and final) outcomes as the computer systems used in support of Flight Operations. Scant resources are often available for the maintenance of complex hardware and software architectures, and these high-availability/high-reliability systems are often expected to function without (and moreover cannot *tolerate*) the regular sorts of software updates expected in other computational environments.

As an example, one of these missions, Cassini, from its launch in October of 1997, would spend seven years crossing the solar system, arriving at and entering into Saturn orbit in June, 2004. It would then orbit Saturn nearly three hundred times over thirteen years, conducting hundreds of targeted flybys of Saturn's largest moons during its mission lifespan, finally coming to a fiery end in Saturn's atmosphere in September of 2017. This operational effort would be conducted on a network of computer systems having a requirement for no more than two minutes of unplanned downtime

*Robert M. Beswick, 4800 Oak Grove Dr., Pasadena, CA 91109 USA, 1-818-393-0539, Robert.M.Beswick@jpl.nasa.gov

https://dx.doi.org/10.25046/aj040245

a year (99.9995% availability) [2]. For a network that could not be upgraded (except in minor incremental steps) during the length of the entire 13-year Saturn orbital tour, maintaining and keeping such a computer network secure, as well as supporting backwards compatibility (and obsolescent hardware) would be a challenging problem. In fact, the systems used over the launch and interplanetary voyage across the Solar System contained less processing power, storage, and *total* memory than the author's current iPhone – and these systems would have to be kept functional and secure in case there was a need for backwards comparison.

While some organizations may have little need for a computational environment larger than a client-server configuration of a few systems, others may require a more complex environment. The Ground Data System for Navigation is constructed in the manner of a classic Development and Operations model with development and production networks of several hundred servers and workstations. This network is used by teams of engineers working, often under critical time pressures, with rigorous requirements for accuracy [2].

For this environment, it should be clear that a particular cryptographic protocol, a set of software, or even an appliance will not solve these security challenges. This is not an application problem but instead a systems problem. As in other engineering disciplines, in such an environment the design must be based on good *principles*, because, like with the pouring of a foundation of a building, you only get one such opportunity.

Part of the effort in this discussion stems from the author's own struggles to find a good systemic set of definitions and guidance while endeavoring to build a more secure network. What you see here is a reflection on the insights I was trying to find for my own efforts. Furthermore, many current efforts in computer security research are based not on building a secure system but tearing a system down. Indeed, a great deal of present investigation in computer security is based around the twin ideas of "if it ain't broke, don't fix it", and "try and see if can be broken". Accordingly, extensive research across the spectrum of computer security is being conducted in the field of penetration testing, where the primary methodology is to break into an existing setup and then fix the discovered problems. While this can be helpful in discovering specific flaws, it does not provide much help in trying to understand a more general architecture model of security.

An example of this is perhaps best exemplified by the software tool known as "Chaos Monkey" – part of an open source suite of tools called "The Simian Army" that was originally designed for the cloud infrastructure of the streaming media service Netflix [3]. This software set comprises a series of tools that help the design of resiliency in a set of virtual machine instances. It does so by randomly shutting down members of the set of virtual machines. By forcing developers and systems engineers to prepare for unexpected failure, a more fault tolerant network design will emerge (it is hoped). This has been further expanded and generalized to even more powerful tools that comprise "Chaos Gorilla", which randomly simulates the shutdown of an entire Amazon Availability Zone, or the even more devastating "Chaos Kong", which simulates the shutdown of an entire Amazon Region [4]. This design is an example of "survival of the fittest", incorporating a genetic algorithm-like approach to the design of secure systems.

Critical questions that should be raised in conjunction with this software are, "How does a developer or systems engineer build a more stable and secure system? What principles should be used? What methods should be avoided?"

Continuing with the metaphors given above, consider an analogy to the above (genetic) algorithm: a team of stone-age architects trying to build a bridge across a river, first by using a captive monkey, then a captive gorilla, and then a giant mythical beast to try throwing stones and batter a pile of rocks into a working bridge. While such a method will produce some results (albeit very slowly), what about other engineering approaches to design? What of the arch and the use of suspension? What about the consideration of tension and compression and the use of different materials in the construction of a bridge?

Clearly other engineering principles can be useful here in order to produce an initial design and improve upon it before bringing someone to attempt to tear it down. In like manner, this paper is a study on security architecture design, and hopes to add to such efforts by discussing principles on "how to build a (better) bridge".

A word about the expected audience of this paper: the design principles discussed in Sections 2 and 3 are aimed at top level design of secure systems, and may be of greatest use for project management and systems engineers (it could also be titled "how to avoid buying crap"), while Section 4 covers an example implementation targeted more for computer systems architects and systems administrators. The paradigms covered in Section 2 and 3 are observed derivations from fault tolerance and have wide applicability in systems engineering, while Section 4 applies this methodology to securing a specific computer system.

2. System design approaches: Fault Tolerance and Security Fault Tolerance

2.1. Fault Tolerance

There are several valuable definitions for the concept of fault tolerance. Fault Tolerance, according to Carl Carson, comprises "...a design that enables a system to continue its intended operation, possibly at a reduced level, rather than failing completely, when some part of the system fails" [5, p. 167].

This has been categorized by Barry Johnson in the approaches taken for fault tolerance in microprocessor design as [6]:

- Minimize the number of points where a single fault will cause the whole system to fail.
- Graceful degradation – known also as "Fail-Gently", a system's ability to continue operating in the event of a failure, having a decrease in operating capacity no worse than necessary for the severity of the failure.
- Redundancy in components – both in space, having multiple parts that can be utilized, and in time, with the repeatability of an operation.

Jim Gray and Daniel Siewiorek help characterize such steps to provide high availability in computer systems by examining single points of failure to promote [7]:

- Independent failure – where each module functions so that if it fails, it does not impact other modules in the system.
- Design diversity – using hardware and software from differing organizations to promote independent failure modes (e.g. differing *types* of failure).

There are abundant examples of fault tolerant design. This is a well understood area of systems engineering. From the 135-year old Brooklyn Bridge in New York [8], to the current Eastern Interconnection power grid of the United States [9], approaches such as these are needed where one must trust the behavior of a system to work, and to work in predictable ways.

As an aspirational example, consider one such computer design further at the highest end of the reliability spectrum. The primary flight control system of the Boeing 777 achieves ultra-high reliability metrics. It is a highly redundant, highly available system comprising the fly-by-wire avionics controls and is a rare example of a true Triple Modular Redundant (TMR) system (with little exception the highest level of redundant design, having three redundant components for each single point of failure), in both computer nodes, software, and hardware. It has service metrics requiring a maximum rate of failure of the flight computers of 1.0×10^{-11} failure/hours (i.e. a failure of the flight computers less than 1 in 100 billion flight hours) [10]. This is an example of what can be done with sufficient effort and due diligence – a computer system millions of passengers a year put their trust in.

2.2. Security Fault Tolerance

In like manner, this paper considers computational systems that one can trust – as is done with the physical systems described above. From fault tolerance, we can derive similar approaches to deal with the actions of intelligent actors [1] rather than random chance or stress failure modes. Such an approach was described affectionately by Ross Anderson and Roger Needham as "Programming Satan's Computer" [11]. While the application of these principles we apply here to the flight computer and network security of our systems, the principles are applicable across the board to security design. Such design promotes:

- Secure systems should be resilient from random chance and predicted stress modes of failure.
- Secure systems should also be resistant to direct action.
- Simplicity of design, known as the popularized KISS principle, is a golden virtue in secure systems [12].

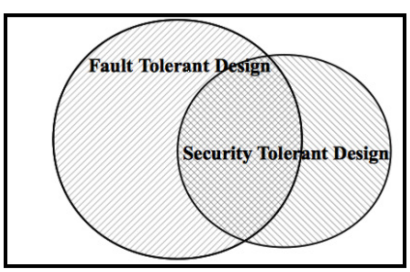

Figure 1: Relation of Fault Tolerant and Security Tolerant Design

These principles can be considered in four approaches:

2.2.1. For the most critical systems, use a machine that has only one function.

This approach has the benefit that in the event of a failure, you have lost only that one function. There are numerous examples in security design. Indeed, "appliance" IT systems, such as web servers, email servers, firewalls, and similar systems use this approach. As a good analogy: in (most) kitchens, refrigerators and ovens are not a part of the same appliance – even though they have the same task of changing and maintaining food temperature.

2.2.2. For redundancy in a security context ideally differing configurations should be used.

This technique considers that the systems in a given setup should not all have the same potential vulnerability (and therefore not truly redundant against a threat). It is an example of the previously discussed design diversity. Examples of this include the use of multiple arrays of web servers – running different OS/web server software, or application servers that use differing configurations and password sets, or multiple (different) backup systems – e.g. tape, disk, and cloud service providers. As an analogy, consider the commute from a major urban center: it is better to have several differing options for transport, be it freeway, commuter train, bus, or even surface streets. In the event one method is impacted, other options are available to return home.

2.2.3. Single points of failure of a system should be few, and truly independent.

As observed above, in a security context, systems that are single points of failure should be truly *independent* of other points of failure. Such single points of failure should be examined closely to ensure that they are actually single, independent, points of failure.

This goes hand in hand with the first point about single use. One example of this can be seen in network file server "appliances" that perform the function of serving files – other application sets such as virus checkers and configuration management tools may be run on the files themselves, but they are seldom loaded on the file servers. This design approach is often misunderstood in poor implementations, especially where security may be seen as a software package or an add on feature. As an analogy consider tires that serve as critical single points of failure for a modern car – in a similar manner, it would be absurd if a failure of the GPS system caused the tires to fail!

2.2.4. Systems should Fail-Safe and/or Fail-Gently.

In case of failure, a security system should degrade safely (known as Fail-Safe), and/or compromise only a limited part of the overall system or otherwise take an "acceptable" amount of time to fail ("Fail-Gently"). Examples of this abound, many of them utilizing cryptography, such as disk and file encryption, password login for most computer systems, firewalls, network segmentation, and network Intrusion Prevention Systems (IPS). An analogy can be found in the mechanical realm in that high grade safes are rated

[1] To be clear: this term is meant here to describe human attackers, not intelligent software agents. They may also be described as malicious actors, or threat actors depending on context. The colloquial and overlapping terms of hackers, crackers, or security hackers are also used in the general news media.

for time against tools, cutting/welding torches, and explosives. Some safes may have mechanisms that break or cause the safe to be unopenable if drilled or otherwise tampered with.

3. Computer Security Design

3.1. Abstract Principles

This computer security design incorporates the above techniques through increasing grades of refinement. Abstract concepts of Confidentiality, Integrity, and Availability (the traditional trinity of security) help to determine the "who, what, when, and where" of the security needs for navigation computation. These principles provide definition for the key concerns for securing a system, not in terms of technique, or subsystem protected, but rather in terms of what features in the computational environment must be protected.

3.1.1. Confidentiality

Confidentiality is referred to as "the concealment of information or resources" [13, p. 4]. This can be of high priority for some financial systems, where customer data is not only a crucial part of business operations, but also where strong legal regulations may come into play for control of customer information. It may be critical in military computer systems (for some cases it may be more desirable to destroy the system than allow the unauthorized release of information). This is significantly less crucial in the field of navigation computation. Such information for navigation comprises mechanisms used to authenticate access to the systems, network and system configuration information (possibly of use to subvert security), and restricted navigation software. An example of a baseline concern for Confidentiality can be seen even in the naming of individual systems, as such host names may reveal a great deal of information about the underlying network design [14]. Consider a hypothetical, badly named example from JPL: the host name "cas-web-serv3", which immediately gives information the system in question is running a web server daemon, for the Cassini project, and that most likely there are (at the minimum), two similar servers.

3.1.2. Integrity

Integrity is "the trustworthiness of data or resources ... usually phrased in terms of preventing improper or unauthorized change" [13, p. 5]. Integrity is particularly critical for navigation computation, as improper or unauthorized modification of the environment could cause very serious problems. Corrupted data sets, results or software could cause terminal errors in spacecraft control. With regard to the accuracy required for navigation of spacecraft missions, the sensitivity placed on the accuracy and integrity of the data, software, and corresponding results cannot be overstated. One such example of the critical nature of Integrity is seen in the previous case of the Cassini project. Integrity was critical on such a mission, which consisted of one of the largest teams of navigation engineers ever assembled, flying on the navigation computer system one of the most complex orbital and interplanetary trajectories ever designed [15].

3.1.3. Availability

Availability is "the ability to use information or resources" [13, p. 6]. Conceptually, it is the most direct derivation of principles coming from fault tolerant design. Availability in the context of navigation computation, has an additional concern that someone could deliberately try to deny access to a system service or data sets. The 24-hour-a-day, 365-day-a-year activity calendar of spacecraft navigation indeed makes this a crucial concern [15]. An event which causes the system to be unavailable, which in other industries might be cause for concern, could lead to the premature end of a multimillion dollar space mission.

3.2. Implementation

From these abstract principles, there are a number of paradigms that are employed for the implementation of better protection. Accordingly, strategic archetypes are used in the work toward good security design.

3.2.1. Defense in Depth

Defense in depth is a military security term with a long historical pedigree. Instead of a single defensive stronghold or chokepoint, this strategic principle is based around a series of overlapping defenses, forming a type of fault tolerant redundancy [16, pp. 40-44] in that a failure of one part of the system does not lead to the failure of the whole system. Considering a networked computer system, this can be seen on a variety of levels in overlapping defenses: starting at the network perimeter firewall, the network segmentation rules used on the network switches, the host based firewall, the protections applied to the processes that connect to the network, and then the internal host security measures that must be bypassed by a potential attacker. This is analogous to a defensive perimeter made up of a series of overlapping walls and fortifications, much like that seen in that of a medieval castle, or World War I trench warfare, presenting so many obstacles to entry that an adversary, having a choice, will pick a less well defended target [17, p. 259].

3.2.2. Defense in Breadth

Defense in breadth is a term serving as the converse for *defense in depth*. It involves the concept that a secure system design must consider the whole system in its implementation, or an attacker will simply ignore a well fortified part of the system and instead chose an easier route into the system. All of the previous paradigms of overlapping defenses, minimization, elimination, and security over the system life, must be considered for *every* part of the system. This is a difficult task and it does lay bare the challenge of the security engineering process. By definition this is an effort to examine the totality of all of the possible attacks against the system. Indeed, this defensive principle is referred to by Sami Saydjari as *Ensure Attack-Space Coverage*. He acknowledges that achieving this comprehensive coverage is a large and challenging problem, and one that is usually not well understood, but he underlines its necessity as a security engineering principle when he remarks "Depth without breadth is useless; breadth without depth weak. " [18, pp. 133-135] Consider an analogy from a failure of this principle: putting a well-locked door with a security system on a Hollywood film set facade; while it is possible to break through the front door, it is much easier to simply walk around the side or back of such a facade because most such sets do not even have a back wall. History is rife with excellent examples of the failure to consider the whole scope of ways an adversary could carry out an attack. One such example can be seen in the WWII failure of the Maginot line on the French-German border. [2]

3.2.3. Least Privilege

The principle of *least privilege* is that subjects (processes and users by extrapolation) should be given only the rights and accesses for the tasks the subjects need to perform, and no more [13, p. 457]. This avoids many possibilities for the manipulation of a process (or manipulation by a user) to get them to do things they were not intended to do. There are many similarities to ideas in finance and accounting where financial mismanagement and corruption in corporations are prevented by not allowing any one person to take charge of all the corporate finances – also known as the "two man" rule. As an example, consider a hypothetical printing utility that can write to a central spooling directory as a privileged user. It is discovered that by manipulating the input files sent to the printer, it is possible to write to other directories on the system. With some effort and cleverness it may become possible to overwrite critical system files or even get remote access to the system. By changing the permissions of the spooling directory and removing the ability to run as a privileged user, the printing utility can continue to function, without enhanced access, thereby removing its capability to be misused. A similar analogy is a classic safe deposit box repository in a bank, where two people (each with a different key) are required for access to a given safe deposit box.

3.2.4. Vulnerability Removal

When we remove potential vulnerabilities, we can elude the many problems that come with those vulnerabilities, and sometimes avoid other issues as well. Matt Bishop refers to this as *The Principle of Economy of Mechanism* [13, pp. 459-460]. An example of *vulnerability removal*: a self-replicating worm that attacks email server processes can do little damage if you do not have an email server on your system. Likewise, if you do not have a web server running on your system, there is no need to monitor for such and keep up with attendant patches. Making sure that (along with the software and its own attendant maintenance) possible vulnerabilities in buggy software are not installed, can save tremendous resources and time over the system lifetime. As an analogy, this is akin to not just locking a side door into a building, but instead never constructing the door into the building in the first place.

3.2.5. Sterility and Absolute Security

We now consider the idea of *sterility.* This is a point along a spectrum of levels of trust in a given system. Understanding how much one can trust such a system may help determine how it should be used and where it should be placed on the network. A few (very rare) systems we consider to be sterile and have *absolute security*, the top of this spectrum, or "security beyond any reasonable doubt". [3] To be clear: this is a theoretical initial state, a starting point for definition, and *no* connected or exposed system can be said to be sterile and in this state. This is a valuable concept, especially as we consider the next paradigm. It is comparable to a definition of an initial starting point (a *t0*) that is useful when considering how that system might evolve over time.

Let us further consider, that a system implemented on a closed network, built from a secure image is secure, or *sterile* to the limits of confidence one has in the hardware (and the hardware vendors), network, and the software media (DVD or secure image and/or patch servers, etc.) used to construct the system. On such a spectrum of trust this system would be seen as approaching *absolute security* considering these limits of confidence. This useful idea can be seen as extrapolated (as systems in miniature) from credentials, passwords, or certificates that also have not been exposed. We can liken this to issues seen in medical care, or food preparation and handling, where much effort for hand washing, cleanliness, or cooking is undertaken to produce sterile areas, or clean food for consumption.

3.2.6. Security over time or robustness

The previous paradigms examine the implementation of a static system. Considering the evolution of a system state over time, one should also consider how the system is secure during its implementation and over its whole lifecycle. How robust is this system? How much can it be trusted and how does that trust change over time? This is similar to principles of Communications Security (COMSEC) and Operations Security (OPSEC). These are military security terms that examine the communications and background operations processes of military organizations, working to prevent compromise of communications, and the processes of such organizations. As in a military organization, our trust in a system will change over time. This is strongly dependent on the environment and networks that connect to this system. It is very important to examine these connections and method of contact to characterize the *security over time* of a system.

This concept is akin to what Winn Schwartau called "Time Based Security" [18, p. 34]. In Time Based Security, a system would be considered "secure" if the time to break through the system protection (Pt) was greater than the time required to detect (Dt) and to respond (Rt) to the intrusion. This can be expressed as:

$$Pt > Dt + Rt \tag{1}$$

Time Based Security suffers in the great difficulty of quantifying these values in (1), for the system protection, detection, and reaction time. Nonetheless Time Based Security does help illustrate well that security over time is a derivation from the fault tolerant concept of Fail-Gently, as discussed above.

Coming from the previous point about sterility, trust in a sterile system must change when it is attached to outside networks. Our confidence in such a system is then based on the security configuration of the external network, internal host, and user

[2] The Maginot line was designed to protect France from a German incursion in the event of a second world war. It was an excellent example of the principles discussed here, providing significant fault tolerant, defense in depth, with carefully considered access and both perimeter and internal security. A marvel of military engineering, its primary construction protected the French-German border. Most elements of the line were operational and fully prepared to continue fighting *after* the fall of France, and had to be ordered to surrender with the French capitulation. The designers famously did not consider (mostly due to the staggering costs to expand the fortification) an assault across the French-Belgian border.

[3] This is a functional term that in our model is akin to, but not the same as, the mathematical term *perfect security* – such as the unbreakable one-time pad [36].

controls of the system. Log mechanisms can help give indications of change to the system. If this trust is misplaced, the system could be compromised, and the system could become untrustworthy and itself a source of security concerns. As in the previous section we consider that this is akin to handling a compromised password or certificate, and in most cases the system must be rebuilt.

There is considerable kinship between these ideas and the study of infection and food-borne illness. The frequent admonition about hand washing before meals comes to mind. What things did one touch or pick up? Do you have a thermometer to see if the food is cooked? A brisket set out too long at a picnic may "go bad" and become a host to viruses, worms and other sources of contagion. It may be possible to sterilize it, or at least to clean the dish containing the item. Much care is required to safely clean dishes under food handling regulations, but having gone bad, food, no matter how savory, almost all of the time must be thrown out.[4]

4. System Evaluation

Keeping these principles of secure system design in mind, we consider an example case: a single computational node and the techniques and mechanisms put to use to create a secure system. Our model system is a server running Red Hat Enterprise Linux 7. Particular care is taken in its construction as it serves as a fundamental "building block" in our system plan. This security design takes on several design principles found in architecture in that the strength of a system can often be improved, not by what one adds, but by what one takes away. Also, this serves as an effective approach in considering the overall security of our environment. Moreover, many systems are actually allocated in a "one engineer, one workstation" ratio. Similar efforts can just as easily be a network segment, implemented in a network group.

It is useful to reiterate here: this is *example*. These security architecture guidelines can be applied in many other approaches and types of system setups. This is an outline that other system architects and system engineers can follow to create their own secure systems. It is hoped that this demonstration will help to make these key concepts and their application in design more clear. This system-design model is a simple one. It is to serve as a means to explain principles and their use in an architecture. As we extrapolate to a network, or a network-of-networks we get a clearer understanding of these principles and their use in a model. Complexity may be introduced in efforts to move towards a particular architecture model.

For example, one such effort called Zero Trust computing, moves towards a very atomic model of trust, that of so called "de-perimeterisation" where the outer defenses of a network system are assumed to be ineffective. Zero Trust uses the same design goals, but with an aggressive application of the principle of *least privilege* applied to every element of a network [20, pp. 2-3, 12-18]. It involves the hardening of every computational node, and every network connection and data access, and moves away from the traditional specialization of gateways, firewalls, and trusted subnets or zones. The model we discuss is agnostic to such efforts, as approaches we take here are equally valid for such designs. A more "classic" network security model is, simpler to explain.

Our fundamental design goal is to create a system that can be trusted and relied upon to perform the difficult task of spacecraft navigation. This design effort sought to find an optimal tradeoff between usability and security, the point of both maximal utility (for the users) and security: a point where users could work without being fettered by obtrusive security measures, while confident that their work is safe. Indeed, it is a mistaken, albeit popular, notion that security must interfere with usability, and that secure systems must necessarily be hard to use. Much of the time this misconception is due to a poor implementation of a secure feature, or a security control that was added on as an afterthought to a software system. Failing to consider these requirements and needs of the users also can lead to the perceived adversarial role of security in an organization. The idea of examining the security controls in consideration with the user environment is referred to by Matt Bishop as the *Principle of Psychological Acceptability* [13, pp. 464-466]. The strategy we consider here strives to find a complementary intersection between usability and security, an optimal point where these two groups of competing requirements reach their maximum effectiveness [21]. This is similar to the concept known as the Center of Percussion (known also as the so-called "sweet spot") as found in weapons, aircraft, sound engineering, and sports equipment design – where multiple factors combine into an optimum response from a given amount of effort [22]. Analogously, these competing needs are similar to the economic concept of the law of supply and demand.

Finding this complementary intersection requires the evaluation of both security and user requirements. For an example of this optimal intersection, consider the often maligned password change requirements of most institutions.[5] Usually eight or more alpha-numeric, and special characters are required, often with other "randomness" requirements. These passwords often have to be changed every 180 to 90 days (or less). As a matter of cryptographic security, the longer the encrypted password hash, the more difficult it becomes to conduct a brute force attack to obtain the unencrypted password. Hand in hand with this, changing the password more frequently helps ensure that even if the password is broken or obtained by some other means, the window of exposure is short before a new password is created. Evaluating these security requirements, without user input, leads to more "random" and longer passwords, approaching something looking akin to line noise, with changes occurring in shorter and shorter time intervals. Taken alone, this might be considered to be a positive trend.

However, it has been widely known for some time that the user response to such policies tends to decrease the security of the system [23]. Users, unable to remember their ever-changing passwords, proceed to create easily guessable password combinations, or worse still, write passwords down in easy-to-find locations such as next to computer monitors or under keyboards. Evaluating both security and user utility requirements can instead lead to an optimal solution for these concerns. This could include

[4] There are limitations to this analogy. One of my associates who is a professional chef cited several counter examples – however he was quick to note that this holds true for 99% of food handling concerns.

[5] A memorable and humorous example of this can be found at http://xkcd.com/936/

a longer password rotation with a longer password, or possibly a smart card and a password (for two- or three-factor authentication).

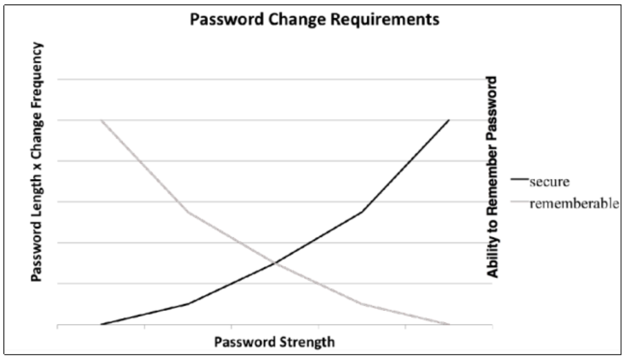

Figure 2: Complementary intersection of password controls.

But how can this optimal intersection point of security and usability for this system be determined? For this system design an initial setup is undertaken stemming from security design requirements and user needs. Numerous manuals for securing systems can be used *a priori* to determine a baseline configuration. We have used recommendations from the National Institutes for Standards and Technology (NIST) [24], the Information Assurance Directorate (previously named the System and Network Attack Center) of the National Security Agency (NSA) [25], or the Center for Internet Security (CIS) [26]. Using the security principles we discuss, these (and other) security approaches are evaluated, determining what user needs are crucial while seeking as secure a configuration as practicable. Areas of conflict (and overlap) are considered and from this iterative changes can be made.

Changes are then evaluated on the privilege, area and criticality of the alteration. Iteration towards an optimal state is a manual process of testing, examination, and consultation with users. For our model, there are three areas of concern: external network access, internal host security, and user level access controls. These areas have differing complementary intersections: the optimum trade-space differs between these areas of concern. Once this optimal state is determined, we then consider the evolution of this security state over time.

4.1. External Network Access

Under the greatest amount of scrutiny, the area of greatest care for the system design is the configuration of external network access. This is an exercise in optimization and extreme minimization. While users will be surveyed for input on desired services, security needs predominate in this area over almost all user concerns. Every access point (open network port or service) is of the highest concern as network access control is the first and best line of defense against intrusion. As we note above this approach can be generalized: this principle applies to both individual computer nodes, as well as networks of computer systems. For an analogy, if the network is compared to a street, an IP address would be the street address of the building and the ports would be the doors of that building. A firewall could be a wall surrounding that building (having its own doors/gates), or around several buildings in a compound. This analogy can be further extended much like that of a design of a military base (or a medieval fortress) with layered defenses. Again, this system design model is a simple one, and other design choices may factor into such an extension. In the area of external network access, the interplay between security controls and user needs will be very heavily tilted toward security because this represents the first, best chance to block an attacker (at the gate).

As mentioned previously this security design could be used in other system approaches. When we examine network access points to the model system, we should also consider other access points, such as physical connections to the system like the ubiquitous USB or Thunderbolt connectors. One can also consider similar methods by extrapolation to evaluate a database system, or a file storage system, by examining the controls on the data, and the access points to that data.

The approach utilized involves cutting down to the absolute minimum the number of open network ports, and then over those ports minimizing the content and amount of data transferred. Among the network testing tools we use, two include the Nmap port scanner (providing a comprehensive scan of all open ports on a machine) [27], and Nessus, a widely available network security scanner that helps probe for security vulnerabilities on the remaining open ports [28]. Indeed, although the user community may with regularity request the installation of numerous software applications that will have their own unique web server on an additional open port, such services will usually be disallowed. This is necessarily an iterative process. Sometimes if taken too far and too many ports are closed off and services shut down, the machine will not be able to communicate over the network. There may be times as well when certain user applications really do need to have a port opened for them. These should be examined most carefully. Those few services that are still available will be expected to be extremely secure against external subversion, such as the SSH remote login/file transfer/port forwarding service. In this approach:

- First test the system absent the host based firewall. This is to ensure the underlying system is secure without it. The firewall should not be the only point where outside connections are minimized and controlled. *Almost all network services can be shut down on a secure system with no real difficulties to the underlying function of the operating system!*
- Next test the system with the host based firewall engaged. In many cases stateful packet filtering can be used to trace (and allow) replies to network calls, which will eliminate the necessity for most holes in the firewall.

Table 1 depicts the results of this process for our example. From more than twenty open network ports on our initial image (which is a great improvement over previous Red Hat Linux versions) we reduced the number of open network services to a bare minimum of essential network services:

Table 1: Number of open network services with and without Firewall – Final Minimum Services

Firewall State	TCP	UDP	ICMP
No Firewall	3	6	2
Firewall	2	3	2

This is an excellent example of the point made earlier that the strength of a system can many times be improved by what is taken away from it. Contrasting these results with the hundreds or thousands of network services on a general home Mac or Windows computer can be enlightening as to the current default state of computer security.

4.2. Internal Host Security

A highly secure system that is impossible to use for its primary duties is not very *useful*. In evaluating our system's internal host security, the interplay between security controls and user requirements must be nearly equal due to the competing concerns to both keep it working as efficiently, and as secure, as possible for the users of the system.

By analogy, inside the building, the use of the building by its inhabitants is an important design consideration. Is it a home? A bank? A police station? Safe construction approaches are dictated for all buildings by fire codes, but how a building is used will determine much of a building's interior design.

For our own computation environment, this process of system hardening considered functions and services the user community required:

- The completion of operational duties such as supplying critical data sets to mission partners and utilization of mission critical flight software.
- The supply of required capability for a task or job role (e.g. visualization and formatting tools, viewers, editors, functional compilers, and third party software).
- The provision of *useful* utility functions and software (e.g. BR/DVD/CD archiving, external export of interesting graphical output, the capacity to safely load removable file systems, and network printing).

From these characterizations, a definition evolved of what behaviors were expected of a user and conduct they should *never* be expected to engage in. With such a set of definitions we removed from the system those privileges and programs a user was never expected to use, and added further constraints so users would have difficulty in performing anomalous activities.

Similar to the approaches used to secure the external network access of the machine, a software tool was used to evaluate the internal security settings of the machine and produce benchmarks for enhancement. Created by the Center for Internet Security (CIS), the CISscan package was used to evaluate the internal host security for the system [26]. It provides a set of metrics for assessing security configurations for a number of package distributions, as well as operating system platforms, allowing comparisons between variant software sets, alternate configurations, and operating systems. Representing an effort to create a "best practices" industry standard guideline to system security, the CISscan package is based around a set of consistent standards, that can be used to evaluate a given system against such metrics. With this tool, it was possible to create a security baseline, make sure that configuration changes and patching continued to meet that baseline, and iterate to a desired system configuration.

Categorical changes to the internal security settings included:

- Removal of extraneous executable permissions. The ability to change users in a program is an especially serious concern. SetGID and SetUID executables have the ability to change the group and user of the process that runs them. With this ability such programs present an extreme security risk. Some programs however, such as the ones that are required for users to log into the system need such a capability. Like our evaluation of open network services, almost all operating systems have a needlessly high amount of these types of programs by default. Even the latest versions of Red Hat Enterprise 7 contain numerous examples of programs with too many privileges. In our system, with effort we reduced the number of these very sensitive programs from 45 SetUID executables in the initial install to a total of 15 in the final secured configuration (see Table 2 for full discussion).
- Limit the installation of new software. Every new software installer has the potential to open up new vulnerabilities. It is far better to avoid such problems by not installing the software at all. As noted, this may minimize many maintenance issues as well, including keeping the software secure and patched. A related question for discussion is, "does your software really *need* its own web server?"
- Limit or otherwise shut down all unnecessary system services. For some minimal operating system configurations, the number of system services running on startup can be counted on one hand. This is a far cry from the average computer, which can have more than a hundred processes running at any given moment before anyone has logged in. Such extraneous processes can represent significant vulnerabilities on a system, especially if they have a network port open.
- Modify key network and kernel data structures. By changing the settings of key network and kernel configuration values, it is possible to significantly increase the protection of the system against denial of service attacks and other security failures with the occasional cost of small increases in memory use. Indeed, lowering user limits (number of users) and per-process (number of processes) on the system, significantly lower the odds an application can harm system function, blocking a denial of service attack by preventing such software from consuming system resources. Fortunately this area is one of the least likely to result in negative feedback and consequent user pushback.
- Restrict file system permissions on untrusted and/or critical file systems, secure application sets, and use caution for removable file systems. Crucial file systems are mounted read-only on most machines in our environment (especially the ones containing critical software). Also, file systems that are removable cannot execute programs with SetGID or SetUID privilege as it is trivial to create such programs that can give the user elevated privileges (thus bypass system security) on a different system and load them from a removable device.

These categorical changes are summarized both from the metrics of the CISscan tool and with direct metrics (where possible). Results of these efforts are shown in Table 2 and Table 3, taken from our model system image at four different revision times.

Table 2 examines direct metrics that can be compared across several differing system images. This includes the total number of SetGID and SetUID programs in the image, the number of "classic" System V and "new" Systemd services, as well as kernel settings (variables) changed for hardening the internal system and network from attack. For the first four rows of metrics, lower is better, for the last two rows, higher is better:

Table 2: Navigation OS Direct Metrics

Metric	**Initial Install** [6]	**June 2016**	**April 2017**	**May 2018** [7]
(Lower numbers are better)				
Total SetUIDs	45	15	15	15
Total SetGIDs	23	18	19	19
Systemd Services	136	55	58	58
Sys V Services	5	2	2	2
(Higher numbers are better)				
Kernel variable changes	3	11	14	14
Network changes	2	4	4	4

Table 3: Navigation Red Hat Enterprise 7 Security Metrics (Center for Internet Security Benchmarks)

CIS category	**May 2015**	**June 2016**	**April 2017**	**May 2018** [6]
Updates, Add. Security	38%	45%	45%	47%
OS	12%	11%	11%	11% (est.)
Special Services	67%	67%	67%	79%
Net Configuration	91%	92%	92%	91%
Log & Audit	50%	55%	55%	57%
System Access	45%	41%	41%	39%
User Account	14%	14%	29%	43%
Tests passed/failed	71/66	87/79	88/78	110/79 [8]

Table 3 tracks more general changes in *types* of configurations, and in order to track such changes over time, the CISscan tool is used. Breaking the OS into areas of concern, these metrics measure how secure such categories are compared to a reference model. For some cases, with the addition of software sets or new features requested by users, these scores went down. While the results are broad and vary by software sets and installed feature, they give the ability to check the aggregate state of security and compare changes over time. This may be invaluable when a software installer decides to reset a host of security settings. Such changes are very apparent in these results, and this tool also proves itself useful in providing aspirational (and safe) examples for academic papers. Relevant CIS categories along with numeric percentages for several system images are given. For these values a higher percentage is better, but it can be nearly impossible, and (mentioned previously) less than useful to reach a 100% score.

4.3. User Access Controls

The controls directly placed on user action in this security model is an area where considerable compromise is necessary in the interplay between system security and user needs. The domain is one where (for the Navigation systems) the need for usability is a greater priority than security. By analogy, consider the use of badge controlled rooms in a building. While such security may be appropriate for certain high security buildings where this type of security is required, it may not be as suitable for a supermarket or a home. Two such systems are in general available for most OS platforms.

4.3.1. Discretionary Access Control

In Linux this user control is based on standard process and file permissions, allowing for access control of critical system files and granting users the ability to manage access to data sets and user files. This mechanism allows for a separation of users and data, with these management controls based on Discretionary Access Control (DAC) mechanisms, such as traditional Unix process and file management. Such controls have been standard on almost all operating systems for some time. Care should be taken to avoid overly restrictive user settings. Unlike the previous areas, it is hard to come up with a general standard for these controls. There might be significant difference in file system and data permissions even for different teams on the same system. Indeed, all that we can recommend here is due diligence in the application of these protections.

4.3.2. Mandatory Access Control

Mandatory Access Control (MAC) is an alternate security mechanism that is available under Linux, referred to as SELinux [29]. Part of a series of research projects out of the United States' National Security Agency, this series of software modules seeks to bring aspects of highly secure operating system designs to the Open Source community [30]. These features, which allow for a second, very granular control over user actions, previously were available only on highly secure and expensive computer designs. These modules are included with the Red Hat Enterprise Linux distribution and are a part of our model image. User access can be granted or revoked to a specific file or process, categorized by role. For example, on a system without SELinux, the critical system password file (/etc/shadow), cannot normally be read, however the time it was last modified and the size can be read by an unprivileged user of the system. Such information, such as when the file was last changed (i.e. the last time a password was modified) could be useful to an attacker. For a machine running SELinux with restrictive settings however that file cannot even be listed by an unprivileged user of such a system: no information about that file will be returned *at all*.

[6] The initial install was not suitable for general use and underwent significant change. It is close but not equivalent to the May 2015 release of Table 3.
[7] It should be noted in both Table 2 and Table 3 (below) that the system contained almost five times as many software packages in the May 2018 release as the initial install due to new feature requests and open source changes.

[8] CISscan was updated and several tests were added and expanded. This category had changed significantly in the new version and the value was derived from the previous test method.

However, as we note, how well the users can use the system is a crucial concern for this area. Unlike the specialized intelligence and military computer systems that utilized Mandatory Access Control initially, users of general purpose engineering machines, like those of the navigation computing environment, typically do not have the same expectations or same security concerns about how such machines should function. The use of such constraints could potentially make the user experience miserable, or simply untenable. Furthermore, familiar applications could fail in unexpected ways. Such controls are also quite difficult to configure in a correct manner to support the Navigation user community. There are few use cases where this level of security restriction for these *User Access Controls* area, has been found useful, in comparison with the application of greater restrictions on the *External Network Access* and *Internal Host Security* subsystems.

A trial run of the SELinux system was undertaken on a limited set of operations workstations to evaluate the utility of these controls. The proposed idea was to apply an iterative process to determine the areas of the system utilized normally by the user base. SELinux was run in permissive mode over the course of several weeks, and the SELinux system was examined to determine those areas where the users would be blocked by the SELinux policy. From these conflicts a model of user activity was built up over several months, which allowed for changes to be made to the SELinux policy rules, or changes to be made to user software and/or user behavior. Over time the sum of these changes helped define *expected* user actions. Areas of the system that users did not use and did not need, would be blocked off from user activity.

In principle this is a good approach. However a formal effort examining this method noted two major difficulties [31] and these difficulties have not changed significantly:

- System analysis and configuration: Getting the computer system and its processes working, and working with the correct permission sets was significantly more technically challenging than expected. Many errors were only solved by trial and error. A considerable amount of time was spent to get the system to a working and stable state.
- User analysis: This process (even on earlier versions of SELinux) was not unusually difficult. However downtime could be required during the analysis iterations, and these iterations could make it difficult to accommodate system and user activity changes (users do not like having to log out of their systems repeatedly). This may be an area that functions better for environments that are more static.

At this time methods of Mandatory Access Control such as SELinux are still being evaluated for use in Navigation. Although it offers much improved control mechanisms, and even allowing the automatic design of user access from user actions, our current examination of the intersection between system security and user utility in this area does not recommend its use at this time.

4.4. Evolution of system security over time

Unlike the previous parts of this section which deal with the issues of creating an initial, secure system state, here we consider the evolution of that state over time. As we observed in our discussion on *security over time* how this state changes is strongly subject to the environments and networks that connect to our system.

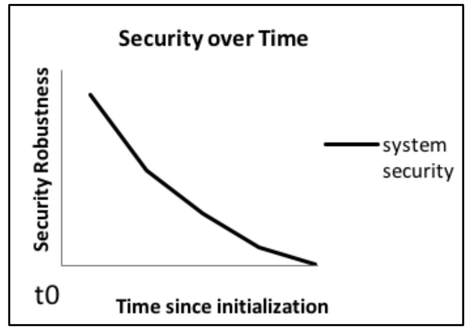

Figure 3: Security over time.

How this confidence in a system changes, and hence the *slope* of the security state in the figure above is very dependent on events in the local environment and the vulnerabilities that emerge over time. It may be nearly linear over time, or an exponential die-off due to newly discovered vulnerabilities. For example, a powered down system on a shelf (or offline storage for a VM) will not change at all. However once connected, many factors will strongly affect the slope of the curve, such as the age of the patching and software set, the security controls, and the environment to which it is connected. This is highly particular to the environmental factors acting on the system: even systems at the same site may have wide variance in this evolution. Understanding this, and remediating such changes is a large part of the maintenance lifecycle of a system. The only clear guidance that can be offered is that, as with a broken password, a system compromise will cause the curve to have a cliff (or stair-step) function in the trust of the system. This will require a system reset or reinstall to resolve.

5. Future Considerations and Conclusions

Considering the evolution of the cyber threat environment and trying to discern what new challenges will arise and how to meet these concerns is a subject of ongoing interest and research for this author. The navigation computational environment conducts critical activity on a 24/7/365 schedule, and cannot afford to be the victim of a security compromise. It is an important system that needs protection. While tips and techniques for security have dramatically changed since this author started as a system administrator, the underlying principles discussed here have changed little in two decades, or not at all. Such archetypes are examined in this paper, and while the particular technical points can change, the foundational ideas will likely remain the same.

One case in point, as noted “de-perimeterisation” approaches like Zero Trust computing may help our approach to computational and network security by encouraging rigorous security at every computational node and network connection. This is a refreshing model which brings to mind some of the most secure intelligence facilities and military fortifications of the last century. It is a vast improvement on the simple, single-defensive layer (sometimes called the hard exterior / soft interior) model which ends up being the most common approach taken in network security. Indeed, we advocate an approach in this paper of being hard on the exterior *and* hard on the interior!

While it is heartening to see such enthusiasm, and much good can come from this, it is important to remember that these efforts (still) need to consider both the complementary intersection of security and user design requirements, as well as the importance of the fault tolerant protection of *all* of the critical computational elements. As we mention above, solving the totality of this defense in breadth problem is a *hard* one. Indeed, not considering these two avenues of concern can lead to situations where the computational environment is perceived by the users as as more akin to something like a prison, or worse still, end up promoting a failure of protection akin to that seen in the previously mentioned Maginot line. Especially in the second case, aggressive efforts as Zero Trust are expensive and challenging to implement and can (from exhaustion of resources in time and effort) lead to the promotion of the failure they sought to prevent! If even a simple approach cannot be executed correctly, attempting to implement a more complex model (like Zero Trust) can be a dubious undertaking.

Another example showcasing this fundamental difference is the spate of attacks based in speculative execution on modern x86 processors (as well as methods to remediate them). These have been of tremendous concern and rapid development for the entire computer industry over the past 12 months [32]. However, the architecture problems at the source of these issues are fundamental design concerns that were identified in their implementation nearly twenty years ago [33].

In addition, a few observations may be derived from the principles espoused above. To the author's mind these should be regarded as obvious and self-evident. Unfortunately, that is often not be the case.

Of these, the most significant is *don't engineer in single points of failure*. For example, after considerable effort to construct a secure, fault tolerant network design, with a hardened firewall and a focused IDS, it is a contradictory effort to then layer a poorly secured Active Directory server for single sign-on for the network (or a poorly configured VPN to access such systems). Such a setup is self-defeating – at best. Fault tolerant and secure design should not be ignored for "just one service". In a similar manner the implementation of a poorly designed security tool designed to examine (or worse, modify) the entire enterprise environment can serve to help implement a large security hole for the entire enterprise. Indeed, as Sami Saydjari relates, there is particular concern with such enterprise security tools as such systems are the highest priority targets of attackers [19, p. 346]. Ease of management of an enterprise network is a nice goal. However, one of the questions that should come up is, "by *whom*?" Single points of failure must be closely, closely watched, as they can be doors that potentially open up the whole network to attack.

This goes with the concept that uniformity of design is not necessarily good. "Balkanization" or the promotion of multiple differing configurations (as long as each of those configurations are secure) promotes design diversity, as discussed in Section 2. While this may not be desirable from a management perspective, such diversity can lead to independent modes of failure, and hence increased security fault tolerance.

Similar to this is the desire to patch often, in the effort to be secure. These two concepts are not, as popularly believed, the same. While this may go against the grain of the currently popular DevOps and Agile software engineering paradigms, it is clear that, absent other testing schemes, it is wise to take the approach of "wait and see" when patching systems. [9] Such updates may introduce bugs, new vulnerabilities, or other unforeseen issues. This is especially true in times of stress after the announcement of major computer security bugs. Large companies can and do make mistakes, and a patch failure that in individual systems may cause pain and irritation could lead to a catastrophic failure or outage if on a critical system. [10]

Finally, one of the bigger trends in current computation lies in the increase in the use of virtual and cloud computing systems. Distributed systems such as these can offer significantly lower costs if (and this is still a big "if") their security and reliability metrics can meet the requirements of their customers. Architecture principles discussed here are (as much as they can be made to be) platform agnostic. One computer security researcher relates the major difference in cloud computing as, "Fundamentally, cloud security is a primary concern due to loss of control ... We've seen this before – [with] outsourcing..." [34, p. 24]. Does the cloud service provider follow fault tolerant and security fault tolerant design principles? Can such questions even be answered by such services?

This loss of control over the configuration for the security environment and for critical events, continues to be problematic for the Navigation use case for cloud computing, especially with concerns over Availability [34, p. 96]. With cloud computing, ownership of the systems and operational processes is by an outside organization. As a part of the operations of our computational environment, it has sometimes taken extraordinary effort to ensure the continuing functioning of our systems in times of stress. This has sometimes meant the difference between mission success and failure. In an emergency, wide latitude is given to operational staff to keep systems running and restore failed systems as fast as possible to meet the needs of flight operations. With an emergency in a remote cloud computing environment, can one even expect to get a responsible engineer on the phone? Without control over that environment, it is obvious we cannot, as Flight Director for NASA Chris Kraft said, ''...take any action necessary for mission success'' [35, p. 392].

It is hoped that the ideas in this paper will provide assistance to administrators and system engineers, and especially the astronautical community. Aspirational goals are presented here, in the hope of providing a guideline to follow for your own design

[9] A major point of defense in depth is that a single failure should not provide the opportunity for compromise on a wide scale. This should be one of the benefits of such an architecture focused approach. Many times a significant vulnerability in our systems crossed our desks with an organizational rallying cry of "patch now!", "patch now!" and we would discover that we had limited to no exposure from the vulnerability because of other defense in depth controls that were in place. Our goal is to be proactive rather than reactive. While we do have emergency patching mechanisms in place, we prefer not to use them unless truly necessary.

[10] It may be instructive to examine the release schedule (and following systems failure reports) for the firmware and software updates for the MELTDOWN/SPECTER vulnerability of 2018. Having a *running* server is in most cases preferable to one that is "currently patched", but "awaiting motherboard replacement."

efforts. These principles can be applied in Ground Data Systems design problems, as well as in other areas of systems engineering. This is particularly valuable in a community of austere budgetary realities where our bespoke systems engineering is based around missions with only a few, or (more often) only a single deliverable.

In an ideal world we would be able to trust our computer systems in the same way that when we drive a car, we trust its brakes. I believe that this optimistic idea is a badly needed one in the design of the increasingly complex and intertwined computer systems that comprise our world today. With the current state of computer security this can appear hopeless, however it is clear, as with the encouraging Boeing flight control system [10], there *are* computer systems that have been designed to be truly fault tolerant. A hard problem is not necessarily an impossible problem. There is no reason we can not also do this in computer security.

Conflict of Interest

The author declares no conflict of interest.

Acknowledgements

To the Systems Engineers and System Administrators who have helped in support of the security architecture discussed here I would like to give my sincere thanks. Additionally, of the editors who assisted with this paper, Zachary Porcu did tremendous service and to him a considerable debt of gratitude is owed. In addition it is important to note that a great deal of appreciation is also due Hal Pomeranz, contributing author of the Center for Internet Security, and senior Fellow of the SANS Institute, who spent valuable time reviewing the ideas in this paper, and raised some insightful questions that helped refine this effort.

This research was carried out at the Jet Propulsion Laboratory, California Institute of Technology, under a contract with the National Aeronautics and Space Administration. Reference to any specific commercial product, process, or service by trade name, trademark, manufacturer or otherwise, does not constitute or imply its endorsement by the United States Government or the Jet Propulsion Laboratory, California Institute of Technology.

References

[1] This paper is an extension of work originally presented in, R. M. Beswick, "Computer Security as an Engineering Practice: A System Engineering Discussion," IEEE: 6th International Conference on Space Mission Challenges for Information Technology (SMC-IT), 27-29 September, 2017. doi: 10.1109/SMC-IT.2017.18

[2] R. Beswick, P. Antreasian, S. Gillam, Y. H. Hahn, D. Roth and J. and Jones, "Navigation Ground Data System Engineering for the Cassini/Huygens Mission," AIAA 2008-3247, SpaceOps 2008 Conference, Heidelberg, Germany, May 12-16, 2008. doi:10.2514/6.2008-3247

[3] The Netflix Tech Blog, "The Netflix Simian Army," Medium, 19 July 2011. [Online]. URL: https://medium.com/netflix-techblog/the-netflix-simian-army-16e57fbab116. [Accessed 3 September 2018].

[4] The Netflix Tech Blog, "Chaos Engineering Upgraded," Medium, 25 September 2015. [Online]. URL: https://medium.com/netflix-techblog/chaos-engineering-upgraded-878d341f15fa. [Accessed 3 September 2018].

[5] C. Carson, Effective FMEA's – Achieving safe, reliable and economical products and processes using Failure Mode and Effects Analysis, Hoboken, NJ: Wiley & Sons, 2012.

[6] B. Johnson, "Fault-Tolerant Microprocessor-Based Systems," *IEEE Micro,* vol. 4, no. 6, IEEE Computer Society Press, Los Alamitos, CA, pp. 6-21, 1984.

[7] J. Gray and D. P. and Siewiorek, "High-Availability Computer Systems," IEEE Computer Society, Los Alamitos, CA, p. 39-48, September 1991. doi: 10.1109/2.84898

[8] D. McCullough, The Great Bridge: The Epic Story of the Building of the Brooklyn Bridge, New York: Simon & Schuster, 2012.

[9] U.S. - Canada Power System Outage Task Force, "Final Report on the August 14th, 2003 Blackout in the United States and Canada – Causes and Recommendations," April 2004. [Online]. URL: https://energy.gov /sites/prod/files/oeprod/DocumentsandMedia/Blackout Final-Web.pdf. [Accessed 25 May 2018].

[10] Y. C. Yeh, "Safety critical avionics for the 777 primary flight controls system," IEEE - Digital Avionics Systems, Daytona Beach, FL, DASC. 20th Conference, October 14-18, 2001. doi: 10.1109/DASC.2001.963311

[11] R. Anderson and R. Needham, "Programming Satan's Computer," *Computer Science Today, Berlin, Springer, Lecture Notes in Computer Science,* vol. 1000, pp. 426-441, 1995.

[12] B. R. Rich, "Clarence Leonard (Kelly) Johnson, 1910-1990, A Biographical Memoir," in *National Academy of Sciences*, Washington, D.C., National Academies Press, p. 231, 1995.

[13] M. Bishop, Computer Security, Art and Science, 2nd. Ed., New York: Addison-Wesley, 2019.

[14] D. Libes, "RFC 1178 – Choosing a name for your computer," August 1990. [Online]. URL: http://www.faqs.org/rfcs/rfc1178.html. [Accessed 25 May 2017].

[15] I. Roundhill, "699-101: Cassini Navigation Plan, JPL D-11621," Jet Propulsion Laboratory, Pasadena, CA, 1 August 2003.

[16] S. Garfinkel, G. Spafford and A. Schwartz, Practical UNIX and Internet Security, 3rd Ed., Sebastopol, CA: O'Reilly and Associates, 2003.

[17] W. R. Cheswick, S. M. Bellovin and A. D. Rubin, Firewalls and Internet Security, Repelling the Wily Hacker, 2nd Ed., New York: Addison-Wesley, 2003.

[18] W. Schwartau, Time Based Security, Seminole, FL: Interpact Press, 1999.

[19] O. S. Saydjari, Engineering Trustworthy Systems, New York: McGraw-Hill Education, 2018.

[20] E. Gilman and D. Barth, Zero Trust Networks, Sebastopol, CA: O'Reilly Media Inc., 2017.

[21] B. Youn and P. Wang, "Complementary Intersection Method for System Reliability Analysis," *ASME Journal Mechanical Design,* vol. 134, no. 4, April 2009. doi: 10.1115/1.3086794

[22] R. Cross, "Center of percussion of hand-held implements," *American Journal of Physics,* vol. 72, no. 5, pp. 622-630, May 2004. doi:10.1119/1.1634965

[23] S. Chiasson and P. C. v. Oorschot, "Quantifying the security advantage of password expiration policies," *Designs, Codes and Cryptography,* vol. 77, Issue 2-3, pp. 401-408, December 2015.doi: 10.1007/s10623-015-0071-9

[24] National Vulnerability Database, "National Checklist Program Repository," National Institiute of Standards and Technology, [Online]. URL: https://nvd.nist.gov/ncp/repository. [Accessed 30 March 2018].

[25] Information Assurance Directorate, " Operating Systems guidance," National Security Agency, [Online]. URL: https://www.iad.gov/iad/library/ia-guidance/security-configuration/operating-systems/index.cfm. [Accessed 20 April 2017].

[26] Center for Internet Security, "CIS - Center for Internet Security," CIS, [Online]. URL: http://www.cisecurity.org. [Accessed 30 March 2018].

[27] NMAP, "Nmap," [Online]. URL: http://www.nmap.org. [Accessed 30 March 2018].

[28] Nessus, "Tenable Security," Tenable Inc, [Online]. URL: http://www.tenable.com/products. [Accessed 30 March 2018].

[29] SELinux, [Online]. URL: http://selinuxproject.org/page/Main_Page. [Accessed 25 May 2018].

[30] NSA, "SELinux," National Security Agency, [Online]. URL: https://www.nsa.gov/what-we-do/research/selinux/.[Accessed 25 May 2018].

[31] R. M. Beswick and D. C. Roth, "A Gilded Cage: Cassini/Huygens Navigation Ground Data System Engineering for Security," AIAA 2012-1267202, SpaceOps 2012 Conference, Stockholm, Sweden, June 11-15, 2012. doi:10.2514/6.2012-1267202

[32] P. Kocher, D. Genkin, D. Gruss, W. Haas, M. Hamburg, M. Lipp, S. Mangard, T. Prescher, M. Schwarz and Y. Yarom, "Spectre Attacks: Exploting Speculative Execution," *arXiv.org:1801.01203,*3 January 2018.

[33] Z. Wang and R. B. Lee, "Covert and Side Channels due to Processor Architecture," *Proceedings of the 22nd Annual Computer Security Applications Conference (ACSAC'06),* 11-15 Dec. 2006. doi:10.1109/ACSAC.2006.20

[34] D. Shackleford, "Security 524: Cloud Security Fundamentals - Day 1," in *[seminar], SANS National Conference*, Orlando, FL, April 7th, 2017.

[35] G. Kranz, in *Failure Is Not an Option: Mission Control From Mercury to Apollo 13 and Beyond*, New York, Simon & Schuster, 2009.

[36] C. E. Shannon, "Communication Theory of Secrecy Systems," *Bell System Technical Journal,* vol. 28, no. 4, pp. 656-715, 1949. doi:10.1002/j.1538-7305.1949.tb00928.x

Advances in Science, Technology and Engineering Systems Journal
Vol. 4, No. 2, 370-379 (2019)
www.astesj.com
Special Issue on Advancement in Engineering and Computer Science

ASTES Journal
ISSN: 2415-6698

Distribution of Bit Patterns in Binary Sequence Generated Over Sub Extension Field

Md. Arshad Ali[*,1], Yuta Kodera[1], Takuya Kusaka[1], Yasuyuki Nogami[1], Satoshi Uehara[2], Robert H. Morelos-Zaragoza[3]

[1]*Graduate School of Natural Science and Technology, Okayama University, 7008530, Japan*

[2]*Faculty of Environmental Engineering, The University of Kitakyushu, 8028577, Japan*

[3]*Department of Electrical Engineering, San Jose State University, CA 95192, United States*

ARTICLEINFO

Article history:
Received: 05 March, 2019
Accepted: 16 April, 2019
Online: 28 April, 2019

Keywords:
Pseudo-random sequence
Distribution of bit patterns
Primitive polynomial
Trace function
Legendre symbol

ABSTRACT

The distribution of bit patterns is an important measure to check the randomness of a sequence. The authors of this paper observed this crucial property in a binary sequence which generated by using a primitive polynomial, trace function, and Legendre symbol defined over the sub extension field. The authors create a new dimension in the sequence generation research area by considering the sub extension field, whereas all our previous works are focused in the prime field. In terms of distribution of bit patterns property, this research work has notable outcomes more specifically the binary sequence (defined over the sub extension field) holds much better (close to uniform) bit distribution than the previous binary sequence (defined over the prime field). Furthermore, the authors theoretically proved the distribution of bit property in this paper.

1 Introduction

In this IoT era, we communicate with each other through the internet. Therefore, secure communication is the major matter of concern. We use symmetric cryptosystems (Advanced Encryption Standard (AES) [1]) and asymmetric cryptosystems (Rivest Shamir Adleman (RSA) [2], and Elliptic Curve Cryptography (ECC) [3]) to establish a secure communication. A pseudo-random number is one of the crucial parts of these cryptosystems. More specifically, in case of cryptography, to generate the keys (public key, private, session key, and so on) a pseudo-random number generator is used. A prominent pseudo-random number generator is essential to generate pseudo-random number having randomness property (along with other good statistical properties). Consequently, the security of these cryptosystems deliberately depends upon the randomness property regarding a sequence. Thus, it is mandatory to evaluate the randomness of a sequence before utilized them in any cryptosystems. Basically, two crucial properties namely the linear complexity [4] and the distribution of bit patterns regarding a sequence are nowadays well-known to check the randomness of a pseudo-random sequence. In this work, the authors restrict the discussion on the distribution of bit patterns property to evaluate the randomness of a sequence.

Most renowned pseudo-random number generators are the Mersenne Twister (MT) [5], Blum-Blum-Shub (BBS) [6], Legendre sequence [7, 8], and M-sequence [9]. Among those the former two pseudo-random number generators (MT and BBS) are well-known considering their applications in cryptography rather than the theoretical aspect. On the other hand, the M-sequence and Legendre sequence are prominent geometric sequences regarding the theoretical aspect. As a result, the authors attracted in the pseudo-random sequence generation research area by observing the theoretical prospect on the M-sequence and Legendre sequences.

The Legendre sequence [7, 8] is generated by applying the Legendre symbol over the odd characteristic field. It has a long period, high linear complexity, and the distribution of bit patterns of the Legendre se-

*Md. Arshad Ali, Graduate School of Natural Science and Technology, Okayama University, 3-1-1, Tsushima-naka, Kita, Okayama, 7008530, Japan, +81-8042661986, arshad@s.okayama-u.ac.jp

https://dx.doi.org/10.25046/aj040246

quence is known to be close to uniform [10, 11]. On the other hand, M-sequence is generated by a linear recurrence relation over the finite field. It has a maximum period but minimum linear complexity. In addition, M-sequence [9] is well-known for its uniform distribution of bit patterns [12]. Our previous work on geometric sequence [13] combines the features of the Legendre sequence and M-sequence. As mentioned previously, linear complexity and distribution of bit patterns are the important measures to evaluate the randomness of a sequence. So, regarding the linear complexity, our previous sequence [13] always possess high value. Unlike the linear complexity, the distribution of bit patterns in [13] doesn't reaches up to the mark alike the Legendre sequence and M-sequence. Hence, its a scope to improve the distribution of bit patterns in our previous sequence.

The trace calculation is an important step during our sequence generation procedure. Lets focus on the important aspect regarding this calculation. In case of prime field $\mathbb{F}_p$, the trace function maps an element of the extension field $\mathbb{F}_{q^M}$ to an element of the prime field $\mathbb{F}_p$. Therefore, the number of possible trace outputs will be in the range of $\{0 \sim p-1\}$. In other words, if we calculate the trace over the prime field, then it will output p kinds of values. On the other hand, in case of the sub extension field $\mathbb{F}_q$, the trace function maps an element of the extension field $\mathbb{F}_{q^M}$ to an element of the sub extension field $\mathbb{F}_q$ and the number of possible trace outputs will be in the range of $\{0 \sim q-1\}$ which means the trace outputs q kinds of values. It should be noted that here $M = m/m'$, $q = p^{m'}$, and m' be one of the factors of m. From the theoretical perspective, more variation in the trace values contribute to the better appearance of bits (0 and 1) in a sequence. This is one of the important aspects to consider the sub extension during the sequence generation procedure to improve the distribution of bit patterns in our previous sequence [13]. After utilizing the sub extension field, the detailed improvement in distribution of bit patterns is introduced in the result and discussion section in this paper.

Recently, the authors started to consider the sub extension field during the sequence generation procedure, which is a new dimension of our research work on generation of pseudo-random sequence (whereas our previous works on binary sequence [13] and multi-value sequence [14, 15] are considered in the prime field). As a result, our recent works on binary sequence [16] and multi-value sequence [17] experimentally observed the linear complexity, autocorrelation properties, respectively. As mentioned previously, the distribution of bit patterns is an important measure to evaluate the randomness of a sequence. Thus, the authors of this paper consider the distribution of bit patterns in a binary sequence which generated over the sub extension field.

The Legendre sequence and M-sequence are the base of the sequence research area. Their properties are already proven, therefore many researchers attracted by those sequences. As mentioned previously, our sequence also generated by the idea of the Legendre and M-sequences. Consequently, the authors thought that its properties can be theoretically proven and fortunately its proven (which shown in the later section of this paper). This is one of the contributions of the authors in this paper. Moreover, they also make a comparison between the binary sequence defined over the sub extension field with their previous work on binary sequence in terms of distribution of bit patterns property. According to the comparison result, binary sequence (defined over sub extension field) holds much better (close to uniform) distribution of bit patterns than the previous binary sequence [13]. Finding this improvement by considering the sub extension field is the major contribution of this paper.

The authors of this paper observed the distribution of bit patterns in a binary sequence which generated by a primitive polynomial, trace function, and Legendre symbol over the sub extension field. In brief, the sequence generation procedure is as follows: at first, it uses a primitive polynomial over the odd characteristic field $\mathbb{F}_p$ to generate maximum length vector sequence as elements in $\mathbb{F}_{q^M}$, then the trace function maps the extension field $\mathbb{F}_{q^M}$ elements to the sub extension field $\mathbb{F}_q$ elements, and finally the Legendre symbol binarizes the sub extension field $\mathbb{F}_q$ elements to a binary sequence. The authors already observed the period, autocorrelation, cross-correlation, and linear complexity properties of the binary sequence (which generated over the sub extension field) in their previous works [16, 17]. Thus, this paper focused on the distribution of bit patterns property. In brief, the authors count the number of appearances for each n-bit patterns (where $1 \leq n \leq (m/m')$). After observing many experimental results, the authors found that the number of appearances of each bit pattern is related to the number of zeros contained in each bit pattern. Furthermore, the authors theoretically proven the distribution of bit patterns equation. Moreover, they also make a comparison with their previous work [13].

Throughout this paper, p and q denote an odd prime number and its power $q = p^{m'}$, respectively, where m be a positive integer which mainly denotes extension degree and m' be one of the factors of m. In addition, $M = m/m'$ and $\mathbb{F}_q^*$ denotes the multiplicative group of $\mathbb{F}_q$, that is $\mathbb{F}_q^* = \mathbb{F}_q - \{0\}$.

2 Preliminaries

This section briefly explains some fundamental concepts of the finite field theory such as group, field, primitive polynomial, trace function, Legendre symbol, and dual bases. Then, binary sequence is introduced along with its period and distribution of bit patterns properties.

2.1 Group

A group is a non-empty set $\mathbb{G}$ with a binary operation $\circ$ on its elements denoted as $< \mathbb{G}, \circ >$, which satisfies the following axioms.

- **Closure** For $\forall_{a,b} \in \mathbb{G}$, the result of $a \circ b$ also exists in $\mathbb{G}$ and it is uniquely given.

- **Associativity** Elements in group $\mathbb{G}$ should follow associativity. i.e. $(a \circ b) \circ c = a \circ (b \circ c)$, where $a, b, c \in \mathbb{G}$.

- **Identity element** There exists an element $e \in \mathbb{G}$ such that $\forall_a \in \mathbb{G}$, $a \circ e = e \circ a = a$.

- **Inverse element** For $\forall_a \in \mathbb{G}$, there exists an element $b \in \mathbb{G}$ such that $a \circ b = e = b \circ a$, where b is called inverse element of a.

Commutative group A group $\mathbb{G}$ will be commutative if $a \circ b = b \circ a$ for all $a, b \in \mathbb{G}$.
Group generator For a given group $\mathbb{G}$ if there is an element $g \in \mathbb{G}$ such that for any $a \in \mathbb{G}$ there exists an unique integer i with $a = g^i$ then g will be called as a generator of $\mathbb{G}$.
Order of a group The order of a group $\mathbb{G}$ often denoted as $\#\mathbb{G}$ is the number of elements in the group $\mathbb{G}$.
Cyclic group A group $\mathbb{G}$ will be cyclic if there exists at least one generator $g \in \mathbb{G}$ and it is denoted as $\mathbb{G} = < g >$. From the definition of cyclic group, it can be visualized that each element in a cyclic group can be generated with iterative operations of generator g which shown in the following Figure 1.

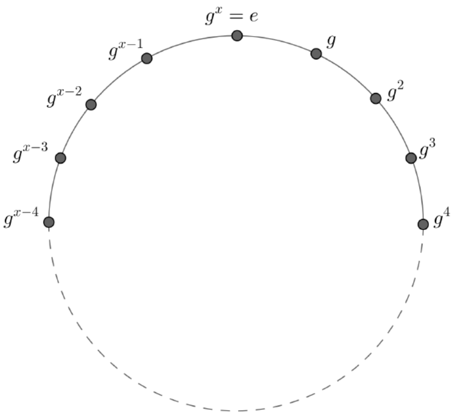

Figure 1: cyclic group.

Multiplicative group A cyclic group is called multiplicative if we tend to write its group operation in the same same way we do multiplication, that is

$$f = g \cdot x \text{ or } f = g^x.$$

2.2 Field

A field $< \mathbb{F}, +, \cdot >$ is a set that obeys two binary operations denoted by + and $\cdot$, such that

- $\mathbb{F}$ is a commutative group with respect to addition (+) having identity element 0.

- Let $\mathbb{F}^*$ is a subset of $\mathbb{F}$ having non-zero elements of $\mathbb{F}$ i.e. $\mathbb{F}^* = \mathbb{F} - \{0\}$. Then $\mathbb{F}^*$ will be called a commutative group with respect to multiplication $(\cdot)$, where every element should have multiplicative inverse in $\mathbb{F}^*$.

- For all $a, b, c \in \mathbb{F}$ the distributive law will be followed, i.e. $a \cdot (b + c) = a \cdot b + a \cdot c$ and $(b + c) \cdot a = b \cdot a + c \cdot a$.

Sub field Let $\mathbb{F}_1$ is a sub field of a field $\mathbb{F}$. Then $\mathbb{F}_1$ will be called a sub field if $\mathbb{F}_1$ obeys the laws of field with respect to the field operation inherited from $\mathbb{F}$. In addition, if $\mathbb{F}_1 \neq \mathbb{F}$, then $\mathbb{F}_1$ is a proper sub field of $\mathbb{F}$.

Prime field Let p be a prime. The ring of integers modulo p is a finite field of characteristic p having field order p denoted as $\mathbb{F}_p$ is called a prime field.

Extension field A subset $\mathbb{F}_0$ of a field $\mathbb{F}$ that is itself a field under the operations of $\mathbb{F}$ will be called a sub field of $\mathbb{F}$. In this case, $\mathbb{F}$ is called an extension field of $\mathbb{F}_0$. An extension field of a prime field $\mathbb{F}_p$ can be represented as m-dimensional vector space that has m elements in $\mathbb{F}_p$. Let the vector space be the m-th extension field be denoted as $\mathbb{F}_{q^M}$. The order of a extension field $\mathbb{F}_{q^M}$ is given as p^m (here $q = p^{m'}$ and $M = m/m'$).

In very brief, it can be said that a prime field $(\mathbb{F}_p)$ is a subset of sub extension field $(\mathbb{F}_q)$ and sub extension field $\mathbb{F}_q$ is also a sub set of extension field $\mathbb{F}_{q^M}$ which shown in Figure 2.

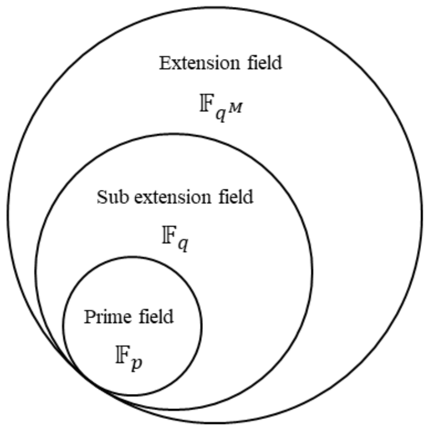

Figure 2: $\mathbb{F}_p \subset \mathbb{F}_q \subset \mathbb{F}_{q^M}$.

2.3 Primitive Polynomial

Consider a polynomial $f(x)$ of degree m over prime field $\mathbb{F}_p$. If it is not factorized into smaller degree polynomials over the prime field $\mathbb{F}_p$, it is called an irreducible polynomial. Consider the smallest number e such that $x^e - 1$ is divisible by $f(x)$ over $\mathbb{F}_p$, it is known that e becomes a factor of $q^M - 1$. Then $f(x)$ is especially called a primitive polynomial, when e is equal to $q^M - 1$. Its zero ω belongs to the extension field $\mathbb{F}_{q^M}$ and it becomes a primitive element in $\mathbb{F}_{q^M}$ that generates every non-zero element in $\mathbb{F}_{q^M}$ as its power ω^i (for $i = 0, 1, 2, \ldots, q^{M-2}$).

2.4 Trace Function

This work utilizes the trace function to map an element of the extension field $X \in \mathbb{F}_{q^M}$ to an element of the sub extension field $x \in \mathbb{F}_q$ as,

$$x = \mathrm{Tr}_{q^M|q}(X) = \sum_{i=0}^{\frac{m}{m'}-1} X^{p^{im'}}. \tag{1}$$

A crucial point, the above trace becomes an arbitrary element in $\mathbb{F}_q$ and the trace function has a linearity property over the sub extension field $\mathbb{F}_q$ as follows,

$$\mathrm{Tr}_{q^M|q}(aX + bY) = a\mathrm{Tr}_{q^M|q}(X) + b\mathrm{Tr}_{q^M|q}(Y), \tag{2}$$

where $a, b \in \mathbb{F}_q$ and $X, Y \in \mathbb{F}_{q^M}$.

2.5 Legendre Symbol

The Legendre symbol $\left({}^{a}\!/\!{}_{q}\right)_2$ is used to check the quadratic residue for any arbitrary element a in $\mathbb{F}_q$. It is defined as,

$$\begin{aligned}\left({}^{a}\!/\!{}_{q}\right)_2 &= a^{(q-1)/2} \\ &= \begin{cases} 0, & \text{if } a = 0, \\ 1, & \text{else if } a \text{ is a QR in } \mathbb{F}_q^*, \\ p-1, & \text{otherwise } a \text{ is a QNR in } \mathbb{F}_q^*. \end{cases}\end{aligned} \tag{3}$$

Here, QR and QNR stand for Quadratic Residue (QR) and Quadratic Non-Residue (QNR), respectively. Additionally, the non-zero element a is called the QR if it has a square root in $\mathbb{F}_q$, otherwise a is called the QNR. In this paper, the Legendre symbol is used for translating a vector sequence generated by the trace function over $\mathbb{F}_q$ to a binary sequence. Above mentioned QR and QNR in $\mathbb{F}_q$ holds the following important property.

Non-zero elements are the roots of $x^{q-1} - 1$ in $\mathbb{F}_q^*$ over $\mathbb{F}_q$ without any duplicates. Since it is factorized as follows:

$$x^{q-1} - 1 = \left(x^{(q-1)/2} - 1\right) - \left(x^{(q-1)/2} - 1\right). \tag{4}$$

It is thus found that the number of QR's and QNR's in $\mathbb{F}_q^*$ are the same and it is given by $(q-1)/2$. In addition, these numbers are important part in proving the theorem in the later section of this paper.

2.6 Dual Bases

The dual bases plays an important role in proving the theorem shown in this paper. It is defined as follows:

Let $\mathbb{F}_{q^M}$ be a finite field and $\mathbb{F}_q$ be a finite extension of $\mathbb{F}_{q^M}$. Then the two bases $\mathcal{A} = \{\alpha_0, \alpha_1, \ldots, \alpha_{m-1}\}$ and $\mathcal{B} = \{\beta_0, \beta_1, \ldots, \beta_{m-1}\}$ of $\mathbb{F}_q$ over $\mathbb{F}_{q^M}$ are said to be the dual (or complementary) bases if

$$\mathrm{Tr}_{q^M|q}\left(\alpha_i \beta_j\right) = \begin{cases} 1, & \text{if } i = j, \\ 0, & \text{otherwise,} \end{cases} \tag{5}$$

where $1 \le i, j \le m-1$.

2.7 Binary Sequence and Its Properties

This paper introduces a binary sequence along with its period and distribution of bit patterns properties as follows.

2.7.1 Generation Procedure and Period

Let ω be a primitive element in the extension field $\mathbb{F}_{q^M}$, where $M = m/m'$, m be a composite number which denotes the extension degree of the primitive polynomial, and m' be one of the factors of m. Then, by utilizing the trace function and Legendre symbol a binary sequence $\mathcal{S}$ is generated as follows:

$$\mathcal{S} = \{s_i\}, s_i = f_2\left(\left({}^{\mathrm{Tr}_{q^M|q}\left(\omega^i\right)}\!/\!{}_{p}\right)\right), \tag{6}$$

where $i = (0, 1, 2, \ldots, \lambda - 1, \ldots)$, $s_i \in 0, 1$ and $f_2(\cdot)$ be a mapping function, which translates the 0, 1, and $p-1$ values sequence generated by the Legendre symbol to a pseudo-random binary sequence. This mapping function is defined as follows:

$$f_2(s) = \begin{cases} 0, & \text{if } x = 0, 1 \bmod q, \\ 1, & \text{otherwise.} \end{cases} \tag{7}$$

After observing many experimental results, the authors derive the equation for the period λ of the binary sequence as,

$$\lambda = \frac{2(q^M - 1)}{q - 1}. \tag{8}$$

2.7.2 Distribution of Bit Patterns

From the viewpoint of security, the distribution of bit patterns is as important as the linear complexity. If a sequence holds the uniform distribution of bit patterns, then it becomes difficult to guess the next bit after observing the previous bit patterns. For example, let's assume a binary sequence having a period of 12 as $\mathcal{S}_{12} = \{1, 0, 1, 0, 1, 0, 1, 0, 1, 0, 1, 0\}$. If we observe the 1-bit pattern in this sequence, then we can find that it has a uniform distribution of 1 and 0. In other words, 1 and 0 appear same in number. However, when we check 2-bit patterns on $\mathcal{S}_{12}$, we find that it only has two types of patterns (10 and 01). In this case, we can easily predict the next bit patterns after observing the previous patterns. For example, let us make a sub-sequence of $\mathcal{S}_{12}$ as $\{1, 0, 1, 0, x_5, x_6\}$, we can easily guess x_5 and x_6 as $x_5 = 1$ and $x_6 = 0$. Therefore, it is also essential to evaluate the distribution of bit patterns of the sequence to confirm its randomness. In other words, the uniformity of the distribution contributes to the randomness from the viewpoint of unpredictability.

3 Distribution of Bit Patterns in Binary Sequence

In this section, we will introduce the bit distribution of binary sequence which generated over the sub extension field. In addition, bit distribution of M-sequence and Legendre sequence is also introduced here. Throughout this section $b^{(n)}$, $Z(b^{(n)})$ and $D_{\mathcal{S}_\lambda}(b^{(n)})$ denotes a bit pattern of length n, number of 0's in $b^{(n)}$, and number of appearance of $b^{(n)}$ in $\mathcal{S}_\lambda$, respectively. For example, in a binary sequence of period 15, a 3-bit pattern $b = 101$ appears 4 times. Then, these notations become $b^{(3)} = 101$, $Z(b^{(3)}) = 1$, and $D_{\mathcal{S}_{15}}(b^{(3)}) = 4$.

3.1 Bit Distribution of M-sequence

The M-sequence [9] is generated by a linear recurrence relation over the finite field. M-sequence has a maximum period and uniform distribution of bit pattern except for the case of $Z(b^{(n)}) = n$ but it has minimum linear complexity. Let, $f(x) = x^4 + x + 1$ be a primitive polynomial over $\mathbb{F}_2$, then using the linear recurrence relation a M-sequence of period 15 becomes as follows.

$$\mathcal{S}_{15} = \{1,0,0,0,1,1,1,1,0,1,0,1,1,0,0\}. \tag{9}$$

The distribution of n-bit pattern in (9) is shown in Table 1, here $1 \le n \le m$. In the case of M-sequence, except the all-zero pattern, every pattern appears same in number. For example, when $n = 3$ all patterns appear 2 times (except 000 pattern). In other words, they are uniformly distributed. Every M-sequence has such good distribution of bit pattern feature.

Table 1: Bit distribution of the M-sequence $\mathcal{S}_{15}$.

n	$b^{(n)}$	$Z(b^{(n)})$	$D_{\mathcal{S}_{15}}(b^{(n)})$
1	0	1	7
	1	0	8
2	00	2	3
	01	1	4
	10	1	4
	11	0	4
3	000	3	1
	001	2	2
	010	2	2
	100	2	2
	011	1	2
	101	1	2
	110	1	2
	111	0	2

3.2 Bit Distribution of LegendreSequence

Legendre sequence [7, 8] is generated by applying the Legendre symbol over the odd characteristic field. Legendre sequence has a long period, high linear complexity, and the distribution of bit pattern is close to uniform. Let, $p = 23$, then the Legendre sequence of period 23 becomes as follows.

$$\mathcal{S}_{23} = \{0,0,0,0,0,1,0,1,0,0,1,1,0,0,1,1,0,1,0,1,1,1,1\}. \tag{10}$$

The distribution of n-bit pattern in (10) is shown in Table 2. In case of Legendre symbol, bit patterns appearance is close to uniform.

Table 2: Bit distribution of the Legendre sequence $\mathcal{S}_{23}$.

n	$b^{(n)}$	$Z(b^{(n)})$	$D_{\mathcal{S}_{23}}(b^{(n)})$
1	0	1	12
	1	0	11
2	00	2	6
	01	1	6
	10	1	5
	11	0	5
3	000	3	3
	001	2	3
	010	2	3
	100	2	3
	011	1	2
	101	1	3
	110	1	2
	111	0	2

3.3 Bit Distribution of the Proposed Binary Sequence

Let $\mathcal{S}_\lambda$ be a binary sequence of having a period of λ. Again, let $b^{(n)}$, $Z(b^{(n)})$, and $D_{\mathcal{S}_\lambda}(b^{(n)})$ denotes a bit pattern of length n, number of 0's in $b^{(n)}$, and number of appearance of $b^{(n)}$ in $\mathcal{S}_\lambda$, respectively. Then, the distribution of bit patterns in the binary sequence which defined over the sub extension field can be given by the following theorem.

$$D_{\mathcal{S}_\lambda}\left(b^{(n)}\right) = \begin{cases} q^{M-(n\cdot m')} \cdot \left(\frac{q-1}{2}\right)^{n-Z\left(b^{(n)}\right)-1} \cdot \left(\frac{q+1}{2}\right)^{Z\left(b^{(n)}\right)} & \text{(11a)} \\ \quad \text{when } 0 \le Z\left(b^{(n)}\right) < n, & \\ \lambda - \sum_{u=0}^{Z\left(b^{(n)}\right)} {}_nC_u \cdot D_{\mathcal{S}_\lambda}\left(b^{(n)}\right) & \text{(11b)} \\ \quad \text{when } Z\left(b^{(n)}\right) = n. & \end{cases}$$

Let ω be a primitive element in the extension field $\mathbb{F}_{q^M}$, where $M = m/m'$, m be a composite number which denotes the extension degree of the primitive polynomial, and m' be one of the factors of m. Then, utilizing the trace function and Legendre symbol one period of a binary sequence is generated as follows.

$$\mathcal{S}_\lambda = \{s_i\}, s_i = f_2\left(\left(\mathrm{Tr}_{q^M|q}\left(\omega^i\right) \big/ p\right)\right), i = 0,1,2,\ldots,\lambda-1,\ldots, \tag{12}$$

Here λ be the period of the sequence and it is given by the following equation as,

$$\lambda = \frac{2(q^M - 1)}{q - 1}. \quad (13)$$

At first, a primitive polynomial is used, then the trace value is calculated, then the Legendre symbol outputs zero, QR or QNR in $\mathbb{F}_q$, and finally the sequence coefficients s_i is given by the mapping function $f_2(\cdot)$.

The authors of this paper observe the distribution of n-bit patterns in a binary sequence. It should be noted that here n satisfies $1 \le n \le (m/m')$ relation. The distribution of n-bit patterns evaluated by observing the consecutive sequence coefficients $(s_i, s_{i+1}, \ldots, s_{i+(n-1)})$. Particularly,

$$\begin{aligned} s_{i+0} &= f_2\left(\left(\mathrm{Tr}\left(\omega^i \cdot \omega^0\right)\Big/p\right)\right), \\ s_{i+1} &= f_2\left(\left(\mathrm{Tr}\left(\omega^i \cdot \omega^1\right)\Big/p\right)\right), \\ &\vdots \\ s_{i+(n-1)} &= f_2\left(\left(\mathrm{Tr}\left(\omega^i \cdot \omega^{n-1}\right)\Big/p\right)\right), \end{aligned}$$

where $0 \le i \le (q^M - 2)$. By observing the above sequence coefficients, the distribution of bit patterns $D_{\mathcal{S}_\lambda}$ is determined by the following trace values.

$$\mathrm{Tr}\left(\omega^i \cdot \omega^0\right), \mathrm{Tr}\left(\omega^i \cdot \omega^1\right), \ldots, \mathrm{Tr}\left(\omega^i \cdot \omega^{n-1}\right). \quad (14)$$

Let $\mathcal{A} = \{\alpha_0, \alpha_1, \ldots, \alpha_{m-1}\}$ be a basis, ω be a primitive element and with this basis ω^i is represented as,

$$\omega^i = \sum_{j=0}^{m-1} a_{i,j}\alpha_j, \text{where } a_{i,j} \in \mathbb{F}_q \text{ and } 0 \le i \le q^M - 2. \quad (15)$$

Again let $\mathcal{B} = \{\omega^0, \omega^1, \ldots, \omega^{n-1}, \beta_n, \ldots, \beta_{m-1}\}$ be a dual basis of $\mathcal{A}$ in $\mathbb{F}_q$ over $\mathbb{F}_{q^M}$. Then we also have

$$\omega^t = \omega^t + \sum_{j=0}^{\frac{m}{m'}-1} 0 \cdot \beta_j, \text{where } 0 \le t < n. \quad (16)$$

Since $\mathcal{A}$ and $\mathcal{B}$ are dual bases to each other, then $\mathrm{Tr}\left(\omega^i \cdot \omega^t\right)$ be calculated as follows.

$$\begin{aligned} \mathrm{Tr}\left(\omega^i \cdot \omega^t\right) &= \mathrm{Tr}\left(\sum_{j=0}^{m-1} a_{i,j}\alpha_j \cdot \left(\omega^t + \sum_{j=0}^{\frac{m}{m'}-1} 0 \cdot \beta_j\right)\right) \\ &= a_{i,t}. \end{aligned}$$

Therefore, by using the dual basis, the distribution of bit patterns $D_{\mathcal{S}_\lambda}\left(b^{(n)}\right)$ determined by the trace values becomes as follows.

$$\begin{aligned} &\mathrm{Tr}\left(\omega^i \cdot \omega^0\right), \mathrm{Tr}\left(\omega^i \cdot \omega^1\right), \ldots, \mathrm{Tr}\left(\omega^i \cdot \omega^{n-1}\right) \\ &= (a_{i,0}, a_{i,1}, \ldots, a_{i,n-1}). \end{aligned}$$

Thus, instead of using sequence coefficients $(s_i, s_{i+1}, \ldots, s_{i+(n-1)})$, we can consider the dual basis representation of these coefficients as $\left(a_{i,0}, a_{i,1}, \ldots, a_{i,(n-1)}\right)$. Additionally, all the above trace values belong to the sub extension field $\mathbb{F}_q$.

Furthermore, $\omega^i \left(0 \le i \le q^M - 2\right)$ in (15) represents every non-zero vectors in the extension field $\mathbb{F}_{q^M}$ as,

$$\left\{\mathrm{Tr}\left(\omega^0\right), \mathrm{Tr}\left(\omega^1\right), \mathrm{Tr}\left(\omega^2\right), \mathrm{Tr}\left(\omega^3\right), \ldots, \mathrm{Tr}\left(\omega^{q^M-2}\right)\right\}. \quad (17)$$

According to the trace property, non-zero $\mathbb{F}_q$ elements appear $q^{M-m'}$ times and zero appears one less than the other elements i.e. $q^{M-m'} - 1$ times in the above equation.

3.3.1 Relation Between the Sequence Coefficients With the Trace Values and Legendre Symbol Calculation

Depending on the three different types of trace values (0, QR, and QNR), the Legendre symbol outputs three different values (0, 1, and $p-1$), and finally the mapping function outputs 0 and 1 as sequence coefficients s_i. This dependency between the trace and Legendre symbol is explained as follows.

Table 3: Relation between the sequence coefficients with trace and Legendre symbol calculation -I.

s_i	$\mathrm{Tr}\left(\omega^i\right)$
0	0 or QR in $\mathbb{F}_q^*$
1	QNR in $\mathbb{F}_q^*$

According to the above table, the sequence coefficient 0 comes from the two cases: one is for the $\mathrm{Tr}(0)$ case and another one is for the QR in $\mathbb{F}_q^*$ case. To deal with this two cases uniquely, let us denote **0** and 0 for the first and second cases, respectively. In addition, 1 comes for QNR in $\mathbb{F}_q^*$ case. Thus the above table can be further modified as follows.

Table 4: Relation between the sequence coefficients with trace and Legendre symbol calculation -II.

s_i	$\mathrm{Tr}\left(\omega^i\right)$
0	0
0	QR in $\mathbb{F}_q^*$
1	QNR in $\mathbb{F}_q^*$

To distinguish the appearance of 0, this paper uses the notation **0**, when zero comes from $\mathrm{Tr}(0)$ and 0 when zero comes from QR. Let the number of **0** be denoted by u and $T_{u,n}$ denotes the number of bit patterns including u times **0** and $Z(b^{(n)}) - u$ times 0. Thus, T_n can be considered as,

$$\sum_{u=0}^{Z\left(b^{(n)}\right)} T_{u,n}. \quad (18)$$

In the following section, the distribution of bit patterns in the binary sequence defined over the sub extension field theoretically proven.

3.3.2 Proof of (11a)

The period of the binary sequence is given by the following equation as,

$$\lambda = \frac{2(q^M-1)}{q-1}. \tag{19}$$

After rewriting the above equation we obtain,

$$q^M - 1 = \lambda \cdot \left(\frac{q-1}{2}\right). \tag{20}$$

To observe the distribution of bit patterns, the above relation becomes as follows.

$$D_{\mathcal{S}_{q^M-1}}\left(b^{(n)}\right) = D_{\mathcal{S}_\lambda}\left(b^{(n)}\right) \cdot \left(\frac{q-1}{2}\right). \tag{21}$$

Thus, we must consider two cases of the sequence length such as $\mathcal{S}_{q^M-1}$ and $\mathcal{S}_\lambda$. Hence, we will observe the distribution of bit patterns in $\mathcal{S}_{q^M-1}$ as $D_{\mathcal{S}_{q^M-1}}\left(b^{(n)}\right)$ and $\mathcal{S}_\lambda$ as $D_{\mathcal{S}_\lambda}\left(b^{(n)}\right)$.

In the previous section, we explained that n-bit patterns can be considered as $b^{(n)} = (a_{i,0}, a_{i,1}, \ldots, a_{i,n-1})$. On the other hand, the remaining $(m-(n \cdot m'))$-bit patterns are composed of $(a_{i,nm'}, a_{i,nm'+1}, \ldots, a_{i,m-1})$ coefficients of ω^i, which is given by the (16). In addition, the number of combinations of $(a_{i,nm'}, a_{i,nm'+1}, \ldots, a_{i,m-1})$ becomes $q^{M-nm'}$. It should be noted that here ω^i represents all of the non-zero coefficients in the extension field $\mathbb{F}_{q^M}$.

As mentioned previously, when the trace value is equal to 0 or QR, then the sequence coefficients becomes **0** and 0, respectively. In addition, if the trace value is equal to QNR, then the sequence coefficients becomes 1. Additionally, u denotes the number of **0** in $b^{(n)}$ $\left(\text{where } 0 \le u \le Z\left(b^{(n)}\right)\right)$ from Tr(0), then the other 0's comes from $Z\left(b^{(n)}\right) - u$ QR's, and finally 1's comes from $n - Z\left(b^{(n)}\right)$ QNR's. Therefore, by separating 0, $T_{u,n}$, and T_n the combination of n-bit patterns can be given as follows.

$$\begin{aligned} T_{u,n} &= {}_nC_u \cdot {}_{n-u}C_{Z(b^{(n)})-u} \cdot \left(\frac{q-1}{2}\right)^{Z(b^{(n)})} \\ &\times {}_{n-Z(b^{(n)})}C_{n-Z(b^{(n)})} \cdot \left(\frac{q-1}{2}\right)^{n-Z(b^{(n)})} \end{aligned} \tag{22}$$

Furthermore, T_n can be derived as,

$$\begin{aligned} T_n &= \sum_{u=0}^{Z(b^{(n)})} T_{u,n} \\ &= \sum_{u=0}^{Z(b^{(n)})} {}_nC_u \cdot {}_{n-u}C_{Z(b^{(n)})-u} \cdot \left(\frac{q-1}{2}\right)^{Z(b^{(n)})} \\ &\times \left(\frac{q-1}{2}\right)^{n-Z(b^{(n)})} \end{aligned} \tag{23}$$

According to the above equation, T_n can be calculated by $Z\left(b^{(n)}\right)$. In addition, there are ${}_nC_{Z(b^{(n)})}$ possible bit patterns that have the same $Z\left(b^{(n)}\right)$. To calculate the $D_{\mathcal{S}_{q^M-1}}\left(b^{(n)}\right)$ for each $b^{(n)}$, T_n needs to be divided by ${}_nC_{Z(b^{(n)})}$.

$$\begin{aligned} D_{\mathcal{S}_{q^M-1}}\left(b^{(n)}\right) &= q^{M-(n \cdot m')} \cdot \frac{T_n}{{}_nC_{Z(b^{(n)})}} \\ &= q^{M-(n \cdot m')} \sum_{u=0}^{Z(b^{(n)})} \frac{{}_nC_u \cdot {}_{n-u}C_{Z(b^{(n)})-u}}{{}_nC_{Z(b^{(n)})}} \\ &\times \left(\frac{q-1}{2}\right)^{Z(b^{(n)})-u} \cdot \left(\frac{q-1}{2}\right)^{n-Z(b^{(n)})} \end{aligned} \tag{24}$$

The above equation can be further modified as follows.

$$\begin{aligned} &\sum_{u=0}^{Z(b^{(n)})} {}_nC_u \cdot {}_{n-u}C_{Z(b^{(n)})-u} \\ &= \frac{n!}{\left(n - Z\left(b^{(n)}\right)\right)!} \cdot \sum_{u=0}^{Z(b^{(n)})} \cdot \frac{1}{u!\left(Z\left(b^{(n)}\right) - u\right)!} \\ &= \frac{n!}{\left(n - Z\left(b^{(n)}\right)\right)!} \cdot \sum_{u=0}^{Z(b^{(n)})} \cdot \frac{1}{u!\left(Z\left(b^{(n)}\right) - u\right)!} \\ &\times \frac{\left(Z\left(b^{(n)}\right)\right)!\left(n - Z\left(b^{(n)}\right)\right)!}{n!} \\ &= \sum_{u=0}^{Z(b^{(n)})} \frac{(Z(b^{(n)}))!}{u!(Z(b^{(n)}))!} = {}_{Z(b^{(n)})}C_{Z(b^{(n)})-u}. \end{aligned} \tag{25}$$

Thus, (24) becomes as follows:

$$\begin{aligned} D_{\mathcal{S}_{q^M-1}}\left(b^{(n)}\right) &= q^{M-(n \cdot m')} \sum_{u=0}^{Z(b^{(n)})} {}_{Z(b^{(n)})}C_{Z(b^{(n)})-u} \\ &\times \left(\frac{q-1}{2}\right)^{Z(b^{(n)})-u} \cdot \left(\frac{q-1}{2}\right)^{n-Z(b^{(n)})} \end{aligned} \tag{26}$$

By using the bilinear theorem, the above equation can be rewritten as,

$$\begin{aligned} D_{\mathcal{S}_{q^M-1}}\left(b^{(n)}\right) &= q^{M-(n \cdot m')} \cdot \left(\frac{q-1}{2}\right)^{n-Z(b^{(n)})} \\ &\times \left(\frac{q-1}{2} + 1\right)^{Z(b^{(n)})} \\ &= q^{M-(n \cdot m')} \cdot \left(\frac{q-1}{2}\right)^{n-Z(b^{(n)})} \cdot \left(\frac{q+1}{2}\right)^{Z(b^{(n)})}. \end{aligned} \tag{27}$$

From the (21), $D_{\mathcal{S}_\lambda}\left(b^{(n)}\right)$ holds the following relation as follows,

$$D_{\mathcal{S}_\lambda}\left(b^{(n)}\right) = D_{\mathcal{S}_{q^M-1}}\left(b^{(n)}\right) \cdot \left(\frac{q-1}{2}\right)^{-1}. \tag{28}$$

Therefore, using the (27), $D_{\mathcal{S}_\lambda}\left(b^{(n)}\right)$ can be given by the following relation as,

$$D_{\mathcal{S}_\lambda}\left(b^{(n)}\right) = q^{M-(n\cdot m')} \cdot \left(\frac{q-1}{2}\right)^{n-Z\left(b^{(n)}\right)} \times \left(\frac{q+1}{2}\right)^{Z\left(b^{(n)}\right)} \cdot \left(\frac{q-1}{2}\right)^{-1}$$
$$= q^{M-(n\cdot m')} \cdot \left(\frac{q-1}{2}\right)^{n-Z\left(b^{(n)}\right)-1} \cdot \left(\frac{q+1}{2}\right)^{Z\left(b^{(n)}\right)}. \quad (29)$$

Thus, the first part of the (11a) is proven.

3.3.3 Proof of (11b)

Let us consider the case that $Z\left(b^{(n)}\right) = n$. Therefore, the combination of n-bit patterns except the all-zero patterns is given as follows:

$$ {}_nC_{Z\left(b^{(n)}\right)}. \quad (30)$$

Thus, the distribution of all-zero patterns becomes

$$D_{\mathcal{S}_\lambda}\left(b^{(n)}\right) = \lambda - \sum_{u=0}^{n-1} {}_nC_u \cdot D_{\mathcal{S}_\lambda}\left(b^{(n)}\right). \quad (31)$$

Thus, the second part of the (11b) is proven. In addition, the theorem in (11) is also proven.

4 Result and Discussion

This section explains the distribution of bit patterns in the binary sequence which generated over the sub extension field based on some experimental results. Then, a comparison between the binary sequence defined over the sub extension field and our previous geometric sequence [13] also introduces in terms of the distribution of bit patterns property. Here, H_{wt} denotes the hamming weight.

4.1 Experimental Results

Let us consider the distribution of bit patterns in the binary sequence, introduced in this paper which generated over the sub extension field in the following examples.

Example 1 *Let $p = 5, m = 4$, and $m' = 2$, then the sequence having a period of* 52 *becomes as follows its distribution of n-bit patterns is shown in Table 5.*

$$\mathcal{S}_{52} = \{0100110100000010101111001 1\ 10110010111110010100001100\}. \quad (32)$$

Table 5: Bit distribution of the binary sequence $\mathcal{S}_{52}$ with $p = 5, m = 4$, and $m' = 2$.

n	$H_{wt}(b^{(n)})$	$Z(b^{(n)})$	$D_{\mathcal{S}_{52}}(b^{(n)})$
1	0	1	27
	1	0	25
2	0	2	14
	1	1	13
	2	0	12

Example 2 *Let $p = 3, m = 6$, and $m' = 2$, then the sequence having a period of* 182 *becomes as follows its distribution of n-bit patterns is shown in Table 6.*

Table 6: Bit distribution of the binary sequence $\mathcal{S}_{182}$ with $p = 3, m = 6$, and $m' = 2$.

n	$H_{wt}(b^{(n)})$	$Z(b^{(n)})$	$D_{\mathcal{S}_{182}}(b^{(n)})$
1	0	1	101
	1	0	81
2	0	2	56
	1	1	45
	2	0	36
3	0	3	31
	1	2	25
	2	1	20
	3	0	16

Example 3 *Let $p = 7, m = 9$, and $m' = 3$, then the sequence having a period of* 235986 *becomes as follows its distribution of n-bit patterns is shown in Table 7.*

Table 7: Bit distribution of the binary sequence $\mathcal{S}_{235986}$ with $p = 7, m = 9$, and $m' = 3$.

n	$H_{wt}(b^{(n)})$	$Z(b^{(n)})$	$D_{\mathcal{S}_{235986}}(b^{(n)})$
1	0	1	118337
	1	0	117649
2	0	2	59341
	1	1	58996
	2	0	58653
3	0	3	29757
	1	2	29584
	2	1	29412
	3	0	29241

4.1.1 Observation

It was found that the experimental results explicitly support the (11). In addition, the number of appearance of each bit pattern is related to the number of zeros contained in each bit pattern. Moreover, $D_{\mathcal{S}_\lambda}(b^{(n)})$

increases in proportion to $Z(b^{(n)})$. To confirm this, let us check the **Example** 2 with $n = 3$.

$Z(b^{(3)}) = 0:$

$$D_{S_{182}}(b^{(3)} = 111) = 3^{6-(3\times2)} \cdot 4^{3-0-1} \cdot 5^{0} = 16.$$

$Z(b^{(3)}) = 1:$

$$D_{S_{182}}(b^{(3)} = 011) = 3^{6-(3\times2)} \cdot 4^{3-1-1} \cdot 5^{1} = 20,$$
$$D_{S_{182}}(b^{(3)} = 101) = 3^{6-(3\times2)} \cdot 4^{3-1-1} \cdot 5^{1} = 20,$$
$$D_{S_{182}}(b^{(3)} = 111) = 3^{6-(3\times2)} \cdot 4^{3-1-1} \cdot 5^{1} = 20.$$

$Z(b^{(3)}) = 2:$

$$D_{S_{182}}(b^{(3)} = 001) = 3^{6-(3\times2)} \cdot 4^{3-2-1} \cdot 5^{2} = 25,$$
$$D_{S_{182}}(b^{(3)} = 010) = 3^{6-(3\times2)} \cdot 4^{3-2-1} \cdot 5^{2} = 25,$$
$$D_{S_{182}}(b^{(3)} = 100) = 3^{6-(3\times2)} \cdot 4^{3-2-1} \cdot 5^{2} = 25.$$

$Z(b^{(3)}) = 3:$

$$D_{S_{182}}(b^{(3)} = 000) = 182 - (1 \times 16 + 3 \times 20 + 3 \times 25) = 31.$$

4.2 Comparison With Our Previous Work

By combining the features of the M-sequence and Legendre sequence our previous work [13] proposed a geometric sequence, namely NTU (Nogami-Tada-Uehara) sequence. According to our previous research work, NTU sequence always holds long period, low correlation, high linear complexity properties which are the important considerations to use any sequence in cryptographic applications. Another crucial consideration before utilizing them in any secure applications, is to judge the randomness of a sequence. To do so, we need to evaluate the distribution of bit patterns property in a sequence. After the experimental observation, it was found that in terms of distribution of bit patterns NTU sequence is not uniformly distributed. In other words, in case of binary NTU sequence, there is much difference in appearance between the 0 and 1. To improve this drawback, instead of prime field (which used in the NTU sequence generation procedure), we focused on the sub extension field during the sequence generation procedure in this research work. As a result, after utilizing the sub extension field, the distribution of bit patterns becomes close to uniform. This comparison is shown in the following tables (Table 8 and Table 9).

It should be noted that the NTU sequence is controlled by 2 parameters (p and m), on the other hand the sequence over the sub extension field is controlled by 3 parameters (p, m, and m'). Therefore, it is not possible to make the comparison between these two sequences in terms of the same length (in other words, the same period λ). The authors kept the difference as minimum as possible.

One of the most notable outcomes of this comparison result is the NTU sequence holds higher difference in terms of the appearance between the 'all zero' and 'all one' patterns. In other words, it also confirms the ununiform distribution of bit patterns. On the other hand, sequence defined over the sub extension field minimizes this difference to make it close to uniform. This comparison graphically shown in Figure 3.

Table 8: Comparison in bit distribution between the sub field binary sequence and NTU sequence -I.

n	$H_{wt}(b^{(n)})$	$D_{S_{182}}(b^{(n)})$	%	$D_{NTU_{242}}(b^{(n)})$	%
1	0	101	55.49	161	66.52
	1	81	44.51	81	33.48
2	0	56	30.76	107	44.21
	1	45	24.72	54	22.31
	2	36	19.78	27	11.15
3	0	31	17.03	71	29.33
	1	25	13.73	36	14.87
	2	20	10.98	18	7.43
	3	16	8.79	9	3.71

Table 9: Comparison in bit distribution between the sub field binary sequence and NTU sequence -II.

n	$H_{wt}(b^{(n)})$	$D_{S_{240200}}(b^{(n)})$	%	$D_{NTU_{275514}}(b^{(n)})$	%
1	0	122551	51.02	156865	56.93
	1	117649	48.98	117649	43.07
2	0	62526	26.03	89637	32.53
	1	60025	24.98	67228	24.40
	2	57624	23.99	50421	18.30
3	0	31901	13.28	51221	18.59
	1	30625	12.74	38416	13.94
	2	29400	12.23	28812	10.45
	3	28224	11.75	21609	7.84
4	0	16276	6.77	29269	10.62
	1	15625	6.50	21952	7.96
	2	15000	6.24	16464	5.97
	3	14400	5.99	12348	4.48
	4	13824	5.75	9261	3.36

Recently, there are lots of considerations to use a long period pseudo-random sequence in cryptographic applications. The use of binary sequence in a stream cipher is one of the most common application. Before applying a sequence in such applications, the linear complexity and distribution of bit patterns are considered as the most important properties regarding a sequence to check its randomness. Among these two, the authors observed the linear complexity property in their previous work [16] and it always holds a maximum value of the linear complexity. As a continuation, the authors focused on the distribution of bit patterns in this paper. According to the comparison results, the binary sequence generated over the sub extension field holds much better (close to uniform) compared to our previous binary sequence in terms of distribution of bit patterns. Therefore, the binary sequence defined over the sub extension field can be a suitable candidate for some cryptographic applications.

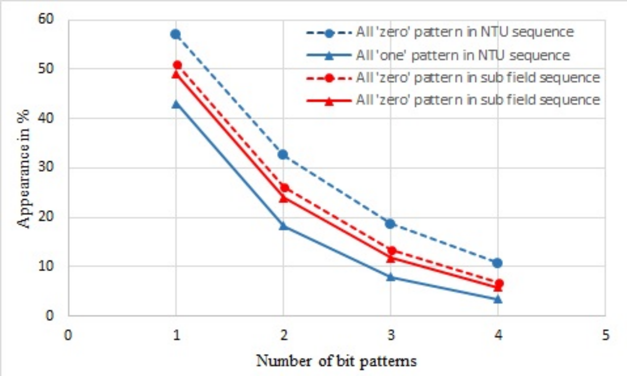

Figure 3: Appearance of 'all zero' and 'all one' bit patterns in the NTU and sub field sequence.

5 Conclusion

In this paper, the authors observed the distribution of bit patterns in a binary sequence which defined over the sub extension. The number of appearances is related to the number of zeros contained in each bit pattern. Furthermore, the authors theoretically prove the distribution of bit patterns property. In addition, they also made a comparison between the binary sequence defined over the sub extension field and our previous work on binary sequence based on distribution of bit patterns property. According to the comparison results, the binary sequence generated over the sub extension field holds much better (close to uniform) compared to our previous binary sequence. As a future work, we would like to consider an efficient implementation to enhance the usability of our proposed sequence a Cryptographically Secure Pseudo Random Number Generator (CSPRNG).

Conflict of Interest The authors declare no conflict of interest.

Acknowledgment This work has been supported by JSPS KAKENHI Grant-in-Aid for Scientific Research (A) Number 16H01723.

References

[1] J. Daemen and V. Rijmen, The Design of Rijndael, Springer-Verlag Berlin Heidelberg, Germany, 2002.

[2] Richard A. Mollin, RSA and Public-Key Cryptography, Chapman & Hall CRC, 2002.

[3] H. Cohen and G. Frey, Handbook of Elliptic and Hyperelliptic Curve Cryptography, Discrete Mathematics and Its Applications, Chapman & Hall CRC, 2005.

[4] V. Edemskiy, On the Linear Complexity of Interleaved Binary Sequences of Period 4p Obtained from Hall Sequences or Legendre and Hall Sequences, IEEE Electronic Letter, 50, 8, 604–605, 2014.

[5] M. Matsumoto and T. Nishimura, "Mersenne Twister: A 623-Dimensionally Equidistributed Uniform Pseudo-Random Number Generator", ACM Trans. on Modeling and Computer Simulation, **8**(1), 3–30, 1998. http://doi.org/10.1145/272991.272995

[6] L. Blum, M. Blum, and M. Shub, "A simple Unpredictable Pseudo-Random Number Generator", SIAM Journal on Computing, **15**(2), 364–383, 1986. http://doi.org/10.1137/0215025

[7] X. Tang and G. Gong, "New Constructions of Binary Sequences with Optimal Autocorrelation Value/Magnitude", IEEE Trans. Inf. Theory, **56**(3), 1278–1286, 2010. http://doi.org/10.1109/TIT.2009.2039159

[8] J. S. No, H. K. Lee, H. Chung, H. Y. Song, and K. Yang, "Trace Representation of Legendre Sequence of Mersenne Prime Period", IEEE Trans. on Inform. Theory, **42**(6 PART 2), 2254–2255, 1996. https://doi.org/10.1109/18.556617

[9] J. Ren, "Design of Long Period Pseudo-Random Sequence from the Addition of m-sequences over $\mathbb{F}_p$", EURASIP Journal on Wireless Communication and Networking, **1**, 12–18, 2004. http://doi.org/10.1155/S1687147204405052

[10] C. Ding, "Pattern Distributions of Legendre Sequences", IEEE Transactions on Information Theory, **44**(4), 1693–1698, 1998. http://doi.org/10.1109/18.681353

[11] B. Z. Moroz, "The distribution of power residues and non-residues", Vestnik Leningrad Univ. Math, **16**, 164–169, 1961. (In Russian with English summary)

[12] T. Helleseth, "Maximal-length sequences", Encyclopedia of Cryptography and Security, 2nd Ed. Springer, 5–14, 2011. https://doi.org/10.1007/978-1-4419-5906-5_359

[13] Y. Nogami, K. Tada, and S. Uehara, "Geometric Sequence Binarized with Legendre Symbol over Odd Characteristic Field and Its Properties", IEICE Trans. on Fund. of Electronics and Computer Sciences, **E97.A**(12), 2336–2342, 2014. https://doi.org/10.1587/transfun.E97.A.2336

[14] Y. Nogami, S. Uehara, K. Tsuchiya, N. Begum, H. Ino, and R. H. Morelos-Zaragoza, "A Multi-value Sequence Generated by Power Residue Symbol and Trace Function over Odd Characteristic Field", IEICE Trans. on Fund. of Electronics, Communications and Computer Sciences, **E99.A**(12), 2226–2237, 2016. https://doi.org/10.1587/transfun.E99.A.2226

[15] A. M. Arshad, Y. Nogami, H. Ino, and S. Uehara, "Auto and Cross Correlation of Well Balanced Sequence Over Odd Characteristic Field", Fourth International Symposium on Computing and Networking (CANDAR), Hiroshima, Japan, 2016. http://doi.org/10.1109/CANDAR.2016.0109

[16] A. M. Arshad, T. Miyazaki, S. Heguri, Y. Nogami, S. Uehara, and R. H. Morelos-Zaragoza, "Linear Complexity of Pseudo Random Binary Sequence Generated by Trace Function and Legendre Symbol Over Proper Sub Extension Field", Eighth International Workshop on Signal Design and Its Applications in Communications (IWSDA), Sapporo, Japan, 2017. http://doi.org/10.1109/IWSDA.2017.8095741

[17] A. M. Arshad, T. Miyazaki, Y. Nogami, S. Uehara, and R. H. Morelos-Zaragoza, "Multi-value Sequence Generated by Trace Function and Power Residue Symbol Over Proper Sub Extension Field", IEEE International Conference on Consumer Electronics - Taiwan (ICCE-TW), Taipei, Taiwan, 2017. http://10.1109/ICCE-China.2017.7991089

Advances in Science, Technology and Engineering Systems Journal Vol. 4, No. 2, 380-386 (2019)

www.astesj.com

Special Issue on Recent Advances in Engineering Systems

ASTESJ

ISSN: 2415-6698

Effects of The Low-Resolution 3D Video Clip on Cerebrum Blood Flow Dynamics

Toru Tanimura[1], Hiroki Takada[1], Akihiro Sugiura[2], Fumiya Kinoshita[3], Masumi Takada[4,*]

[1]Department of Human & Artificial Intelligence Systems, Graduate School of Engineering, University of Fukui, Fukui 910-8507, Japan

[2]Department of Radiological Technology, Faculty of Health Science, Gifu University of Medical Science, Gifu 501-3892, Japan

[3]Department of Electrical and Computer Engineering, Faculty of Engineering, Toyama Prefectural University, Toyama 939-0398 Japan

[4]Department of Nursing, Faculty of Nursing, Yokkaichi Nursing and Medical Care University, Mie 512-8043, Japan

A R T I C L E I N F O

Article history:
Received:20 December, 2018
Accepted:05 April, 2019
Online: 26 April, 2019

Keywords:
Near-Infrared Imaging (fNIRS),
body sway,
head-mounted display (HMD),
low-resolution,
3D video clip.

A B S T R A C T

We have already succeeded in findings that stereoscopic video clips enhance brain activity. We herein increase the knowledge about the influence of 3D and blurred images on the human body, especially on brain activity. From of old, it has been pointed out that the motion sickness is induced by the blurred images. In this study, stabilogram and cerebral blood flow are measured to investigate the process in the brain during the 3D sickness. Activity in the ventral and dorsal streams is enhanced. The most suitable cutoff frequency for viewing the effects of the dorsal stream are estimated between 0.1–0.3 Hz in a Fourier-Shuffle surrogate data analysis of the cerebral blood flow.

1. Introduction

In recent years, various three-dimensional (3D) video display systems have been developed. Generally, they require 3D glasses, but some recent displays can present binocular and multiaspect autostereoscopic images. However, in either case, there are issues: (1) unpleasant symptoms such as headaches, vomiting, and eyestrain, (2) and a lack of ambience and realism. Especially with Japanese 3D televisions, binocular disparity is set to 1º or less; therefore, dynamic movements cannot be fully expressed. The reason for the eyestrain induced by 3D video viewing is not fully known yet; thus, without an appropriate manufacturing standard for 3D videos and their display systems, excessive measures against visually induced motion sickness (VIMS) have been implemented.

With natural vision, accommodation and vergence are consistent. However, it is generally understood that in 3D video viewing, while the lens is accommodated to the position of the screen that displays the image, the eyes converge at the position of the 3D object (a common reason for eyestrain during 3D image viewing). This discrepancy between the accommodation and vergence is considered to be the reason for the eyestrain from 3D viewing and visually induced motion sickness [1–4].

We can easily view stereoscopic video clips in daily life; however, it has been reported that symptoms such as headaches, nausea, dizziness, and vomiting occurred from VIMS [5]. It is said that the abovementioned symptom is induced by the vestibulo-vegetative reflex [6]. The vestibulo-vegetative system is closely accompanied by the vestibular nuclei, which is also involved in body balance. Compensatory movements in this equilibrium function are controlled by the vestibule-spinal reflex and the vestibule-ocular reflex. In these, the outputs from the vestibular nuclei are projected to the antigravitational muscles and the extraocular muscle, respectively. Therefore, body sway is affected by motion sickness, although there are some processes that control the antigravitational muscles through other nervous pathways (see [7]).

According to Patterson [8], if the viewing conditions are sufficiently bright, the depth of field of a target has a mean difference on the order of 1.0 D (diopter), and the

* Masumi Takada, Email: takada@y-nm.ac.jp

accommodation-vergence conflict discussed above is a problem unique to proximity displays. Factors associated with the depth of field are the pupil diameter and resolution, and viewing conditions of images influence the pupil diameter. Most previous studies used a deep depth of field to prevent blurriness, resulting in a measurement environment quite different from that of everyday life.

Moreover, distribution of the vergence fusional stereoscopic limits in stereoscopic images is desired [9]. Eighty-four percent of all subjects could see a stereoscopic image of two planar images with a binocular disparity of 2º. The target under such a condition is a single target without a surrounding image. When there is no other parallax image, an accommodation-vergence process that creates an image from a double image is considered to function as a positive feedback system [10].

With developments such as the miniaturization of diagnostic equipment, brain science is developing rapidly, and a variety of brain activities are being defined [11]. Brain functional imaging using near-infrared spectroscopy (NIRS) has been developed of late years [12]. This technique is known to be a noninvasive measurement of brain activity, which utilizes the property of a hemoglobin which absorbs near infrared light, detecting the time course of the overall reactivity to activation of the cerebral cortex in subjects in a natural state [13–17]. Applying this to surfaces on the brain, we can observe changes in cerebral blood flow (CBF) within a 2–3 cm depth from the scalp, and recorded polygraph as time series data.

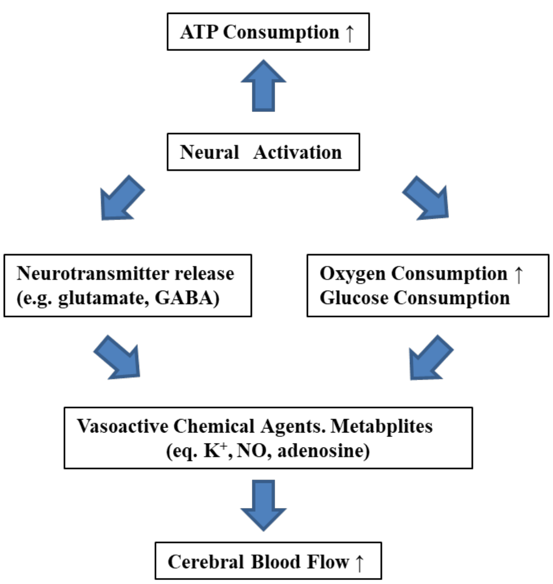

Figure 1: Physiological structure of neurovascular coupling.

The impacts of viewing 3D images on equilibrium function and brain activities were investigated in order to elucidate the cause for 3D sickness, which is induced during the peripheral vision more readily. Potential changes in brain activity can be measured by using fNIRS. Here, peripheral vision for the entire screen was compared to tracking a target while viewing 3D images [18] in accordance with neurovascular coupling (See Figure 1), which was known to be the relationship between subsequent changes in the CBF and local neural activity [19]. Tight temporal and amplitudinal linkages have been observed between the CBF supply and demand of the neuronal activity for over a century [20–22]. According to previous studies [23–25], the regional blood flow is likely controlled by multiple mechanisms such as the feedforward involving neural signaling via neurotransmitters.

In this study, we investigated effects of 3D video clips on human body. In this experiment, we recorded a stabilogram from which the severity of the VIMS could be estimated. The brain function, especially in the hemodynamics in the CBF, was also measured.

2. Material and Method

Biometric data were obtained for the center of pressure (CoP), heart rate variability, and hemodynamics on the surface of the cerebrum in 11 healthy young individuals (mean ± standard deviation: 22.6 ± 1.0 years) with no abnormalities in the extremities and no past medical history of ear or nervous system disease. Moreover, the visual acuity of subjects with the naked eye and/or contact lenses had to be greater than 0.8 and capable of stereoscopic vision. This experiment was fully explained to the subjects beforehand, and written consent was obtained. The experiment was approved by the Ethics Committee of the Department of Human and Artificial Intelligent Systems in the Graduate School of the Engineering University of Fukui (No. H2018010-11).

In this study, subjects wore a head-mounted display (HMD) GOOVIS G2 (Lets-co.jp, Nagoya), and the following video clips (VCs) were projected to the HMD:

VC1) stereoscopic video clip with a resolution of 1080p

VC2) stereoscopic video clip with a resolution of 360p

A resolution of 1080p (1920 × 1080 px; also known as Full HD (high definition video) or FHD (full high definition 2K) and BT.709 (broadcasting service television 709)) is a set of HDTV (high-definition television) high-definition video modes characterized by 1,920 pixels displayed across the screen horizontally and 1,080 pixels down the screen vertically. The *p* stands for progressive scan, *i.e.* noninterlaced [26]. Contents using as visual stimuli in this experiment was supplied by Sky Crystal (Olympus Memory Works Ltd. Co., Tokyo), which was modified with the company's permission. A sphere in a video clip was ambulated in a complex manner.

Biometric data such as the stabilogram, electrocardiogram (ECG), and oxy-/deoxygenated hemoglobin concentrations on the CBF were recorded while the participant viewed high-resolution video clip VC1 and low-resolution video clip VC2. At a sampling frequency of 100 Hz, each sway of the CoP was recorded by using a Wii balance board (Nintendo, Kyoto). Subjects were instructed to maintain the Romberg posture during the duration of the trials. The subjects were asked to use peripheral vision for VC1 for the first 60 s and VC2 for the next 60 s, and to stand when there were no images (resting state). This trial was repeated five times (Figure 2).

In addition to the electrocardiogram (ECG), the CBF on was recorded on the surface of the frontal lobe (1–12 ch), on that of left temporal lobe (13–24 ch), on that of the right temporal lobe (25–36 ch), and on that of the occipital lobe (37–48 ch) in accordance with the fNIRS; channels in the prove of the FOIRE-3000 (Shimadzu, Kyoto) were arranged as shown in Figure 3. Our previous study gave a description of the position where the probe cap was attached in detail [27, 28]. Observing cross-section MRI shots in the brain, we have also confirmed the field on which the CBF changes [29]. Time series data of the CBF were smoothed by the low-pass filtering whose cutoff frequency was set to be 0.15 Hz.

Viewing high-resolution video clip	Viewing low-resolution video clip	Static Upright Posture	
60 s	60 s	30 s	× 5 times
Stabilogram, fNIRS, ECG			

Figure 2: Experimental protocol.

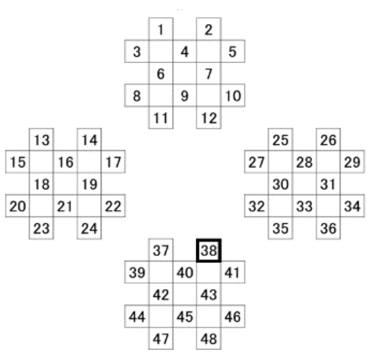

Figure 3: NIRS measurement channel layout.

3. Results

Sway values such as the area of sway, total locus length, total locus length per unit area, and sparse density [30,31] were estimated from the stabilograms (Figures 4–5). By using the Wilcoxon signed-rank test, we compared the sway values while viewing the VCs for a trial as follows. The statistical significance was herein set to be 0.05.

There was no statistical significance in the difference between the sway values while viewing the VCs during the trials except for the total locus (Figure 6b). In the third trial, the total locus length per unit area while viewing VC1 tended to be different from that while viewing VC2 ($p < 0.1$).

(a)

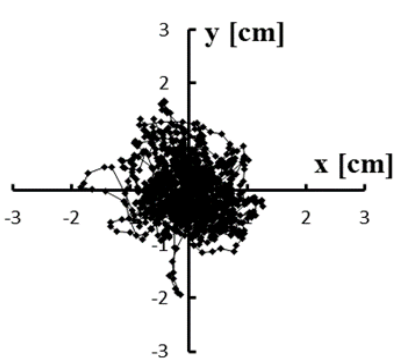

(b)

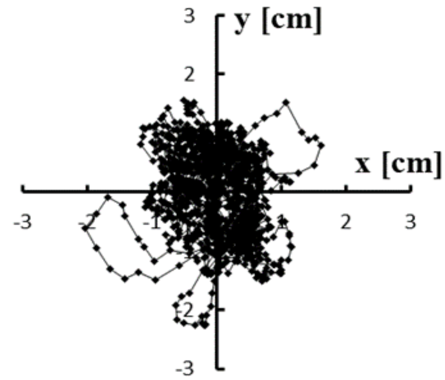

(c)

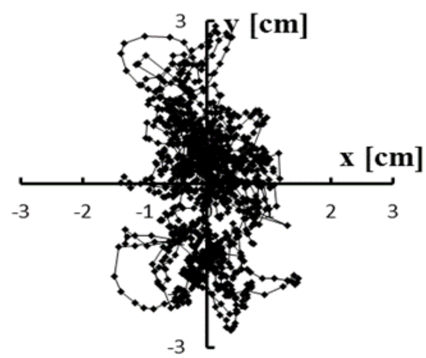

(d)

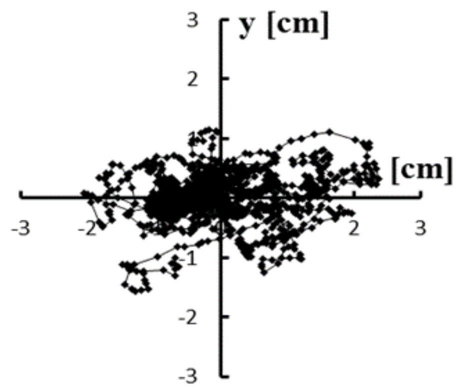

(e)

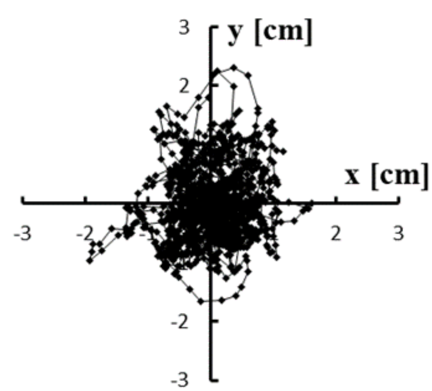

Figure 4: (a–e) Typical stabilograms while viewing VC1 for first to fifth trials, respectively

The oxygenated hemoglobin concentration in the CBF recorded while viewing VC2 was compared to that while viewing VC1. Significant changes were observed in the frontal lobe, temporal lobe, and upper occipital lobe (Figure 7).

For area of sway, sparse density, and total locus length, the sway values for the n-th trial (n = 3, 4, 5) were significantly greater than those for the first trial while viewing VC1 ($p < 0.05$). In addition, all sway values for the n-th trial (n = 3, 4, 5) were significantly greater than those for the first trial while viewing VC2, as shown in Figure 6 ($p < 0.05$).

4. Discussion

In this study, we investigated effects of 3D video clips on the equilibrium function and the brain function, especially in the hemodynamics in the CBF. Video clips were projected on an HMD.

In this experiment, no statistical differences were observed between the sway values while viewing the high-resolution video clip (VC1) and those while viewing the low-resolution video clip (VC2). The VIMS did not result from differences between the resolutions in this study. In addition, there was a statistical significance between the sway values of the n-th trial and those of the first trial (n = 3, 4, 5) while viewing any video clip. The changes in the sway values were considered to be owing to acclimatization in the upright posture.

Time series data are prone to noise with measurement errors, and biological signals are no exception. Noise including in the biological signals should be removed. We have already conducted a study for a nonlinear analysis of the changes in the CBF using fNIRS in order to determine an appropriate cutoff frequency for the low-pass filtering of the CBF. In the experiment, subjects did not view stereoscopic VCs through the HMD but those on a liquid crystal display (LCD) through polarizing spectacles, following a test with subjects' eyes closed (*Cnt*). The VCs were played back for 70 s in visual pursuit and for 70 s in the peripheral vision in succession, which were classified as the resting, the visual pursuit, and the peripheral vision terms. This protocol was repeated five times. Changes in the CBF were recorded in the measurements taken from 10 healthy persons that sat in a dark room. Sampling frequency and the arrangement of the probes were set to be same as shown in this study (Figure 3). Also, the study focused on the dorsal stream, which can be measured around the channel 38. Low-pass filters with some cutoff frequencies were applied to the original CBF for 38-ch, and the translation errors of the smoothed CBF were estimated using the Wayland algorithm [32]. We herein focused on the first set of results from each subject to compare among translation errors during the resting, the visual pursuit, and the peripheral vision terms Because the regularity of the changes in the CBF were indicated through the experiment. Using the Fourier shuffle surrogate data method, the nonlinearity of the results was also analyzed [33].

In each instance, the translation error peaked at cutoff frequencies of 0.3–0.5 Hz [34]. Statistically significant differences were noted between mathematical models of the raw data in the CBF and their surrogate sequences. In addition, statistically significant differences/tendencies were also observed between mathematical models of the surrogate data and the CBF time series smoothed by the low-pass filtering whose cutoff frequencies ≤ 1 Hz. We believed that the CBF data were affected by noises with high frequencies > 1Hz, owing to muscular activities in the extraocular muscles and physical artifacts.

The translation errors were compared according to the cutoff frequencies f_0 (Figure 8). At f_0 = 0.2 Hz, translation errors estimated in the visual pursuit and in the peripheral vision were significantly greater than those observed while the eyes were closed (*Cnt*). Hence, the visual effect is thought to lie in the 0.1–0.3 Hz band.

In order to evaluate the difference between raw data and surrogate data, a t-value was herein calculated at f_0 = 0.2 Hz. The values were estimated as 6.77, 3.52, and 1.09 for the *Cnt*, the peripheral vision, and the visual pursuit, respectively. For the visual pursuit and peripheral vision, the t-value was reduced compared to the *Cnt*. Thus, it was difficult to observe the nonlinearity in the CBF while viewing stereoscopic video clips. Compared to that for the peripheral vision, the t-value was reduced for the visual pursuit. This is thought to be the effect of increased activity in the dorsal stream that governs subjects' spatial awareness with respect to the object being viewed [35]. This manifested itself more strongly when viewing stereoscopic video clips. For this reason, it is thought that a low-pass filter with a cutoff frequency of approximately 0.2 Hz is suitable for observing the nonlinearity and changes in the CBF during the viewing of stereoscopic video clips.

Presently, we investigated effects of 3D video clips on the equilibrium function [27] and the CBF [28,34]. In the former, video clips were projected on the screen. The images were composed of a number of balls. A virtual evoked postural response (VEPR) was expected to be induced by their periodic motion with 0.25 Hz. Severity of the VIMS could be measured as a VEPR. We confirmed that the motion sickness was occurred while viewing 3D video clips. Based on the results of the stabilometry frequency analysis, we observed a reduction in the intensity of power spectral density for 0.25 Hz with the course of the noise amplitudes. The frequency seemed to be synchronized with the periodic motion of the balls in the video clips. In the latter, subjects viewed video clips on LCDs of the video game and the television, respectively. Except for the video game, subjects viewed video clips through shutter/polarizing spectacles in this paragraph.

We investigated the effects of 3D video clips on the brain function, especially in the hemodynamics in the CBF which was remarkably increased while viewing the stereoscopic video clip, compared to while viewing the 2D.

(a)

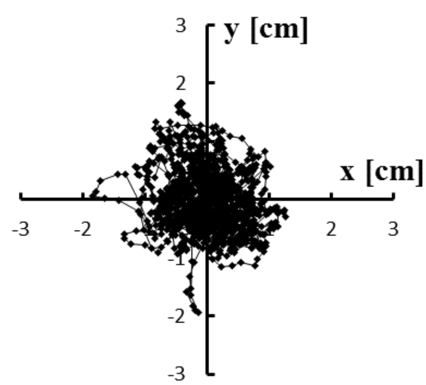

(b)

(c)

(d)

(e)

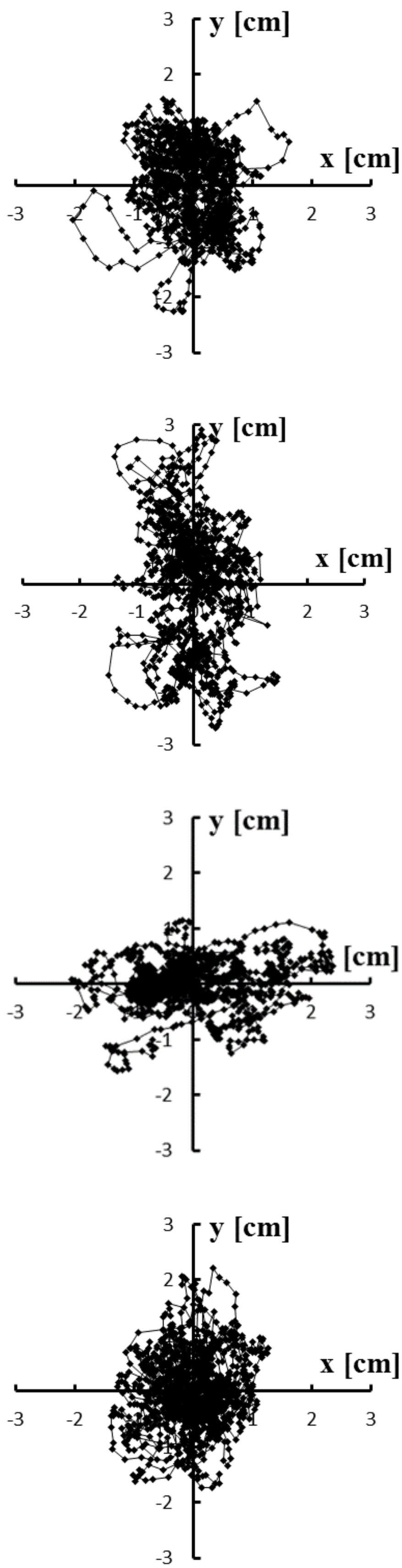

Figure 5: (a–e) Typical stabilograms while viewing VC2 for first to fifth trials, respectively

One question remains: compared with the impact of viewing 3D videos with peripheral vision on the balance system, the amount of sway during viewing is small. Presently, we have not directly captured the instability in the balance system during the peripheral viewing of 3D videos. Therefore, it would be meaningful to improve the measurement precision of the impact on the balance system through numerical models. Considering research ethics, as it would lessen the burden on the subjects, this would not be limited to the design evaluation analysis of ultrahigh-definition images and VR, but could also contribute to hygiene and biomedical engineering.

(a)

(b)

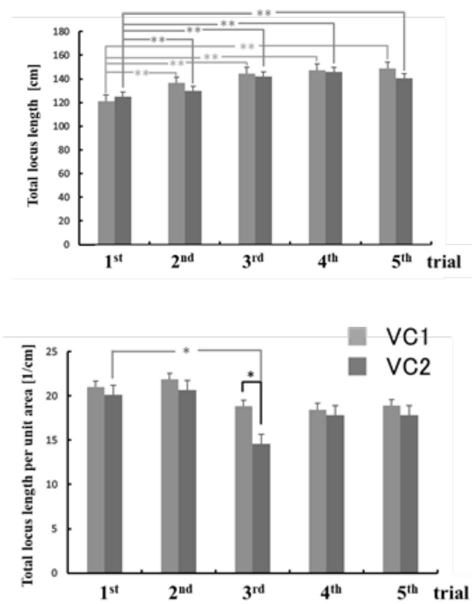

Figure 6: Comparison of sway values while viewing VCs for each trial: total locus length (a); total locus length per unit area (b).

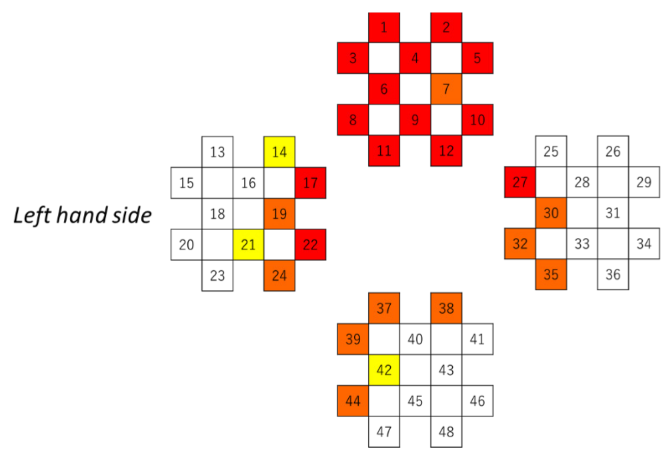

Figure 7: Changes in oxygenated hemoglobin concentration in the CBF recorded while viewing VC2 compared to that while viewing VC1: significant increase ($p < 0.01$ and $p < 0.05$) marked by ■ and ■, respectively; increase tendency ($p < 0.1$) marked by ■.

In this study, by continuing the research challenges described above, we verified the illusion of self-motion (vection) induced by 3D video viewing. As an application, we determined new research topics. Is vection induced by 3D video viewing caused selectively by peripheral vision? Does uncoordinated movement of central and peripheral vision cause vection, inducing visually induced motion sickness? We plan to elucidate these questions. By working on new research topics, we may be able to propose a guideline for the safe viewing of 3D videos.

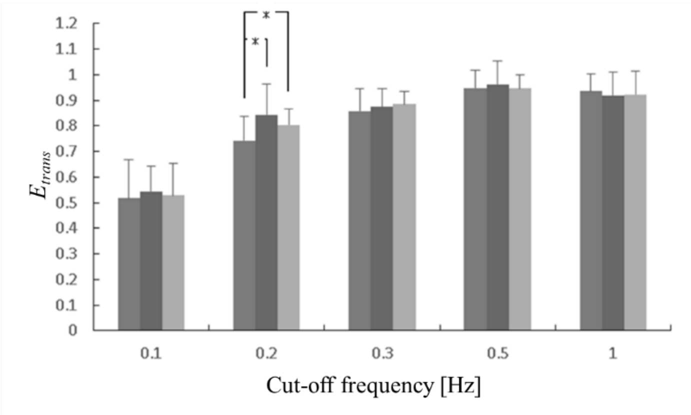

Figure 8: Comparison of translation errors estimated from CBF with eyes closed as control (*Cnt*) ■ with those of the visual pursuit ■, and of the peripheral vision ■.

According to the fNIRS measurement, as shown in Figure 7, significant changes were observed in the temporal lobe and upper occipital lobe that corresponded to the ventral and dorsal streams, respectively [35]. It is difficult to recognize the visual objects and motion processes owing to the low resolution of the video clip. Activity in the ventral and dorsal streams was enhanced, and theircooperativeness might be expected to be found in the next step.

The number of elderly people with dementia in Japan is estimated to reach approximately 7 million people by 2025. It is important to diagnose/respond dementia in early stage. Games for people with mild cognitive impairments (MCIs) has been developed in accordance with the previous. Epidemiologic research [36]; Untreated poor vision is associated with cognitive decline, particularly Alzheimer disease. It is important to take care the decline in the visual acuity. Protecting eyesight also keep our brain function. Their medical evaluations are now conducting, using fNIRS and electroencephalograms (EEG) [37-38]. The basic experiments will be also stated in detail for the virtual space and the video games in the next paper.

5. Conclusion

We focused on the visual consciousness and examined whether the hemodynamics in the CBF depend on the consciousness. Despite the consciousness, the CBF contains body artifacts owing to the cardiovascular system and extraocular muscles in accordance with a nonlinear analysis of the CBF filtered at cutoff frequencies >0.5 Hz. In other words, noise at high frequency (>0.5 Hz) exhibits regularity.

Conflict of Interest

The authors declare no conflict of interest.

Acknowledgment

This work was supported in part by the Takeuchi Scholarship Foundation and the Descente and Ishimoto Memorial Foundation for the Promotion of Sports Science; the Japan Society for the Promotion of Science, Grant-in-Aid for Scientific Research (C) Number 17K00715 and Young Scientists (B) Number 15H06711.

References

[1]. F. M. Toates, “Vergence eye movements” Doc. Ophthalmol., 37, 153–214, 1974.

[2]. C. Cruz-Neira, D. J. Sanding, T. A. DeFanti, “Virtual reality: The design and implementation of the CAVE,” in Proceedings of the 20th Annual Conference on Computer Graphics and Interactive Techniques, SIGGRAPH ’93, 135–142, 1993.

[3]. D. M. Hoffman, A. R. Girshick, K. Akeley, M. S. Banks, “Vergence-accommodation conflicts hinder visual performance and cause visual fatigue” J. Vis., 8(3): 33.1–30, 2018. doi: 10.1167/8.3.33

[4]. T. Shibata, J. Kim, D. M. Hoffman, M. S. Banks, “The zone of comfort: Predicting visual discomfort with stereo displays” J. Vis., 11(8), 1–29, 2011.

[5]. International Standard Organization, “IWA3:2005 Image safety-reducing determinism in a time series” Phys. Rev. Lett., 70, 530–582, 1993.

[6]. K. R. Brizzee, “Mechanics of vomiting: A mini review” Can. J. Physiol. Pharmacol., 68: 221–229, 1990.

[7]. H. Takada, M. Miyao, S. Fateh (eds.), Stereopsis and Hygiene, Springer Nature, 2018.

[8]. R. Patterson, “Human factors of stereo displays: An update” J. SID, 17(12), 987–996, 2009.

[9]. S. Nagata, “Distribution of vergence fusional stereoscopic limits (VFSL) of disparity in a stereoscopic display” TVRSJ, 7, 239–46, 2002 (in Japanese).

[10]. S. Nagata, “The binocular fusion of human vision on stereoscopic displays: Field of view and environments” Ergonomics, 39(11), 1273–1284, 1996.

[11]. A. M. Chiarelli, F. Zappasodi, F. Di Pompeo, A. Merla, “Simultaneous functional near-infrared spectroscopy and electroencephalography for monitoring of human brain activity and oxygenation” Neurophot., 4(4), 041411, 2017.

[12]. M. Fukuda, M. Mikuni, “A study of near-infrared spectroscopy in depression” J. Clinical and Exp. Med., 219, 1057–1062, 2006.

[13]. A. Zardecki, “Multiple scattering corrections to the Beer-Lambert Law” in Proc. SPIE, 103–110, 1983.

[14]. S. Wray, M. Cope, D. T. Delpy, J.S. Wyatt, E. O. Reynolds, “Characterization of the near infrared absorption spectra of cytochrome AA 3 and hemoglobin for the non-invasive monitoring of cerebral oxygenation” Biochemica et Biophysica A., 933, 184–192, 1988.

[15]. T. Kato, A. Kamei, S. Takashima, T. Ozaki, “Human visual cortical function during photic stimulation monitoring by means of near-infrared spectroscopy” J. Cereb. Blood Flow Metab., 13, 516–520, 1993.

[16]. Y. Hoshi, M. Tamura, “Detection of dynamic changes in cerebral oxygenation coupled to neural function during mental work in man” Neurosci. Lett., 150, 5–8, 1993.

[17]. C. E. Elwell, C. E. Cooper, M. Cope, D. T. Delpy, “Performance comparison of several published tissue near-infrared spectroscopy algorithms” Anal. Biochem., 227, 54 –68, 1995.

[18]. M. Takada, Y. Fukui, Y. Matsuura, M. Sato, H. Takada, “Peripheral viewing during exposure to a 2D/3D video clip: Effects on the human body” Env. Health Prev. Med., 20, 79–89, 2015.

[19]. A. A. Phillips, F. H. N. Chan, M. M. Z. Zheng, A. V. Krassioukov, P. N. Ainslie, “Neurovascular coupling in humans: Physiology, methodological advances and clinical implications” J. Cerebral Blood Flow & Metabol., 36, 647–664, 2016.

[20]. F. C. Donders, “Die bewegungen des gehirns und die vera: Nderungen der gefa¨ssfu¨llung der pia mater” Schmid’s Fahrbucher., 69, 16–20, 1851.

[21]. A. Mosso, “Sulla circolazione del cervello dell’uomo” Atti R Accad Lincei., 5, 237–358, 1880.

[22]. C. S. Roy, C. S. Sherrington, “On the regulation of the blood-supply of the brain” J. Physiol., 11, 85–158, 1890.

[23]. D. Attwell, C. Iadecola, “The neural basis of functional brain imaging signals” Trends in Neurosci., 25, 621–625, 2002.

[24]. M. Lauritzen, “Reading vascular changes in brain imaging: Is dendritic calcium the key?” Nature Rev., 6, 77–85, 2005.

[25]. K. Uludag, D. J. Dubowitz, E. J. Yoder, K. Restom, T. T. Liu, R. B. Buxton, “Coupling of cerebral blood flow and oxygen consumption during physiological activation and deactivation measured with fMRI” Neuro Im., 23, 148–155, 2004.

[26]. R. Silva, “720p vs. 1080p: A comparison” Lifewire.com, 2018, last accessed 2016/11/21.

[27]. M. Takada, K. Ito, T. Tanimura, H. Tahara, A. Sugiura, H. Takada, “The impact of 3D games on brain blood flow dynamics and its utilization” in 13th international conference on computer science and education (ICCSE),

828-833, 2018.
[28]. M. Takada, Y. Mori, F. Kinoshita, H. Takada, “Changes in brain blood flow by the use of 2D/3D games” in Universal Accessin Human-Computer Interaction (UAHCI/HCII2016), PartII (eds. A. Margherita, S. Constantin) LNCS9738, 516-523, 2016.
[29]. Y. Matuura, T. Taniguchi, A. Sugiura, M. Miyao, H. Takada, “Distribution of cerebral blood flow during gum-chewing” Forma, 27, 1-4, 2012.
[30]. H. Takada, Y. Kitaoka, S., M. Miyao, “Physical meaning on geometrical index for stabilometry” Equil. Res., 62(3), 168–180, 2003.
[31]. Japan Society for Equilibrium Research (ed.), “Standard of Stabilometry” Equil. Res., 42, 367–369, 1983.
[32]. R. Wayland, D. Bromley, D. Pickett, A. Passamante, “Recognizing determinism in a time series”, Phys. Rev. Lett., 70, 580-582, 1993.
[33]. J. Theiler, S. Eubank, A. Longtin, B. Galdrikian, J. D. Farmer, “Testing for nonlinearity in time series: The method of surrogate data” Physica D, 58, 77-94, 1992.
[34]. T. Tanimura, D. Iida, Y. Jono, M. Takada, Y. Matsuura, H. Takada, “Nonlinear analysis using multiple cutoff frequencies for local cerebral blood flow during biofeedback training” JAMMR, 28(6), 1-12, 2018.
[35]. L. G. Ungerleider, M. Mishkin, “Two cortical visual systems” in Analysis of visual behavior (ed. D. J. Ingle et al.), MIT Press, 1982.
[36]. M. A. M. Rogers, K. M. Langa, “Untreated poor vision: A contributing factor to late-life dementia” Am. J. Epidemiol., 171(6), 728–735, 2010.
[37]. G. R. Mendez, I. Dunwell1, E. A. M. Mirón, M. D. V. Cerdán, S. de Freitas, F. Liarokapis, A. R. G. Gaona, “Assessing NeuroSky’s usability to detect attention levels in an assessment exercise” in Human-Computer Interaction (UAHCI/HCII 2009), Part I (ed. J. A. Jacko), LNCS 5610, 149–158, 2009.
[38]. S. J. Johnstone, S. Roodenrys, R. Blackman, E. Johnston, K. Loveday, S. Mantz, M. F. Barratt, “Neurocognitive training for children with and without AD/HD” ADHD Atten. Def. Hyp. Disord., 4, 11–23, 2012.

Advances in Science, Technology and Engineering Systems Journal Vol. 4, No. 2, 387-394 (2019)

www.astesj.com

Special Issue on Advancement in Engineering and Computer Science

ASTESJ

ISSN: 2415-6698

A Formal Ontology-based Framework Towards an Intelligent Temporal Scheduler

Patience Usoro Usip*, Udoinyang Godwin Inyang, Daniel Ekpenyong Asuquo, Enobong Umoren

University of Uyo, Computer Science Department, Faculty of Science, PMB 1017, 520003, Uyo, Nigeria

A R T I C L E I N F O

Article history:
Received:04 February, 2019
Accepted:05 April, 2019
Online: 26 April, 2019

Keywords:
Time Complexities and Scheduling
Formal Representations
Qualitative Reasoning
Timetabling Process
Allen's Interval Logic

A B S T R A C T

Time scheduling as seen in timetabling processes with few and/or competing resources has exposed complex interoperable time scheduling. Attempts to resolving these time scheduling processes has been undertaken, using several classical methods, with difficulty due to inherent complexities, constraints and conflicting issues. The use of ontology-based approaches to resolve time complexity is recently adopted due to its ease in interoperability and reuse of data. The probability weighted ontology provides the various types of complexity as a requirement for the complexity reduction. To determine the optimality of the resulting timetable required the evaluation of its criteria using the analytical hierarchy process. The need for a formal representation to explicate the intelligent behaviour of the ontology-based framework of the temporal scheduler arises. Hence, this work is aimed at providing that formal representation of the logical part of the ontology. The basic rules handling the constraints in the timetabling process are outlined with the corresponding formal representations of the interval-based logic using first-order logic. The semantic model of the temporal scheduler is further described following Guarino's formal ontology model. The unified modeling language (UML) design of a system framework prototype that adopts the formal model is also given. Through the formal ontology-based framework, all constraints that will give optimality are explicated and incorporated into the allocation reasoned, which results in an optimal formal ontology-based model. This will ensure reliability, ease of use and the likelihood of re-usability of the resulting timetable.

1. Introduction

This paper is an extension of work originally presented in a conference [1]. Scheduling is a constrained allocation of resources to objects in space and time, aimed at minimizing the total cost of a set of used resources [2]. This involves creating schedules by temporarily assigning activities to resources considering one or more objectives and some constraints. Project scheduling in [3] with emphasis on testing the dependencies of ordered activities using Pearson's Correlation Coefficient (PCC) is not centered on temporal scheduling which is the focus of this paper. Basically, PCC is used in [3] to obtain weights for activities and then classify them as dependent or independent so as to avoid frequent usage of same resources multiple times thereby reducing expenses and project duration. Temporal reasoning is a suitable methodology to synchronize operations, make allocations for resources, determine sequences of operations, and evaluate average earliness or tardiness of a schedule. Time, which is modeled by quantitative values and constraints, is used to represent every schedule [4, 5]. Formalizing time scheduling process is a complex task that involves different reasoning strategies, structures and elements from multiple languages. Several attempts of formalizing time schedules using classical techniques exist in the literature (simulated annealing [6], genetic algorithm [7], Tabu search [8, 9], case-based reasoning [10], and graph coloring approach [11, 12, 13, 14]. However, these approaches lack formalization and are not simple to implement needed semantics during problem solving. Moreso, their solutions, though functional, may be error prone when considering new sets of constraints. Ontology-based approaches are emerging to resolving such complexities due to their ease in interoperability and reuse of data. The identified time complexities in [1] can be resolved in the allocation reasoner

*Daniel Ekpenyong Asuquo: Department of Computer Science, University of Uyo, Nigeria; +2348035680549; danielasuquo@uniuyo.edu.ng

(AR) by implementing the represented formal notations that describe the embedded semantics in the given rules applicable for inference in the weighted ontology framework. In this work, the heuristics are formalized through ontology [15], by explicitly incorporating all constraints that will give valid answers to the competency questions in the AR and to enable their execution by ontology reasons.

The focus of this work is to construct the basic rules handling the constraints in the timetabling process with the corresponding formal representations of the interval-based logic [16, 17] using first-order logic. Furthermore, the semantic model of the temporal scheduler is further described following Guarino's formal ontology model.

The rest of the paper is organized as follows. Section 2 reviews related works and the use of ontology in scheduling problems including publishing meetings and event, resource allocation and timetabling while section 3 presents a formalization of the complexity reduction rules using first order logic and Allen's interval relations for optimal time scheduling process. Section 4 presents the semantic model of the formal time scheduling ontology with different components for obtaining optimality of time, with a mathematical description of the conceptual model. In section 5, unified modeling language (UML) diagrams are used for structural and behavioral description of the time scheduling ontology (TSONT) while section 6 concludes the paper.

2. Related works

Ontology is a model building tool for specifying the scope of an application domain as well as it entities with the attributes or desired system features. Formally, it represents knowledge as a hierarchy of concepts within a domain and uses shared vocabulary to denote the concepts' types, properties, functionalities and interrelationships. Ontology has been used as a structural tool to organize information and represent knowledge about the world in many areas, such as Artificial Intelligence (AI), Semantic Webs, Information Architecture, System Engineering, Library Science and so on. The formalization of rules enables the complexities found in the production of timetable to be managed and optimized. Ontology is capable of uniquely combining inherent techniques such as semantic search, ontology matching and ontology mapping to reduce the timescale and cost complexity in data and resolve conflicts that always occur. A typical complexity reduction case between two departmental ontologies is shown using the Anchor-PROMPT mapping technique [18]. The representation of the complexity types using the probability weighted ontology (PWO) [19] and the evaluation of its gold standard criteria using analytic hierarchy process (AHP) model [1] provide users with the window to reschedule any time based on the level of identified complexity to attain optimality. The various users' windows for rescheduling are formally represented in the following sections.

Anchor-PROMPT is a conventional ontology mapper that automatically finds semantically similar features (described by terms) between two ontologies, taking a set of pairs of related terms from the source ontologies as input. Commonalities in two different departmental ontologies are mapped together to expose the causes of conflict or clash and resolve them. Consider the mapping of two departmental ontologies shown in figure 1 with Computer Science department in Faculty of Science as an anchor department, owning a certain course, CSC211. This course, CSC 211, is also being offered by students of the departments of Mathematics, Statistics and Physics in the same faculty, Vocational Education in faculty of Education, and Geo-Informatics in faculty of Environmental Studies. Ontology mapping involves linking the interactions around the course in the anchor department with that of the departments it is providing services to. In case of any clash or conflict with other courses offered by the students of any cooperating departments, the Time Scheduler or Allocation Reasoner (AR) along with the interval-based reasoning formally represented in this paper will re-schedule either of the courses concerned to resolve the conflict.

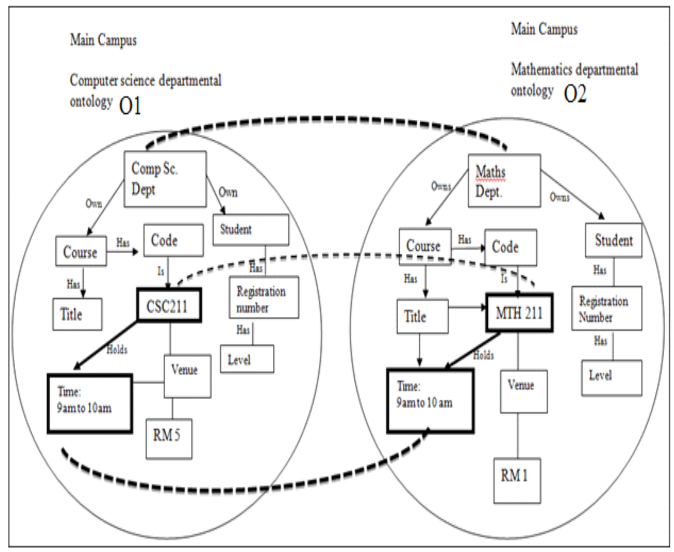

Figure 1. Mapping of two departmental ontologies

As shown in Figure 1, the mapping of ontology O_1 and ontology O_2 by Anchor- PROMPT involves accepting pairs of related terms called anchors, defined by the user or automatically identified by lexical and syntactic matching, as input, from the source graph (ontology); and traversing the path between the anchors in the corresponding ontology. The link between the classes (nodes) defined by the hierarchical relations forms a path. The Anchor-PROMPT then compares the terms along these paths to find similar terms frequently appearing in similar positions on similar paths. In a nutshell, once the sets of similar terms are generated, e.g. {CSC211, MTH211}, scheduled for the same time$\{t_1, t_1\}$and in the same venue $\{v_1,v_1\}$ which is also scheduled, the AR will be notified, and with the help of the interval-based reasoning, the AR will automatically reschedule either CSC211 or MTH211 for another time and venue respectfully giving priority to CSC211 on account that the high number of cooperating departments produces more complexities, as identified in PWO [1].The identified time complexities as resolved in the AR are expressively represented using formal notations to describe the embedded semantics in the given rules applicable for inference in the weighted ontology framework [1].

2.1 Ontology in scheduling and timetabling

Ontology has been applied in several scheduling task. The ontological framework in [20] specifies a meta-model that provides a vocabulary for formulating application model in a problem domain as well as a set of constraints on what can be expressed. The authors proposed the use of ontology to structure and simplify the process of constructing domain-specific problem-solving tools. Their work focused specifically on the task of scheduling, which ultimately led to the development of OZONE - a toolkit for configuring constraint-based scheduling systems.

With OZONE, it was possible to define domains, constraints as well as reusable and extensible concepts for describing and representing scheduling problem. In [21], a brief review of ontology for scheduling and publishing meetings and events was presented with a framework having a single consistent representation with a hierarchical structure capable of capturing some uncertainty and complexity that occur in real world system. The work attempts to present a balance between logical complexity in the ontology and the content language.

In [22], a generic task ontology for scheduling problems was proposed, expressing that ontology is generic if it is both domain and application independent. The work clearly described the class of scheduling tasks, independently of various ways by which these tasks can be solved. The given ontological framework provided a fairly fine-grained structure needed to build the scheduling system. The given cost related axioms ensure that an optimal solution or result is constructed by subsuming the various preferences in a scheduling task specification. Also, resource availability axiom was used to tackle the conflict between various jobs for the use of same resources depending on their overlapped time range.

An ontology-driven system for solving resources-constrained scheduling problems, orders-oriented and lean mass customization-based manufacturing was presented in [23]. This aimed at getting an easily customizable scheduling system that could be richly exploited by different manufacturers. Within the project Model Based Java Software Development Technology, it assumed the commencement of system development from the ontological conceptualization of the domain, constructing the models of the problem and implementing the system through transformation of models into codes.

In [24], a generic library problem solving method for scheduling application, following the limited coverage provided by different attempts made in the past in developing the libraries of scheduling problem-solvers was proposed. They subscribed to the Task-Method-Domain-Application knowledge modeling framework which provides a structured organization for the different components of the library and approached the work at two different levels – the task level and the method level. At the task level, a generic scheduling task ontology was constructed to formalize the space of scheduling problem. At the method level, a generic problem solving model of scheduling that generalize from the variety of approaches to scheduling problem-solving was constructed. In their work, they subscribed to a top down approach of scheduling construction and analyzed the importance of scheduling research both from the theoretical and engineering perspectives.

The authors in [25] proposed a framework which brought a step toward a generic semi-automatic timetabling tool. They investigated different types of timetabling problems and developed a framework for timetabling application with a central domain ontology tagged "ontology for timetabling". The work developed a local search component that can deal with the search space based on problem characteristics passed on by the semantic components and was simplified into steps in order to generate good quality timetables in a reasonable amount of time. The first step was towards solving general problem that consists of mapping their data representation onto the ontology. The next step was using the tools to assists in determining the constraints and object of the problem. Custer *et al*. [25] based their timetabling ontology on the general OZONE scheduling ontology in [20] and developed a generic algorithmic component to generate a solution for real world problems.

The formal relationship between different components in a particular universe of discourse is described using formal languages. These descriptions are the basis for any ontology. An explicit description of the domain of discourse is formally represented in the formal ontology model in Figure 2 [26]. This model is adapted in this work for the semantic model of the formal time scheduling ontology in section 4, as it gives an explicit description of the domain of discourse.

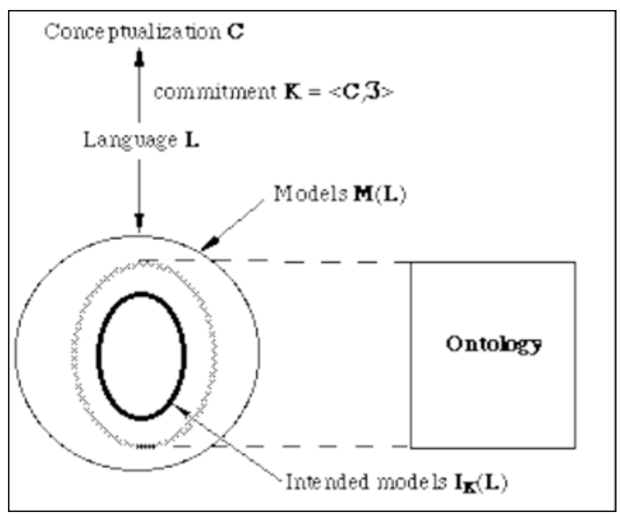

Figure 2. Formal ontology model [26]

3 Complexity reduction rules and axiomatization

The set of competency questions - which are constraints to be satisfied, introduces the time complexities under consideration. Some of the commonly applied competency questions include: Are students from other cooperating departments or faculty offering this course with students of the host department? Is the said course scheduled for the same time with course(s) in the serviced or cooperating department? Is the said course scheduled to hold in the same venue with course(s) in the other department? Are there students in other levels in the cooperating departments who enroll for this course? Is a particular lecturer scheduled to teach more than one course at the same time? Is the venue for the lecture on different campuses from that of students offering the course? Is more than one course allotted a particular venue at the same time? The Rule set comprises rules that address the constraints /complexities and also proposes axioms for their resolutions through the application of Allen's interval relations. The assumption that a faculty has all its constituent (departments) within the same locality (campus) hold for this work: A sub-set of the rules is given as follows:

R1: IF student of $dept_1$ *offers* $course_1$ AND $dept_1$ NOT *owns* $course_1$ THEN $time_1$ for $course_1$ **NOT *overlaps*** $time_2$ for $course_2$ in $dept_2$.

R2: IF $course_1$ *holds* at $time_1$ and $course_2$ holds at $time_2$ AND $time_1$ ***equals*** $time_2$ AND students offer $course_1$ and $course_2$ THEN $time_1$ and $time_2$ ***overlaps***.

R3 IF $course_1$ *holds* at $time_1$ and $course_2$ holds at $time_2$ AND time1 is ***during*** $time_2$ AND students offer $course_1$ and $course_2$ THEN $time_1$ and $time_2$ ***overlaps***.

R4: IF $course_1$ *holds* at $time_1$ and $course_2$ holds at $time_2$ AND $time_1$ ***starts*** with $time_2$ AND students offer $course_1$ and $course_2$ THEN $time_1$ and time2 ***overlaps***.

R5: IF $course_1$ *holds* at $time_1$ and $course_2$ holds at $time_2$ AND $time_1$ ***finishes*** at $time_2$ AND students offer $course_1$ and $course_2$ THEN $time_1$ and $time_2$ ***overlaps***.

R6: IF $course_1$ and $course_2$ are of the same department, $dept_1$, THEN reschedule $course_2$ to a different time from $course_1$ (**NOT *overlaps***).

R7: IF $course_1$ and $course_2$ are in the same faculty but different departments ($dept_1$ and $dept_2$), THEN $time_1$ and $Time_2$ for $course_1$ and $course_2$ respectivelyshould **NOT *overlaps*** or $course_1$ **NOT *during*** $course_2$.

R8: IF $course_1$ and $course_2$ are not in the same faculty, THEN time for $course_1$ and time for $course_2$**NOT *overlaps*** and **NOT *meets***.

R9: IF $time_1$ for $course_1$ and $time_2$ for $course_2$ ***meet***, THEN $time_2$ for $course_2$ or $time_1$ for $course_1$ will be re-scheduled for next available time (**NOT *meets***)

R10: IF time for $course_1$ and $course_2$ are ***equal*** AND venue for $course_1$ is the same venue as venue for $course_2$, THEN $course_2$ should be re-scheduled for the next available time or $course_2$ re-scheduled for the next available venue

R11: IF time for $course_1$ and $course_2$ are ***equal*** or ***meet***, AND the lecturer teaching $course_1$ in $campus_1$ is also scheduled to teach $course_2$ in $campus_2$ within the space of a period, THEN $course_2$ should be res-scheduled for another time greater than a period.

R12: IF $course_1$ is fixed to hold at $time_1$ at $campus_1$ AND $course_2$ $time_2$ at $campus_2$ THEN $time_1$ **NOT *meets*** $time_2$.

R13: IF students who previously failed $course_1$ offer $course_1$ again, and are taking lectures at $time_1$ THEN $time_2$, for their current level course, **NOT *overlaps*** $time_1$.

R14: IF $course_1$ in $campus_1$ and $course_2$ in $campus_2$, THEN $time_1$ for $course_1$ and $time_2$ for $course_2$ **NOT *meets*** or **NOT *overlaps.***

R15: IF venue capacity is less than students' enrolment in $course_1$ THEN re-schedule $course_1$ another suitable venue.

Formalizing the complexity reduction rules in the previous section explicitly and expressively using First-Order Logic(FOL) yields the following AX1 to AX15 as axioms. The conventional approach of conceptualizing domain concepts; **lecturer, student, venue and time** with relations specific to the domain under consideration: *owns, has, offers, holds* and *teaches,* results in a non-optimal time scheduling. This therefore calls for the inclusion and utilization of the Allen's interval relations; ***overlaps, meets, equals, during*** and their negations. Axioms AX1 to AX15 are rule instances that form the basis for the AR based on ontology and produces an optimal time-scheduling process.

Let S,V,T,C, L represent students, venue, time, course and levels respectively. Let S={s_1, s_2, … s_n} be the set of students, V={v_1, v_2, … v_n} be the set of venues, CS={cs_1, cs_2, … cs_n} be the set of courses, T={t_1, t_2, … t_n} be the set of time slots , P = {p1, p2, …, p3} be the set of campuses and L={L_1, L_2, … L_n} be the set of students level

AX1: *s, d1, cs1, t1, cs2, d2, t2,*
offers(s,cs1)owns(d1,cs1)offers(s,cs2)
owns(d2,cs2)
cooperates(d1, Host, d2, Serviced).

AX2: *s, cs1, t1, cs2, t2.*
holds(cs1,t1)holds(cs2,t2)
equals(t1,t2)offers(s, cs1) offers(s, cs2)
overlaps(t1, t2).

AX3: *s, cs1, t1, cs2, t2.*
holds(cs1,t1)holds(cs2,t2)
during(t1,t2) offers(s, cs1)
offers(s, cs2)overlaps(t1, t2).

AX4: *s, cs1, t1, cs2, t2.*
holds(cs1,t1)holds(cs2,t2)
starts(t1,t2) offers(s, cs1) offers(s, cs2)
overlaps(t1, t2).

AX5: S, cs1, t1, cs2, t2.
holds(cs1,t1)holds(cs2,t2)
finishes(t1,t2)offers(s, cs1) offers(s, cs2)overlaps(t1, t2).

AX6: cs1, t1, d1, cs2, t2.
owns(d1,cs1)owns(d1,cs2)
holds(cs1,t1)holds(cs2,t2)equals(t1,t2)
equals(l1, l2)overlaps(t1, t2).

AX7: cs1, t1, d1, fac1, cs2,t2, d2. fac2.
owns(d1,fac1,cs1)owns(d2, fac2, cs2)
overlaps(t1,t2) during(holds(cs1, cs2)) .

AX8: cs1, t1, cs2, t2, t.
holds(cs1,t1)holds(cs2,t2) finishes(t1,t)
starts(t2,t) meets(t1, t2).

AX9: cs1, t1, d1, fac1, cs2, t2, d2. fac2.
owns(d1, fac1, cs1) owns(d2, fac2, cs2)
equals(f1,f2)
meets(t1,t2) overlaps(t1, t2).

AX10: cs1, t1, v1, cs2, t2, v2.
holds(cs1,t1)holds(cs2, t2) equals (v1, v2)
equals(t1, t2).

AX11: cs1, t1, p1, cs2, t2, p2.
holds(cs1,t1, p1) holds(cs2, t2, p1) equals (t1, t2) equals(p1,p2) teaches(lect,p2) teaches (lect, p2)
overlaps (t1, t2)meets (t1, t2)

AX12: cs1, t1, p1, cs2, t2, p2.
holds(cs1,t1,p1) holds(cs2, t2, p2) equals (t1, t2) equals (p1, p2) meets (t1, t2)

AX13: s, cs1, t1, d1, cs2, t2.
offers(s,cs1,t1) offers(s, cs2, t2) owns(d1, c1)
equals(t1, t2) equals(l1, l2) overlaps(t1, t2).

AX14: s, cs1, t1, d1, cs2, t2.
offers(s,cs1,cs2)
holds(cs1, p1) holds(cs2, p2)
meets(t1,t2)overlaps(t1, t2).

AX15: s, cs1,v1, t1, nos, v2, vcap.
offers(s, cs1, v1) holds(cs1, v1, t1) (nos>vcap)
holds(cs1, v2)

As an interpretation, axiom *AX6* can be read thus*: 'For all students, courses and departments, there exist course cs2, such that cs2 is offered by student and department owns student and cs2 is not own by department. It therefore follows that time$_1$ for cs1 should not overlap with time$_2$ for cs2".*

This formalism utilizes *offers and owns as* domain-specific relations. It also explored a reverse relation to *owns* between students and departments. The power of Allen's interval relation, ***overlaps***, is also brought into consideration not forsaking the expressive tools in FOL. The use of the universal and the existential qualifiers gave life to the axiom. Putting all these together in Protégé ontology tool where the departmental timetable ontology has been developed and mapped together with reasoning to make the task of responding to the earlier proposed competency questions an easy one. A general and optimal lecture timetable with clear semantics as described in the formal representation is thus achieved.

4 Semantic modeling of the formal time scheduling ontology

Figure 3 represents the semantic model of the formal time scheduling ontology with different components which are related accordingly to show how an optimality of time can be obtained. The semantic model of the formal time scheduling ontology is adapted from the semantic model by Guarino [26], where, Time Scheduling Ontology (TSONT) is defined as the conceptualization of the domain concepts expressed mathematically in equation (1). Further description of the conceptual model is explicated in equations (2) to (4), where a set of conceptual relations, R is on a structure, S being the model of the language L with vocabulary V.

$$C_{TS} =< D_T , T_C , R > \qquad (1)$$

$$<D_T , T_C> = DSR + AIR \qquad (2)$$

The resulting model is given as < S, I > w*here,*

$$S = <D_T , R > \qquad (3)$$

and the usual interpretation function, I is expressed as I = V → D_T R. Fixing the intentional Time Schedule by means of a structure such as < C_{TS}, P> where,

C_{TS} = < D_T, T_C, R> and P:V → D_T R is an intentional interpretation, hence, K = < C_{TS}, P > is an Ontological commitment for L. That is, L commits to C_{TS} by means of K and C_{TS} is the underlying conceptualization of K. With the commitment,

$$C_{TS} =< D_T, T_C, R, I > \qquad (4)$$

where, C_{TS} is the time scheduling conceptualization, D_T is the timetabling domain, T_C *is the* interdepartmental allocation complexities, *R* is the relations, *DSR* is the Domain Specific Relation, *AIR* is the Allen Interval Relations, *I* is the Interpretation, *P* is the Intentional Interpretation, *S* is the Structure, and *K* is the Ontological Commitment. The mathematical model in equation (1) is used to give a semantic interpretation that will further explicate the logic behind ontology.

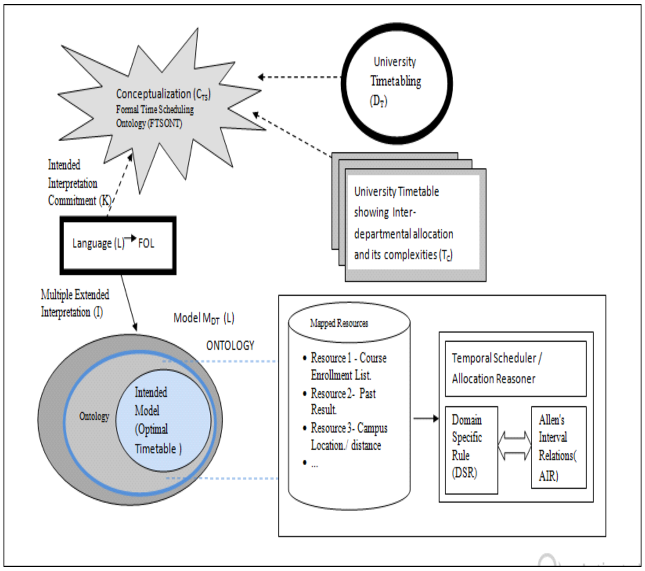

Figure 3. Semantic model of the formal time scheduling Ontology

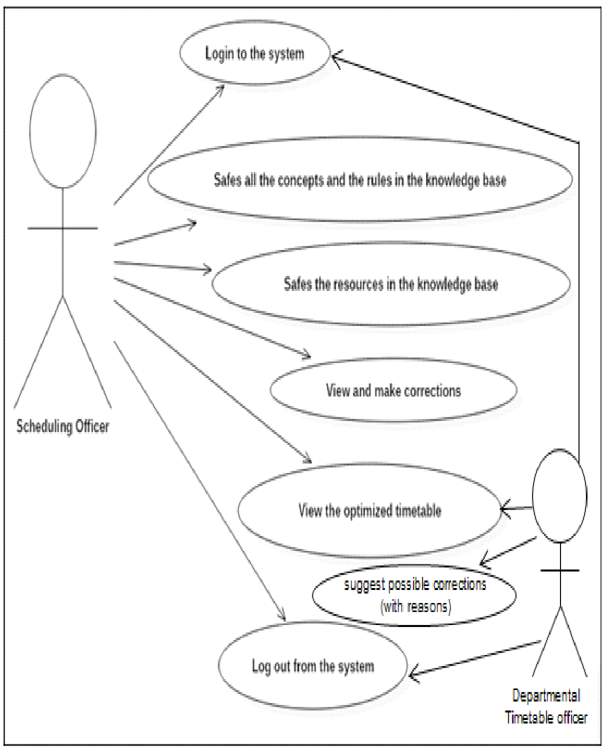

Figure 4. Use case diagram for the TSONT framework

5. System design for TSONT model

5.1 Use case description

The Use Case diagram in figure 4 gives a clear understanding of the developed time scheduling ontology (TSONT) system. The concepts and the resources of the timetable are saved into the knowledge base by the scheduling officer, after a successful log in. The scheduling officer then sends the resources to the allocation reasoner or time scheduler for proper allocation of time. Furthermore, the officer can view the system outcomes, make corrections where necessary, and then review for optimized timetable, and then logs out. The departmental timetable officers can in turn log in to view the optimized timetable, suggest possible corrections for consideration and effect by the scheduling officer, and logs out.

5.2 Class diagram for TSONT framework

Figure 5 represents the class diagram of the TSONT framework, which shows the interactions between classes that constitute the domain of discourse. The student offers courses and the courses are taught by the lecturers. Courses are held in venues, and each venue has an interval of time assigned for it. The venue also has its capacity which informs the number of students that can be allocated to the venue.

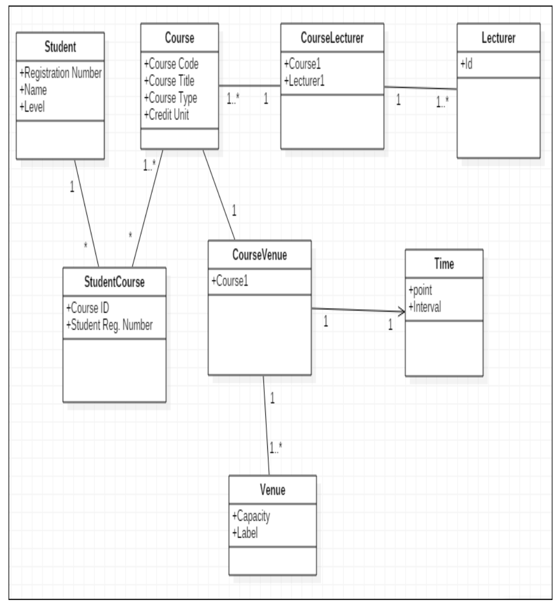

Figure 5. Class diagram for TSONT framework

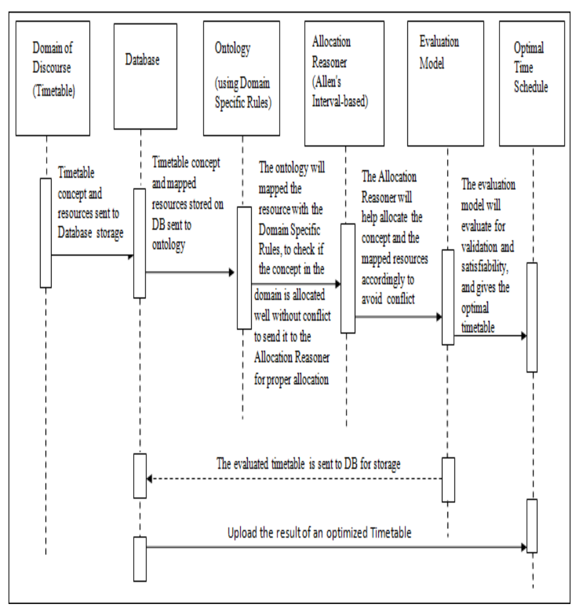

Figure 6. Sequence diagram for the TSONT framework

5.3 Sequence diagram

Figure 6 represents the sequence diagram of how the proposed TSONT system works. The resources used for time schedule and the concepts of the domain of discourse are sent to the database (DB) for storage. The ontology picks the concepts and resources needed for time schedule and sends them to the AR, which helps the rule-based and the interval-based relations, check and allocate the courses, lecturers, venue to the time-slots and to a particular set of students, considering the students who failed or dropped course at a lower level.

The AR sends the results to be evaluated by an ontology evaluation tool, for validation and satisfiability, after which the conclusion of a time complexity free time schedule is sent back to the DB for storage and future reuse. The DB uploads the optimized time schedule for printing and distribution.

6. Conclusion

The university timetabling, an instance of space-time related conflicts or complexities, requires the design of an interval-based temporal ontology to help in its resolution demands full understanding of how the ontology handles the constraints that will answer the stated competency questions. The formal axioms from the stated rules update the constraints in the ontology using the interval based relations. The implementation of the represented formal notations to describe the embedded semantics in the given rules is applicable for inference in the weighted ontology framework. It aims at formalizing the heuristics through ontology, by explicitly incorporating all constraints that will give valid answers to the competency questions in the AR and enabling their analysis and resolution by the ontology-based reasoners. The formal semantic model further explicates the ontology and shows how it is applicable for intelligent complexity reduction and resolution in time scheduling process. The time scheduling ontology based on this formal semantic model will provide an optimal time table schedule.

Conflict of Interest:

The authors declare no conflict of interest

References

[1] P. U. Usip, U. G. Inyang, D. E. Asuquo, E. M. Umoren, "An evaluation model for a probability weighted ontology of temporal complexities", in Proceedings of 2nd IEEE International Conference on Computational Systems and Information Technology for Sustainable Solutions (CONTISS 2017), Bengaluru, India, 159-165, 2017.

[2] A. Wren, "Scheduling, timetabling and rostering - A special relationship"? International Conference on the Practice and Theory of Automated Timetabling (PATAT 1995), 46-75, 1995.

[3] J. Shafi, A. Waheed and S. Sanober (2016). Dependency Test: Portraying Pearson's Correlation Coefficient Targeting Activities in Project Scheduling. International Journal of Advanced Computer Science and Applications. 7(9). 351-356. 10.14569/IJACSA.2016.070948.

[4] A. Modupe, O. Olusayo, and O. Olantunde, "Development of a University lecture timetable using modified genetic algorithm approach", International Journal of Advanced Research in Computer Science and Software Engineering, (4), 163-168, 2014.

[5] S. Kristiansen and T. R. Stidsen, "A comprehensive study of educational timetabling: A survey", Department of Management Engineering, Technical University of Denmark, DTU Management Engineering Report, (8), 2013.

[6] D. Abramson, "Constructing school timetable using simulated annealing: sequential and parallel algorithm", Management Science, 37(1), 98-113, 1994.

[7] A. Colorni, M. Dorigo, and V. Manniezzo, "A genetic algorithm to solve the timetable problem", Journal of Computational Optimization and Applications, 1, 90-92, 1992.

[8] N. Ibaraki, "Tabu Search for the constraint satisfaction problem as a general problem solver", European Journal of Operational Research, 599-623, 1998.

[9] E. K. Burke and J. Newall, "Enhancing timetable solutions with local search methods", In: Burke, E. K., DeCausmaecker, P. (eds.): Selected papers from the 4th International conference on the Practice and Theory of Automated Timetabling. Lecture Notes in Computer Science, Vol. 2740, Springer-Verlag, Berlin Heidelberg New York, 344- 354, 2003.

[10] Q. Rong, "Case-base reasoning for course timetabling problem", PhD Thesis, University of Nottingham, 2002.

[11] J. P. Rickman, "The design of a course-timetabling system using graph-coloring and artificial intelligence", Honors Program Theses, Paper 15, 2014. https://scholarship.rollins.edu/cgi/viewcontent.cgi?article=1014 HYPERLINK "https://scholarship.rollins.edu/cgi/viewcontent.cgi?article=1014&context =honors"& HYPERLINK "https://scholarship.rollins.edu/cgi/viewcontent.cgi?article=1014&context =honors"context=honors

[12] R. Ganguli and S. Roy, "A study on course timetable scheduling using graph coloring approach", International Journal of Computational and Applied Mathematics, 12(2), 469-485, 2017.

[13] R. K. Bania and P. Duarah, "Exam time table scheduling using graph coloring approach", International Journal of Computer Sciences and Engineering, 6(5), 84-93, 2018.

[14] R. P. Badoni, and D. K. Gupta, "A graph edge colouring approach for school timetabling problems", International Journal of Mathematics in Operational Research, 6(1), 117–132, 2014.

[15] J. Roa, E. Reynares, C. M. Laura and P. D. Villarreal, "Ontology-based heuristics for process behavior: formalizing false positive scenarios", 2017. Available from: https://www.researchgate.net/publication/316743617 [accessed Jan 13 2019].

[16] J. Allen, "Maintaining knowledge about temporal intervals", Communications of the ACM. 26(11), 832-843, 1983.

[17] M. Hemalatha, V. Uma and G. Aghila, "Time ontology with reference event based temporal relations", International Journal of Web and Semantic Technology, 3(1), 23-31, 2012.

[18] N. Noy and M. Musen, "Anchor-PROMPT: using non local context for semantic matching", in Proceedings of the Workshop on Ontologies and Information Sharing at the International Joint Conference on Artificial Intelligence (IJCAI), Seattle, Washington, 2001.

[19] A. Formica, M. Missikoff, E. Pourabbas and F. Taglino, "Bayesian approach for weighted ontologies and semantic search", in Proceedings of the 8th International Joint Conference on Knowledge Discovery, Knowledge Engineering and Knowledge Management (2), 171-178, 2016.

[20] S. Smith and A. Becker, "An ontology for constructing scheduling system", AAAI, Spring, 120 Symposium on Ontology Engineering, Newport Beach, California, 129, 1997.

[21] C. Sayers and R. Letsinger, "An ontology for publishing and scheduling events and the lessons learned in developing it", in Workshop on Ontologies in Agent Systems, 1st International Joint Conference on Autonomous Agents and Multi-Agent Systems (AAMAS 2002), Bologna, Italy, 2002.

[22] D. Rajpathak, E. Motta and R. Roy, "A generic task ontology for scheduling applications", in Proceedings of the International Conference on Artificial Intelligence, Las Vegas, 2001.

[23] J. Sanko and V. Kotkas, "Ontology-driven scheduling system for manufacturing", Baltic Journal of Modern Computing, 4(3), 508 – 522, 2016.

[24] D. G. Rajpathak, E. Motta, Z. Zdrahal and R. Roy, "A generic library of problem solving methods for scheduling applications", IEEE Transactions on Knowledge and Data Engineering, 18(6), 815-828, 2006.

[25] N. Custers, P. De Causmaecker, P. Demeester, and G. Berghe, "Semantic component for timetabling", International Conference on the Practice and Theory of Automated Timetabling (PATAT 2004), 17-33, 2004.

[26] N. Guarino, (Ed.), "Formal ontology", in Proceedings of the First International Conference on information systems (FOIS'98), 46, 3-15, Trento, Italy, 1998.

Advances in Science, Technology and Engineering Systems Journal Vol. 4, No. 2, 395-401 (2019)

www.astesj.com

ASTESJ

ISSN: 2415-6698

Relational Databases Versus HBase: An Experimental Evaluation

Zakaria Bousalem[*,1], Inssaf El Guabassi[2], Ilias Cherti[1]

[1]*Faculty of Sciences and Technologies, Hassan 1st University, Settat, Morocco*

[2]*Faculty of Sciences, Abdelmalek Essaadi University, Morocco*

A R T I C L E I N F O

Article history:
Received:21 February, 2019
Accepted:07 April, 2019
Online: 26 April, 2019

Keywords:
Relational database
HBase
NoSQL
Comparative study
Benchmarking
YCSB

A B S T R A C T

Relational database management systems (RDBMS) have been imposed for more than three decades as a facto standard for data storage, management, and analysis. They have a good reputation by supporting ACID properties (Atomicity, Consistency, Isolation, and Durability) and by adopting the SQL language which has become a standardized language. However, despite their power, RDBMS have failed to meet the modern application's requirements. That's why the need arises for new database management systems that support the manipulation of large amounts of data. NoSQL database systems allow a flexible schema, whereas RDBMSs require a strictly defined schema. They support horizontal scalability and prioritize data availability over consistency (BASE properties) and have performance that remains good with scalability. In this paper, we present an experimental comparison between a relational database (MySQL) and a NoSQL database (HBase) in terms of runtime and latency in different scenarios using the YCSB Framework.

1. Introduction

For more than three decades Relational databases has been the de-facto standard in the database management systems market thanks to its maturity[1], [2]. Nowadays, with a constant growth of data generated by modern web applications such as social networks, e-commerce sites, and mobile applications; the management, querying and analysis data have become a real challenge for relational database management systems (RDBMS). Besides, these data are recorded in several formats (structured, semi-structured and unstructured), whereas the traditional database management systems based on a rigid schema. These limitations of the relational model led the leaders of the internet such as Google, Amazon, eBay, Alibaba and Facebook to develop a new model named NoSQL databases[3], in order to overcome the weakness of relational database management systems towards the variety, the velocity and the large volume of new data captured. "NoSQL" databases are not usually a replacement, but rather a complementary complement to RDBMS and SQL. The NoSQL model is based on the CAP theorem (Consistency Availability Partition Tolerance) as opposed to RDBMS based on ACID properties (Atomicity, Coherence, Isolation, Durability). NoSQL databases management systems (DBMS) can be classified into four categories: Key-Value databases, Document Oriented databases, Column Oriented databases and Graph databases. This classification is due to the fact that each type of database arises in a specific context and based on different architectures [4]. Comparing different models provides a clear vision for choosing the most appropriate model for a given context. The purpose of this article is to compare the relational model (MySQL) and the NoSQL model (HBase)[5] in terms of runtime and latency in different scenarios using the YCSB Framework. We will measure the latency of three cases of operations: 100% read operations, 100% update operations, and a mix of 50% reads and 50% updates with two scenarios. The first is increasing the number of records however the total number of operations remains fixed at 10000. The second is increasing the number of operations while fixing the total number of records at 1 million records in order to reveal how the number of operations and number of records affect the performance in terms of the latency metric and runtime for data loading. In order to make an efficient approach for migration from Relational databases to HBase database, we have started by a feasibility assessment[6], and in this paper, we have made an experimental comparison between relational databases and HBase database. The goal of this comparison is clearly identifying which case is better to migrate from relational to HBase.

The rest of the paper is structured as follows: In section 2 we introduce the basic definitions starting with an introduction to the NoSQL databases after we present the HBase database, so we will see what Databases Benchmarking is, then we provide a brief presentation of YCSB Framework. In section 3 we introduce the experimental strategy used in our paper. In section 4 we describe

*Zakaria Bousalem, Faculty of Sciences and Technologies, Hassan 1st University, Settat, Morocco, zakaria.bousalem@gmail.com

https://dx.doi.org/10.25046/aj040249

the experimental setup for evaluation. In Section 5 we present the MySQL and HBase evaluation results. In Section 6, a summary and general observations about the results of this evaluation are provided. Finally, Section 7 concludes our paper.

2. Basic definitions

2.1. NoSQL Databases

NoSQL (Not Only SQL) is a broad category of next-generation database management systems, as they are typically non-relational, distributed, open source, and support horizontal scaling. Unlike relational databases, they can better respond to big data problems. These database systems do not rely on a rigid relational schema and the database can therefore grow without constraint.

There are various classes of NoSQL DBMS [7]:

- **Key / Value:** These databases function as a key/value associative array. This structure makes it a simple database to set up and allows quick access to information. The value can be a string or an object. It offers high scalability thanks to schema-less approach. E.g. Riak, Azure Table Storage, and Redis.
- **Document-Oriented databases:** These databases management systems are an extension of the key/value databases. Document-oriented engines do not associate a key with a value but with a schema-less document like JSON and XML. The flexibility of these databases makes them polyvalent. E.g. MongoDB, Couchbase Server, and OrientDB.
- **Column-oriented databases:** The data representation is done by columns contrary to traditional DBMS. This structure makes it easier to add a column to a table and manage millions of columns. These databases are known for their ability to scale and to store a large volume of data. These DBMSs are mainly used in environments where it is necessary to access many columns. They are especially useful for streaming data and Real-time analytics. E.g. HBase, Cassandra, and BigTable.
- **Graph databases:** Store data based on graph theory using graph structures (nodes, arcs, and properties). This storage model facilitates the representation of all highly connected data, which is particularly well adapted to the social networks data processing, fraud detection, and recommendation engine[8]. E.g. AllegroGraph, Neo4j, and FlockDB.

2.2. HBase

HBase is a distributed database management system, developed on top of the HDFS file system. It belongs to the column-oriented databases category. HBase is designed to provide real-time access to data stored on HDFS. It supports horizontal scalability which allows it to support extremely large database tables[9]. It was based on "BigTable" DBMS [10].

As shown in Figure 1, the HBase data model is based on six concepts [11]:

- **Table:** HBase was organizing data in tables.
- **Row:** Within tables, the data is organized in rows. RowKey is the identifier for each row.
- **Column Family:** In each row, data is grouped by "Column Families ". All rows have the same "Column Families". The "Column Family" is set when the table is created in HBase.
- **Column Qualifier:** Access to data within a "Column Family" is done via the "column qualifier". It's specified at the data insertion phase.
- **Cell:** Cell is identified by the combination of the "RowKey", the "Column Family" and the "Column Qualifier". It's Stores the values.
- **Version:** The values within a cell are versioned. The versions are identified by their timestamp.

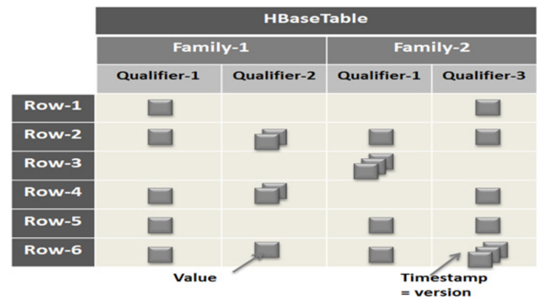

Figure 1: HBase model [12]

2.3. Databases Benchmarking

Database benchmarks (Performance evaluation by experimentation on a real system) [13] are an important tool for database researchers, designers, and users. Its role is to generate application-specific workloads and to test databases in order to assess the relative performance and ease the process of making comparisons between different database specifications. As mentioned by [14] the big data benchmarking process is composed of five steps: Planning, Generating data, Generating tests, Execution and Analysis, and evaluation Figure 2[14].

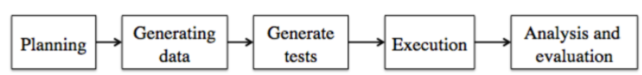

Figure 2: Benchmarking process for big data systems [14]

There are many existing tools for Big Data benchmark [15] like BigBench [16], TPC-C[17] , TPC-E[18], TPC-H[19], TPC-D[20], Bigdatabench [21] and YCSB [22]. In this paper, we are going to use Yahoo! Cloud Serving Benchmark (YCSB) because is currently the most popular choice for benchmarking performance of big data databases [23].

2.4. YCSB

YCSB benchmark is an extensible, modular benchmarking tool, it was developed by Yahoo teams for the aim of measuring the performance of various storage solutions, with adapters for a variety database systems such as Relational databases (with JDBC driver), Big data databases(HBase, Mongo, Cassandra, Redis, HyperTable, Couchbase, DynamoDB, Accumulo, etc) and others.

As shown in Figure 3 YCSB client is composed of four modules: the executor workload, client-threads module, Database interface module and statistics module. After generating the data to be loaded to the database by YCSB client, the executor workload will launch several client threads that execute a series of operations (client-threads module) by using the (Database Interface Layout). The statistics module will retrieve statistics from each operation and analyze them.

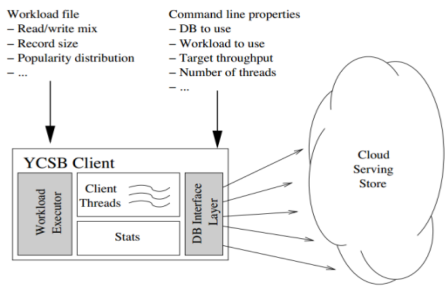

Figure 3: YCSB client architecture [22]

YCSB benchmark varies the proportion of read, write, update, insertion, and scan operations in a series of queries named workloads. The YCSB distribution includes six workloads:

- **Workload A:** A mixed workload with 50% of reads and 50% of writes
- **Workload B:** A mixed workload with 95% of reads and 5% of writes.
- **Workload C:** A workload of 100% read
- **Workload D:** A mixed workload with 95% of reads and 5% of inserts.
- **Workload E:** A mixed workload with 95% of scans and 5% of inserts.
- **Workload F: Read-modify-write:** A mixed workload with 50% of reads and 50% of read-modify-writes

3. Experimental strategy

Much work on the potential of comparing database performances by YCSB has been carried out [24]–[26]. Abramova et al [24] compare five NoSQL databases (Redis, Cassandra, HBase, MongoDB, and OrientDB) in terms of their capabilities, based on read and update operations. They affirm that MongoDB, Redis, and OrientDB are better for reads, Cassandra and HBase are optimized for updates. Yassien and Desouky [26] compare MySQL, MongoDB, and HBase by using YCSB for the aim to study the effect of varying the operation and thread count with respect to runtime, throughput, and latency. The authors state that each database performs at its best in different circumstances. They recommend HBase to use for the applications that require the high update and insert operations, MySQL for the applications whose perform mostly reads operations and MongoDB for the applications that require both adequate read and write performance. Matallah et *al* [25] compare MongoDB and HBase in order to evaluate loading and running time of five workloads. According to their results, when performing reads, MongoDB showed good performance, unlike HBase which showed good performance for updates.

Latency means the time of response can get user when sending a request. It's one of the essential metrics to evaluate databases performance [27]. Consequently, we chose in our paper to compare MySQL and HBase in terms of runtime and response time (latency) based on read and update operations since they are the most used operations[24] while increasing the number of records however the total number of operations remains fixed at 10000. Then we will increase the number of operations while fixing the total number of records at 1 million records in order to reveal how the number of operations and number of records affect the performance in terms of latency and runtime for data loading.

4. Experimental setup

In order to perform our comparative study, we present the experimental setup for evaluation. The experiments were run using a single physical machine with Ubuntu operating system, YCSB benchmark, Cloudera Hadoop, Cloudera HBase, and, MySQL. All specifications are listed in Table1.

Table 1 Experimental specifications

CPU	Intel® Xeon(R) CPU E5504 @ 2.00GHz × 8
Memory	16 GB
Hard disk	237 GB SSD
Operating system	Ubuntu 14.04 (64-bit)
Java version	1.8.0_16
YCSB version	0.14
CDH version	5.14.1
Cloudera HBase version	1.2.0
Cloudera Hadoop version	2.6.0
MySQL	5.6.26

The main focus of this study is to evaluate read and update operations since they are the most used operations [24]. Therefore this comparison mainly consists of three workloads namely A and B included in the YCSB project and we create new workload G proposed by [24] to evaluate the Update Only case. Table 2 shows the tested workloads:

Table 2 Used workloads

Workload	Operations
Workload A	50% of reads and 50% of writes
Workload C	100% read: Read Only
Workload G	100% update : Update Only

The dataset used in this databases benchmarking is generated by YCSB data generator which is a part of YCSB client. The dataset records are composed of 10 fields. Each field is filled by a random string with 100 bytes which give 1 KB per record. The 'YCSB_KEY' is the primary key for each row[22]. Table 3 shows the YCSB dataset structure.

Table 3 YCSB Dataset structure

	YCSB_KEY	FIELD1	FIELD2	FIELD3	FIELD4	FIELD5	FIELD6	FIELD7	FIELD8	FIELD9
Row 1										
Row 2										
……										

Row N										

5. Experimental results

We performed three tests. The first is loading data, the second is running workloads while increasing the number of records and fix the number of operations at 10000 and the last is running workloads while increasing the number of operations and set the number of records to 1 million.

5.1. Loading data

- **Runtime (less is better):** As shown in Figure 4 as the size of data increases the runtime of loading data for MySQL and HBase increases, HBase exhibited an immense increase but MySQL shows starting from 100000 records a dramatic increase. Additionally, HBase has the lowest runtime. In the first test (Record number=1000) MySQL and HBase have almost identical runtime. As the record number increases, the runtime for MySQL to load data ranges from 2 times slower than HBase for the second test(Record number=10000), to more than 4 times slower for MySQL for the third test and more than 5 times for the fourth test.

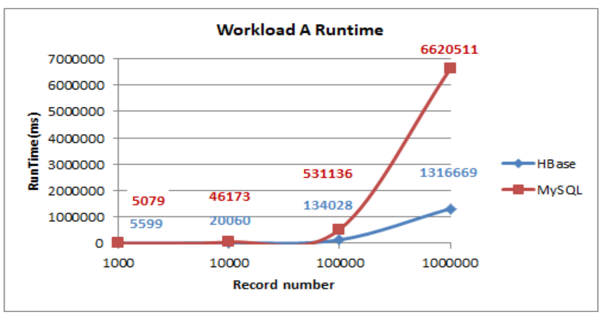

Figure 4: Loading data Runtime

- **Insert latency (less is better):** decreases as the size of data increases for HBase. Unlike MySQL that shows a steadiness initially and then it exhibited a decline and increase thereafter. As shown in Figure 5 HBase has the shortest insert latency.

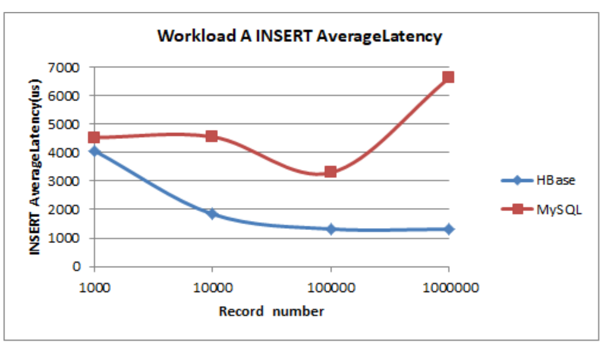

Figure 5: Loading data Insert latency

5.2. Increasing the number of records

5.2.1. Workload A

- **Runtime:** As illustrated in Figure 6 as the size of data increases the runtime of MySQL for data loading increases. MySQL exhibits a slight steady increase in runtime, unlike HBase that shows a slight decline and increase thereafter. HBase has the lowest runtime.
- **Read latency (less is better):** HBase shows a slight decline and increases thereafter, unlike MySQL that exhibits a slight steady increase as shown in Figure 7. MySQL has the shortest read latency.

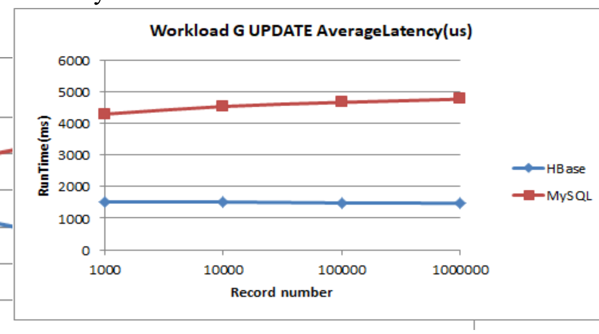

Figure 12: Workload G Latency

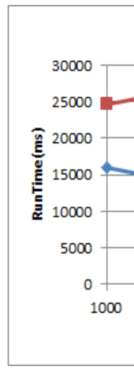

Figure 6: Workload A Runtime

- **Update latency (less is better):** As shown in Figure 8, like runtime in update latency MySQL exhibits a slight steady increase in runtime, unlike HBase that shows a slight decline and increase thereafter. HBase has the lowest update latency.

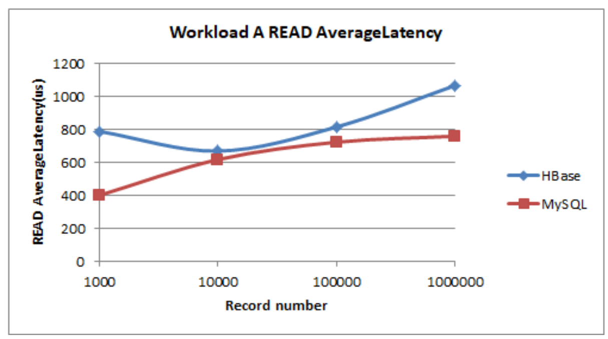

Figure 7: Workload A Read Latency

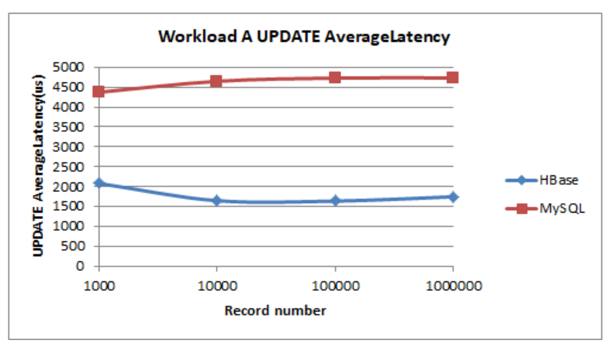

Figure 8: Workload A Update Latency

5.2.2. Workload C

As illustrated in Figure 9 and Figure 10 HBase exhibits a slightly decline initially, it shows an alternating increase and decline thereafter in terms of runtime and read latency, unlike MySQL that shows a steadiness initially, then it exhibited a slight increase after reaching 100000 records. MySQL has the shortest run time and read latency.

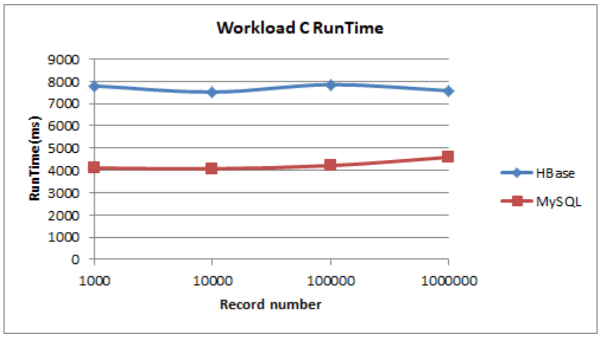

Figure 9: Workload C Runtime

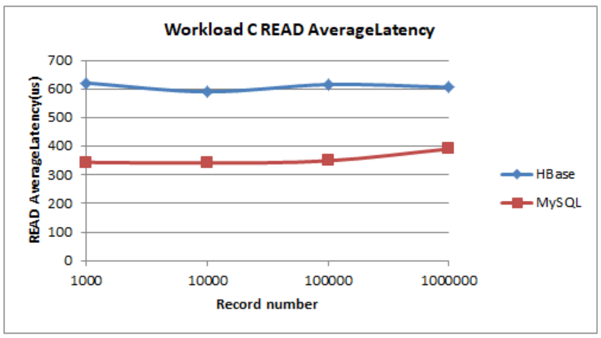

Figure 10: Workload C Read Latency

5.2.3. *Workload G*

As illustrated in Figure 11 and Figure 12 the HBase exhibits a steadiness both for runtime and update latency, unlike MySQL that shows a slight increase. HBase has the lowest value of runtime and read latency.

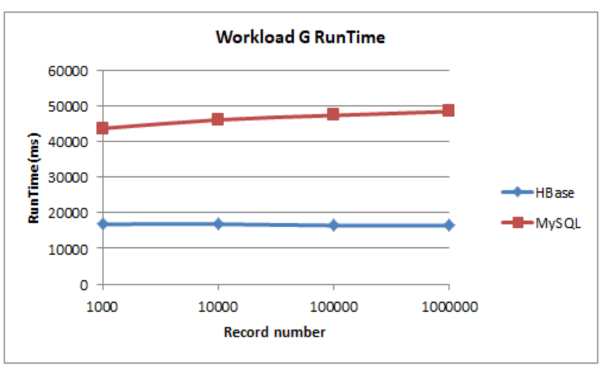

Figure 11: Workload G Runtime

5.3. Increasing the number of operations

5.3.1. *Workload A*

- **Runtime:** As shown in Figure 13 as the number of operations increases the runtime of MySQL and HBase increases, HBase and MySQL show an immense increase but MySQL exhibits starting from 100000 operations a dramatic increase. HBase has the lowest runtime.

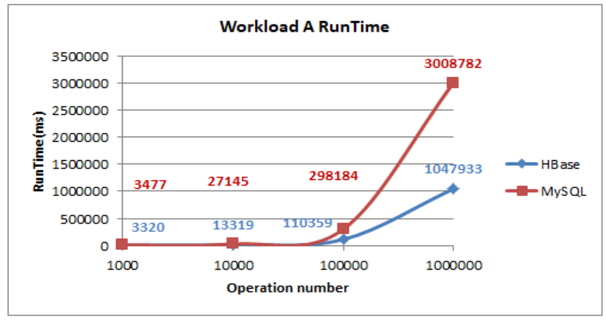

Figure 13: Workload A Runtime

- **Read latency (less is better):** HBase and MySQL show an immense decline until reaching 10000 records, then exhibit slightly decline as shown in Figure 14. MySQL has the shortest read latency.

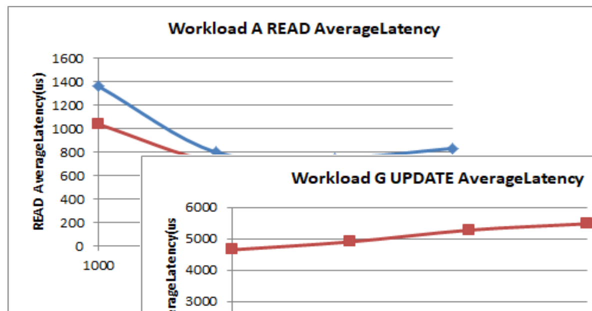

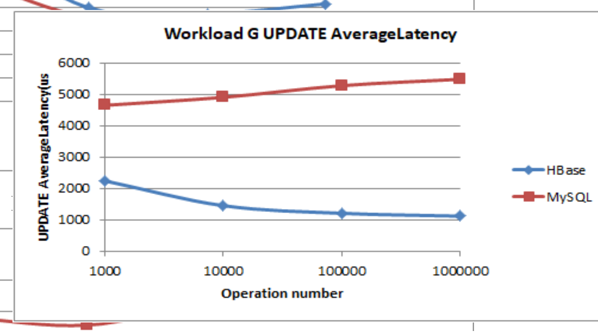

Figure 19: Workload G Update Latency

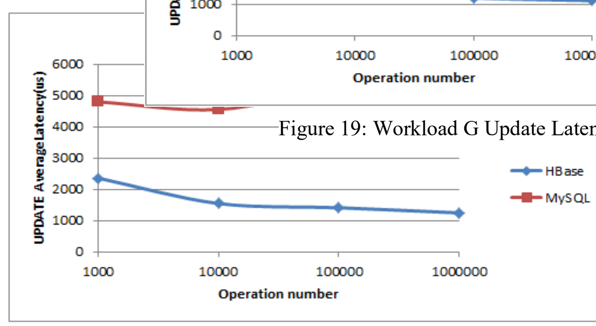

Figure 15: Workload A Update Latency

- **Update latency (less is better):** As illustrated in Figure 15 as the number of operations increases the update latency of HBase decline. MySQL exhibits a slightly decline initially, it shows an alternating increase and a steadiness thereafter in terms of update latency. HBase has the lowest update latency.

5.3.2. *Workload C*

- **Runtime:** As shown in Figure 16 as the number of operations increases the runtime of MySQL and HBase increases, HBase and MySQL show an immense growth but starting from 100000 operations they exhibit a dramatic increase. MySQL has the lowest runtime.

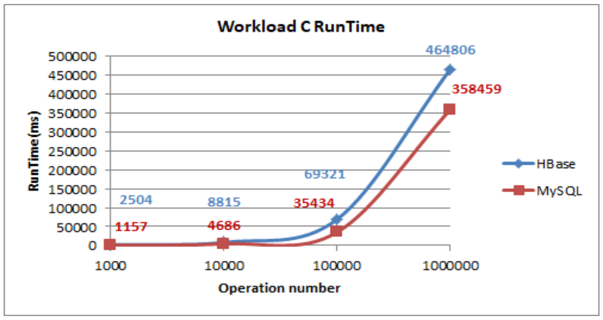

Figure 16: Workload C Runtime

- **Read latency(less is better):** HBase shows an immense decrease, unlike MySQL that exhibits a steady decline as shown in Figure 17. MySQL has the shortest read latency.

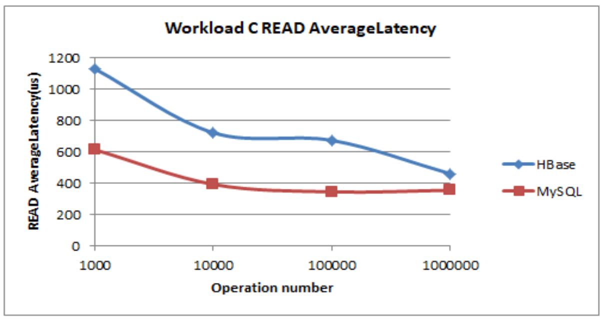

Figure 17: Workload C Read Latency

5.3.3. *Workload G*

- **Runtime:** As shown in Figure 18 as the number of operations increases the runtime of MySQL and HBase increases, HBase and MySQL show an immense increase but MySQL exhibits starting from 100000 operations a dramatic increase. HBase has the lowest runtime.

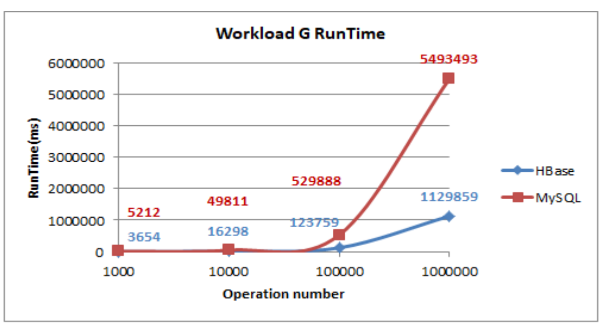

Figure 18: Workload G Runtime

- **Update latency (less is better):** HBase shows an immense decrease, unlike MySQL that exhibits a steady increase as shown in Figure 19. HBase has the shortest update latency.

6. General observations

According to our experimental results, it can be observed that MySQL runtime is higher in all scenarios for data loading and HBase performed far better compared to MySQL. Concerning read/write latencies, it can be stated that MySQL's latency is lower for read operations and HBase's latency is lower for write operations. In terms of the running workloads runtime; HBase beats the competition in all cases except for the read-only workload. Also from our experimental results it can be stated that on the one hand the increasing the number of records seems to have mediocre effects on read latency for MySQL and HBase, no consequences in term of read latency and great impact with respect to runtime data loading (Taken into account that number of records tested was not of a real large size). On the other hand, increasing the number of operations seems to have a significant impact on read and write latency for MySQL and HBase, and immense effects on the running workloads runtime. Consequently, we believe that HBase outperforms MySQL on I/O bound ('write') operations but lagged behind in bound ('read') operations with respect to runtime and latency metrics. HBase exhibits good performance in update operations thanks to using the log files and cache memories to store all transactions and then write only the log files on disk which reduce the input/output operations [25], contrary to MySQL that stores data directly on disk. Additionally, HBase lagged behind in reads capabilities due to comparing all copies by HBase before running a read operation in order to return the most recent copy, which affects database performance [25]. So, according to our experimental results, we can say that is better to migrate from Relational databases (MySQL) to HBase in case of the applications that require a heavy update, most update and high insert operations like session store in order to record recent actions.

7. Conclusion and future work

In this paper, we present an experimental comparison between a relational database (MySQL) and a NoSQL database (HBase) with respect to runtime and latency in different scenarios using the YCSB Framework. Based on the above results we can deduce that HBase performed far better compared to MySQL in data loading because MySQL runtime is higher in all scenarios for this kind of operation. Additionally, we have found that HBase outperforms MySQL on I/O bound ('write') operations but lagged behind in bound ('read') operations with respect to runtime and latency metrics. In perspective, we envisage to compare MySQL and HBase in terms of database performance of the aggregate functions and also pass to higher scales by using a very large database and performing the evaluation in a really distributed and parallel environment.

References

[1] Z. Bousalem and I. Cherti, "XMap: A Novel Approach to Store and Retrieve XML Document in Relational Databases.," *JSW*, vol. 10, no. 12, pp. 1389–1401, 2015.

[2] Z. Bousalem, I. El Guabassi, and I. Cherti, "Toward Adaptive and Reusable Learning Content Using XML Dynamic Labeling Schemes and Relational Databases," in *Advanced Intelligent Systems for Sustainable Development (AI2SD'2018)*, 2019, pp. 787–799.

[3] D. J. Abadi, "Data management in the cloud: Limitations and opportunities.," *IEEE Data Eng Bull*, vol. 32, no. 1, pp. 3–12, 2009.

[4] J. R. Lourenço, B. Cabral, P. Carreiro, M. Vieira, and J. Bernardino, "Choosing the right NoSQL database for the job: a quality attribute evaluation," *J. Big Data*, vol. 2, no. 1, p. 18, 2015.

[5] L. George, *HBase: the definitive guide: random access to your planet-size data*. O'Reilly Media, Inc., 2011.

[6] Z. Bousalem, I. Cherti, and G. Zhao, "Migration from Relational Databases to HBase: A Feasibility Assessment," in *International Conference on Advanced Information Technology, Services and Systems*, 2017, pp. 383–395.

[7] A. B. M. Moniruzzaman and S. A. Hossain, “NoSQL Database: New Era of Databases for Big data Analytics - Classification, Characteristics and Comparison,” *ArXiv13070191 Cs*, Jun. 2013.
[8] J. Webber and I. Robinson, “The Top 5 Use Cases of Graph Databases,” *Neo Technol.*, 2015.
[9] N. Dimiduk, A. Khurana, M. H. Ryan, and M. Stack, *HBase in action*. Manning Shelter Island, 2013.
[10] F. Chang *et al.*, “Bigtable: A distributed storage system for structured data,” *ACM Trans. Comput. Syst. TOCS*, vol. 26, no. 2, p. 4, 2008.
[11] A. Khurana, “Introduction to HBase schema design,” *White Pap. Cloudera*, 2012.
[12] Blandine Larbret, “Hadoop Hbase - Introduction,” 09:09:39 UTC.
[13] J. Darmont, “Data-Centric Benchmarking,” in *Encyclopedia of Information Science and Technology, Fourth Edition*, IGI Global, 2018, pp. 1772–1782.
[14] R. Han, X. Lu, and J. Xu, “On big data benchmarking,” in *Workshop on Big Data Benchmarks, Performance Optimization, and Emerging Hardware*, 2014, pp. 3–18.
[15] R. Han, L. K. John, and J. Zhan, “Benchmarking big data systems: A review,” *IEEE Trans. Serv. Comput.*, vol. 11, no. 3, 2018.
[16] A. Ghazal *et al.*, “BigBench: towards an industry standard benchmark for big data analytics,” in *Proceedings of the 2013 ACM SIGMOD international conference on Management of data*, 2013, pp. 1197–1208.
[17] “Tpc-c.” [Online]. Available: http://www.tpc.org/tpcc/.
[18] “Tpc-e.” [Online]. Available: http://www.tpc.org/tpce/.
[19] “Tpc-h.” [Online]. Available: http://www.tpc.org/tpch/.
[20] “Tpc-ds.” [Online]. Available: http://www.tpc.org/tpcds/.
[21] L. Wang *et al.*, “Bigdatabench: A big data benchmark suite from internet services,” in *High Performance Computer Architecture (HPCA), 2014 IEEE 20th International Symposium on*, 2014, pp. 488–499.
[22] B. F. Cooper, A. Silberstein, E. Tam, R. Ramakrishnan, and R. Sears, “Benchmarking cloud serving systems with YCSB,” in *Proceedings of the 1st ACM symposium on Cloud computing*, 2010, pp. 143–154.
[23] D. Bermbach, E. Wittern, and S. Tai, “Getting Started in Cloud Service Benchmarking,” in *Cloud Service Benchmarking*, Springer, 2017, pp. 151–153.
[24] V. Abramova, J. Bernardino, and P. Furtado, “Which nosql database? a performance overview,” *Open J. Databases OJDB*, vol. 1, no. 2, pp. 17–24, 2014.
[25] H. Matallah, G. Belalem, and K. Bouamrane, “Experimental comparative study of NoSQL databases: HBASE versus MongoDB by YCSB,” *Comput Syst Sci Eng*, vol. 32, no. 4, pp. 307–317, 2017.
[26] A. W. Yassien and A. F. Desouky, “RDBMS, NoSQL, Hadoop: A Performance-Based Empirical Analysis,” in *Proceedings of the 2nd Africa and Middle East Conference on Software Engineering*, 2016, pp. 52–59.
[27] X. Tian, R. Han, L. Wang, G. Lu, and J. Zhan, “Latency critical big data computing in finance,” *J. Finance Data Sci.*, vol. 1, no. 1, pp. 33–41, 2015.

Advances in Science, Technology and Engineering Systems Journal Vol. 4, No. 2, 402-412 (2019)

www.astesj.com

ASTESJ

ISSN: 2415-6698

Behavioral Analysis of Bitcoin Users on Illegal Transactions

Zuha Samsudeen, Dhanushka Perera, Mgnas Fernando*

University of Colombo School of Computing, 00700, Sri Lanka

ARTICLE INFO

Article history:
Received:19 February, 2019
Accepted:09 April, 2019
Online: 26 April, 2019

Keywords:
Analysis
Behavior
Bitcoin
Blockchain
Illegal

ABSTRACT

Bitcoin is a popular crypto currency that is used as a mode of investment and a medium for trading goods and services. Anonymity, security and decentralization are significant features of Bitcoin. This creates several opportunities for criminals to involve in illegal and fraudulent activities. This research study aimed to automate the process of gaining the interconnected illegal transactions from Bitcoin Blockchain; which also identified the behavioral patterns and significant facts among illegal incidents that are of varied nature.

The motivation for choosing this study was lack of literature that covers illegal incidents that are of various natures. In addition, the lack of literature on spending patterns common to several illegal incidents is also one of the motivations. For this study, an inductive approach was carried out. Initially the illegal incident and transaction data extracted from publicly available sources were parsed into BlockSci. In BlockSci scripts were written to gain the details on related illegal incidents. In visualizing the relationship of derived interconnected transaction indexes, Gephi tool was used in which the most significant indexes were summarized for further interpretation of data. Thereafter, traversing data back in the Blockchain was the method used in deriving patterns and significant facts. Finally, the common patterns obtained were evaluated based on previous findings. Consequently, the study recognized common spending patterns and popular exchanges used.

1. Introduction

Many crypto currencies have come into usage in recent years for multiple purposes. Bitcoin developed by Satoshi Nakamoto came into usage from 2009 [1] and it is the most prominent crypto currency in terms of market capitalization with $250 billion as of January 2018 [2]. Bitcoin is discussed mostly based on its negative aspect [3] since Bitcoin systems are being targeted by hackers and fraudsters [4] thus making it easy to compromise [3, 4]. Among the negative discussion, aspects such as darknet marketplaces [5, 6, 7], Ponzi scheme [8, 9, 10], ransomware [11, 12, 13], Bitcoin Exploits [10, 14], Denial-Of-Service (DOS) attack [15], thefts [14, 16] and Money Laundering [9, 17, 18] have been discussed widely by previous researches and media. These negative aspects can be briefed as illegal activities.

The literature reveals in detail about illegal activities separately based on its nature or as a case study focusing on a single incident. According to careful investigation of the literature, it reveals that there is no or evidences have not been documented properly by analyzing several illegal incidents as a study. Thereby, this study focuses on providing an analysis of different illegal incident categories by highlighting user transactions behavior in dissimilar natured incidents as depicted in Figure. 1. The curves among incidents represent any possible patterns among incidents of dissimilar nature.

This study is important to provide a more comprehensive idea about real-world user behavior of those who involve in illegal transactions which is a real-world requirement. It will specify the view of the relationship among incidents of different nature. In addition, it will mainly assist Bitcoin Miners or protocol designers to make changes in protocol to reduce the illegal activities. In addition, it would assist relevant officials to impose new rules and controls on Bitcoin exchanges or services, Bitcoin users and potential Bitcoin users will become aware of illegal incidents and how related each incident are to another.

The goal of the study is to provide a behavioral analysis of Bitcoin users involving in illegal incidents that are varied in nature.

* Mgnas Fernando, University of Colombo School of Computing,00700, Sri Lanka | Email: nas@ucsc.cmb.ac.lk

The main question to be addressed is 'What are the behavioral patterns among Bitcoin users involving in different types of illegal incidents?' by answering sub-questions such as 'What are the illegal incidents involving Bitcoin and how they can be categorized into various categories?', 'What are the significant facts for each illegal incident?'.

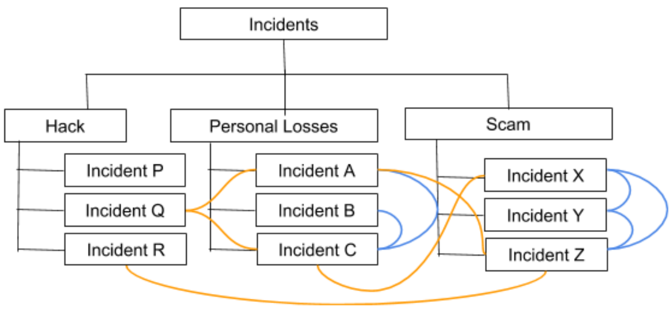

Figure. 1: An example of analysis considering different types of illegal incidents

2. Background

Bitcoin is the crypto currency that works based on the principle of a public ledger called Blockchain [2] which provides security using Blockchain technology [14]. Each Block in Blockchain consists of Bitcoin transactions [1] and information about transactions is publicly visible. The blocks in the Blockchain can be uniquely identified by the block hash or the block height. The Merkle Tree is the data structure which is used to summarize all the Bitcoin transactions in the block [19]. The processing of transactions involves solving a computation problem to put the transactions included in a confirmed block to be included in Blockchain. This is called mining [20]. The transactions between users are registered, validated and maintained via the entire network which is called Bitcoin mining.

The usage of Bitcoin became substantial due to the various reasons such as speed [21], anonymity, security, convenience [22] and decentralization with less transaction cost as there is no middle party involved to control the Bitcoin in comparison to traditional payment methods [1]. But [14] critiques that while Bitcoin exist as a decentralized system; it requires a formal structure, rules and a proper line of communication for better management. But still, Bitcoin is lack of legal interpretation in the Bitcoin user community and Bitcoin exchanges. In addition, there is no coordination among the Bitcoin Exchanges as well [14]. Regardless of several criticisms and concerns on the legality of Bitcoin, currently not only online businesses, but also traditional retailers are also beginning to accept Bitcoins as a payment method [22]. However, Bitcoins have their own risks such as major exchange rate fluctuations and hacking of major Bitcoin exchanges [13].

Bitcoin payments or transfers are carried out by generating transactions. Bitcoin addresses are used in performing transactions [23]. A user generally has hundreds of different Bitcoin addresses which are usually stored in their digital Bitcoin wallet [22, 24]. The addresses that are used only once are termed as disposable addresses. Bitcoin addresses can be reused as well [25]. But, reusing Bitcoin address is traceable because the flow of Bitcoin can be traced from one known or unknown address to another [12] leading to privacy leaks. Therefore, Bitcoin community and previous researches has encouraged using a different Bitcoin address for every transaction [25]. However, if users use strategies such as CoinJoin [12, 25] or Mixing Services or tumblers [12], it is difficult to trace by identifying Bitcoin addresses accordingly. A Bitcoin transaction happens in the form of an input or set of inputs pointing to an output or set of outputs [25]. The total values of the inputs must be distributed to the output. In Bitcoin Blockchain, for a transaction to be valid the total value of the outputs should not exceed the total value of the inputs.

2.1. Bitcoin Exchanges

A Bitcoin exchange is an online platform where anybody can buy and sell Bitcoins using fiat currencies. Some of the exchanges behave like a bank where they offer fixed interest on the customer savings. The exchange creates a wallet for every customer in their system and one can sell or buy Bitcoins with this wallet [20]. But, major risk of hacking Bitcoin exchanges still prevails [13]. However, [14] concludes on recommending exchanges to clearly disclose all the details of the cyber-attacks on them to their customers. Thus, leading to better transparency in the way they operate. Some of the instances for the major attack on exchanges were Mt. Gox attack losing 450 million dollars, attack on Bitfinex exchange leading to reduction in value of Bitcoin by 23% and DDoS attack on Bitfinex and Bitcoin-e Exchanges [14], Bitfloor loss of 24,000 Bitcoins in an attack [20].

2.2. Illegal Activities

The illegal activities related to Bitcoin cover a wide range of crimes such as murders for hire, funding terrorism, drug, weapon, organ trafficking, ponzi schemes, forgeries, unlawful gambling, money laundering, illegal mining, computer hacking, spreading ransomware and outright theft [2, 6, 26].

At least 25% of Bitcoin users and around 44% of Bitcoin transactions are associated mainly with illegal activities as previous researches shows [5]. It is discovered there are 24 million Bitcoin users; use Bitcoin primarily for illegal purposes [5]. Another research [2] said that exactly half of Bitcoin transactions are illegal. However, a study mentioned that Bitcoin will become less used in illegal activities in future as it will be accepted as a common medium in near future since the need for exchanges will be reduced to a certain extent. A recent study [2] reveals that the illegal users tend to transact more in smaller amounts repeatedly with a certain party to avoid getting noticed. In addition, it is noted that the illegal users are holding less Bitcoin due to Bitcoin seizure incidents by FBI [2]. As [5] highlight that the users who are spending Bitcoin on illegal goods had about 25%-45% more Bitcoin (with the 95% confidence interval) than those who doesn't spend Bitcoin on illegal goods [5].

Therefore, it is timely needed to have a look on the illegal activities. Following is a literature review on some major illegal activities which involves Bitcoin.

- *Ransomware*

Ransomware are similar to other computer virus such as trojan horse, worms and spyware [27, 28] and it is defined as the emergence of cyber hack jacking threat in new form in the cyberspace. Ransomware has become a significant problem

[13] due to its rapid growth in global level [29]. In [30], it mentions one of the main reasons for the growth of ransomware is due to the increasing ease of use of Bitcoin systems for payment purposes. In addition, for example CryptoLocker [11], according to [31], there is an existence of connections between CryptoLocker to Bitcoin services namely Bitcoin Fog and BTC-e, and to the Sheep Marketplace scam happened in 2013. A pattern that has been already revealed is that most ransomware related transactions occur multiple times with the same party and Xapo.com, BTC-e.com, LocalBitcoin.com and Kraken.com are frequently used Bitcoin exchanges. Also, Helix Mixer has been used in purifying tainted coins. A notable finding indicates that some ransomware attackers directly sent the ransom payments received to known parties such as exchange services and gambling [12].

- *Theft*

Over one-third (⅓) of money in the Bitcoin system was lost [14] due to Bitcoin being vulnerable to software hacks and network-based attacks [3]. These attacks are commonly termed as Cyber-Attacks referring to any action that violates the security of the exchange system. Cyber-attacks on Bitcoin wallets can be due to security flaws in system, mistakes of Bitcoin users such as negligence or ignorance and a Denial of Service (DoS) attack [14]. The patterns that have been identified so far related to DOS are; sending Bitcoins in tiny amounts to the same set of addresses and transaction rate attack forming the parasitic worm structures [32]. The studies [3, 8] highlighted that the transactions are not reversible. It is an advantage for criminals because it is impossible to correct errors occurred due to a theft. Thus, allowing funds being stolen or taking without the permission of Bitcoin owners [8].

- *Scam*

Scams based on Bitcoin can be classified into mainly four groups such as high yield investment programs or ponzi scheme, mining investment scams, wallet scams and exchanges scams according to a classification identified by studying 192 scam incidents [10].

- *Darknet*

Darknet refers to a network that is encrypted and existing on internet which can be accessed only by using special browsers [7]. The research [33] proves 57% of content in darknet is illegal, whereas 47% of all Bitcoin transactions involve illegal trading on darknet [2]. So the deeper layers; deep web, dark web and darknet are mainly with the illegal content [33].

As per study of [7], Ross Ulbricht the main operator of Silk Road was traced down and seized by FBI in October 2013. In addition, after the closure, as [7] mention, Silk Road 2.0 emerged, following the darknet marketplaces such as 'The evolution' evolved quickly where in some cases the operators disappeared along with Bitcoins held in escrow.

In studies of [14] and [34], authors highlight that mainly anonymity of Bitcoin transactions give criminals as an enabler tool to operate without getting noticed by legal authorities. Even though numerous real-world incidents prove some criminals use only Bitcoin to conduct illegal activities, [6] says the same will be applicable even for cash transactions conducted using fiat currencies indicating less necessity to implement additional rules and regulations especially for Bitcoin.

2.3. Tainted Coins

Tainted are Bitcoins which has involved in some sort of crime [35]. If a Bitcoin address is tainted, it is visible across the network. This is due to the digital signature mechanism in Bitcoin. The publicly available transaction history can be used to examine how a tainted Bitcoin behave in the network [36]. When a Bitcoin user receive Bitcoins from a sender, the Bitcoin user can check whether the receiving Bitcoins has involved in fraudulent activity in past. Thereafter, determine whether to continue the transaction with accepting Bitcoin or not [35]. An example would be Mt. Gox, a Bitcoin exchange based in Japan locked Bitcoin holder's account with tainted coins after an incident of theft where 43,000 Bitcoins were robbed from another Bitcoin trading platform Bitcoinica [36].

According to [4] the more 'tainted' the chain of transactions is, the stronger the link in between the Bitcoin addresses is. For example, if a wallet is stolen, whenever the robber tries to bank the money at an exchange, they can be arrested as [37] pointed out.

3. Methodology

3.1. Research Design

The research design shows the important stages followed to answer the research problem (Figure. 2). Each block in Figure. 2 represent a main stage in addressing the research problem.

This is a summary how the research was carried out. The incident data was extracted from publicly available data sources whereas transaction data was from the Bitcoin Blockchain. Definition of illegal incident based upon incident data extracted was helpful to categorize the incidents.

During the process of resource setting, Blockchain data was parsed into BlockSci which was imported into Jupyter to run python scripts. The scripts included filtering of non coinjoin incident transactions using heuristic parameter, gaining transaction data using chain classes in BlockSci, gaining significant index details using address classes in BlockSci. Thereafter, through traversing back in the Blockchain the initial data derived from Blockchain was verified. To visualize the data, Gephi was used along with various metrics. The most significant indexes were then summarized for further interpretation of data using Address classes in BlockSci which consisted of addresses and address types. Traversing data back in the Blockchain was the method used in deriving patterns and significant facts. Finally, some of the patterns obtained were evaluated based on previous findings. In addition, new findings were evaluated using user feedback obtained via a survey and some test cases. Let's look at on detailed description on stages.

3.2. *Resource Set Up*

The following configurations made the analysis easier: A Cloud Virtual Machine with the specifications of (i) Ubuntu 18.04

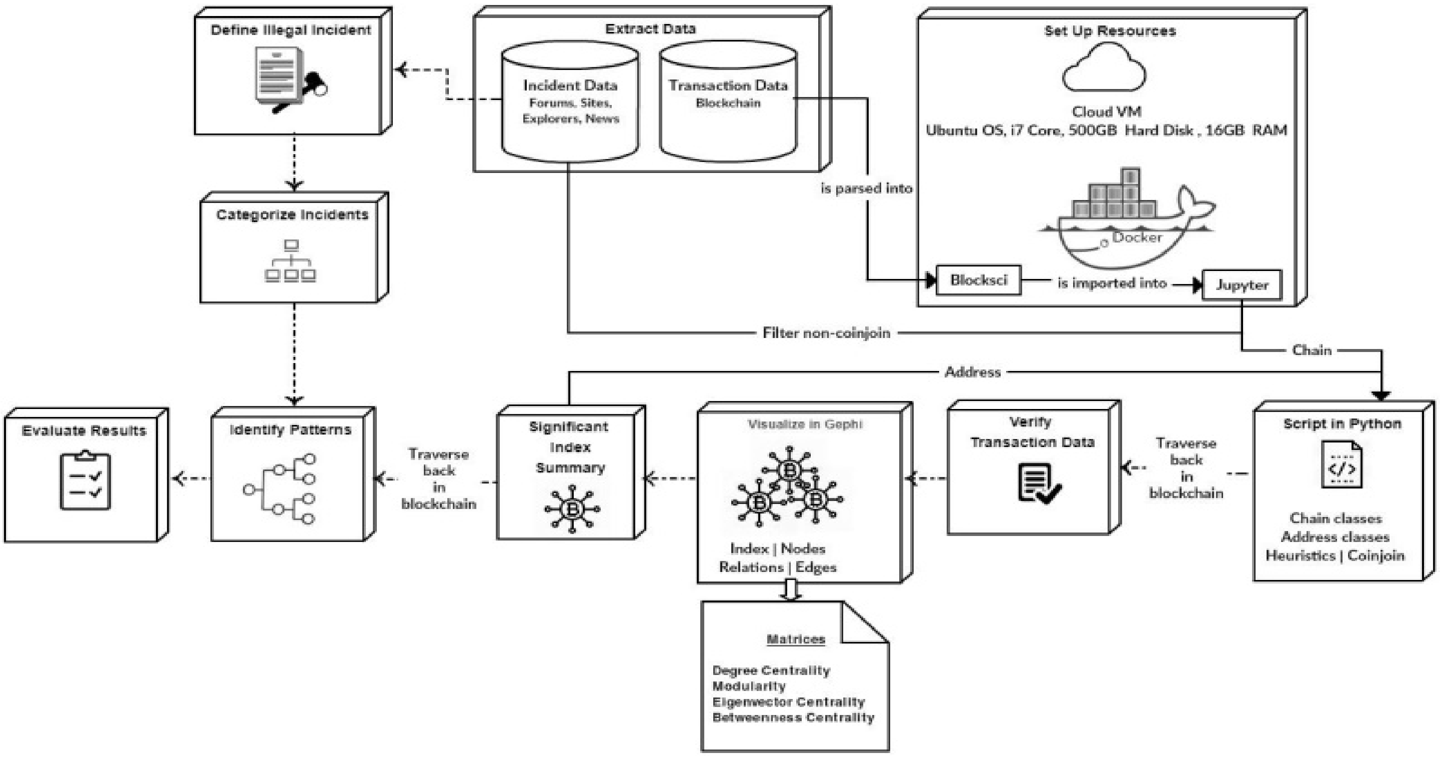

Figure. 2: Research design

LTS Server Version as the Operating System (OS), (ii) i7 as core processor, (iii) 500GB as Hard Disk, (iv) 16GB as RAM and (v) Docker as the OS level virtualization, (vi) Blocksci as Blockchain analysis tool, (vii) Jupyter as Notebook, (viii) Gephi as visualization tool.

3.3. Blocksci

BlockSci is a tool developed with the intention of analyzing the transactions of Bitcoin in Blockchain [38] which was in use at Princeton for research and educational purposes [39]. According to a research paper [40], BlockSci library has used to analyze the Bitcoin Blockchain from 2009 till August in 2017. To examine how the Bitcoin usage has grown over time by the original developer of the tool and to identify whether there is a diverse community present and thereon to investigate whether they differ in important factors. Accordingly, this research study was carried out using the Blocksci tool by parsing transaction data inside it.

3.4. Data Extraction and Pre-processing

Since the Bitcoin Blockchain is decentralized, no authorized party is responsible for reporting illegal endeavors involving bitcoin. So, the publicly available data is the sole data source from where the details of illegal incidents can be obtained. Initially the details such as Incident Name, Date, Value (USD), Coins (Bitcoin), Transaction Id, Bitcoin Address, Nature /Description of Incident, Countermeasures were collected from public data sources via surfing through internet. Among those collected incidents, from 2012 to 2018[1], there were 33 illegal incidents that were available with respective 331 transaction ids which were mandatory in uniquely identifying the incidents. The data for the period from 2012 to 2014 was extracted mostly from publicly available forum called Bitcointalk and prepared to a homogeneous format in an Excel sheet manually. Online forums Bitcointalk, discussion websites, Reddit in [10, 41], blogs, Bitcoinwhoswho Bitcoin Blockchain explorer, Walletexplorer in[12] and additional sites coindesk.com, bleepingcomputer.com in [11] were used to extract data which are mentioned in several previous types of researches and completed the majority of data for the period from 2015 to 2018. Finally, all collected data was cross-checked with multiple sources that were available publicly and confirmed the reliability of data.

Along with that on parallel, Blockchain[2] up to the block height of 514463 (157.3GB as at March 2018) was downloaded to gain internal transaction data related to illegal incidents like input index, output index and unspent index.

3.5. Definition of Illegal Incident

Based on the details of illegal incidents and previous studies, a definition for illegal activity was formulated. It is defined for illegal incident categorization.

"Any activity that involves Bitcoin which brings a financial disadvantage to one or more parties with or without their knowledge while the opposite party gains benefits financially from its outcome with their knowledge is defined as an illegal incident".

[1] https://docs.google.com/spreadsheets/d/1fOUIA9J4-lJKhgXqh2_zH6__t1BBRjaPMExH3GeFi6w/edit?usp=sharing

[2] https://www.blockchain.com/explorer

3.6. Incident Categorization

The incidents those were defined as illegal were categorized into different sub categories based on the nature of incidents referring to the basic categorization of heists in Bitcointalk till 2014 and with further reading on incidents.

3.6. 1. Hack - Wallets owned to an exchange or a platform is hacked by outsiders led to the collapse of the exchange.

3.6.2. Ransomware - Malware is spread to lock or encrypt the database, files, PC or any electronic copy and demand ransoms in Bitcoin to enable access.

3.6.3. Known Theft - Bitcoin holder knowingly sends Bitcoin to criminal because of threatening or blackmail.

3.6.4. Scams - The exchange or the platform steal the users' wallet and disappear by closing their exchange.

3.6.5. Fake Agencies - Scammers pretend to be an already existing popular exchange or government organization and steal Bitcoin either by communicating with customers or pretending to be honest.

The Sub Categories were put into main categories to enable better analysis. It was based on how the financial loss was committed to the other party. That is, whether the dishonest party obtained an advantage by directly dealing with Bitcoin user or via being a third party and another fact considered is whether the Bitcoin user loss his Bitcoins with his knowledge or not.

3.6.6. Hack - Dishonest party comes in between the Bitcoin holder and the exchange as a third party and collapses the exchange. It causes harm to both the Bitcoin holder and exchange without their knowledge.

3.6.7. Personal Losses - Includes subcategories of 'Ransomware' and 'Known Theft' where the effect of the Bitcoin loss is solely for the individual or a group of Bitcoin users committed by a third party with victims' knowledge.

3.6.8. Scams - Includes subcategories of 'Scam' and 'Fake Agencies' where frauds are done by exchange or platform itself or by a scammer. Exchange would purposefully close by issuing a notice by falsely claiming that they were hacked. Sometimes the exchange would make their website unavailable either by issuing a notice or without issuing a notice. This would lead to the financial loss to the Bitcoin holders of that exchange without their knowledge.

The following Table 1 summarizes the main similarities and differences of Main Categories.

3.7. Main Scripts

The n-ary tree chart as in Figure 3 represents how transactions are interconnected and it led to try out scripts. For an example, in T2 169...Tig address sends 5 Bitcoins to 1DV...NQs address holding the transaction id 118du….2a8u7. In T3 1DV...NQs address sends 4.52809038 Bitcoins to 1Nc...ytD address holding the transaction id 7d5uc….5c2e1 and sends 1.28 Bitcoins to 1xt...vsn address holding the transaction id 1frtu.…. ud2e1. Every output address can spend its Bitcoins like in T5, T6, T7 and T8 or else it can keep Bitcoins unspent as in T9 (Figure. 3).

Table 1: Summary of main categories

Main Category	***Sub Category/ies***	***Attacker***	***Victim***	***Knowingly happened?***
Hack	Hack	Third Party	Bitcoin Holder + Exchange	No
Personal Loss	Ransomware Known Theft	Third Party	Bitcoin Holder	Yes
Scam	Scam Fake Agencies	Exchange	Bitcoin Holder	No

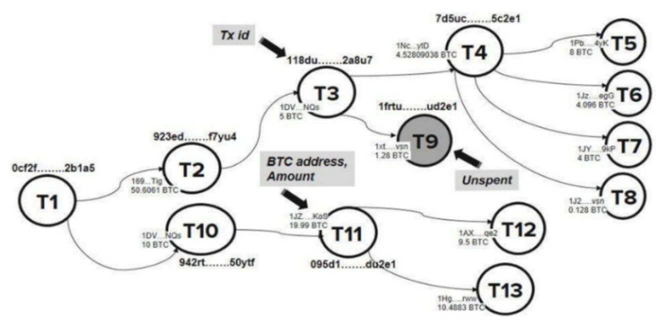

Figure. 3: N-ary tree chart for bitcoin transactions

The n-ary tree chart triggered to use recursion in the scripts to get chained transaction data. First the focus was on the circulation of the illegal input addresses and output addresses inputting illegal transaction ids. The results come out from the script were computationally expensive because these illegal transaction ids often result out ScriptHashAddress along with wrapped_addresses with different types of address requirements. One such example is represented in Table 2.

When a result was with a ScriptHashAddress, only the first address was needed. The rest was an additional security for the transaction. So as the next effort, it was considered to output related transaction ids. But still transaction ids resulted out 256-bit hash which had longer number of digits leading to slow up of results. So, the circulation of the input and output indexes was created as the solution. The index was a few digits number (lesser than 9 digits in this dataset). It was more convenient in terms of consumption of computing resources.

3.8. Data Processing

Pseudocode 1 was used to automate gaining related illegal input and output indexes after the data processing for a given transaction id.

Table 2. Different Address Types

	Output Address
Result Obtained	ScriptHashAddress(344...1Md[3], wrapped_address=MultisigAddress(2 of 4 multisig with addresses 13d...Vrc[4], 1Da...SbB[5], 1Gv...WbU[6], 18V...BAJ[7]))
Result Expected	344p...1Md (Recipient Address)

Pseudocode 1: Related illegal input and output indexes for a given transaction id

Input: Transaction id related to illegal incident; txid

Output: Related index details to a given txid; input index, output index, unspent index

```
Extract details from chain tx
Define results (tx)
If any tx has output:
   for each output:
        If any output is spent:
             Write input index, output index
                  Do results recursively for every output
        Else:
             Return unspent index
Else:
   Return unspent index
```

Each transaction id under main categories was input to the script. It resulted out the details i.e. input index and output index of the transaction undertaken or unspent index in a state of unspent.

The script extracted data from stored Blockchain transaction data considering the hash value for a given transaction id. Then the function 'results' was called. In this function, simply there was an initial selection construct identifying whether there were outputs i.e. whether the transaction was continued. If so, for those each output, script checked whether the resulting outputs of first if condition were also spent through the use of second if statement. If, then a file was appended with the details of input and output index pairs, according to the outcome of secondary condition of 'if'. Here, two selections were used to prevent the repetition of the records appended in the file while maintaining the connectivity of the transaction chain. Then the function was recursively called for each output index identified in both first and second selections. Recursion got terminated when the transaction had no more transaction relationship further as denoted in T9 as "Unspent" (Figure. 3). Approximately 1 million records on input-output indexes were obtained per each illegal transaction id. There was a variable number of transaction ids per incident considered in inserting into the script according to the availability of extracted transaction ids in dataset.

3.9. Transaction Data Verification

The output transaction data from the script was verified by traversing back in the Blockchain and sketching up an n-ary tree manually for the chain.

3.10. Data Visualization

Gephi[8] considered 'indexes' as the nodes, the 'relationships between indexes' as the edges and 'directed' as graph type. The noisy data was removed through filters considering the degree range under topology. The ForceAtlas 2 layout was chosen. It is a continuous graph layout algorithm suitable for handy network visualizations as recommended in study [32]. Fruchterman-Reingold layout improved the viewing and the perception of the network [42]. Thereon, metrics in statistics such as Degree Centrality, Modularity, Eigenvector Centrality and Betweenness Centrality were computed to obtain further insights [42, 43].

In the graphs, the Degree represents the number of direct or 'one hop' connections each index has to other indexes which also considered as illegal under Poison heuristics i.e. the related party are also considered as illegal meaning all the outputs are completely tainted by all illegal inputs. The size of the node denotes the strength of the connectivity meaning the total number of input and output indexes that is linked with. Modularity in the study measures how well the network decomposes into modular communities of illegal Bitcoin users. Eigenvector Centrality measures the importance of an index in terms of connectivity of other indexes. For instance, an index with high eigenvector score is connected to many indexes who themselves have high number of connections. Betweenness Centrality measures how often an index is required to go to another index. If an index is with a high betweenness, it often appears on shortest paths between indexes in the network. If the high betweenness indexes are removed, the graph may cut into multiple unconnected components losing the connectivity.

As a summary, these metrics demonstrated the connectivity of the illegal indexes i.e. degree and eigenvector score represent the number of direct and indirect connections respectively, modularity measures number of modular communities of illegal Bitcoin users, betweenness represents how an index is needed to maintain the connectivity. So, indexes scored higher for the above metrics were taken into consideration as the most significant indexes in the graph. Then corresponding Bitcoin addresses were output for those indexes through scripts and started investigation of those addresses in the Blockchain and obtained the results as explained in results section.

---

[3] 344pUP56enuGjbPdyubYEqoxB6VaFmD1Md
[4] 13dCNU7T38Ca3zp4mMBSmP6FGyBzq6vVrc
[5] 1DayuQZkBCt4MYYA5Hr8awXvmJDXLndSbB
[6] 1GvFkgaLV69PtrTcMC9XznqcXZxRHWvWbU
[7] 18VibwUc5CNG8TFZNRMSY6LMadED3qGBAJ
[8] https://gephi.org/

3.11. Justification for Methodology

The motivation for choosing this study was lack of literature that covers analysis for patterns and significant facts in patterns on illegal incidents of various nature. Since the inductive approaches usually focus on exploring new phenomena that have not been investigated or previously explored, it was best suited to this research. To identify new patterns based on the information, detailed data on each illegal incident was gathered and preliminary patterns from separate incidents were obtained first. Once the data analysis has been completed for each incident, generalized conclusions were produced based on the patterns and facts derived from the analyzed individual cases. It required extensive and repeated sifting through the data and analyzing and re-analyzing multiple times to identify new patterns.

However, the few patterns that were discovered so far in literature also got confirmed in this study. Since deduction begins with expected patterns (already defined patterns in prior researches in this study) and is able to test them against observations, this study is following deductive approach too. Thus, a combination of inductive and deductive approaches was practiced in this research study.

4. Results

In this study, 10 illegal incidents were analyzed thoroughly, and results were obtained. The results are shown below in incident wise along with its main category.

4.1. NiceHash / Hack

NiceHash, is a cryptocurrency mining marketplace. During the early December 2017, NiceHash has been hacked due to a security breach, causing a loss of 4,736.42 bitcoins[9] [46].

The analysis of results shows that the illegal party has been transferring in small amounts to new wallets and different addresses in subsequent transactions. Thereafter, subsequently Bitcoins are being sent out to an exchange or a service.

The Bitcoins have been distributed in a constant amount or by a percentage. For instance, 100 of Bitcoins are sent constantly whereas the rest to another wallet and to fresh wallets simply for transacting in small amounts.

4.2. Shapeshift.io / Hack

Shapeshift.io is a Switzerland based cryptocurrency exchange service that offers trading cryptocurrencies through its website and its API globally. On 7th April 2016, it faced a security breach which compromised on the server infrastructure of platform[10].

The analysis of results shows that the illegal party has been transferring in small amounts to new wallets and different addresses in subsequent transactions. Thereafter, subsequently Bitcoins are being sent out to an exchange or a service. The transactions traversed indicate that Bitcoin services such as Helix Mixer, Polenix.com and Bittrex have been used to cash out. In addition, one of the significant results is that next transaction that comes out from exchange has been made with the address 344...1Md[11] that has been tagged in 'Richest Bitcoin Address'. In addition, we can identify an address 1DU…. Uru[12] tagged as sixth richest on the Tether crypto list has also been involved in transaction traversal.

4.3. Gatecoin / Hack

Gatecoin is an exchange established in Hong Kong, mainly facilitating services for Bitcoin and Ethereum tokens. The hackers accessed the hot wallets of both Bitcoins and Ethereum stealing 250 Bitcoins and 185,000 ethers[13].

As per the analysis, a major portion of the immediately sent inputs is still unspent. Due to that reason, a clear insight on the tainted Bitcoin circulation cannot be obtained. However, the minor number of Bitcoins that were spent indicates that mostly Poloniex.com, OKCoin.com, Bter.com, Xapo.com have been used very commonly to cash out immediately.

4.4. WannaCry / Personal Losses

WannaCry Ransomware is a type of malicious software. According to statistics of this attack 300,000 computers including entities such as hospitals, companies, universities and government organization across 150 countries had a loss of hundreds of millions to billions of dollars [47].

The analysis of results shows that the illegal party has been transferring in small amounts to fresh wallets in subsequent transactions. Thereafter subsequently Bitcoins are being sent out to an exchange or a service.

In addition, the transaction traversal shows that there are few popular Bitcoin services that have been commonly used. They are Poloniex.com, Bittrex.com, HaoBTC.com, BTC-e.com, Xapo.com, CoinGaming.io and bitfinex.com.

Another notable result would be that there are addresses in their respective wallets have involved in conjoin transactions to mix their coins which is usually used to makes it harder for outside parties to determine which party or parties were making a particular transaction.

4.5. CryptorLocker / Personal Losses

CryptorLocker Ransomware started spreading since September 2013 that encrypted files and demanded ransom. This created almost USD 519,991 of direct financial impact. CryptoLocker opened the gates to many other ransomware variants [12].

In the study of the incident Cryptor Locker, it could be discovered that one single wallet has been used to obtain and transfer Bitcoins. Thereafter, gambling services such as SatoshiDice.com and LuckyB.it has been used to cash out. In addition, the results also indicate that an address 121...PM4[14] has obtained Bitcoins from Agora and Evolution darknet market and paid in the medium of Bitcoins to Agora market and Black bank

[9] https://bitcointalk.org/index.php?topic=2535366.0;all
[10] https://news.bitcoin.com/looting-fox-sabotage-shapeshift/
[11] 344pUP56enuGjbPdyubYEqoxB6VaFmD1Md
[12] 1DUb2YYbQA1jjaNYzVXLZ7ZioEhLXtbUru
[13] https://news.bitcoin.com/gatecoin-official-statement-hot-wallet-breach-losses-estimated-2m-usd/
[14] 121dBo5epQEDJZVpZDuBYBwV5Y2xeXTPM4

market. Thereby, it is possibly a wallet belonging to a darknet market supplier.

4.6. VenusLocker / Personal Losses

VenusLocker is a ransomware type virus which was spreader via an infectious email letter [47]. The analysis of results shows that the illegal party has been transferring in small amounts to fresh wallets in subsequent transactions. Thereafter subsequently Bitcoins are being sent out to an exchange or a service.

In addition, the transaction traversal shows that there are few popular Bitcoin services that have been commonly used. They are Poloniex.com, Luno.com, korbit.co.kr, Xapo.com and HelixMixer.

4.7. Blackmail / Personal Losses

Several people received different versions of emails claiming that the recipient's computer has been used to create a video of adult websites that the recipient visiting and threaten that it will be sent to recipients' contacts if they do not pay $200-$400 in BTC within 20-24 hours[15].

As per analysis, it can be noted that majority of the transactions have been performed directly through exchanges such as Poloniex.com, Matbea.com, Cubits.com. Among the blackmail incidents, it is significant that the Bitcoins are immediately cashed out via exchanges since the money received on blackmailing is not relatively a notable large Bitcoin amount.

4.8. BTGwallet.com / Scam

Bitcoin Gold (BTG) is one of the forks of Bitcoin which was released on 24th October 2017 [16]. MyBTGwallet.com is an online wallet creator that only stores data on the browser. This website cheated investors out of $3.3 million in November 2017 by promising to allow them to claim their Bitcoin Gold[17].

The analysis of results shows that the illegal party has been transferring in small amounts to fresh wallets in subsequent transactions. Thereafter subsequently Bitcoins are being sent out to an exchange or a service. The results of transaction traversal show that, there are few popular exchanges such as Bittrex and Bitflyer.jp that are involved in the transactions. In addition, the results highlight that there have been continuous transactions from the exchange 'hitbtc.com' to another address 3Jj...4FC [18] belonging to wallet [457b8ced80]. From further analysis, it was evident that this is another incident where a malware was installed in Hitbtc website which automatically changed the Bitcoin addresses of users to another address when an address was copied from Hitbtc.com.

4.9. Fake Agency Support / Scam

This includes a Coinbase support phone scam where a phone number '1-888-455-1155' which is not a real Coinbase support number were shown up in a lot of web search results. When users search in Google typing "coinbase phone support" they obtained a phone number from Google search results that leads them to this scam in which an operator tells them to send money in Bitcoin[19] .

The analysis reveals that the transactions have been performed directly through exchanges such as Cex.io, Luno.com and Bittrex.

4.10. Alphabay / Scam

AlphaBay Market operated in Thailand was an online darknet market which was launched in December 2014. It operated under an escrow system which paved the way for the scam. Alpha Bay went offline due to a scam with 1,479 Bitcoins transferred from a Bitcoin wallet which were identified to be used by those behind the darknet site to other Bitcoin wallets. During that period, there are numerous orders pending in its escrow system. It was shut down by 13th July 2017 [20].

The analysis reveals that the transactions have been performed directly through exchanges such as Bitstamp.net, Xapo.com, Bitfinex.com

Accordingly, the analysis reveals that the incidents which are of high number of users involved have high severity. Since, it would create panic situations among the Bitcoin community. During these incidents, we can observe, the illegal users tend to cash out the tainted Bitcoins indirectly through an exchange. Whereas, the incidents that had affected fewer users tends to be with less severe. Thus, enabling illegal users to cash out directly via an exchange. However, one exception would be the incident Alphabay. Even though, it had affected large user base and created a tense situation; it had been cashing out directly through an exchange.

A summary of incident results is depicted in Table 3 based on the common factors identified in all incidents.

Table 3: Summary of Incident Results

	Direct to Exchange / Mixer	Indirectly to Exchange / Mixer	Small Amount	New wallets
NiceHash		✓	✓	✓
ShapeShift		✓	✓	✓
Gatecoin				
WannaCry		✓	✓	✓
CryptoLocker				
Venuslocker		✓	✓	✓
Blackmailing	✓			
BTGwallet		✓	✓	✓
Fake Agency	✓			
AlphaBay	✓			

[15] https://bitcoinwhoswho.com/blog/2017/10/09/blackmail-scam-run-on-russian-wallet-matbea/#more-540

[16] https://99bitcoins.com/the-bitcoin-gold-hard-fork-explained-coming-october-25th/

[17] https://news.bitcoin.com/bitcoin-gold-wallet-stole-private-keys-scooped-3-3-million/, https://bitcointalk.org/index.php?topic=2412182.0, https://www.reddit.com/r/CryptoCurrencies/comments/7db42c/httpsmybtgwallet com_seems_to_be_scam/

[18] 3JjPf13Rd8g6WAyvg8yiPnrsdjJt1NP4FC

[19] https://bitcoinwhoswho.com/blog/2017/12/17/fake-coinbase-support-phone-number-1-888-455-1155/, https://www.reddit.com/r/Bitcoin/comments/77hxl0/my_bitcoin_at_coinbase_got_hacked/

[20] https://www.reddit.com/r/AlphaBay/comments/6lbu32/alphabay_down_shit_vendor_review_as_well_buyer/, https://news.bitcoin.com/major-darknet-marketplace-alphabay-goes-down-exit-scam-speculations-arise/

5. Discussion

The findings of this study reveal that there are common patterns that can be identified among different illegal incidents. The study highlights novel findings along with validation previous studies result. The discussion section highlights the previous study findings and novel key findings from this study by comparing both.

According to previous study [12], It has been identified that "Ransomware criminals' cash out via a Bitcoin services, gambling and mixing services".

According to this study, it has been revealed that "criminals" cash out via a Bitcoin services, gambling and mixing services. But, when they are cashing out there are mainly two ways, as

- Illegal users directly transfer illegally obtained Bitcoins to exchanges
- Another way is that, criminal will not directly transfer illegally obtained Bitcoins to exchanges or mixtures. But, they would first transfer to several other unidentified Bitcoins address and later they would transfer exchanges or mixtures"

The next discussion point would be that according to previous study, it was recognized that "Generally users have hundreds of different Bitcoin addresses [22, 44].

Whereas, according to this study, the notable novel finding is that "Illegal users do not only have hundreds of different Bitcoins addresses but they also create new wallets to transfer their tainted Bitcoins'.

In addition, another discussion fact would be that according to previous study,

Illegal users "Transact more in smaller amounts" [12, 32].

According to this study, it is revealed that illegal users do not only transfer in small amounts, but they transfer the small amounts in constant or in a certain proportion in the subsequent transactions".

In addition, the final discussion point is that the previous studies have recognized exchanges such as Xapo.com, BTC-e.com, LocalBitcoin.com, Kraken.com as popularly used by Ransomware attackers. The studies also reveal the mixing services Helix Mixer has been repetitively used by illegal users. [12, 45].

According to this study, it has identified additional exchange services such as Poloniex.com, Bittrex, Cex.io, Bitfinex and Helix Mixer being popular used across illegal users.

6. Evaluation

As in [48], it has been highlighted that many of the proposed solutions in Blockchain related researches are lack of solid evaluation on their effectiveness. However, recent researches in [49], [50], [51] has used deep neural network and unsupervised feature learning approach to evaluate the results obtained.

As in recent research study [49], on Bitcoin address linking; authors used deep neural network for testing the efficiency of the method used. In addition, as in [50] and [51], for frauds detection in Bitcoin network, a feature learning approach of K-means has been used. Whereas in [52], feature learning approach along with performance measures and validation techniques have been used for evaluation.

But, accordingly the approach of machine learning cannot be implemented as only few results can be tested using some features. Therefore, in this study two evaluation methods were used for testing the results obtained. The two techniques were obtaining feedback from real Bitcoin users regarding the Bitcoin usage. The next approach is by using a sample test dataset to evaluate the results instead of a machine learning approach.

6.1. User Feedback

This approach is to obtain feedback from real Bitcoin users about their spending patterns of Bitcoins by issuing an online survey. This technique assumed all the survey respondents are legal. The Survey targeted on validating the findings from this study. This was posted to Bitcoin forum using the username "Rosecuppy123". There were about 27 complete responses for the survey.

The user feedback highlights that frequent users send Bitcoins to their own addresses in existing wallets before sending someone else. In addition, over 75% of respondents use 2 to 5 wallets for the security purposes. But, they do not create new wallets for every single transaction unlike illegal users. Thus, confirming that illegal users create several new wallets, addresses to spread their tainted coins.

Generally, an illegal person can pretend to be a legal individual and can provide feedback which can mislead. Most of the respondents were not willing to provide reliable information. Therefore, this approach was not productive.

Due to the lack of reliability in user feedback evaluation technique, another evaluation technique of using sample test incident dataset was used.

6.2. Test Cases

Sample incidents were tested to check whether the same patterns are resulted out for each main category. Sample hack incident called Linode repeated the pattern of transferring in small amounts to new wallets alike in NiceHash, ShapeShift hacks. Samsam ransomware replicated the same pattern as in WannaCry, Venuslocker; ransomwares which were analysed in the study. Btc-e is also used in this incident as in WannaCry. TradeRoute scam also transacted directly through several exchanges and Bitfinex.com was popular as in Alphabay. Fake Coinbase scam replicated the same pattern as was in Fake Agency, AlphaBay. Bittrex exchange was popular same as BTGwallet, Fake Agency scams.

7. Conclusion

Bitcoin is a crypto currency that is being used by millions of people for both legal and illegal intentions. The decentralized and anonymized feature of Bitcoin has drastically increased the rate of Bitcoin being misused, particularly its involvement in illegal activities. This triggered to conduct a comprehensive analysis of several illegal incidents of different nature. The aim of study is to identify behavioral patterns among illegal incidents that are dissimilar in nature.

Based on the results, it can be identified that there are mainly three patterns identified as,

1. Illegal users directly use exchanges to cash out tainted Bitcoins as shown in Figure. 4.

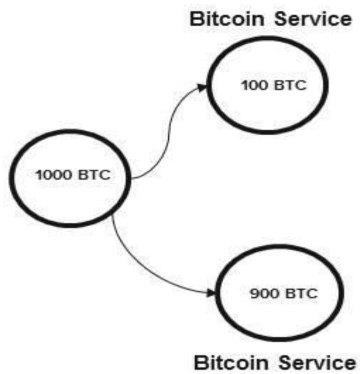

Figure. 4: Use exchange directly

2. Illegal users cash out tainted Bitcoins after sending to intermediate addresses in small amount as shown in Figure. 5.

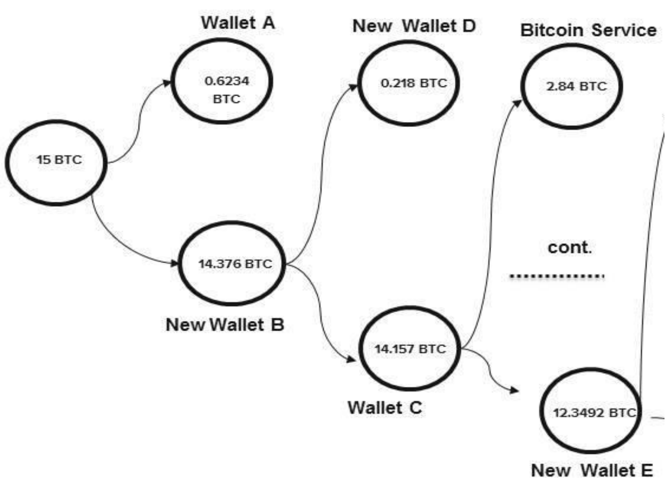

Figure. 5: Use intermediate addresses

3. Illegal users cash out tainted Bitcoins by transferring to new wallets in small amount as shown in Figure. 6.

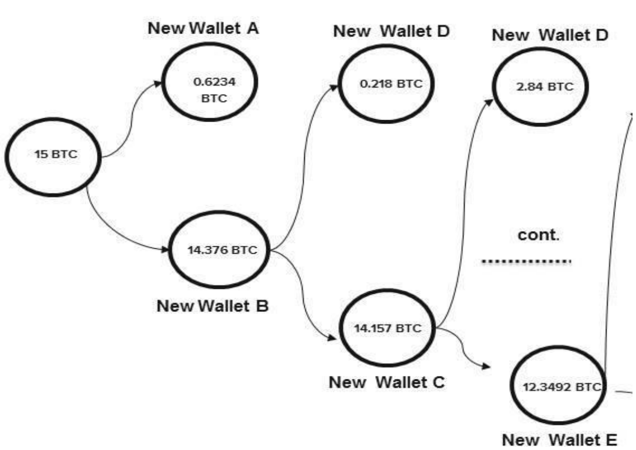

Figure. 6: Use new wallets

Accordingly, the two findings 1 and 2 validate with previous researches. The novel finding of this study is that illegal users "create new wallets to transfer the tainted Bitcoins before sending to an exchange or a service". The study also revealed significant exchanges from the analysis. The Evaluation techniques results also indicate similar patterns as the analysis.

Thereby, it can be concluded that "The behavior of an illegal user in spending tainted Bitcoins can generalized among different natured incident". However, "The patterns tend to vary when the 'severity' of the illegal incident differs". However, this study has been limited to certain limitations in scope and implementations.

7.1. Delimitations

In this research, the illegal incidents considered were limited to the definition of 'Illegal Activity' (i.e. this study does not consider every single illegal activity defined in accordance with general definition of law authorities).

In addition, specific country rules will not be considered because legality of Bitcoin is different according to the country law. For example, some countries consider Bitcoin as legal or illegal or restricted whereas some other countries are neutral on legality status of Bitcoin.

7.2. Contributions

The main contributions of this study are the novel findings from the analysis of illegal incidents regarding the spending behavior patterns of illegal users. The novel findings from this study are that the Illegal users send tainted Bitcoins in mainly two ways, as

2.Using intermediate addresses and then transferring Bitcoins to exchanges or mixtures. While they are transferring Bitcoins, Illegal users create new wallets to transfer their tainted Bitcoins.

In addition, the study also highlights popular exchanges or services used across illegal users such as Poloniex.com, Cex.io, Bittrex, Bitfinex and Helix Mixer.

In addition, a major contribution to the research community would be the illegal Incident data collection for 33 incidents along with 331 transaction id[21].

References

[1] Nakamoto, S., 2008. Bitcoin: A Peer-to-Peer Electronic Cash System. https://bitcoin.org/en/bitcoin-paper (accessed 7 February 2018).

[2] Foley, S. M., Karlsen, J. R. M., Putniņš, T. J. M., 2018. Sex, Drugs, and Bitcoin: How Much Illegal Activity Is Financed Through Cryptocurrencies? SSRN Electronic Journal.

[3] Spagnuolo, M., Maggi, F., Zanero, S., 2014. BitIodine: Extracting Intelligence from the Bitcoin Network. 18th Conference on Financial Cryptography and Data Security. 457-468.

[4] Raeesi, R., 2018. The Silk Road, Bitcoins and the Global Prohibition Regime on the International Trade in Illicit Drugs: Can this Storm Be Weathered? Glendon Journal of International Studies. 8, 1.

[5] Bohr, J., Bashir, M., 2014. Who Uses Bitcoin? An Exploration of the Bitcoin Community. 2014 Twelfth Annual International Conference on Privacy, Security and Trust.

[6] Janze, C., 2017. Are Cryptocurrencies Criminals Best Friends? Examining the Co-Evolution of Bitcoin and Darknet Markets. Proceedings of the Americas Conference on Information Systems (AMCIS). https://aisel.aisnet.org/cgi/viewcontent.cgi?article=1041&context=amcis2017 (accessed 10 August 2018).

[7] Kethineni, S., Cao, Y., Dodge, C., 2017. Use of Bitcoin in Darknet Markets: Examining Facilitative Factors on Bitcoin-Related Crimes. American Journal of Criminal Justice. 43, 2, 41-157.

[8] Moore, T., Christin, N., 2013. Beware the Middleman: Empirical Analysis of Bitcoin-Exchange Risk. 18th Conference on Financial Cryptography and Data Security. 25-33.

[9] Vasek, M., Thornton, M., Moore, T., 2014. Empirical Analysis of Denial-of-Service Attacks in the Bitcoin Ecosystem. 18th Conference on Financial Cryptography and Data Security. 57-71.

[10] Vasek, M., Thornton, M., Moore, T., 2015. There's No Free Lunch, Even Using Bitcoin: Tracking the Popularity and Profits of Virtual Currency Scam. 18th Conference on Financial Cryptography and Data Security. 44-61.

[11] Huang, D., Aliapoulios, M., Li, V., Invernizzi, L., Bursztein, E., McRoberts, K., Levin, J., Levchenko, K., Snoeren, A., McCoy, D., 2018. Tracking Ransomware End-to-end. 2018 IEEE Symposium on Security and Privacy (SP).

[12] Paquet-Clouston, M., Haslhofer, B., Dupont, B., 2018. Ransomware Payments in the Bitcoin Ecosystem. https://arxiv.org/abs/1804.04080 (accessed 15 August 2018).

[13] Richardson, R., North, M., 2018. Ransomware: Evolution, Mitigation and Prevention. Scholars' Press. http://scholarspress.us/journals/IMR/pdf/IMR-1-2017.%20pdf/IMR-v13n1art2.pdf (accessed 12 August 2018).

[14] Marella, V., 2017. Bitcoin: A Social Movement Under Attack. Selected Papers of the IRIS - European Journal of Philosophy and Public Debate. http://aisel.aisnet.org/iris2017/1/ (accessed 17 August 2018).

[15] Karami, M., McCoy, D., 2018. Understanding the Emerging Threat of DDoS-as-a-Service | USENIX. https://www.usenix.org/conference/leet13/workshop-program/presentation/karami (accessed 12 August 2018).

[16] Barber, S., Boyen, X., Shi, E., 2012. Bitter to Better—How to Make Bitcoin a Better Currency. Financial Cryptography and Data Security. 399–414.

[17] Bryans, D., 2018. Bitcoin and Money Laundering: Mining for an Effective Solution. Digital Repository @ Maurer Law. https://www.repository.law.indiana.edu/ilj/vol89/iss1/13/ (accessed 12 August 2018).

[18] Gifari, A., Anggorojati, B., Yazid, S., 2017. On preventing bitcoin transaction from money laundering in Indonesia: Analysis and recommendation on regulations. 2017 International Workshop on Big Data and Information Security (IWBIS).

[19] Gipp. B., Meuschke, N., Gernandt, A., 2015. Decentralized Trusted Timestamping using the Crypto Currency Bitcoin. iConference 2015, Newport Beach, CA, USA.

[20] 20*Bhaskar, N., Chuen, D., 2015. Bitcoin Exchanges. Handbook of Digital Currency, pp. 559-573.

[21] Trautman, L., 2014. Virtual Currencies Bitcoin & What Now After Liberty Reserve, Silk Road, and Mt. Gox. Richmond Journal of Law and Technology. 1-108.

[22] Ly, M., 2014. COINING BITCOIN'S "LEGAL-BITS": EXAMINING THE REGULATORY FRAMEWORK FOR BITCOIN AND VIRTUAL CURRENCIES. Harvard Journal of Law & Technology. 27, 2.

[23] Androulaki, E., Karame, G., Roeschlin, M., Scherer, T., Capkun, S., 2013. Evaluating User Privacy in Bitcoin. Financial Cryptography and Data Security. 34-51.

[24] Karame, G., Androulaki, E., Capkun, S., 2012. Double-spending fast payments in bitcoin. 2012 ACM conference on Computer and communications security - CCS '12.

[25] Barcelo, J., 2018. User Privacy in the Public Bitcoin Blockchain. https://pdfs.semanticscholar.org/549e/7f042fe0aa979d95348f0e04939b2b451f18.pdf (accessed 15 August 2018).

[26] Hurlburt, G., Bojanova, H., 2014. Bitcoin: Benefit or Curse? IEEE Computer Society.

[27] Pathak, P. B., 2016. A Dangerous Trend of Cybercrime: Ransomware Growing Challenge. International Journal of Advanced Research in Computer Engineering & Technology (IJARCET). 5(2). http://ijarcet.org/wp-content/uploads/IJARCET-VOL-5-ISSUE-2-371-373.pdf (accessed 12 August 2018).

[28] Upadhyaya, R., Jain, A., 2016. Cyber ethics and cybercrime: A deep dwelved study into legality, ransomware, underground web and bitcoin wallet. 2016 International Conference on Computing, Communication and Automation (ICCCA).

[29] Kharraz, A., Robertson, W., Balzarotti, D., Bilge, L., Kirda, E., 2015. Cutting the Gordian Knot: A Look Under the Hood of Ransomware Attacks. Detection of Intrusions and Malware, and Vulnerability Assessment. 3-24.

[30] Everett, C., 2016. Ransomware: to pay or not to pay? Computer Fraud & Security. 4, 8-12.

[31] Liao, K., Zhao, Z., Doupe, A. Ahn, G., 2016. Behind closed doors: measurement and analysis of CryptoLocker ransoms in Bitcoin. 2016 APWG Symposium on Electronic Crime Research (eCrime).

[32] McGinn, D., Birch, D., Akroyd, D., Molina-Solana, M., Guo, Y., Knottenbelt, W., 2016. Visualizing Dynamic Bitcoin Transaction Patterns. Big Data. 4, 2.

[33] Weimann, G., 2015. Going Dark: Terrorism on the Dark Web. Studies in Conflict & Terrorism. 39, 3, 195-206.

[34] Ron, D., Shamir, A., 2018. How Did Dread Pirate Roberts Acquire and Protect his Bitcoin Wealth?

[35] Fromknecht, C., 2015. One-Time, Zero-Sum Ring Signature. https://scalingbitcoin.org/papers/one-time-zero-sum-ring-signature-conner-fromknecht-2015.pdf (accessed 15 August 2018).

[36] Gervais, A., Karame, G., Capkun, S., Capkun, V., 2014. Is Bitcoin a Decentralized Currency? IEEE Security & Privacy. 12, 3, 6-7. https://eprint.iacr.org/2013/829.pdf (accessed 13 August 2018).

[37] Anderson, R., Shumailov, I., Ahmed, M., Making Bitcoin Legal. https://www.cl.cam.ac.uk/~rja14/Papers/making-bitcoin-legal.pdf (accessed 13 August 2018).

[38] Kalodner, H., Goldfeder, S., Chator, A., Möser, M., Narayanan, A., 2017. BlockSci: Design and applications of a blockchain analysis platform. https://arxiv.org/abs/1709.02489 (accessed 12 August 2018).

[39] Reid, F., Harrigan, M., 2012. An Analysis of Anonymity in the Bitcoin System. Security and Privacy in Social Networks. 197-223.

[40] Stanford, G., Stanford, T., 2018. Cointopia: Blockchain Analysis using Online Forums. https://web.stanford.edu/class/cs224w/projects/cs224w-87-final.pdf (accessed 12 August 2018).

[41] Böhme, R., Christin, N., Edelman, B., 2015. Bitcoin: Economics, Technology, and Governance. Journal of Economic Perspectives. 213-238.

[42] Rodrigues, M., Gama, J., Ferreira, C.A., 2012. Identifying Relationships in Transactional Data, in: Pavón, J., Duque-Méndez, N.D., Fuentes-Fernández, R. (Eds.), Advances in Artificial Intelligence – IBERAMIA 2012. Lecture Notes in Computer Science, Springer, Berlin, Heidelberg, 7637.

[43] Rojas, E., Gorton, D., Axelsson, S., 2015. Using the RetSim simulator for fraud detection research. International Journal of Simulation and Process Modelling. 10, 2.

[44] Rose, C., 2015. The Evolution of Digital Currencies: Bitcoin, A Cryptocurrency Causing A Monetary Revolution. International Business & Economics Research Journal (IBER). 14, 4, 617.

[45] Hong, Y., Kwon, H., Lee, S., Hur, J., 2018. Poster: De-mixing Bitcoin Mixing Services. https://pdfs.semanticscholar.org/5425/fb2c0a039bc16e5a4fe31a1b493094631462.pdf (accessed 22 August 2018).

[46] CoinDesk. (2017, Dec. 6). Cryptocurrency Mining Market NiceHash Hacked [Online]. Available: https://www.coindesk.com/62-million-gone-cryptocurrency-mining-market-nicehash-hacked [Accessed: Oct. 18, 2018].

[47] M. Conti, A. Gangwal, and S. Ruj, ―On the Economic Significance of Ransomware Campaigns: A Bitcoin Transactions Perspective,‖ Computers & Security, vol. 79, pp. 162-189, 2018. doi: 10.1016/j.cose.2018.08.008

[48] J. Yli-Huumo, D. Ko, S. Choi, S. Park, and K. Smolander, ―Where Is Current Research on Blockchain Technology? A Systematic Review,‖ PLoS ONE, vol. 11, no. 10, 2016. doi: 10.1371/journal.pone.0163477

[49] W. Shao, H. Li, M. Chen, C. Jia, C. Liu, and Z. Wang, ―Identifying Bitcoin Users Using Deep Neural Network,‖ in: J. Vaidya, and J. Li (eds), Algorithms and Architectures for Parallel Processing, ICA3PP 2018. Lecture Notes in Computer Science, Springer, Cham, 2018, vol. 11337, pp. 178-192.

[50] V. R. Patil, A. P. Nikam, J. S. Pawar, and M. S. Pardhi, ―Bitcoin Fraud Detection using Data Mining Approach,‖ Journal of Information Technology and Sciences, vol.4, no. 2, 2018.

[51] D. Zambre, and A. Shah, ―Analysis of Bitcoin Network Dataset for Fraud,‖ 2013. [Online]. Available: http://snap.stanford.edu/class/cs224w-2013/projects2013/cs224w-030-final.pdf [Accessed: Oct. 21, 2018].

[52] M. Bartoletti, B. Pes, and S. Serusi, ―Data mining for detecting Bitcoin Ponzi schemes, ‖ 2018. [Online]. Available: https://arxiv.org/pdf/1803.00646 [Accessed: Oct. 21, 2018].

Advances in Science, Technology and Engineering Systems Journal Vol. 4, No. 2, 413-421 (2019)

www.astesj.com

ASTESJ

ISSN: 2415-6698

A Novel Rule Based Technique to Detect Electricity Theft in India

Priyamvada Chandel[*,1], Tripta Thakur[2]

[1]Central Power Research Institute, Bhopal, India

[2]Maulana Azad National Institute of Technology, Bhopal, India

ARTICLE INFO

Article history:
Received:19 March, 2019
Accepted:12 April, 2019
Online: 26 April, 2019

Keywords:
Distributed power generation
Threshold current
Energy conservation
Data acquisition
Electricity

ABSTRACT

It is high time to control and prevent power theft by manipulating the meter reading and tampering of the meter. It is possible to deal power theft by developing Advanced Metering Infrastructure (AMI) and smart grids. For most of the distribution companies, utility smart meters' data is serving as wealthy source of information beyond billing. There are numerous methods for detection of meter inconsistencies and dishonest behavior like meter tampering based on past data. This paper proposes a "Rule Based" electricity theft detection methodology based on the detection of abnormal readings of phase voltages, currents and power factor communicated by smart energy meters to the central server of the utility in constant time interval of fifteen minute. Individual customer theft detection rate of 94.8% is achieved with 10% False Positive Rate, which is low. The proposed method is tested on real time data collected from smart meters installed in Raipur city of Chhattisgarh State Electricity Board India.

1. Introduction

In the process of market and regulatory reforms for electricity sector the most focused segment of value chain is "Distribution sector", due to its importance in financial flow. However, despite attention, Indian sector of distribution continues to be the weakest link and undergoes suffering from common drawbacks like high aggregate technical and commercial (AT&C)[1] losses. The current high level of AT&C losses incurred by the Indian distribution companies (DISCOM) is a matter of concern. Unfortunately non-technical losses (NTL)[2], are the most difficult to estimate as they include loss component which are not associated with system's physical features [1]. Due to losses as on 30 September 2015 Indian DISCOMs had an exceptional debt of Rs.4.3 trillion [2].

To take care of the financial viabilities of DISCOMs, which were in 'red' due to increased losses, Ministry of Power, Government of India launched ambitious Ujjwal DISCOM Assurance Yojana (UDAY) program in November 2015 to aim debt reductions of DISCOMs. The financial losses of utilities have cut down from Rs. 515.9 billion (~$8.14 billion) in 2016 Financial Year (FY) to Rs. 348.3 billion (~$5.49 billion) in the FY 2017 due to UDAY [3,4].

The ultimate sufferer due to NTL is the consumer as these losses are converted into economic losses by DISCOM, which further resulted as imposition of extra tariffs. Therefore; electric utility grids should be encouraged for developing programs to reduce NTL. The traditional way of detecting fraud is to carry out on-site inspection but the cost of onsite inspection for a number of customers may not be compensated with the value of the energy recovered. Another approach is observation of 'load profile[3]' of consumers. By customer's load-profile data, it is possible to detect significant deviations in the behavior that can be associated with NTL.

Wider use of smart energy meters has increased possibilities of detecting power theft by using power consumption data

[*]Corresponding Author: Priyamvada Chandel, Central Power Research Institute, Bhopal, India, Email Id: priyamvada@cpri.in

[1] Aggregate Technical and Commercial (AT&C) losses comprises of two components (a)Technical Losses (b) Non-Technical or Commercial losses. Technical losses occur due to power dissipation in the resistive elements of the network and transformer losses whereas the commercial losses occur due to improper meter readings, faulty meters, meter tampering, power theft etc.

[2] Theft is the main component of NTL

3 Utilities have customer energy consumption records to support their billing activities. One type of data is that of load profiles, which represents the behavioral characteristics of customers' electric power consumption during a specific period

https://dx.doi.org/10.25046/aj040251

communicated by smart meters to the utility server within a constant time interval. These meters may be subjected to anomalies related to meter securities, measurement interruptions and network intrusions. Advanced Metering Infrastructure (AMI) has made it possible to sense and store large amount of data communicated by smart meters. By applying suitable machine learning technique on such a large amount of smart meter data it has become possible to detect anomalies related to NTL.

Since the evolution of algorithms of machine learning, AMI have been widely applied for the assessment of the security of power system to overcome the disadvantages of conventional methods [5]. This section provides the overview of the reported work for NTL detection by using both conventional and modern data analytics methods. There has been an increasing interest in the development of techniques on the basis of extraction of patterns of consumer consumption behavior from historical data. These methods can be supervised, unsupervised or semi-supervised [6]. Unsupervised methods determine anomalies without prior knowledge about customers' behavior, and supervised methods determine both normal as well as abnormal behavior using a supervised classification that requires pre-classified data [7]. In [8], the development of representative load-profiles is presented as a reference for the analysis of NTL using classification algorithms, decision trees, and Naïve Bayes classifier. In [9,10], the authors propose the use of support vector machines (SVMs) to identify fraudulent customers. Load profiles are classified based on the typical or atypical content of their behavior. In [11], a methodology based on extreme learning machines (ELM) is presented. The characteristic load profile of a customer is developed on the basis of measurements obtained from customer load curve.

A methodology on the basis of Genetic Algorithm (GA) and SVM is presented in [12]. In another work a methodology deals with the variability of customer consumption, trend of consumption, and other contributions for NTL detection is presented [13]. In [14], the effectiveness of the SVM technique is compared with the extreme learning machine (ELM) technique. In [15] a hybridized classifier which utilizes grouping (clustering), Euclidean distance, dynamic time warp (DTW), and a weighted curve comparison algorithm were used.

In [16] two methods were suggested; one based on clustering with decision trees and other simpler approach permits users to be detected with severe consumption drops. In [17] a combinational approach is proposed using a fusion of statistical techniques, neural-networks (NNs) and text mining for the recognition of NTL. An optimal forest classifier (OPF) and its learning algorithm for the identification of NTL are reported in [18].

In [19] a methodology for the detection of NTL is presented using vector support machines (SVM). In [20] Hybrid selection algorithm between Harmony Search and Optimal Road Forest has been proposed. A two-step methodology that combines diffuse clustering based on C-means and a fuzzy classification is proposed in [21]. In [22], authors suggested improved methodology proposed in [14] by introducing a diffuse inference system. In [23], the authors present an integrated expert system (IES7) consisting different modules. Vector support machine trained with information gathered from smart meters, representing all available forms of fraud is presented in [24].

In [25] a mining-based methodology to identify NTL is described based on the statistical characterization of the energy patterns of consumers. A relative comparison study for the identification of NTL by the use of supervised machine learning techniques is discussed in [26]. In [27] the Pearson coefficient is used for evolution of user consumption and a model is developed based on Bayesian network and decision trees.

In [28] the customer data was analyzed using an Autoregressive (AR) model so as to predict the amount of energy consumed within a specific interval and then compare the result obtained against the user's current record that is low. A technique based on diffuse clustering is proposed in [29] in which number of clusters or groups is predefined. In [30] an artificial neural network is applied to the user classification process to be inspected. In [31] SVM and probabilistic neural networks (PNN) are used for the detection of energy theft. Extreme Learning Machines (ELM) and SVM are proposed in [32].

In [33], a knowledge-based system (KBS) is proposed, which is developed on the basis of knowledge and experience of inspectors and uses data mining, statistical-techniques and neural-networks (NNs). A methodology that uses a Time domain reflector meter (TDR) to determine the theft of energy is proposed in [34].

A surveillance system based on live machine learning techniques and automatic meter reading is proposed in [35, 36]. NTL are reviewed thoroughly and different methods have been recommended in [37]. Dynamic time wrap (DTW of non-technical losses in the electricity grid is review [38]. Detection of electricity theft detection in Indian) based approach suggested in smart meter data base nontechnical loss detection [39]. Various solution for detection of detection state is discussed in [40] by empirical analysis.

In [41], Random Matrix Theory is proposed for the detection of electricity theft in a system. Customer consumption pattern based detection of electricity theft in AMI is discussed in [42]. Decision tree and advanced data analytics based SVM for identification of theft is introduced in [43]. In [44], various methods of electricity theft and abnormalities in customer consumption patterns have been discussed.

It is evident from the reported literature that most of the techniques are based on supervised learning. These supervised approaches make use of such cases which have been detected previously to achieve equivalent patterns, that is, the techniques require pre-labeled data.

This paper suggests rule based theft detection technique for the utilities by using data mining and feature extraction tools if their customers are connected through smart meter. Data mining is a process whose major goal is to investigate, extract and store correlated data from huge databases, which contain histories of energy consumption through probabilistic and statistical tools. Feature extraction is the process of extracting special features from the measured data, such that it helps in the improvement of accuracy of the detection model. Parameters like three phase voltage, current and power factor are extracted and stored in the feature vector. This feature matrix is compared with the threshold values. Rule based theft detection technique frames a set of rules according to the result of comparison with threshold values. Thus, a Novel Rule Based Theft Detection Technique is suggested so as to improve the accuracy in individual electricity theft detection.

Following are the contributions of this paper:

- A new automated model using data mining is introduced with high percentage of probability of fraud detection in an agile, timely manner using MATLAB simulation, and the result obtained supports the decision-making and future investigations for improving the productivity of electric service companies, which will have a positive influence on financial sustainability and quality of service.
- The introduced model has a high percentage of specificity and sensitivity. In addition, it will help the electric energy recovery section to improve the NTL detection process in less time and lower costs with lesser quantity of field staff and thus avoid subjectivity.

The paper has introduction followed by review of the research in data mining to detect electricity theft in section I. In section II system model is proposed for electricity theft detection including data preparation, rules for type of meter tampering attempts mainly based on meter measurement interruption techniques. Section III includes model for individual electricity theft detection. Section IV presents results of the simulation and its comparison with other data mining methods. Section V presents a final conclusions and future scope of the work.

2. System Model for Electricity Theft Detection

A novel threshold based detection model for electricity theft detection has been prepared for analyzing the per phase voltage, current and aggregate power factor readings sent by three phase direct connected smart energy meters connected at individual customer premises for whole year. The analysis process is based on a systematic approach divided in sequential steps to get correct results of theft. Following are the steps for novel threshold based theft analysis.

2.1. Data Preparation

A distribution network with 'n' no. of buses is considered each of which is equipped with three phase direct connected smart meters. Every smart meter generates the time-series data of the respective bus, which includes the amplitude of the three-phase voltage, current, power factor, reactive and active power measurements.

The matrix V serves as system state data formulated as:

$$V^R = [v^1, v^2, ..., v^{(t)}]$$

$$V^Y = [v^1, v^2, ..., v^{(t)}]$$

$$V^B = [v^1, v^2, ..., v^{(t)}]$$

$$V^i = [V^R, V^Y, V^B] \tag{1}$$

$V^i = [V^R, V^Y, V^B]$

$V^1 = [V^R, V^Y, V^B]$

Similarly, current can be represented as:

$$I^i = [I^R, I^Y, I^B] \tag{2}$$

And power factor:

$$PF^i = [PF^R, PF^Y, PF^B] \tag{3}$$

The three-phase data matrix serves as the input factor for threshold based theft detection formulated as:

$$p = [V, I, PF] \tag{4}$$

p

The sequence of 12 months of the three-phase data matrix for independent user serves as the factor data formulated as:

$$P = [p_t^1, p_t^2, ..., p_t^{12}] \tag{5}$$

P

p_t

Once data matrix is formulated then next approach is to define the threshold according to certain rules for detection of theft. Initially, the central server gathers the current, voltage and power factor measurement data from the region. The signal patterns according to the formulated predictions matrix are compared with the instantaneous threshold patterns. If the signal patterns exceed the threshold values, then it is considered as electricity theft.

2.2. Rules for Threshold Detection

Threshold values of electrical parameters measured by smart meter for logging the abnormal meter tampering conditions are formulated by cumulating the meter tampering threshold values gathered from the requirements of various major Indian DISCOMs throughout the country.

This analysis has taken three major tampering conditions which are frequently used for power theft in the country out of various tampering methods.

As the voltage and current related tampering are the major causes which can affect the meter power measurements hence, illegal consumers would frequently try to decrease the amount of these parameters to decrease the consumption bills.

These tampering can be understood by following:

a) Voltage Link Missing

Theft condition can take place when either single phase or any two phase voltages are intentionally missing or reached a value less than a particular threshold value.

b) CT Bypass

This theft condition takes place when either one phase, any two phases or all three phases CT's of the smart meter externally/internally bypassed by putting external shorting link of low resistance between the source side and load side terminals of one or more phases of the meter. Due to low resistance of the shorting link most of the phase current passes through it and meter measures lesser current and hence records less energy consumed.

c) CT Open Phase Wise

This theft condition can take place when either single phase, two-phase currents are intentionally missing or reached a value less than a particular threshold value.

The smart meters used considered for this analysis are direct connected three phase four wire type, with 3x240volt as the reference voltage from supply side denoted by V_{ref} on the name plate of the meter, basic current I_b is 10Amp, maximum current rating of the meter is Imax=40Amp and the meter is of class 1. All the above discussed theft conditions are summarized in Table 1.

Table 1 Various Theft Conditions

Sl. no.	**Tamper Conditions**		
	Type of Tamper	**Occurrence Threshold**	**Restoration Threshold**
1	Link Miss phase wise	Vx < 60% Vref (Vx <144V)Ix > 20% Ib (Ix >2A)Any other Phase Voltage > 75 % Vref (Vp >180V)	Vx > 85 % Vref (Vx >204V) Any other Phase Voltage > 75 % Vref (Vall>180V
2	**CT Bypass**	Iavg > 2% Ibasic (Iavg >0.2A) Ibypass > 25 % Ibasic (Ibypass >2.5A)	Iavg > 2 % Ibasic (Iavg>0.2A) Ibypass < 20 % Ibasic(Ibypass <2A)
3	**CT Open phase wise**	Vx > 60 % Vref (Vx >144V) Ix < 2 % Ibasic (Ix <0.2A) Ibypass > 25 % Ibasic (Ibypass >2.5A)	Vx > 60 % Vref (Vx >144V) Ix > 2 % Ibasic (Ix >0.2A)

Pseudo Code of rules according to threshold values are discussed in Appendix - A.

3. Proposed Model for Individual Electricity Theft Detection

Fig.1 represents the structure of the distribution network used in this paper for preparing theft model and further theft analysis.

The communication between the AMI and the substation real-time monitoring of specific area is carried out with the Remote Terminal Units (RTU). This unit lists the total energy consumption registered by all the connected meters in that particular zone.

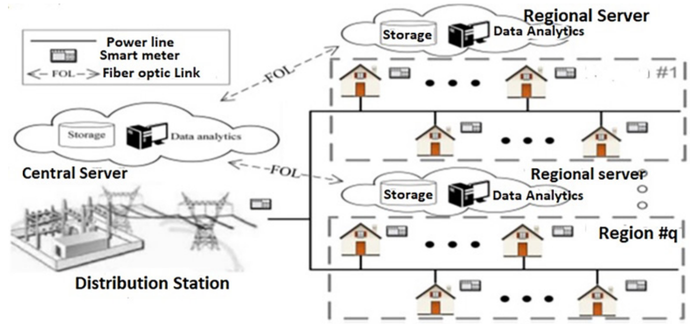

Figure 1 Distribution network processing and Data acquisition

The comparison of combined energy consumed by consumers belong to particular distribution supply system with the supplied energy appears as less accurate and impractical method, hence this paper proposes theft analysis for each customer individually by comparing instantaneous values of all three phase voltages, currents and aggregate power factor communicated by smart meters connected at each consumer premises. A novel rule based theft detection technique for the utility grids using feature extraction combined data mining technique is formulated. Obtained feature matrix is an augmented matrix of three features namely three phase voltage, current and aggregate power factor. These features are compared with the threshold of those parameters and a rule base is framed using those comparison results.

Initially, the network is separated into ns geographical regions. Each region is comprised of set of buses represented as B1, B2, …… Bn. After the successful detection of area of fraud, each user is individually investigated for the detection of electricity theft. The real-time process of analysis is identical to the regional method of theft detection approach, which is used to monitor anomalies in the pattern of consumption of all the customers. At the time step k, the values of the total three-phase voltages, currents along with power factor that can be used in qt region from equation (4) is given as:

$$P_q^k = [V_m^k, I_m^k, PF_m^k]$$

$I_m^{(k)}$ $V_m^{(k)}$

$PF_m^{(k)}$ m^{th}

P_q^k

$$t(i) = P_q^k =<$$

Where t(i) is the outcome of set of rules according to threshold for theft detection.

There are three different rules are presented for theft detection according to the cognitive pattern signal of electricity. The outcome of rules can be depicted as:

$$T^1 = \sum_1^3 t(i) \tag{8}$$

$$T^2 = t(i) \tag{9}$$

$$T^3 = \sum_1^2 t(i)$$

$$T^1, T^2 and T^3$$

Theft detection further estimated according to the voting of all saved values. The majority decision will be considered as final outcome for theft. In order to ensure automatic detection of anomalies, a threshold must be set. The threshold is obtained using the min-max criteria (i.e. minimizing FPR and maximizing the DR) to obtain a solution with high-performance for detecting theft of electricity[4].

With respect to Rules described in equations, the Theft can be defined as follows:

$$Theft = \max(T)$$

With the above discussion it is clear that theft detection is sequential procedure and each step got its own importance. Flow chart of the proposed detection method for electricity theft and its detailed function are mentioned in Appendix- B.

4. Simulation Results

The simulation results obtained from rule based threshold model have been discussed in this section. Performance of the proposed model is calculated in terms of percentage accuracy, precision and sensitivity. Based on the calculated parameters the method is compared with the other existing theft detection methods.

4.1. Dataset Explanation

Utilities have customer energy consumption records to support their billing activities. Load profile data represents the behavioral characteristics of customer's electric power consumption during a specific period. By using this data, it is possible to detect significant deviations in the behavior that can be associated with NTL. Handling such a big amount of data and extracting useful information from it is a new challenge. However, utilities are using data mining methods to correlate data from huge databases, which contain histories of energy consumption through statistical and probabilistic approaches.

In the proposed approach the smart meter dataset is collected from Raipur city of Chhattisgarh State Electricity Board (CSEB) India. The collected data is communicated to the central server of the utility by 41 three phase whole current smart energy meters for the period of one year (01.01.2017 to 01.01.2018), with 15 minutes of time interval. Each meter data information consists of Unique Meter Identity Number (MID), all three phase voltages, currents, consumed power and power factor for whole year with date and time.

4.2. Performance of Rule Based Theft Detection Method

The proposed performance of the rule based theft detection method is represented by confusion matrix. The confusion matrix comprises of information regarding predicted and actual classification values done by the classification system. The performance of the system is generally assessed using the matrix data. Theft event is logged by meter when value of any phase voltage or current crosses the pre decided threshold values discussed in table I. Theft event represented by value 1 and normal event by value 0.

Fig.2 represents the Confusion Matrix obtained by the proposed method; here rows and the columns are the labels of theft and normal detection from dataset. The matrix contains Output Class and Target Class. The confusion-matrix of proposed approach depicts that total 10,000 randomly picked samples from self-collected dataset have been considered, from which detection of 81 samples is wrongly considered as Normal which is represented by False Negatives (FN). False negative refer to undetected fraud committing consumers, creating financial loss for utility. The detection of 5565 samples is accurately detected as Normal called True Positive (TP).

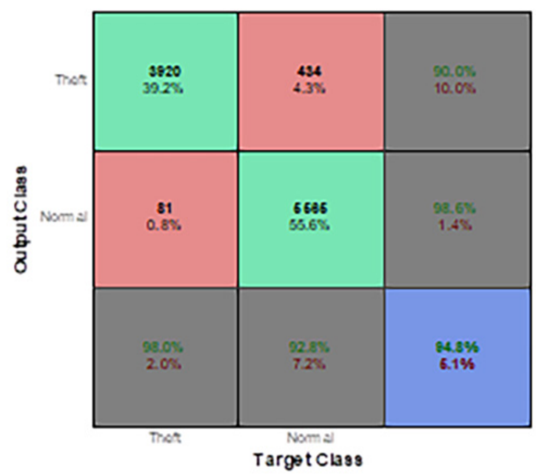

Figure 2 Confusion Matrix for Rule Based Theft Detection

$$\text{FPR (False Positive Rate)} = \frac{FP}{FP+TN} = \frac{434}{434+3920} = 10.0\%$$

$$\text{FNR (False Negative Rate)} = = \frac{FN}{FN+TN} = \frac{91}{91+3920} = 2.02\%$$

$$\text{TP (True Positive Rate)} = \frac{TP}{TP+FN} = \frac{5565}{5565+91} = 98.6\%$$

$$\text{Miss Rate} = \frac{FN}{TP+FN} = \frac{91}{5565+91} = 1.4\%$$

$$\text{Error Rate} = \frac{FN+FP}{TOTAL} = \frac{91+434}{1000} = 5.1\%$$

Finally, complete content and organizational editing before formatting. Please take note of the following items when proofreading spelling and grammar.

4 Although the Cyber-Physical System (CPS) facilitates a direct viewpoint about the correlations between voltage amplitude and energy consumption.

Calculations from the confusion matrix for the proposed method are obtained as per the formulae given in [45]:

The other important parameters calculated from the above confusion matrix are theft detection accuracy, precision and sensitivity of the proposed method.

Theft detection accuracy is the fraction of rightly classified instances by the classification model. For the proposed rule based detection method the theft detection accuracy is calculated as follows:

$$\text{Accuracy} = \frac{TP + TN}{TP + +TN + FP + FN} = \frac{3920 + 5565}{10000} = 94.8\%$$

Fig.3 represents the accuracy graph of the proposed method based on the above calculation for two class labels one is normal and other is theft. Theft represented by class number 1 and normal data represented by class number 2 in the graph.

Precision is defined as the fraction of true positive instances among the overall identified instances as positive by the theft detection method.

$$\text{Precision} = \frac{TP}{TP + FP} = \frac{5565}{5565 + 434} = 92.76\%$$

Fig.3 represents the precision graph of the proposed method based on the above calculation for two class labels one is normal and other is theft.

Sensitivity of the detection method represents its ability to correctly detect the theft cases. Sensitivity is known as the fraction of true positive instances among the true positive and false negatives. For the detection of fraudulence both false negative (FN) and false positive (FP) predictions must be controlled.

$$\text{Sensitivity} = \frac{TP}{TP + FN} = \frac{5565}{5565 + 91} = 98.56\%$$

Fig.3 represents the sensitivity graph of the proposed method based on the above calculation for two class labels one is normal and other is theft. Theft represented by class number 1 and normal data represented by class number 2 in the graph.

4.3. Comparing the Proposed Method with Existing Theft Identification Methods

Comparison between the results of the suggested methodology and other existing methods discussed in [41,42,43,44] are presented in Table II. The performance evaluation is done on the basis of accuracy of detection, false positives, used strategy, privacy and implementation and maintenance costs. It is found that the Random Matrix Theory (RMT) based method (with a threshold of 1.5) is defined as an efficient technique compared to other techniques.

Moreover, the suggested approach produces efficient outputs than RMT and other techniques with FPR 10%. Hence, setting the threshold is an efficient way to ensure automatic detection of low FPR anomalies.

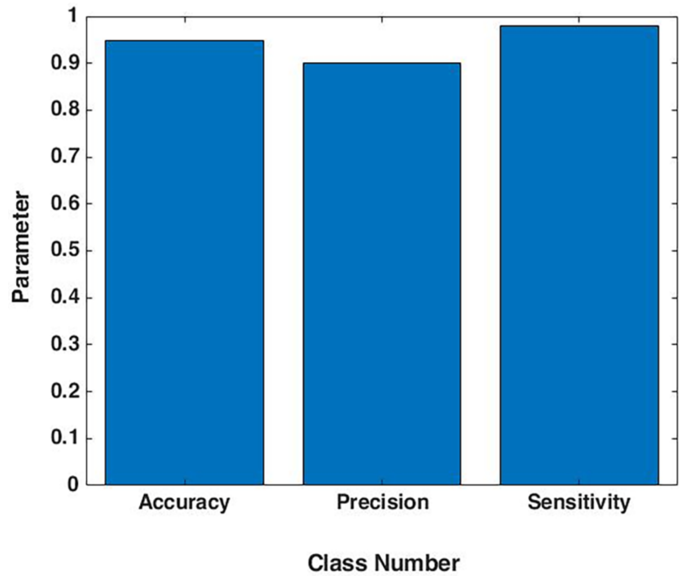

Figure 3 Accuracy, Precision and Sensitivity graph for Rule Based Theft Detection

The accuracy of the proposed technique is 94.8%, which is better compared to the SVM approach. In addition, the power management system ensures that the efficiency of the proposed technique complies with the standard and aggregated data at the substation. low voltage either illegally or anomalously. Hence, the process used here is appropriate to detect electricity consumption abnormalities at multiple levels.

Table 2 Comparative Analysis of Proposed and existing theft detection methods

Parameters	**Proposed Method**	**RMT [41]**	**Multi class SVM [42]**	**DT couple SVM [43]**	**One-class SVM [42]**	**Fuzzy classification [44]**
Detection Rate (DR)%	94.8	91.5	94.0	92.5	76.0	74.5
False Positive Rate (FPR) %	10.0	1.5	11.0	5.1	29.0	33.1
Approach Used	Region and Customer level	Region and Customer level	Region and Customer level	Distribution and Customer level	Region and Customer level	Customer level
Privacy Preservation	Medium	Medium	Medium	Weak	Medium	Weak
Cost	Medium	Medium	Medium	High	Medium	Low

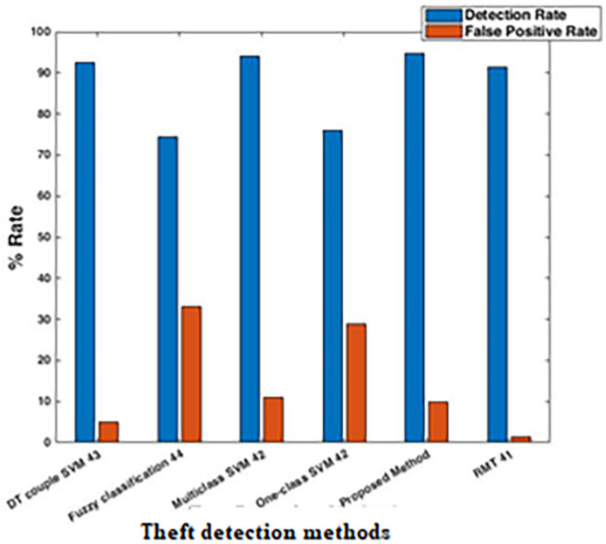

Figure. 4 Comparative analysis of proposed and existing theft detection methods

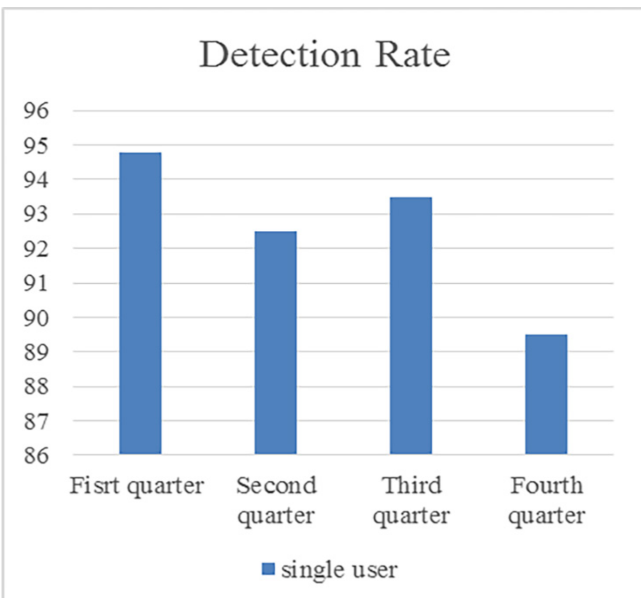

Figure. 5 Detection Rate with different time periods

4.4. Effect of Seasons on Theft Detection Rate

To analyze the seasonal effect on theft detection rate (DTR) the entire smart meter data is divided in equal time periods of three months' duration hence the whole year data is represented by four subsets.

On calculations of DTR for whole year it is found that the first quarter data claims approximately 94.8 % of detection rate, a higher accuracy compare to other quarters for the same region whereas the fourth quarter claims minimum accuracy i.e. 89 %.

Fig. 5 shows the detection rate of proposed algorithm for twelve months' data.

4.5. Analysis of Percentage Loss and Received Values in Units

Theoretically calculation of losses is done by determining supplied electricity then deducting the energy billed/paid from it. Moreover, NTL are calculated as follows:

$$Total.Energy.Losses = Energy.Supplied - Bills.paid \tag{12}$$

$$Total.Energy.Losses = NTL + TL \tag{13}$$

Combining equations (12) and (13), we get:

$$NTL = Energy.Supplied - Bills.Paid - TL \tag{14}$$

Percentage losses are calculated as:

$$Percentage.loss = \left(\frac{ReceivedValue - SoldValue}{ReceivedValue}\right)*100 \tag{15}$$

Fig. 6 shows the decline of percentage loss with increase in the received values. According to equation (15), Fig. 6 claims that when received values i.e. bill collection from defaulters or all users of electricity are high, then the percentage losses to the utility will be low.

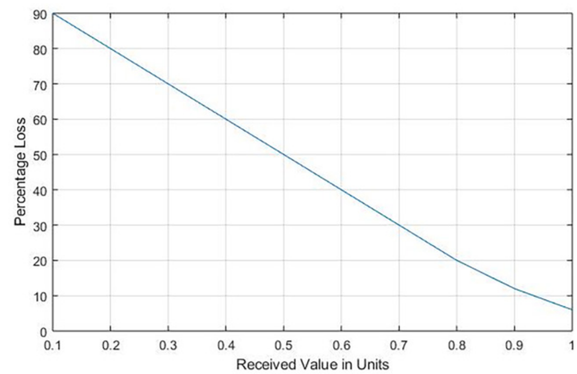

Figure. 6 Percentage Loss vs. Received Value

5. Conclusion

In the above paper, a novel data based approach for theft detection is suggested and comparison of its performance with existing methods in different types of electricity theft and operational conditions is done. Since it only requires measurement of the voltage, current and power factor-amplitudes as communicated by smart-meters, the suggested method is very viable and authentic. Moreover, the method doesn't depend on the power-system modeling and the pre-classification of the load. It is observed from simulation studies that the proposed method detects dishonest customers with an accuracy of 94.8% (high) with false positive rate of 10% (low). The presented method not only recognizes the inconsistencies in the consumption of electricity, but also shows the type of electricity theft at the customer-end. The above method encourages creating an automated model that detects cases of electric power fraud with greater efficiency, quick inspection of supplies which will help ailing DISCOM in India, to overcome financial losses due to AT&C losses and have a positive impact on financial sustainability and quality of service.

Conflict of Interest

The authors declare no conflict of interest.

Acknowledgment

The authors are grateful to Central Power Research Institute Bhopal, and MANIT Bhopal for providing the necessary facilities to carry out this research work.

References

[1] Tooraj Jamasb, Tripta Thakur, Baidyanath Bag, "Smart electricity distribution networks, business models, and application for developing countries," Energy Policy,Vol. 114, Pages 22-29, 2018.

[2] Baidyanath Bag, Tripta Thakur, "A Utility Initiative based Method for Demand Side Management and Loss Reduction in a Radial Distribution Network Containing Voltage Regulated Loads, " IEEE International Conference on Electrical Power and Energy Systems, Bhopal, Pages 52- 57, 2016.

[3] Government of India, Power Finance Corporation Ltd. Report on, " The Performance of State Power Utilities for the years 2016 ". [Online] Available: http://www.pfcindia.com/.

[4] Government of India, Power Finance Corporation Ltd. Report on, " The Performance of State Power Utilities for the years 2017, " [Online] Available: http://www.pfcindia.com/

[5] Venkatesh T, Trapti Jain, " Synchronized measurements-based wide-area static security assessment and classification of power systems using case based reasoning classifiers," Computers and Electrical Engineering, Vol. 68, Pages 513-525, 2018.

[6] Thomas B Smith, " Electricity theft: a comparative analysis, " Energy Policy, Vol. 32, Issue 18, Pages 2067-2076, 2004.

[7] V. J. Hodge and J. Austin, "A Survey of Outlier Detection Methodologies," Artificial Intelligence Review, Vol. 22, Issue 2, Pages 85-126, 2004.

[8] A. H. Nizar, Z. Y. Dong, J. H. Zhao and P. Zhang, "A Data Mining Based NTL Analysis Method," IEEE Power Engineering Society General Meeting, Tampa, FL, Pages 1-8, 2007.

[9] A. H. Nizar, Z. Y. Dong and P. Zhang, "Detection rules for Non-technical losses analysis in power utilities," IEEE Power and Energy Society General Meeting - Conversion and Delivery of Electrical Energy in the 21st Century, Pittsburgh, PA, Pages 1-8, 2008.

[10] J. Nagi, A. M. Mohammad, K. S. Yap, S. K. Tiong and S. K. Ahmed, "Non-Technical Loss analysis for detection of electricity theft using support vector machines," IEEE Power and Energy Conference, Johor Bahru, Pages 907-912, 2008.

[11] A. H. Nizar, Z. Y. Dong and Y. Wang, "Power Utility Non-Technical Loss Analysis with Extreme Learning Machine Method," IEEE Transactions on Power Systems, Vol. 23, Issue 3, Pages 946-955, 2008.

[12] J. Nagi, K. S. Yap, S. K. Tiong, S. K. Ahmed and A. M. Mohammad, "Detection of abnormalities and electricity theft using genetic Support Vector Machines," TENCON– 2008, IEEE Region 10 Conference, Pages 1-6, 2008.

[13] Biscarri, F., Monedero, Í., León, C., Guerrero, J. I., "A Mining Framework to Detect Non-Technical Losses in Power Utilities, " Proceedings of the 11th International Conference on Enterprise Information Systems, Pages 96– 101, 2009.

[14] A. H. Nizar and Z. Y. Dong, "Identification and detection of electricity customer behaviour irregularities," IEEE Power Systems Conference and Exposition, Seattle, Pages 1-10, 2009.

[15] F. Fabris, L. R. Margoto and F. M. Varejao, "Novel Approaches for Detecting Frauds in Energy Consumption," Third International Conference on Network and System Security, Gold Coast, Pages 546-551, 2009.

[16] I. Monedero, F. Biscarri, C. León, J.I. Guerrero, J. Biscarri, and R. Millán, " New Methods to Detect Non-Technical Losses on Power Utilities", Proceeding (683) IASTED Artificial Intelligence and Soft Computing, Sept. 2009, Spain.

[17] J. I. Guerrero, C. León, F. Biscarri, I. Monedero, J. Biscarri and R. Millán, "Increasing the efficiency in Non-Technical Losses detection in utility companies," 15th IEEE Mediterranean Electrotechnical Conference, Pages 136-141, April 2010, Valletta.

[18] Caio C. O. Ramos, André N. Souza, João P. Papa, Alexandre X. Falcão," Learning to Identify Non-Technical Losses with Optimum-Path Forest," IWSSIP 2010, 17th International Conference on Systems, Signals and Image Processing, Pages 154-157, 2010.

[19] J. Nagi, K. S. Yap, S. K. Tiong, S. K. Ahmed and M. Mohamad, "Nontechnical Loss Detection for Metered Customers in Power Utility Using Support Vector Machines," IEEE Transactions on Power Delivery, Vol. 25, Issue 2, Pages 1162-1171, 2010.

[20] Caio C.O. Ramos, André N. Souza, Giovani Chiachia, Alexandre X. Falcão, João P. Papa, "A novel algorithm for feature selection using Harmony Search and its application for non-technical losses detection, " Computers & Electrical Engineering, Vol. 37, Issue 6, Pages 886-894, 2011.

[21] E. W. S. Angelos, O. R. Saavedra, O. A. C. Cortés and A. N. de Souza, "Detection and Identification of Abnormalities in Customer Consumptions in Power Distribution Systems," IEEE Transactions on Power Delivery, Vol. 26, Issue 4, Pages 2436-2442, 2011.

[22] J. Nagi, K. S. Yap, S. K. Tiong, S. K. Ahmed and F. Nagi, "Improving SVM-Based Nontechnical Loss Detection in Power Utility Using the Fuzzy Inference System," IEEE Transactions on Power Delivery, Vol. 26, Issue 2, Pages 1284-1285, 2011.

[23] Carlos León, Félix Biscarri, Iñigo Monedero, Juan I. Guerrero, Jesús Biscarri, Rocío Millán, "Integrated expert system applied to the analysis of non-technical losses in power utilities, " Expert Systems with Applications, Vol. 38, Issue 8, Pages 10274-10285, 2011.

[24] S. S. S. R. Depuru, L. Wang and V. Devabhaktuni, "Support vector machine based data classification for detection of electricity theft," IEEE/PES Power Systems Conference and Exposition (PSCE), Phoenix, Pages 1-8, 2011.

[25] C. Leon, F. Biscarri, I. Monedero, J. I. Guerrero, J. Biscarri and R. Millan, "Variability and Trend-Based Generalized Rule Induction Model to NTL Detection in Power Companies," IEEE Transaction on Power Systems, Vol. 26, Issue 4, Pages 1798-1807, 2011.

[26] Yap K.S., Tiong S.K., Nagi J., Koh J.S.P., Nagi F., "Comparison of Supervised Learning Techniques for Non-Technical Loss Detection in Power Utility, " International Review on Computers and Software, Vol. 7. Issue 2, Pages 626-636, 2012.

[27] Iñigo Monedero, Félix Biscarri, Carlos León, et al., "Detection of frauds and other non-technical losses in a power utility using Pearson coefficient, Bayesian networks and decision trees, " International Journal of Electrical Power & Energy Systems, Vol. 34, Issue 1, Pages 90-98, 2012.

[28] Abdullateef, A.I. and Salami, M. J., Eyiomika, et al., "Electricity theft Prediction on Low Voltage Distribution System Using Autoregressive Technique," International Journal of Research in Engineering and Technology, Vol. 1, Issue 5, Pages 250-254, 2012.

[29] T. V. Babu, T. S. Murthy and B. Sivaiah, "Detecting unusual customer consumption profiles in power distribution systems — APSPDCL," IEEE International Conference on Computational Intelligence and Computing Research (ICCIC), Enathi, Pages 1-5, 2013.

[30] Breno C. Costa, Bruno. L. A. Alberto, et al., "Fraud Detection in Electric Power Distribution Networks Using an Ann-based Knowledge-Discovery Process," International Journal of Artificial Intelligence & Applications (IJAIA), Vol. 4, Issue. 6, Pages 17-23, 2013.

[31] Mandava, Srihari, Vanishree J. and Ramesh V., "Automation of Power Theft Detection Using PNN Classifier," International Journal of Artificial Intelligence and Mechatronics, Vol. 3, Issue 4, Pages 118-122, 2014.

[32] D. Dangar, S.K.Joshi, "Electricity Theft Detection Techniques for Distribution System in GUVNL," International Journal of Engineering Development And Research, Pages 11-18, 2014dd.

[33] Juan I. Guerrero, Carlos León, Iñigo Monedero, et al., "Improving Knowledge-Based Systems with statistical techniques, text mining, and neural networks for non-technical loss detection, " Knowledge-Based Systems, Vol. 71, Pages 376-388, 2014.

[34] Hossein Pourarab M, Alishahi S, Aghli N, " Electric power theft detection using time domain reflectometer," 23rd International Conference on Electricity Distribution, June 2015, Lyon.

[35] T. Hartmann et al., "Suspicious electric consumption detection based on multi- profiling using live machine learning," IEEE International Conference on Smart Grid Communications (SmartGridComm), Miami, Pages 891-896, 2015.

[36] McDaniel, Patrick, and Stephen McLaughlin, "Security and privacy challenges in the smart grid," IEEE Security & Privacy, Vol.7, Issue 3, Pages 75-77, 2009.

[37] Messinis, G.M. and Hatziargyriou, N.D.,"Review of non-technical loss detection methods, " Electric Power Systems Research, Vol.158, Pages 250-266, 2018.

[38] Villar-Rodriguez, E., Del Ser, J., Oregi, et al., " Detection of non-technical losses in smart meter data based on load curve profiling and time series analysis, " Energy, Vol.137, Pages 118-128, 2017.

[39] Viegas, J.L., Esteves, P.R., Melício, R., et al., " Solutions for detection of non-technical losses in the electricity grid: A review, " Renewable and Sustainable Energy Reviews, Vol. 80, Pages 1256-1268, 2017.

[40] Gaur, V. and Gupta, E., " The determinants of electricity theft: An empirical analysis of Indian states, " Energy Policy, Vol.93, Pages 127-136, 2016.

[41] Xiao, Fei, and Qian Ai, "Electricity theft detection in smart grid using random matrix theory," IET Generation, Transmission & Distribution, Vol. 12, Issue 2, Pages 371-378, 2018.

[42] Jokar, P., Arianpoo, N., Leung, V.C.M., " Electricity theft detection in AMI using customer's consumption patterns, " IEEE Transaction on Smart Grid, Vol.7, Issue 1, Pages 216–226, 2016.

[43] Jindal, A., Dua, A., Kaur, K., et al., " Decision tree and SVM-based data analytics for theft detection in smart grid, " IEEE Transaction on Industrial Informatics, Vol. 12, Issue 3, Pages 1005–1016, 2016.

[44] Angelos, E.W.S., Saavedra, O.R., Cortés, O.A.C., et al., " Detection and identification of abnormalities in customer consumptions in power distribution systems, " IEEE Transaction on Power Delivery Vol. 26, Issue 4 , Pages 2436–2442, 2011.

[45] Miller, Harvey J., and Han, J. "Geographic Data Mining and Knowledge Discovery." Geographic data mining and knowledge discovery (2001): 1.

Appendix-A

Pseudo Code of rules according to threshold

*Vref = 3*240;*

Ibasic = 10;

% RULES for Theft Detection

a) *% RULE-1 for* Voltage Link Missing

```
if sum([Vr, Vy, Vb] < 0.6*Vref)
dec(1) = dec(1)+1;
end
if sum([Ir, Iy, Ib] > 0.2*Ibasic)
dec(1) = dec(1)+1;
end
if sum([Vr, Vy, Vb] > 0.75*Vref)
dec(1) = dec(1)+1;
end
```

b) *% RULE-2 for* CT Bypass

```
if sum([Ir, Iy, Ib])/3 > 0.02*Ibasic
dec(2) = dec(1)+1;
if sum([Irbypass,Iybypass,Ibbypass] > 0.25*Ibasic
dec(2) = dec(1)+1;
end
```

c) *% RULE-3 for* CT Open Phase Wise

```
if sum([Vr, Vy, Vb] > 0.6*Vref)
dec(3) = dec(3)+1;
end
if sum([Ir, Iy, Ib] < 0.02*Ibasic)
dec(3) = dec(3)+1;
end
```

Appendix-B

Steps of proposed Rule Based Theft Detection Method for electricity theft and its detailed function

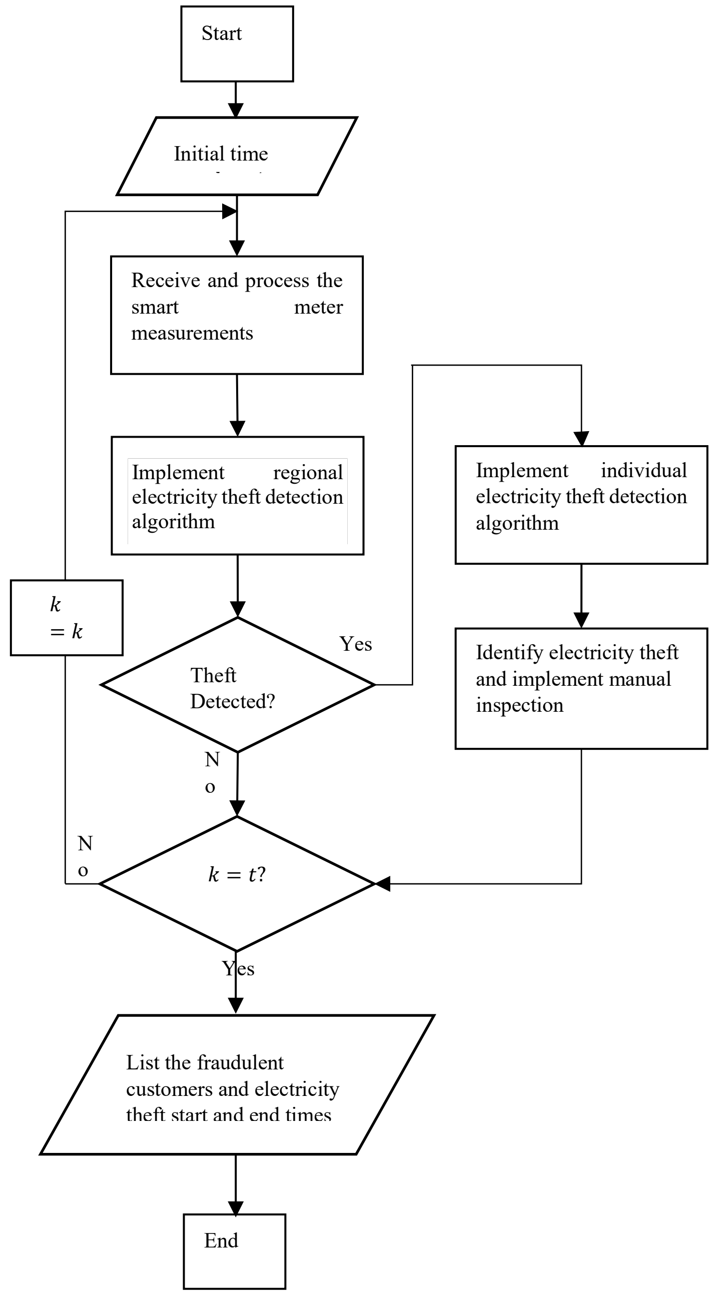

Advances in Science, Technology and Engineering Systems Journal Vol. 4, No. 2, 422-428 (2019)

www.astesj.com

ASTESJ

ISSN: 2415-6698

Evaluation of IEEE 802.11n and IEEE 802.11p based on Vehicle to Vehicle Communications

Danilo Caceres*, Edgar Murillo[1], Hector Poveda[2], Kang-Hun Jo[3]

[1]*Facultad de Ingenieria Eléctrica, Universidad Tecnológica de Panamá, Panamá*

[2]*Facultad de Ingeniería Eléctrica Universidad Tecnológica de Panamá, Panamá*

[3]*A Kang-Hyun Jo Intelligent Systems Laboratory, University of Ulsan South Korea*

A R T I C L E I N F O

Article history:
Received:03 March, 2019
Accepted:26 March, 2019
Online: 26 April, 2019

Keywords:
Vehicle to vehicle communications
Wireless communication
80211n
802.11p
Intelligent vehicle systems

A B S T R A C T

This Journal is an extension of work originally presented in conference on Human System Interaction (HSI), although the current standard for vehicular communication is the 802.11p, those devices are still very expensive. To achieve our goal we simulated the wave propagation using Win Pro Solutions which include Proman, Wallman software and field test of 802.11n.

1. Introduction

This section we focus in the properties of propagation of electromagnetic waves, second section related works, third section simulation of the standard that we want to compare and in the final section the results.

Radio propagation is the behavior of electromagnetic waves in the radio spectrum when propagating, from one point to another. Like light waves, radio waves are affected by the phenomena of reflection, refraction, diffraction, absorption, polarization and dispersion and interference. Understanding the effects of different conditions on the propagation of the radio has many practical applications such as: frequency selection, power, type of modulation, type of antenna, among others. To simulate how electromagnetic waves propagate the WinProp software was used, this software includes a set of tools for simulation in the domain of wireless propagation and radio network planning. To solve this problem, the Friis equation was used to calculate the power received from an antenna, when it is transmitted from another antenna, as follows:

$$P_r = P_t G_t G_r (\lambda/4\pi R)^2 \text{ (Dbm)} \quad (1)$$

Where P_r is the power at the receiving antenna, P_t is the transmitted power, G_t is the gain in the transmitted antenna, G_r is the gain in the received antenna, R is the distance from the transmitted antenna to the received antenna, λ is the wavelength. This is the equation used by the PROMAN software to calculate the behavior of the propagation of the different wireless systems.

Our real objective was design a low cost vehicular communication system to prevent for frontal and read collision, the system designed allow to send vital information between vehicles that are within the coverage and limitations of the communication protocol used. The system to be designed will be able will be able to establish a vehicular communication between the mobile nodes. Because the V2V network does not behave like a conventional star network with a main node assigning the IP addresses, other alternatives such as Ad-Hoc networks will be searched.

2. Related Works

Considering the above-mentioned paragraph, the initiatives are addressing the problem of how to improve monitoring vehicle communication capacities in order to reduce accident risk. The ongoing studies are focused mainly on calculating the performance of communication [1], [2], [3], understanding of the environment surrounding [4], [5], the geometry-based vehicular propagation modeling and simulation [6], [7], as well as a vehicular cloud-based communication

Researchers [8] used the Friis equation to estimate the distance between the mobile device and the access point within an indoor environment using a trilateration strategy. Researchers in [9] analyzed how the performance of the V2V communication system

* Danilo Caceres, Email: danilo.caceres@utp.ac.pa

https://dx.doi.org/10.25046/aj040252

in a controlled or not environment. To do this, the author uses the Network Simulator (NS2). In that sense, Authors in [10] proposed to use the optimized network engineering tools (OPNET) simulator to introduce a modeling and solution of a large scale vehicle communication problem.

The main difference of our journal is that in most of the cases investigation for vehicular communication where based using 802.11a standard that is no longer being used. We also focus our investigation in the possibility to use 802.11n for V2V because the 802.11p standard hardware are too expensive.

3. Simulation Analysis

To mesure the cause and effect between the urban environment and the V2V/V2I communication model a performance evaluation between both IEEE 802.11n and IEEE 802.11p standards were developed. The statistical measurement analysis was conducted at the Causeway Islands, Amador, Panamá, see Figure 1. To do that a database of the urban scenario was created using WinProp software. The 3D model of the urban environment was edited and generated using WallMan software, while to predict the propagation the ProMan software was used. The electrical specifications of the Raspberry Pi that has been used in the simulation process are shown in Table I and Table II.

TABLE I
ANTENNA PARAMETERS FOR THE RASPBERRY PI

Frequency range	2400 to 2500 MHz
Impedance	50 Ω
SWR	2.0 max.
Gain	1.5 dBi max.
Polarization	Linear
Beam width	Omni-directional

Note: FCC ID Web [11]

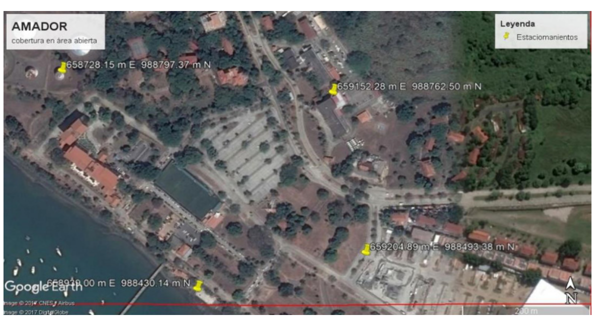

Figure 1. Satellite image of open area , Panama

Figure 2. Satellite image urban area, Panamá.

TABLE II
WIFI MODULE PARAMETERS FOR THE RASPBERRY PI

1Frequency of operation	2400 to 2483.5 MHz
Modulation types	GFSK / BPSK
Occupied channel bandwidth	1 MHz
Channel spacing	1 MHz
ITU emission designator	1MF1D/1MG1D
Declared output power	8 dBm

Note: FCC ID Web [11]

3.1. Image Reference

To get the reference image to be used in the IEEE 802.11n and IEEE 802.22p simulation task the satellite image of the following places located in Panama City were used: Amador and Via España. Google Earth Maps was used to get the satellite imagery and geospatial information of the selected areas. The information was added to Wallman Sofware as follows:

- Height in meters. Building, trees and objects are limited to a height of 732 meters.
- Width and Length in meters. This was done by subtracting the UTM coordinates, in case of the width from the East to the West, to extract the length the coordinates from the North to the South were subtracted.
- Finally, the process was repeated for all those areas within the image were the propagation model should be computed.

3.2. Scenery Recreation

In this section we proceed to create the database that will be used in the Proman to determine the propagation of the following way.

- To define the environment information, the indoor database and draw option was selected. It is important to emphasize that to perform the simulation with different urban scenarios the indoor database option should be used. Using this option, objects such as trees, bulk, building, as well as other objects are added into the database.
- Due to the absence of 3D maps information of the urban area, the option draw was used to describe the 3D environment data.
- Then the catalog material properties for different frequency bands of materials [12].
- Once the catalog is imported into the database, the georeferenced image was created by specifying units in meters. This process can also be done by using UTM coordinates (X,Y), however it will cause some difficulties viewing images because pixels are not correctly mapped into the simulator.
- Finally, database information of buildings and other objects were added.

Figure 3 and 4 shows the process result. The information related to the trees was shown into the image using a cylinder shapes in green.

TABLE III
REAL TEST RESULTS.

D^a [m]	t_1 [m]	t_2 [m]	t_3 [m]	t_4 [m]	t_5 [m]	t_6 [m]	t_7 [m]	t_8 [m]	t_9 [m]	t_{10} [m]	A [m]
0.5	24	25	24	23	24	23	22	23	21	22	23.1
1.0	40	54	42	40	44	46	42	40	53	41	44.2
2.5	51	44	45	47	45	47	46	49	47	46	46.7
5.0	50	52	49	50	49	49	51	50	52	51	50.3
10.0	66	69	69	64	66	65	67	63	62	60	65.1
20.0	63	78	80	77	75	76	80	73	71	73	74.6
30.0	78	77	74	75	78	76	77	75	72	77	75.9
40.0	78	78	79	80	78	77	82	75	74	75	77.6
50.0	83	81	79	80	78	81	80	80	81	82	80.5
60.0	83	81	78	84	84	83	84	75	76	80	80.8
70.0	83	78	78	80	80	78	86	82	80	79	80.4
80.0	85	84	83	86	83	86	86	84	85	81	84.3
90.0	83	84	84	83	86	82	83	80	79	80	82.4
100.0	81	83	84	79	78	79	84	81	82	80	81.1

Note: D is the distance between the antennas, from t1 to t2 are the samples results in meters, A are the average in meters.

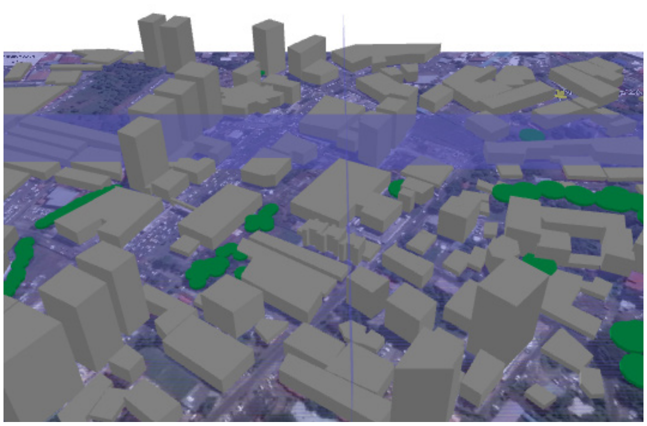

3.3. *Simulation Process*

To analyze the effect of the 3D urban environment under the propagation model used in the V2V/V2I communication systems a simulation was developed as follows:

- Firstly, select the connection to the database that it was created in the previous section. To do that, in the scenario section the indoor database was selected while in the indoor 3D section the database previously created was the selected one.
- Secondly, the propagation point was added. Here in the simulation option choose the time variant.
- Thirdly, the type of transmitter site and antenna were selected considering an omni-directional type which is the Raspberry Pi 3 antenna.
- Fourthly, the Raspberry PI 3 transmitter parameters were defined. This task was done using channel 1, the frequency is 2.41GHz and the transmission power is 8 dBm and the antenna 1.5 dBi. The parameters of the WIFI module BCM43438 since both are from the same manufacture, Raspberry does not provide enough information about it.
- Finally, at this step the propagation can be computed.

Here, the tasks consist in verifying the radiated power. To do that the test involves measuring the power intensity receive in a notebook using a Raspberry Pi 3 as a transmitter. This process starts by taken measures at every certain distance by measuring the power intensity received in a laptop with a WiFi analyzer. Figure 3 shows the tests from 0.5 to 100 meters that were made to the Raspberry Pi 3. Table III shows the results of this task.

4. Experimental Results

The results of the comparison is presented in this section. To do that, the error between both IEEE standards were computed using MatLab. Figure 5 and Figure 6 show the expected result between the both IEEE standards, 802.11n and 802.11p respectively. In case of the simulation task it can be observed that at the same power transmission, the more distance increase, the more attenuated the signal is in the IEEE 802.11p. It should be clearly noticed that those differences are basically due to the fact that the 802.11p standards were developed for data quality while the 802.11n was designed for transmission speeds.

The results in Figure 7 have shown that for the practical results (data in blue) there is high attenuation (over 16%) compared with the simulations using the 802.11p and 802.11n standards. Since the vehicle-to-vehicle prototype system is taken into consideration to work with a low data rate, the proposed V2V prototype system is a promising strategy to deal with the problem of vehicle communication. Although there is a drawback of the proposed implementation of the V2V over the IEEE 802.11n standards, the problem of oversaturation on 2.4GHz band due to the presence of devices is compensated with the use of OFDM.

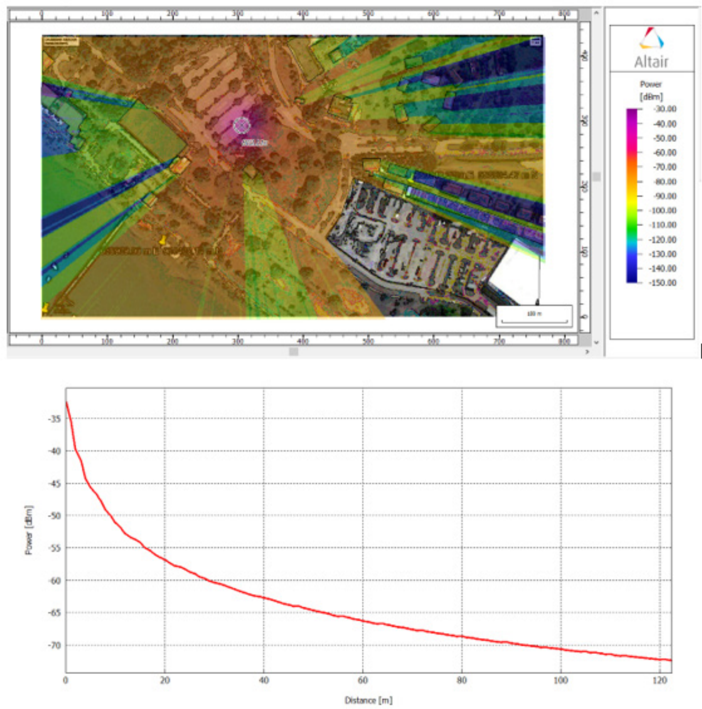

Figure 5. Experimental results using the IEEE standard 802.11n. In the Top right hand, we can see that there is the scale of color intensity according to the power in dBm. The height at which the propagation was simulated was about 1.3 meters. The region where colors are not visible is due to the existence of an installed metal fence about 4 meters high.

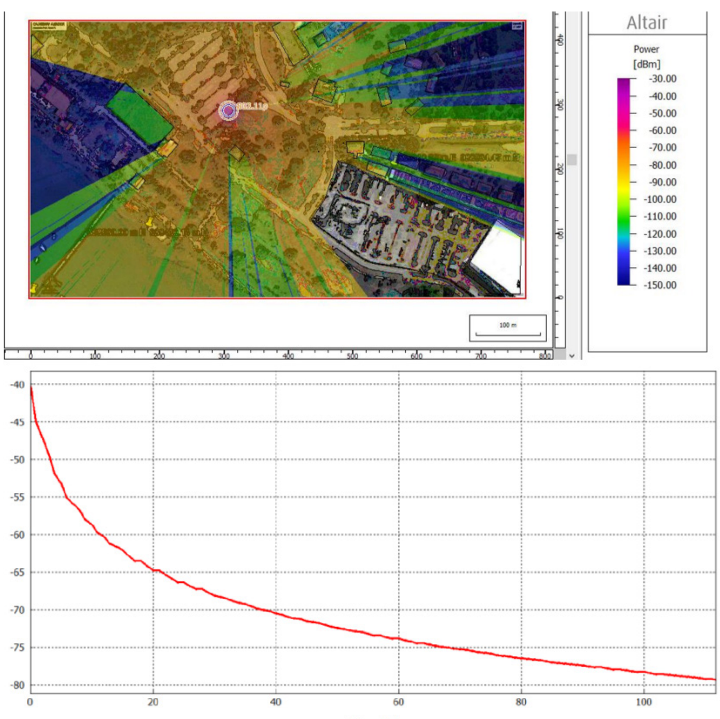

Figure 6. Experimental results using the IEEE standard 802.11p. If we compare with the previous figure we see clearly that the 802.11p signal at the same power weakens more quickly

At this point it is important to mention that the 802.11p standard uses a transmission power above 13 dBm but for comparative purposes between both standards we will place the power and gain parameters of the antenna at the same value. The 802.11p standard uses more power as it aims to cover from 300 meters to 1000 meters above all to compensate for the loss in urban spaces.

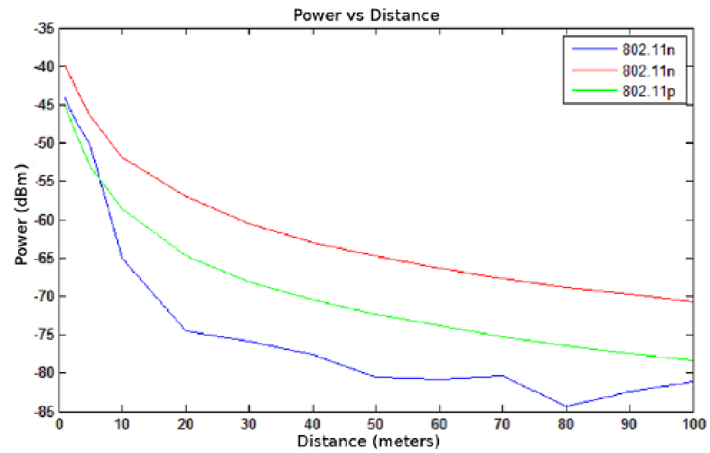

Figure 7. Experimental results using the IEEE standard 802.11p. If we compare with the previous figure we see clearly that the 802.11p signal at the same power weakens more quickly

5. Implementation:

At present there are different types of vehicle control algorithms, we will limit ourselves to determining the collision time (TTC). The condition of collision can occur when the driver in front suddenly stops or slows downs when the driver behind is going too fast. This type of collisions represents 23% of the collisions that occur on the roads.

Figure 8 is an example of the type of collisions that can occur on the road. The vehicle A in an accident case suffered a rear collision, while the vehicle B a front collision.

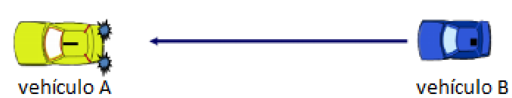

Figure 8. Vehicle A Vehicle B

- **Microcontroller:** For this task the Raspberry PI 3 reduced board computer with Linux Rasbian operating system and Python programming language will be used. This will be responsible for processing the information acquired, formatting, sending and receiving information through the network and finally send alarms or alerts to the driver about possible risks.

- **Acquisition of data:** This task will be performed by the serial receiver of the Global Positioning System (GPS) and the bluetooth reader of the vehicular diagnostic port (OBD II) that will allow us to access the vehicle's data bus (CAN Bus).

- **Wireless communication:** The communication will be made using the 802.11n module integrated in the Raspberry Pi 3 in the 2.4GHz band. The network topology will be Ad-Hoc.

- **Alerts:** the alert system will be used to indicate the distance and time of collision and if the event is a rear or front collision.

Figure 9 details the components to be used in the development of our prototype and the way in which everyone interacts and communicates with each other:

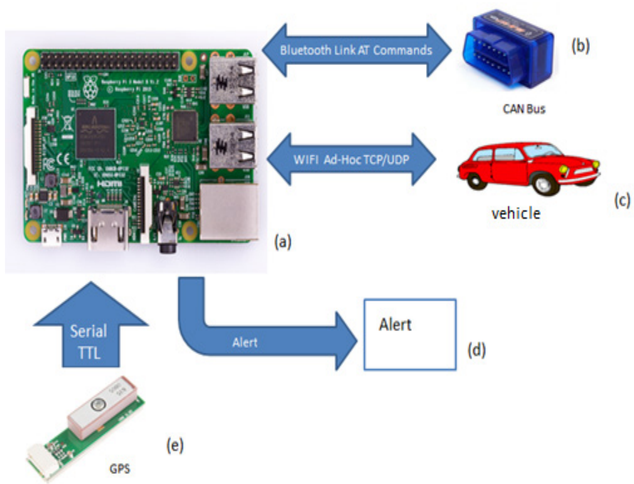

Figure 9. V2V prototype

In order to calculate and predict the collision is important to know each of the factors involves that may cause failure to our algorithm.

Latency due to the transmission of data, acquisition times and information processing are factors of vital relevance for our algorithm since when the data is received it has been some time since it was captured. Table IV of times involved to be considered in the calculation of collision time.

Table IV Latency Times

Tiempo de latencia a considerar.
T0: Time when the vehicle data is available in the electronic systems of the vehicle.
T1: Data capture of CAN bus and time at which the GPS position information is updated. This is the real time the event was detected, and it will be the information that will be sent
T2: Time taken by the message to be processed and sent to the wireless network
T3: Time in which the message is received in the access layer (antenna level) in the receiver.
T4: Time the decoding of the received message data and it is ready for processing
T5: Time in which the processing of the received data is completed. The application can request a driver action, if applicable.
T6: Time is that it takes the information processed in giving an alert the driver either sonorously or visually

With these 6 times involved we can easily predict the trajectory of the vehicles involved in a possible collision. Figure 10 below shows how the information flows between the vehicles involved in a possible collision

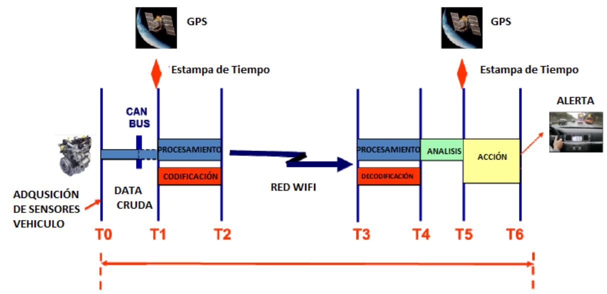

Figure 10. Processing time.

6. Experimental Results V2V communication

In order to verify the results of systems already in operation, the equipment was installed in two vehicles. Figure 11 and Figure 12 show the result of the GPS positions of the X-Trail vehicle and the data received from the Kicks vehicle.

Figure 11. GPS track of prototype installed in Nissan Kicks

Figure 12. GPs track of prototype installed in Nissan Kicks received by Nissan X-trail

Based on the results obtained, we passed the data acquired by a Kalman filter to determine the accuracy of the GPS positions of the path used. Figure 13 and Figure 14 below show the real data in red and the result of the prediction using the Kalman filter.

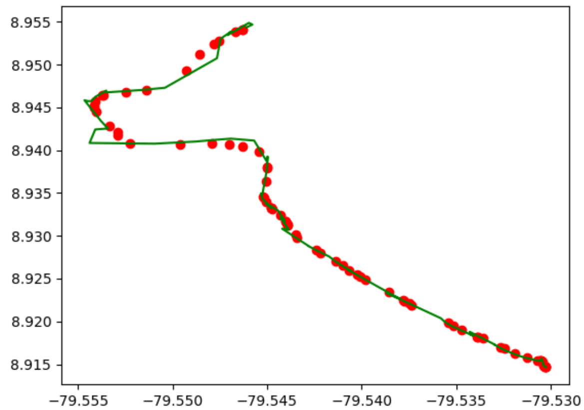

Figure 13. First track

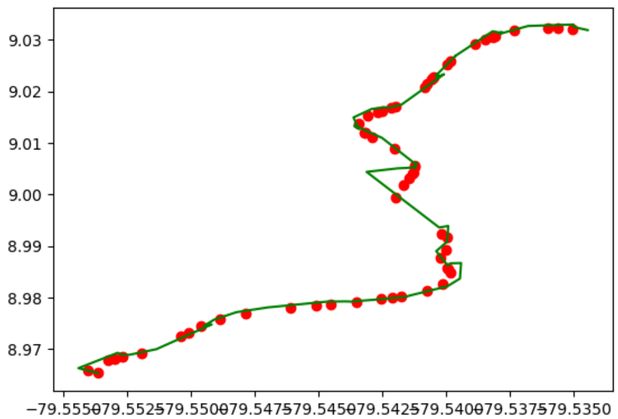

Figure 14. Second Track

We proceed do a statistical analysis of the results obtained for each of the tracks. These results are shown below in the table

Table V. First track statistical results

Data	Result
Average absolute error of latitude	6.36607E-05 %
Average absolute error of the length	53.2094E-05 %
Correlation coefficient of latitude	0.999
Coefficient of correlation of length	0.997

Table VI. Second track statistical results

Data	Result
Average absolute error of latitude	6.36607E-05 %
Average absolute error of the length	53.2094E-05 %
Correlation coefficient of latitude	0.999
Coefficient of correlation of length	0.997

From the previous figure and the statistical analysis, we can realize that where there is loss of data or information for the Kalman filter it is difficult to make an accurate prediction especially if this path involves curves.

TABLE VII. Summary of the changes/additions made to the extended version.

Applications: Including the final implementation we were looking for with the 802.11n propagation study

Graphical material: Including simulation graphics of the propagation environment, graphs of actual tests of the V2V communication system designed, Kalman filter path graphs

Tables: including table of the statistical results of the V2V system designed

Motivation: The main motivation to study the propagation of 802.11n was to design a low-cost vehicular communication system

a. Context: Added more information related with the implementation.

b. Conclusions: Added conclusion related use 802.11n in vehicular environments

c. Introduction: Additional information related with the final implementation.

Acknowledgment

The authors would like to thank the National Bureau of Science, Technology and Innovation of Panamá (SENACYT) and the Sistema Nacional de Investigación (SNI) of Panama (SNI 168-2017, SNI 153-2017).

In both analytical and simulation results, the IEEE 802.11n standards achieved a good performance of propagation studies than the IEEE 802.11p standard. Future analysis of the proposed systems will be focused on the effects of the weather conditions.

References

[1] Y. R. Hidayanti, N.A. Siswandari, and O. Puspitorini. N. Sneddon, "An analysis of simulation-based vehicle to vehicle (V2V) communication system in main street of Surabaya," In 2015 International Electronics Symposium. Indonesia, pp. 183–188.
[2] R. I. Meneguette, and A. Boukerche, "Peer to peer protocol for allocated resources in vehicular cloud based on V2V communication", In 2007 IEEE Wireless Communications and Networking Conference. Spain, pp. 1–6.
[3] M. Cheong, Y. Lee, W. Park, and I. Yeom, "Analysis of V2V communication for ADAS," IN 2017 Ninth International Conference on Ubiquitous and Future Networks. Czech Republic, pp. 248-246.
[4] Z. H. Mir and F. Filali, "Simulation and perfomance evaluation of vehicle-to-vehicle (V2V) propagation model in urban environment," In 2016 7th International Conference on Intelligent Systems, Modelling and Simulation. Thailand, pp. 394-399.
[5] B. U. Rani, and S. Tarannum, " A channel modelling considering varied environmental model for dsrc based V2V application services," In 2016 International Conference on Devices, Circuits and Systems. India, pp. 48-53.
[6] L. Chen, B. E. Henty, F. Bai, and D. D. Stancil, "Highway and rural propagation channel modeling for vehicle-to-vehicle communications at 5.9 Ghz," In 2008 IEEE Antennas and Propagation Society International Symposium. United States, pp. 1-4.
[7] T. Abbas, J. Nuckelt, T. Kaijrner, T. Zemen, C.F. Mecklenbrauker, and F. Tufvesson, "Simulation and measurement-based vehicle-to-vehicle channel characterization: accuracy and constraint analysis," IEEE Transactions on Antennas and Propagation, 63(7), pp. 3208-3218, July 2015.

[8] F. Lassabe, P. Canalda, P. Chatonnay, F. Spies, and O. Baala, "A Friss-based calibrated model for wifi terminals positioning," In IEEE International Symposium on a World of Wireless Mobile and Multimedia Networks. Italy, pp. 382-387.
[9] V. Khairnar, and K. Kotecha, "Propagation models for V2V communication," In Vehicular ad-hoc Networks, 61, pp. 686-695, January, 2014.
[10] T. Islam, Y. Hu, E. Onur, B. Boltjes, and J. F. C. M. de Jongh, "Realistic simulation of IEEE 802.11 p channel in mobile vehicle to vehicle communication," In 2013 Conference on Microwave Techniques. Czech Republic, pp. 156-161.
[11] FCC ID, "FCC ID 2ABCB-RPI3BP". [Online]. https://fccid.io/2ABCB-RPI3BP
[12] GlobalMaterial-Catalogue.mcb. https://connect.altair.com/

Conference Papers:
[13] E. Murillo, D. Caceres, H. Poveda, K. Jo, "Evaluation of IEEE 802.11n and IEEE 802.11p based on Vehicle to Vehicle Communications," In International Conference on Human System Interaction (HIS), 2018.